TECHNISCHE UNIVERSITÄT MÜNCHEN

Lehrstuhl für Anorganische Chemie mit Schwerpunkt Neue Materialien

Reactions of Ge_9 Clusters –

Functionalization, Linkage and Cluster Expansion

Sabine Frischhut

Vollständiger Abdruck der von der Fakultät für Chemie der Technischen Universität München zur Erlangung des akademischen Grades eines

Doktors der Naturwissenschaften (Dr. rer. nat.)

genehmigten Dissertation.

Vorsitzender: Prof. Dr. Thomas Brück

Prüfer der Dissertation:

1. Prof. Dr. Thomas F. Fässler
2. Hon.-Prof. Dr. Richard W. Fischer
3. Prof. Dr. Peter Jutzi

Die Dissertation wurde am 22.11.2018 bei der Technischen Universität München eingereicht und durch die Fakultät für Chemie am 13.12.2018 angenommen.

Die vorliegende Arbeit wurde im Zeitraum von November 2015 bis Dezember 2018 erstellt.

„Die Tatsache, dass man etwas über den Himmel weiß, ändert an seinem Zauber nichts.“

(Harald Lesch, Ludwig Maximilians Universität München, 2009)

DANKSAGUNG

Zuallererst möchte ich einen ganz besonderen Dank an meinen Doktorvater **Prof. Dr. Thomas F. Fässler** aussprechen, der mir die Möglichkeit gegeben hat, dieses überaus interessante und herausfordernde Thema zu bearbeiten, der mich immer wieder aufs Neue motivieren konnte und, der mir mit seinen Ratschlägen jederzeit zur Seite stand. Durch die Freiheiten, die er mir gab, konnte ich mich uneingeschränkt entfalten.

Des Weiteren möchte ich noch denjenigen danken, die wertvolle Beiträge zum Entstehen dieser Arbeit beigetragen haben:

Manuela Donaubauer danke ich für die hervorragende Organisation sämtlicher bürokratischer Angelegenheiten, sowie für die freundliche und schnelle Hilfe bei sämtlichen Fragen. Kleine Plauderminuten gaben mir immer wieder neuen Schwung für den Tag.

Ein herzliches Dankeschön gilt **Dr. Manuel M. Bentlohner**, der mich für das Thema begeistern konnte und, durch den ich letztendlich an den Lehrstuhl gekommen bin. Er stand mir besonders zu Beginn meiner Promotion stets mit hilfreichen Ratschlägen zur Seite.

Dr. Wilhelm Klein danke ich für seine schnellen Hilfen bei kristallographischen Fragestellungen und Problemen und für seinen Humor, der mich immer wieder zum Lachen brachte.

Dr. Annette Schier danke ich für die aufmunternden Worte und gute Zusammenarbeit, auch im Praktikumsbetrieb des ACIII Praktikums, sowie für die Inspiration bezüglich neuer Reiseziele.

Für nette Gespräche und Karrieretipps danke ich **Dr. Nathalie Kunkel**.

Prof. Dr. Peter Jutzi danke ich für die hilfreichen Diskussionen und das großzügige Decamethylsilicocen-Geschenk. Seine Ideen lieferten Beiträge zu einigen faszinierenden Ergebnissen.

Bedanken möchte ich mich auch bei **Dr. Markus Drees**, **Prof. Dr. Antti J. Karttunen** und **Jasmin Dums** für die Durchführung der zahlreichen quantenmechanischen Rechnungen.

Prof. Dr. Fritz E. Kühn und **Dr. Felix Kaiser** möchte ich für die fruchtbare Zusammenarbeit danken.

Prof. Dr. Bernhard Rieger und **Markus Pschenitza** danke ich für die Bereitstellung des UV-Vis Spektrometers und die Einführung in das Gerät.

Ein Dankeschön geht auch an **Prof. Dr. Roland A. Fischer** und **Konstantin Epp** für die nette Zusammenarbeit innerhalb eines Kooperationsprojektes.

Die unterstützende Arbeit durch Studenten hat nicht nur diese Arbeit, sondern auch mich stets bereichert. Deswegen danke ich meinen Masteranden, meiner Bachelorandin und meinen Studenten **João Guilherme Machado de Carvalho**, **Kevin Frankiewicz**, **Nicole Willeit**, **Melanie Ripsam**, **Catharina Theiß**, **Florian Petermichl**, **Louis Hartmann** und **Lilla Koser** für die engagierte Mitarbeit, sowie die Durchführung zahlreicher Synthesen und Messungen.

Dr. Patrick Woidy danke ich für die Einführung in die Glasbläserei und die nette Fahrt mit dem Feuerwehrauto.

Für zahlreiche Messungen danke ich **Maria Weindl** und **Christine Schwarz** (VT-NMR), **Lorenz Schiegerl** und **Christina Fischer** (ESI-MS), **Ulrike Ammari** und **Bircan Dilki** (Elementaranalyse), **Prof. Dr. Manfred Scheer** und **Felix Riedlberger** (CV-Messungen), **Katia Rodewald** (EDX, SEM), **Maria Müller** (EDX), **Dr. Gabriele Raudaschl-Sieber** (MAS-NMR), **Dr. Carmen Haeßner** (EPR) sowie allen Angestellten der **Feinmechanikwerkstatt** und der **Glasbläserei** für die Ausführung sämtlicher Aufträge.

An dieser Stelle will ich auch ein großes Danke an den **Verband der Chemischen Industrie** aussprechen, der mich mit dem FCI-Stipendium (**F**onds der **C**hemischen **I**ndustrie) großzügig finanziell und auch ideell gefördert hat. Des Weiteren danke ich der **TUM Graduate School** für die Finanzierung einiger Soft Skills Kurse, der **Gesellschaft Deutscher Chemiker** für die erteilten Reisestipendien, sowie der **TU München** für die Auszeichnung durch den Manchot Studienpreis.

Ein herzliches Dankeschön geht auch an **Prof. Dr. Richard W. Fischer**, der mich mit seinem Engagement und seiner Persönlichkeit begeistert. Danke für das offene Ohr bei zahlreichen Problemen und Fragestellungen.

Besonders danken möchte ich meinen Laborkollegen **Sebastian Geier** und **Michael Giebel** für den Spaß im Labor, der dem Arbeitsalltag einen schönen Ausgleich gab. Durch dich Sebastian konnte ich auch meinem niederbayerischen Temperament freien Lauf lassen. **Marina Boyko** danke ich für netten Plauderminuten und gemeinsame Weinabende und **Benedikt Witzel** für seine ansteckende Leichtigkeit.

Mein besonderer Dank geht an meine Kollegin und Freundin **Kerstin Mayer** für die ständige Hilfsbereitschaft, wenn es Probleme sämtlicher Art gab. Die zahlreichen Diskussionen, Plauderstunden und gemeinsamen Sportaktivitäten lieferten immer wieder neue Kraft und Motivation.

Ich möchte mich bei der gesamten **Fässler-** und **Nilges-Gruppe** für die angenehme Arbeitsatmosphäre bedanken. Auch die gemeinschaftlichen Konferenzbesuche, die netten Grillabende, die jährlichen Drachenbootrennen, Oktoberfestbesuche und Feiern waren stets unterhaltsam und ein hervorragender Ausgleich zur Arbeit.

Ein riesengroßes Dankeschön geht an meine Eltern, **Susanne** und **Siegfried**, die mir die Promotion durch ihre mentale und finanzielle Unterstützung erst ermöglicht haben. Ihr Stolz war Teil meiner treibenden Kraft während meiner gesamten Ausbildung bis hin zur Promotion. Ebenso möchte ich meinen Geschwistern **Bettina** und **Sascha** für den Zusammenhalt in der Familie danken.

Außerdem will ich an dieser Stelle auch meine **Freunde** und **Verwandte** erwähnen, die mir immer wieder gezeigt haben, dass es auch ein Leben außerhalb der Arbeit gibt. Ich möchte dabei insbesondere meinen unternehmungslustigen Reisepartnern **Christine**, **Mary**, **Dane** und meinen Freundinnen **Catharina** und **Lidia** danken, die immer für mich da sind und immer wieder für ein Abenteuer gut sind. **Karen** danke ich für die Freundschaft, die sogar über eine Distanz von 7500 km hält.

Danke möchte ich auch meinen verstorbenen **Großeltern** und meiner **Oma Elisabeth** sagen, die mich z.T. bis zum Abschluss meiner Promotion begleitet haben. Ihr unermesslicher Stolz hat mich immer angetrieben.

Zuletzt möchte ich mich bei **Philippe** bedanken, der mir zu jeder Zeit Rückhalt gibt, und mir mit seiner Fürsorge das Gefühl verleiht, jedes Hindernis überwinden zu können.

ZUSAMMENFASSUNG

Deltaedrische homoatomare Tetrelelement-Cluster sind eng verwandt mit den Fullerenen und stellen daher interessante Moleküle bezüglich ihrer elektronischen Struktur und ihrer Reaktivität gegenüber organischen Verbindungen dar. Analog zu Fullerenen können Ge_9 Cluster verschiedene Ladungen annehmen ($[Ge_9]^{n-}$, n = 2-4) und können unter Bildung von Zintl Triaden untereinander kovalent verknüpft werden. Aufgrund dieser Eigenschaften wurden Fullerene intensiv als Materialien für Solarzellen untersucht. Obwohl Ge_9 Cluster schon seit langer Zeit bekannt sind, steckt die Herstellung maßgeschneiderter Ge_9-Cluster-basierender Materialien immer noch in den Anfängen.

Vergleichende UV-Vis spektroskopische Studien von simplen $[Ge_9]^{2-}$-Clustern und Fullerenkäfigen zeigten ähnliche elektronische Strukturen für C_{60} Fullerene und $[Ge_9]^{2-}$-Cluster auf, was die enge Verwandtschaft zwischen den beiden Gerüststrukturen bekräftigt. Inspiriert von der Analogie zwischen Ge_9-Zintl-Clustern und Fullerenen wurde die erste Fulleren-analoge Zintl Triade $[R-Ge_9-CH=CH-CH=CH-Ge_9-R]^{4-}$ (R = (2*Z*,4*E*)-7-amino-5-azahepta-2,4-dien-2-yl) synthetisiert und genauer untersucht. In diesem Zusammenhang wurde die Reaktivität von 1,4-Bis(trimethylsilyl)butadiin gegenüber Ethylendiamin (*en*) und $[Ge_9]^{4-}$ mittels *in situ* NMR-Spektroskopie untersucht. Für diese Reaktion wurde festgestellt, dass kleinen Mengen an Wasser, die in *en* enthalten sind, eine bedeutende Rolle zukommt. In diesem Zusammenhang wurde die Rolle von Wasser in der Reaktion zwischen 1,4-Bis(trimethylsilyl)butadiin und *en* aufgeklärt. Dabei wurde eine Methode für die qualitative Wasserbestimmung in *en* entwickelt. *In situ* NMR Studien gaben Einblicke in den Mechanismus der Bildung des 1,3-butadien-1,4-diyl Linkers und erlaubten den Zugang zur neuen Zintl Triade $[Ge_9-CH=CH-CH=CH-Ge_9]^{6-}$ durch Reaktion von A_4Ge_9 (*A* = K, Rb) mit 1,4-Bis(trimethylsilyl)butadiin in *en*, welches unter Anderem strukturell bestimmt wurde. Basierend auf diesen Ergebnissen ging die Zintl Triade $[H_2C=CH-Ge_9-CH=CH-CH=CH-Ge_9-CH=CH_2]^{4-}$ aus der Reaktion von K_4Ge_9 mit Bis(trimethyl)acetylen und 1,4-Bis(trimethylsilyl)butadiin in *en* hervor. Die Struktur des Anions zeigt ein ausgedehntes, konjugiertes π-Elektronen System.

Die Reaktion von $[\{(Me_3Si)_3Si\}_3Ge_9]^-$ mit Alkylbromiden lieferten sowohl die erzielten neutralen Verbindungen $\{(Me_3Si)_3Si\}_3Ge_9(CH_2)_nCH=CH_2$ (n = 1, 2, 3), die terminale Doppelbindungen tragen, als auch $\{(Me_3Si)_3Si\}_3Ge_9(CH_2)_2CH_3$ und $\{(Me_3Si)_3Si\}_3Ge_9(CH_2)_3Ph$.

Als wesentlich einfachere und übertragbare Methode zur spezifischen organo-Funktionalisierung stellte sich die Acylierung von $[\{(Me_3Si)_3Si\}_3Ge_9]^-$ mit Säurechloriden heraus, wodurch eine Reihe an acyl-substituierter Cluster $\{(Me_3Si)_3Si\}_3Ge_9(CO)R'$ (R' = Me, *i*Pr, *t*Bu, Ph, Bz, cyclopropylmethyl, $(CH_2)_2Ph$, 4-vinylphenyl) zugänglich wurde. Die erhaltenen Produkte zeigten, gestützt von Temperatur-abhängigen NMR Studien, dynamisches Verhalten in Lösung an. Mittels röntgenographischer Untersuchungen wurde insbesondere für $\{(Me_3Si)_3Si\}_3Ge_9(CO)tBu$ eine Decarbonylierung in Lösung nachgewiesen.

Daneben wurde auch eine synthetische Methode zur Herstellung von geladenen organo-funktionalisierten Ge_9 Clustern entwickelt, die noch reaktive Stellen zur weiteren Cluster-Substitution tragen. Die Reaktion von $[\{(Me_3Si)_3Si\}_2Ge_9]^{2-}$ mit Ethylbromid in thf führte zur Bildung von $[\{(Me_3Si)_3Si\}_2Ge_9CH_2CH_3]^-$, das in einem Folgeschritt nach Zugabe von 2,2,2-crypt einen Silyl-Liganden abstrahiert, wodurch das Anion $[\{(Me_3Si)_3Si\}Ge_9CH_2CH_3]^{2-}$ gebildet wird. Auch die Reaktion von $[\{(Me_3Si)_3Si\}_2Ge_9]^{2-}$ mit Säurechloriden lieferte eine Reihe neuer Verbindungen $[\{(Me_3Si)_3Si\}_2Ge_9(CO)R']^-$ (R' = *t*Bu, Ph, CH_2Ph, $(CH_2)_2Ph$, 9-anthracenyl, C_5H_4-Fe-C_5H_5), die mittels NMR-Spektroskopie und Massenspektrometrie untersucht wurden.

Neben der spezifischen Funktionalisierung von Ge_9 Clustern wurde erstmals ein Beispiel einer 3D Verknüpfung von Ge_9 Zintl Clustern gezeigt, bei der vier Ge_9 Cluster dreidimensional kovalent untereinander über ein zentrales Ge Atom verknüpft sind. Aus der Umsetzung von $[\{(Me_3Si)_3Si\}_2Ge_9]^{2-}$ mit $[SiCp^*][B(C_6F_5)_4]$ in Fluorbenzol in Anwesenheit von $[Li(OEt_2)_x][B(C_6F_5)_4]$ ging $[[\{(Me_3Si)_3Si\}_2Ge_9]_4Ge]^{4-}$ hervor. Die Struktur des Anions wurde mittels Einkristalldiffraktometrie bestimmt.

Für elektronisches Feintuning von Ge_9-Cluster-basierten, nanostrukturierten Materialien ist Dotierung nicht wegzudenken. Zu diesem Zweck zeigten wir die Eingliederung von Übergangsmetallen in das *nido*-Ge_9-Clustergerüst von $\{(Me_3Si)_3Si\}_3Ge_9CH_2CH_3$ durch dessen Reaktion mit η^2-Ethylen-Bis(triphenylphosphan)nickel(0) und dem entsprechenden Pt-Analogon. Dabei wurden die Verbindungen $\{(Me_3Si)_3Si\}_3CH_3CH_2[Ge_9M]PPh_3$, die einen *closo*-[$MGe_9$]-Kern enthalten, erhalten (M = Ni, Pt). Aus einer weiteren Synthese ging das erste Beispiel hervor, bei dem ein niedervalentes Tetrelelement in das deltaedrische Ge_9 Clustergerüst integriert wurde. Durch Reaktion von $[\{(Me_3Si)_3Si\}_2Ge_9]^{2-}$ mit $[SiCp^*][B(C_6F_5)_4]$ in Fluorbenzol in Anwesenheit von Li Kationen wurde die Verbindung $\{(Me_3Si)_3Si\}_2Cp^*[LiSiGe_9](SiCp^*)_2[Ge_9SiLi]Cp^*\{(Me_3Si)_3Si\}_2$ erhalten.

ABSTRACT

Deltahedral homoatomic tetrel element clusters are closely related to fullerenes, and thus are interesting molecules with respect to their electronic structure as well as their reactivity towards organic compounds. Analogously to fullerenes, Ge_9 clusters can adopt different charges ($[Ge_9]^{n-}$, n = 2-4) and can be covalently linked to form Zintl triads. Due to these features, organo-fullerenes have been thoroughly investigated as materials in solar cells. Even though, Ge_9 Zintl clusters have been known for a long time, the generation of tailor-made Ge_9 cluster-based materials through specific functionalization, for example, is still in its infancy.

Comparative UV-Vis spectroscopic investigations of bare Ge_9 clusters and fullerene cages revealed similar electronic structures for C_{60} fullerenes and $[Ge_9]^{2-}$ clusters reinforcing the close relation between them. Inspired by the analogy between Ge_9 Zintl clusters and fullerenes, the first fullerene analogous Zintl triad $[R-Ge_9-CH=CH-CH=CH-Ge_9-R]^{4-}$ (R = (2*Z*,4*E*)-7-amino-5-azahepta-2,4-dien-2-yl) was synthesized and further investigated. In this respect, the reactivity of 1,4-bis(trimethylsilyl)butadiyne towards ethylenediamine (*en*) and $[Ge_9]^{4-}$ was studied by *in situ* NMR spectroscopy. Traces of water in *en* play a significant role in this reaction. In this context, the role of water in the reaction of 1,4-bis(trimethylsilyl)butadiyne with *en* was enlightened. Thereby, a method for qualitatively tracing water-contents in *en* was developed. *In situ* NMR investigations gave insights into the mechanism of the formation of the 1,3-butadien-1,4-diyl linker and gave access to the new Zintl triad $[Ge_9-CH=CH-CH=CH-Ge_9]^{6-}$ by the reaction of A_4Ge_9 (A = K, Rb) with 1,4-bis(trimethylsilyl)butadiyne in *en*, which was among others structurally characterized. Based on these results, the Zintl triad $[H_2C=CH-Ge_9-CH=CH-CH=CH-Ge_9-CH=CH_2]^{4-}$ emerged from the reaction of K_4Ge_9 with bis(trimethylsilyl)acetylene and 1,4-bis(trimethylsilyl)butadiyne in *en*. The structure of the Zintl anion comprises an extended conjugated π-electronic system.

The reaction of $[\{(Me_3Si)_3Si\}_3Ge_9]^-$ with alkyl bromides afforded the targeted neutral compounds $\{(Me_3Si)_3Si\}_3Ge_9(CH_2)_nCH=CH_2$ (n = 1, 2, 3) comprising terminal double bonds, as well as $\{(Me_3Si)_3Si\}_3Ge_9(CH_2)_2CH_3$ and $\{(Me_3Si)_3Si\}_3Ge_9(CH_2)_3Ph$. A more straightforward approach towards specific organo-functionalization emerged from the acylation of $[\{(Me_3Si)_3Si\}_3Ge_9]^-$ with acyl chlorides, successfully yielding a row of acyl-decorated clusters $\{(Me_3Si)_3Si\}_3Ge_9(CO)R'$ (R' = Me, *i*Pr, *t*Bu, Ph, Bz, cyclopropylmethyl, $(CH_2)_2Ph$, 4-vinylphenyl).

According to variable temperature NMR studies, the obtained products showed dynamic behavior in solution. In particular for $\{(Me_3Si)_3Si\}_3Ge_9(CO)tBu$, decarbonylation in solution was shown by X-ray structure analysis.

Besides, also a synthetic approach towards charged organo-functionalized Ge_9 clusters was developed, which still provide reactive sites for further cluster-substitution. The reaction of $[\{(Me_3Si)_3Si\}_2Ge_9]^{2-}$ with bromoethane in thf afforded $[\{(Me_3Si)_3Si\}_2Ge_9CH_2CH_3]^-$, which in a follow-up step abstracts one silyl ligand upon addition of 2,2,2-crypt, forming $[\{(Me_3Si)_3Si\}Ge_9CH_2CH_3]^{2-}$. Also, the reaction of $[\{(Me_3Si)_3Si\}_2Ge_9]^{2-}$ with acyl chlorides gave access to a row of new compounds $[\{(Me_3Si)_3Si\}_2Ge_9(CO)R']^-$ (R' = *t*Bu, Ph, CH_2Ph, $(CH_2)_2Ph$, 9-anthracenyl, C_5H_4-Fe-C_5H_5), which were characterized by NMR spectroscopy and ESI mass spectrometry.

Besides specific organo-functionalization of Ge_9 clusters, the first example of 3D linkage of Ge_9 clusters was achieved, where four Ge_9 clusters are three-dimensionally covalently interconnected by a central Ge atom. The reaction of $[\{(Me_3Si)_3Si\}_2Ge_9]^{2-}$ with $[SiCp^*][B(C_6F_5)_4]$ in fluorobenzene containing $[Li(OEt_2)_x][B(C_6F_5)_4]$ yielded $[[\{(Me_3Si)_3Si\}_2Ge_9]_4Ge]^{4-}$. The structure of the anion was characterized by single crystal X-ray crystallography.

For electronic fine-tuning of such Ge_9 cluster-based nanostructured materials, doping is inevitable. For this purpose, we showed the incorporation of late transition metals into the *nido*-Ge_9 cluster scaffold of $\{(Me_3Si)_3Si\}_3Ge_9CH_2CH_3$ by reaction of the latter with η^2-ethylene-bis(triphenylphosphine)nickel(0) and the respective Pt-analogue yielding $\{(Me_3Si)_3Si\}_3CH_3CH_2[Ge_9M]PPh_3$ containing a *closo*-$[MGe_9]$ core (M = Ni, Pt). From a further synthesis, the first example of integration of a low-valent tetrel-element atom into the deltahedral Ge_9 cluster scaffold is shown. The reaction of $[\{(Me_3Si)_3Si\}_2Ge_9]^{2-}$ with $[SiCp^*][B(C_6F_5)_4]$ in fluorobenzene in the presence of Li cations afforded $\{(Me_3Si)_3Si\}_2Cp^*[LiSiGe_9](SiCp^*)_2[Ge_9SiLi]Cp^*\{(Me_3Si)_3Si\}_2$.

LIST OF ABBREVIATIONS

Å	ångstrom
A	alkaline metal
a	amorphous
a, b, c; α, β, γ	cell parameters
acn	acetonitrile
Ar'	2,6-bis(dipp)phenyl
BTS	copper oxide catalyst for gas regeneration
Ch.	chapter
chess	chessboard
COSY	correlation spectroscopy
Cp*	pentamethylcyclopentadienyl
18-crown-6	1,4,7,10,13,16-hexaoxacyclooctadecane
2,2,2-crypt	4,7,13,16,21,24-Hexaoxa-1,10-diazabicyclo[8.8.8]hexacosane
1D	one dimensional
2D	two dimensional
3D	three dimensional
DFT	density functional theory
Dipp	2,6-diisopropylphenyl
Dis	bis[bis(trimethylsilyl)methyl](methyl)silyl
DSD	diamond square diamond
ΔG	free activation energy for rotation
EDX	energy-dispersive X-ray spectroscopy
e.g.	*exempli gratia*
en	ethylenediamine
equiv.	equivalents
ESI	electron spray ionization
Fc	ferrocenyl
fw	formula weight
η	hapticity
h	hour(s)

HMBC	heteronuclear multiple bond correlation
HSQC	heteronuclear single quantum coherence
*i*Pr	*iso*-propyl
K	Kelvin
λ	wavelength
lab	laboratory
μ	absorption coefficient
M	transition metal
Me	methyl
Mes	1,3,5-trimethylphenyl
MHz	megahertz
mg	milligram
ml	millilitre
µl	microlitre
mmol	millimole
MOF	metal organic framework
n	number of vertices
n/a	not available
no	number
NMR	nuclear magnetic resonance
ppm	parts per million
PCBM	phenyl-C_{61}-butyric acid methyl acid
Ph	phenyl
PMMA	poly(methyl methacrylate)
P3HT	poly(3-hexylthiophen-2,5-diyl)
ρ	density
R	reliability factor
R	all isomers of 7-amino-5-azahepta-2,4-dien-2-yl
R^{Si}	tris(trimethylsilyl)silyl
r.t.	room temperature
SPS	solvent purification system
T	temperature

*t*Bu	*tert*-butyl
T_C	coalescence temperature
thf	tetrahydrofurane
Tip	2,4,6-triisopropylphenyl
TMS	trimethylsilyl
Tt	tetrel element
TWh	terawatt hour
UV	ultraviolet
V	volume
Vis	visible light
Z	number of formula units

TABLE OF CONTENTS

DECLARATION

This dissertation is written as a publication-based thesis. The bibliographic data of articles published in peer-reviewed journals is compiled in Chapter 5. In case of unpublished work, corresponding manuscripts prepared for publication are included. The relevance of this work for science and research as well as the scope and outline are presented as introductory part in Chapter 1. The experimental section in Chapter 2 gives details on the synthesis and characterization of materials as well as computational methods. Contributions from coauthors are explicitly stated in Chapter 5. The results and discussion are presented in Chapter 3. The subsections 3.1, 3.2, 3.4 and 3.5 are structured as follows: i) review of relevant literature, ii) results (summary of articles) and discussion across the respective topics, iii) references. An overall summary and conclusion is given in Chapter 4.

1 INTRODUCTION

1.1 Changing Times - Energy Reform

Harald Lesch is one of the most famous German detractors of human beings exploiting the earth without future thinking. The human beings of nowadays are totally aware of the consequences of intervention in nature, however, they mainly have not changed their attitude towards conservation or preservation of earth.[1] The growing threat of global warming, caused by the exorbitant release of anthropogenic greenhouse gases, such as water vapor, methane, nitrous gas and CO_2, is already noticeable by progressive ocean acidification,[2] ongoing melting of the polar ice caps,[3] as well as increasing extreme weather events.[4] The ecosystem can hardly adapt to this rapid change of the environment leading to enormous species extinction.[5]

The rapidly rising concentration of the greenhouse gas CO_2 in the atmosphere, as is shown in Figure 1.1.1, is alarming. The 400 ppm mark has already been exceeded in 2015 and further exponential rise is expected in the next years.[6]

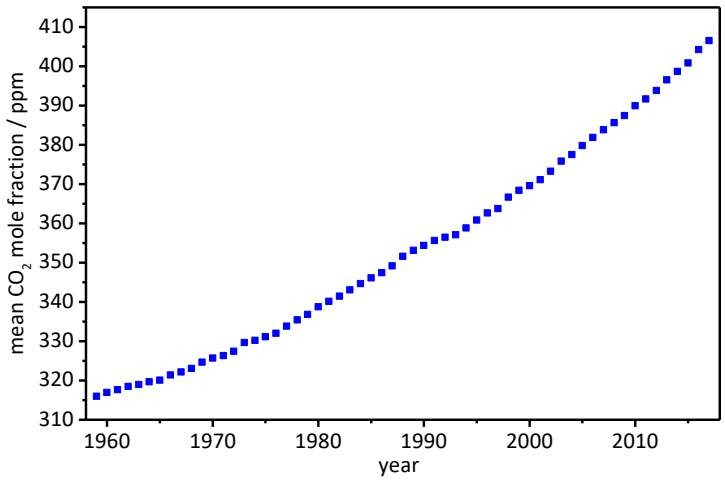

Figure 1.1.1. Trend of the mean CO_2 mole fraction in dry air from 1959 until 2017 recorded at Mauna Loa Observatory, Hawaii.[6]

A constantly increasing anthropogenic CO_2 emission, which had been preliminary initiated by the industrialization in the 19th century and heavily advanced throughout World War I,[1] is mainly caused by human beings by burning fossil fuels for power generation. However, the thereby ongoing climate change demands for fast response to the massive emissions problems at a simultaneously rising energy demand. The major approach to “clean” energy consumption, which minimizes environmental impact, would be the conversion to renewable energy technologies.[7]

In Germany the energy transition includes the reduction of greenhouse gas emission by at least 80-95% by the year 2050.[8] Throughout the recent decades, much effort has been put into wind power, solar energy and biomass, whereby renewable energy sources constituted 33.3% of the total energy gross production in Germany in 2017. The value increased by almost 10% throughout the recent ten years (Figure 1.1.2).[9]

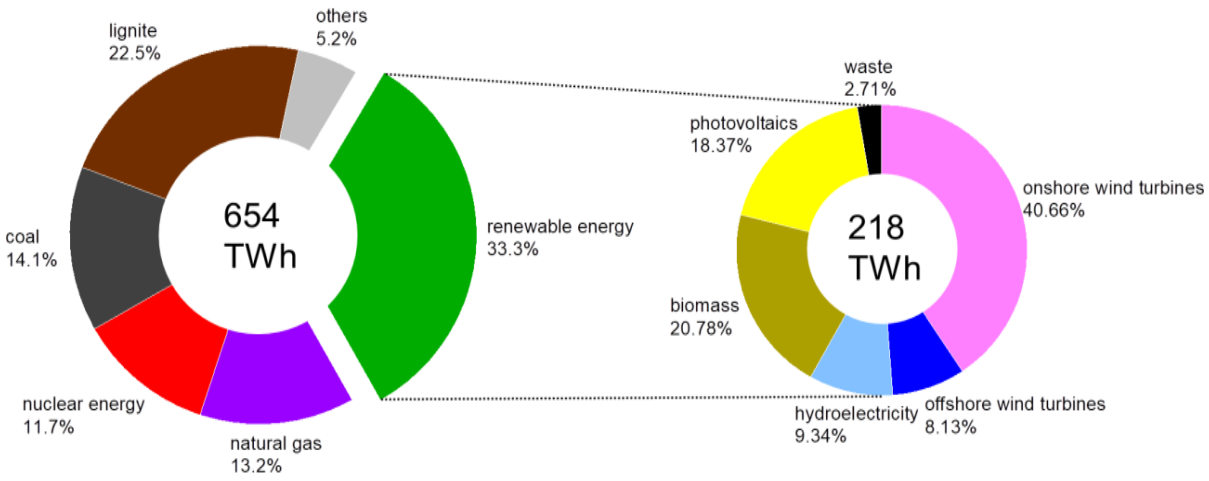

Figure 1.1.2. Total energy gross production by energy source in Germany in 2017.[9]

This energy transition towards renewable energy generation often implies dependency on special environmental conditions, such as wind power or solar energy. For this purpose, but also for electro-mobility, energy storage systems are inevitable.[10]

For the purposes of world-wide's energy transition, semiconductor materials are highly demanding. Even though germanium was the first element which was used for transistors and other microelectronic materials,[11] the lighter homologue silicon, which is abundantly available (21.22% in the earth's crust)[12], mainly took over its function. This is traced back to the comparatively low price of silicon due to enormous resources and mature production technologies.[13] Germanium is quite uncommon in the earth's crust with approximately 0.0003%[14] and is industrially obtained as by-product from processing zink ores.[15] However, germanium shows better optoelectronic properties and higher charge carrier mobility,[16-17] wherefore a constantly rising amount has been applied in photovoltaics[18-23] and lithium ion batteries[24-28] in recent years. This is nicely reflected by the world's annual production of silicon (7.4 million tons in 2017) and germanium (134 tons in 2017) with the very diverged average prices of $243 per kg (metallurgical grade) and $1358 per kg in 2017, respectively.[29-30]

To make photovoltaics more appealing, the costs need to be shrunk by more efficient devices. This can be achieved by increasing the number of band gaps or by favoring charge separation, which can be realized by utilizing nanostructured materials with tunable electronic properties and multi-junction solar cells.[21, 31] Ge_9 clusters represent soluble sources for processing of Ge, for example as inverse opal structured thin films.[32-33] Fullerenes have been thoroughly investigated as acceptor materials in organic solar cells.[34] Due to the close relation of nine-atomic deltahedral Zintl clusters to fullerenes,[35] especially deltahedral Ge_9 clusters represent interesting potential candidates for application in hybrid solar cells.

1.2 Clusters – Definition and Significance

Expressed in casual terms, chemical reactions imply the oxidation of elemental metals to simple monoatomic cations and the reduction of elemental nonmetals to simple monoatomic anions. Metalloids in the transition area might do both. However, the reality appears to be different. On the basis of several boron and phosphorous examples, chemical reactions from main group elements to simple ions or compounds appear to often run through intermediate states elucidated by crystallization of polyatomic networks, chains, clusters or rings. Partial retention of homoatomic bonding situations of the elemental structure in these intermediates clearly indicates a stepwise breakup of the structure of the element.[36-38] In other words, clusters provide insights into the transitional region between elemental bulk material and molecular chemistry. To improve chemical understanding of microscopic surface processes in elemental bulk material, investigations on clusters which comprise unsaturated “naked” vertices and therefore serve as model structures are inevitable. In this manner, a relation between structural motives and the auspicious novel chemical and physical properties, which clusters involve, can be established. The investigations might have a significant impact on developments in catalysis[39-40] and nanotechnology.[41] Another positive effect might be the savings of precious resources by an increase of the ratio of active surface atoms to bulk atoms, which is exactly the case in clusters.

Definition Cluster

According to Cotton’s first definition, a metal atom cluster, which he referred to transition elements, is a group of a finite number of metal atoms held together by bonds directly

between the metal atoms, including triangular structures as the smallest metal atom cluster.[42] In further definitions he clarified that not all metal atoms need to be identical and even binuclear clusters are to be called clusters.[43] In case of transition metal clusters the formal oxidation state (the lower the better) as well as the homophilicity (especially pronounced for late and heavier transition metal atoms) contributes to the stability of the cluster resulting in greater metal-metal interactions.[43-44] It was unclear whether a polymeric chain, electron deficiency or the minimum number of interconnected metal atoms is two or three are conditions to claim a group of atoms as cluster. However, von Schnering was putting it straight, saying that we should keep boundaries open. We should not spend too much time on finding a clear definition of clusters, but should focus on the essentials. Nevertheless, he also states that the term "cage" only refers to structures which most certainly can embed a metal atom in the center, such as fullerenes.[36] In the following, the most relevant main-group metal cluster types are distinguished from each other.

Metalloid Clusters

According to Schnöckel, metalloid clusters include metal clusters with more direct metal-metal bonds than metal-ligand bonds.[45] As indicated in the term "metalloid", they exhibit structural motives which are similar to those of the solid metals, but characteristic metallic properties such as conductivity are not necessarily given.[46-47] Therefore, metalloid clusters represent the ideal atomic arrangements in the elements at a molecular level. Such clusters require an average oxidation state between 0 and +1 for all vertices.[48-49] The term was originally introduced for group 13 elements. Most recently, this definition had been transferred to also group 14 and group 12 metal clusters.[50-51] Metalloid clusters are preliminary synthesized *via* redox processes starting from metastable subvalent metal halides.

Siliconoid Clusters

Lately, a separate subclass of metalloid clusters was defined by Scheschkewitz, the so-called siliconoids, which imply silicon clusters that bear at least one hemispheroidal cluster atom.[52-53] The synthesis of such clusters proceeds either by utilization of disilenides or by full reductive coupling of suitable halogenated silane precursors.[53]

The main challenge in the synthesis of metalloid clusters is given by the synthetic approach towards clusters which bear an incompletely saturated coordination sphere, and thus are still available for follow-up reactions.

INTERMETALLOID CLUSTERS

The definition for intermetalloid clusters was given by Fässler *et al.*[54] and describes especially endohedral clusters comprising at least two different metal or metalloid atoms of low oxidation states. This class of cluster compounds, where metal atoms are embedded in the cluster's center can even comprise structural motives which resemble segments of related intermetalloid phases, as is the case in $[Pt@Pd_{12}]^{2-}$.[55-56] The definition was further extended to ligand-stabilized or ligand-free cluster species comprising more metal−metal than metal−ligand bonds. Even onionskin-like structures, e.g. $[Sn@Cu_{12}@Sn_{20}]^{12-}$ are representatives of such intermetalloid clusters.[57]

ZINTL CLUSTERS

Generally speaking, the term "Zintl cluster" is referred to clusters that are derived from the so-called "Zintl phases".[37] Laves was the first who applied the term "Zintl phase",[58] according to the investigations made by Eduard Zintl in the 1930s.[59-62] Zintl phases imply salt-like binary compounds consisting of alkali or alkaline-earth elements and p-block (semi)metals. According to the Zintl-Klemm concept, electrons are formally transferred from the metal of group 11 or group 12 to the electronegative component, following the (8−*N*) electron rule for the atoms of the polyanionic substructure, amongst others the Zintl clusters.[63-67] Early investigations showed that these clusters are accessible by reaction of the elements in liquid ammonia,[68] or by extraction from the Zintl phases by dissolution in liquid ammonia and later on also in ethylenediamine (*en*)[69] and dimethylformamide (dmf)[70] making these clusters accessible for further investigations. The oxidation states of the Ge vertices range from 0 to −1. Regarding the fact, that Zintl clusters bear only hemispheroidal vertices, Zintl clusters are one of the leading species in terms of imitating the surface of the respective elemental bulk phase, and thus the most promising ones in terms of outstanding electronic properties they might possess.

1.3 Zintl Clusters – Structure, Properties and Reactivity

STRUCTURE AND PROPERTIES

The binary Zintl phases with the nominal composition A_4Tt_4 (*A* = K, Rb; *Tt* = Si-Pb), A_4Tt_9 (*A* = K-Cs; *Tt* = Ge-Pb) and $A_{12}Tt_{17}$ (*A* = K-Cs; *Tt* = Si-Pb) comprise the isolated cluster anions $[Tt_4]^{4-}$, $[Tt_9]^{4-}$, and both, $[Tt_4]^{4-}$ as well as $[Tt_9]^{4-}$ in a 2:1 ratio in the crystal structures, respectively. They are accessible by alloying of stoichiometric amounts of the elements.[71] The phases are at least partially soluble in rather inconvenient highly polar solvents, such as liquid ammonia,[38, 59-60, 72-75] *en*[69] and dmf[70], whereby by this extraction process, the Zintl clusters are transferred from the solid state into solution, making them accessible for reactions.[76] The tetrahedral structure of $[Tt_4]^{4-}$ in A_4Tt_4 is easy to explain since according to the (8−*N*) electron rule they are isovalence electronic to the P_4 tetrahedra in the white phosphorous modification.[77-79] The structure of $[Tt_9]^{4-}$ is more complex and is explained by the Wade-Mingos rules, which have been preliminary developed for deltahedral boranes.[80-82] $[Tt_9]^{4-}$ also depict delocalized and electron deficient cluster systems analogous to boranes, exhibiting $2n+4 = 22$ (*n* = number of vertices) skeleton bonding electrons, whereas each vertex contributes two electrons to the cluster bonding system, plus four additional electrons coming from the charge, resulting in a *nido*-$[Tt_9]^{4-}$ cluster. Besides, the stability of the bare $[Ge_9]^{4-}$ cluster is explainable by the superatom concept based on the spherical jellium model. Accordingly, $[Ge_9]^{4-}$ bears 40 valence electrons, and thus has a favorable jellium closed shell configuration.[83-84] Due to the lower atom-to-charge ratio in $[Tt_9]^{4-}$ compared to $[Tt_4]^{4-}$ the nine-atomic clusters show better solubility and higher stability towards reactants. Therefore, the focus of Zintl cluster research was set on $[Tt_9]^{4-}$. The addition of sequestering agents such as 2,2,2-crypt or 18-crown-6 to $[Tt_9]^{4-}$ solutions allowed for (re)crystallization of these clusters[85-86] and therefore numerous interesting and at the same time promising structures emerged throughout reactivity studies.[37, 76, 87-88] As has been shown by X-ray structure analysis, the $[Tt_9]^{4-}$ cluster cores show structural flexibility and can adopt either a mono-capped square antiprism with C_{4v} symmetry, or a D_{3h} symmetric three-fold capped trigonal prism. $[Tt_9]^{4-}$ clusters often appear distorted. The structural flexibility entails that the $[Tt_9]^{n-}$ anions can adopt different charges (*n* = −4 to −2) accompanied with structural changes. $[Tt_9]^{2-}$ adopts a D_{3h} symmetric threefold capped trigonal prismatic *closo*-structure with elongated prism heights with 20 skeleton bonding, electrons which is consistent with Wade's rules (Figure 1.3.1).[89]

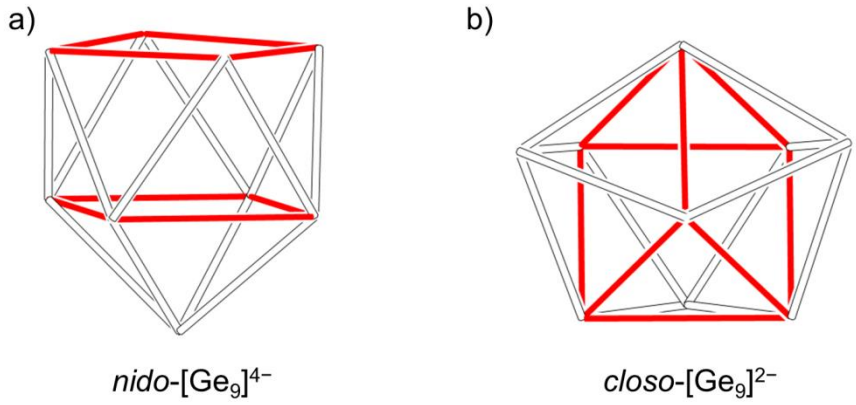

Figure 1.3.1. Schematic representation of a) C_{4v} symmetric *nido*-$[Ge_9]^{4-}$[90] cluster with the square planes being highlighted in red, and of b) D_{3h} symmetric *closo*-$[Ge_9]^{2-}$[89] with the in red denoted trigonal prism.

By contrast, the structure of $[Tt_9]^{3-}$ with 21 skeleton bonding electrons evades from Wade's rules, but adopts structures which lie between C_{4v} and D_{3h} symmetry.[76, 91-92] Even a coexistence of the three discussed Ge_9 clusters according to the equilibrium $[Ge_9]^{4-} \rightleftharpoons [\cdot Ge_9]^{3-} + e^{-1} \rightleftharpoons [Ge_9]^{2-} + 2\ e^{-1}$ in *en*-solutions, analogous to alkali metals dissolved in *en*, was stated.[93]

REACTIVITY IN SOLUTION – SPECIFIC ORGANO-FUNCITONALIZATION

Recent investigations highlighted the multifaceted, but also often unforeseen reactivity of $[Tt_9]^{4-}$ Zintl clusters. So far, the $[Ge_9]^{4-}$ clusters are the most well-known Zintl clusters, wherefore the present chapter only covers the reactivity of these structures. As is shown in Figure 1.3.2, there had been only a few methods for specific organo-functionalization of $[Ge_9]^{4-}$ Zintl clusters, which are addressed in the following.

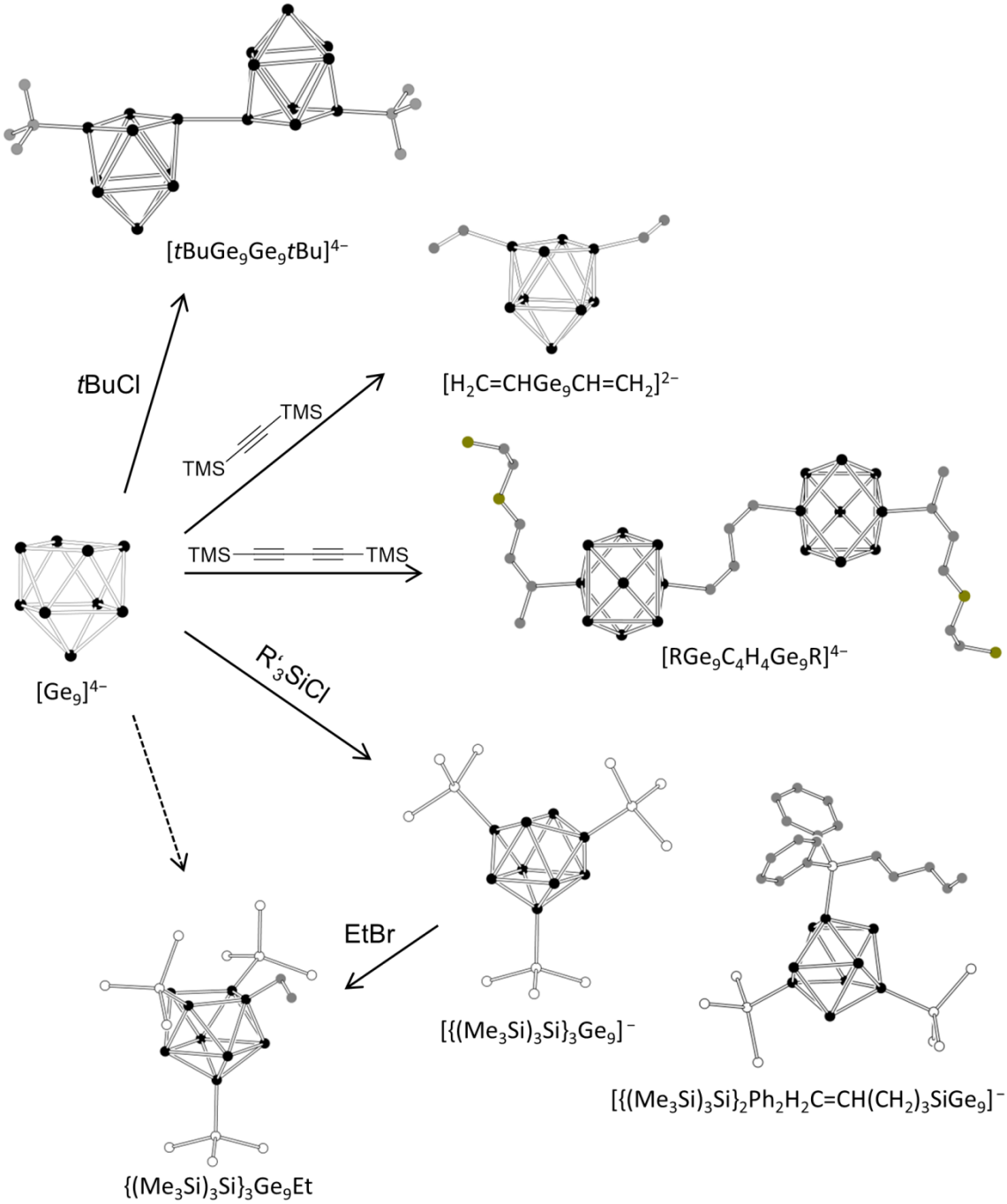

Figure 1.3.2. State-of-the-art specific organo-functionalized Ge_9 Zintl clusters. The following Zintl clusters are depicted: $[tBuGe_9Ge_9tBu]^{4-}$,[94] $[H_2C=CHGe_9CH=CH_2]^{2-}$,[95] $[RGe_9C_4H_4Ge_9R]^{4-}$,[96] $[\{(Me_3Si)_3Si\}_3Ge_9]^{-}$[97], $[\{(Me_3Si)_3Si\}_2Ph_2H_2C=CH(CH_2)_3SiGe_9]^{-}$[98], and $\{(Me_3Si)_3Si\}_3Ge_9Et$.[99] For reasons of clarity, all hydrogen atoms as well as the methyl groups attached to the silyl ligands are omitted for clarity. R represents (2*Z*,4*E*)-7-amino-5-azahepta-2,4-dien-2-yl. Ge – black, Si – colorless, C – grey, N – khaki spheres.

In the early stage, but still about 100 years after the discovery of the Zintl ions in solution, the first covalent *exo*-bond to the Ge_9 cluster was reported in the oxidatively coupled Ge_9 clusters $[Ge_9{-}Ge_9]^{6-}$,[70, 100-103] followed by the oligomers $[Ge_9{=}Ge_9{=}Ge_9]^{6-}$[104-105] as well as

$[Ge_9{=}Ge_9{=}Ge_9{=}Ge_9]^{8-}$[106-107] and the polymer $^{1}_{\infty}[Ge_9^{2-}]$.[101, 108-110] X-ray structure analysis revealed the interconnection of Ge_9 clusters in $[Ge_9{-}Ge_9]^{6-}$ and $^{1}_{\infty}[Ge_9^{2-}]$ *via* single bonds, whereas the trimer $[Ge_9{=}Ge_9{=}Ge_9]^{6-}$ and the corresponding tetramer show bond orders of <1 for the *exo*-bonds, and thus the anions comprise a delocalized bonding system throughout the whole anions. The first example of a $[Ge_9]^{4-}$ cluster derivative was achieved in $[Ph_2Bi{-}Ge_9{-}BiPh_2]^{2-}$,[111] followed by the first report of an organo-substituted Ge_9 Zintl cluster with a $Ge_9{-}C$ single bond in $[Ph{-}Ge_9{-}SbPh_2]^{2-}$.[93, 112] The first approach towards targeted attachment of organyl substituents to $[Ge_9]^{4-}$ was made, when $[Ge_9]^{4-}$ was reacted with alkyl chlorides R'Cl in a nucleophilic substitution reaction in *en*, affording $[R'{-}Ge_9{-}Ge_9{-}R']^{2-}$ (R' = *t*Bu, *s*Bu, *n*Bu, *t*Am).[94] The thus obtained anions were mostly only characterized by ESI mass spectrometry. The synthesis strategy turned out to be very unselective. However, the reaction of $[Ge_9]^{4-}$ with monoalkynes in *en* yielded at a maximum twofold alkenylated Ge_9 clusters,[95, 113-115] and even allowed for specific functionalization for follow-up reactions.[116] The alkenylation proceeds *via* nucleophilic *anti*-addition to the triple-bond.[117] The most prominent example is given by $[(H_2C{=}CH)_nGe_9]^{(4-n)-}$ (*n* = 1, 2), which are obtained from reactions of $[Ge_9]^{4-}$ with bis(trimethylsilyl)acetylene in *en*.[95, 118] Only very recently, the first fullerene analogous Zintl triad $[R{-}Ge_9{-}CH{=}CH{-}CH{=}CH{-}Ge_9{-}R]^{4-}$ (R = (2*Z*,4*E*)-7-amino-5-azahepta-2,4-dien-2-yl), comprising an extended conjugated π-electronic system was achieved by a complex, not yet fully understood, reaction between $[Ge_9]^{4-}$ clusters and 1,4-bis(trimethylsilyl)butadiyne.[96] Such triad systems are promising materials as electron acceptors in hybrid solar cells. Still, the high purification efforts, as well as low yields and limited solubility of the products were not satisfying, seeking for an improved method for targeted organo-functionalization.

For the first time, improved solubility of the Ge_9 clusters in less polar solvents was achieved by a heterogeneous silylation reaction of $[Ge_9]^{4-}$ with two or three equiv. of chloro-tris(trimethylsilyl)silane in acetonitrile forming $[\{(Me_3Si)_3Si\}_nGe_9]^{(4-n)-}$ (*n* = 2, 3).[97, 119] $[\{(Me_3Si)_3Si\}_3Ge_9]^{-}$ was originally discovered by Schnepf through co-condensation of metastable Ge halides.[120] The mono-anion is easily soluble in acetonitrile, thf and toluene, and thus, gave access to a whole new chemistry, which has also been shown by an increasing number of publications in recent years. Variation of silyl ligands with altered steric shielding as well as electronic effects lead to a diversity of threefold silylated cluster cores.[121-124] Specific organo-functionalization of Ge_9 clusters through alkenyl substituted silyl ligands was

shown with $[\{(Me_3Si)_3Si\}_2Ph_2H_2C{=}CH(CH_2)_nGe_9]^-$ (n = 1, 3).[98] Schnepf and co-workers even showed the linkage of two Ge_9 clusters *via* a silyl ligand.[125] Despite the improvements made with the silylation reaction, the obtained clusters are still charged, which might become a hindrance in follow-up reactions. With this respect, neutral Ge_9 clusters are of special interest. The only organo-substituted Ge_9 cluster present in literature had been $\{(Me_3Si)_3Si\}_3Ge_9Et$ comprising dynamic behavior in solution at r.t.[126] Only very recently, a new method for specific functionalization has been shown *via* the introduction of organo-decorated phosphine ligands to the Ge_9 cluster core.[127-129]

All in all, even though the clusters show an electron deficient system their reactivity is still not driven by electrophilicity. They readily react with several electrophiles to form substituted clusters, which still had the potential to be extended to further organic reactants.

REACTIVITY IN SOLUTION – CLUSTER EXPANSION

In principle, the chemistry of Ge_9 Zintl clusters is restricted to a nine-atomic functionalized scaffold. However, attempts to expand such clusters have been made to show possible fine-tuning of the electronic properties of the clusters. Therefore, Ge_9 clusters have been treated with a series of transition metal complexes. There are many different coordination modes a Ge_9 cluster can adapt (η^1-η^5). This fact even allows for linkage of Ge_9 clusters *via* a transition metal, forming dimeric $[Ge_9Au_3Ge_9]^{5-}$[130] and $[\{(Me_3Si)_3Si\}_3Ge_9MGe_9\{Si(SiMe_3)\}_3]^{n-}$ (M = Cu, Ag, Au, n = 1; M = Zn, Cd, Hg, Mn, n = 0),[131-134] oligomeric $[Hg_3(Ge_9)_4]^{10-}$[135] or even polymeric cables, such as $^1_\infty\{[MGe_9]^{2-}\}$ (M = Hg, Zn).[136-138]

Probably the most interesting transition metal Ge_9 cluster structures are given by those where the transition metal is directly integrated into the cluster scaffold forming a heteroatomic cage. Examples for three different types of such structures are shown in Figure 1.3.3, namely a bare *closo*-$[MGe_9]$ (M = Ni, Zn, Pd, Cu) core where the transition metal atom caps the open square face,[139-143] a silyl ligand decorated *closo*-$[MGe_9]$ (M = Cr, Mo, W) core where the transition metal is coordinated in an η^5-fashion[144-145] and a silylated and ethyl substituted *closo*-$[PdGe_9]$ core with the transition metal being also η^5-coordinated.[146]

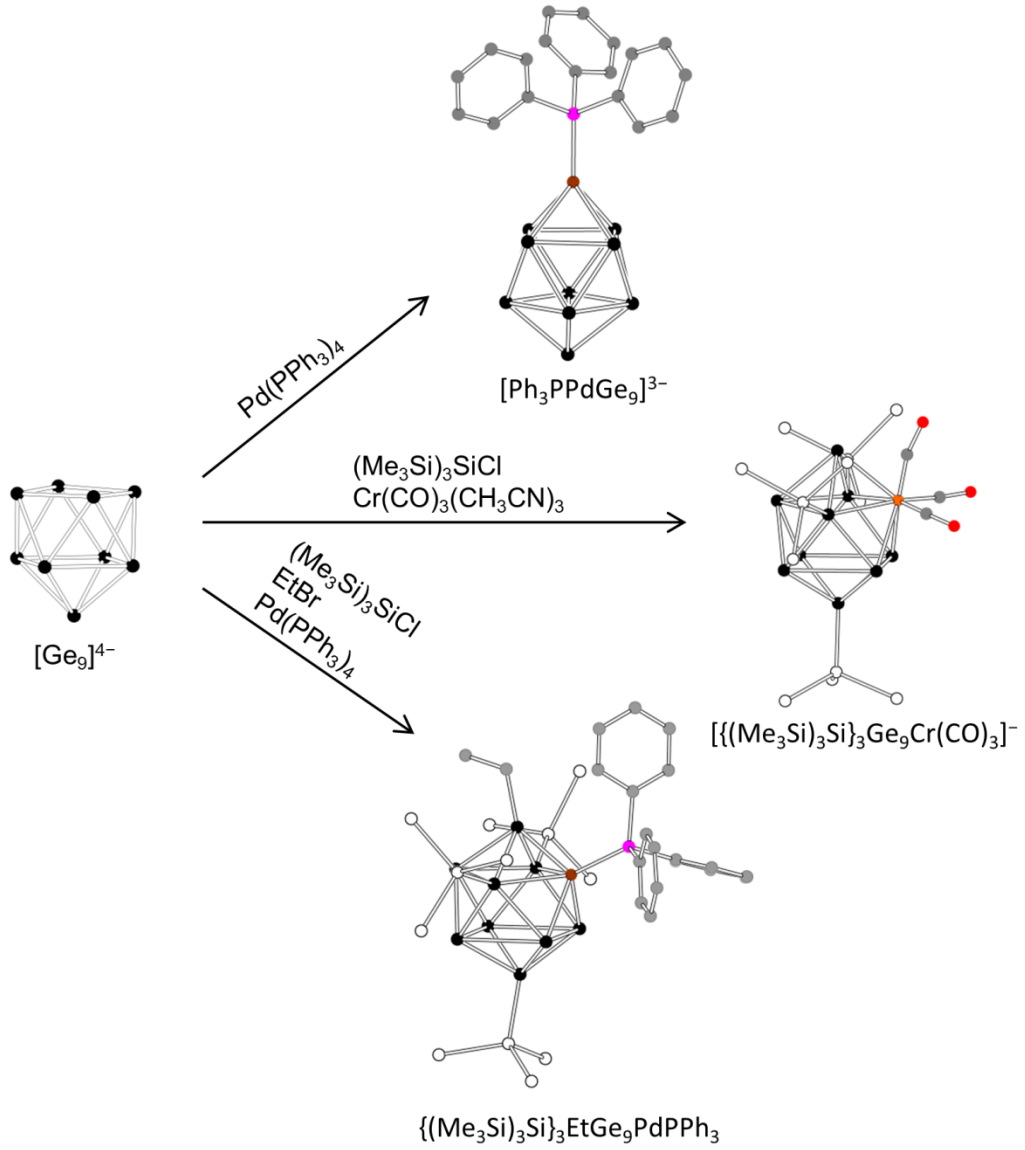

Figure 1.3.3. State-of-the-art closo-[*M*Ge$_9$] clusters. The clusters [PdGe$_9$]$^{3-}$,[142] [{(Me$_3$Si)$_3$Si}$_3$Ge$_9$Cr(CO)$_3$]$^-$[144-145], and {(Me$_3$Si)$_3$Si}$_3$EtGe$_9$PdPPh$_3$[146] are illustrated. All hydrogen atoms as well as the methyl groups attached to the silyl ligands are omitted for clarity. Ge – black, Si – colorless, C – grey, Pd – brown, Cr – orange, P – purple spheres.

Besides transition metals being embedded in the cluster scaffold, metal atoms that are encapsulated into the cluster's center have been observed, which is also accompanied with cluster fragmentation and expansion to a *closo*-[Ge$_{10}$] core[147-148] or the endohedral [Ru@Ge$_{12}$]$^{3-}$.[149-150]

Precisely, the *closo*-[Ge$_{10}$]$^{2-}$ cluster was crystallized from a reaction solution containing Rb$_4$Ge$_9$ and 7-amino-1-(trimethylsilyl)-5-azahepta-3-en-1-yne in *en*, hinting at a cluster fragmentation accompanied with cluster expansion.[151] Even though the reaction has not

been fully understood, it offers totally new pathways of generating expanded Ge_9 Zintl clusters.

1.4 Low-Valent Group 14 Compounds for Cluster Growth

Cluster growth has become a major topic in main group metal cluster chemistry, since its elucidation would allow for design and control of the syntheses of cluster-based materials.[152] In contrast to Zintl clusters, which can be easily extracted from the Zintl phases,[76] the synthesis of metalloid clusters by disproportionation or reduction of low-valent main group metal compounds requires several steps and as a negative side-effect, they bear a stabilizing ligand sphere, which is often fully saturated.[53] However, there are a few metalloids or siliconoids reported in literature, which bear at least one hemispheroidal vertex. The first germanium-based metalloid clusters were reported by Schnepf and Köppe applying germanium(I) bromide yielding $Ge_8\{N(SiMe_3)_2\}_6$[153] as well as $[\{(Me_3Si)_3Si\}_3Ge_9]^-$.[120] and by Power and co-workers through reduction of GeClAr' and $GeCl_2$·dioxane with KC_8 affording $Ge_6Ar'_2$ (Ar' = C_6H_3-2,6-$Dipp_2$; Dipp = C_6H_3-2,6-*i*Pr_2).[154] In 2005, also siliconoids were reported for the first time by Scheschkewitz[155] and by Veith and Wiberg[156] which were accessible by reaction of a disilenide with $SiCl_4$ and by treating a tetrahedrotetrasilane with an oxidizing agent, respectively. The synthesis of siliconoids is more complex due to the lower stability of low-valent silicon compounds. The discovery of the first stable and isolable low-valent pentamethylcyclopentadienyl silicon (II) cation by Jutzi *et al.* opened novel pathways for cluster growth and expansion.[157-158] As demonstrated in the reaction of $[Cp^*Si][B(C_6F_5)_4]$ with the disilenide **A**, the cation can serve as stoichiometric source in siliconoid cluster buildup (Scheme 1.4.1).[159]

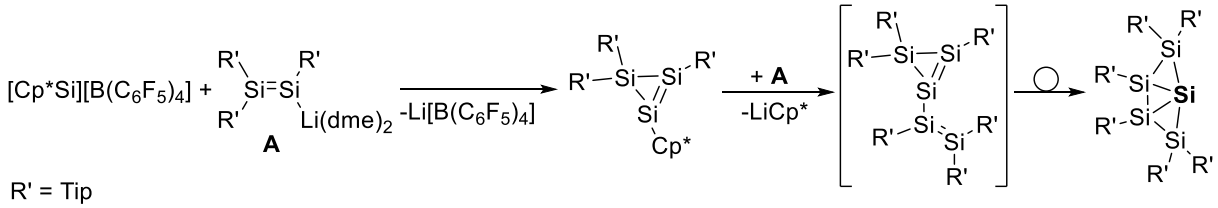

Scheme 1.4.1. Reaction of $[Cp^*Si][B(C_6F_5)_4]$ with the disilenide **A** yielding the Si_5 hemispheroidal siliconoid (Tip = 2,4,6-triisopropylphenyl). The unsubstituted Si vertex is depicted in bold.[159]

One step further towards closing the gap between siliconoids and silicon-based Zintl clusters has been made by the synthesis of the unsaturated anionic siliconoid by e.g. lithiation of a

dismutational hexasilabenzene isomer. The anionic siliconoid shows considerable nucleophilicity allowing for specific functionalization.[160]

Heteronuclear siliconoids emerged for example from the reaction of the disilenide **A** with $GeCl_2$·dioxane and subsequent reduction with lithium/naphthalene resulting in the dismutational Ge_2Si_4 isomer which undergoes thermal isomerization.[161]

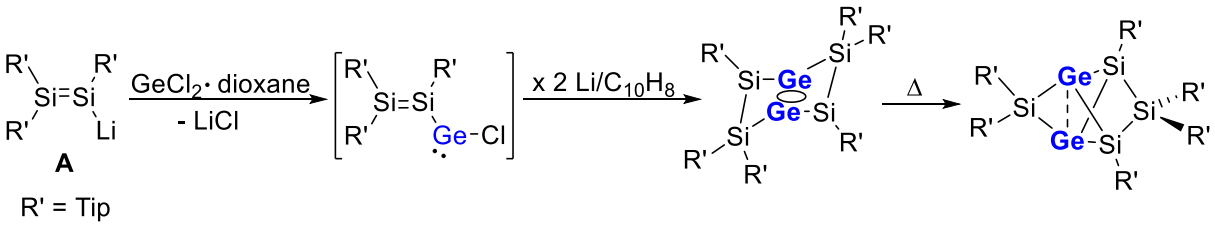

Scheme 1.4.2. Reaction of the disilenide **A** with $GeCl_2$·dioxane yielding the dismutational Ge_2Si_4 isomer (Tip = 2,4,6-triisopropylphenyl), which thermally isomerizes. The Ge atoms are shown in blue. Unsubstituted Ge atoms are depicted in bold.[161]

1.5 $[Ge_9]^{4-}$ Zintl Clusters as Precursors for Nanostructured Materials

$[Ge_9]^{4-}$ Zintl clusters exhibit a high surface-to-bulk ratio, and thus are believed to have unique optical and electronic properties.[162] Therefore, these semiconductor materials have been used to build high-surface nanostructured germanium-based non-oxide materials. Tolbert and Kanatzidis presented the first synthetic approach towards hexagonal nanoporous germanium-based semiconductors through surfactant-driven assembly of the polymeric $^1_\infty[Ge_9^{2-}]$ and $[Ge_9]^{4-}$ Zintl clusters, respectively.[163-164] The size-dependent energy band gap as well as the observed photoluminescence, they possess, can be attributed to size-induced quantum confinement.[165] These materials can be electronically tuned by doping through utilization of a specific linker,[166] or absorption of donors or acceptors in the interior of the structures, generating host-guest interactions.[167]

To make such materials applicable in electronic devices, research was done on generation of thin films. Sevov and co-workers prepared amorphous germanium thin films by anodic electrodeposition from a K_4Ge_9/*en* solution.[168] However, the first well-defined porous inverse opal structured germanium thin films starting from $[Ge_9]^{4-}$ have been reported by the Fässler group. The template-driven method, where PMMA beats are used as template material and a K_4Ge_9/*en* solution as germanium source, produces honeycomb like high-surface structures upon treating with a cross-linker.[32] These germanium thin films have

been investigated as anode materials for lithium ion batteries providing high capacity retention.[33]

1.6 Motivation, Scope and Outline

1.6.1 Motivation and Scope

Since the discovery of the Buckminsterfullerene C_{60} in 1985,[169] this field of research has attracted great interest. Fullerenes exhibit outstanding properties with respect to the intensively discussed spherical aromaticity and the associated electronic and magnetic properties.[170-172] They can serve as electron reservoirs adapting charges from 0 to −6, including reversible oxidation.[173-174] Possible C_{60} interconnection to obtain 1D cables, as well as 2D or even 3D structures has already been shown.[175] A wide range of specifically functionalized fullerene compounds emerged, such as organo-functionalized C_{60} cages, so-called fullerene dyads and triads, comprising electroactive spacers for application in semiconductor devices, such as organic solar cells, spintronics or artificial photosynthesis.[174, 176-178]

Deltahedral Zintl clusters feature, unlike fullerenes with their rigid σ-bonded scaffold, delocalized bonds throughout the whole cluster core.[54] The fluctuation of bonds associated with the fast exchange of atomic positions within the core was NMR spectroscopically proven for Zintl clusters in case of $[Sn_9]^{4-}$ and $[Pb_9]^{4-}$.[179] The D_{3h} cages can smoothly rearrange into the C_{4v} structures. However, still, there exist parallels between the delocalized bonding system of the Zinl ions and the delocalized π-electrons of fullerenes.[180] To further explore the electronic structure of Ge_9 cluster compounds in comparison to fullerenes, UV-Vis spectroscopic investigations were performed.

The remarkable existing analogy between deltahedral Ge_9 clusters and fullerene cage molecules, which had already been stated by Fässler in 2001, gives motivation to further explore the reactivity of Ge_9 Zintl clusters.[35] Compared to C_{60} fullerenes, deltahedral Ge_9 clusters represent electron-delocalized and simultaneously electron-deficient systems with exceptional properties. They possess structural flexibility and the associated ability of reversibly adopting different charges (from −2 to −4). The reported $^{1}_{\infty}[Ge_9]^{2-}$[108-109] polymer, as well as the oligomers $[Ge_9{=}Ge_9{=}Ge_9]^{6-}$[104-105] and $[Ge_9{=}Ge_9{=}Ge_9{=}Ge_9]^{8-}$[106-107] might open up possibilities for “bottom up” synthesis of new Ge-allotropes consisting of 2D layers or 3D frameworks.[35] In 2015, the analogy was further enforced by the successful synthesis of the fullerene triad analogous Zintl triad $[RGe_9{-}CH{=}CH{-}CH{=}CH{-}Ge_9R]^{4-}$ (R = (2*Z*,4*E*)-7-amino-5-

azahepta-2,4-dien-2-yl).[96] However, the formation of the organic conjugated linker had not been fully understood. The formation of the side-chain R was rather unforeseen.

Therefore in the present work, the knowledge about the Zintl triads was expanded to fully elucidate the mechanism on the formation of the linking unit, as well as the generation of the additional functionality attached to the Ge_9 cluster. Based on the basic studies, the transferability of the Zintl triad formation to the synthesis of other Zintl triads was intensively studied.

Fullerenes decorated with certain organic donor moieties distinguish themselves through intramolecular electronic communication. Also grafting on surfaces or polymerization reactions of organo-fullerene cages has been reported.[181-182] Functionalization of fullerenes is involved with the loss of π-system, compared to Ge_9 Zintl clusters, which retain the delocalized bonding system. However, specific functionalization of deltahedral Ge_9 Zintl clusters had always been a challenge due to often observed unexpected reactions. Straight-forward approaches towards organically functionalized deltahedral Ge_9 clusters had remained unexplored and therefore, were major goals within this thesis.

Fullerene based 2D and 3D architectures with remarkable opto- and electroactive features have been intensively studied.[175] Therefore, analogous potentially available Ge_9 Zintl cluster based structures attract great attention due to expected outstanding properties. However, 2D and 3D linkage had not been reported, hence studies on cluster assemblies became part of this work.

The existing analogy between C_{60} fullerenes and Ge_9 Zintl clusters highlighting the prior to this work missing pieces of the respective Zintl compounds are schematically displayed in Figure 1.6.1.

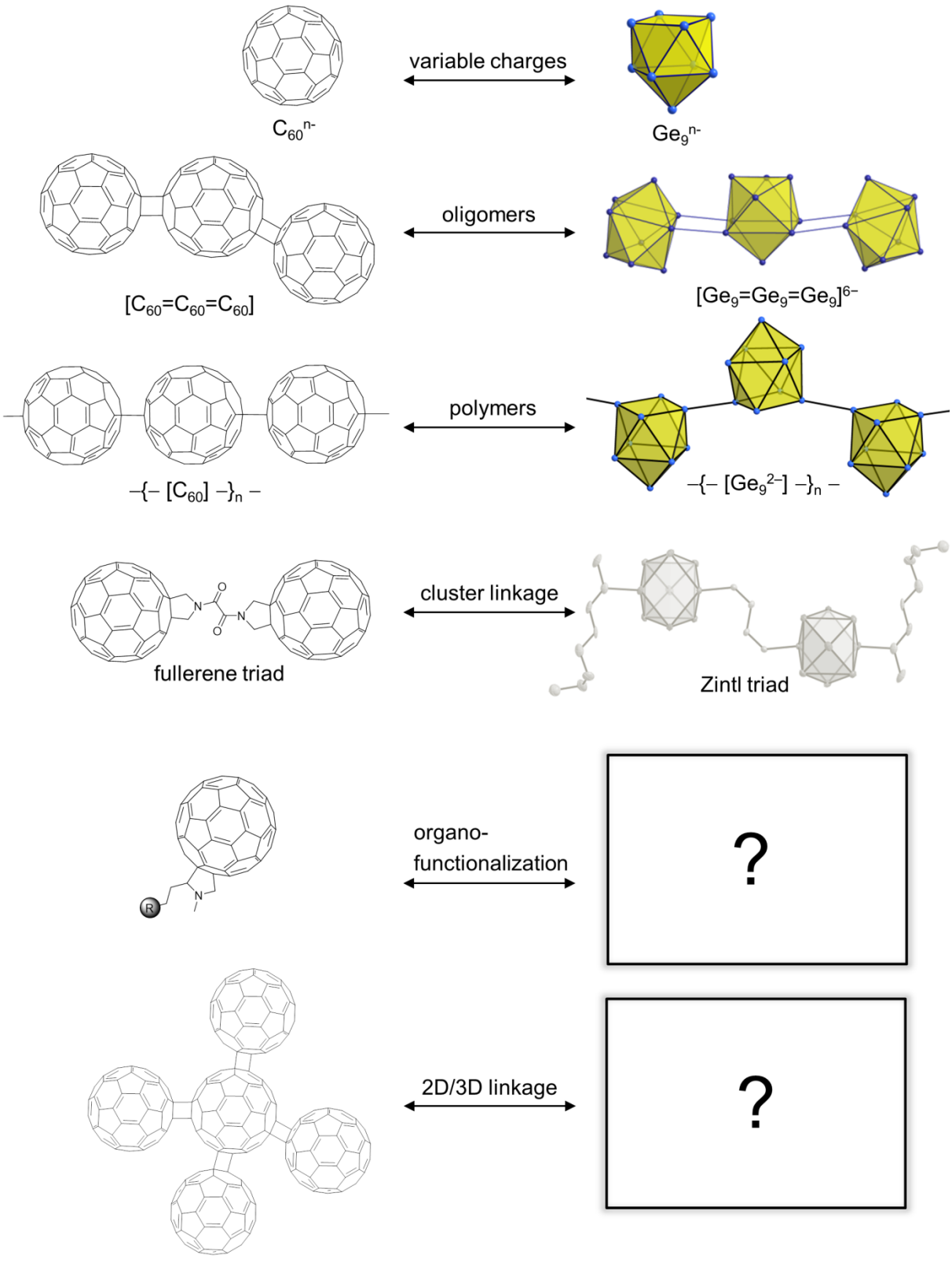

Figure 1.6.1. Analogy between C_{60} fullerenes and Ge_9 Zintl clusters and the missing items.

Cluster species represent the connecting link between elemental bulk material and molecules. As has been shown, nanoparticles exhibit unexpected optical and electronic properties. Related to nanoparticles, clusters embody a segment of surface atoms of a bulk species with a controllable number of vertices.

The synthesis of unsaturated metalloid clusters, which bear at least one vertex with a hemispheroidal coordination sphere, is complex and requires several steps.[48, 52] In contrast, deltahedral $[Ge_9]^{4-}$ Zintl clusters, which bear exclusively naked vertices, are easily accessible in one-step syntheses. These clusters are well investigated and show flexibility towards incorporation of mostly transition metal atoms into the cluster scaffold.[76, 146] So far, targeted E_9 Zintl cluster expansion (E = Si-Pb) with low-valent main-group metal atoms has been mainly unexplored, but was of special interest within this work, as this offers an easy and controllable way to access optionally heteroatomic cluster structures with a distinct number of vertices. The development of such synthesis approaches is aimed at to allow for controlled doping of cluster structures.

1.6.2 Outline

Chapter 3.1 deals with the synthesis of fullerene triad analogous Zintl triads comprising extended conjugated π-electronic systems implying the reactivity of 1,4-bis(trimethylsilyl)butadiyne with A_4Ge_9 (*A* = K, Rb) in *en*. In particular, **Chapter 3.1.2** compares the *closo*-$[Ge_9]^{2-}$ cluster with fullerene C_{60} in solution in terms of their electronic structures applying UV-Vis spectroscopy. **Chapter 3.1.3** discusses the reactivity of 1,4-bis(trimethylsilyl)butadiyne in *en* and the role of water therein. Based on the results, a qualitative and easy method to detect water-traces in *en* was developed. The first unfunctionalized Zintl triad $[Ge_9{-}CH{=}CH{-}CH{=}CH{-}Ge_9]^{6-}$ is presented in this chapter, which resulted from the reaction of A_4Ge_9 with 1,4-bis(trimethylsilyl)butadiyne in *en* under prevention of the reaction of the dialkyne with *en*. The new Zintl triad is characterized in terms of crystal structure and Raman spectroscopy. *In situ* ^{1}H NMR spectroscopic studies revealed the mechanism of the formation of the conjugated buta-1,3-diene-1,4-diyl bridge. The deep understanding, gained on the formation of the linking unit, gave access to the vinyl-decorated Zintl triad $[H_2C{=}CH{-}Ge_9{-}CH{=}CH{-}CH{=}CH{-}Ge_9{-}CH{=}CH_2]^{4-}$, which is only the second of its kind. The triad emerged by simultaneous reaction of 1,4-bis(trimethylsilyl)butadiyne and bis(trimethylsilyl)acetylene with K_4Ge_9 in *en* and is characterized by singly crystal X-ray crystallography and NMR spectroscopy.

In **Chapter 3.2** different methods of organo-functionalization of Ge_9 Zintl clusters are presented, which lead to further shrinkage of the existing gap in the analogy of fullerenes and Ge_9 Zintl clusters. Investigations on organo-functionalization of $[\{(Me_3Si)_3Si\}_3Ge_9]^-$ with alkyl bromides and acyl chlorides are given in **Chapter 3.2.2**. The neutral alkenyl functionalized cluster compounds $\{(Me_3Si)_3Si\}_3Ge_9(CH_2)_3CH{=}CH_2$ is presented in terms of crystal structure and NMR spectroscopic characterization. This chapter introduces also the newly achieved compounds $\{(Me_3Si)_3Si\}_3Ge_9(CH_2)_2CH_3$, $\{(Me_3Si)_3Si\}_3Ge_9(CH_2)_nCH{=}CH_2$ (*n* = 1, 2) and $\{(Me_3Si)_3Si\}_3Ge_9(CH_2)_3C_6H_5$, which are characterized by NMR spectroscopy. Alkyl halides turned out to lead to rather unexpected reactions towards Ge_9 Zintl clusters. Therefore, the newly developed straight-forward specific functionalization of Ge_9 clusters *via* acylation of $[\{(Me_3Si)_3Si\}_3Ge_9]^-$ is covered in this chapter leading to the selective formation of neutral and specifically functionalized Ge_9 clusters, which might allow for follow-up reactions. The obtained products $\{(Me_3Si)_3Si\}_3Ge_9(CO)Me$, $\{(Me_3Si)_3Si\}_3Ge_9(CO)i\text{Pr}$, $\{(Me_3Si)_3Si\}_3Ge_9(CO)t\text{Bu}$ and $\{(Me_3Si)_3Si\}_3Ge_9(CO)Ph$ are presented in terms of crystal

structure and NMR spectroscopy. Time-resolved ^{1}H NMR spectroscopy, as well as X-ray structure analysis show a conversion of {$(Me_3Si)_3Si$}$_3Ge_9(CO)t$Bu into {$(Me_3Si)_3Si$}$_3Ge_9t$Bu in solution at r.t. Several possible reaction mechanisms for the observed decarbonylation reaction are discussed with the aid of quantum chemical calculations. Temperature-dependent ^{1}H NMR studies give information about the dynamic behavior for all obtained neutral functionalized Ge_9 clusters. In **Chapter 3.2.3**, results on the reaction of $[\{(Me_3Si)_3Si\}_2Ge_9]^{2-}$ with bromo ethane and acyl chlorides are reported. The compound $[\{(Me_3Si)_3Si\}Ge_9CH_2CH_3]^{2-}$ is presented including its crystal structure and ESI mass spectrometric investigations. The transferability of the acylation to $[\{(Me_3Si)_3Si\}_2Ge_9]^{2-}$ was examined, wherefore, the chapter summarizes the NMR spectroscopic and ESI mass spectrometric investigations on the obtained charged acyl-decorated cluster anions $[\{(Me_3Si)_3Si\}_2Ge_9(CO)R']^-$ (R' = *t*Bu, Ph, CH_2Ph, $(CH_2)_2Ph$, 9-anthracenyl, C_5H_4-Fe-C_5H_5).

Chapter 3.3 demonstrates the first example of three-dimensional cluster linkage, where four $[\{(Me_3Si)_3Si\}_2Ge_9]^{2-}$ entities are interconnected *via* a central Ge atom. The synthesis of $K_4[\{(Me_3Si)_3Si\}_2Ge_9]_4Ge$, as well as its characterization by single crystal X-ray crystallography are given therein. Such three-dimensionally linked Ge_9 cluster structures represent promising building blocks to approach nanostructured materials.

Finally, **Chapter 3.4** covers two different approaches towards Ge_9 Zintl cluster expansions. **Chapter 3.4.2** deals with the transfer of the *nido*-[Ge_9] cluster core into a *closo*-[*M*Ge_9] (*M* = Ni, Pt) cluster core by integration of a transition metal into the cluster scaffold. The compounds [{$(Me_3Si)_3Si$}$_3Ge_9CH_2CH_3$]*M*(PPh_3) were achieved by reaction of the neutral compound {$(Me_3Si)_3Si$}$_3Ge_9CH_2CH_3$ with η^2-ethylene-bis(triphenylphosphine) nickel(0) and η^2-ethylene-bis(triphenylphosphine) platinum(0). Temperature-dependent ^{1}H NMR spectroscopy, as well as quantum chemical calculations support the therein stated dynamic behavior of the nickel analogue in solution. In contrast, **Chapter 3.4.3** addresses cluster growth by reaction of $[\{(Me_3Si)_3Si\}_2Ge_9]^{2-}$ with the low-valent silicon compound [SiCp*][$B(C_6F_5)_4$] in the presence of lithium cations in fluorobenzene. The presented structure represents the first example of cluster growth of deltahedral Ge_9 clusters with a low-valent tetrel-element compound (Figure 1.6.2).

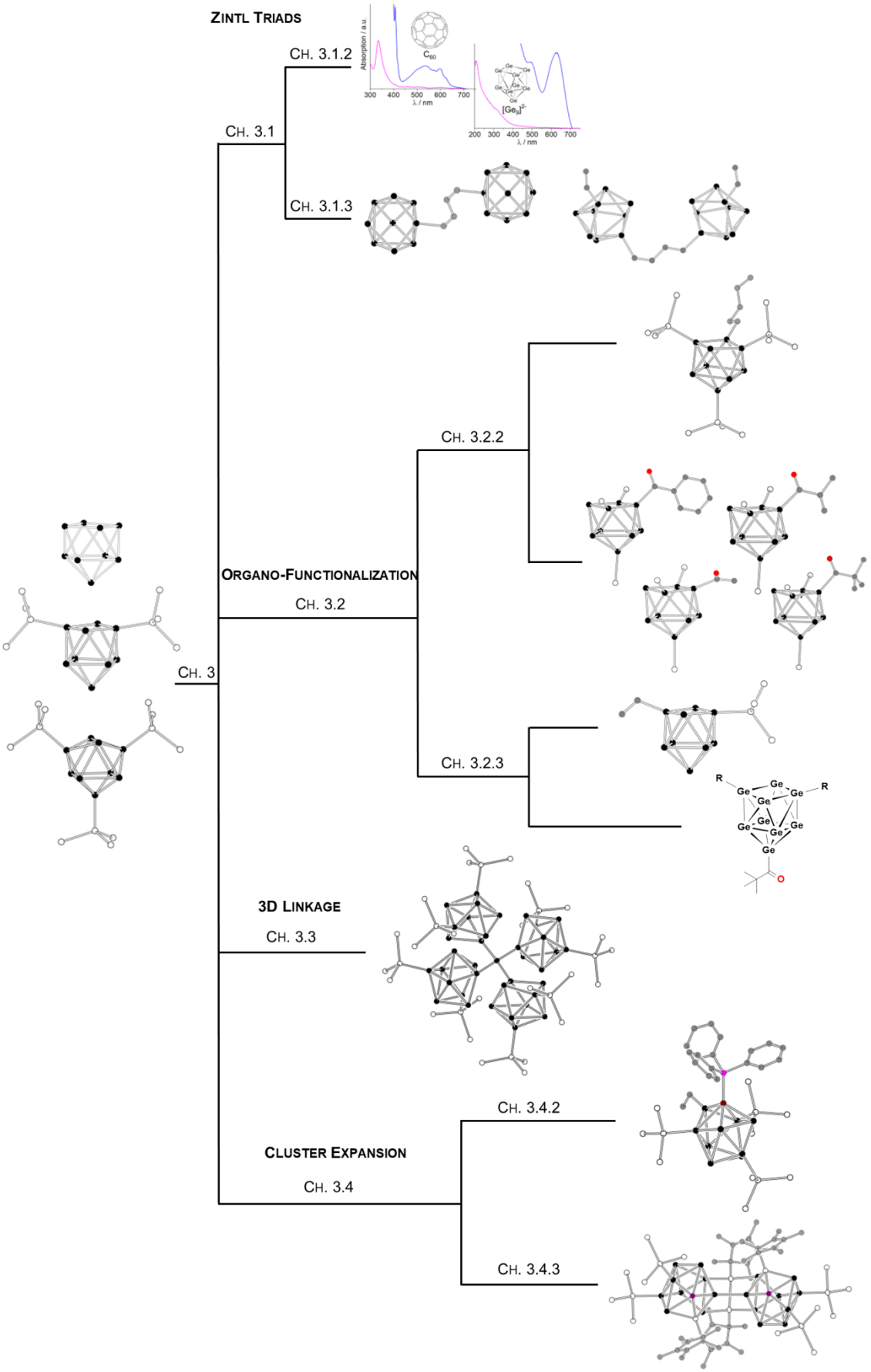

Figure 1.6.2. Overview of the results presented in this thesis. Ge, Si, C and O are shown as black, colorless, grey and red spheres, respectively.

1.7 References

[1] H. Lesch, K. Kamphausen, *Die Menschheit schafft sich ab: die Erde im Griff des Anthropozän*, Komplett-Media, **2016**.

[2] O. Hoegh-Guldberg, J. F. Bruno, *Science* **2010**, *328*, 1523-1528.

[3] H. Pritchard, S. Ligtenberg, H. Fricker, D. Vaughan, M. Van den Broeke, L. Padman, *Nature* **2012**, *484*, 502.

[4] D. R. Easterling, J. Evans, P. Y. Groisman, T. R. Karl, K. E. Kunkel, P. Ambenje, *Bull. Am. Meteorol. Soc.* **2000**, *81*, 417-426.

[5] J. R. Malcolm, C. Liu, R. P. Neilson, L. Hansen, L. Hannah, *Conserv. Biol.* **2006**, *20*, 538-548.

[6] P. Tans, R. Keeling, NOAA/ESRL and Scripps Institution of Oceanography, retrieved from www.esrl.noaa.gov/gmd/ccgg/trends/data.html, **2018**.

[7] I. Dincer, *Renew. Sust. Energ. Rev.* **2000**, *4*, 157-175.

[8] The Energy of the Future: Fourth "Energy Transition" Monitoring Report - Summary. Berlin, Germany: Federal Ministry for Economic Affairs and Energy (BMWi). **November, 2015**.

[9] AG Energiebilanzen e.V., Stromerzeugung nach Energieträgern, retrieved from www.ag-energiebilanzen.de/, **February 2018**.

[10] B. Dunn, H. Kamath, J.-M. Tarascon, *Science* **2011**, *334*, 928-935.

[11] E. Haller, *Mater. Sci. Semicond. Process.* **2006**, *9*, 408-422.

[12] H. Palme, H. S. C. O'Neill, *Treatise on Geochemistry* **2003**, *2*, 568.

[13] C. Claeys, E. Simoen, *Germanium-Based Technologies: from Materials to Devices*, Elsevier, **2011**.

[14] R. Höll, M. Kling, E. Schroll, *Ore Geology Reviews* **2007**, *30*, 145-180.

[15] R. Moskalyk, *Miner. Eng.* **2004**, *17*, 393-402.

[16] A. Stein, *Nature* **2006**, *441*, 1055-1056.

[17] R. Pillarisetty, *Nature* **2011**, *479*, 324.

[18] A. Du Pasquier, D. D. Mastrogiovanni, L. A. Klein, T. Wang, E. Garfunkel, *Appl. Phys. Lett.* **2007**, *91*, 183501.

[19] M. G. Kanatzidis, *Adv. Mater.* **2007**, *19*, 1165-1181.

[20] W. Guter, J. Schöne, S. P. Philipps, M. Steiner, G. Siefer, A. Wekkeli, E. Welser, E. Oliva, A. W. Bett, F. Dimroth, *Appl. Phys. Lett.* **2009**, *94*, 223504.

[21] S. Ossicini, M. Amato, R. Guerra, M. Palummo, O. Pulci, *Nanoscale Res. Lett.* **2010**, *5*, 1637.

[22] B. Hekmatshoar, D. Shahrjerdi, M. Hopstaken, K. Fogel, D. K. Sadana, *Appl. Phys. Lett.* **2012**, *101*, 032102.

[23] K. Ramasamy, P. G. Kotula, A. F. Fidler, M. T. Brumbach, J. M. Pietryga, S. A. Ivanov, *Chem. Mater.* **2015**, *27*, 4640-4649.

[24] S. Goriparti, E. Miele, F. De Angelis, E. Di Fabrizio, R. P. Zaccaria, C. Capiglia, *J. Power Sources* **2014**, *257*, 421-443.

[25] K. H. Seng, M. H. Park, Z. P. Guo, H. K. Liu, J. Cho, *Angew. Chem. Int. Ed.* **2012**, *51*, 5657-5661.

[26] T. Kennedy, E. Mullane, H. Geaney, M. Osiak, C. O'Dwyer, K. M. Ryan, *Nano Lett.* **2014**, *14*, 716-723.

[27] X. Li, Z. Yang, Y. Fu, L. Qiao, D. Li, H. Yue, D. He, *ACS Nano* **2015**, *9*, 1858-1867.

[28] R. Mo, D. Rooney, K. Sun, H. Y. Yang, *Nature Commun.* **2017**, *8*, 13949.

[29] Silicon Statistics and Information, U.S. Department of the Interior, U.S. Geological Survey, retrieved from https://minerals.usgs.gov/minerals/pubs/commodity/silicon/, **2018**.
[30] Germanium Statistics and Information, U.S. Department of the Interior, U.S. Geological Survey, retrieved from https://minerals.usgs.gov/minerals/pubs/commodity/germanium/, **2018**.
[31] M. A. Green, S. P. Bremner, *Nature Materials* **2017**, *16*, 23.
[32] M. M. Bentlohner, M. Waibel, P. Zeller, K. Sarkar, P. Müller-Buschbaum, D. Fattakhova-Rohlfing, T. F. Fässler, *Angew. Chem. Int. Ed.* **2016**, *55*, 2441-2445.
[33] S. Geier, R. Jung, K. Peters, H. A. Gasteiger, D. Fattakhova-Rohlfing, T. F. Fässler, *Sustainable Energy Fuels* **2018**, *2*, 85-90.
[34] B. C. Thompson, J. M. Fréchet, *Angew. Chem. Int. Ed.* **2008**, *47*, 58-77.
[35] T. F. Fässler, *Angew. Chem. Int. Ed.* **2001**, *40*, 4161-4165.
[36] H. G. von Schnering, *Angew. Chem. Int. Ed. Engl.* **1981**, *20*, 33-51.
[37] J. D. Corbett, *Chem. Rev.* **1985**, *85*, 383-397.
[38] E. B. Peck, *J. Am. Chem. Soc.* **1918**, *40*, 335-347.
[39] E. Muetterties, *Bull. Soc. Chim. Belg.* **1975**, *84*, 959-986.
[40] E. L. Muetterties, M. J. Krause, *Angew. Chem. Int. Ed. Engl.* **1983**, *22*, 135-148.
[41] *Cluster and Colloids* (Ed.: G. Schmid), Wiley-VCH, Weinheim, 1994; Metal Clusters in Chemistry (Eds.: P. Braunstein, L. A. Oro, P. R. Raithby), Wiley-VCH, Weinheim, **1999**.
[42] F. A. Cotton, *Inorg. Chem.* **1964**, *3*, 1217-1220.
[43] F. Cotton, *Q. Rev. Chem. Soc.* **1966**, *20*, 389-401.
[44] F. Cotton, N. Curtis, C. Harris, B. Johnson, S. Lippard, J. Mague, W. Robinson, J. Wood, *Science* **1964**, *145*, 1305-1307.
[45] A. Schnepf, H. Schnöckel, *Angew. Chem. Int. Ed.* **2002**, *41*, 3532-3554.
[46] A. Schnepf, G. Stößer, H. Schnöckel, *J. Am. Chem. Soc.* **2000**, *122*, 9178-9181.
[47] A. Purath, R. Köppe, H. Schnöckel, *Angew. Chem. Int. Ed.* **1999**, *38*, 2926-2928.
[48] A. Schnepf, *Chem. Soc. Rev.* **2007**, *36*, 745-758.
[49] A. Schnepf, *New J. Chem.* **2010**, *34*, 2079-2092.
[50] C. Schrenk, A. Schnepf, *Rev. Inorg. Chem.* **2014**, *34*, 93-118.
[51] T. Kruczyński, F. Henke, M. Neumaier, K. Bowen, H. Schnöckel, *Chem. Sci.* **2016**, *7*, 1543-1547.
[52] K. Abersfelder, A. Russell, H. S. Rzepa, A. J. White, P. R. Haycock, D. Scheschkewitz, *J. Am. Chem. Soc.* **2012**, *134*, 16008-16016.
[53] Y. Heider, D. Scheschkewitz, *Dalton Trans.* **2018**.
[54] T. F. Fässler, S. D. Hoffmann, *Angew. Chem. Int. Ed.* **2004**, *43*, 6242-6247.
[55] N. Korber, *Angew. Chem. Int. Ed.* **2009**, *48*, 3216-3217.
[56] E. N. Esenturk, J. Fettinger, Y. F. Lam, B. Eichhorn, *Angew. Chem. Int. Ed.* **2004**, *43*, 2132-2134.
[57] S. Stegmaier, T. F. Fässler, *J. Am. Chem. Soc.* **2011**, *133*, 19758-19768.
[58] F. Laves, *Die Naturwissenschaften*, Springer, **1941**, pp. 244-256.
[59] E. Zintl, J. Goubeau, W. Dullenkopf, *Z. Phys. Chem., Abt. A* **1931**, *154*, 1-46.
[60] E. Zintl, A. Harder, *Z. Phys. Chem., Abt. A* **1931**, *154*, 47-91.
[61] E. Zintl, W. Dullenkopf, *Z. Phys. Chem., Abt. B* **1932**, *16*, 183-194.
[62] E. Zintl, H. Kaiser, *Z. Anorg. Allg. Chem.* **1933**, *211*, 113-131.
[63] A. F. Holleman, E. Wiberg, N. Wiberg*, Lehrbuch der Anorganischen Chemie*, *Vol. 101*, Walter de Gruyter, Berlin, New York, **1995**, p. 866.
[64] E. Zintl, *Angew. Chem.* **1939**, *52*, 1-6.

[65] W. Klemm, E. Busmann, *Z. Anorg. Allg. Chem.* **1963**, *319*, 297-311.
[66] H. Schäfer, B. Eisenmann, W. Müller, *Angew. Chem. Int. Ed. Engl.* **1973**, *12*, 694-712.
[67] R. Nesper, *Z. Anorg. Allg. Chem.* **2014**, *640*, 2639-2648.
[68] M. Joannis, *C. R. Hebd. Séances Acad. Sci.* **1891**, *113*, 795-798.
[69] D. Kummer, L. Diehl, *Angew. Chem. Int. Ed. Engl.* **1970**, *9*, 895.
[70] A. Nienhaus, S. D. Hoffmann, T. F. Fässler, *Z. Anorg. Allg. Chem.* **2006**, *632*, 1752-1758.
[71] C. Hoch, M. Wendorff, C. Röhr, *J. Alloys Compd.* **2003**, *361*, 206-221.
[72] F. H. Smyth, *J. Am. Chem. Soc.* **1917**, *39*, 1299-1312.
[73] C. A. Kraus, *J. Am. Chem. Soc.* **1922**, *44*, 1216-1239.
[74] C. Kraus, *Trans. Am. Electrochem. Soc* **1924**, *45*, 175-186.
[75] K. Wiesler, K. Brandl, A. Fleischmann, N. Korber, *Z. Anorg. Allg. Chem.* **2009**, *635*, 508-512.
[76] S. Scharfe, F. Kraus, S. Stegmaier, A. Schier, T. F. Fässler, *Angew. Chem. Int. Ed.* **2011**, *50*, 3630-3670.
[77] E. Busmann, *Naturwissenschaften* **1960**, *47*, 82-82.
[78] J. Witte, H. v. Schnering, W. Klemm, *Z. Anorg. Allg. Chem.* **1964**, *327*, 260-273.
[79] H. von Schnering, M. Schwarz, J.-H. Chang, K. Peters, E.-M. Peters, R. Nesper, *Z. Kristallogr. - New Cryst. Struct.* **2005**, *220*, 525-527.
[80] K. Wade, *Inorganic and Nuclear Chemistry Letters* **1972**, *8*, 559-562.
[81] K. Wade, *Advances in Inorganic Chemistry and Radiochemistry, Vol. 18*, Elsevier, **1976**, pp. 1-66.
[82] J. D. Corbett, *Prog. Inorg. Chem.* **1976**, *21*, 129-158.
[83] R. King, I. Silaghi-Dumitrescu, *Dalton Trans.* **2008**, 6083-6088.
[84] K. Mayer, J. Weßing, T. F. Fässler, R. A. Fischer, *Angew. Chem. Int. Ed.* **2018**, *57*, 14372-14393.
[85] J. D. Corbett, D. G. Adolphson, D. J. Merryman, P. A. Edwards, F. J. Armatis, *J. Am. Chem. Soc.* **1975**, *97*, 6267-6268.
[86] T. F. Fässler, R. Hoffmann, *Angew. Chem. Int. Ed.* **1999**, *38*, 543-546.
[87] T. F. Fässler, *Coord. Chem. Rev.* **2001**, *215*, 347-377.
[88] S. C. Sevov, J. M. Goicoechea, *Organometallics* **2006**, *25*, 5678-5692.
[89] J. Akerstedt, S. Ponou, L. Kloo, S. Lidin, *Eur. J. Inorg. Chem.* **2011**, 3999-4005.
[90] S. Ponou, T. F. Fässler, *Z. Anorg. Allg. Chem.* **2007**, *633*, 393-397.
[91] T. Fässler, M. Hunziker, M. Spahr, H. Lueken, H. Schilder, *Z. Anorg. Allg. Chem.* **2000**, *626*, 692-700.
[92] T. F. Fässler, U. Schütz, *Inorg. Chem.* **1999**, *38*, 1866-1870.
[93] A. Ugrinov, S. C. Sevov, *Chem. Eur. J.* **2004**, *10*, 3727-3733.
[94] M. W. Hull, A. Ugrinov, I. Petrov, S. C. Sevov, *Inorg. Chem.* **2007**, *46*, 2704-2708.
[95] M. W. Hull, S. C. Sevov, *Inorg. Chem.* **2007**, *46*, 10953-10955.
[96] M. M. Bentlohner, W. Klein, Z. H. Fard, L.-A. Jantke, T. F. Fässler, *Angew. Chem. Int. Ed.* **2015**, *54*, 3748-3753.
[97] F. Li, S. C. Sevov, *Inorg. Chem.* **2012**, *51*, 2706-2708.
[98] K. Mayer, L. J. Schiegerl, T. Kratky, S. Günther, T. F. Fässler, *Chem. Commun.* **2017**, *53*, 11798-11801.
[99] F. Li, S. C. Sevov, *J. Am. Chem. Soc.* **2014**, *136*, 12056-12063.
[100] L. Xu, S. C. Sevov, *J. Am. Chem. Soc.* **1999**, *121*, 9245-9246.
[101] R. Hauptmann, T. F. Fässler, *Z. Anorg. Allg. Chem.* **2003**, *629*, 2266-2273.

[102] C. Suchentrunk, J. Daniels, M. Somer, W. Carrillo-Cabrera, N. Korber, *Z. Naturforsch. B* **2005**, *60*, 277-283.
[103] S. Scharfe, T. F. Fässler, *Z. Anorg. Allg. Chem.* **2011**, *637*, 901-906.
[104] A. Ugrinov, S. C. Sevov, *J. Am. Chem. Soc.* **2002**, *124*, 10990-10991.
[105] L. Yong, S. D. Hoffmann, T. F. Fässler, *Z. Anorg. Allg. Chem.* **2005**, *631*, 1149-1153.
[106] A. Ugrinov, S. C. Sevov, *Inorg. Chem.* **2003**, *42*, 5789-5791.
[107] L. Yong, S. D. Hoffmann, T. F. Fässler, *Z. Anorg. Allg. Chem.* **2004**, *630*, 1977-1981.
[108] C. Downie, Z. Tang, A. M. Guloy, *Angew. Chem. Int. Ed.* **2000**, *39*, 337-340.
[109] C. Downie, J.-G. Mao, H. Parmar, A. M. Guloy, *Inorg. Chem.* **2004**, *43*, 1992-1997.
[110] A. Ugrinov, S. C. Sevov, *C. R. Chim.* **2005**, *8*, 1878-1882.
[111] A. Ugrinov, S. C. Sevov, *J. Am. Chem. Soc.* **2002**, *124*, 2442-2443.
[112] A. Ugrinov, S. C. Sevov, *J. Am. Chem. Soc.* **2003**, *125*, 14059-14064.
[113] M. W. Hull, S. C. Sevov, *Angew. Chem. Int. Ed.* **2007**, *46*, 6695-6698.
[114] M. W. Hull, S. C. Sevov, *J. Organomet. Chem.* **2012**, *721*, 85-91.
[115] C. B. Benda, H. He, W. Klein, M. Somer, T. F. Fässler, *Z. Anorg. Allg. Chem.* **2015**, *641*, 1080-1086.
[116] M. W. Hull, S. C. Sevov, *Chem. Commun.* **2012**, *48*, 7720-7722.
[117] M. W. Hull, S. C. Sevov, *J. Am. Chem. Soc.* **2009**, *131*, 9026-9037.
[118] C. B. Benda, J. Q. Wang, B. Wahl, T. F. Fässler, *Eur. J. Inorg. Chem.* **2011**, *27*, 4262-4269.
[119] O. Kysliak, A. Schnepf, *Dalton Trans.* **2016**, *45*, 2404-2408.
[120] A. Schnepf, *Angew. Chem. Int. Ed.* **2003**, *42*, 2624-2625.
[121] O. Kysliak, C. Schrenk, A. Schnepf, *Inorg. Chem.* **2015**, *54*, 7083-7088.
[122] K. Mayer, L. J. Schiegerl, T. F. Fässler, *Chem. Eur. J.* **2016**, *22*, 18794-18800.
[123] O. Kysliak, T. Kunz, A. Schnepf, *Eur. J. Inorg. Chem.* **2017**, *4*, 805-810.
[124] L. J. Schiegerl, F. S. Geitner, C. Fischer, W. Klein, T. F. Fässler, *Z. Anorg. Allg. Chem.* **2016**, *642*, 1419-1426.
[125] O. Kysliak, C. Schrenk, A. Schnepf, *Inorg. Chem.* **2017**, *56*, 9693-9697.
[126] F. Li, A. Muñoz-Castro, S. C. Sevov, *Angew. Chem. Int. Ed.* **2012**, *51*, 8581-8584.
[127] F. S. Geitner, J. V. Dums, T. F. Fässler, *J. Am. Chem. Soc.* **2017**, *139*, 11933-11940.
[128] F. Geitner, C. Wallach, T. F. Fässler, *Chem. Eur. J.* **2018**, *24*, 4103-4110.
[129] F. S. Geitner, W. Klein, T. F. Fässler, *Angew. Chem. Int. Ed.* **2018**, *57*, 14509-14513.
[130] A. Spiekermann, S. D. Hoffmann, F. Kraus, T. F. Fässler, *Angew. Chem. Int. Ed.* **2007**, *46*, 1638-1640.
[131] C. Schenk, A. Schnepf, *Angew. Chem. Int. Ed.* **2007**, *46*, 5314-5316.
[132] C. Schenk, F. Henke, G. Santiso-Quiñones, I. Krossing, A. Schnepf, *Dalton Trans.* **2008**, 4436-4441.
[133] F. Henke, C. Schenk, A. Schnepf, *Dalton Trans.* **2009**, 9141-9145.
[134] O. Kysliak, C. Schrenk, A. Schnepf, *Chem. Eur. J.* **2016**, *22*, 18787-18793.
[135] M. S. Denning, J. M. Goicoechea, *Dalton Trans.* **2008**, 5882-5885.
[136] A. Nienhaus, R. Hauptmann, T. F. Fässler, *Angew. Chem. Int. Ed.* **2002**, *41*, 3213-3215.
[137] M. B. Boeddinghaus, S. D. Hoffmann, T. F. Fässler, *Z. Anorg. Allg. Chem.* **2007**, *633*, 2338-2341.
[138] K. Mayer, L.-A. Jantke, S. Schulz, T. F. Fässler, *Angew. Chem. Int. Ed.* **2017**, *56*, 2350-2355.
[139] J. M. Goicoechea, S. C. Sevov, *J. Am. Chem. Soc.* **2006**, *128*, 4155-4161.
[140] J. M. Goicoechea, S. C. Sevov, *Organometallics* **2006**, *25*, 4530-4536.
[141] B. Zhou, M. S. Denning, C. Jones, J. M. Goicoechea, *Dalton Trans.* **2009**, 1571-1578.

[142] Z.-M. Sun, Y.-F. Zhao, J. Li, L.-S. Wang, *J. Cluster Sci.* **2009**, *20*, 601-609.
[143] S. Scharfe, T. F. Fässler, *Eur. J. Inorg. Chem.* **2010**, *2010*, 1207-1213.
[144] C. Schenk, A. Schnepf, *Chem. Commun.* **2009**, 3208-3210.
[145] F. Henke, C. Schenk, A. Schnepf, *Dalton Trans.* **2011**, *40*, 6704-6710.
[146] F. Li, A. Muñoz-Castro, S. C. Sevov, *Angew. Chem. Int. Ed.* **2016**, *55*, 8630-8633.
[147] J. Q. Wang, S. Stegmaier, T. F. Fässler, *Angew. Chem. Int. Ed.* **2009**, *48*, 1998-2002.
[148] B. Zhou, M. S. Denning, D. L. Kays, J. M. Goicoechea, *J. Am. Chem. Soc.* **2009**, *131*, 2802-2803.
[149] G. Espinoza-Quintero, J. C. Duckworth, W. K. Myers, J. E. McGrady, J. M. Goicoechea, *J. Am. Chem. Soc.* **2014**, *136*, 1210-1213.
[150] J. M. Goicoechea, J. E. McGrady, *Dalton Trans.* **2015**, *44*, 6755-6766.
[151] M. M. Bentlohner, C. Fischer, T. F. Fässler, *Chem. Commun.* **2016**, *52*, 9841-9843.
[152] B. Weinert, S. Mitzinger, S. Dehnen, *Chem. Eur. J.* **2018**, *24*, 8470-8490.
[153] A. Schnepf, R. Köppe, *Angew. Chem. Int. Ed.* **2003**, *42*, 911-913.
[154] A. F. Richards, H. Hope, P. P. Power, *Angew. Chem. Int. Ed.* **2003**, *42*, 4071-4074.
[155] D. Scheschkewitz, *Angew. Chem. Int. Ed.* **2005**, *44*, 2954-2956.
[156] G. Fischer, V. Huch, P. Mayer, S. K. Vasisht, M. Veith, N. Wiberg, *Angew. Chem. Int. Ed.* **2005**, *44*, 7884-7887.
[157] P. Jutzi, A. Mix, B. Rummel, W. W. Schoeller, B. Neumann, H.-G. Stammler, *Science* **2004**, *305*, 849-851.
[158] P. Jutzi, *Chem. Eur. J.* **2014**, *20*, 9192-9207.
[159] K. Leszczyńska, K. Abersfelder, M. Majumdar, B. Neumann, H.-G. Stammler, H. S. Rzepa, P. Jutzi, D. Scheschkewitz, *Chem. Commun.* **2012**, *48*, 7820-7822.
[160] P. Willmes, K. Leszczyńska, Y. Heider, K. Abersfelder, M. Zimmer, V. Huch, D. Scheschkewitz, *Angew. Chem. Int. Ed.* **2016**, *55*, 2907-2910.
[161] D. Nieder, C. B. Yildiz, A. Jana, M. Zimmer, V. Huch, D. Scheschkewitz, *Chem. Commun.* **2016**, *52*, 2799-2802.
[162] A. P. Alivisatos, *Science* **1996**, *271*, 933-937.
[163] D. Sun, A. E. Riley, A. J. Cadby, E. K. Richman, S. D. Korlann, S. H. Tolbert, *Nature* **2006**, *441*, 1126.
[164] G. S. Armatas, M. G. Kanatzidis, *Nature* **2006**, *441*, 1122.
[165] G. S. Armatas, M. G. Kanatzidis, *Nano Lett.* **2010**, *10*, 3330-3336.
[166] G. S. Armatas, M. G. Kanatzidis, *J. Am. Chem. Soc.* **2008**, *130*, 11430-11436.
[167] G. S. Armatas, M. G. Kanatzidis, *Adv. Mater.* **2008**, *20*, 546-550.
[168] N. Chandrasekharan, S. C. Sevov, *J. Electrochem. Soc.* **2010**, *157*, C140-C145.
[169] H. W. Kroto, J. R. Heath, S. C. O'Brien, R. F. Curl, R. E. Smalley, *Nature* **1985**, *318*, 162-163.
[170] A. Hirsch, Z. Chen, H. Jiao, *Angew. Chem. Int. Ed.* **2000**, *39*, 3915-3917.
[171] M. Bühl, A. Hirsch, *Chem. Rev.* **2001**, *101*, 1153-1184.
[172] Z. Chen, R. B. King, *Chem. Rev.* **2005**, *105*, 3613-3642.
[173] Q. Xie, F. Arias, L. Echegoyen, *J. Am. Chem. Soc.* **1993**, *115*, 9818-9819.
[174] N. Martín, L. Sánchez, B. Illescas, I. Pérez, *Chem. Rev.* **1998**, *98*, 2527-2548.
[175] F. Giacalone, N. Martin, *Chem. Rev.* **2006**, *106*, 5136-5190.
[176] J. L. Segura, N. Martín, *Chem. Soc. Rev.* **2000**, *29*, 13-25.
[177] M. A. Lebedeva, T. W. Chamberlain, E. S. Davies, B. E. Thomas, M. Schröder, A. N. Khlobystov, *Beilstein J. Org. Chem.* **2014**, *10*, 332-343.
[178] Y. Kanai, J. C. Grossman, *Nano Lett.* **2007**, *7*, 1967-1972.

[179] W. L. Wilson, R. W. Rudolph, L. L. Lohr, R. C. Taylor, P. Pyykko, *Inorg. Chem.* **1986**, *25*, 1535-1541.
[180] A. Hirsch, Z. Chen, H. Jiao, *Angew. Chem. Int. Ed.* **2001**, *39*, 3915-3917.
[181] Y. Zhang, L. Ren, S. Wang, A. Marathe, J. Chaudhuri, G. Li, *J. Mater. Chem.* **2011**, *21*, 5386-5391.
[182] C. Wang, Z.-X. Guo, S. Fu, W. Wu, D. Zhu, *Prog. Polym. Sci.* **2004**, *29*, 1079-1141.

2 EXPERIMENTAL SECTION

2.1 General Experimental Procedure

2.1.1 Inert Gas Technique

Most of the used educts are moisture and air sensitive. Therefore all manipulations were carefully performed under inert conditions in an argon-filled glovebox (MBraun, $O_2 \leq 0.5$ ppm, $H_2O \leq 0.5$ ppm) or using standard Schlenk technique. For Schlenk techniques Argon (Westfalen, purity grade 4.8) was used as inert gas. Argon was passed through a BTS catalyst, and was dried over molecular sieve (4 Å) and P_2O_5 for further purification prior to use. Glassware and spatulas were cleaned in a KOH/isopropanol bath, stored in a furnace at 120 °C for at least one day, baked at 650 °C in fine vacuum (< 10^{-3} mbar) and purged with Argon for three times. The glass junctions were lubricated with silicon high-vacuum grease (DOW Corning).

2.1.2 Filtration Technique

Reaction solutions were filtered over glass fiber filters (Pall Corporation, A/B 1 µm) stuffed in a Pasteur pipette to remove precipitate. For this purpose, the solution was pushed through the prepared filter, which was dried for at least one day at 120 °C, into a thoroughly dried Schlenk tube in a glovebox. For volumes > 6 mL or in case the solid product needed to be filtered off, a different filtration method was applied. In this case, a Whatman filter (Whatmanfilter™ GE Healthcare Life Sciences, GD 1 µm) was placed at one end of a Teflon cannula and fixed with Teflon tape. The prepared filter was dried in vacuum at 650 °C for three times and purged with Argon in between. The filtration was executed by using Argon pressure to push the reaction solution through the glass fiber.

2.1.3 Reagents

Table 2.1.1 below lists all used reagents and solvents. Fluorobenzene was dried over calciumhydride for at least 17 h, distilled and stored over molecular sieve (3 Å) in a glovebox. Potassium was freed from oxide layers in a glovebox prior to use. Acetonitrile, diethylether, hexane, pentane, tetrahydrofurane and toluene were taken from a Solvent Purification System (SPS, MBraun). 2,2,2-crypt was dried in vacuum for at least 17 h. 18-crown-6 was sublimed in dynamic vacuum at 80 °C. Deuterated solvents were stored over molecular sieve (3 Å) for at least one day. For reactions with low-valent silicon compounds all solvents

(including deuterated solvents) were degassed applying freeze-pump-thaw technique prior to use.

Table 2.1.1. Overview of all used reagents and solvents.

Chemical	Supplier	Morphology	Purity	Storage
acetone	VWR Chemicals	liquid	≥ 99.8%	glovebox, stored over molecular sieve (3 Å)
acetonitrile	Merck	liquid	SPS	glovebox, stored over molecular sieve (3 Å)
acetyl chloride	AlfaAesar	liquid	98%	glovebox
benzoyl chloride	Acros Organics	liquid	≥ 98%	
bis(trimethylsilyl)acetylene	Sigma Aldrich	liquid	99%	glovebox
1,4-bis(trimethylsilyl)butadiyne	AlfaAesar	powder	98%	glovebox
bromoethane	Sigma Aldrich	liquid	98%	glovebox
4-bromo-1-butene	AlfaAesar	liquid	97%	glovebox
bromoethane	Sigma Aldrich	liquid	98%	glovebox
5-bromopent-1-ene	Sigma Aldrich	liquid	95%	glovebox
1-bromo-3-phenylpropane	Acros Organics	liquid	98%	glovebox
1-bromopropane	Merck	liquid	n/a	glovebox
3-bromoprop-1-ene	Sigma Aldrich	liquid	97%	glovebox
calciumhydride	Merck	chunks	n/a	lab
chloro-*tris*(trimethylsilyl)silane	TCI Chemicals	powder	> 95.0%	glovebox
C_{60} fullerene	Hoechst	powder	> 99%	glovebox
Cis-dichloro-*bis*-(triphenylphosphine)-platinum(II)	Sigma Aldrich	powder	n/a	glovebox
18-crown-6	Merck	powder	sublimed	glovebox
2,2,2-crypt	Merck	powder	dried in vacuum	glovebox
diethylether	-	liquid	SPS	glovebox, stored over molecular sieve (3 Å)
ethylene	Sigma Aldrich	gaseous	≥ 99.5%	gas cylinder
ethylenediamine	AlfaAesar	liquid	dried over CaH_2, freshly distilled	laboratory
fluorobenzene	AlfaAesar	liquid	dried over CaH_2 and molecular sieve (3 Å)	glovebox
Ge	Evochem	pieces	99.999%	glovebox
hexane	-	liquid	SPS	glovebox
hydrocinnamoyl chloride	Sigma Aldrich	liquid	98%	glovebox
hydrogen chloride dissolved in diethyl ether	Alfa Aesar	liquid	1 M	refrigerator (−32 °C)
isobutyryl chloride	Acros Organics	liquid	98%	glovebox
K	Merck	chunks	98%	glovebox
K_4Ge_9	self-made	powder	phase-pure	glovebox
Lithium *tetrakis*(pentafluorophenyl)borate	TCI Chemicals	powder	> 70.0%	glovebox

- ethyl ether complex				
nickel(II) acetylacetonate	lab inventory	powder	sublimed *in vacuo*	glovebox
pentane	-	liquid	SPS	glovebox
phenylacetyl chloride	Sigma Aldrich	liquid	98%	glovebox
pivaloyl chloride	Sigma Aldrich	liquid	99%	glovebox
Rb	lab inventory	ductile	liquated	glovebox
Rb_4Ge_9	self-made	powder	phase-pure	glovebox
tetrahydrofurane	Bernd Kraft	liquid	SPS	Glovebox, stored over molecular sieve (3 Å)
toluene	Merck	liquid	SPS	glovebox
triphenylphosphine	lab inventory	powder	recrystallized	glovebox
acetone-d_6	Deutero GmbH	Liquid	99.5%	Glovebox, stored over molecular sieve (3 Å)
acetonitrile-d_3	Deutero GmbH	liquid	99.8%	glovebox, stored over molecular sieve (3 Å)
benzene-d_6	Deutero GmbH	liquid	99.5%	glovebox, stored over molecular sieve (3 Å)
chloroform-*d*	Deutero GmbH	liquid	99.8%	glovebox, stored over molecular sieve (3 Å)
dichloromethane-d_2	Deutero GmbH	liquid	99.6%	glovebox, stored over molecular sieve (3 Å)
tetrahydrofurane-d_8	Deutero GmbH	liquid	99.5%	glovebox, stored over molecular sieve (3 Å)
toluene-d_8	Deutero GmbH	liquid	99.5%	glovebox, stored over molecular sieve (3 Å)

2.1.3.1 Purification of Ethylenediamine

In the Fässler group a method to determine the overall water content of *en* was established. Due to the high basicity of *en*, the water content cannot be determined by the common well-known Karl-Fischer titration.

Ethylenediamine with an initial water-content of < 1% was refluxed over calciumhydride for 72 h and freshly distilled in an appropriate glass apparatus prior to use. The water content of the solvent was determined dissolving 35 mg 1,4-bis(trimethylsilyl)butadiyne in 3 mL *en*. After stirring for 17 h at r.t. a ^{1}H NMR spectrum was recorded directly from the reaction solution. In case no water is present in the reaction solution 1,4- bis(trimethylsilyl)butadiyne

reacts exclusively to 7-amino-1-(trimethylsilyl)-5-azahepta-3-en-1-yne. Trace amounts of water lead to the formation of 2,3-dihydro-5-methyl-*H*-1,4-diazepine out of 7-amino-1-(trimethylsilyl)-5-aza-hepta-3-en-1-yne. The higher the water content in *en* the faster the conversion (see chapter 5.2).[1]

2.1.3.2 Preparation of the Zintl Phases A_4Ge_9 (A = K, Rb)

K_4Ge_9 was synthesized heating a stoichiometric mixture of the elements potassium and germanium to 650 °C for 46 h (ramp rate for heating: 2 K/min, ramp rate for cooling: −1 K/min) in a stainless steel autoclave.[2-3] The latter was placed in a corundum tube, which was evacuated in fine vacuum for three times and purged with Ar (Figure 2.1.1). The Ar-filled corundum tube, equipped with a football bladder for pressure compensation, was placed in a tube furnace (*HTM Reetz GmbH*) combined with a temperature controller (*Eurotherm Deutschland GmbH*).

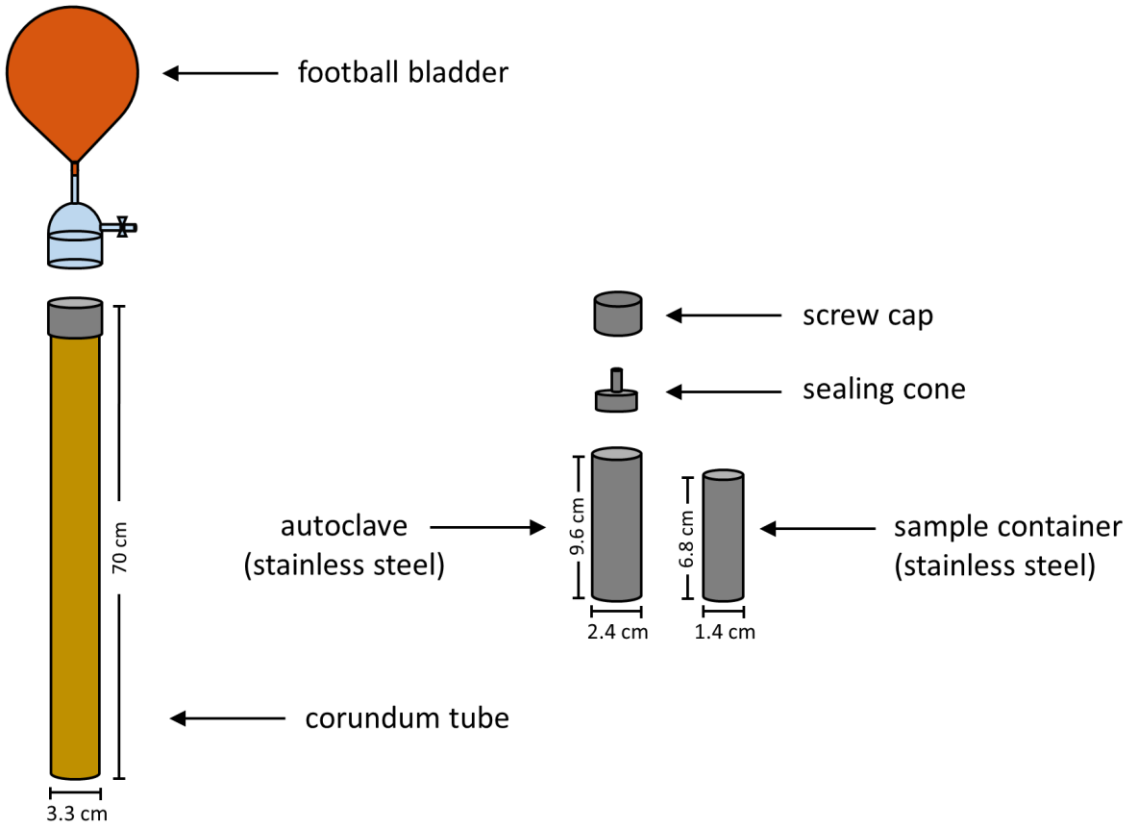

Figure 2.1.1. Corundum tube and stainless steel autoclave used for the synthesis of K_4Ge_9.

Rb_4Ge_9 was synthesized heating a stoichiometric mixture of the elements rubidium and germanium to 650 °C for 48 h in a tantalum ampoule.[2] The tantalum ampoules were prepared as follows: cylinders were cut from a tantalum tube (diameter 10 mm, wall

thickness: 0.5 mm) to a smaller size of 5 cm, cleaned with acetic acid, water and acetone by sonication, dried in an oven at 120 °C for at least one day and sealed on one side by crimping and subsequent welding with an arc melting furnace (*Edmund Bühler, MAM 1*) in a glovebox. After loading, the second end was sealed accordingly. The loaded tantalum ampoule was placed into a fused silica tube which was additionally equipped with an inner fused silica tube for safety reasons. The loaded fused silica tube was placed into a tube furnace (*HTM Reetz GmbH*) which is combined with a temperature controller (*Eurotherm Deutschland GmbH*). The obtained products were grinded in an agate mortar and analyzed by X-ray powder diffraction for purity.

2.2 Characterization

2.2.1 Single Crystal X-Ray Diffraction, Structure Solution, and Refinement

Single crystal X-ray diffraction (SC-XRD) is one of the best methods to identify and to determine the exact structure of newly found compounds. All structures presented in this work were determined by using this method. SC-XRD data were recorded on Xcalibur3 (Oxford), FR591 APEX II (Bruker) and Stoe StadiVari diffractometer with $Mo_{K\alpha}$ radiation ($\lambda = 0.71073$). The diffractometers are equipped with a CCD (charge coupled device), except for the Stoe StadiVari diffractometer which is equipped with a Pilatus 300K detector. Data collection was controlled with the Crysalis RED,[4] the APEX[5] and X-Area software package,[6] respectively. The crystal structures were solved with Direct Methods (SHELXS) and refined with full-matrix least squares on F^2 (SHELXL).[7] Strongly disordered solvent molecules were treated with the SQUEEZE option of the program PLATON.[8-9] Due to the air- and moisture-sensitivity of the investigated compounds single crystals were picked and prepared under exclusion of air and all measurements were carried out under inert gas atmosphere. Crystals which grew at r.t. were transferred from the mother liquor into a perfluoropolyalkylether (abcr GmbH, viscosity 1800 cSt) in a glovebox. Under a microscope one single crystal was separated and fixed on top of a glass fiber and mounted in a cold N_2 stream (100 – 150 K). Crystals which grew at temperatures below r.t. were transferred from the mother liquor into a cooled perfluorinated polyether (Galden®, Solvay Solexis). One single crystal was separated under a microscope, fixed on a capillary loop (Hampton Research) and positioned on the goniometer in a cold N_2 stream.

Depending on the crystallization temperatures different single crystal-preparations were applied which are further specified in the relevant publications/manuscripts.

Detailed information about the used devices for determination of the individual single crystal structures are also given in the particular publications/manuscripts.

Visualization of the obtained structures was done with the Diamond software.[10]

2.2.2 Powder X-Ray Diffraction

X-ray powder diffraction (P-XRD) was used to analyze crystalline samples for purity. In a glovebox samples were ground to fine powder in an agate mortar and filled into glass capillaries (Hilgenberg, diameter: 0.3-0.5 mm, wall thickness: 0.01 mm), which were then sealed airtight by fusing with a heated tungsten wire and an additional wax droplet on top of the capillary. P-XRD patterns were recorded in Debey-Scherrer geometry on a STOE STADI P diffractometer equipped with a Ge(111) monochromator for Cu $K_{\alpha 1}$ radiation (λ = 1.54056 Å) and a Dectris MYTHEN DCS 1K solid-state detector. The P-XRD patterns were analyzed using the WINXPOW software package.[11] The measured diffractograms are compared with respective theoretical P-XRD patterns, which were calculated from single crystal X-ray diffraction data.

2.2.3 Electron Dispersive X-Ray Analysis

Electron dispersive X-ray (EDX) serves for determination of the elemental composition (for all elements heavier than boron) in the single crystals which were used to determine the single crystal structure by SC-XRD. Therefore a Hitachi TM-1000 tabletop microscope was applied.

For EDX measurements a graphite tape loaded with the single crystal was fixed on an aluminum stub and transferred to the microscope facility in air. Since only the elemental compositions of the crystals were needed, oxidation in air did not play a major role for this procedure.

2.2.4 Elemental Analysis

Elemental analysis was performed by the microanalytical laboratory at the Department of Chemistry of the Technische Universität München. The elements C and H were determined with a combustion analyzer (elementar vario EL, Bruker Corp.). Platinum was determined photometrically with tin(II) chloride at 404 nm. Nickel was determined *via* atomic absorption spectroscopy.

2.2.5 Nuclear Magnetic Resonance Spectroscopy

Nuclear magnetic resonance (NMR) spectroscopy is the fastest and most practicable method to analyze reaction solutions as well as the obtained compounds. As soon as the clusters carry organic or silyl functionalities they are decorated with an antenna which offers the possibility to detect the formed cluster species in solution. The 1D and 2D NMR spectra were recorded on Bruker Avance Ultrashield AV400, Bruker Avance DRX 400, Bruker Avance Ultrashield AV500 and Bruker Avance Ultrashield AV500C spectrometers for complete characterization and structure elucidation.

All obtained isolated products (approx. 10 mg) were dissolved in 0.5 mL deuterated solvents and investigated applying NMR spectroscopy. For highly moisture and air sensitive products J Young NMR tubes were used to prevent oxidation processes in solution.

For *in situ* investigations of reactions which were carried out in non-deuterated solvents (e.g. *en* or fluorobenzene) an aliquot of approx. 150 µL of the reaction solution was filtered and filled into a Norell® NMR tube (Deutero GmbH, outer diameter 3 mm) which was sealed with a cap and placed into a common NMR tube (inner diameter 4 mm) (Figure 2.2.1). The outer NMR tube was filled with 0.3 mL chloroform-*d* or dichloromethane-d_2. The corresponding NMR spectra were referenced to the signals of the non-deuterated solvent *en* (-CH_2-, s, 2.645 ppm) and fluorobenzene (m, 7.080 ppm; m, 6.890). All NMR spectra were processed with the program MNova.[12]

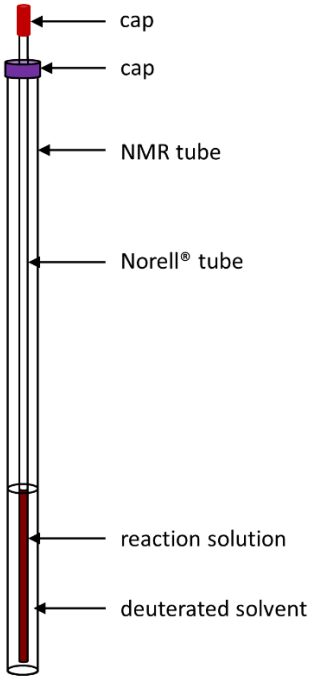

Figure 2.2.1. NMR setup for *in situ* investigations of reactions carried out in non-deuterated solvents.

2.2.6 Electron Spray Ionization Mass Spectrometry

Electron spray ionization mass spectrometry (ESI-MS) represents a very helpful method to detect charged cluster compounds in solution. ESI mass spectra were recorded on a HCT mass spectrometer (Bruker Daltronic) in the negative ion mode (−). Acetonitrile- or thf-solutions of the samples of approximate concentrations of 0.8-1.7 M were prepared and filtered over glass fiber syringe filters. The solutions were then injected into the ESI-MS device with an injection rate of 240 µL/h. The obtained mass spectra were compared to the simulated ones. The measurement conditions are given in detail in the relevant publications/manuscripts. Lorenz Schiegerl and Christina Fischer partly assisted during ESI mass spectrometric measurements. The spectra were processed using the program Origin.[13]

2.2.7 Raman Spectroscopy

As has been shown earlier, “naked”, as well as functionalized Ge_9 clusters show characteristic signals in Raman spectra, wherefore Raman spectroscopic investigations were performed on a Renishaw inVia Raman microscope RE04 on single crystals sealed in glass capillaries (Hilgenberg, diameter: 0.3-0.5 mm, wall thickness: 0.01 mm). Specific details on laser adjustments are given in the respective publications. Sebastian Geier carried out the Raman measurements. The spectra were processed with the program Origin.[13]

2.2.8 UV-Vis Spectroscopy

UV-Vis spectroscopy serves to investigate the electronic structure of molecules. Prior to this work, UV-Vis spectra of Zintl clusters had only scarcely been reported. UV-Vis spectra of diluted solutions of the Ge_9 Zintl compounds were recorded using a Cary® 50 spectrophotometer from Varian. Standard solutions were prepared using the respective solvents. Crystals of each substance were weighed out and transferred to volumetric flasks and dissolved in the relevant solvent. All solutions were homogenized before filling up the volumetric flask. All dilutions were realized using volumetric flasks. For measurement the solutions were transferred into a tailor-made Schlenk cuvette with a thickness of 10 mm. The UV-Vis spectra were processed using the program Origin.[13]

2.2.9 Quantum-Chemical Calculations

Quantum-chemical calculations to elucidate the reaction mechanism of the decarbonylation reaction of $\{(Me_3Si)_3Si\}_3Ge_9(CO)tBu$ were performed by Dr. Markus Drees using the software package Gaussian 09.[14] Throughout the study, the hybrid density functional PBE1PBE[15] together with the basis set Def2TVPP[16] were used. All energies are unscaled and reported as ΔG for 298.15 K and gas-phase relative to the starting material. Frequency calculations also ensure either optimized structures of intermediates (NImag=0) or transition states (NImag=1).

Calculations to investigate dynamic processes in solution in the case of $[\{(Me_3Si)_3Si\}_3Ge_9CH_2CH_3]Ni(PPh_3)$ have been carried out with the software package Gaussian 09.[14] The level of theory contains the gradient approximated functional PBE[17] and the def2-SV(P)[16, 18] basis set for all elements. All optimized structures have been proved by frequency analysis, if we have a ground state (NImag=0) or a transition state (NImag=1).

Prof. Dr. Antti J. Karttunen performed quantum-chemical structural optimizations and UV-Vis spectrum calculations on $[Ge_9]^{2-}$ and $[Ge_9{=}Ge_9{=}Ge_9]^{6-}$ anions, which were carried out using the TURBOMOLE program package.[19-20] PBE0 hybrid density functional method and a triple-zeta-valence quality basis set with polarization functions (def2-TZVP) were used.[16-17, 21] Resolution-of-the-identity technique was used to speed up the calculations.[18, 22] The $[Ge_9]^{2-}$ and $[Ge_9{=}Ge_9{=}Ge_9]^{6-}$ anions were fully optimized within D_{3h} and C_1 point group symmetries, respectively. The COSMO continuum solvation model was used to counter the negative charge of the anions.[23] The excited states were investigated using the Time-Dependent DFT

formalism.[24] The singlet excitations were determined at the optimized ground state S_0 geometries. In the UV-Vis calculations, the effect of COSMO was taken into account for the ground state, but not when calculating the vertical excitations. The final UV-Vis spectra were obtained by applying a Gaussian broadening of 0.25 eV.

The computational analysis of $\{(Me_3Si)_3Si\}_2Cp^*[LiSiGe_9](SiCp^*)_2[Ge_9SiLi]Cp^*\{(Me_3Si)_3Si\}_2$ was performed using the TURBOMOLE V7.3 program package[25], with exchange correlation hybrid function after Perdew, Burke and Ernzerhof (PBE0) and def2-TZVP basis sets for all considered elements Li, Ge, Si, C and H.[16, 26] Multipole-accelerated resolution-of-the-identity technique was used to speed up the calculations.[18, 22, 27] Natural population analysis (NPA)[28] and Paboon charges[29], as well as an intrinsic bonding orbital (IBO)[30] analysis were carried out. For data processing and visualization Jmol[31] and IBOview[32] were used.

Details on calculations are displayed in the relevant publications.

2.3 References

[1] S. Frischhut, M. M. Bentlohner, T. F. Fässler, *The Reaction of Ethylenediamine with 1,4-Bis(trimethylsilyl)butadiyne and the Role of Water: A Qualitative Method for the Determination of Water in Ethylenediamine*, *manuscript for publication*.

[2] C. Hoch, M. Wendorff, C. Röhr, *J. Alloys Compd.* **2003**, *361*, 206-221.

[3] S. Ponou, T. F. Fässler, *Z. Anorg. Allg. Chem.* **2007**, *633*, 393-397.

[4] C. RED, Version 1.171.33.34d ed., Oxford Diffraction, Abingdon, UK **2009**.

[5] APEX Suite of Crystallographic Software, Bruker AXS Inc., Madison, WI, USA **2008**.

[6] X-Area, *STOE & Cie GmbH*, Version 1.76, **2015**.

[7] G. M. Sheldrick, *Acta Cryst. C* **2015**, *71*, 3-8.

[8] A. L. Spek, *Acta Cryst. D* **2009**, *65*, 148-155.

[9] A. L. Spek, *Acta Cryst. C* **2015**, *71*, 9-18.

[10] K. Brandenburg, *Crystal Impact Gbr*, Version 3.2k ed., Bonn, Germany **2014**.

[11] WinXPow, *Stoe & Cie GmbH*, Version 2.08, **2003**.

[12] MestReNova, *Mestrelab Research S. L.*, Version 8.1.0-11315, **2012**.

[13] OriginPro, *OriginLab Cop.*, **2016**.

[14] Gaussian o0, **E.**03. M. J. Frisch, G. W. Trucks, H. B. Schlegel, G. E. Scuseria, M. A. Robb, J. R. Cheeseman, G. Scalmani, V. Barone, G. A. Petersson, H. Nakatsuji, X. Li, M. Caricato, A. V. Marenich, J. Bloino, B. G. Janesko, R. Gomperts, B. Mennucci, H. P. Hratchian, J. V. Ortiz, A. F. Izmaylov, J. L. Sonnenberg, D. Williams-Young, F. Ding, F. Lipparini, F. Egidi, J. Goings, B. Peng, A. Petrone, T. Henderson, D. Ranasinghe, V. G. Zakrzewski, J. Gao, N. Rega, G. Zheng, W. Liang, M. Hada, M. Ehara, K. Toyota, R. Fukuda, J. Hasegawa, M. Ishida, T. Nakajima, Y. Honda, O. Kitao, H. Nakai, T. Vreven, K. Throssell, J. Montgomery, J. A. , J. E. Peralta, F. Ogliaro, M. J. Bearpark, J. J. Heyd, E. N. Brothers, K. N. Kudin, V. N. Staroverov, T. A. Keith, R. Kobayashi, J. Normand, K. Raghavachari, A. P. Rendell, J. C. Burant, S. S. Iyengar, J. Tomasi, M. Cossi, J. M. Millam, M. Klene, C. Adamo, R. Cammi, J. W. Ochterski, R. L. Martin, K. Morokuma, O. Farkas, J. B. Foresman, D. J. Fox, *Gaussian, Inc.*, Wallingford CT **2016**.

[15] M. Ernzerhof, G. E. Scuseria, *J. Chem. Phys.* **1999**, *110*, 5029-5036.

[16] F. Weigend, R. Ahlrichs, *PCCP* **2005**, *7*, 3297-3305.

[17] J. P. Perdew, K. Burke, M. Ernzerhof, *Phys. Rev. Lett.* **1996**, *77*, 3865.

[18] F. Weigend, *PCCP* **2006**, *8*, 1057-1065.

[19] TURBOMOLE V7.2 2017, 1989-2007, TURBOMOLE GmbH, since 2007; available from www.turbomole.com.

[20] R. Ahlrichs, M. Bär, M. Häser, H. Horn, C. Kölmel, *Chem. Phys. Lett.* **1989**, *162*, 165-169.

[21] C. Adamo, V. Barone, *J. Chem. Phys.* **1999**, *110*, 6158-6170.

[22] K. Eichkorn, O. Treutler, H. Öhm, M. Häser, R. Ahlrichs, *Chem. Phys. Lett.* **1995**, 283-290.

[23] A. Klamt, G. Schüürmann, *J. Chem. Soc., Perkin Trans. 2* **1993**, 799-805.

[24] F. Furche, D. Rappoport, J. Theor. *Comput. Chem.* **2005**, *16*, 93-128.

[25] TURBOMOLE V7.3; University of Karlsruhe and Forschungszentrum Karlsruhe GmbH, **2016**.

[26] F. Weigend, M. Häser, H. Patzelt, R. Ahlrichs, *Chem. Phys. Lett.* **1998**, *294*, 143-152.

[27] M. Sierka, A. Hogekamp, R. Ahlrichs, *J. Chem. Phys.* **2003**, *118*, 9136-9148.

[28] A. E. Reed, R. B. Weinstock, F. Weinhold, *J. Chem. Phys.* **1985**, *83*, 735-746.

[29] C. Ehrhardt, R. Ahlrichs, *Theor. Chim. Acta* **1985**, *68*, 231-245.

[30] G. Knizia, *J. Chem. Theory Comput.* **2013**, *9*, 4834-4843.

[31] *Jmol - An Open-Source Java Viewer for Chemical Structures in 3D*, The Jmol Team, **2017**.

[32] G. Knizia, J. E. Klein, *Angew. Chem. Int. Ed.* **2015**, *54*, 5518-5522.

3 RESULTS AND DISCUSSION

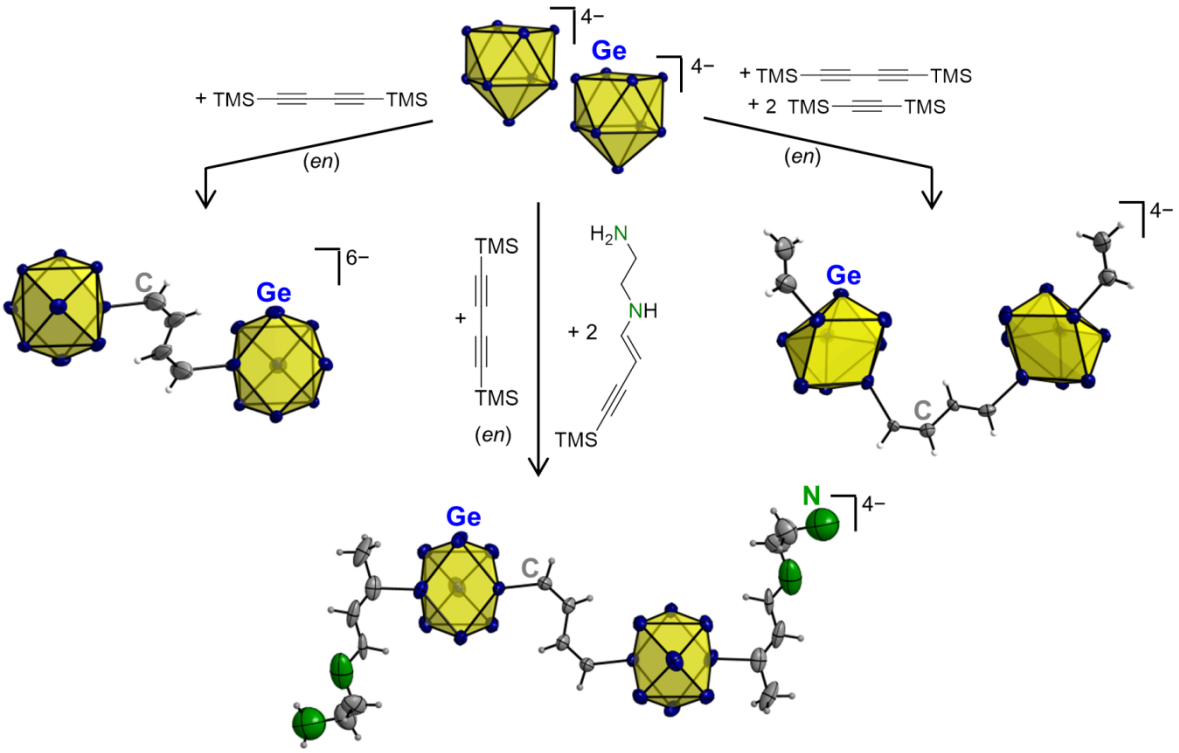

3.1 Linkage of $[Ge_9]^{4-}$ Zintl Ions with Conjugated Organic Building Blocks

3.1.1 Review of Relevant Literature

3.1.1.1 Reaction of $[Ge_9]^{4-}$ and Amines with Alkynes

Sevov and co-workers first explored the reaction of $[Ge_9]^{4-}$ clusters with monoalkynes by treating K_4Ge_9 with 2 eq. of Fc−C≡CH in *en* to form the anion [Fc−CH=CH−Ge_9−CH=CH−Fc] (Fc = ferrocenyl).[1] The alkenylation reaction was further investigated by the reaction of $[Ge_9]^{4-}$ clusters with the simplest conceivable monoalkyne bis(trimethylsilyl)acetylene to obtain the vinylated cluster $[(CH_2{=}CH)_nGe_9]^{(4-n)-}$ (n = 1,2) in good yields. Depending on the applied equivalents of the monoalkyne onefold or twofold substitution can be achieved.[2-3] So far, a threefold alkenylation could not be observed in *en*. The elucidation of the reaction mechanism revealed that $[Ge_9]^{4-}$ undergoes a nucleophilic attack at the most electrophilic *sp*-hybridized carbon atom, which provides a low-lying and unoccupied π^*-orbital, resulting in the alkenyl-anion which abstracts a proton from *en*, generating an amide and the corresponding *cis*-product. The *cis*-stereoselectivity can be explained by the repulsion of the cluster-electrons and the negative charge at the carbanion of the alkenyl anion (Scheme 3.1.1 a). The *in situ* generated amide, which had not been unequivocally proven, yet, step-wisely abstracts the trimethylsilyl groups, whereby the as generated alkenylanions are protonated by *en*.[4] This alkenylation reaction at Ge_9 clusters is further transferable to a wide range of monoalkynes, thus a variety of alkenylated Ge_9 cluster compounds was accessible.[5-6] A *trans*-product is exceptionally observed for $[Ge_9(Me)C{=}CHPh]^{3-}$ which is traced back to the conjugated system in the organic tether, which stabilizes the intermediary formed alkenyl anion.[7]

Besides $[Ge_9]^{4-}$ clusters, also amines (e.g. *en*) can serve as nucleophiles and can principally react with alkynes to form C−N-bonds. The so-called hydroamination proceeds in presence of homogenous catalysts, e.g. late transition metal complexes. The reaction of primary amines with alkynes yields enamines, which are further transferred to the corresponding imines by prototropic tautomerism (Scheme 3.1.1 b). In contrast, the hydroamination reaction with secondary amines leads to the enamines due to the impossibility of prototropic tautomerism within the molecule.[8-10]

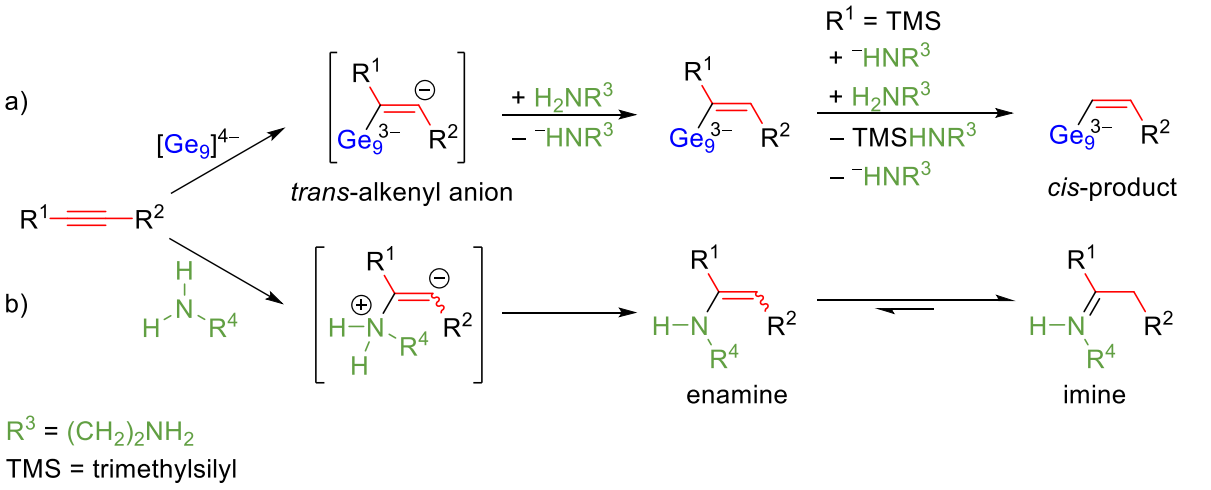

Scheme 3.1.1. Nucleophilic addition of a) $[Ge_9]^{4-}$ and b) primary amines to alkynes.[4, 8-9] Red: Carbon skeleton, blue: Ge_9 cluster, green: *en* or any primary amine.

3.1.1.2 Fullerene Triads versus Zintl Triads

Already in 2001, an analogy between fullerenes and $[Ge_9]^{4-}$ Zintl clusters was stated. They both can serve as electron reservoirs due to their flexibility upon oxidation. Fullerenes are well-known for their exceptional electronic properties.[11] C_{60} fullerenes which are linked through electroactive spacers can display interesting electronic and optical properties. With regard to application in organic photovoltaics the stabilization of charge-separated states can be provided by covalently linked fullerenes which can offer intramolecular electronic communication, the so-called fullerene triads (Figure 3.1.1 a).[12-13] Therefore, these materials have been investigated for application in organic photovoltaics as electron acceptor materials (especially PCBM) in combination with the semiconductive polymer P3HT, but also in molecular spintronics and electron-spin-based quantum computing.[14-16] Ge_9 clusters can also adapt different charges, and thus count as interesting materials for application in semiconductor devices.[17] Ge shows better semiconductor properties than carbon which leads to the assumption that, compared to fullerenes, Ge_9 clusters might have similar potential for application in hybrid solar cells. Therefore, the synthesis of fullerene analogous Zintl triads has been investigated. In 2015, the first Zintl triad was reported, namely $[R–Ge_9–CH=CH–CH=CH–Ge_9–R]^{4-}$ (R = (2*Z*,4*E*)-7-amino-5-azahepta-2,4,dien-2-yl) (**1a**) (Figure 3.1.1 b), which was achieved by reaction of K_4Ge_9 with 2 eq. of the dialkyne 1,4-bis(trimethylsilyl)butadiyne (**2**) in *en*. According to quantum chemical calculations the latter provides an extended conjugated π-electronic system. However, cyclovoltammetric measurements did not reveal reversible oxidation in solution.[18]

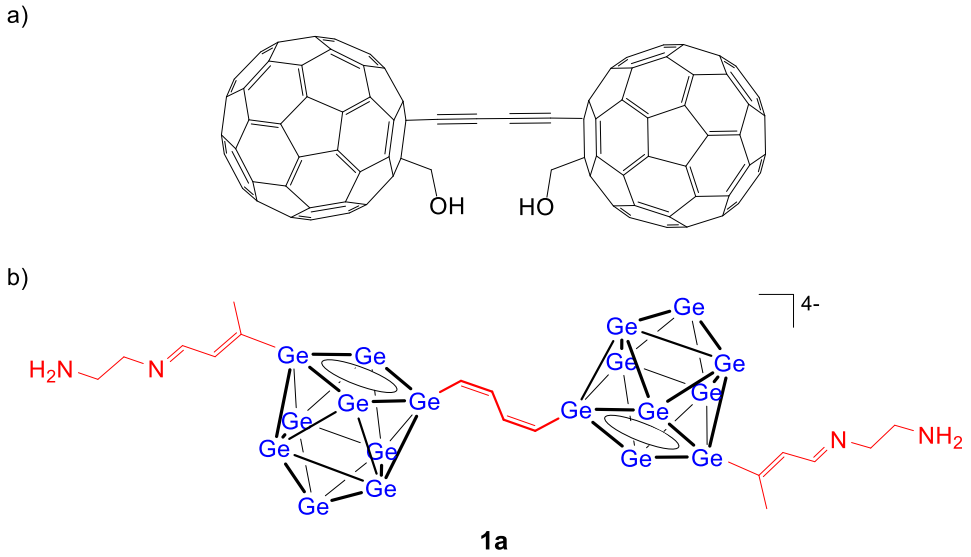

Figure 3.1.1. a) Fullerene triad and b) Zintl triad $[R–Ge_9–CH=CH–CH=CH–Ge_9–R]^{4–}$ (R = (2*Z*,4*E*)-7-amino-5-azahepta-2,4,dien-2-yl) (**1a**).[12, 18]

The formation of the side-chain of the Zintl triad **1a** shown in Figure 3.1.1 b involving the solvent *en* was initially not understood. Therefore, the targeted synthesis of the first Zintl triad to obtain higher yields, the elucidation of the reaction mechanism of the formation of the linking unit, as well as the synthesis of further Zintl triads comprising extended π-electronic systems was aimed at.

3.1.2 UV-Vis Spectroscopic Investigations on the *closo*-$[Ge_9]^{2-}$ Cluster

see chapter 5.1

S. Frischhut, J. G. Machado de Carvalho, A. J. Karttunen, T. F. Fässler, *Z. Anorg. Allg. Chem.*, **2018**, *644*, 1337-1343.

The close relation between fullerenes and deltahedral Ge_9 clusters had been pointed out before.[11] C_{60} and C_{70} fullerenes have been scarcely investigated *via* UV-Vis spectroscopy in solution. Hare *et al.* reported UV-Vis spectra of these compounds in hexane and benzene solutions for the first time. However, the recorded spectra had not been fully understood by the authors. Pronounced signals had been observed at wavelengths of 213, 257 and 329 nm in hexane solutions. Very weak broad features at high concentrations had been reported in the region of 400 to 700 nm, which had been assigned to either first-order forbidden transitions or to small impurities in the used C_{60} sample.[19] A UV-Vis electronic spectrum of deltahedral Ge_9 clusters had only been reported for $[\{(Me_3Si)_3Si\}_3Ge_9]^-$, which appeared to be rather featureless.[20] To further investigate the electronic structure of Ge_9 clusters, UV-Vis electronic spectra of C_{60} fullerene in toluene-solutions were reproduced and compared to those of the *closo*-$[Ge_9]^{2-}$ (**3a**) deltahedral cluster within this work (Figure 3.1.2).

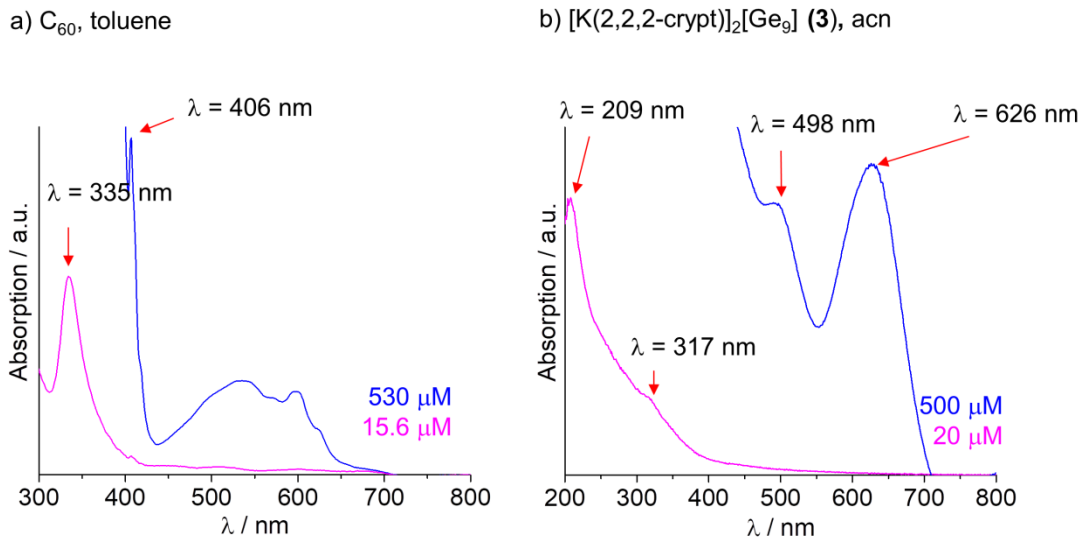

Figure 3.1.2. UV-Vis electronic spectra of a) C_{60} in toluene at concentrations of 530 and 15.6 µM in the region of 300 to 800 nm and of b) $[K(2,2,2\text{-crypt})]_2[Ge_9]$ (**3**) in acetonitrile (acn) at concentrations of 500 and 20 µM in the region of 200 to 800 nm. The figure was modified on the basis of ref. [21].

The spectrum of the "naked" *closo*-$[Ge_9]^{2-}$ cluster **3a** in highly diluted acetonitrile-solutions (c = 10 μM) shows a strong absorption at wavelengths of 209 nm and a weaker absorption at 317 nm, which are in good agreement with the calculated UV-Vis spectrum of **3a**. The obtained broad signals are in accordance with the high flexibility of the deltahedral Ge_9 clusters in solution. Upon further concentration of the *closo*-$[Ge_9]^{2-}$ acetonitrile solutions up to c = 500 μM, weaker absorption bands at 498 and 626 nm appear. According to DFT calculations the very weak absorptions at 498 and 626 nm are assigned to the agglomerate $[Ge_9{=}Ge_9{=}Ge_9]^{6-}$, which is formed due to further concentration. As a consequence, an equilibrium according to 3 $[Ge_9]^{2-} \rightleftharpoons [Ge_9{=}Ge_9{=}Ge_9]^{6-}$ is present in solution.

All in all **3a** shows a similar UV-Vis spectrum compared to C_{60}, concluding that both cage molecules possess similar electronic structures.[21]

3.1.3 The Zintl Triads $[Ge_9–CH=CH–CH=CH–Ge_9]^{6–}$, $[CH_2=CH–Ge_9–CH=CH–CH=CH–Ge_9–CH=CH_2]^{4–}$ and $[R–Ge_9–CH=CH–CH=CH–Ge_9–R]^{4–}$ (R = (2*Z*,4*E*)-7-amino-5-azahepta-2,4-dien-2-yl) – Investigations on the Formation and the Role of Water

see chapter 5.2 S. Frischhut, M. M. Bentlohner, T. F. Fässler, *manuscript for publication*.

see chapter 5.3 M. M. Bentlohner, S. Frischhut, T. F. Fässler, *Chem. Eur. J.* **2017**, *23*, 17089-17094.

see chapter 5.4 S. Frischhut, M. M. Bentlohner, W. Klein, T. F. Fässler, *Inorg. Chem.* **2017**, *56*, 10691-10698.

The reaction of 1,4-bis(trimethylsilyl)butadiyne (**2**) with A_4Ge_9 (A = K, Rb) in *en* afforded the first Zintl triad $[R–Ge_9–CH=CH–CH=CH–Ge_9–R]^{4–}$ (R = (2*Z*,4*E*)-7-amino-5-azahepta-2,4,dien-2-yl) (**1a**).[18] The formation of the side chain R was unforeseen at first sight, but indicated the ready reaction of **2** with *en*. Therefore, investigations on the reaction of **2** with *en* were performed to prevent these side-reactions, and thus to be able to design and synthesize specifically functionalized Zintl triads.

NMR spectroscopic investigations revealed that **2** readily reacts with *en* at r.t. One molecule *en* adds to the most electrophilic carbon of **2** following a hydroamination reaction, which results in the formation of the two isomers (3*Z*)- and (3*E*)-1-trimethylsilyl-7-amino-5-azahepta-3-en-1-yne (**4**) in an isomers ratio of *Z*/*E* = 30/70. An enamide is not generated throughout this reaction. In water-free *en* the reaction stops at this stage (Scheme 3.1.2 a). In the presence of traces of water, two follow-up reaction pathways were observed: on the one hand **4** can undergo an intramolecular hydroamination reaction to form the cyclization product 2,3-dihydro-5-methyl-*H*-1,4-diazepine (**5**), on the other hand a second molecule *en* can nucleophilically add to **4** to form 1,9-di-amino-4-methyl-3,7-diaza-nonadiene (**6**) (Scheme 3.1.2 b) at r.t.[22] The formation of product **5** had already been reported in 1969, but the significant role of water in the cyclization reaction had not been considered.[23]

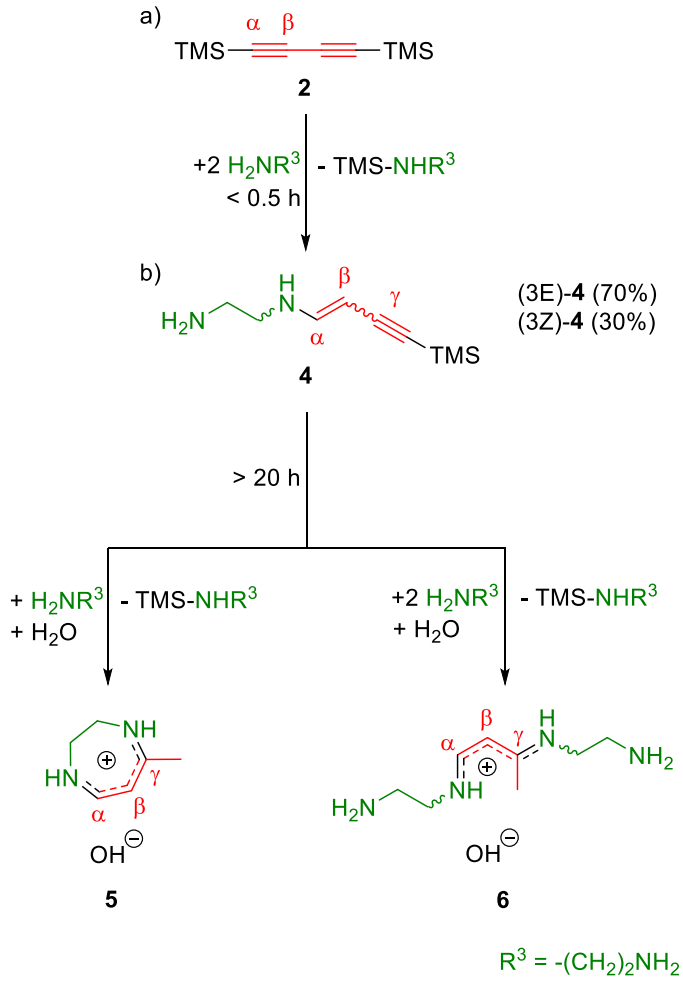

Scheme 3.1.2. a) Reaction of 1,4-bis(trimethylsilyl)butadiyne (**2**) with *en* at r.t. In the absence of water-traces the reaction stops at product (3*Z*/3*E*)-1-trimethylsilyl-7-amino-5-azahepta-3-en-1-yne (**4**). b) Follow-up reaction of **4** to the cyclization product 2,3-dihydro-5-methyl-*H*-1,4-diazepine (**5**) and to the product 1,9-di-amino-4-methyl-3,7-diaza-nonadiene (**6**), which results from the addition of a second molecule *en* to **4** in the presence of water.

The reaction of **2** with *en* at r.t. can serve as easy method to trace water-contents in *en*. The traditional Karl-Fischer method cannot be easily transferred to amines such as *en*,[24-25] which would lead to several side reactions.[26]

These investigations provided further contributions to the elucidation of the reaction mechanism of the nucleophilic addition of $[Ge_9]^{4-}$ to alkynes in *en*. Prior to this work, the formation of the enamide throughout this reaction was predicted, but could not be unequivocally shown. **6** forms out of **4** in the presence of water-traces in *en*, but is also formed throughout the reaction of $[Ge_9]^{4-}$ with **4** in *en* as a dominant side-product. The addition of $KHN(CH_2)_2NHK$ to a solution of **4** in water-free *en* also yields **6**. Therefore, the enamide must be formed throughout the reaction of $[Ge_9]^{4-}$ with **4**.[22]

As has been presented in chapter 3.1.1.2, the reaction of K_4Ge_9 with a solution of 4 eq. of 1,4-bis(trimethylsilyl)butadiyne (**2**) in *en* lead to the formation of the Zintl triad $[R{-}Ge_9{-}CH{=}CH{-}CH{=}CH{-}Ge_9{-}R]^{4-}$ (R = (2*Z*,4*E*)-7-amin-azahepta-2,4-dien-2-yl) (**1a**), which was at first sight unforeseen as the hydroamination reaction between *en* and **2** was unexpected.[18] Also, the formation of the linking unit had been unclear. Therefore, an improved synthesis protocol needed to be developed, as well as the elucidation of the mechanism of the linkage had been asked for.

The presented reactivity studies between **2** and *en* gave access to a new Zintl triad. When A_4Ge_9 (*A* = K, Rb) and 0.25-0.5 eq. of **2** were simultaneously dissolved in *en* at r.t., the hydroamination reaction between *en* and the dialkyne was prevented and a linkage of two Ge_9 clusters was achieved without further attachment of the (2*Z*,4*E*)-7-amino-azahepta-2,4-dien-2-yl (R) functionality. Besides the (1*Z*,3*Z*)-, also the (1*E*,3*Z*)-configured conformer of $[Ge_9{-}CH{=}CH{-}CH{=}CH{-}Ge_9]^{6-}$ (**7a** and **7b**, respectively) were monitored by ^{1}H NMR spectroscopic investigations in the reaction solution in an isomer ratio of 20:80. Crystallization of **7a** was achieved by layering the reaction solution with a solution of 4 eq. of 2,2,2-crypt in toluene (Scheme 3.1.3).

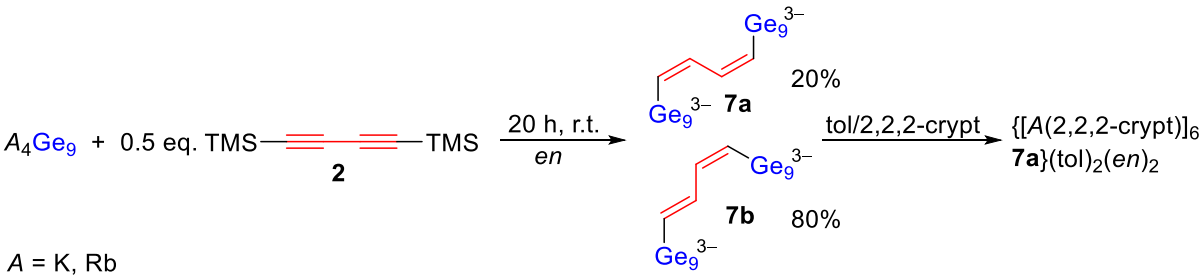

Scheme 3.1.3. Reaction of A_4Ge_9 with 1,4-bis(trimethylsilyl)butadiyne (**2**) in *en* yielding the Zintl triads **7a** and **7b**. Red: organic skeleton originating from **2**, blue: Ge_9 cluster. The scheme was modified on the basis of ref. [27].

The formation of **7a** was unequivocally shown by the crystal structure which contains solely the anion $[Ge_9{-}CH{=}CH{-}CH{=}CH{-}Ge_9]^{6-}$ in (1*Z*,3*Z*)-configuration (**7a**), whereby **7a** appears strongly disordered in three superimposing conformers. The Ge_9 cluster entity of **7a** adopts C_S-symmetry, which is typical of onefold substituted Ge_9 cluster anions which show a compression of the open square face Ge1/Ge2/Ge3/Ge4 at the substituted Ge1 atom (Figure 3.1.3).[3]

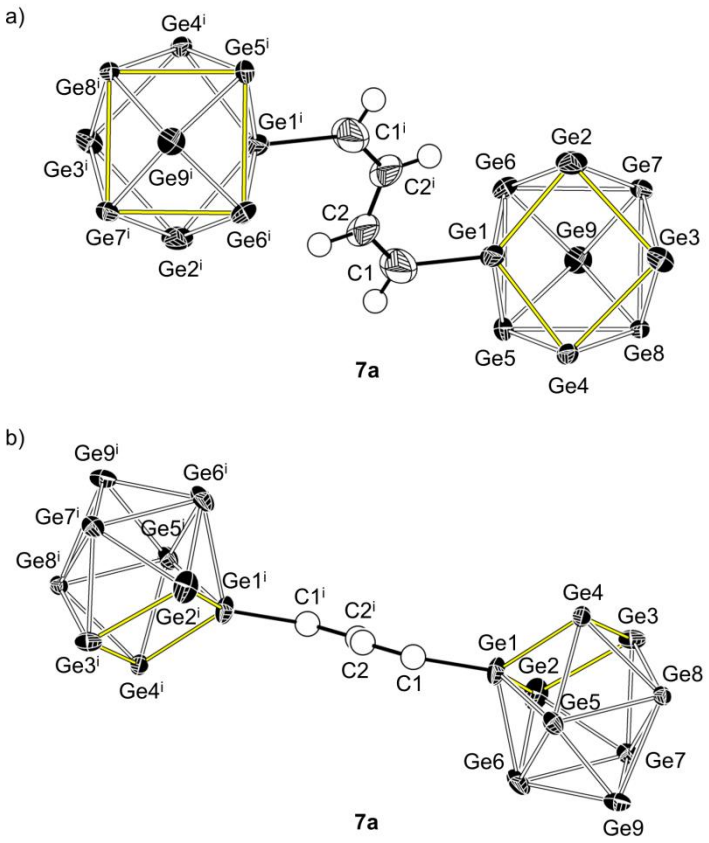

Figure 3.1.3. Structure of **7a**. a) view perpendicular and b) view parallel to the plane Ge1i/C1i/C2i/C2/C1/Ge1. All ellipsoids are shown at a probability level of 50%. In a) hydrogen atoms are shown as empty spheres. In b) carbon atoms are shown as empty spheres and hydrogen atoms are omitted for clarity. The frame of the open square is highlighted in yellow. The figure was modified on the basis of ref. [27].

To track linkage of the two Ge_9 Zintl clusters *via* the conjugated organic buta-1,3-dien-1,4-diyl bridge to form **7a** and **7b** time-resolved *in situ* ^{1}H NMR studies were performed. The formation of **7a** and **7b** occurs to be a step-wise process, where first, one $[Ge_9]^{4-}$ anion very rapidly adds to **2** to form two isomers of an alkenyl-anion, which in a subsequent step is protonated by *en*. The formation of the *anti*-product can be easily explained by the repulsion of the negative charges of the cluster anion and the carbanion. The *syn*-product is a result of isomerization by stabilization of the conjugated anion. This has been observed previously for $[Ge_9MeC{=}CHPh]^{3-}$.[7] After TMS group abstraction by the *in situ* generated amide a second $[Ge_9]^{4-}$ cluster adds slowly to the second triple bond, solely in *anti*-fashion (Scheme 3.1.4).

The formation of the Zintl anions **7a** and **7b** is complete within 20 h.[27]

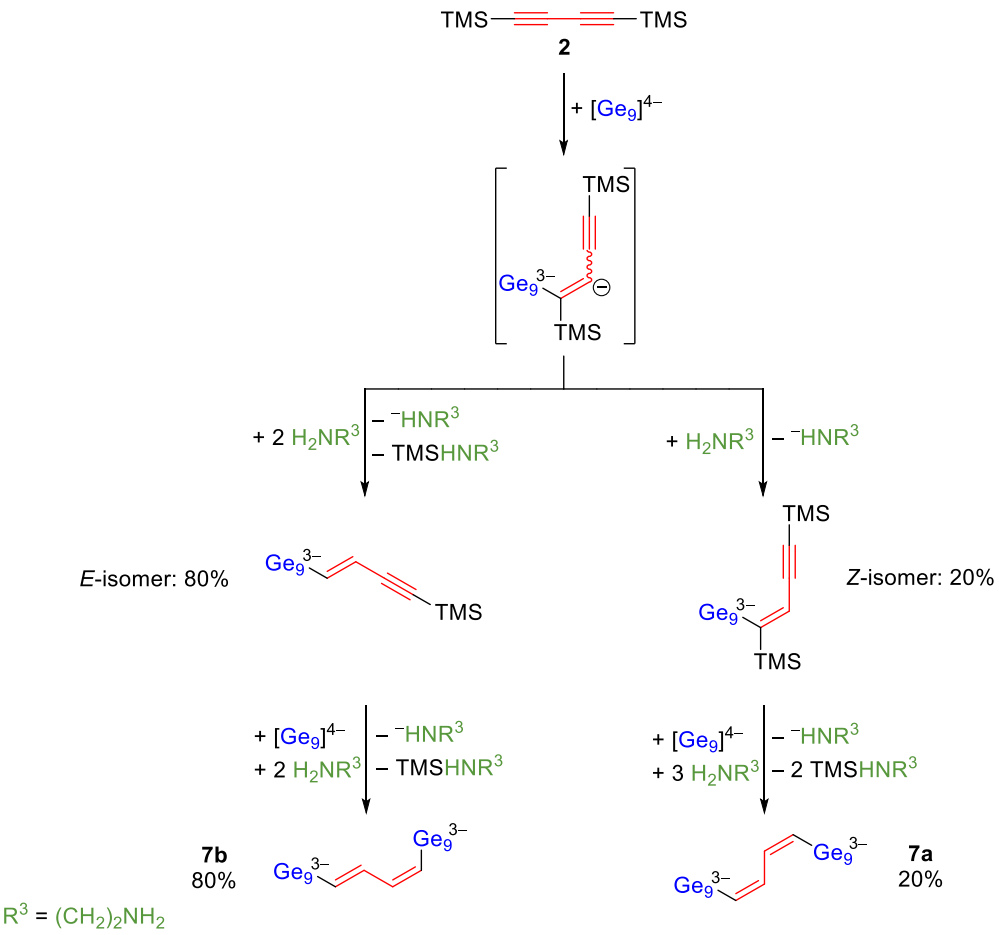

Scheme 3.1.4. Reaction mechanism of the formation of the buta-1,3-dien-1,4-diyl linker in **7a** and **7b**. Red: organic skeleton originating from **2**, blue: Ge_9 cluster, green: *en*. The scheme was modified on the basis of ref. [27].

The results show, that only if an excess of $[Ge_9]^{4-}$ compared to **2** is applied, and both reactants are dissolved simultaneously in *en*, the hydroamination reaction between **2** and *en* to form 1-trimethylsilyl-7-amino-5-azahepta-3-en-1-yne (**4**) is prevented.

The insight into the reaction mechanism of the formation of the buta-1,3-dien-1,4-diyl linking unit, as well as the investigations on the reactivity of **2** towards *en* allowed for the design and synthesis of a novel Zintl triad with potential application in hybrid solar cells.

The reaction of K_4Ge_9 with 0.5 eq. of **2** and 2 eq. of bis(trimethylsilyl)acetylene (**8**) lead to the newly found Zintl triads (1*E*,3*Z*)- and (1*Z*,3*Z*)-$[H_2C{=}CH{-}Ge_9{-}CH{=}CH{-}CH{=}CH{-}Ge_9{-}CH{=}CH_2]^{4-}$ (**9a**, **9b**) (Scheme 3.1.5 a). A more direct synthesis strategy of the first Zintl triad $[R{-}Ge_9{-}CH{=}CH{-}CH{=}CH{-}Ge_9{-}R]^{4-}$ (**1a**) (R = (2*Z*,4*E*)-7-amin-azahepta-2,4-dien-2-yl), which was previously reported,[18] was developed where Rb_4Ge_9 and 0.5 eq. of **2** were treated with a

solution of 2 eq. of (3Z/3E)-7-amino-1-(trimethylsilyl)-5-azahepta-3-en-1-yne (**4**) in *en* (Scheme 3.1.5 b). Both triads were crystallized and characterized by single-crystal X-ray diffraction and NMR spectroscopy.

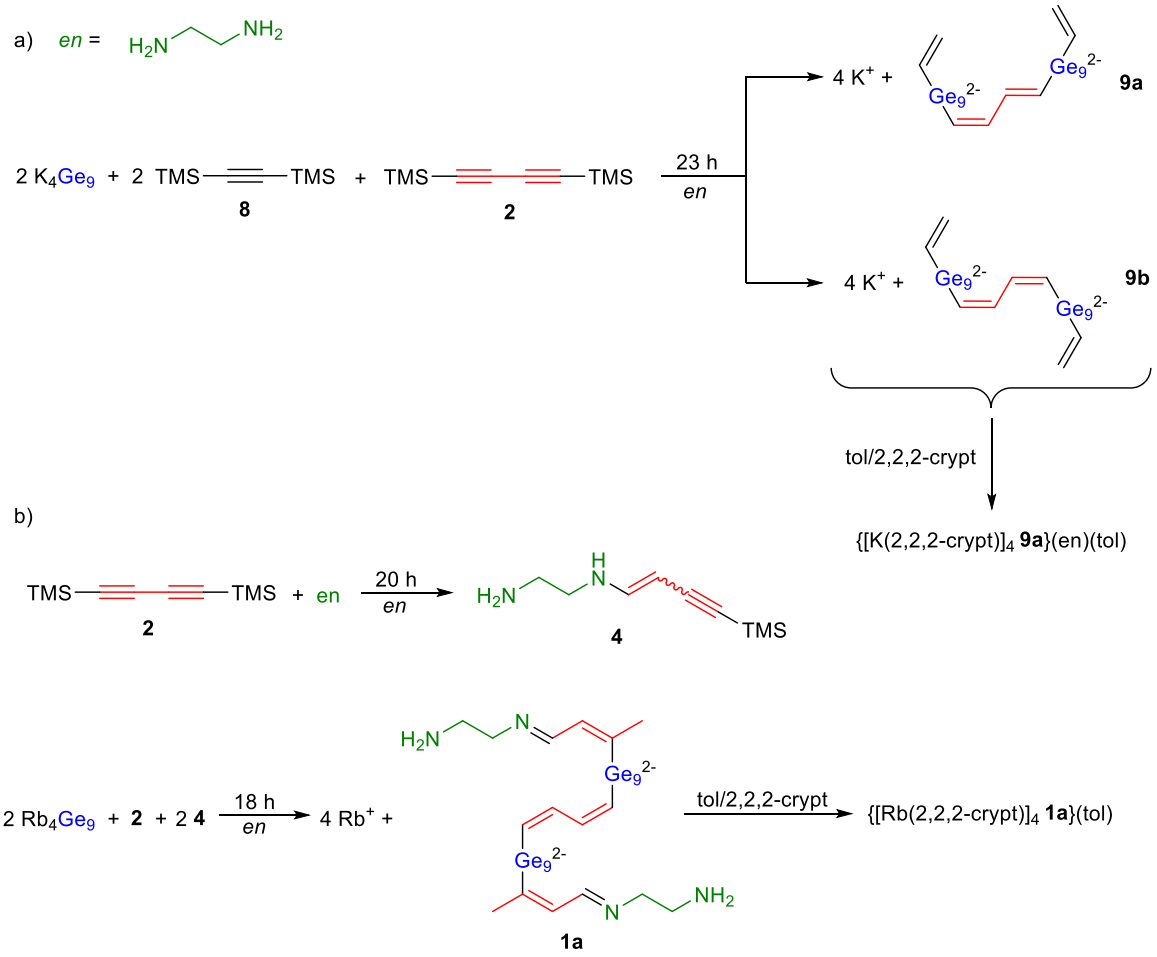

Scheme 3.1.5. Reaction of a) K_4Ge_9 with 1,4-bis(trimethylsilyl)butadiyne (**2**) and bis(trimethylsilyl)acetylene (**8**) in *en* yielding the anions **9a** and **9b** and b) Rb_4Ge_9 with (3Z/3E)-1-trimethylsilyl-7-amino-5-azahepta-3-en-1-yne (**4**) and 1,4-bis(trimethylsilyl)butadiyne (**2**) in *en* yielding the anion **1a**. The scheme was modified on the basis of ref. [28].

Step-by-step synthesis of **9a**/**b** by change of the order of addition of the reactants was not successful and lead to several side reactions. Also, the reaction turned out to be very sensitive towards the applied equivalents of the reactants. Often the formation of the vinylated cluster species $[(CH_2{=}CH)_nGe_9]^{(4-n)-}$ (n = 1,2) was observed as the reaction of $[Ge_9]^{4-}$ with **8** is preferred over the reaction with **2**. This shows that an understanding of the interplay of all reactants including solvent molecules is of great importance for further developing synthesis strategies for analogous linked Zintl anions.

Even though both isomers **9a** and **9b** were present in the reaction solution, only **9a** could be crystallized, whereas in the synthesis of $[R{-}Ge_9{-}CH{=}CH{-}CH{=}CH{-}Ge_9{-}R]^{4-}$ (R = (2*Z*,4*E*)-7-amin-azahepta-2,4-dien-2-yl) (**1a**) was the only detected Zintl triad anion isomer in solution. In the crystal structure of $\{[K(2,2,2\text{-crypt})]_4$ **9a**$\}(en)(tol)$ the (1*Z*,3*E*)-buta-1,3-diene-1,4-diyl bridge (C1/C2/C3/C4) of **9a** appears in two orientations resulting in two different conformers, whereby the second conformer carries the (1*E*,3*Z*)-buta-1,3-diene-1,4-diyl bridge (C4'/C3'/C2'/C1') which is mirrored on a virtual plane crossing the bond between C2 and C3. As expected for conjugated systems, the atoms C1/C2/C3/C4 and C4'/C3'/C2'/C1' lie in one plane, respectively. Both Ge_9 clusters adopt almost perfect C_{2v}-symmetry, which results from the compression of the *exo*-bond-substituted Ge atoms Ge1 and Ge10. These observations are consistent with the reported structures of twofold substituted Ge_9 clusters.[1-6, 18] Remarkably, the open square faces of the clusters are tilted toward each other (Figure 3.1.4 a and b). Unlike **9a**, the crystal structure of **1a** reveals an inverted spatial orientation of the two linked Ge_9 clusters (Figure 3.1.4 c and d).[28] Otherwise, the structure of **1a** is isotypic to the respective potassium salt of the Zintl triad, which had already been reported.[18]

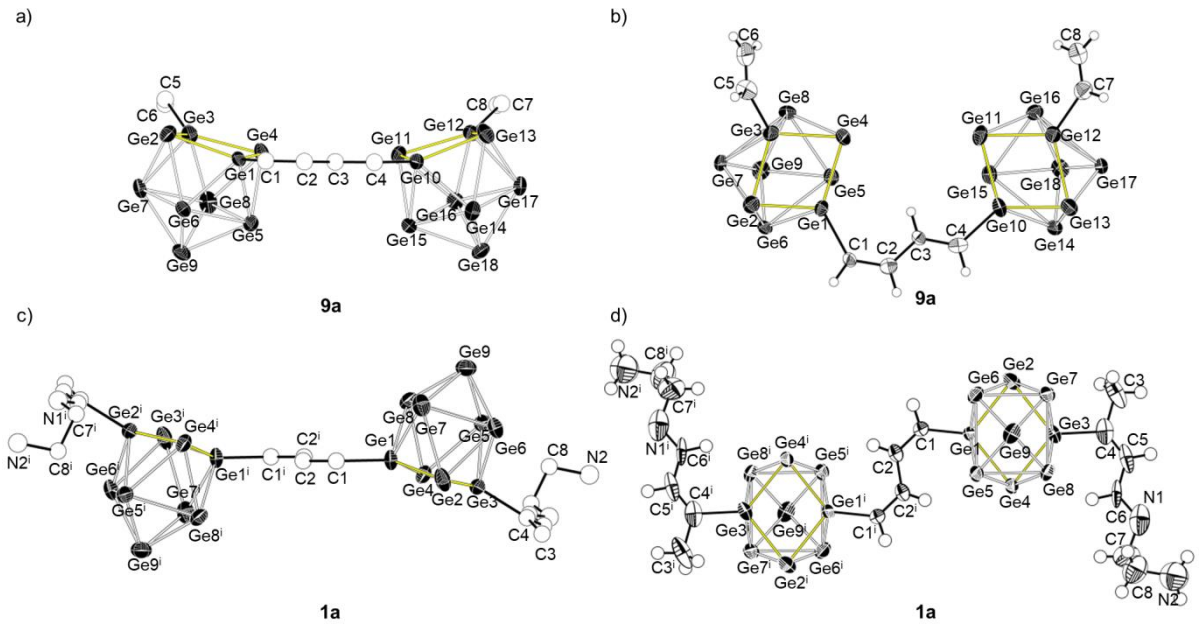

Figure 3.1.4. Structures of the Zintl triads **9a** and **1a**. a) and c) view parallel to the plane in which the linking unit is located. All carbon atoms are shown as empty spheres. Hydrogen atoms are omitted for clarity. b) and d) view perpendicular to the plane in which the linking unit is located. Hydrogen atoms are shown as empty spheres. The frame of the open square is highlighted in yellow. All displacement vectors are shown at a probability level of 50%. The figure was modified on the basis of ref. [28].

Quantum chemical calculations revealed, that the anion **9a** comprises a conjugated π-electronic system which is extended over the whole anion, which makes this compound an interesting candidate for further investigations in application in semiconductor devices.[18]

3.1.4 References

[1] M. W. Hull, S. C. Sevov, *Angew. Chem. Int. Ed.* **2007**, *46*, 6695-6698.
[2] M. W. Hull, S. C. Sevov, *Inorg. Chem.* **2007**, *46*, 10953-10955.
[3] C. B. Benda, J. Q. Wang, B. Wahl, T. F. Fässler, *Eur. J. Inorg. Chem.* **2011**, *27*, 4262-4269.
[4] M. W. Hull, S. C. Sevov, *J. Am. Chem. Soc.* **2009**, *131*, 9026-9037.
[5] M. W. Hull, S. C. Sevov, *J. Organomet. Chem.* **2012**, *721*, 85-91.
[6] M. W. Hull, S. C. Sevov, *Chem. Commun.* **2012**, *48*, 7720-7722.
[7] M. M. Gillett-Kunnath, I. Petrov, S. C. Sevov, *Inorg. Chem.* **2009**, *49*, 721-729.
[8] T. E. Muller, K. C. Hultzsch, M. Yus, F. Foubelo, M. Tada, *Chem. Rev.* **2008**, *108*, 3795-3892.
[9] T. E. Müller, M. Beller, *Chem. Rev.* **1998**, *98*, 675-704.
[10] F. Alonso, I. P. Beletskaya, M. Yus, *Chem. Rev.* **2004**, *104*, 3079-3160.
[11] T. F. Fässler, *Angew. Chem. Int. Ed.* **2001**, *40*, 4161-4165.
[12] J. L. Segura, N. Martín, *Chem. Soc. Rev.* **2000**, *29*, 13-25.
[13] N. Martín, L. Sánchez, B. Illescas, I. Pérez, *Chem. Rev.* **1998**, *98*, 2527-2548.
[14] M. A. Lebedeva, T. W. Chamberlain, E. S. Davies, B. E. Thomas, M. Schröder, A. N. Khlobystov, *Beilstein J. Org. Chem.* **2014**, *10*, 332-343.
[15] P. Vanlaeke, A. Swinnen, I. Haeldermans, G. Vanhoyland, T. Aernouts, D. Cheyns, C. Deibel, J. D'Haen, P. Heremans, J. Poortmans, *Sol. Energy Mater. Sol. Cells* **2006**, *90*, 2150-2158.
[16] Y. Kanai, J. C. Grossman, *Nano Lett.* **2007**, *7*, 1967-1972.
[17] T. Fässler, M. Hunziker, M. Spahr, H. Lueken, H. Schilder, *Z. Anorg. Allg. Chem.* **2000**, *626*, 692-700.
[18] M. M. Bentlohner, W. Klein, Z. H. Fard, L.-A. Jantke, T. F. Fässler, *Angew. Chem. Int. Ed.* **2015**, *54*, 3748-3753.
[19] J. P. Hare, H. W. Kroto, R. Taylor, *Chem. Phys. Lett.* **1991**, *177*, 394-398.
[20] M. Klinger, C. Schenk, F. Henke, A. Clayborne, A. Schnepf, A.-N. Unterreiner, *Chem. Commun.* **2015**, *51*, 12278-12281.
[21] S. Frischhut, J. G. Machado de Carvalho, A. J. Karttunen, T. F. Fässler, *Z. Anorg. Allg. Chem.* **2018**, *644*, 1337-1343.
[22] S. Frischhut, M. M. Bentlohner, T. F. Fässler, *The Reaction of Ethylenediamine with 1,4-Bis(trimethylsilyl)butadiyne and the Role of Water: A Qualitative Method for the Determination of Water in Ethylenediamine*, *manuscript for publication*.
[23] W. W. Paudler, A. G. Zeiler, *J. Org. Chem.* **1969**, *34*, 999-1001.
[24] K. Fischer, *Angew. Chem.* **1935**, *48*, 394-396.
[25] A. Meyer, C. Boyd, *Anal. Chem.* **1959**, *31*, 215-219.
[26] M. Conceição, P. Lima, M. Spiro, *Anal. Chim. Acta* **1976**, *81*, 429-431.
[27] M. M. Bentlohner, S. Frischhut, T. F. Fässler, *Chem. Eur. J.* **2017**, *23*, 17089-17094.
[28] S. Frischhut, M. M. Bentlohner, W. Klein, T. F. Fässler, *Inorg. Chem.* **2017**, *56*, 10691-10698.

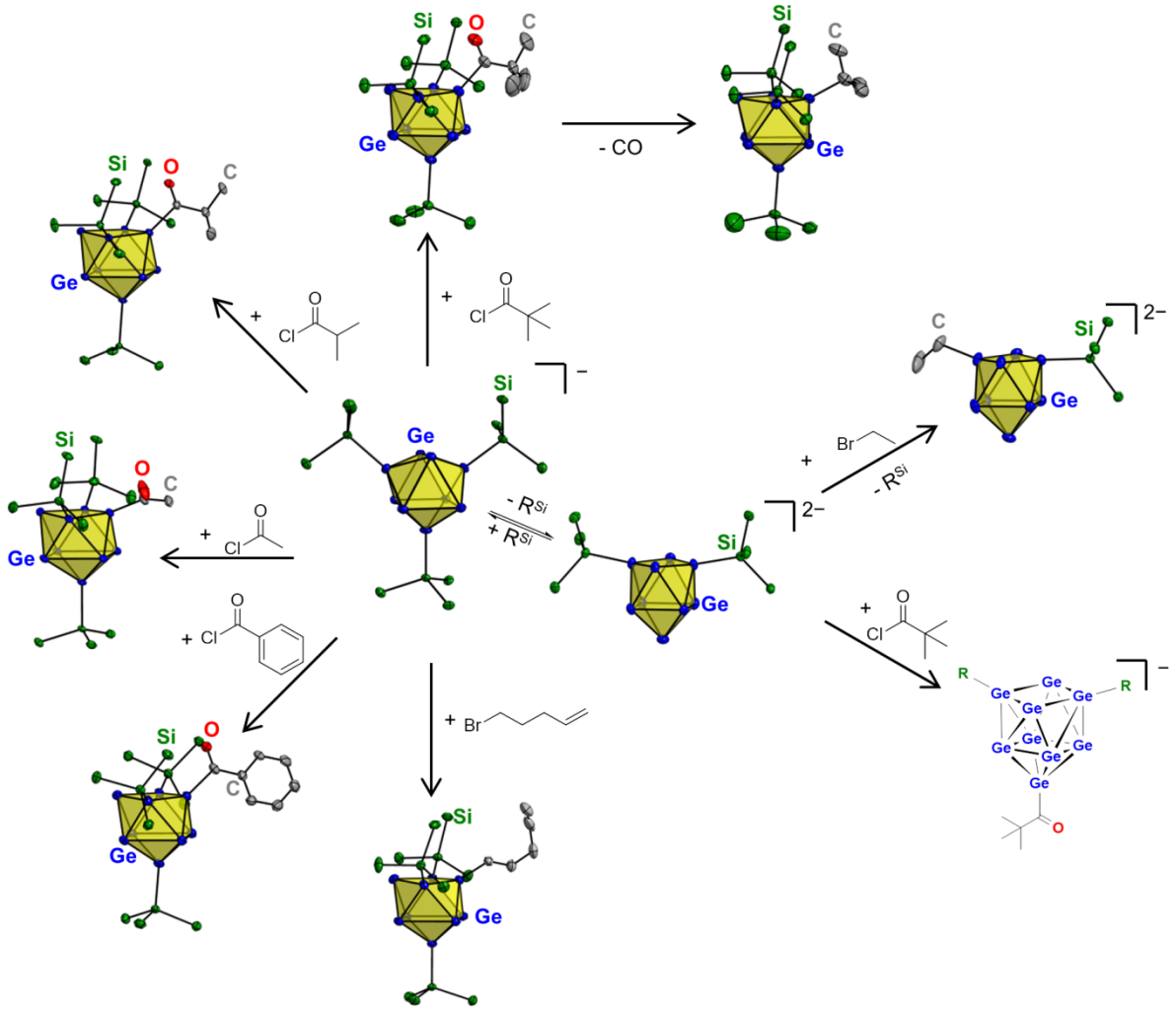

3.2 Organo-Functionalization of Silylated Ge_9 Clusters

3.2.1 Review of Relevant Literature

The comparatively highly charged Ge_9 cluster compounds, such as $[R{-}Ge_9{-}CH{=}CH{-}CH{=}CH{-}Ge_9{-}R]^{4-}$ (R = vinyl, (2*Z*,4*E*)-7-amino-5-azahepta-2,4-dien-2-yl) (**9a**/**9b**, **1a**),[1-2] as described in chapter 3.1 show only low solubility in less polar and more convenient solvents, and are therefore difficult to handle in solution for follow-up reactions. Also, reactions with K_4Ge_9 in liquid ammonia or *en* are often accompanied with redox-processes in solution, which often lead to multiple side-reactions and low yields of the desired product.[3]

A straightforward synthesis protocol to achieve specifically functionalized and at the same time easily soluble and at best neutral R_4Ge_9 clusters had not been developed prior to this work. Therefore these investigations are crucial for application of functionalized Ge_9 clusters in follow-up reactions, e.g. grafting on surfaces and polymerization reactions to build up higher cluster aggregates. Also, the generation of systems comprising intramolecular electronic communication between a specific functionality and the Ge_9 cluster is of great interest. Such properties are known for porphyrine-decorated fullerenes.[4]

In 2003, Schnepf discovered the threefold silylated cluster $[\{(Me_3Si)_3Si\}_3Ge_9]^-$ (**10a**) which he obtained from co-condensation of low-valent germanium halides.[5] This rather complicated bottom-up synthesis strategy was replaced by the easier "top-down" method by Sevov and coworkers where K_4Ge_9 was reacted with 3 equiv. of chloro-tris(trimethylsilyl)silane in thf or acetonitrile at r.t. in a heterogeneous reaction.[6] The Ge_9 cluster core of **10a** adapts D_{3h}-geometry. Applying only 2 equiv. of chloro-tris(trimethylsilyl)silane, the twofold silylated Ge_9 cluster $[\{(Me_3Si)_3Si\}_2Ge_9]^{2-}$ (**11a**) was achieved, which shows C_{2v}-symmetry. **10a** can be transferred into **11a** by adding additional K_4Ge_9 to an acetonitrile solution of $K[\{(Me_3Si)_3Si\}_3Ge_9]$ (**10**) (Scheme 3.2.1). This shows, that the silyl ligands can be abstracted in solution.[7] Remarkably, the mono-silylated cluster $[\{(Me_3Si)_3Si\}Ge_9]^{3-}$ has not been reported, yet.

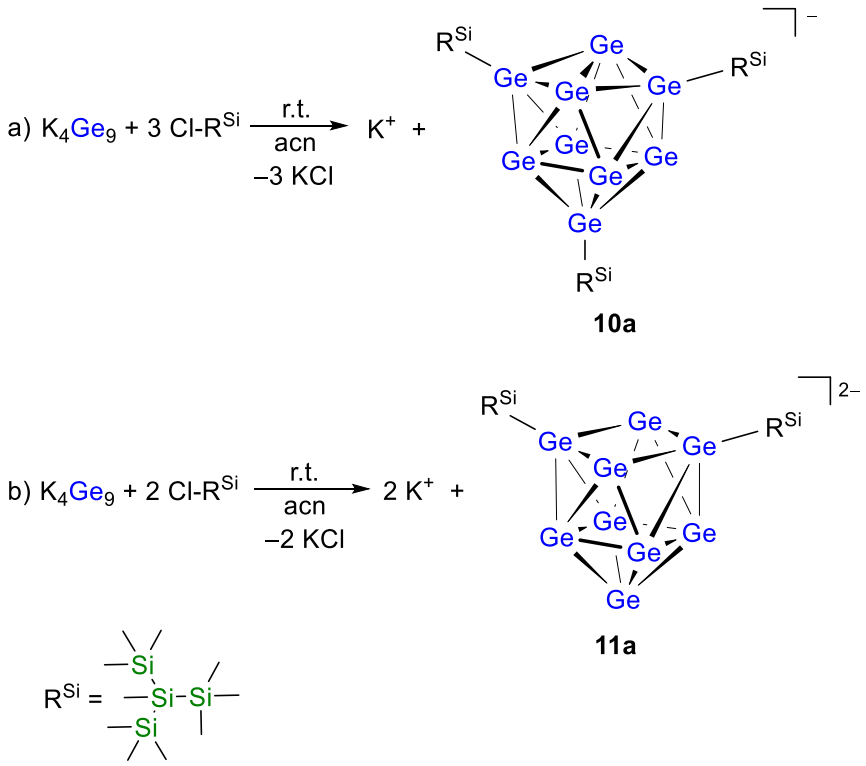

Scheme 3.2.1. Reaction of K_4Ge_9 with cloro-tris(trimethylsilyl)silane in acetonitrile yielding a) $K[\{(Me_3Si)_3Si\}_3Ge_9]$ (**10**) and b) $K_2[\{(Me_3Si)_3Si\}_2Ge_9]$ (**11**). R^{Si} depicts the tris(trimethylsilyl)silyl ligand.[6-7]

The syntheses of the two described silylated Ge_9 clusters $[\{(Me_3Si)_3Si\}_nGe_9]^{(4-n)-}$ (n = 2, 3) (**10a** and **11a**) opened completely new possibilities of functionalizing Ge_9 Zintl clusters. The silylation of $[Ge_9]^{4-}$ clusters is regarded as an outstanding option to, on the one hand transfer Ge_9 clusters into less polar solvents, such as thf, acetonitrile and optionally toluene, and on the other hand to stabilize them by steric shielding and by electronic effects. Therefore the silylated Ge_9 clusters have been applied as starting material for several follow-up reactions, especially in reactions with transition metal complexes or to attach phosphine ligands to the Ge_9 cluster core.[8-12]

The silyl ligands have been varied by replacement with sterically less demanding substituents.[13-16] $[(tBu_2HSi)_3Ge_9]^-$ turned out to contain the less sterically shielded Ge_9 cluster core.[15] Even the linkage of two $[\{(Me_3Si)_3Si\}_2Ge_9]^{2-}$ (**11a**) entities by a reaction with a chlorodisilane has been realized.[17] Specific functionalization by using silyl ligands equipped with organic tethers, which carry terminal double bonds, has been shown with $[\{(Me_3Si)_3Si\}_2\{Ph_2(CH_2{=}CH(CH_2)_3)Si\}Ge_9]^-$.[18] Nevertheless the cluster is still onefold

negatively charged, which can be a disadvantage in specific follow-up reactions, e.g. polymerization reactions.

The only neutral organo-substituted Ge_9 Zintl cluster known in literature had been the ethyl-decorated Ge_9 cluster $\{(Me_3Si)_3Si\}_3Ge_9CH_2CH_3$, however, without carrying a specific functionalization for follow-up reactions (Scheme 3.2.2).

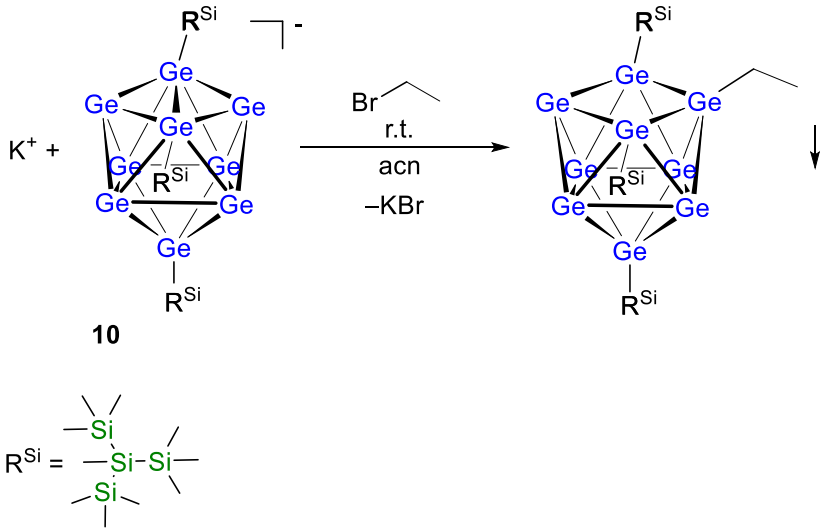

Scheme 3.2.2. Reaction of $K[\{(Me_3Si)_3Si\}_3Ge_9]$ (**10**) with bromo-ethane in acetonitrile yielding $\{(Me_3Si)_3Si\}_3Ge_9CH_2CH_3$. R^{Si} depicts the tris(trimethylsilyl)silyl ligand.[19]

Dynamic behavior has been observed for neutral, substituted Ge_9 cluster compounds. According to literature, this is traced back to the either labile-bound silyl groups which scramble around the cluster surface in one plane (Figure 3.2.1), or dynamic processes within the cluster core.[19-20]

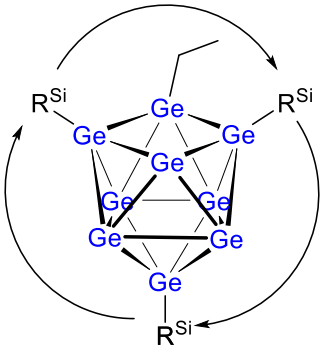

Figure 3.2.1. The Proposed dynamic processes by labile-bound silyl groups in the neutral compound $\{(Me_3Si)_3Si\}_3Ge_9CH_2CH_3$.[19]

3.2.2 Neutral Organo-Substituted Ge_9 Clusters – Reactions of $K[\{(Me_3Si)_3Si\}_3Ge_9]$ with Alkyl Bromides and Acyl Chlorides

see chapter 5.1

S. Frischhut, J. G. Machado de Carvalho, A. J. Karttunen, T. F. Fässler, *Z. Anorg. Allg. Chem.*, **2018**, *644*, 1337-1343.

see chapter 5.5

S. Frischhut, T. F. Fässler, *Dalton Trans.* **2018**, *47*, 3223-3226.

see chapter 5.6

S. Frischhut, W. Klein, M. Drees, T. F. Fässler, *Chem. Eur. J.* **2018**, *24*, 9009-9014.

As has already been stated in chapter 3.2.1, the only organo-substituted neutral Ge_9 cluster, prior to this work, had been given by $\{(Me_3Si)_3Si\}_3Ge_9CH_2CH_3$, which was synthesized by a nucleophilic substitution reaction of $K[\{(Me_3Si)_3Si\}_3Ge_9]$ with bromo-ethane in acetonitrile.[19]

Further transferability of the reaction of $K[\{(Me_3Si)_3Si\}_3Ge_9]$ (**10**) with various alkyl bromides was investigated within this work. Reaction conditions had to be optimized for each applied alkyl bromide. However, new compounds, such as $\{(Me_3Si)_3Si\}_3Ge_9(CH_2)_2CH_3$ (**12**) and $\{(Me_3Si)_3Si\}_3Ge_9(CH_2)_3Ph$ (**13**) emerged by reaction of **10** with the respective alkyl bromides bromo-propane and 1-bromo-3-phenylpropane in acetonitrile at r.t. (Figure 3.2.2).[21]

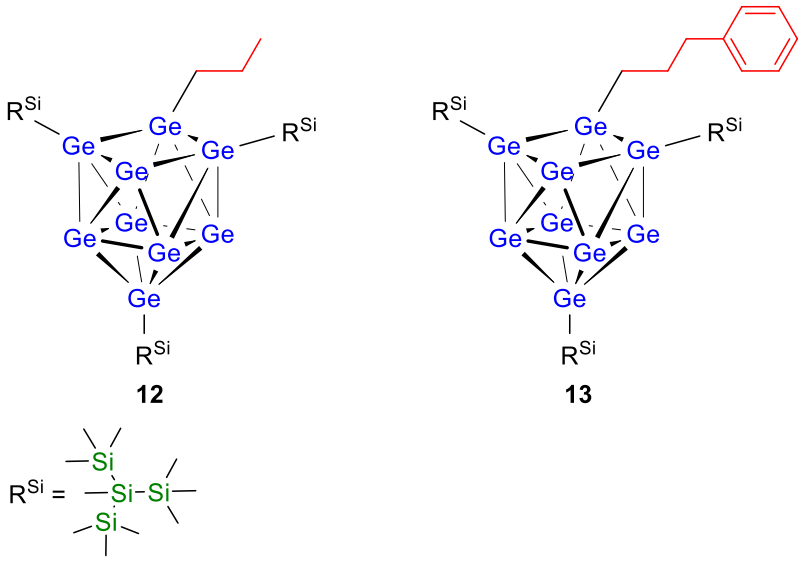

Figure 3.2.2. The proposed structures of $\{(Me_3Si)_3Si\}_3Ge_9(CH_2)_2CH_3$ (**12**) and $\{(Me_3Si)_3Si\}_3Ge_9(CH_2)_3Ph$ (**13**). Ge vertices – blue, organic functionality – red. R^{Si} depicts the tris(trimethylsilyl)silyl ligands attached to the Ge_9 cluster.[21]

12 was synthesized analytically pure, whereas **13** shows besides the expected sharp signals in the ^1H NMR spectrum also broad signals which hint at the formation of radicals. Both compounds, **12** and **13**, carry an organic moiety, which however, can hardly be involved in follow-up reactions due to the lack of highly reactive organic functionalities.

Terminal double bonds are, in principle, accessible for a wide range of organic reactions, e.g. Diels-Alder,[22] catalytic polymerization,[23-24] catalyzed hydrosilylation[25] and many others. Therefore, the alkenyl-substituted compounds $\{(Me_3Si)_3Si\}_3Ge_9(CH_2)_nCH{=}CH_2$ (n = 1, 2, 3) (**14**-**16**) were synthesized according to a modified synthesis protocol of $\{(Me_3Si)_3Si\}_3Ge_9CH_2CH_3$ which implied the nucleophilic substitution reaction of $K[\{(Me_3Si)_3Si\}_3Ge_9]$ (**10**) with the respective alkyl halides, allyl bromide, 4-bromo-1-butene and 5-bromo-1-pentene, in acetonitrile (Scheme 3.2.3).[21, 26]

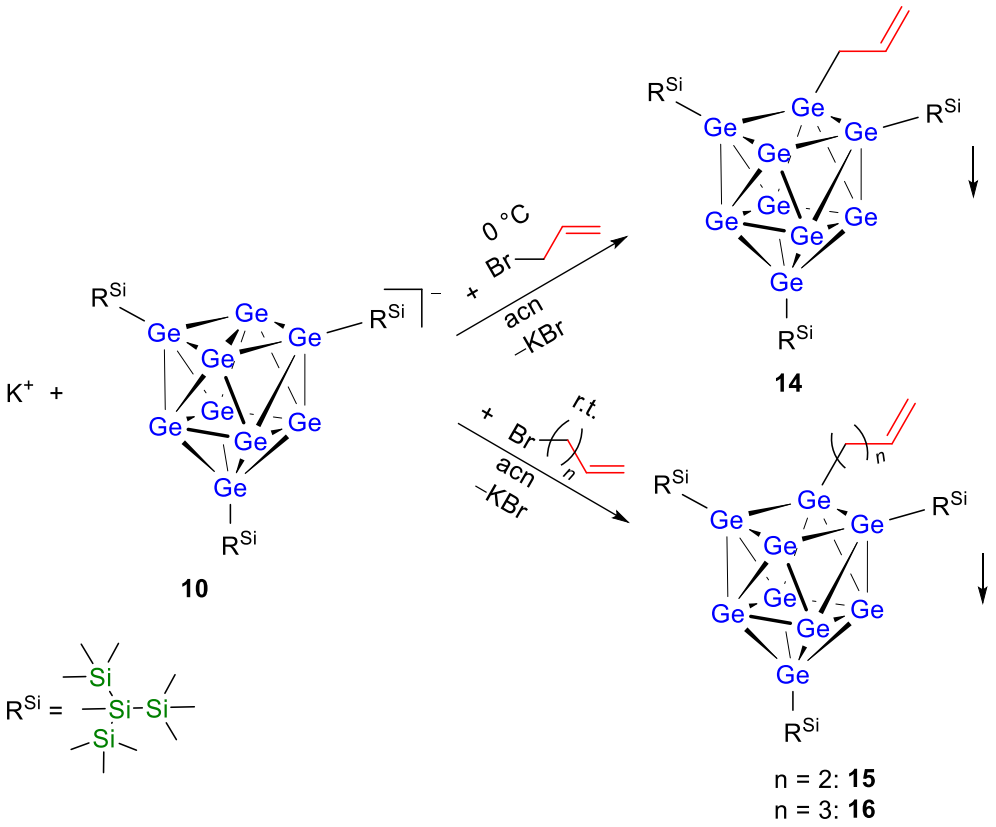

Scheme 3.2.3. Reaction of K[{(Me$_3$Si)$_3$Si}$_3$Ge$_9$] (**10**) with allyl bromide, 4-bromo-1-butene and 5-bromo-1-pentene yielding [{(Me$_3$Si)$_3$Si}$_3$Ge$_9$CH$_2$CH=CH$_2$ (**14**), [{(Me$_3$Si)$_3$Si}$_3$Ge$_9$(CH$_2$)$_2$CH=CH$_2$ (**15**) and [{(Me$_3$Si)$_3$Si}$_3$Ge$_9$(CH$_2$)$_3$CH=CH$_2$ (**16**), respectively. R^{Si} depicts the tris(trimethylsilyl)silyl ligands attached to the Ge$_9$ cluster. Ge vertices – blue, organic functionality – red.[21, 26]

Due to the high reactivity of allyl bromide towards **10**, **14** is only accessible by reaction of 2 equiv. of allyl bromide with **10** at 0 °C. In contrast, **15** and **16** are accessible by reaction of 5 equiv. of 4-bromo-1-butene and 5-bromo-1-pentene with **10** at r.t., respectively.

Compared to **14**, which could not be obtained in crystalline form due to the instability of the compound in solution, **16** forms orange block-shaped crystals from toluene-solutions at −32 °C in a comparatively good yield of 50%. The structure of **16** is shown in Figure 3.2.3.[26]

Reactions of alkyl bromides with K[{(Me$_3$Si)$_3$Si}$_3$Ge$_9$] (**10**) turned out to be hardly transferable to a wide range of alkyl bromides as reaction conditions had to be adjusted for every single alkyl bromide which was applied. ^{1}H NMR spectroscopic studies often revealed broad signals, which most likely resulted from formed radical species.

Therefore, an easier and more controllable synthesis strategy for specific organo-functionalized neutral Ge$_9$ clusters was sought for. Especially, the easily accessible acyl

chlorides, which are well-known in the organic chemistry,[27] in principle, offer a good opportunity to transfer functionalities to a nucleophile, such as the Ge_9 cluster **10**.

The reaction of $K[\{(Me_3Si)_3Si\}_3Ge_9]$ (**10**) with pivaloyl chloride in hexane at 0 °C lead to the formation of $\{(Me_3Si)_3Si\}_3Ge_9(CO)tBu$ (**17**), which, upon warming to r.t., releases CO to form $\{(Me_3Si)_3Si\}_3Ge_9tBu$ (**18**). This synthesis proceeds *via* an addition-elimination mechanism followed by a decarbonylation reaction (Scheme 3.2.4).[28]

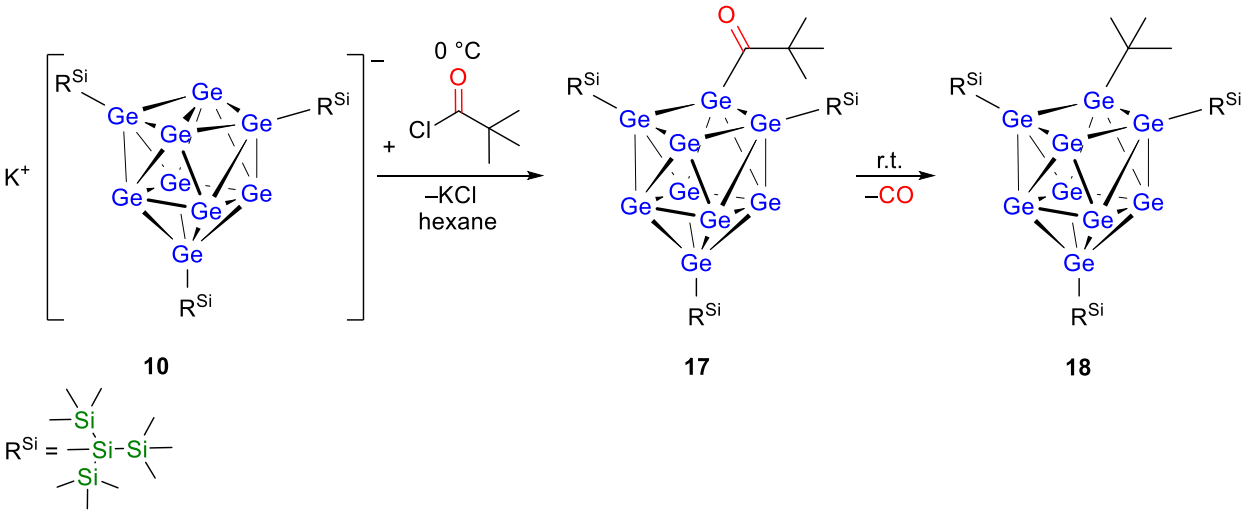

Scheme 3.2.4. Reaction of $K[\{(Me_3Si)_3Si\}_3Ge_9]$ (**10**) with pivaloyl chloride yielding $\{(Me_3Si)_3Si\}_3Ge_9(CO)tBu$ (**17**). Subsequent decarbonylation yields $\{(Me_3Si)_3Si\}_3Ge_9tBu$ (**18**). Ge vertices – blue, CO fragment – red. R^{Si} depicts the tris(trimethylsilyl)silyl ligands attached to the Ge_9 cluster. The scheme was modified on the basis of ref. [28].

Both compounds, **17** and **18**, were crystallized and characterized by single crystal X-ray diffraction.

To further investigate the reaction mechanism of the decarbonylation reaction, quantum chemical calculations were performed. Scheme 3.2.5 shows three conceivable reaction pathways, which include a radical Norrish type I α-bond cleavage, as known for ketones,[29] and a concerted reaction mechanism.

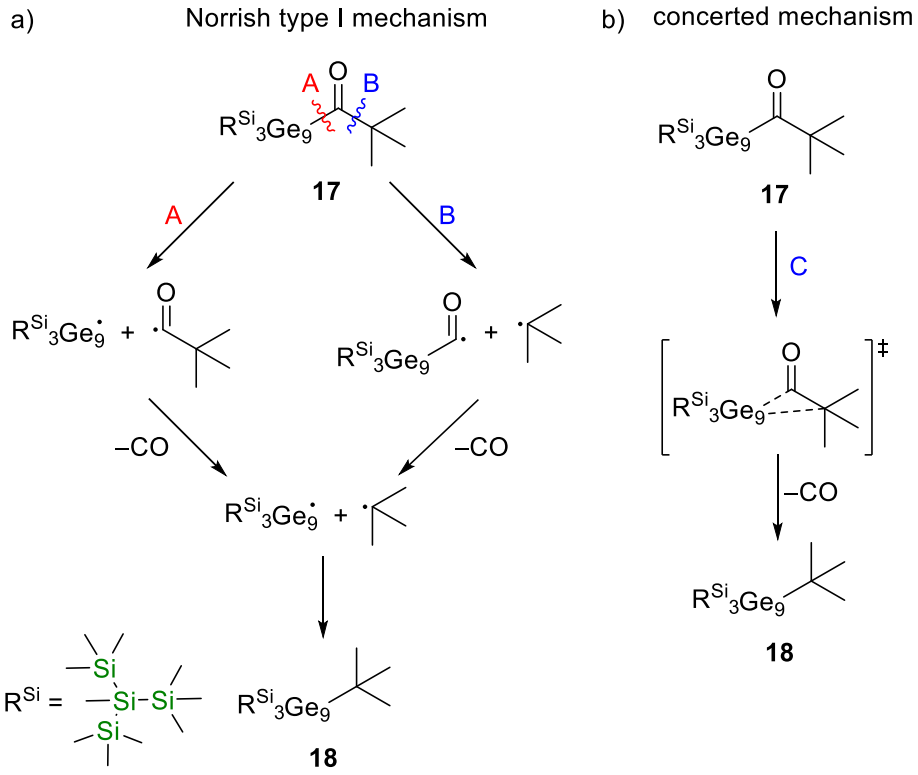

Scheme 3.2.5. Three possible reaction pathways of the conversion of $\{(Me_3Si)_3Si\}_3Ge_9(CO)tBu$ (**17**) to $\{(Me_3Si)_3Si\}_3Ge_9tBu$ (**18**) a) following a Norrish type I mechanism, implying a radical α-bond cleavage (pathway A and B) and b) running through a concerted transition state (pathway C). R^{Si} depicts the tris(trimethylsilyl)silyl ligands attached to the Ge_9 cluster. The scheme was modified on the basis of ref. [28].

According to the performed DFT calculations the decarbonylation mechanism of **17** most likely runs through pathway A (Scheme 3.2.5). Thereby an activation barrier of 40.3 kJ/mol is required to form $\{(Me_3Si)_3Si\}_3Ge_9\cdot$ and $\cdot(CO)tBu$ in the first step. $\cdot(CO)tBu$ is known to readily release CO forming $\cdot tBu$,[30] which again can recombine with $\{(Me_3Si)_3Si\}_3Ge_9\cdot$ yielding **18**.

To further probe the scope of the presented reaction type, the acylation of **10** was further conducted with different acyl chlorides R'(CO)Cl (R' = Me, *i*Pr, Ph, Bz, cyclopropylmethyl, phenethyl, 4-vinylphenyl). In all cases, except for R' = Bz, the carbonyl products $\{(Me_3Si)_3Si\}_3Ge_9(CO)Me$ (**19**), $\{(Me_3Si)_3Si\}_3Ge_9(CO)iPr$ (**20**), $\{(Me_3Si)_3Si\}_3Ge_9(CO)Ph$ (**21**), $\{(Me_3Si)_3Si\}_3Ge_9(CO)CH_2C_3H_5$ (**22**), $\{(Me_3Si)_3Si\}_3Ge_9(CO)(CH_2)_2Ph$ (**23**) and $\{(Me_3Si)_3Si\}_3Ge_9(CO)C_6H_4CH{=}CH_2$ (**24**) were obtained, which was unequivocally shown by single crystal X-ray diffraction (for **19**-**21**, Figure 3.2.3) and in addition by (temperature-dependent) NMR spectroscopy (**19**-**24**). Most likely in case of R' = Bz decarbonylation occurs but does not expectedly lead to $\{(Me_3Si)_3Si\}_3Ge_9CH_2C_6H_5$, instead, decomposition of the products is observed.

Notably, cyclopropylacetyl chloride is known as radical clock. Once the cyclopropylcarbinyl radical is formed, it immediately reacts further to the homoallylcarbinyl radical with a rate constant of $1.2 \cdot 10^8$ s^{-1} at 25 °C.[31] In our case, only the cyclopropylacetyl derivative **22** was obtained, which leads to the assumption that the Ge−(CO) bond remains intact in solution, wherefore a release of CO does not occur.[28]

The following Figure 3.2.3 shows the molecular structures of all crystallized neutral organo-functionalized Ge_9 clusters.

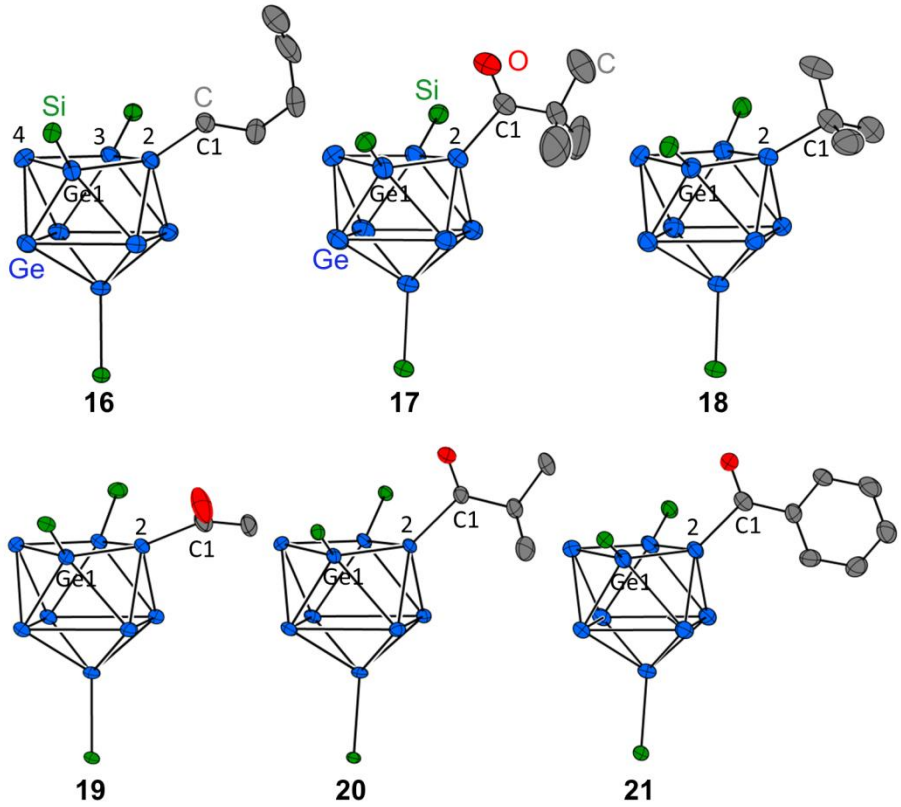

Figure 3.2.3. Molecular structures of compounds **16** and **17**-**21**. All hydrogen atoms as well as the trimethylsilyl groups on the silyl ligands are omitted for clarity. All ellipsoids are shown at a probability level of 50%. Ge – blue, Si – green, C – grey, O – red.[26, 28]

The crystal structures of **16** and **17**-**21** revealed C_S-symmetric cluster cores in the shape of mono-capped square-antiprisms. Each organo-functionalized cluster carries three silyl ligands and an organic moiety attached to Ge2, being part of the open square (Ge1-Ge2-Ge3-Ge4) (Figure 3.2.3). The Ge2−C1 bond distance of 1.970(3) Å in **16** is indicative of a 2-center-2-electron Ge−C(sp^3) bond.[1, 32-33] In comparison, the respective bond lengths of 2.054(9) Å in **17**, 2.05(1) Å in **18**, 2.036(9) Å in **19**, 2.058(6) Å in **20** and 2.047(5) Å in **21** are slightly elongated. The binding of the fourth substituent leads to lowering in the symmetry

of the cluster cores compared to K[{(Me$_3$Si)$_3$Si}$_3$Ge$_9$] (**10**) (D_{3h}) and results in a compression of the bond lengths of Ge1−Ge2 and Ge2−Ge3, which are adjacent to the organo-substituted Ge2 atom, compared to the oppositely positioned bonds Ge1−Ge4 and Ge3−Ge4 [**16**: d(Ge1−Ge2) = 2.4472(4) Å and d(Ge2−Ge3) = 2.4532(4) Å], compared to d(Ge1−Ge4) = 2.5901(4) Å and d(Ge3−Ge4) = 2.6034(4) Å].[26, 28] The geometries of the cluster cores are similar to those observed for other neutral organo-functionalized Ge$_9$ clusters.[19] The distance between the two sp^2-atoms C4 and C5 of **16** is 1.322(7) Å and lies in the typical range of C=C double bonds.[34] The crystal structure of **16** shows an easily accessible double bond, which hints at further possible follow-up reactions.[26]

All obtained neutral organo-functionalized Ge$_9$ cluster compounds show dynamic behavior in [D$_8$]toluene-solutions at r.t., which was revealed by temperature-dependent ^{1}H NMR spectroscopy.[26, 28] This had already been observed for other neutral Ge$_9$ clusters.[19] The following Table 3.2.1 compares the coalescence temperatures and the calculated free activation energies for rotation (ΔG) of selected neutral alkylated and acylated Ge$_9$ cluster compounds.

Table 3.2.1. Coalescence temperatures (T_C) and calculated free activation energies for rotation (ΔG) of the alkylated Ge$_9$ compounds [{(Me$_3$Si)$_3$Si}$_3$Ge$_9$(CH$_2$)$_2$CH$_3$ (**12**), [{(Me$_3$Si)$_3$Si}$_3$Ge$_9$CH$_2$CH=CH$_2$ (**14**), [{(Me$_3$Si)$_3$Si}$_3$Ge$_9$(CH$_2$)$_3$CH=CH$_2$ (**16**), and {(Me$_3$Si)$_3$Si}$_3$Ge$_9$*t*Bu (**18**), as well as of the acylated compounds {(Me$_3$Si)$_3$Si}$_3$Ge$_9$(CO)*t*Bu (**17**), {(Me$_3$Si)$_3$Si}$_3$Ge$_9$(CO)Me (**19**), {(Me$_3$Si)$_3$Si}$_3$Ge$_9$(CO)*i*Pr (**20**), {(Me$_3$Si)$_3$Si}$_3$Ge$_9$(CO)Ph (**21**), {(Me$_3$Si)$_3$Si}$_3$Ge$_9$(CO)CH$_2$C$_3$H$_5$ (**22**) and {(Me$_3$Si)$_3$Si}$_3$Ge$_9$(CO)C$_6$H$_4$CH=CH$_2$ (**24**) in [D$_8$]toluene.[21, 26, 28]

compound	**12**	**14**	**16**	**18**	**17**	**19**	**20**	**21**	**22**	**24**
T_C [K]	273	258	273	286	218	218	203	233	213	243
ΔG [kJ/mol]	57.5	55.4	58.1	56.9	46.4	46.5	43.1	48.8	46.4	50.6

The values of ΔG for neutral alkylated Ge$_9$ clusters (**12**, **14**, **16**, **18**) are higher than those for the acylated ones (**17**, **19**-**22**, **24**), concluding that the latter are more dynamic in solution.

Especially compounds **16** and **24** represent promising candidates for application in follow-up reactions, such as polymerization. All in all, the well-investigated and well-understood acylation reaction towards organo-functionalized Ge$_9$ clusters provides access to so far unexplored interesting candidates for specific applications due to the transferability to a wide range of acyl chlorides.

In addition, a few selected substituted Ge_9 clusters were UV-Vis spectroscopically investigated. The UV-Vis electronic spectra of $[K(18\text{-c-}6)]_2[(H_2C{=}CH)_2Ge_9]$ (**25**), [K(2,2,2-crypt)][{$(Me_3Si)_3Si$}$_3Ge_9$] (**10**), {$(Me_3Si)_3Si$}$_3Ge_9CH_2CH_3$ (**26**), {$(Me_3Si)_3Si$}$_3Ge_9(CH_2)_2CH_3$ (**12**), {$(Me_3Si)_3Si$}$_3Ge_9(CH_2)_3CH{=}CH_2$ (**16**) and [{$(Me_3Si)_3Si$}$_3Ge_9CH_2CH_3$]$Pt(PPh_3)$ (**27**) appear to be very similar. They all show one very strong absorption band in the range of 203 to 221 nm and a weaker absorption in the region of 250 to 290 nm. Compared to $[K(2,2,2\text{-crypt})]_2[Ge_9]$ (**3**), weak bands in the region of 490 to 630 nm were not observed, concluding that an agglomeration of the clusters does not occur for substituted Ge_9 clusters at higher concentrations.[21]

3.2.3 Charged Organo-Substituted Ge_9 Clusters – Reactions of $K_2[\{(Me_3Si)_3Si\}_2Ge_9]$ with bromoethane and acyl chlorides

see chapter 5.7 — S. Frischhut, W. Klein, T. F. Fässler, *C. R. Chim.* **2018**, *21*, 932-937.

see chapter 5.8 — S. Frischhut, K. Frankiewicz, T. F. Fässler, *manuscript for publication*.

Besides $K[\{(Me_3Si)_3Si\}_3Ge_9]$ (**10**), $K_2[\{(Me_3Si)_3Si\}_2Ge_9]$ (**11**), in principle, provides two reactive sites for organo-functionalization, which makes this starting material an interesting candidate.

Therefore, $K_2[\{(Me_3Si)_3Si\}_2Ge_9]$ (**11**) was reacted with 1 equiv. of bromo-ethane in acetone yielding $[\{(Me_3Si)_3Si\}_2Ge_9CH_2CH_3]^-$ (**28a**). The latter was characterized by NMR spectroscopy and ESI mass spectrometry (Figure 3.2.4).

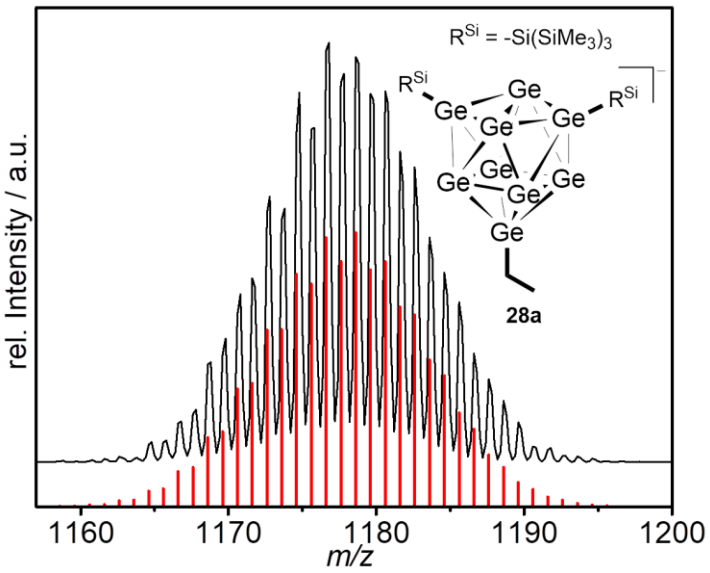

Figure 3.2.4. ESI mass spectrum of $[\{(Me_3Si)_3Si\}_2Ge_9CH_2CH_3]^-$ (**28a**) in black and calculated pattern as bar graph in red below. A proposed structure of **28a** is given in the figure. R^{Si} depicts the tris(trimethylsilyl)silyl ligands attached to the Ge_9 cluster. The figure was modified on the basis of ref. [35].

Crystallization of **28a** failed. However, the addition of 2,2,2-crypt to an acetone-solution of **28a** lead to the abstraction of one silyl ligand resulting in the crystallization of $[K(2,2,2\text{-crypt})]_2[\{(Me_3Si)_3Si\}Ge_9CH_2CH_3]$ (**29**) (Scheme 3.2.6), which was shown by single crystal X-ray

diffraction of the obtained red-brown needle-shaped crystals after storage at −32 °C (8% yield).

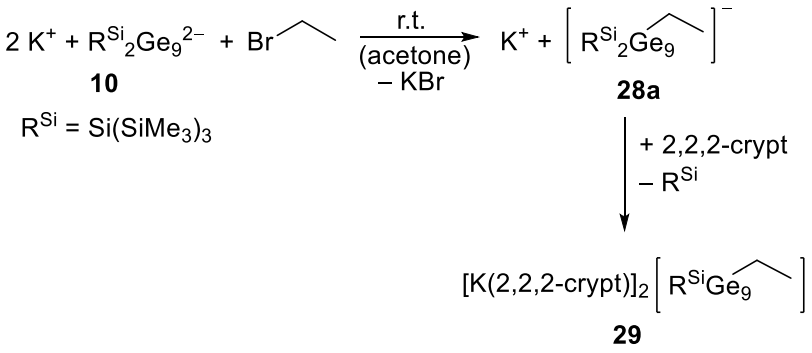

Scheme 3.2.6. Reaction of $K_2[\{(Me_3Si)_3Si\}_2Ge_9]$ (**10**) with bromo-ethane in acetone yielding $[\{(Me_3Si)_3Si\}_2Ge_9CH_2CH_3]^-$ (**28a**). Addition of 2,2,2-crypt yields $[K(2,2,2\text{-crypt})]_2[\{(Me_3Si)_3Si\}Ge_9CH_2CH_3]$ (**29**). R^{Si} depicts the tris(trimethylsilyl)silyl ligands attached to the Ge_9 cluster. The scheme was modified on the basis of ref. [35].

The structure of the anion $[\{(Me_3Si)_3Si\}Ge_9CH_2CH_3]^{2-}$ (**29a**) is depicted in Figure 3.2.5 and contains a C_{2v} symmetric Ge_9 cluster core, which is typical of twofold substituted Ge_9 clusters.[36-37]

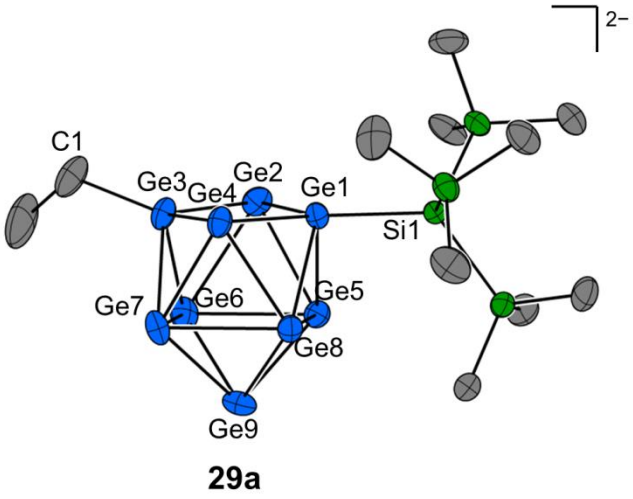

Figure 3.2.5. The molecular structure of $[\{(Me_3Si)_3Si\}Ge_9CH_2CH_3]^{2-}$ (**29a**). Ge – blue, Si – green, C – grey. The figure was modified on the basis of ref. [35].

The bonds adjacent to the substituted Ge atoms Ge1 and Ge3 at the open square appear compressed, compared to the bonds forming the capped square. The Ge1-Si1 distance of 2.423(2) Å is elongated compared to the structures of $[\{(Me_3Si)_3Si\}_2Ge_9]^{2-}$ (**11a**) [d(Ge−Si) = 2.4097(9) and 2.4071(9) Å][7] and $[\{(Me_3Si)_3Si\}_3Ge_9]^-$ (**10a**) [d(Ge−Si) = 2.363(2)–2.369(1) Å][6]. Remarkably, the Ge1−Si1 bond does not as usual point radially away from the

cluster core, but lies in the plane Ge1-Ge2-Ge3-Ge4. Regarding the desilylation reaction in case of **28a**, interesting new structures might emerge, containing several different functionalities attached to one core.[35]

Besides the attachment of a simple ethyl functionality to the cluster $[\{(Me_3Si)_3Si\}_2Ge_9]^{2-}$ (**11a**), the decoration with different acyl moieties was achieved within this thesis. As was the case for organo-functionalization of **10a**, the functionalization of **11a** appeared to be also more straight-forward with acyl chlorides compared to alkyl bromides. The reaction of **11a** with pivaloyl chloride, benzoyl chloride, phenylacetyl chloride, hydrocinnamoyl chloride, 9-anthracenoyl chloride and ferrocenoyl chloride in thf or acetone at r.t. afforded $[\{(Me_3Si)_3Si\}_2Ge_9(CO)R']^-$ (R' = *t*Bu, Ph, CH_2Ph, $(CH_2)_2Ph$, 9-anthracenyl, Fc) (**30a**-**35a**), respectively (Scheme 3.2.7).

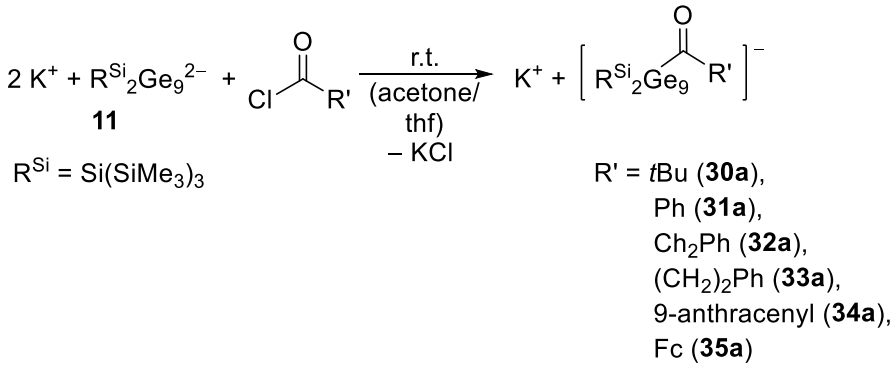

Scheme 3.2.7. Reaction of $K_2[\{(Me_3Si)_3Si\}_2Ge_9]$ (**11**) with Cl(CO)R' in acetone or thf at r.t. yielding $[\{(Me_3Si)_3Si\}_2Ge_9(CO)R']^-$ (R' = *t*Bu, Ph, CH_2Ph, $(CH_2)_2Ph$, 9-anthracenyl, Fc) (**30a**-**35a**).

Desilylation upon addition of 2,2,2-crypt was not observed. Remarkably, decarbonylation of $[\{(Me_3Si)_3Si\}_2Ge_9(CO)tBu]^-$ (**30a**) in solution, as occurred in the case of $[\{(Me_3Si)_3Si\}_3Ge_9(CO)tBu]$ (**17**), did not take place even at elevated temperatures (Scheme 3.2.8).

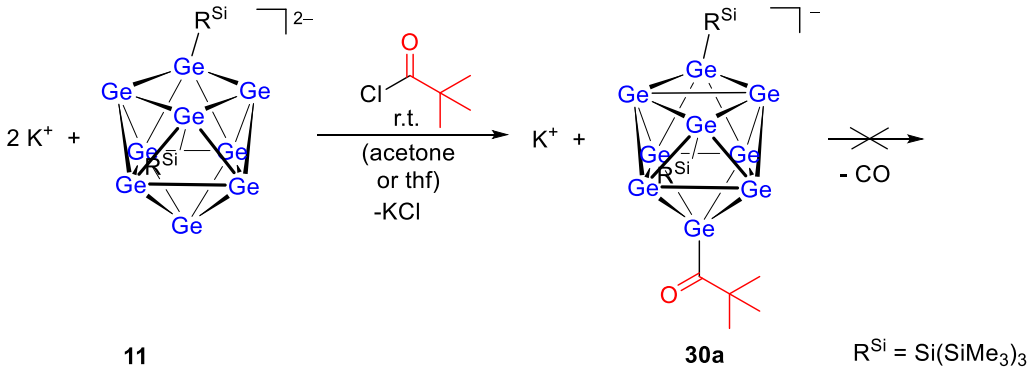

Scheme 3.2.8. Reaction of $K_2[\{(Me_3Si)_3Si\}_2Ge_9]$ (**11**) with pivaloyl chloride yielding $[\{(Me_3Si)_3Si\}_2Ge_9(CO)R']^-$ (**30a**).

The anions **30a**-**35a** were characterized by ESI mass spectrometry (Figure 3.2.6), as well as by NMR spectroscopy. Crystallization of the anions **30a**-**35a** failed.[38]

As a conclusion, the reaction of **11** with acyl chlorides again shows an easy straight-forward approach towards targeted functionalization of Ge_9 cluster compounds, which allows for the synthesis of a wide range of charged specifically functionalized Ge_9 cluster compounds.

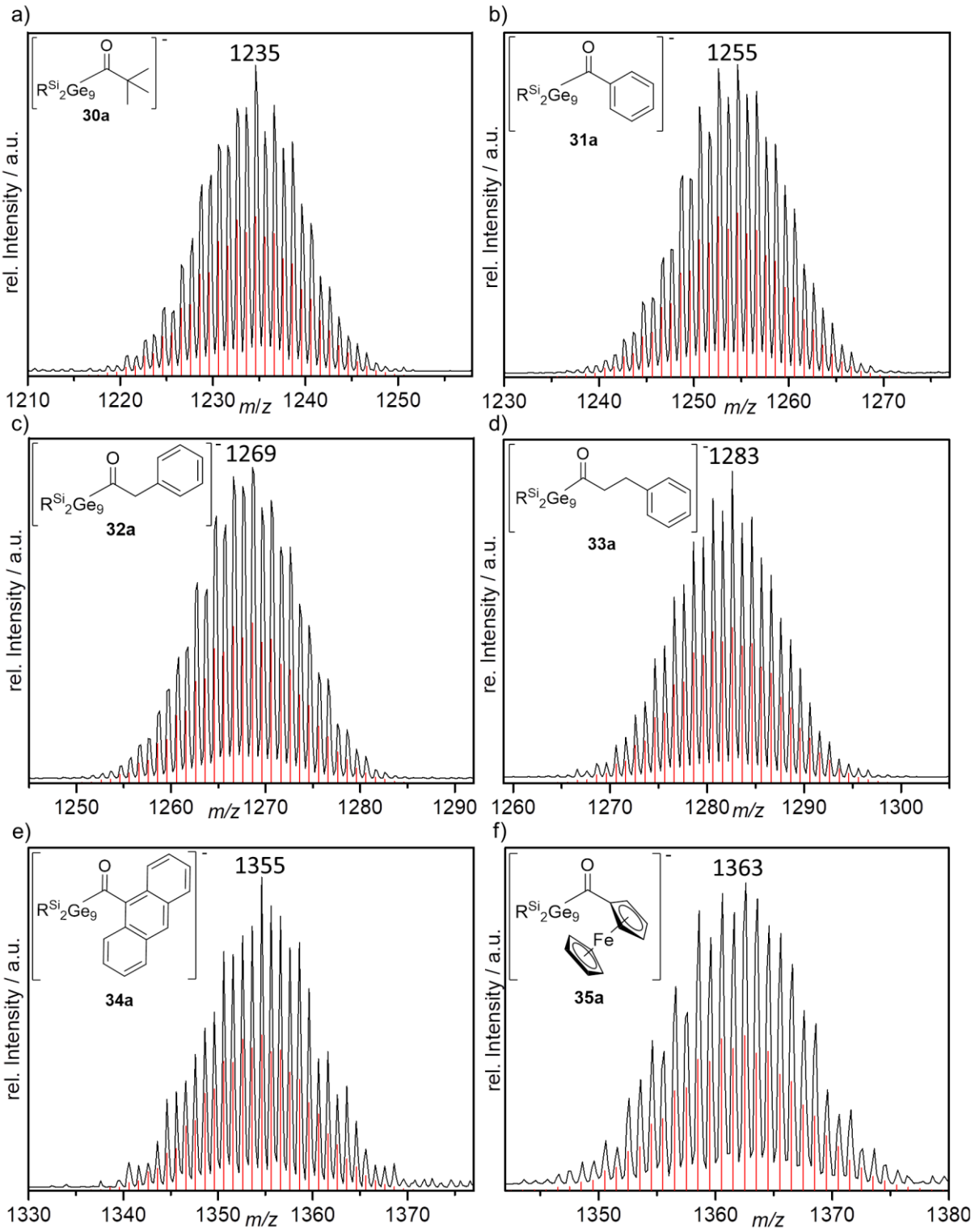

Figure 3.2.6. ESI mass spectra of the anions **30a**-**35a** recorded in thf-solutions in the negative ion mode (a – f). The measured spectra are shown in black and the corresponding simulated patterns are shown as bar graphs below. R^{Si} represents the tris(trimethylsilyl)silyl ligands.

3.2.4 References

[1] M. M. Bentlohner, W. Klein, Z. H. Fard, L.-A. Jantke, T. F. Fässler, *Angew. Chem. Int. Ed.* **2015**, *54*, 3748-3753.

[2] S. Frischhut, M. M. Bentlohner, W. Klein, T. F. Fässler, *Inorg. Chem.* **2017**, *56*, 10691-10698.

[3] S. C. Sevov, J. M. Goicoechea, *Organometallics* **2006**, *25*, 5678-5692.

[4] D. M. Guldi, *Chem. Soc. Rev.* **2002**, *31*, 22-36.

[5] A. Schnepf, *Angew. Chem.* **2003**, *115*, 2728-2729.

[6] F. Li, S. C. Sevov, *Inorg. Chem.* **2012**, *51*, 2706-2708.

[7] O. Kysliak, A. Schnepf, *Dalton Trans.* **2016**, *45*, 2404-2408.

[8] F. Henke, C. Schenk, A. Schnepf, *Dalton Trans.* **2009**, 9141-9145.

[9] C. Schenk, F. Henke, G. Santiso-Quiñones, I. Krossing, A. Schnepf, *Dalton Trans.* **2008**, 4436-4441.

[10] C. Schenk, A. Schnepf, *Angew. Chem. Int. Ed.* **2007**, *46*, 5314-5316.

[11] F. S. Geitner, J. V. Dums, T. F. Fässler, *J. Am. Chem. Soc.* **2017**, *139*, 11933-11940.

[12] F. Geitner, C. Wallach, T. F. Fässler, *Chem. Eur. J.* **2018**, *24*, 4103-4110.

[13] K. Mayer, L. J. Schiegerl, T. F. Fässler, *Chem. Eur. J.* **2016**, *22*, 18794-18800.

[14] L. J. Schiegerl, F. S. Geitner, C. Fischer, W. Klein, T. F. Fässler, *Z. Anorg. Allg. Chem.* **2016**, *642*, 1419-1426.

[15] O. Kysliak, T. Kunz, A. Schnepf, *Eur. J. Inorg. Chem.* **2017**, *4*, 805-810.

[16] O. Kysliak, C. Schrenk, A. Schnepf, *Inorg. Chem.* **2015**, *54*, 7083-7088.

[17] O. Kysliak, C. Schrenk, A. Schnepf, *Inorg. Chem.* **2017**, *56*, 9693-9697.

[18] K. Mayer, L. J. Schiegerl, T. Kratky, S. Günther, T. F. Fässler, *Chem. Commun.* **2017**, *53*, 11798-11801.

[19] F. Li, S. C. Sevov, *J. Am. Chem. Soc.* **2014**, *136*, 12056-12063.

[20] F. Li, A. Muñoz-Castro, S. C. Sevov, *Angew. Chem. Int. Ed.* **2016**, *55*, 8630-8633.

[21] S. Frischhut, J. G. Machado de Carvalho, A. J. Karttunen, T. F. Fässler, *Z. Anorg. Allg. Chem.* **2018**, *644*, 1337-1343.

[22] H. Holmes, *The Diels-Alder Reaction Ethylenic and Acetylenic Dienophiles*, Wiley Online Library, **1948**.

[23] W. Kaminsky, M. Arndt, *Polymer Synthesis/Polymer Catalysis*, Springer, **1997**, pp. 143-187.

[24] W. Kaminsky, *J. Chem. Soc., Dalton Trans.* **1998**, 1413-1418.

[25] B. Marciniec, *Hydrosilylation: A Comprehensive Review on Recent Advances, Vol. 1*, Springer Science & Business Media, **2008**.

[26] S. Frischhut, T. F. Fässler, *Dalton Trans.* **2018**, *47*, 3223-3226.

[27] N. O. Sonntag, *Chem. Rev.* **1953**, *52*, 237-416.

[28] S. Frischhut, W. Klein, M. Drees, T. F. Fässler, *Chem. Eur. J.* **2018**, *24*, 9009-9014.

[29] W. M. Horspool, P.-S. Song, *CRC Handbook of Organic Photochemistry and Photobiology, Vol. 1*, CRC press, Boca Raton, **1995**.

[30] C. Chatgilialoglu, D. Crich, M. Komatsu, I. Ryu, *Chem. Rev.* **1999**, *99*, 1991-2070.

[31] V. W. Bowry, J. Lusztyk, K. Ingold, *J. Am. Chem. Soc.* **1991**, *113*, 5687-5698.

[32] M. W. Hull, A. Ugrinov, I. Petrov, S. C. Sevov, *Inorg. Chem.* **2007**, *46*, 2704-2708.

[33] M. W. Hull, S. C. Sevov, *J. Am. Chem. Soc.* **2009**, *131*, 9026-9037.

[34] E. V. Anslyn, D. A. Dougherty, *Modern Physical Organic Chemistry*, University Science, Sausalito, CA, **2006**.

[35] S. Frischhut, W. Klein, T. F. Fässler, *C. R. Chim.* **2018**, *21*, 932-937.

[36] C. B. Benda, H. He, W. Klein, M. Somer, T. F. Fässler, *Z. Anorg. Allg. Chem.* **2015**, *641*, 1080-1086.

[37] M. W. Hull, S. C. Sevov, *Inorg. Chem.* **2007**, *46*, 10953-10955.

[38] S. Frischhut, K. Frankiewicz, T. F. Fässler, *Acyl-Functionalized Deltahedral Ge_9 Clusters - [{$(Me_3Si)_3Si$}$_2Ge_9(CO)R']^-$ (R' = tBu, Ph, CH_2Ph, $(CH_2)_2Ph$, 9-anthracenyl, Fc)*, *Manuscript for publication*.

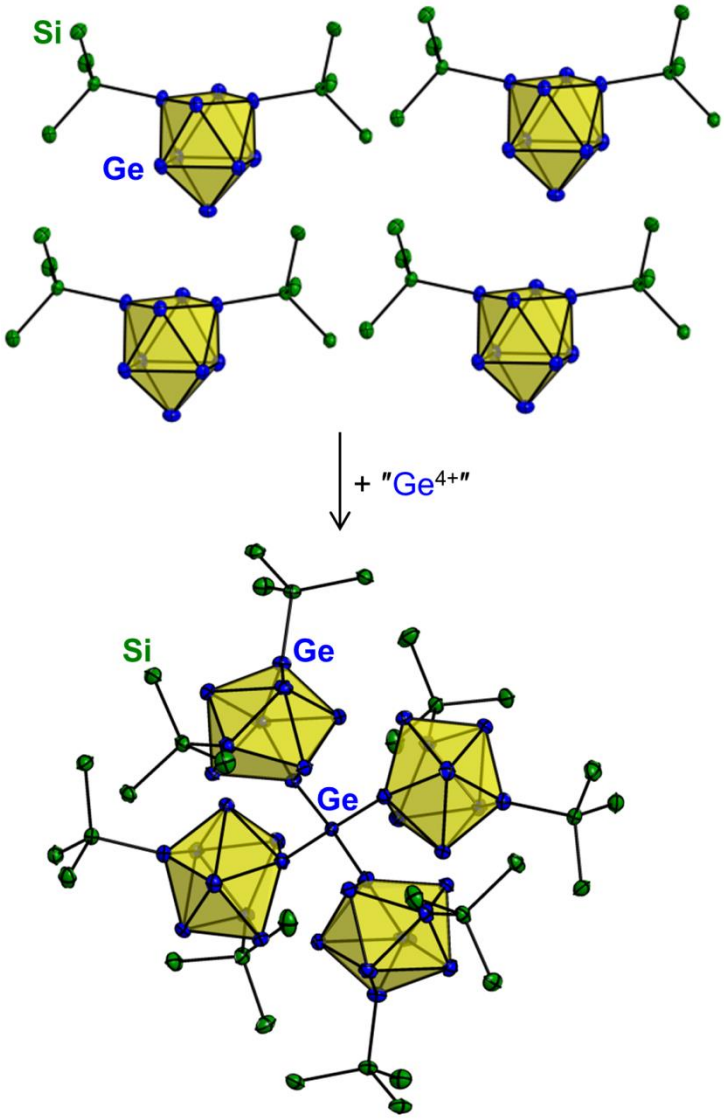

3.3 Interconnection of Ge_9 Clusters for Potential Three-Dimensional Cluster Networks

3.3.1 Review of Relevant Literature

3.3.1.1 Interconnection of Deltahedral Ge_9 Zintl Clusters

Already in the early stage of the investigations on the reactivity of $[Ge_9]^{4-}$ Zintl clusters in solution, the first interconnected deltahedral Ge_9 clusters were reported, namely the dimer $[Ge_9{-}Ge_9]^{6-}$,[1-3] trimer $[Ge_9{=}Ge_9{=}Ge_9]^{6-}$,[4] tetramer $[Ge_9{=}Ge_9{=}Ge_9{=}Ge_9]^{8-}$ [5] and polymer $^{1}_{\infty}[Ge_9]^{2-}$[6-7] (Figure 3.3.1). These anions are products obtained from oxidative coupling of $[Ge_9]^{4-}$ Zintl clusters. They consist of 1D cables, where the clusters are interconnected by one or two covalent bonds. Remarkably, in an acetonitrile-solution of $[Ge_9]^{2-}$, agglomeration according to 3 $[Ge_9]^{2-} \rightleftharpoons [Ge_9{=}Ge_9{=}Ge_9]^{6-}$ occurs at higher concentrations.[8]

2D or even 3D linkage of bare deltahedral Ge_9 clusters had not been reported, yet, however, would open up outstanding new possibilities of creating novel porous frameworks, which might exhibit interesting electronic properties.

Further covalent linkage of Ge_9 clusters is shown in the fullerene triad analogous Zintl triads $[Ge_9{-}CH{=}CH{-}CH{=}CH{-}Ge_9]^{6-}$[9] (Figure 3.3.1) and $[RGe_9{-}CH{=}CH{-}CH{=}CH{-}Ge_9R]^{4-}$ (R = (2*Z*,4*E*)-7-amino-5-azahepta-2,4,dien-2-yl, vinyl)[10-11], where two Ge_9 clusters are covalently linked by a conjugated organic bridge (Figure 3.3.1). The anions bear an extended conjugated π-electronic system, where the electrons are delocalized throughout the whole anion. 2D and 3D linkage applying respective organic linkers, which allow for such connectivities, has not been successful to date.

The covalent interconnection of four Ge_9 clusters by Ge bridges was realized in the complex anionic structure of $[Au_3Ge_{45}]^{9-}$ (Figure 3.3.1). The Ge_9 clusters were partly oxidized in the reaction of K_4Ge_9 with $[AuCl(PPh_3)]$ in ethylenediamine.[12]

A different type of Ge_9 cluster linkage was shown by coordination of Ge_9 clusters to late transition metals. Prominent examples are given by $^{1}_{\infty}[Ge_9Hg]^{2-}$,[13-14] $[Ge_9Zn{-}Ge_9{-}ZnGe_9]^{8-}$[15] and $^{1}_{\infty}[Ge_9Zn]^{2-}$[15].

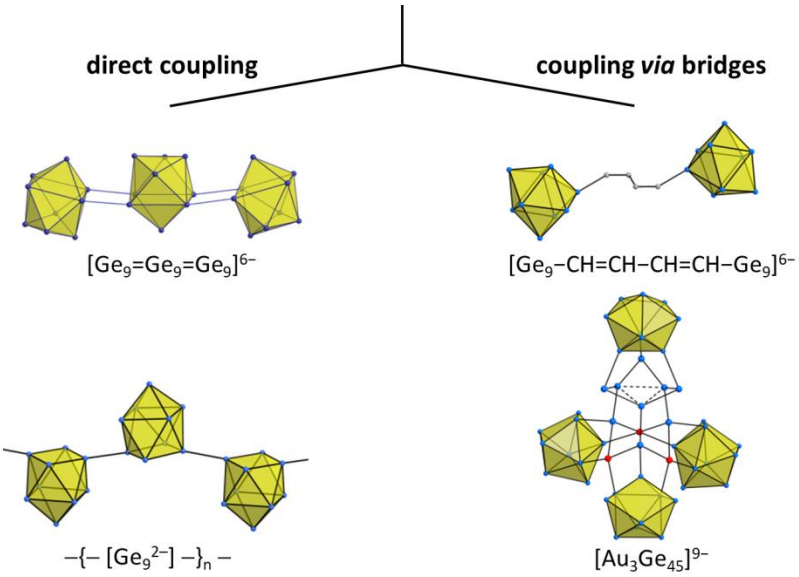

Figure 3.3.1. Comparison of the state-of-the-art linked Ge_9 structures containing interconnected deltahedral Ge_9 clusters.

Since the discovery of the silylated Ge_9 clusters, more covalently and coordinatively linked Ge_9 cluster species emerged, e.g. $[\{(Me_3Si)_3Si\}_2Ge_9{-}SiMe_2{-}C_6H_4{-}Me_2Si{-}Ge_9\{Si(SiMe_3)_3\}_2]^{2-}$[16] and $[\{(Me_3Si)_3Si\}_3Ge_9MGe_9\{(Me_3Si)_3Si\}_3]^{n-}$ ($n = 1$, M = Cu, Ag, Au; $n = 0$, M = Mn, Zn, Cd, Hg)[17-19], respectively.

Additional theoretical studies revealed the potential accessibility of 2D linkage of $[Ge_9]^{4-}$ analogous $[Si_9]^{4-}$ clusters *via* a central sp^3 hybridized Si atom leading to the chessboard network $^2_\infty\{[Si_9]Si_2\}_n$ (Figure 3.3.2 a). Cutting out a unit of four interconnected Si_9 clusters, $[(Si_9)_4Si]^{12-}$ is obtained, which is shown in Figure 3.3.2 b.[20] Experimentally, the realization of such interconnections under retention of the clusters has still remained a challenge.

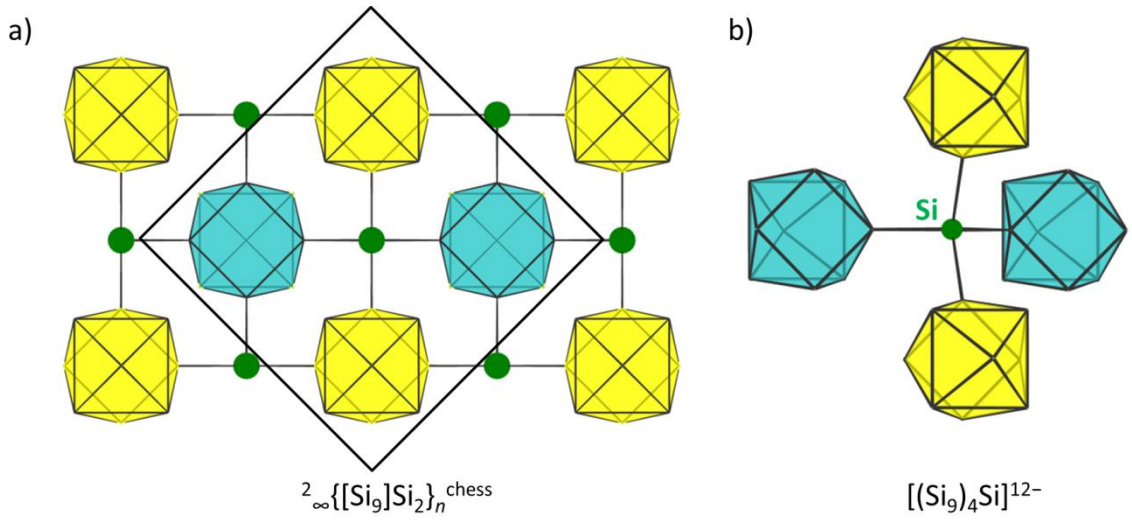

Figure 3.3.2. Calculated structures of a) the 2D chessboard network $^2_\infty\{[Si_9]Si_2\}_n$ and b) $[(Si_9)_4Si]^{12-}$. The two different colors of the polyhedra show different orientations. [20]

3.3.1.2 From Deltahedral Ge_9 Zintl Clusters to Nanostructured Materials

In principle, deltahedral $[Ge_9]^{4-}$ clusters serve as ideal candidates to create porous high-surface structures. According to Muñoz-Castro *et al.*, especially the well-investigated Zintl anion $[\{(Me_3Si)_3Si\}_3Ge_9]^-$ (**10a**) has the potential to serve as building block to form honeycomb-like 2D structures with well-defined pores.[21]

A few approaches towards Ge-based nanostructured high-surface materials have been made, making use of deltahedral Ge_9 Zintl clusters. Oxidative self-polymerization of Ge_9 cages lead to mesoporous Ge structures, with tunable electronic properties.[22] In addition, inverse opal structured layers for application in semiconductor devices has been reported, which were made from $[Ge_9]^{4-}$ clusters, treated with $GeCl_4$ resulting in a-Ge-based structures.[23-24]

3.3.2 Three-Dimensional Linkage of Ge_9 Clusters *via* a Central Ge(IV) Atom

see chapter 5.9

S. Frischhut, P. Jutzi, T. F. Fässler, **2018**, *manuscript for publication*.

3D linkage of deltahedral Ge_9 clusters is of great interest for the potential generation of nanostructured frameworks as had already been reported in theoretical studies.[20, 25] A synthetic approach towards such materials, which might exhibit outstanding electronic properties, had not been reported prior to this work.

The reaction of $K_2[\{(Me_3Si)_3Si\}_2Ge_9]$ (**11**) with $[SiCp^*][B(C_6F_5)_4]$ in the presence of $[Li(OEt_2)_x][B(C_6F_5)_4]$ in fluorobenzene reproducibly, however unexpectedly, yielded $K_4[\{(Me_3Si)_3Si\}_2Ge_9]_4Ge$ (**36**) as block-shaped, deep-brown crystals in low yields after crystallization at −32 °C. **36** was characterized by single crystal X-ray structure analysis and by temperature-dependent ^1H NMR spectroscopy.

The crystal structure of **36** contains four potassium cations, which is consistent with a fourfold negatively charged entity $[[\{(Me_3Si)_3Si\}_2Ge_9]_4Ge]^{4-}$ (**36a**). It exhibits four interconnected disilylated Ge_9 clusters *via* a central Ge atom. Each cluster bears one negative charge (Figure 3.3.3 a). The clusters adopt C_{2v}-symmetry, which is rather unusual for threefold substituted Ge_9 clusters. The clusters are arranged around the central Ge atom in the shape of a distorted tetrahedron. The four potassium cations, which are placed in the interspaces between the clusters, are coordinated by three clusters in a η^1-, η^2- and η^4-fashion, each. The potassium cations themselves also form a distorted tetrahedron which interpenetrates with the tetrahedron framed by the $Ge_{cluster}$ atoms (Ge2, Ge11, Ge20, Ge29) directly connected to the central Ge1 atom (Figure 3.3.3 b).

An *in situ* oxidation of Ge_9 clusters to Ge(IV) is reported by this example. So far, cluster fragmentation accompanied with partial oxidation of the Ge_9 cluster has been observed in $[Ge_{10}]^{2-}$ [26] and $[Au_3Ge_{45}]^{9-}$ [12].

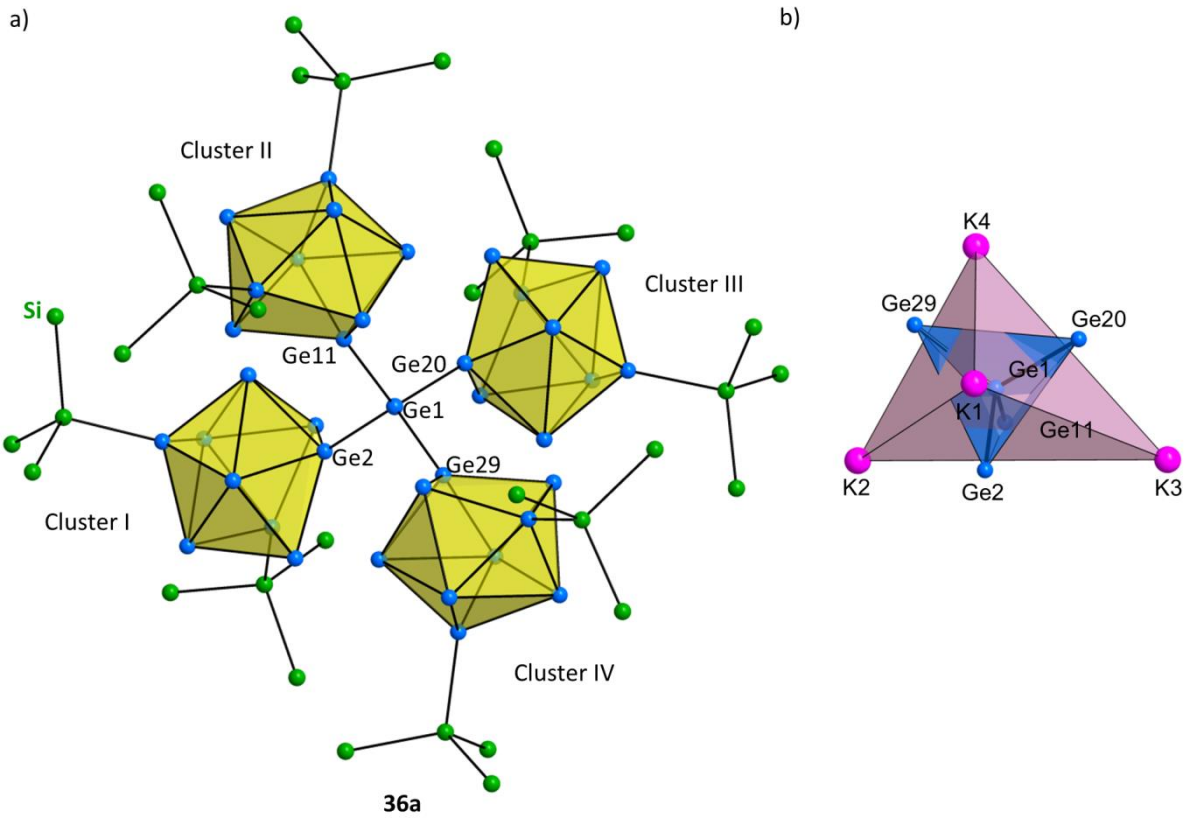

Figure 3.3.3. a) Molecular structure of $[[\{(Me_3Si)_3Si\}_2Ge_9]_4Ge]^{4-}$ (**36a**). The Ge_9 clusters are shown as yellow polyhedra. The methyl groups of the silyl ligands are omitted for clarity. b) Interpenetrating tetrahedrons formed by the coordinated potassium cations (depicted in purple) and the germanium atoms bound to the central Ge1(IV) (depicted in blue). Ge – blue, Si – green, K – purple.

Temperature-dependent ^{1}H NMR studies revealed that **36** does not show dynamic behavior in solution. Only one singlet is observed in the ^{1}H NMR spectrum, which is unexpected due to the magnetically independent silyl ligands attached to the Ge_9 core.

The 3D linked Ge_9 clusters in **36a** still bear a negative charge. Therefore, **36a** might serve as building block in follow-up substitution reactions to generate highly porous structures consisting of Ge_9 clusters.[27] **36a** shows a to $[(Si_9)_4Si]^{12-}$ similar structure, however bears different orientations of the interconnected clusters (Figure 3.3.4). **36** represents a further approach towards the already predicted Ge analogous 2D chessboard structure $^2_\infty\{[Ge_9]Ge_2\}_n$ presented in Figure 3.3.2 a.

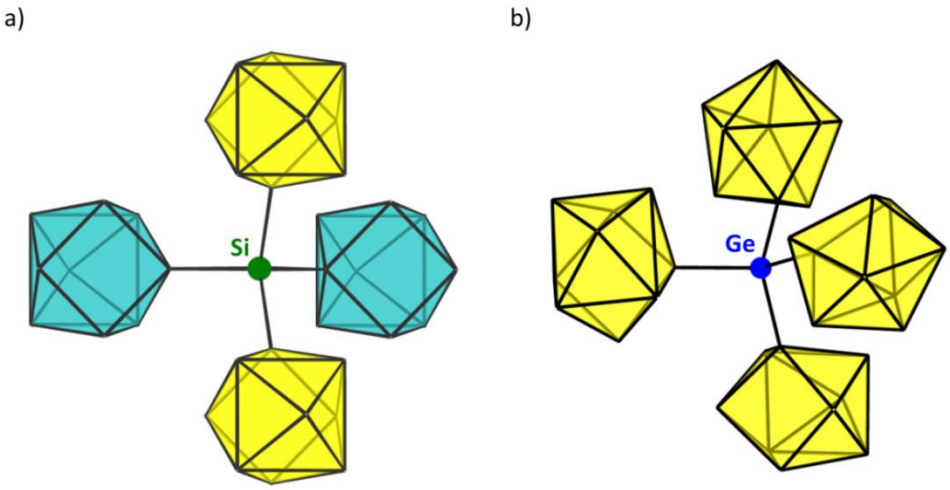

Figure 3.3.4. Schematic comparison of interconnected clusters in a) predicted $[(Si_9)_4Si]^{12-}$[20] and b) $[[\{(Me_3Si)_3Si\}_2Ge_9]_4Ge]^{4-}$ (**36a**). The silyl ligands are omitted for clarity.

3.3.3 References

[1] L. Xu, S. C. Sevov, *J. Am. Chem. Soc.* **1999**, *121*, 9245-9246.

[2] R. Hauptmann, T. F. Faessler, *Z. Anorg. Allg. Chem.* **2003**, *629*, 2266-2273.

[3] A. Nienhaus, S. D. Hoffmann, T. F. Fässler, *Z. Anorg. Allg. Chem.* **2006**, *632*, 1752-1758.

[4] A. Ugrinov, S. C. Sevov, *J. Am. Chem. Soc.* **2002**, *124*, 10990-10991.

[5] A. Ugrinov, S. C. Sevov, *Inorg. Chem.* **2003**, *42*, 5789-5791.

[6] C. Downie, Z. Tang, A. M. Guloy, *Angew. Chem. Int. Ed.* **2000**, *39*, 337-340.

[7] C. Downie, J.-G. Mao, H. Parmar, A. M. Guloy, *Inorg. Chem.* **2004**, *43*, 1992-1997.

[8] S. Frischhut, J. G. Machado de Carvalho, A. J. Karttunen, T. F. Fässler, *Z. Anorg. Allg. Chem.* **2018**, *644*, 1337-1343.

[9] M. M. Bentlohner, S. Frischhut, T. F. Fässler, *Chem. Eur. J.* **2017**, *23*, 17089-17094.

[10] M. M. Bentlohner, W. Klein, Z. H. Fard, L.-A. Jantke, T. F. Fässler, *Angew. Chem. Int. Ed.* **2015**, *54*, 3748-3753.

[11] S. Frischhut, M. M. Bentlohner, W. Klein, T. F. Fässler, *Inorg. Chem.* **2017**, *56*, 10691-10698.

[12] A. Spiekermann, S. D. Hoffmann, T. F. Fässler, I. Krossing, U. Preiss, *Angew. Chem. Int. Ed.* **2007**, *46*, 5310-5313.

[13] A. Nienhaus, R. Hauptmann, T. F. Fässler, *Angew. Chem. Int. Ed.* **2002**, *41*, 3213-3215.

[14] M. B. Boeddinghaus, S. D. Hoffmann, T. F. Fässler, *Z. Anorg. Allg. Chem.* **2007**, *633*, 2338-2341.

[15] K. Mayer, L-A. Jantke, S. Schulz, T. F. Fässler, *Angew. Chem. Int. Ed.* **2017**, *56*, 2350-2355.

[16] O. Kysliak, C. Schrenk, A. Schnepf, *Inorg. Chem.* **2017**, *56*, 9693-9697.

[17] C. Schenk, F. Henke, G. Santiso-Quiñones, I. Krossing, A. Schnepf, *Dalton Trans.* **2008**, 4436-4441.

[18] O. Kysliak, C. Schrenk, A. Schnepf, *Chem. Eur. J.* **2016**, *22*, 18787-18793.

[19] F. Henke, C. Schenk, A. Schnepf, *Dalton Trans.* **2009**, 9141-9145.

[20] L.-A. Jantke, T. F. Fässler, *Inorganics* **2018**, *6*, 31.

[21] A. Muñoz-Castro, K. Takahashi, *J. Phys. Chem. C* **2017**, *121*, 1934-1940.

[22] G. S. Armatas, M. G. Kanatzidis, *Adv. Mater.* **2008**, *20*, 546-550.

[23] M. M. Bentlohner, M. Waibel, P. Zeller, K. Sarkar, P. Müller-Buschbaum, D. Fattakhova-Rohlfing, T. F. Fässler, *Angew. Chem. Int. Ed.* **2016**, *55*, 2441-2445.

[24] S. Geier, R. Jung, K. Peters, H. A. Gasteiger, D. Fattakhova-Rohlfing, T. F. Fässler, *Sustainable Energy Fuels* **2018**, *2*, 85-90.

[25] A. J. Karttunen, T. F. Fässler, M. Linnolahti, T. A. Pakkanen, *ChemPhysChem* **2010**, *11*, 1944-1950.

[26] M. M. Bentlohner, C. Fischer, T. F. Fässler, *Chem. Commun.* **2016**, *52*, 9841-9843.

[27] S. Frischhut, P. Jutzi, T. F. Fässler, Three-dimensional Covalent Linkage of Four Deltahedral Ge_9 Clusters *via* a Central sp^3 Hybridized Ge Atom: Synthesis and Crystal Structure of $K_4[\{Me_3Si)_3Si\}_2Ge_9]_4Ge$, *Manuscript for publication*.

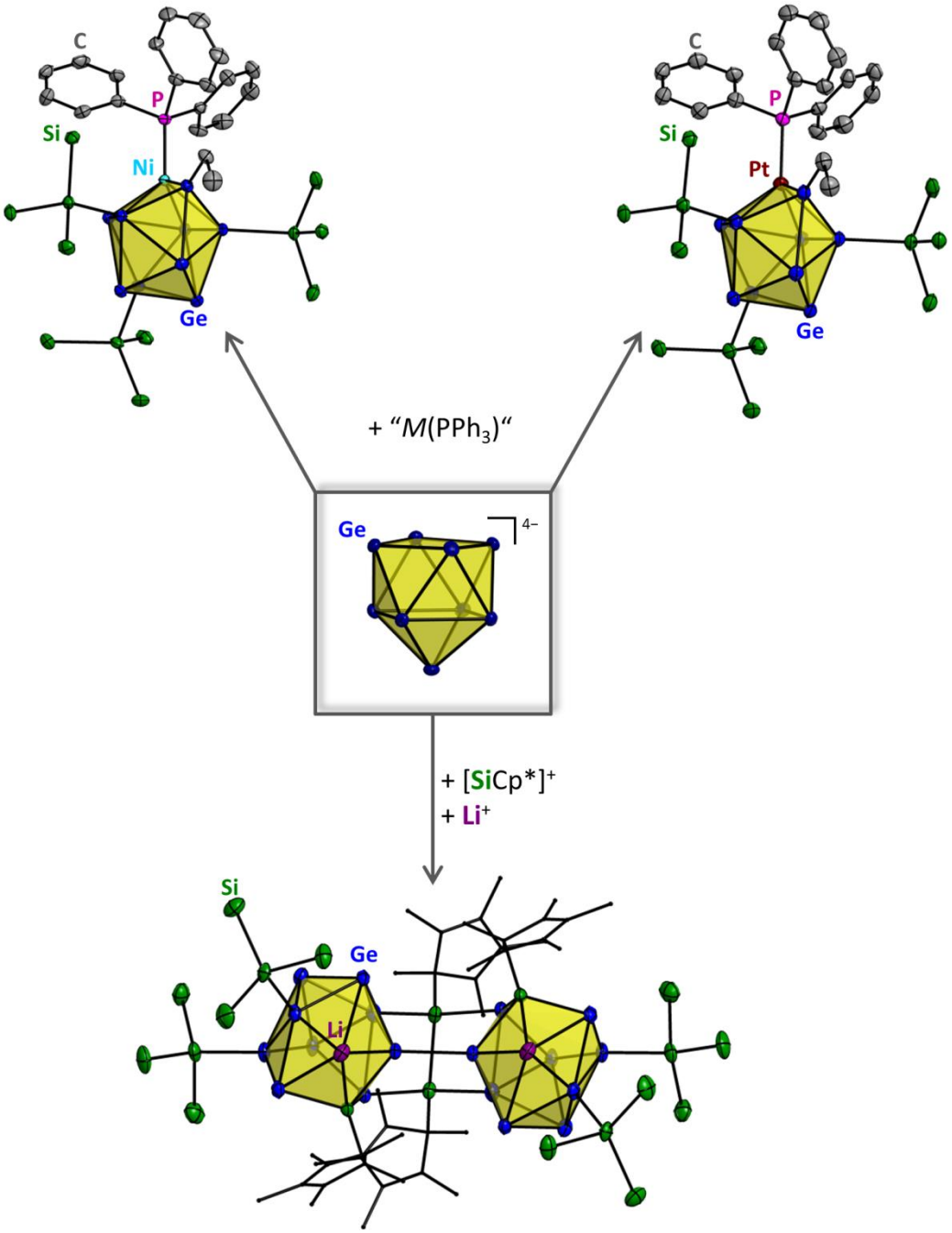

3.4 Ge_9 Cluster Expansion

3.4.1 Review of Relevant Literature

3.4.1.1 Bottom-up Synthesis of Siliconoids

Clusters are fascinating constructs, reflecting the transitional region between molecular chemistry and bulk material, and thus, provide deeper insight into the relation between structural and electronic changes. Clusters exhibit outstanding electronic properties and therefore attract great interest. The possibility of specifically doping clusters with a distinct number of vertices, as well as the presence of a maximum number of hemispheroidal vertices is a remaining challenge in cluster chemistry research.

There are two different major approaches to achieve such cluster structures in solution, on the one hand, the bottom-up synthesis of metalloid clusters utilizing low-valent metal atoms[1-2], and on the other hand the extraction of Zintl clusters from solid state Zintl phases.[3-4]

The first method has been preliminary applied for the synthesis of silicon clusters bearing at least one hemispheroidal vertex, the so-called siliconoids, implying the utilization of low-valent silicon compounds, which have progressively emerged in recent decades and gave access to several siliconoids, heteronuclear siliconoids as well as negatively charged siliconoids (Figure 3.4.1).[2]

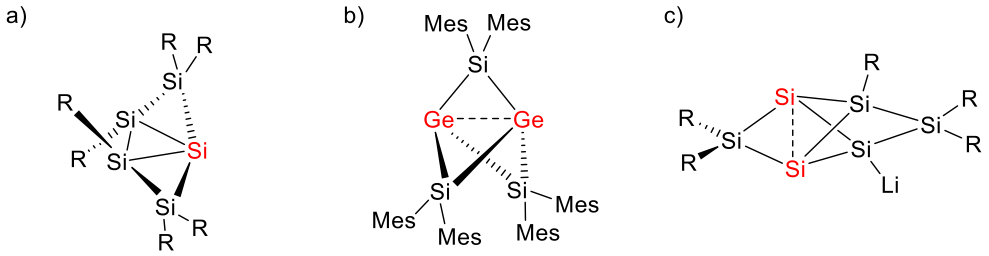

Figure 3.4.1. Structure of a) the first siliconoid;[5] b) a heteronuclear siliconoid;[6] c) anionic siliconoid.[7] Hemispheroidal atoms are marked in red.

The prediction of the cluster structure is rather impossible, but they predominantly show overall propellane-like structures.[2] Also, the number of "naked" vertices is often unforeseen. Such syntheses are comparatively complex and require several steps.

As a special remark, the salt [SiCp*][$B(C_6F_5)_4$] has turned out to be a stoichiometric silicon source, which had been predicted to allow for a targeted expansion of nucleophilic clusters, such as E_9 Zintl clusters.[8]

3.4.1.2 Ge_9 Zintl Cluster Expansion

Especially $[Ge_9]^{4-}$ clusters are well investigated with respect to reactivity and specific functionalization.[3, 9-12] Compared to metalloid clusters, their vertices carry negative formal oxidation states. Recent advances had shown, that they provide flexibility towards incorporation of mostly transition metal atoms into the cluster scaffold.

A method to expand the *nido*-Ge_9 Zintl cluster is given by the reaction of Ge_9 clusters with transition metal complexes yielding bare *closo*-[*M*Ge_9] clusters (*M* = Cu, Sn, Zn, Pd),[13-18] of $[\{(Me_3Si)_3Si\}_3Ge_9]^-$ resulting in *closo*-$[\{(Me_3Si)_3Si\}_3Ge_9M(CO)_3]^-$ for *M* = Cr, Mo, W,[19-20] or neutral Ge_9 clusters yielding *closo*-$[\{(Me_3Si)_3Si\}_3Ge_9CH_2CH_3]M(PPh_3)$ (*M* = Pd).[21] In all cases the transition metal is introduced into the polyhedral arrangement forming a distorted bicapped square antiprismatic [*M*Ge_9] core. Especially, the bare *closo*-[*M*Ge_9] clusters, where the *M*-vertex displays the capping atom of the originally open square face, differs in the position of *M* from the other [*M*Ge_9] cores, where *M* becomes part of a capped square (Figure 3.4.2 a-c).

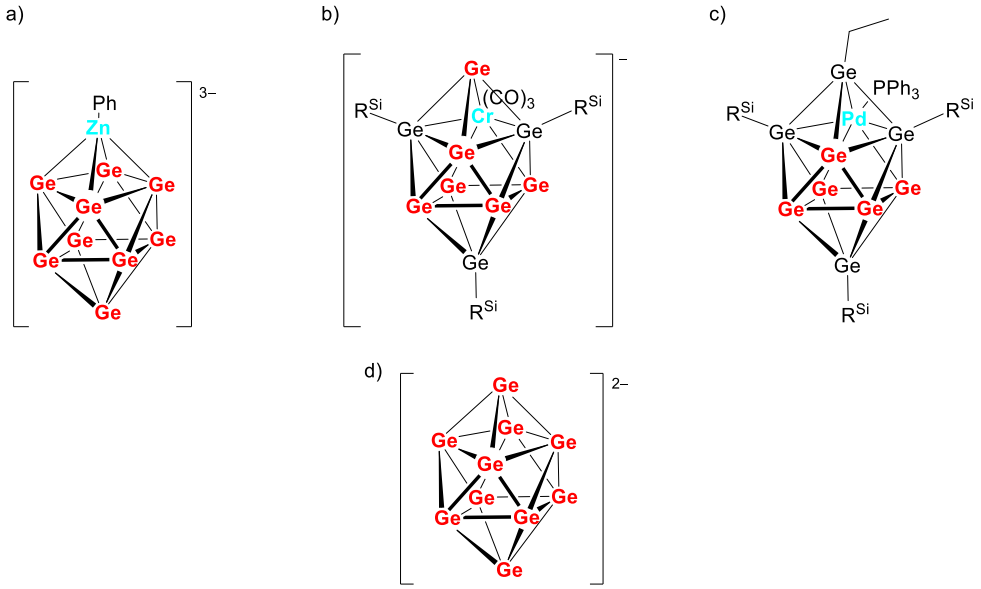

Figure 3.4.2. Structure of a) *closo*-$[Ge_9ZnPh]^{3-}$,[17] b) *closo*-$[\{(Me_3Si)_3Si\}_3Ge_9Cr(CO)_3]^-$,[20] c) closo-$[\{(Me_3Si)_3Si\}_3EtGe_9Pd(PPh_3)]$, and d) *closo*-$[Ge_{10}]^{2-}$.[22] The unsubstituted, "naked" vertices are highlighted in red. R^{Si} depicts the tris(trimethylsilyl)silyl ligands attached to the cluster core.

As a special remark, [{$(Me_3Si)_3Si$}$_3$$EtGe_9Pd(PPh_3)$] as shown in Figure 3.4.2 c does not show dynamic behavior as was observed for other neutral and tetrafunctionalized Ge_9 cluster compounds.[9-10, 23]

So far, E_9 Zintl cluster expansion with low-valent main group metal atoms has been mainly unexplored, but is of special interest as this offers an easy and controllable way to access cluster structures with a distinct number of vertices and at the same time might allow for doping and fine-tuning of the electronic structure of the expanded Zintl clusters. The first Ge_9 Zintl cluster expansion with a group 13 metal atom was achieved by reaction of $[Ge_9]^{4-}$ with TlCp forming *closo*-$[Ge_9Tl]^{3-}$.[24]

The first example of $[Ge_9]^{4-}$ cluster expansion with a main group metal atom combined with cluster fragmentation was reported by Bentlohner *et al.* and is presented by $[Ge_{10}]^{2-}$ (Figure 3.4.2 d).[22] The mechanism of the formation of the ten-atomic *closo*-cluster has been unknown to date.

Applying such cluster expansion reactions, the Ge_9 Zintl cluster chemistry is no longer restricted to only nine-atomic germanium cluster scaffolds.

3.4.2 The *closo*-Clusters [{$(Me_3Si)_3Si$}$_3Ge_9CH_2CH_3$]*M*(PPh_3) (*M* = Ni, Pt) and Dynamic Processes in Solution

see chapter 5.10

S. Frischhut, F. Kaiser, W. Klein, M. Drees, T. F. Fässler, *Organometallics*, **2018**, *37*, 4560-4567.

[{$(Me_3Si)_3Si$}$_3Ge_9CH_2CH_3$]Pd(PPh_3) was synthesized by reaction of {$(Me_3Si)_3Si$}$_3Ge_9CH_2CH_3$ with tetrakis(triphenylphosphine)palladium(0) in toluene. The compound, which has already been introduced in chapter 3.4.1.2, presents a pentafunctionalized *closo*-Ge_9Pd core, which, compared to tetrafunctionalized deltahedral neutral Ge_9 cluster compounds,[9-10, 23] does not show dynamic processes in solution.[21] As a result, Sevov and coworkers were able to show that even the neutral cluster compound {$(Me_3Si)_3Si$}$_3Ge_9CH_2CH_3$ does not show a completely saturated coordination sphere. The syntheses of the analogous Ni and Pt derivatives had not been accomplished prior to this work.

Therefore {$(Me_3Si)_3Si$}$_3Ge_9CH_2CH_3$ was treated with the respective tetrakis(triphenylphosphine)nickel(0) and tetrakis(triphenylphosphine)platinum(0), but the desired compounds did not form. Consequently, the application of the educt complexes η^2-ethylene-bis-(triphenylphosphine)-nickel(0) and η^2-ethylene-bis-(triphenylphosphine)-platinum(0), instead, successfully lead to the formation of [{$(Me_3Si)_3Si$}$_3Ge_9CH_2CH_3$]Ni(PPh_3) (**37**) and [{$(Me_3Si)_3Si$}$_3Ge_9CH_2CH_3$]Pt(PPh_3) (**38**) (Scheme 3.4.1).[25] Both compounds were crystallized from hexane solutions and characterized by single crystal X-ray diffraction, NMR spectroscopy and elemental analysis.

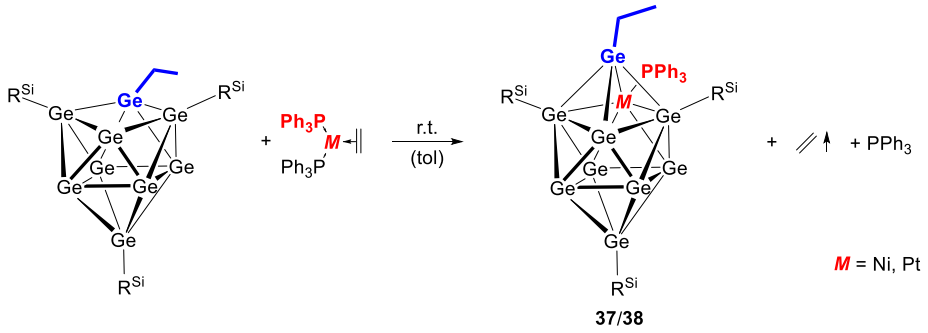

Scheme 3.4.1. Reaction of $\{(Me_3Si)_3Si\}_3Ge_9CH_2CH_3$ with η^2-ethylene-bis-(triphenylphosphine)-nickel(0) or η^2-ethylene-bis-(triphenylphosphine)-platinum(0) yielding $[\{(Me_3Si)_3Si\}_3Ge_9CH_2CH_3]Ni(PPh_3)$ (**37**) and $[\{(Me_3Si)_3Si\}_3Ge_9CH_2CH_3]Pt(PPh_3)$ (**38**). The scheme was modified on the basis of ref. [25]. R^{Si} depicts the tris(trimethylsilyl)silyl ligands attached to the cluster core.

The structures of **37** and **38** are shown in Figure 3.4.3.

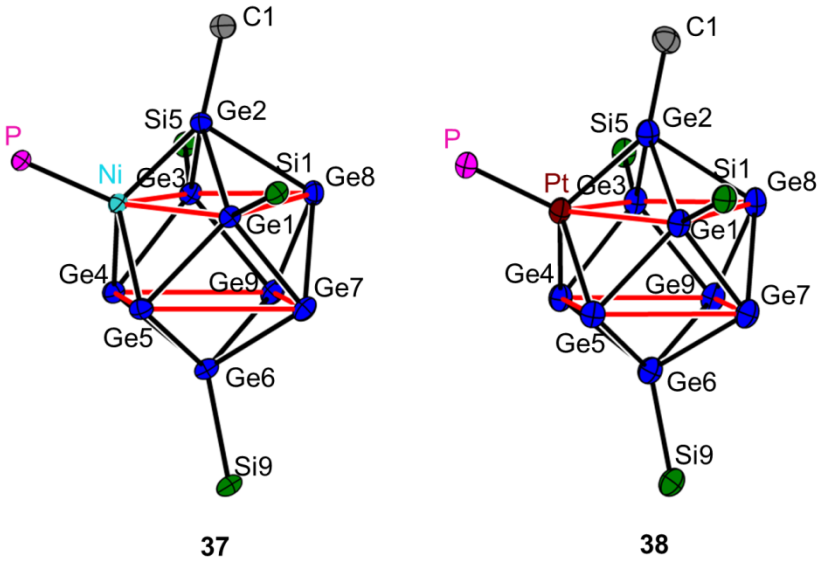

Figure 3.4.3. The molecular structures of $[\{(Me_3Si)_3Si\}_3Ge_9CH_2CH_3]Ni(PPh_3)$ (**37**) and $[\{(Me_3Si)_3Si\}_3Ge_9CH_2CH_3]Pt(PPh_3)$ (**38**). Hydrogen atoms, TMS groups of the silyl ligands, the phenyl groups of the phosphine ligand, as well as the methyl group of the ethyl ligand are omitted for clarity. The capped squares of the cluster cores are highlighted in red. All ellipsoids are shown at a probability level of 50%. Ge – blue, Si – green, C – grey, P – purple, Ni – turquoise, Pt – brown. The figure was modified on the basis of ref. [25].

38 shows an almost to $[\{(Me_3Si)_3Si\}_3Ge_9CH_2CH_3]Pd(PPh_3)$ identical structure, which is traced back to the almost identical atom radii of Pd and Pt due to the lanthanide contraction. In contrast, the *closo*-$[NiGe_9]$ cluster **37** does not fit into the series very well. The cluster core of **37** is distorted compared to **38** most likely caused by the smaller atom radius of Ni. But most importantly, **37** shows highly dynamic processes in toluene-solution at r.t. which was

revealed by temperature-dependent ^{1}H NMR studies. Upon cooling to −40 °C two sharp signals with an integrals ratio of 1:2 corresponding to the silyl ligands of **37** appear in the ^{1}H NMR spectra. Upon heating to r.t. the sharp signals vanish and only broad signals are observed in the spectrum. At temperatures above 60 °C two new sharp signals appear for the silyl ligands which are assigned to an isomer of **37**. The observed temperature-dependent behavior of **37** in solution is reversible. These studies imply that both isomers which are involved in these dynamic processes show C_S-symmetry. This was identified through the appearance of two signal sets corresponding to the silyl ligands of two isomers with each an integral ratio of 1:2. The relevant section of the temperature-dependent ^{1}H NMR spectra is shown in Figure 3.4.4.

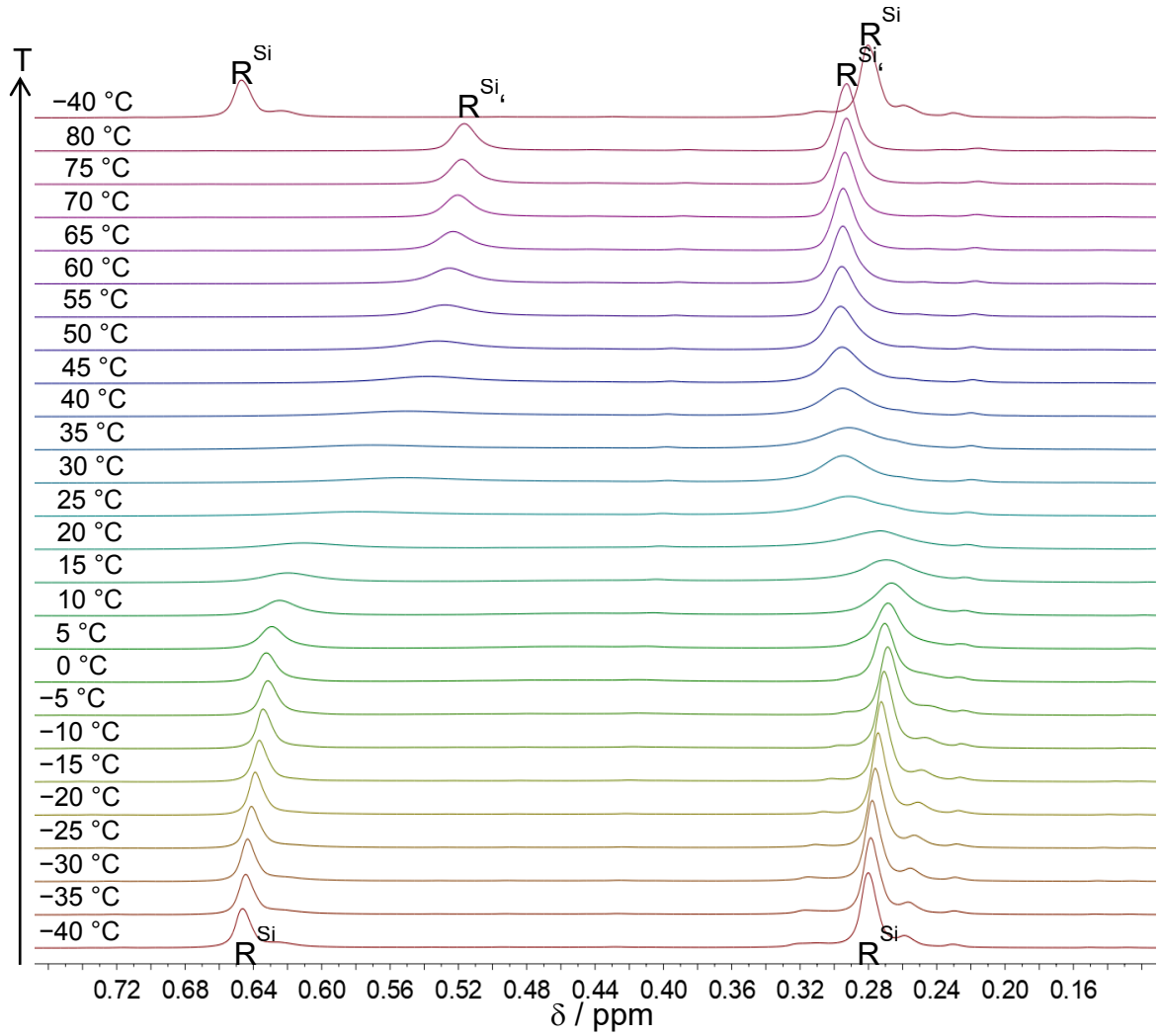

Figure 3.4.4. Stacked excerpt of the relevant section of the temperature-dependent ^{1}H NMR spectra of **37** recorded in [D_8]toluene. R^{Si} depicts the silyl ligands of **37** and $R^{Si'}$ the silyl ligands of the high-temperature-isomer of **37**. The figure was modified on the basis of ref. [25].

Due to the close structural and electronic relationship between Ge_9 Zintl clusters and boranes or carboranes, a diamond-square-diamond (DSD) rearrangement mechanism is feasible leading to temperature-dependent changes of connectivities within the cluster core, and therefore to different constitutional isomers.[26]

3.4.3 Ge_9 Zintl Cluster Expansion with Low-Valent Silicon Compounds

see chapter 5.11

S. Frischhut, J. V. Dums, W. Klein, P. Jutzi T. F. Fässler, *manuscript for publication*.

The reaction of deltahedral Ge_9 clusters with low-valent main group compounds offers an alternative way of Ge_9 Zintl cluster expansion. Compared to the bottom-up synthesis of metalloid clusters with low-valent main group metal compounds, as has been intensively studied for siliconoids in the past decades,[2] the herein presented synthesis approach ensures the presence of hemispheroidal vertices in the cluster scaffold, as well as a predictable distinct number of vertices, forming the architecture of the cluster core. Both demands for metalloid cluster build-up have been a remaining challenge in the synthesis of siliconoids.

The first example of Ge_9 Zintl cluster expansion with a low-valent tetrel-element compound ever, succeeded by reaction of $K_2[\{(Me_3Si)_3Si\}_3Ge_9]$ with $[SiCp^*][B(C_6F_5)_4]$ in the presence of lithium cations in fluorobenzene at r.t. for 3 h. Storage of the reaction solution at −32 °C yielded one deep-brown block-shaped crystal, which was used for single crystal X-ray crystallography. The structure revealed the formed compound $\{(Me_3Si)_3Si\}_2Cp^*[LiSiGe_9](SiCp^*)_2[Ge_9SiLi]Cp^*\{(Me_3Si)_3Si\}_2$ (**39**), which contains two coupled *arachno*-$[Ge_9Si]$ icosahedra each of which bearing two open pentagonal faces (Figure 3.4.5). One Li atom caps one of the two five-membered rings of each cluster. The two icosahedra are further linked by a side-on covalently bonded Cp*Si2−Si2'Cp* bridge, which contains silicon atoms of the formal oxidation state of +IV. Besides, the cluster bears two further $\{(Me_3Si)_3Si\}$ ligands attached to two neighbored Ge atoms of the cluster (Ge4 and Ge8), as well as an η^1-Cp* ligand bound to the low-valent silicon atom which had been integrated into the cluster scaffold.

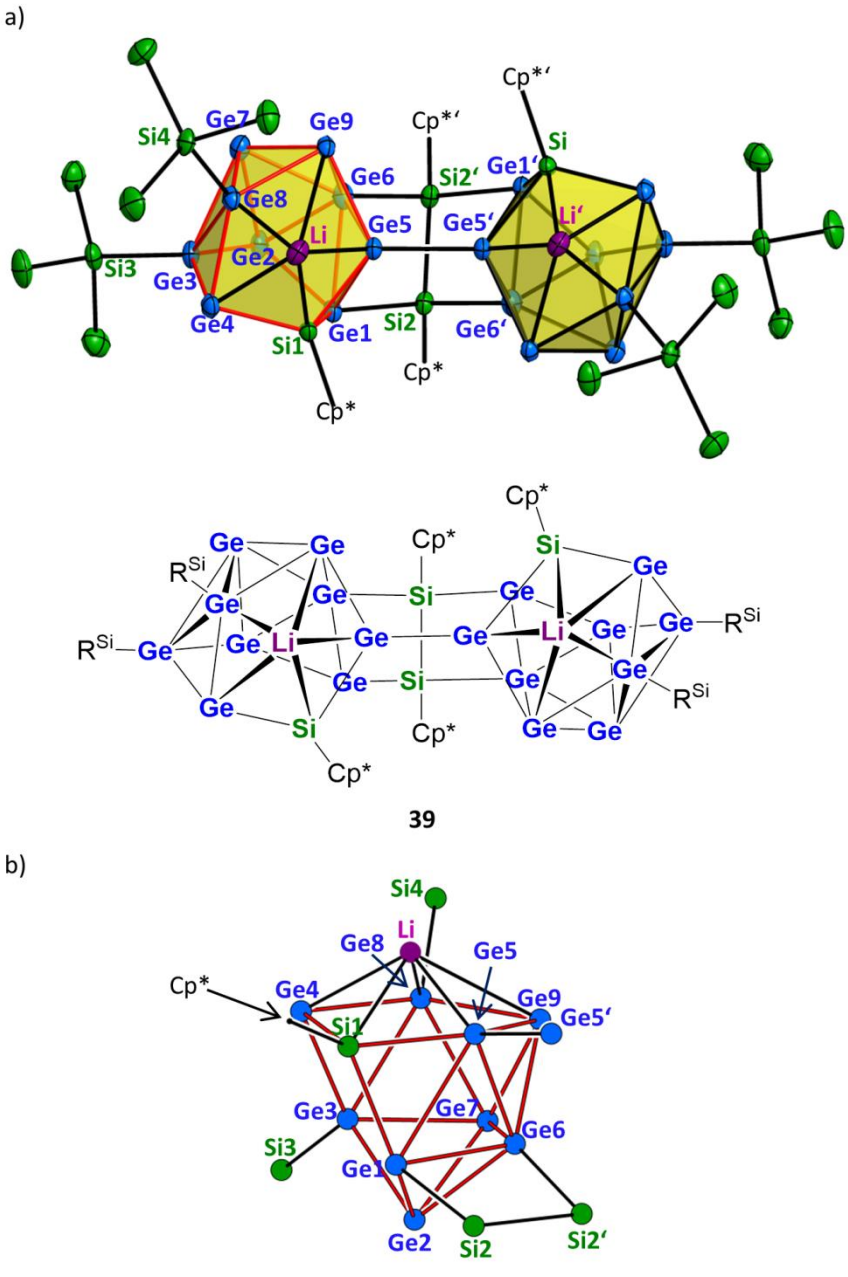

Figure 3.4.5. a) Molecular structure of $\{(Me_3Si)_3Si\}_2Cp^*[LiSiGe_9](SiCp^*)_2[Ge_9SiLi]Cp^*\{(Me_3Si)_3Si\}_2$ (**39**). The *nido*-[$LiGe_9Si$] icosahedra are shown as yellow polyhedra. The methyl groups of the tris(trimethylsilyl)silyl ligands are omitted for clarity. All Cp* ligands are coordinated to Si1 or Si2 in η^1-fashion (R^{Si} = tris(trimethylsilyl)silyl; Cp* = pentamethylcyclopentadienyl). All ellipsoids are shown at a probability level of 50%. b) *Arachno*-[Ge_9Si] icosahedron highlighted in red. Ge – blue, Si – green, Li – purple.

The structure of the *arachno*-[Ge_9Si] cluster does not follow Wade-Mingos rules. The mechanism of the formation of the icosahedron of **39** most likely involves cluster opening and a diamond-square-diamond (DSD) mechanism according to Lipscomb,[26] concluding from the fact that the Ge4 and Ge8 atoms, which were originally positioned oppositely to each other, are now neighbored vertices.[27]

The *arachno*-icosahedron bears an incompletely saturated cluster core with four naked vertices (Ge2, Ge4, Ge7, Ge9) and thus, represents the first heteronuclear siliconoid synthesized from the parent Ge_9 Zintl cluster.

These results open up further possibilities toward selective doping of Ge_9 Zintl clusters with main group metal atoms, other than group 14. Several new structures with fascinating electronic properties might now be available.

3.4.4 References

[1] A. Schnepf, *Chem. Soc. Rev.* **2007**, *36*, 745-758.
[2] Y. Heider, D. Scheschkewitz, *Dalton Trans.* **2018**.
[3] S. Scharfe, F. Kraus, S. Stegmaier, A. Schier, T. F. Fässler, *Angew. Chem. Int. Ed.* **2011**, *50*, 3630-3670.
[4] S. C. Sevov, J. M. Goicoechea, *Organometallics* **2006**, *25*, 5678-5692.
[5] D. Scheschkewitz, *Angew. Chem. Int. Ed.* **2005**, *44*, 2954-2956.
[6] D. Nied, P. Oña-Burgos, W. Klopper, F. Breher, *Organometallics* **2011**, *30*, 1419-1428.
[7] P. Willmes, K. Leszczyńska, Y. Heider, K. Abersfelder, M. Zimmer, V. Huch, D. Scheschkewitz, *Angew. Chem. Int. Ed.* **2016**, *55*, 2907-2910.
[8] K. Leszczyńska, K. Abersfelder, M. Majumdar, B. Neumann, H.-G. Stammler, H. S. Rzepa, P. Jutzi, D. Scheschkewitz, *Chem. Commun.* **2012**, *48*, 7820-7822.
[9] S. Frischhut, T. F. Fässler, *Dalton Trans.* **2018**, *47*, 3223-3226.
[10] S. Frischhut, W. Klein, M. Drees, T. F. Fässler, *Chem. Eur. J.* **2018**, *24*, 9009-9014.
[11] K. Mayer, L. J. Schiegerl, T. Kratky, S. Günther, T. F. Fässler, *Chem. Commun.* **2017**, *53*, 11798-11801.
[12] F. S. Geitner, J. V. Dums, T. F. Fässler, *J. Am. Chem. Soc.* **2017**, *139*, 11933-11940.
[13] Z.-M. Sun, Y.-F. Zhao, J. Li, L.-S. Wang, *J. Cluster Sci.* **2009**, *20*, 601-609.
[14] S. Scharfe, T. F. Fässler, *Eur. J. Inorg. Chem.* **2010**, *2010*, 1207-1213.
[15] M. M. Bentlohner, L. A. Jantke, T. Henneberger, C. Fischer, K. Mayer, W. Klein, T. F. Fässler, *Chem. Eur. J.* **2016**, *22*, 13946-13952.
[16] K. Mayer, L.-A. Jantke, S. Schulz, T. F. Fässler, *Angew. Chem. Int. Ed.* **2017**, *56*, 2350-2355.
[17] J. M. Goicoechea, S. C. Sevov, *Organometallics* **2006**, *25*, 4530-4536.
[18] B. Zhou, M. S. Denning, C. Jones, J. M. Goicoechea, *Dalton Trans.* **2009**, 1571-1578.
[19] F. Henke, C. Schenk, A. Schnepf, *Dalton Trans.* **2011**, *40*, 6704-6710.
[20] C. Schenk, A. Schnepf, *Chem. Commun.* **2009**, 3208-3210.
[21] F. Li, A. Muñoz-Castro, S. C. Sevov, *Angew. Chem. Int. Ed.* **2016**, *55*, 8630-8633.
[22] M. M. Bentlohner, C. Fischer, T. F. Fässler, *Chem. Commun.* **2016**, *52*, 9841-9843.
[23] F. Li, S. C. Sevov, *J. Am. Chem. Soc.* **2014**, *136*, 12056-12063.
[24] D. Rios, M. M. Gillett-Kunnath, J. D. Taylor, A. G. Oliver, S. C. Sevov, *Inorg. Chem.* **2011**, *50*, 2373-2377.
[25] S. Frischhut, F. Kaiser, W. Klein, M. Drees, F. E. Kühn, T. F. Fässler, *Organometallics* **2018**, *37*, 4560-4567.
[26] W. N. Lipscomb, *Science* **1966**, *153*, 373-378.
[27] S. Frischhut, J. V. Dums, W. Klein, P. Jutzi, T. F. Fässler, *Deltahedral Ge_9 Cluster Expansion with Pentamethylcyclopentadienylsilicon(II) Cation*, m*anuscript for publication*.

4 SUMMARY AND CONCLUSION

In the time of climate change the need for semiconductors with tunable electronic properties encourages the field of research to develop tailor-made materials with outstanding properties for specific applications to enable improved energy storage. Fullerenes, which are closely related to Ge_9 Zintl clusters, have attracted great interest in recent years. Way more effort had been put into the development of fullerene-containing materials due to the easier handling of these cage molecules with respect to specific functionalization. However, as has gradually been shown, Ge_9 Zintl clusters are without doubt at least as promising as fullerenes. But the incontrollable reaction of the deltahedral Ge_9 clusters towards many reagents and the associated instability, as well as the limited solubility in convenient solvents let only a few scientists face the challenge, resulting only in slow progress.

The present work deals with investigations on the affinity between fullerenes and Ge_9 Zintl clusters, including studies on Zintl triads, specific organo-functionalization, and the approach towards 2D and 3D cluster networks for the fabrication of nanoporous materials. Moreover, studies on Ge_9 cluster expansion gives new insights into the possibility of the synthesis of heteroatomic deltahedral cluster cages, which, in principle, allows for doping and, therefore, fine-tuning of the electronic properties.

The first fullerene-analogous functionalized Zintl triad $[R{-}Ge_9{-}CH{=}CH{-}CH{=}CH{-}Ge_9{-}R]^{4-}$ (R = (2*Z*,4*E*)-7-amino-5-azahepta-2,4-dien-2-yl) showing an extended conjugated π-electronic system let raise questions on the formation of the butadienyl linker, as well as regarding the formation of the side-chain R, which had been rather unexpected. In this respect, the reactivity of the reagent 1,4-bis(trimethylsilyl)butadiyne towards *en* and $[Ge_9]^{4-}$ was comparatively studied, respectively. According to *in situ* NMR studies, $[Ge_9]^{4-}$ more likely adds to 1,4-bis(trimethylsilyl)butadiyne than *en*. Upon dissolution of 1,4-bis(trimethylsilyl)butadiyne in *en* in the absence of Ge_9 clusters, *en* adds to the dialkyne forming the monoalkyne (3*Z*)-7-amino-1-(trimethylsilyl)-5-azahepta-3-en-1-yne, which upon addition of Ge_9 forms the side-chain R. Moreover, the role of water present in the solvent *en* upon addition of 1,4-bis(trimethylsilyl)butadiyne was investigated. Depending on the water-content, different reaction products are formed. In this context, a qualitative method of tracing water-contents in *en* was developed which has become an important common method at our group to test the suitability of the dried solvent *en* for reactions with highly moisture sensitive Zintl phases. Throughout the investigations on the reactivity of 1,4-

bis(trimethylsilyl)butadiyne with A_4Ge_9 (*A* = K, Rb) in *en*, the first unfunctionalized Zintl triad $[Ge_9–CH=CH–CH=CH–Ge_9]^{6–}$ emerged. *In situ* NMR studies revealed the mechanism on the formation of the 1,3-butadien-1,4-yl linker. For the first time, *cis*- and *trans*-isomers of the Zintl triad were obtained. Based on the therein gained information, the second functionalized Zintl triad $[H_2C=CH–Ge_9–CH=CH–CH=CH–Ge_9–CH=CH_2]^{4–}$, which had already been predicted in a recent publication, was successfully synthesized. Theoretical calculations revealed an extended conjugated π-electronic system throughout the whole vinylated Zintl triad anion, highlighting the potential application as electron acceptor material in hybrid solar cells. As a consequence, the order of addition of the reactants, as well as the applied equivalents play major roles in the targeted synthesis of germanium-based electroactive Zintl triad systems. With these investigations the basis is set for the exploration of further functionalized Zintl triads allowing for the transfer of the reaction to attach specific functional groups to the organically linked Ge_9 clusters. However, so far, the reversible oxidation as was shown for fullerene triads has not been proven, yet, which might be due to the limited solubility and stability in less polar solvents.

In the further course of the exploration of the substantial analogy between fullerenes and Ge_9 Zintl clusters, a method for specific functionalization of Ge_9 clusters was aimed at. The reaction of $[\{(Me_3Si)_3Si\}_3Ge_9]^-$ with allyl bromide, 4-bromo-1-butene and 5-bromo-1-pentene in acetonitrile yielded the respective neutral organo-functionalized clusters $\{(Me_3Si)_3Si\}_3Ge_9(CH_2)_nCH=CH_2$ (*n* = 1, 2, 3) decorated with a terminal double bond, which should in principle allow for follow-up reactions, such as grafting on surfaces or polymerization reactions. Consuming screening-work, as well as adjustments on the reaction conditions gave access to two more alkyl functionalized clusters, namely $\{(Me_3Si)_3Si\}_3Ge_9(CH_2)_2CH_3$ and $\{(Me_3Si)_3Si\}_3Ge_9(CH_2)_3Ph$. The reaction of Ge_9 clusters with alkyl halides was not suitable for straight-forward reactions for specific functionalization due to often unforeseen reactions accompanied with the formation of radicals. In contrast, the decoration of $[\{(Me_3Si)_3Si\}_3Ge_9]^-$ with acyl functionalities proceeded straightforwardly in toluene or hexane by reaction with the respective acyl chlorides. A row of new neutral Zintl compounds $\{(Me_3Si)_3Si\}_3Ge_9(CO)R'$ emerged (R = Me, *i*Pr, *t*Bu, Ph, Bz, cyclopropylmethyl, phenethyl, 4-vinylphenyl). Single crystal X-ray structures of $\{(Me_3Si)_3Si\}_3Ge_9(CO)tBu$ and $\{(Me_3Si)_3Si\}_3Ge_9tBu$, as well as the detection of CO in the gas phase unequivocally displayed the decarbonylation of $\{(Me_3Si)_3Si\}_3Ge_9(CO)tBu$ in solution. The mechanism of this reaction

most likely proceeds according to a Norrish type I α-bond cleavage, forming $\{(Me_3Si)_3Si\}_3Ge_9\cdot$ and $\cdot(CO)t$Bu, which was revealed by DFT calculations. The latter radical easily releases CO forming the stable radical $\cdot t$Bu. Due to geminal processes, the two formed radicals recombine to form $\{(Me_3Si)_3Si\}_3Ge_9t$Bu. The decarbonylation was only observed for the pivaloyl functionalized Ge_9 cluster and most likely for the phenylacetyl-derivatized one. The latter, however, decomposes in solution. The observations are consistent with the stability of the formed organic radicals. All neutral obtained cluster structures show highly dynamic behavior in solution, which we believe occurs according to diamond-square-diamond rearrangement processes as had been stated for (car)boranes. The transferability to an arbitrary acyl chloride shows the significance of this derivatization reaction of Ge_9 Zintl clusters, which is the first one ever reported that shows such a wide-ranged transferability. Therefore, coupling of deltahedral Ge_9 clusters to porphyrine systems, which had already been reported for fullerenes, might be available. Both systems provide molecular architectures which hold great expectations on account of their electronic properties. The coupling of both *via* an acyl-functionality attached to the porphyrine-system might allow for multicomponent systems which can undergo photo-induced charge-separation and thus, are promising with respect to the development of photovoltaics. These speculations were corroborated by the UV-Vis spectroscopic comparison between C_{60} fullerenes and (un)functionalized $[Ge_9]^{2-}$ clusters, performed in the scope of this thesis, which according to the obtained spectra show analogous electronic structures.

During the course of this thesis a synthetic approach towards charged specifically functionalized Ge_9 clusters was developed. They still carry reactive sites, being available for further functionalization, making these materials interesting candidates. Besides organo-functionalization of $[\{(Me_3Si)_3Si\}_2Ge_9]^{2-}$ with bromoethane yielding $[\{(Me_3Si)_3Si\}_2Ge_9CH_2CH_3]^-$, which in a subsequent step upon addition of the sequestering agent 2,2,2-crypt abstracts one silyl ligand to form $[\{(Me_3Si)_3Si\}Ge_9CH_2CH_3]^{2-}$, also acyl-derivatization to obtain $[\{(Me_3Si)_3Si\}_2Ge_9(CO)R']^-$ (R' = *t*Bu, Ph, CH_2Ph, $(CH_2)_2$Ph, 9-anthracenyl, Fc) was devised. Remarkably, no CO elimination takes place for charged acyl-decorated Ge_9 clusters. Silyl ligand abstraction from the Ge_9 cluster core might become of high relevance for future follow-up reactions of functionalized Ge_9 clusters and should be further investigated in future.

Nanostructured semiconductor-based materials have attracted great interest for application in energy storage systems. Regarding this fact, the first example of 3D covalent linkage of deltahedral Ge_9 clusters was reported. The obtained Zintl anion $[[\{(Me_3Si)_3Si\}_2Ge_9]_4Ge]^{4-}$ comprises four *via* a central Ge(IV) atom interconnected Ge_9 clusters, each of which bearing one negative charge. The anion offers high potential to serve as building block for Ge_9 cluster assembly to higher porous MOF-like structures providing high surface areas and flexibility upon volume change.

For fine-tuning of the electronic properties of the discussed nanostructured materials doping of such materials is inevitable. For this purpose, the neutral compound $\{(Me_3Si)_3Si\}_3Ge_9CH_2CH_3$ was reacted with transition-metal complexes to extend the cluster to a *closo*-[*M*Ge_9] core (*M* = Ni, Pt). In addition, the reactivity of charged Ge_9 clusters towards pentamethylcyclopentadienyl silicon (II) cation was investigated in the presence of lithium cations. The targeted integration of a low-valent tetrel-element atom, in this case silicon, into the Ge_9 cluster scaffold is successfully recorded for the first time. The structure comprises two coupled distorted *arachno*-[Ge_9Si] icosahedra which are additionally linked *via* a side-on bonded Cp*Si−SiCp* bridge. One of the two open pentagonal faces is capped by a Li atom. Heteroatomic polyhedral structures with a distinct number of vertices are auspicious regarding intriguing novel properties. Compared to the bottom-up synthesis of clusters with hemispheroidal vertices starting with low-valent molecules, the use of K_4Ge_9 as precursor material provides only “naked” vertices, thus, saving several reaction steps. As we showed, the number of vertices can be adjusted by reaction with low-valent tetrel-element atoms, which can now be transferred to also other metal atoms.

To put it in a nutshell, this work has again confirmed the close relation between C_{60} fullerene cage molecules and deltahedral Ge_9 clusters. We provided insight into several missing or still unclear facts extending the expectations on potential application of Ge_9 Zintl clusters in semiconductor devices (Figure 3.4.1). This class of compounds has an enormous potential for unusual structures with novel properties.

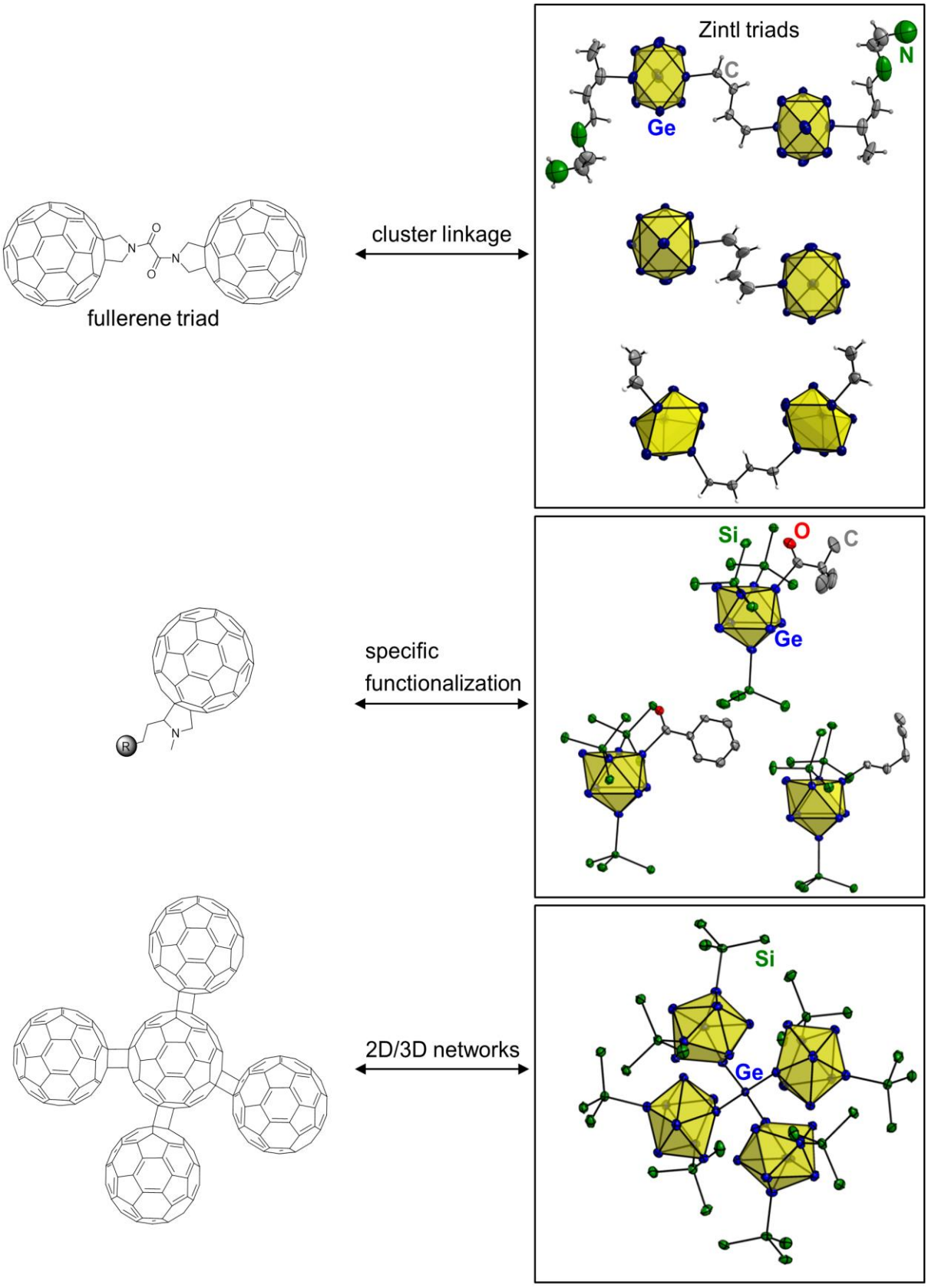

Figure 3.4.1. Schematic display of the newly confirmed analogy between fullerenes and deltahedral Ge_9 Zintl clusters. The Ge_9 clusters are shown as yellow polyhedra. Color code: Ge – blue, Si/N – green, C – grey, O – red.

5 PUBLICATIONS AND MANUSCRIPTS

5.1 On the Affinity between Fullerenes and Deltahedral Zintl Ions: a UV-Vis Spectroscopic Investigation

Sabine Frischhut[+], João G. Machado de Carvalho[+], Antti J. Karttunen, and Thomas F. Fässler

[+] These authors contributed equally to this work.

published in:

Z. Anorg. Allg. Chem. **2018**, 644, 1337-1343.

CONTENT AND CONTRIBUTION

Within the scope of this publication, further targeted functionalization of $[\{(Me_3Si)_3Si\}_3Ge_9]^-$ with alkyl halides was aimed at. The synthesis of three new neutral functionalized compounds, $\{(Me_3Si)_3Si\}_3Ge_9(CH_2)_2CH_3$, $\{(Me_3Si)_3Si\}_3Ge_9(CH_2)_2CH{=}CH_2$ and $\{(Me_3Si)_3Si\}_3Ge_9(CH_2)_3Ph$, was achieved. Only $\{(Me_3Si)_3Si\}_3Ge_9(CH_2)_2CH_3$ was successfully synthesized analytically pure. All compounds were synthesized and NMR spectroscopically characterized by M.Sc. João G. Machado de Carvalho within a Master's thesis supervised within this work.

For the first time the unsubstituted *closo*-$[Ge_9]^{2-}$ cluster was UV-Vis-spectroscopically investigated within this publication. The UV-Vis spectrum of acetonitrile solutions show strong absorption bands at wavelengths of $\lambda = 209$ and 317 nm at low concentrations of 20 μM. Upon further concentration of the acetonitrile solution, additional weak bands appear at wavelengths of 498 and 626 nm, which according to DFT calculations are assigned to the agglomerate $[Ge_9{=}Ge_9{=}Ge_9]^{6-}$. Quantum chemical calculations were carried out by Prof. Dr. Antti J. Karttunen. The UV-Vis spectra of *closo*-$[Ge_9]^{2-}$ were compared to reproduced UV-Vis spectra of C_{60} fullerene and to substituted and functionalized Ge_9 clusters, namely $[(H_2C{=}CH)_2Ge_9]^{2-}$, $[\{(Me_3Si)_3Si\}_3Ge_9]^-$, $\{(Me_3Si)_3Si\}_3Ge_9CH_2CH_3$, $\{(Me_3Si)_3Si\}_3Ge_9(CH_2)_2CH_3$, $\{(Me_3Si)_3Si\}_3Ge_9(CH_2)_3CH{=}CH_2$ and $[\{(Me_3Si)_3Si\}_3Ge_9CH_2CH_3]Pt(PPh_3)$. $\{(Me_3Si)_3Si\}_3Ge_9(CH_2)_3CH{=}CH_2$ and $[\{(Me_3Si)_3Si\}_3Ge_9CH_2CH_3]Pt(PPh_3)$ were synthesized within this thesis and UV-Vis spectroscopic investigations were performed by M.Sc. João G. Machado de Carvalho within the scope of a Master's thesis, which was assisted throughout these doctoral studies. Data evaluation was done within this work and by M.Sc. João G. Machado de Carvalho.

The publication was authored within this work and by M.Sc. João G. Machado de Carvalho. The manuscript was revised by Prof. Dr. Thomas F. Fässler.

Journal of Inorganic and General Chemistry
ZAAC
Zeitschrift für anorganische und allgemeine Chemie
DOI: 10.1002/zaac.201800293
ARTICLE

On the Affinity between Fullerenes and Deltahedral Zintl Ions: A UV/Vis Spectroscopic Investigation

Sabine Frischhut,[a][‡] João G. Machado de Carvalho,[a][‡] Antti J. Karttunen,[b] and Thomas F. Fässler*[a]

Dedicated to Professor Werner Uhl on the Occasion of his 65th Birthday

Abstract. The close relationship of C_{60} and deltahedral tetrel element cluster anions has been pointed out before. We report herein on UV/Vis spectra of the Zintl anions and compounds $[Ge_9]^{2-}$, $[(CH_2{=}CH)_2Ge_9]^{2-}$, $[\{(Me_3Si)_3Si\}_3Ge_9]^-$, $\{(Me_3Si)_3Si\}_3Ge_9CH_2CH_3$, $\{(Me_3Si)_3Si\}_3Ge_9(CH_2)_2CH_3$, $\{(Me_3Si)_3Si\}_3Ge_9(CH_2)_3CH{=}CH_2$, and $[\{(Me_3Si)_3Si\}_3Ge_9CH_2CH_3]Pt(PPh_3)$. The spectra are compared to those of the C_{60} fullerene, which were recorded under the same conditions. The UV/Vis spectrum of pristine $[Ge_9]^{2-}$ resembles that of C_{60} and at higher concentration hint at the known trimeric $[(Ge_9)_3]^{6-}$. The influence of ligand substitution at the Ge_9 cluster-core is highlighted. For this, the synthesis of the specifically functionalized deltahedral Ge_9 clusters $\{(Me_3Si)_3Si\}_3Ge_9(CH_2)_2CH_3$, $\{(Me_3Si)_3Si\}_3Ge_9(CH_2)_2CH{=}CH_2$, and $\{(Me_3Si)_3Si\}_3Ge_9(CH_2)_3C_6H_5$ are reported for the first time and is achieved by the reaction of $K[\{(Me_3Si)_3Si\}_3Ge_9]$ with the respective alkyl halides in acetonitrile. The newly synthesized products were characterized by NMR spectroscopy.

Introduction

Fullerenes have been thoroughly investigated for application in semiconductor devices due to their outstanding electronic properties, e.g. organic solar cells. Specific organo-functionalization of fullerenes allowed for an electronic fine-tuning to make these materials more suitable for specific applications.[1] The analogy between fullerenes and deltahedral Ge_9 clusters is remarkable. This close relationship was already pointed out in 2001.[2] Both, fullerenes and deltahedral Ge_9 clusters, can adopt different charges (from –6 to –1 and from –4 to –2, respectively) and can be oxidatively coupled.[2–3] In case of the Ge_9 clusters, in analogy to C_{60} coupled products of pristine clusters like the dimer $[Ge_9{-}Ge_9]^{6-}$,[4] the trimer $[Ge_9{=}Ge_9{=}Ge_9]^{6-}$ or the anionic polymeric chain $^1_\infty\{[Ge_9]^{2-}\}$ are known,[5] which have their fullerene counterpart in dimeric C_{60}–C_{60},[6] the predicted $[C_{60}]_3$,[7] and polymeric C_{60},[8] respectively (Figure 1). Furthermore, only recently, the linkage of two Ge_9 clusters via an electroactive spacer embodied in the so-called fullerene triad analogous Zintl triads $[RGe_9{-}CH{=}CH{-}CH{=}CH{-}Ge_9R]^{4-}$ [*R* = vinyl, (2*Z*,4*E*)-7-amino-5-azahepta-2,4-dien-2-yl] and $[Ge_9{-}CH{=}CH{-}CH{=}CH{-}Ge_9]^{6-}$ was reported (Figure 1).[9] This again reinforces the assumption of the close relationship between fullerenes and Ge_9 Zintl clusters.

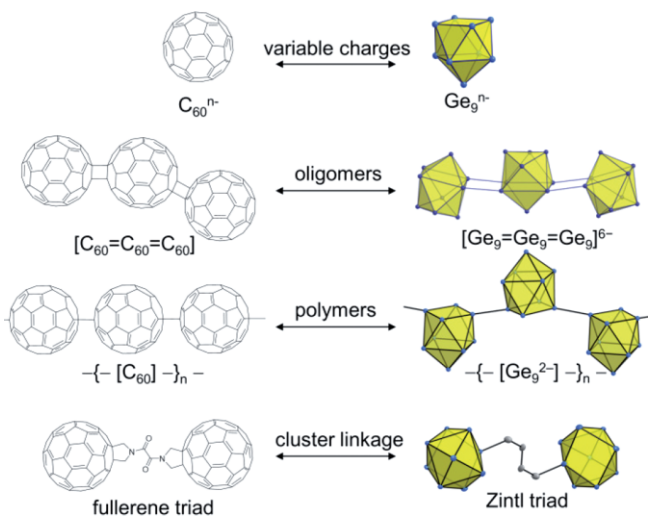

Figure 1. Schematic representation of the analogy between fullerenes and deltahedral Ge_9 Zintl clusters.

In recent years, specific functionalization of deltahedral Ge_9 clusters has become one of the major goals in its cluster chemistry. The reduction of the negative charges of the Zintl anions under retention of the number of delocalized electrons in the cluster orbitals and the better solubility in less polar solvents allowing now also for a more detailed investigation of the electronic properties. Application of functionalized nine-atomic germanium cluster frameworks in optoelectronic devices[10] or hybrid solar cells[11] might in principle also be feasible.

The first organo-functionalization of Ge_9 Zintl clusters from binary phases was introduced by *Sevov* and co-workers, who

* Prof. Dr. T. F. Fässler
E-Mail: thomas.faessler@lrz.tum.de
[a] Department of Chemistry
Technical University of Munich
Lichtenbergstraße 4
85747 Garching, Germany
[b] Department of Chemistry and Materials Science
Aalto University
P.O. Box 16100
00076 Aalto, Finland
[‡] These authors contributed equally to this work.
Supporting information for this article is available on the WWW under **http://dx.doi.org/10.1002/zaac.201800293** or from the author.

reacted A_4Ge_9 (A = K, Rb) with alkynes to afford alkenylation of Ge_9 clusters. According to this reaction scheme several new organo-functionalized Ge_9 cluster compounds emerged. Either one- or twofold substituted or, as already mentioned above, even linked Ge_9 cages were discovered.[12] Especially the vinylated species $[(CH_2{=}CH)_nGe_9]^{(4-n)-}$ (n = 1, 2)[13] and the fullerene analogous Zintl triads $[R{-}Ge_9C_4H_4Ge_9{-}R]^{4-}$ [R = vinyl, (2*Z*,4*E*)-7-amino-5-azahepta-2,4-dien-2-yl][9] comprising a π-electronic system are to be mentioned here. Also, the reaction of the Zintl phase A_4Ge_9 with alkyl halides gave alkylated Ge_9 cluster anions, which were mostly only characterized by ESI mass spectrometry.[14]

The discovery of the threefold silylated Ge_9 cluster $[\{(Me_3Si)_3Si\}_3Ge_9]^-$ by *Schnepf* was made for the first time accessible by co-condensation of germanium halides.[15] *Sevov* and co-workers introduced a high-yield synthesis strategy where the Zintl phase K_4Ge_9 was reacted with three equivalents of chloro-tris(trimethylsilyl)silane.[16] Using the trisilylated Ge_9 cluster as starting point, also neutral organo-functionalized Ge_9 cluster compounds were reported, which resulted from a nucleophilic substitution reaction with alkyl halides, e.g. $\{(Me_3Si)Si\}_3Ge_9CH_2CH_3$ and $\{(Me_3Si)Si\}_3Ge_9(CH_2)_3CH{=}CH_2$.[17] Furthermore, only very recently, the acylation of $[\{(Me_3Si)_3Si\}_3Ge_9]^-$ with acyl chlorides was shown to be a very efficient way of specifically functionalizing these deltahedral cage molecules.[18] Neutral alkylated Ge_9 clusters can still be reacted with late transition metal complexes, such as tetrakis(triphenylphosphine)palladium(0), to form the pentafunctionalized cluster $[\{(Me_3Si)_3Si\}_3Ge_9CH_2CH_3]Pd(PPh_3)$.[19] Only recently, it was shown that also silyl groups with unsaturated ligands as well as phosphine groups can be attached to the Ge cluster core.[20]

Once, specifically functionalized deltahedral Ge_9 cluster compounds are synthesized they can be studied to be used in composite materials with potential interesting electronic properties. UV/Vis spectroscopic investigations on deltahedral Ge_9 cluster compounds have barely been reported, but are crucial to investigate electronic structures. So far, only $[\{(Me_3Si)_3Si\}_3Ge_9]^-$ among functionalized and naked Ge_9 clusters has been characterized by UV/Vis spectroscopy in a thf solution. A broad and almost featureless absorption is reported for this compound. According to quantum chemical calculations, the optical transitions originate from the atomic orbital contributions in the cluster core.[21]

Herein we report further neutral alkyl-substituted Ge_9 cages, namely $\{(Me_3Si)_3Si\}_3Ge_9(CH_2)_2CH_3$ (**1**), $\{(Me_3Si)_3Si\}_3Ge_9(CH_2)_2CH{=}CH_2$ (**2**), and $\{(Me_3Si)_3Si\}_3Ge_9(CH_2)_3C_6H_5$ (**3**), which were synthesized by treating $K[\{(Me_3Si)_3Si\}_3Ge_9]$ with the respective alkyl bromides in acetonitrile at room temperature. Moreover, UV/Vis spectra of $[Ge_9]^{2-}$ (**4a**), $[(CH_2{=}CH)_2Ge_9]^{2-}$ (**5a**), $[\{(Me_3Si)_3Si\}_3Ge_9]^-$ (**6a**), $\{(Me_3Si)_3Si\}_3Ge_9CH_2CH_3$ (**7**), $\{(Me_3Si)_3Si\}_3Ge_9(CH_2)_2CH_3$ (**1**), $\{(Me_3Si)_3Si\}_3Ge_9(CH_2)_3CH{=}CH_2$ (**8**), as well as $[\{(Me_3Si)_3Si\}_3Ge_9CH_2CH_3]Pt(PPh_3)$ (**9**) are shown and discussed in comparison to UV/Vis spectra of C_{60} fullerenes, which we recorded under the same conditions. The effect of Ge_9-cluster substitution is highlighted. An overview of all herein investigated Ge_9 clusters is given in Figure 2.

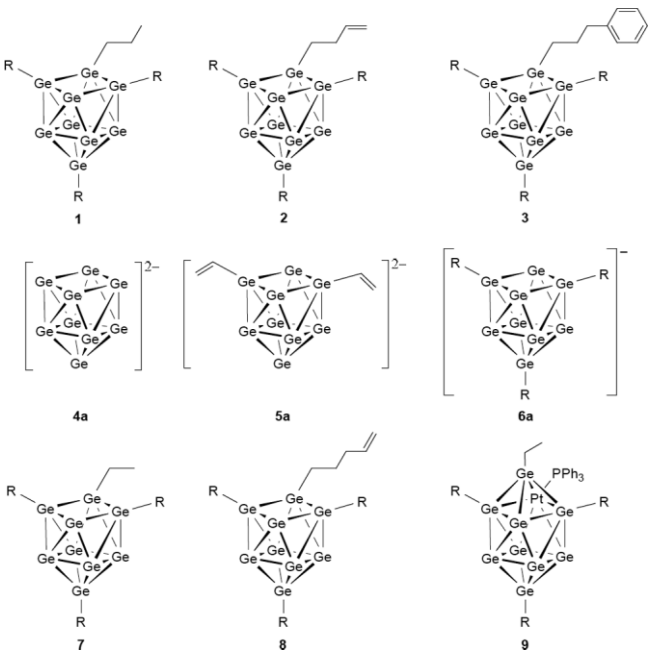

Figure 2. Overview of the structures of the herein investigated Ge_9 clusters **1**–**9**. *R* depicts the $\{(Me_3Si)_3Si\}$-groups.

Results and Discussion

For specific functionalization of silylated Ge_9 clusters, $[\{(Me_3Si)_3Si\}_3Ge_9]^-$ was treated with the alkyl bromides 1-bromopropane, 4-bromo-1-butene, and 1-bromo-3-phenylpropane in acetonitrile according to the nucleophilic substitution reaction in the synthesis of $\{(Me_3Si)_3Si\}_3Ge_9CH_2CH_3$. It turned out that the reaction type was not transferable to a wide range of alkyl bromides. Often, broad signals were observed in the ^{1}H NMR spectra of the obtained precipitates. Nevertheless, after optimization of the reaction conditions the propyl-substituted Ge_9 cluster $\{(Me_3Si)_3Si\}_3Ge_9(CH_2)_2CH_3$ (**1**) was obtained in good yield and high purity. In contrast, the syntheses of $\{(Me_3Si)_3Si\}_3Ge_9(CH_2)_2CH{=}CH_2$ (**2**) and $\{(Me_3Si)_3Si\}_3Ge_9(CH_2)_3C_6H_5$ (**3**) were less selective and besides the sharp signals of the neutral product, also broad peaks are visible in the ^{1}H NMR spectra. Since compounds **2** and **3** could not be obtained analytically pure due to fail of attempted crystallization experiments, the compounds were not used for UV/Vis measurements, even though their existence in solution was verified. Temperature-dependent ^{1}H NMR studies of dissolved crystals of **1** in [D_8]toluene revealed dynamic processes in solution as has already been observed for other neutral Ge_9 cluster compounds (Figure 3).[17,18]

The coalescence temperature of **1** is determined to be 0 °C affording an exchange rate of 53.3 s^{-1} and an activation free energy of rotation of 57.5 kJ·mol^{-1}. Raman spectroscopic investigations of crystals of **1** show a comparable spectrum to **8** (see Figure S3, Supporting Information).[17b]

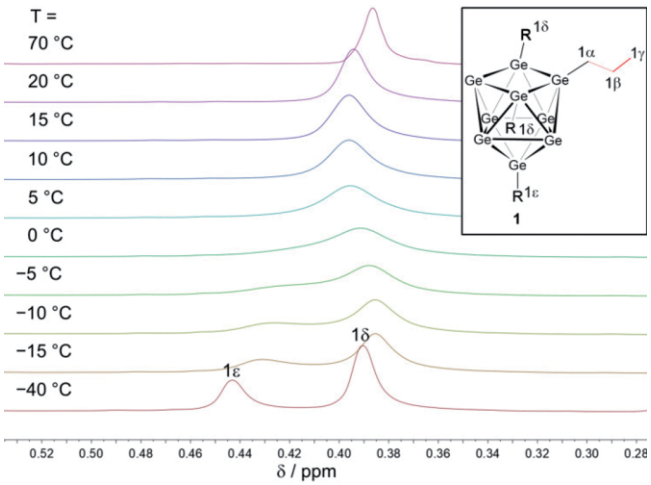

Figure 3. Temperature-dependent ^{1}H NMR study of dissolved crystals of **1** in [D_8]toluene. For reasons of clarity only the signals of the silyl ligands *R* are depicted.

In particular, fullerenes of the formulae C_{60} and C_{70}, which are closely related to Ge_9 Zintl clusters, show characteristic behavior in UV/Vis absorption in benzene- and hexane solutions. Therefore, we recorded UV/Vis spectra of C_{60} in toluene and obtained spectra which are in full agreement with the ones presented in literature (Figure 4).

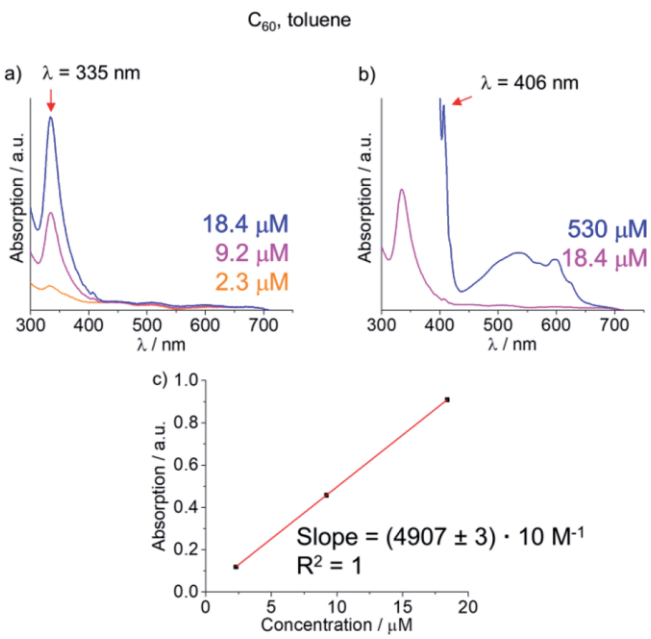

Figure 4. (a) UV/Vis electronic spectrum of C_{60} in toluene (λ = 300–750 nm), emphasazing the absorption at λ = 335 nm. (b) UV/Vis electronic spectra of C_{60} in toluene (λ = 300–750 nm) at higher concentration. (c) Linear regression for *A* vs. c_M plot for λ = 335 nm.

Figure 4a displays a strong absorption band at 350 nm with an extinction coefficient of approximately 49000 $cm^{-1}M^{-1}$. The spectra in Figure 4b obtained at higher concentrated C_{60}/toluene solutions show a weak band at 406 nm and a very weak absorption band in the region of 450 to 650 nm, which is in accordance with the literature. Back then, it was unclear whether the appearance of the broad band at 450 to 650 nm originated from little impurity in the C_{60} fullerene or is related to first-order forbidden transitions.[22]

The obtained spectra of acetonitrile solutions of various concentrations of $[Ge_9]^{2-}$ (**4a**) obtained from the dissolution of $[K(2,2,2\text{-crypt})]_2[Ge_9]$ crystals (**4**) are shown in Figure 5. The bulk species of **4** was characterized by powder X-ray diffraction (see Figure S8, Supporting Information).

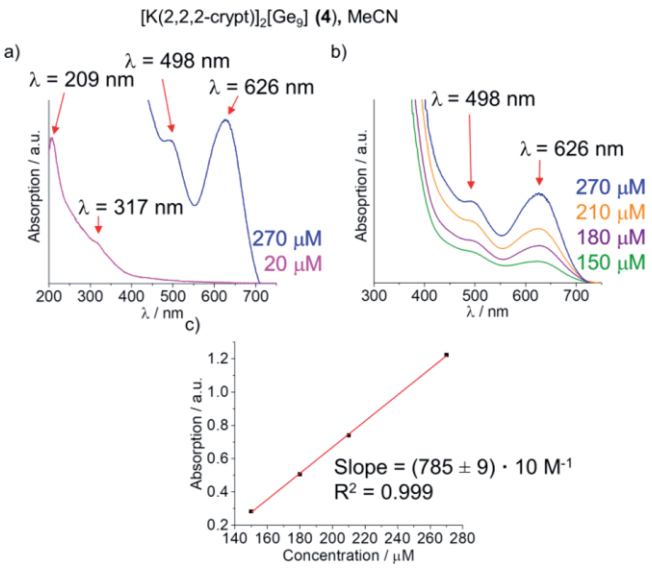

Figure 5. (a) UV/Vis electronic spectra of $[K(2,2,2\text{-crypt})]_2[Ge_9]$ (**4**) in acetonitrile (λ = 200–750 nm). (b) UV/Vis electronic spectra of **4** in acetonitrile (λ = 400–750 nm, c_M = 150–270 µM). (c) Linear regression for *A* vs. c_M plot for λ = 626 nm.

The Zintl anion **4a** shows a pronounced absorption band at λ = 209 nm and a less resolved absorption at around 317 nm (Figure 5a and b), which according to DFT calculations arise from the cluster. The broadness of these bands confirms the flexibility of the Ge_9 clusters in solution, allowing for a great number of excited states and transitions (see Figure S16, Supporting Information). Dynamic processes in solution at room temperature have already been reported for other Ge_9 cluster compounds.[17,18] The pronounced band at 209 nm is in good agreement with the absorption at 215 nm in the theoretical UV/Vis spectrum of **4a**. The named absorptions at 209 nm and 317 nm are rather similar to the ones for C_{60}. At higher concentrations weak absorption bands at 498 nm and 626 nm appear (Figure 5b). The latter absorption bands are in accordance with the deep green colored solutions at concentrations above 50 µM. However, compared to the theoretical UV/Vis spectrum, these absorptions cannot be assigned to **4a**. Yet, the theoretical UV/Vis spectrum of the agglomerate $[Ge_9{=}Ge_9{=}Ge_9]^{6-}$ with its absorptions at 418, 516, and 678 nm matches well with the UV/Vis spectrum in the region of 400 to 750 nm of **4a** at higher concentrations (see Figure S17, Supporting Information), concluding that agglomeration and oligomerization of **4a** at higher concentrations occurs. Therefore, an equilibrium according to 3 $[Ge_9]^{2-} \leftrightharpoons [Ge_9{=}Ge_9{=}Ge_9]^{6-}$ is present in solution, which is evidently shifted upon change of concentration.

For the measured concentrations, the cation $[K(2,2,2\text{-crypt})]^+$ does not show relevant absorptions in the UV/Vis window. Quantitative analysis revealed an extinction coefficient of $\varepsilon_{max} = (785 \pm 9) \cdot 10\ cm^{-1} \cdot M^{-1}$ for the absorption observed at 626 nm.

The UV/Vis spectra of charged functionalized Ge_9 clusters in $[K(18c\text{-}6)]_2[(CH_2{=}CH)_2Ge_9]$ (**5**) and $[K(2,2,2\text{-crypt})][\{(Me_3Si)_3Si\}_3Ge_9]$ (**6**) in acetonitrile solutions are shown in Figure 6. The isolated crystals of **5** and **6** were characterized by NMR spectroscopy in solution (see Figures S9 and S10, Supporting Information).

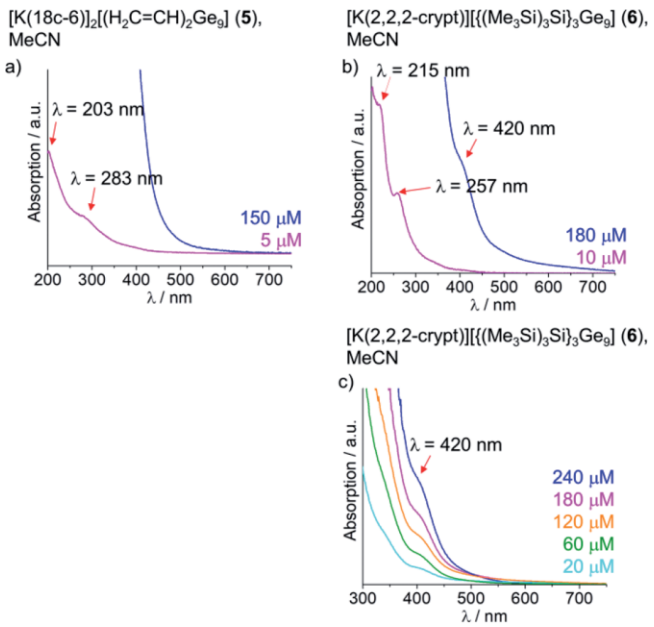

Figure 6. (a) UV/Vis electronic spectra of $[K(18c\text{-}6)]_2[(H_2C{=}CH)_2Ge_9]$ (**5**) in acetonitrile (λ = 200–750 nm). (b) UV/Vis electronic spectra of $[K(2,2,2\text{-crypt})][\{(Me_3Si)_3Si\}_3Ge_9]$ (**6**) in acetonitrile (λ = 200–750 nm). (c) UV/Vis electronic spectrum of **6** in acetonitrile (λ = 300–750 nm, c_M = 20–240 µM).

Figure 6a and b display broad absorption between 200 nm and 300 nm for $[(CH_2{=}CH)_2Ge_9]^{2-}$ **5a** and $[\{(Me_3Si)_3Si\}_3Ge_9]^-$ **6a**, which are comparable to the broad bands of the unsubstituted Ge_9 cluster **4a**, suggesting that these transitions are related to the Ge_9 core. A slight hypsochromic shift is observed for **5a** and **6a**, compared to the pristine cluster **4a**. For the broad absorption of **6a**, a bathochromic shift compared to **5a** is displayed, which is associated with the higher charge in **5a**. The band at 420 nm is in good agreement with the pale yellow colored solutions of **5** and **6**. However, no extinction coefficients could be determined due to the overlap of absorption bands. Similar behavior was observed for **6** in toluene (Figure S14, Supporting Information).

Neutral functionalized Ge_9 cluster compounds were also investigated by UV/Vis spectroscopy in hexane, namely $\{(Me_3Si)_3Si\}_3Ge_9CH_2CH_3$ (**7**), $\{(Me_3Si)_3Si\}_3Ge_9(CH_2)_2CH_3$ (**1**), $\{(Me_3Si)_3Si\}_3Ge_9(CH_2)_3CH{=}CH_2$ (**8**), and $[\{(Me_3Si)_3Si\}_3Ge_9CH_2CH_3]Pt(PPh_3)$ (**9**) (Figure 7). All compounds were characterized by NMR spectroscopy in solution (see Figures S11, S1, S12 and S13, Supporting Information).

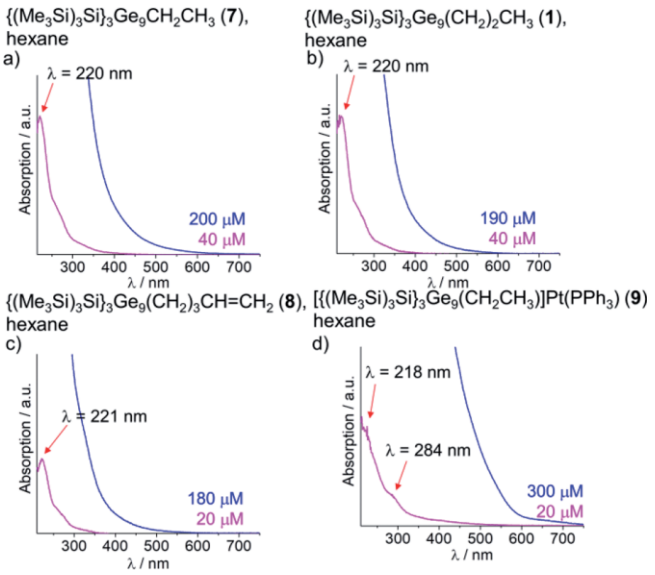

Figure 7. (a) UV/Vis electronic spectrum of $\{(Me_3Si)_3Si\}_3Ge_9(CH_2CH_3)$ (**7**) in hexane (λ = 210–750 nm). (b) UV/Vis electronic spectrum of $\{(Me_3Si)_3Si\}_3Ge_9(CH_2)_2CH_3$ (**1**) in hexane (λ = 210–750 nm). (c) UV/Vis electronic spectrum of $\{(Me_3Si)_3Si\}_3Ge_9(CH_2)_3CH{=}CH_2$ (**8**) in hexane (λ = 210–750 nm). (d) UV/Vis electronic spectrum of $[\{(Me_3Si)_3Si\}_3Ge_9(CH_2CH_3)]Pt(PPh_3)$ (**9**) in hexane (λ = 210–750 nm).

From the spectra we conclude, that due to the resemblance of the absorption bands at around 220 nm the chain length of the organic substituent does not noticeably affect the electronic situation within the cluster core. In contrast, for the *closo*-$[PtGe_9]$ cluster **9** (Figure 7d) an absorption at 284 nm is more evident than in the case of the neutral clusters **1**, **7**, and **8** (Figure 7a, b, and c). Hence, the UV/Vis spectrum suggests that the electronic situation of the cluster core is slightly influenced upon coordination. In all four cases, with increasing concentrations a weaker absorption band, as could be observed for **4a**, is not observed for the measured concentrations.

Conclusions

The three new organo-substituted neutral Ge_9 clusters, $\{(Me_3Si)_3Si\}_3Ge_9(CH_2)_2CH_3$, $\{(Me_3Si)_3Si\}_3Ge_9(CH_2)_2CH{=}CH_2$, and $\{(Me_3Si)_3Si\}_3Ge_9(CH_2)_3C_6H_5$, were successfully synthesized. Especially the latter two represent interesting candidates in terms of follow-up reactions, aiming for cluster aggregation through successive reactions including the side groups.

The pristine non-functionalized Ge_9 cluster anion, $[Ge_9]^{2-}$ (**4a**), shows, similarly to fullerenes, very intense absorptions in the UV region and two very weak bands at 498 nm and 626 nm, which are assigned to $[Ge_9{=}Ge_9{=}Ge_9]^{6-}$ occurring from agglomeration of **4a** at higher concentrations. The higher the degree of substitution at the Ge_9 cluster, starting with $[(CH_2{=}CH)_2Ge_9]^{2-}$ and $[\{(Me_3Si)_3Si\}_3Ge_9]^-$ through to $\{(Me_3Si)_3Si\}_3Ge_9CH_2CH_3$, $\{(Me_3Si)_3Si\}_3Ge_9(CH_2)_2CH_3$, and $\{(Me_3Si)_3Si\}_3Ge_9(CH_2)_3CH{=}CH_2$, the more intense the band in the UV region becomes. This leads to a strong overlap of the bands at $\lambda < 450$ nm. The *closo*-cluster

[{$(Me_3Si)_3Si$}$_3Ge_9CH_2CH_3$]Pt(PPh_3) shows slightly different UV/Vis spectra compared to the other investigated neutral clusters. As expected, the presence of a transition metal has a greater influence on the electronic structure of the cluster. All substituted Ge_9 cluster compounds do not show the weak bands in the region of 400 to 750 nm, concluding agglomeration of the latter at higher concentrations does not take place. The similarity of the spectra of the pristine Ge_9 cluster anion with C_{60} hints for similar interesting possibilities for optoelectronic applications.

Experimental Section

General: All manipulations were carried out in a purified argon atmosphere using standard Schlenk techniques. The Zintl phase with the nominal composition K_4Ge_9 was synthesized heating a stoichiometric mixture of the elements K and Ge (99.999 %, Chempur) at 650 °C for 46 h in a stainless steel autoclave.[23] The solvents acetonitrile, toluene, and hexane were dried with molecular sieves in a solvent purification system MB-SPS. C_{60} (> 99 %, Hoechst), chloro-tris(trimethylsilyl)silane (≥ 95.0 %, TCI Chemicals), 1-bromopropane (Merck), 4-bromo-1-butene (97 %, Alfa Aesar), and 1-bromo-3-phenylpropane (98 %, Acros Organics) were used as received. [K(2,2,2-crypt)]$_2$[Ge_9] (**4**),[24] [K(18c-6)]$_2$[(CH_2=CH)$_2Ge_9$] (**5**) (contains one molecule ethylenediamine per formula unit),[13a] [K(2,2,2-crypt)][{$(Me_3Si)_3Si$}$_3Ge_9$] (**6**) (the isolated bulk species contains 0.5 molecules 2,2,2-crypt per formula unit),[16] {$(Me_3Si)_3Si$}$_3Ge_9CH_2CH_3$ (**7**),[17a] {$(Me_3Si)_3Si$}$_3Ge_9(CH_2)_3CH$=CH_2 (**8**),[17b] and [{$(Me_3Si)_3Si$}$_3Ge_9CH_2CH_3$]Pt(PPh_3) (**9**) (contains 1.5 molecules of hexane per formula unit)[25] were synthesized according to literature procedures. The successful synthesis of **4** was proven by determination of the unit cell parameters by single-crystal X-ray diffraction. Moreover, the isolated bulk species of **4** was characterized by powder X-ray diffraction (Figure S8, Supporting Information).[26] The purity of compounds **5**–**9** was checked by ^{1}H NMR spectroscopy and optionally by elemental analysis (for further information see Supporting Information). The deuterated solvents [D_3]acetonitrile, [D_6]benzene, and [D_8]toluene were purchased from Deutero GmbH and stored over molecular sieves (3 Å) for at least one day.

NMR Spectroscopy: NMR spectra were recorded with a BRUKER Avance Ultrashield AV400 spectrometer. The signals were referenced to the residual proton signal of the deuterated solvents [D_6]benzene (δ = 7.16 ppm) and [D_8]toluene (δ_{CH3} = 2.09 ppm). The chemical shifts are given in δ values in parts per million (ppm).

Electrospray Ionization Mass Spectrometry (ESI MS): ESI mass spectra were recorded using an Esquire HCT spectrometer from Bruker. Measurements were carried out in the negative ion mode under a capillary voltage of 4500 V using thf as solvent. Samples were prepared in a glovebox (c_M: 0.5–2 mg·mL^{-1}) and filtered through 0.2 µm PTFE syringe filters before measurement.

Raman Spectroscopy: Crystals were sealed in a glass capillary (diameter: 0.5 mm) with paraffin wax. The measurements were carried out with a Renishaw inVia Raman microscope RE04 equipped with a CCD detector (λ = 532 nm, laser power during measurement = 5.0 mW).

UV/Vis Spectroscopy: UV/Vis spectra were recorded using a Cary® 50 spectrophotometer from Varian. Standard solutions were prepared using the respective solvents. Crystals of each substance were weighed out and transferred to volumetric flasks and dissolved in the relevant solvent. All solutions were homogenized before filling up the volumetric flask. All dilutions were realized using volumetric flasks. For measurement the solutions were transferred into a taylormade Schlenk cuvette with a thickness of 10 mm.

Powder X-ray Diffraction Analysis: A PXRD pattern of **4** was recorded with a Stoe STADI P diffractometer equipped with a Ge(111) monochromator for Cu-K_α radiation (λ = 1.54056 Å) and a Dectris MYTHEN DCS 1 K solid-state detector. The crystalline isolated bulk material of **4** was ground in an agate mortar and filled into a 0.3 mm glass capillary, which was sealed. The sample was measured within a 2θ range of 4–84° (PSD steps, 0.3°; time per step, 5 s). The diffraction pattern is shown in Figure S8 (Supporting Information).

Elemental Analysis: Elemental analysis was carried out at the Department of Chemistry of the Technische Universität München. The elements C and H were determined with a combustion analyzer (Elementar vario EL, Bruker Corp.). Platinum was determined photometrically with tin(II) chloride at 404 nm.

Computational Details: Quantum-chemical structural optimizations and UV/Vis spectrum calculations on $[Ge_9]^{2-}$ and $[Ge_9$=Ge_9=$Ge_9]^{6-}$ anions were carried out using the TURBOMOLE program package.[27] We used PBE0 hybrid density functional method and a triple-zeta-valence quality basis set with polarization functions (def2-TZVP).[28] Resolution-of-the-identity technique was used to speed up the calculations.[29] The $[Ge_9]^{2-}$ and $[Ge_9$=Ge_9=$Ge_9]^{6-}$ anions were fully optimized within D_{3h} and C_1 point group symmetries, respectively. The COSMO continuum solvation model was used to counter the negative charge of the anions.[30] The excited states were investigated using the Time-Dependent DFT formalism.[31] The singlet excitations were determined at the optimized ground state S_0 geometries. In the UV/Vis calculations, the effect of COSMO was taken into account for the ground state, but not when calculating the vertical excitations. The final UV/Vis spectra were obtained by applying a Gaussian broadening of 0.25 eV.

Synthesis of K[{$(Me_3Si)_3Si$}$_3Ge_9$]:[16] Predissolved chloro-tris(trimethylsilyl)silane (101 mg, 0.36 mmol) in 3 mL acetonitrile was added to K_4Ge_9 (96 mg, 0.12 mmol). The resulting suspension was stirred at room temperature for at least 8 h. Subsequently, the reaction solution was filtered to yield a deep-red solution, which was used as obtained in further reactions.

Synthesis of {$(Me_3Si)_3Si$}$_3Ge_9(CH_2)_2CH_3$ (1): 1-Bromopropane (51 µL, 0.56 mmol) diluted in 0.5 mL acetonitrile were added to the obtained acetonitrile solution of K[{$(Me_3Si)_3Si$}$_3Ge_9$]. The mixture was stirred for 4 h at room temperature yielding a brown suspension. The suspension was left to rest at –32 °C to allow the precipitate to settle down. The supernatant was decanted and the precipitate washed three times with a total amount of 6 mL acetonitrile. The solid was dried in vacuo yielding a brown solid (65 % yield). The obtained brown solid was dissolved in toluene, filtered through glass fiber filter, concentrated under vacuum and stored at –32 °C for crystallization. Dark-orange, block-shaped crystals were obtained after three weeks (30 % yield). The crystals were separated from the mother liquor, washed with a little amount of acetonitrile and dried in vacuo. **^{1}H NMR** (400 MHz, [D_6]benzene, 298 K): δ = 1.83 (m, 2 H, -CH_2–CH_2–CH_3), 1.77 (m, 2 H, –CH_2–CH_2–CH_3), 0.97 (t, 3 H, ^3J = 7.2 Hz, –CH_2–CH_2–CH_3), 0.42 [s, 81 H, –Si(CH_3)$_3$]. **^{29}Si NMR** (79 MHz, [D_6]benzene, 298 K): δ = –8.28 [–Si(CH_3)$_3$], –105.93 [–Si(Si(CH_3)$_3$)$_3$]. **^{13}C NMR** (101 MHz, [D_6]benzene, 298 K): δ = 30.7 (–CH_2–CH_2–CH_3), 18.6 (–CH_2–CH_2–CH_3), 13.7 (–CH_2–CH_2–CH_3), 2.7 [Si(CH_3)$_3$]. **ESI-MS** (*m*/*z*): 1397 [{$(Me_3Si)_3Si$}$_3Ge_9$]$^-$, 1193

$[\{(Me_3Si)_3Si\}_2Ge_9(CH_2)_2CH_3]^-$. **Raman**: $\tilde{\nu}$ = 2948 [ν_a(C–H)], 2890 [ν_s(C–H)], 740 [ν_a(Si–C)], 691 [ν_a(Si–C)], 624 [δ_s(Si–C)], 241 (Ge_9 cluster), 149 (Ge_9 cluster) cm^{-1}.[32]

Synthesis of $\{(Me_3Si)_3Si\}_3Ge_9(CH_2)_2CH{=}CH_2$ (2): 4-Bromo-1-butene (68 µL, 0.67 mmol) diluted in 0.5 mL acetonitrile were added to the obtained acetonitrile solution of $K[\{(Me_3Si)_3Si\}_3Ge_9]$. The mixture was stirred for 4 h at room temperature yielding a brown suspension. The suspension was left to rest at –32 °C to allow the precipitate to settle down. The supernatant was decanted and the precipitate washed three times with a total amount of 6 mL acetonitrile. The solid was dried in vacuo yielding a brown solid (58 % yield). A little amount of the obtained brown solid was dissolved in [D_6]benzene NMR spectroscopically investigated. **^{1}H NMR** (400 MHz, [D_6]benzene, 298 K): δ = 5.77 [ddt, ^3J = 16.4, 10.0, 6.4 Hz, 1 H, $-(CH_2)_2CH{=}CH_2$], 5.00 [dd, ^3J = 16.4, 1.6 Hz, 1 H, $-(CH_2)_2CH{=}CH_{cis}H_{trans}$], 4.93 [d, ^3J = 10.0 Hz, 1 H, $-(CH_2)_2CH{=}CH_{cis}H_{trans}$], 2.52 (m, 2 H, $-CH_2CH_2CH{=}CH_2$), 1.91 (m, 2 H, $-CH_2CH_2CH{=}CH_2$), 0.41 [s, 81 H, $Si(CH_3)_3$]. **^{29}Si NMR** (79 MHz, [D_6]benzene, 298 K): δ = –8.22 [$-Si(CH_3)_3$], –105.73 [$-Si(Si(CH_3)_3)_3$]. **ESI-MS** (*m*/*z*): 1397 $[\{(Me_3Si)_3Si\}_3Ge_9]^-$, 1205 $[\{(Me_3Si)_3Si\}_2Ge_9(CH_2)_2CH{=}CH_2]^-$.

Synthesis of $\{(Me_3Si)_3Si\}_3Ge_9(CH_2)_3C_6H_5$ (3): 1-Bromo-3-phenylpropane (18 µL, 0.12 mmol) diluted in 0.5 mL acetonitrile were added to the obtained acetonitrile solution of $K[\{(Me_3Si)_3Si\}_3Ge_9]$. The mixture was stirred for 4 h at room temperature yielding a brown suspension. The suspension was left to rest at –32 °C to allow the precipitate to settle down. The supernatant was decanted and the precipitate washed three times with a total amount of 6 mL acetonitrile. The solid was dried in vacuo yielding a brown solid (58 % yield). A little amount of the obtained brown solid was dissolved in [D_6]benzene NMR spectroscopically investigated. **^{1}H NMR** (400 MHz, [D_6]benzene, 298 K): δ = 7.09 [overlap with C_6H_6, $-(CH_2)_3C_6H_5$], 2.64 [t, ^3J = 7.2 Hz, 2 H, $-CH_2CH_2CH_2C_6H_5$], 2.09 (m, 2 H, $-CH_2CH_2CH_2C_6H_5$), 1.83 (m, 2 H, $-CH_2CH_2CH_2C_6H_5$), 0.40 [s, 81 H, $Si(CH_3)_3$]. **ESI-MS** (*m*/*z*): 1397 $[\{(Me_3Si)_3Si\}_3Ge_9]^-$, 1269 $[\{(Me_3Si)_3Si\}_2Ge_9(CH_2)_3C_6H_5]^-$.

Supporting Information (see footnote on the first page of this article): NMR spectroscopic characterization of **1**, **2**, **3**, **5**, **6**, **7**, **8**, and **9;** electron-spray ionization mass spectra of **1**, **2**, and **3**; elemental analysis for **8** and **9**; Raman spectrum of **1**; P-XRD of crystals of **4,** UV-Vis electronic spectrum of **7**, simulated UV-Vis spectra of $[Ge_9]^{2-}$ and $[Ge_9{=}Ge_9{=}Ge_9]^{6-}$.

Acknowledgements

The authors thank the "Bayerische Staatsministerium für Wirtschaft und Medien, Energie und Technologie" within the program "Solar Technologies go Hybrid" for financial support. We further thank *Prof. Dr. Bernhard Rieger* (Wacker-Chair of Macromolecular Chemistry, Technical University of Munich) and *M.Sc. Markus Pschenitza* for provision of and introduction into the UV/Vis spectrometer. Furthermore, the authors acknowledge *Maria Weindl* for temperature-dependent NMR-studies, as well as *M.Sc. Sebastian Geier* for Raman measurements.

Keywords: Cluster compounds; Germanium, Functionalities, UV/Vis spectroscopy; Agglomeration

References

[1] a) J. L. Segura, N. Martín, *Chem. Soc. Rev.* **2000**, *29*, 13–25; b) M. A. Lebedeva, T. W. Chamberlain, E. S. Davies, B. E. Thomas, M. Schröder, A. N. Khlobystov, *Beilstein J. Org. Chem.* **2014**, *10*, 332–343.
[2] T. F. Fässler, *Angew. Chem. Int. Ed.* **2001**, *40*, 4161–4165.
[3] S. Scharfe, F. Kraus, S. Stegmaier, A. Schier, T. F. Fässler, *Angew. Chem. Int. Ed.* **2011**, *50*, 3630–3670.
[4] L. Xu, S. C. Sevov, *J. Am. Chem. Soc.* **1999**, *121*, 9245–9246.
[5] C. Downie, Z. Tang, A. M. Guloy, *Angew. Chem. Int. Ed.* **2000**, *39*, 337–340.
[6] K. Komatsu, G.-W. Wang, Y. Murata, T. Tanaka, K. Fujiwara, K. Yamamoto, M. Saunders, *J. Org. Chem.* **1998**, *63*, 9358–9366.
[7] D. S. Sabirov, *RSC Adv.* **2013**, *3*, 19430–19439.
[8] F. Giacalone, N. Martin, *Chem. Rev.* **2006**, *106*, 5136–5190.
[9] a) M. M. Bentlohner, W. Klein, Z. H. Fard, L.-A. Jantke, T. F. Fässler, *Angew. Chem. Int. Ed.* **2015**, *54*, 3748–3753; b) S. Frischhut, M. M. Bentlohner, W. Klein, T. F. Fässler, *Inorg. Chem.* **2017**, *56*, 10691–10698; c) M. M. Bentlohner, S. Frischhut, T. F. Fässler, *Chem. Eur. J.* **2017**, *23*, 17089–17094.
[10] L. M. Wheeler, L. M. Levij, U. R. Kortshagen, *J. Phys. Chem. Lett.* **2013**, *4*, 3392–3396.
[11] M. Pelton, Y. Tang, O. M. Bakr, F. Stellacci, *J. Am. Chem. Soc.* **2012**, *134*, 11856–11859.
[12] a) M. W. Hull, S. C. Sevov, *Angew. Chem. Int. Ed.* **2007**, *46*, 6695–6698; b) M. W. Hull, S. C. Sevov, *J. Am. Chem. Soc.* **2009**, *131*, 9026–9037; c) M. W. Hull, S. C. Sevov, *Chem. Commun.* **2012**, *48*, 7720–7722.
[13] a) M. W. Hull, S. C. Sevov, *Inorg. Chem.* **2007**, *46*, 10953–10955; b) C. B. Benda, J. Q. Wang, B. Wahl, T. F. Fässler, *Eur. J. Inorg. Chem.* **2011**, *27*, 4262–4269.
[14] M. W. Hull, A. Ugrinov, I. Petrov, S. C. Sevov, *Inorg. Chem.* **2007**, *46*, 2704–2708.
[15] A. Schnepf, *Angew. Chem. Int. Ed.* **2003**, *42*, 2624–2625.
[16] F. Li, S. C. Sevov, *Inorg. Chem.* **2012**, *51*, 2706–2708.
[17] a) F. Li, S. C. Sevov, *J. Am. Chem. Soc.* **2014**, *136*, 12056–12063; b) S. Frischhut, T. F. Fässler, *Dalton Trans.* **2018**, *47*, 3223–3226.
[18] S. Frischhut, W. Klein, M. Drees, T. F. Fässler, *Chem. Eur. J.* **2018**, *24*, 9009–9014.
[19] F. Li, A. Muñoz-Castro, S. C. Sevov, *Angew. Chem. Int. Ed.* **2016**, *55*, 8630–8633.
[20] a) K. Mayer, L. J. Schiegerl, T. Kratky, S. Günther, T. F. Fässler, *Chem. Commun.* **2017**, *53*, 11798–11801; b) F. S. Geitner, J. V. Dums, T. F. Fässler, *J. Am. Chem. Soc.* **2017**, *139*, 11933–11940; c) F. Geitner, C. Wallach, T. F. Fässler, *Chem. Eur. J.* **2018**, *24*, 4103–4110; d) F. Geitner, W. Klein, T. F. Fässler, Angew. Chem. Int. Ed. **2018**, online (DOI: 10.1002/anie.201803476).
[21] M. Klinger, C. Schenk, F. Henke, A. Clayborne, A. Schnepf, A.-N. Unterreiner, *Chem. Commun.* **2015**, *51*, 12278–12281.
[22] J. P. Hare, H. W. Kroto, R. Taylor, *Chem. Phys. Lett.* **1991**, *177*, 394–398.
[23] C. Hoch, M. Wendorff, C. Röhr, *J. Alloys Compd.* **2003**, *361*, 206–221.
[24] J. Åkerstedt, S. Ponou, L. Kloo, S. Lidin, *Eur. J. Inorg. Chem.* **2011**, *2011*, 3999–4005.
[25] S. Frischhut, F. Kaiser, W. Klein, M. Drees, F. E. Kühn, T. F. Fässler, submitted.
[26] An NMR spectroscopic proof of the presence of the $[Ge_9]^{4-}$ clusters in acetonitrile solutions cannot be provided. Also, mass spectrometry does not allow for a statement about the presence of **4** in acetonitrile solutions.
[27] a) TURBOMOLE V7.2 2017, 1989–2007, TURBOMOLE GmbH, since 2007; available from www.turbomole.com; b) R. Ahlrichs, M. Bär, M. Häser, H. Horn, C. Kölmel, *Chem. Phys. Lett.* **1989**, *162*, 165–169.
[28] a) J. P. Perdew, K. Burke, M. Ernzerhof, *Phys. Rev. Lett.* **1996**, *77*, 3865; b) C. Adamo, V. Barone, *J. Chem. Phys.* **1999**, *110*, 6158–6170; c) F. Weigend, R. Ahlrichs, *Phys. Chem. Chem. Phys.* **2005**, *7*, 3297–3305.
[29] a) K. Eichkorn, O. Treutler, H. Öhm, M. Häser, R. Ahlrichs, *Chem. Phys. Lett.* **1995**, *232–247*, 283–290; b) F. Weigend, *Phys. Chem. Chem. Phys.* **2006**, *8*, 1057–1065.

[30] A. Klamt, G. Schüürmann, *J. Chem. Soc. Perkin Trans. 2* **1993**, 799–805.
[31] F. Furche, D. Rappoport, *Density Functional Methods for Excited States: Equilibrium Structure and Electronic Spectra*, in *Computational Photochemistry*, vol. 16 *Computational and Theoretical Chemistry* (Ed.: M. Olivucci), ch. III. Elsevier, Amsterdam, **2005**.
[32] a) B. H. Boo, *J. Korean Phys. Soc.* **2011**, *59*, 3192–3200; b) H. Von Schnering, M. Baitinger, U. Bolle, W. Carrillo-Cabrera, J. Curda, Y. Grin, F. Heinemann, J. Llanos, K. Peters, A. Schmeding, *Z. Anorg. Allg. Chem.* **1997**, *623*, 1037–1039; c) C. Fischer, W. Klein, L.-A. Jantke, L. J. Schiegerl, T. F. Fässler, *Z. Anorg. Allg. Chem.* **2016**, *642*, 1314–1319.

Received: July 5, 2018
Published online: August 16, 2018

Z. Anorg. Allg. Chem. **2018** · ISSN 0044–2313

SUPPORTING INFORMATION

Title: On the Affinity between Fullerenes and Deltahedral Zintl Ions: A UV/Vis Spectroscopic Investigation

Author(s): S. Frischhut, J. G. Machado de Carvalho, A. J. Karttunen, T. F. Fässler*

Ref. No.: z201800293

On the Affinity between Fullerenes and Deltahedral Zintl Ions: a UV-Vis Spectroscopic Investigation

Sabine Frischhut[+[a]], João G. Machado de Carvalho[+[a]], Antti J. Karttunen[[b]], and Thomas F. Fässler[[a]*]

[a] Sabine Frischhut, João G. Machado de Carvalho, Thomas F. Fässler

Department Chemie, Technische Universität München

Lichtenbergstraße 4, 85747 Garching, Germany

E-mail: thomas.faessler@lrz.tum.de

[b] Prof. Dr. Antti J. Karttunen

Department of Chemistry and Materials Science, Aalto University

P.O. Box 16100, FI-00076 Aalto, Finland

Content

1 Characterization of **1**

1.1 NMR spectroscopic characterization of **1**

Figure S1. a) ^{1}H, b) ^{1}H ^{1}H COSY, c) ^{29}Si, d) 13C, e) ^{1}H ^{13}C HSQC and f) ^{1}H ^{13}C HMBC NMR spectrum of crystals of **1** dissolved in [D_6]benzene recorded at r.t.

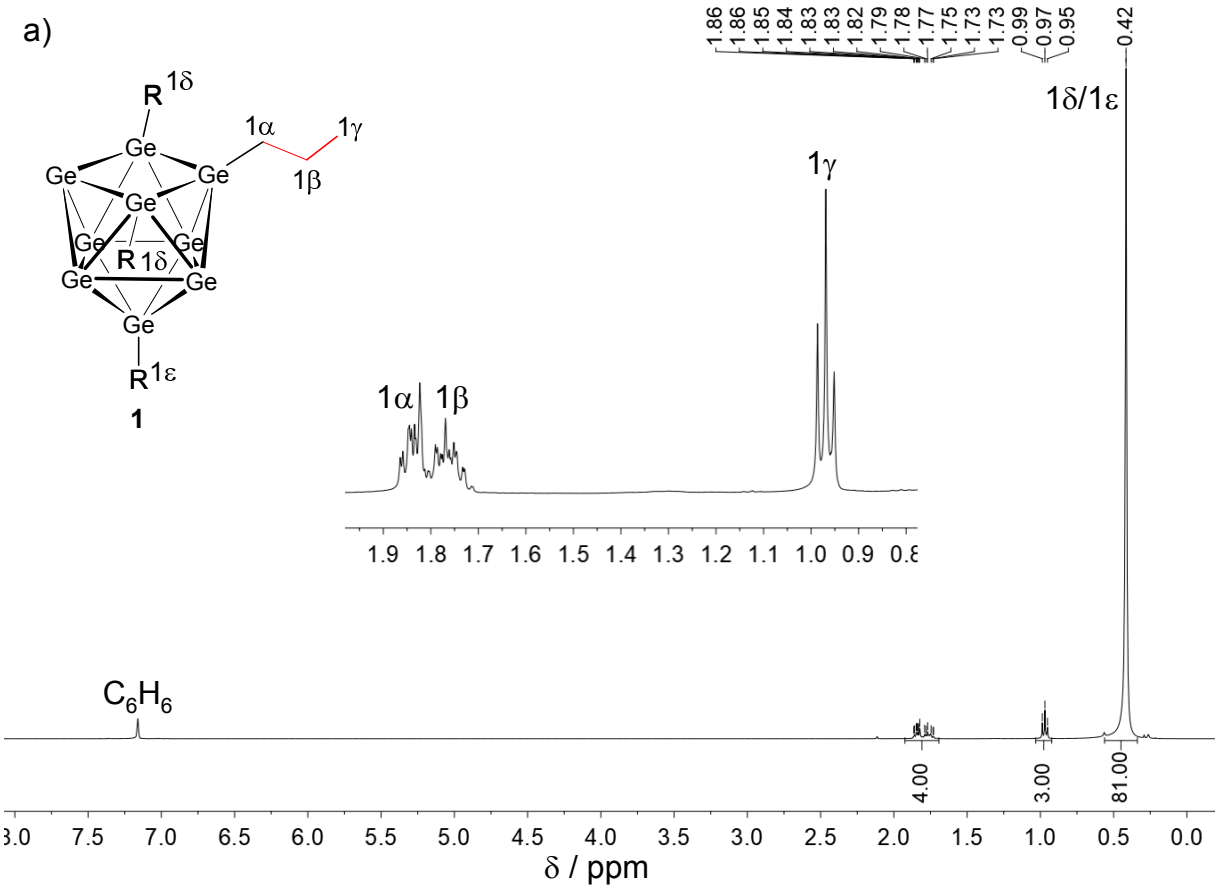

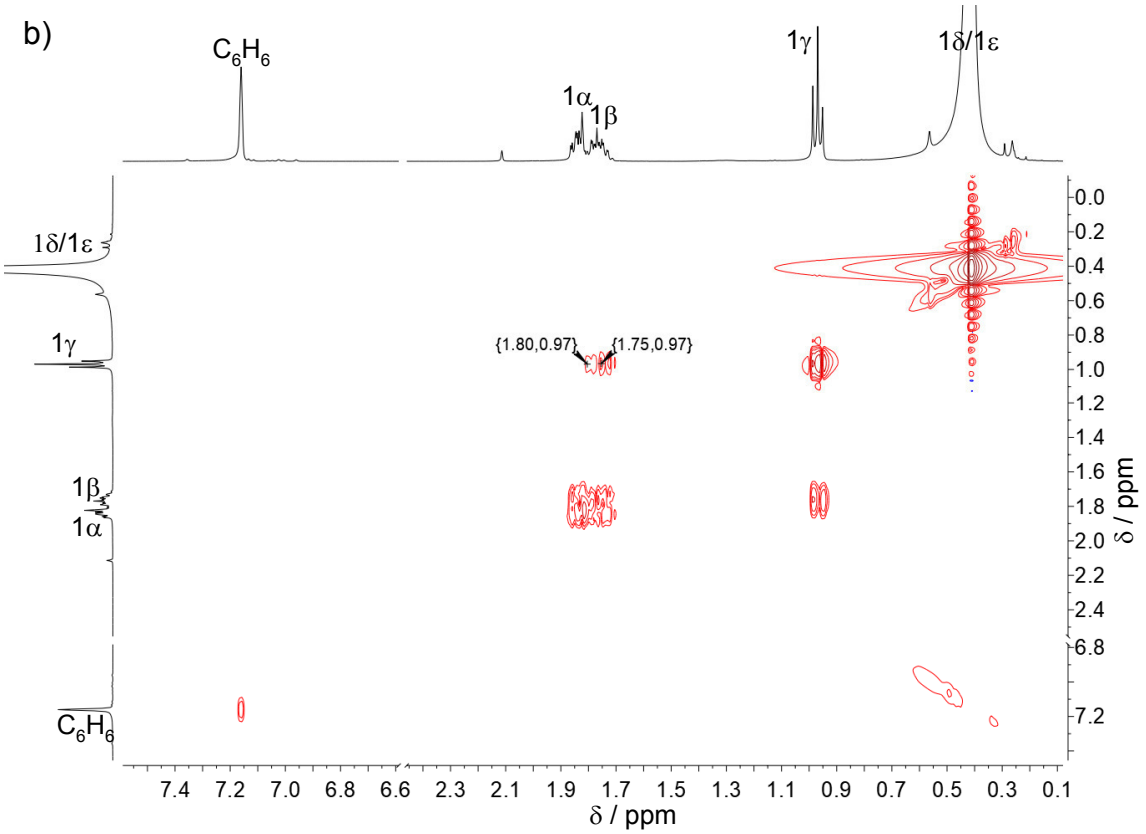
b)
C6H6
1α
1β
1γ
1δ/1ε
{1.80,0.97}
{1.75,0.97}
δ / ppm

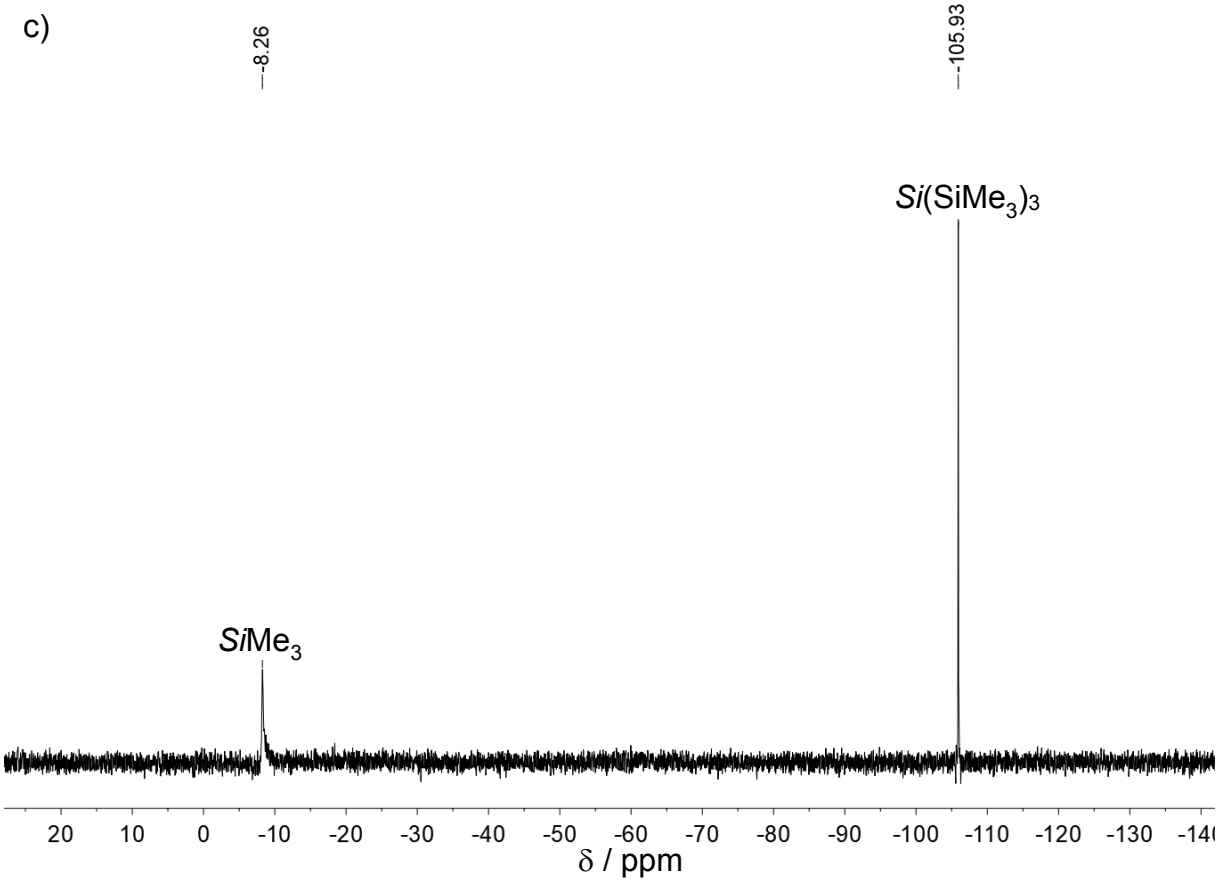
c)
8.26
105.93
Si(SiMe3)3
SiMe3
δ / ppm

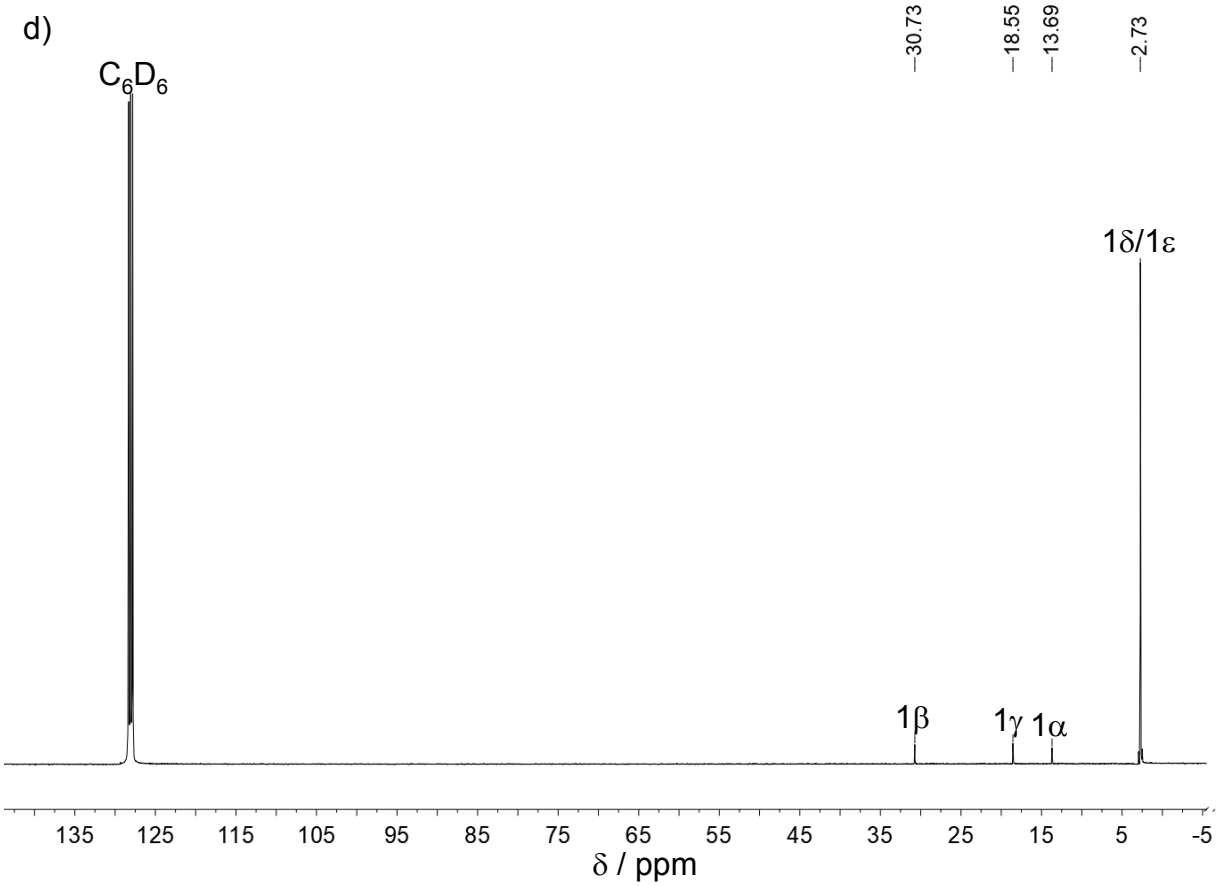
d)
C6D6
30.73
18.55
13.69
2.73
1δ/1ε
1β
1γ
1α
135 125 115 105 95 85 75 65 55 45 35 25 15 5 -5
δ / ppm

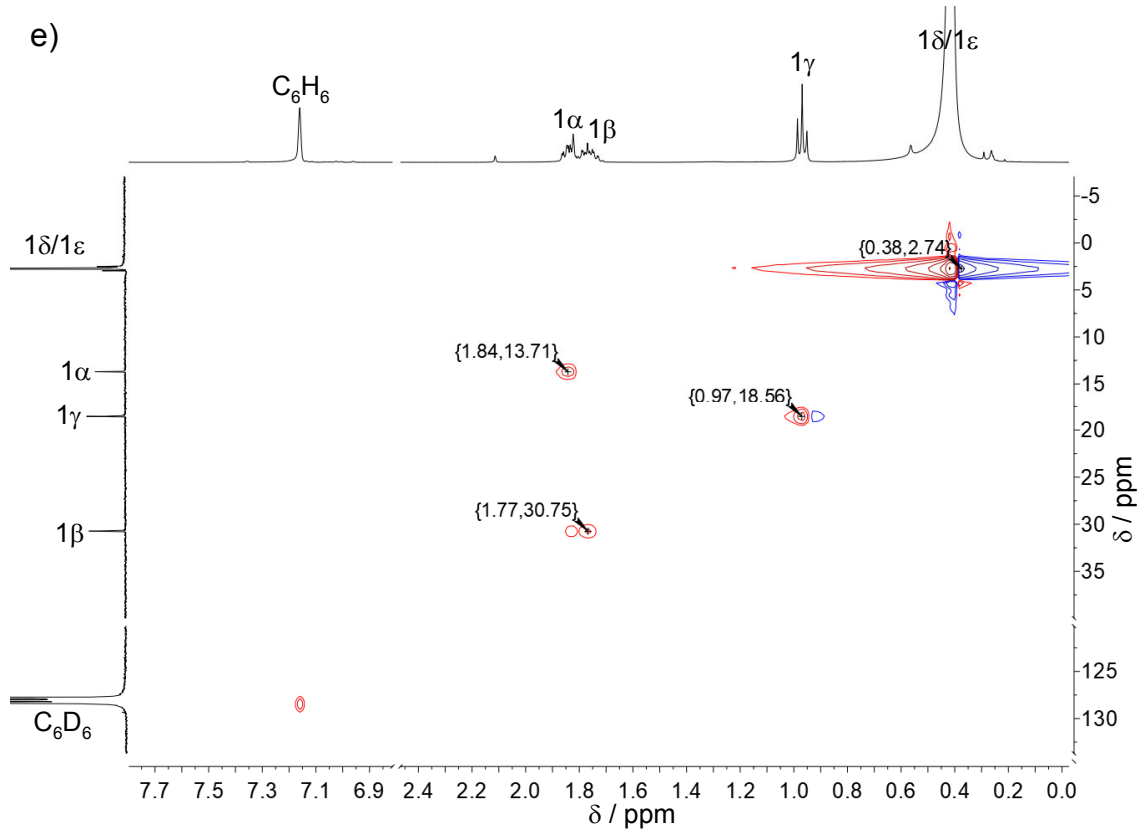
e)
C6H6
1α
1β
1γ
1δ/1ε
{0.38,2.74}
{1.84,13.71}
{0.97,18.56}
{1.77,30.75}
C6D6
7.7 7.5 7.3 7.1 6.9 2.4 2.2 2.0 1.8 1.6 1.4 1.2 1.0 0.8 0.6 0.4 0.2 0.0
δ / ppm
-5 0 5 10 15 20 25 30 35 125 130
δ / ppm

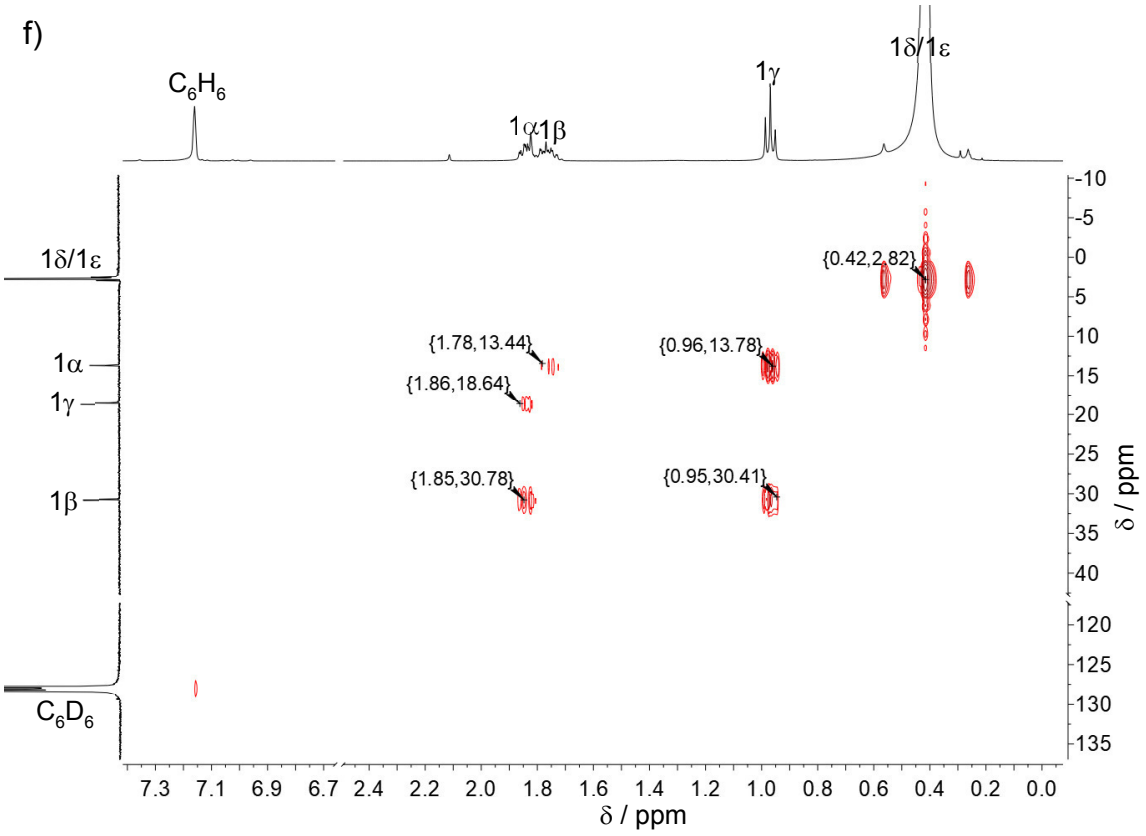

1.2 Electron-spray ionization mass spectrum of **1**

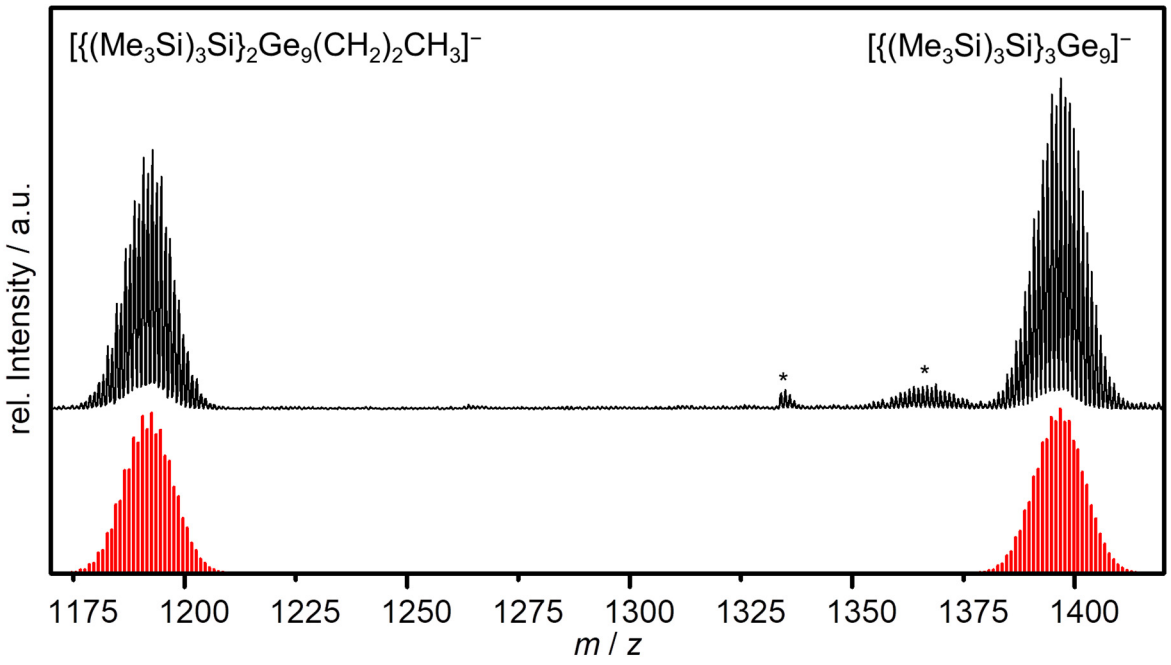

Figure S2. ESI mass spectrum of dissolved crystals of **1** in thf in black recorded in the negative ion mode. Simulated patterns of $[\{(Me_3Si)_3Si\}_2Ge_9(CH_2)_2CH_3]^-$ and $[\{(Me_3Si)_3Si\}_3Ge_9]^-$ are depicted in red below. The signals marked with * could not be assigned.

1.3 Raman spectrum of **1**

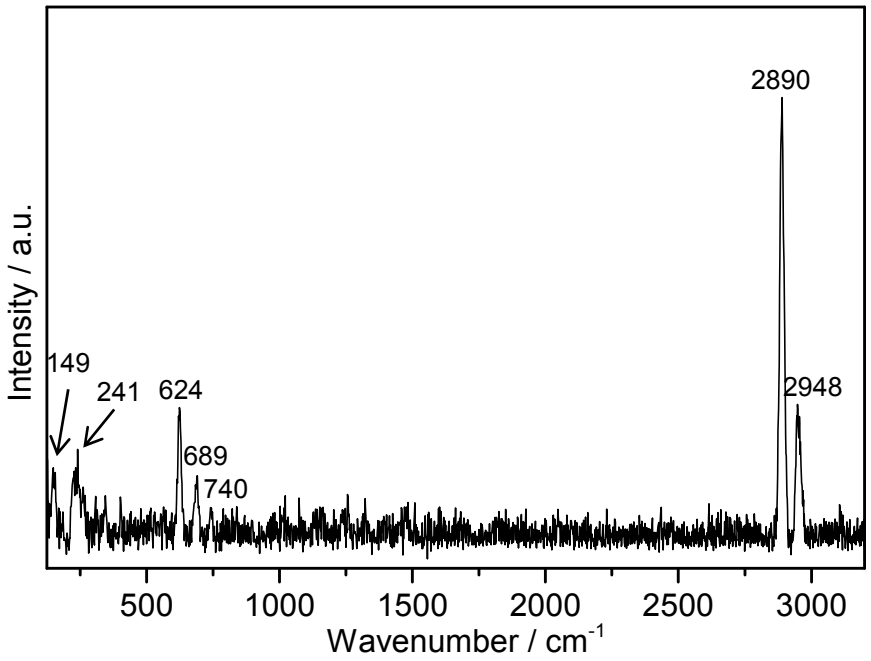

Figure S3. Raman spectrum of crystals of **1**.

2 Characterization of **2**

2.1 NMR spectroscopic characterization of **2**

Figure S4. a) ^{1}H, b) ^{1}H ^{1}H COSY and c) ^{29}Si NMR spectrum of dissolved precipitate of **2** in [D_6]benzene recorded at r.t. Signals marked with * could not be assigned.

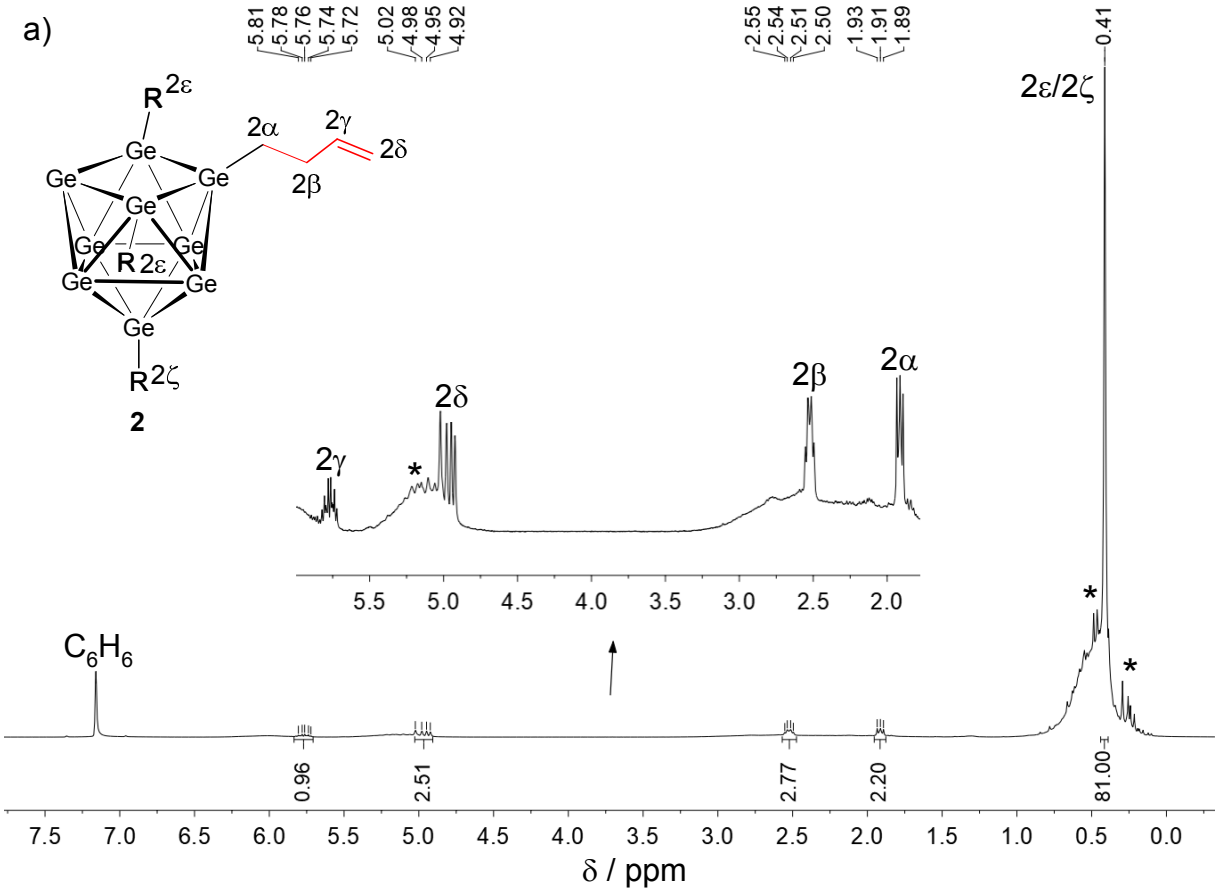

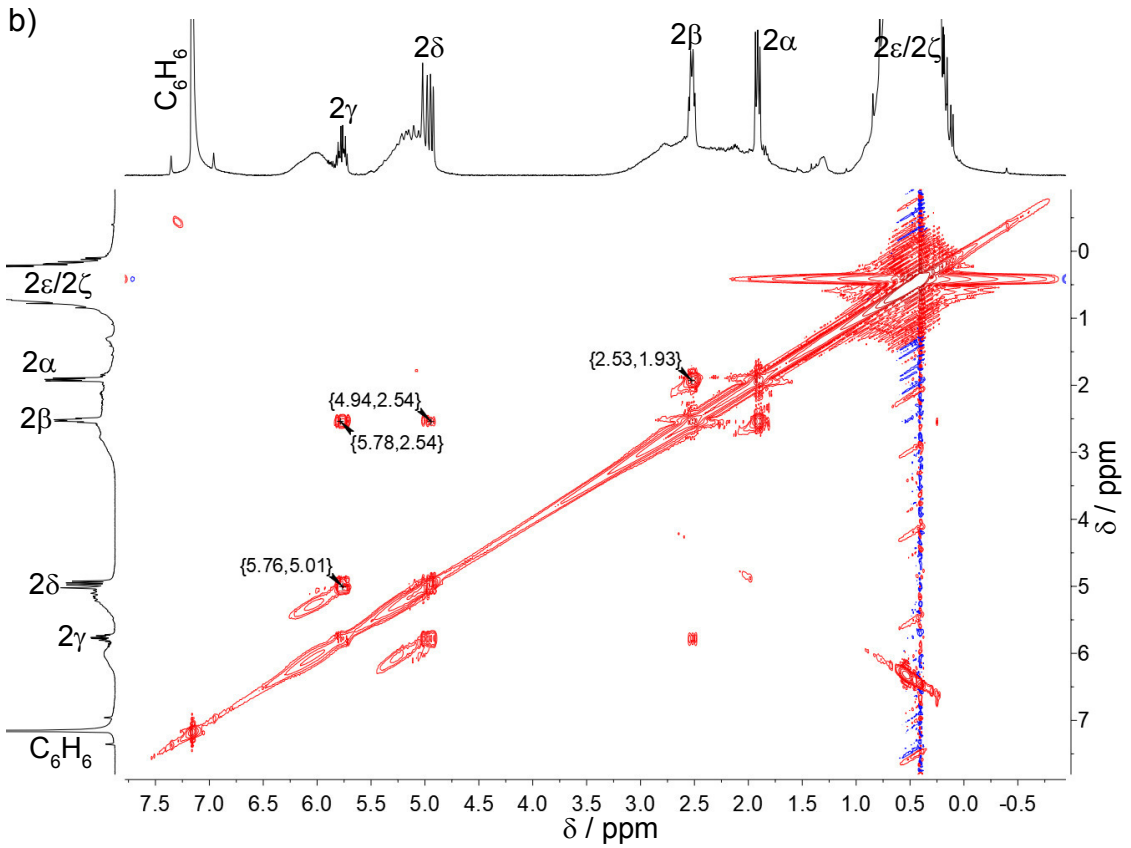
b)
C6H6
2γ
2δ
2β
2α
2ε/2ζ
{2.53,1.93}
{4.94,2.54}
{5.78,2.54}
{5.76,5.01}
δ / ppm

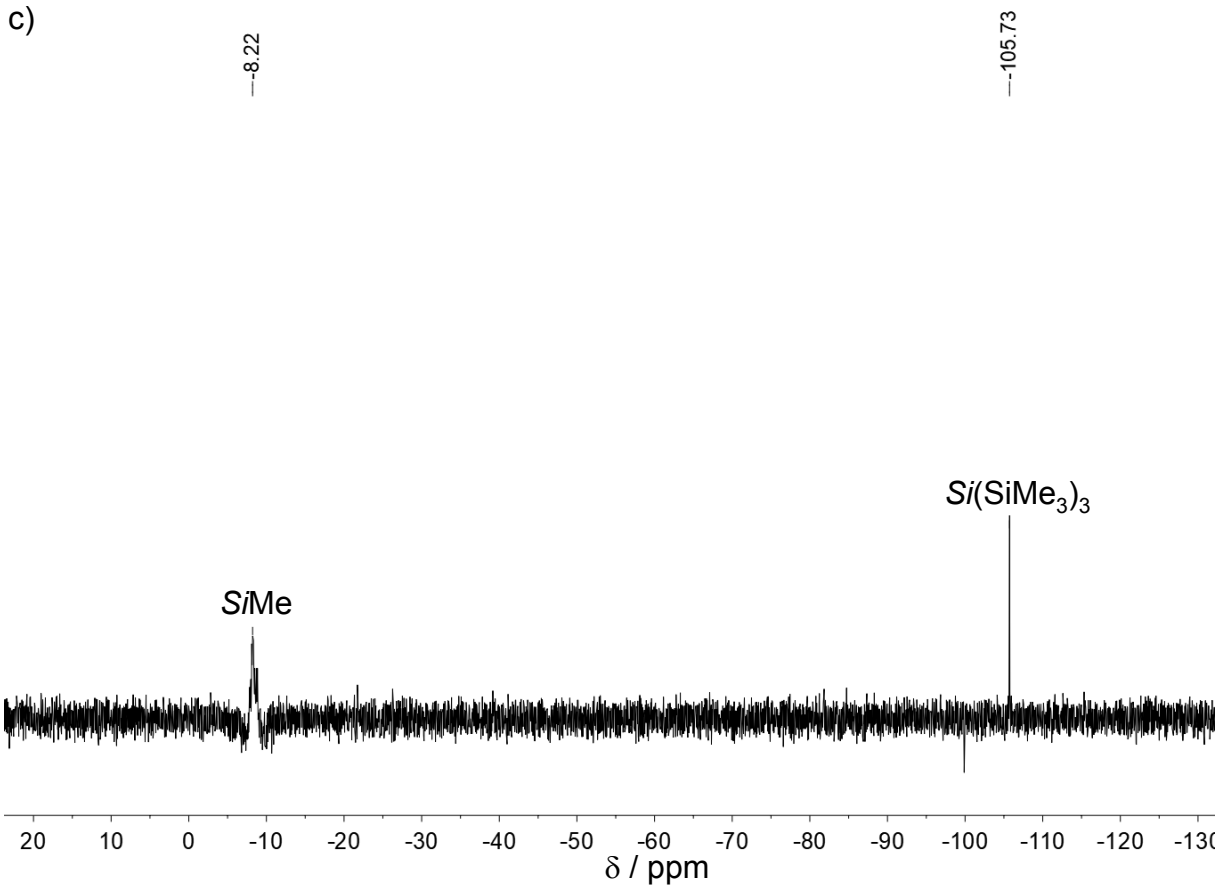
c)
-8.22
-105.73
SiMe
Si(SiMe3)3
δ / ppm

2.2 Electron-spray ionization mass spectrum of **2**

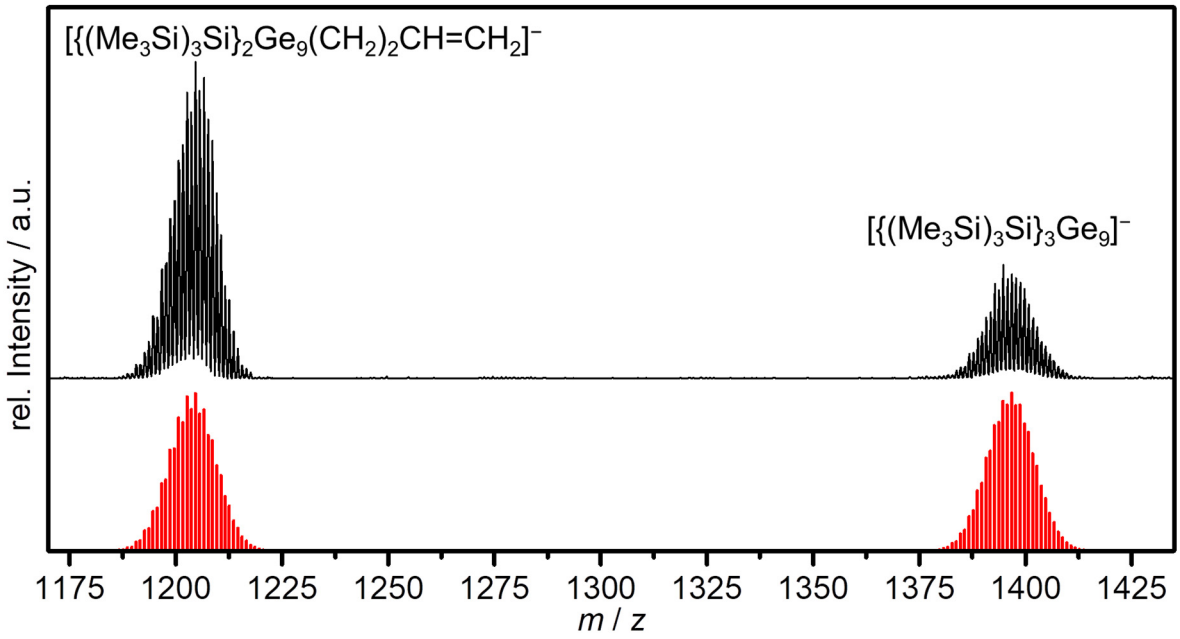

Figure S5. ESI mass spectrum of dissolved precipitate of **2** in thf in black recorded in the negative ion mode. Simulated patterns of $[\{(Me_3Si)_3Si\}_2Ge_9(CH_2)_2CH=CH_2]^-$ and $[\{(Me_3Si)_3Si\}_3Ge_9]^-$ are depicted in red below.

3 Characterization of 3

3.1 NMR spectroscopic characterization of 3

Figure S6. a) ^{1}H and b) ^{1}H ^{1}H COSY spectrum of dissolved precipitate of **3** in [D6]benzene recorded at r.t. Signals marked with * could not be assigned.

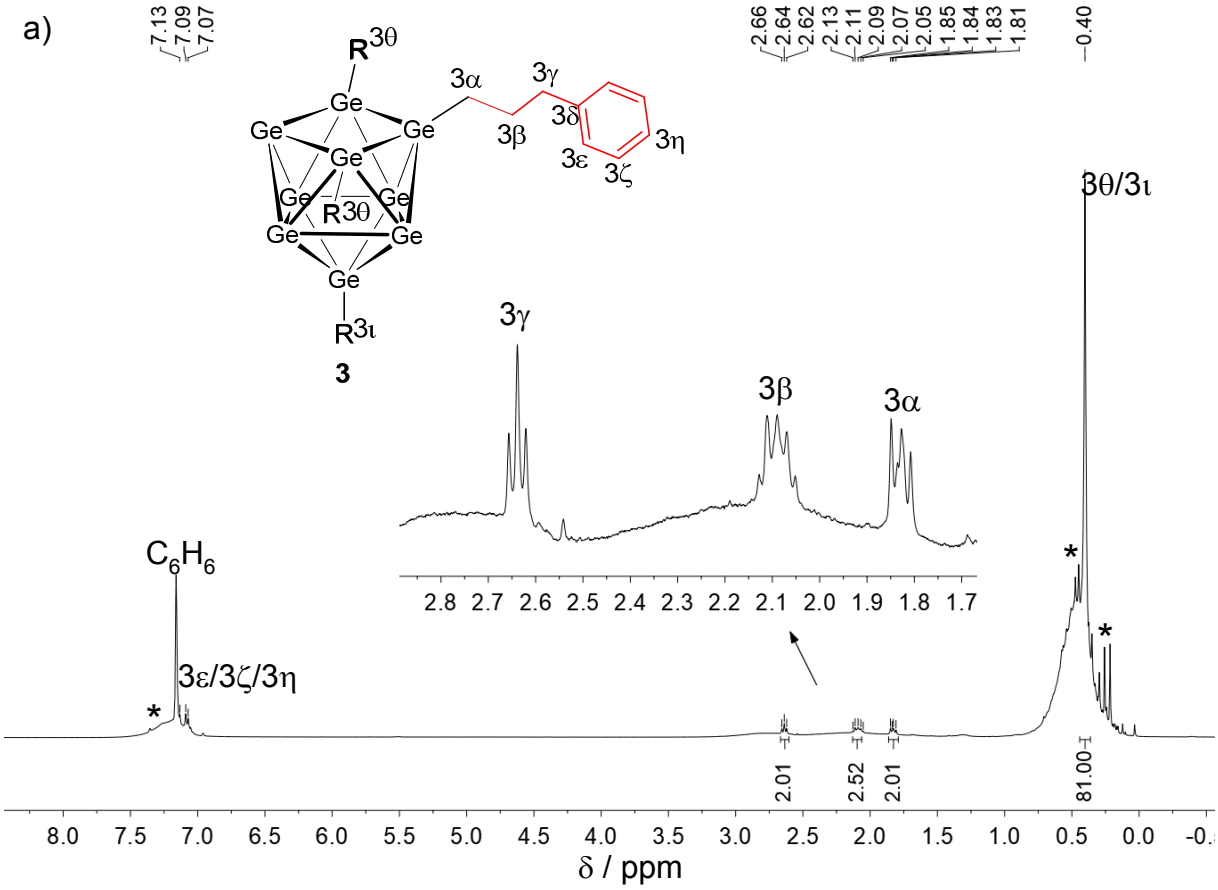

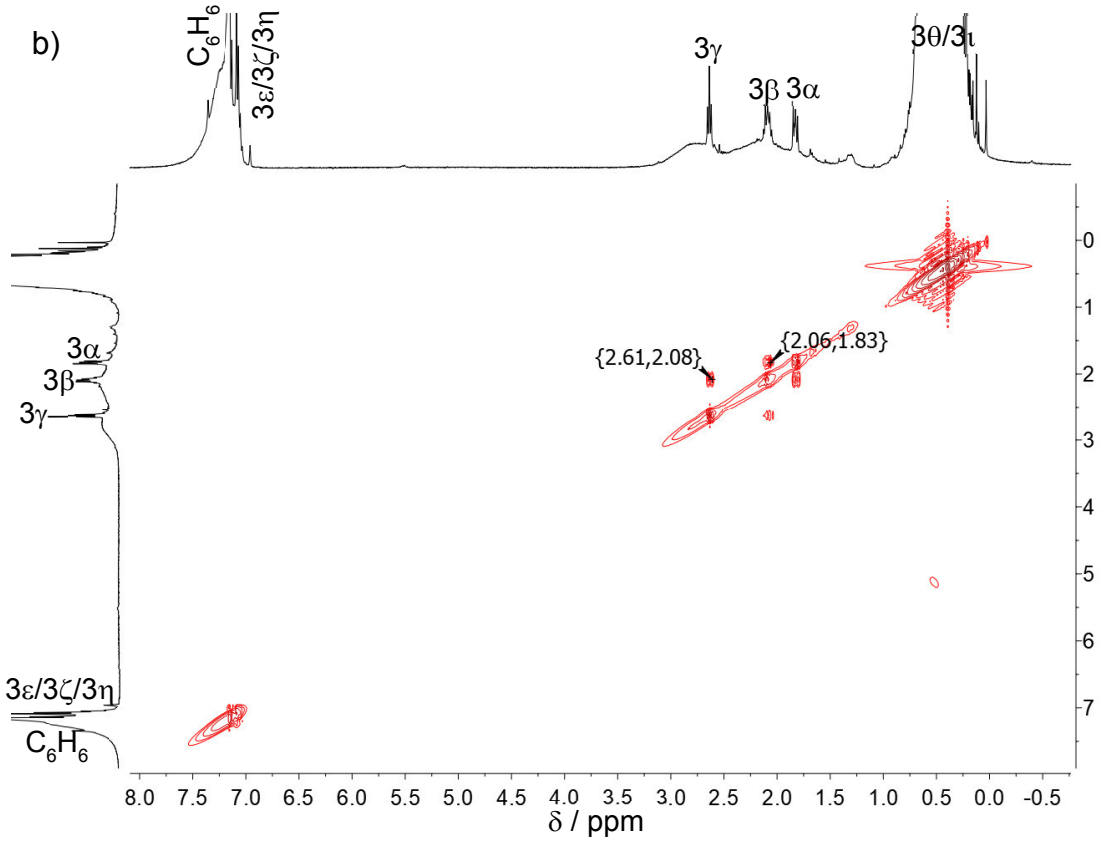

3.2 Electron-spray ionization mass spectrum of **3**

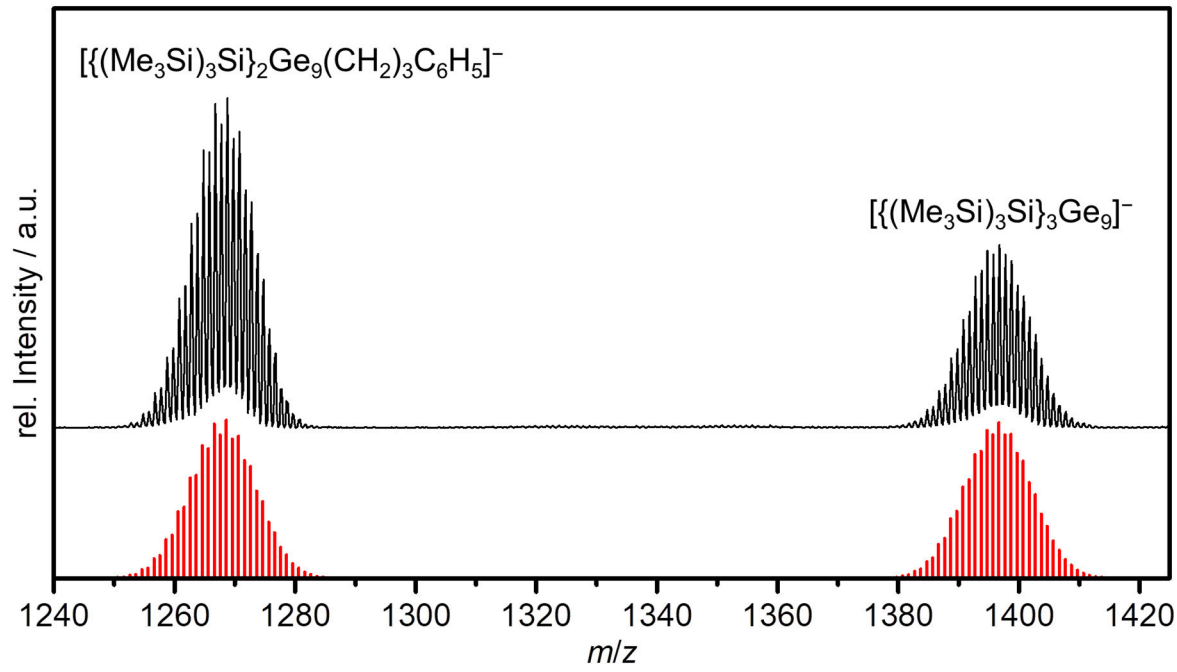

Figure S7. ESI mass spectrum of dissolved precipitate of **3** in thf in black recorded in the negative ion mode. Simulated patterns of $[\{(Me_3Si)_3Si\}_2Ge_9(CH_2)_3C_6H_5]^-$ and $[\{(Me_3Si)_3Si\}_3Ge_9]^-$ are depicted in red below.

4 Analytical Data of compounds **4**-**9**

4.1 Compound **4**

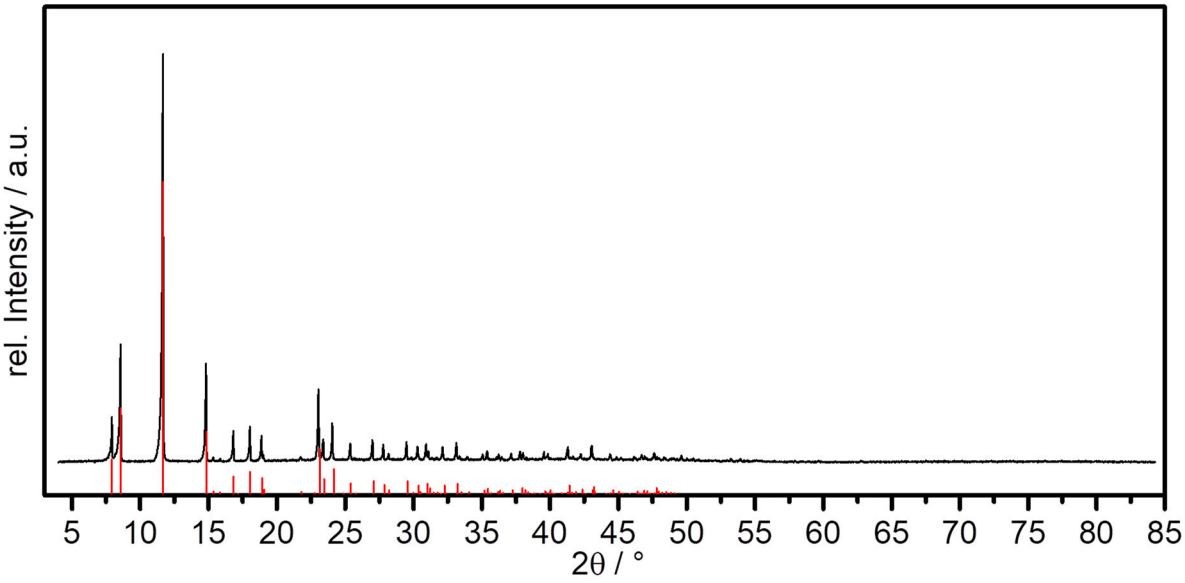

Figure S8. P-XRD pattern of crystals of **4** (black) and theoretical pattern taken from the single crystal data (rot).[1]

4.2 Compound **5**

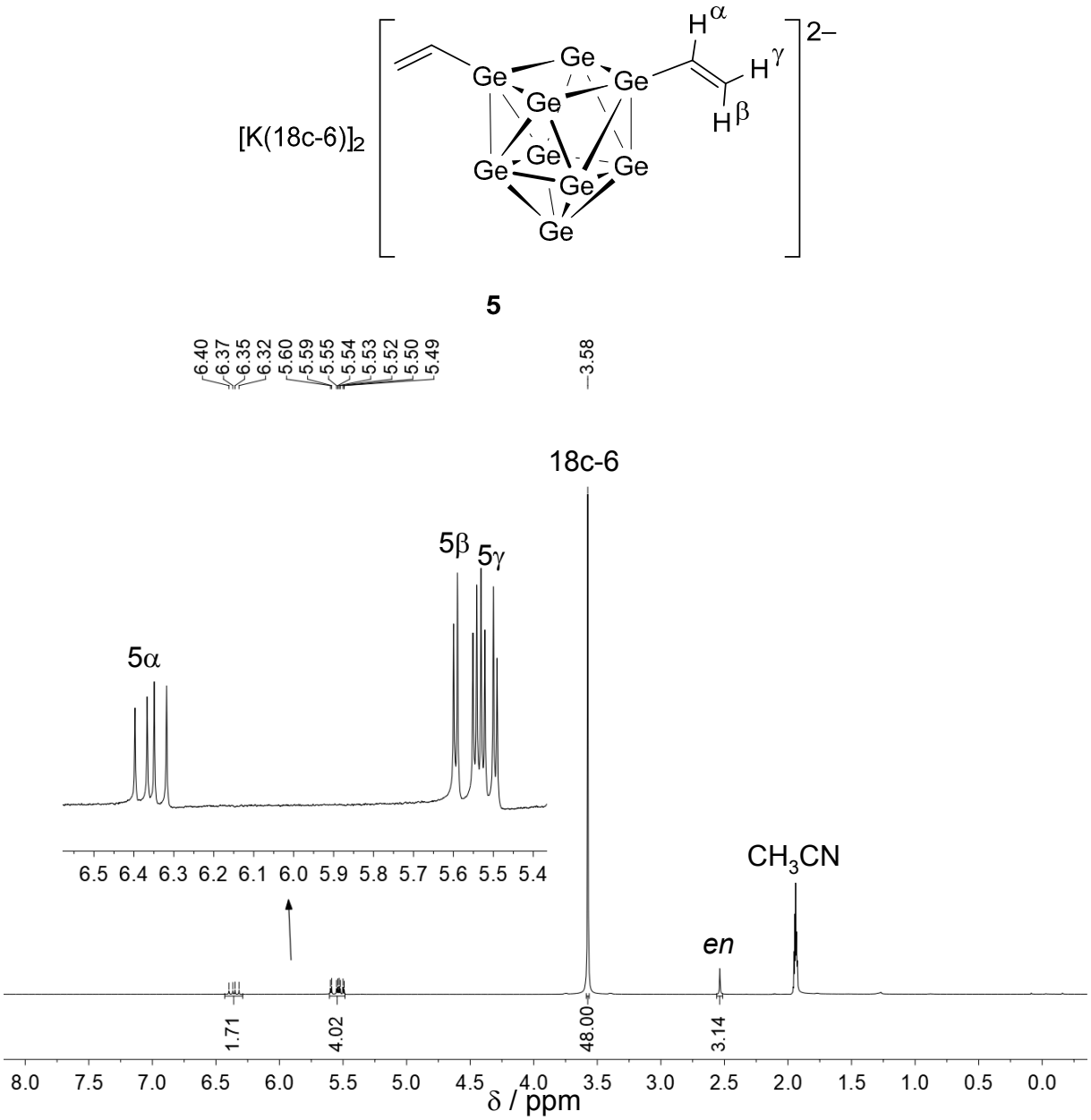

Figure S9. ^{1}H NMR spectrum of crystals of **5** recorded in [D_3]acetonitrile at r.t.

4.3 Compound 6

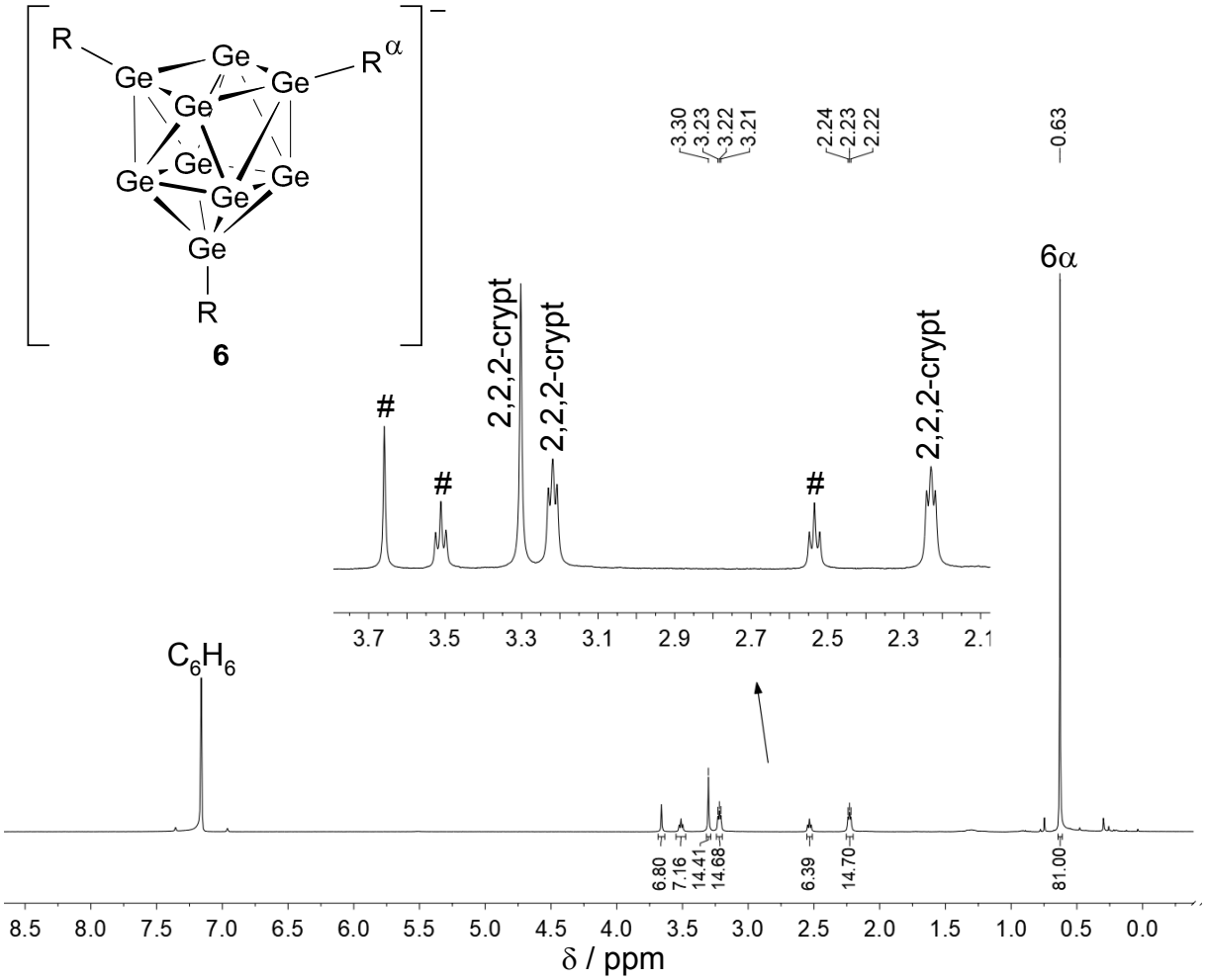

Figure S10. ^{1}H NMR spectrum of crystals of **5** recorded in [D_6]benzene at r.t.

4.4 Compound **7**

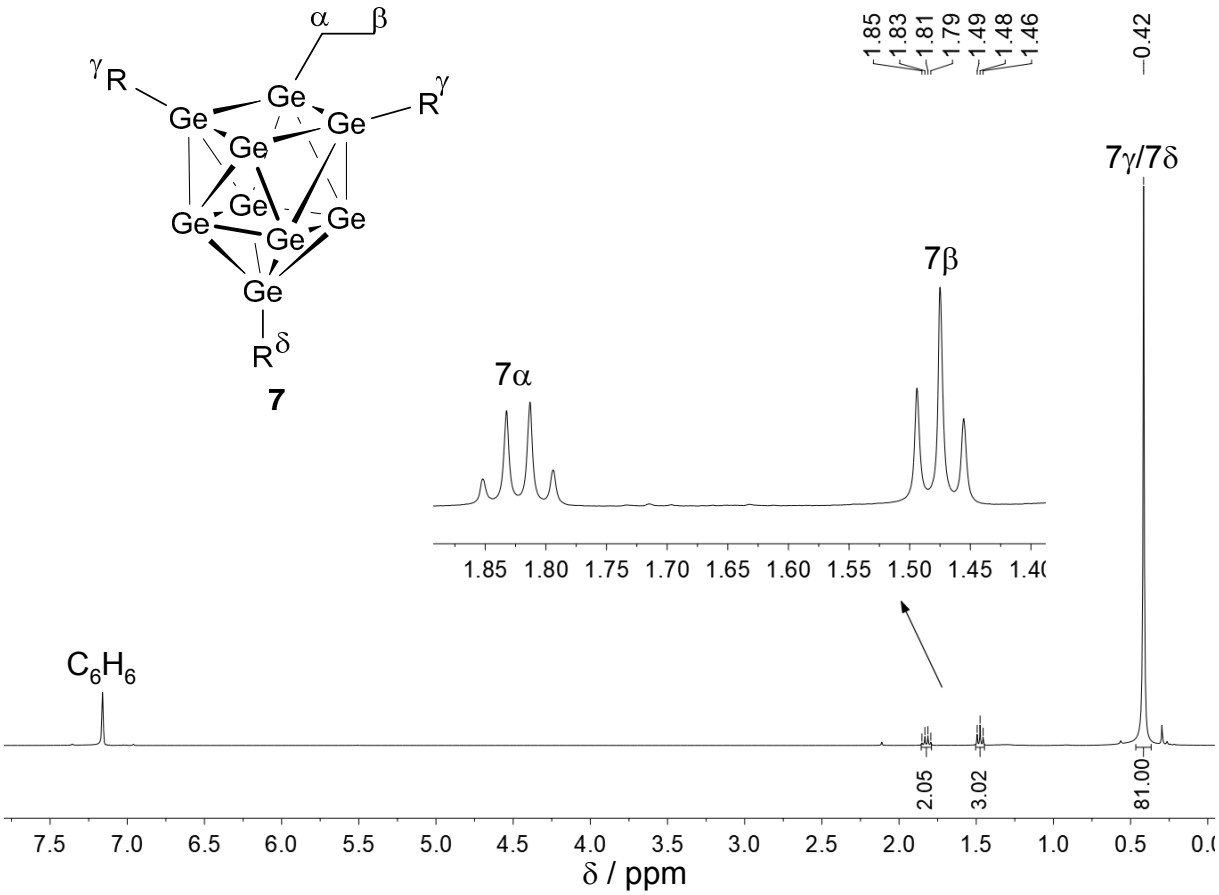

Figure S11. ^{1}H NMR spectrum of crystals of **7** recorded in [D_6]benzene at r.t.

4.5 Compound **8**

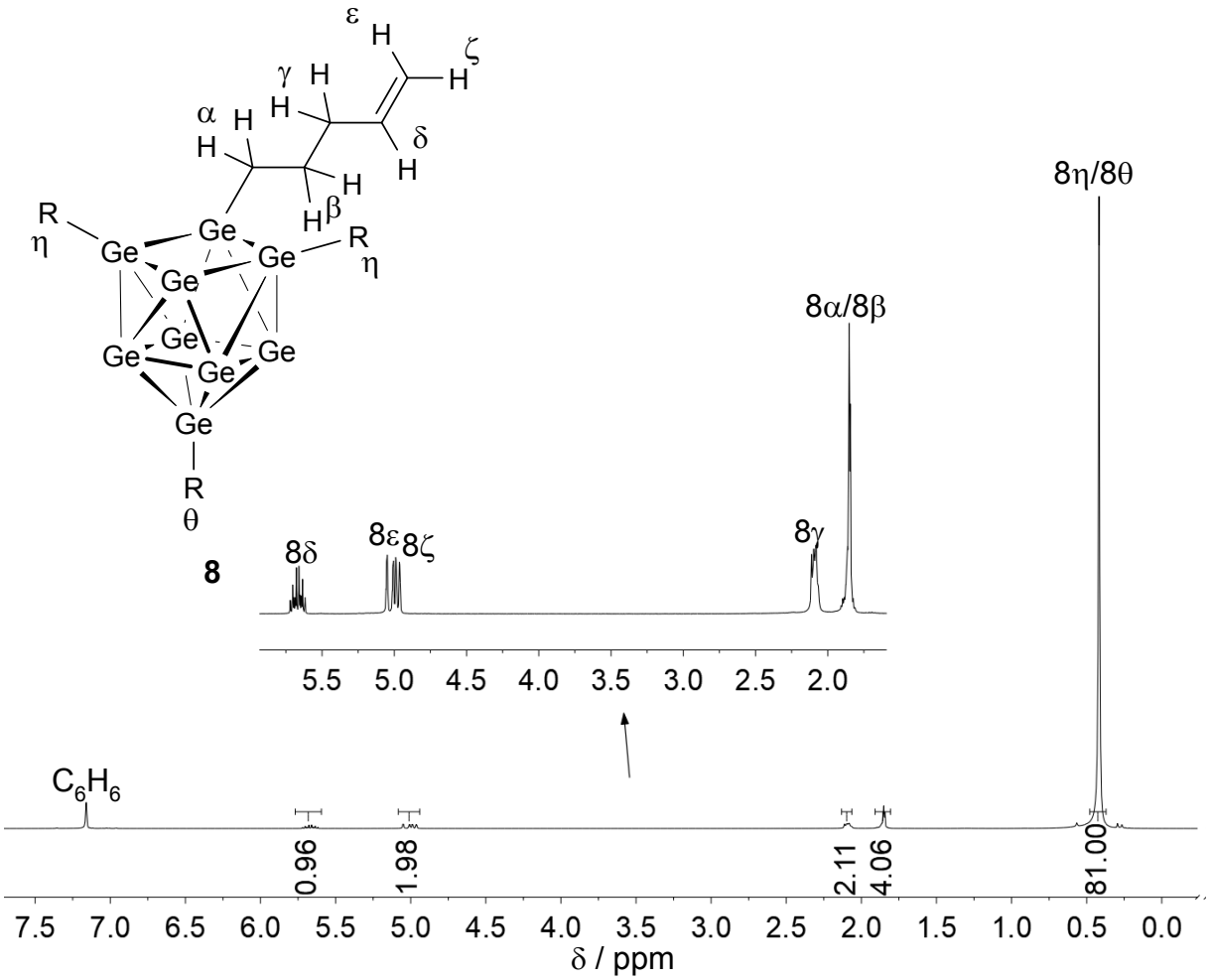

Figure S12. ^{1}H NMR spectrum of crystals of **8** recorded in [D_6]benzene at r.t.

Elemental analysis of **8**: elemental analysis calcd (%): C 26.22, H 6.19; found: C 26.35, H 6.22.

4.6 Compound **9**

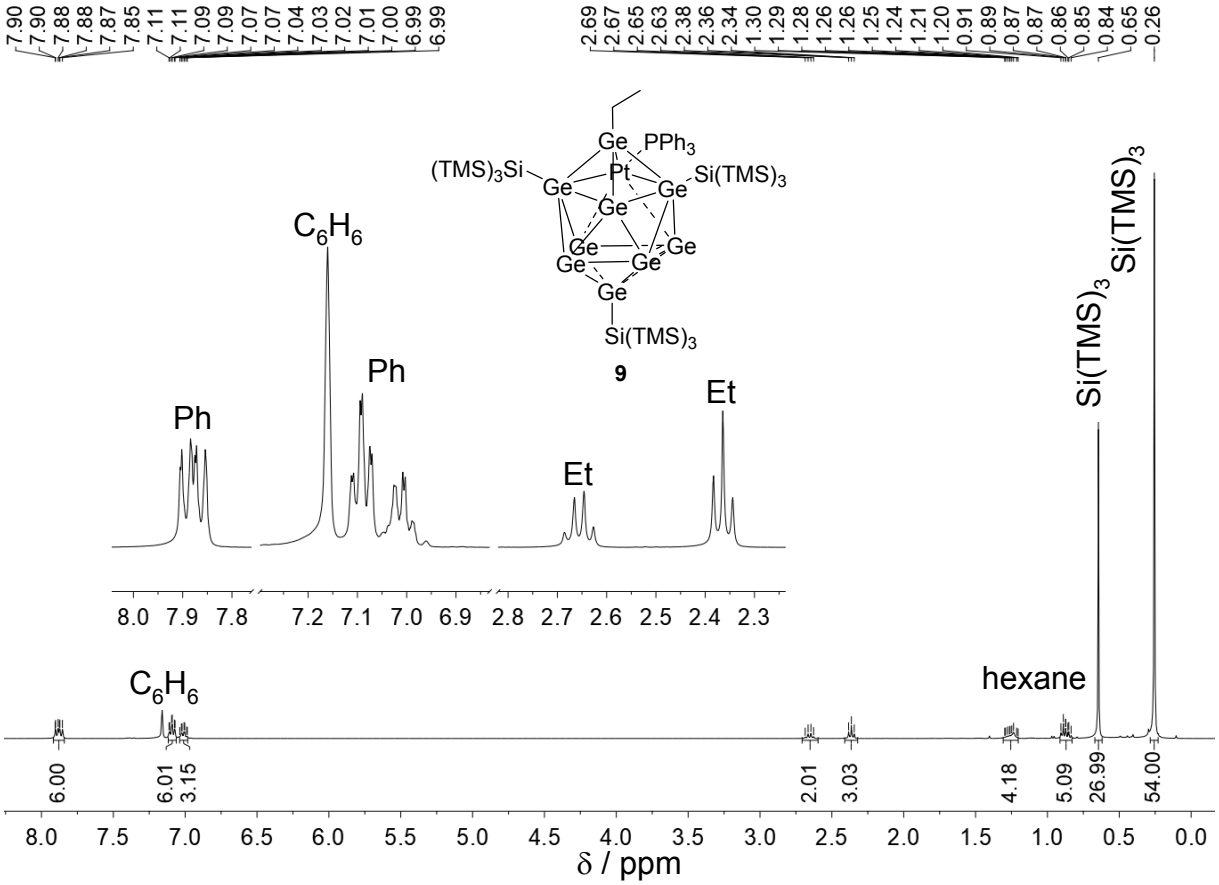

Figure S13. ^{1}H NMR spectrum of crystals of **9** recorded in [D_6]benzene at r.t.

Elemental analysis calcd for **9**·1.5 hex (%): C 33.42, H 6.11, Pt 9.69; found: C 32.84, H 5.80, Pt 9.6.

5 UV-Vis spectroscopic data

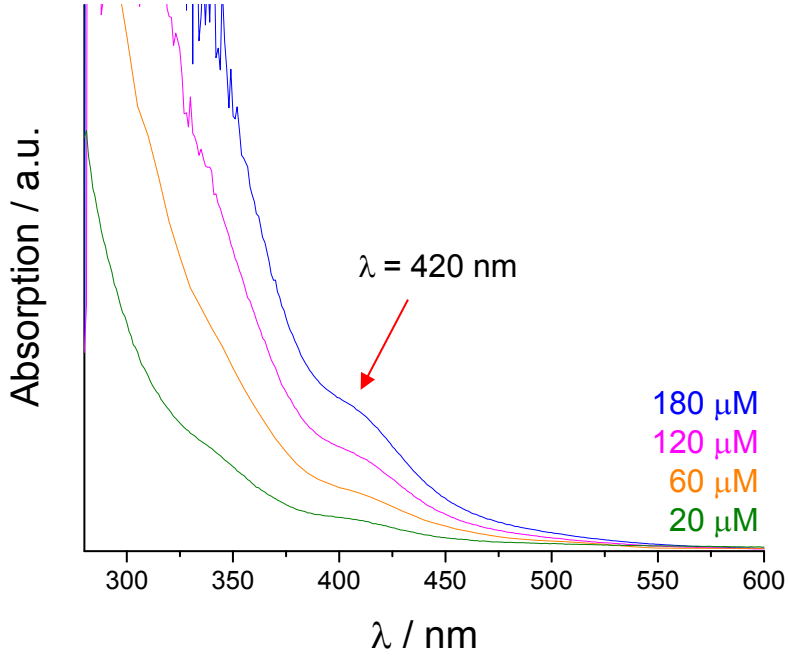

Figure S15. UV-Vis electronic spectrum of [K(2,2,2-crypt)][{(Me$_3$Si)$_3$Si}$_3$Ge$_9$] (**7**) in toluene (λ = 280 – 600 nm, c_M = 20 –180 μM).

6 Computational Details

Simulated UV-Vis spectra

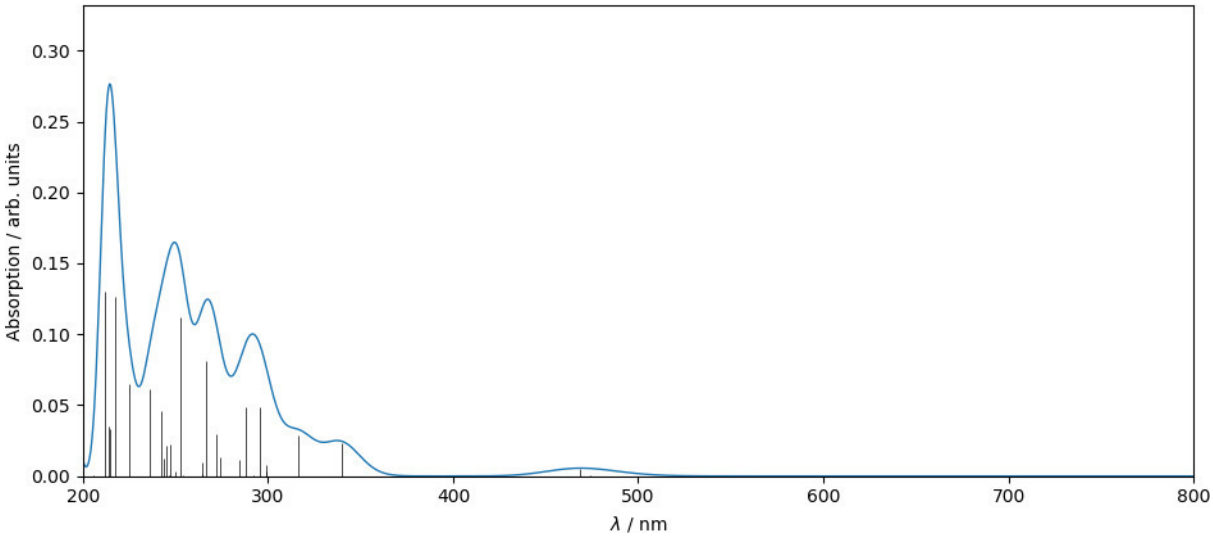

Figure S16. Simulated UV-Vis spectrum of $[Ge_9]^{2-}$ in the range 200–800 nm. The black peaks are the raw data, the blue curve has been obtained from the peak data by applying Gaussian broadening of 0.25 eV.

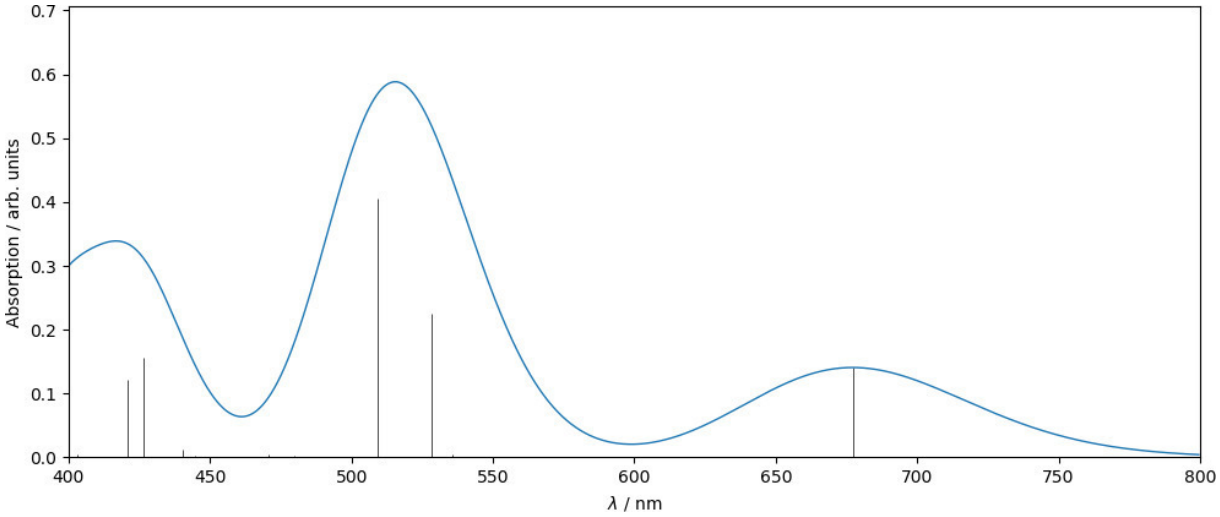

Figure S17. Simulated UV-Vis spectrum of $[Ge_9{=}Ge_9{=}Ge_9]^{6-}$ in the range 400–800 nm.

Cartesian Coordinates of the studied systems (Å units)

$[Ge_9]^{2-}$ (D_{3h})

9

D_{3h}

Ge	1.5948755	0.0000000	1.3627423
Ge	1.5948755	0.0000000	-1.3627423
Ge	-0.7974378	1.3812027	1.3627423
Ge	-0.7974378	1.3812027	-1.3627423
Ge	-0.7974378	-1.3812027	1.3627423
Ge	1.2543663	-2.1726262	-0.0000000
Ge	-2.5087326	0.0000000	-0.0000000
Ge	-0.7974378	-1.3812027	-1.3627423
Ge	1.2543663	2.1726262	-0.0000000

$[Ge_9{=}Ge_9{=}Ge_9]^{6-}$ (C_1)

27

C_1

Ge	-2.2650698	-3.0672321	5.0328549
Ge	1.1440373	-0.6605280	6.1731680
Ge	-0.1098035	0.4661662	4.3098228
Ge	0.1288686	-2.2347025	4.3240310
Ge	-0.7280886	-2.2627884	6.9455951
Ge	-1.0835556	0.4141935	7.1602087
Ge	-2.1759140	-0.9911081	3.6196051
Ge	-3.0791316	-0.9933134	6.4909587
Ge	-2.4727058	1.1245862	5.0187059
Ge	-2.8424542	0.4463052	-0.7074025
Ge	-1.7607998	1.9427325	1.1523333
Ge	-1.4881904	-0.7660670	1.1316356
Ge	-0.7024629	-0.4653638	-1.8340600
Ge	-1.0638157	2.2096941	-1.4806724
Ge	0.5573154	0.6780985	1.8162074
Ge	0.8699816	-1.2823395	0.1003110
Ge	1.3424024	0.9783426	-1.1489651

Ge	0.5869296	2.8690224	0.4449185
Ge	4.0482381	0.4502165	-4.8253405
Ge	2.5334963	1.7920774	-6.5562251
Ge	2.8761426	-0.8920182	-6.6945918
Ge	2.3429291	-1.3918609	-4.0352866
Ge	1.9880330	1.2678373	-3.6415180
Ge	0.5419424	0.3775576	-7.2227211
Ge	0.6449482	-1.9671367	-5.9625490
Ge	-0.0733948	-0.1960067	-4.3315427
Ge	0.2401220	2.1536352	-5.2794814

7 References

[1] J. Åkerstedt, S. Ponou, L. Kloo, S. Lidin, *Eur. J. Inorg. Chem.* **2011**, *2011*, 3999-4005.

5.2 The Reaction of Ethylenediamine with 1,4-Bis(trimethylsilyl)butadiyne and the Role of Water: A Qualitative Method for the Determination of Water in Ethylenediamine

Sabine Frischhut[+], Manuel M. Bentlohner[+], and Thomas F. Fässler

[+] These authors contributed equally to this work.

Manuscript for publication

5.2.1 Content and contribution

In the scope of this publication a closer look was taken at the reactivity of 1,4-bis(trimethylsilyl)butadiyne towards *en* and the role of water in the reaction mixture. Water-traces were found to significantly influence the reaction outcome. Based on these investigations, a comparatively simple method for tracing water-contents in *en* was developed, which is inevitable for reactions with the Zintl phases A_4Ge_9 (*A* = K, Rb) in *en* due to their moisture-sensitivity.

Within this work for the first time we proved the formation of the enamide $K[HN(CH_2)_2NH_2]$ in the alkenylation reaction of $[Ge_9]^{4-}$ clusters with alkynes in *en*. The evaluation of the data was partly carried out within this work. The associated investigations, as well as the elucidation of data were carried out within this thesis (approximately 50% of the experimental work) and by Dr. Manuel M. Bentlohner.

The manuscript was authored within this work and partly by Dr. Manuel M. Bentlohner. The manuscript was revised by Prof. Dr. Thomas F. Fässler.

5.2.2 Manuscript for publication

The Reaction of Ethylenediamine with 1,4-Bis(trimethylsilyl)butadiyne and the Role of Water: A Qualitative Method for the Determination of Water in Ethylenediamine

Sabine Frischhut[+], Manuel M. Bentlohner[+], and Thomas F. Fässler*

[*]

Sabine Frischhut, Dr. Manuel M. Bentlohner, Prof. Dr. Thomas F. Fässler

Department Chemie, Technische Universität München

Lichtenbergstraße 4, 85747 Garching, Germany

E-mail: thomas.faessler@lrz.tum.de

[+] These authors contributed equally to this work.

Keywords

Ethylenediamine / Water / Butadiyne / Hydroamination / Enamine-Imine

ABSTRACT

The hydroamination reaction between 1,3-butadiyne and ethylenediamine and subsequent cyclization to form the dihydrodiazepine has been known for a long time. But the role of water in this reaction type has not been considered, yet. Herein we present the reaction of ethylenediamine with 1,4-bis(trimethylsilyl)butadiyne and discuss the formation of different reaction products depending on the water-content in ethylenediamine. NMR spectroscopic investigations revealed that the cyclization product 1,9-di-amino-4-methyl-3,7-di-aza-nonadiene is only formed in presence of water-traces in the reaction mixture. Based on these results, we developed a fast method to trace water in ethylenediamine, supported by ^{1}H NMR spectroscopy. Besides, for the first time we could proof the formation of the enamide throughout the nucleophilic reaction of $[Ge_9]^{4-}$ with alkynes in ethylenediamine.

INTRODUCTION

Amines have been shown to be outstanding solvents for highly polar Zintl phases. Already in 1891, Joannis stated for the first time green- and red-colored solutions upon dissolution of elemental sodium and lead or antimony in liquid ammonia.[1] His observations were reinforced by further investigations by Smyth, Peck, Kraus and Zintl.[2-6] The latter was the first who recognized the close relation of salt-like intermetallic phases and soluble polyanions.[7] In 1970, Kummer *et al.* reported the solubility of the Zintl phase Na_4Sn_9 in amines, other than liquid ammonia, for the first time, whereby deep-red solutions in ethylenediamine (*en*) were observed.[8] These discoveries allowed for the transfer of Zintl cluster chemistry into the solvent *en* which is easier to handle than liquid ammonia. Therein organo-functionalization of polyanions, especially of $[Ge_9]^{4-}$ clusters, had been intensively studied.

Monoalkynes readily react with the Zintl phase K_4Ge_9 in *en* to form at a maximum twofold alkenylated cluster species. The most prominent example is given by the vinylated species $[Ge_9(CH{=}CH_2)_n]^{(4-n)-}$.[9-10] The mechanism follows a nucleophilic addition of $[Ge_9]^{4-}$ to one carbon atom of the triple bond of bis(trimethylsilyl)acetylene. Due to steric repulsion the subsequent protonation takes place in *anti*-fashion leading to the formation of the respective *syn*-product. The proton is delivered by *en*, which itself turns into an amide, which again initiates the exchange of the trimethylsilyl groups by protons. The intermediates could be identified by ESI mass spectrometry, except the formation of the amide had not been unequivocally proven, yet.[11] Especially the dialkyne 1,4-bis(trimethylsilyl)butadiyne has been applied in reactions with the Zintl phase K_4Ge_9 in *en*. Due to the addition of the Ge_9 cluster to the sterically less hindered carbon atom of the triple bond, organically linked Ge_9 clusters *via* a conjugated organic bridge can be achieved, namely $[R{-}Ge_9{-}CH{=}CH{-}CH{=}CH{-}Ge_9{-}R]^{4-}$ (R = vinyl, (2*Z*,4*E*)-7-amino-5-azahepta-2,4-dien-2-yl) (Figure 1).[12-14]

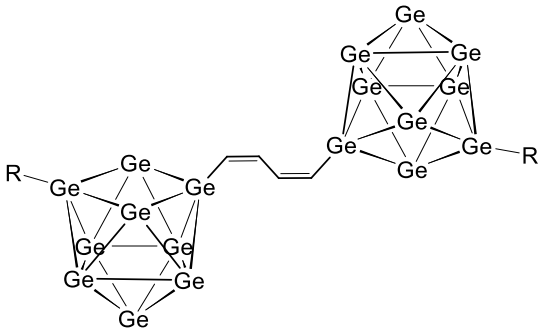

Figure 1. The Zintl triad [R–Ge_9–CH=CH–CH=CH–Ge_9–R]$^{4-}$ (R = vinyl, (2*Z*,4*E*)-7-amino-5-azahepta-2,4-dien-2-yl).[12]

1,4-Bis(trimethylsilyl)butadiyne does not physically dissolve in *en*, but undergoes a hydroamination reaction with the solvent *en*. However, variation of applied equivalents of 1,4-bis(trimethylsilyl)butadiyne and order of addition of reactants allows for a control of formation of specific products.[12] The alkenylation of $[Ge_9]^{4-}$ proceeds only in *en* and variation of the alkyne showed that even coupling products of the alkyne and *en* are formed. Therefore, we have deeply investigated the coupling reactions and showed that therein water impurity plays a decisive role.

The preferred reaction of alkynes is the addition of electrophiles due to their electron rich carbon triple bond. Low-lying and unoccupied π*-orbitals, however, allow the addition of nucleophiles,[15-16] such as amines[17-18] and $[Ge_9]^{4-}$ Zintl anions.[11]

In hydroamination reactions, amines nucleophilically add to an alkyne's triple bond generating a C–N bond. Depending on the type of amine, different products are obtained. Application of primary amines yields enamines, which tautomerize to the corresponding imines by a prototropic shift. By using instead secondary amines, the reaction stops at the enamine. Additions of amines at alkynes are of high technical relevance as enamines and imines are important intermediates for the synthesis of commercially available chemicals and pharmaceuticals. Accordingly, a wide range of catalysts has been developed to enhance the yield and selectivity of such reactions.[17-18]

In such reactions with highly moisture sensitive reactants it is of great importance to ensure that the applied *en* is water-free. Otherwise oxidation of $[Ge_9]^{4-}$ clusters is observed. These Zintl clusters can carry different charges and are in equilibrium with solvated electrons in *en*.[19] This has already been pointed out by Fässler and co-workers.[20] The conventional Karl-Fischer method of coulometric determination of the water-content is not applicable for amines,[21-22] which would lead to side-reactions of *en* with the titration-reagents.[23]

Herein we present an alternative and comparatively easy way of tracing water in *en* by mixing 1,4-bis(trimethylsilyl)butadiyne with *en* and stirring the reaction solution at r.t. for 20 h. *In situ* NMR studies on reaction solutions containing 1,4-bis(trimethylsilyl)butadiyne and optionally water in *en* are provided. In addition, we prove the formation of potassium ethylenediamide as a side product throughout the reaction of $[Ge_9]^{4-}$ clusters with alkynes in *en*.

RESULTS AND DISCUSSION

As monitored by NMR, the reaction of 1,4-bis(trimethylsilyl)butadiyne (**1**) with water-free *en* quantitatively forms (3*Z*)- and (3*E*)-1-trimethylsilyl-7-amino-5-aza-hepta-3-en-1-yne (**2**) in an approximate isomers ratio of *Z*/*E* = 30/70 (Scheme 1, reaction I). Under water-free conditions, **2** is the final product, emerging from the nucleophilic addition of *en* at the terminal carbon atom of **1**. The availability of the alkyne-functionality of **2** has been shown by reaction with $[Ge_9]^{4-}$ and **1** to obtain the Zintl triad $[R–Ge_9–CH=CH–CH=CH–Ge_9–R]^{4-}$ (R = (2*Z*,4*E*)-7-amino-5-azahepta-2,4-dien-2-yl).[12-13]

In the presence of water, **2** further reacts to 2,3-dihydro-5-methyl-*H*-1,4-diazepine (**3**) (Scheme 1, reaction II) and 1,9-di-amino-4-methyl-3,7-di-aza-nonadien (**4**) (Scheme 1, reaction III). In an earlier described synthesis, **3** was obtained by reaction of *en* with 1,3-butadiyne, however the role of water has not been discussed.[24] Obviously, **3** and **4** arise from water-catalyzed intramolecular amine addition and addition of another *en* molecule at carbon γ, respectively. According to ^{13}C chemical shifts the electrophilicity of the γ carbons for both (3E)-**2** and (3Z)-**2** is higher than for the δ carbons {^{13}C chemical shifts [ppm] (3*E*)-**2**: 109.1 (γ), 86.1 (δ); (3*Z*)-**2**: 105.8 (γ), 93.9 (δ)}. Hence, addition of a second amino group at **2**, preferentially proceeds at the γ carbon. A catalytic effect of water in hydroaminations has been also reported in previous publications dealing with the synthesis of imidazo[1,2-*a*]pyridines.[25-26]

The influence of water on the reaction of **1** with *en* was exploited for the qualitative determination of water in the solvent. Due to moisture sensitivity, the chemistry of $[E_9]^{4-}$ in solution requires thoroughly dried reactants and solvents in order to achieve reproducible results. As has already been pointed out, the determination of the water content in *en* by classical Karl-Fischer titration methods is difficult, due to side reactions of the solvent with the titration-reagents.[23]

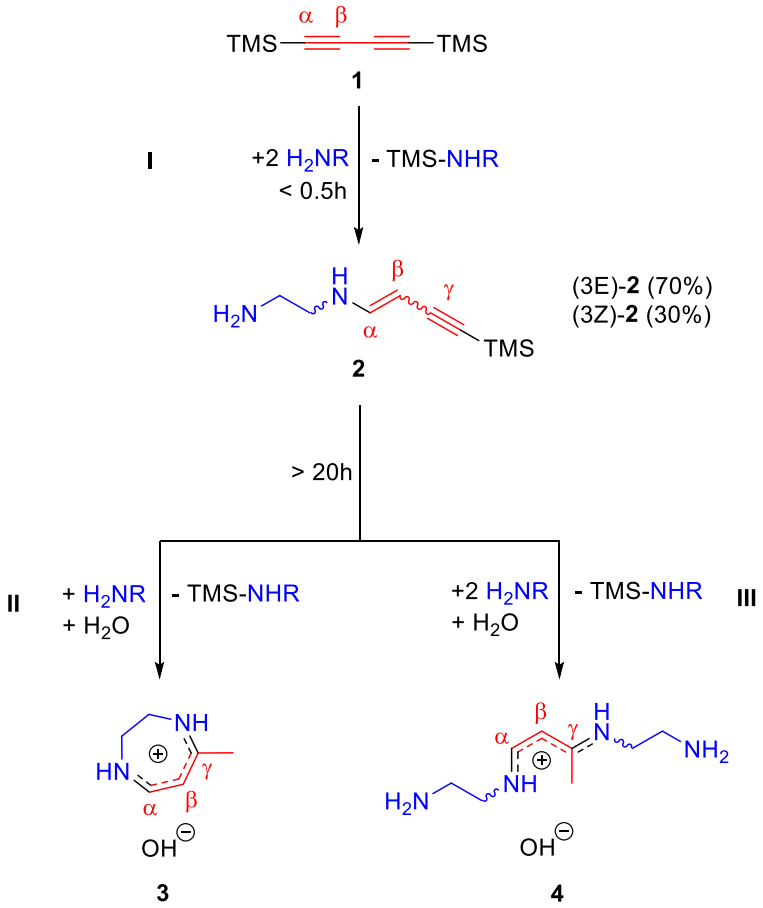

Scheme 1. Reaction of 1,4-bis(trimethylsilyl)butadiyne (**1**) with *en* in the absence of $[Ge_9]^{4-}$ Zintl anions and the influence of water. I) Formation of **2** by addition of one *en*-molecule to **1**. II) Intramolecular cyclization of **2** to form **3** in the presence of water. III) Reaction of **2** with *en* to form **4** in the presence of water. With regard to the NMR time-scale, **3** and **4** quickly isomerize/tautomerize in presence of water, as can be seen by a signal broadening in the ^{1}H NMR spectrum.

In the absence of $[Ge_9]^{4-}$ clusters the reaction of **1** with *en* quantitatively forms (3*Z*)-**2** and (3*E*)-**2** (*Z*/*E* = 30/70) by *anti*- and *syn*-addition of the amino-functionality of *en* to the α C-atom of **1** and exchange of the trimethylsilyl (TMS) group by protons (supporting information, Figure S1). The addition of *en* to **1** does not form an amide as a side product since the proton which is required for protonation of the intermediate alkenyl-anion is provided by the incoming *en* itself. Under water-free conditions **2** is the final product, whereas in presence of water-traces the reaction proceeds further to 2,3-Dihydro-5-methyl-H-1,4-diazepine (**3**) and 1,9-di-amino-4-methyl-3,7-di-aza-nonadien (**4**) (supporting information, Figure S2/3). Species **4** rapidly isomerizes/tautomerizes in presence of water (supporting information, Scheme S3), which can be derived from the broadened signals of the corresponding ^{1}H NMR spectrum. In the NMR spectrum four different isomers/tautomers of **3** appear by four distinct signal sets, which show characteristic

coupling patterns (supporting information, Figure S2/S3). That is in contrast to solutions of **4** in *en* containing water-traces, where the latter quickly isomerizes/tautomerizes and only broadened ^{1}H NMR signals are visible (supporting information, Figure S2/3). Under water-free conditions isomerization/tautomerization might be possible, however, appears slowly with respect to NMR time scale.

According to the ^{13}C chemical shifts of **2** [^{13}C chemical shifts [ppm] (3*E*)-**2**: 109.1 (γ), 86.1 (δ); (3*Z*)-**2**: 109.1 (γ), 86.1 (δ)] (supporting information, Table S1), the electrophilicity of the γ position is higher than for the δ position and nucleophilic additions preferably take place at the γ C atom.

For the nucleophilic addition of *en* to **2**, additional protons from *en* are required for protonation of the intermediate alkenyl-anion. Consequently, the reaction itself forms another amide and the formation of **4** is self-sustaining and triggered by trace amounts of amide.

The absence of **2** in the reaction mixtures points out, that nucleophilic addition of $[Ge_9]^{4-}$ to **1** is favored over *en*-addition, and formation of side chains R (R = (2*Z*,4*E*)-7-amino-5-azahepta-2,4-dien-2-yl) is not possible under such conditions. To shed also more light on the formation of **2** and, in particular, its side chains R, we performed investigations on the reactivity of $[Ge_9]^{4-}$ towards **2**, which was separately prepared by the reaction of **1** with water-free *en* in the absence of clusters. According to NMR and ESI-MS the reaction of $[Ge_9]^{4-}$ with **2** in water-free *en* leads to the Zintl anions $[(Ge_9)–(R)]^{3-}$ and $[(R)–(Ge_9)–(R)]^{2-}$ as well as species **4**.[27] The formation of $[(Ge_9)–(R)]^{3-}$ is attributed to regioselective addition of $[Ge_9]^{4-}$ to the most electrophilic carbon atom γ of **2**. [40] In an analogous reaction $[(R)–(Ge_9)–(R)]^{2-}$ is formed by addition of the clusters of $[(Ge_9)–(R)]^{3-}$ at the γ carbon of **2**. In contrast to the reaction of $[Ge_9]^{4-}$ with **3**, species **4** arises as a dominant side-product from the reaction of clusters with **2**. **4** is the formal result of a twofold *en*-addition at **1** in α and γ position. However, in the absence of water, *en* is unable to add to **2**, pointing to the addition of the stronger nucleophile *en*, which has been postulated as a side product in additions of clusters at alkynes. Indeed, the reaction of potassium ethylenediamide with **2** quantitatively forms species **4** in water-free *en* (supporting information, Figure S4). Hence, the latter provides the first evidence for the postulated *en* deprotonation in additions of $[E_9]^{4-}$ Zintl clusters to alkynes.

Each freshly distilled *en*-batch was qualitatively tested according to its water-content by mixing an aliquot of the solvent with **1** and monitoring the reaction with ^{1}H NMR for at least 24 h. As long as **2** was the only product after 24 h, *en* was considered as water-free and used for further reactions.

CONCLUSION

A viable example of a hydroamination reaction between *en* and 1,4-bis(trimethylsilyl)butadiyne (**1**) depending on the water-content is reported. In water-free *en* **1** adds one molecule *en* to form (3*Z*/3*E*)-7-amino-1-(trimethylsilyl)-5-azahepta-3-en-1yne (**2**) and stops at this stage. In the presence of water-traces, **2** can add an additional molecule *en* to form 1,9-di-amino-4-methyl-3,7-di-aza-nonadiene (**4**), or can undergo a cyclization reaction to form 2,3-dihydro-5-methyl-*H*-1,4-diazepine (**3**). Therefore, the reaction of **2** to form **3** and **4** in *en* at r.t. provides an indicator to trace water-contents in the solvent *en*. The reaction of **2** with potassium ethylenediamide to form **4** proves the formation of amides throughout the alkenylation of $[Ge_9]^{4-}$ Zintl clusters in *en*.

EXPERIMENTAL SECTION

General Methods. All manipulations were carried out under a purified argon atmosphere using a glove box and standard Schlenk technique. 1,4-bis(trimethylsilyl)butadiyne (Alfa Aesar 98%) was used as received. Potassium was purified by liquation and stored in a glove box.

Purification of *en*. *En* (Merck) with an initial water content of ≤ 1% was refluxed over calcium hydride (Merck) and freshly collected prior to use. Water free *en* was obtained after refluxing for 72 h. The sample tubes were thoroughly cleaned and dried at 120°C immediately before the *en* collection. *En* containing trace amounts of water was obtained after refluxing for 2-6 h. The sample tubes were stored under ambient conditions.

Qualitative water-test in *en*: preparation of (3*Z*/3*E*)-7-amino-1-(trimethylsilyl)-5-azahepta-3-en-1yne (2).[13] Solutions with 60, 120, 240 µmol **2**/ml *en* were obtained by reacting 23.4 mg (120 µmol), 46.7 mg (240 µmol) and 93.4 mg (480 µmol) of **1** with each 2 ml *en* in a Schlenk tube for 5-20 h, respectively. Thereby pale yellow colored transparent solutions

were obtained. Prior to application of **2** for further syntheses the solutions were filtered over glass wool in order to remove traces of unreacted **1**. ^{1}H NMR (500 MHz, ethylendiamine (non-deuterated), 296 K): Isomer ^{Z}**2** δ(ppm) 6.40 (dd, *J* = 8.6 Hz, 12.2 Hz, 1H, -NH-C*H*=CH-), 3.96 (d, *J* = 8.6 Hz, 1H, -NH-CH=C*H*-), 6.67 (s(broad), -N*H*-CH=CH-), 3.21 (pseudo q, *J* = 6.0 Hz, 2H, NH_2-CH_2-CH_2-), 2.76 (NH_2-CH_2-CH_2-, covered by en and revealed by COSY), 0.23 (s, 9H, C-Si-(CH_3)$_3$-); Isomer ^{E}**2**: δ(ppm) 6.91 (dd, *J* = 13.6 Hz, 7.4 Hz, 1H, -NH-C*H*=CH-), 4.23 (d, *J* = 13.6 Hz, 1H, -NH-CH=C*H*-), 7.54 (s(broad), 1H, -N*H*-CH=CH-), 2.96 (pseudo q, *J* = 6.0 Hz, 2H, NH_2-CH_2-CH_2-), 2.79 (covered by *en* and revealed by COSY, NH_2-CH_2-CH_2-), 0.19 (s, 9H, C-Si-(CH_3)$_3$-).

Supporting Information. The Supporting Information contains details on the *in situ* studies and detailed descriptions of NMR-data are given.

ACKNOWLEDGMENT

The authors are grateful to the SolTech (Solar Technologies go Hybrid) program of the State of Bavaria for its financial support. Moreover, the authors thank M. Sc. Lorenz Schiegerl and Maria Weindl for helping with the preparation of reaction solutions and NMR-investigations.

TOC

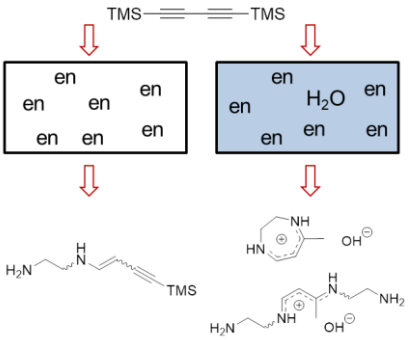

REFERENCES

[1] M. Joannis, *C. R. Hebd. Séances Acad. Sci.* **1891**, *113*, 795-798.
[2] F. H. Smyth, *J. Am. Chem. Soc.* **1917**, *39*, 1299-1312.
[3] E. B. Peck, *J. Am. Chem. Soc.* **1918**, *40*, 335-347.
[4] C. A. Kraus, *J. Am. Chem. Soc.* **1922**, *44*, 1216-1239.
[5] C. A. Kraus, *Trans. Am. Electrochem. Soc* **1924**, *45*, 175-186.
[6] E. Zintl, J. Goubeau, W. Dullenkopf, *Z. Phys. Chem., Abt. A* **1931**, *154*, 1-46.
[7] E. Zintl, A. Harder, *Z. Phys. Chem.* **1931**, *14*, 265-284.
[8] D. Kummer, L. Diehl, *Angew. Chem. Int. Ed. Engl.* **1970**, *9*, 895.
[9] M. W. Hull, S. C. Sevov, *Inorg. Chem.* **2007**, *46*, 10953-10955.
[10] C. B. Benda, J. Q. Wang, B. Wahl, T. F. Fässler, *Eur. J. Inorg. Chem.* **2011**, *27*, 4262-4269.
[11] M. W. Hull, S. C. Sevov, *J. Am. Chem. Soc.* **2009**, *131*, 9026-9037.
[12] M. M. Bentlohner, W. Klein, Z. H. Fard, L.-A. Jantke, T. F. Fässler, *Angew. Chem. Int. Ed.* **2015**, *54*, 3748-3753.
[13] S. Frischhut, M. M. Bentlohner, W. Klein, T. F. Fässler, *Inorg. Chem.* **2017**, *56*, 10691-10698.
[14] M. M. Bentlohner, S. Frischhut, T. F. Fässler, *Chem. Eur. J.* **2017**, *23*, 17089-17094.
[15] R. Bruckner, *Organic Mechanisms: Reactions, Stereochemistry and Synthesis*, Springer, Berlin, Heidelberg, **2010**.
[16] K. P. C. Vollhardt, N. E. Schore, *Organische Chemie*, 4. ed., John Wiley & Sons, **2009**.
[17] T. E. Müller, M. Beller, *Chem. Rev.* **1998**, *98*, 675-704.
[18] T. E. Muller, K. C. Hultzsch, M. Yus, F. Foubelo, M. Tada, *Chem. Rev.* **2008**, *108*, 3795-3892.
[19] S. C. Sevov, J. M. Goicoechea, *Organometallics* **2006**, *25*, 5678-5692.

[20] M. M. Bentlohner, M. Waibel, P. Zeller, K. Sarkar, P. Müller-Buschbaum, D. Fattakhova-Rohlfing, T. F. Fässler, *Angew. Chem. Int. Ed.* **2016**, *55*, 2441-2445.
[21] K. Fischer, *Angew. Chem.* **1935**, *48*, 394-396.
[22] A. Meyer, C. Boyd, *Anal. Chem.* **1959**, *31*, 215-219.
[23] M. Conceição, P. Lima, M. Spiro, *Anal. Chim. Acta* **1976**, *81*, 429-431.
[24] W. W. Paudler, A. G. Zeiler, *J. Org. Chem.* **1969**, *34*, 999-1001.
[25] D. C. Mohan, N. B. Sarang, S. Adimurthy, *Tetrahedron Lett.* **2013**, *54*, 6077-6080.
[26] D. Chandra Mohan, S. Nageswara Rao, S. Adimurthy, *J. Org. Chem.* **2013**, *78*, 1266-1272.
[27] M. M. Bentlohner, C. Fischer, T. F. Fässler, *Chem. Commun.* **2016**, *52*, 9841-9843.

SUPPORTING INFORMATION

The Reaction of Ethylenediamine with 1,4-Bis(trimethylsilyl)butadiyne and the Role of Water: A Qualitative Method for the Determination of Water in Ethylenediamine

Sabine Frischhut[+], Manuel M. Bentlohner[+], and Thomas F. Fässler*

[*]

Sabine Frischhut, Dr. Manuel M. Bentlohner, Prof. Dr. Thomas F. Fässler

Department Chemie, Technische Universität München

Lichtenbergstraße 4, 85747 Garching, Germany

E-mail: thomas.faessler@lrz.tum.de

Contents

Figures

Tables

Schemes

1 *In situ* Studies

The reactivity of *en*, $KNH(CH_2)_2NHK$ towards 1,4-bis(trimethylsilyl)butadiyne (**1**) was tested. Therefore, test mixtures according to section 1.2 Scheme S1 were prepared. The reactions were investigated *in situ* by NMR spectroscopy. For methodologic details on NMR spectroscopic investigations, see section 1.1. In section 1.3, an overview on all the species, which were identified by NMR, is given together with detailed descriptions of NMR-data. In Table S1-S3 the corresponding ^{1}H and ^{13}C NMR-data are summarized. In section 1.4 Table S3 the outcomes of *in situ* NMR-investigations are broken down for the different types of test-mixtures. In section 1.5 Figure S1-S3 the NMR-spectra are shown together with experimental details on the preparation of the test mixtures.

1.1 General

NMR spectroscopy. ^{1}H, COSY, HSQC and HMBC NMR spectra were recorded on 500 MHz (Bruker AV-500) and 400 MHz (Bruker AV-400) NMR spectrometers, respectively. Aliquots of ca. 150 µl of the filtered test mixture (solvent: non-deuterated *en*) were filled into a Norell® NMR tube (outer diameter: 3 mm). The Norell® NMR tube was put into a NMR tube with a diameter of 4 mm (denoted as outer tube) and the outer NMR tube was filled with 0.4 ml of chloroform-d_1. Due to the application of non-deuterated *en* as solvent, the spectra show dominant signals at. 2.5-3.0 ppm (s, *en*, -CH_2-) and 1.3-1.9 ppm (s, *en*, -NH_2-), respectively. Samples for time-resolved ^{1}H-NMR-spectroscopy were taken immediately after the reactants entirely dissolved (ca. 15 min) and the NMR measurements immediately were started.

1.2 Test-mixtures

Scheme S1. Overview on test-mixtures, prepared for investigating the reactivity of *en* and $KNH(CH_2)_2NHK$ towards **1** and **2**, respectively. Reaction time and stoichiometry was varied. For experimental details on the preparation of each test mixture as well as the NMR spectra see section 1.5 Figures S1-S3. Different types of mixtures are assigned with capital letters for distinction. Mixture type "A" and "B": **1** either was dissolved in water free *en* ("A") or *en* containing 0.5-1% water ("B"); Mixture type "C": 1 eq. $KNH(CH_2)_2NHK$ was dissolved in an *en*-solution containing 1 eq. **2**.

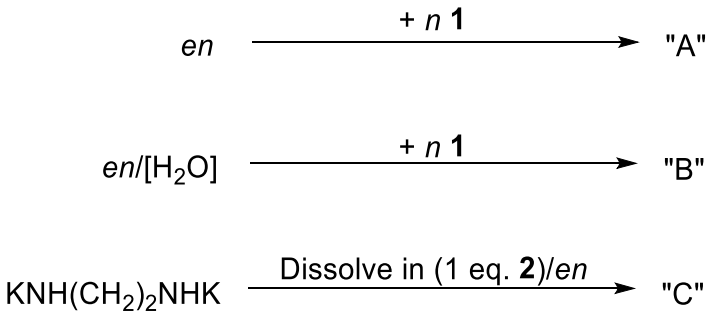

1.3 Identified organic molecules/functionalities and NMR-descriptions

In this chapter the NMR-data of organic molecules and functionalities which were identified in the test-mixtures by *in-situ* NMR are summarized and described in detail (Scheme S2 and Table S1-S2)

Scheme S2. a-c) Organic-molecules identified by *in situ* NMR. The molecules are denoted with bold capital letters and bold numbers, respectively. Protons/carbons are labeled with greek-letters for distinction. Color code: Red: C_4-backbone originating from **1**, Blue: *en*-substituent.

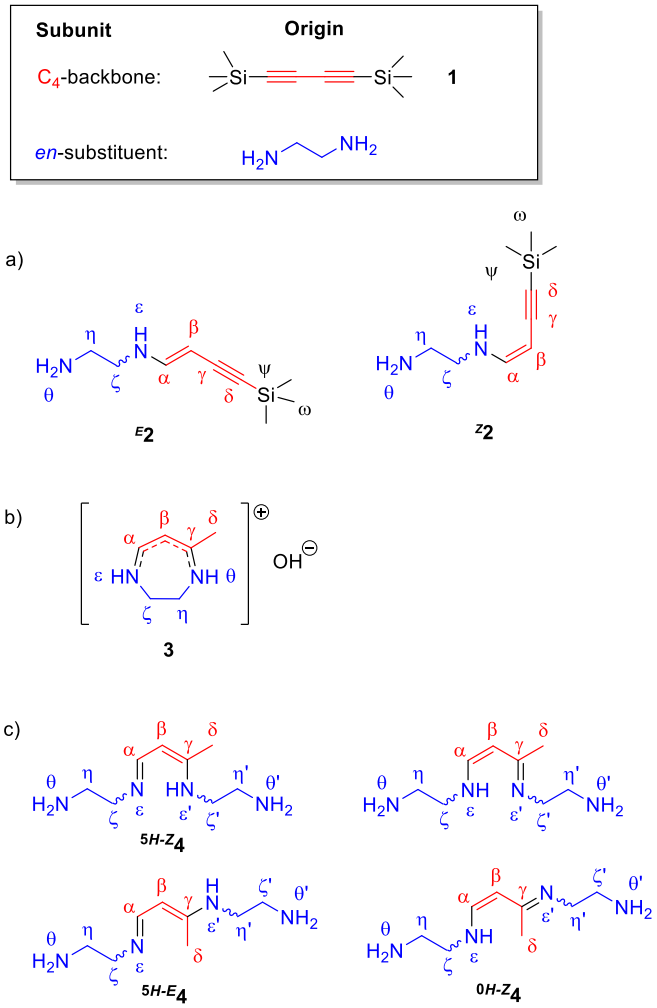

1.3.1 ^{E}2/^{Z}2

Table S1. Summary of the ^{1}H (upper rows) and ^{13}C NMR (lower rows) chemical shifts (ppm) of ^{E}**2**/^{Z}**2** (*E*/*Z* = 70/30). The ^{1}H NMR data are given together with the coupling pattern (s = singlet, d = doublet, dd = doublet of doublet, t = triplet, q = quartet), coupling constants (Hz) and integrals. Grey layered boxes: no signals are expected in ^{1}H and ^{13}C NMR for that atom positions. The NMR spectra are shown in ref. [1].

	^{E}**2**	^{Z}**2**
α	6.91 (dd, *J* = 13.6 Hz/7.4 Hz, 1H)	6.40 (dd, *J* = 8.6 Hz/12.2 Hz, 1H)
	147.6	146.9
β	4.23 (d, *J* = 13.6 Hz, 1H)	3.96 (d, *J* = 8.6 Hz, 1H)
	70.7	70.1
γ		
	109.1	105.8
δ		
	86.1	93.9
ε	7.54 (s(broad), 1H)	6.67 (s(broad))
ζ	2.96 (pseudo q, *J* = 6.0 Hz, 2H)	3.21 (pseudo q, *J* = 6.0 Hz, 2H)
	46.3	49.7
η	2.79	2.76
	40.3	42.7
Θ	covered by *en*	covered by *en*
ω	0.19 (s, 9H)	0.23 (s, 9H)
	0	0
ω'		

Molecule ^{E}2 and ^{Z}2.

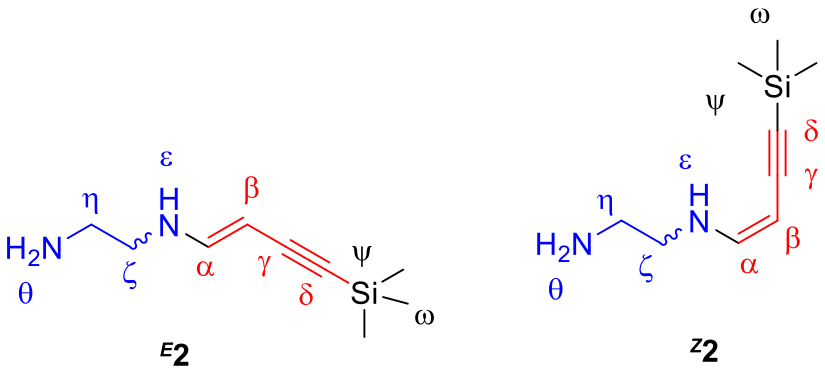

^{E}2 ^{Z}2

1D- and 2D-NMR data as well as detailed description of the data see ref. [1].

1.3.2 **3** and **4**

Table S2. Summary of the ^{1}H (upper rows) and ^{13}C NMR (lower rows) chemical shifts (ppm) of a) **4** under water-free conditions and b) **4** and **3** in presence of water traces. Different isomers/tautomers of **4** appear in the NMR spectra by similar signal sets. NMR data do not reveal which signal set belongs to which isomer/tautomer and consequently the signal sets are distinguished by superscripted numbers. The signals $^{2\text{-}7}$**4** severely interfere with *en* and consequently NMR-data are incomplete. Grey layered boxes: no signals are expected.

a)	**4**			
	^{1}4 (65%)	^{2}4 (35%)	^{3}4 (80%)	^{4}4(20%)
α	7.79 (d, *J* = 11.6 Hz, 1H)	7.83 (d, *J* = 10.8 Hz, 1H)	7.46 (d, *J* = 11.5 Hz)	7.51 (d, *J* = 11.5 Hz)
	157.9	161.5	161.7	Intensity too low
β	4.24 (d, *J* = 11.6 Hz, 1H)	4.56 (d, *J* = 10.5 Hz, 1H)	3.11	3.33
	79.5	82.0	ca. 64	ca. 64
γ				
	163.0	161.5	169.6	Intensity to low
δ	2.05 (s)	2.00 (s)	2.05 or 2.0	2.05 or 2.0
	22.3	22.3	22.3	22.3
ε	proton exchange	proton exchange	proton exchange	proton exchange
ζ	2.95 (t)	3.21 (t, *J* = 5.6 Hz, 1H)	covered by *en*	covered by *en*
	53.3	64.1	covered by *en*	covered by *en*
η	covered by *en*	covered by *en*	covered by *en*	covered by *en*
	covered by *en*	covered by *en*	covered by *en*	covered by *en*
Θ	covered by *en*	covered by *en*	covered by *en*	covered by *en*
ε'	proton exchange	proton exchange	proton exchange	proton exchange
ζ'	2.98 (t)	covered by *en*	covered by *en*	covered by *en*
	53.2	covered by *en*	covered by *en*	covered by *en*
η'	covered by *en*	covered by *en*	covered by *en*	covered by *en*
	covered by *en*	covered by *en*	covered by *en*	covered by *en*
Θ'	proton exchange	proton exchange	proton exchange	proton exchange

b)	**4**			**3**
	^{5}4 (Figure S2)	^{6}4 (Figure S2)	^{7}4 (Figure S2)	3 (Figure S2)
α	7.88 (s, broad, variable)	7.88 (s, broad, variable)	7.5	6.87 (d, *J* = 7.4 Hz, 1H)
	in 2D NMR invisible	in 2D NMR invisible	in 2D NMR invisible	148.7
β	4.49 (s, broad, variable)	5.11 (s, broad, variable)	overlap with en, ca. 3	4.55 (d, *J* = 7.4 Hz, 1H)
	in 2D NMR invisible	in 2D NMR invisible	in 2D NMR invisible	91.9
γ				
	in 2D NMR invisible	in 2D NMR invisible	in 2D NMR invisible	161.6

δ	2.06 (s, broad, variable)	2.06 (s, broad, variable)	2.06 (s, broad, variable)	2.0 (s, 9H)
	in 2D NMR invisible	in 2D NMR invisible	in 2D NMR invisible	25.3
ε	fast proton exchange	fast proton exchange	fast proton exchange	fast proton exchange
ζ	3.32 (s, broad, variable)	3.13 (s, broad, variable)	covered by *en*	3.55 (s(broad))
	in 2D NMR invisible	in 2D NMR invisible	in 2D NMR invisible	52.3
η	covered by *en*	covered by *en*	covered by *en*	covered by *en*
	in 2D NMR invisible	in 2D NMR invisible	in 2D NMR invisible	covered by *en*
Θ	fast proton exchange	fast proton exchange	fast proton exchange	fast proton exchange
ε'	fast proton exchange	fast proton exchange	fast proton exchange	
ζ'	3.32 (s, broad, variable)	3.13 (s, broad, variable)	covered by *en*	
	in 2D NMR invisible	in 2D NMR invisible	in 2D NMR invisible	
η'	covered by *en*	covered by *en*	covered by *en*	
	in 2D NMR invisible	in 2D NMR invisible	in 2D NMR invisible	
Θ'	fast proton exchange	fast proton exchange	fast proton exchange	

Scheme S3. Supposed mechanism of a) water-triggered tautomerization/isomerization of **4** and b) tautomerization of **3**. Due to the open structure of **4**, the conformation of the C_4-backbone can change, whereas in case of **3** the conformation of the molecule is fixed because of its ring structure, and only tautomerization can occur. For the C_4-backbone both the configuration of the double bond as well as its conformation are given by superscripted prefixes.

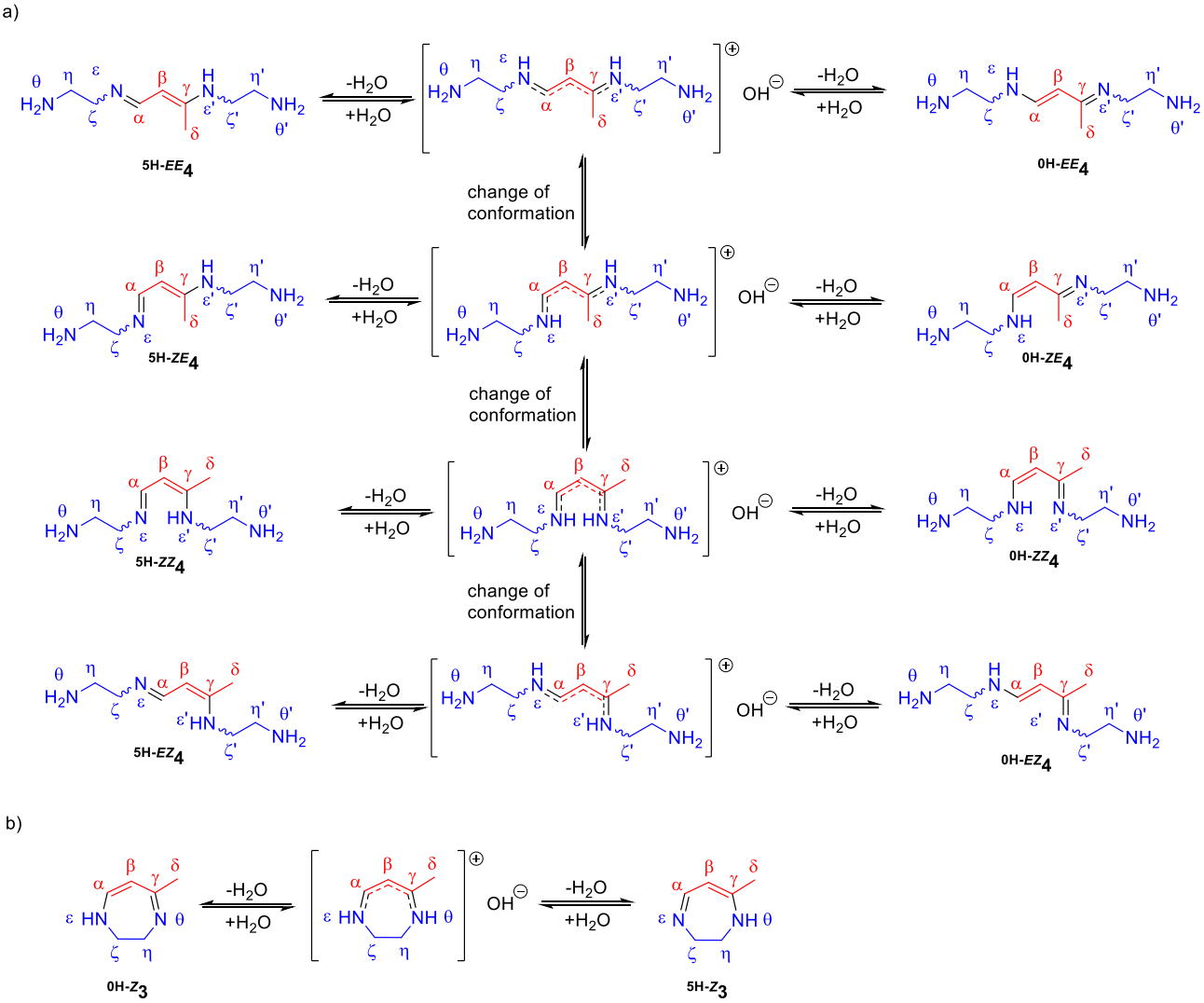

Molecule 4 in presence of water traces.

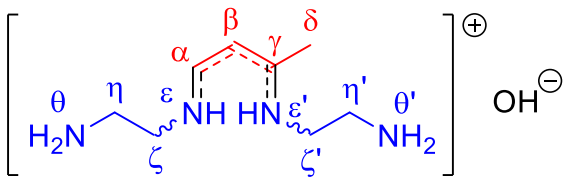

4

1D NMR data: see Table S2

2D NMR data: no couplings visible

NMR description: In water-free *en* the tautomerization/isomerization of **4** is slow, with respect to NMR time scale. However, in *en* containing water traces the signals of **4** broaden (signals denoted by $^{5\text{-}7}$4) and the coupling patterns disappear. We suppose that in presence of water, molecule **4** tautomerizes/isomerizes fast according to the mechanism described in Scheme S3a. Due to the open structure of **4** the configuration/conformation of the C_4-backbone can change. As a further consequence of fast tautomerization the average chemical surroundings of the protons ζ and ζ' are almost identical (the only difference is the position of the methyl-group), and in ^{1}H NMR both protons appear at almost identical chemical shifts. The same argumentation is valid for protons η/η' and θ/θ', however these signals cannot be detected due to overlaps with *en*-peaks.

Molecule 3 in presence of water traces.

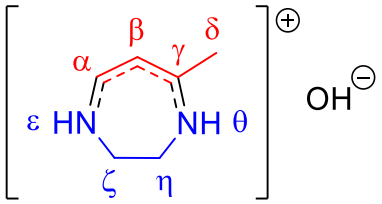

3

1D NMR data: see Table S2.

2D NMR data: COSY (500 MHz, chloroform-d_1, 296 K), δ(ppm): 6.87/4.55 (^3J, 3α/3β); HMBC (500 MHz, chloroform-d_1, 296 K), δ(ppm): 6.87/161.6 (^3J, 3α/3γ), 4.54/161.6 (^2J, 3β/3γ), 2.01/161.6 (^2J, 3δ/3γ), 4.56/148.6 (^2J, 3β/3α), 6.87/91.9 (^2J, 3α/3β), 2.00/91.9 (^3J, 3δ/3β), 6.87/52.3 (^3J, 3α/3ζ), 4.56/25.3 (^3J, 3β/3δ); HSQC (500 MHz, chloroform-d_1, 296 K), δ(ppm): 6.87/148.7 (^1J, 3α/3α), 4.55/91.9 (^1J, 3β/3β), 3.55/52.4 (^1J, 3ζ,η/3ζ,η), 2.01/25.2 (^1J, 3δ/3δ).

NMR description: Analogously to **4**, molecule **3** can tautomerize fast in *en* containing water traces. In ^{1}H NMR (Figure S2a) the protons 3α, 3β and 3δ of the C_4-backbone appear by two doublets (J = 7.4 Hz) at 6.87 ppm and 4.55 ppm as well as a singlet at 2.0 ppm, respectively. Due to the ring structure, the configuration of the C_4-backbone is fixed and no isomerization can occur upon tautomerization (Scheme S3b). Consequently, the resonances of the protons of the C_4-backbone exhibit coupling patters. For 3α and 3β, the chemical shifts and coupling constant of 7.4 Hz are typical for *cis*-orientated olefinic protons. The tautomerization of **3** is associated with fast proton exchange at the nitrogen atoms 3ε/3θ, and delocalization of the double bonds among the nitrogen and carbon atoms 3ε/3α/3β/3γ/3θ, respectively. Due to fast proton exchange, no couplings of the -N*H* groups to the C_4-backbone and *en*-substituent are visible, respectively. As a further consequence of fast tautomerization, the averaged chemical surroundings of the protons 3ζ and 3η of the *en*-substituent (blue) are almost identical (the only difference is the position of methyl-group), and in ^{1}H NMR solely one signal (3ζ/3η: 3.55 ppm, superposition of two close laying triplets, integral 4H) appears, respectively. For the C_4-backbone and *en*-substituent, ^{13}C chemical shifts of 148.7 (3α), 91.9 (3β), 161.6 (3γ), 25.2 (3δ) ppm and 52.3 (3ζ/3η) ppm were derived from the HSQC/HMBC-spectra (Figure S2c/d), respectively. In HMBC the C_4-backbone is indicated by ^2J and ^3J

couplings between proton 3α/carbon 3β (6.87 ppm/91.9 ppm), proton 3β/carbon 3γ (4.54 ppm/161.6 ppm) and proton 3β/carbon 3δ (4.56 ppm/25.3 ppm), respectively. Moreover, the connection of the C_4-backbone to the *en*-substituent is indicated by a cross-peak at 6.87 ppm/52.3 ppm, which is attributed to a ^3J coupling of proton 3α with carbon 3ζ.

1.4. Summary of *in situ* NMR

In Table S3 the outcomes of *in situ* NMR investigations are broken down for the different mixtures and references to the figures, showing the corresponding NMR spectra, are given.

Table S3. Molecules and functionalities identified in test mixtures A-B

Test mixture					**Results: NMR**	
Type	**Nucleophile**	**1**	**2**	**Reaction time [h]**	**Molecules/ Funct.**	**Figure S**
A	*en* 1ml	60-240 µmol	-	20	**2**	5a
	en 1ml	240 µmol	-	3-147	**2**	5b
B	*en*/[H_2O] 1ml	120 µmol	-	3-100	**2**, **3**, **4**	7
	en/[H_2O] 1ml	120 µmol	-	>20	**3**, **4**	6

1.5 NMR spectra and details on the preparation of test mixtures of the reaction of *en* with 1

In the following the NMR spectra of the test mixtures are shown. Experimental details on the preparation of the mixtures are given in the figure captions. In most cases only sections of the spectra are given and the intensity scales of different spectral regions were adjusted in a way that all relevant signals can be seen. r.t. = reaction time.

1.5.1 water-free *en* [1]

The following spectra correspond to test mixtures type A.

Figure S1. a) ^{1}H NMR spectra of test mixtures prepared by reacting 23.4 mg (60 µmol), 46.7 mg (120 µmol) and 93.4 mg (240 µmol) of **1** with each 1 ml of water-free *en* (r.t. = 20 h). **1** dissolved in *en* within 1 h and transparent pale yellow solutions were obtained. The mixtures contain ^{Z}**2** and ^{E}**2**, and the overall concentration of **2** in the solution increases with the initial amount of **1**; b) ^{1}H NMR spectra of a mixture obtained by dissolving 93.4 mg (240 µmol) in 1 ml water-free *en* after reaction times of 3, 24 and 147 h. After a reaction time of 3 h the maximal concentration of $^{E/Z}$**2** is reached and remains constant.

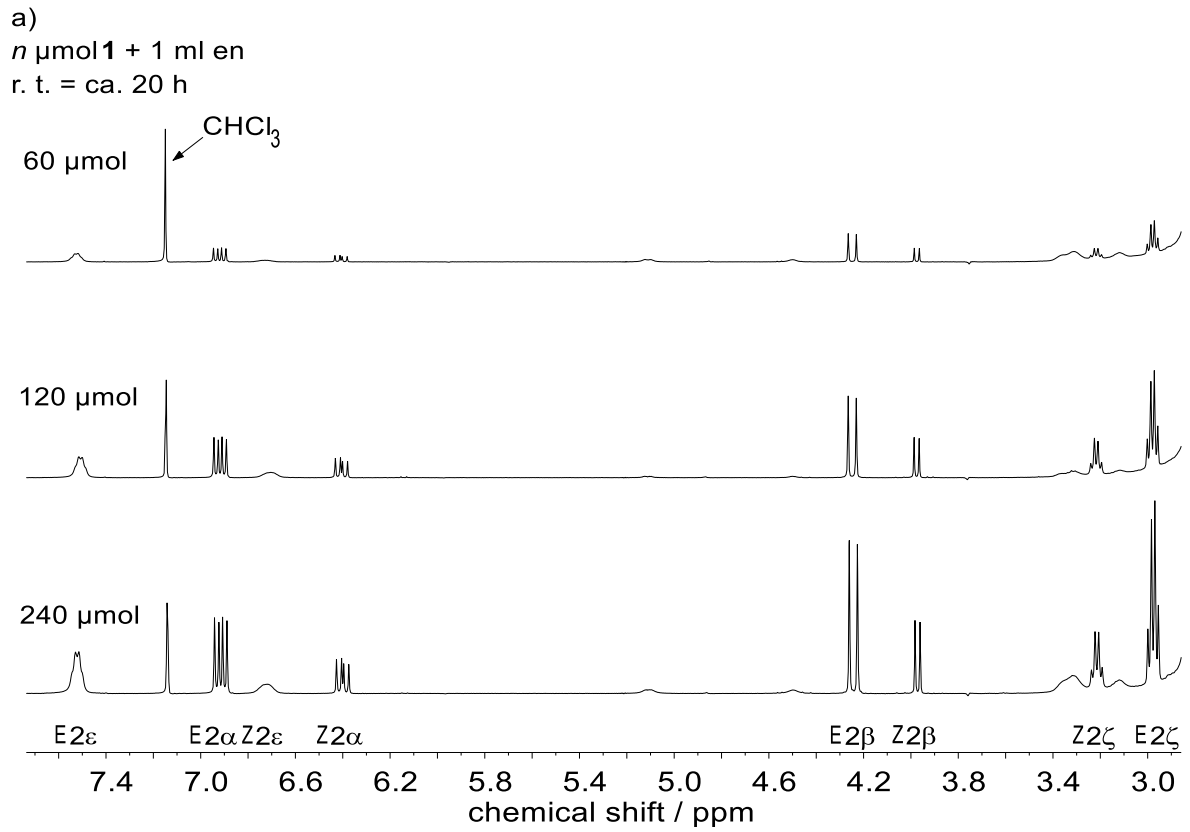

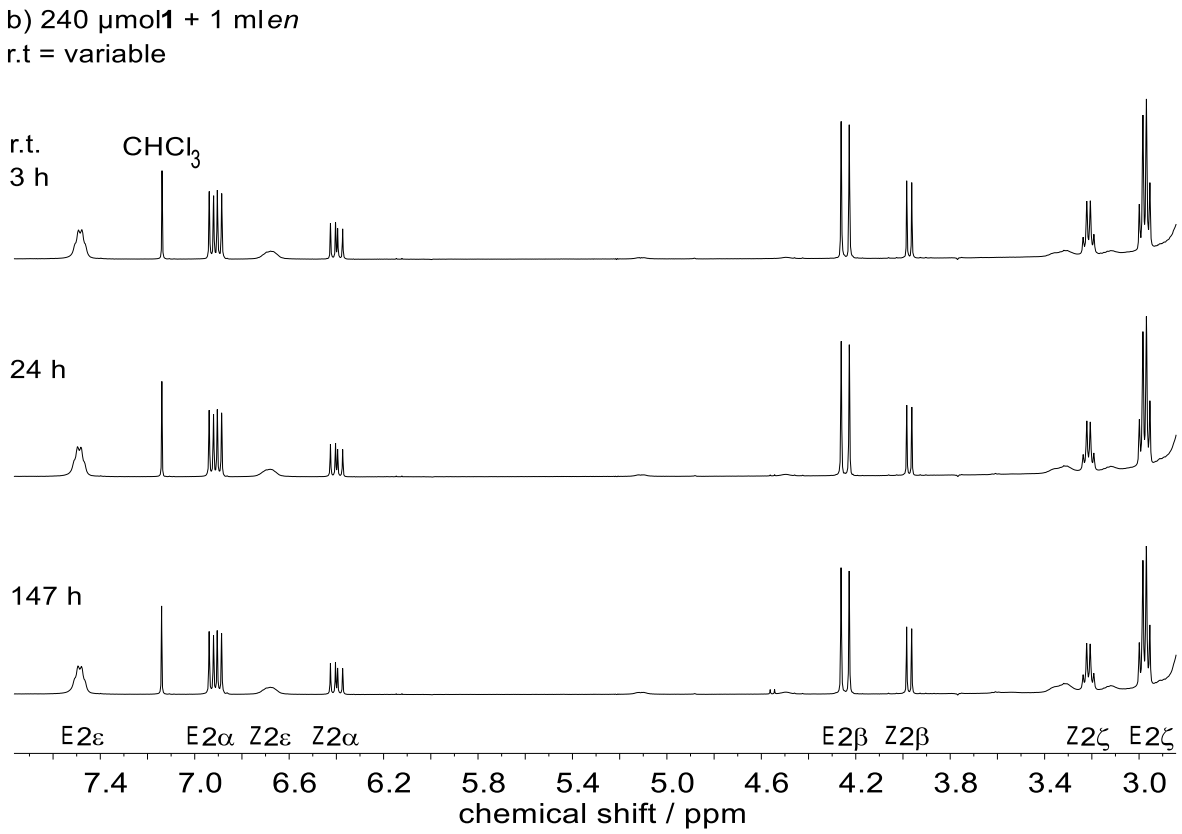
b) 240 µmol 1 + 1 ml en
r.t = variable
r.t.
3 h
CHCl3
24 h
147 h
E2ε
E2α
Z2ε
Z2α
E2β
Z2β
Z2ζ
E2ζ
7.4
7.0
6.6
6.2
5.8
5.4
5.0
4.6
4.2
3.8
3.4
3.0
chemical shift / ppm

1.5.2 *en* containing water traces

The following spectra correspond to test mixtures type B.

Figure S2. a) ^{1}H, b) COSY, c) HMBC and d) HSQC spectra of a test mixture, prepared by dissolving 46.7 mg (240 µmol) of **1** in 2 ml *en* containing ca. 0.5-1% water (r.t. > 20 h). Initially, the colour of the mixture was pale yellow, but turned into intensive orange after 100 h. The NMR spectra exhibit signals of **3** and **4**, which both tautomerize/isomer fast in presence of water.

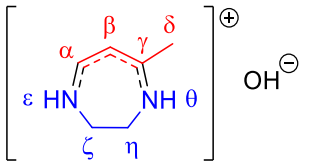

3

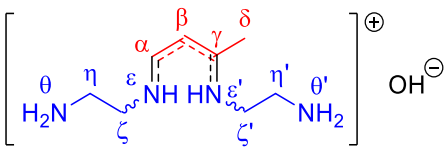

4

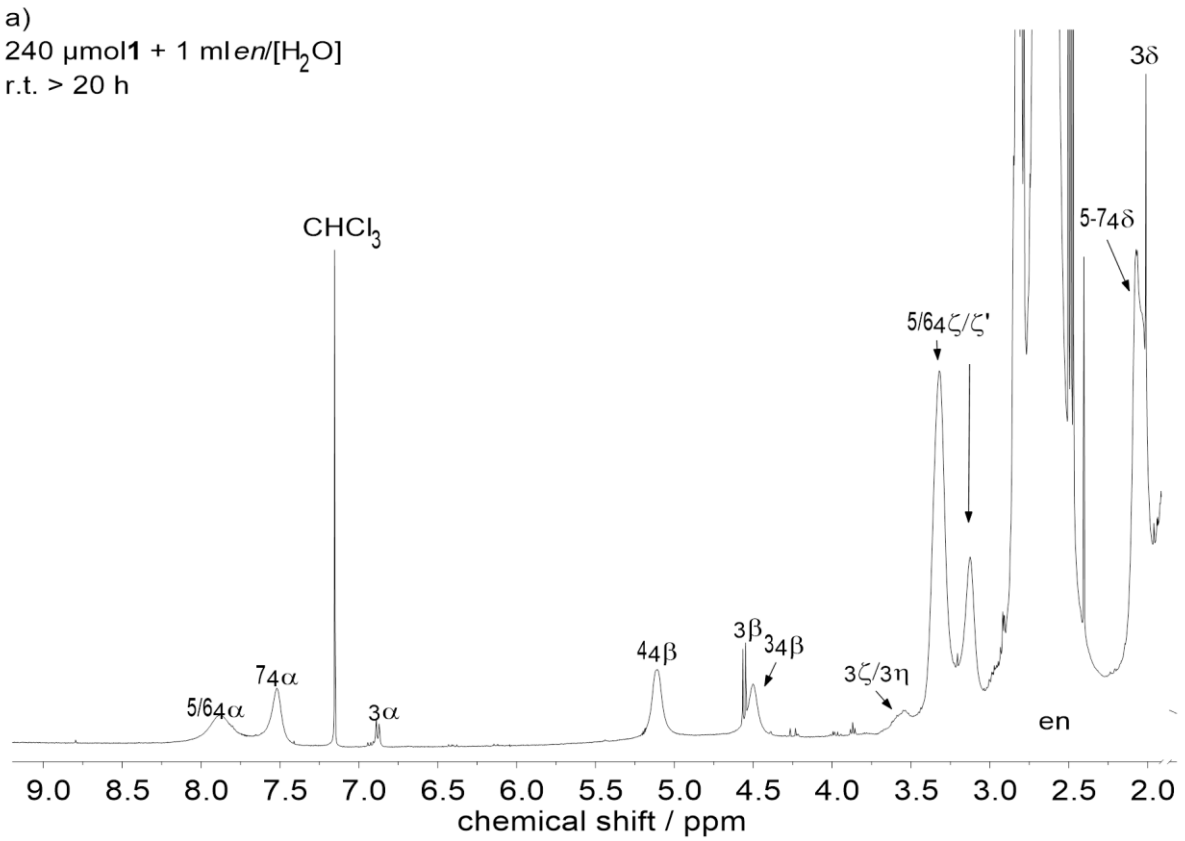

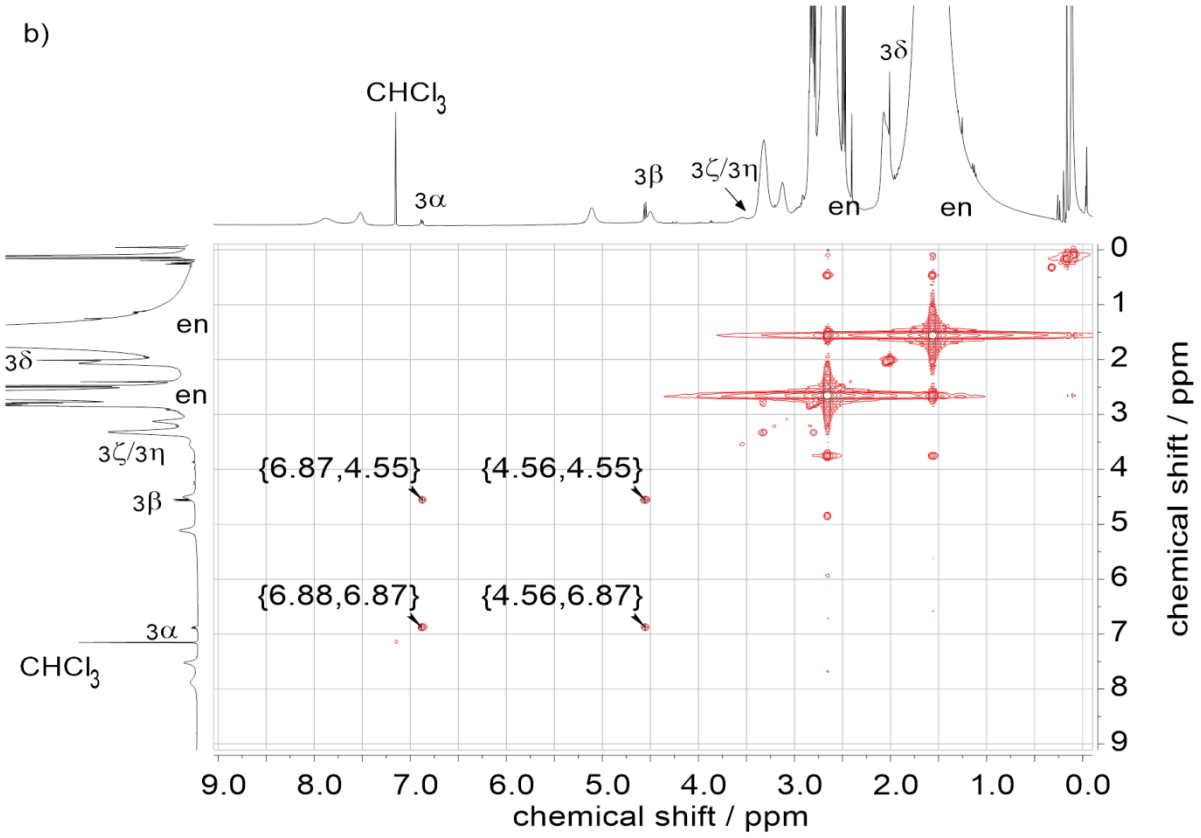
b)
CHCl3
3α
3β
3ζ/3η
en
en
3δ
en
3δ
en
3ζ/3η
3β
3α
CHCl3
{6.87,4.55}
{4.56,4.55}
{6.88,6.87}
{4.56,6.87}
chemical shift / ppm
chemical shift / ppm

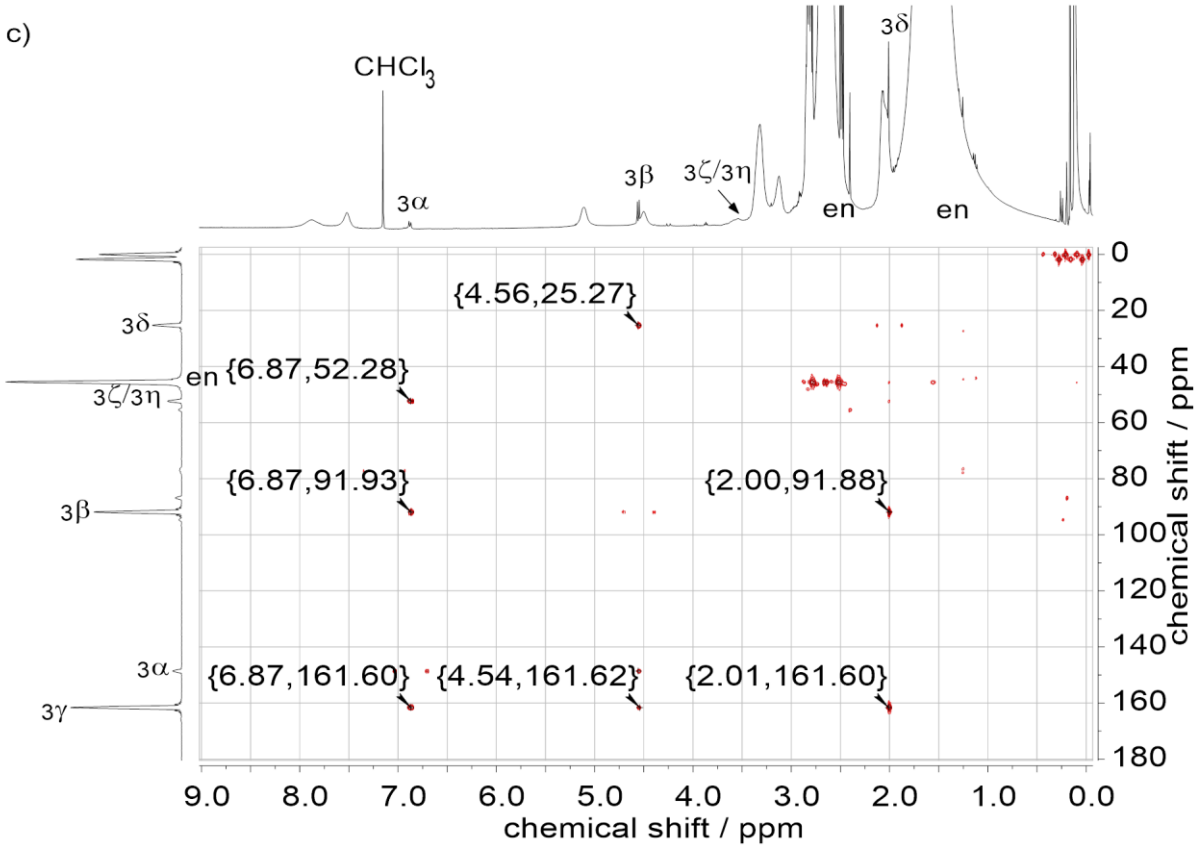
c)
CHCl3
3α
3β
3ζ/3η
en
en
3δ
3δ
en
3ζ/3η
3β
3α
3γ
{4.56,25.27}
{6.87,52.28}
{6.87,91.93}
{2.00,91.88}
{6.87,161.60}
{4.54,161.62}
{2.01,161.60}
chemical shift / ppm
chemical shift / ppm

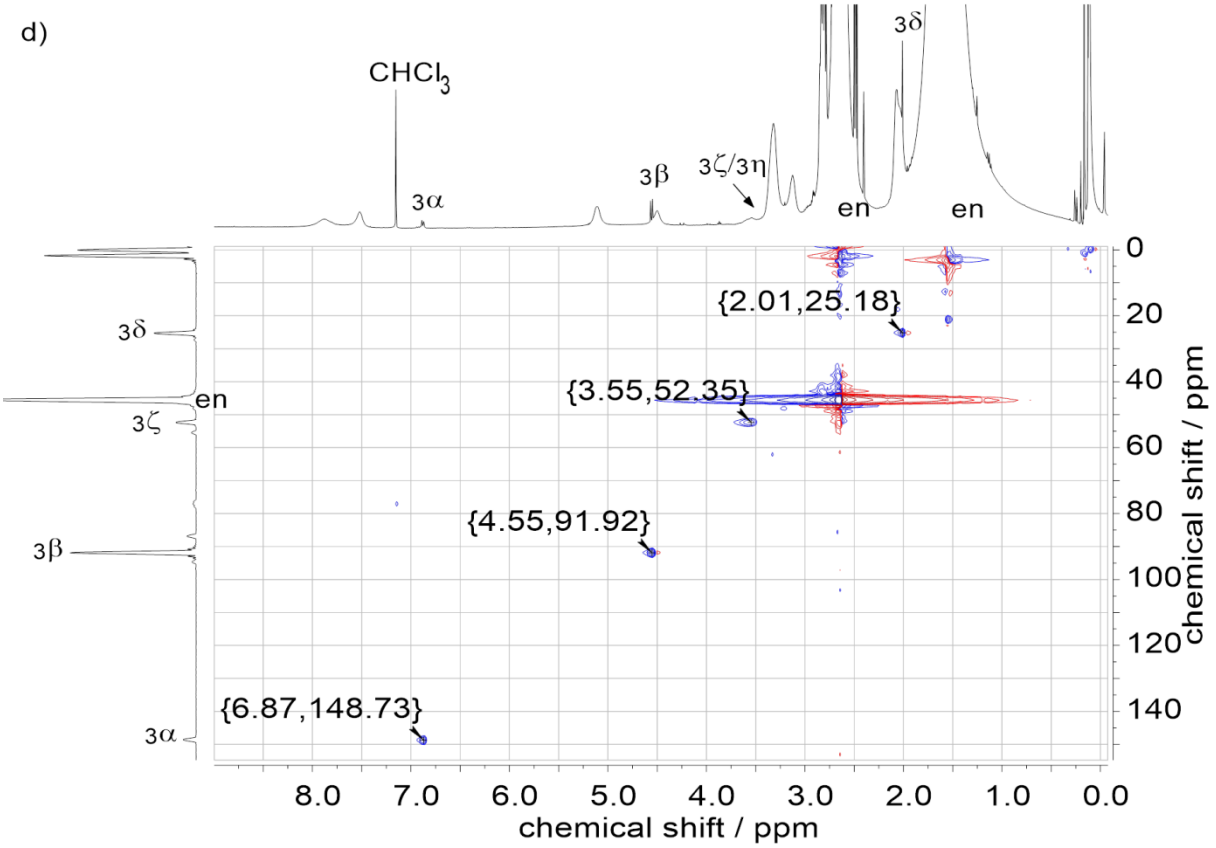
d)
CHCl3
3α
3β
3ζ/3η
en
en
3δ
{2.01,25.18}
{3.55,52.35}
{4.55,91.92}
{6.87,148.73}
3δ
en
3ζ
3β
3α
8.0
7.0
6.0
5.0
4.0
3.0
2.0
1.0
0.0
chemical shift / ppm
0
20
40
60
80
100
120
140
chemical shift / ppm

Figure S3. ^{1}H NMR spectra of a test mixture, prepared by dissolving 46.7 mg (240 µmol) of **1** in 2 ml *en* containing ca. 0.5-1% water, in dependence of reaction time (3, 20, 100 h). After reaction times of 3 h, signals of **2**, **3** and **4** are visible. With increasing reaction time the concentration of **2** decreases and after 100 h solely **3** and **4** are visible.

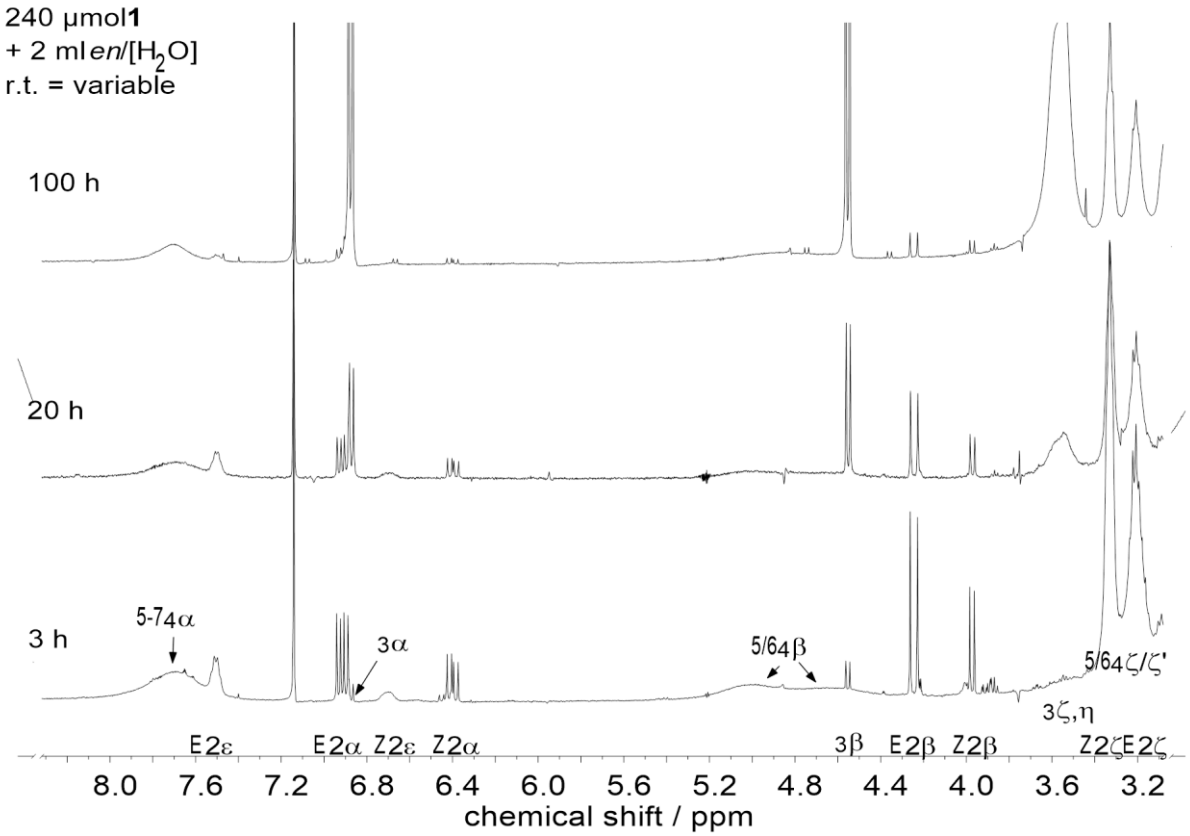

1.6 Reaction of $KHN(CH_2)_2NHK$ with 2 in water-free *en*

The following spectra correspond to test mixtures type C

Figure S4. a) ^1H, b) COSY, c) HMBC and d) HSQC NMR spectra of a test mixture, prepared by dissolving $KNH(CH_2)_2NHK$ (6.1 mg , 45 µmol, 1 eq.) in 0.75 ml of an *en*-solution (water-free) containing 60 µmol/ml **2** (4: 45 µmol, 1 eq.). Immediately upon addition of $KNH(CH_2)_2NHK$ the color of the solution turned into intensive deep-orange. The mixture was stirred for 30 min, before a sample for NMR was taken. The NMR spectra show signals of **4**.

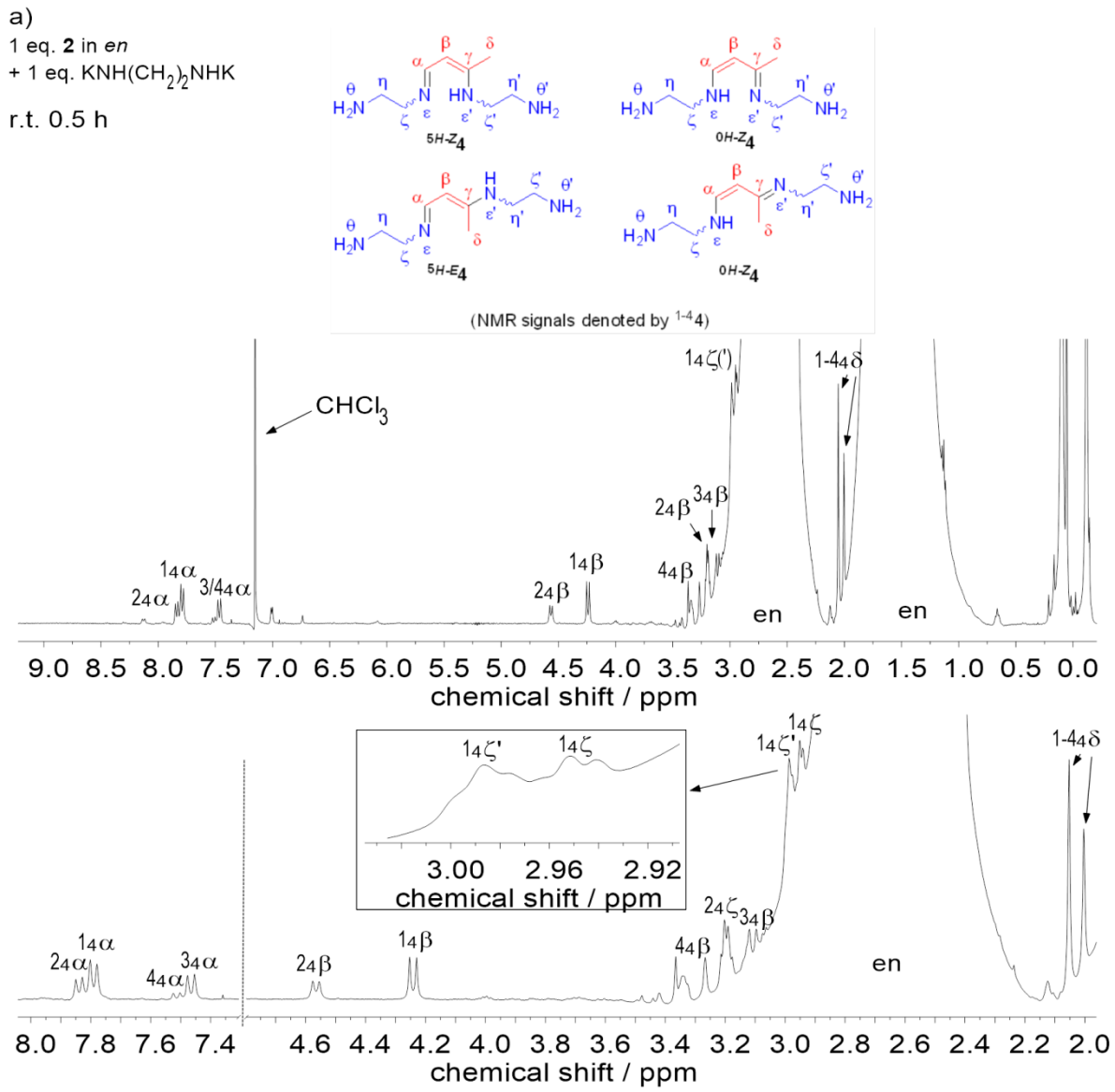

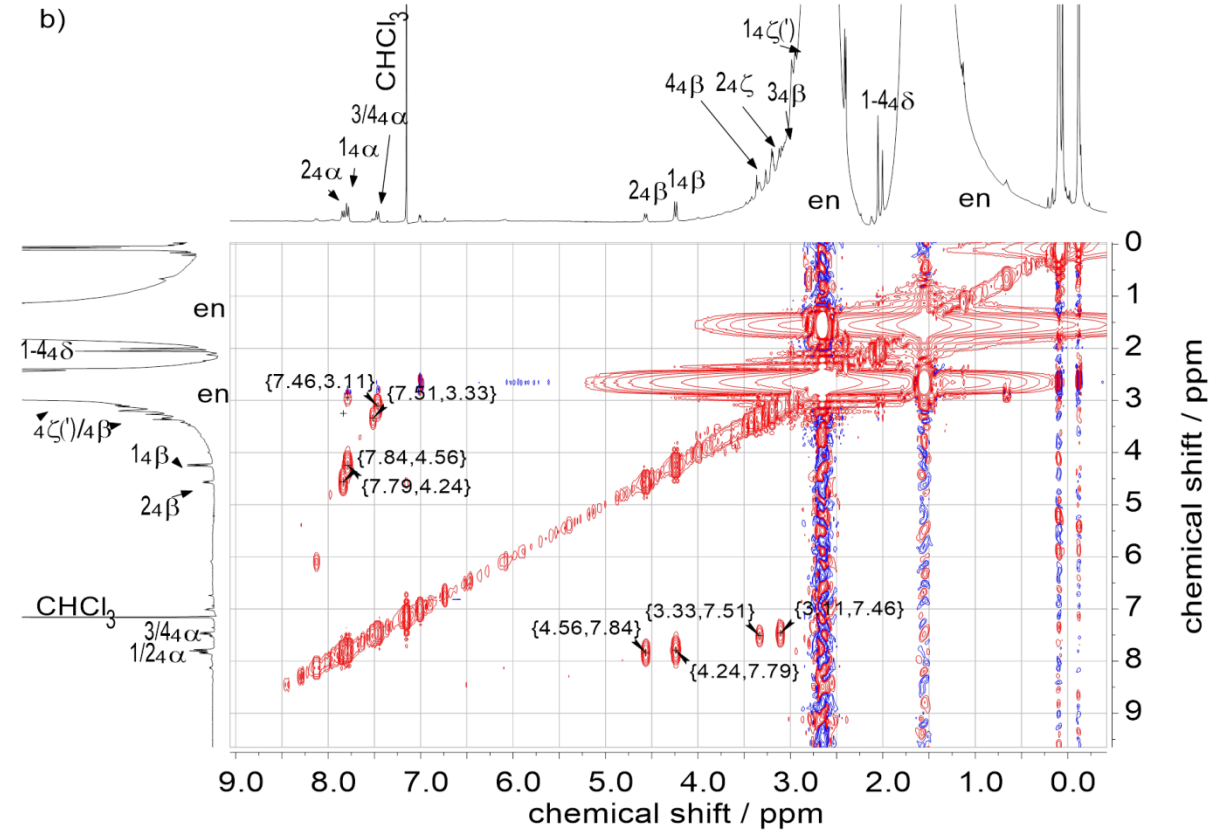
b)
CHCl3
1₄ζ(')
4₄β 2₄ζ 3₄β
1-4₄δ
3/4₄α
1₄α
2₄α
2₄β 1₄β
en
en
en
en
1-4₄δ
4ζ(')/4β
1₄β
2₄β
CHCl3
3/4₄α
1/2₄α
{7.46,3.11}
{7.51,3.33}
{7.84,4.56}
{7.79,4.24}
{4.56,7.84}
{3.33,7.51}
{3.11,7.46}
{4.24,7.79}
chemical shift / ppm
chemical shift / ppm

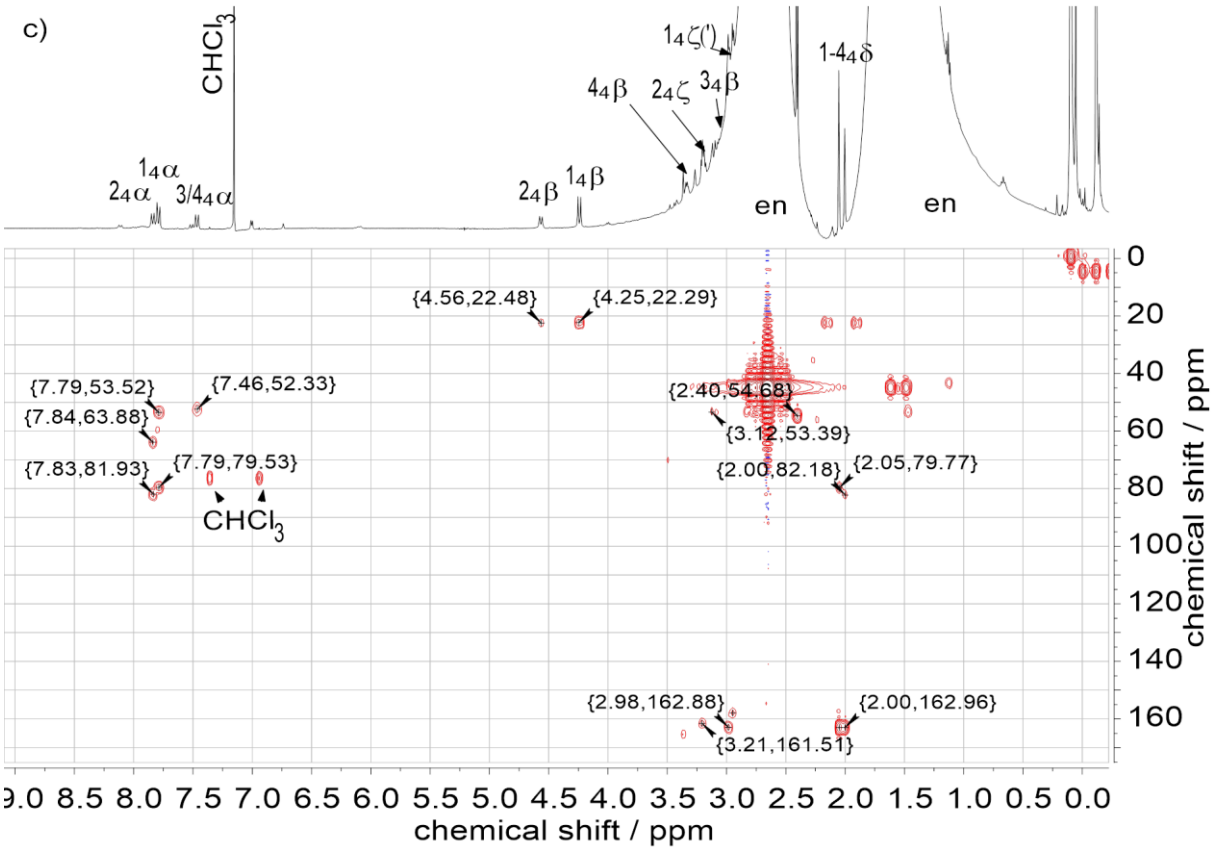
c)
CHCl3
1₄ζ(')
1-4₄δ
4₄β 2₄ζ 3₄β
1₄α
2₄α 3/4₄α
2₄β 1₄β
en
en
{4.56,22.48}
{4.25,22.29}
{7.79,53.52}
{7.46,52.33}
{7.84,63.88}
{2.40,54.68}
{3.12,53.39}
{7.83,81.93}
{7.79,79.53}
{2.00,82.18}
{2.05,79.77}
CHCl3
{2.98,162.88}
{2.00,162.96}
{3.21,161.51}
chemical shift / ppm
chemical shift / ppm

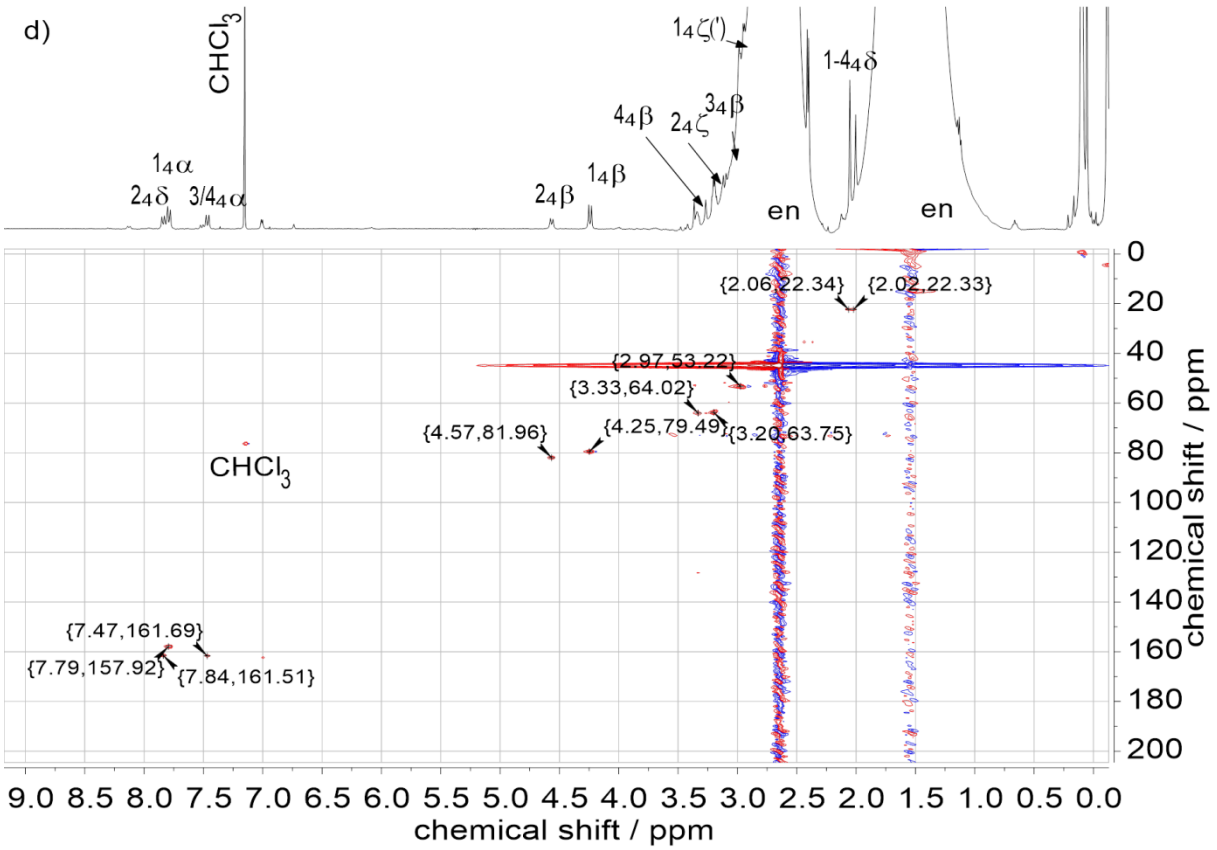

2 References

[1] M. M. Bentlohner, W. Klein, Z. H. Fard, L.-A. Jantke, T. F. Fässler, *Angew. Chem. Int. Ed.* **2015**, *54*, 3748-3753.

5.3 On the Mechanism of Connecting Deltahedral Zintl Clusters *via* Conjugated Buta-1,3-dien-1,4-diyl Functionalities: Synthesis and Structure of $[Ge_9–CH=CH–CH=CH–Ge_9]^{6–}$

Manuel M. Bentlohner[+], Sabine Frischhut[+], and Thomas F. Fässler

[+] These authors contributed equally to this work.

published in:

Chem. Eur. J. **2017**, *23*, 17089-17094.

CONTENT AND CONTRIBUTION

In the scope of this publication the synthesis of the first unfunctionalized Zintl triad $[Ge_9–CH=CH–CH=CH–Ge_9]^{6–}$ comprising two Ge_9 Zintl clusters linked by a conjugated buta-1,3-diene-1,4-diyl bridge was achieved by reaction of A_4Ge_9 (*A* = K, Rb) with 0.25 equiv. of 1,4-bis(trimethylsilyl)butadiyne in *en* at r.t. The synthesis strategy of adding *en* to a pre-mixture of A_4Ge_9 and 1,4-bis(trimethylsilyl)butadiyne turned out to be decisive for a successful synthesis and to prevent the reaction of 1,4-bis(trimethylsilyl)butadiyne with *en*. The choice of equivalents of the dialkyne was also significant for successful crystallization of $[Ge_9–CH=CH–CH=CH–Ge_9]^{6–}$, which was carried out in the scope of this work. The novel compound was the second of its kind. The crystal structure was determined by single crystal X-ray diffraction and was carried out by Dr. Manuel M. Bentlohner, who also completed structure refinement.

In addition, the mechanism of the formation of the conjugated organic linker moiety was elucidated for the first time by *in situ* ^{1}H NMR investigations, which were carried out by Dr. Manuel Bentlohner.

Dr. Herta Slavik and M.Sc. Sebastian Geier performed Raman measurements on single crystals of $[Ge_9–CH=CH–CH=CH–Ge_9]^{6–}$. The elucidation of the data was carried out in the scope of this work and by Dr. Manuel M. Bentlohner.

The publication was equally authored within this work and by Dr. Manuel M. Bentlohner. The manuscript was revised by Prof. Dr. Thomas F. Fässler.

Cluster Compounds

On the Mechanism of Connecting Deltahedral Zintl Clusters via Conjugated Buta-1,3-dien-1,4-diyl Functionalities: Synthesis and Structure of $[Ge_9–CH=CH–CH=CH–Ge_9]^{6-}$

Manuel M. Bentlohner[+], Sabine Frischhut[+], and Thomas F. Fässler*[a]

Dedicated to Professor Dieter Fenske on the occasion of his 75th birthday

Abstract: We report on the synthesis and structure, as well as on the mechanism of formation of the $[Ge_9–CH=CH–CH=CH–Ge_9]^{6-}$ unit. As shown by in situ NMR spectroscopy (^{1}H, COSY, HSQC, HMBC), both (1*Z*,3*Z*)- and (1*E*,3*Z*)-$[Ge_9–CH=CH–CH=CH–Ge_9]^{6-}$ are formed during the reaction of a mixture of 1,4-bis(trimethylsilyl)butadiyne and A_4Ge_9 (A = K, Rb) with ethylenediamine. However, upon layering of the obtained solution with 222-crypt/toluene (222-crypt = 4,7,13,16,21,24-hexaoxa-1,10-diazabicyclo-[8.8.8]hexacosan) only the (1*Z*,3*Z*)-isomer crystallizes as $\{[A(222\text{-crypt})]_6[(1Z,3Z)\text{-}(Ge_9–CH=CH–CH=CH–Ge_9)]\}(tol)_2(en)_2$ (A = K, Rb) salts. Single crystals of these salts were characterized by X-ray structure analysis and Raman spectroscopy, indicating the presence of three superimposed conformers of (1*Z*,3*Z*)-$[Ge_9–CH=CH–CH=CH–Ge_9]^{6-}$, which show different orientations of the cluster units with respect to the planar (1*Z*,3*Z*)-buta-1,3-dien-1,4-diyl linker unit.

Introduction

$[E_9]^{4-}$ Zintl anions (E = Si, Ge, Sn, Pb) are accessible by the dissolution of the Zintl phases A_4E_9 (A = K, Rb, Cs; E = Ge, Sn, Pb) and $A_{12}E_{17}$ (A = K, Rb, Cs; E = Si, Ge) in ethylenediamine (en), *N*,*N*-dimethylformamide (dmf) or liquid ammonia.[1,2] Similar to the closely related fullerenes, E_9 cages can adopt different oxidation states and occur as $[E_9]^{2-}$, $[E_9]^{3-}$ and $[E_9]^{4-}$ Zintl anions, with 20, 21 and 22 skeleton-bonding electrons (SE), respectively.[3,4] According to the Wade–Mingos rules, $[E_9]^{4-}$ (22 SE) and $[E_9]^{2-}$ (20 SE) are *nido* and *closo* clusters, whereas the paramagnetic $[E_9]^{3-}$ radical anion evades this description.[1,2]

The homologous fullerenes have been thoroughly investigated as components in systems for artificial photosynthesis, spintronics, and photovoltaics.[5,6] By covalent binding of the fullerenes to organic donor and acceptor molecules and by the coupling of two fullerene entities via organic spacers, a variety of electroactive dyads and triads has been synthesized.[5–7] An outstanding example is [6,6]-phenyl-C_{61}-butyric acid methyl ester (PCBM), which has been applied as an electron-acceptor molecule in organic photovoltaics.[7,8] The flexibility of the E_9 cages with respect to their number of electrons makes these molecules to interesting alternatives for fullerenes.

The possible functionalization of Ge_9 Zintl anions with organic tethers by nucleophilic addition to alkynes[9–14], as well as their substitution with alkyl halides,[15] point towards the synthesis of fullerene-analogous Zintl triads. Recently, we reported the first representatives of such Zintl triads, $[CH_2=CH–(Ge_9)–(^{ZE}\mathbf{B})–(Ge_9)–CH=CH_2]^{4-}$ [$^{ZE}\mathbf{B}$ = (1*Z*,3*E*)-buta-1,3-dien-1,4-diyl)][16] and $[(^{Z}\mathbf{R})–(Ge_9)–(^{ZZ}\mathbf{B})–(Ge_9)–(^{Z}\mathbf{R})]^{4-}$ [$^{ZZ}\mathbf{B}$ = (1*Z*,3*Z*)-buta-1,3-dien-1,4-diyl; $^{Z}\mathbf{R}$ = (2*Z*,4*E*)-7-amino-5-aza-hepta-2,4-dien-2-yl] (**C**)[17] (Scheme 1). **C** was obtained by the reaction of K_4Ge_9 with a mixture of 1,4-bis(trimethylsilyl)butadiyne and 1-trimethylsilyl-7-amino-5-aza-hepta-3-en-1-yne in en solvent.[17] Besides the

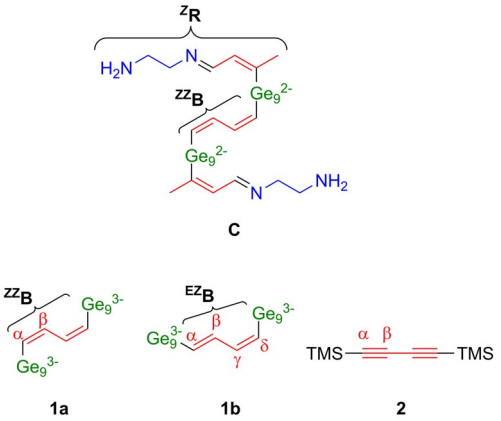

Scheme 1. The chemical composition of $[(^{Z}\mathbf{R})–(Ge_9)–(^{ZZ}\mathbf{B})–(Ge_9)–(^{Z}\mathbf{R})]^{4-}$ (**C**), $[(Ge_9)–(^{ZZ}\mathbf{B})–(Ge_9)]^{6-}$ (**1 a**), $[(Ge_9)–(^{EZ}\mathbf{B})–(Ge_9)]^{6-}$ (**1 b**) and 1,4-bis(trimethylsilyl)-butadiyne (**2**).

[a] *M. M. Bentlohner,[+] S. Frischhut,[+] Prof. Dr. T. F. Fässler*
Department Chemie, Technische Universität München
Lichtenbergstraße 4, 85747 Garching (Germany)
E-mail: thomas.faessler@lrz.tum.de
[+] *These authors contributed equally to this work.*
Supporting information and the ORCID identification number for the author of this article can be found under: https://doi.org/10.1002/chem.201703494. The Supporting Information contains detailed crystallographic material on the compounds $\{[A(222\text{-crypt})]_6\mathbf{1a}\}(tol)_2(en)_2$ and details on the in situ NMR investigations.

linkage of the two cluster units by a diene, the reaction of 1,4-bis(trimethylsilyl)butadiyne with the solvent en led to the formation of the functional group ^{Z}**R** as part of the Zintl triad **C**.

Herein we studied the reaction mechanism that leads to the formation of the Zintl triads $[(Ge_9)–(^{ZZ}\mathbf{B})–(Ge_9)]^{6-}$ (**1 a**), and $[(Ge_9)–(^{EZ}\mathbf{B})–(Ge_9)]^{6-}$ (**1 b**) [^{EZ}**B** = (1*E*,3*Z*)-buta-1,3-dien-1,4-diyl] without a subsequent reaction resulting in additional side chains at the clusters. The entities **1 a** and **1 b** were identified in solution by NMR spectroscopy (^{1}H, COSY, HSQC, HMBC), and **1 a** which was isolated as its potassium and rubidium salts $\{[A(222\text{-crypt})]_6\mathbf{1a}\}(tol)_2(en)_2$ (A = K, Rb), was characterized by means of single crystal X-ray structure analysis and Raman spectroscopy.

Results and Discussion

Synthesis

The Zintl triads **1 a** and **1 b** were synthesized by stirring pre-mixtures of the solids A_4Ge_9 (1 equiv) and 1,4-bis(trimethylsilyl)-butadiyne (**2**) (0.25–0.5 equiv) with water-free en solvent[17] for 20 h (Scheme 1 and Equation 1). In former experiments leading to the Zintl triads with ^{Z}**R** side chains in **C**, suspensions of **2** in en were treated with solid A_4Ge_9.[17] By contrast, the method presented herein avoids a pre-mixing of **2** with en, and focuses on the direct addition of en to a mixture of **2** with A_4Ge_9. According to the results of in situ NMR spectroscopic investigations, **1 a** and **1 b** are formed in an isomer ratio of 20:80 (see Supporting Information, Figure S6). The layering of the dark brown reaction mixture with 222-crypt in toluene resulted in bundles of dark red crystals of $\{[A(222\text{-crypt})]_6\mathbf{1a}\}(tol)_2(en)_2$ (A = K, Rb) (yield ca. 10%) within 1–2 weeks, whereas no crystals containing **1 b** could be isolated.

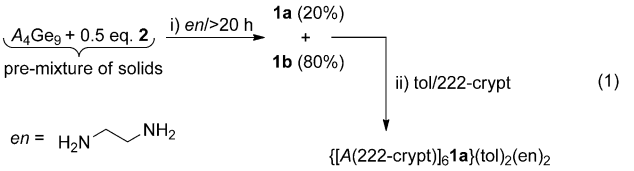

(1)

Crystal structure

Single crystals of $\{[Rb(222\text{-crypt})]_6\mathbf{1a}\}(tol)_2(en)_2$ suitable for X-ray structure analysis and Raman spectroscopy were isolated from a mixture of Rb_4Ge_9 (1 equiv) and **2** (0.25 equiv) which was treated with en for 23 h and layered with 222-crypt in toluene. The presence of six $[Rb(222\text{-crypt})]^+$ counterions clearly indicate a six- fold negative charge to the cluster anion **1 a**.[19] The crystalline compound contains two toluene and two en molecules per formula unit, which are enclosed in channels formed by the $[Rb(222\text{-crypt})]^+$ units along the crystallographic *a* axis (Figure 1). The anionic entity **1 a** (Figure 2) consists of two clusters that are linked by a C_4 chain via covalent Ge–C bonds. The anionic entity is arranged around a crystallographic center of inversion, which is located in the middle of the C_4 linker.

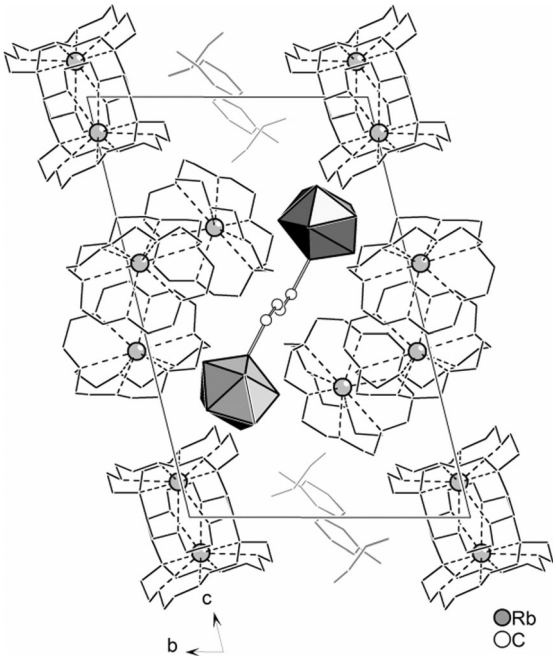

Figure 1. The unit cell of $\{[Rb(222\text{-crypt})]_6\mathbf{1a}\}(tol)_2(en)_2$. Conformer **1 a**^{I} is depicted, and the minority components **1 a**^{II} and **1 a**^{III} are omitted for clarity. The Ge_9 clusters are shown as dark-grey polyhedra. The atoms of the organic functionalities ^{ZZ}**B** are shown as empty spheres. The 222-crypt and solvent molecules are shown schematically. Hydrogen atoms are omitted for clarity.

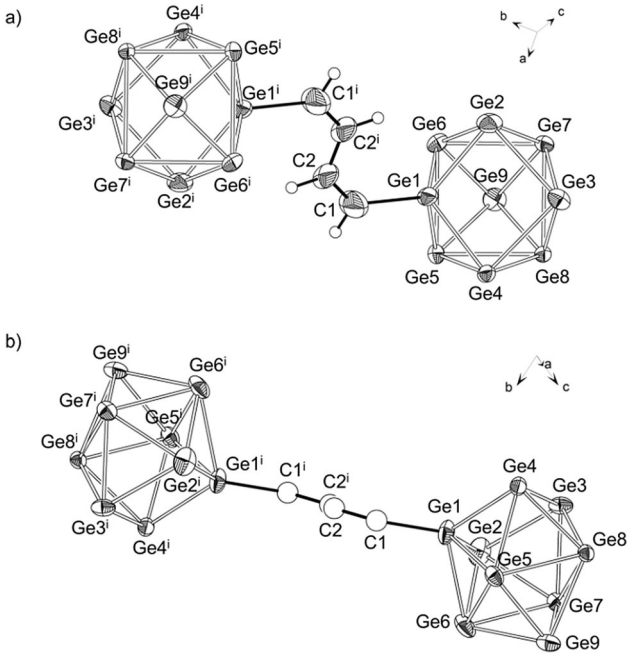

Figure 2. X-ray structure of **1 a**^{I} Views: a) perpendicular, and b) parallel to the [Ge-^{ZZ}**B**-Ge] plane. Thermal ellipsoids are shown at a probability level of 50%. In b) carbon and nitrogen atoms are shown as empty spheres, and hydrogen atoms are omitted for clarity.

In the crystal structure the anion **1 a** is disordered. The disorder is caused by three superimposed Ge_9 clusters [**I** (61.9%), **II** (25.1%) and **III** (13.0%)] which show rather similar shapes but different orientations (Figure S2). For each cluster the center of

inversion generates a symmetry equivalent cluster **I**^{i}, **II**^{i} and **III**^{i}. The shortest inter-cluster Ge–Ge^{i} distances between each cluster-pair **I**/**I**^{i}, **II**/**II**^{i} and **III**/**III**^{i} are 6.376 Å (Ge1–Ge1^{i}), 6.583 Å (Ge10–Ge10^{i}), and 6.582 Å (Ge19–Ge19^{i}) (see also Supporting Information, Figure S3). Ge–Ge distances in that range are typical of clusters connected by a planar conjugated (1*Z*,3*Z*)-buta-1,3-dien-1,4-diyl unit in *s-trans* configuration (**^{ZZ}B**)[20], and thus the inter-cluster distances point towards a superposition of three conformers **1a**^{I} (Figure 2), **1a**^{II}, and **1a**^{III} with different orientations (Figure S2). In the conformers **1a**^{I} and **1a**^{II} the clusters **I** (61.9%) and **II** (25.1%), are both attached to the **^{ZZ}B** functionality (C1–C2–C2^{i}–C1^{i}), which therefore shows 87% occupancy. The Ge_9 clusters of **1a**^{I} and **1a**^{II} are rotated by 165° (for details see Supporting Information, Figure S4). The Ge–C distances are in the range of covalent Ge–C(sp^2) bonds,[9,21] whereby d(Ge1–C1) = 2.001(9) Å and d(Ge10–C1) = 1.918(9) Å. Moreover, the Ge1–C1–C2 and Ge10–C1–C2 bond angles of 130.1° and 139.1°, respectively, indicate that the clusters **I** and **II** are connected to **^{ZZ}B**. Further structural parameters are given in the Supporting Information (Table S1). The significantly different bond lengths within the C1–C2–C2^{i}–C1^{i} chain of 1.343(1) Å (C1–C2) and 1.447(2) Å (C2–C2^{i}) correspond to a double bond and a short single bond with multiple bond character, respectively.[21,22]

However, the minority cluster **III** (Figures S2 and S3) with an occupancy of 13% does not show any reasonable Ge–C distances to the C1–C2–C2^{i}–C1^{i} chain [d(Ge19–C1) = 2.703 Å, ∢(Ge19–C1–C2) = 109°], but a corresponding second, differently orientated, **^{ZZ}B** bridge (resulting in conformer **1a**^{III}) could not be unequivocally identified. The alternative possibility of an isolated $[Ge_9]^{3-}$ cluster cannot be unequivocally ruled out from the results of the Raman spectrum of {[Rb(222-crypt)]$_6$ **1a**}$(tol)_2(en)_2$ (Figure 3), even though the presence of isolated $[Ge_9]^{3-}$ clusters aside from the functionalized ones should lead to additional Raman signals, which, however, could not be detected. Therefore we assume that cluster **III** is also connected to **III**^{i} via a corresponding **^{ZZ}B** bridge, which due to its low occupancy of 13% could not be detected as significant electron density in the difference Fourier map located between the heavy atom clusters.

For the majority component **1a**^{I} the Ge–Ge distances of cluster **I** are in the range from 2.476(2) to 2.857(5) Å (for details see Supporting Information, Tables S1 and S3). Cluster **I** is best described as a distorted mono-capped quadratic antiprism with the square planes being defined by Ge1 to Ge4 [d(Ge–Ge) = 2.476(2)–2.673(5) Å] and Ge5 to Ge8 [d(Ge–Ge) = 2.757(5)–2.857(5) Å]. The deviation of the cluster shape from a tricapped trigonal prism with D_{3h} symmetry is indicated by maximum torsion angles of 178.8° and 179.8° for the square planes Ge1 to Ge4 and Ge5 to Ge8, respectively, as well as by the heights of the central trigonal prisms of 3.390 Å (Ge1–Ge3), 2.767 Å (Ge6–Ge7) and 2.757 Å (Ge5–Ge8). The square plane Ge1 to Ge4 is significantly compressed at the atom Ge1, which bears the **^{ZZ}B** functionality: d(Ge1–Ge2) = 2.476(2) Å and d(Ge1–Ge4) = 2.499(4) Å versus d(Ge3–Ge2) = 2.656(6) Å and d(Ge3–Ge4) = 2.673(5) Å. Correspondingly, **I** adopts C_S symmetry and derives from a C_{4v} symmetric mono-capped square antiprism with 22 skeleton-electrons by compression of the Ge1/Ge2/Ge3/Ge4 square plane at Ge1.[14,23]

By an analogous synthetic procedure single crystals of {[K(222-crypt)]$_6$**1a**}$(tol)_2(en)_2$ were obtained and characterized by X-ray structure analysis. It turned out that both {[A(222-crypt)]$_6$**1a**}$(tol)_2(en)_2$ are isotypic for A = K, Rb, and thus both show the same disorder of the anionic entity **1a** with slightly different occupancies; **1a**^{I}: 65.4%, **1a**^{II}: 18.0%, and **1a**^{III}: 16.6%.Thus, the structural parameters of the potassium salt are given only in the Supporting Information.

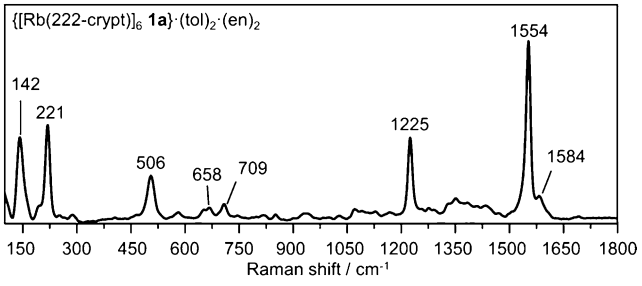

Figure 3. The Raman spectrum of single crystals of {[Rb(222-crypt)]$_6$**1a**}$(tol)_2(en)_2$. The most intensive signals are labelled with the corresponding Raman shift.

Raman spectroscopy

The Raman spectrum of crystals of {[Rb(222-crypt)]$_6$**1a**}-$(tol)_2(en)_2$ is shown in Figure 3. The intensive signals at 142 and 221 cm^{-1} are indicative of the Ge_9 clusters. Similar Raman signals in this region are observed for isolated $[Ge_9]^{4-}$ clusters,[24–26] and thus we assign the signals to the Ge_9 units in **1a**. The covalent connection of the Ge_9 units to carbon atoms are displayed by the signal at 506 cm^{-1}, which is typical of Ge–C valence vibrations.[27–30] Moreover, intensive signals at 1225 and 1554 cm^{-1} are indicative of symmetric C=C and C–C valence vibrations of the **^{ZZ}B** functionality.[31,32]

In situ NMR studies

In order to track the formation of the buta-1,3-dien-1,4-diyl cluster linkage we carried out time-resolved in situ NMR investigations involving mixtures of A_4Ge_9 and **2** in water-free en[18] with different stoichiometries (for details see Supporting Information, chapter 2).

Within less than 30 minutes, the reaction of **2** with an excess of A_4Ge_9 (A_4Ge_9/**2** = 1:0.25, 1:0.5) in en leads to a mixture of $[(Ge_9)–\mathbf{A}']^{3-}$ [**A**′ = 1,4-bis(trimethylsilyl)-buta-3-yne-1-en-1-yl] (**1**′**a**)[33] and $[(Ge_9)–(^{E}\mathbf{A})]^{3-}$ [^{E}**A** = (1*E*)-4-trimethylsilyl-buta-3-yne-1-en-1-yl] (**1**′**b**) in a 20:80 ratio (Figure 4 and Supporting Information, Figures S5–S7). Product **1**′**a** results from the addition of a $[Ge_9]^{4-}$ cluster to **2** before the trimethylsilyl (TMS) group at the double bond is exchanged by protons originating from en. With increasing reaction time the concentrations of **1**′**a** and **1**′**b** decrease, and the signals of the final products **1a** and **1b** emerge. The integrals of the ^{1}H NMR signals during the reaction indicate that **1a** originates from **1**′**a**, whereas **1b** arises

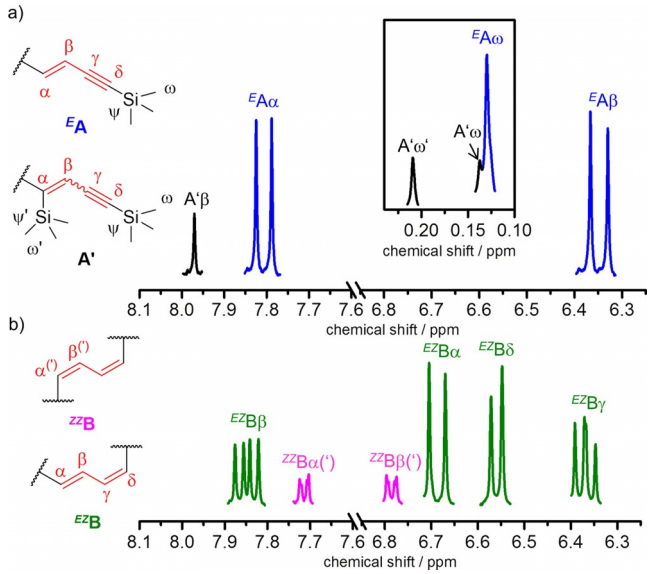

Figure 4. a) Relevant signals of the ^{1}H NMR spectrum of a solution, prepared by dissolving a pre-mixture of the neat solids K_4Ge_9 (97.2 mg, 120 μmol, 1 equiv) and **2** (11.6 mg, 60 μmol, 0.5 equiv) in 2 mL en, after reaction times of: a) < 8 h, and b) > 17 h. The reactants dissolved within 15 min, and a homogeneous dark-brown solution was obtained. In the NMR spectrum a), signals corresponding to the organic functionalities ^{E}**A** and **A**′ appear, and after reaction times of > 17 h the signals of functionalities ^{E}**A** and **A**′ had entirely transformed into the signals of ^{EZ}**B** and ^{ZZ}**B**, respectively. Unassigned signals have been omitted in the figure. The assignments of the signals have been achieved by additional COSY, HMBC and HSQC NMR spectra, which are shown and described in detail in the Supporting Information.

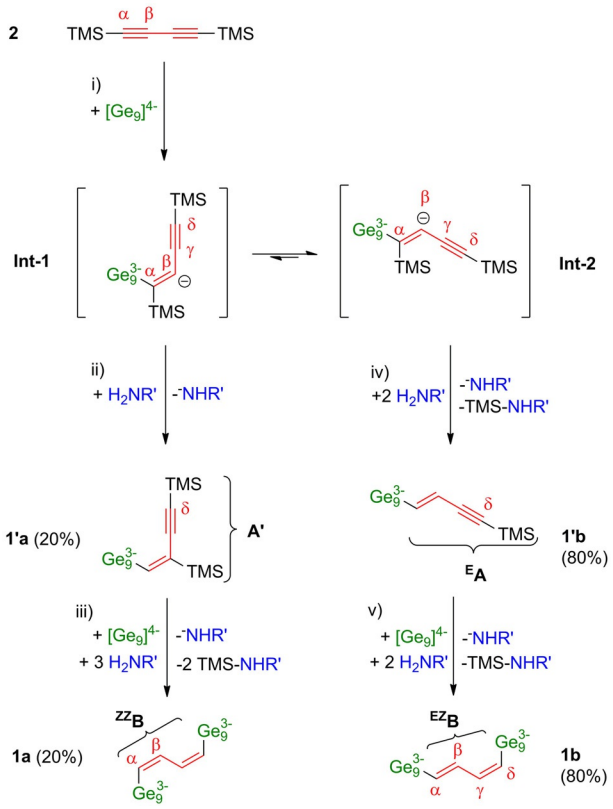

Scheme 2. Reaction scheme illustrating the formation of the buta-1,3-dien-1,4-diyl (**B**) cluster linkages. i) Addition of $[Ge_9]^{4-}$ to the α carbon of **2** in an *anti*-fashion leading to the alkenyl anion **Int-1** (*trans*-geometry with regard to cluster and lone pair at carbon β), which is supposed to be in an equilibrium with **Int-2** (*cis*-geometry with regard to cluster and lone pair at carbon β). ii/iv) Protonation of the alkenyl anions **Int-1** and **Int-2** by en as well as TMS exchange in case of **Int-2**, leading to **1**′**a** and **1**′**b**, respectively. iii/v) Addition of a second $[Ge_9]^{4-}$ cluster to the δ carbon of **1**′**a** and **1**′**b**, respectively, in an *anti*-fashion (intermediate alkenyl anions are not shown), resulting in the Zintl triads **1a** (*anti*,*anti*-product) and **1b** (*syn*,*anti*-product).

from **1**′**b**. After 20 h the reaction is completed, and only the signals of the final products **1a** and **1b** can be detected (**1a**/**1b** = 20:80).

The in situ NMR data show that the linking of Ge_9 clusters by the reaction of $[Ge_9]^{4-}$ with **2** is a stepwise process. Concretely, **1a** emerges from the step-by-step addition of two $[Ge_9]^{4-}$ clusters in an *anti*-fashion to the terminal carbon atoms of **2**.[11,34] According to the time-resolved ^{1}H NMR studies, the first cluster addition in α position proceeds very fast and results in **1**′**a** (*anti*-product). In a much slower consecutive reaction, **1**′**a** adds a second cluster in the δ position, and the *anti*/*anti*-product **1a** is formed.[35]

The formation of *anti*-products in the addition of clusters to alkynes is most dominant, whereas the formation of *syn*-products—as is the case for **1**′**b** and **1b**—is seldom but can occur in the presence of conjugated alkynes, as has been previously shown by the synthesis of *cis*/*trans*-[Ge_9-MeC=CHPh)]$^{3-}$ which is accessible by the reaction of MeC≡CPh with K_4Ge_9 in en.[11,36] According to these investigations, the occurrence of also the *syn*-product **1**′**b** can be interpreted by the intermediate formation of a *cis*-alkenyl-anion from its *trans*-configured correspondent (Scheme 2: **Int-1** and **Int-2**). Subsequent, slow addition of a second cluster in *anti*-fashion at the δ carbon atom of **1**′**b** and TMS exchange therefore results in the final *syn*/*anti*-product **1b**. Formally, the formation of **1a** and **1b** requires an excess of clusters, as two $[Ge_9]^{4-}$ units per molecule **2** are added. Indeed **1a** and **1b** are not formed in mixtures with an excess of **2** (A_4Ge_9/**2** = 1:2) (Supporting Information, Figure S7b) and solely species bearing the organic fragment ^{E}**A** are present.

As reported previously, 1-trimethylsilyl-7-amino-5-aza-hepta-3-en-1-yne (**3**) is formed quantitatively in the reaction of en with **2** (Scheme 3).[17] Thus, the absence of **3** in the reaction mixtures prepared by dissolving pre-mixtures of A_4Ge_9 and **2** in en demonstrates that the nucleophilic addition of $[Ge_9]^{4-}$ to **2** is favored over an en-addition, and the formation of **3** does not take place under such conditions.

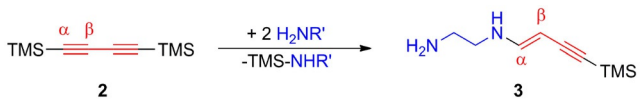

Scheme 3. Reaction of **2** with water-free en in the absence of $[Ge_9]^{4-}$ clusters.

Conclusions

We presented a straightforward synthesis of Zintl triads composed of two homoatomic nine-atom germanium clusters that

are covalently connected via a conjugated π-electron system. The investigations highlight the influence of, firstly, the order of the addition of the reactants A_4Ge_9, 1,4-bis(trimethylsilyl)butadiyne and en, and secondly, of the reaction time on the formation of the buta-1,3-dien-1,4-diyl cluster linkage. The formation of the buta-1,3-dien-1,4-diyl functionality paves the way for the synthesis of molecules with more than two interconnected clusters and offers the chance of a transfer of the reaction to other polyynes. Such reactions are favorable for the development of a supramolecular Zintl-chemistry and the assembly of larger molecular structures similar to metal-organic frameworks. In this context, it is feasible to use Ge_9-linker-Ge_9 Zintl triads in metal-organic reactions and coordinate transition-metal centers at the π-bonds. From such compounds a multifaceted and valuable redox chemistry can be expected. In order to further increase the field of possible chemical transformations, it is necessary to transfer the Zintl triads into less-polar solvents.

Experimental Section

General methods

All manipulations were carried out under a purified argon atmosphere using glove box and standard Schlenk techniques. The Zintl compounds of the nominal composition A_4Ge_9 (A = K, Rb) were synthesized by heating a stoichiometric mixture of the elements K, Rb and Ge (99.999% Chempur) at 650 °C for 48 h in an iron autoclave.[37] 1,4-Bis(trimethylsilyl)butadiyne (Alfa Aesar 98%) was used as received. Toluene was dried over molecular sieves (4 Å) in a solvent purifier (MBraun MB-SPS), and 222-crypt (Merck) was dried in a vacuum for 8 h.

Purification of en

en (Merck) with an initial water content of ≤1% was refluxed over calcium hydride (Merck) and freshly collected prior to use. Water-free en was obtained after refluxing for 72 h. The sampling tubes were thoroughly cleaned and dried at 120 °C immediately before the en collection. Schlenk tubes were heated in a fine vacuum and purged with thoroughly dried argon.

Synthesis

Synthesis of {[K(222-crypt)]$_6$[Ge$_9$–CH=CH–CH=CH–Ge$_9$]}·(tol)$_2$·(en)$_2$: A mixture of K_4Ge_9 (85.0 mg, 105 μmol) and **2** (5.1 mg, 26.3 μmol, 0.25 equiv) was dissolved in 1.75 mL en and stirred for at least 20 h. The dark, red–brown reaction mixture was filtered over glass fibers, and an aliquot of 0.75 mL was layered with a solution of 222-crypt (67.8 mg, 180 μmol, 4 equiv) in toluene (3 mL). After one week, red crystals of {[K(222-crypt)]$_6$**1 a**}(tol)$_2$(en)$_2$ (yield ca. 10%) were obtained and used for X-ray structure analysis (Table 1).

Synthesis of {[Rb(222-crypt)]$_6$[Ge$_9$–CH=CH–CH=CH–Ge$_9$]}·(tol)$_2$·(en)$_2$: A mixture of Rb_4Ge_9 (74.7 mg, 75 μmol) and **2** (3.7 mg, 19 μmol, 0.25 equiv) was dissolved in 1.25 mL en and stirred for at least 20 h. The dark-brown reaction mixture was filtered over glass fibers, and an aliquot of 0.8 mL was layered with a solution of 222-crypt (72.3 mg, 192 μmol, 4 equiv) in toluene (3.2 mL). Bundles of red crystals of {[Rb(222-crypt)]$_6$**1 a**}(tol)$_2$(en)$_2$ (yield ca. 10%) were obtained after two weeks and used for X-ray structure analysis (Table 1) and Raman spectroscopy. Raman $\tilde{\nu}$ = 142 (s, Ge_9-cluster), 221 (s, Ge_9-cluster, breathing mode), 506 (m, *exo*-Ge–C), 658 (w), 709 (w), 1225 (s, ^{zz}**B**, C–C valence), 1554 (vs, ^{zz}**B**, C=C valence), 1584 cm^{-1} (w).

X-ray data collection and structure determination

Single crystals were fixed on the top of a glass fiber with perfluorinated ether and positioned in a cold N_2 stream at 123 K. The single

Table 1. Crystallographic data of {[A(222-crypt)]$_6$**1 a**}(en)$_2$(tol)$_2$ (A = K, Rb).

	{[K(222-crypt)]$_6$**1 a**}(tol)$_2$(en)$_2$	{[Rb(222-crypt)]$_6$**1 a**}(tol)$_2$(en)$_2$
formula	$C_{129.37}H_{251.37}N_{16}O_{36}Ge_{18}K_6$	$C_{129.45}H_{251.45}N_{16}O_{36}Ge_{18}Rb_6$
f_w [g mol^{-1}]	4148.5	4427.8
space group (no)	$P\bar{1}$ (2)	$P\bar{1}$ (2)
a [Å]	14.5799(2)	14.5699(4)
b [Å]	15.4866(2)	15.5121(4)
c [Å]	22.1328(3)	22.1316(6)
α [°]	75.386(1)	75.148(2)
β [°]	84.145(1)	84.305(2)
γ [°]	66.815(2)	66.769(2)
V [Å^3]	4445.2(1)	4442.8(2)
Z	1	1
T [K]	123(2)	100(2)
λ [Å]	0.71073	0.71073
ρ_{calcd} [g cm^{-3}]	1.550	1.655
μ [mm^{-1}]	3.20	4.70
collected rflns	85505	143971
independent rflns	16516	17443
R_{int}	0.075	0.050
parameters/restraints	1039/125	1039/118
R_1 [$I > 2\sigma(I)$/all data]	0.055/0.106	0.049/0.080
wR_2 [$I > 2\sigma(I)$/all data]	0.129/0.142	0.128/0.147
GoF	0.935	1.062
max./min. diff. el. density [e Å^{-3}]	0.99/−0.72	1.34/−1.24

crystal X-ray diffraction data were recorded on an Oxford-Diffraction Xcalibur3 diffractometer (Mo-Kα radiation). All crystal structures were solved by Direct Methods using the SHELX software.[38] The positions of the hydrogen atoms were calculated and refined using a riding model. All non-hydrogen atoms were treated with anisotropic displacement parameters. CCDC 1563545 ({[K(222-crypt)]$_6$**1 a**}(tol)$_2$(en)$_2$) and 1563546 ({[Rb(222-crypt)]$_6$**1 a**}(tol)$_2$(en)$_2$) contain the supplementary crystallographic data for this paper. These data are provided free of charge by The Cambridge Crystallographic Data Centre.

Raman spectroscopy

Raman measurements were performed on single crystals sealed in glass capillaries with a Raman microscopy spectrometer (Senterra Raman spectrometer: Bruker Corporation; diode laser: 785 nm, 1 mW).

Acknowledgements

The authors are grateful to the SolTech (Solar Technologies go Hybrid) program of the Bavarian State Ministry of Education, Science and the Arts for financial support. For the help with the single crystal X-ray structure analyses and the treatment of disorder in the crystal structures the authors are grateful to Dr. Wilhelm Klein and Dr. Viktor Hlukhyy. Moreover, the authors thank Dr. Herta Slavik and M. Sc. Sebastian Geier for Raman-spectroscopic measurements as well as M.Sc. Lorenz Schiegerl for help with the preparation of the reaction solutions and NMR investigations. The authors also thank Maria Weindl for NMR measurements and the Graduate School of the Technical University of Munich for support. S.F. is further grateful to the Fonds der Chemischen Industrie for her fellowship.

Conflict of Interest

The authors declare no conflict of interest.

Keywords: buta-1,3-dien-1,4-diyl · crystal structures · germanium · Raman spectroscopy · Zintl triads

[1] S. C. Sevov, J. M. Goicoechea, *Organometallics* **2006**, *25*, 5678 – 5692.
[2] S. Scharfe, F. Kraus, S. Stegmaier, A. Schier, T. F. Fässler, *Angew. Chem. Int. Ed.* **2011**, *50*, 3630 – 3670; *Angew. Chem.* **2011**, *123*, 3712 – 3754.
[3] T. F. Fässler, *Angew. Chem. Int. Ed.* **2001**, *40*, 4161 – 4165; *Angew. Chem.* **2001**, *113*, 4289 – 4293.
[4] J. M. Goicoechea, S. C. Sevov, *Inorg. Chem.* **2005**, *44*, 2654 – 2658.
[5] J. L. Segura, N. Martin, *Chem. Soc. Rev.* **2000**, *29*, 13 – 25.
[6] M. A. Lebedeva, T. W. Chamberlain, E. S. Davies, B. E. Thomas, M. Schröder, A. N. Khlobystov, *Beilstein J. Org. Chem.* **2014**, *10*, 332 – 343.
[7] N. Martín, L. Sánchez, B. Illescas, I. Pérez, *Chem. Rev.* **1998**, *98*, 2527 – 2548.
[8] Y. Kanai, J. C. Grossman, *Nano Lett.* **2007**, *7*, 1967 – 1972.
[9] M. W. Hull, S. C. Sevov, *Angew. Chem. Int. Ed.* **2007**, *46*, 6695 – 6698; *Angew. Chem.* **2007**, *119*, 6815 – 6818.
[10] M. W. Hull, S. C. Sevov, *Inorg. Chem.* **2007**, *46*, 10953 – 10955.
[11] M. W. Hull, S. C. Sevov, *J. Am. Chem. Soc.* **2009**, *131*, 9026 – 9037.
[12] M. W. Hull, S. C. Sevov, *Chem. Commun.* **2012**, *48*, 7720 – 7722.
[13] M. W. Hull, S. C. Sevov, *J. Organomet. Chem.* **2012**, *721*, 85 – 91.
[14] C. B. Benda, J.-Q. Wang, B. Wahl, T. F. Fässler, *Eur. J. Inorg. Chem.* **2011**, 4262 – 4269.
[15] M. W. Hull, A. Ugrinov, I. Petrov, S. C. Sevov, *Inorg. Chem.* **2007**, *46*, 2704 – 2708.
[16] S. Frischhut, M. M. Bentlohner, W. Klein, T. F. Fässler, *Inorg. Chem.* **2017**, *56*, 10691 – 10698.
[17] M. M. Bentlohner, W. Klein, Z. H. Fard, L.-A. Jantke, T. F. Fässler, *Angew. Chem. Int. Ed.* **2015**, *54*, 3748 – 3753; *Angew. Chem.* **2015**, *127*, 3819 – 3824.
[18] M. M. Bentlohner, M. Waibel, P. Zeller, K. Sarkar, P. Müller-Buschbaum, D. Fattakhova-Rohlfinger, T. F. Fässler, *Angew. Chem. Int. Ed.* **2016**, *55*, 2441 – 2445; *Angew. Chem.* **2016**, *128*, 2487 – 2491.
[19] The crystal structures of {[K(222-crypt)]$_6$**1 a**}(tol)$_2$(en)$_2$ and {[Rb(222-crypt)]$_6$**1 a**}(tol)$_2$(en)$_2$ are isotypic. In the main paper the structure of {[Rb(222-crypt)]$_6$**1 a**}(tol)$_2$(en)$_2$ is discussed and for details on {[K(222-crypt)]$_6$**1 a**}(tol)$_2$(en)$_2$, see the Supporting Information, chapter 1.
[20] In [K(222-crypt)]$_4$[RGe$_9$-CH=CH–CH=CH-Ge$_9$R](tol)[17] the distance between the Ge atoms of the *s-trans*[(Ge-(**ZZB**)-(Ge] building unit is 6.281 Å.
[21] B. Cordero, V. Gomez, A. E. Platero-Prats, M. Reves, J. Echeverria, E. Cremades, F. Barragan, S. Alvarez, *Dalton Trans.* **2008**, 2832 – 2838.
[22] E. V. Anslyn, D. A. Dougherty, *Modern Physical Organic Chemistry*, University Science, **2006**.
[23] For the clusters **II** and **III** of the minority components **1 a**^{II} and **1 a**^{III} the structural parameters are analogous to that of the majority component **1 a**^{I}, as these clusters were refined by the SAME instructions within Shelx97 (ref. [38]). For details see Table S1.
[24] Signals of 222-crypt are expected at 1040–1080 cm^{-1} (C–O–C, valence), 1374 cm^{-1} (C–N valence) and 1425–1475 cm^{-1} (C–C, valence); see ref. [31].
[25] H. G. Von Schnering, M. Baitinger, U. Bolle, W. Carrillo-Cabrera, J. Curda, Y. Grin, F. Heinemann, J. Llanos, K. Peters, A. Schmeding, M. Somer, *Z. Anorg. Allg. Chem.* **1997**, *623*, 1037 – 1039.
[26] M. Somer, W. Carrillo-Cabrera, E. M. Peters, K. Peters, H. G. Von Schnering, *Z. Anorg. Allg. Chem.* **1998**, *624*, 1915 – 1921.
[27] H. Siebert, *Z. Anorg. Allg. Chem.* **1952**, *271*, 75 – 75.
[28] E. R. Lippincott, M. C. Tobin, *J. Am. Chem. Soc.* **1953**, *75*, 4141 – 4147.
[29] L. A. Leites, S. S. Bukalov, A. V. Zabula, D. V. Lyubetskii, I. V. Krylova, M. P. Egorov, *Russ. Chem. Bull.* **2004**, *53*, 33 – 44.
[30] C. Benda, PhD Thesis Technical University of Munich, **2013**.
[31] E. Benedetti, M. Aglietto, S. Pucci, Y. N. Panchenko, Y. A. Pentin, O. T. Nikitin, *J. Mol. Struct.* **1978**, *49*, 293 – 299.
[32] G. Gundersen, P. Klaeboe, A. Borg, Z. Smith, *Spectrochim. Acta A* **1980**, *36*, 843 – 852.
[33] The double-bond configuration of **A**′ cannot be obtained from the NMR data, because no couplings to the α proton are visible due to non-hydrogen atoms at the neighboring β and ε positions.
[34] As follows from mechanistic studies of Sevov et al., en acts as a proton source in additions of clusters to alkynes, and the formation of an amide as the side product has been postulated but not evidenced so far. Moreover, TMS groups are exchanged by protons from en, and NH$_2$(CH$_2$)$_2$NH–TMS is formed as a second side product; see ref. [12].
[35] According to the ^{13}C NMR chemical shifts for **A**′ and ^{E}**A** {^{13}C chemical shifts [ppm] **A**′: 108.6 (γ), 89.4 (δ); ^{E}**A**: 108.9 (γ), 86.8 (δ), Table S5} the electrophilicity of the γ carbon atom is higher than that of the δ carbon, and thus nucleophilic additions are expected to proceed in γ position. However, it is feasible that steric demands and repulsive interactions between the negatively charged cluster units prohibit cluster-addition to the more electrophilic γ position.
[36] M. M. Gillett-Kunnath, I. Petrov, S. C. Sevov, *Inorg. Chem.* **2009**, *48*, 721 – 729.
[37] C. Hoch, M. Wendorff, C. Röhr, *J. Alloys Compd.* **2003**, *361*, 206 – 221.
[38] G. M. Sheldrick, *Acta Crystallogr. A* **2008**, *64*, 112 – 122.

Manuscript received: July 27, 2017
Accepted manuscript online: September 14, 2017
Version of record online: November 6, 2017

CHEMISTRY
A European Journal

Supporting Information

On the Mechanism of Connecting Deltahedral Zintl Clusters via Conjugated Buta-1,3-dien-1,4-diyl Functionalities: Synthesis and Structure of $[Ge_9–CH=CH–CH=CH–Ge_9]^{6-}$

Manuel M. Bentlohner[+], Sabine Frischhut[+], and Thomas F. Fässler*[a]

chem_201703494_sm_miscellaneous_information.pdf

On the Mechanism of Connecting Deltahedral Zintl Clusters via Conjugated Buta-1,3-dien-1,4-diyl Functionalities: Synthesis and Structure of $[Ge_9–CH=CH–CH=CH–Ge_9]^{6–}$

Manuel M. Bentlohner[+], Sabine Frischhut[+] and Thomas F. Fässler*[a]

Contents

1 Crystallographic details

Figure S1. The unit cells of a) {[K(222-crypt)]$_6$ **1a**}·(tol)$_2$·(en)$_2$, b) {[Rb(222-crypt)]$_6$ **1a**}·(tol)$_2$·(en)$_2$. Only conformer **1a^{I}** is shown, and the minority components **1a^{II}** and **1a^{III}** are omitted for clarity. Ge$_9$ clusters are shown as dark-grey polyhedra. Atoms of ^{zz}**B** are shown as empty spheres, and 222-crypt and solvent molecules are shown schematically, whereas hydrogen atoms are omitted for clarity.

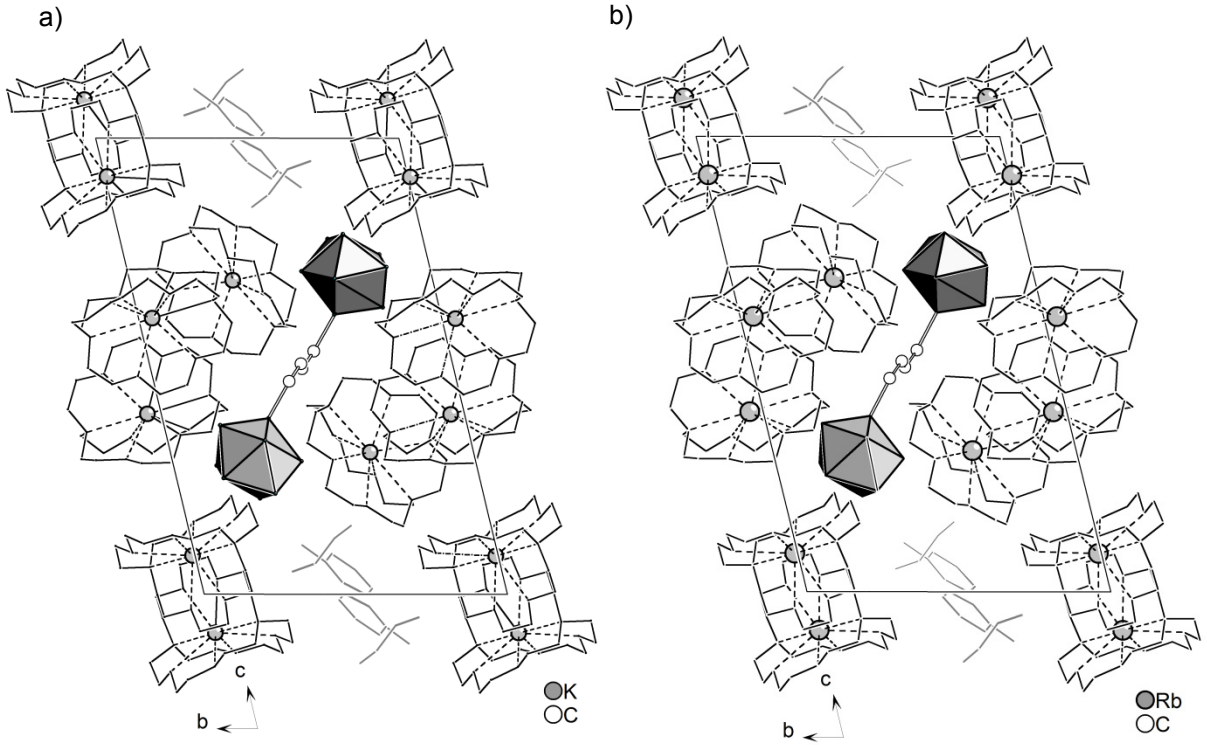

Figure S2. a) The disordered anion **1a**. The inversion center between C2 and C2^{i} is marked with *. The germanium atoms of the superimposed cluster components are depicted with different colors and are shown individually in b). **I** (blue), **II** (green) and **III** (grey). The squares of the quadratic antiprism of the clusters are depicted by bold lines. Ellipsoids are shown at the probability level of 50%. c) The C1/C2/C2^{i}/C1^{i} chain (red atoms) as well as Ge1/Ge1^{i} and Ge10/Ge10^{i}, which together give the *s-trans* [(Ge)-(**^{ZZ}B**)-(Ge)] building units of the conformers **1a^{I}** and **1a^{II}**, respectively. Planes through the atoms Ge1/C1/C2/C2^{i}/C1^{i}/Ge1^{i} (blue) and Ge10/C1/C2/C2^{i}/C1^{i}/Ge10^{i} (green) indicate the spatial orientations of **1a^{I}** and **1a^{II}** around the inversion center. Due to the almost identical spatial location of both **^{ZZ}B** functionalities of **1a^{I}** and **1a^{II}**, individual C_4 chains cannot be resolved by X-ray diffraction, and only a superposition of both chains appears in the crystal structures. As a consequence the occupancy of the C1/C2/C2^{i}/C1^{i} chain is 87% (sum **I** and **II**). d) Clusters **III**/**III^{i}** are not related to the C1/C2/C2^{i}/C1^{i} chain (see bond length and angles in Table S1). The shortest Ge-Ge^{i} distance of 6.572(8) Å (Ge19-Ge19^{i}) is indicative of another conformer **1a^{III}**, however, due to the low contribution of **III** (13%) it is unclear from the X-ray data whether there is another, differently orientated **^{ZZ}B** bridge, or whether **III** is a $[Ge_9]^{3-}$ cluster. For the conformer **1a^{III}** the terminal carbon atoms of the C_4 chain are expected to be located in the grey plane.

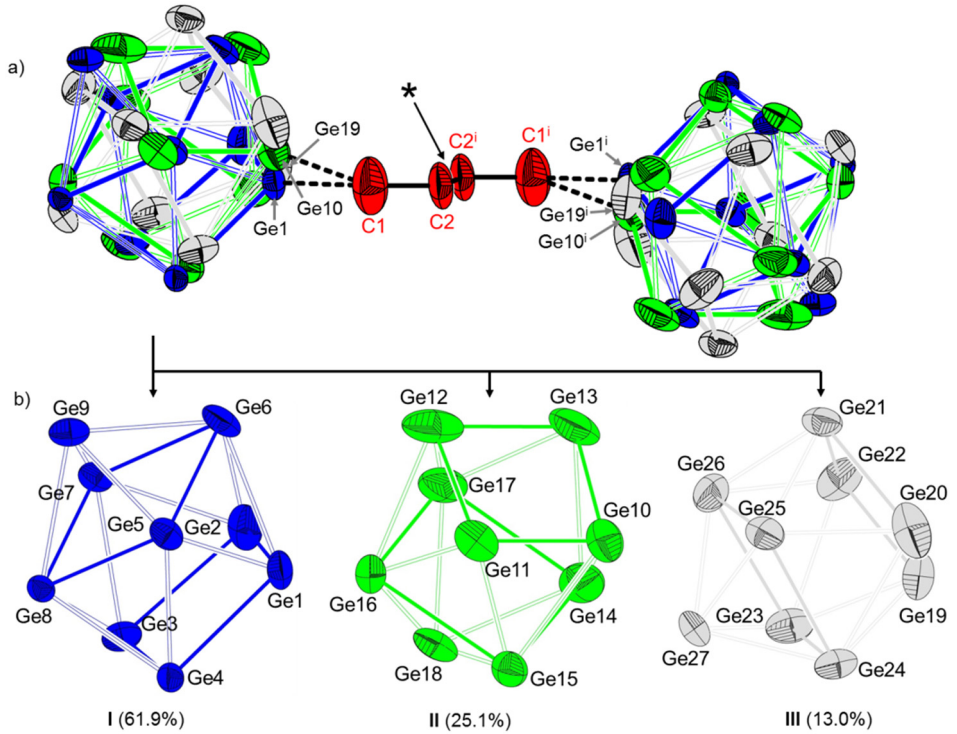

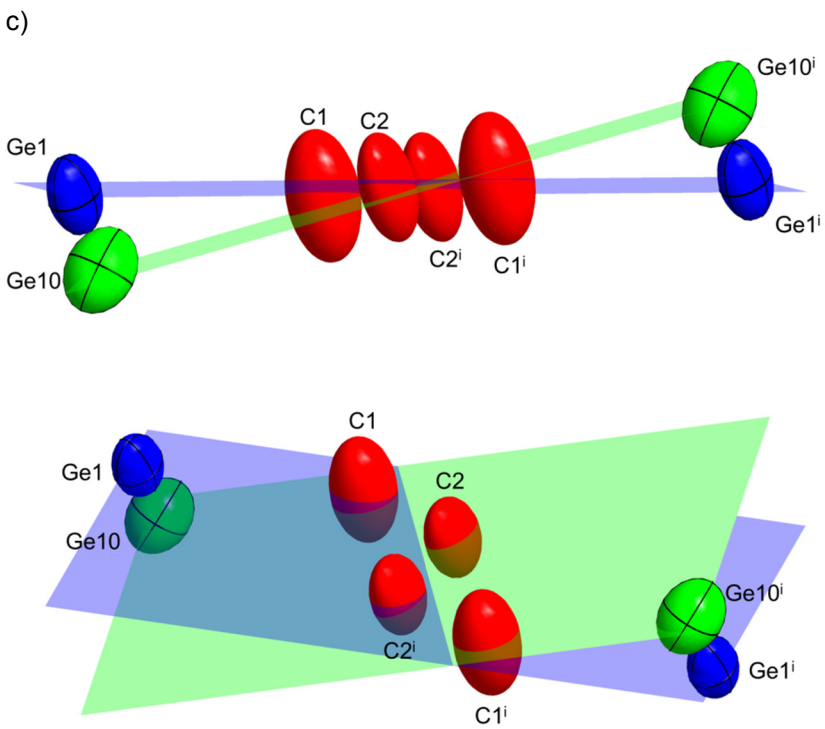
c)
Ge1
Ge10
C1
C2
C2i
C1i
Ge10i
Ge1i
C1
Ge1
C2
Ge10
C2i
C1i
Ge10i
Ge1i

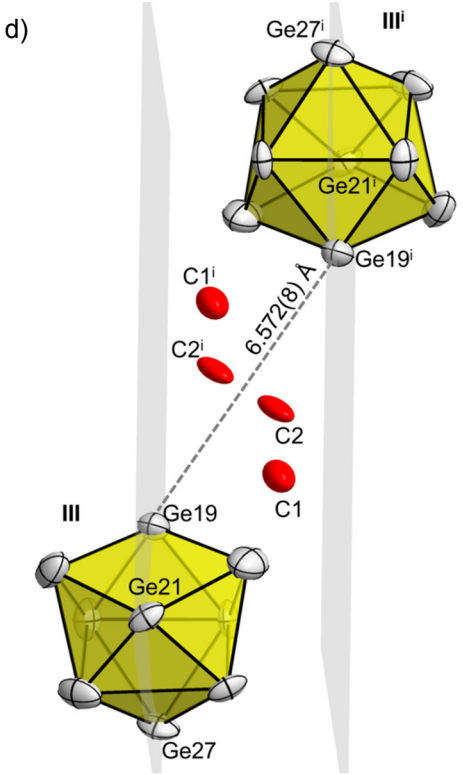
d)
Ge27i
IIIi
Ge21i
Ge19i
C1i
C2i
6.572(8) Å
C2
C1
III
Ge19
Ge21
Ge27

I

Figure S3. The conformers of **1a** differing by the orientation of the Ge_9 cluster units with respect to the [(Ge)-(**^{ZZ}B**)-(Ge)] plane. The shortest Ge-Ge^i distances are emphasized by a doted grey line, and the corresponding distances are given.

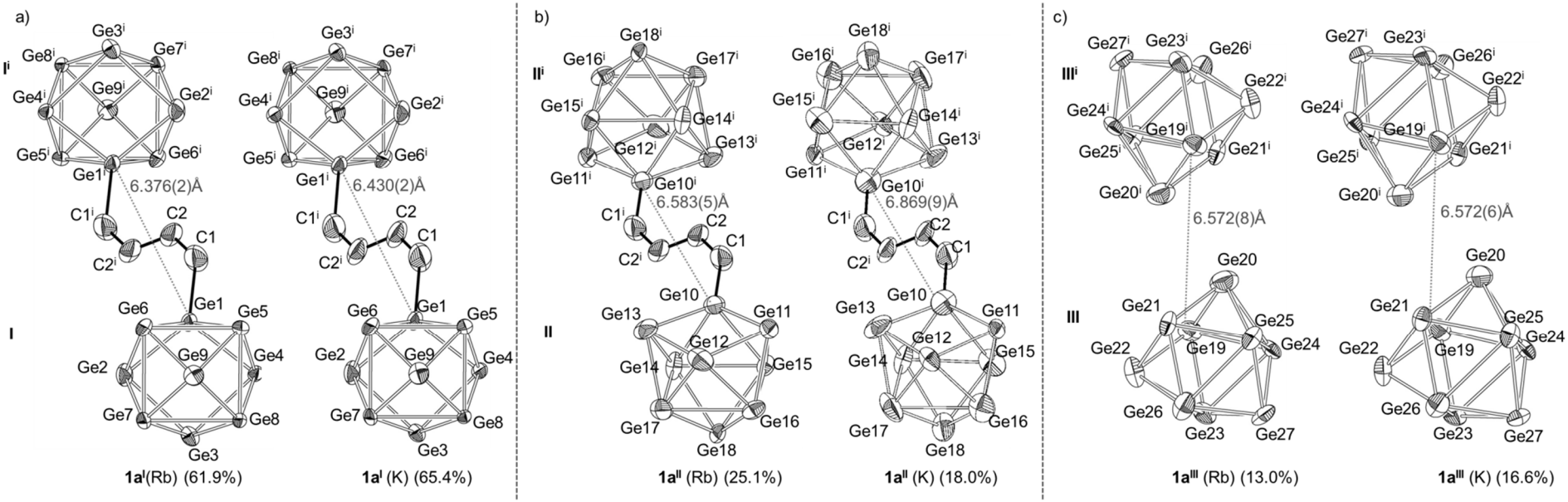

Figure S4. The absolut orientation of the Ge_9 clusters of **1a^{I}** and**1a^{II}**. The rotation angle of the clusters is defined by the angle between the face normals (dashed arrows) of the depicted planes. a) Conformer **1a^{I}**; red plane: Ge1/C1/C2/C2^{i}/C1^{i}/Ge1^{i}; blue plane: Ge1/Ge3/Ge9. b) Conformer **1a^{II}**; red plane: Ge10/C1/C2/C2^{i}/C1^{i}/Ge10^{i}, green plane: Ge10/Ge12/Ge18. The difference between the rotation angles of **1a^{I}** and**1a^{II}** is 165°. Displacement ellipsoids are shown at a probability level of 50%.

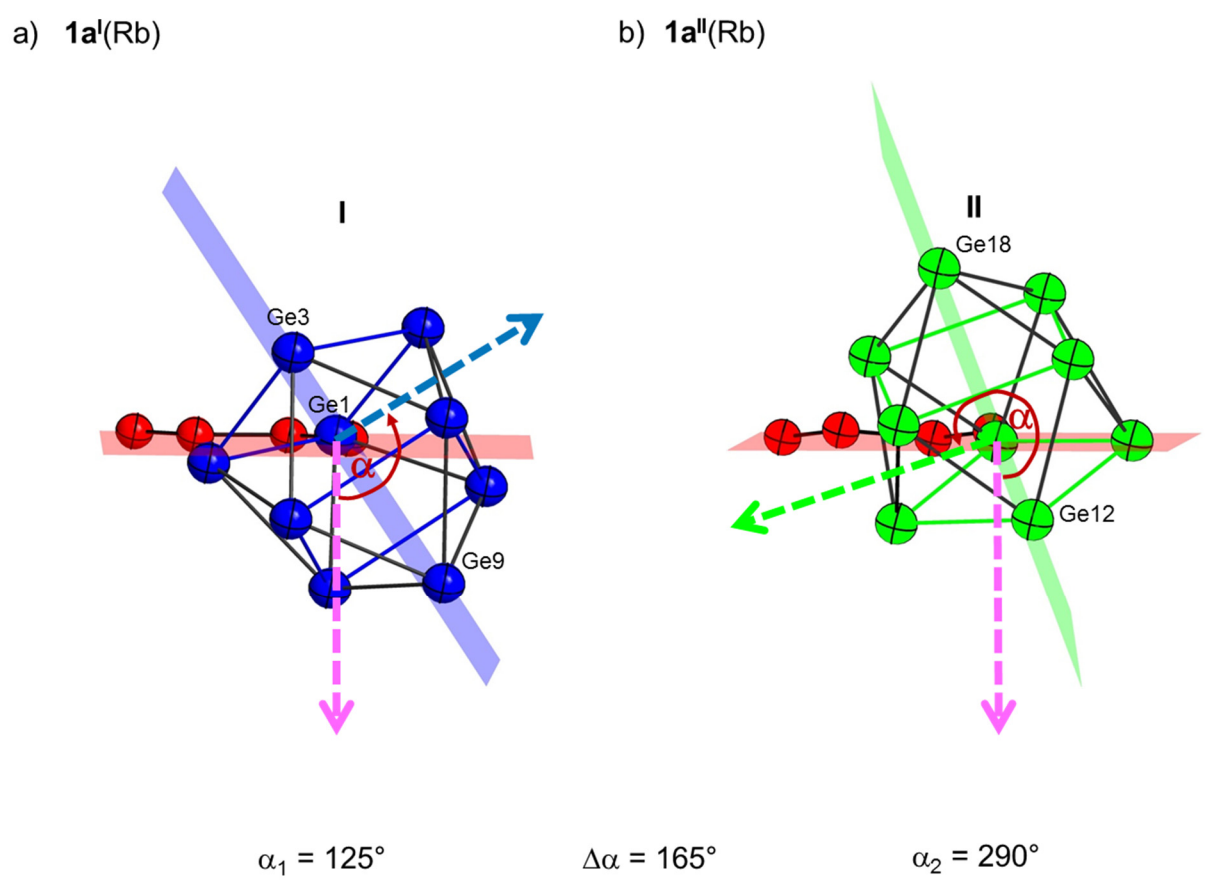

Table S1: Geometrical parameters of the cluster units in the crystal structures of {[A(222-crypt)]$_6$ **1a**}·(tol)$_2$·(en)$_2$ (A = K, Rb). The parameters of the minority clusters **II** and **III** in the crystal structures of {[A(222-crypt)]$_6$ **1a**}·(tol)$_2$·(en)$_2$ (A = K, Rb) were coupled to the geometrical parameters of the majority component **I** by applying the SAME instruction in shelxl97[1].

cluster	Symmetry	c[%][a]	α [°][b]	β [°][c]	ω [°][d]	c_1/c_2[e]	d_1/d_2[f]	h_1 [Å][g]	h_2 [Å][g]	h_3 [Å][g]	$(a_1+a_2)/(b_1+b_2)$
{[Rb(222-crypt)]$_6$ **1a**}·(tol)$_2$·(en)$_2$											
I	C_s	61.9	178.8	130.1	158.7	1.06	1.14	3.390	2.767	2.757	0.93
II	C_s	25.1	177.3	139.1	161.8	1.00	1.16	3.340	2.745	2.720	0.95
III	C_s	13.0	178.7	109.0	98.6	0.43	1.18	3.297	2.794	2.732	0.93
{[K(222-crypt)]$_6$ **1a**}·(tol)$_2$·(en)$_2$											
I	C_s	65.4	178.5	131.5	159.9	1.04	1.13	3.416	2.746	2.743	0.93
II	C_s	18.0	177.7	143.8	163.7	1.05	1.13	3.398	2.878	2.746	0.95
III	C_s	16.6	178.8	110.2	98.7	0.44	1.19	3.296	2.821	2.762	0.93

a) occupancy

b) α is defined as the dihedral angle closest to 180° in the cluster.

c) is defined as the angle between 1/C1/C2.

d) defines the out-of-plane angle ω of the *exo*-bonded ^{zz}**B** bridge.

e) A c_1/c_2 ratio of 1 indicates that the C1 atom of ^{zz}**B** is located in the plane through 1/3/9. This is expected for the carbon atom of organic functionalities attached to the open square face of Ge_9 clusters [2].

f) d_1 and d_2 are the diagonals of the open square face that includes α.

g) h is the height of the central trigonal prisms of the clusters. $h_1 = d_1$.

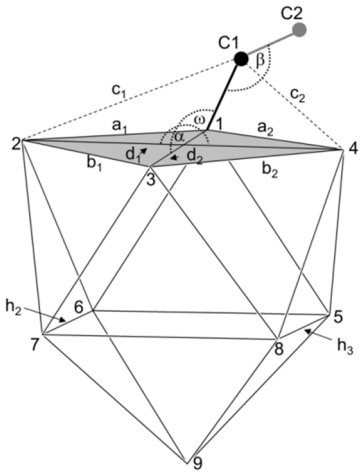

Table S2. Bond lengths [Å] of **1a** in {K(222-crypt)]$_6$ **1a**}·(tol)$_2$·(en)$_2$.

1a^{I}		**1a**^{II}		**1a**^{III}	
Ge1—Ge2	2.480 (1)	Ge10—Ge13	2.457 (9)	Ge19—Ge20	2.463 (8)
Ge1—Ge4	2.492 (3)	Ge10—Ge11	2.530 (1)	Ge19—Ge22	2.488 (6)
Ge1—Ge6	2.575 (2)	Ge10—Ge14	2.549 (8)	Ge19—Ge23	2.563 (7)
Ge1—Ge5	2.615 (3)	Ge10—Ge15	2.599 (1)	Ge19—Ge24	2.614 (9)
Ge2—Ge7	2.532 (3)	Ge11—Ge16	2.564 (1)	Ge20—Ge25	2.535 (9)
Ge2—Ge3	2.674 (4)	Ge11—Ge12	2.611 (1)	Ge20—Ge21	2.680 (7)
Ge2—Ge6	2.700 (2)	Ge11—Ge15	2.724 (1)	Ge20—Ge24	2.733 (1)
Ge3—Ge8	2.579 (4)	Ge12—Ge17	2.571 (1)	Ge21—Ge26	2.551 (7)
Ge3—Ge7	2.589 (3)	Ge12—Ge16	2.620 (1)	Ge21—Ge25	2.591 (7)
Ge3—Ge4	2.669 (3)	Ge12—Ge13	2.646 (9)	Ge21—Ge22	2.625 (6)
Ge4—Ge8	2.562 (4)	Ge13—Ge17	2.602 (1)	Ge22—Ge26	2.537 (7)
Ge4—Ge5	2.642 (4)	Ge13—Ge14	2.643 (8)	Ge22—Ge23	2.663 (7)
Ge5—Ge9	2.570 (3)	Ge14—Ge18	2.559 (1)	Ge23—Ge27	2.549 (1)
Ge5—Ge8	2.742 (4)	Ge14—Ge15	2.853 (1)	Ge23—Ge24	2.817 (9)
Ge5—Ge6	2.852 (3)	Ge14—Ge17	2.878 (1)	Ge23—Ge26	2.822 (7)
Ge6—Ge9	2.571 (3)	Ge15—Ge18	2.560 (1)	Ge24—Ge27	2.563 (1)
Ge6—Ge7	2.746 (2)	Ge15—Ge16	2.747 (1)	Ge24—Ge25	2.762 (1)
Ge7—Ge9	2.609 (4)	Ge16—Ge18	2.591 (2)	Ge25—Ge27	2.613 (1)
Ge7—Ge8	2.844 (4)	Ge16—Ge17	2.896 (1)	Ge25—Ge26	2.906 (9)
Ge8—Ge9	2.572 (4)	Ge17—Ge18	2.566 (1)	Ge26—Ge27	2.564 (1)
Ge1—C1	2.007 (9)	Ge10—C1	1.989(1)		
C1—C2	1.337 (2)				
C2—C2^{i}	1.50 (2)				

Table S3. Bond lengths [Å] of **1a** in {Rb(222-crypt)]$_6$ **1a**}·(tol)$_2$·(en)$_2$.

1a^{I}		**1a^{II}**		**1a^{III}**	
Ge1—Ge2	2.476 (2)	Ge10—Ge13	2.489 (5)	Ge19—Ge20	2.434 (1)
Ge1—Ge4	2.499 (4)	Ge10—Ge11	2.506 (1)	Ge19—Ge22	2.491 (7)
Ge1—Ge6	2.573 (2)	Ge10—Ge14	2.576 (6)	Ge19—Ge23	2.570 (1)
Ge1—Ge5	2.608 (5)	Ge10—Ge15	2.586 (1)	Ge19—Ge24	2.610 (1)
Ge2—Ge7	2.554 (3)	Ge11—Ge16	2.570 (1)	Ge20—Ge25	2.528 (9)
Ge2—Ge3	2.656 (6)	Ge11—Ge12	2.595 (1)	Ge20—Ge21	2.676 (9)
Ge2—Ge6	2.703 (2)	Ge11—Ge15	2.690 (1)	Ge20—Ge24	2.715 (1)
Ge3—Ge8	2.573 (5)	Ge12—Ge17	2.579 (1)	Ge21—Ge26	2.565 (9)
Ge3—Ge7	2.586 (5)	Ge12—Ge16	2.590 (1)	Ge21—Ge25	2.602 (8)
Ge3—Ge4	2.673 (5)	Ge12—Ge13	2.649 (7)	Ge21—Ge22	2.621 (7)
Ge4—Ge8	2.540 (5)	Ge13—Ge17	2.546 (1)	Ge22—Ge26	2.515 (9)
Ge4—Ge5	2.635 (5)	Ge13—Ge14	2.662 (5)	Ge22—Ge23	2.662 (9)
Ge5—Ge9	2.570 (5)	Ge14—Ge18	2.561 (1)	Ge23—Ge27	2.594 (2)
Ge5—Ge8	2.757 (5)	Ge14—Ge17	2.747 (1)	Ge23—Ge26	2.794 (1)
Ge5—Ge6	2.857 (5)	Ge14—Ge15	2.882 (9)	Ge23—Ge24	2.817 (1)
Ge6—Ge9	2.568 (2)	Ge15—Ge18	2.580 (1)	Ge24—Ge27	2.564 (2)
Ge6—Ge7	2.767 (4)	Ge15—Ge16	2.720 (1)	Ge24—Ge25	2.732 (1)
Ge7—Ge9	2.602 (3)	Ge16—Ge18	2.562 (1)	Ge25—Ge27	2.587 (1)
Ge7—Ge8	2.838 (4)	Ge16—Ge17	2.890 (1)	Ge26—Ge27	2.580 (1)
Ge8—Ge9	2.578 (6)	Ge17—Ge18	2.586 (1)		
Ge1—C1	2.001 (9)	Ge10—C1	1.918 (9)		
C1—C2	1.343 (1)				
C2—C2^{i}	1.447 (2)				

2 *In situ* NMR Studies

In order to shed light on the formation of **1a** and **1b** the reactivity of $[Ge_9]^{4-}$ towards **2** in *en* was investigated. Therefore, test mixtures according to section 2.2 Scheme S1 were prepared. The reactions were investigated by *in situ* NMR spectroscopy. For methodologic details on NMR experiments, see section 2.1. In section 2.3, an overview of all the species, which were identified by NMR spectroscopy, is given together with detailed descriptions of the NMR data. In section 2.4 the outcomes of the *in situ* NMR investigations are broken down for the different stoichiometries and reaction times. In section 2.5 Figure S5-S7 the NMR spectra are shown together with experimental details on the preparation of the test mixtures.

2.1 General

NMR spectroscopy. ^{1}H, COSY, HSQC and HMBC NMR spectra were recorded on 500 MHz (Bruker AV-500) and 400 MHz (Bruker AV-400) NMR spectrometers, respectively. Aliquots of ca. 150 µL of the filtered test mixture (solvent: non-deuterated *en*) were filled into a Norell® NMR tube (outer diameter: 3 mm). The Norell® NMR tube was put into a NMR tube with a diameter of 4 mm (denoted as outer tube), and the outer NMR tube was filled with 0.4 mL of chloroform-d_1. Due to the application of non-deuterated *en* as solvent, the spectra show dominant signals at 2.5-3.0 ppm (s, *en*, -C*H*$_2$-) and 1.3-1.9 ppm (s, *en*, -N*H*$_2$-). Samples for time-resolved ^{1}H NMR spectroscopy were taken immediately after the reactants had entirely dissolved (ca. 15 min), and the NMR measurements were started immediately.

2.2 Test mixtures

Scheme S1. Overview of test mixtures. Reaction time (*t*) and stoichiometry was varied. For experimental details on the preparation of the mixtures as well as the NMR-spectra see section 2.5 Figures S5-S7. In the figure captions S5-S7 the preparation of each of the 2 mL reaction solutions are shown. The concentration of A_4Ge_9 (A = K, Rb) in *en* was set constant at 60 µmol/mL in order to provide comparability. Mixtures: The neat solids A_4Ge_9 and **2** (*n* = 0.25, 0.5, 2) were pre-mixed and dissolved in *en*.

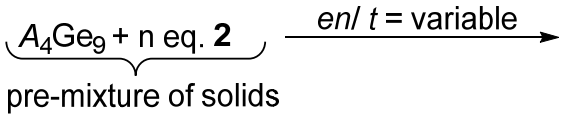

2.3 Identified organic functionalities and NMR spectra

The NMR data of organic functionalities which were identified in the test mixtures by *in-situ* NMR spectroscopy are summarized and described in detail (Scheme S2 and Tables S4-S5)

Scheme S2. a/b) Organic functionalities identified by *in situ* NMR spectroscopy. Proton/carbon atoms are labelled with Greek-letters for distinction. Red: C_4 backbone originating from **2**.

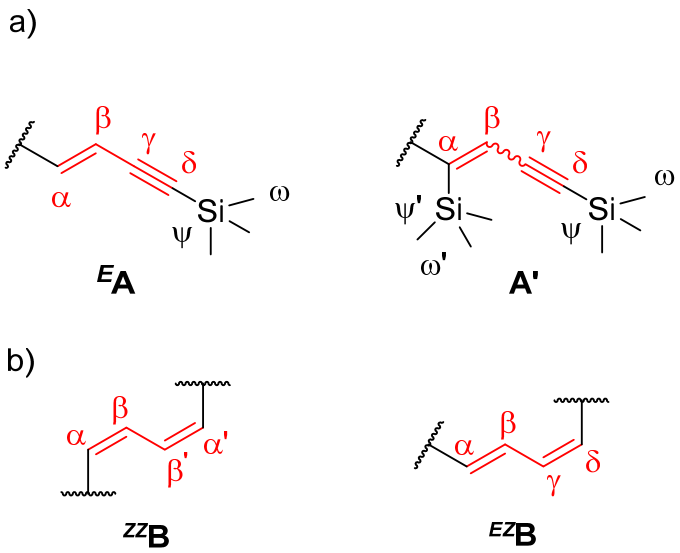

2.3.1 *E*A and A’

Table S4. Summary of the ^{1}H (upper rows) and ^{13}C NMR (lower rows) chemical shifts (ppm) of ***E*A** and **A’** (***E*A**/**A’** = 80/20). The ^{1}H NMR data are given together with the coupling pattern (s = singlet, d = doublet, dd = doublet of doublet, t = triplet, q = quartet), coupling constants (Hz) and integrals. Figures showing the NMR spectra are referenced, respectively. Grey layered boxes: no signals are expected in the ^{1}H and ^{13}C NMR spectra for that atom positions.

	***E*A** (Figure S7)	**A'** (Figure S7)
α	7.81 (d, *J* = 18.3 Hz, 1H)	
	169.9	186.4
β	6.35 (d, *J* = 18.3 Hz, 1H)	7.97 (s 1H)
	116.5	124.5
γ		
	108.9	108.6
δ		
	86.8	89.4
ω	0.13 (s)	0.14 (s)
	-0.7	-0.7
ω'		0.21 (s)
		-0.7

Functionality ^{E}A.

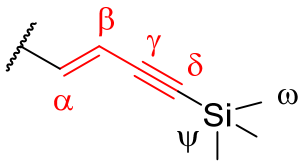

^{E}**A**

1D NMR data: see Table S4

2D NMR data: COSY (500 MHz, chloroform-d_1, 296 K), δ(ppm): 7.82/6.34 (^{3}J, ^{E}Aα/^{E}Aβ); HMBC (500 MHz, chloroform-d_1, 296 K), δ(ppm): 7.78/116.6 (^{2}J, ^{E}Aα/^{E}Aβ), 7.80/108.9 (^{3}J, ^{E}Aα/^{E}Aγ), 6.36/108.9 (^{2}J, ^{E}Aβ/^{E}Aγ), 6.35/86.8 (^{3}J, ^{E}Aβ/^{E}Aδ), 0.13/86.7 (^{3}J, ^{E}Aω/^{E}Aδ); HSQC (500 MHz, chloroform-d_1, 296 K), δ(ppm): 7.79/169.9 (^{1}J, ^{E}Aα/^{E}Aα), 6.33/116.5 (^{1}J, ^{E}Aβ/^{E}Aβ), 0.12/-0.73 (^{1}J, ^{E}Aω/^{E}Aω).

NMR description: In the ^{1}H NMR spectrum (Figure S5a), ^{E}**A** generates three resonances, namely at 7.81 ppm (^{E}Aα), 6.35 ppm (^{E}Aβ) and 0.13 ppm (^{E}Aω). Both signals ^{E}Aα and ^{E}Aβ feature a doublet structure with a coupling constant of 18.3 Hz, being in the typical range for *trans*-orientated olefinic protons[4] and indicating a 1*E*[3] configuration for ^{E}**A**. The signal ^{E}Aω at 0.13 ppm is a singlet, which is expected for the methyl protons of TMS connected to a carbon atom. From the HMBC and HSQC NMR spectra (Figure 5c/d) ^{13}C chemical shifts of 169.9 ppm (^{E}Aα), 116.5 ppm (^{E}Aβ), 108.9 ppm (^{E}Aγ), and 86.8 ppm (^{E}Aδ) were derived, respectively. In the HMBC experiment (Figure S9c) the -C≡C- unit is indicated by cross-peaks at 7.8 ppm/108.9 ppm and 6.35 ppm/86.8 ppm, corresponding to ^{3}J couplings of proton ^{E}Aα with carbon ^{E}Aγ and proton ^{E}Aβ with carbon ^{E}Aδ, respectively. Another, cross-peak at 0.13 ppm/86.7 ppm, corresponds to the ^{3}J coupling between proton ^{E}Aω and carbon ^{E}Aδ and indicates the connection of the TMS group to the -C≡C- unit.

Functionality A'.

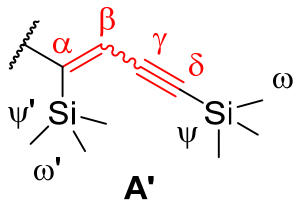

A'

1D NMR data: see Table S4

2D NMR data: HMBC (500 MHz, chloroform-d_1, 296 K), δ(ppm): 7.96/108.6 (^2J, A'β/A'γ), 7.97/89.4 (^3J, A'β/A'δ), 0.2/186.4 (^3J, A'ω/A'α), 0.13/86.7 (probably overlap of ^3J, Aω/Aδ and ^3J, A'ω/A'δ); HSQC (500 MHz, chloroform-d_1, 296 K), δ(ppm): 7.97/124.5 (^1J, A'β/ A'β), 0.14/-0.7 (^1J, A'ω/A'ω), 0.2/-0.7 (^1J, A'ω'/A'ω').

NMR description: In the ^{1}H NMR (Figure S5a) spectrum functionality **A'** exhibits singlets at 7.97 ppm (A'β), 0.21 ppm (A'ω') and 0.14 ppm (A'ω), respectively. From the HMBC and HSQC spectra (Figure S5c/d) ^{13}C chemical shifts of 186.4 ppm (A'α), 124.5 ppm (A'β), 108.6 ppm (A'γ), and 89.4 ppm (A'δ) were derived. In the HMBC experiment, cross-peaks at 7.97 ppm/108.6 ppm and 7.97 ppm/89.4 ppm correspond to ^2J and ^3J couplings of proton A'β with carbon atoms A'γ and A'δ of the -C≡C- unit, respectively. Moreover, a cross-peak at 0.2 ppm/186.4 ppm is visible and originates from the ^3J coupling of proton A'ω' to carbon A'α. Due to similar ^{1}H and ^{13}C chemical shifts for the δ and ω protons/carbons of ^{E}**A** and **A'**, in the HMBC experiment appears (at 0.13 ppm/86.7 ppm) a superposition of ^3J couplings of proton A'ω with carbon A'δ and proton ^{E}Aω with carbon ^{E}Aδ, respectively. The configuration of the double bond of **A'** cannot be derived from the NMR data, as no couplings to proton A'α are visible due to non-hydrogen atoms at the neighboring β and ε positions.

2.3.2 ^{EZ}B and ^{ZZ}B

Table S5. Summary of the ^{1}H (upper rows) and ^{13}C NMR (lower rows) chemical shifts (ppm) of ^{EZ}**B** and ^{ZZ}**B** (*EZ*/*ZZ* = 80/20). The ^{1}H NMR data are given together with the coupling pattern (s = singlet, d = doublet, dd = doublet of doublet, t = triplet, q = quartet), coupling constants (Hz) and integrals. Figures showing the NMR spectra are referenced, respectively. Grey layered boxes: no signals are expected in ^{1}H and ^{13}C NMR spectra for these atom positions.

	^{EZ}**B** (Figure S10)	^{ZZ}**B** (Figure S10)
α	6.69 (d, *J* = 17.2 Hz, 1H)	7.71 (dd, *J* = 8.7/2.0 Hz, 1H)
	142.4	142.1
β	7.85 (dd, *J* = 17.3/10.0 Hz, 1H)	6.78 (dd, *J* = 8.6/2.1 Hz, 1H)
	143.6	142.8
γ	6.38 (dd, *J* = 11.1/10.1 Hz, 1H)	
	142.2	
δ	6.56 (d, *J* = 11.3 Hz, 1H)	
	139.0	

Functionality ^{ZZ}B.

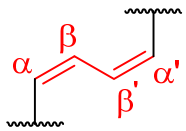

^{ZZ}**B**

1D NMR data: see Table S5

2D NMR data: COSY (500 MHz, chloroform-d$_1$, 296 K), δ(ppm): 7.71/6.79 (^{3}*J*, ^{ZZ}Bα/ ^{ZZ}Bβ); HMBC (500 MHz, chloroform-d$_1$, 296 K), δ(ppm): 6.78/142.8 (^{2}*J*, ^{ZZ}Bα/ ^{ZZ}Bβ); HSQC (500 MHz, chloroform-d$_1$, 296 K), δ(ppm): 7.72/142.1 (^{1}*J*, ^{ZZ}Bα/ ^{ZZ}Bα), 6.78/142.8 (^{1}*J*, ^{ZZ}Bβ/ ^{ZZ}Bβ).

NMR description: In the ^{1}H NMR spectrum (Figure S6a), the C$_4$-backbone (red) of ^{ZZ}**B** generates two resonances at 7.71 ppm (^{ZZ}Bα$^{(')}$) and 6.78 ppm (^{ZZ}Bβ$^{(')}$). We assume that proton ^{ZZ}Bα$^{(')}$, which is closest to the NMR inactive substituent (Ge$_9$ cluster), is largest deep field shifted, however an unambiguous assignment is not possible from the NMR experiment. Both signals ^{ZZ}Bα$^{(')}$ and ^{ZZ}Bβ$^{(')}$ feature a doublet of doublets structure with coupling constants of 8.6 and 2.1 Hz, respectively. The chemical shifts and the 8.6 Hz coupling constant are indicative of *cis*-orientated olefinic protons.[4] Moreover, the 2.1 Hz fine structure is typical of *cis*,*cis*-buta-1,3-dienes, and originates from couplings between the magnetically non-equivalent

protons ^{ZZ}Bα/^{ZZ}Bβ and ^{ZZ}Bα'/^{ZZ}Bβ'.[4] The ^{3}J coupling of ^{ZZ}Bα$^{(')}$ and ^{ZZ}Bβ$^{(')}$ can also be seen in the COSY experiment (Figure S6b) by cross-peaks at 7.71 ppm/6.79 ppm and 6.79 ppm/7.71 ppm, respectively. From the HSQC and HMBC spectra (Figure S6c/d) ^{13}C chemical shifts of 142.1 ppm (^{ZZ}Bα$^{(')}$) and 142.8 ppm (^{ZZ}Bβ$^{(')}$) were derived, which is in the typical region of olefinic carbons.[4]

Functionality ^{EZ}B.

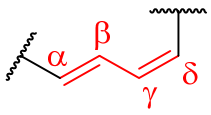

^{EZ}B

1D NMR data: see Table S5

2D NMR data: COSY (500 MHz, chloroform-d$_1$, 296 K), δ(ppm): 7.85/6.69 (^{3}J, ^{EZ}Bβ / ^{EZ}Bα), 7.85/6.36 (^{3}J, ^{EZ}Bβ / ^{EZ}Bγ), 6.34/6.55 (^{3}J, ^{EZ}Bγ / ^{EZ}Bδ); HMBC (500 MHz, chloroform-d$_1$, 296 K), δ(ppm): 7.86/142.7 (^{2}J, ^{EZ}Bβ/ ^{EZ}Bα), 6.68/143.1 (assumed overlap of ^{2}J, ^{EZ}Bα/ ^{EZ}Bβ and ^{3}J, ^{EZ}Bα/ ^{EZ}Bγ), 6.56/144.4 (^{3}J, ^{EZ}Bδ/^{EZ}Bβ), 6.38/143.8 (assumed overlap of ^{3}J, ^{EZ}Bγ/ ^{EZ}Bα and ^{2}J, ^{EZ}Bγ/ ^{EZ}Bβ); HSQC (500 MHz, chloroform-d$_1$, 296 K), δ(ppm): 7.86/143.6 (^{1}J, ^{EZ}Bβ / ^{EZ}Bβ), 6.68/142.4 (^{1}J, ^{EZ}Bα / ^{EZ}Bα), 6.56/139.0 (^{1}J, ^{EZ}Bδ / ^{EZ}Bδ), 6.38/142.2 (^{1}J, ^{EZ}Bγ / ^{EZ}B).

NMR description: In the ^{1}H NMR spectrum (Figure S6a) the C$_4$ backbone (red) of **^{EZ}B** exhibits four resonances at 6.69 ppm (^{EZ}Bα), 7.85 ppm (^{EZ}Bβ), 6.38 ppm (^{EZ}Bγ) and 6.56 ppm (^{EZ}Bδ). ^{EZ}Bβ and ^{EZ}Bγ feature doublet of doublet structures with coupling constants of 17.3/10.0 Hz and 11.1/10.0 Hz, respectively, whereas the signals corresponding to ^{EZ}Bα and ^{EZ}Bδ are doublets with coupling constants of 17.3 and 10.0 Hz, respectively. The chemical shifts and coupling constants of 17.3 and 11.1/10.0 Hz are typical of *trans*- and *cis*-orientated olefinic protons, respectively, indicating an 1,4-disubstituted (1*E*,3*Z*)-buta-1,3-dien (for COSY see Figure S6b).[4] From the HSQC and HMBC spectra (Figure S6c/d) ^{13}C chemical shifts of 139.0 – 143.6 ppm were derived for the carbon atoms, indicative of olefins.[4]

2.4. Summary of *in situ* NMR experiments

In Table S6 the outcome of the *in situ* NMR investigations are summarized for the different mixtures, and references to the figures showing the corresponding NMR spectra are given.

Table S6. Overview of identified functionalities in the test mixtures.

Test Mixture			**Result**	
Nucleophile	**n 2 [eq.]**	***t* [h]**	**Func-tionality**	**Figure S**
K_4Ge_9	0.5	<8	^{E}**A**, **A'**	5
K_4Ge_9	0.25-0.5	>20	^{EZ}**B**/^{ZZ}**B**	6/7
Rb_4Ge_9	0.25-0.5	>20	^{EZ}**B**/^{ZZ}**B**	7
K_4Ge_9	2	>20	^{E}**A**	7

2.5 NMR spectra and details on the preparation of the test mixtures

The NMR spectra of the test mixtures are shown. Experimental details on the preparation of the mixtures are given in the figure captions. In most cases only sections of the spectra are given, and the intensity scales of different spectral regions were adjusted in a way that all relevant signals can be seen.

Figure S5. a) ^{1}H NMR spectrum with magnified relevant signals below, b) COSY, c) HMBC and d) HSQC NMR spectra of a solution, prepared by dissolving a pre-mixture of the neat solids K_4Ge_9 (97.2 mg , 120 µmol, 1 eq.) and **2** (11.6 mg, 60 µmol, 0.5 eq.) in 2 mL *en*, after t < 8h. The reactants dissolved within 15 min, and a homogenous dark-brown solution was obtained. In the NMR spectra, signals corresponding to the organic functionalities ^{E}**A** and **A'** appear. Unassigned signals are marked with ‡. Unmarked signals of very low intensity in the region of 8.0-6.0 ppm belong to the already formed species **1a** and **1b** (see Figure S6).

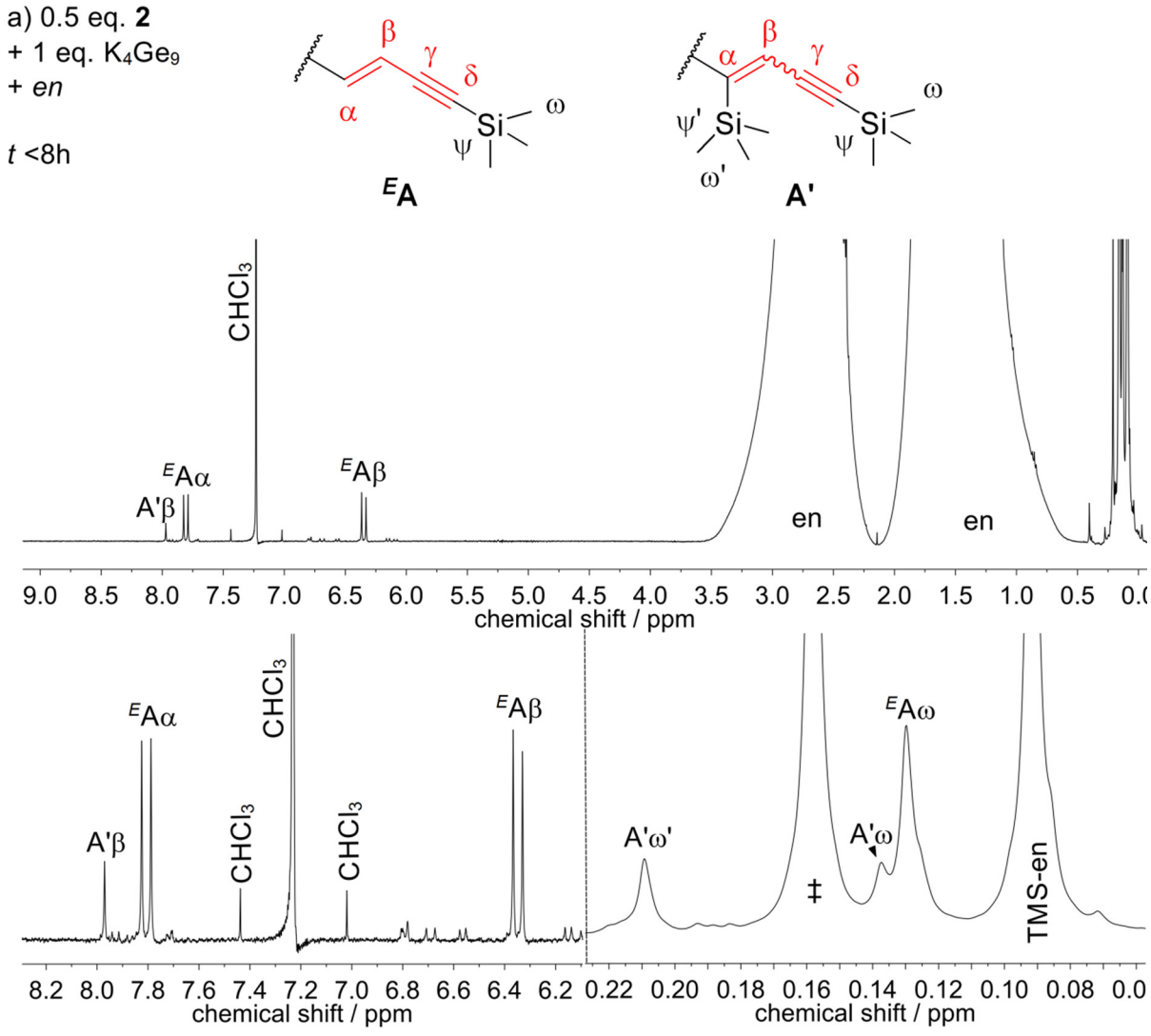

b)

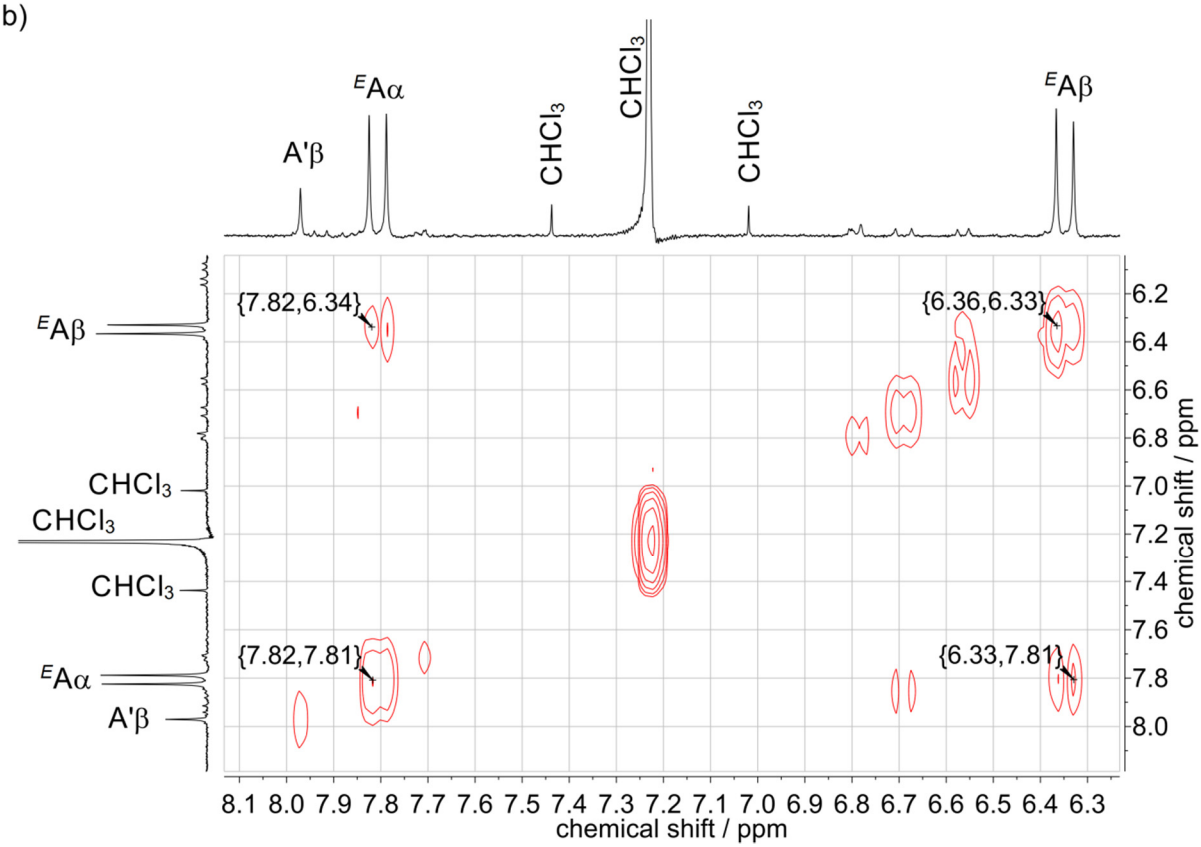
^{E}Aα
A'β
CHCl$_3$
CHCl$_3$
CHCl$_3$
^{E}Aβ
{7.82,6.34}
{6.36,6.33}
{7.82,7.81}
{6.33,7.81}
^{E}Aβ
CHCl$_3$
CHCl$_3$
CHCl$_3$
^{E}Aα
A'β
chemical shift / ppm
chemical shift / ppm

c)

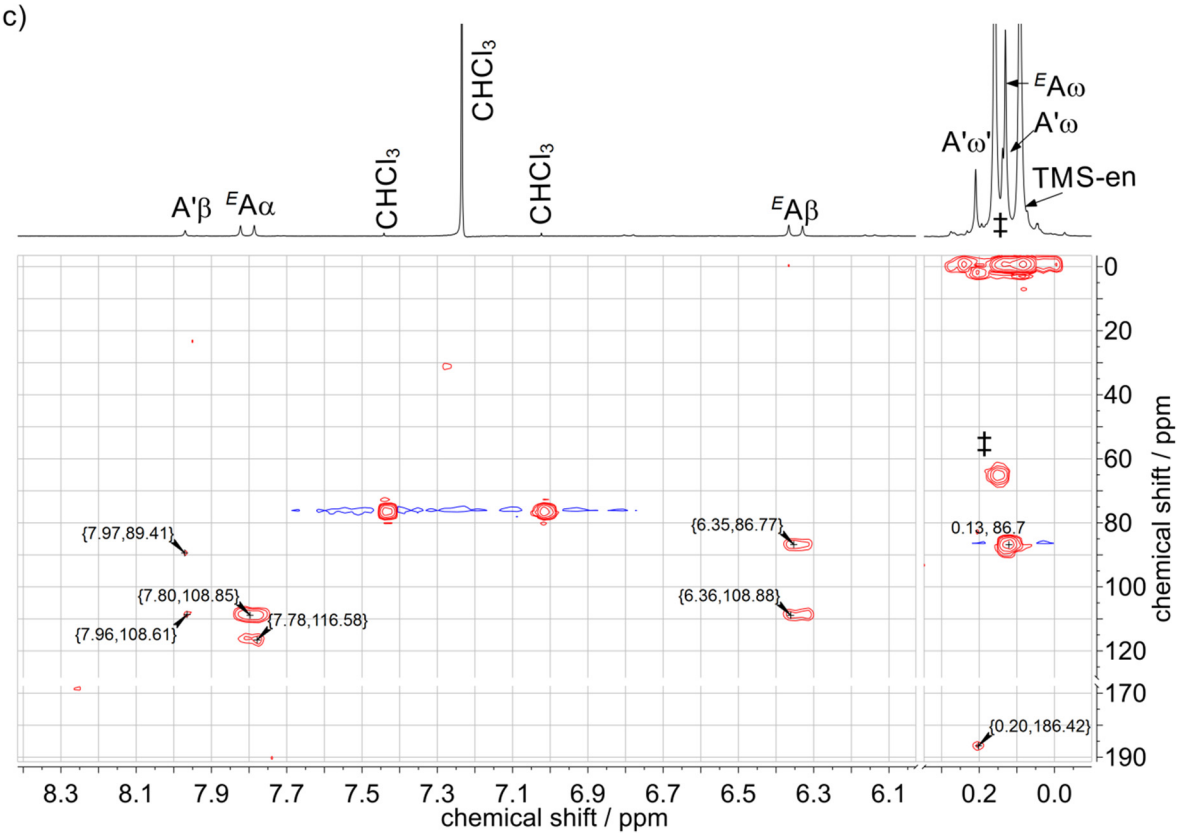
A'β
^{E}Aα
CHCl$_3$
CHCl$_3$
CHCl$_3$
^{E}Aβ
^{E}Aω
A'ω'
A'ω
TMS-en
‡
‡
{7.97,89.41}
{7.80,108.85}
{7.96,108.61}
{7.78,116.58}
{6.35,86.77}
{6.36,108.88}
0.13, 86.7
{0.20,186.42}
chemical shift / ppm
chemical shift / ppm

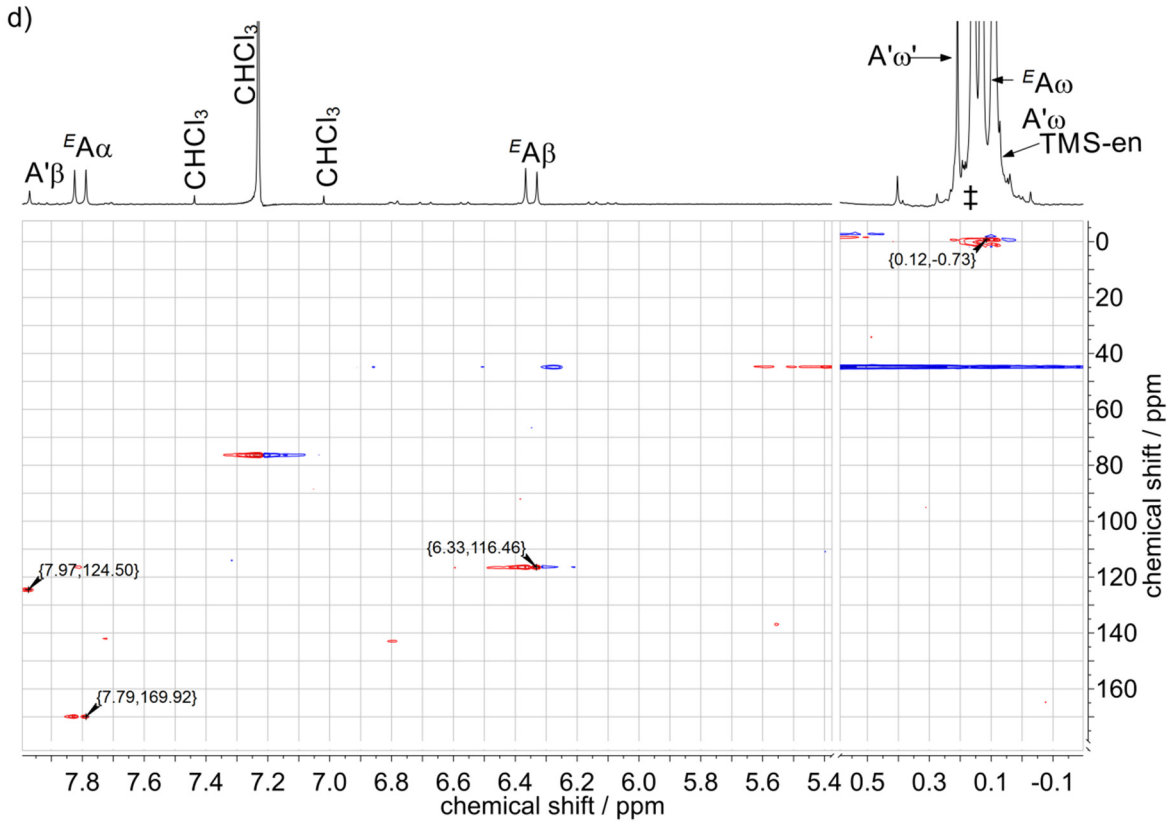
d)
A'β
EAα
CHCl3
CHCl3
CHCl3
EAβ
A'ω'
EAω
A'ω
TMS-en
‡
{0.12,-0.73}
{6.33,116.46}
{7.97,124.50}
{7.79,169.92}
chemical shift / ppm
chemical shift / ppm

Figure S6. a) ^{1}H NMR spectrum with magnified relevant signals below, b) COSY, c) HMBC and d) HSQC spectra of a solution, prepared by dissolving a pre-mixture of the neat solids K_4Ge_9 (97.2 mg , 120 µmol, 1 eq.) and **2** (11.6 mg, 60 µmol, 0.5 eq.) in 2 mL *en*, after *t* > 20 h. The reactants dissolved within 15 min, and a homogenous dark-brown solution was obtained, which turned into deep-red after 20 h. In the NMR spectra, signals corresponding to the organic functionalities ^{ZZ}**B** and ^{EZ}**B** appear. Unassigned signals are marked with ‡.

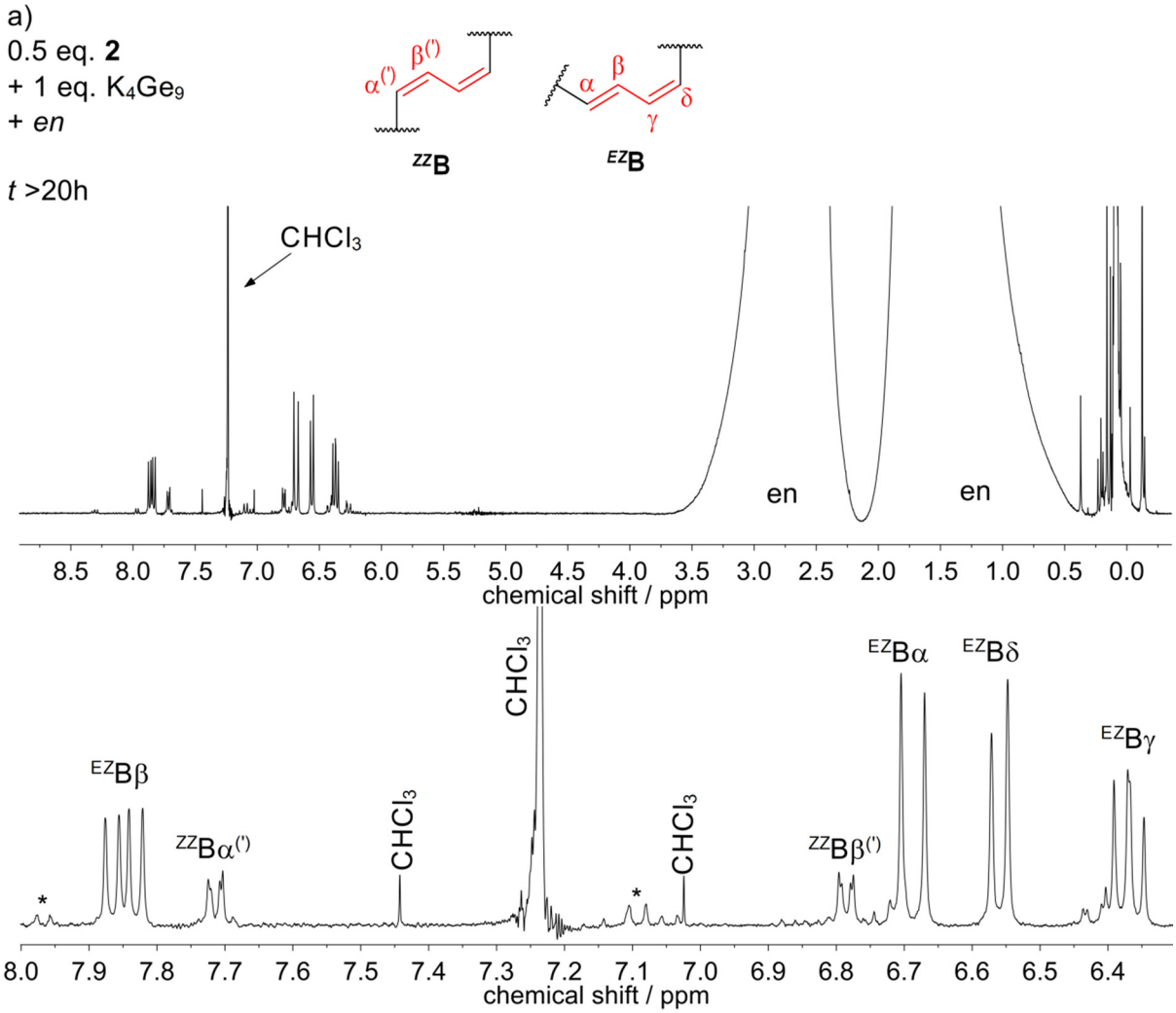

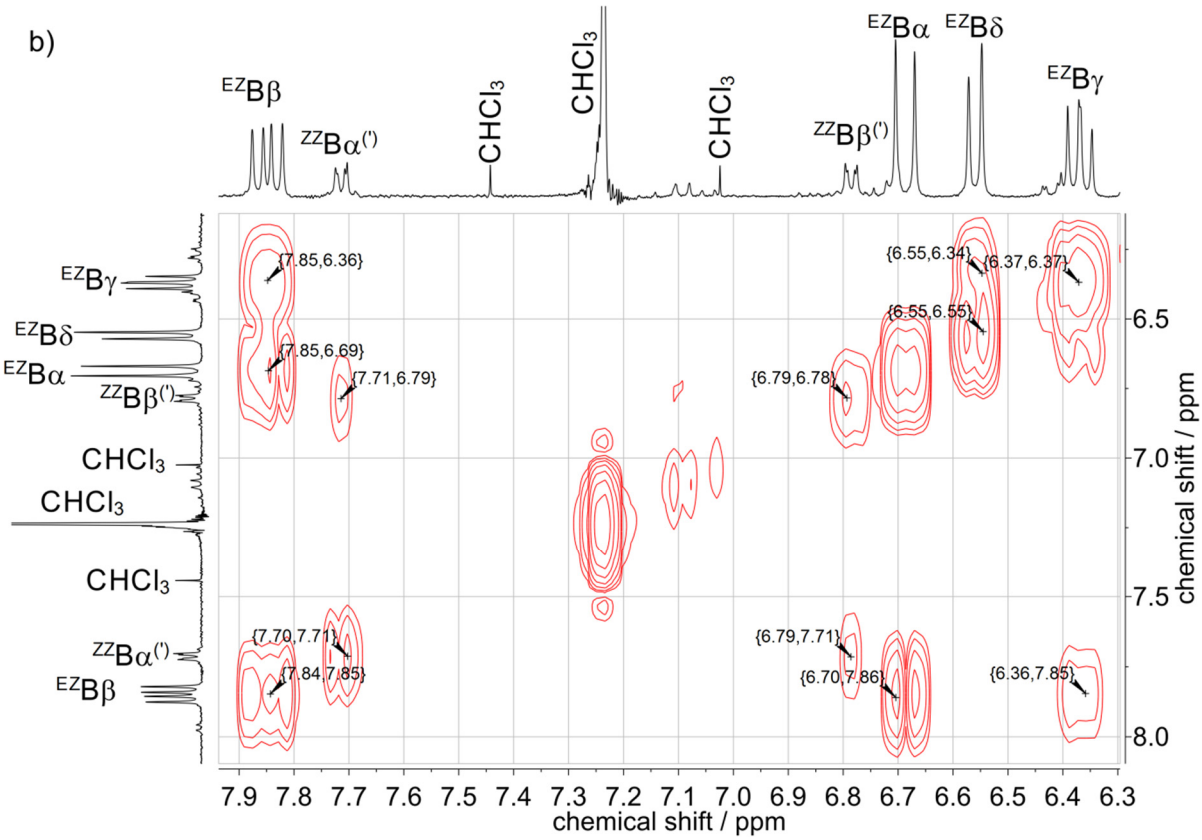
b)
EZBβ
ZZBα(')
CHCl3
CHCl3
CHCl3
ZZBβ(')
EZBα
EZBδ
EZBγ
{7.85,6.36}
{7.85,6.69}
{7.71,6.79}
{6.55,6.34}
{6.37,6.37}
{6.55,6.55}
{6.79,6.78}
{7.70,7.71}
{7.84,7.85}
{6.79,7.71}
{6.70,7.86}
{6.36,7.85}
chemical shift / ppm
chemical shift / ppm

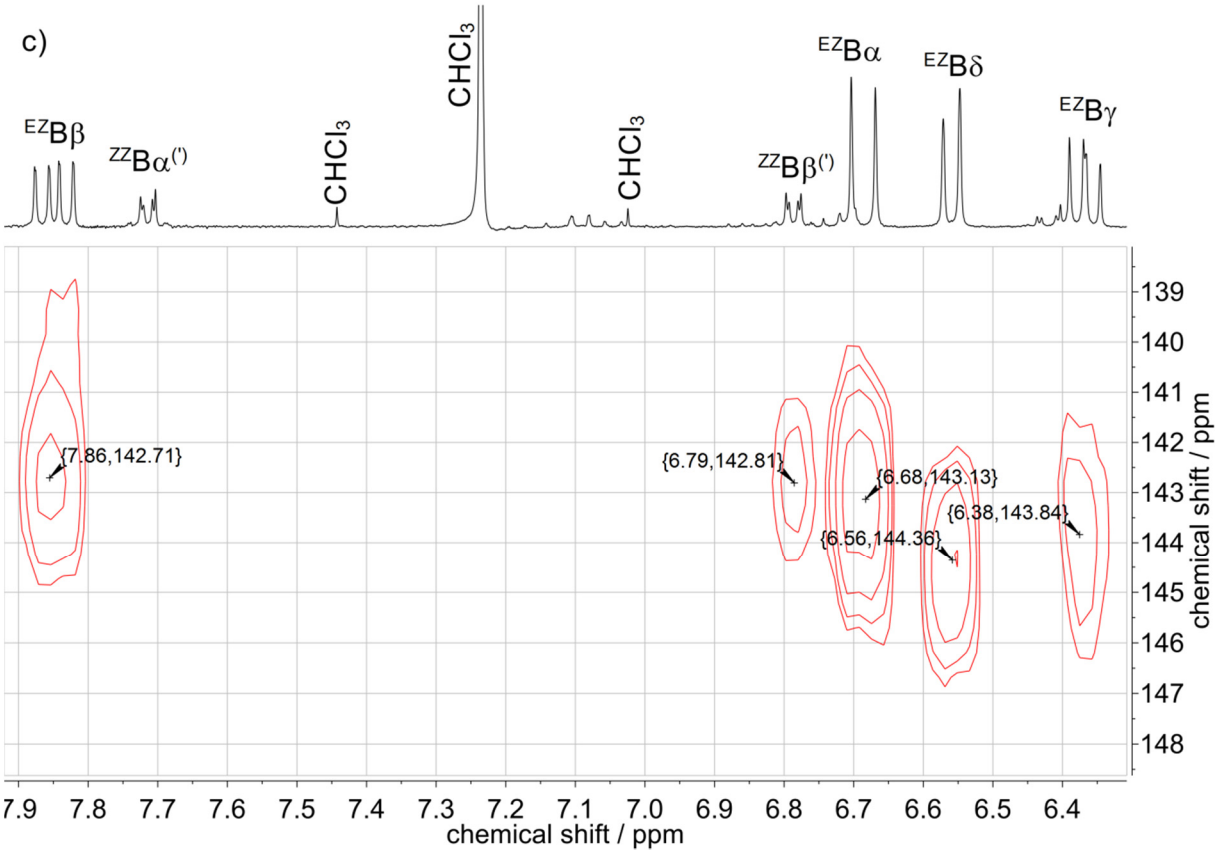
c)
EZBβ
ZZBα(')
CHCl3
CHCl3
CHCl3
ZZBβ(')
EZBα
EZBδ
EZBγ
{7.86,142.71}
{6.79,142.81}
{6.68,143.13}
{6.38,143.84}
{6.56,144.36}
chemical shift / ppm
chemical shift / ppm

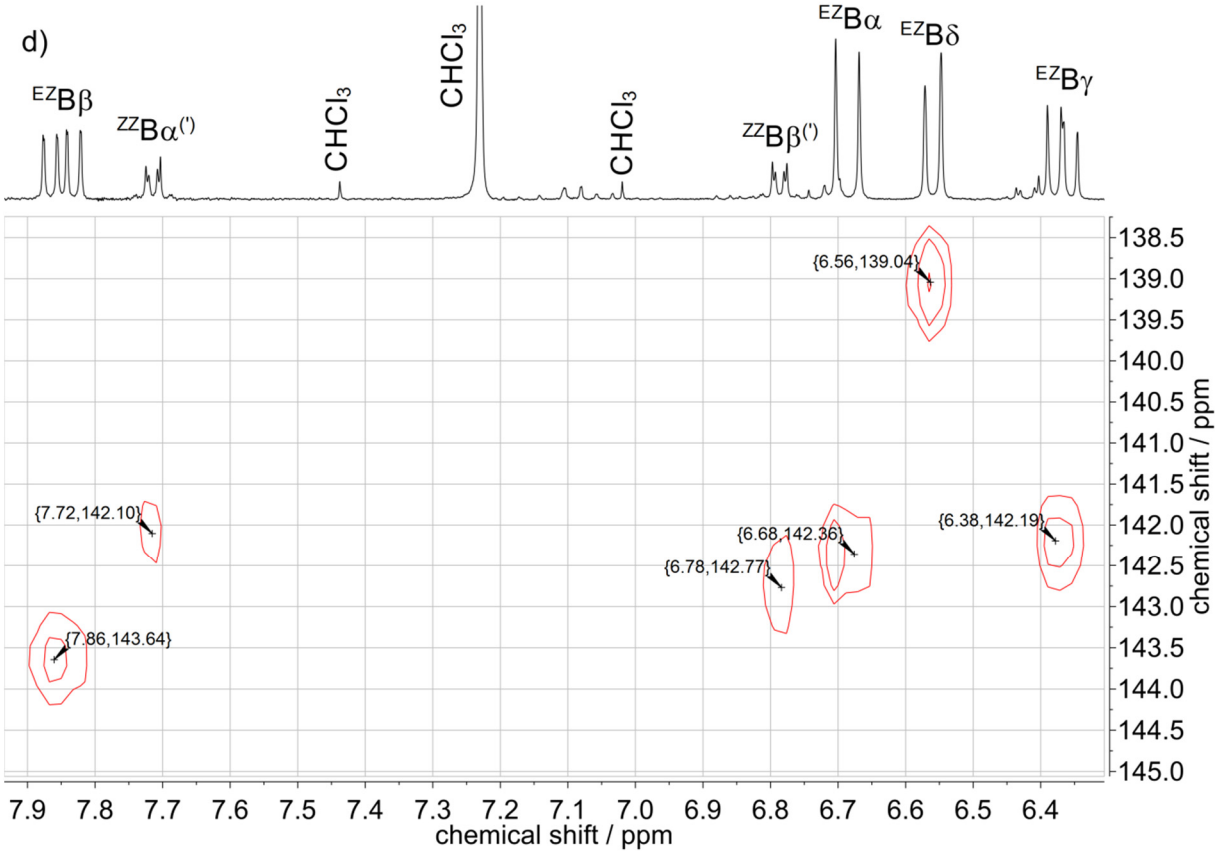
d)
EZBβ
ZZBα(')
CHCl3
CHCl3
CHCl3
ZZBβ(')
EZBα
EZBδ
EZBγ
{6.56,139.04}
{7.72,142.10}
{6.68,142.36}
{6.78,142.77}
{6.38,142.19}
{7.86,143.64}
chemical shift / ppm
chemical shift / ppm

Figure S7. a) Time-dependent ^{1}H NMR spectra (t = 0.5 h - 20 h) of a solution, prepared by dissolving a pre-mixture of the neat solids K_4Ge_9 (97.2 mg , 120 µmol, 1 eq.) and **2** (11.6 mg, 60 µmol, 0.5 eq.) in 2 mL *en*. For t = 0.5 h the signals corresponding to ^{E}**A**/**A'** are dominating. With increasing t signals ^{E}**A**/**A'** decrease, whereas signals of ^{ZZ}**B**/^{EZ}**B** increase. After 20 h the signals of ^{E}**A**/**A'** had vanished and the ones of ^{ZZ}**B**/ ^{EZ}**B** are dominating. In the Table below the absolute integrals of the signals corresponding to ^{E}**A**/**A'** and ^{ZZ}**B**/ ^{EZ}**B** are shown. b) ^{1}H NMR spectra of solutions, prepared by dissolving a pre-mixture of A_4Ge_9 (A = K: 97.2 mg , 120 µmol, 1 eq.; A = Rb: 119.4 mg, 120 µmol, 1 eq.) and different amounts of **2** (5.8 mg, 30 µmol, 0.25 eq.; 11.6 mg, 60 µmol, 0.5 eq.; 46.7 mg, 240 µmol, 2 eq) in 2 mL *en*. t > 20 h. In the NMR spectra of mixtures containing ≤ 0.5 eq. of **2** signals corresponding to ^{ZZ}**B**/ ^{EZ}**B** appear. In case of the Rb_4Ge_9 precursor the signals of ^{ZZ}**B**/ ^{EZ}**B** are slightly down-field shifted. For the mixture containing 2 eq. of **2** solely signals corresponding to functionality ^{E}**A** but no signals of ^{ZZ}**B**/ ^{EZ}**B** are visible. Unassigned signals are marked with ‡.

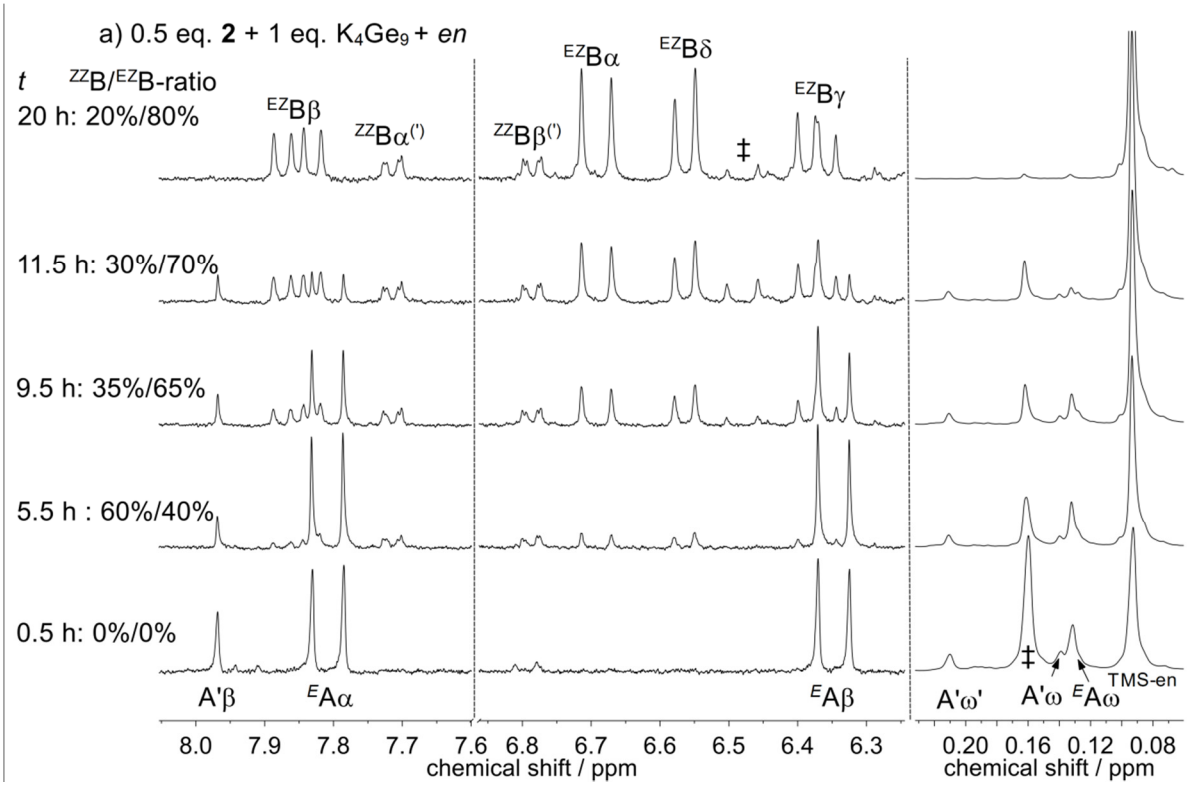

t [h]	abs. Integral [a.u.] **A'**	abs. Integral [a.u.] ^{ZZ}**B**	abs. Integral [a.u.] ^{E}**A**	abs. Integral [a.u.] ^{EZ}**B**
0.5	0.20	0	0.75	0
20	0	0.22	0	0.74

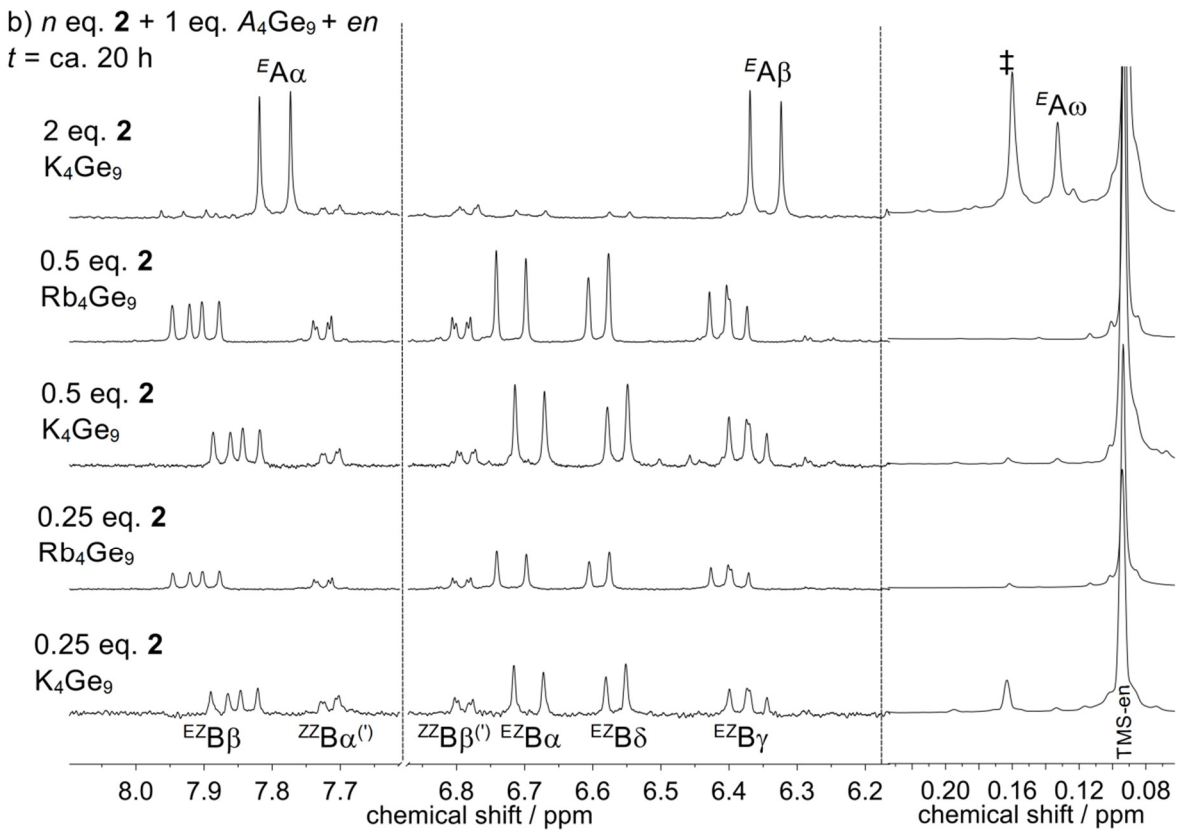

3 References

[1] G. M. Sheldrick, *Acta Crystallogr.* **2008**, *A64*, 112.

[2] C. B. Benda, J.-Q. Wang, B. Wahl, T. F. Fässler, *Eur. J. Inorg. Chem.* **2011**, 4262-4269.

[3] Numbering: The positions of the C=C double bonds are counted with respect to the C_4-backbone: α = 1, β = 2, γ = 3, δ = 4.

[4] M. Hesse, H. Meier, B. Zeeh, *Spektroskopische Methoden in der organischen Chemie*, Thieme, **2005**.

5.4 Synthesis of Zintl Triads Comprising Extended Conjugated π-Electronic Systems: $[RGe_9–CH=CH–CH=CH–Ge_9R]^{4–}$ (R = $–CH=CH_2$, $–C(CH_3)–CH–CH=N(CH_2)_2NH_2$)

Sabine Frischhut, Manuel M. Bentlohner, Wilhelm Klein, and Thomas F. Fässler

published in:

Inorg. Chem. **2017**, *56*, 10691-10698.

CONTENT AND CONTRIBUTION

In the scope of this publication the functionalized Zintl triad $[H_2C{=}CH{-}Ge_9{-}CH{=}CH{-}CH{=}CH{-}Ge_9{-}CH{=}CH_2]^{4-}$ was synthesized for the first time, which was only the second example of its kind. The Zintl triad was synthesized by reaction of 2 eq. of bis(trimethylsilyl)acetylene with 1,4-bis(trimethylsilyl)butadiyne and K_4Ge_9 in *en*. The latter comprises two Ge_9 clusters linked by a conjugated organic 1,3-butadien-1,4-diyl bridge. Each cluster carries an additional vinyl-functionality. $[H_2C{=}CH{-}Ge_9{-}CH{=}CH{-}CH{=}CH{-}Ge_9{-}CH{=}CH_2]^{4-}$ was characterized by single crystal X-ray crystallography as well as NMR spectroscopy. *In situ* NMR investigations provided insight into the formation of the Zintl triad. All measurements, investigations on the new Zintl triad as well as data evaluation were performed within this work. Dr. Wilhelm Klein assisted with structure elucidation. The existence of this compound had already been predicted in a different publication by DFT calculations, which were carried out by Dr. Laura-Alice Jantke. The quantum chemical calculations revealed that the Zintl triad comprises a conjugated π-electronic system, which is extended throughout the whole anion.

Furthermore, a more direct synthesis protocol for the formation of the first-reported Zintl triad $[R{-}Ge_9{-}CH{=}CH{-}CH{=}CH{-}Ge_9{-}R]^{4-}$ (R = (2Z,4E)-7-amino-5-azahepta-2,4-dien-2-yl) is reported within this publication. Investigations on the reactivity of 1,4-bis(trimethylsilyl)butadiyne towards *en* compared to the reactivity of 1,4-bis(trimethylsilyl)butadiyne towards A_4Ge_9 (*A* = K, Rb) allowed for the development of a synthesis strategy, which implied higher yields of the desired product. The simultaneous reaction of the Zintl phase A_4Ge_9 with 1,4-bis(trimethylsilyl)acetylene and (3*Z*/3*E*)-7-amino-1-(trimethylsilyl)-5-azahepta-3-en-1-yne, which itself is a reaction product between *en* and 1,4-bis(trimethylsilyl)butadiyne, in *en* gave access to $[R{-}Ge_9{-}CH{=}CH{-}CH{=}CH{-}Ge_9{-}R]^{4-}$ in comparatively good yields. These investigations were carried out by Dr. Manuel M. Bentlohner.

The publication was authored within this work and revised by Dr. Manuel M. Bentlohner, Dr. Wilhelm Klein and Prof. Dr. Thomas F. Fässler.

Inorganic Chemistry

Article

pubs.acs.org/IC

Synthesis of Zintl Triads Comprising Extended Conjugated π-Electronic Systems: $[RGe_9–CH=CH–CH=CH–Ge_9R]^{4-}$ (R = $–CH=CH_2$, $–C(CH_3)=CH–CH=N(CH_2)_2NH_2$)

Sabine Frischhut, Manuel M. Bentlohner, Wilhelm Klein, and Thomas F. Fässler*

Department of Chemistry, Technische Universität München, Lichtenbergstraße 4, 85747 Garching, Germany

Supporting Information

ABSTRACT: Triads with extended conjugated π-electronic systems between polyhedral cage molecules possess promising electronic properties. In contrast to the known fullerene–bridge–fullerene triads, fewer synthetic procedures are known for the related homoatomic deltahedral cage molecules of the heavier homologues of carbon. The synthesis of the organo-Zintl triads $[RGe_9–CH=CH–CH=CH–Ge_9R]^{4-}$ with R = $–CH=CH_2$ (R_1), $–C(CH_3)=CH–CH=N(CH_2)_2NH_2$ ((2*Z*,4*E*)-7-amino-5-azahepta-2,4-dien-2-yl) (R_2) is reported, in which the deltahedral Ge_9 cages carry an additional functional group, allowing for further connections. Both anionic cage entities bear a butadiene-1,4-diyl bridge which is formed by reacting the Zintl ion $[Ge_9]^{4-}$ with 1,4-bis(trimethylsilyl)butadiyne in ethylenediamine. The organic tethers can be attached by nucleophilic attack of the Ge_9 clusters at the bis(trimethylsilyl)acetylene and (3*Z*/3*E*)-7-amino-1-(trimethylsilyl)-5-azahepta-3-en-1-yne, respectively, in ethylenediamine, and the products *cis*/*trans*-$[R_1Ge_9–CH=CH–CH=CH–Ge_9R_1]^{4-}$ and *cis*/*cis*-$[R_2Ge_9–CH=CH–CH=CH–Ge_9R_2]^{4-}$ have been isolated as $[A(2,2,2\text{-crypt})]^+$ salts with *A* = K, Rb, respectively. Crystals containing the novel anions $[RGe_9–CH=CH–CH=CH–Ge_9R]^{4-}$ have been structurally characterized by X-ray diffraction methods, and the compounds have been investigated by ^1H and ^{13}C NMR as well as by Raman spectroscopy. The *cis*/*cis* configurational isomer of $[R_1Ge_9–CH=CH–CH=CH–Ge_9R_1]^{4-}$ was characterized by means of NMR spectroscopy. Via in situ NMR measurements, we shed some light on the formation of the Zintl triads $[RGe_9–CH=CH–CH=CH–Ge_9R]^{4-}$ bearing supplemental organic tethers.

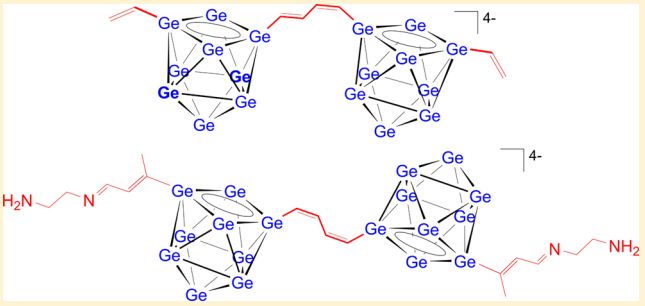

INTRODUCTION

There exists a striking similarity between the carbon fullerenes and the homoatomic deltahedral cage compounds of the heavier homologues of carbon.[1−3] Both represent spherical atom clusters solely composed of one atom type. Carbon fullerenes C_n have a covalent σ-bonded framework and *n* π-bonding electrons which are, however, only free to delocalize for specific *n*; deltahedral cage compounds, Si_n to Pb_n, which exist as anions for various *n*, possess delocalized cluster bonds which are best described applying Wade's skeletal-electron-number rules.[4−6] In addition to the comparable possibility of appearing with various charges, both compound classes are able to incorporate heteroatoms, forming endohedrally filled clusters.[7,8] In addition, fullerenes form exohedral adducts, which has been known for a long time,[9−11] and the related organo-functionalized deltahedral tetrel clusters are also known but have been less investigated. The first organo-functionalized deltahedral Ge_9 Zintl cluster anion, $[Ph–Ge_9–SbPh_2]^{2-}$, was reported in 2003 by Sevov et al.,[12] giving the signal for the synthesis of further interesting Ge_9 cluster entities bearing other organic functionalities. Reactions of deltahedral Ge_9 Zintl clusters with the alkyl halides R–Cl (R = *t*Bu, *n*Bu, *s*Bu, *t*Am) and *c*PrMe–Cl led to the formation of small amounts of the cluster anions $[R–Ge_9–Ge_9–R]^{6-}$[13] and $[Ge_9–(CH_2–CH–(CH_2)_2)_2]^{2-}$,[14] respectively. In particular the alkenylation of $[Ge_9]^{4-}$ Zintl clusters has become a widely explored reaction which can be carried out by treating $[Ge_9]^{4-}$ clusters with alkynes in ethylenediamine. Thus, a limited number of alkene-functionalized, negatively charged cluster entities have become accessible through the reaction of $[Ge_9]^{4-}$-containing solutions, namely $[Ge_9(CH=CH_2)_n]^{4-n}$ (*n* = 1, 2),[15,16] $[CH_2=CH–Ge_9–Ge_9–CH=CH_2]^{4-}$,[17] $[Ge_9–C(CH_3)=CH–CH_2CH_3]^{3-}$,[14] and $[Ge_9R''_2]^{2-}$ (R″ = –CH=CH–Im(Me), –CH=CH–C_6H_4–OMe, –CH=CH–Fc, –CH=CH–$(CH_2)_4$–C≡CH, –CH=CH–C_6H_4–C≡CH, –CH=CH–C_6H_4–NH_2, –CH=CH–Py, –CH=CH–$(CH_2)_3$–C≡N, –CH=CHCH$(OEt)_2$, –$C(CH_3)_2$C≡CH, –CH=CH–CH_2NH_2).[18−20] According to mechanistic studies the addition of the Ge_9 cluster and the accompanied protonation of the triple bond entail a *cis*-configured product with respect to the second organic substituent bound to the double bond.[14] Treatment with dialkynes instead of monoalkynes in the alkenylation reaction led to the formation of the first representative of deltahedral tetrel clusters that are linked by an organic group—the Ge_9 Zintl cluster analogous to the

Received: June 29, 2017
Published: August 24, 2017

DOI: 10.1021/acs.inorgchem.7b01643
Inorg. Chem. 2017, 56, 10691−10698

Scheme 1. (a) Reaction of K_4Ge_9 with Bis(trimethylsilyl)acetylene (3) and 1,4-Bis(trimethylsilyl)butadiyne (4) in *en* To Give the Anionic Entities 1a,b and (b) Reaction of Rb_4Ge_9 with 1,4-Bis(trimethylsilyl)butadiyne (4) and (3*Z*/3*E*)-1-Trimethylsilyl-7-amino-5-azahepta-3-en-1-yne (5) Resulting in the Anionic Entity 2a

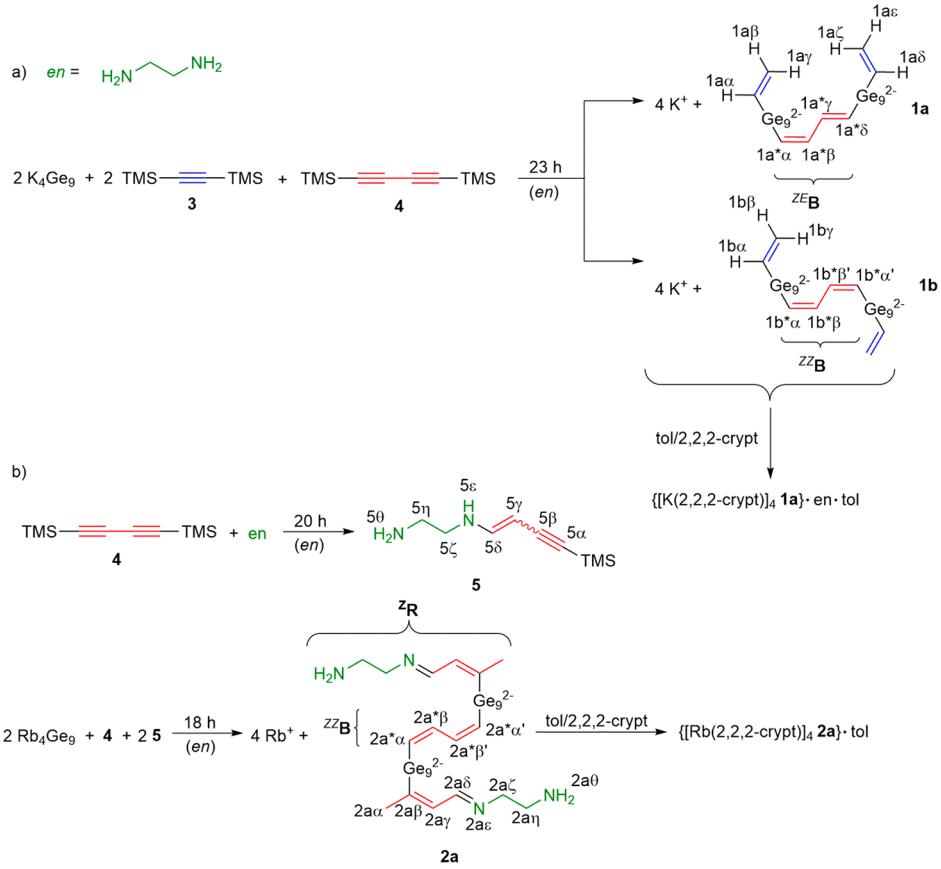

known fullerene–linker–fullerene triads.[21] These fullerene–linker–fullerene triads have been widely explored in terms of their outstanding ability of charge generation and separation, which are useful properties in photovoltaic devices.[21−24] Due to the interesting analogy between fullerenes and deltahedral tetrel clusters—the latter are in addition to other properties also capable of adopting different charges[1,2]—the novel Ge_9 Zintl triads similarly represent promising candidates for applications in diverse molecular electronic devices, photovoltaics, and photodynamic therapy.

The $[Ge_9–Ge_9]^{6-}$ dimer and the $_{1\infty}[Ge_9]^{2-}$ polymer represent examples of directly coupled Ge_9 Zintl clusters.[25,26] Additionally, the linkage of deltahedral Ge_9 Zintl clusters via coordination to late transition metals is present in $[Hg_3(Ge_9)_4]^{10-}$[27] and $[MGe_9]^{2-}$ (M = Hg, Zn).[28,29]

So far only the coupling of Zintl clusters by organic linkers has been realized in $[R_2Ge_9–CH=CH–CH=CH–Ge_9R_2]^{4-}$ (R_2 = (2*Z*,4*E*)-7-amino-5-azahepta-2,4-dien-2-yl) comprising an organic (1*Z*,3*Z*)-buta-1,3-dien-1,4-diyl linking unit (^{ZZ}**B**). In addition also an unforeseen reaction of the linker unit with the solvent ethylenediamine has occurred.[30] In order to get a better insight into the formation of the cluster linkages, we systematically investigated this reaction and show here that the formation of the side groups can be controlled. An understanding of the formation of Zintl triads carrying organic tethers allows the directed synthesis of new types of linked cluster entities and the design of electronically tuned Zintl triads. Such materials comprising functionalities within their organic tethers, e.g. a double bond or an amine, have a high potential for the adsorption or grafting onto surfaces of thin films as well as onto nanoparticles for semiconductor applications.

Herein we report the synthesis and characterization of Zintl triads holding organic tethers and being linked by the conjugated butadiene-1,4-diyl bridge $[RGe_9–CH=CH–CH=CH–Ge_9R]^{4-}$ (R = R_1, R_2; **1a**, R_1 = vinyl; **2a**, R_2 = (2*Z*,4*E*)-7-amino-5-azahepta-2,4-dien-2-yl). **1a** is accessible by reacting K_4Ge_9 with bis(trimethylsilyl)acetylene (**3**) and 1,4-bis(trimethylsilyl)butadiyne (**4**) in ethylenediamine. The known Zintl triad **2a** is reproduced in a more direct synthesis strategy by reacting Rb_4Ge_9 with 1,4-bis(trimethylsilyl)-butadiyne (**4**) and (3*Z*/3*E*)-7-amino-1-(trimethylsilyl)-5-aza-hepta-3-en-1-yne (**5**) in ethylenediamine (Scheme 1). The Zintl triads crystallize as {$[K(2,2,2\text{-crypt})]_4$ **1a**}·tol·en (**1**) comprising a (1*Z*,3*E*)-butadien-1,4-yl bridge (^{ZE}**B**) and as {$[Rb(2,2,2\text{-crypt})]_4$ **2a**}·tol (**2**), which contains a (1*Z*,3*Z*)-butadien-1,4-yl bridge (^{ZZ}**B**). The $[A(2,2,2\text{-crypt})]^+$ salts (*A* = K, Rb) have been structurally characterized by single-crystal X-ray diffraction methods and investigated by Raman spectroscopy in the solid state and by ^{1}H and ^{13}C NMR spectroscopy in solution (2,2,2-crypt = 4,7,13,16,21,24-hexaoxa-1,10-diazabicyclo[8.8.8]hexacosane). The formation mechanisms of **1a** and **2a** (Scheme 1) have been examined by 1D and 2D NMR spectroscopy. In solution **1a** also appears with a ^{ZZ}**B** linking unit, which in the following is labeled as **1b** (Scheme 1).

DOI: 10.1021/acs.inorgchem.7b01643
Inorg. Chem. 2017, 56, 10691−10698

RESULTS AND DISCUSSION

Synthesis. {[K(2,2,2-crypt)]$_4$ **1a**}·tol·en (**1**) was synthesized by stirring a mixture of K_4Ge_9, bis(trimethylsilyl)acetylene (**3**), and 1,4-bis(trimethylsilyl)butadiyne (**4**) in the molar ratio of 1/2/0.5 in water-free *en*[31] for 23 h at ambient temperature. Red block-shaped crystals suitable for X-ray crystallography were obtained after layering of the resulting brown solution with a solution of 2,2,2-crypt in toluene (Scheme 1a) in an approximate yield of 10% (based on the amount of K_4Ge_9) within 2 months. In order to shed some light on the formation of the Zintl triad isomers **1a**,**b**, in situ NMR spectroscopic investigations were performed. For this purpose reaction solutions with various amounts of reactant **3** (0−5.9 equiv) were prepared. Time-resolved NMR spectroscopy was also used to help in partially elucidating the reaction mechanism of the formation of **1a**,**b**.

In a further synthesis we reproduced the already known Zintl triad **2a** $[R_2Ge_9{-}CH{=}CH{-}CH{=}CH{-}Ge_9R_2]^{4-}$ (R_2 = (2*Z*,4*E*)-7-amino-5-azahepta-2,4-dien-2-yl) by using a more direct synthesis protocol, which led to the isolation of the new compound {[Rb(2,2,2-crypt)]$_4$ **2a**}·tol (**2**) (Scheme 1b). In a prestep (in the absence of the cluster units), a mixture of 1,4-bis(trimethylsilyl)butadiyne (**4**) and water-free *en*[30,31] gives compound **5**. In a second step the 1-(trimethylsilyl)-7-amino-5-azahepta-3-en-1-yne (**5**)/*en* solution (2 equiv of **5** with respect to Rb_4Ge_9) was added to a 2/1 premixture of the neat solids Rb_4Ge_9 and 1,4-bis(trimethylsilyl)butadiyne (**4**). After stirring of the combined mixtures for 18 h, the orange-red reaction solution was layered with 2,2,2-crypt/toluene solution. Orange plates of {[Rb(2,2,2-crypt)]$_4$ **2a**}·tol grew within several weeks (yield ca. 30%, based on the amount of Rb_4Ge_9), which were characterized by Raman and NMR spectroscopy. In addition, time-resolved NMR spectroscopic measurements were performed to study the reaction mechanism.

Crystal Structures. The crystal structure of {[K(2,2,2-crypt)]$_4$ **1a**}·tol·en contains, in addition to two solvent molecules (toluene and *en*), the anionic entity **1a** and four $[K(2,2,2\text{-crypt})]^+$ cations, which is consistent with the 4-fold negatively charged anionic entity **1a**. The latter consists of two 2-fold negatively charged Ge_9 clusters connected by a conjugated organic (1*Z*/3*E*)-buta-1,3-diene-1,4-diyl bridge (^{ZE}**B**) (C1/C2/C3/C4). Both Ge_9 clusters carry an additional vinyl group. In the crystal structure the linking chain appears in two orientations and two different conformers are present: the major component comprises the 1*Z*,3*E*-configured bridge ^{ZE}**B** (**1a**, occupancy 61.0%), whereas the less frequent conformer shows the 1*E*,3*Z* bridge ^{EZ}**B** (**1a**, occupancy 39.0%) (Figure 1). In other words, the linking unit ^{ZE}**B** is mirrored on a virtual plane crossing the bond between the atoms C2 and C3.[32] The bond lengths of 1.34(1) Å (C1−C2), 1.34(2) Å (C1′−C2′) and 1.36(1) Å (C3−C4), 1.29(2) Å (C3′−C4′) reveal a double bond, and 1.41(1) Å (C2−C3) and 1.46(2) Å (C2′−C3′) display a single-bond character.[33] The atoms of the linking entities ^{ZE}**B** (C1/C2/C3/C4) and ^{EZ}**B** (C4′/C3′/C2′/C1′) and the connecting atoms Ge1 and Ge10 of the two clusters lie on the idealized plane through these atoms with a maximum deviation of 0.0185 Å for C3 and 0.0421 Å for C4′ (Figure S2a,b in the Supporting Information). The Ge−C(sp^2) distances of 1.90(2)−2.10(1) Å are in the typical range of a single bond.[16,30] The cluster units appear with almost perfect C_{2v} point symmetry, as indicated by the compression of their square planes, which are significantly compressed along the diagonal between the atoms that are connected to the organic entities (Figure 2a).[16,30] The plane Ge1/Ge2/Ge3/Ge4 possesses a shorter Ge1−Ge3 diagonal of 3.126 Å in comparison to the Ge2−Ge4 distance of 4.001 Å (for the second cluster unit: *d*(Ge10−Ge12) = 3.140 Å and *d*(Ge11−Ge13) = 3.995 Å). This effect is typically observed for Ge_9 clusters with two covalently bound organic substituents.[14−16,18−20,30,34] The other Ge−Ge distances within the clusters are in the typical range of 2.5289(7) and 2.7021(7) Å except for the two elongated bonds Ge5−Ge6 (2.9228(6) Å) and Ge7−Ge8 (2.9294(7) Å) (second cluster unit: *d*(Ge14−Ge15) = 2.9308(7) Å and *d*(Ge16−Ge17) = 2.9721(7) Å).

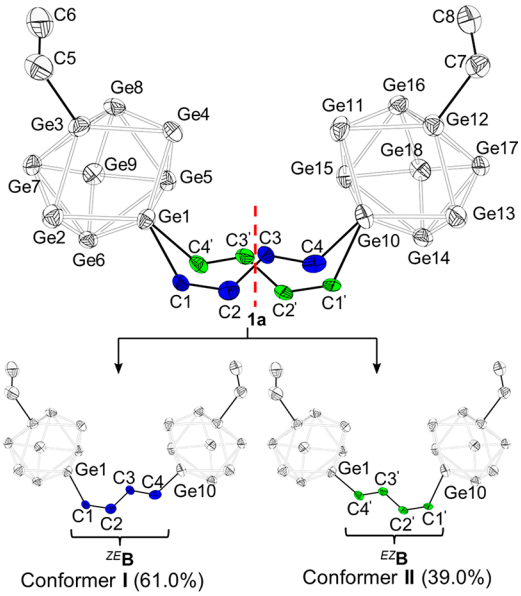

Figure 1. Disordered anion **1a**. The disordered organic conjugated bridge is marked in color. The two resulting conformers are shown individually: ^{ZE}**B** conformer **I** in blue and ^{EZ}**B** conformer **II** in green. Displacement ellipsoids are shown at a probability level of 50%. Hydrogen atoms are omitted for clarity. The virtual mirror plane is marked in red.

The ^{ZE}**B** linkage of the two Ge_9 clusters significantly affects their spatial orientation. A remarkable difference from the currently known functionalized *cis*/*cis*-linked Ge_9 clusters linked by the ^{ZZ}**B** entity is given by the spatial proximity of the Ge_9 clusters shown by a comparatively short intercluster distance of Ge4−Ge11 of 4.649 Å (Figure S2b in the Supporting Information). In contrast, in **2a** as well as in the known Zintl triad $[(^{Z}\mathbf{R})-(Ge_9)-(^{ZZ}\mathbf{B})-(Ge_9)-(^{Z}\mathbf{R})]^{4-}$ [30] the intercluster distances are much longer and occur in **2a** between Ge1 and Ge1′ (6.281 Å), the two atoms which are connected to the cluster linkage ^{ZZ}**B**. In **1a** the open faces of the two Ge_9 cluster units are tilted toward each other (Figure 2b). The dihedral angle between the defined planes Ge1/Ge3/Ge9 and Ge10/Ge12/Ge18 is 80.2° (Figure S3 in the Supporting Information).

In addition, anion **2a** has also been obtained and characterized as the $[Rb(2,2,2\text{-crypt})]^+$ salt. Orange single crystals of the compound {[Rb(2,2,2-crypt)]$_4$ **2a**}·tol (Scheme 1b) were characterized by X-ray structure analysis, revealing isotypism with the previously reported {[K(2,2,2-crypt)]$_4$ **2a**}·tol.[30,35] Both compounds contain the molecular anion **2a** (Figure 2c,d), which is 4-fold negatively charged and located around a crystallographic inversion center. The anion consists

DOI: 10.1021/acs.inorgchem.7b01643
Inorg. Chem. 2017, 56, 10691−10698

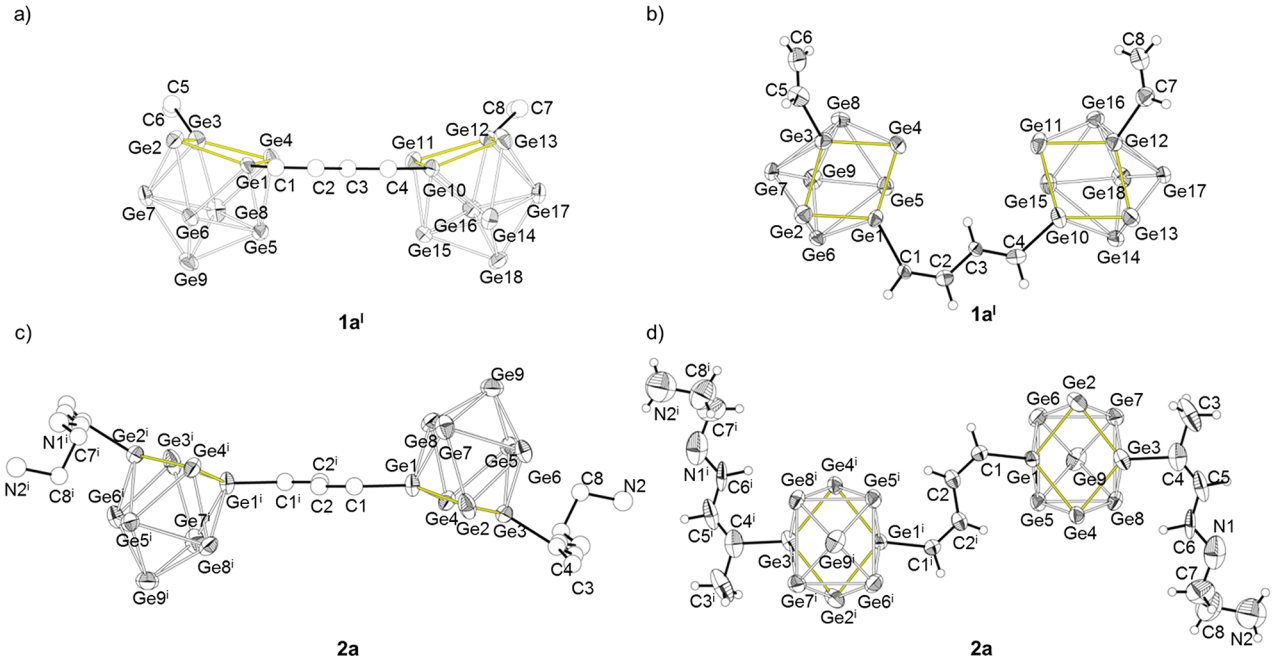

Figure 2. Structure details of **1** and **2**: (a) **1aI** with view parallel to the plane [Ge1−^{ZE}**B**−Ge10]; (b) **1aI** with view perpendicular to the plane [Ge1−^{ZE}**B**−Ge10]; (c) **2a** viewed parallel to the plane [Ge1−^{ZZ}**B**−Ge1^{i}]; (d) **2a** with view perpendicular to the plane [Ge1−^{ZZ}**B**−Ge1^{i}]. In (a) and (c) hydrogen atoms are omitted for clarity and carbon atoms are shown as empty spheres. The frame of the open square is highlighted in yellow. Displacement vectors are shown at a probability level of 50%.

of two Ge_9 units, which are connected by a ^{ZZ}**B** bridge, and each cluster carries a ^{Z}**R** side chain. The structural parameters of **2** in both {[Rb(2,2,2-crypt)]$_4$ **2a**}·tol and {[K(2,2,2-crypt)]$_4$ **2a**}·tol are almost identical. The open square (atoms Ge1−Ge4) of the Ge_9 unit is compressed at the atoms Ge1 and Ge3, which bear the ^{ZZ}**B** and ^{Z}**R** functionalities. Accordingly the cluster adapts, analogously to the clusters in **1a**, C_{2v} symmetry and derives from a C_{4v}-symmetric monocapped square antiprism with 22 skeletal electrons which is compressed at the atoms Ge1 and Ge3 of the open square.

NMR Spectroscopic Characterization of {[K(2,2,2-crypt)]$_4$ 1a}·tol·en. Red block-shaped crystals of **1** were separated under a microscope, dissolved in acetonitrile-d_3, and investigated by ^{1}H, ^{13}C, and 2D NMR spectroscopy (Figure 3 and the Supporting Information).

In the ^{1}H NMR spectrum of {[K(2,2,2-crypt)$_4$]**1a**}·tol·en the integral ratio of the signals of the protons of 2,2,2-crypt and the signals of the protons of the vinyl groups as well as the linking unit makes a total of 144:9 (expected: 144:10). This lets us assume that the crystals could not be separated from all side products by hand. This is also shown by the additional signals that are marked with asterisks in Figure 3. The protons of the linking unit ^{ZE}**B**/^{EZ}**B** appear as four signals. The signals associated with the olefinic protons 1a*α and 1a*δ show doublets with coupling constants of 11.8 and 17.1 Hz, which are typical for *cis*- and *trans*-located olefinic protons, respectively.[36] A doublet of doublets with coupling constants of 17.0 and 10.5 Hz is observed for the signal corresponding to 1a*γ. The same splitting pattern with different coupling constants is expected for the superimposed signal related to 1a*β. The protons of the vinyl functionality bound to the Ge_9 clusters of **1a** show a signal pattern which is already known for the vinylated cluster species $[Ge_9(CH{=}CH_2)_n]^{(4-n)-}$ (n = 1, 2).[15,16] The signal corresponding to 1a(α/δ) occurs as a doublet of doublets of doublets with coupling constants of 19.3

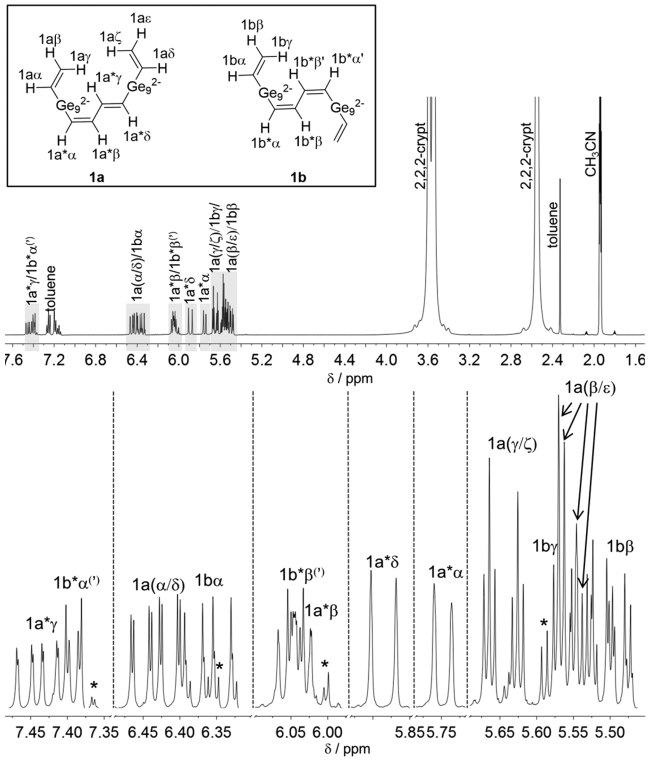

Figure 3. ^{1}H NMR spectrum of {[K(2,2,2-crypt)]$_4$ **1a**}·tol·en recorded in acetonitrile-d_3. The resonances highlighted in gray are magnified in the lower part of the figure. Signals marked with asterisks could not be assigned.

and 12.3 Hz, which is in good agreement with *trans*- and *cis*-oriented vinyl protons, respectively. As a special remark, the signal also shows a fine structure which arises from the asymmetric linking unit ^{ZE}**B** and therefore causes a slight

DOI: 10.1021/acs.inorgchem.7b01643
Inorg. Chem. 2017, 56, 10691−10698

Scheme 2. Two Pathways Resulting in the Formation of 1a,b[a]

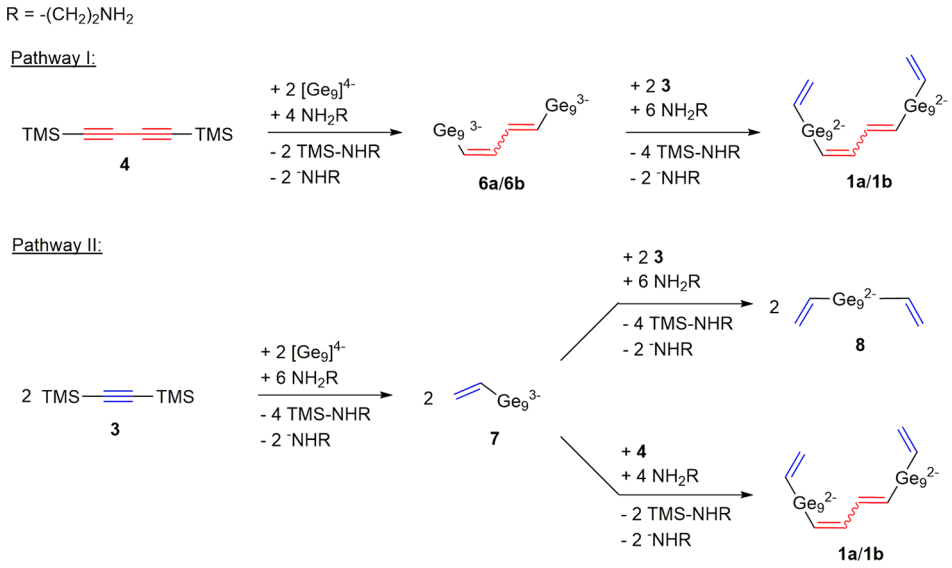

[a]Pathway II also includes the side reaction leading to the divinylated cluster **8**.

difference in the chemical shift of the vinyl protons 1aα and 1aδ. In contrast to expectations, the resonances of the protons 1a(γ/ζ) appear as doublets of triplets with coupling constants of 19.3 and 3.7 Hz. Temperature-dependent NMR investigations revealed the expected doublet of doublets of doublets splitting of the signal 1a(γ/ζ) with corresponding coupling constants of 19.3 and 3.9 Hz (Figure S5 in the Supporting Information).

The ^{1}H NMR spectrum in Figure 3 also shows the signals of **1b** containing the ^{ZZ}**B** linking unit with the ratio **1a**/**1b** = 70/30. Although no single crystals containing **1b** suitable for a single-crystal X-ray structure analysis could be found, the signals of **1b** appear in the ^{1}H NMR spectrum of selected and dissolved crystals of compound **1**. On comparison of the ratio of the conformers in the reaction solution (also **1a**/**1b** = 70/30) and in the solution of the dissolved single crystals with that for **1a**, it is possible that an equilibrium between **1a** and **1b** is achieved in solution. However, temperature-dependent NMR studies in the temperature range of −20 to +60 °C did not show a shift of a potential equilibrium between the isomers **1a** and **1b**. Light-induced *cis*−*trans* isomerization can be excluded, as the isomer ratio of the dissolved crystals did not show any change within a period of 2.5 months. The resonances of the olefinic protons 1b*$\alpha^{(\prime)}$ and 1b*$\beta^{(\prime)}$ of the linking unit ^{ZZ}**B** of **1b** appear as doublets of doublets with a coupling constant of 8.5 Hz, showing the same characteristic fine structure as the protons of ^{ZZ}**B** in {[*A*(2,2,2-crypt)$_4$] **2a**} (*A* = K, Rb).[30] The latter is the only conformer that has been found for the Zintl triad **2** both in solution and in the solid state. Due to superimposition of the signals of the vinyl functionality bound to the Ge$_9$ clusters of **1b** and those of **1a**, the multiplets cannot be identified properly.

In Situ NMR Studies. The synthesis of the vinylated Zintl triad implies an extensive study, because the reaction of $[Ge_9]^{4-}$ with bis(trimethylsilyl)acetylene (**3**) and 1,4-bis(trimethylsilyl)-butadiyne (**4**) in *en* is rather complex. The reaction rate of the reaction between $[Ge_9]^{4-}$ and **3** to give $[Ge_9(CH{=}CH_2)_2]^{2-}$ (**8**) (reaction completed within 2 h[16]) is higher than that of the reaction between $[Ge_9]^{4-}$ and **4** to give $[Ge_9{-}CH{=}CH{-}CH{=}CH{-}Ge_9]^{6-}$ (**6**) (reaction completed within 20 h[37]) when no species other than the respective mentioned reactants are present in the reaction solution. Therefore, a variation of the amounts used of the reactants as well as a variation of the order of addition of the reactants was carried out. An excess of **4** in the reaction with respect to **1** favors the formation of (3*Z*/3*E*)-7-amino-1-(trimethylsilyl)-5-azahepta-3-en-1-yne (**5**), which results in even more unwanted side reactions. Therefore, the numerous side reactions need to be limited by a variation of the amounts of **3** and also by a variation of the order of addition.

A series of experiments was performed in which the *z* equiv amounts of bis(trimethylsilyl)acetylene (**3**) (*z* = 0, 0.5, 1, 1.5, 2, 2.9, 4, 5.9) which were reacted with the Zintl phase K_4Ge_9 and 1,4-bis(trimethylsilyl)butadiyne (**4**) in *en* were varied. The in situ NMR spectroscopic investigations revealed that significant amounts of the vinylated Zintl triad **1a,b** are only formed when at least 1.5 equiv of bis(trimethylsilyl)acetylene (**3**) is used, whereas an even larger amount of **3** leads to an increase in the concentration of **1a,b** in the reaction solution, and at the same time the reaction toward the divinylated cluster $[Ge_9(CH{=}CH_2)_2]^{2-}$ (**8**) is favored (Figure S7 in the Supporting Information). Contrary to expectations, the compound with the Zintl triad **1a** crystallizes only in case of reacting 4 equiv of **3** with 2 equiv of K_4Ge_9 and 1 equiv of **4**. After a certain reaction time this mixture contains many different species according to the ^{1}H NMR spectrum of the reaction solution: namely **1a,b**, the *cis,trans* and *cis,cis* isomers of $[Ge_9{-}CH{=}CH{-}CH{=}CH{-}Ge_9]^{6-}$ (**6a,b**), the vinylated cluster species $[Ge_9(CH{=}CH_2)]^{3-}$ (**7**), and most likely also the divinylated cluster $[Ge_9(CH{=}CH_2)_2]^{2-}$ (**8**).

In order to examine the mechanism leading to the formation of the Zintl triad **1a,b**, time-resolved in situ NMR studies were performed. According to the ^{1}H NMR spectra of the reaction solutions the reaction rates of the reactions of $[Ge_9]^{4-}$ with **3** or **4** are different when more than only one of the mentioned reactants are present in the reaction solution. The first step including the reaction of two $[Ge_9]^{4-}$ clusters with **4** to form the Zintl triad **6a,b** proceeds comparatively quickly and is complete within 0.5 h (Scheme 2, pathway I). Within the same time in a second reaction pathway the vinylated anionic entity **7**

DOI: 10.1021/acs.inorgchem.7b01643
Inorg. Chem. 2017, 56, 10691−10698

is formed by the reaction of $[Ge_9]^{4-}$ with one molecule of **3** and reaches its maximum concentration (Scheme 2, pathway II).

In both reaction pathways the subsequent second step takes at least 3.5 h and is therefore significantly slower. With decreasing intensities of the signals of **6a,b** the signals assigned to **1a,b** increase in intensity. This observation suggests that **6a,b** subsequently reacts with **3**, resulting in **1a,b**. As specified by the integrals of the signals of **6a,b** and **1a,b** the reactivity of **6a** (*cis*/*trans* product) toward **3** is higher than that of **6b** (*cis*/*cis* product); thus the *cis*/*trans* isomer **1a** is formed more quickly than the corresponding *cis*/*cis* isomer **1b**. The second step of reaction pathway II implies the subsequent reaction of **7** with **3** or **4**. With advanced reaction time the divinylated cluster species **8** is formed in noticeable quantity, which leads to the conclusion that the reaction of **7** with **3** is preferred over the reaction with **4**.

Step by step addition of the reaction components **3** and **4** to K_4Ge_9 according to reaction pathways I and II given in Scheme 2 leads to side reactions so that the Zintl triad **1a,b** is not among the major products in the reaction solution. A variation of the order of the addition of the reaction components **3** and **4** to K_4Ge_9 according to the reaction pathways given in Scheme 2 leads in both cases to the required product **1a,b** as minor components. Throughout the reaction of $[Ge_9]^{4-}$ with **4** the presence of **3** outstandingly affects the reaction time, which is lowered by 11 h.[37] As a result it was necessary to dissolve all reaction components simultaneously in *en* in order to mainly obtain **1a,b**. It should be noted that *trans*-configured alkenylated Ge_9 cluster species as in **1a** are rare. The syn addition of Ge_9 clusters to a triple bond can occur when the triple bond is part of a conjugated π-electronic system.[34] The formation of the ^{ZE}**B** linking entity could also be observed in the ^{1}H NMR spectrum of the reaction solution of 1 equiv of A_4Ge_9 (A = K, Rb) and 0.5 equiv of **4**, leading to $[Ge_9C_4H_4Ge_9]^{6-}$ (**6a,b**).

CONCLUSIONS

Herein we present the synthesis and characterization of the Zintl triads $[R{-}Ge_9{-}CH{=}CH{-}CH{=}CH{-}Ge_9{-}R]^{4-}$ (**1**, **2**) bearing supplemental organic tethers (R: R_1 = $-CH{=}CH_2$, R_2 = $-C(CH_3){=}CH{-}CH{=}N(CH_2)_2NH_2$). For their formation the reactants $[Ge_9]^{4-}$, 1,4-bis(trimethylsilyl)butadiyne (**4**), bis(trimethylsilyl)acetylene (**3**), and (3*Z*/3*E*)-7-amino-1-(trimethylsilyl)-5-azahepta-3-en-1-yne (**5**), respectively, are simultaneously required. Understanding the interplay of the applied alkyne reactants toward $[Ge_9]^{4-}$ clusters including solvent molecules as well as the interplay between the various organic reactants now allows for the synthesis of a wider range of Zintl triads. According to quantum chemical calculations the anionic entity **1a** bears a conjugated π-electron system which is extended throughout the whole Zintl triad.[30] This interesting electronic structure makes these new materials, in analogy to fullerenes, interesting candidates for application in electronic devices. The reported Zintl triads have the potential to be grafted or adsorbed on surfaces via their organic tethers, which bear the relevant functionality. In addition, the coordination of double bonds, which are included in the organic tethers, to transition metals is feasible.

EXPERIMENTAL SECTION

Materials and Techniques. All manipulations were carried out under a purified argon atmosphere using standard Schlenk techniques and an argon-filled glovebox with a moisture and oxygen level below 0.1 ppm. The Zintl phases A_4Ge_9 (A = K, Rb) were synthesized by heating a stoichiometric mixture of the elements K or Rb and Ge (99.999% Chempur) at 650 °C for 48 h in an iron autoclave.[38] 1,4-Bis(trimethylsilyl)butadiyne (Alfa Aesar 98%) was used as received. Bis(trimethylsilyl)acetylene (Sigma-Aldrich 99%) was stored over molecular sieves (3 Å). Toluene was dried over molecular sieves (4 Å) in a solvent purification system (MBraun MB-SPS). 2,2,2-crypt (Merck) was dried under vacuum for 8 h. The reactions were carried out in ethylenediamine (*en*). *en* (Merck) with an initial water content of ≤1% was refluxed over calcium hydride (Merck) for 48 h and stored in a Schlenk tube under an argon atmosphere.

Synthesis of {[K(2,2,2-crypt)]$_4$ 1a}·tol·en (1). **4** (9.0 mg, 46 μmol, 0.5 equiv) was weighed into a Schlenk tube and partially dissolved in **3** (39 μL, 180 μmol, 2 equiv). K_4Ge_9 (73.0 mg, 90 μmol, 1 equiv) was subsequently added to the Schlenk tube, and the mixture was dissolved in 1.5 mL of *en*, resulting in a brown solution after stirring for 23 h. After filtration 1 mL of the reaction solution was layered with a solution of 2,2,2-crypt (91.0 mg, 240 μmol, 4 equiv) in 4 mL of toluene and left undisturbed at room temperature. After 2 months red block-shaped crystals of {[K(2,2,2-crypt)]$_4$ **1a**}·tol·en suitable for X-ray crystallography were obtained (yield ca. 10%). Crystals of {[K(2,2,2-crypt)]$_4$ **1a**}·tol·en were separated from side products by hand and used for X-ray structure analysis (Table 1).

Table 1. Crystallographic Data for Compounds {[K(2,2,2-crypt)]$_4$ 1a}·en·tol (1) and {[Rb(2,2,2-crypt)]$_4$ 2a}·tol (2)

	1	2
fw (g mol^{-1})	3227.36	3520.99
space group (No.)	$P\bar{1}$ (2)	$P\bar{1}$ (2)
a (Å)	16.3459(2)	11.9068(2)
b (Å)	17.0533(2)	12.8103(2)
c (Å)	24.9891(3)	24.5724(6)
α (deg)	99.003(1)	104.534(2)
β (deg)	101.014(1)	92.040(2)
γ (deg)	101.601(1)	109.352(2)
V (Å^3)	6558.7(1)	3394.0(1)
Z	2	1
T (K)	153(2)	123(2)
λ (Å)	0.71073	0.71073
ρ_{calcd} (g cm^{-3})	1.634	1.723
μ (mm^{-1})	4.24	5.41
R_{int}	0.059	0.094
R_1 ($I > 2\sigma(I)$/all data)	0.037/0.073	0.085/0.136
wR_2 ($I > 2\sigma(I)$/all data)	0.075/0.079	0. 218/0.242
goodness of fit	0.909	1.035

Crystals used for Raman and NMR spectroscopy were washed with toluene and dried at ambient pressure. Raman ν [cm^{-1}]: 145 (m, Ge_9 cluster), 185 (m, Ge_9 cluster breathing), 516 (w, exo-Ge−C). 568 (w, exo-Ge−C), 851 (w, vinyl, $=CH_2$ valence), 990 (w, vinyl, $=CH_2$ valence), 1070 (m, en, C−N stretching), 1206 (w, ^{ZE}**B**/^{EZ}**B**, C−C valence), 1279 (s, ^{ZE}**B**/^{EZ}**B**, C=C valence), 1421 (w, vinyl, $=CH_2$ valence), 1560 (vs, ^{ZE}**B**/^{EZ}**B**, C=C valence). ^{1}H NMR (500 MHz, acetontirile-d_3, 296 K): δ (ppm) 7.44 (ddd, J = 17.0 Hz, 10.5 Hz, 1.0 Hz, 1H, 1a*γ), 7.21 (m, Ar*H*, tol), 6.43 (ddd, J = 19.3 Hz, 12.3 Hz, 1.9 Hz, 2H, 1a(α/δ)), 6.04 (m, superimposed with 1b*β and revealed by COSY NMR spectrum, 1a*β), 5.89 (d, J = 17.1 Hz, 1H, 1a*δ), 5.75 (d, J = 11.8 Hz, 1H, 1a*α), 5.65 (pseudo dt, J = 19.3 Hz, 3.7 Hz, 2H, 1a(γ/ζ)), 5.55 (dd, J = 12.0 Hz, 4.0 Hz, 2H, 1a(β/ε)), 3.59 (s, crypt), 3.54 (s, crypt), 2.55 (s, crypt), 2.33 (s, − C*H*$_3$, tol). COSY (500 MHz, acetonitrile-d_3, 296 K): δ (ppm) 6.05/7.39 (^3J, 1a*β/1a*γ), 5.90/7.43 (^3J, 1a*δ/1a*γ), 5.75/6.04 (^3J, 1a*α/1a*β), 5.66/6.41 (^3J, 1a(γ/ζ)/ 1a(α/δ)), 5.56/6.39 (^3J, 1a(β/ε)/ 1a(α/δ)). ^{13}C NMR (126 MHz, acetonitrile-d_3, 296 K): δ (ppm) 146.26 (1a*γ), 145.74−145.62 (1a(α/δ), cannot be assigned properly), 145.08 (1a*β), 138.71

DOI: 10.1021/acs.inorgchem.7b01643
Inorg. Chem. 2017, 56, 10691−10698

(1a*δ), 134.31 (1a*α), 129.84 (C2/6$_{ar}$, tol), 129.14 (C3/5$_{ar}$, tol), 129.09−128.84 (1a(γ/ζ)/1a(β/ε), cannot be assigned properly), 126.18 (C4$_{ar}$, tol), 71.26 (2,2,2-crypt), 68.45 (2,2,2-crypt), 54.68 (2,2,2-crypt), 45.83 (en), 21.39 (−CH$_3$, tol). HSQC (500 MHz, 126 MHz, acetontirile-d_3, 296 K): δ (ppm) 7.44/146.18 (^1J, 1a*γ/1a*γ), 7.25/129.19 (^1J, tol), 7.19/129.76 (^1J, tol), 6.43/145.69 (^1J, 1a(α/δ)/1a(α/δ)), 6.05/145.26 (^1J, 1a*β/1a*β), 5.90/138.69 (^1J, 1a*δ/1a*δ), 5.76/134.27 (^1J, 1a*α/1a*α), 5.66/128.87 (^1J, 1a(γ/ζ)/1a(γ/ζ)), 5.56/128.85 (^1J, 1a(β/ε)/1a(β/ε)).

Preparation of (3*Z*/3*E*)-7-Amino-1-(trimethylsilyl)-5-azahepta-3-en-1-yne (5).[30] Solutions of 120 μmol/4 mL *en* were prepared by stirring 46.7 mg (240 μmol) of **4** with 2 mL of *en* in a Schlenk tube for 20 h. Thereby a pale yellow, transparent solution of **5** was obtained. Prior to the application of **5** in further synthesis the solution was filtered over glass wool in order to remove traces of unreacted **4**. ^{1}H NMR (500 MHz, ethylenediamine (nondeuterated), 296 K): isomer ^{Z}**5** δ (ppm) 6.40 (dd, *J* = 8.6 Hz, 12.2 Hz, 1H, 5δ), 3.96 (d, *J* = 8.6 Hz, 1H, 5γ), 6.67 (s(broad), 5ε), 3.21 (pseudo q, *J* = 6.0 Hz, 2H, 5ζ), 2.76 (5η, covered by en and revealed by COSY), 0.23 (s, 9H, C−Si−(CH_3)$_3$−); isomer ^{E}**5** δ (ppm) 6.91 (dd, *J* = 13.6 Hz, 7.4 Hz, 1H, 5δ), 4.23 (d, *J* = 13.6 Hz, 1H, 5γ), 7.54 (s(broad), 1H, 5ε), 2.96 (pseudo q, *J* = 6.0 Hz, 2H, 5ζ), 2.79 (covered by *en* and revealed by COSY, 5η), 0.19 (s, 9H, C−Si−(CH_3)$_3$).

Synthesis of {[Rb(2,2,2-crypt)]$_4$ 2a}·tol (2). In a Schlenk tube 1.3 mL of a **5**/*en* solution (120 μmol/mL, 156 μmol, 2 equiv) was dropped onto a mixture of Rb_4Ge_9 (77.6 mg, 78 μmol, 1 equiv) and **4** (7.6 mg, 39 μmol, 0.5 equiv). Immediately, a dark red suspension was obtained, which was stirred for 18 h. After it was stirred, the orange-red reaction solution was filtered over glass fibers. An aliquot of 1 mL was layered with a solution of 2,2,2-crypt (90.4 mg, 240 μmol, 4 equiv) in toluene (4 mL). After 1 week orange crystals of {[Rb(2,2,2-crypt)]$_4$ **2a**}·tol were found in the Schlenk tube (yield ca. 30%) and used for X-ray structure analysis (Table 1) and Raman and NMR spectroscopy. Raman ν [cm^{-1}]: 145 (s, Ge$_9$-cluster), 214 (s, Ge$_9$-cluster, breathing), 522 (m, *exo*-Ge−C), 1183 (w, ^{Z}**R$_2$**, C−C valence), 1225 (s, ^{ZZ}**B**, C−C valence), 1561 (vs, ^{ZZ}**B**, C═C valence), 1611 (m, ^{Z}**R$_2$**, C═N/C═C valence). ^{1}H NMR (500 MHz, py-d_5, 296 K), δ (ppm): 10.14 (d, *J* = 9.0 Hz, 2H, 2aδ), 8.78 (covered by py revealed by COSY, 2a*$\alpha^{(\prime)}$), 7.22 (covered by py revealed by COSY, 2a*$\beta^{(\prime)}$), 6.92 (d, *J* = 8.9 Hz, 2H, 2aγ), 3.81 (t, *J* = 5.9 Hz, 4H, 2aζ), 3.00 (pseudo q, *J* = 6.1, 7.3 Hz, 4H, 2aη), 2.48 (s, 6H, 2aα), 1.45 (covered and revealed by COSY, 2aθ), 7.2−7.3 (m, tol, ArH), 2.23 (s, tol, − CH_3), 3.47 (m, crypt), 3.42 (m, crypt), 2.43 (m, crypt).

Structure Determination. A single crystal was fixed on the top of a glass fiber with perfluorinated ether and positioned in a cold N_2 stream. The single-crystal X-ray diffraction data were recorded on an Oxford-Diffraction Xcalibur3 diffractometer (Mo Kα radiation). The crystal structure was solved by direct methods using the SHELX software.[39] CCDC 1551572 and CCDC 1551573 contain the supplementary crystallographic data for this paper. The positions of the hydrogen atoms were geometrically calculated and refined using a riding model. All non-hydrogen atoms were treated with anisotropic displacement parameters. In the crystal structure of **1** a disordered solvent molecule was treated with the SQUEEZE option in PLATON.[40,41] Due to the observed conformational disorder of the linking entity in the crystal structure of {[K(2,2,2-crypt)]$_4$ **1a**}·tol·en (**1**), there is an uncertainty in the distances between the carbon atoms of the linking units ^{ZE}**B** and ^{EZ}**B**. Further crystallographic details are given in Table 1.

NMR Spectroscopy. The NMR solvents acetonitrile-d_3 (Deutero GmbH 99.8%) and pyridine-d_5 (Deutero GmbH 99.5%) were dried over molecular sieves (3 Å) for at least 1 day and stored in a glovebox. Chloroform-*d* (Deutero GmbH 99.8%) was used as received. The ^{1}H, ^{13}C, and 2D NMR spectra were recorded on a Bruker 400 MHz and a Bruker 500 MHz spectrometer. For ^{1}H NMR and 2D NMR spectra of the reaction solutions in *en* the reaction solution was filtered. An aliquot was taken (approximately 0.20 mL) and filled into a Norell tube (with an outer diameter of 3 mm). The Norell tube was set into a common NMR tube (with an inner diameter of 4 mm) filled with chloroform-*d*.

■ ASSOCIATED CONTENT

Ⓢ Supporting Information

The Supporting Information is available free of charge on the ACS Publications website at DOI: 10.1021/acs.inorgchem.7b01643.

Full experimental procedures on the compounds {[K-(2,2,2-crypt)]$_4$ **1a**}·tol·en (**1**) and {[Rb(2,2,2-crypt)]$_4$ **2a**}·tol (**2**), detailed crystallographic material and in situ NMR studies on the compound {[K(2,2,2-crypt)]$_4$ **1a**}·tol·en (**1**), and Raman spectra of the compounds **1** and **2** (PDF)

Accession Codes

CCDC 1551572−1551573 contain the supplementary crystallographic data for this paper. These data can be obtained free of charge via www.ccdc.cam.ac.uk/data_request/cif, or by emailing data_request@ccdc.cam.ac.uk, or by contacting The Cambridge Crystallographic Data Centre, 12 Union Road, Cambridge CB2 1EZ, UK; fax: +44 1223 336033.

■ AUTHOR INFORMATION

Corresponding Author

*E-mail for T.F.F.: thomas.faessler@lrz.tum.de.

ORCID

Thomas F. Fässler: 0000-0001-9460-8882

Notes

The authors declare no competing financial interest.

■ ACKNOWLEDGMENTS

The authors acknowledge support through the research network "Solar Technologies go Hybrid" (Bavarian Ministry of Economic Affairs and Media, Energy and Technology, Germany) via TUM.solar and are grateful to M.Sc. Thomas Henneberger for his help with the structure determination as well as to M.Sc. Sebastian Geier and Dr. Herta Slavik for performing Raman measurements. The authors also thank Maria Weindl for carrying out NMR measurements. S.F. is further grateful to the Fonds der Chemischen Industrie for her fellowship.

■ REFERENCES

(1) Fässler, T. F. Homoatomic Polyhedra as Structural Modules in Chemistry: What Binds Fullerenes and Homonuclear Zintl Ions? *Angew. Chem., Int. Ed.* **2001**, *40*, 4161−4165; *Angew. Chem.* **2001**, *113*, 4289−4293.

(2) Fässler, T. F. The Renaissance of Homoatomic Nine-Atom Polyhedra of the Heavier Carbon-Group Elements Si−Pb. *Coord. Chem. Rev.* **2001**, *215*, 347−377.

(3) Segura, J. L.; Martín, N. [60] Fullerene Dimers. *Chem. Soc. Rev.* **2000**, *29*, 13−25.

(4) Wade, K. The Structural Significance of the Number of Skeletal Bonding Electron-Pairs in Carboranes, the Higher Boranes and Borane Anions, and Various Transition-Metal Carbonyl Cluster Compounds. *J. Chem. Soc. D* **1971**, 792−793.

(5) Wade, K. J. Structural and Bonding Patterns in Cluster Chemistry. *Adv. Inorg. Chem. Radiochem.* **1976**, *18*, 1−66.

(6) Hirsch, A.; Chen, Z.; Jiao, H. Spherical Aromaticity in I_h Symmetrical Fullerenes: the 2 $(N+1)^2$ Rule. *Angew. Chem., Int. Ed.* **2000**, *39*, 3915−3917; *Angew. Chem.* **2000**, *112*, 4079−4085.

(7) Goicoechea, J. M.; Sevov, S. C. [(Ni-Ni-Ni)@(Ge$_9$)$_2$]$^{4-}$: A Linear Triatomic Nickel Filament Enclosed in a Dimer of Nine-Atom Germanium Clusters. *Angew. Chem., Int. Ed.* **2005**, *44*, 4026−4028; *Angew. Chem.* **2005**, *117*, 4094−4096.

DOI: 10.1021/acs.inorgchem.7b01643
Inorg. Chem. 2017, 56, 10691−10698

(8) Scharfe, S.; Kraus, F.; Stegmaier, S.; Schier, A.; Fässler, T. F. Zintl Ions, Cage Compounds, and Intermetalloid Clusters of Group 14 and Group 15 Elements. *Angew. Chem., Int. Ed.* **2011**, *50*, 3630−3670; *Angew. Chem.* **2011**, *123*, 3712−3754.
(9) Suzuki, T.; Li, Q.; Khemani, K. C.; Wudl, F.; Palmarsson, O. Systematic Inflation of Buckminsterfullerene C60: Synthesis of Diphenyl Fulleroids C61 to C66. *Science* **1991**, *254*, 1186−1188.
(10) Balch, A. L.; Catalano, V. J.; Lee, J. W.; Olmstead, M. M.; Parkin, S. R. $(\eta^2\text{-}C_{70})Ir(CO)Cl(PPh_3)_2$: The Synthesis and Structure of an Iridium Organometallic Derivative of a Higher Fullerene. *J. Am. Chem. Soc.* **1991**, *113*, 8953−8955.
(11) Hirsch, A.; Grösser, T.; Skiebe, A.; Soi, A. Synthesis of Isomerically Pure Organodihydrofullerenes. *Chem. Ber.* **1993**, *126*, 1061−1067.
(12) Ugrinov, A.; Sevov, S. C. Derivatization of Deltahedral Zintl Ions by Nucleophilic Addition: $[Ph\text{-}Ge_9\text{-}SbPh_2]^{2-}$ and $[Ph_2Sb\text{-}Ge_9\text{-}Ge_9\text{-}SbPh_2]^{4-}$. *J. Am. Chem. Soc.* **2003**, *125*, 14059−14064.
(13) Hull, M. W.; Ugrinov, A.; Petrov, I.; Sevov, S. C. Alkylation of Deltahedral Zintl Clusters: Synthesis of $[R\text{-}Ge_9\text{-}Ge_9\text{-}R]^{4-}$ (R= *t*Bu, *s*Bu, *n*Bu, *t*Am) and Structure of $[t\text{Bu-}Ge_9\text{-}Ge_9\text{-}t\text{Bu}]^{4-}$. *Inorg. Chem.* **2007**, *46*, 2704−2708.
(14) Hull, M. W.; Sevov, S. C. Functionalization of Nine-Atom Deltahedral Zintl Ions with Organic Substituents: Detailed Studies of the Reactions. *J. Am. Chem. Soc.* **2009**, *131*, 9026−9037.
(15) Benda, C. B.; Wang, J. Q.; Wahl, B.; Fässler, T. F. Syntheses and ^{1}H NMR Spectra of Substituted Zintl Ions $[Ge_9R_n]^{(4-n)-}$: Crystal Structures of $[Ge_9R]^{3-}$ (R = 2,4,6-$Me_3C_6H_2$, $CHCH_2$) and Indication of Tris-Vinylated Clusters. *Eur. J. Inorg. Chem.* **2011**, *27*, 4262−4269.
(16) Hull, M. W.; Sevov, S. C. Organo-Zintl Clusters Soluble in Conventional Organic Solvents: Setting the Stage for Organo-Zintl Cluster Chemistry. *Inorg. Chem.* **2007**, *46*, 10953−10955.
(17) Benda, C. B.; He, H.; Klein, W.; Somer, M.; Fässler, T. F. Bisvinylated $[R\text{−}Ge_9\text{−}Ge_9\text{−}R]^{4-}$ Cluster Dimers. *Z. Anorg. Allg. Chem.* **2015**, *641*, 1080−1086.
(18) Hull, M. W.; Sevov, S. C. Developing Organo-Zintl Deltahedral Clusters as Ligands for Coordination to Transition-Metals via their Organic Tethers. *J. Organomet. Chem.* **2012**, *721-722*, 85−91.
(19) Hull, M. W.; Sevov, S. C. Water Compatibility and Organic Transformations of Organo-Zintl Deltahedral Clusters. *Chem. Commun.* **2012**, *48*, 7720−7722.
(20) Hull, M. W.; Sevov, S. C. Addition of Alkenes to Deltahedral Zintl Clusters by Reaction with Alkynes: Synthesis and Structure of $[Fc\text{−}CH{=}CH\text{−}Ge_9\text{−}CH{=}CH\text{−}Fc]^{2-}$, an Organo-Zintl−Organometallic. *Angew. Chem., Int. Ed.* **2007**, *46*, 6695−6698; *Angew. Chem.* **2007**, *119*, 6815−6818.
(21) Lebedeva, M. A.; Chamberlain, T. W.; Davies, E. S.; Thomas, B. E.; Schröder, M.; Khlobystov, A. N. Tuning the Interactions between Electron Spins in Fullerene-Based Triad Systems. *Beilstein J. Org. Chem.* **2014**, *10*, 332−343.
(22) Yu, G.; Gao, J.; Hummelen, J. C.; Wudl, F.; Heeger, A. J. Polymer Photovoltiac Cells: Enhanced Efficiencies via a Network of Internal Donor-Acceptor Heterojunctions. *Science* **1995**, *270*, 1789−1791.
(23) Xie, Q.; Arias, F.; Echegoyen, L. Electrochemically-Reversible, Single-Electron Oxidation of C60 and C70. *J. Am. Chem. Soc.* **1993**, *115*, 9818−9819.
(24) Martín, N.; Sánchez, L.; Illescas, B.; Pérez, I. C60-Based Electroactive Organofullerenes. *Chem. Rev.* **1998**, *98*, 2527−2548.
(25) Nienhaus, A.; Hoffmann, S. D.; Fässler, T. F. First Synthesis of Group-14 Polyanions by Extraction of a Binary Alloy with dmf and a Novel Conformation of the $(Ge_9\text{−}Ge_9)^{6-}$ Dimer: Crystal Structures of $[K_6(Ge_9\text{−}Ge_9)](dmf)_{12}$, $[Rb_6(Ge_9\text{−}Ge_9)](dmf)_{12}$ and $[K2.5Cs3.5\text{-}(Ge_9\text{−}Ge_9)](dmf)_{12}$. *Z. Anorg. Allg. Chem.* **2006**, *632*, 1752−1758.
(26) Downie, C.; Tang, Z.; Guloy, A. M. An Unprecedented $_{1\infty}[Ge_9]^{2-}$ Polymer: A Link between Molecular Zintl Clusters and Solid-State Phases. *Angew. Chem., Int. Ed.* **2000**, *39*, 337−340; *Angew. Chem.* **2000**, *112*, 346−348.
(27) Denning, M. S.; Goicoechea, J. M. $[Hg_3(Ge_9)_4]^{10-}$: A Nanometric Molecular Rod Precursor to Polymeric Mercury-Linked Cluster Chains. *Dalton Trans.* **2008**, 5882−5885.
(28) Nienhaus, A.; Hauptmann, R.; Fässler, T. F. $^1{}_\infty[HgGe_9]^{2-}$−A Polymer with Zintl Ions as Building Blocks Covalently Linked by Heteroatoms. *Angew. Chem., Int. Ed.* **2002**, *41*, 3213−3215; *Angew. Chem.* **2002**, *114*, 3352−3355.
(29) Mayer, K.; Jantke, L.-A.; Schulz, S.; Fässler, T. F. Retention of the Zn−Zn bond in $[Ge_9Zn\text{−}ZnGe_9]^{6-}$ and Formation of $[(Ge_9Zn)\text{−}(Ge_9)\text{−}(ZnGe_9)]^{8-}$ and Polymeric $^1{}_\infty[-(Ge_9Zn)^{2-}-]^1$. *Angew. Chem., Int. Ed.* **2017**, *56*, 2350−2355; *Angew. Chem.* **2017**, *129*, 2390−2395.
(30) Bentlohner, M. M.; Klein, W.; Fard, Z. H.; Jantke, L.-A.; Fässler, T. F. Linking Deltahedral Zintl Clusters with Conjugated Organic Building Blocks: Synthesis and Characterization of the Zintl Triad $[R\text{-}Ge_9\text{-}CH{=}CH\text{−}CH{=}CH\text{-}Ge_9\text{-}R]^{4-}$. *Angew. Chem., Int. Ed.* **2015**, *54*, 3748−3753; *Angew. Chem.* **2015**, *127*, 3819−3824.
(31) Bentlohner, M. M.; Waibel, M.; Zeller, P.; Sarkar, K.; Müller-Buschbaum, P.; Fattakhova-Rohlfing, D.; Fässler, T. F. Zintl Clusters as Wet-Chemical Precursors for Germanium Nanomorphologies with Tunable Composition. *Angew. Chem., Int. Ed.* **2016**, *55*, 2441−2445; *Angew. Chem.* **2016**, *128*, 2487−2491.
(32) It is likely that the two conformers **I** and **II** lie in one crystallographic position so that not only the linking unit ^{ZE}**B** but also the clusters are split with occupancies of 61.0% and 39.0%, respectively.
(33) Anslyn, E. V.; Dougherty, D. A. *Modern Physical Organic Chemistry*; University Science: Sausalito, CA, 2006.
(34) Gillett-Kunnath, M. M.; Petrov, I.; Sevov, S. C. Heteroatomic Deltahedral Zintl Ions of Group 14 and their Alkenylation. *Inorg. Chem.* **2010**, *49*, 721−729.
(35) Regarding the better quality of the present crystals, we assume that the potassium analogue of the same compound as reported in ref 30, $\{K(222\text{-crypt})]_4\mathbf{2}\}\cdot(tol)_2$, also contains one solvent molecule.
(36) Hesse, M.; Meier, H. *Spektroskopische Methoden in der Organischen Chemie*, 8th ed.; Georg Thieme Verlag: Stuttgart, Germany, 2014.
(37) Bentlohner, M. M. Dissertation, Technische Universität München, Garching, Germany, 2016.
(38) Hoch, C.; Wendorff, M.; Röhr, C. Synthesis and Crystal Structure of the Tetrelides $A_{12}M_{17}$ (A = Na, K, Rb, Cs; M = Si, Ge, Sn) and A_4Pb_9 (= K, Rb). *J. Alloys Compd.* **2003**, *361*, 206−221.
(39) Sheldrick, G. M. Crystal Structure Refinement with SHELXL. *Acta Crystallogr., Sect. C: Struct. Chem.* **2015**, *71*, 3−8.
(40) Spek, A. L. Structure Validation in Chemical Crystallography. *Acta Crystallogr., Sect. D: Biol. Crystallogr.* **2009**, *65*, 148−155.
(41) Spek, A. L. PLATON SQUEEZE: A Tool for the Calculation of the Disordered Solvent Contribution to the Calculated Structure Factors. *Acta Crystallogr., Sect. C: Struct. Chem.* **2015**, *71*, 9−18.

DOI: 10.1021/acs.inorgchem.7b01643
Inorg. Chem. 2017, 56, 10691−10698

Synthesis of *Zintl* Triads Comprising Extended Conjugated π-Electronic Systems – $[RGe_9–CH=CH–CH=CH–Ge_9R]^{4–}$ (R: $–CH=CH_2$, $–C(CH_3)=CH–CH=N(CH_2)_2NH_2$)

*Sabine Frischhut, Manuel M. Bentlohner, Wilhelm Klein, and Thomas F. Fässler**

[*] Prof. Dr. Thomas F. Fässler, Department of Chemistry, Technische Universität München, Lichtenbergstraße 4, 85747 Garching, Germany; Email: thomas.faessler@lrz.tum.de

Contents

Figures

Figure S1. Unit cells of the crystal structures of a) {[K(2,2,2-crypt)]$_4$ **1a**}·tol·en and b) {[Rb(2,2,2-crypt)]$_4$ **2a**}·tol.

Figure S2. a) Depiction of the atoms Ge1/C1/C2/C3/C4/Ge10 and Ge1/C4'/C3'/C2'/C1'/Ge10 which form the ^{ZE}**B** and the ^{EZ}**B** entity of **1a**, respectively. b) Anionic entity **1a**.

Figure S3. Spatial orientation of the Ge$_9$ clusters in the anionic entity **1a**.

Figure S4. Selected ranges of a) ^{1}H b/c) COSY d/e) ^{13}C f) HSQC NMR spectra of {[K(2,2,2-crypt)]$_4$ **1a**}·tol·en dissolved in acetonitrile-*d*$_3$.

Figure S5. Temperature-dependent ^{1}H NMR study of {[K(2,2,2-crypt)]$_4$ **1a**}·tol·en dissolved in acetonitrile-*d*$_3$ (T = –20 °C – 60 °C). Only the relevant signal 1a(γ/ζ) which shows the expected signal splitting at elevated temperature is magnified.

Figure S6. ^{1}H NMR spectrum of crystals of {[Rb(2,2,2-crypt)]$_4$ **2a**}·tol dissolved in pridine-*d*$_5$. The resonances originating from **2** highlighted in grey are magnified below.

Figure S7. Comparison of the ^{1}H NMR spectra of reaction solutions of 1 eq. of K$_4$Ge$_9$, 0.5 eq. of **4** and *z* eq. of **3** in en after stirring for at least 16 h at r.t. (z = 0 - 5.9). In the test-mixtures the anionic entities **1a**, **1b**, **6a**, **6b**, **7** and **8** were identified.

Figure S8. ^{1}H NMR spectra of reaction solutions of 1 eq. of K$_4$Ge$_9$, *z* eq. of **3** and 0.5 eq. of **4** in en. *z* = 0: Spectrum of the reaction solution after a reaction time of 23 h. *z* = 4: time-resolved ^{1}H NMR spectra of the reaction solution after reaction time t (t = 0.5 h – 21 h).

Figure S9. Time-resolved ^{1}H NMR spectra (t = 0.5 h – 16 h) of test-mixtures prepared by dissolving a pre-mixture of the neat solids K$_4$Ge$_9$ (97.2 mg, 120 μmol, 1 eq.) and **4** (11.6 mg, 60 μmol, 0.5 eq.) in 2 mL of an en-solution containing 120 μmol **5**/mL en (**5**: 240 μmol, 2 eq.).

Figure S10. Raman spectra of selected crystals of a) {[K(2,2,2-crypt)]$_4$ **1a**}·tol·en (**1**) and b) {[Rb(2,2,2-crypt)]$_4$ **2a**}·tol (**2**) in glass capillaries at r.t..

Scheme

Scheme S1. Conformers **1a** and **1b** comprising ^{ZE}**B** and ^{ZZ}**B** units, respectively.

Tables

.

1 Crystallographic details

Figure S1. Unit cells of the crystal structures of a) {[K(2,2,2-crypt)]$_4$ **1a**}·tol·en and b) {[Rb(2,2,2-crypt)]$_4$ **2a**}·tol. Atoms of the linking unit ^{ZE}**B**/^{EZ}**B** and ^{ZZ}**B** as well as the additional functionalities bound to the clusters are shown as empty spheres. The alkali cations are shown as grey spheres. The Ge_9 clusters are shown as gray polyhedra. 2,2,2-crypt as well as solvent molecules are shown schematically. Hydrogen atoms are omitted for clarity.

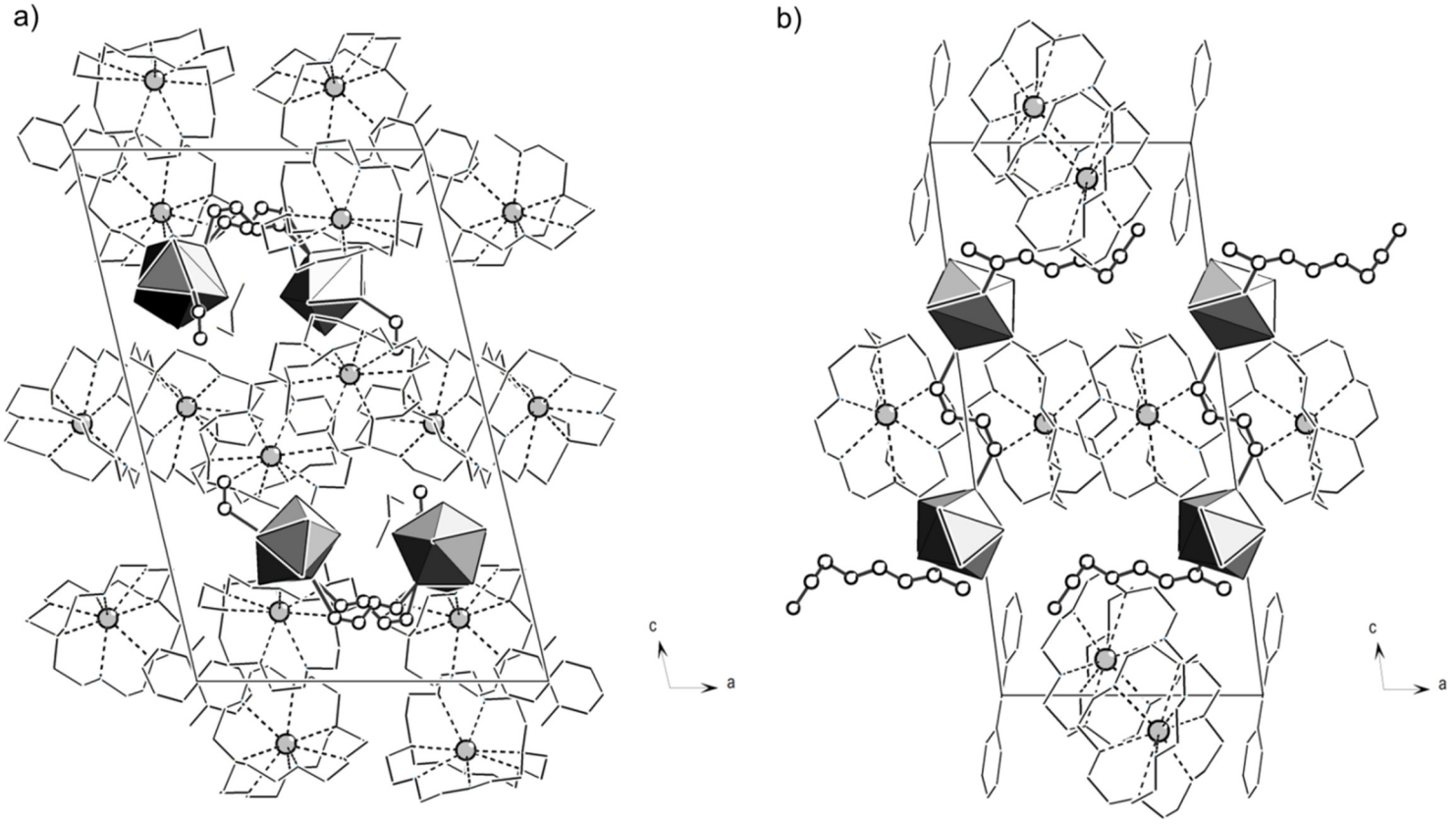

Table S1. Geometrical parameters of the clusters in the crystal structures of {[K(2,2,2-crypt)]$_4$ **1a**}·tol·en and {[*A*(2,2,2-crypt)]$_4$ **2a**}·tol (*A* = Rb, K). Cluster 1 contains the atoms Ge1 – Ge9, cluster 2 the atoms Ge10 – Ge18. α is defined as the dihedral angle closest to 180°. β is defined as the angle Ge1/$C_{\mathbf{B1}}$/$C_{\mathbf{B2}}$ or Ge10/$C_{\mathbf{B1}}$/$C_{\mathbf{B2}}$, whereas $C_{\mathbf{B2}}$ represents carbon atoms of the linking unit **B**. ω represents the out-of-plane angle of the *exo*-bonded linking entity **B** (β and ω are listed for the majority conformer **1a$^{\mathbf{I}}$**). d_1 and d_2 depict the diagonals of the open square marked in grey. $h_1 = d_1$, h_2 and h_3 are specified as the heights of the central trigonal prism of the cluster. Ideally the ratio c1/c2 is 1, which is the case for $C_{\mathbf{B1}}$ being located in the plane Ge1/Ge3/Ge9 and Ge10/Ge12/Ge18, respectively.[1]

Cluster	Symmetry	α[°]	β[°]	ω[°]	c_1/c_2	d_1/d_2	h_1[Å]	h_2[Å]	h_3[Å]	$(a_1+a_2)/(b_1+b_2)$
{[K(2,2,2-crypt)]$_4$ **1a**}·tol·en										
Conformer I										
Cluster 1	C_{2v}	177.0	127.9	165.0	0.93	0.78	3.126	2.702	2.685	1.00
Cluster 2	C_{2v}	176.6	126.3	160.2	1.01	0.79	3.140	2.671	2.685	0.99
Conformer II										
Cluster 1	C_{2v}	177.0	130.1	160.9	0.90	0.78	3.126	2.702	2.685	1.00
Cluster 2	C_{2v}	176.6	124.6	159.5	0.89	0.79	3.140	2.671	2.685	0.99
{[Rb(2,2,2-crypt)]$_4$ **2**}·tol										
	C_{2v}	173.8	132.1	161.4	1.04	1.25	3.144	2.670	2.686	1.00
{[K(2,2,2-crypt)]$_4$ **2**}·tol[2]										
	C_{2v}	174.0	131.3	160.3	1.04	1.26	3.149	2.676	2.690	1.00

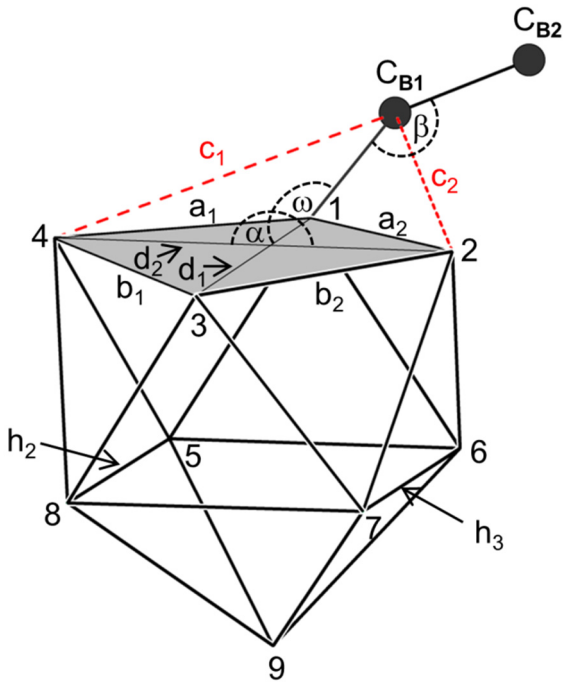
C_B2
C_B1
β
c_1
c_2
a_1
ω
1
a_2
α
4
2
d_2
d_1
b_1
b_2
3
h_2
5
6
8
7
h_3
9

Table S2. Selected bond lengths [Å] of **1a** in {[K(2,2,2-crypt)]$_4$ **1a**}·tol·en.

Atoms	Distances	Atoms	Distances	Atoms	Distances
Ge1 – C1	1.993(9)	C7 – C8	1.271(6)	K2 – O10	2.730(3)
C1 – C2	1.34(1)	C7 – H7	0.95	K2 – O11	2.740(3)
C1 – H1	0.95	C8 – H8A	0.95	K2 – O12	2.770(3)
C2 – C3	1.41(1)	C8– H8B	0.95	N3 – C27	1.458(5)
C2 – H2	0.95	K1 – N1	3.027(4)	C27 – C28	1.493(6)
C3 – C4	1.36(1)	K1 – N2	2.992(3)	C28 – O7	1.416(5)
C3 – H3	0.95	K1 – O1	2.818(3)	O7 – C29	1.419(5)
C4 – H4	0.95	K1 – O2	2.769(3)	C29 – C30	1.474(7)
Ge10 – C4	1.91(1)	K1 – O3	2.867(3)	C30 – O8	1.412(5)
Ge1 – C4'	1.90(2)	K1 – O4	2.838(3)	O8 – C31	1.415(6)
C4' – C3'	1.29(2)	K1 – O5	2.840(3)	C31 – C32	1.463(6)
C4' – H4'	0.95	K1 – O6	2.871(3)	C32 – N4	1.470(6)
C3' – C2'	1.46(2)	N1 – C9	1.457(6)	N4 – C33	1.466(6)
C3' – H3'	0.95	C9 – C10	1.510(7)	C33 – C34	1.465(7)
C2' – C1'	1.34(2)	C10 – O1	1.429(5)	C34 – O9	1.429(5)
C2' – H2'	0.95	O1 – C11	1.427(5)	O9 – C35	1.426(5)
C1' – H1'	0.95	C11 – C12	1.473(6)	C35 – C36	1.450(6)
Ge10 – C1'	2.10(1)	C12 – O2	1.400(5)	C36 – O10	1.438(5)
Ge1 – Ge2	2.5487(7)	O2 – C13	1.413(5)	O10 – C37	1.414(5)
Ge2 – Ge3	2.5289(7)	C13 – C14	1.504(6)	C37 – C38	1.498(6)
Ge3 – Ge4	2.5492(7)	C14 – N2	1.465(5)	C38 – N3	1.479(5)
Ge4 – Ge1	2.5357(7)	N2 – C15	1.463(5)	N3 – C39	1.469(5)
Ge1 – Ge5	2.5836(6)	C15 – C16	1.495(6)	C39 – C40	1.497(6)
Ge1 – Ge6	2.5764(6)	C16 – O3	1.417(5)	C40 – O11	1.420(5)
Ge2 – Ge6	2.6506(6)	O3 – C17	1.427(5)	O11 – C41	1.421(5)
Ge2 – Ge7	2.6610(7)	C17 – C18	1.502(6)	C41 – C42	1.484(7)
Ge3 – Ge7	2.5998(6)	C18 – O4	1.430(5)	C42 – O12	1.425(5)
Ge3 – Ge8	2.5849(7)	O4 – C19	1.417(5)	O12 – C43	1.429(5)
Ge4 – Ge8	2.6880(7)	C19 – C20	1.509(6)	C43 – C44	1.504(7)
Ge4 – Ge5	2.6323(7)	C20 – N1	1.475(5)	C44 – N4	1.465(6)
Ge5 – Ge6	2.9228(6)	N1 – C21	1.476(6)	K3 – N5	2.957(4)
Ge6 – Ge7	2.7021(7)	C21– C22	1.506(6)	K3 – N6	2.967(3)
Ge7 – Ge8	2.9294(7)	C22 – O5	1.431(5)	K3 – O13	2.919(3)
Ge8 – Ge5	2.6848(7)	O5 – C23	1.423(5)	K3 – O14	2.837(3)
Ge5 – Ge9	2.5844(7)	C23 – C24	1.489(6)	K3 – O15	2.852(3)
Ge6 – Ge9	2.5810(7)	C24 – O6	1.428(5)	K3 – O16	2.821(3)
Ge7 – Ge9	2.5891(7)	O6 – C25	1.424(5)	K3 – O17	2.804(3)
Ge8 – Ge9	2.6039(7)	C25 – C26	1.503(6)	K3 – O18	2.866(3)
Ge3 – C5	1.988(6)	C26 – N2	1.461(5)	N5 – C45	1.474(6)
C5 – C6	1.240(6)	K2 – N3	2.982(3)	C45 – C46	1.489(7)
C5 – H5	0.95	K2 – N4	2.995(4)	C46 – O13	1.447(5)
C6 – H6A	0.95	K2 – O7	2.851(3)	O13 – C47	1.437(5)
C6 – H6B	0.95	K2 – O8	2.832(3)	C47 – C48	1.483(6)
Ge12 – C7	1.989(5)	K2 – O9	3.011(3)	C48 – O14	1.421(5)

Atoms	Distances	Atoms	Distances	Atoms	Distances
O14 – C49	1.415(5)	C61 – C62	1.484(6)	N8 – C69	1.461(6)
C49 – C50	1.492(6)	C62 – N6	1.467(5)	C69 – C70	1.492(7)
C50 – N6	1.465(5)	K4 – N7	3.018(4)	C70 – O21	1.420(6)
N6 – C51	1.468(5)	K4 – N8	3.015(4)	O21 – C71	1.423(5)
C51 – C52	1.511(6)	K4 – O19	2.812(3)	C71 – C72	1.468(7)
C52 – O15	1.430(5)	K4 – O20	2.859(3)	C72 – O22	1.427(5)
O15 – C53	1.419(5)	K4 – O21	2.870(3)	O22 – C73	1.405(5)
C53 – C54	1.493(6)	K4 – O22	2.832(3)	C73 – C74	1.494(6)
C54 – O16	1.429(5)	K4 – O23	2.838(3)	C74 – N7	1.473(5)
O16 – C55	1.411(5)	K4 – O24	2.809(3)	N7 – C75	1.446(5)
C55 – C56	1.493(6)	N7 – C63	1.479(6)	C75 – C76	1.494(7)
C56 – N5	1.465(6)	C63 – C64	1.506(6)	C76 – O23	1.430(6)
N5 – C57	1.476(5)	C64 – O19	1.421(6)	O23 – C77	1.430(5)
C57 – C58	1.501(6)	O19 – C65	1.425(6)	C77 – C78	1.473(7)
C58 – O17	1.426(5)	C65 – C66	1.496(7)	C78 – O24	1.432(5)
O17 – C59	1.415(5)	C66 – O20	1.416(6)	O24 – C79	1.411(6)
C59 – C60	1.494(6)	O20 – C67	1.439(6)	C79 – C80	1.520(7)
C60 – O18	1.435(5)	C67 – C68	1.523(8)	C80 – N8	1.496(6)
O18 – C61	1.415(5)	C68 – N8	1.463(6)		

Table S3. Selected bond angles [deg] of **1a** in {[K(2,2,2-crypt)]$_4$ **1a**}·tol·en.

Atoms	Angles	Atoms	Angles
Ge1 – C1 – C2	127.9(7)	Ge3 – Ge4 – Ge5	96.18(2)
C2 – C1 – H1	116.1	Ge2 – Ge1 – Ge6	62.28(2)
Ge1 – C1 – H1	116.1	Ge4 – Ge1 – Ge5	61.88(2)
C1 – C2 – C3	127.5(9)	Ge2 – Ge3 – Ge7	62.49(2)
C1 – C2 – H2	116.3	Ge4 – Ge3 – Ge8	63.14(2)
C3 – C2 – H2	116.3	Ge1 – Ge2 – Ge6	59.37(2)
C2 – C3 – C4	126(1)	Ge3 – Ge2 – Ge7	60.06(2)
C2 – C3 – H3	117.0	Ge1 – Ge4 – Ge5	59.95(2)
C4 – C3 – H3	117.0	Ge3 – Ge4 – Ge8	59.08(2)
C3 – C4 – Ge10	126.4(9)	Ge5 – Ge1 – Ge6	69.01(2)
C3 – C4 – H4	116.8	Ge6 – Ge2 – Ge7	61.16(2)
Ge10 – C4 – H4	116.8	Ge7 – Ge3 – Ge8	68.80(2)
Ge1 – C4' – C3'	130(1)	Ge8 – Ge4– Ge5	60.60(2)
C3' – C4' – H4'	115.0	Ge4 – Ge5 – Ge1	58.17(2)
Ge1 – C4'– H4'	115.0	Ge1 – Ge6 – Ge2	58.35(2)
C4' – C3' – C2'	128(2)	Ge2 – Ge7 – Ge3	57.45(2)
C4' – C3' – H3'	116.1	Ge3 – Ge8 – Ge4	57.78(2)
C2' – C3' – H3'	116.1	Ge1 – Ge5 – Ge8	95.74(2)
C3' – C2' – C1'	129(1)	Ge1 – Ge6 – Ge7	95.53(2)
C3' – C2' – H2'	115.7	Ge3 – Ge7 – Ge6	93.87(2)
C1' – C2' – H2'	115.7	Ge3 – Ge8 – Ge5	94.05(2)
C2' – C1' – Ge10	125(1)	Ge4 – Ge5 – Ge6	102.04(2)
C2' – C1' – H1'	117.7	Ge2 – Ge6 – Ge5	101.49(2)
Ge10 – C1' – H1'	117.7	Ge2 – Ge7 – Ge8	101.39(2)
Ge4 – Ge1 – Ge2	103.78(2)	Ge4 – Ge8 – Ge7	101.70(2)
Ge1 – Ge2 – Ge3	75.99(2)	Ge1 – Ge5 – Ge6	55.38(2)
Ge2 – Ge3 – Ge4	103.96(2)	Ge1 – Ge6 – Ge5	55.61(2)
Ge3 – Ge4 – Ge1	75.86(2)	Ge3 – Ge7 – Ge8	55.36(2)
Ge8 – Ge5 – Ge6	90.37(2)	Ge3 – Ge8 – Ge7	55.84(2)
Ge5 – Ge6 – Ge7	89.77(2)	Ge4 – Ge5 – Ge8	60.72(2)
Ge6 – Ge7 – Ge8	89.89(2)	Ge2 – Ge6 – Ge7	59.61(2)
Ge7 – Ge8 – Ge5	89.96(2)	Ge2 – Ge7 – Ge6	59.23(2)
Ge2 – Ge1 – Ge5	114.61(2)	Ge4 – Ge8 – Ge5	58.67(2)
Ge4 – Ge1 – Ge6	115.45(2)	Ge1 – Ge5 – Ge9	104.65(2)
Ge2 – Ge3 – Ge8	115.68(2)	Ge1 – Ge6 – Ge9	104.95(2)
Ge4 – Ge3 – Ge7	115.68(2)	Ge3 – Ge7 – Ge9	104.06(2)
Ge1 – Ge2– Ge7	97.21(2)	Ge3 – Ge8 – Ge9	104.06(2)
Ge3 – Ge2 – Ge6	96.80(2)	Ge4 – Ge5 – Ge9	114.29(2)
Ge1 – Ge4 – Ge8	96.80(2)	Ge2 – Ge6 – Ge9	112.86(2)

Atoms	Angles	Atoms	Angles
Ge2 – Ge7 – Ge9	112.26(2)	Ge6 – Ge9 – Ge7	63.02(2)
Ge4 – Ge8 – Ge9	111.80(2)	Ge7 – Ge9 – Ge8	68.68(2)
Ge6 – Ge5 – Ge9	55.48(2)	Ge8 – Ge9 – Ge5	62.33(2)
Ge5 – Ge6 – Ge9	55.59(2)	Ge5 – Ge9 – Ge7	100.32(2)
Ge8 – Ge7 – Ge9	55.90(2)	Ge6 – Ge9 – Ge8	100.34(2)
Ge7 – Ge8– Ge9	55.42(2)	C5 – Ge3 – Ge2	122.3(2)
Ge8 – Ge5 – Ge9	59.19(2)	C5 – Ge3 – Ge4	125.4(2)
Ge7 – Ge6 – Ge9	58.64(2)	C5 – Ge3 – Ge7	110.8(2)
Ge6 – Ge7 – Ge9	58.34(2)	C5 – Ge3 – Ge8	112.5(2)
Ge5 – Ge8 – Ge9	58.48(2)	C6 – C5 – Ge3	127.4(5)
Ge5 – Ge9 – Ge6	68.92(2)		

Figure S2. a) Depiction of the atoms Ge1/C1/C2/C3/C4/Ge10 and Ge1/C4'/C3'/C2'/C1'/Ge10 which form the ^{ZE}**B** and the ^{EZ}**B** entity of **1a**, respectively. Planes through the selected atoms (grey). The ^{ZE}**B** unit shows an occupancy of 61.0%. b) Anionic entity **1a**. The distances between the atoms Ge1 and Ge10 as well as Ge4 and Ge11 is marked. All atoms are shown at a probability level of 50%.

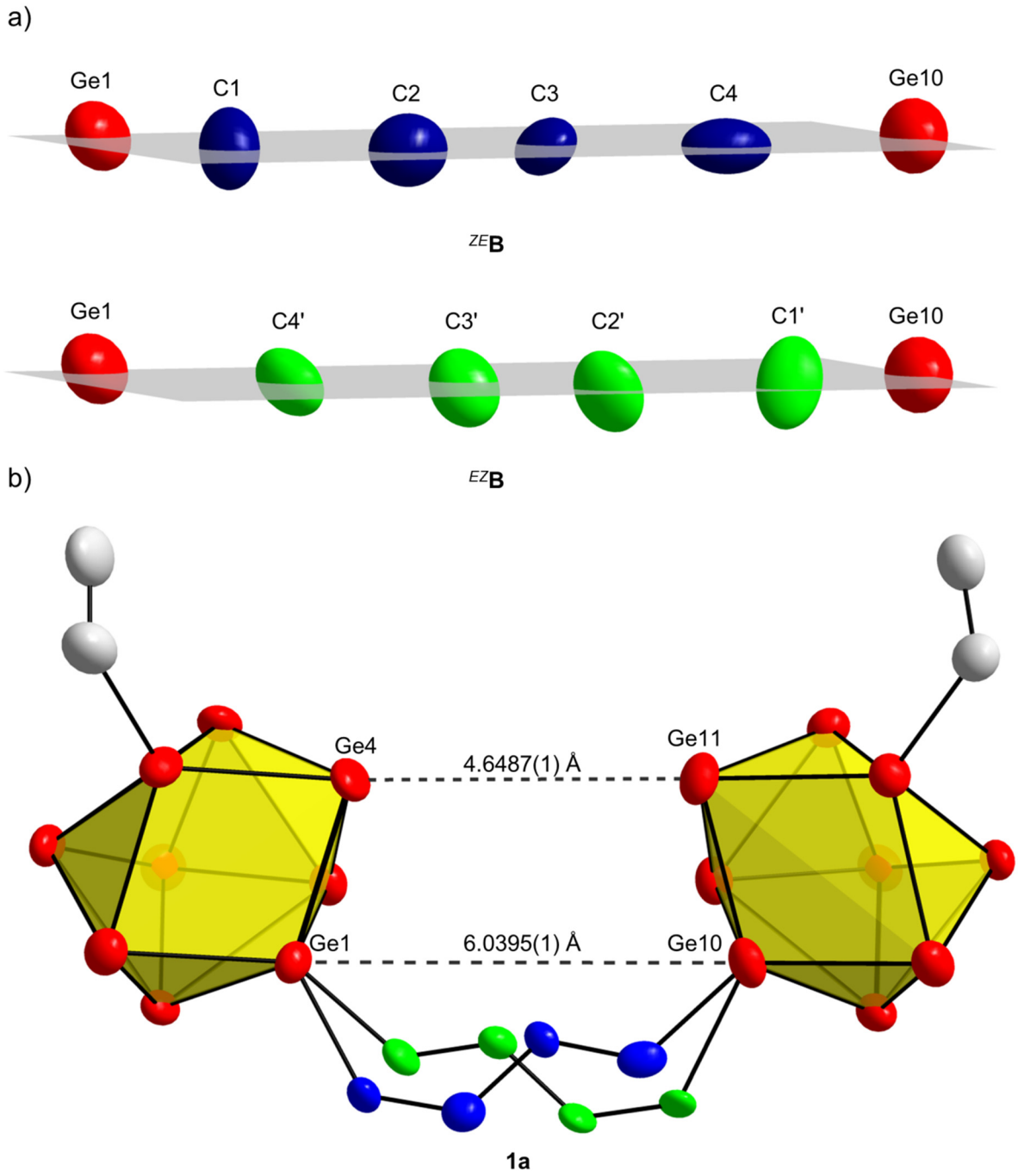

Figure S3. Spatial orientation of the Ge_9 clusters in the anionic entity **1a**. Planes through the atoms Ge1/Ge3/Ge9 and Ge10/Ge12/Ge18 (grey). The angle between the intersecting planes is labelled with α. The clusters in the already known *Zintl* triad $[R_2Ge_9C_4H_4Ge_9R_2]^{2-}$ (R_2 = (2*Z*/4*E*)-7-amino-5-aza-hepta-2,4-dien-2-yl) are not twisted. The corresponding planes run parallel.

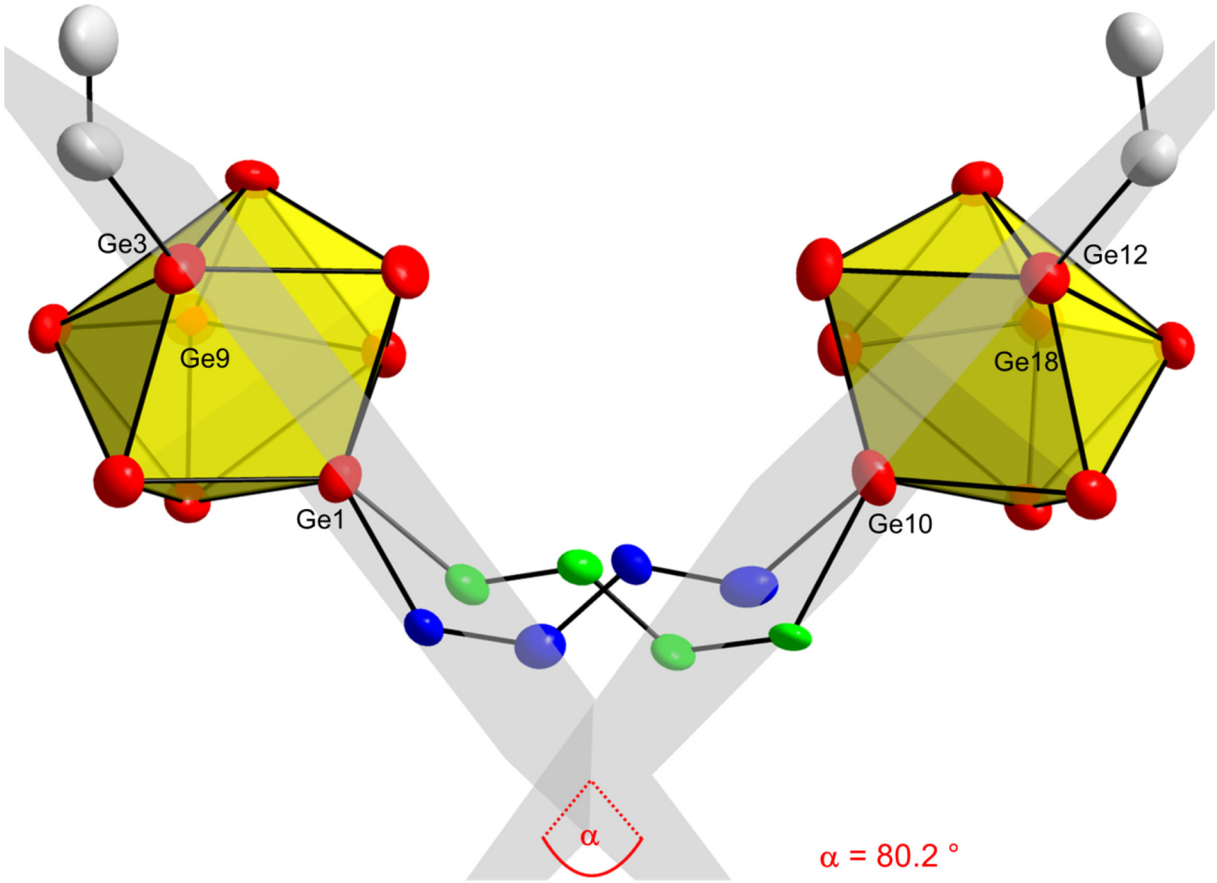

1a

2 NMR studies

2.1 General

NMR spectroscopy. ^{1}H, COSY, ^{13}C, HSQC and HMBC NMR spectra were recorded on 500 MHz (Bruker AV-500) and 400 MHz (Bruker AV-400) NMR spectrometers. For *in situ* NMR studies aliquots of 200 µL of the filtered reaction solution (solvent: non-deuterated *en*) were filled into a Norell® NMR tube (outer diameter: 3 mm). The latter was put into a common NMR tube filled with 0.3 mL of chloroform-d_1. The NMR spectra show dominant signals at 2.5-3.0 ppm (s, *en*, –CH_2–) and 1.3-1.9 ppm (s, *en*, –NH_2) which are caused by the non-deuterated solvent *en* in the reaction solution. Samples for time-resolved ^{1}H NMR spectroscopy were taken right after the reactants were completely dissolved (ca. 15 min). The NMR measurements were started immediately.

2.2 NMR spectroscopic characterization of {[K(2,2,2-crypt)]$_4$ 1a}·tol·en and of the anionic entity 1b

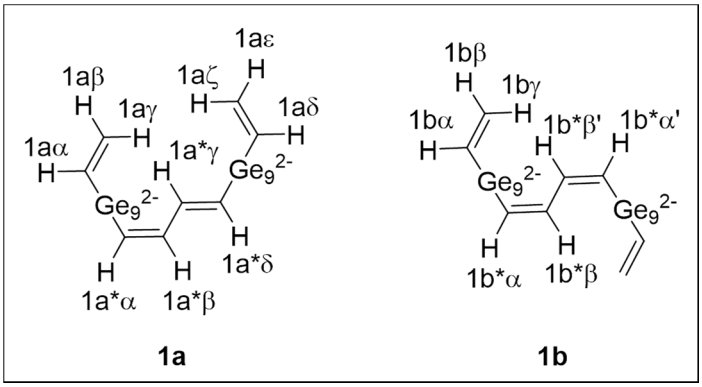

Scheme S1. Conformers **1a** and **1b** comprising ^{ZE}**B** and ^{ZZ}**B** units, respectively. The hydrogen atoms are labelled with the corresponding compound letter and Greek letters for assignment.

Figure S4. Selected ranges of a) ^{1}H b/c) COSY d/e) ^{13}C f) HSQC NMR spectra of {[K(2,2,2-crypt)]$_4$ **1a**}·tol·en dissolved in acetonitrile-*d*$_3$. Signals marked with * could not be assigned.

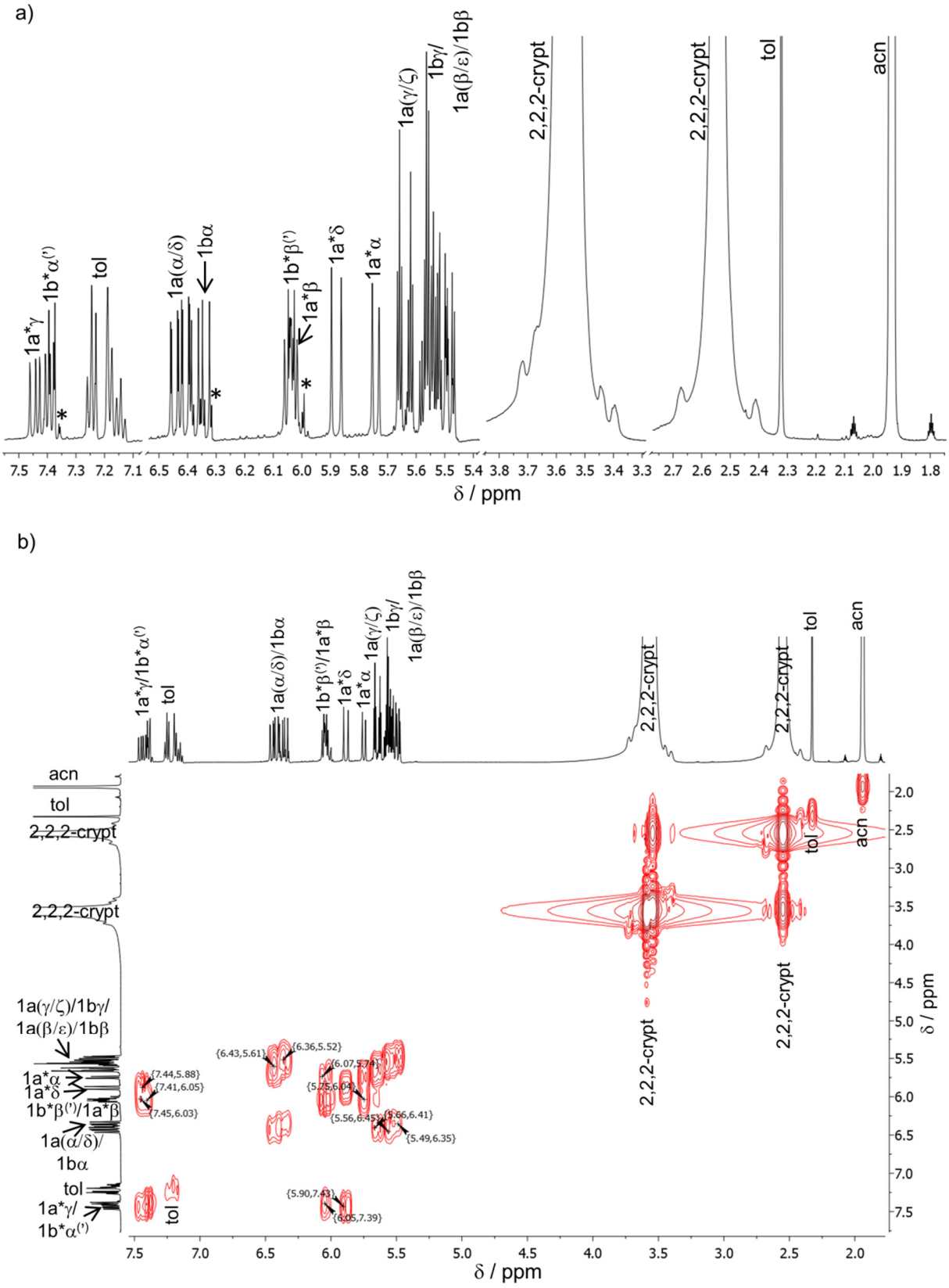

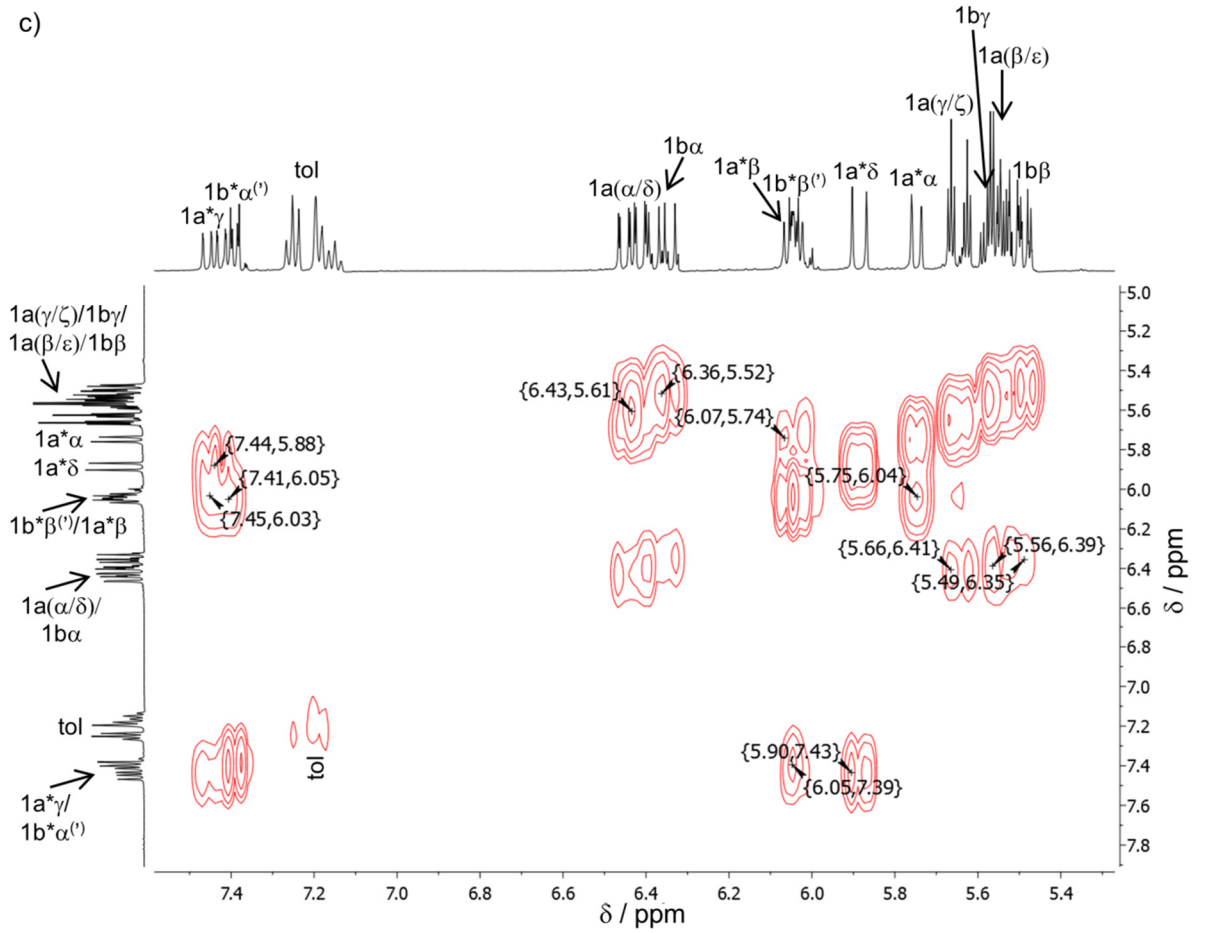
c)
1bγ
1a(β/ε)
1a(γ/ζ)
1bα
1a*β
1a*δ
1a*α
1bβ
1b*α(')
1a*γ
tol
1a(α/δ)
1b*β(')
1a(γ/ζ)/1bγ/
1a(β/ε)/1bβ
1a*α
1a*δ
1b*β(')/1a*β
1a(α/δ)/
1bα
tol
1a*γ/
1b*α(')
{7.44,5.88}
{7.41,6.05}
{7.45,6.03}
{6.43,5.61}
{6.36,5.52}
{6.07,5.74}
{5.75,6.04}
{5.66,6.41}
{5.56,6.39}
{5.49,6.35}
{5.90,7.43}
{6.05,7.39}
δ / ppm
δ / ppm

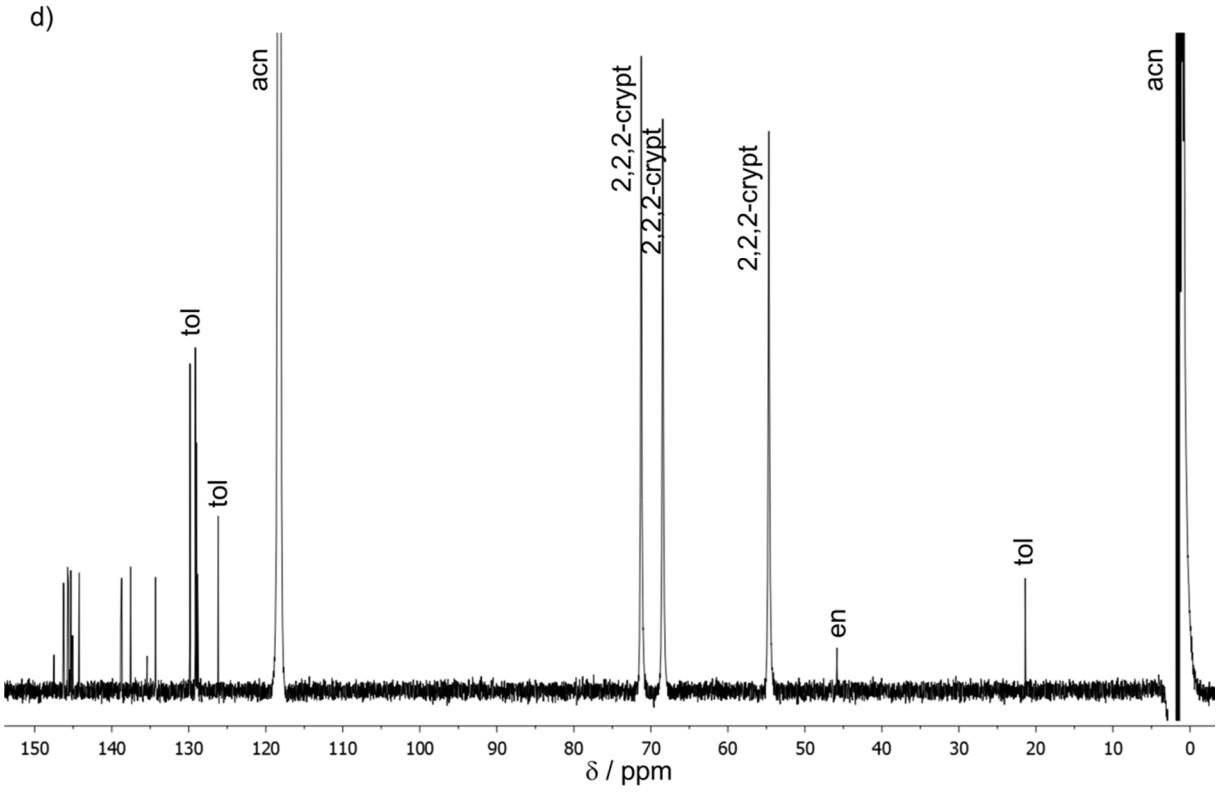
d)
acn
tol
tol
2,2,2-crypt
2,2,2-crypt
2,2,2-crypt
en
tol
acn
δ / ppm

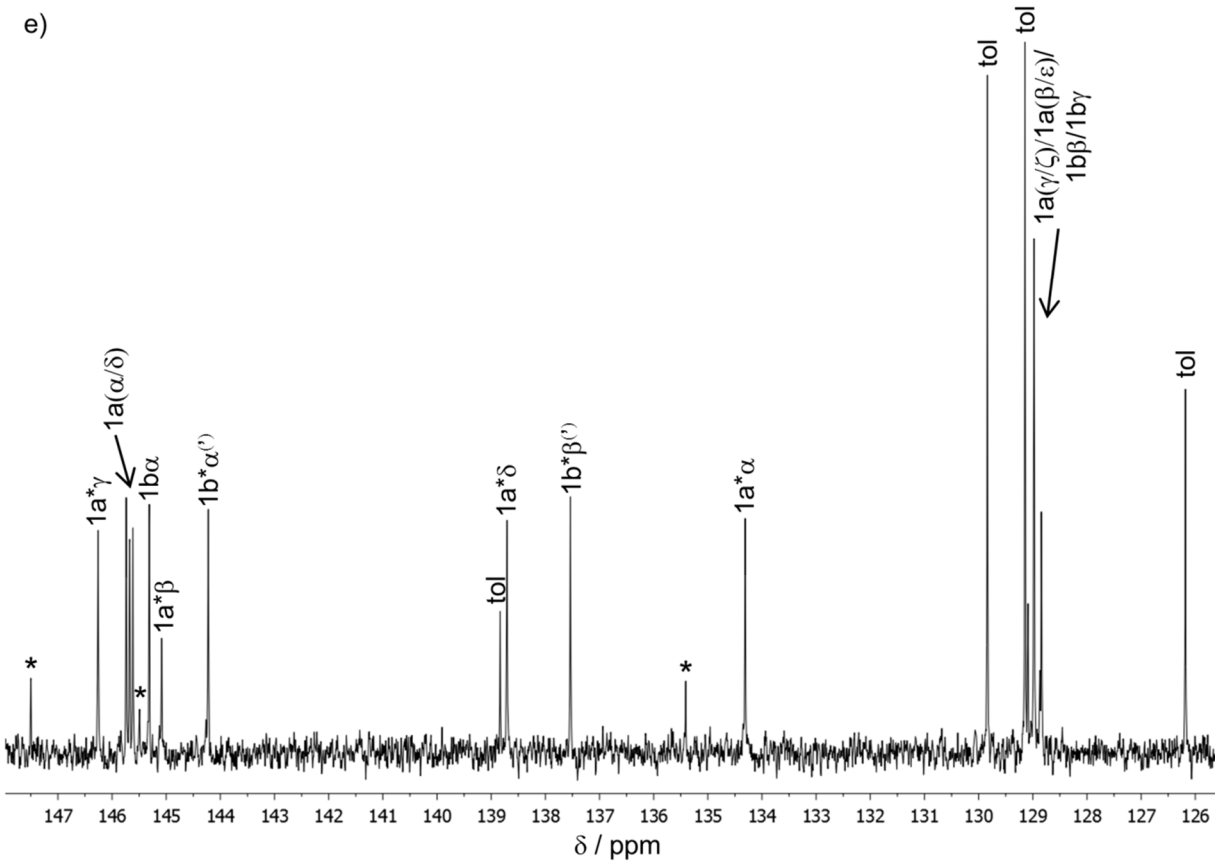
e)
tol
tol
1a(γ/ζ)/1a(β/ε)/
1bβ/1bγ
tol
1a(α/δ)
1a*γ
1bα
1b*α(')
1a*β
1a*δ
tol
1b*β(')
1a*α
*
*
*
147 146 145 144 143 142 141 140 139 138 137 136 135 134 133 132 131 130 129 128 127 126
δ / ppm

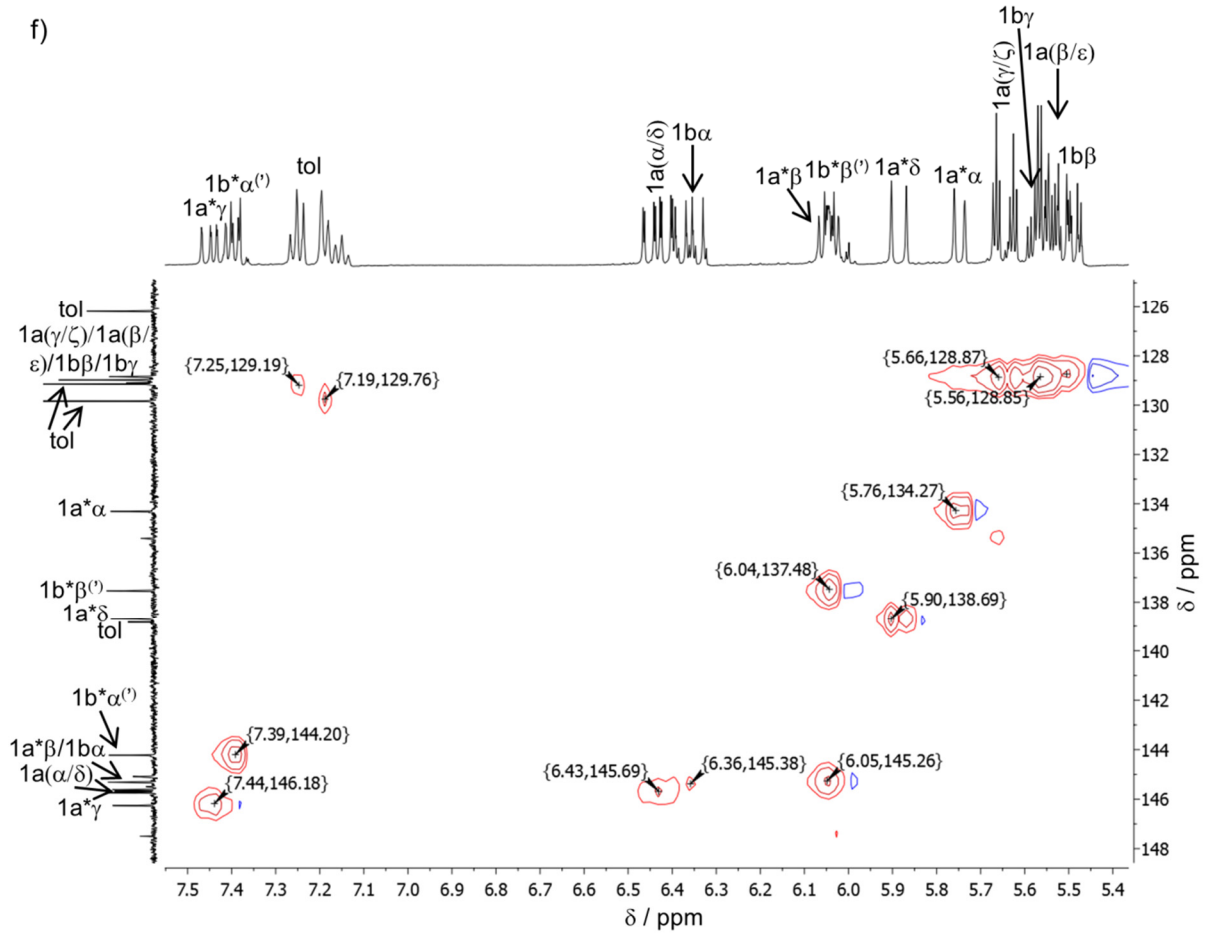
f)
1bγ
1a(β/ε)
1a(γ/ζ)
1bβ
1a(α/δ)
1bα
1b*α(')
tol
1a*γ
1a*β
1b*β(')
1a*δ
1a*α
tol
1a(γ/ζ)/1a(β/
ε)/1bβ/1bγ
tol
1a*α
1b*β(')
1a*δ
tol
1b*α(')
1a*β/1bα
1a(α/δ)
1a*γ
{7.25,129.19}
{7.19,129.76}
{5.66,128.87}
{5.56,128.85}
{5.76,134.27}
{6.04,137.48}
{5.90,138.69}
{7.39,144.20}
{7.44,146.18}
{6.43,145.69}
{6.36,145.38}
{6.05,145.26}
7.5 7.4 7.3 7.2 7.1 7.0 6.9 6.8 6.7 6.6 6.5 6.4 6.3 6.2 6.1 6.0 5.9 5.8 5.7 5.6 5.5 5.4
δ / ppm
126 128 130 132 134 136 138 140 142 144 146 148
δ / ppm

NMR spectroscopic characterization of the anionic entity **1b**.

^{1}H NMR (500 MHz, acetontirile-d_3, 296 K): δ (ppm) 7.39 (dd, J = 8.5 Hz, 2.5 Hz, 2H, 1b*α$^{(')}$), 6.36 (dd, J = 19.3 Hz, 12.3 Hz, 2H, 1bα), 6.04 (dd, J = 8.5 Hz, 2.0 Hz, 2H, 1b*β$^{(')}$), 5.55 (dd, J = 19.5 Hz, 12.5 Hz, 2H, 1bγ), 5.49 (dd, J = 12.5 Hz, 4.0 Hz, 2H, 1bβ). COSY (500 MHz, acetontirile-d_3, 296 K): δ (ppm) 6.05/7.39 (^{3}J, 1b*β$^{(')}$/1b*α$^{(')}$), 5.49/6.35 (^{3}J, 1bβ/1bα). ^{13}C NMR (500 MHz, acetontirile-d_3, 296 K): δ (ppm) 145.31 (1bα), 144.22 (1b*α$^{(')}$), 137.54 (1b*β$^{(')}$), 129.09-128.84 (1bγ/1bβ, cannot be assigned accurately). HSQC (500 MHz, acetontirile-d_3, 296 K): δ (ppm) 7.39/144.20 (^{1}J, 1b*α$^{(')}$/ 1b*α$^{(')}$), 6.36/145.38 (^{1}J, 1bα/1bα), 6.04/137.48 (^{1}J, 1b*β$^{(')}$/ 1b*β$^{(')}$), 5.50/128.74 (^{1}J, 1bβ/1bβ).

2.3 Temperature-dependent NMR study of {[K(2,2,2-crypt)]$_4$ 1a}·tol·en

Figure S5. Temperature-dependent ^{1}H NMR measurements of {[K(2,2,2-crypt)]$_4$ **1a**}·tol·en dissolved in acetonitrile-d_3 (T = –20 °C – 60 °C). Only the relevant signal 1a(γ/ζ) which shows the expected signal splitting at elevated temperature is shown magnified.

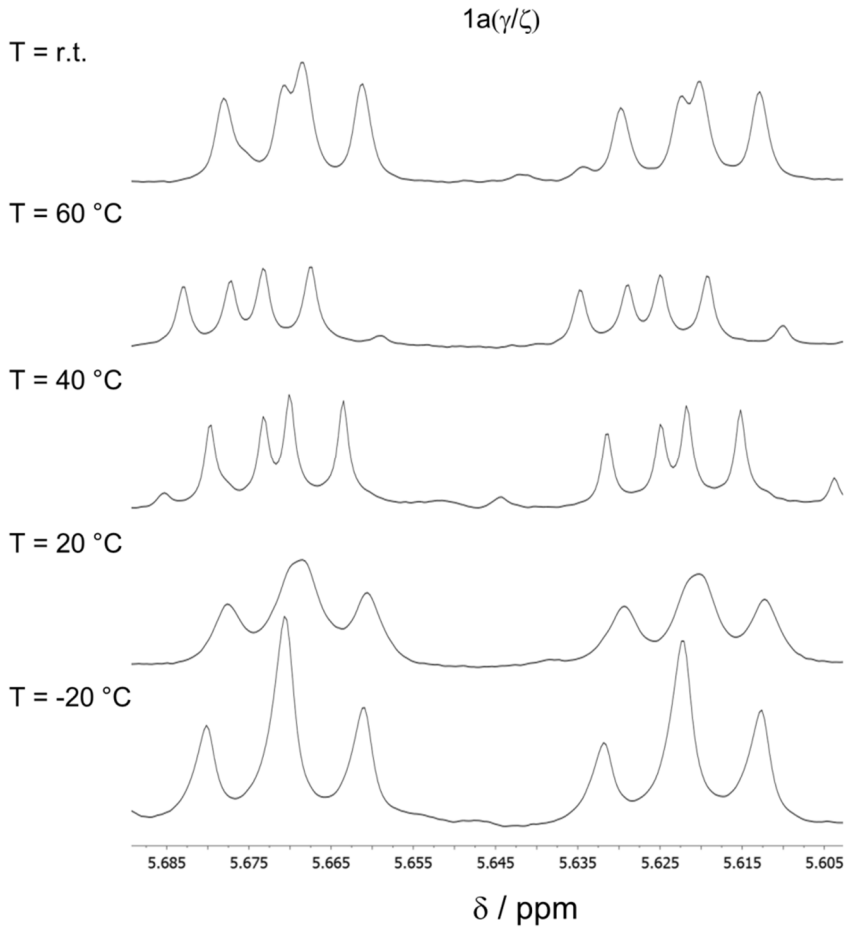

2.4 NMR spectroscopic characterization of {[Rb(2,2,2-crypt)]$_4$ 2a}·tol

Figure S6. ^{1}H NMR spectrum of crystals of {[Rb(2,2,2-crypt)]$_4$ **2a**}·tol dissolved in pyridine-d_5. The resonances originating from **2a** highlighted in grey are magnified below. Signals marked with * could not be assigned.

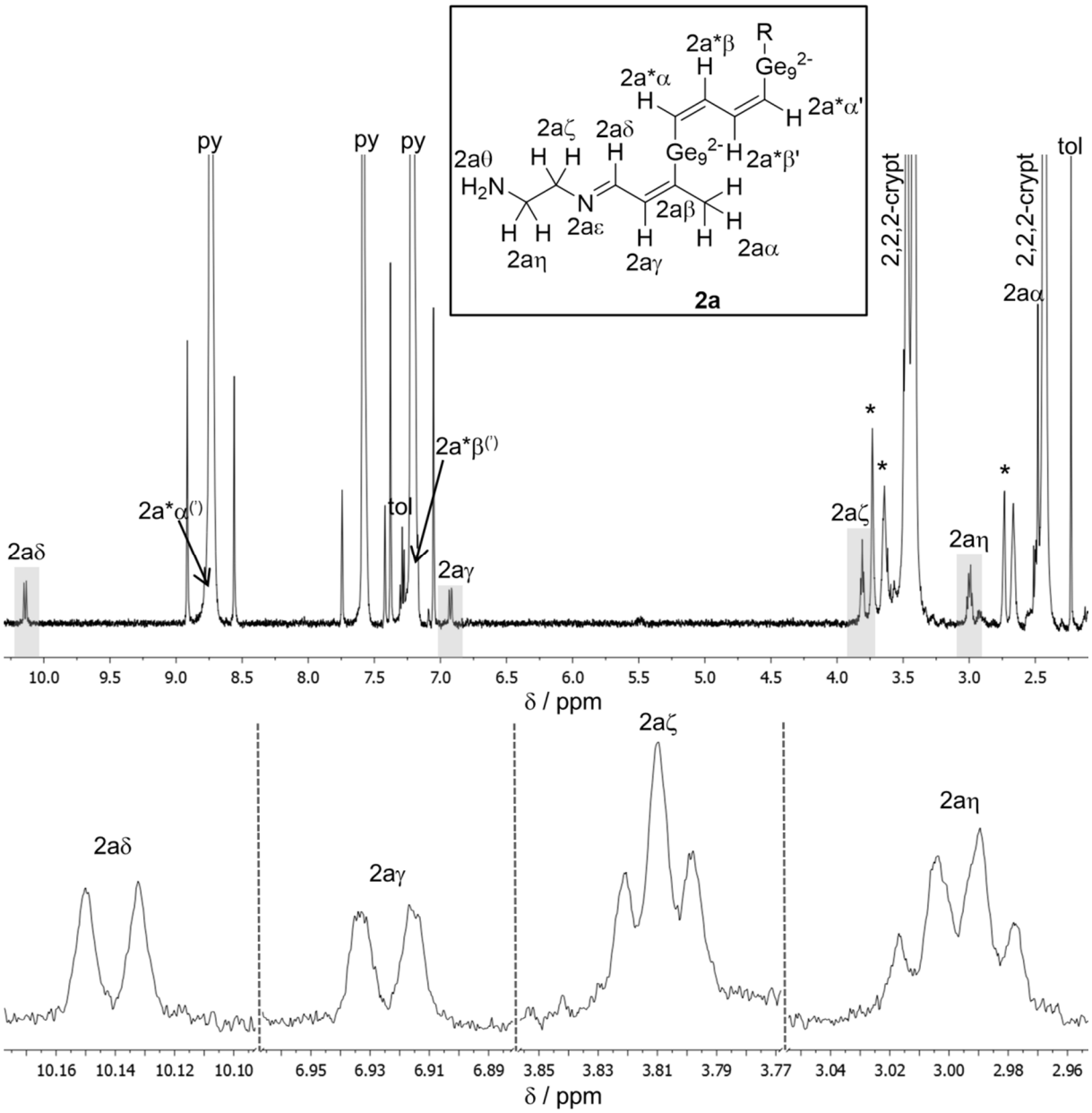

2.5 Mechanistic investigation on the formation of $[R_1–Ge_9–CH=CH–CH=CH–Ge_9–R_1]^{4–}$ (1a/1b) (R_1 = –CH=CH_2)

2.5.1 Variation of equivalents of reactants in solution

The effect of varying the equivalents of bis(trimethylsilyl)acetylene in the reaction solution on the formation of **1a**/**1b** is shown. All reactants (1 eq. of K_4Ge_9, 0.5 eq. of 1,4-bis(rimethylsilyl)butadiyne and *z* eq. of bis(trimethylsilyl)acetylene, with $z = 0 - 5.9$) were mixed simultaneously, subsequently dissolved in *en* (0.06 M based on K_4Ge_9) and stirred for at least 16 h at r.t.. After the reaction the test-mixtures were investigated by means of ^{1}H NMR spectroscopy.

Figure S7. Comparison of the ^{1}H NMR spectra of the reaction solution containing 1 eq. of K_4Ge_9, 0.5 eq. of **4** and *z* eq. of **3** in *en* after stirring for at least 16 h at r.t. (*z* = 0-5.9). The

spectra of the test-mixtures show the signals of the anionic entities **1a**, **1b**, **6a**, **6b**, **7**, and **8**.[1, 3, 4]

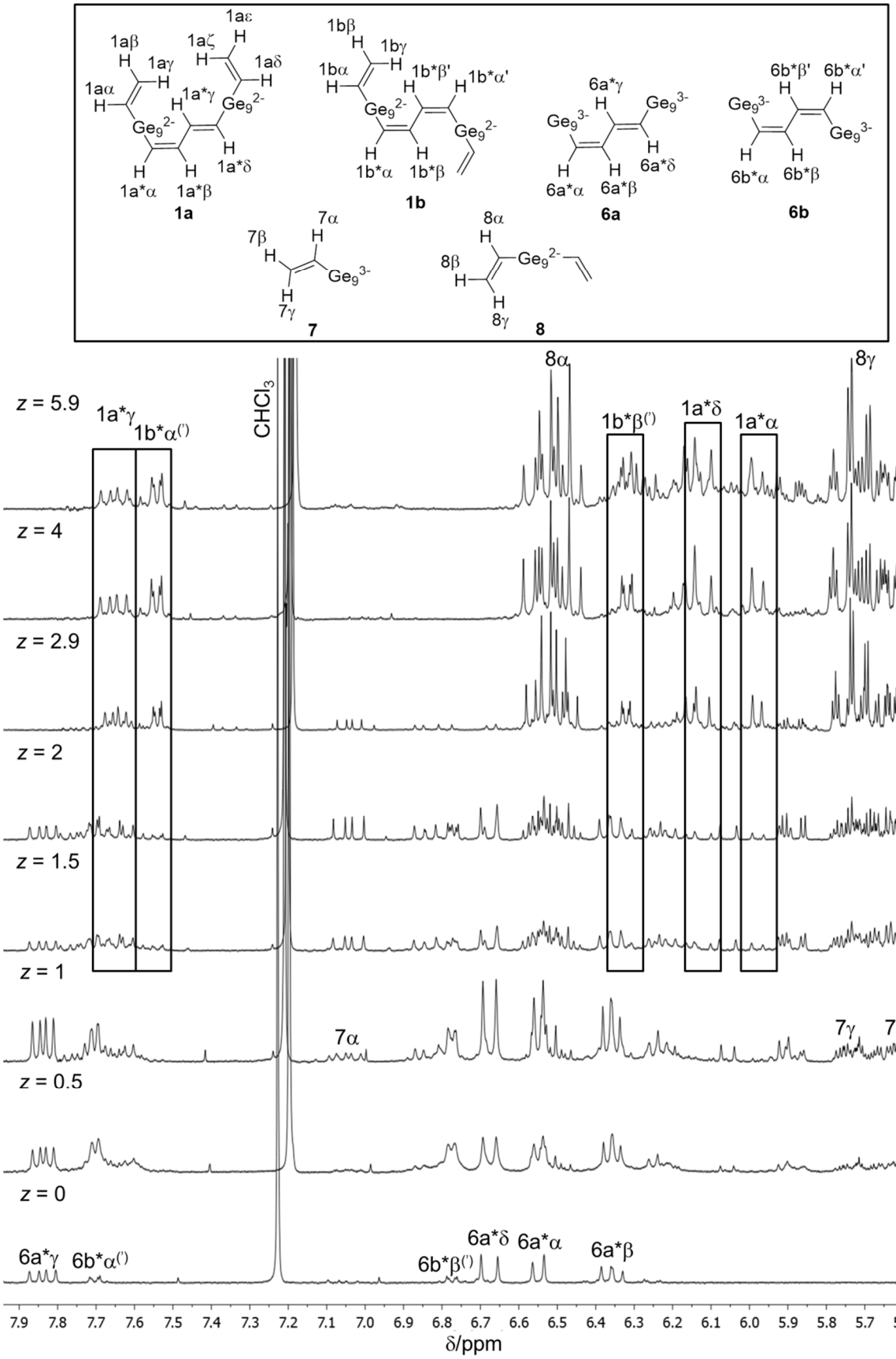

2.5.2 Time-resolved NMR study

Figure S8. ^{1}H NMR spectra of the reaction solutions of 1 eq. of K_4Ge_9, *z* eq. of **3** and 0.5 eq. of **4** in *en*. *z* = 0: The spectrum of the reaction solution after a reaction time of 23 h. *z* = 4: time-resolved ^{1}H NMR spectra of the reaction solution after reaction time t (t = 0.5 h – 21 h). The test-mixtures were prepared by dissolving a mixture of **3** (82 µL, 360 µmol, 4 eq.; in case of *z* = 0: 0 eq.), **4** (8.9 mg, 46 µmol, 0.5 eq.) and K_4Ge_9 (73.0 mg, 90 µmol, 1 eq.) in 1.5 mL *en*. The residual proton signal of the deuterated solvent $CHCl_3$ shows a shift for *z* = 0 which is due to the referencing of the most intense *en* signal (δ = 2.65 ppm). The reaction to **6a**/**6b** proceeds very fast (reaction complete within 0.5 h). The reaction to **1a** is significantly faster than the reaction to **1b** which can be clearly derived from the ratio of the integrals of the signals assigned to 1a*γ and 1b*α$^{(')}$.

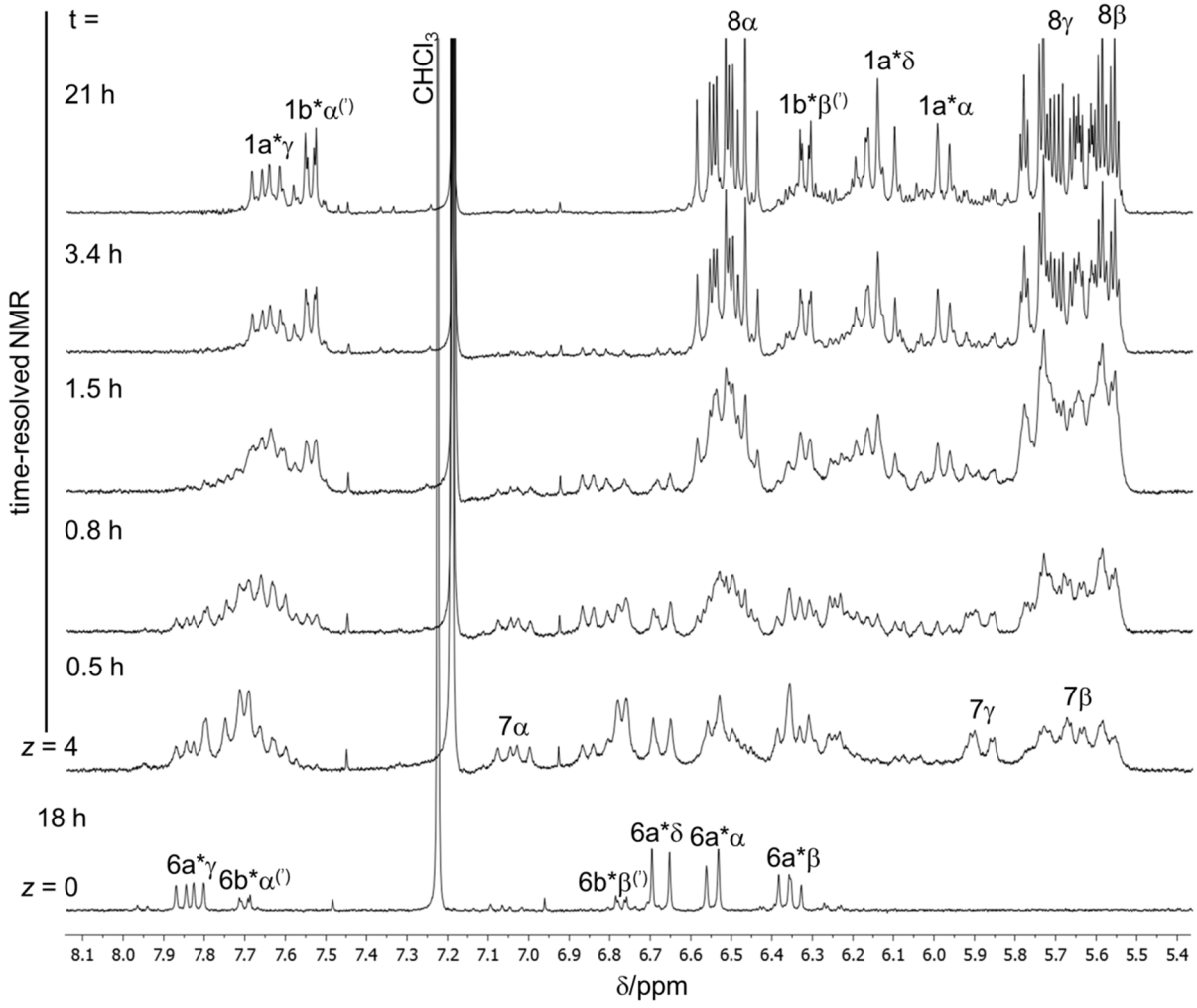

2.6 Mechanistic investigations on the formation of $[R_2Ge_9C_4H_4Ge_9R_2]^{4-}$ (2a) (R_2 = (2*Z*,4*E*)-7-amino-5-aza-hepta-2,4-dien-2-yl)

Figure S9. Time-resolved ^{1}H NMR spectra (t = 0.5 h – 16 h) of test-mixtures prepared by dissolving a pre-mixture of the neat solids K_4Ge_9 (97.2 mg, 120 µmol, 1 eq.) and **4** (11.6 mg, 60 µmol, 0.5 eq.) in 2 mL of an *en*-solution containing 120 µmol **5**/mL en (**5**: 240 µmol, 2 eq.).

The spectra show signals corresponding to **R** and **B**. Signals labelled with * could not be assigned.

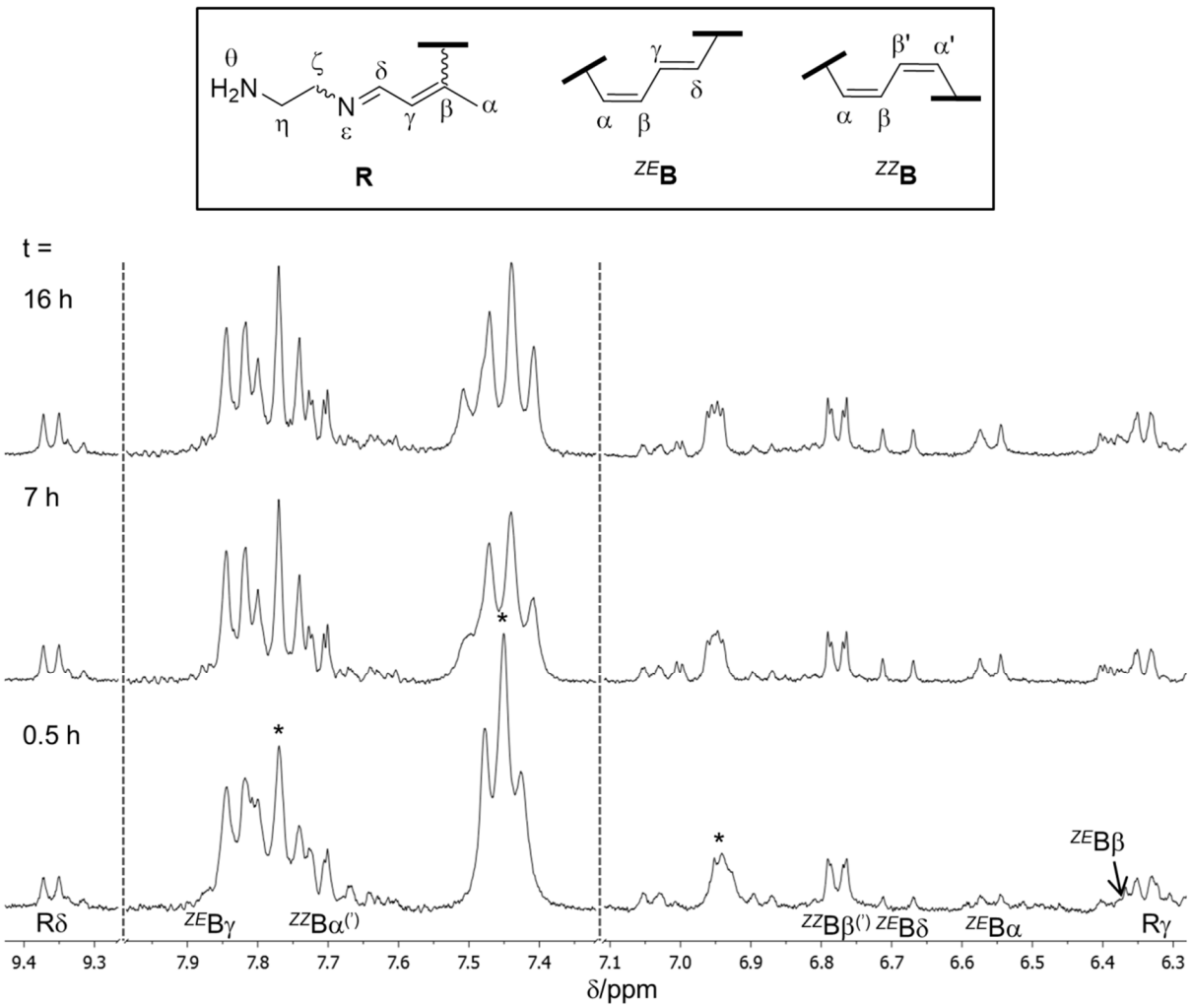

3 Raman spectra of compounds 1 and 2

Raman measurements were performed on single crystals sealed in glass capillaries with a Raman microscopy spectrometer ({[K(2,2,2-crypt)]$_4$ **1a**}·tol·en (**1**): Renishaw inVia Raman Microscope RE04: 532 nm, laser power 1%; {[Rb(2,2,2-crypt)]$_4$ **2a**}·tol (**2**): Senterra Raman spectrometer: Bruker Corporation; diode laser: 785 nm, 1 mW).

Crystals of the *Zintl* triads {[K(2,2,2-crypt)]$_4$ **1a**} ·tol ·en and {[Rb(2,2,2-crypt)]$_4$ **2a**} ·tol were further characterized by Raman spectroscopy (Figure 3). Up to now no Raman spectra of Ge_9 clusters bearing organic tethers have been reported.

Figure S10. Raman spectra of selected crystals of a) {[K(2,2,2-crypt)]$_4$ **1a**}·tol·en (**1**) and b) {[Rb(2,2,2-crypt)]$_4$ **2a**}·tol (**2**) in glass capillaries at r.t.. The relevant signals are labelled with the corresponding Raman shift.

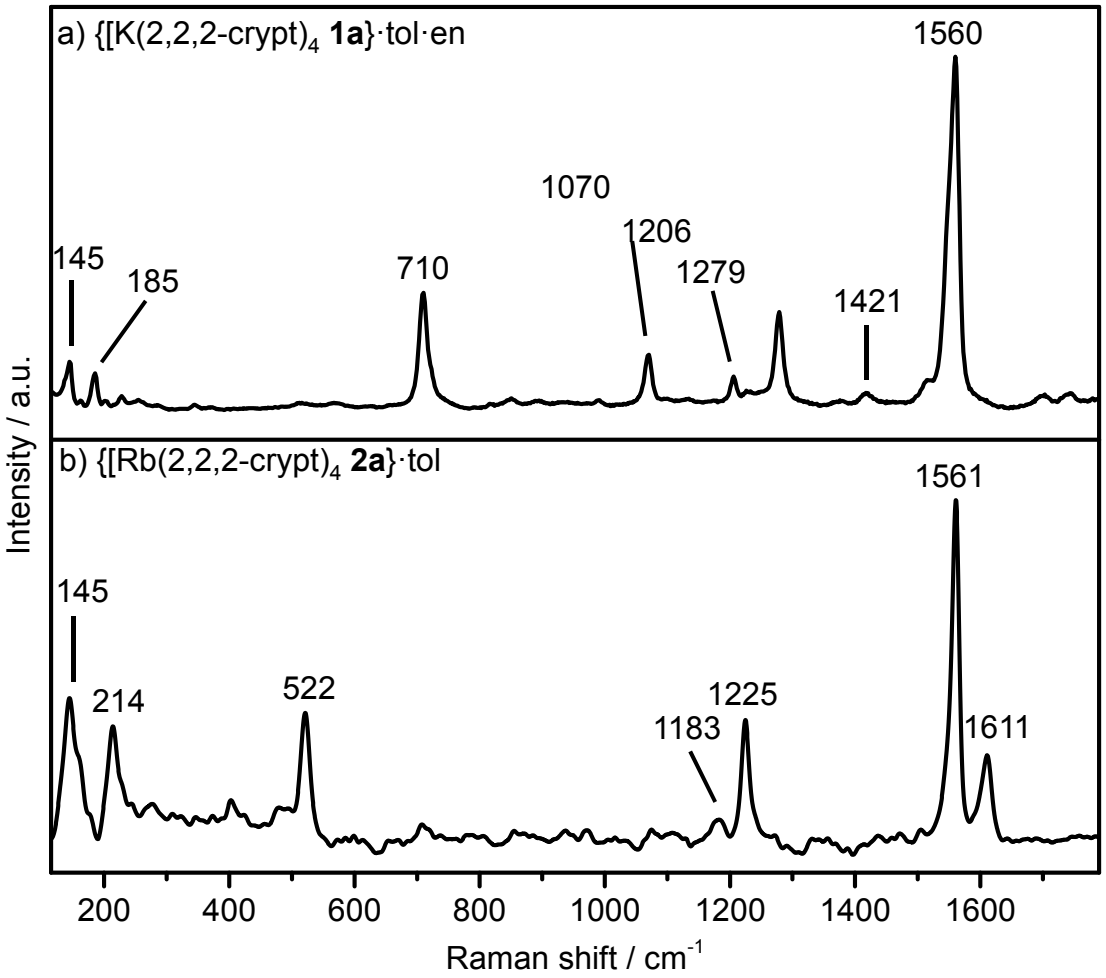

The signals at 145 and 185 cm^{-1} for **1a** and at 145 and 214 cm^{-1} for **2a** are in the range of the skeletal vibrations of bare Ge_9 clusters.[5] The band at 522 cm^{-1} is indicative of the *exo*-Ge–C

valence vibrations.[6-8] The signal at 710 cm^{-1} in the Raman spectrum of {[K(2,2,2-crypt)]$_4$ **1a**}·tol·en points at an *exo*-Ge–C valence vibration with partial double bond character.[9, 10] The absorption band at 1206 cm^{-1} as well as the comparatively strong signals at 1279 and 1560 cm^{-1} are assigned to the symmetric C–C and C=C valence vibrations of the ^{EZ}**B**/^{ZE}**B** entity, respectively.[11, 12] The symmetric C=C and C–C valence vibrations of the linking unit ^{ZZ}**B** of **2a** are displayed by the signals at 1225 and 1561 cm^{-1}, respectively.[11, 12] A comparatively strong signal of the C=C valence vibration of the vinyl functionality of **1a** is expected to be at around 1562 cm^{-1} and thus superimposes with the very strong signal at 1560 cm^{-1}.[13-15] The signal at 1070 cm^{-1} hints at the C–N stretching mode of the solvent molecule *en* in {[K(2,2,2-crypt)]$_4$ **1a**}·tol·en.[16] Additional signals at 1183 and 1611 cm^{-1} in the Raman spectrum of {[Rb(2,2,2-crypt)]$_4$ **2a**}·tol indicate C–C as well as C=C and C=N valence vibrations of the ^{Z}**R** side chain.

4 References

1. Benda, C. B.; Wang, J. Q.; Wahl, B.; Fässler, T. F. Syntheses and ^{1}H NMR Spectra of Substituted Zintl Ions $[Ge_9R_n]^{(4-n)-}$: Crystal Structures of $[Ge_9R]^{3-}$ (R= 2,4,6-$Me_3C_6H_2$, $CHCH_2$) and Indication of Tris-Vinylated Clusters. *Eur. J. Inorg. Chem.* **2011,** *2011*, 4262-4269.
2. Bentlohner, M. M.; Klein, W.; Fard, Z. H.; Jantke, L.-A.; Fässler, T. F. Linking Deltahedral Zintl Clusters with Conjugated Organic Building Blocks: Synthesis and Characterization of the Zintl Triad $[R-Ge_9-CH=CH-CH=CH-Ge_9-R]^{4-}$. *Angew. Chem. Int. Ed.* **2015,** *54*, 3748-3753; *Angew. Chem.* **2015**, *127*, 3819-3824.
3. Hull, M. W.; Sevov, S. C. Organo-Zintl Clusters Soluble in Conventional Organic Solvents: Setting the Stage for Organo-Zintl Cluster Chemistry. *Inorg. Chem.* **2007,** *46*, 10953-10955.
4. Bentlohner, M. M. Dissertation, Technische Universität München, Garching, 2016.
5. Von Schnering, H.; Baitinger, M.; Bolle, U.; Carrillo-Cabrera, W.; Curda, J.; Grin, Y.; Heinemann, F.; Llanos, J.; Peters, K.; Schmeding, A. Binary Alkali Metal Compounds with the Zintl Anions $[Ge_9]^{4-}$ and $[Sn_9]^{4-}$. *Z. Anorg. Allg. Chem.* **1997,** *623*, 1037-1039.
6. Vilcarromero, J.; Marques, F.; Andreu, J. Bonding Properties of rf-co-Sputtering Amorphous Ge–C Films Studied by X-ray Photoelectron and Raman Spectroscopies. *J. Non-Cryst. Solids* **1998,** *227*, 427-431.
7. Lippincott, E. R.; Tobin, M. C. The Vibrational Spectra and Thermodynamic Functions of Lead Tetramethyl, Tin Tetramethyl and Germanium Tetramethyl. *J. Am. Chem. Soc.* **1953,** *75*, 4141-4147.
8. Spiro, T. G.; Fontal, B. Raman Spectra and Metal-Metal Bonds. Force Constants and Bond Polarizability Derivatives for Hexamethyldisilicon, -germanium, -tin, and -lead. *Inorg. Chem.* **1971,** *10*, 9-13.
9. Lazraq, M.; Escudié, J.; Couret, C.; Satgé, J.; Dräger, M.; Dammel, R. (Mesityl)$_2$Ge (fluorenylidene)–Stabilization of a Ge–C Double Bond by Charge Transfer into an

Aromatic System. *Angew. Chem. Int. Ed.* **1988,** *27*, 828-829; *Angew. Chem.* **1988,** *100*, 885-887.

10. Barrau, J.; Escudie, J.; Satge, J. Multiply Bonded Germanium Species. Recent Developments. *Chem. Rev.* **1990,** *90*, 283-319.

11. Benedetti, E.; Aglietto, M.; Pucci, S.; Panchenko, Y. N.; Pentin, Y. A.; Nikitin, O. Vibrational Spectra of *trans*,*trans*-, *cis*,*cis*- and *cis*,*trans*-1,4-dideuterobuta-1,3-dienes. *J. Mol. Struct.* **1978,** *49*, 293-299.

12. Borg, A.; Smith, Z.; Gundersen, G.; Klaeboe, P. The Vibrational Spectra of *cis*- and *trans*-1-chloro-1, 3-butadiene. *Spectrochim. Acta A* **1980,** *36*, 119-130.

13. Signals of 2,2,2-crypt are expected at 1040-1080 cm^{-1} (C-O-C, valence), 1374 cm^{-1} (C-N valence) and 1425-1475 cm^{-1} (C-C, valence).

14. Benda, C. B. Dissertation, Technische Universität München, Garching, 2013.

15. Glockling, F.; Lyle, M. A.; Stobart, S. R. Vinyl Derivatives of Silicon, Germanium, and Tin. *J. Chem. Soc., Dalton Trans.* **1974**, 2537-2542.

16. Giorgini, M. G.; Pelletti, M. R.; Paliani, G.; Cataliotti, R. S. Vibrational Spectra and Assignments of Ethylenediamine and its Deuterated Derivatives. *J. Raman Spectrosc.* **1983,** *14*, 16-21.

5.5 Synthesis of Low-Oxidation-State Germanium Clusters Comprising a Functional Anchor Group - Synthesis and Characterization of $[(Ge^0)_5(Ge–R)_3(Ge–(CH_2)_n–CH=CH_2)]$ with R = $Si(SiMe_3)_3$

Sabine Frischhut and Thomas F. Fässler

published in:

Dalton Trans. **2018**, *47*, 3223-3226.

CONTENT AND CONTRIBUTION

Specific organo-functionalization of deltahedral Ge_9 clusters had only been scarcely reported. Therefore, within the scope of this publication, the reactivity of the threefold silylated cluster $K[\{(Me_3Si)Si\}_3Ge_9]$ towards alkyl halides, comprising terminal double bonds was investigated. Two new alkenyl functionalized Ge_9 clusters, namely $\{(Me_3Si)_3Si\}_3Ge_9(CH_2)_nCH=CH_2$ (n = 1, 3), emerged. Both compounds were characterized by NMR spectroscopy (^1H, ^{29}Si, ^{13}C, COSY, HMBC, HSQC). The pentenyl substituted cluster (n = 3) was further characterized by single crystal structure analysis, as well as ESI mass spectrometry. $\{(Me_3Si)_3Si\}_3Ge_9(CH_2)_3CH=CH_2$ could not be detected by ESI mass spectrometric investigations. Nevertheless, the mass spectrum shows $[(Me_3Si)_3Si\}_2Ge_9(CH_2)_3CH=CH_2]^-$ which is formed upon abstraction of one silyl ligand. All investigations, including NMR spectroscopy, crystal structure determination, structure refinement and ESI mass spectrometric investigations were carried out within this thesis.

The allylic substituted Ge_9 cluster turned out to be very instable in solution, therefore crystallization of the latter failed.

Temperature-dependent ^1H NMR studies, which were carried out within this thesis, revealed dynamic processes for both alkenyl-substituted cluster compounds in solution.

Both neutral alkenyl functionalized Ge_9 clusters provide interesting candidates for follow-up reactions, e.g. grafting on surfaces or polymerization reactions.

The publication was authored within this work and revised by Prof. Dr. Thomas F. Fässler.

Dalton Transactions

COMMUNICATION

View Article Online
View Journal | View Issue

Cite this: *Dalton Trans.*, 2018, **47**, 3223

Received 24th January 2018,
Accepted 26th January 2018

DOI: 10.1039/c8dt00321a

rsc.li/dalton

Synthesis of low-oxidation-state germanium clusters comprising a functional anchor group – synthesis and characterization of $[(Ge^0)_5(Ge\text{-}R)_3(Ge\text{-}(CH_2)_n\text{-}CH{=}CH_2)]$ with $R = Si(SiMe_3)_3$†

Sabine Frischhut and Thomas F. Fässler *

The first alkenyl-functionalized, uncharged deltahedral germanium clusters $[\{Si(SiMe_3)_3\}_3Ge_9(CH_2)_nCH{=}CH_2]$ (n = 1 or 3) comprising five Ge^0 atoms are presented. All compounds were NMR-spectroscopically and mass-spectrometrically characterized. $[\{Si(SiMe_3)_3\}_3Ge_9(CH_2)_3CH{=}CH_2]$ was further characterized by X-ray structure analysis and Raman spectroscopy. Temperature-dependent NMR studies reveal dynamic behavior for both compounds in solution at room temperature. The propenyl derivative $[\{Si(SiMe_3)_3\}_3Ge_9CH_2CH{=}CH_2]$ undergoes fast decomposition in solution. The possibility of the comparatively stable pentenyl-substituted Ge_9 cluster as a candidate for follow-up reactions is highlighted.

One of the recent challenging aspects in main group chemistry of tetrel elements has been the design and synthesis of tetrel-element rich molecules with atoms in low oxidation states or at best with ligand-free tetrel atoms. In the case of silicon, the first compound featuring a "naked" silicon vertex (siliconoid[1]) was synthesized in 2005 by Scheschkewitz *et al. via* reaction of a disilenide with $SiCl_4$, and also by Wiberg and Veith through complete reductive dehalogenation of a (pentaiodo)tetrasilabutane.[2] The concept of metalloid clusters of group 13 and group 14 elements has been summarized in reviews.[3] In recent years, small diatomic clusters with Si(0) and Ge(0) have also come to the forefront.[4] Also, larger neutral Ge clusters which comprise tetrel atoms of the formal oxidation state 0 have been reported, *e.g.* $[Ge_8\{N(SiMe_3)_2\}_6]$,[5] $Ge_6Ar'_2$ [6] and $[Ge_{12}\{FeCp(CO)_2\}_8\{FeCp(CO)\}_2]$.[7] In contrast, a large number of ligand-free Si and Ge clusters exists in *Zintl* phases such as alkali–metal (A) tetrelides comprising atoms with zero but also negative oxidation states.[8] Even though the usage of *Zintl* phases has been proposed many times and the direct relationship of $[Si_4]^{4-}$ in the neat solid NaSi and the possible formation of tetrahedro-tetrasilane molecules was pointed out many years ago,[9] only one example of a reaction of Si_4 clusters employing the *Zintl* phase $Rb_{12}Si_{17}$ and liquid ammonia as solvent has emerged in the form of the characterization of $[(MesCu)_2(\eta^3\text{-}Si_4)]^{4-}$.[10] In contrast, ligand-free Ge_9 clusters are easily accessible from *Zintl* phases in good yields *via* dissolution of binary phases such as K_4Ge_9 in ethylenediamine and DMF. Pristine Ge_9 clusters, which show a multifaceted reactivity in solution, have been intensively investigated,[11] and recently the reaction of Ge_9^{4-} with chloro-tris(trimethylsilyl) silane led to the mono-anionic compound $[R_3Ge_9]^{1-}$ (R = $Si(SiMe_3)_3$),[12] which had been obtained for the first time by Schnepf *et al.* in low yields using a different synthetic approach.[13] Variation of the silyl-ligand led to several other derivatives of the trisilylated Ge_9 cluster.[14] In principle, $[R_3Ge_9]^{1-}$ allows for the introduction of another ligand with organic functionalities which has not been utilized yet. Vinyl groups have been attached by reacting the *Zintl* phase A_4Ge_9 (A = K or Rb) with 1,2-bis(trimethylsilyl)acetylene in ethylenediamine resulting in the anionic species $[(CH_2{=}CH)_xGe_9]^{(4-x)-}$ (x = 1 or 2)[15] and $[(CH_2{=}CH)Ge_9\text{–}Ge_9(CH{=}CH_2)]^{4-}$,[16] and the linkage of deltahedral Ge_9 clusters *via* a conjugated organic bridge has been achieved by the reaction of Ge_9^{4-} with 1,4-bis(trimethylsilyl)butadiyne (and optionally also with 1,2-bis(trimethylsilyl)acetylene) in ethylenediamine, giving the *Zintl* triads $[R\text{–}Ge_9\text{–}CH{=}CH\text{–}CH{=}CH\text{–}Ge_9\text{–}R]^{4-}$ (R = (2*Z*,4*E*)-7-amino-5-aza-hepta-2,4-dien-2-yl or vinyl)[17] and $[Ge_9\text{–}CH{=}CH\text{–}CH{=}CH\text{–}Ge_9]^{6-}$.[18] However, although these Ge_9 clusters carry the desired alkene functionality, their formation does not occur by a straightforward approach and the products are still charged, which drastically limits their solubility in convenient solvents and their application for follow-up reactions. Besides, alkenyl-functionality has also been attached to the Ge_9 cluster *via* a silylation reaction resulting in the one-fold negatively charged species $[R_2Ge_9SiPh_2alkenyl]^-$.[19]

Technische Universität München, Department Chemie, Lichtenbergstraße 4, 85747 Garching, Germany. E-mail: thomas.faessler@lrz.tum.de

†Electronic supplementary information (ESI) available: Experimental details, crystallographic details, NMR spectra, Raman spectrum and ESI-MS spectra. CCDC 1565461. For ESI and crystallographic data in CIF or other electronic format see DOI: 10.1039/c8dt00321a

So far, investigations of $[R_3Ge_9]^-$ have focused on subsequent reactions with late transition metals in order to obtain the corresponding transition metal complexes; they led *e.g.* to the synthesis of $[R_6Ge_{18}M]$ (M = Zn, Cd or Hg)[20] and $[R_3Ge_{18}M]^-$ (M = Cu, Ag or Au),[21] both of which contain two $[R_3Ge_9]^-$ clusters connected by M^{II} or M^{I} *via* the triangular face of the Ge_9 clusters, and of $[R_6Ge_{18}Pd]$ and $[R_6Ge_{18}Cu_2(PPh_3)]$ which have been synthesized by the reaction of $[R_3Ge_9]^-$ with $Pd(PPh_3)_4$ and $[Cu(PPh_3)_3Br]$, respectively. In the case of $[R_6Ge_{18}Cu_2(PPh_3)]$, the two linked Ge_9 clusters are η^3-coordinated to a $Cu(PPh_3)$ entity.[22] Examples of species with only one $[R_3Ge_9]^-$ cluster unit connected to a transition metal are $[R_3Ge_9Cr(CO)_5]^-$, $[R_3Ge_9Cr(CO)_3]^-$, $[R_3Ge_9Cu(P\textit{i}Pr_3)]$, and $[R_3Ge_9ZnCp^*]$.[20b,23]

Coinage metal units with NHC-ligands have also been attached to three-fold silylated Ge_9 *Zintl* clusters, namely $[R_3Ge_9M(NHC)]$ (M = Cu, Ag or Au; NHC = *N*-heterocyclic carbene) and $[\{Si(i\text{Pr})_3\}_3Ge_9Cu(NHC^{Dipp})]$ (Dipp = 2,6-diisopropylphenyl).[14b,24] Also, the trisubstituted cluster $[(Sn\textit{i}Pr_3)_3Ge_9]^-$ has been synthesized, and after its reaction with $Pd(PPh_3)_4$ the twinned icosahedral unit $[(Sn\textit{i}Pr_3)_3Ge_{18}Pd_3]$ with an internal Pd_3 triangle could be isolated.[25]

Until now, only a few approaches towards tetrasubstituted Ge_9 *Zintl* clusters have been reported, and the reaction of $[R_3Ge_9]^-$ with ethyl bromide, $^nBu_3SnCl/Ph_3SnCl$ and TlCp yielded $[R_3Ge_9CH_2CH_3]$, $[R_3Ge_9Sn^nBu_3]/[R_3Ge_9SnPh_3]$ and $[R_3Ge_9Tl]$, respectively.[26] In this series, the reaction towards the ethyl-functionalized neutral cluster compound $[R_3Ge_9CH_2CH_3]$ is by far the most promising one for obtaining uncharged functionalized molecules with low valent Ge atoms in good yields and of excellent solubility.

Herein, we report the synthesis and characterization of $[R_3Ge_9(CH_2)_3CH{=}CH_2]$ (**1**) and $[R_3Ge_9CH_2CH{=}CH_2]$ (**2**) (R = $Si(SiMe_3)_3$, hereinafter referred to as "hypersilyl"), which represent the first alkenyl-functionalized neutral deltahedral Ge_9 cluster compounds. **1** was characterized by single crystal X-ray diffraction analysis, and NMR and Raman spectroscopy as well as electrospray ionization mass spectrometry (ESI-MS). **2** was characterized using NMR spectroscopy, and the dynamic behavior of **1** and **2** in solution was investigated using temperature-dependent NMR spectroscopy.

$K[R_3Ge_9]$[12] was reacted with 5-bromopent-1-ene (5 eq.) in acetonitrile at r.t. to give a brown precipitate which was separated and dissolved in toluene. The solution was concentrated *in vacuo* and stored at −32 °C, which led to the formation of orange, block-shaped crystals of **1** in good yields suitable for single crystal X-ray crystallography. For the synthesis of **2**, $K[R_3Ge_9]$ was reacted with 3-bromoprop-1-ene (2 eq.) at 0 °C. The obtained brown precipitate was filtered off and characterized using NMR spectroscopy (Scheme 1).

Crystals of **1** (Fig. S1, ESI†) solely contain the neutral entity $[R_3Ge_9(CH_2)_3CH{=}CH_2]$ (**1**). The unit cell contains 4 molecules of **1** which all appear in the shape of a mono-capped square-antiprismatic Ge_9 cluster unit with C_S symmetry. The mirror plane is defined by the atoms Ge2, Ge4 and Ge9. The Ge_9 cluster carries three hypersilyl groups, one of which is located

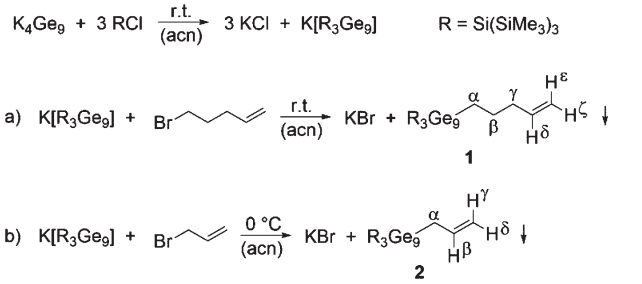

Scheme 1 Reaction of (a) $K[R_3Ge_9]$ with 5-bromopent-1-ene to form **1** and (b) $K[R_3Ge_9]$ with 3-bromoprop-1-ene to form **2** (R = $Si(SiMe_3)_3$). Hydrogen atoms are labelled with Greek letters.

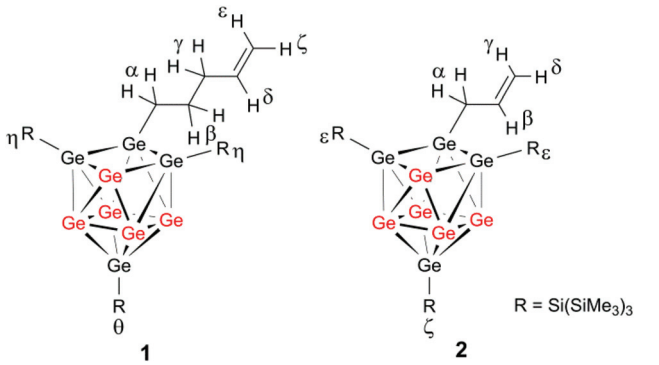

Scheme 2 Fourfold-substituted Ge_9 cluster cores with R = $Si(SiMe_3)_3$ and a pentenyl (**1**) or allyl (**2**) anchor group. Unsubstituted, ligand-free Ge atoms are marked in red.

at the capping atom Ge9, whereas the other two are bonded to the facing atoms Ge1 and Ge3 placed at the open square of the cluster unit (containing the atoms Ge1–Ge2–Ge3–Ge4). The pentenyl entity with its terminal double bond is connected to the cluster core *via* Ge2, which is also part of the open square of the cluster (Scheme 2).

The pentenyl substituent is *exo*-bonded to the cluster, and the Ge2–C28 bond points radially away from the cluster core. The distance between the atoms Ge2 and C28 is 1.970(3) Å and thus indicative of a typical 2-center-2-electron Ge–C(sp^3) bond.[17a,27] The distance between the two sp^2-hybridized atoms C31 and C32 of 1.322(7) Å lies in the typical range of a double bond.[28] The lowering in the symmetry of the cluster core compared to that of $K[R_3Ge_9]$ (D_{3h}) is caused by the fourth substituent: the binding of the organic substituent to Ge2 of the Ge_9 cluster causes a compression of the lengths of the edges of the open square directly adjacent to Ge2, leading to Ge–Ge distances of *d*(Ge1–Ge2) = 2.4472(4) Å and *d*(Ge2–Ge3) = 2.4532(4) Å, whereas the other edges which include the naked atom Ge4 are longer [*d*(Ge3–Ge4) = 2.6034(4) Å and *d*(Ge1–Ge4) = 2.5901(4) Å] (Fig. 1).

As expected and shown by the crystal structure determination, the additional alkene functionality is readily accessible and should thus be available for possible follow-up reactions for building up higher cluster number aggregates.

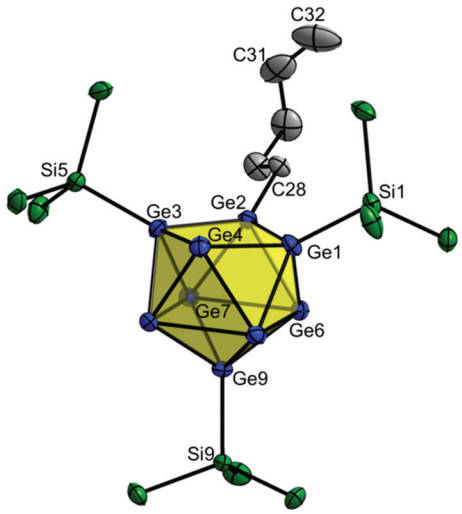

Fig. 1 The structure of $[R_3Ge_9(CH_2)_3CH{=}CH_2]$ (**1**) (Ge, blue; Si, green; C, grey). All carbon atoms connected to Si as well as all hydrogen atoms are omitted for clarity. All ellipsoids are shown at a probability level of 50%.

1 has also been characterized in solution by NMR spectroscopic investigations (Fig. S2–S7, ESI†). The ^{1}H NMR spectrum of a benzene-d_6 solution of crystals of **1** shows a significant up-field shift of the 1α protons at the C atom, on which the bromide was replaced by the Ge_9 cluster. The remaining signals for 1β, 1γ, 1δ, 1ε and 1ζ appear slightly down-field-shifted which is consistent with a relatively wide-range electron-withdrawing effect of the Ge_9 cluster. At the same time, the increased electron density within the cluster core causes an up-field shift of the singlet signal for the hypersilyl protons (1η and 1θ) compared to the corresponding signal for $K[R_3Ge_9]$.

Crystals of **2** could not be obtained so far. Nevertheless, compound **2** was characterized using NMR spectroscopy (Fig. S9–S14, ESI†). Compound **2** was obtained in good purity, since only a few signals of very low intensity originating from by-products could be detected in the ^{1}H NMR spectrum. In the ^{1}H NMR spectrum, all of the signals except for that for the 2δ protons are significantly down-field-shifted. As also observed for **1**, the 2ε/2ζ -signal is up-field-shifted compared to that for $K[R_3Ge_9]$.

Temperature-dependent ^{1}H NMR studies confirm the expected dynamic behavior of **1** and **2** in solution with coalescence temperatures of 273 K and 258 K, respectively, in toluene-d_8 (Fig. S8 and S15, ESI†). The dynamic behavior is indicated by the splitting of the broadened singlet signal corresponding to the three hypersilyl ligands connected to the Ge_9 cluster into two signals of a 2 : 1 ratio in the ^{1}H NMR spectrum at reduced temperatures. Fluctional behavior has also been reported for other *Zintl* clusters.[26a] This dynamic behavior is probably caused by the fluctuation of the hypersilyl ligands in the Ge1–Ge3–Ge9 plane,[26a,29] but dynamic behavior of the total cluster core through exchanging Ge atom positions is also feasible.[30] Compound **1** is remarkably stable even at elevated temperatures (up to 70 °C), whereas compound **2** easily decomposes under the same conditions.

In the ESI-MS spectrum of the crude product of **1** fragmentation of the compound is observed. Besides the peak corresponding to $\{[R_3Ge_9]\}^-$, a peak at the mass-to-charge ratio for the anion $\{[R_2Ge_9(CH_2)_2CH{=}CH_2]\}^-$ is registered, whereas the ESI-MS spectrum of **2** only shows the peak for the anionic entity $[R_3Ge_9]^-$ (Fig. S17 and S18, ESI†).

The reported neutral, functionalized *Zintl* molecules $[R_3Ge_9(CH_2)_3CH{=}CH_2]$ (**1**) and $[R_3Ge_9CH_2CH{=}CH_2]$ (**2**) both comprise an organic substituent with a terminal C–C double bond. The crystal structure of **1** reveals a sterically easily accessible terminal double bond which makes this compound a promising candidate for subsequent reactions including immobilization on surfaces and nanoparticles. **1** and **2** are readily soluble in non-polar solvents such as THF, toluene and hexane, which is very convenient for follow-up reactions and may open up access to new electronically and structurally interesting cluster compounds or even to higher cluster number aggregates.

Conflicts of interest

The authors declare no conflict of interests.

Acknowledgements

The authors are grateful to the SolTech (Solar Technologies go Hybrid) program of the Bavarian State Ministry of Education, Science and the Arts for financial support. S.F. is further grateful to the Fonds der Chemischen Industrie for her fellowship. The authors acknowledge Dr Wilhelm Klein for his help with structure determination and M.Sc. Sebastian Geier for performing Raman measurements. Moreover, the authors thank Maria Weindl for carrying out temperature-dependent NMR studies and M.Sc. Christina Fischer for performing ESI-MS measurements. The authors are grateful to B.Sc. Melanie Ripsam, Catharina Theiß and B.Sc. Kevin Frankiewicz for the preparation of reaction solutions.

References

1 K. Abersfelder, A. Russell, H. S. Rzepa, A. J. White, P. R. Haycock and D. Scheschkewitz, *J. Am. Chem. Soc.*, 2012, **134**, 16008.

2 (*a*) D. Scheschkewitz, *Angew. Chem., Int. Ed.*, 2005, **44**, 2954, (*Angew. Chem.*, 2005, **117**, 3014); (*b*) G. Fischer, V. Huch, P. Mayer, S. K. Vasisht, M. Veith and N. Wiberg, *Angew. Chem., Int. Ed.*, 2005, **44**, 7884, (*Angew. Chem.*, 2005, **117**, 8096); (*c*) D. Scheschkewitz, *Functional Molecular Silicon Compounds I: Regular Oxidation States*, Springer-Verlag, Heidelberg, 2014, vol. 155; (*d*) D. Scheschkewitz, *Functional*

Molecular Silicon Compounds II, Springer-Verlag, Heidelberg, 2014, vol. 156.
3 (*a*) H. Schnöckel, *Dalton Trans.*, 2005, 3131; (*b*) A. Schnepf, *Chem. Soc. Rev.*, 2007, **36**, 745.
4 (*a*) Y. Wang, Y. Xie, P. Wei, R. B. King, H. F. Schaefer, P. v. R. Schleyer and G. H. Robinson, *Science*, 2008, **321**, 1069; (*b*) A. Sidiropoulos, C. Jones, A. Stasch, S. Klein and G. Frenking, *Angew. Chem., Int. Ed.*, 2009, **48**, 9701, (*Angew. Chem.*, 2009, **121**, 9881); (*c*) L. Pu, A. D. Phillips, A. F. Richards, M. Stender, R. S. Simons, M. M. Olmstead and P. P. Power, *J. Am. Chem. Soc.*, 2003, **125**, 11626; (*d*) P. Ghana, M. I. Arz, U. Das, G. Schnakenburg and A. C. Filippou, *Angew. Chem., Int. Ed.*, 2015, **54**, 9980, (*Angew. Chem.*, 2015, **127**, 10118).
5 A. Schnepf and R. Köppe, *Angew. Chem., Int. Ed.*, 2003, **42**, 911, (*Angew. Chem.*, 2003, **115**, 940).
6 A. F. Richards, H. Hope and P. P. Power, *Angew. Chem., Int. Ed.*, 2003, **42**, 4071, (*Angew. Chem.*, 2003, **115**, 4205).
7 C. Schenk, F. Henke and A. Schnepf, *Angew. Chem., Int. Ed.*, 2013, **52**, 1834, (*Angew. Chem.*, 2013, **125**, 1883).
8 (*a*) R. Nesper, *Prog. Solid State Chem.*, 1990, **20**, 1; (*b*) J. Evers, *Zintl Phases: Principles and Recent Developments, Book Series: Structure and Bonding*, ed. T. F. Fässler, Springer-Verlag, Heidelberg, 2011, vol. 139.
9 N. Wiberg, C. M. Finger and K. Polborn, *Angew. Chem., Int. Ed. Engl.*, 1993, **32**, 1054, (*Angew. Chem.*, 1993, **105**, 1140).
10 M. Waibel, F. Kraus, S. Scharfe, B. Wahl and T. F. Fässler, *Angew. Chem., Int. Ed.*, 2010, **49**, 6611, (*Angew. Chem.*, 2010, **122**, 6761).
11 (*a*) J. D. Corbett, *Chem. Rev.*, 1985, **85**, 383; (*b*) T. F. Fässler and S. D. Hoffmann, *Angew. Chem., Int. Ed.*, 2004, **43**, 6242, (*Angew. Chem.*, 2004, **116**, 6400); (*c*) S. C. Sevov and J. M. Goicoechea, *Organometallics*, 2006, **25**, 5678; (*d*) S. Scharfe, F. Kraus, S. Stegmaier, A. Schier and T. F. Fässler, *Angew. Chem., Int. Ed.*, 2011, **50**, 3630, (*Angew. Chem.*, 2011, **123**, 3712); (*e*) T. F. Fässler, *Coord. Chem. Rev.*, 2001, **215**, 347.
12 F. Li and S. C. Sevov, *Inorg. Chem.*, 2012, **51**, 2706.
13 A. Schnepf, *Angew. Chem., Int. Ed.*, 2003, **42**, 2624, (*Angew. Chem.*, 2003, **115**, 2728).
14 (*a*) O. Kysliak, C. Schrenk and A. Schnepf, *Inorg. Chem.*, 2015, **54**, 7083; (*b*) L. J. Schiegerl, F. S. Geitner, C. Fischer, W. Klein and T. F. Fässler, *Z. Anorg. Allg. Chem.*, 2016, **642**, 1419; (*c*) O. Kysliak, T. Kunz and A. Schnepf, *Eur. J. Inorg. Chem.*, 2017, **4**, 805.
15 (*a*) M. W. Hull and S. C. Sevov, *Inorg. Chem.*, 2007, **46**, 10953; (*b*) C. B. Benda, J. Q. Wang, B. Wahl and T. F. Fässler, *Eur. J. Inorg. Chem.*, 2011, **27**, 4262.
16 C. B. Benda, H. He, W. Klein, M. Somer and T. F. Fässler, *Z. Anorg. Allg. Chem.*, 2015, **641**, 1080.
17 (*a*) M. M. Bentlohner, W. Klein, Z. H. Fard, L.-A. Jantke and T. F. Fässler, *Angew. Chem., Int. Ed.*, 2015, **54**, 3748, (*Angew. Chem.*, 2015, **127**, 3819); (*b*) S. Frischhut, M. M. Bentlohner, W. Klein and T. F. Fässler, *Inorg. Chem.*, 2017, **56**, 10691.
18 M. M. Bentlohner, S. Frischhut and T. F. Fässler, *Chem. – Eur. J.*, 2017, **23**, 17089.
19 K. Mayer, L. J. Schiegerl, T. Kratky, S. Günther and T. F. Fässler, *Chem. Commun.*, 2017, **53**, 11798.
20 (*a*) F. Henke, C. Schenk and A. Schnepf, *Dalton Trans.*, 2009, 9141; (*b*) K. Mayer, L. J. Schiegerl and T. F. Fässler, *Chem. – Eur. J.*, 2016, **22**, 18794.
21 C. Schenk, F. Henke, G. Santiso-Quiñones, I. Krossing and A. Schnepf, *Dalton Trans.*, 2008, 4436.
22 F. Li and S. C. Sevov, *Inorg. Chem.*, 2015, **54**, 8121.
23 C. Schenk and A. Schnepf, *Chem. Commun.*, 2009, 3208.
24 F. S. Geitner and T. F. Fässler, *Eur. J. Inorg. Chem.*, 2016, **2016**, 2688.
25 L. G. Perla and S. C. Sevov, *J. Am. Chem. Soc.*, 2016, **138**, 9795.
26 (*a*) F. Li and S. C. Sevov, *J. Am. Chem. Soc.*, 2014, **136**, 12056; (*b*) F. Li, A. Muñoz-Castro and S. C. Sevov, *Angew. Chem., Int. Ed.*, 2012, **51**, 8581, (*Angew. Chem.*, 2012, **124**, 8709).
27 (*a*) M. W. Hull, A. Ugrinov, I. Petrov and S. C. Sevov, *Inorg. Chem.*, 2007, **46**, 2704; (*b*) M. W. Hull and S. C. Sevov, *J. Am. Chem. Soc.*, 2009, **131**, 9026.
28 E. V. Anslyn and D. A. Dougherty, *Modern Physical Organic Chemistry*, University Science, Sausalito, CA, 2006.
29 F. Li, A. Muñoz-Castro and S. C. Sevov, *Angew. Chem., Int. Ed.*, 2016, **55**, 8630, (*Angew. Chem.*, 2016, **51**, 8581).
30 (*a*) R. Rudolph, W. Wilson, F. Parker, R. C. Taylor and D. Young, *J. Am. Chem. Soc.*, 1978, **100**, 4629; (*b*) S. Scharfe, T. F. Fässler, S. Stegmaier, S. D. Hoffmann and K. Ruhland, *Chem. – Eur. J.*, 2008, **14**, 4479; (*c*) B. Eichhorn, *Zintl ions: Principles and Recent Developments, Book Series: Structure and Bonding*, ed. T. F. Fässler, Springer-Verlag, Heidelberg, 2011, vol. 140; (*d*) J. D. Corbett, *J. Am. Ceram. Soc.*, 2011, **133**, 19562.

Electronic Supplementary Material (ESI) for Dalton Transactions.

Supplementary Information

Synthesis of Low-Oxidation-State Germanium Clusters Comprising a Functional Anchor Group − Synthesis and Characterization of $[(Ge^0)_5(Ge\text{-}R)_3(Ge\text{-}(CH_2)_n\text{-}CH{=}CH_2)]$ with $R = Si(SiMe_3)_3$

Sabine Frischhut, and Thomas F. Fässler*[a]

Contents

Figures and Tables

1 Experimental details

General Methods: All manipulations were carried out under a purified argon atmosphere using glove box and standard schlenk techniques. The *Zintl* phase with the nominal composition K_4Ge_9 was synthesized by heating a stoichiometric mixture of the elements K and Ge (99.999% Chempur) at 650 °C for 46 h in a steel autoclave.[1] The trisilylated cluster compound $K[R_3Ge_9]$ was synthesized according to a modified literature procedure.[2] 5-Bromo-1-pentene (Sigma-Aldrich 95%), 3-bromoprop-1-ene (Sigma-Aldrich 97%) and chlorotris(trimethylsilyl)silane (TGI Chemicals >95%) were used as received. Toluene and acetonitrile were dried over molecular sieve (3 Å), and thf was dried over a special drying material in a solvent purificator (MBraun MB-SPS). All solvents were stored over molecular sieve (3 Å) for at least one day. The NMR solvents toluene-d_8 (Deutero GmbH 99.5%) and benzene-d_6 (Deutero GmbH 99.5%) were dried over molecular sieve (3 Å) for at least one day and stored in a glove box.

Synthesis of $[\{Si(SiMe_3)_3\}_3Ge_9(CH_2)_3CH=CH_2]$ (1): K_4Ge_9 (341 mg, 0.42 mmol) was weighed out in a Schlenk tube in the glovebox. 12 mL of an acetonitrile solution of chlorotris(trimethylsilyl)silane (357 mg, 1.26 mmol) was added. The suspension was stirred for 12 h at r.t. and filtered over a glass-fiber filter. To the deep-red filtrate 5-bromo-1-pentene (285 µL, 2.10 mmol) dissolved in 2 mL acetonitrile was slowly dropped upon rigorously stirring. A brown precipitate started to form immediately. The reaction mixture was stirred for 4 h at r.t. The precipitate was then allowed to settle down, and the supernatant solution was decanted. The precipitate was washed three times with 16 mL of acetonitrile in total. The residue was dried in a vacuum to give 401 mg of a dark brown solid. For crystallization 200 mg of the solid were dissolved in 3 mL of toluene resulting in a deep-brown solution. After filtration the solution was concentrated in *vacuo* and stored at -32 °C. Orange block-shaped crystals were obtained after one month (yield 50%). Crystal size: 0.4 x 0.2 x 0.2 mm^3; unit cell parameters: a = 16.0667(7), b = 17.5351(8), c = 23.815(1), $\alpha = \beta = \gamma = 90°$, V = 6709.3(5) $Å^3$, orthorhombic space group $P2_12_12_1$; Z = 4, ρ_{calc} = 1.451 $g \cdot cm^{-1}$, μ = 4.21 mm^{-1}, θ_{max} = 28.00°, 286703 measured reflections, 16198 independent reflections, R_{int} = 0.042, R_1 = 0.017, wR_2 = 0.042 for $I > 2\sigma(I)$, R_1 = 0.020, wR_2 = 0.044 for all data. Min/max residual electron density: 0.46/0.80 $e \cdot Å^{-3}$. CCDC 1565461 contains the supplementary crystallographic data for this paper. These data can be

obtained free of charge from The Cambridge Crystallographic Data Center via www.ccdc.cam.ac.uk/data_request/cif. The presence of the elements Si and Ge in the measured single crystal was confirmed by EDX. ^{1}H NMR (400 MHz, benzene-d_6, 296 K): δ(ppm) 5.67 (ddt, ^{3}J = 17.2 Hz, 10.4 Hz, 6.8 Hz, 1H, 1δ), 5.03 (ddd, ^{3}J = 16.8 Hz, 2.0 Hz, ^{4}J = 1.6 Hz (allylic proton coupling), 1H, 1ε), 4.97 (m, 1H, 1ζ), 2.09 (m, 2H, 1γ), 1.85 (m, 4H, superimposition of 1α and 1β), 0.42 (s, 81H, 1η and 1θ); ^{1}H ^{1}H COSY (400 MHz, benzene-d_6, 296 K): δ(ppm)/δ(ppm) 5.66/5.01 (^{3}J, 1ε/1δ and 1ζ/1δ), 5.65/2.09 (^{3}J, 1γ/1δ), 5.05/2.09 (^{4}J, 1ε/1γ), 4.96/2.10 (^{4}J, 1ζ/1γ), 2.10/1.86 (^{3}J, 1γ/1β); ^{13}C{^{1}H} NMR (101 MHz, benzene-d_6, 296 K): δ(ppm) 137.30 (1Cδ), 115.32 (1Cε/ζ), 37.88 (1Cγ), 36.06 (1Cα), 10.39 (1Cβ), 2.34 (1Cη/1Cθ); ^{1}H ^{13}C HSQC (400 MHz, 101 MHz, benzene-d_6, 296 K): δ(ppm)/δ(ppm) 5.67/137.33 (^{1}J, 1δ/1Cδ), 5.05/115.48 (^{1}J, 1ε/1Cε/ζ and 1ζ/1Cε/ζ), 2.09/37.69 (^{1}J, 1γ/1Cγ), 1.85/35.86 (^{1}J, 1α/1Cα), 1.85/10.25 (^{1}J, 1β/1Cβ), 0.43/2.17 (^{1}J, 1η/1Cη and 1θ/1Cθ); ^{1}H ^{13}C HMBC (400 MHz, 101 MHz, benzene-d_6, 296 K): δ(ppm)/δ(ppm) 2.08/11.03 (^{2}J, 1γ/1Cβ), 1.84/137.86 (^{3}J, 1β/1Cδ), 1.84/38.04 (^{3}J, 1α/1Cγ; ^{2}J, 1β/1Cγ), 1.85/36.24 (^{2}J, 1β/1Cα); ^{29}Si NMR (79 MHz, benzene-d_6, 296 K): δ(ppm) -8.38 (*Si*Me$_3$), -105.78 (*Si*(SiMe$_3$)$_3$); elemental analysis calcd (%): C 26.22, H 6.19; found: C 26.35, H 6.22. ESI-MS (negative ion mode, 4500 V, 300 °C): *m*/*z* (%): 1397 {[{Si(SiMe$_3$)$_3$}$_3$Ge$_9$]}$^-$, 1219 {[{Si(SiMe$_3$)$_3$}$_2$Ge$_9$(CH$_2$)$_3$CH=CH$_2$]}$^-$; Raman ν [cm^{-1}] = 77 (s), 114 (vs, Ge$_9$ cluster), 146 (vs, Ge$_9$ cluster), 245 (s, Ge$_9$ cluster), 400 (w), 626 (m, ν_s(Si–C)), 687 (w, ν_{as}(Si–C) and Si–C–H bending), 742 (w, ν_{as}(Si–Si)), 838 (w), 1238 (w, br), 1412 (w, br, sp^{2}CH$_2$), 2888 (vs, ν(sp^{3}CH$_2$)), 2950 (s, ν(sp^{3}CH$_2$)).[3]

Synthesis of [{Si(SiMe$_3$)$_3$}$_3$Ge$_9$CH$_2$CH=CH$_2$] (2): In a glove box chlorotris(trimethylsilyl)silane (194 mg, 0.68 mmol) dissolved in 6 mL acetonitrile was added to K$_4$Ge$_9$ (185 mg, 0.23 mmol), and the mixture was stirred at r.t. for 19 h. The suspension was filtered over a glass-fiber filter. The resulting deep-red filtrate was cooled to 0 °C, and 3-bromoprop-1-ene (39 mL, 0.47 mmol) dissolved in 3 mL acetonitrile was added dropwise within 5.5 h under rigorous stirring. A brown solid precipitated slowly. The suspension was stirred at 0 °C for additional 23 h. The precipitate was allowed to settle down at -32 °C, and the supernatant solution was decanted. The solid was washed three times with a total amount of 12 mL acetonitrile under constant cooling at 0 °C. The residue was dried in *vacuo* and characterized by means of NMR spectroscopy. ^{1}H NMR (400 MHz, benzene-d_6, 296 K): δ(ppm) 6.12

(ddt, ^3J = 16.8 Hz, 9.6 Hz, 8.0 Hz, 1H, 2β), 5.03 (dd, ^3J = 16.8 Hz, 1.2 Hz, 1H, 2γ), 4.70 (d, ^3J = 9.8 Hz, 1H, 2δ), 2.70 (d, ^3J = 8.0 Hz, 1H, 2α), 0.41 (s, 81H, 2ε and 2ζ); ^{1}H ^{1}H COSY (400 MHz, benzene-d_6, 296 K): δ(ppm)/δ(ppm) 6.10/5.04 (^3J, 2β/1γ), 6.13/4.71 (^3J, 2β/1δ), 6.12/2.69 (^3J, 2β/1α), 5.01/4.69 (^3J, 2γ/1δ), 5.04/2.69 (^3J, 2γ/1α), 4.69/2.70 (^3J, 2δ/1α); ^{13}C{^{1}H} NMR (101 MHz, benzene-d_6, 296 K): δ (ppm) 140.25 (2Cβ), 114.10(2Cγ/δ), 15.25 (2Cα), 2.71 (2Cε/2Cζ); ^{1}H ^{13}C HSQC (400 MHz, 101 MHz, benzene-d_6, 296 K): δ(ppm)/δ(ppm) 6.11/139.79 (^1J, 2β/2Cβ), 5.03/113.87 (^1J, 2γ/2Cγ/δ), 4.71/113.60 (^1J, 2δ/2Cγ/δ), 2.71/14.98 (^1J, 2α/2Cα), 0.43/2.36 (^1J, 2ε/2Cε and 2ζ/2Cζ); ^{1}H ^{13}C HMBC (400 MHz, 101 MHz, benzene-d_6, 296 K): δ(ppm)/δ(ppm) 5.01/15.26 (^3J, 2γ/2Cα), 2.70/140.39 (^2J, 2α/2Cβ), 2.69/14.13 (^3J, 2α/2Cγ/δ); ^{29}Si NMR (79 MHz, benzene-d_6, 296 K): δ(ppm) -8.22 (*Si*Me$_3$), -105.64 (*Si*(SiMe$_3$)$_3$).

X-Ray data collection and structure determination: Crystals of **1** were transferred from the mother liquor into perfluoropolyalkylether oil under a cold N_2 stream. For data collection a single crystal was selected, fixed on top of a glass capillary and positioned in a cold N_2 stream. The single crystal X-ray diffraction data were recorded on a Bruker APEX II diffractometer equipped with a rotating anode (MoK_α radiation) and a CCD-detector at 151 K. The crystal structure was solved by Direct Methods using the SHELX software.[4] The positions of the hydrogen atoms were calculated and refined using a riding model. All non-hydrogen atoms were treated with anisotropic displacement parameters. One methyl group bound to one of the three hypersilyl groups is disordered.

Electron-dispersive X-ray (EDX) analysis: EDX analysis of the single crystal of **1** which was used for X-ray structure analysis was carried out on a Hitachi TM-1000 tabletop microscope.

NMR spectroscopic investigations: The NMR spectra were recorded on a Bruker Avance Ultrashield 400 MHz spectrometer. Temperature-dependent NMR studies were performed on a Bruker DPX 400 MHz spectrometer. Chemical shifts are reported in δ values as parts per million (ppm) relative to TMS. Coupling constants *J* are given in Hz. ^{1}H, ^{13}C and 2D NMR spectra were referenced to the residual signal of the used deuterated solvent (benzene-d_6 and toluene-d_8). Signal multiplicities are abbreviated as follows: singlet (s), doublet (d), triplet (t) and multiplet (m).

Elemental analysis: elemental analysis was carried out at the Department of Chemistry of the Technische Universität München. The elements C and H were determined with a combustion analyzer (elementar vario EL, Bruker Corp.).

Electrospray ionization mass spectrometry (ESI-MS) investigations: ESI-MS measurements were carried out on a HCT mass spectrometer (Bruker Daltronic) in the negative ion mode (-). In a glove box a small amount of the brown solid was dissolved in thf giving a pale-brown solution. The solution was filtered over glass fiber and injected into the ESI-MS. Measurement conditions: capillary voltage: 4.5 V, capillary exit: -166 V, drying gas temperature: 300 °C, injection rate: 240 μL/h.

Raman spectroscopy: Raman measurements were performed on crystals of **1** sealed in glass capillaries with a Raman microscopy spectrometer (Renishaw inVia Raman Microscope RE04: 532 nm, laser power 0.5% of a total power of 500 mW).

2 Crystallographic details

Table S1. Selected crystallographic details of **1**.

Compound	**1**
formula	$Ge_9Si_{12}C_{32}H_{90}$
fw ($g \cdot mol^{-1}$)	1465.42
space group (no.)	*P* 2_1 2_1 2_1 (19)
a (Å)	16.0667(7)
b (Å)	17.5351(8)
c (Å)	23.815(1)
V ($Å^3$)	6709.3(5)
Z	4
T (K)	151(2)
λ (Å)	0.71073
ρ_{calcd} ($g \cdot cm^{-3}$)	1.451
μ (mm^{-1})	4.21
collected reflections	286703
independent reflections	16198
R_{int}	0.042
parameters / restraints	517 / 0
R_1 [all data / $I > 2\,\sigma(I)$]	0.020 / 0.017
wR_2 [all data / $I > 2\,\sigma(I)$]	0.044 / 0.042
goodness of fit	1.092
max. / min. diff. el. density ($e \cdot Å^{-3}$)	0.80 / -0.46

Figure S1. Unit cell of **1**. Ge_9 clusters are shown as dark-grey polyhedra. The functionalities bound to the cluster are shown schematically. Hydrogen atoms are omitted for clarity.

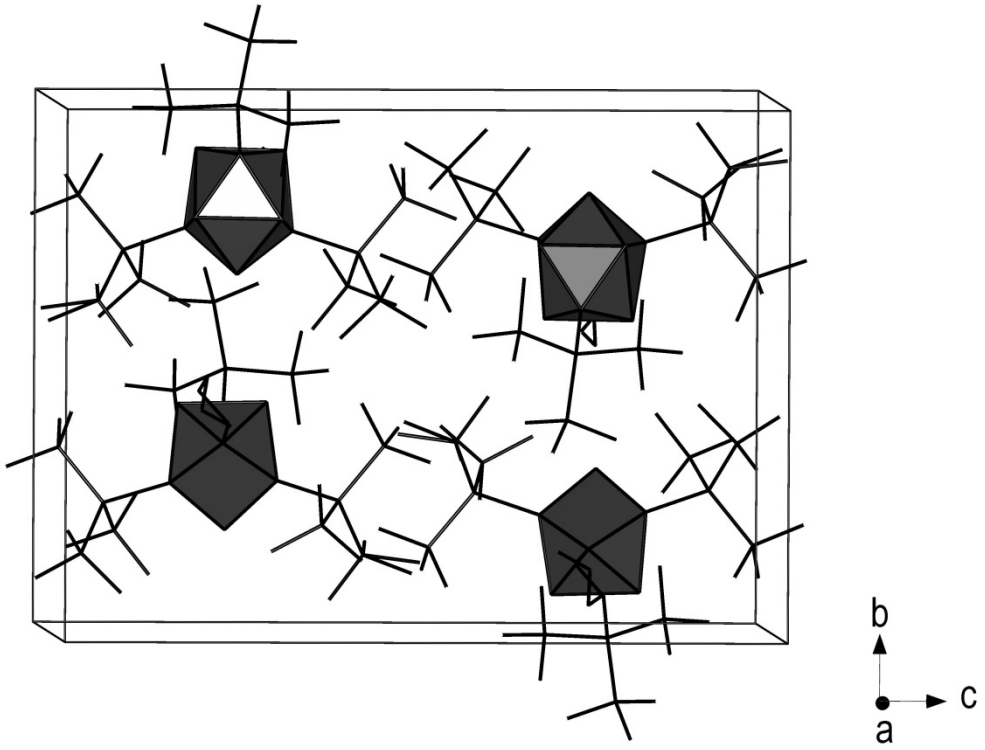

Table S2. Selected bond lengths [Å] in **1**.

Ge1—Si1	2.3803(8)	Ge2—Ge3	2.4532(4)
Si1—Si2	2.346(1)	Ge2—Ge6	2.5911(4)
Si2—C1	1.862(4)	Ge2—Ge7	2.5834(4)
Si2—C2	1.868(4)	Ge3—Si5	2.3901(8)
Si2—C3	1.879(4)	Ge3—Ge4	2.6034(4)
Si1—Si3	2.355(1)	Ge3—Ge7	2.6768(5)
Si1—Si4	2.358(1)	Ge3—Ge8	2.5252(4)
Ge1—Ge2	2.4472(4)	Ge4—Ge5	2.6450(4)
Ge1—Ge4	2.5901(4)	Ge4—Ge8	2.6457(4)
Ge1—Ge5	2.5267(4)	Ge5—Ge8	2.8415(4)
Ge1—Ge6	2.6595(5)	Ge5—Ge9	2.5455(4)
Ge2—C28	1.970(3)	Ge6—Ge7	2.9182(4)
C28—C29	1.514(4)	Ge6—Ge9	2.4967(4)
C29—C30	1.540(5)	Ge7—Ge9	2.5156(4)
C30—C31	1.485(6)	Ge8—Ge9	2.5447(4)

C31—C32	1.322(7)	Ge9—Si9	2.3694(7)

3 NMR spectra of [{Si(SiMe$_3$)$_3$}$_3$Ge$_9$(CH$_2$)$_3$CH=CH$_2$] (1)

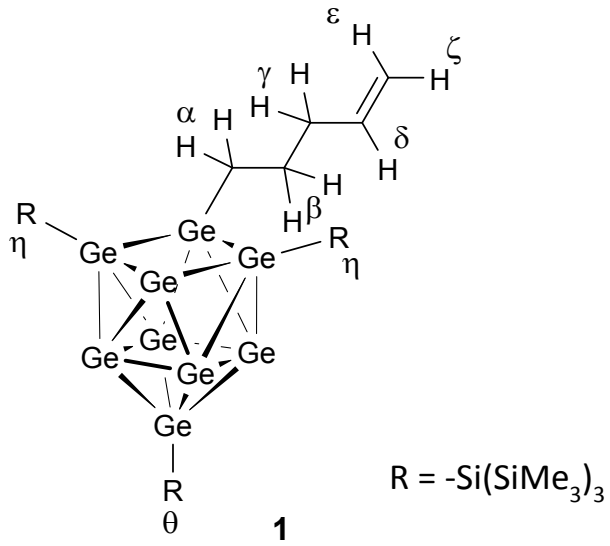

1

Scheme S1. Neutral cluster compound [{Si(SiMe$_3$)$_3$}$_3$Ge$_9$(CH$_2$)$_3$CH=CH$_2$] (**1**). Hydrogen atoms are labelled with Greek letters.

Figure S2. ^{1}H NMR spectrum of dissolved crystals of **1** in benzene-d_6 recorded at 296 K. The signals highlighted in grey are magnified below. The assignment of the signals is effected by the corresponding COSY NMR spectrum shown in figure S3.

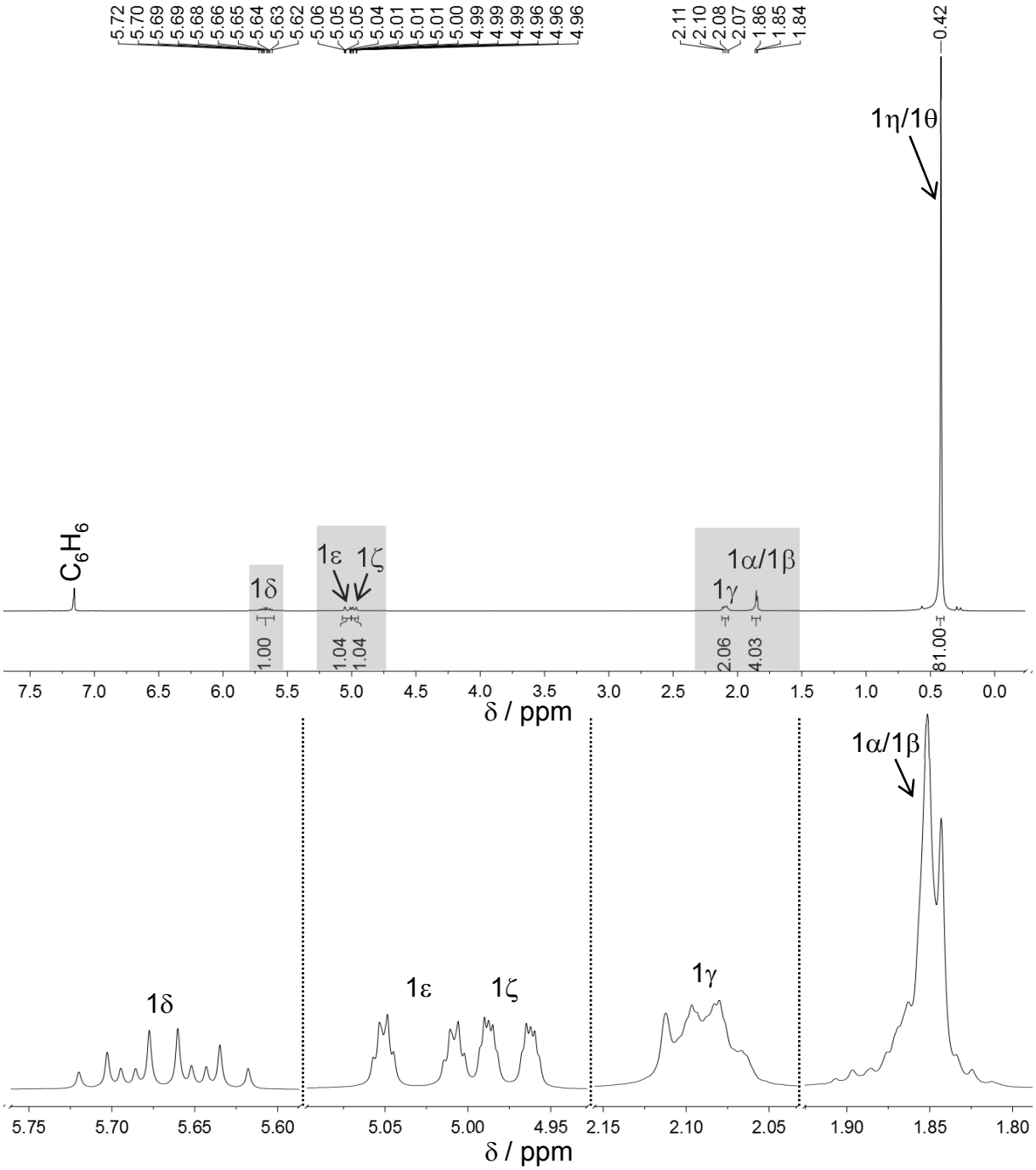

Figure S3. ^{1}H ^{1}H COSY NMR spectrum of dissolved crystals of **1** in benzene-d_6 recorded at 296 K. The signal marked with * couldn't be assigned.

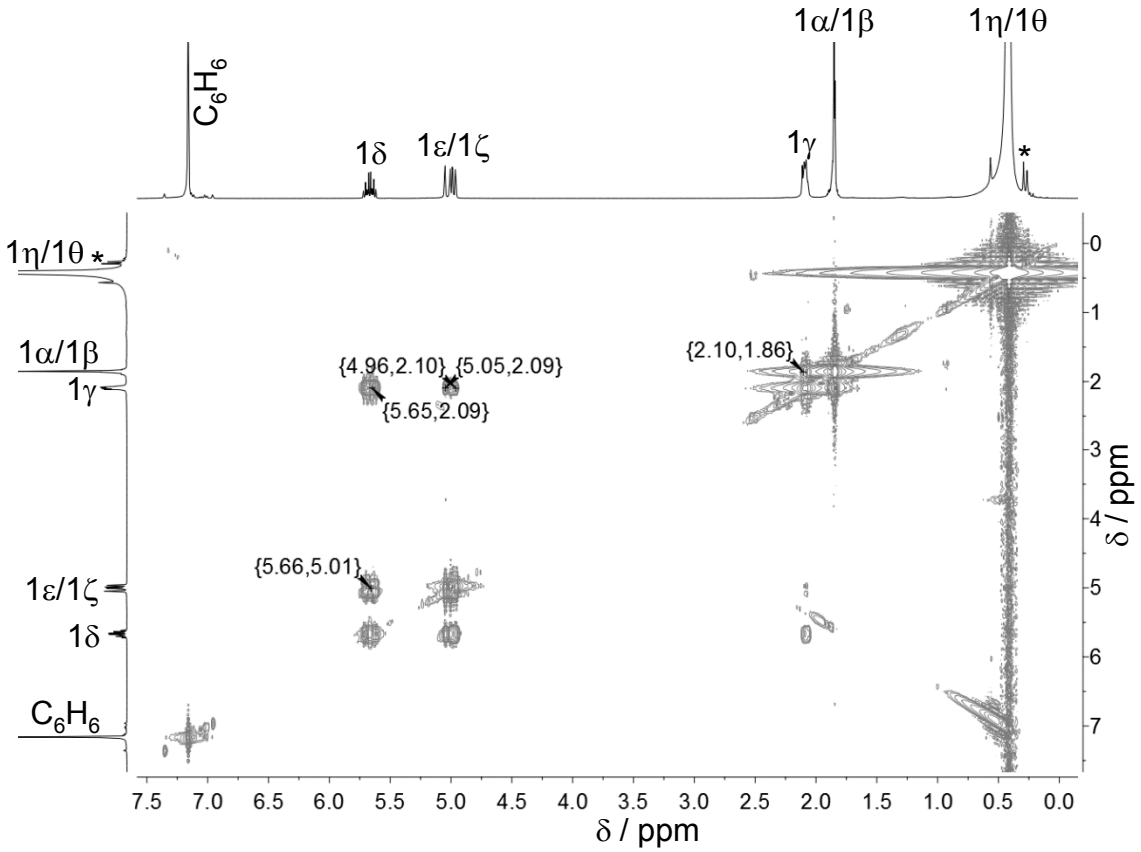

Figure S4. ^{13}C NMR spectrum of dissolved crystals of **1** in benzene-d_6 recorded at 296 K. The assignment of the signals was carried out under consideration of the corresponding HSQC and HMBC NMR spectra shown in figure S6 and figure S7.

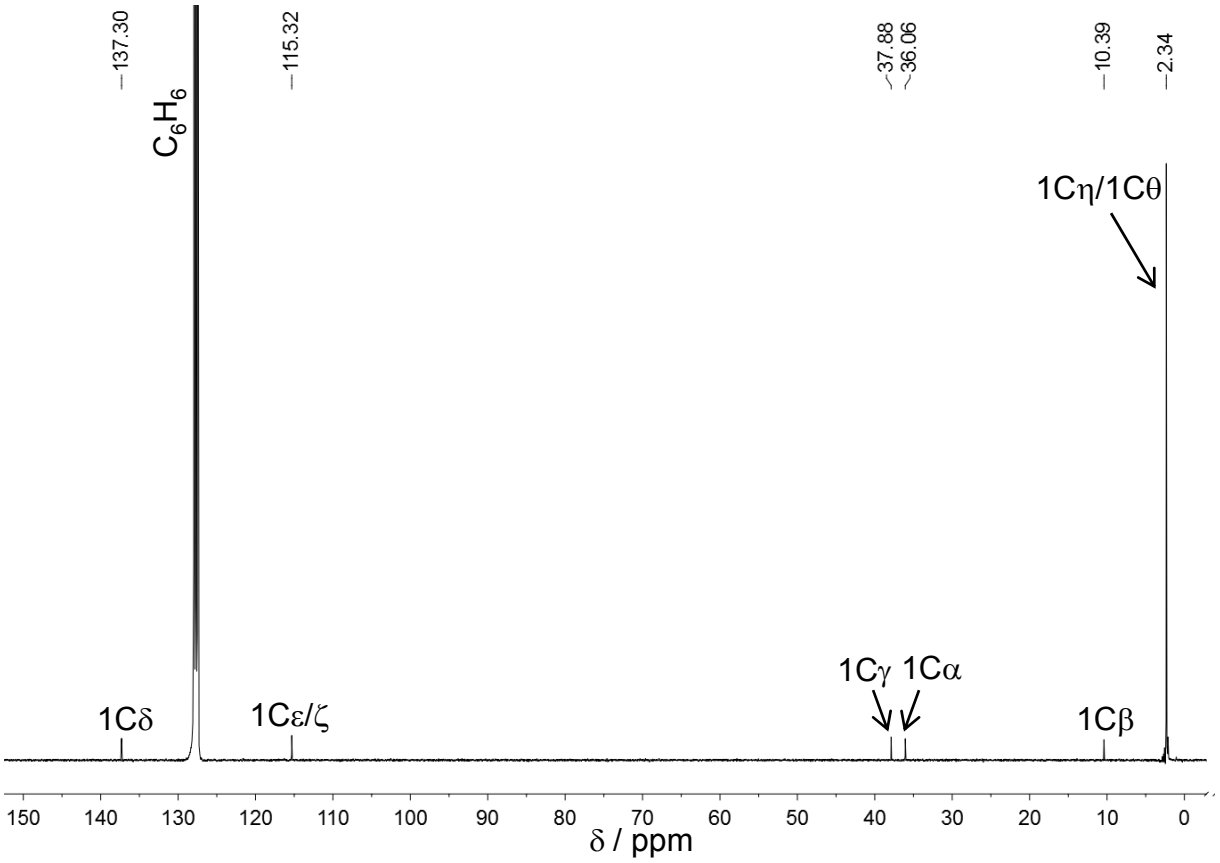

Figure S5. HSQC NMR spectrum of dissolved crystals of **1** in benzene-d_6 recorded at 296 K. The signal marked with * couldn't be assigned.

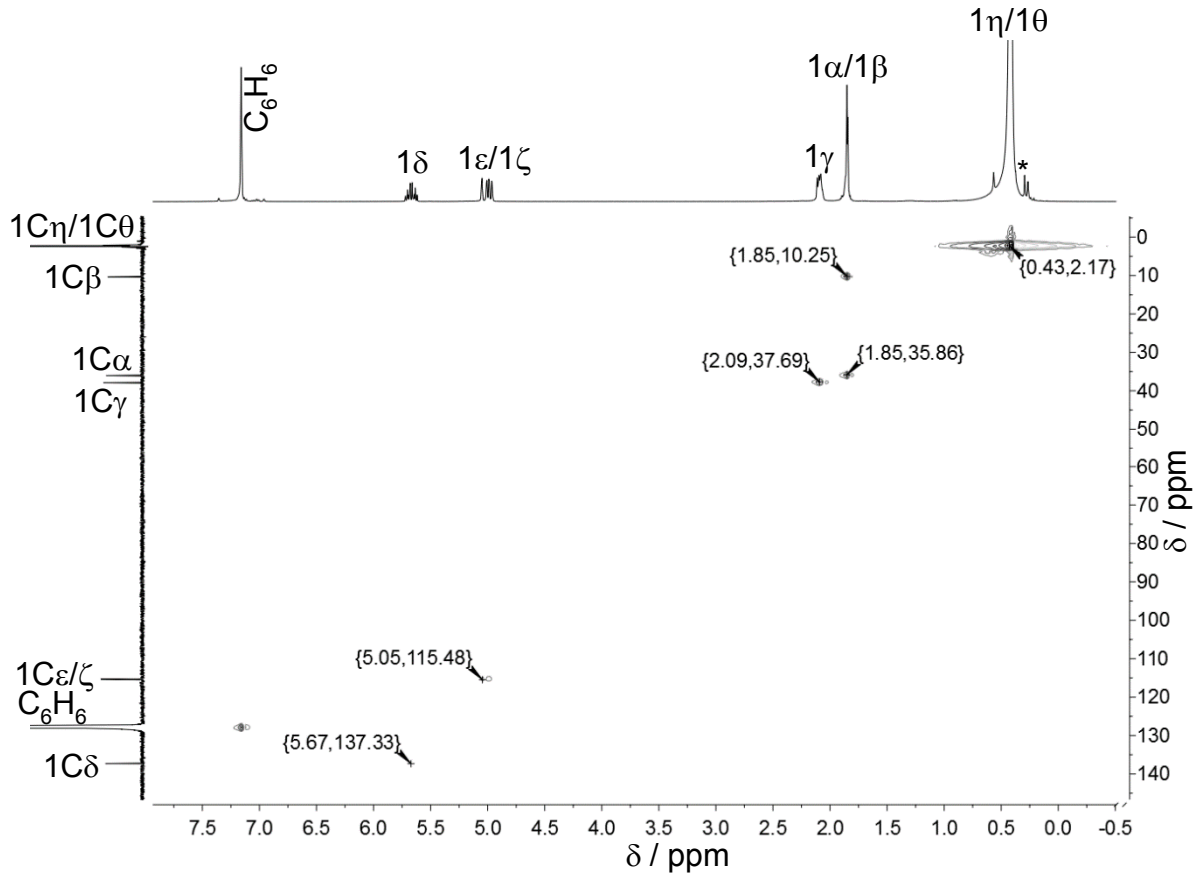

Figure S6. HMBC NMR spectrum of dissolved crystals of **1** in benzene-d_6 recorded at 296 K. The signal marked with * couldn't be assigned.

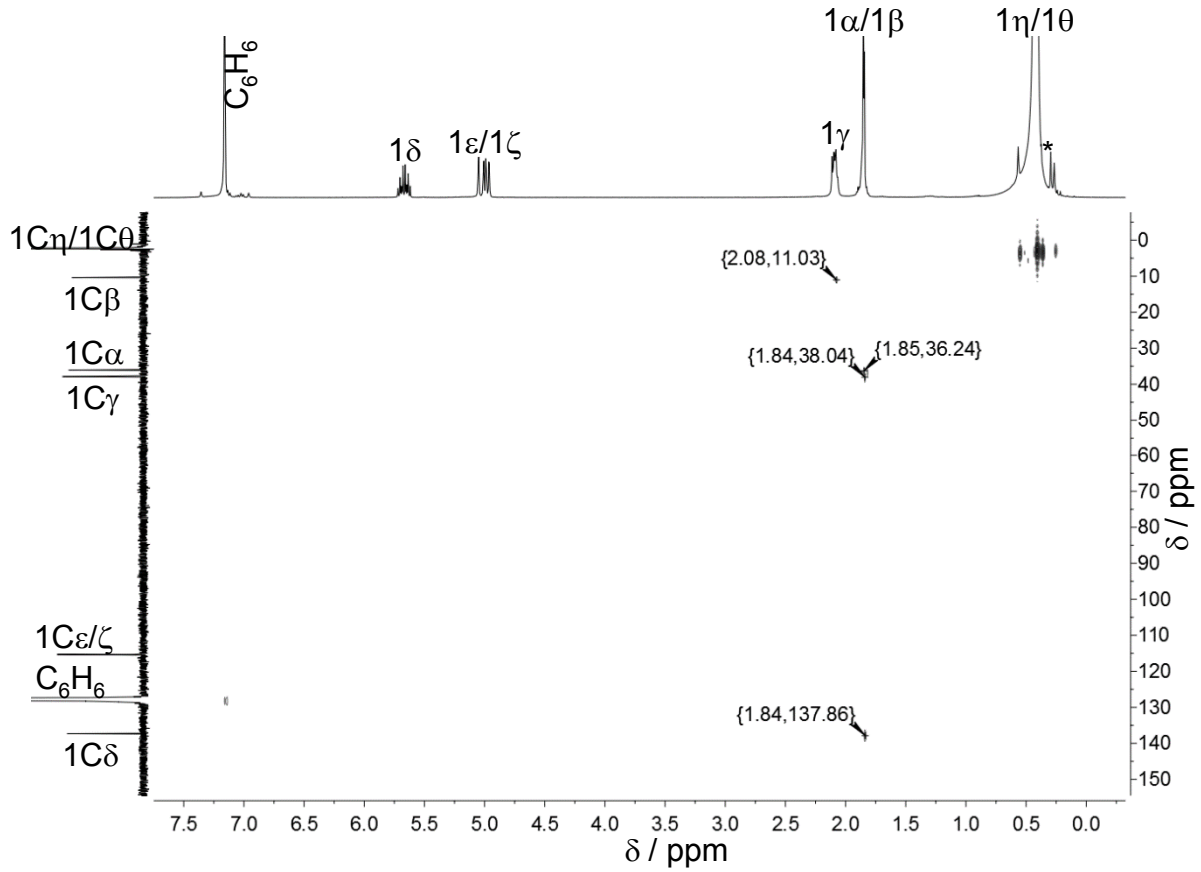

Figure S7. ^{29}Si NMR spectrum of dissolved crystals of **1** in benzene-d_6 recorded at 296 K.

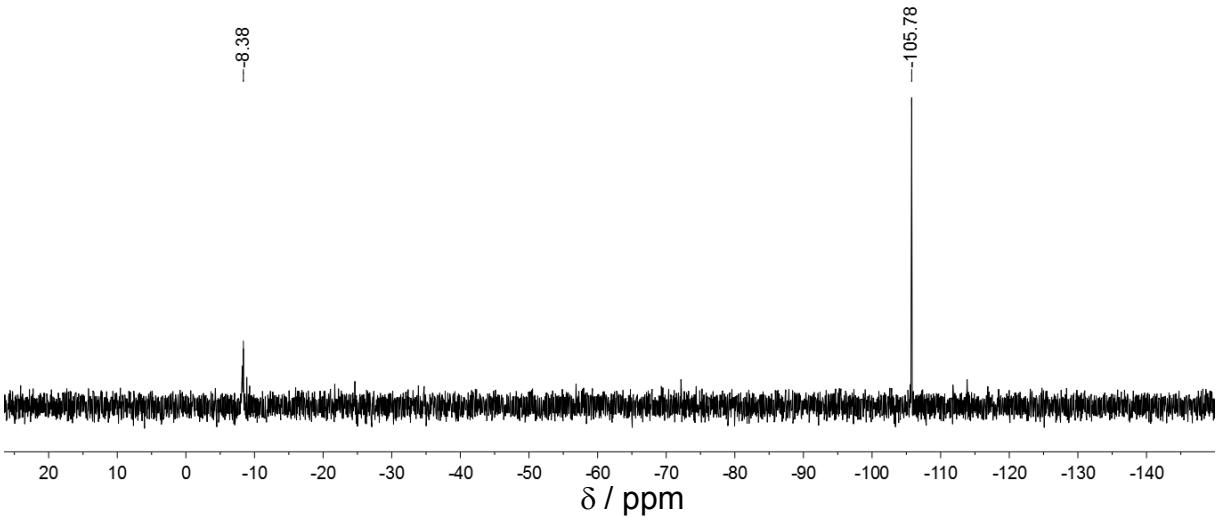

Figure S8. Temperature-dependent ^{1}H NMR study of dissolved crystals of **1** in toluene-d_8. For reasons of clarity only the relevant signals of the hypersilyl groups are depicted.

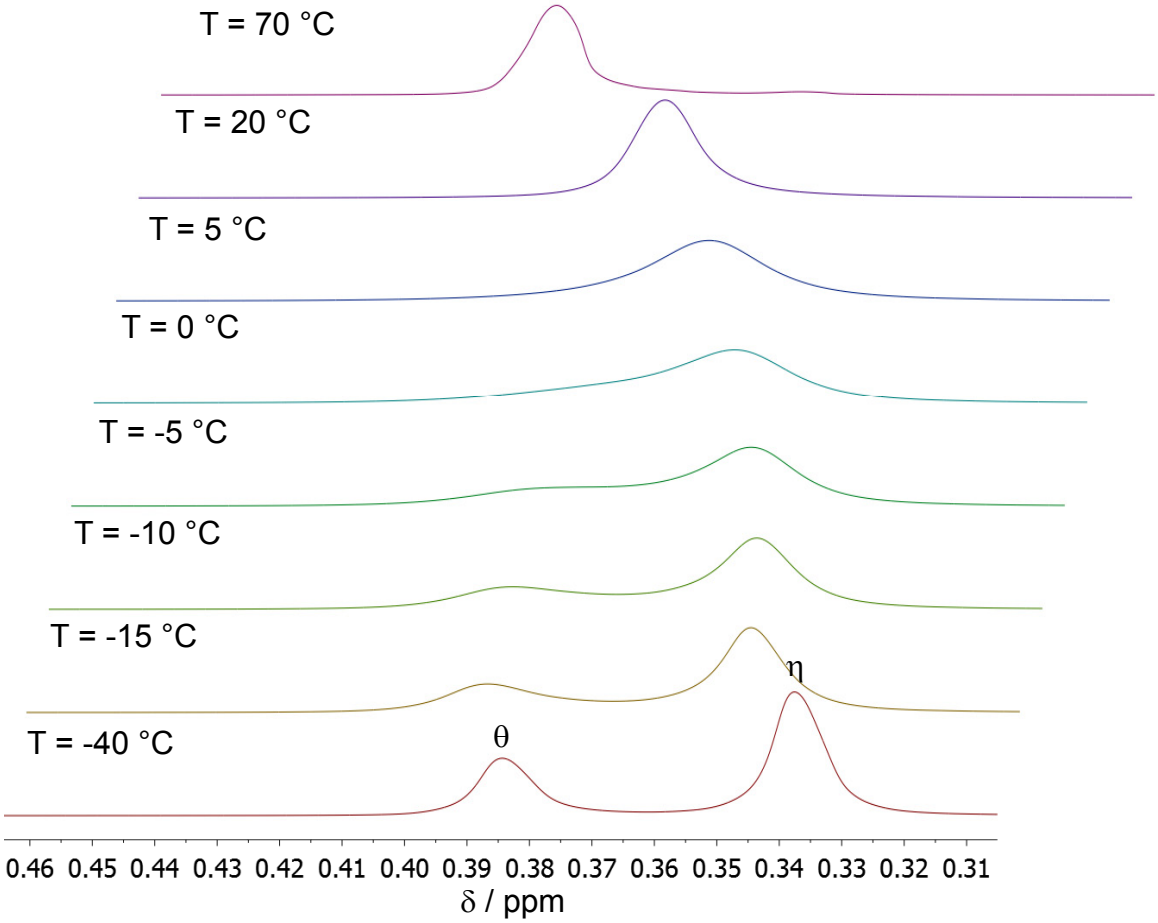

According to the temperature-dependent ^{1}H NMR spectra (figure S8) the coalescence temperature T_c is determined to be 273 K. Assuming that the rotation obeys the rate law of a first order reaction the rate constant of the rotation k_r at T_c according to Eyring equation is 40.9 s^{-1}. Therefore the Free Gibbs Energy of the rotation (ΔG_{273}) is calculated to be 58.1 kJ mol^{-1}.

Figure S9. ^{1}H NMR spectrum of crystals of **1** in toluene-d_8 recorded at r.t. after stepwise heating to 70 °C (see Figure S8), and subsequent cooling to r.t.. Signals marked with * are assigned to decomposition products.

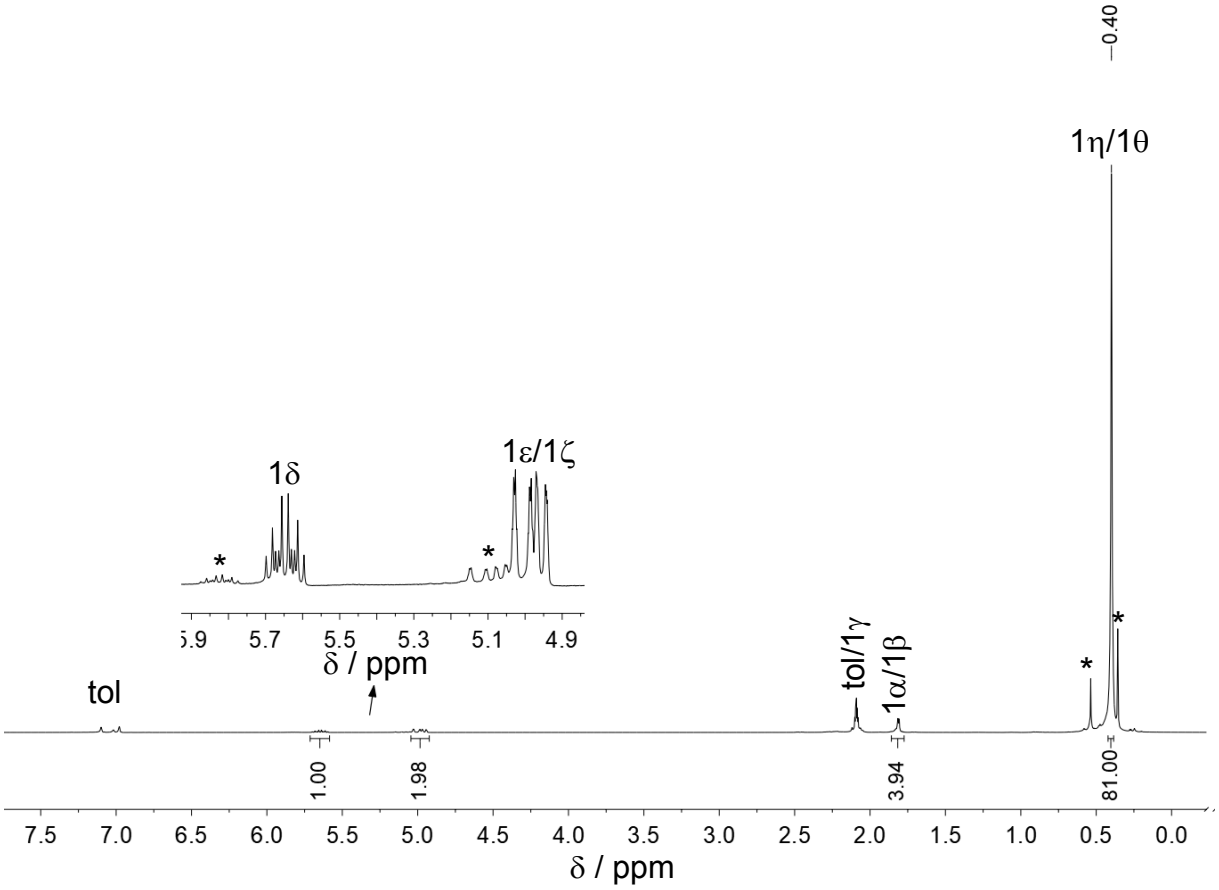

4 NMR spectra of [{Si(SiMe$_3$)$_3$}$_3$Ge$_9$CH$_2$CH=CH$_2$] (2)

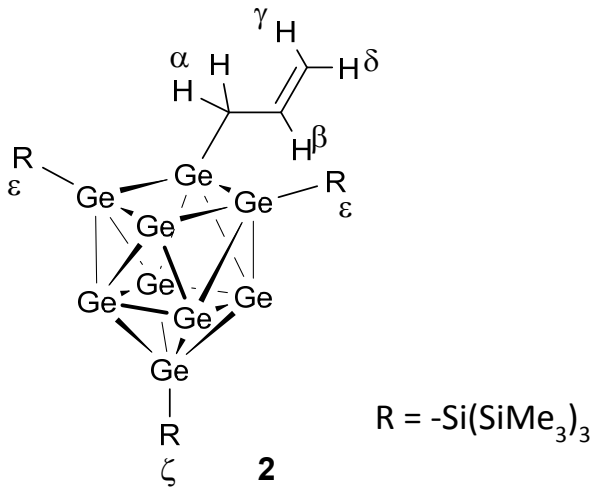

Scheme S2. The neutral cluster compound [{Si(SiMe$_3$)$_3$}$_3$Ge$_9$CH$_2$CH=CH$_2$] (**2**). Hydrogen atoms are labelled with Greek letters.

Figure S10. ^{1}H NMR spectrum of the crude product of **2** in benzene-d_6 recorded at 296 K. The signals highlighted in grey are magnified below. The assignment of the

signals is effected by the corresponding COSY NMR spectrum shown in figure S10. The signals marked with * could not be assigned.

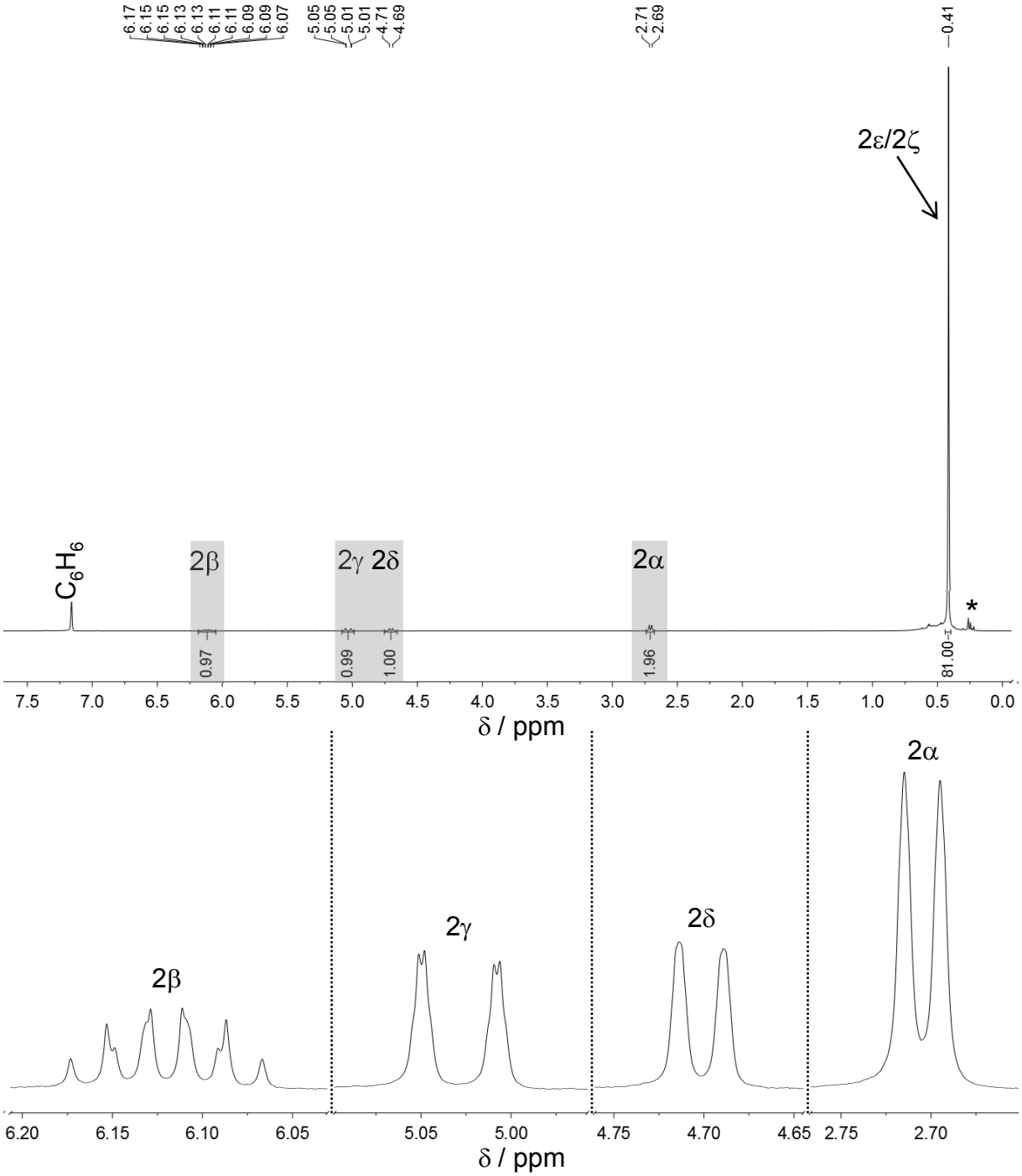

Figure S11. ^{1}H ^{1}H COSY NMR spectrum of the crude product of **2** in benzene-d_6 recorded at 296 K. The signals marked with * could not be assigned.

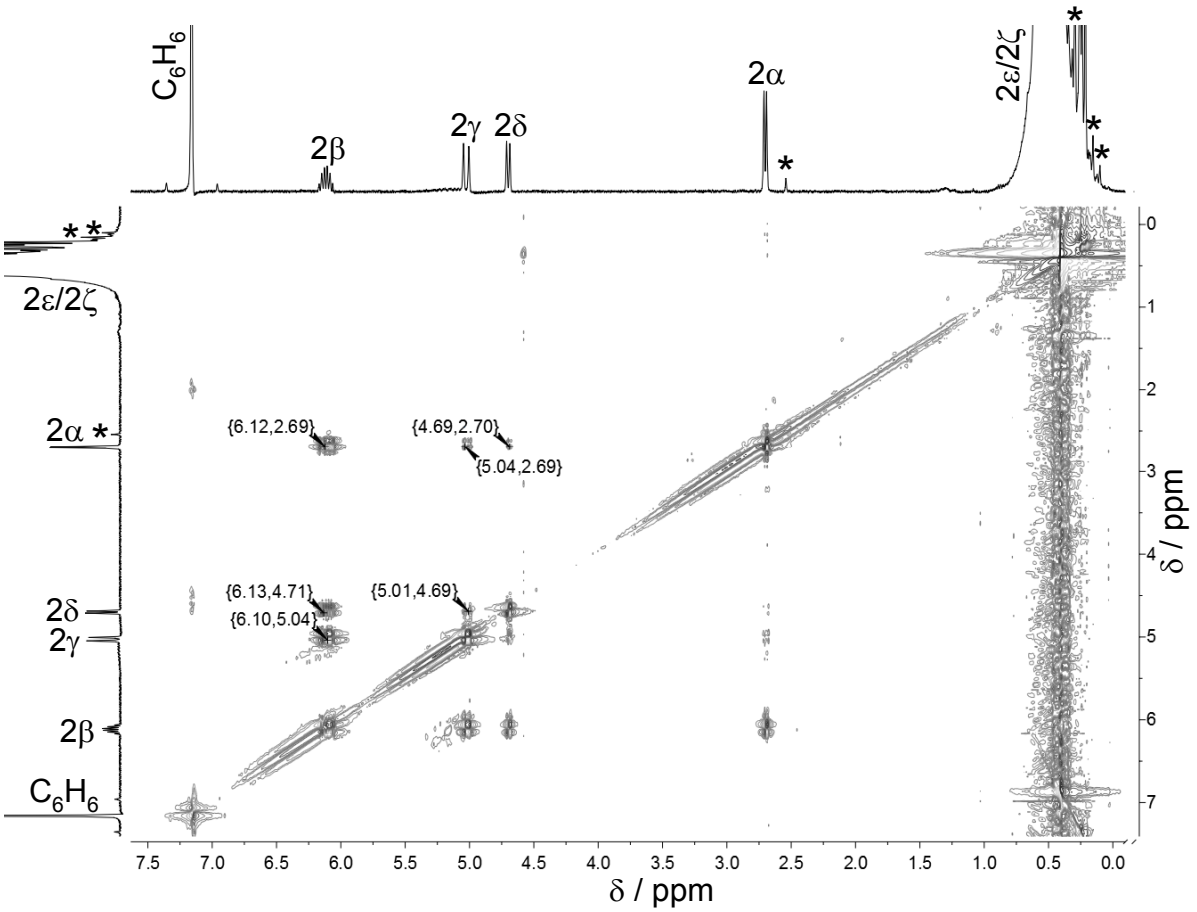

Figure S12. ^{13}C NMR spectrum of the crude product of **2** in benzene-d_6 recorded at 296 K. The assignment of the signals was carried out under consideration of the corresponding HSQC and HMBC NMR spectra shown in figures S12 and S13.

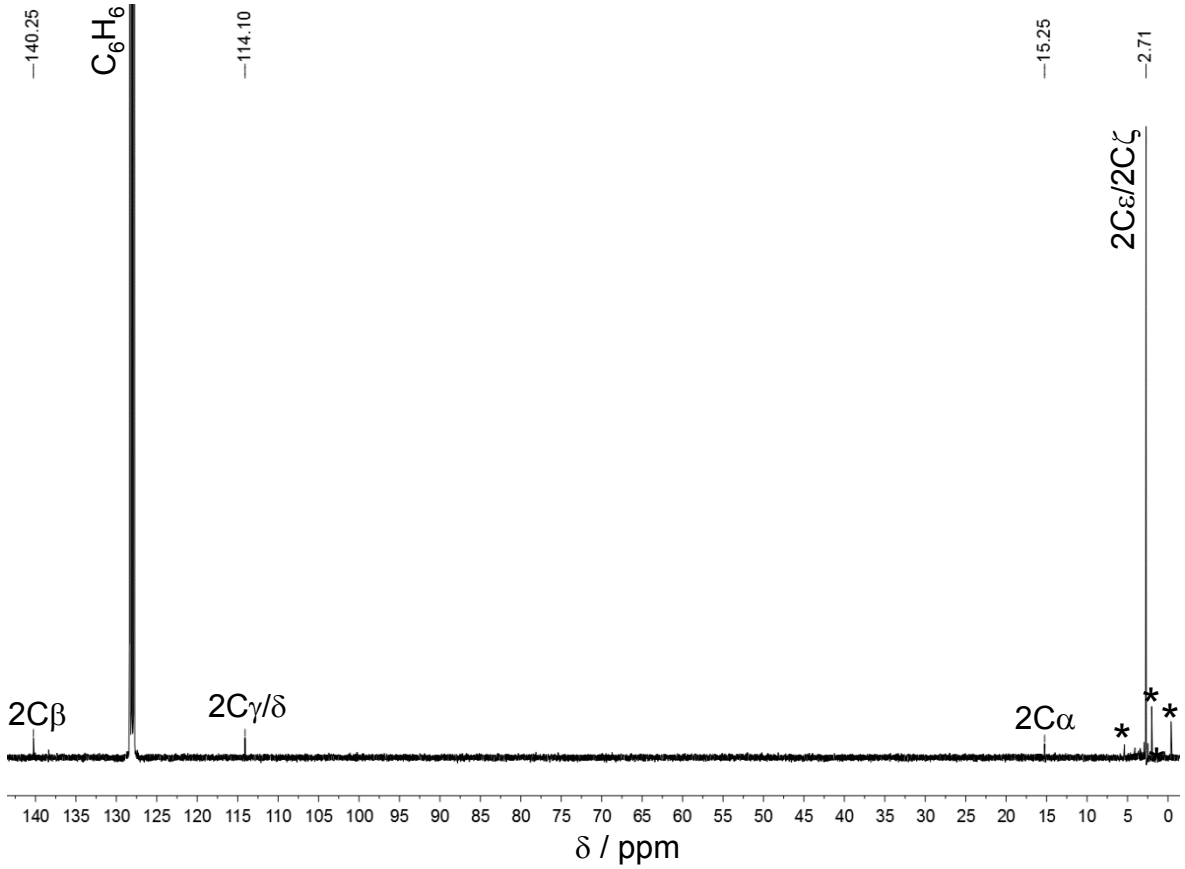

Figure S13. HSQC NMR spectrum of the crude product of **2** in benzene-d_6 recorded at 296 K. The signals marked with * could not be assigned.

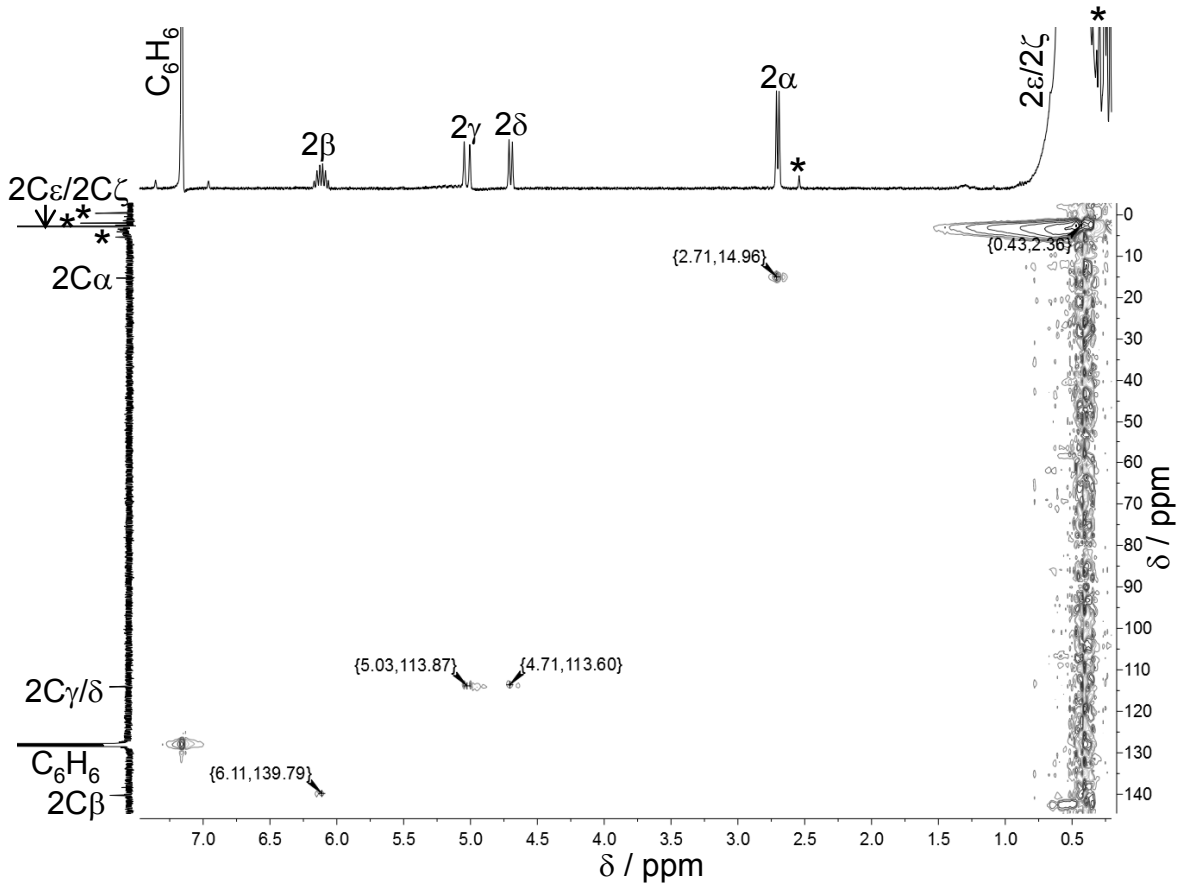

Figure S14. HMBC NMR spectrum of the crude product of **2** in benzene-d_6 recorded at 296 K. The signals marked with * could not be assigned.

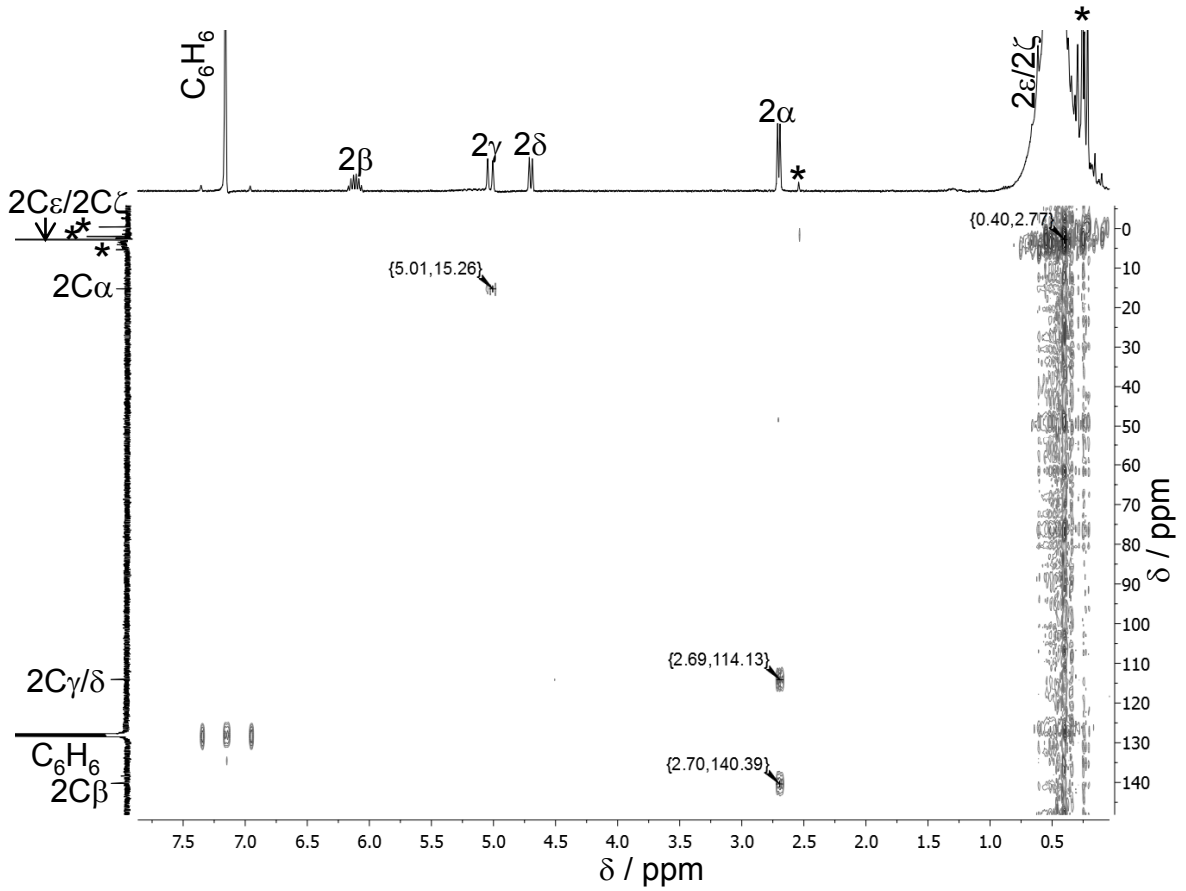

Figure S15. ^{29}Si NMR spectrum of the crude product of **2** dissolved in benzene-d_6 recorded at 296 K.

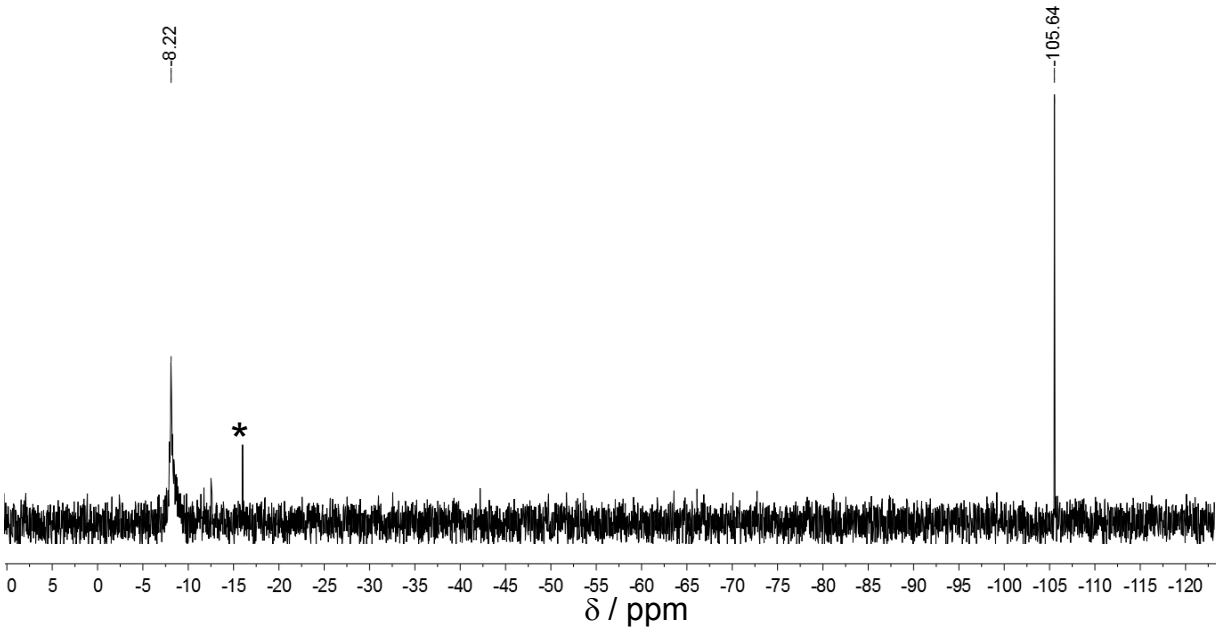

Figure S16. Temperature-dependent ^{1}H NMR study of the crude product of **2** in toluene-d_8. For reasons of clarity only the relevant signals of the hypersilyl groups are shown.

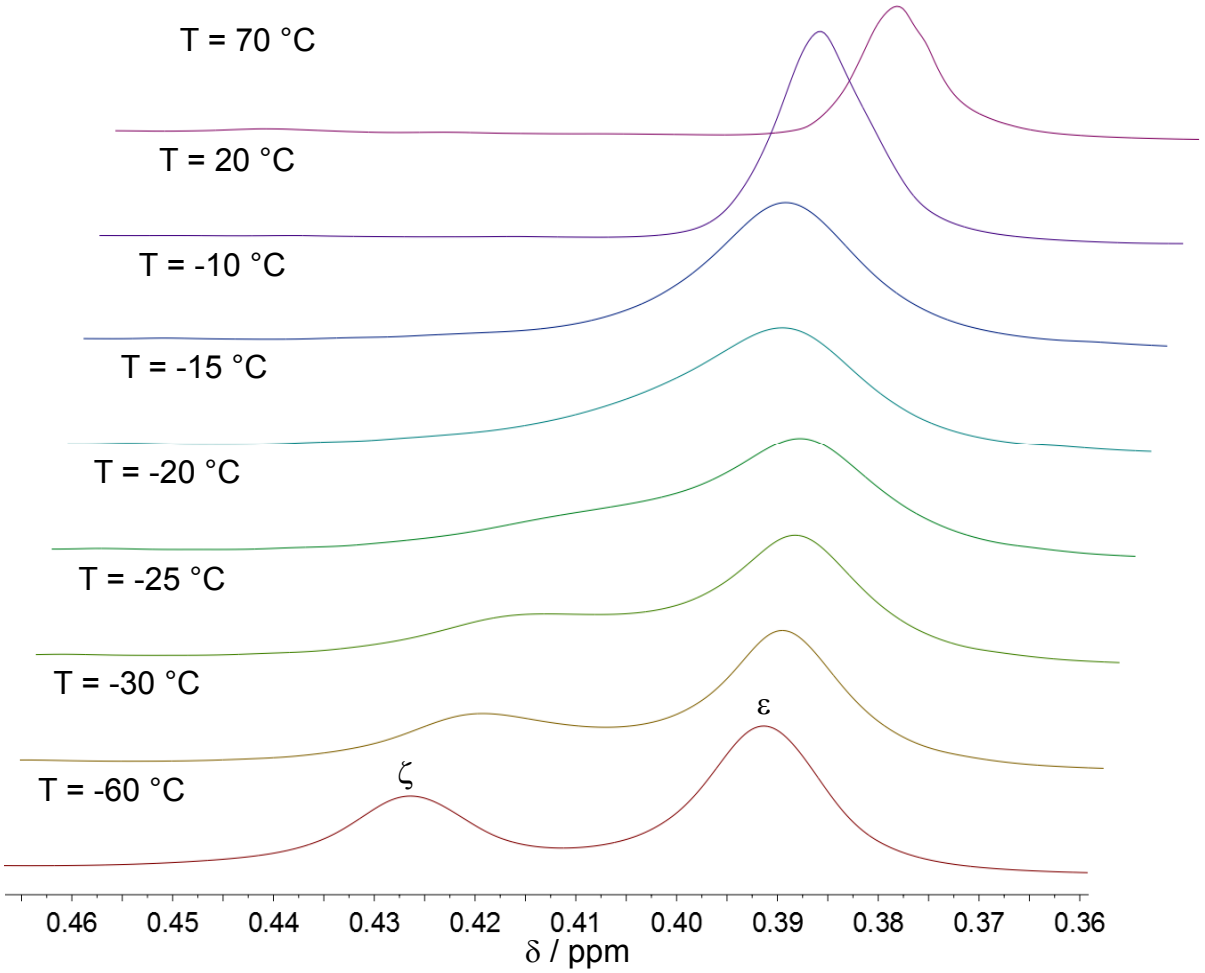

According to the temperature-dependent ^{1}H NMR spectra in figure S14 the coalescence temperature T_c is regarded to be 258 K. Assuming that the rotation obeys the rate law of a first order reaction the rate constant of the rotation k_r at T_c according to Eyring equation is 31.1 s^{-1}. Therefore the Free Gibbs Energy of the rotation (ΔG_{258}) is determined to be 55.4 kJ mol^{-1}.

Figure S17. ^{1}H NMR spectrum of the crude product of **2** in toluene-d_8 recorded at r.t. after stepwise heating to 70 °C (see Figure S16), and subsequent cooling to r.t.. Signals marked with * are assigned to decomposition products.

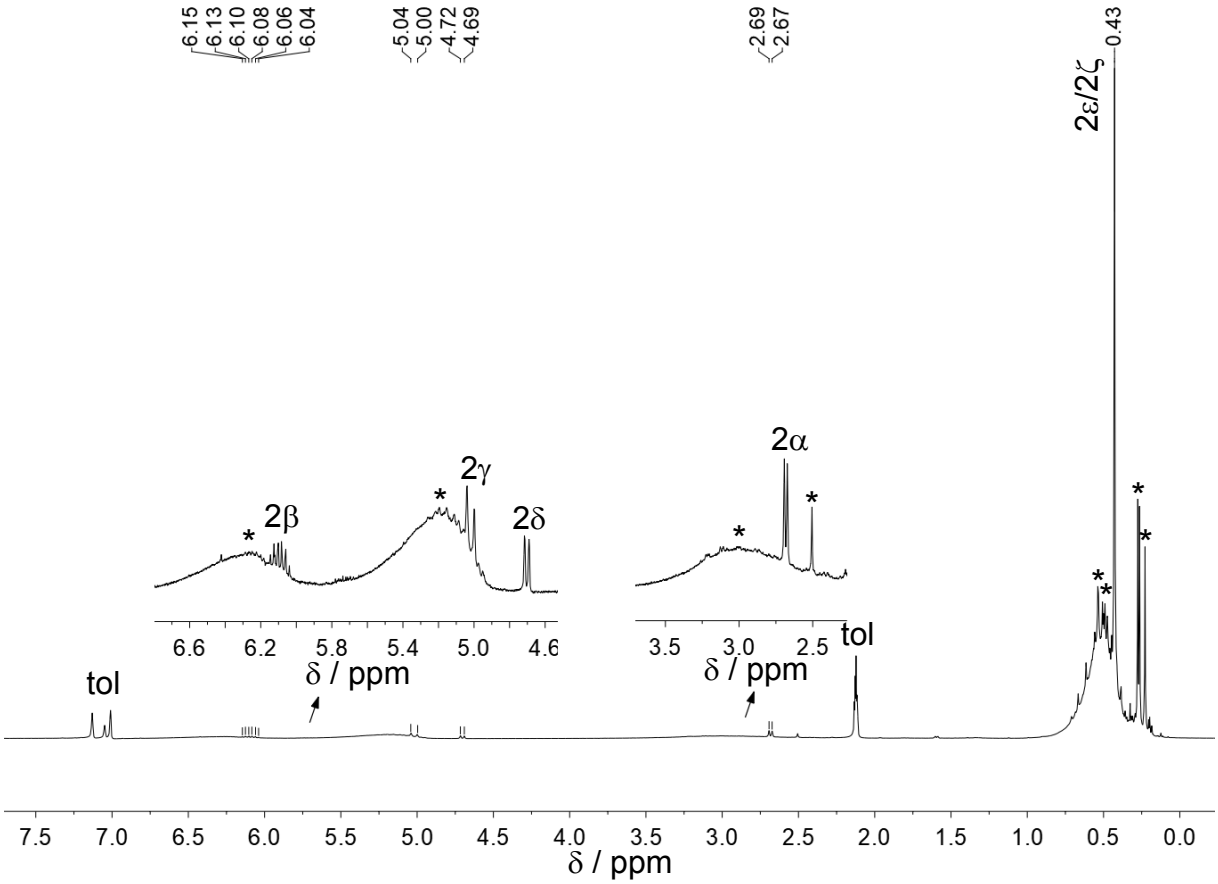

5 Raman spectrum

Figure S18. Raman spectrum of crystals of **1**.

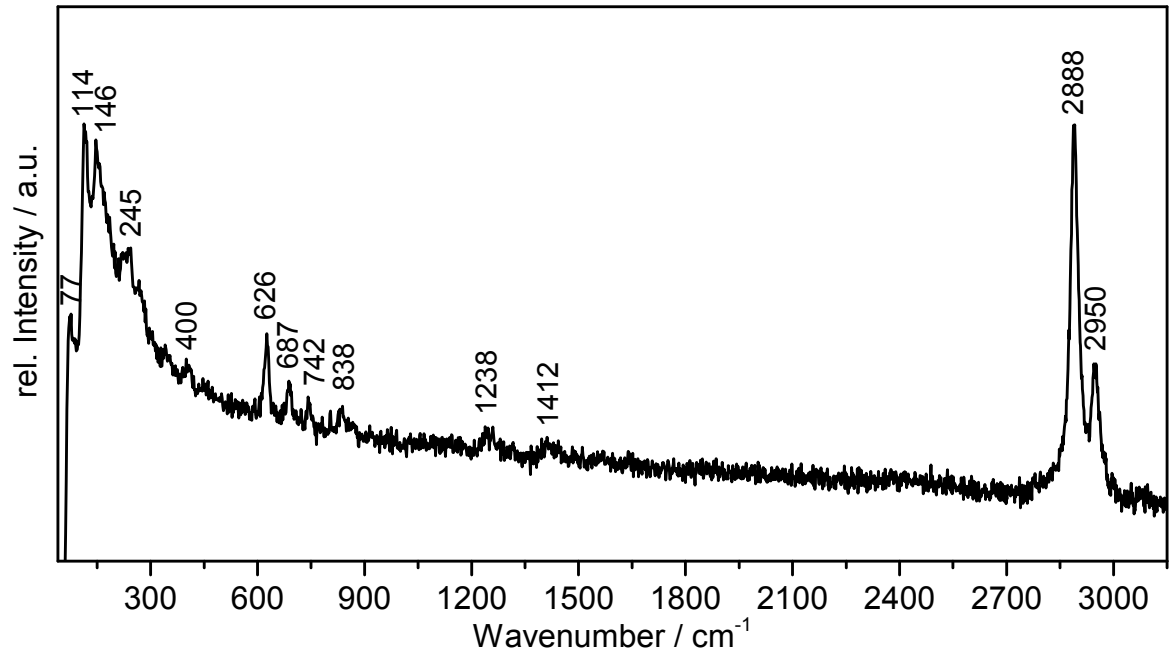

6 Electrospray-ionization mass spectra (ESI-MS)

Figure 19. ESI-MS spectrum (-) of the crude product of **1** in thf. Comparison of the measured spectrum (shown in black) and the corresponding simulated patterns (shown in red columns below).

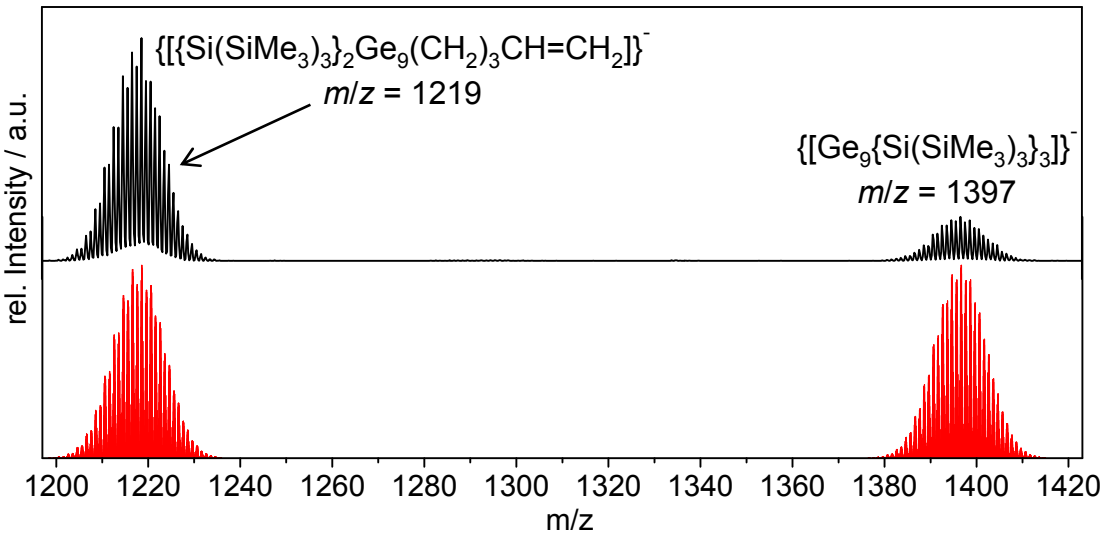

Figure S20. ESI-MS spectrum (-) of the crude product of **2** in thf. Comparison of the measured spectrum (shown in black) and the corresponding simulated patterns (shown in red columns below).

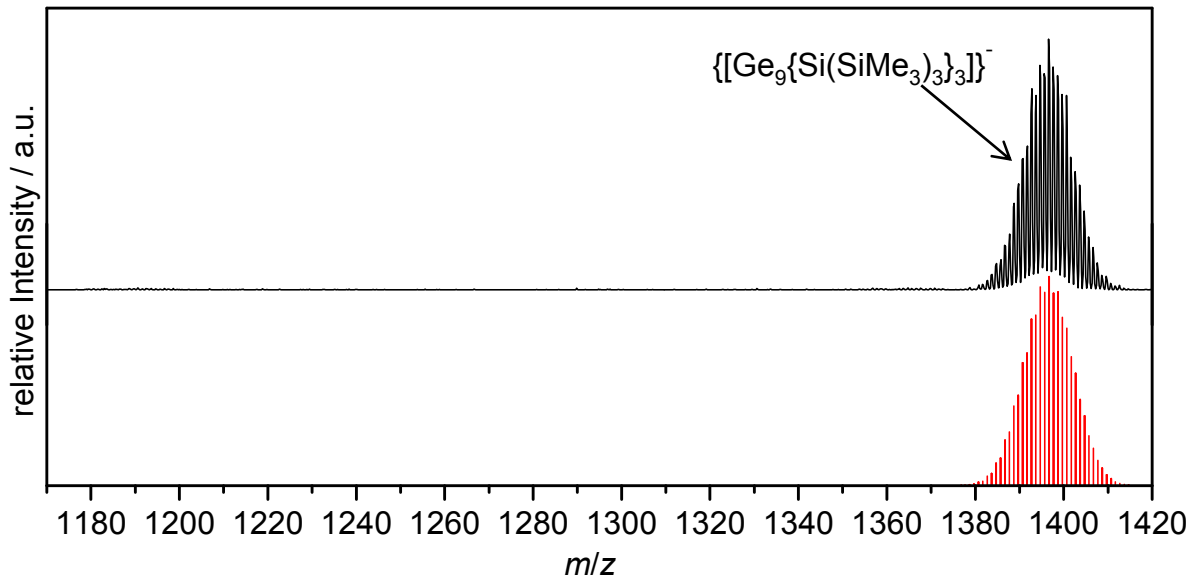

7 References

1 C. Hoch, M. Wendorff and C. Röhr, *J. Alloys Compd.*, 2003, **361**, 206.

2 F. Li and S. C. Sevov, *Inorg. Chem.*, 2012, **51**, 2706.

3 (a) P. Clifford, R. D. Bowen, H. G. Edwards and D. W. Farwell, *Anal. Chim. Acta*, 2007, **598**, 268; (b) B. H. Boo, *J. Korean Phys. Soc.*, 2011, **59**, 3192; (c) H. Von Schnering, M. Baitinger, U. Bolle, W. Carrillo-Cabrera, J. Curda, Y. Grin, F. Heinemann, J. Llanos, K. Peters and A. Schmeding, *Z. Anorg. Allg. Chem.*, 1997, **623**, 1037; (d) C. Fischer, W. Klein, L.-A. Jantke, L. J. Schiegerl and T. F. Fässler, *Z. Anorg. Allg. Chem.*, 2016, **642**, 1314.

4 G. M. Sheldrick, *Acta Cryst. C*, 2015, **71**, 3.

5.6 Acylation of Homoatomic Ge_9 Cages and Subsequent Decarbonylation

Sabine Frischhut, Wilhelm Klein, Markus Drees, and Thomas F. Fässler

published in:

Chem. Eur. J. **2018**, *24*, 9009-9014.

CONTENT AND CONTRIBUTION

Within the scope of this publication a new synthesis approach to specifically functionalize Ge_9 Zintl clusters is reported. The reaction of K[{$(Me_3Si)_3Si$}$_3Ge_9$] with various acyl chlorides in hexane or toluene selectively resulted in the formation of acyl functionalized Ge_9 clusters, namely {$(Me_3Si)_3$}$_3Ge_9$(CO)Me, {$(Me_3Si)_3$}$_3Ge_9$(CO)*i*Pr, {$(Me_3Si)_3$}$_3Ge_9$(CO)*t*Bu, {$(Me_3Si)_3$}$_3Ge_9$(CO)Ph, {$(Me_3Si)_3$}$_3Ge_9$(CO)CHC_3H_4, {$(Me_3Si)_3$}$_3Ge_9$(CO)CH_2Ph, {$(Me_3Si)_3$}$_3Ge_9$(CO)$(CH_2)_2$Ph, {$(Me_3Si)_3$}$_3Ge_9$(CO)$C_6H_4CH{=}CH_2$. All compounds were characterized by NMR spectroscopy (^{1}H, ^{29}Si, ^{13}C, COSY, HMBC, HSQC) within this work, including investigations on dynamic behavior *via* temperature-resolved ^{1}H NMR spectroscopic studies, which revealed dynamic behavior for all obtained neutral Ge_9 cluster products. {$(Me_3Si)_3$}$_3Ge_9$(CO)Me, {$(Me_3Si)_3$}$_3Ge_9$(CO)*i*Pr, {$(Me_3Si)_3$}$_3Ge_9$(CO)*t*Bu, {$(Me_3Si)_3$}$_3Ge_9$(CO)Ph were additionally characterized by single crystal X-ray crystallography. Dr. Wilhelm Klein assisted with structure determination.

Remarkably, {$(Me_3Si)_3$}$_3Ge_9$(CO)*t*Bu undergoes decarbonylation at r.t forming {$(Me_3Si)_3$}$_3Ge_9$*t*Bu, which was characterized by NMR spectroscopy and single crystal X-ray diffraction. The release of CO gas was detected by injecting the gas phase into an aqueous solution of $PdCl_2$. Most likely, {$(Me_3Si)_3$}$_3Ge_9$(CO)CH_2Ph also undergoes decarbonylation, however, due to decomposition of the product the decarbonylation could not be unequivocally shown. Time-resolved and temperature-dependent *in situ* ^{1}H NMR investigations on the decarbonylation were performed within this work.

Quantum chemical calculations revealed that the mechanism of the decarbonylation of {$(Me_3Si)_3$}$_3Ge_9$(CO)*t*Bu proceeds most likely according to a Norrish type I radical mechanism, where the α-bond is cleaved forming {$(Me_3Si)_3$}$_3Ge_9$· and ·(CO)*t*Bu. The latter easily releases CO resulting in ·tBu, which recombines with {$(Me_3Si)_3$}$_3Ge_9$· to form {$(Me_3Si)_3$}$_3Ge_9$*t*Bu. Dr. Markus Drees performed the DFT calculations on the decarbonylation reaction of {$(Me_3Si)_3$}$_3Ge_9$(CO)*t*Bu.

Data evaluation was carried out within this work. The publication was authored within this thesis. The manuscript was revised by Prof. Dr. Thomas F. Fässler.

ChemPubSoc Europe

DOI: 10.1002/chem.201802318

CHEMISTRY A European Journal Communication

Germanium Clusters

Acylation of Homoatomic Ge_9 Cages and Subsequent Decarbonylation

Sabine Frischhut,[a] Wilhelm Klein,[a] Markus Drees,[b] and Thomas F. Fässler*[a]

Abstract: The direct acylation of Ge_9 Zintl clusters by the reaction of $K[Ge_9\{Si(SiMe_3)_3\}_3]$ with acyl chlorides in hexane or toluene solutions is presented, leading to the neutral, carbonyl-derivatized products $[\{Si(SiMe_3)_3\}_3Ge_9(CO)R']$ (R′= Me, *i*Pr, *t*Bu, Ph, Bz, cyclopropylmethyl, phenethyl, 4-vinylphenyl). This reaction is applicable to a wide range of acyl chlorides and allows for diverse functionalization of Ge_9 Zintl clusters. $[\{Si(SiMe_3)_3\}_3Ge_9(CO)tBu]$ readily releases CO at ambient conditions under formation of $[\{Si(SiMe_3)_3\}_3Ge_9tBu]$. This temperature-dependent decarbonylation most likely proceeds via a radical Norrish-type I α-bond cleavage. Except for R′=*t*Bu and Bz all obtained acyl-derivatized Ge_9 cluster compounds do not release CO even at elevated temperatures. All compounds were characterized by NMR spectroscopy. $[\{Si(SiMe_3)_3\}_3Ge_9(CO)R']$ (R′=*t*Bu, Ph, Me, *i*Pr) as well as $[\{Si(SiMe_3)_3\}_3Ge_9tBu]$ were further structurally characterized by single crystal X-ray diffraction.

Fullerenes have attracted great interest due to their outstanding properties since their discovery in the 1980's.[1] As was stated in the early 2000's, there is a striking similarity between fullerenes and the homoatomic tetrel E_9 deltahedral cage molecules of the heavier homologues of carbon *E* despite the different electronic bonding properties within the cage structures.[2] Both classes of compounds retain their structures in solution and are flexible upon reversible oxidization, and in both cases oxidative coupling leads to the formation of anionic polymeric chains such as $^1{}_\infty\{C_{70}{}^{2-}\}$[3] and $^1{}_\infty\{[Ge_9]^{2-}\}$.[4] Fullerenes and Ge_9 Zintl clusters therefore present excellent "superatomic" building blocks for the bottom-up synthesis of complex structures with switchable electronic properties. Many different synthetic approaches have been developed to obtain organofunctionalized fullerenes, which have been summarized in various review articles.[5] Special notice is drawn on the acyl-functionalization of fullerenes that allows for a selective derivatization.[6] Even though Ge_9 Zintl clusters have been discovered long before fullerenes,[7] their functionalization has still only been vaguely explored. Nevertheless, only recently, the linkage of Ge_9 Zintl clusters via a conjugated organic 1,3-butadiene-1,4-diyl bridge, forming the so-called fullerene triad-analogous (non-)functionalized Zintl triads $[A(2,2,2\text{-crypt})]_6[Ge_9C_4H_4Ge_9]$[8] and $[A(2,2,2\text{-crypt})]_4[RGe_9C_4H_4Ge_9R]$ (R = (2*Z*,4*E*)-7-amino-5-aza-hepta-2,4-dien-2-yl, vinyl; *A* = K, Rb),[9] was achieved. The latter species comprise of extended conjugated π-electronic systems and are accessible by treating A_4Ge_9 (*A* = K, Rb) with 1,4-bis(trimethylsilyl)butadiene, (3*Z*/3*E*)-7-amino-1-(trimethylsilyl)-5-aza-hepta-3-en-1-yne or bis(trimethylsilyl)acetylene in ethylenediamine. The alkenylation of such clusters was intensively studied by Sevov and co-workers and is carried out by treating K_4Ge_9 with bis(trimethylsilyl)acetylene in ethylenediamine.[10] However, the above-mentioned Zintl triads are still highly charged and therefore show only limited solubility in less polar solvents. The decoration of Ge_9 clusters with silyl ligands reduces this charge, and thus compounds like $\{K(thf)\}\{[Si(SiMe_3)]_2Ge_9\text{-}SiMe_2\text{-}(C_6H_4)\text{-}SiMe_2\text{-}Ge_9[Si(SiMe_3)]_2K\}$ are much more soluble.[11]

Straightforward synthesis strategies for functionalized neutral Ge_9 Zintl clusters as in the case of fullerenes have not yet been developed, but are of crucial interest for the investigation of the physical properties of the products for potential applications in semiconductor devices.

The chemistry of Ge_9 Zintl clusters has been extended more and more towards common organic chemistry. Besides the already mentioned alkenylation of $[Ge_9]^{4-}$ clusters in ethylenediamine, alkylation can be achieved by the treatment of K_4Ge_9 with certain alkyl halides in ethylenediamine yielding at most doubly alkylated Ge_9 clusters which are still bearing two negative charges.[12] Reactions in ethylenediamine are often unpredictable and accompanied by the formation of side-products and low yields of the desired products.

The heterogeneous reaction of K_4Ge_9 with chloro-tris(trimethylsilyl)silane in acetonitrile to give, depending on the applied equivalents of the chlorosilane, the one- or twofold negatively charged silylated cluster species $K_{(4-n)}[Ge_9\{Si(SiMe_3)_3\}_n]$ (*n* = 2, 3) in high yields leads to a significant improvement of the solubility of the cluster compounds in common organic solvents, such as acetonitrile, tetrahydrofurane, and, for *n* = 3, also in toluene.[13] $[Ge_9\{Si(SiMe_3)_3\}_3]^-$ was first synthesized by Schnepf et al. in low yields applying metastable germanium halides.[14]

The functionalization of the Ge_9 cluster unit by silyl ligands has been thoroughly investigated in recent years,

[a] S. Frischhut, Dr. W. Klein, Prof. Dr. T. F. Fässler
Lehrstuhl für Anorganische Chemie mit Schwerpunkt Neue Materialien
Fakultät für Chemie, Technische Universität München
Lichtenbergstraße 4, 85747 Garching (Germany)
E-mail: Thomas.Faessler@lrz.tu-muenchen.de

[b] Dr. M. Drees
Lehrstuhl für Anorganische und Metallorganische Chemie
Fakultät für Chemie, Technische Universität München
Lichtenbergstraße 4, 85747 Garching (Germany)

Supporting information and the ORCID identification number(s) for the author(s) of this article can be found under:
https://doi.org/10.1002/chem.201802318.

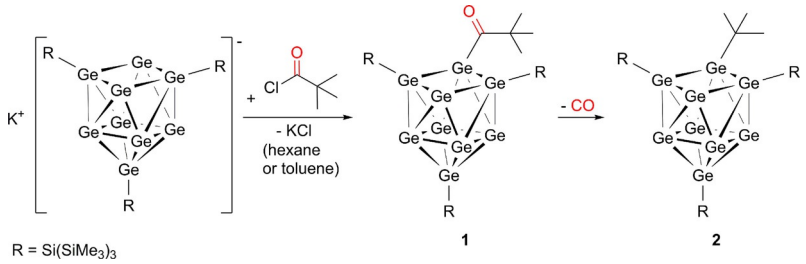

Scheme 1. Reaction of $K[Ge_9\{Si(SiMe_3)_3\}_3]$ with pivaloyl chloride in hexane or toluene yielding **1**. Subsequent release of CO leads to the formation of **2**.

with $[Ge_9\{Si(SiMe_3)_2(SiPh_3)\}_3]^-$,[15] $[Ge_9(SiHtBu_2)_3]^-$[16] and $[Ge_9\{Si(SiMe_3)_3\}_2(SiPh_2pentenyl)]^-$[17] as the most prominent products. Such silylated Ge_9 cluster entities show higher stability due to the shielding of the cluster core and the electronic effect of the ligands, but are still negatively charged and lack a direct organo-functionality. Only recently, phosphine-decorated $[Ge_9\{Si(SiMe_3)_3\}_n]^{(4-n)-}$ ($n=2$, 3) cluster compounds have been reported. The neutral species $[Ge_9\{Si(SiMe_3)_3\}_3PR_2]$ (R=Cy, *i*Pr) are of special interest as they carry a free electron pair at the phosphine ligand which allows for further reactions with Lewis acids to form for example the zwitterionic compounds $[Ge_9\{Si(SiMe_3)_3\}_3tBu_2P]M(NHC^{Dipp})$ (*M*=Cu, Ag, Au).[18]

$[Ge_9\{Si(SiMe_3)_3\}_3]^-$ is still reactive enough to undergo a nucleophilic substitution reaction with bromoethane in acetonitrile to give the cluster species $[\{Si(SiMe_3)_3\}_3Ge_9Et]$.[19] The latter is obtained in high yields and presents the first neutral and organo-functionalized Ge_9 cluster species which is soluble in non-polar solvents. Recent studies have shown that the introduction of an alkenyl functionality to the $[Ge_9\{Si(SiMe_3)_3\}_3]^-$ cluster core is also possible.[20] However, organo-functionalized neutral Ge_9 Zintl clusters are still rare.

The reactivity of Ge_9 clusters with other organic functionalities has remained widely unexplored. Even though acyl chlorides are widely used in organic syntheses, no attempts for the carbonyl-derivatization of Ge_9 Zintl clusters have been made yet. By contrast, the acyl-functionalization of mono-germanides by the reaction of $K[Ge(SiMe_3)_3]$ with acid fluorides to give $[(SiMe_3)_3Ge(CO)R]$ (R=mesityl, phenyl) has been published. Especially tetraacyl-germanides have a high potential as highly efficient photoinitiators for free-radical polymerization reactions.[21]

Herein we present a new approach to carbonyl-derivatized Ge_9 cluster compounds. $[Ge_9\{Si(SiMe_3)_3\}_3]^-$ is heterogeneously reacted with several Cl(CO)R′ compounds in hexane or toluene solutions resulting in the respective neutral carbonyl-functionalized Ge_9 cluster compounds $[\{Si(SiMe_3)_3\}_3Ge_9(CO)R']$ which are characterized by NMR spectroscopy and by single crystal X-ray diffraction. For $[\{Si(SiMe_3)_3\}_3Ge_9(CO)tBu]$ a radical decarbonylation reaction under formation of the *t*Bu-functionalized Ge_9 Zintl cluster $[\{Si(SiMe_3)_3\}_3Ge_9tBu]$ is observed, which opens a new pathway for the addition of organic ligands to tetrel cluster cores. Quantum-chemical calculations were carried out to give an indication for the mechanism of this decarbonylation reaction.

The functionalization of clusters by treatment of $[Ge_9\{Si(SiMe_3)_3\}_3]^-$ with alkyl halides in acetonitrile following the protocol of the syntheses of $[\{Si(SiMe_3)_3\}_3Ge_9Et]$[19] and $[\{Si(SiMe_3)_3\}_3Ge_9(CH_2)_nCHCH_2]$ ($n=1,3$)[20] turned out to be difficult, and NMR spectroscopic investigations of the respective precipitates obtained from the acetonitrile solutions showed the formation of unknown species as side-products. Therefore, we targeted a more efficient method for the synthesis of organo-functionalized neutral Ge_9 cluster species.

Fullerene-C_{60} can be selectively derivatized with acyl functionalities by a photochemical method using aldehydes and tetrabutylammonium decatungstate $[(nBu_4N)_4W_{10}O_{32}]$ as a catalyst. This reaction proceeds via a radical mechanism, and therefore the acyl addition to fullerenes often competes with the precedent decarbonylation.[6] In contrast to fullerenes, $[Ge_9\{Si(SiMe_3)_3\}_3]^-$ acts due to its negative charge as a nucleophile and thus should in principle be able to undergo reactions with acyl chlorides in an addition–elimination mechanism.

The reaction of $K[Ge_9\{Si(SiMe_3)_3\}_3]$ with 1 equivalent pivaloyl chloride at RT in [D8]toluene proceeded readily and afforded almost exclusively the mono-acylated Ge_9 cluster compound $[\{Si(SiMe_3)_3\}_3Ge_9(CO)tBu]$ (**1**) within 45 min (Scheme 1, Supporting Information). Remarkably, upon the storage of the reaction solution in an NMR tube at RT a decarbonylation of **1** occurs yielding almost exclusively $[\{Si(SiMe_3)_3\}_3Ge_9tBu]$ (**2**) after 23 d.

Exclusion of light did not noticeably prevent the decarbonylation of **1** (Supporting Information), and the decarbonylation proceeds much faster in hexane than in toluene or benzene (Supporting Information). However, a cooling of the solution of **1** to 2 °C inhibited the release of carbon monoxide, and the rate constant of the formation of **2** out of **1** is significantly lowered, the conversion from **1** to **2** proceeds much faster when the solution of the reaction of $K[Ge_9\{Si(SiMe_3)_3\}_3]$ with pivaloyl chloride in $[D_8]$toluene is heated (Supporting Information). In order to proof the release of CO during the conversion, a well-known, highly sensitive qualitative detection reaction for CO was applied[22] in which the gas phase after conversion of **1** into **2** was passed into an aqueous solution of $PdCl_2$. The precipitation of elemental Pd displayed CO in the injected gas phase. The decarbonylation reaction of **1** to yield **2** thus leads to the formation of a *t*Bu-decorated Ge_9 cluster which cannot be obtained directly via the treatment of $K[\{Si(SiMe_3)_3\}_3Ge_9]$ with *t*BuBr in acetonitrile in an S_N2 reaction analogous to the synthesis of $[\{Si(SiMe_3)_3\}_3Ge_9Et]$.

Compounds **1** and **2** were crystallized. The respective derivatized Ge_9 cluster compounds are shown in Figure 1. They both comprise three hypersilyl ligands and one organic moiety bound to Ge1 which is part of the open square of the C_s-symmetric Ge_9 clusters. The C_s-symmetric cluster shape is typical of Ge_9 clusters which bear four ligands.

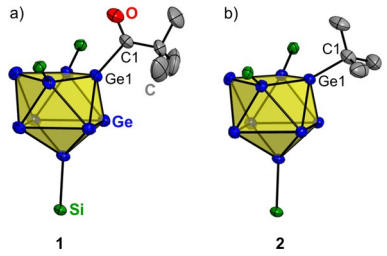

Figure 1. Structures of clusters a) [{Si(SiMe$_3$)$_3$}$_3$Ge$_9$(CO)*t*Bu] (**1**) and b) [{Si(SiMe$_3$)$_3$}$_3$Ge$_9$*t*Bu] (**2**). The Ge_9 units are drawn as yellow polyhedra. All atoms are shown at a probability level of 50%. Hydrogen atoms as well as the trimethylsilyl groups attached to the Ge_9-bound Si atoms are omitted for clarity.

In the following we consider three different reaction pathways to obtain **2** from **1**, which are summarized in Scheme 2.

Since compound **1** can be considered as a ketone, a radical decarbonylation reaction is reasonable in accordance with the Norrish-type I reaction. In this case the weakest α-bond is homolytically cleaved, thus leading to the most stable radicals with [{Si(SiMe$_3$)$_3$}$_3$Ge$_9$]$^\bullet$ and $^\bullet$(CO)*t*Bu or [{Si(SiMe$_3$)$_3$}$_3$Ge$_9$CO]$^\bullet$ and *t*Bu$^\bullet$ as the possible candidates (Scheme 2).[23] Acyl radicals are well-established species in organic syntheses.[24] The pivaloyl radical is known to readily release CO yielding *t*Bu$^\bullet$, which then can recombine again with [{Si(SiMe$_3$)$_3$}$_3$Ge$_9$]$^\bullet$ to give **2**. The driving force of the radical α-bond cleavage upon the release of CO is the formation of a stabilized new carbon-centered radical.[24,25] A recombination of two *t*Bu$^\bullet$ radicals is also feasible but due to the geminate processes the recombination of the initially formed radical pair is more likely. The decarbonylation of the pivaloyl radical occurs with a rate constant of $8.3\times10^5\ s^{-1}$ at 23 °C in hexane.[26] Normally an α-bond cleavage occurs upon irradiation to excite the ketone. In our case the cleavage is dependent on temperature but independent on irradiation with visible light, that is, the α-bond cleavage here is a thermal rather than a photochemical process, and the presence of the Ge_9 cluster therefore seems to have an influence on the radical cleavage of the ketone-like compound **1**.[27]

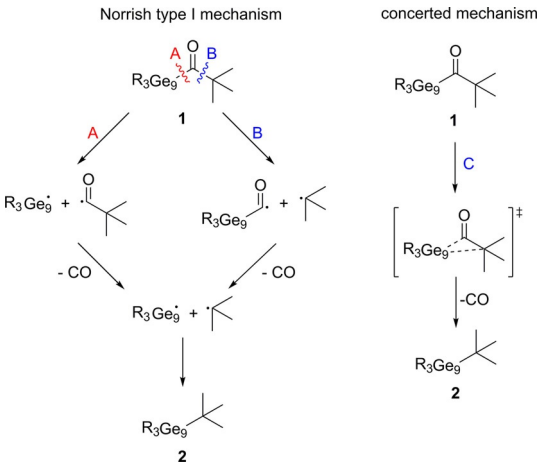

Scheme 2. Three conceivable reaction pathways of the decarbonylation of **1** yielding **2**. Reaction pathways A and B follow a Norrish-type I α-bond cleavage. Reaction pathway C runs through a concerted transition state.

Besides the radical processes (reaction pathways A and B in Scheme 2), also a concerted reaction mechanism with a cyclopropanoyl-like transition state, which leads to a weakening of the Ge_9–(CO) bond and subsequent release of CO, can be formulated (reaction pathway C).

To elucidate the reaction mechanism of the decarbonylation of the acylated Ge_9 Zintl cluster **1**, quantum-chemical calculations were performed. To apply cost-effective quantum-chemical methods, the bulky Si(SiMe$_3$)$_3$ groups were replaced by Me$_3$Si- groups, thus still retaining the Ge–Si bond character (Supporting Information). Pathway B (Scheme 2) could not be investigated by quantum-chemical methods as the key intermediate of this route, [{Si(SiMe$_3$)$_3$}$_3$Ge$_9$CO]$^\bullet$, did not appear as a local minimum on the potential hypersurface. Therefore, pathways A and C remain for comparison (Schemes 2 and Figure 2).

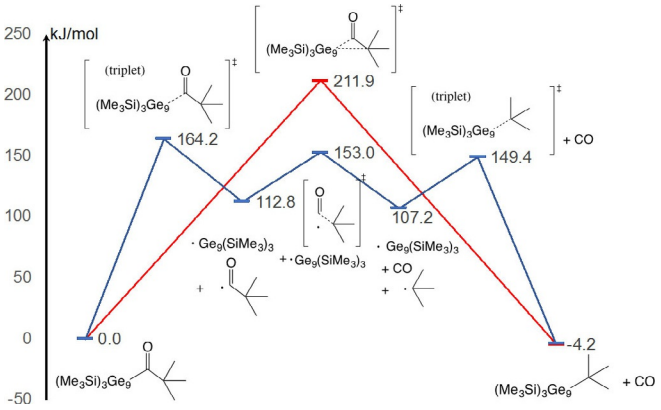

Figure 2. Free Energy (Δ*G*, kJ mol^{-1}) plot over the two compared pathways—red: concerted; blue: stepwise.

Based on our PBEPBE/Def2TVPP calculations, the total reaction to the *t*Bu adduct **2** is exergonic by $\Delta G = -4.2$ kJ mol^{-1}. The concerted pathway C is unlikely to occur because of a high barrier at its transition state of $\Delta G = +211.9$ kJ mol^{-1}. The stepwise mechanism A is therefore energetically more favored. The first step is the formation of the radicals Me$_3$Si–Ge$_9^\bullet$ and $^\bullet$CO–*t*Bu. The transition state of this homolytical bond cleavage between Ge_9 and CO–*t*Bu has a barrier of $\Delta G^{\neq} = +164.2$ kJ mol^{-1}. The radical pair as intermediate has a free energy of $+112.8$ kJ mol^{-1}. The next step, namely the decarbonylation of the CO–*t*Bu radical, to yield the *t*Bu radical requires an activation barrier of 40.3 kJ mol^{-1} (total free energy $\Delta G^{\neq} = +153.0$ kJ mol^{-1}). In sum, the intermediates Me$_3$Si–Ge$_9^\bullet$, $^\bullet$CO*t*Bu and CO have a Free Energy of formation of

+107.2 kJ mol^{-1}. Finally, recombination of the remaining radicals and formation of the product Me_3Si–Ge_9–*t*Bu as the final step requires an activation energy of 42.2 kJ mol^{-1} ($\Delta G^{\neq}$ = +149.4 kJ mol^{-1}) and leads to the overall exergonic product.

The scope of the acylation and subsequent decarbonylation was further explored by studying the reaction of K[{Si(SiMe$_3$)$_3$}$_3$Ge$_9$] with primary and secondary acyl chlorides Cl(CO)R′ (R′=Ph, Me, *i*Pr, Bz, cyclopropylmethyl, phenethyl, 4-vinylphenyl) as an easy way for specific functionalizations of Ge_9 Zintl clusters.

However, the reactions of K[{Si(SiMe$_3$)$_3$}$_3$Ge$_9$] with benzoyl chloride, acetyl chloride and isobutyryl chloride lead in all cases to the carbonyl products [{Si(SiMe$_3$)$_3$}$_3$Ge$_9$(CO)C$_6$H$_5$] (**3**), [{Si(SiMe$_3$)$_3$}$_3$Ge$_9$(CO)CH$_3$] (**4**) and [{Si(SiMe$_3$)$_3$}$_3$Ge$_9$(CO)CH(CH$_3$)$_2$] (**5**), and no release of CO could be detected even at elevated temperatures up to 60 °C (Figure 2).

This observation can be explained either by the higher stability of the acyl-derivatized Ge_9 compounds or by a slow CO elimination of the theoretically generated radicals upon Norrish-type I α-bond cleavage. In the supporting information, DFT calculations for the mechanism similar to Figure 2 are presented for compound **3**. The decarbonylation rates of several acyl radicals are summarized in the literature.[28]

Compounds **3**, **4** and **5** were crystallized (Supporting Information). All neutral acyl-derivatized Ge_9 cluster compounds, which are shown in Figure 3, comprise three hypersilyl ligands and one organic moiety bound to Ge1 which is part of the open square of the C_s-symmetric Ge_9 clusters.

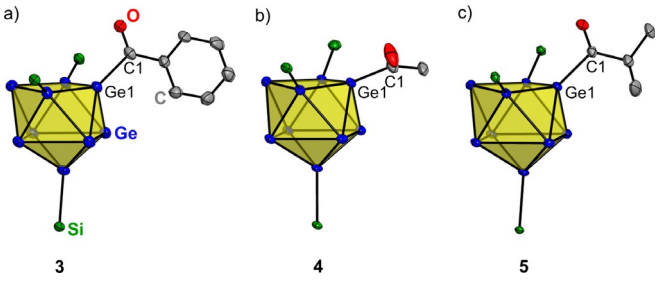

Figure 3. Structures of the clusters a) [{Si(SiMe$_3$)$_3$}$_3$Ge$_9$(CO)C$_6$H$_5$] (**3**), b) [{Si(SiMe$_3$)$_3$}$_3$Ge$_9$(CO)Me] (**4**) and c) [{Si(SiMe$_3$)$_3$}$_3$Ge$_9$(CO)*i*Pr] (**5**). The Ge_9 clusters are drawn as yellow polyhedra. All atoms are shown at a probability level of 50%. Hydrogen atoms as well as the trimethylsilyl groups attached to the Ge_9-bound Si atoms are omitted for clarity.

The Ge–Ge distances within the cluster cores are similar in all structures and are in the range from 2.4523(4) to 3.126(2) Å. The Ge1–C1 bond lengths of 2.054(9) Å (**1**), 2.05(1) Å (**2**), 2.036(9) Å (**3**), 2.058(6) Å (**4**), and 2.047(5) Å (**5**) are slightly elongated compared to Ge–C bonds in other organo-functionalized neutral Ge_9 cluster compounds (e.g. [{Si(SiMe$_3$)$_3$}$_3$Ge$_9$Et]: 1.973(4) Å, [{Si(SiMe$_3$)$_3$}$_3$Ge$_9$(CH$_2$)$_3$CH=CH$_2$): 1.970(3) Å).[19–20] The C=O bond lengths in **1**, **3**, **4**, and **5** of 1.22(1), 1.21(1), 1.202(8), and 1.192(5) Å, respectively, are typical of acyl chlorides.[31]

K[{Si(SiMe$_3$)$_3$}$_3$Ge$_9$] was also reacted with phenylacetyl chloride. The phenylacetyl radical shows a rate constant of 5.3×10^6 s^{-1} in hexane at 23 °C for the decarbonylation which is significantly higher than that of the pivaloyl radical, which is traced back to the high stability of the generated benzylic radical.[26] A mechanism discussion with DFT for this compound **6** is again presented in the Supporting Information. However, the treatment of K[{Si(SiMe$_3$)$_3$}$_3$Ge$_9$] with phenylacetyl chloride in [D$_6$]benzene at RT did not lead to the desired respective products, [{Si(SiMe$_3$)$_3$}$_3$Ge$_9$(CO)CH$_2$C$_6$H$_5$] and [{Si(SiMe$_3$)$_3$}$_3$Ge$_9$CH$_2$C$_6$H$_5$], respectively. The corresponding ^{1}H NMR spectra show broad signals which could not be assigned but hint at the presence of radicals in the solution. However, when the reaction is carried out at 0 °C in [D$_8$]toluene, the expected acyl derivative [{Si(SiMe$_3$)$_3$}$_3$Ge$_9$(CO)CH$_2$C$_6$H$_5$] (**6**) is obtained (Supporting Information), which is consistent with a fast radical α-bond cleavage. The solution may contain many radicals, which enhances unwanted radical recombinations and thus leads to a degradation of the phenylacetyl-derivatized Ge_9 cluster.

In order to probe the mechanism of the acylation of the Ge_9 cluster in K[Ge$_9${Si(SiMe$_3$)$_3$}$_3$], it was treated with cyclopropylacetyl chloride. The latter has been applied to trap radicals upon a reaction. Once the cyclopropylcarbinyl radical, known as a radical clock, is formed, it undergoes a fast rearrangement to the homoallylcarbinyl radical with a rate constant of 1.2×10^8 s^{-1} at 25 °C.[29] Only the cyclopropylacyl-derivatized Ge_9 cluster [{Si(SiMe$_3$)$_3$}$_3$Ge$_9$(CO)CH$_2$(C$_3$H$_5$)] (**7**) was obtained as could be concluded from the NMR spectra of the reaction solution (Supporting Information). Clearly, the Ge–(CO) bond remains intact, and the formation of the butenyl-functionalized Ge_9 cluster does not occur.

The acylation of Ge_9 Zintl clusters under formation of neutral functionalized clusters proceeds with a variety of acyl chlorides. The acylation with hydrocinnamoyl chloride and 4-vinylbenzoic acyl chloride leads to the cluster compounds [{Si(SiMe$_3$)$_3$}$_3$Ge$_9$(CO)(CH$_2$)$_2$(C$_6$H$_5$)] (**8**) and [{Si(SiMe$_3$)$_3$}$_3$Ge$_9$(CO)(C$_6$H$_4$)(CH=CH$_2$)] (**9**), respectively (Supporting Information).

The acylation of fullerenes is thermally controllable, and in contrast to compound **1**, the analogous fullerene species is stable at RT, does not release CO after the formation of the acylated compound, and a Norrish-type I bond cleavage does not proceed in the case of fullerenes.[6]

Temperature-dependent NMR spectroscopic investigations revealed that all neutral acylated cluster compounds **1** and **3**–**9** as well as the *t*Bu-functionalized compound **2** show dynamic behavior in solution (Supporting Information). The dynamic behavior of compounds **1**–**9** is due to a dynamic cluster framework and/or labile-bound silyl groups.[19,30] The acylated Ge_9 cluster species seem to be more flexible in solution than the alkylated species **2**, [{Si(SiMe$_3$)$_3$}$_3$Ge$_9$(CH$_2$)$_3$CH=CH$_2$] (ΔG= 58.1 kJ mol^{-1}) and [{Si(SiMe$_3$)$_3$}$_3$Ge$_9$CH$_2$CH$_3$] (ΔG = 63.9 kJ mol^{-1}), which show higher free activation energies for rotation.[19,20]

In conclusion, we have found a new route for the functionalization of Ge_9 Zintl clusters. The direct acylation proceeds by treating K[Ge$_9${Si(SiMe$_3$)$_3$}$_3$] with acyl chlorides in a one-step reaction in very good yields. The described reaction was found to be highly effective and applicable to a wide range of acyl chlorides leading to the acyl-derivatized Ge_9 Zintl cluster as the

major product. Exceptions are given by the pivaloyl- and phenylacetyl-functionalized Ge_9 clusters. The pivaloyl-functionalized and most likely also the phenylacetyl-functionalized Ge_9 cluster compound undergo a radical decarbonylation reaction which was shown by in situ NMR spectroscopic investigations. Quantum-chemical calculations suggested a radical Norrish-type I α-bond cleavage of the pivaloyl-functionalized Ge_9 cluster and subsequent CO elimination. The pivaloyl-functionalized Ge_9 cluster degrades to the *t*Bu-derivatized cluster, whereas the phenylacetyl-functionalized species decomposes. The decarbonylation was found to be a thermochemical process which can be suppressed by lowering the temperature. All in all, the acylation of Ge_9 Zintl clusters provides a new route towards a variety of neutral, with electron-withdrawing groups derivatized and previously unexplored Ge_9 Zintl cluster-based materials. The decarbonylation reaction of the pivaloyl-functionalized Ge_9 cluster compound suggests an influence of the cluster unit on the radical cleavage of bound organic moieties and therefore offers more interesting follow-up reactions to come. The Ge_9 Zintl clusters can now be decorated with electron-donor functionalities to build up fullerene-analogous neutral Ge_9 Zintl cluster-based donor–acceptor dyad systems with excellent solubility in convenient solvents, and the obtained derivatives $[\{Si(SiMe_3)_3\}_3Ge_9(CO)C_6H_5]$, $[\{Si(SiMe_3)_3\}_3Ge_9(CO)CH_2C_6H_5]$, $[\{Si(SiMe_3)_3\}_3Ge_9(CO)(CH_2)_2(C_6H_5)]$, and $[\{Si(SiMe_3)_3\}_3Ge_9(CO)(C_6H_5)(CH{=}CH_2)]$ may be ideal candidates for the formation of higher aggregates. The 4-vinylphenyl-derivatized Ge_9 cluster could even allow the synthesis of covalently linked polymers consisting of Ge_9 clusters.

Experimental Section

The supporting information includes experimental procedures, crystallographic details as well as computational details. CCDC 1812804 (**1**), 1812805 (**2**), 1812806 (**3**), 1812807 (**4**), and 1812808 (**5**) contain the supplementary crystallographic data for this paper. These data are provided free of charge by The Cambridge Crystallographic Data Centre.

Acknowledgements

S.F. is grateful to the Fonds der Chemischen Industrie for her fellowship. The authors thank the Bayerische Staatsministerium für Wirtschaft und Medien, Energie und Technologie within the program "Solar Technologies go Hybrid" for financial support. M.D. acknowledges the computing center of the Leibniz Rechenzentrum of the Bavarian Academy of Sciences for the provision of computing time on the HPC machines. The authors thank B.Sc. Kevin Frankievicz, B.Sc. Florian Petermichl and B.Sc. Louis Hartmann for their help in the syntheses and for fruitful discussions. Maria Weindl is acknowledged for temperature-dependent NMR measurements, and Dr. Annette Schier for revising the manuscript.

Conflict of interest

The authors declare no conflict of interest.

Keywords: acylation · functionalization · germanium clusters · radical decarbonylation · Zintl

[1] H. W. Kroto, J. R. Heath, S. C. O'Brien, R. F. Curl, R. E. Smalley, *Nature* **1985**, *318*, 162 – 163.
[2] a) T. F. Fässler, *Angew. Chem. Int. Ed.* **2001**, *40*, 4161 – 4165; *Angew. Chem.* **2001**, *113*, 4289 – 4293; b) T. F. Fässler, *Coord. Chem. Rev.* **2001**, *215*, 347 – 377.
[3] H. Brumm, E. Peters, M. Jansen, *Angew. Chem. Int. Ed.* **2001**, *40*, 2069 – 2071; *Angew. Chem.* **2001**, *113*, 2117 – 2119.
[4] C. Downie, Z. Tang, A. M. Guloy, *Angew. Chem. Int. Ed.* **2000**, *39*, 337 – 340; *Angew. Chem.* **2000**, *112*, 346 – 348.
[5] a) A. Hirsch, M. Brettreich, *Fullerenes, Chemistry and Reactions*, Wiley-VCH, Weinheim, **2005**; b) D. Bonifazi, O. Enger, F. Diederich, *Chem. Soc. Rev.* **2007**, *36*, 390 – 414; c) C. Thilgen, F. Diederich, *Chem. Rev.* **2006**, *106*, 5049 – 5135; d) N. Martín, *Chem. Commun.* **2006**, 2093 – 2104; e) F. Wudl, *J. Mater. Chem.* **2002**, *12*, 1959 – 1963; f) K. E. Geckeler, S. Samal, *Polym. Int.* **1999**, *48*, 743 – 757.
[6] M. D. Tzirakis, M. Orfanopoulos, *J. Am. Chem. Soc.* **2009**, *131*, 4063 – 4069.
[7] a) M. Joannis, *Comptes Rendus Acad. Sci.* **1891**, *113*, 795 – 798; b) C. Kraus, *Trans. Am. Electrochem. Soc.* **1924**, *45*, 175 – 186; c) E. Zintl, J. Goubeau, W. Dullenkopf, *Z. Phys. Chem.* **1931**, *154A*, 1 – 46; d) L. Diehl, K. Khodadadeh, D. Kummer, J. Strähle, *Chem. Ber.* **1976**, *109*, 3404 – 3418.
[8] M. M. Bentlohner, S. Frischhut, T. F. Fässler, *Chem. Eur. J.* **2017**, *23*, 17089 – 17094.
[9] a) M. M. Bentlohner, W. Klein, Z. H. Fard, L.-A. Jantke, T. F. Fässler, *Angew. Chem. Int. Ed.* **2015**, *54*, 3748 – 3753; *Angew. Chem.* **2015**, *127*, 3819 – 3824; b) S. Frischhut, M. M. Bentlohner, W. Klein, T. F. Fässler, *Inorg. Chem.* **2017**, *56*, 10691 – 10698.
[10] a) M. W. Hull, S. C. Sevov, *Inorg. Chem.* **2007**, *46*, 10953 – 10955; b) M. W. Hull, S. C. Sevov, *J. Am. Chem. Soc.* **2009**, *131*, 9026 – 9037.
[11] O. Kysliak, C. Schrenk, A. Schnepf, *Inorg. Chem.* **2017**, *56*, 9693 – 9697.
[12] M. W. Hull, A. Ugrinov, I. Petrov, S. C. Sevov, *Inorg. Chem.* **2007**, *46*, 2704 – 2708.
[13] a) F. Li, S. C. Sevov, *Inorg. Chem.* **2012**, *51*, 2706 – 2708; b) O. Kysliak, A. Schnepf, *Dalton Trans.* **2016**, *45*, 2404 – 2408.
[14] A. Schnepf, *Angew. Chem. Int. Ed.* **2003**, *42*, 2624 – 2625; *Angew. Chem.* **2003**, *115*, 2728 – 2729.
[15] O. Kysliak, C. Schrenk, A. Schnepf, *Inorg. Chem.* **2015**, *54*, 7083 – 7088.
[16] O. Kysliak, T. Kunz, A. Schnepf, *Eur. J. Inorg. Chem.* **2017**, 805 – 810.
[17] K. Mayer, L. J. Schiegerl, T. Kratky, S. Günther, T. F. Fässler, *Chem. Commun.* **2017**, *53*, 11798 – 11801.
[18] F. S. Geitner, J. V. Dums, T. F. Fässler, *J. Am. Chem. Soc.* **2017**, *139*, 11933 – 11940.
[19] F. Li, S. C. Sevov, *J. Am. Chem. Soc.* **2014**, *136*, 12056 – 12063.
[20] S. Frischhut, T. F. Fässler, *Dalton Trans.* **2018**, *47*, 3223 – 3226.
[21] J. Radebner, A. Eibel, M. Leypold, C. Gorsche, L. Schuh, R. Fischer, A. Torvisco, D. Neshchadin, R. Geier, N. Moszner, *Angew. Chem. Int. Ed.* **2017**, *56*, 3103 – 3107; *Angew. Chem.* **2017**, *129*, 3150 – 3154.
[22] A. F. Holleman, E. Wiberg, N. Wiberg, *Vol. 101*, de Gruyter, Berlin, New York, **1995**, p. 866.
[23] W. M. Horspool, P.-S. Song, *CRC Handbook of Organic Photochemistry and Photobiology, Vol. 1*, CRC Press, Boca Raton, FL, **1995**.
[24] C. Chatgilialoglu, D. Crich, M. Komatsu, I. Ryu, *Chem. Rev.* **1999**, *99*, 1991 – 2070.
[25] a) H. Fischer, H. Paul, *Acc. Chem. Res.* **1987**, *20*, 200 – 206; b) C. Chatgilialoglu, C. Ferreri, M. Lucarini, P. Pedrielli, G. Pedulli, *Organometallics* **1995**, *14*, 2672 – 2676.
[26] Y. P. Tsentalovich, H. Fischer, *J. Chem. Soc. Perkin Trans. 2* **1994**, 729 – 733.
[27] In case of the pristine $[Ge_9]$ clusters, stable $[Ge_9]^{3-}$ radicals are known. a) C. H. E. Belin, J. D. Corbett, A. Cisar, *J. Am. Chem. Soc.* **1977**, *99*, 7163 – 7169; b) T. F. Faessler, M. Hunziker, *Inorg. Chem.* **1994**, *33*, 5380 – 5381.

[28] I. Ryu, N. Sonoda, *Angew. Chem. Int. Ed. Engl.* **1996**, *35*, 1050 – 1066; *Angew. Chem.* **1996**, *108*, 1140 – 1157.
[29] V. W. Bowry, J. Lusztyk, K. Ingold, *J. Am. Chem. Soc.* **1991**, *113*, 5687 – 5698.
[30] F. Li, A. Muñoz-Castro, S. C. Sevov, *Angew. Chem. Int. Ed.* **2016**, *55*, 8630 – 8633; *Angew. Chem.* **2016**, *128*, 8772 – 8775.
[31] N. O. Sonntag, *Chem. Rev.* **1953**, *52*, 237 – 416.

Manuscript received: May 8, 2018
Accepted manuscript online: May 13, 2018
Version of record online: June 1, 2018

CHEMISTRY
A European Journal

Supporting Information

Acylation of Homoatomic Ge_9 Cages and Subsequent Decarbonylation

Sabine Frischhut,[a] Wilhelm Klein,[a] Markus Drees,[b] and Thomas F. Fässler*[a]

chem_201802318_sm_miscellaneous_information.pdf

SUPPORTING INFORMATION

Table of Contents

1 Experimental Procedures

General: All manipulations were carried out under a purified argon atmosphere using standard Schlenk techniques. The Zintl phase with the nominal composition K_4Ge_9 was synthesized by heating a stoichiometric mixture of the elements K and Ge (99.999%, Chempur) at 650 °C for 46 h in a stainless steel autoclave.[1] The solvents acetonitrile, toluene and hexane were dried over molecular sieve in a solvent purification system MB-SPS. The deuterated solvents [D6]benzene and [D8]toluene were purchased from Deutero GmbH and stored over molecular sieve (3 Å) for at least one day. The commercially available reagents acetyl chloride (Alfa Aesar, 98%), benzoyl chloride (Acros Organics, ≥98%), chloro-tris(trimethylsilyl)silane (TCI Chemicals, ≥95.0%), hydrocinnamoyl choride (Sigma-Aldrich, 98%), isobutyryl chloride (Acros Organics, 98%), phenylacetyl chloride (Sigma-Aldrich, 98%) and pivaloyl chloride (Sigma-Aldrich, 99%) were used as received. Cyclopropylacetic acid[2] and 4-vinylbenzoic acyl chloride[3] were synthesized according to literature procedures.

Synthesis of [{Si(SiMe$_3$)$_3$}$_3$Ge$_9$(CO)^{t}Bu] (1)
First, compound K[Ge$_9${Si(SiMe$_3$)$_3$}$_3$] was synthesized according to a literature procedure.[4] K_4Ge_9 (93 mg, 0.11 mmol) was weighed out in a Schlenk tube in a glove box. A solution of chlorotris(trimethylsilyl)silane (97 mg, 0.34 mmol) in 3 mL acetonitrile was added to the Zintl phase, and the obtained suspension was stirred overnight. The resulting solution was filtered over a glass fiber filter, and the solvent was evaporated in a vacuum. In a second step, the obtained solid was suspended in 3 mL hexane. A solution of pivaloyl chloride (14 μL, 0.11 mmol) dissolved in 3 mL hexane was prepared. Both solutions were cooled to 0 °C. While stirring, the pivaloyl chloride/hexane solution was added dropwise to the suspension containing K[{Si(SiMe$_3$)$_3$}$_3$Ge$_9$] within 5 min whereupon a deep-brown solution was formed. The solution was stirred for additional two hours at 0 °C, transferred to a glove box and filtered over glass fiber filter. The filtrate was stored at –32 °C for crystallization. Within one month a small amount of deep-orange block-shaped crystals suitable for X-ray diffraction analysis were obtained. ^{1}H NMR (400 MHz, [D8]toluene, 298 K): δ(ppm) 1.14 (s, 9H, C(CH_3)$_3$), 0.41 (s, 81H, CH_3 on hypersilyl).

Synthesis of [{Si(SiMe$_3$)$_3$}$_3$Ge$_9$^{t}Bu] (2)
K[Ge$_9${Si(SiMe$_3$)$_3$}$_3$] was synthesized according to the procedure described above for compound **1** using the same amounts of reactants. The as obtained K[{Si(SiMe$_3$)$_3$}$_3$Ge$_9$] was suspended in 3 mL hexane. A solution of pivaloyl chloride (14 μL, 0.11 mmol) dissolved in 3 mL hexane was added dropwise to the suspension within 5 min upon stirring. The obtained deep-brown solution was stirred for additional 17 h at r.t. and then filtered over a glass fiber filter in a glove box. The solvent was removed in a vacuum. The obtained solid was dissolved in 3.5 mL toluene and stored at −32 °C for crystallization. Within 3 weeks block-shaped crystals suitable for X-ray diffraction analysis were obtained (yield 40%). The crystals were separated from the mother liquor and washed three times with a total amount of 2 mL acetonitrile, dried in a vacuum, dissolved in a deuterated solvent and characterized by NMR spectroscopy. ^{1}H NMR (400 MHz, [D8]toluene, 298 K): δ(ppm) 1.63 (s, 9H, C(CH_3)$_3$), 0.43 (s, 81H, CH_3 on hypersilyl); ^{13}C{^{1}H} NMR (101 MHz, [D8]toluene, 298 K): δ(ppm) 39.66 (s, *C*(CH$_3$)$_3$), 39.38 (q, C(*C*H$_3$)$_3$), 3.43 (q, Si(*C*H$_3$)$_3$); ^{29}Si NMR (79 MHz, [D8]toluene, 298 K): δ(ppm) −8.12 (*Si*(CH$_3$)$_3$); ^{1}H ^{13}C HSQC (400 MHz/101 MHz, [D8]toluene, 298 K): δ(ppm)/δ(ppm) 1.63/38.59 (^1J, C(C*H*$_3$)$_3$/C(*C*H$_3$)$_3$), 0.43/2.62 (^1J, Si(C*H*$_3$)$_3$/Si(*C*H$_3$)$_3$); ^{1}H ^{13}C HMBC (400 MHz/101 MHz, [D8]toluene, 298 K): δ(ppm)/δ(ppm) 1.64/39.43 (^2J, C(C*H*$_3$)$_3$/*C*(CH$_3$)$_3$), 0.43/3.43 (^1J, Si(C*H*$_3$)$_3$/Si(*C*H$_3$)$_3$). elemental analysis calcd (%): C 25.61, H 6.24; found: C 26.36, H 6.25.

Synthesis of [{Si(SiMe$_3$)$_3$}$_3$Ge$_9$(CO)C$_6$H$_5$] (3)
K_4Ge_9 (47 mg, 0.06 mmol) was weighed out into a Schlenk tube in a glove box. A solution of chlorotris(trimethylsilyl)silane (49 mg, 0.17 mmol) in 1.5 mL acetonitrile was added to the Zintl phase. The resulting suspension was stirred for 21 h. The solution was filtered over a glass fiber filter and the solvent removed in a vacuum. In a following heterogeneous reaction the solid containing K[Ge$_9${Si(SiMe$_3$)$_3$}$_3$] was suspended in 1.5 mL hexane. A solution of benzoyl chloride (6.6 μL, 0.06 mmol) in 1.5 mL hexane was added dropwise to the suspension. A deep red-brown solution was immediately formed. The solution was stirred for 64 h and then filtered over a glass fiber filter. After concentration in a vacuum the solution was stored at -32 °C. A small amount of orange needles suitable for X-ray diffraction analysis were obtained within 5 months. ^{1}H NMR (400 MHz, [D6]benzene, 298 K): δ(ppm) 8.33 (m, 2H, 3γ), 6.98 (m, 3H, 3α/β), 0.40 (s, 81H, CH_3 on hypersilyl); ^{1}H ^{1}H COSY (400 MHz, [D6]benzene, 298 K): δ(ppm)/δ(ppm) 8.33/6.99 (^3J, 3γ/3α,β); ^{13}C{^{1}H} NMR (126 MHz, [D6]benzene, 298 K): δ(ppm) 227.09 (s, 3ε), 143.94 (s, 3α), 134.23 (m, 3δ), 130.00 (m, 3γ), 128.68 (m, 3β), 2.77 (q, 3ζ/η); ^{29}Si NMR (79 MHz, [D6]benzene, 298 K): δ(ppm) −8.33 (s, *Si*(CH$_3$)$_3$), −103.03 (s, *Si*(Si(CH$_3$)$_3$)$_3$); ^{1}H ^{13}C HSQC (400 MHz/101 MHz, [D6]benzene, 298 K): δ(ppm)/δ(ppm) 8.33/129.70 (^1J, 3γ/3γ), 6.99/133.97 (^1J, 3δ/3δ), 6.99/128.37 (^1J, 3β/3β), 0.40/2.39 (^1J, 3ζ/3ζ and 3η/3η); ^{1}H ^{13}C HMBC (400 MHz/101 MHz, [D6]benzene, 298 K): δ(ppm)/δ(ppm) 8.31/134.07, 6.98/142.91, 6.98/128.44, 0.38/2.87.

Synthesis of [{Si(SiMe$_3$)$_3$}$_3$Ge$_9$(CO)CH$_3$] (4)
In a glove box K[Ge$_9${Si(SiMe$_3$)$_3$}$_3$] (160 mg, 0.11 mmol) was weighed out in a Schlenk tube and suspended in 3 mL hexane. A solution of acetyl chloride (8.1 μL, 0.11 mmol) in 3 mL hexane was added to the suspension. The resulting red-brown reaction solution was stirred at r.t. for 23 h. After filtration the filtrate was concentrated to dryness in a vacuum. The residue was dissolved in 1 mL toluene and stored at −32 °C for crystallization. Red block-shaped crystals suitable for X-ray crystallography were obtained within one month. The crystals were separated from the mother liquor, washed for three times with a total amount of 3 mL acetonitrile and dried in a

vacuum. 30 mg of compound **4** (yield: 19%) were isolated. ^{1}H NMR (400 MHz, [D6]benzene, 298 K): δ(ppm) 2.54 (s, 3H, C*H*$_3$), 0.43 (s, 81H, C*H*$_3$ on hypersilyl); ^{13}C{^{1}H} NMR (126 MHz, [D6]benzene, 298 K): δ(ppm) 229.95 (s, *C*O), 53.04 (q, *C*H$_3$), 2.68 (q, *C*H$_3$ on hypersilyl); ^{29}Si NMR (79 MHz, [D6]benzene, 298 K): δ(ppm) −8.04 (s, *Si*(CH$_3$)$_3$), −104.28 (s, *Si*(Si(CH$_3$)$_3$)$_3$)). elemental analysis calcd (%): C 24.19, H 5.88; found: C 24.04, H 5.88.

Synthesis of [{Si(SiMe$_3$)$_3$}$_3$Ge$_9$(CO)CH(CH$_3$)$_2$] (5)
In a glove box K[Ge$_9${Si(SiMe$_3$)$_3$}$_3$] (160 mg, 0.11 mmol) was weighed out in a Schlenk tube and suspended in 3 mL hexane. A solution of isobutyryl chloride (11.9 μL, 0.11 mmol) in 3 mL hexane was added to the suspension. The solution was stirred at r.t. for 21 h. After filtration the red-brown filtrate was concentrated in a vacuum and stored at −32 °C for crystallization. Deep-red crystals were obtained within three days. The crystals were separated from the mother liquor and washed three times with a total amount of 2 mL acetonitrile. 62 mg of compound **5** (yield: 37%) were isolated. ^{1}H NMR (400 MHz, [D6]benzene, 298 K): δ(ppm) 2.87 (hept, 1H, C*H*), 1.13 (d, 6H, C*H*$_3$), 0.43 (s, 81H, C*H*$_3$ on hypersilyl); ^{1}H ^{1}H COSY (400 MHz, [D6]benzene, 298 K): δ(ppm)/δ(ppm) 2.89/1.12 (^{3}*J*, C*H*/C*H*$_3$); ^{13}C{^{1}H} NMR (126 MHz, [D6]benzene, 298 K): δ(ppm) 236.71 (s, *C*O), 61.08 (d, *C*H), 18.57 (q, *C*H$_3$), 2.71 (q, *C*H$_3$ on hypersilyl); ^{29}Si NMR (79 MHz, [D6]benzene, 298 K): δ(ppm) −8.13 (*Si*(CH$_3$)$_3$), −103.98 (*Si*(Si(CH$_3$)$_3$)$_3$)); ^{1}H ^{13}C HSQC (400 MHz/101 MHz, [D6]benzene, 298 K): δ(ppm)/δ(ppm) 2.89/60.73 (^{1}*J*, C*H*/*C*H), 1.13/18.16 (^{1}*J*, C*H*$_3$/*C*H$_3$), 0.44/2.37 (^{1}*J*, C*H*$_3$/CH$_3$ on hypersilyl); ^{1}H ^{13}C HMBC (400 MHz/101 MHz, [D6]benzene, 298 K): δ(ppm)/δ(ppm) 2.88/18.63 (^{2}*J*, C*H*/*C*H$_3$), 1.12/61.06 (^{2}*J*, C*H*$_3$/*C*H). elemental analysis calcd (%): C 25.37, H 6.04; found: C 25.20, H 6.04.

X-ray Data Collection and Structure Determination: The crystals were transferred from the mother liquor into perfluoropolyalkylether under a cold stream of N_2. A single crystal was fixed on a glass fiber and positioned in a cold stream of N_2. The intensity data were recorded on a Stoe StadiVari diffractometer (Mo K_α radiation (λ = 0.71073 Å), Pilatus 300K detector), by using the X-Area software package.[5] The crystal structures were solved by Direct Methods and refined using the SHELX software.[6] The positions of the hydrogen atoms were calculated and refined using a riding model. All non-hydrogen atoms were treated with anisotropic displacement parameters. In the crystal structure of **1** one methyl group is disordered, and the crystal structure of **2** contains one disordered hypersilyl ligand. All ligands of **4** are disordered, and in compound **3** two hexane molecules per formula unit are disordered and therefore not refined, the corresponding electron density was taken care of using the Squeeze option of the program Platon.[7] Crystallographic details on compounds **1**-**5** are listed in Table S1. CCDC 1812804 (**1**), CCDC 1812805 (**2**), CCDC 1812806 (**3**), CCDC 1812807 (**4**), and CCDC 1812808 (**5**) contain the supplementary crystallographic data. These data can be obtained free of charge from The Cambridge Crystallographic Data Centre via www.ccdc.cam.ac.uk/data_request/cif.

Electron-Dispersive X-ray (EDX) Analysis: The composition concerning the elements Si and Ge of the single crystals of **1**, **2**, **3**, **4**, and **5** which were used to determine the crystal structure was analyzed with a Hitachi TM-1000 tabletop microscope.

Elemental Analysis: Elemental analysis was performed by the microanalytical laboratory at the Department of Chemistry of the Technische Universität München. The elements C and H were determined with a combustion analyzer (elementar vario EL, Bruker Corp.).

NMR Spectroscopy: NMR spectra were recorded on a BRUKER Avance Ultrashield AV400 spectrometer and a BRUKER Avance Ultrashield AV500C spectrometer. The signals were referenced to the residual proton signal of the deuterated solvents [D$_6$]benzene (δ = 7.16 ppm) and [D$_8$]toluene (δ_{CH3} = 2.09 ppm). The chemical shifts are given in δ values in parts per million (ppm). The multiplicities are depicted as follows: s – singlet, d – doublet, q – quartet, m – multiplet.

DFT calculations: All calculations were performed using the software package Gaussian 09[8]. Throughout the study, the hybrid density functional PBE1PBE[9] together with the basis set Def2TVPP[10] were used. All energies are unscaled and reported as ΔG for 298.15 K and gas-phase relative to the starting material. Frequency calculations also ensure either optimized structures of intermediates (NImag=0) or transition states (NImag=1). The details of the calculations can be found in the Supporting Information (see below).

2 Crystallographic Details on the Crystal Structures of 1, 2, 3, 4 and 5

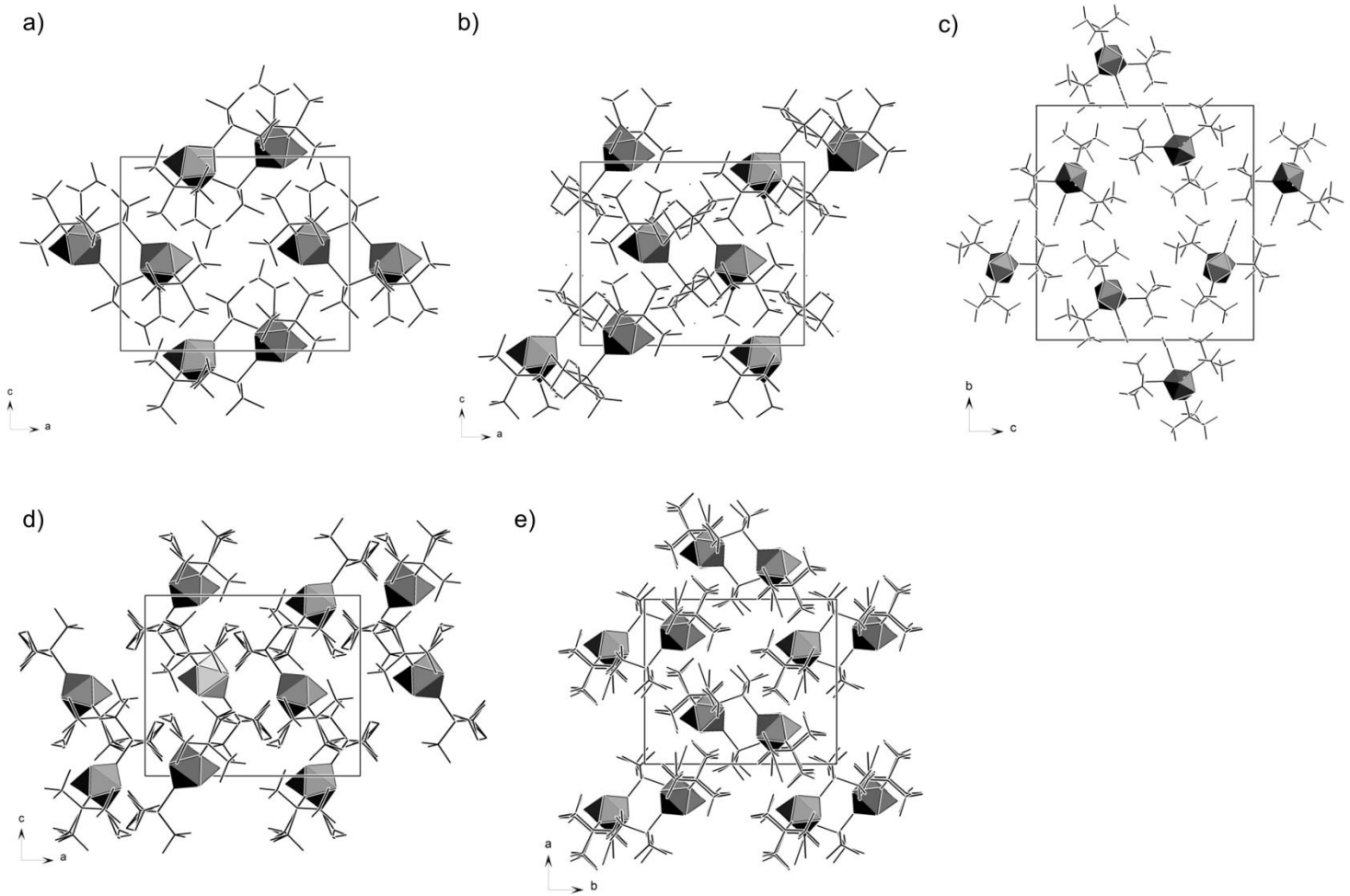

Figure S1. Unit cells of the crystal structures of a) **1**, b) **2**, c) **3**, d) **4** and e) **5**. The Ge_9 clusters are drawn as grey polyhedra. The ligands bound to the clusters are shown schematically. Hydrogen atoms are omitted for clarity.

SUPPORTING INFORMATION

Table S1. Crystallographic details of compounds **1**, **2**, **3**, **4** and **5**.

Compound	[{Si(SiMe$_3$)$_3$}$_3$Ge$_9$(CO)^{t}Bu] (**1**)	[{Si(SiMe$_3$)$_3$}$_3$Ge$_9$^{t}Bu] (**2**)	[{Si(SiMe$_3$)$_3$]$_3$Ge$_9$(CO)C$_6$H$_5$] (**3**)	[{Si(SiMe$_3$)$_3$]$_3$Ge$_9$(CO)Me] (**4**)	[{Si(SiMe$_3$)$_3$]$_3$Ge$_9$(CO)iPr] (**5**)
formula	$C_{32}H_{90}Ge_9OSi_{12}$	$C_{31}H_{90}Ge_9Si_{12}$	$C_{34}H_{86}Ge_9OSi_{12}$	$C_{29}H_{84}Ge_9OSi_{12}$	$C_{31}H_{88}Ge_9OSi_{12}$
fw (g·mol^{-1})	1481.42	1453.41	1501.41	1439.35	1467.40
space group (no.)	*Pnma* (62)	*Pnma* (62)	$P2_1/c$ (14)	*Pnma* (62)	$P2_12_12_1$ (19)
a (Å)	18.142(1)	18.004(1)	9.7368(9)	17.7234(7)	15.2687(4)
b (Å)	24.055(2)	24.646(1)	28.341(3)	24.0883(9)	17.7885(5)
c (Å)	15.320(1)	14.764(1)	26.621(3)	14.9067(6)	23.9737(7)
α (deg)	90	90.00	90	90	90
β (deg)	90	90	99.781(8)	90	90
γ (deg)	90	90	90	90	90
V (Å^3)	6686.3(9)	6551.3(7)	7239(1)	6364.1(4)	6511.4(3)
Z	4	4	4	4	4
T (K)	150(2)	100(2)	150(2)	100(2)	100(2)
ρ_{calcd} (g·cm^{-3})	1.472	1.474	1.378	1.502	1.497
μ (mm^{-1})	4.223	4.308	3.902	4.435	4.336
collected reflections	173213	98101	211982	153689	162817
independent reflections	6730	6596	14189	6414	12785
R_{int}	0.1909[a]	0.1516[a]	0.219[a]	0.0801	0.1020
parameters / restraints	278 / 0	316 / 63	533 / 0	317 / 0	509 / 0
R_1 / wR_2 [$I > 2\ \sigma(I)$]	0.052/0.126	0.057/ 0.131	0.060/0.138	0.029/0.066	0.025/0.056
goodness of fit	1.031	1.036	1.019	1.075	1.078
max. / min. diff. el. Density (e·Å^{-3})	0.86 / -1.17	2.45 / -1.15	1.05 / -1.51	0.97 / −0.83	0.53 / −0.43

[a] the comparatively high R_{int} value originates from a bad crystal quality.

Table S2. Selected bond lengths [Å] in compounds **1**, **2**, and **4**.

Atoms	**1**	**2**	**4**
Ge1–Ge2	2.4589(9)	2.4550(10)	2.4523(4)
Ge2–Ge3	2.5988(10)	2.5859(11)	2.5895(4)
Ge3–Ge2^{i}	2.5988(10)	2.5859(11)	2.5895(4)
Ge2^{i}–Ge1	2.4589(9)	2.4550(10)	2.4524(4)
Ge1–Ge3	3.5901(14)	3.6392(15)	3.5955(6)
Ge2–Ge2^{i}	3.5490(14)	3.4823(14)	3.5256(7)
Ge1–Ge5	2.6029(10)	2.5897(11)	2.6034(5)
Ge2–Ge5	2.6704(10)	2.6726(10)	2.6535(4)
Ge2–Ge4	2.5240(9)	2.5322(11)	2.5282(4)
Ge3–Ge4	2.6483(11)	2.6498(12)	2.6585(5)
Ge3–Ge4^{i}	2.6483(11)	2.6498(12)	2.6585(5)
Ge2^{i}–Ge4^{i}	2.5240(9)	2.5322(11)	2.5282(4)
Ge2^{i}–Ge5^{i}	2.6704(10)	2.6726(10)	2.6535(4)
Ge1–Ge5^{i}	2.6029(10)	2.5897(11)	2.6034(5)
Ge5^{i}–Ge5	2.9248(15)	2.9221(14)	2.9419(7)
Ge5–Ge4	3.1335(10)	3.0621(11)	3.0699(4)
Ge4–Ge4^{i}	2.7881(15)	2.8314(14)	2.8621(7)
Ge4^{i}–Ge5^{i}	3.1335(10)	3.0621(11)	3.0699(4)
Ge5^{i}–Ge6	2.5100(10)	2.5009(11)	2.5143(5)
Ge5–Ge6	2.5100(10)	2.5009(11)	2.5143(5)
Ge4–Ge6	2.5487(11)	2.5316(11)	2.5299(5)
Ge4^{i}–Ge6	2.5487(11)	2.5316(11)	2.5299(5)
Ge1–C1	2.051(9)	2.050(12)	2.058(6)
Ge2–Si1	2.3950(19)	2.3944(19)	2.3846(9)
Ge6–Si5	2.376(2)	2.364(3)	2.3675(11)
C1–O	1.221(12)	-	1.202(7)
C1–C2	1.518(14)	1.519(18)	1.475(8)
C2–C3	1.533(17)	-	-
C2–C4	1.502(13)	-	-
C2–C4^{i}	1.502(13)	-	-
C1–C3	-	1.539(13)	-
C1–C3^{i}	-	1.539(13)	-

Symmetry operation: (i) *x*, -*y*+0.5, *z*.

Table S3. Selected bond lengths [Å] in compounds **3** and **5**.

Atoms	**3**	**5**
Ge1–Ge2	2.4701(12)	2.4547(7)
Ge2–Ge3	2.5930(13)	2.5989(7)
Ge3–Ge4	2.5847(13)	2.5927(7)
Ge4–Ge1	2.4635(12)	2.4562(7)
Ge1–Ge3	3.6639(12)	3.6265(6)
Ge2–Ge4	3.4789(14)	3.5079(7)
Ge1–Ge6	2.5938(13)	2.5959(7)
Ge2–Ge6	2.6873(13)	2.6732(7)
Ge2–Ge7	2.5324(12)	2.5254(7)
Ge3–Ge7	2.6356(13)	2.6481(7)
Ge3–Ge8	2.6669(12)	2.6407(7)
Ge4–Ge8	2.5377(12)	2.5273(7)
Ge4–Ge5	2.7214(13)	2.6669(7)
Ge1–Ge5	2.5890(12)	2.5933(7)
Ge5–Ge6	2.9311(13)	2.9620(7)
Ge6–Ge7	3.1244(13)	3.0797(8)
Ge7–Ge8	2.8289(13)	2.8040(6)
Ge8–Ge5	3.0576(12)	3.1225(7)
Ge5–Ge9	2.5176(13)	2.5107(7)
Ge6–Ge9	2.5155(12)	2.5116(7)
Ge7–Ge9	2.5430(12)	2.5506(7)
Ge8–Ge9	2.5452(13)	2.5436(7)
Ge1–C1	2.046(8)	2.047(5)
Ge2–Si1	2.394(2)	2.3934(14)
Ge4–Si5	2.394(2)	2.3843(14)
Ge9–Si9	2.377(2)	2.3776(11)
C1–O	1.203(10)	1.192(5)
C1–C2	1.510(11)	1.519(6)
C2–C3	1.384(12)	1.487(8)
C3–C4	1.399(12)	-
C4–C5	1.363(13)	-
C5–C6	1.391(14)	-
C6–C7	1.387(13)	-
C7–C2	1.392(11)	-
C2–C4	-	1.520(7)

3 NMR spectra of compounds 1-9

3.1 NMR spectroscopic characterization of [{Si(SiMe$_3$)$_3$}$_3$Ge$_9$(CO)^{t}Bu] (1)

Compound **1** was characterized in the reaction solution due to the little amount of crystals which were obtained. Therefore a solution of pivaloyl chloride (0.021 mmol, 2.64 μL) dissolved in 0.3 mL [D8]toluene was added to a suspension of K[Ge$_9$\{Si(SiMe$_3$)$_3$\}$_3$] (0.021 mmol, 30 mg) in 0.3 mL [D8]toluene and reacted for 3 h 20 min. The NMR spectrum was then recorded.

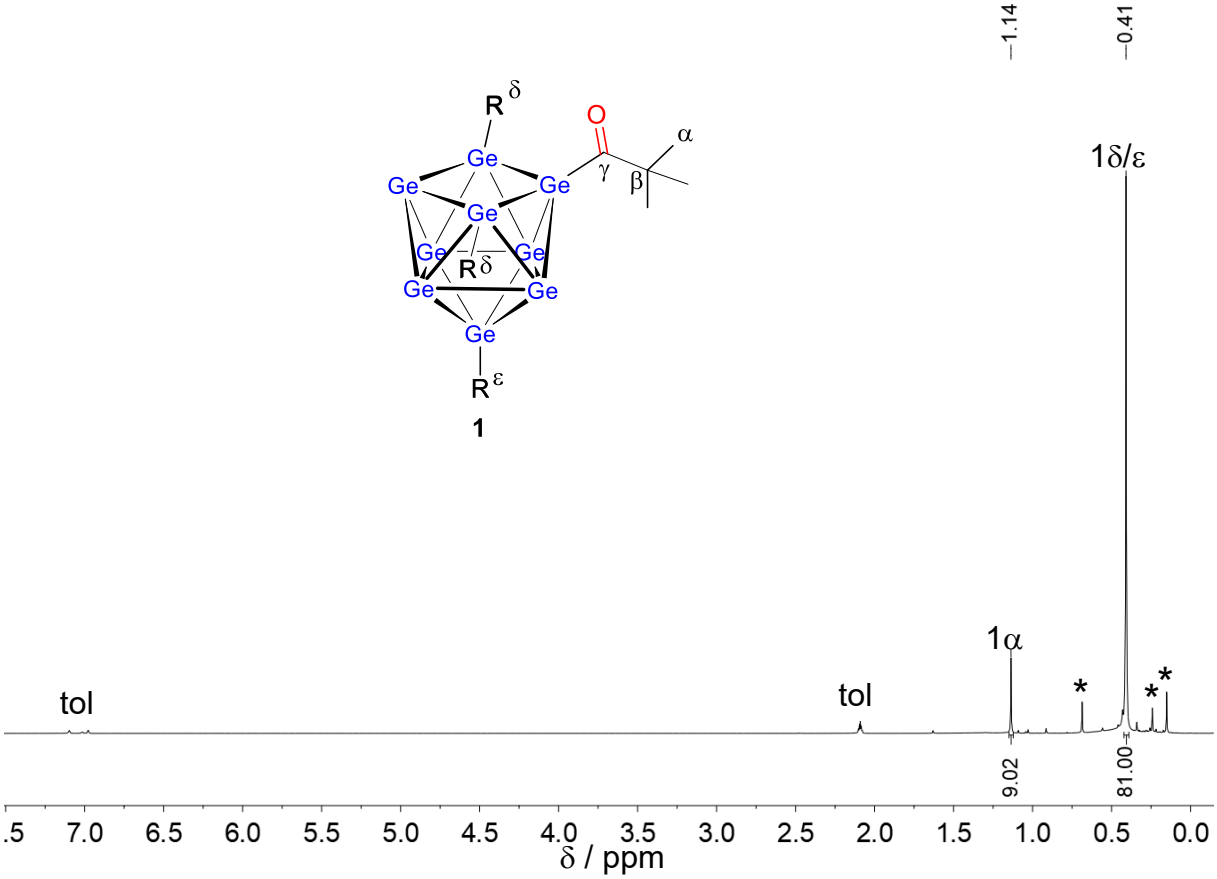

Figure S2. ^{1}H NMR spectrum of **1** in a [D8]toluene reaction solution recorded at r.t.. Signals marked with * could not be assigned. R depicts the hypersilyl (hyp) moiety bound to the Ge$_9$ cluster.

3.2 NMR spectroscopic Characterization of [{Si(SiMe$_3$)$_3$}$_3$Ge$_9$^{t}Bu] (2)

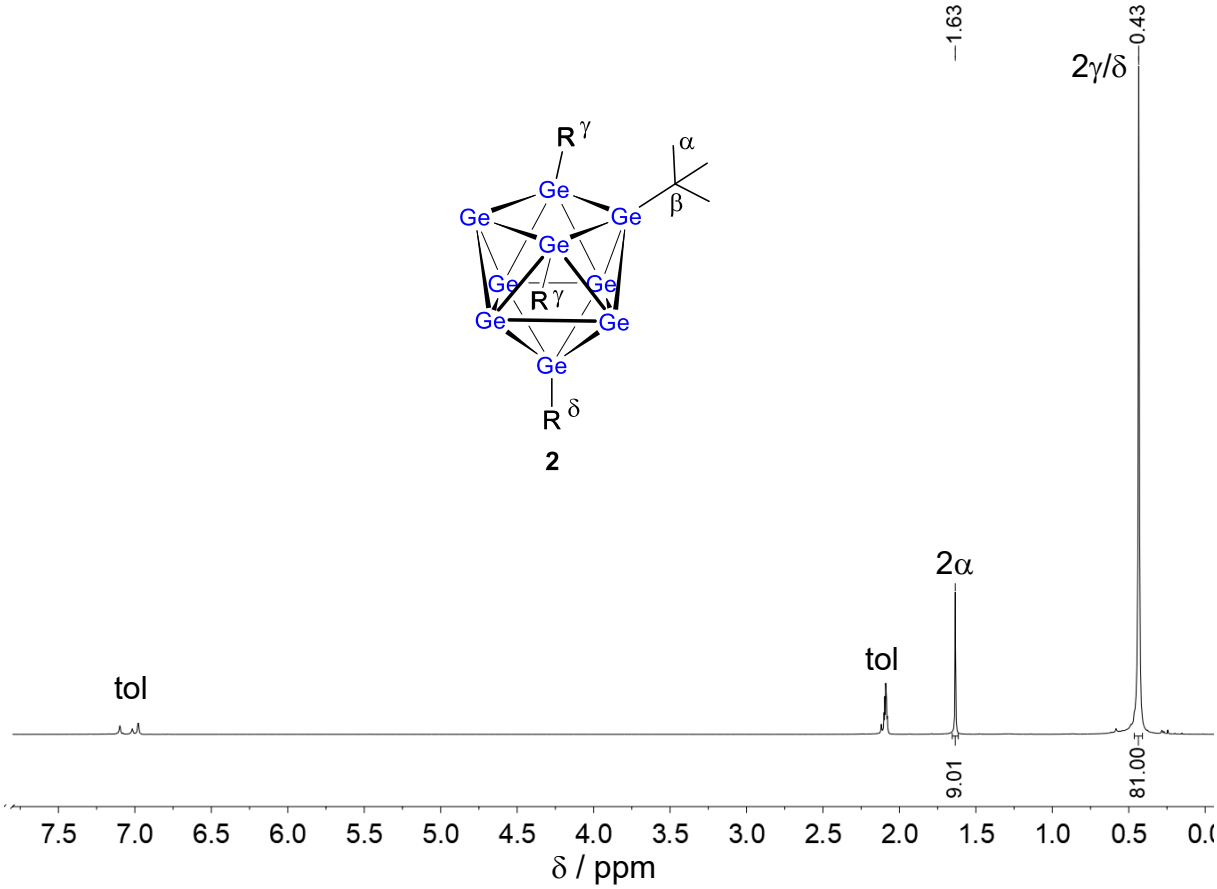

Figure S3. ^{1}H NMR spectrum of dissolved crystals of **2** in [D8]toluene at r.t.. R represents the hypersilyl (hyp) moiety bound to the Ge$_9$ cluster.

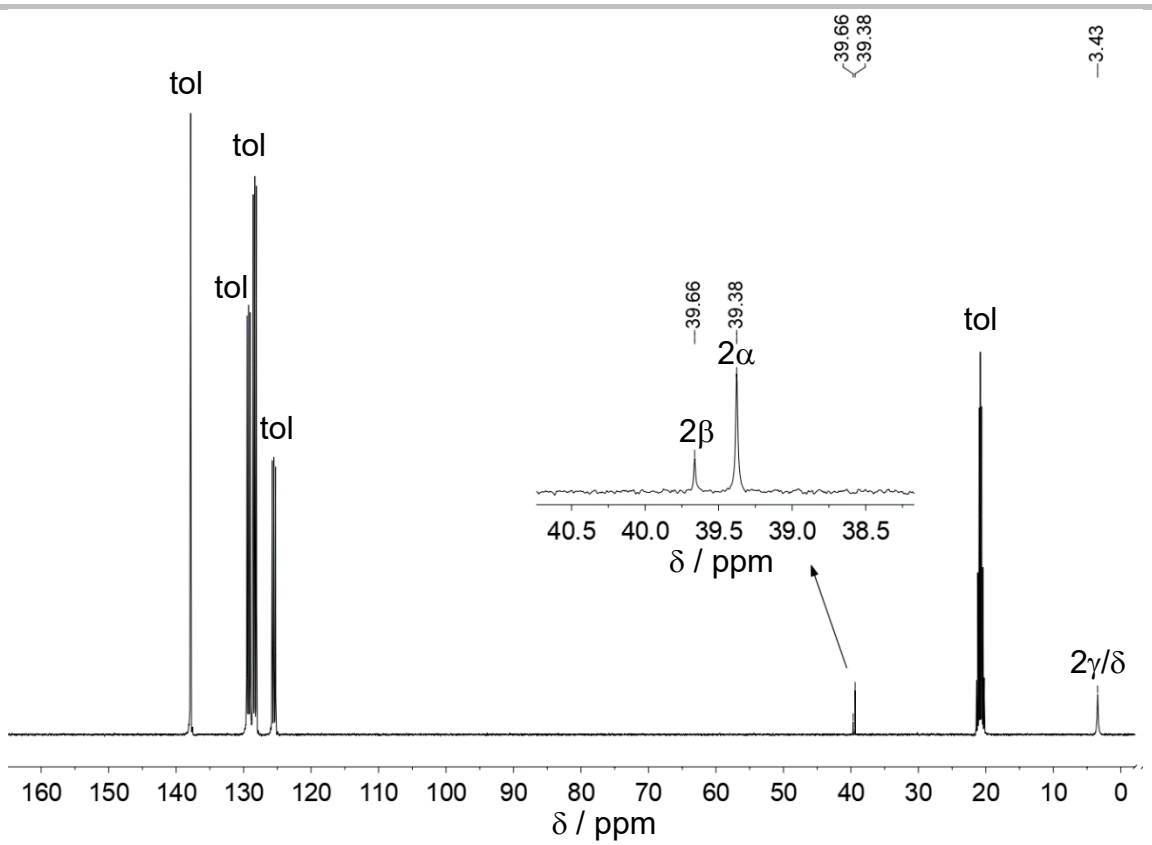

Figure S4. ^{13}C NMR spectrum of dissolved crystals of **2** in [D8]toluene at r.t..

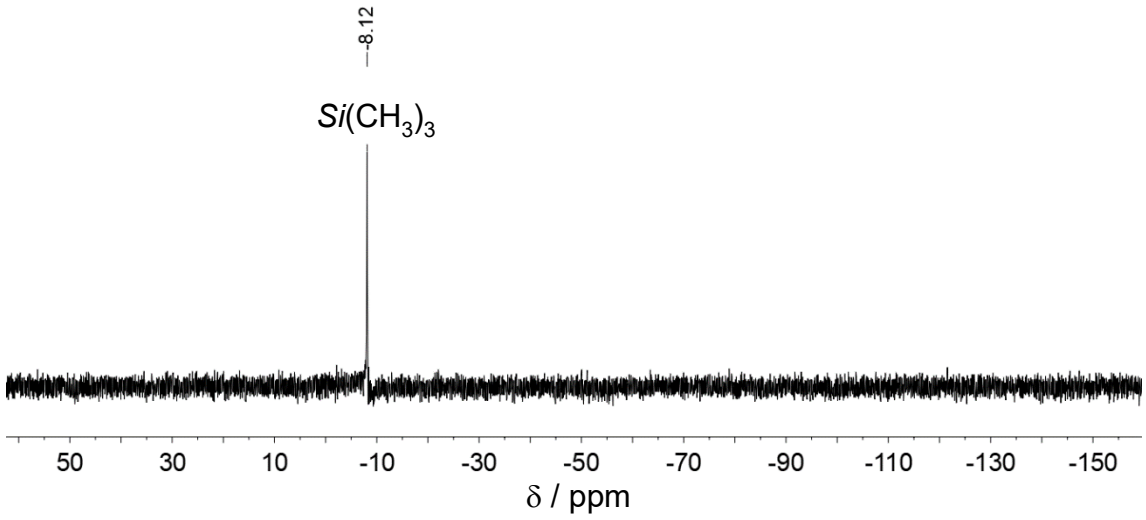

Figure S5. ^{29}Si NMR spectrum of dissolved crystals of **2** in [D8]toluene at r.t..

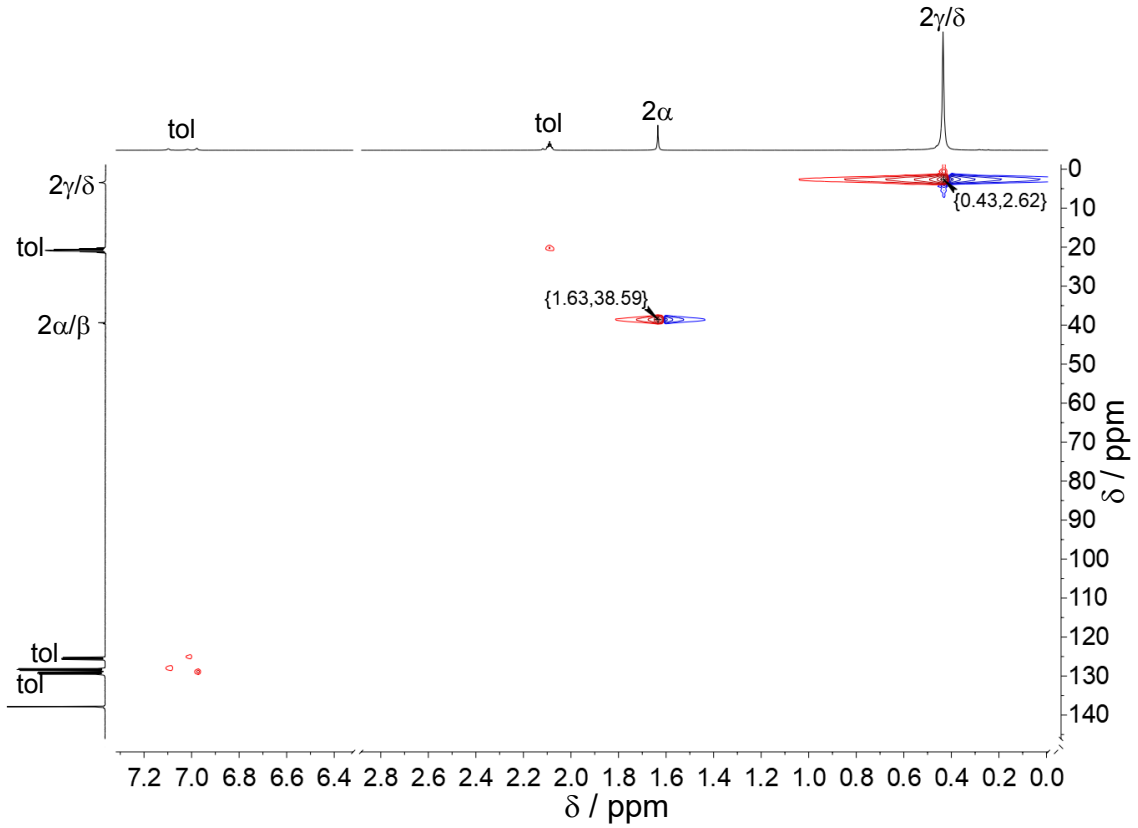

Figure S6. Relevant sections of ^{1}H ^{13}C HSQC NMR spectrum of dissolved crystals of **2** in [D8]toluene at r.t..

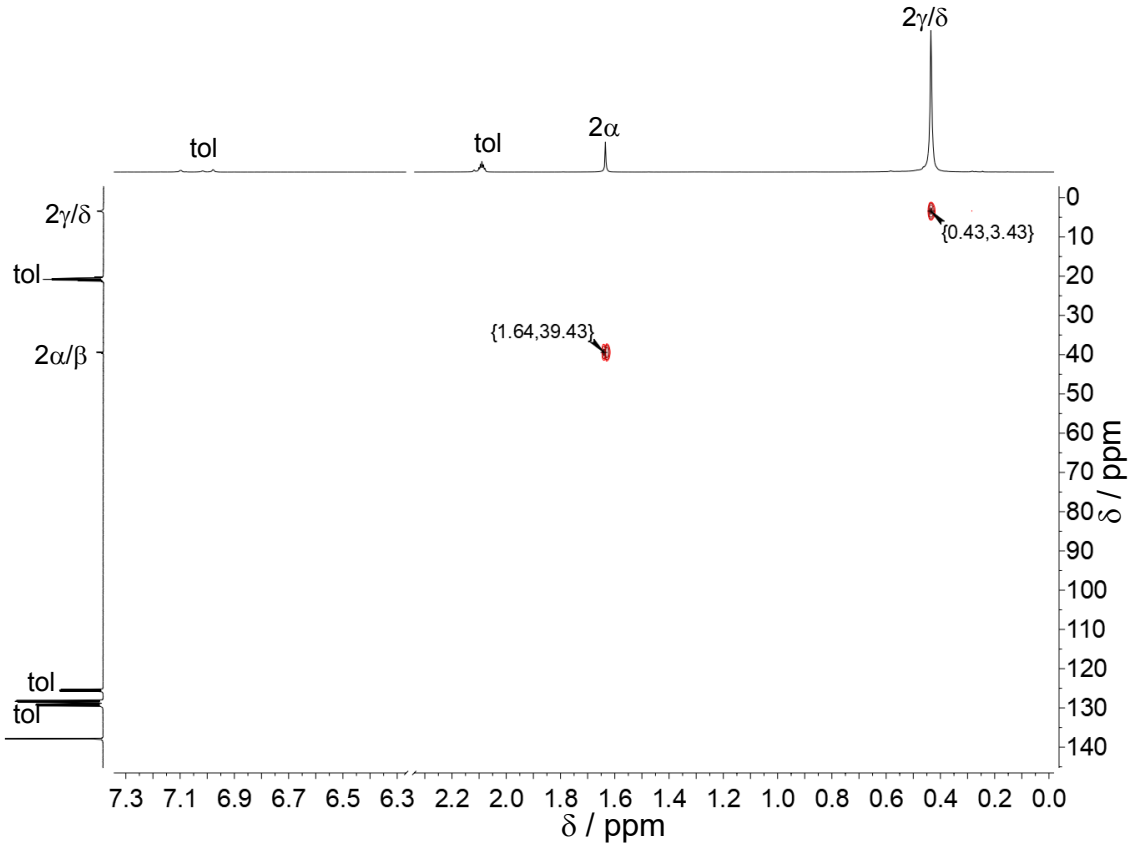

Figure S7. Relevant sections of ^{1}H ^{13}C HMBC NMR spectrum of dissolved crystals of **2** in [D8]toluene at r.t..

3.3 NMR spectroscopic characterization of [{Si(SiMe$_3$)$_3$]$_3$Ge$_9$(CO)phenyl] (3)

Compound **3** was characterized in the reaction solution due to the little amount of crystals which were obtained. Therefore a solution of benzoyl chloride (0.021 mmol, 2.44 μL) dissolved in 0.6 mL [D6]benzene was added to K[Ge$_9${Si(SiMe$_3$)$_3$}$_3$] (0.021 mmol, 30 mg) and reacted for 30 min. The NMR spectra were then recorded.

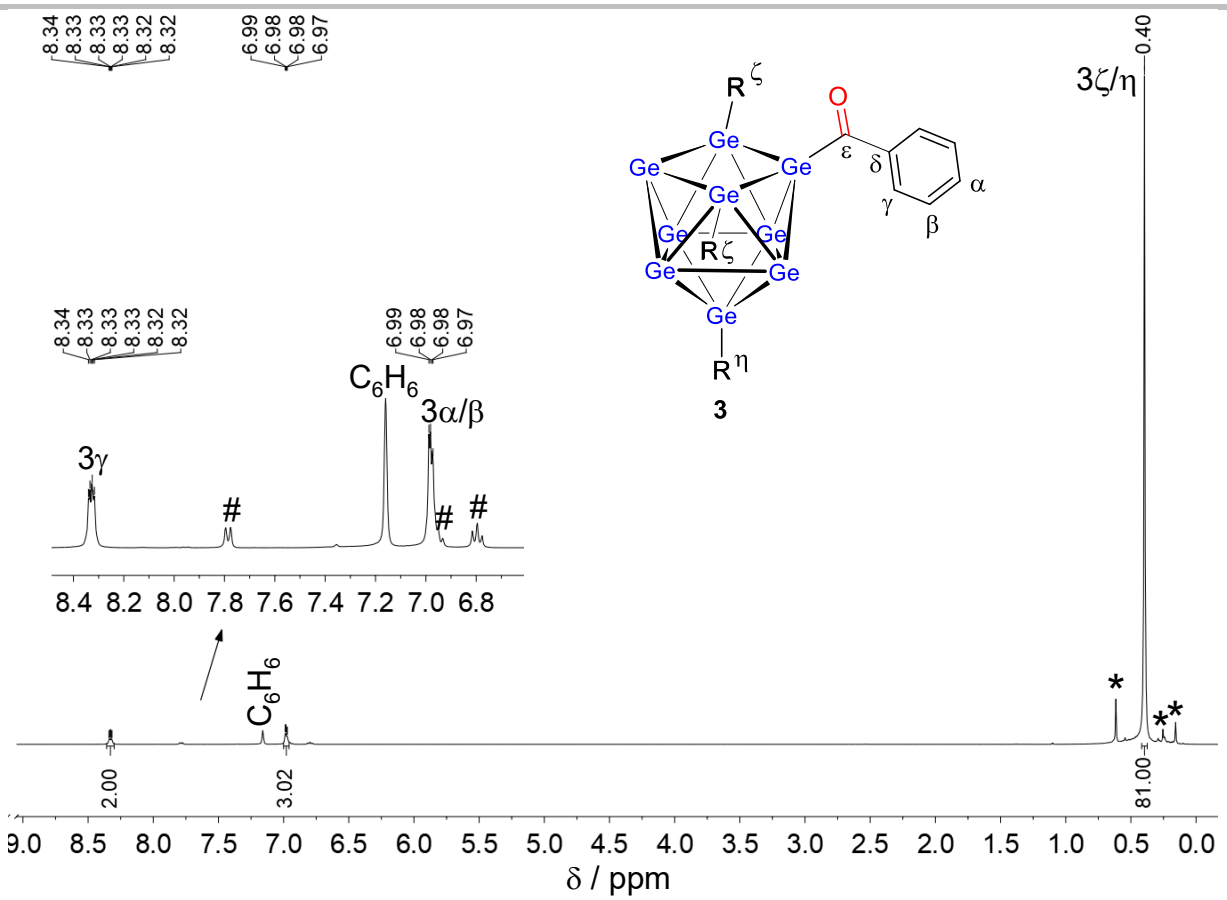

Figure S8. ^{1}H NMR spectrum of **3** in a [D6]benzene reaction solution recorded at r.t.. Signals marked with # are assigned to unreacted benzoyl chloride. Signals marked with * could not be assigned. R represents the hypersilyl (hyp) moiety bound to the Ge_9 cluster.

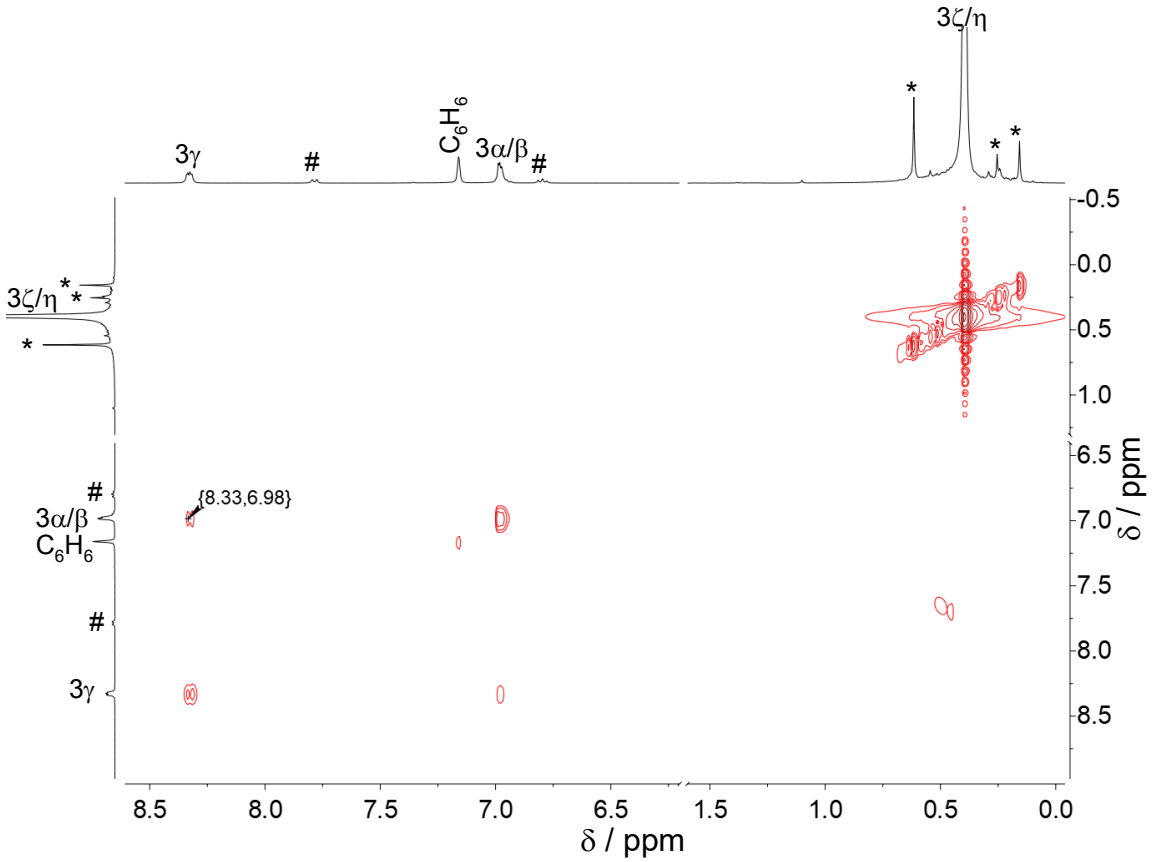

Figure S9. Relevant sections of the ^{1}H ^{1}H COSY spectrum of **3** in a [D6]benzene reaction solution recorded at r.t.. Signals marked with # are assigned to unreacted benzoyl chloride. Signals marked with * could not be assigned.

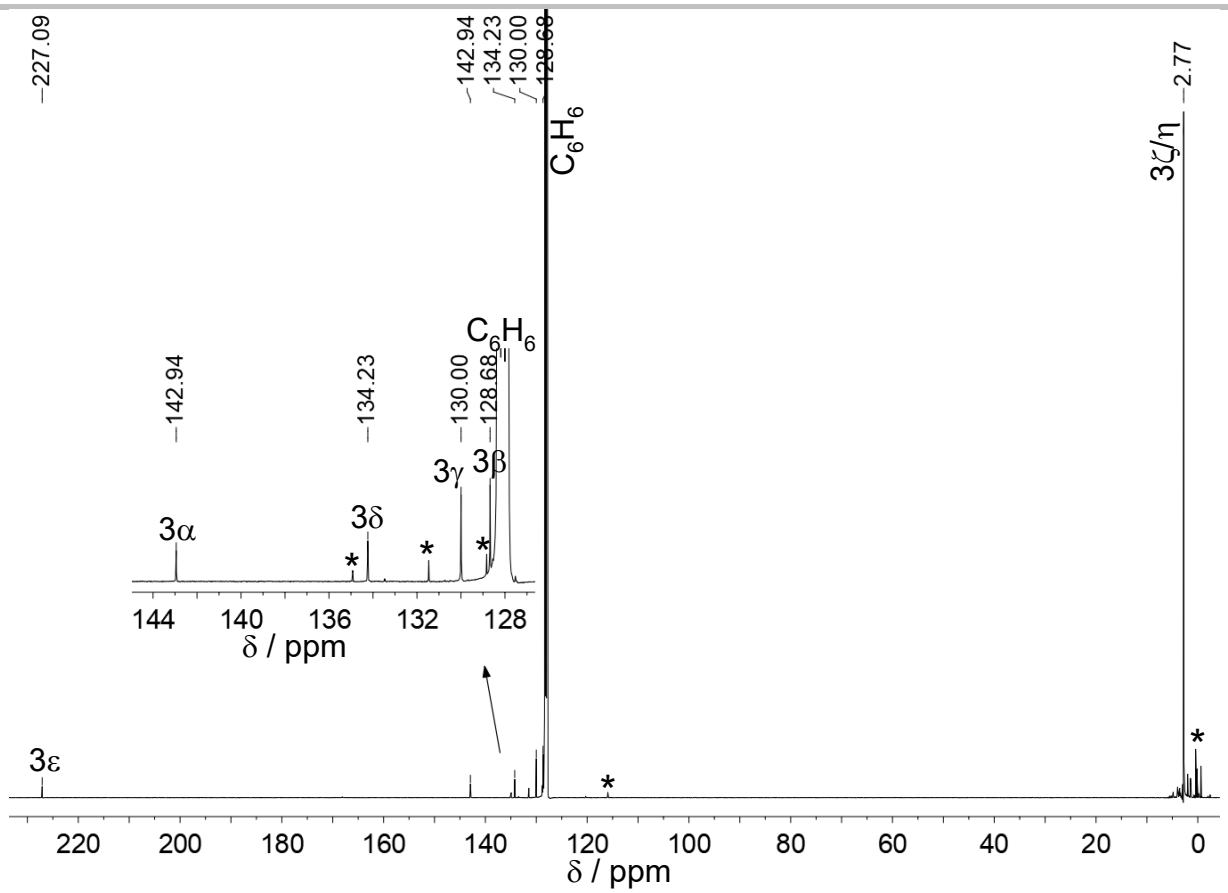

Figure S10. ^{13}C NMR spectrum of **3** in a [D6]benzene reaction solution recorded at r.t.. Signals marked with * could not be assigned.

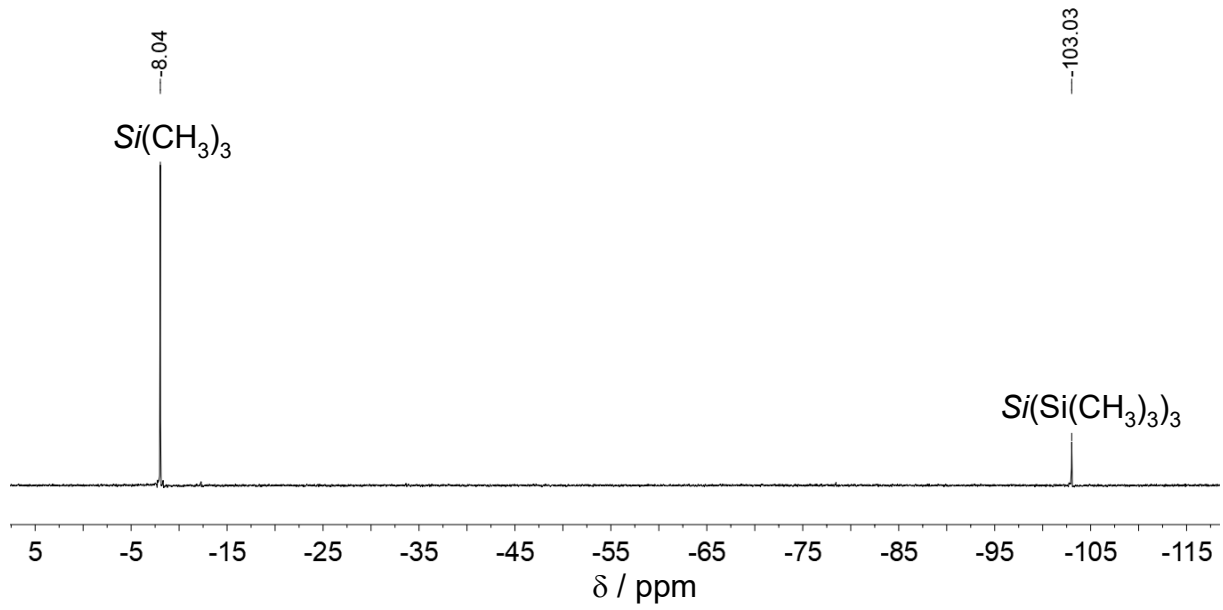

Figure S11. ^{29}Si NMR spectrum of **3** in a [D6]benzene reaction solution recorded at r.t..

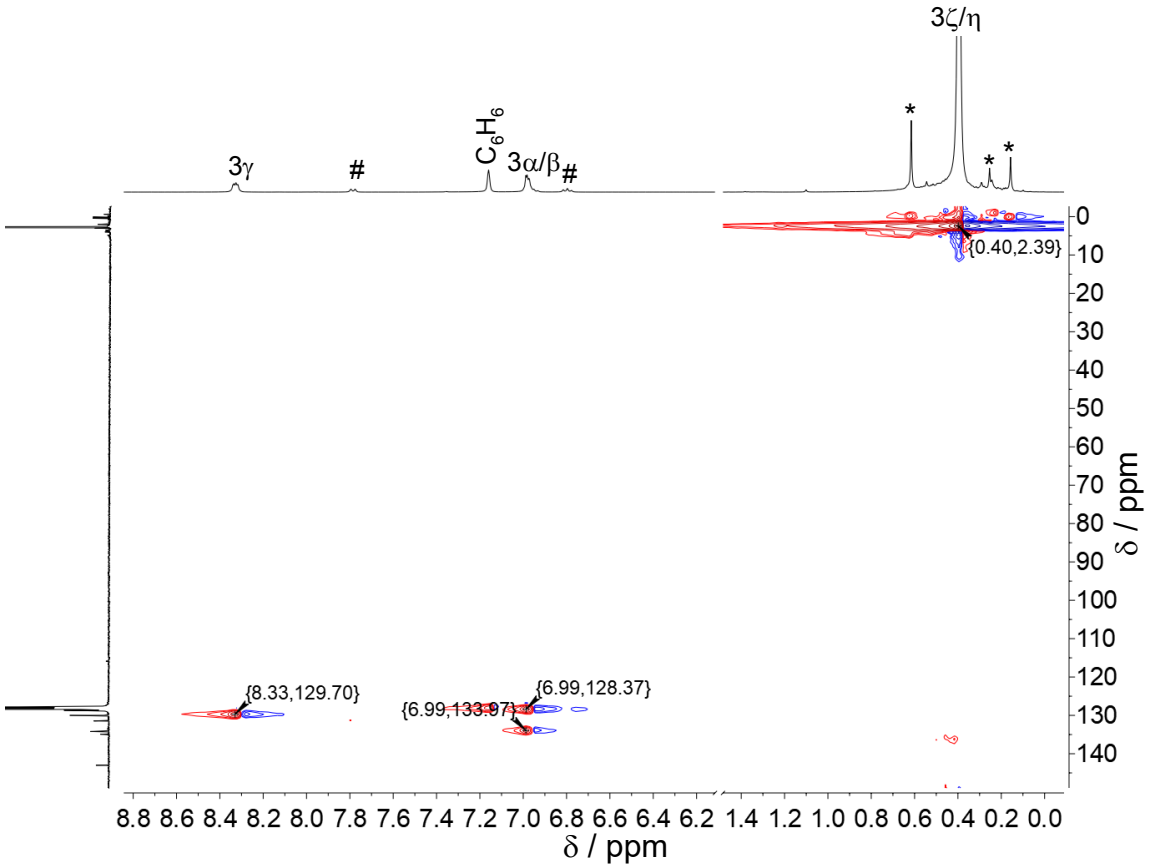

Figure S12. Relevant sections of the ^{1}H ^{13}C HSQC spectrum of **3** in a [D6]benzene reaction solution recorded at r.t.. Signals marked with # are assigned to unreacted benzoyl chloride. Signals marked with * could not be assigned.

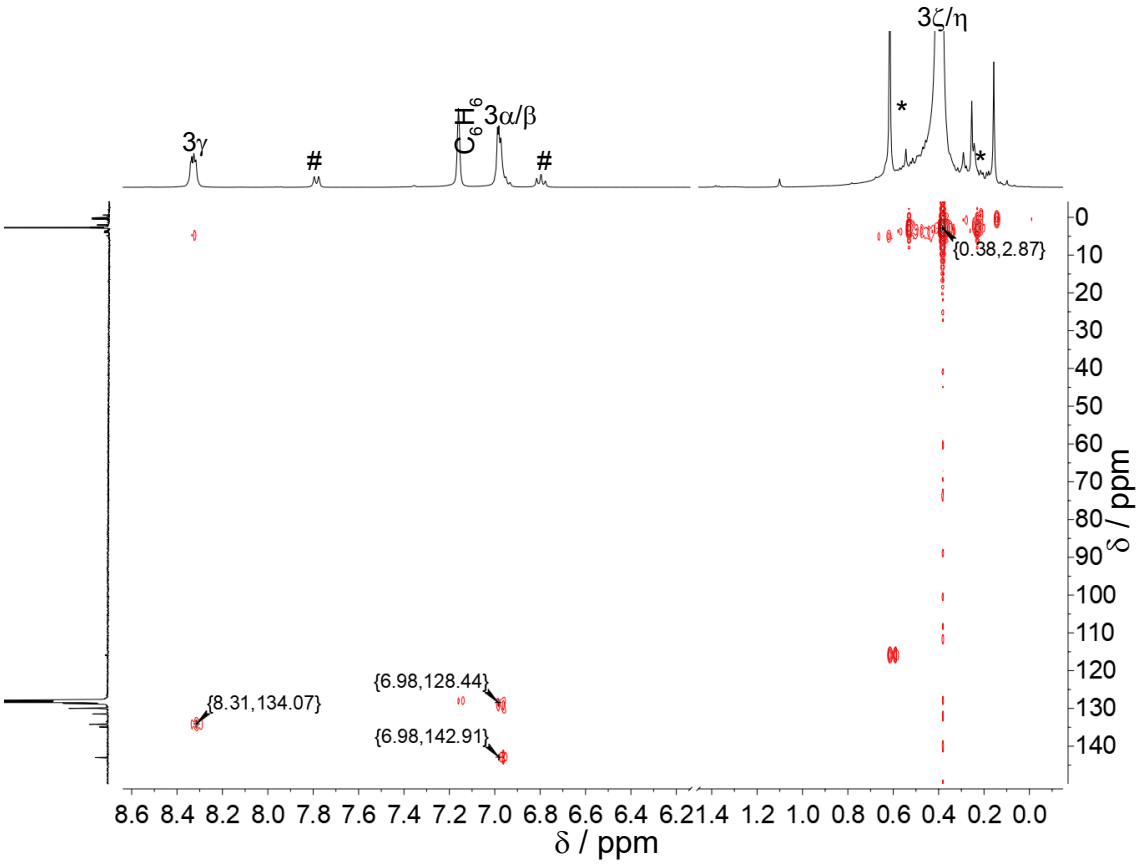

Figure S13. Relevant sections of the ^{1}H ^{13}C HMBC spectrum of **3** in a [D6]benzene reaction solution recorded at r.t.. Signals marked with # are assigned to unreacted benzoyl chloride. Signals marked with * could not be assigned.

3.4 NMR spectroscopic characterization of 4

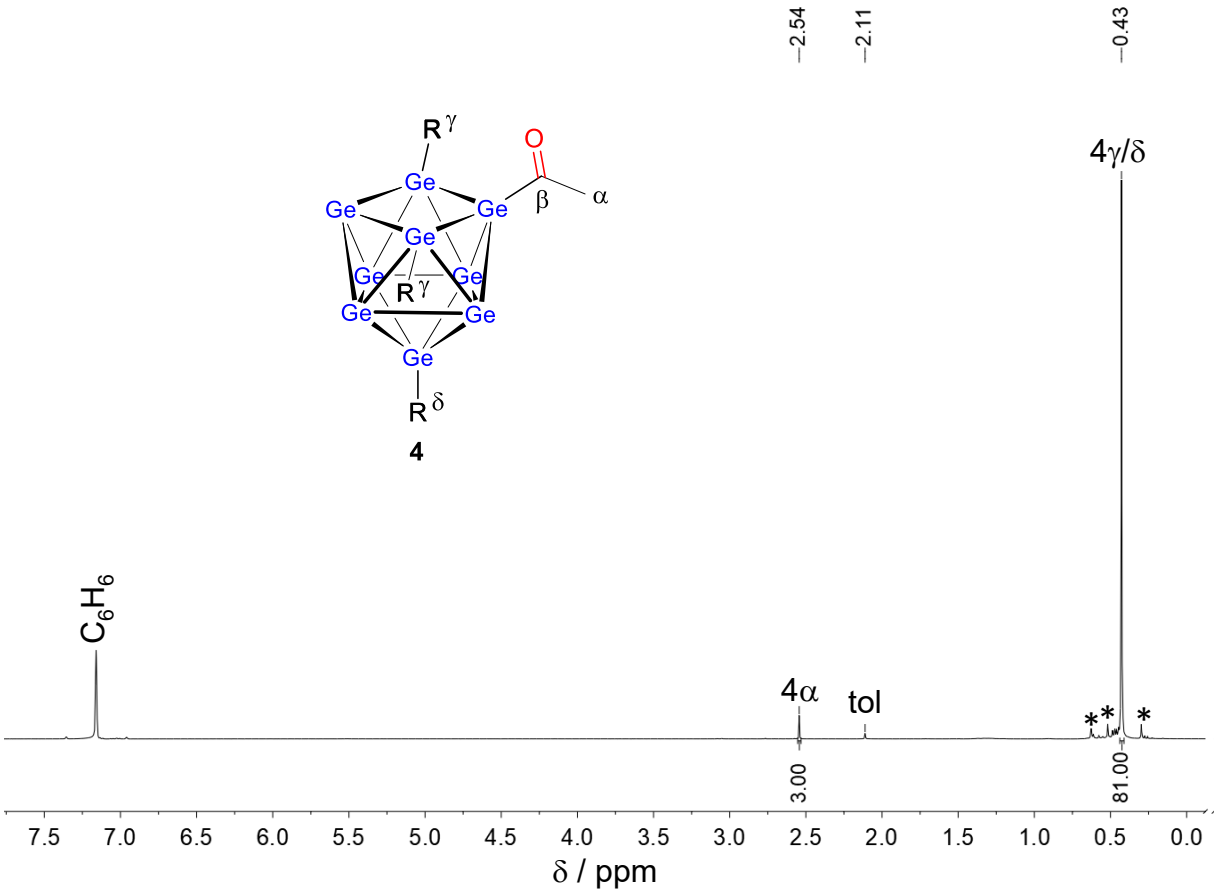

Figure S14. ^{1}H NMR spectrum of **4** in a [D6]benzene reaction solution recorded at r.t.. Signals marked with * could not be assigned. R represents the hypersilyl (hyp) moiety bound to the Ge_9 cluster.

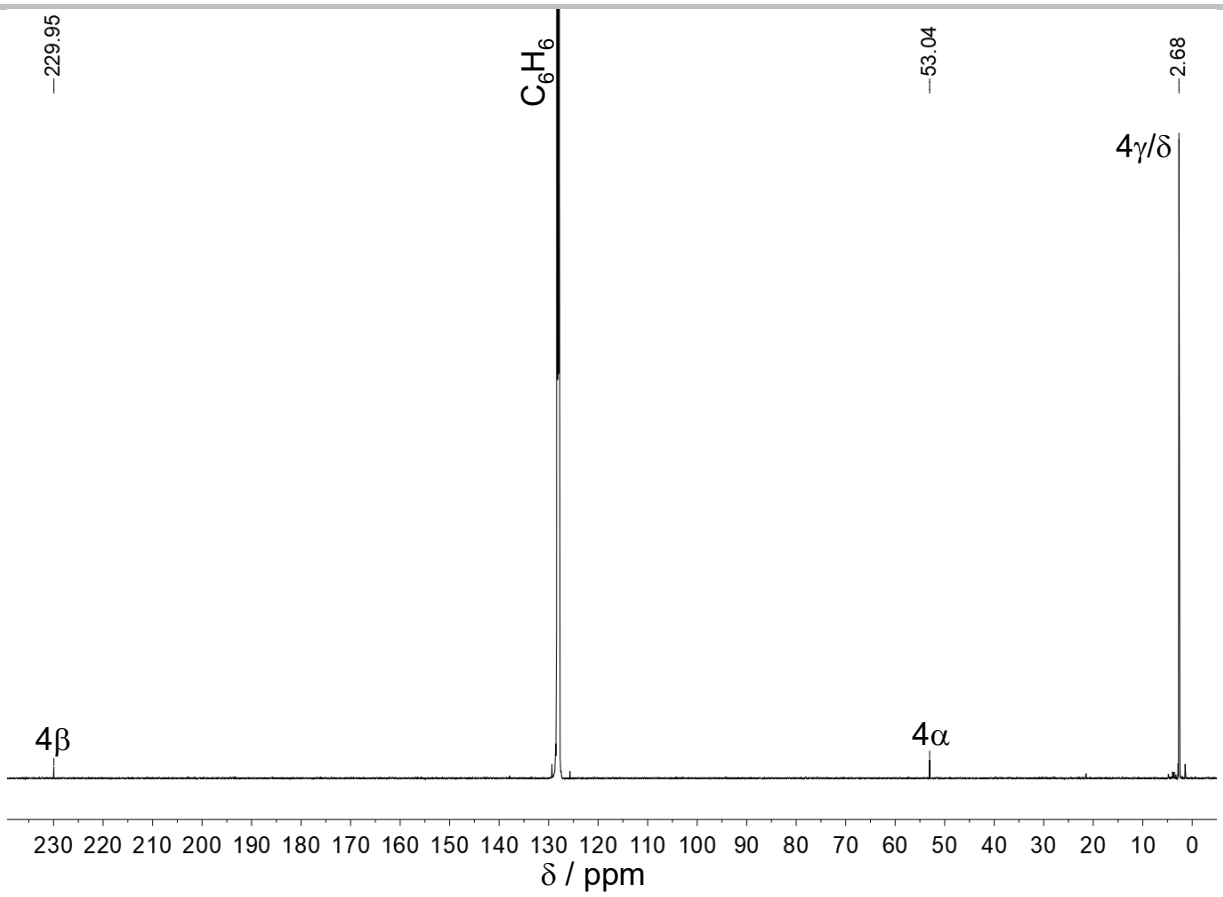

Figure S15. ^{13}C NMR spectrum of crystals of **4** in [D6]benzene recorded at r.t..

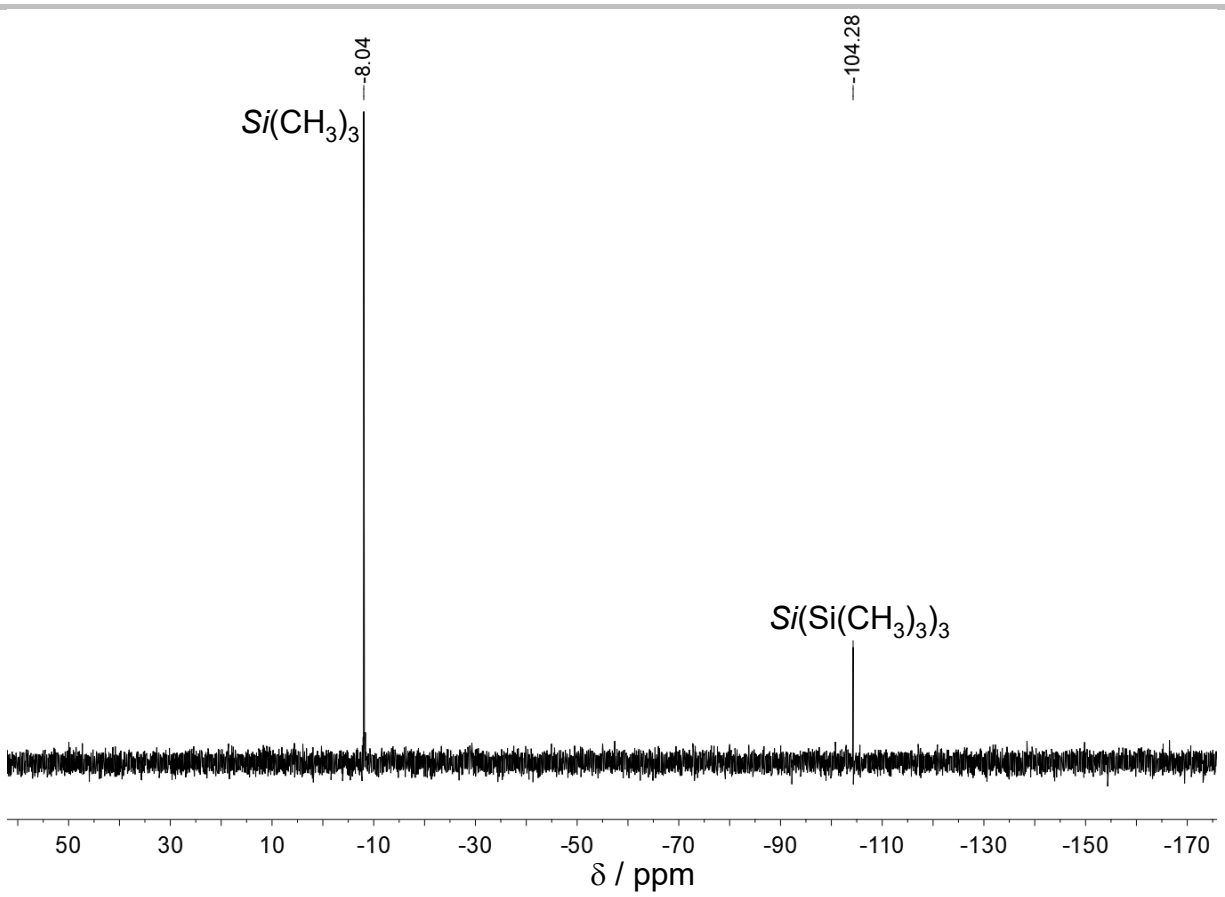

Figure S16. ^{29}Si NMR spectrum of dissolved crystals of **4** in [D6]benzene at r.t..

3.5 NMR spectroscopic characterization of 5

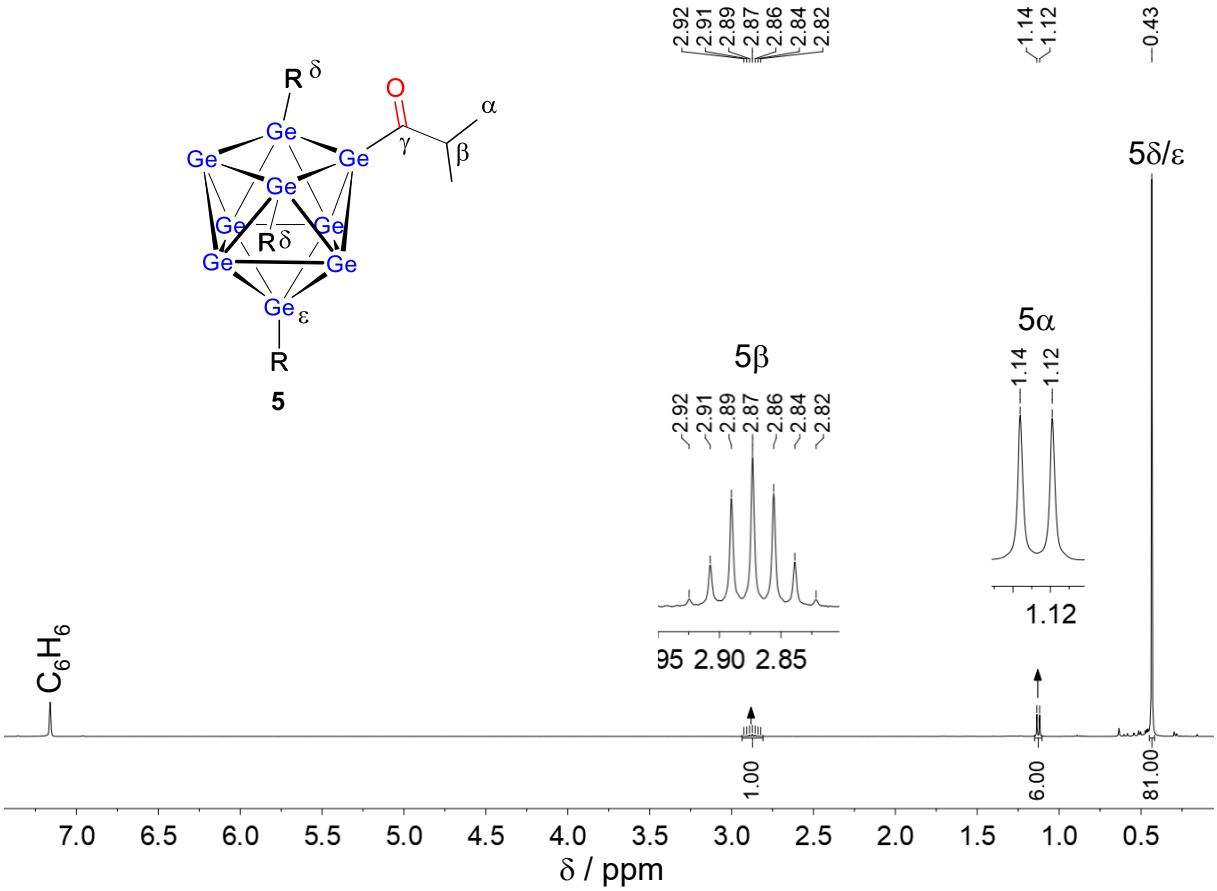

Figure S17. ^{1}H NMR spectrum of dissolved crystals of **5** in [D6]benzene at r.t.. R represents the hypersilyl (hyp) moiety bound to the Ge_9 cluster. Relevant signals are shown enlarged.

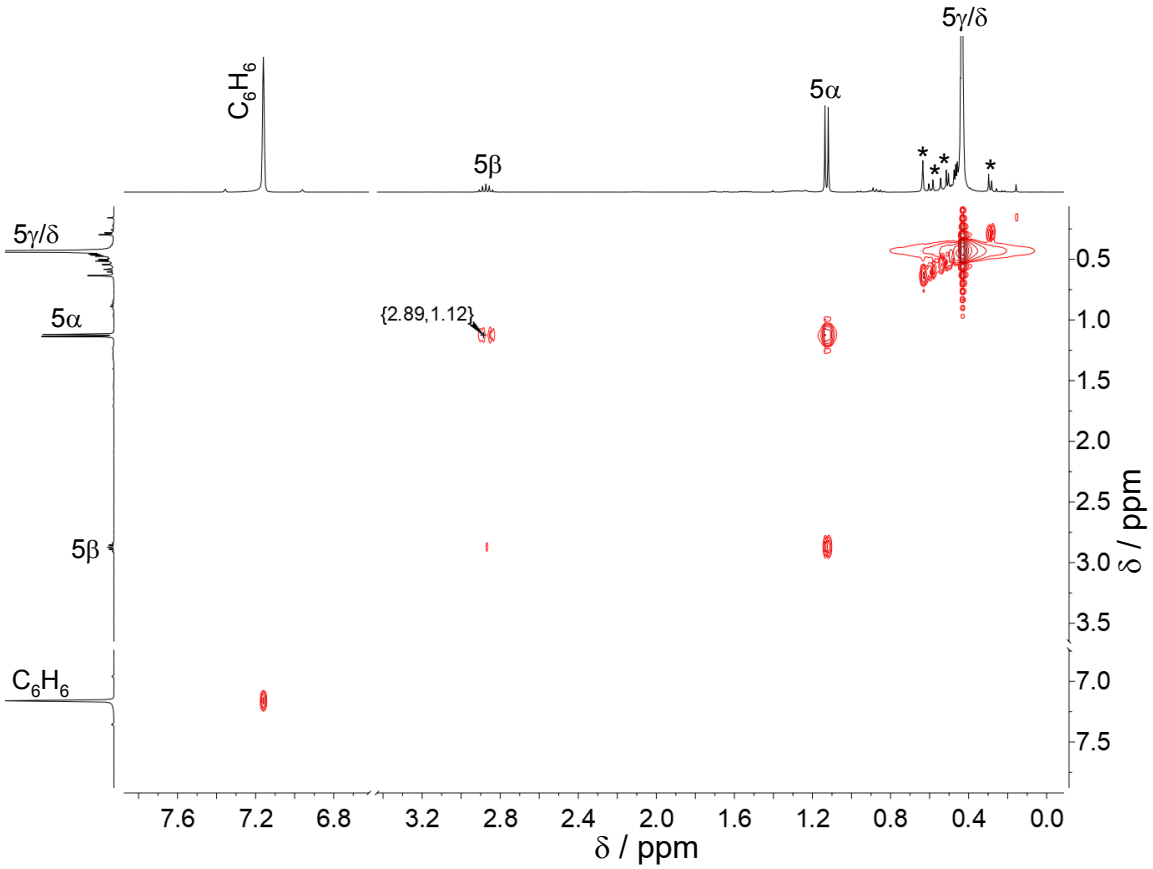

Figure S18. Relevant sections of the ^{1}H ^{1}H COSY NMR spectrum of dissolved crystals of **5** in [D6]benzene at r.t..

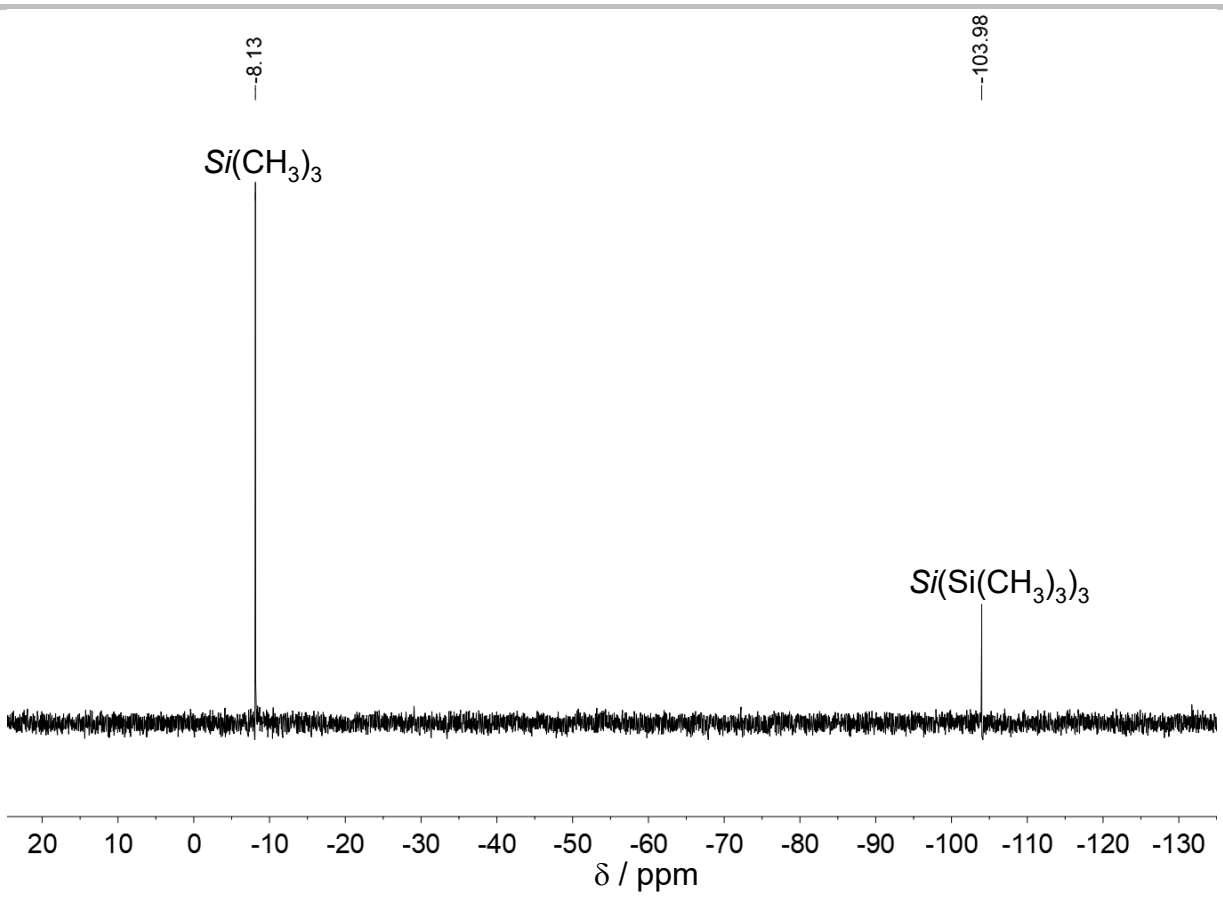

Figure S19. ^{29}Si NMR spectrum of dissolved crystals of **5** in [D6]benzene at r.t..

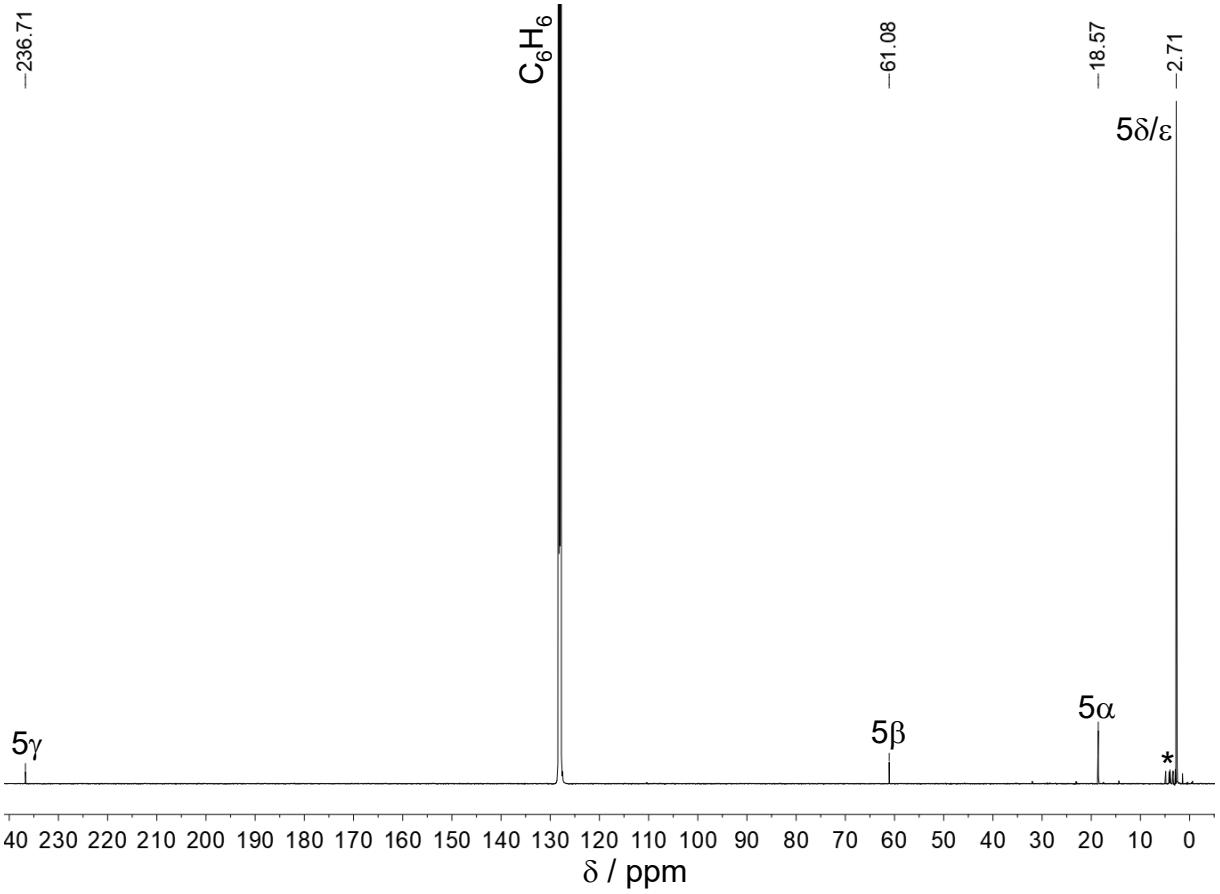

Figure S20. ^{13}C NMR spectrum of crystals of **5** recorded in [D6]benzene at r.t..

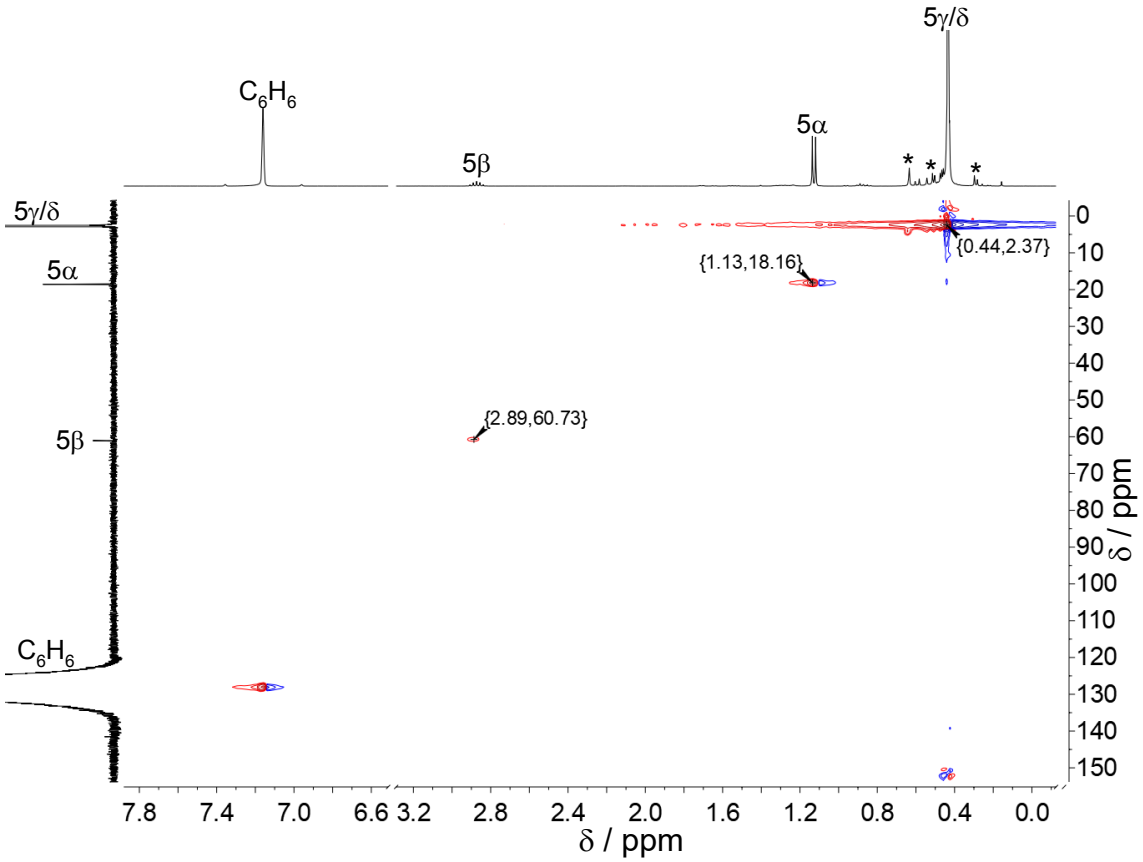

Figure S21. Relevant sections of ^{1}H ^{13}C HSQC NMR spectrum of crystals of **5** recorded in [D6]benzene at r.t..

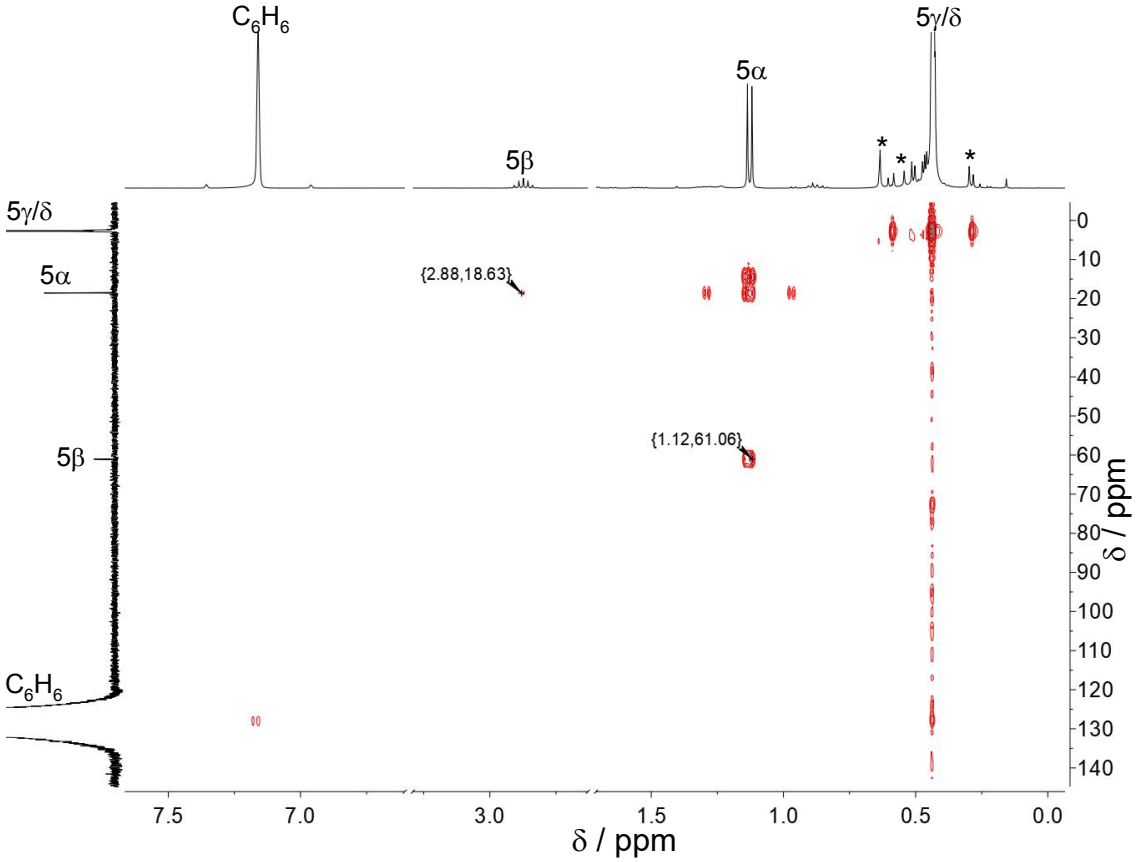

Figure S22. Relevant sections of ^{1}H ^{13}C HMBC NMR spectrum of crystals of **5** recorded in [D6]benzene at r.t..

3.6 NMR spectroscopic characterization of 6

In a glove box K[Ge_9{$Si(SiMe_3)_3$}$_3$] (30 mg, 0.021 mmol) was weighed out in a Schlenk tube, suspended in 0.3 mL [D8]toluene and cooled to 0 °C. A solution of phenylacetylchloride (2.8 μL, 0.021 mmol) in 0.3 mL [D8]toluene was added dropwise to the cooled suspension within 10 min. After stirring at 0 °C for additional 15 h the solution was investigated by NMR spectroscopy. ^{1}H NMR (400 MHz, [D8]toluene, 298 K): δ(ppm) 7.14-6.98 (m, 5H, 6α/β/γ), 4.23 (s, 2H, 6ε), 0.40 (s, 81H, 6η/θ).

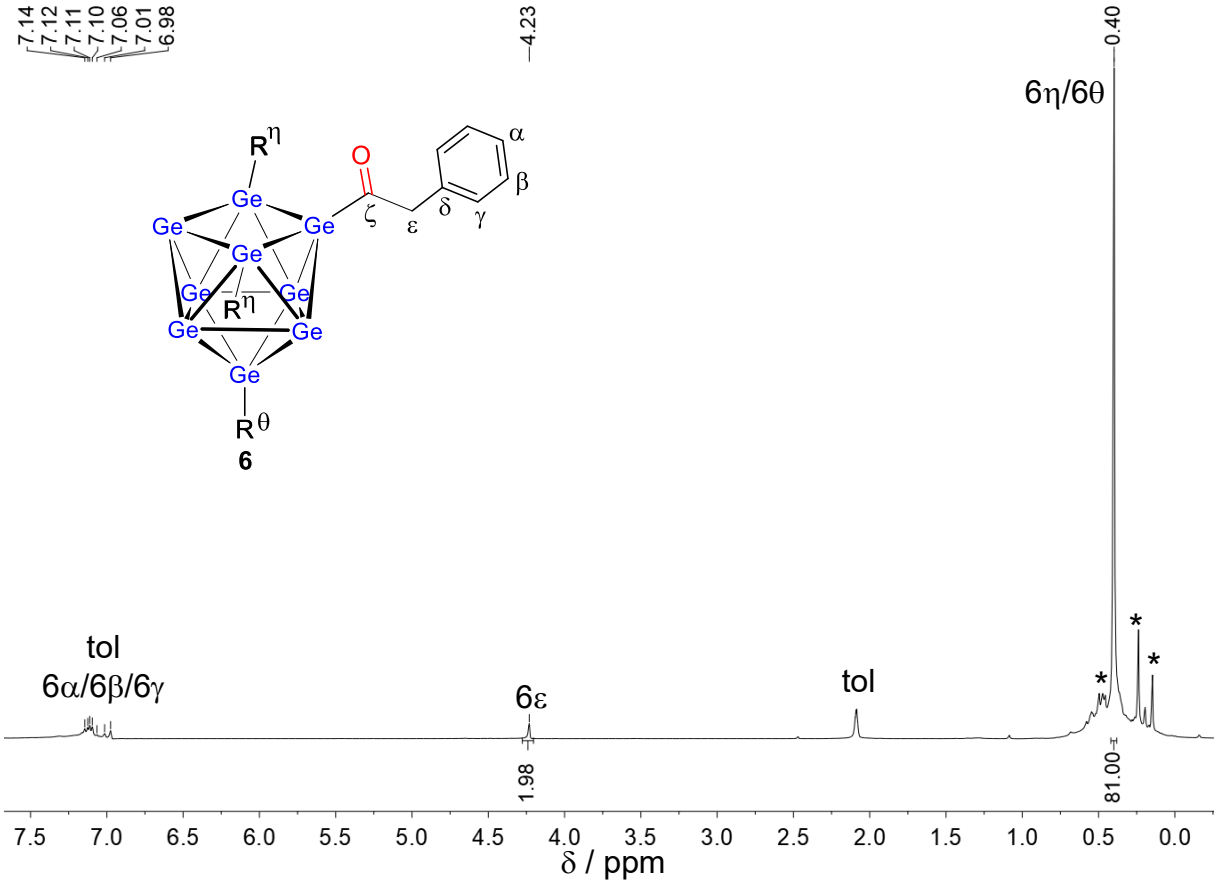

Figure S23. ^{1}H NMR spectrum of **6** in a [D8]toluene reaction solution recorded at r.t.. Signals marked with * could not be assigned. R represents the hypersilyl (hyp) moiety bound to the Ge_9 cluster.

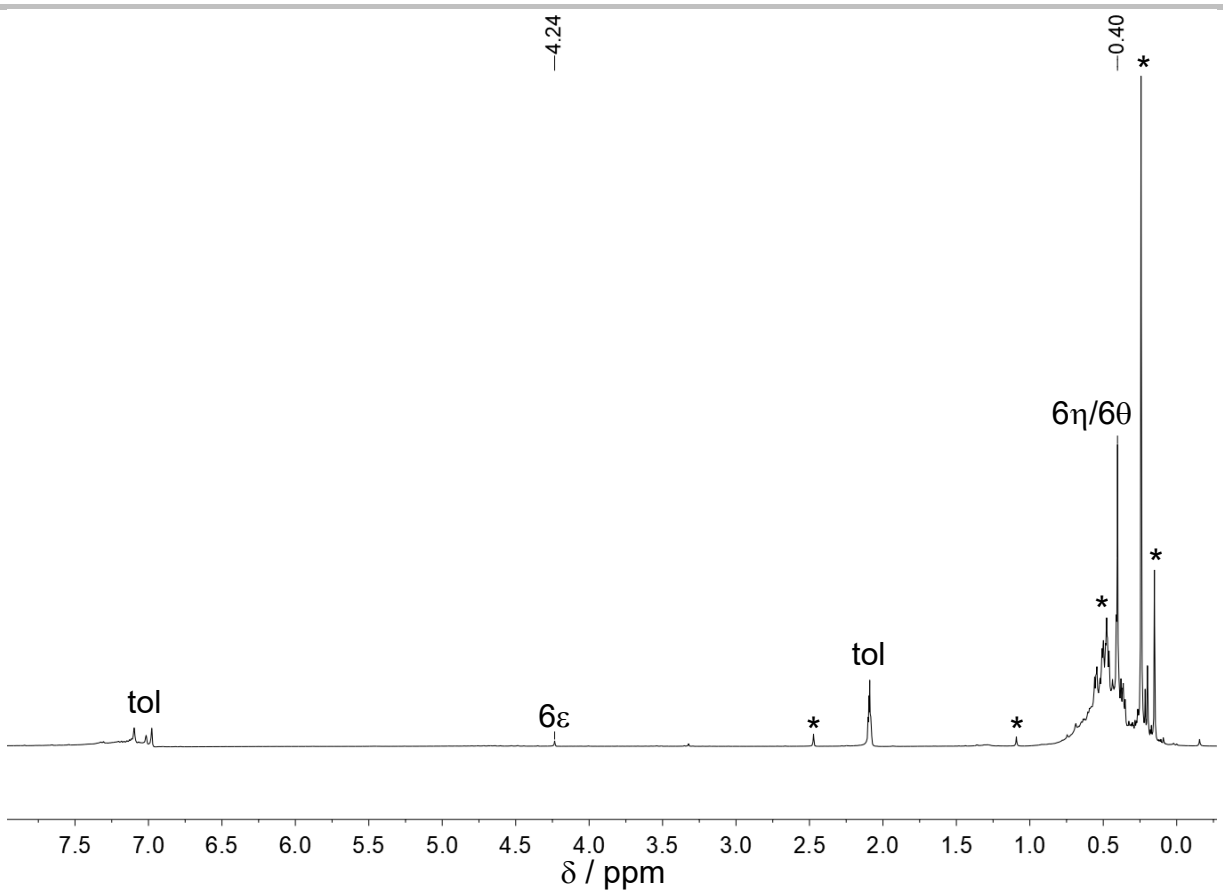

Figure S24. ^{1}H NMR spectrum of the reaction solution described in Figure S23 at r.t. after storage of the NMR tube for 1 h at r.t.

3.7 NMR spectroscopic characterization of 7

A solution of cyclopropylacyl chloride (2.08 *µ*L, 0.021 mmol) in 0.6 mL [D6]benzene was added to K[Ge_9{$Si(SiMe_3)_3$}$_3$] (30 mg, 0.021 mmol). The red-brown solution was stirred for 16 h at r.t.. After filtration the NMR spectroscopic characterization of **7** was performed. ^{1}H NMR (400 MHz, [D6]benzene, 298 K): δ(ppm) 3.02 (d, 2H, 7δ), 1.05 (m, 1H, 7γ), 0.43 (s, 81H, 7ζ/η), 0.33 (m, 2H, 7α/β), -0.01 (m, 2H, 7α/β); ^{1}H ^{1}H COSY (400 MHz, [D6]benzene, 298 K): δ(ppm)/δ(ppm) 3.01/1.05 (^{3}J, 7γ/7δ), 1.04/0.30 (^{3}J, 7γ/7α/β), 1.05/-0.02 (^{3}J, 7γ/7α/β), 0.33/-0.02 (^{3}J, 7α/β/7β/α); ^{29}Si NMR (79 MHz, [D6]benzene, 298 K): δ(ppm) −8.12 (*Si*$(CH_3)_3$), −104.16 (*Si*(Si$(CH_3)_3)_3$)); ^{13}C{^{1}H} NMR (101 MHz, [D6]benzene, 298 K): δ(ppm) 230.86 (s, 7ε), 72.85 (t, 7δ), 7.65 (d, 7γ), 4.88 (m, 7α/β), 2.72 (q, 7ζ/η); ^{1}H ^{13}C HSQC (400 MHz/101 MHz, [D6]benzene, 298 K): δ(ppm)/δ(ppm) 3.03/72.52 (^{1}J, 7δ/7δ), 1.06/7.30 (^{1}J, 7γ/7γ), 0.44/12.32 (^{1}J, 7ζ/η/7ζ/η), 0.33/4.81 (^{1}J, 7α/β/7α/β), −0.01/4.57 (^{1}J, 7α/β/7α/β); ^{1}H ^{13}C HMBC (400 MHz/101 MHz, [D6]benzene, 298 K): δ(ppm)/δ(ppm) 3.01/7.73 (^{2}J, 7δ/7γ).

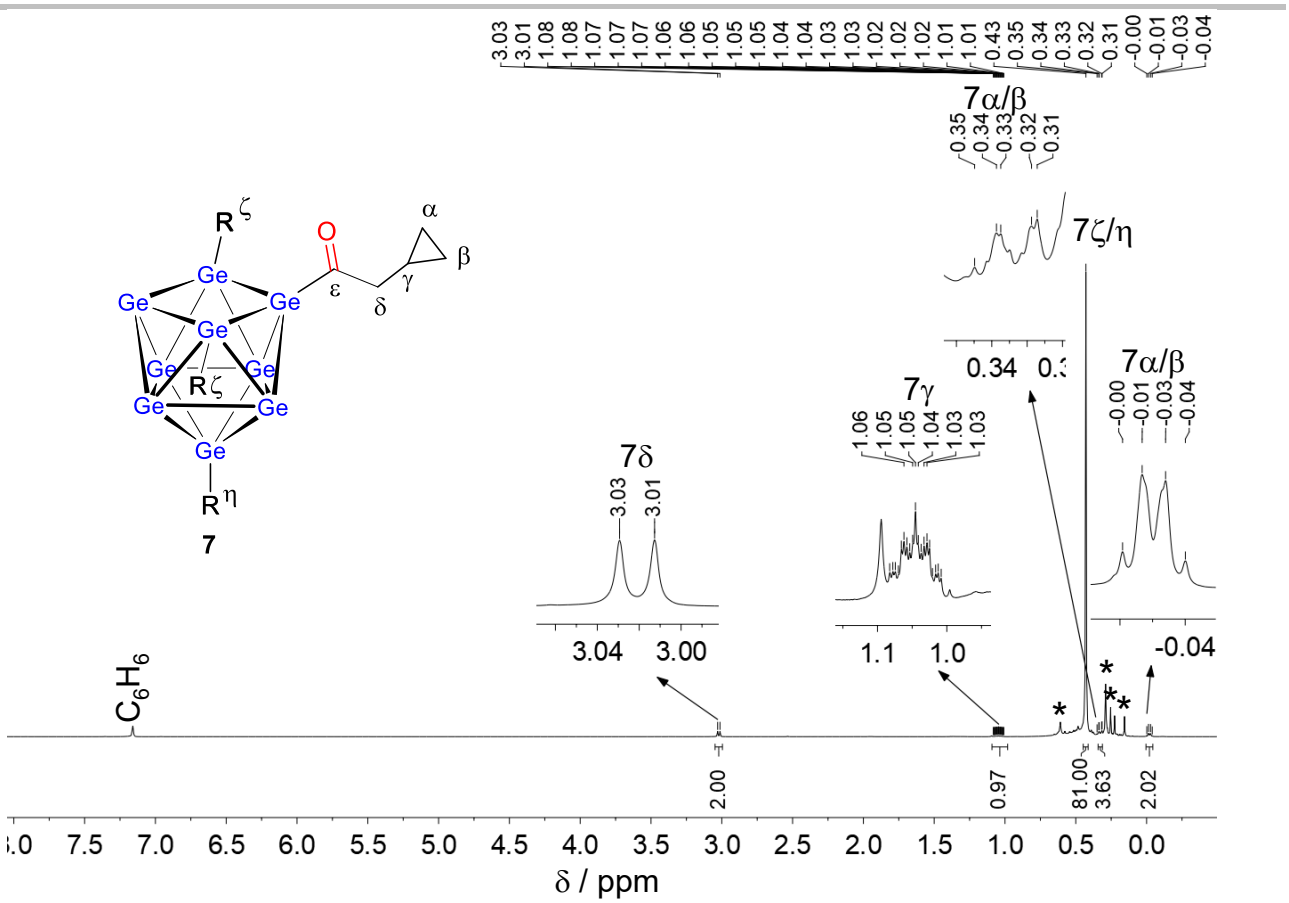

Figure S25. ^{1}H NMR spectrum of **7** in a [D6]benzene reaction solution recorded at r.t.. Signals marked with * could not be assigned. R represents the hypersilyl (hyp) moiety bound to the Ge_9 cluster.

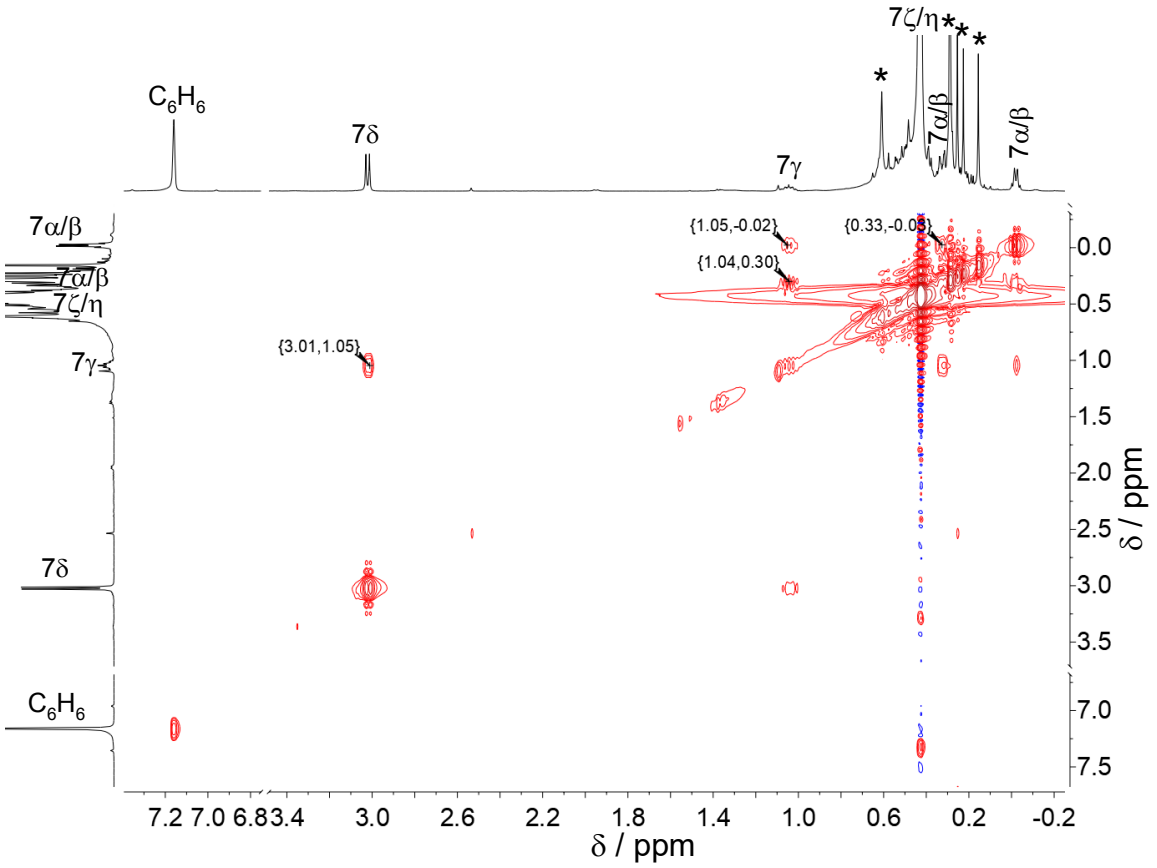

Figure S26. Relevant sections of the ^{1}H ^{1}H COSY NMR spectrum of **7** in a [D6]benzene reaction solution recorded at r.t.. Signals marked with * could not be assigned.

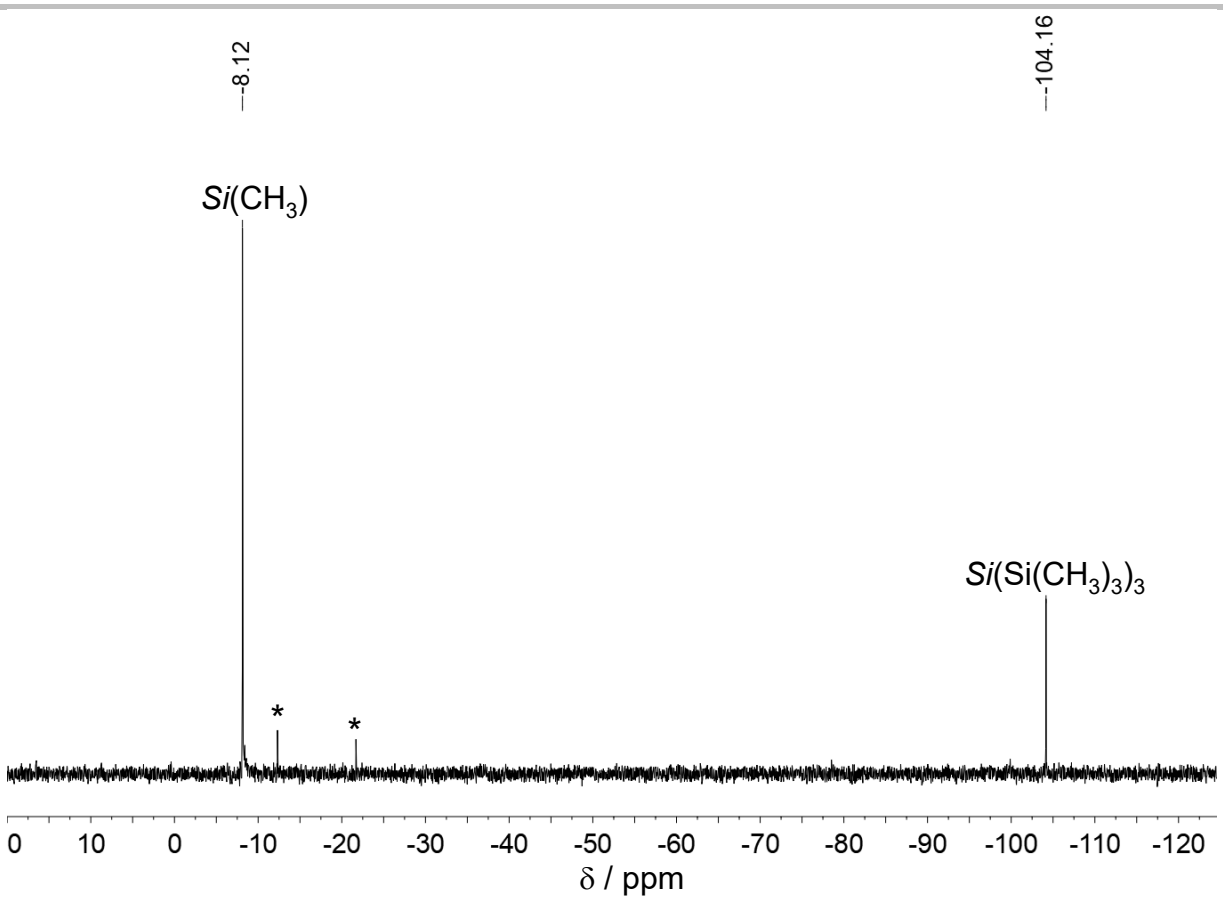

Figure S27. ^{29}Si NMR spectrum of **7** in [D6]benzene at r.t.. Signals marked with * could not be assigned.

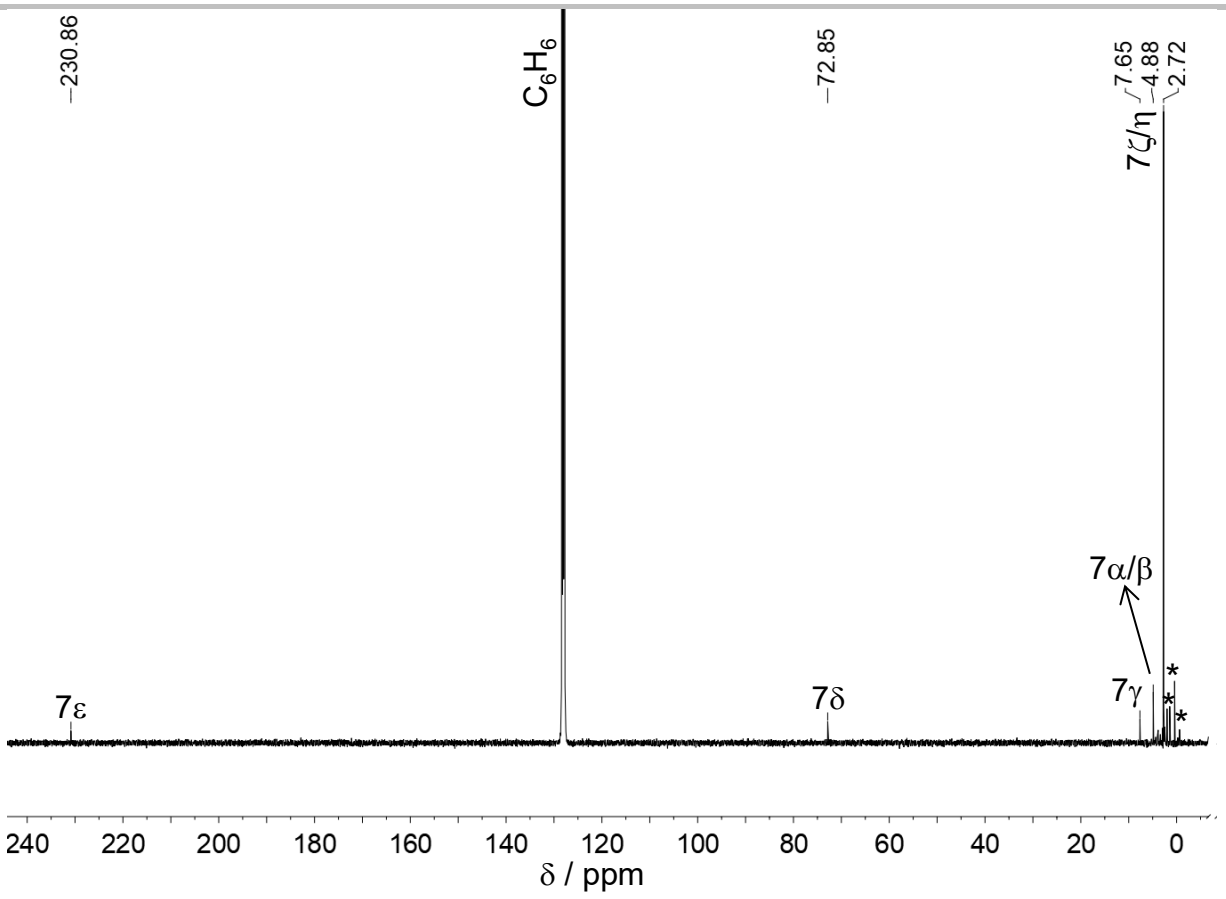

Figure S28. ^{13}C NMR spectrum of **7** in [D6]benzene at r.t.. Signals marked with * could not be assigned.

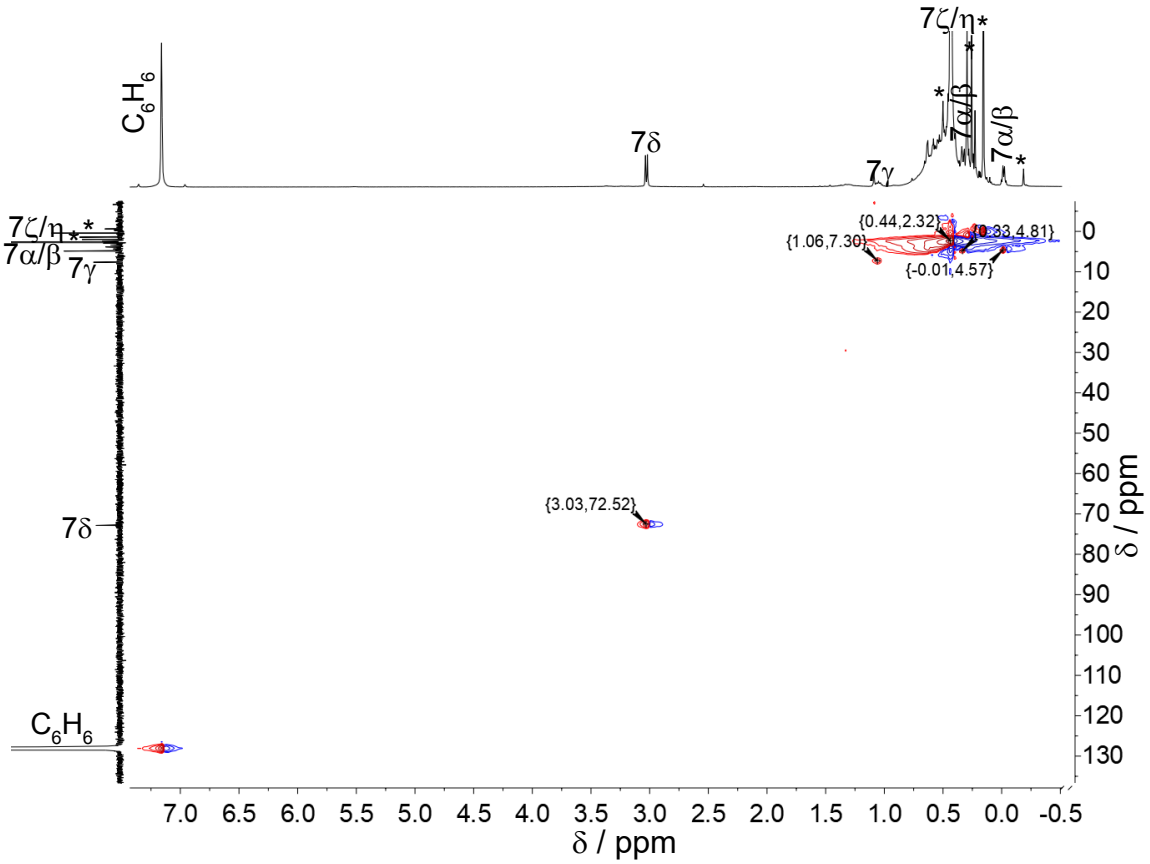

Figure S29. ^{1}H ^{13}C HSQC NMR spectrum of **7** in [D6]benzene at r.t.. Signals marked with * could not be assigned.

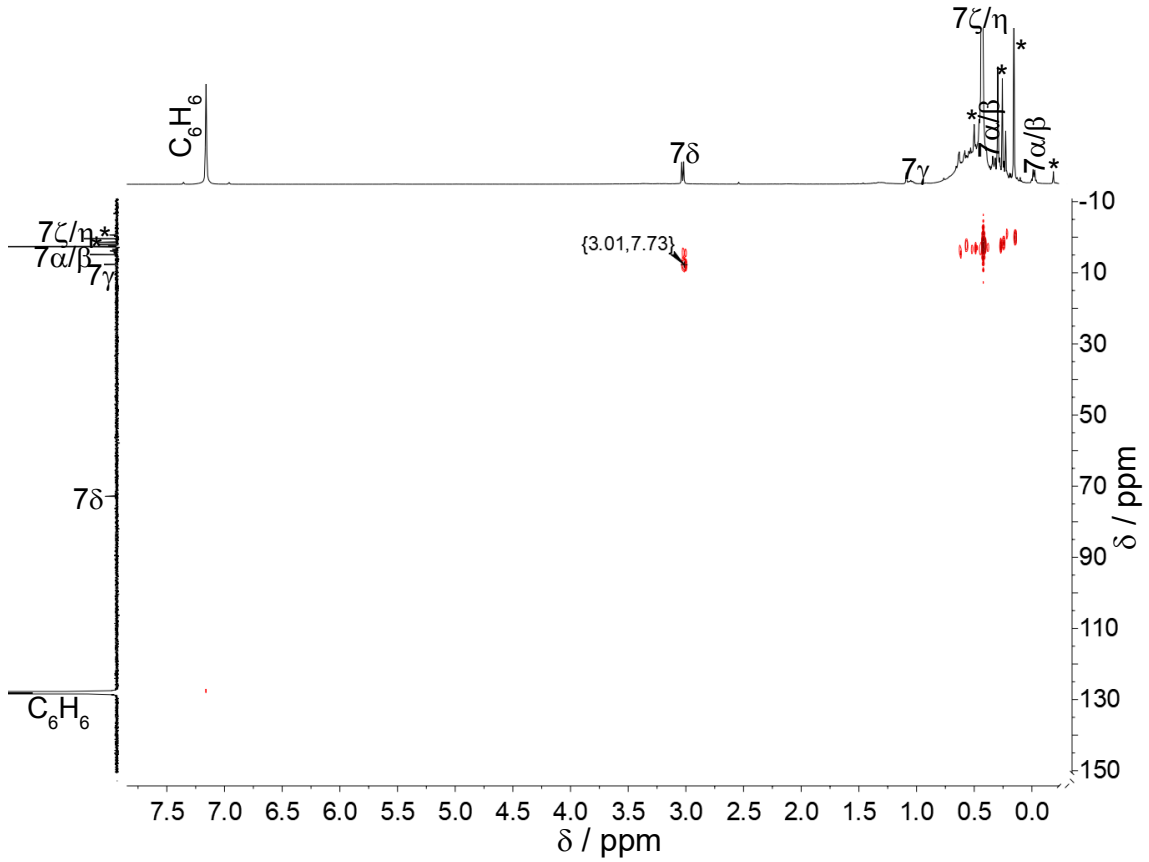

Figure S30. ^{1}H ^{13}C HMBC NMR spectrum of **7** in [D6]benzene at r.t.. Signals marked with * could not be assigned.

3.8 NMR spectroscopic characterization of 8

A solution of hydrocinnamoyl chloride (6.24 μL, 0.042 mmol) in 1.2 mL [D6]benzene was added to K[Ge_9{$Si(SiMe_3)_3$}$_3$] (60 mg, 0.042 mmol). The deep red-brown solution was stirred for 14 h at r.t.. The solution was characterized by NMR spectroscopy. ^{1}H NMR (400 MHz, [D6]benzene, 298 K): δ(ppm) 7.04 (m, 5H, 8α/β/γ), 3.43 (t, 2H, 8ζ), 2.85 (t, 2H, 8ε), 0.42 (s, 81H, 8θ/ι); ^{1}H ^{1}H COSY (400 MHz, [D6]benzene, 298 K): δ(ppm)/δ(ppm) 3.41/2.85 (^{3}J, 8ζ/8ε); $^{13}C\{^{1}H\}$ NMR (101 MHz, [D6]benzene, 298 K): δ(ppm) 231.56 (s, 8η), 128.93 (m, C_{Ar}), 128.78 (m, C_{Ar}), 126.44 (m, C_{Ar}), 69.12 (t, 8ζ), 31.00 (t, 8ε), 2.70 (q, 8θ/ι); ^{29}Si NMR (79 MHz, [D6]benzene, 298 K): δ(ppm) −8.13 (*Si*$(CH_3)_3$), −104.01 (*Si*$(Si(CH_3)_3)_3$)); ^{1}H ^{13}C HSQC (400 MHz/101 MHz, [D6]benzene, 298 K): δ(ppm)/δ(ppm) 7.09/128.50 (^{1}J, H_{Ar}/C_{Ar}), 7.02/126.06 (^{1}J, H_{Ar}/C_{Ar}), 7.00/128.60 (^{1}J, H_{Ar}/C_{Ar}), 3.44/68.71 (^{1}J, 8ζ/8ζ), 2.86/30.61 (^{1}J, 8ε/8ε), 0.42/2.28 (^{1}J, 8θ/ι/8θ/ι).

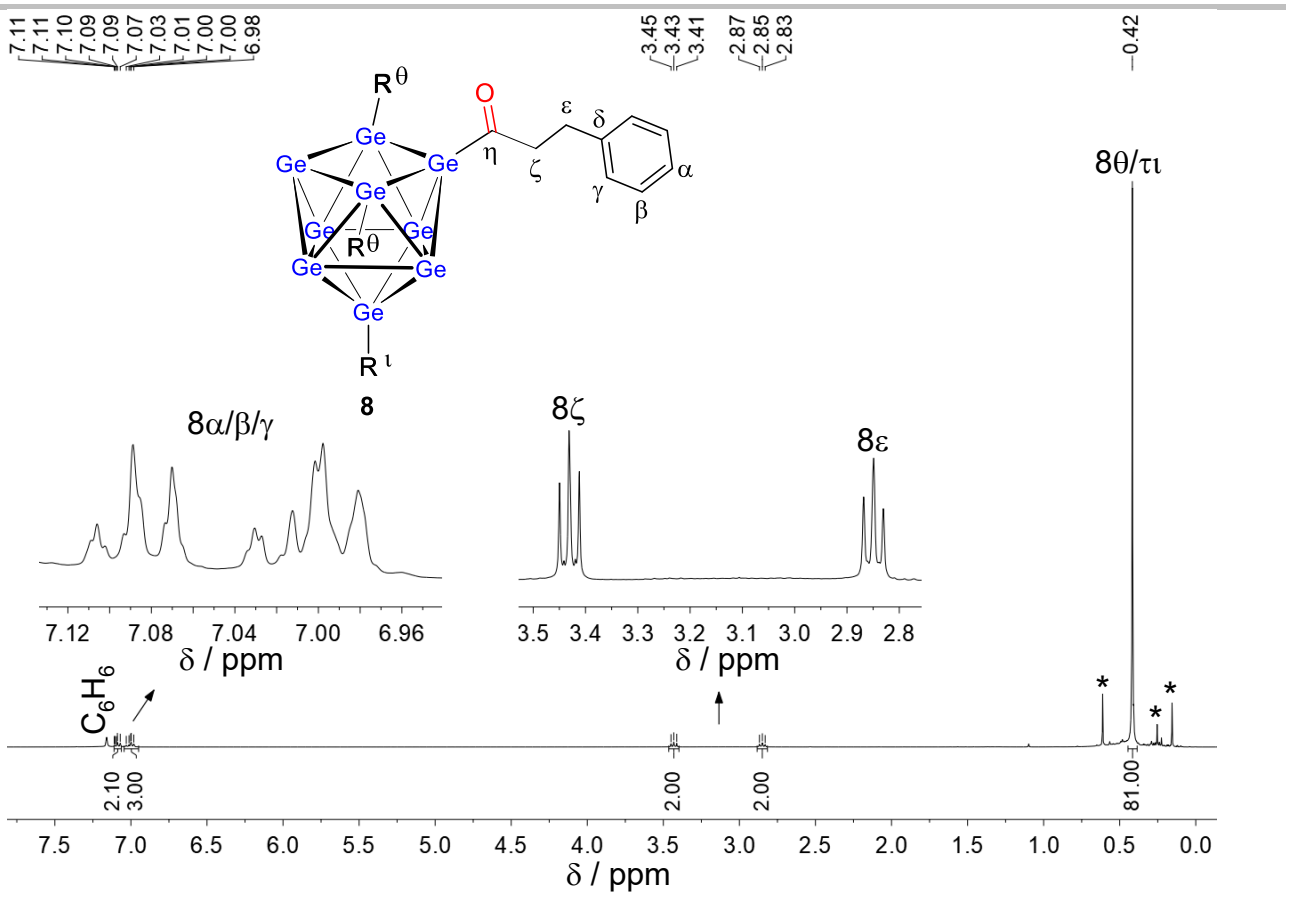

Figure S31. ^{1}H NMR spectrum of the reaction solution of **8** in [D6]benzene recorded at r.t.. Signals marked with * could not be assigned. R represents the hypersilyl (hyp) moiety bound to the Ge_9 cluster.

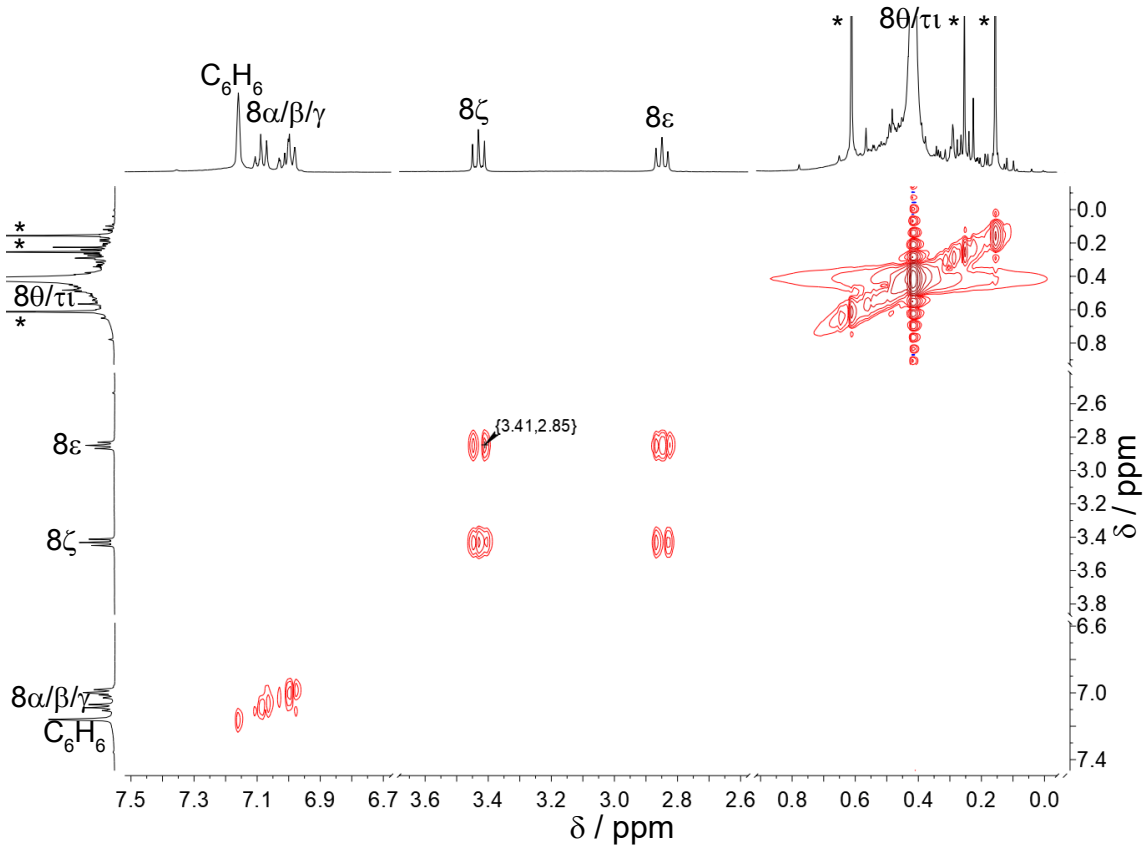

Figure S32. Relevant sections of the ^{1}H ^{1}H COSY NMR spectrum of the reaction solution of **8** in [D6]benzene recorded at r.t.. Signals marked with * could not be assigned.

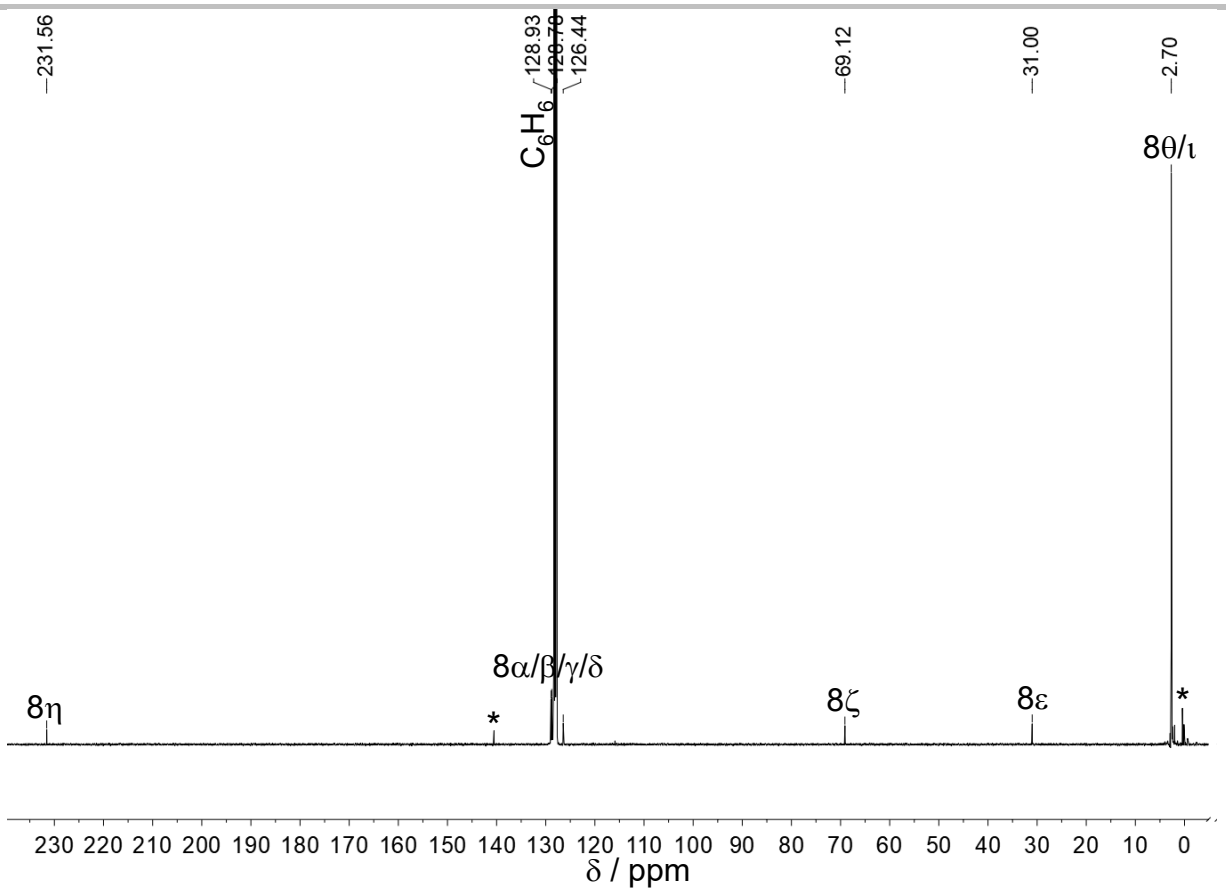

Figure S33. ^{13}C NMR spectrum of the reaction solution of **8** in [D6]benzene recorded at r.t.. Signals marked with * could not be assigned.

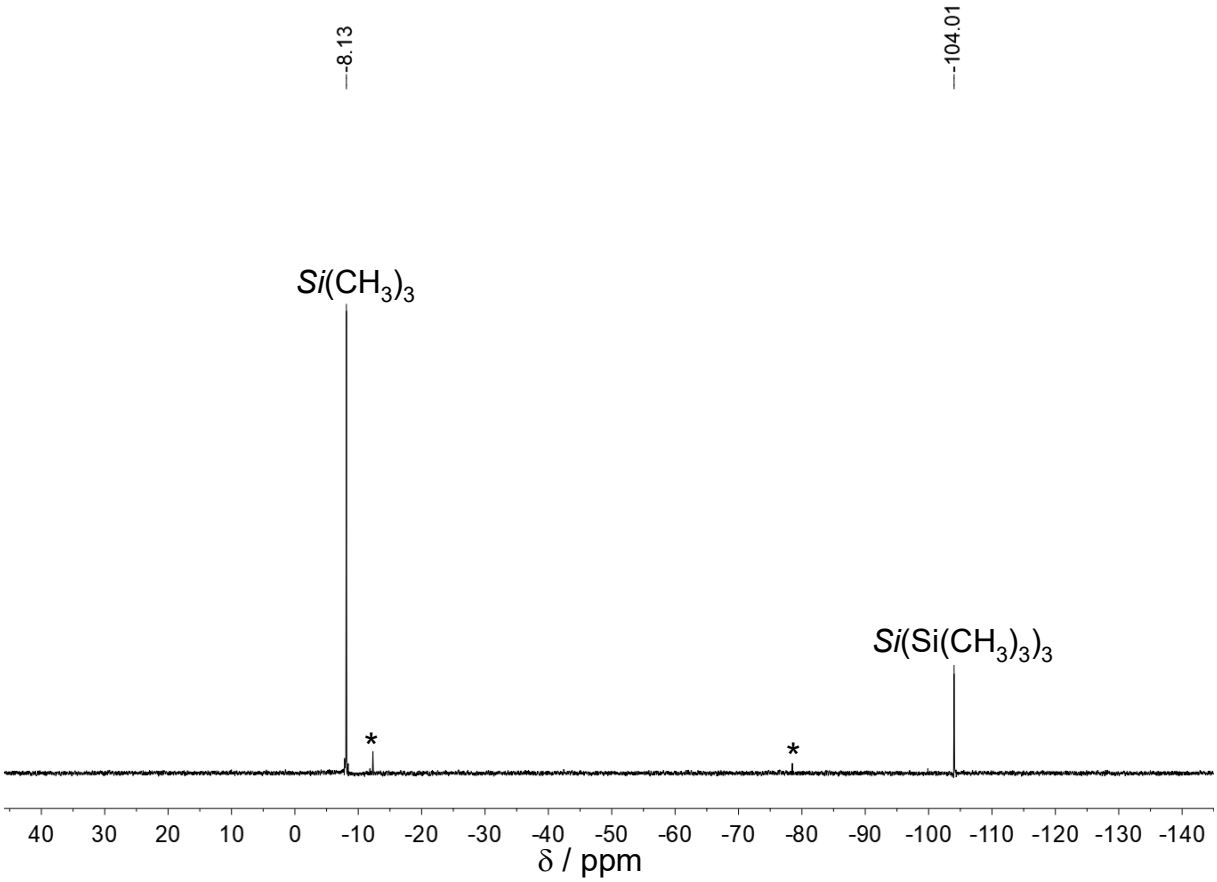

Figure S34. ^{29}Si NMR spectrum of the reaction solution of **8** in [D6]benzene recorded at r.t.. Signals marked with * could not be assigned.

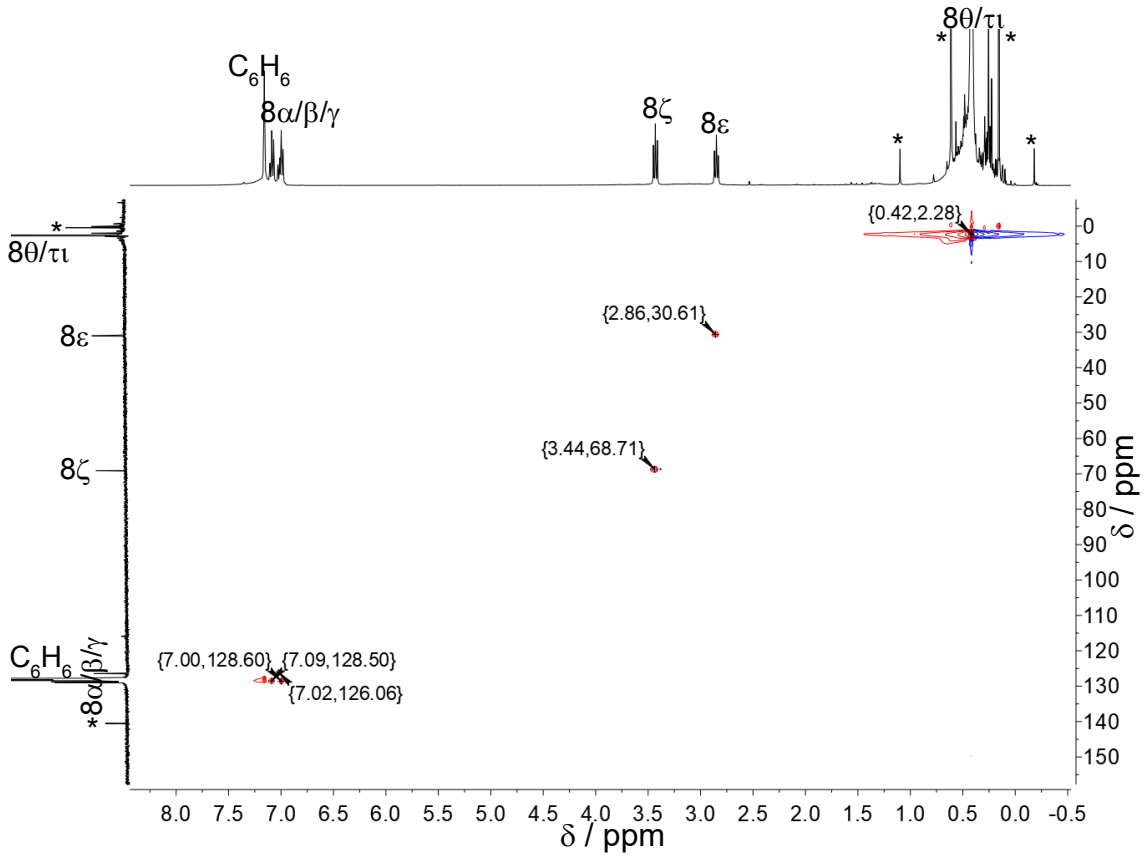

Figure S35. ^{1}H ^{13}C HSQC NMR spectrum of the reaction solution of **8** in [D6]benzene recorded at r.t.. Signals marked with * could not be assigned.

3.9 NMR spectroscopic characterization of 9

A solution of 4-vinylbenzoyl chloride (5.8 μL, 0.042 mmol) in 0.6 mL toluene was added to K[Ge$_9${Si(SiMe$_3$)$_3$}$_3$] (60 mg, 0.042 mmol). The deep red-brown solution was stirred for 14 h at r.t.. The solvent was evaporated in a vacuum. The resulting solid was dissolved in a deuterated solvent and characterized by NMR spectroscopy. ^{1}H NMR (400 MHz, [D6]benzene, 298 K): δ(ppm) 8.32 (d, ^{3}J = 8.4 Hz, 9ζ, 2H), 7.02 (d, ^{3}J = 8.4 Hz, 9ε, 2H), 6.33 (dd, ^{3}J = 17.6 Hz, 11.2 Hz, 9γ, 1H), 5.47 (d, ^{3}J = 17.6 Hz, 9β, 1H), 5.03 (d, ^{3}J = 11.2 Hz, 9α, 1H), 0.41 (s, 9ι/κ, 81H); ^{1}H ^{1}H COSY (400 MHz, [D6]benzene, 298 K): δ(ppm)/δ(ppm) 8.34/7.01 (^{3}J, 9ζ/9ε), 6.36/5.45 (^{3}J, 9γ/9β), 6.36/5.01 (^{3}J, 9γ/9α); ^{13}C{^{1}H} NMR (101 MHz, [D6]benzene, 298 K): δ(ppm) 225.98 (s, 9θ), 143.36 (s, 9δ), 142.02 (s, 9η), 136.03 (d, 9γ), 130.49 (d, 9ζ), 126.61 (d, 9ε), 117.18 (dd, 9α/β), 2.80 (q, 9ι/κ); ^{29}Si NMR (79 MHz, [D6]benzene, 298 K): δ(ppm) −8.02 (*Si*(CH$_3$)$_3$), −103.11 (*Si*(Si(CH$_3$)$_3$)$_3$)); ^{1}H ^{13}C HSQC (400 MHz/101 MHz, [D6]benzene, 298 K): δ(ppm)/δ(ppm) 8.32/130.20 (^{1}J, 9ζ/9ζ), 7.03/126.28 (^{1}J, 9ε/9ε), 6.36/135.72 (^{1}J, 9γ/9γ), 5.49/116.86 (^{1}J, 9β/9β), 5.04/116.86 (^{1}J, 9α/9α); ^{1}H ^{13}C HMBC (400 MHz/101 MHz, [D6]benzene, 298 K): δ(ppm)/δ(ppm) 8.31/143.34 (^{3}J, 9ζ/9δ), 7.01/142.12 (^{3}J, 9ε/9η), 7.00/135.90 (^{3}J, 9ε/9γ), 6.33/126.49 (^{3}J, 9γ/9ε), 5.47/143.41 (^{3}J, 9β/9δ), 5.48/135.82 (^{2}J, 9β/9γ), 5.02/143.36 (^{3}J, 9α/9δ).

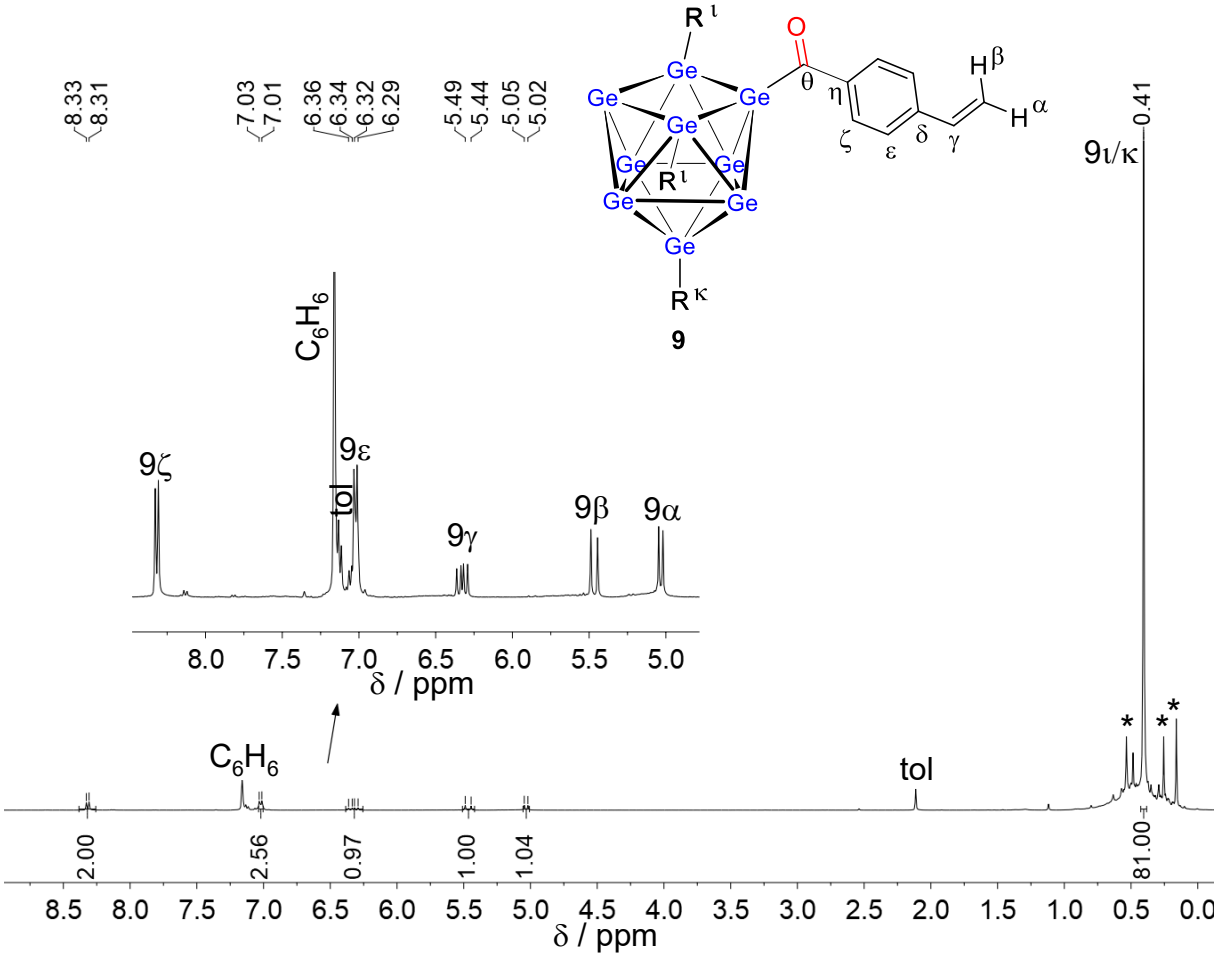

Figure S36. ^{1}H NMR spectrum of the reaction solution of **9** in [D6]benzene recorded at r.t.. Signals marked with * could not be assigned. R represents the hypersilyl (hyp) moiety bound to the Ge_9 cluster.

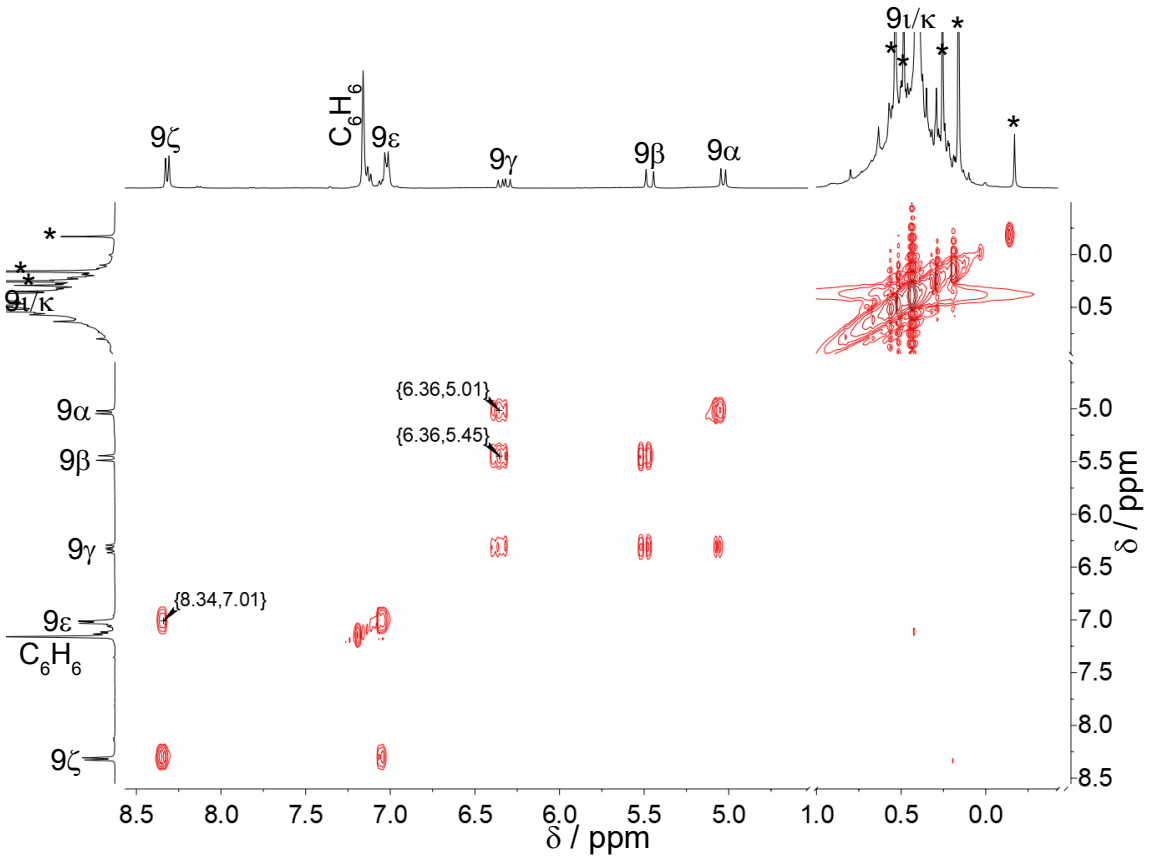

Figure S37. Relevant sections of the ^{1}H ^{1}H COSY NMR spectrum of the reaction solution of **9** in [D6]benzene recorded at r.t.. Signals marked with * could not be assigned.

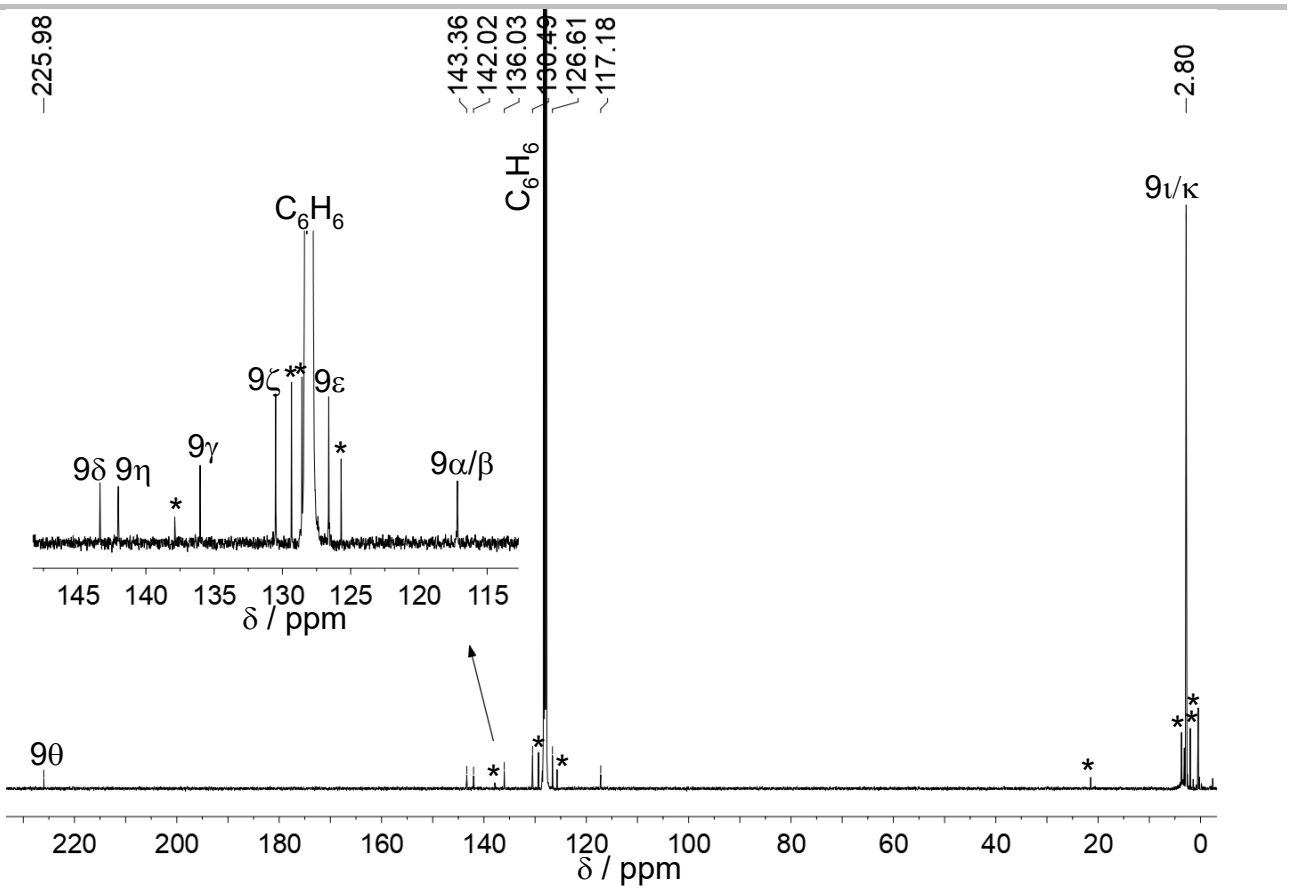

Figure S38. ^{13}C NMR spectrum of the reaction solution of **9** in [D6]benzene recorded at r.t.. Signals marked with * could not be assigned.

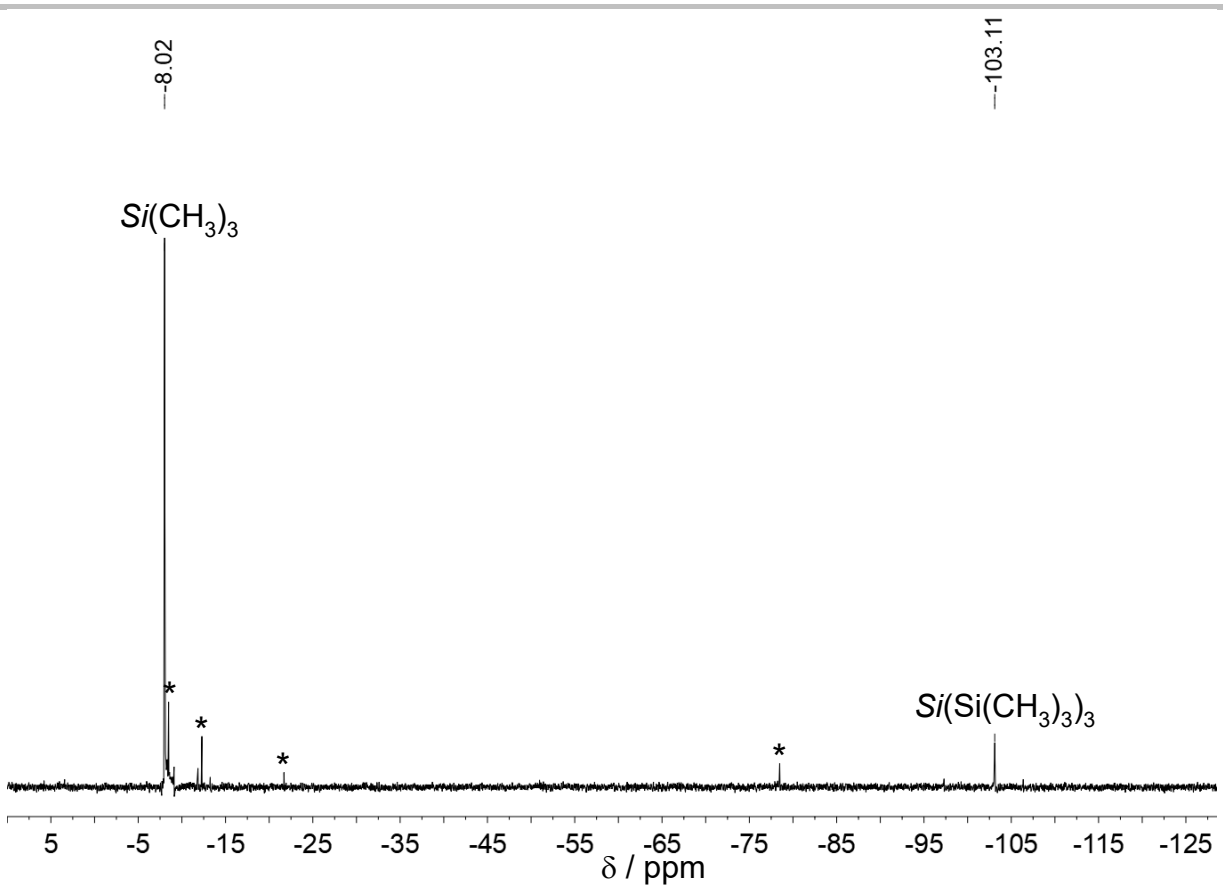

Figure S39. ^{29}Si NMR spectrum of the reaction solution of **9** in [D6]benzene recorded at r.t.. Signals marked with * could not be assigned.

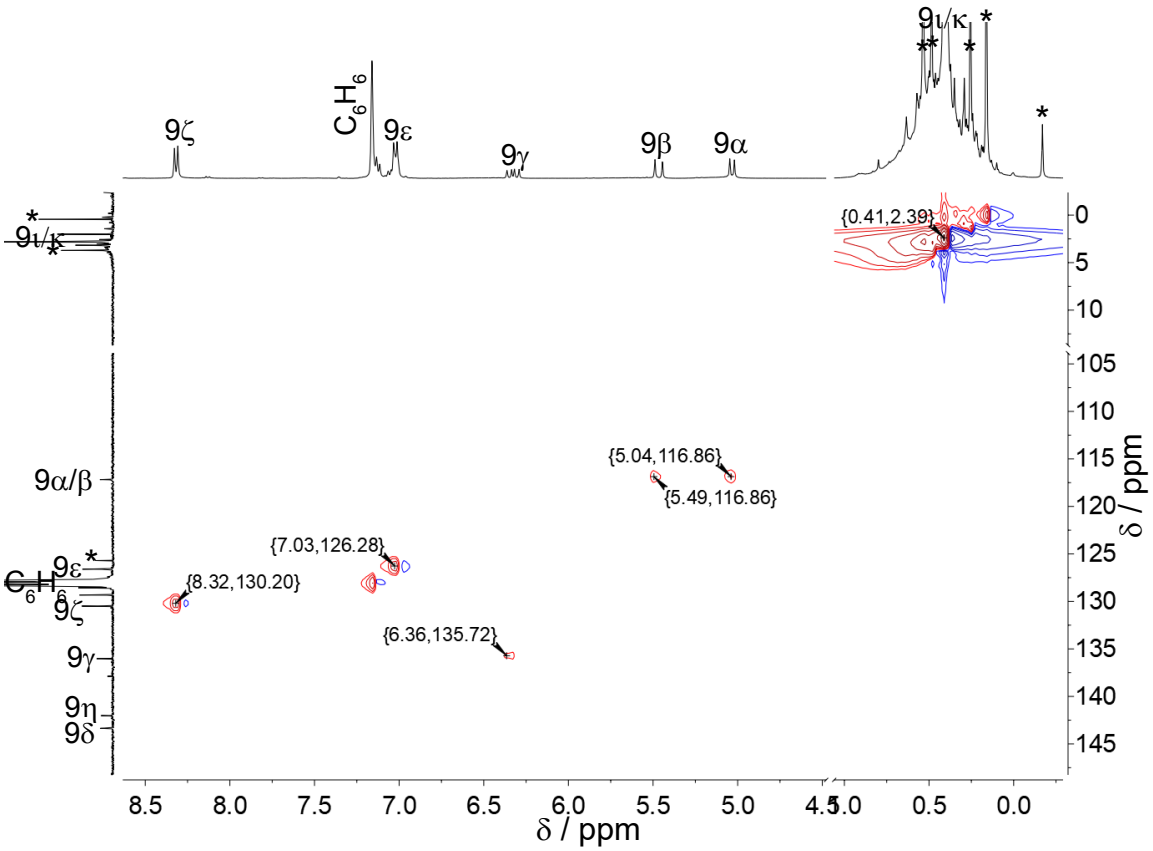

Figure S40. ^{1}H ^{13}C HSQC NMR spectrum of the reaction solution of **9** in [D6]benzene recorded at r.t.. Signals marked with * could not be assigned.

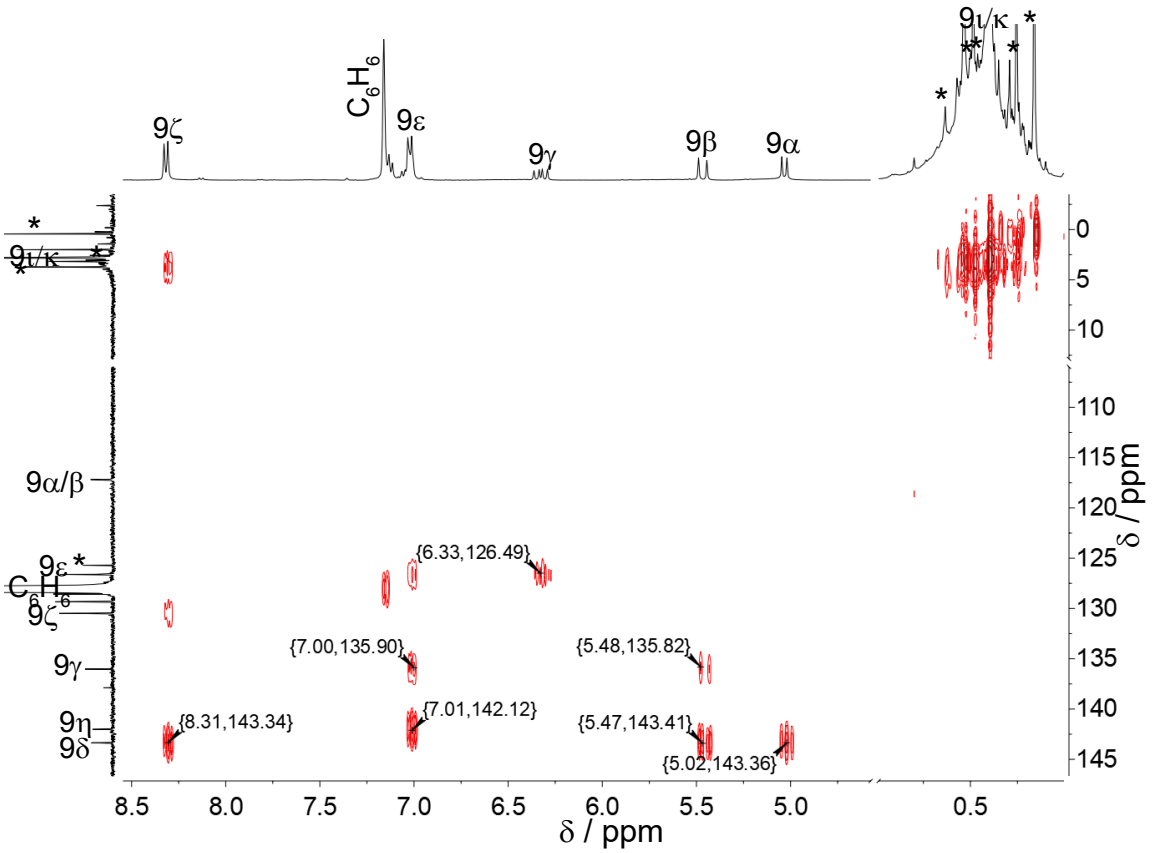

Figure S41. Relevant Sections of the ^{1}H ^{13}C HMBC NMR spectrum of the reaction solution of **9** in [D6]benzene recorded at r.t.. Signals marked with * could not be assigned.

4 Time-resolved ^{1}H NMR Spectroscopic Studies of Compound 1

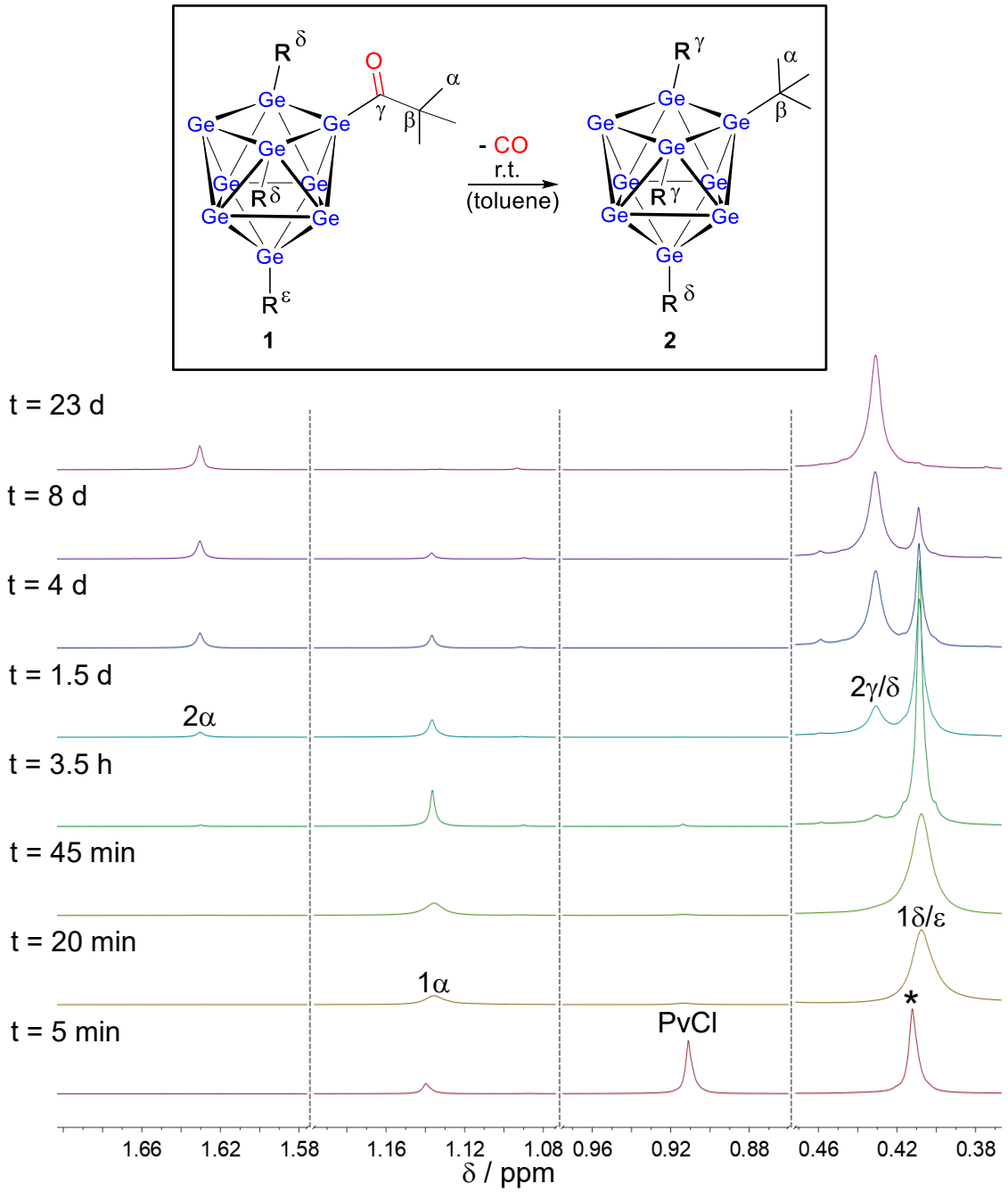

Figure S42. Relevant sections of the time-resolved ^{1}H NMR study of the reaction solution of K[Ge_9{$Si(SiMe_3)_3$}$_3$] (30 mg, 0.021 mmol) and pivaloyl chloride (2.6 μL, 0.021 mmol) in 0.6 mL [D8]toluene at r.t.. The signal marked with * could not be assigned.

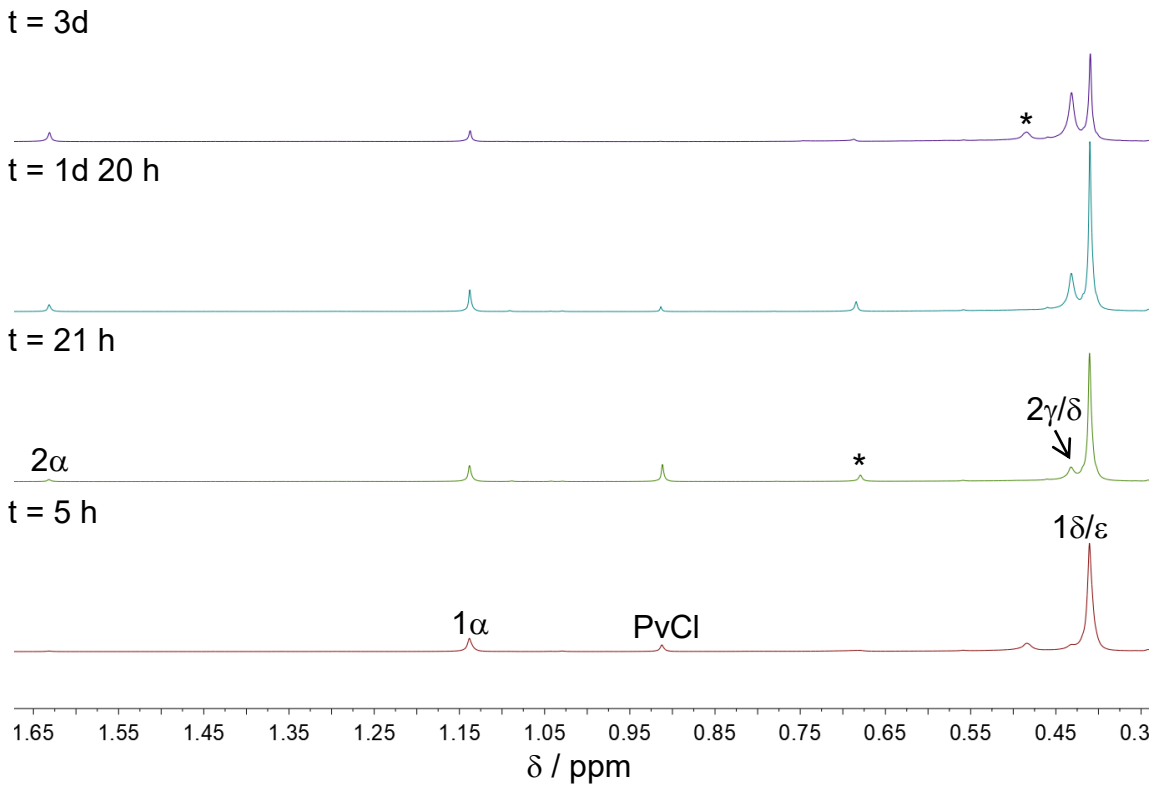

Figure S43. Time-resolved ^{1}H NMR study of the reaction solution of K[Ge$_9${Si(SiMe$_3$)$_3$}$_3$] (30 mg, 0.021 mmol) and pivaloyl chloride (2.6 μL, 0.021 mmol) in 0.6 mL [D8]toluene at r.t. after reaction time t under exclusion of light. Signals marked with * could not be assigned.

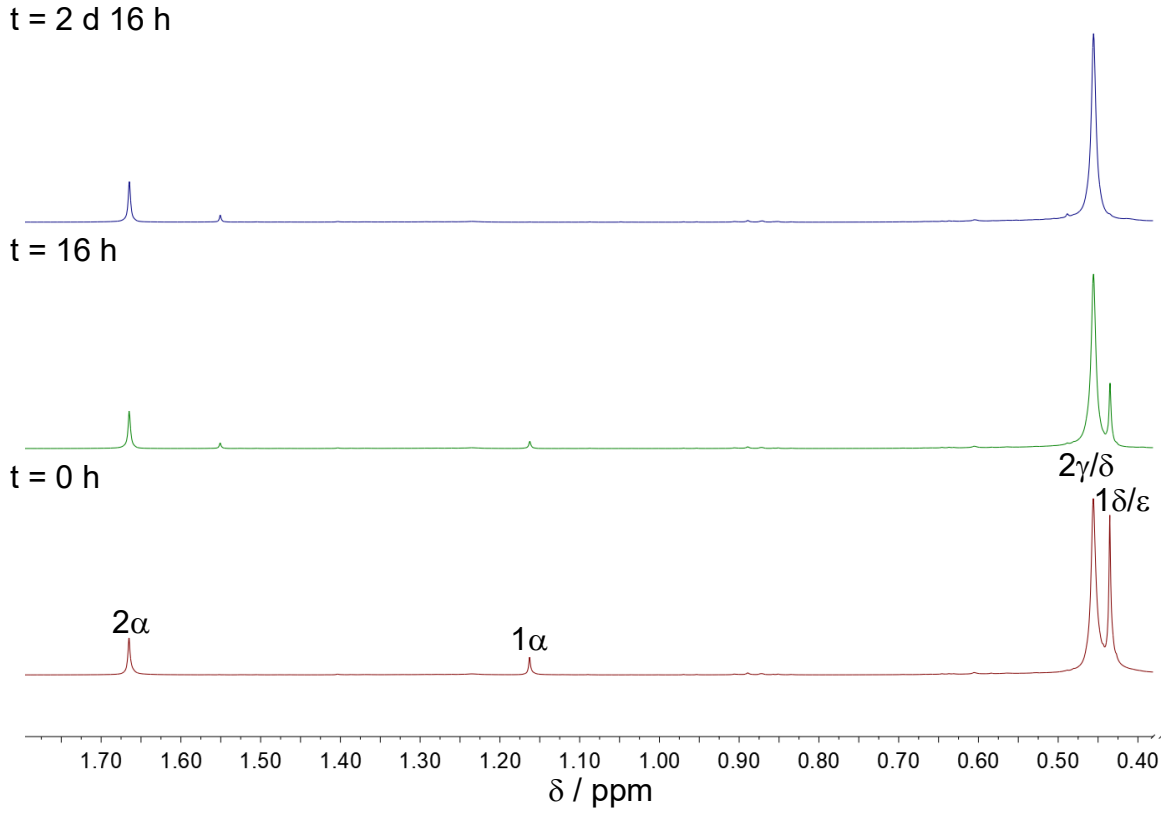

Figure S44. Time-resolved ^{1}H NMR study in [D6]benzene of the dissolved residue of the reaction of 1 eq. of K[Ge$_9${Si(SiMe$_3$)$_3$}$_3$] with 1 eq. of pivaloyl chloride in hexane after a reaction time of 17 h at r.t. and after evaporation of hexane to dryness. t abbreviates the period after redissolving of products 1 and 2 in [D6]benzene.

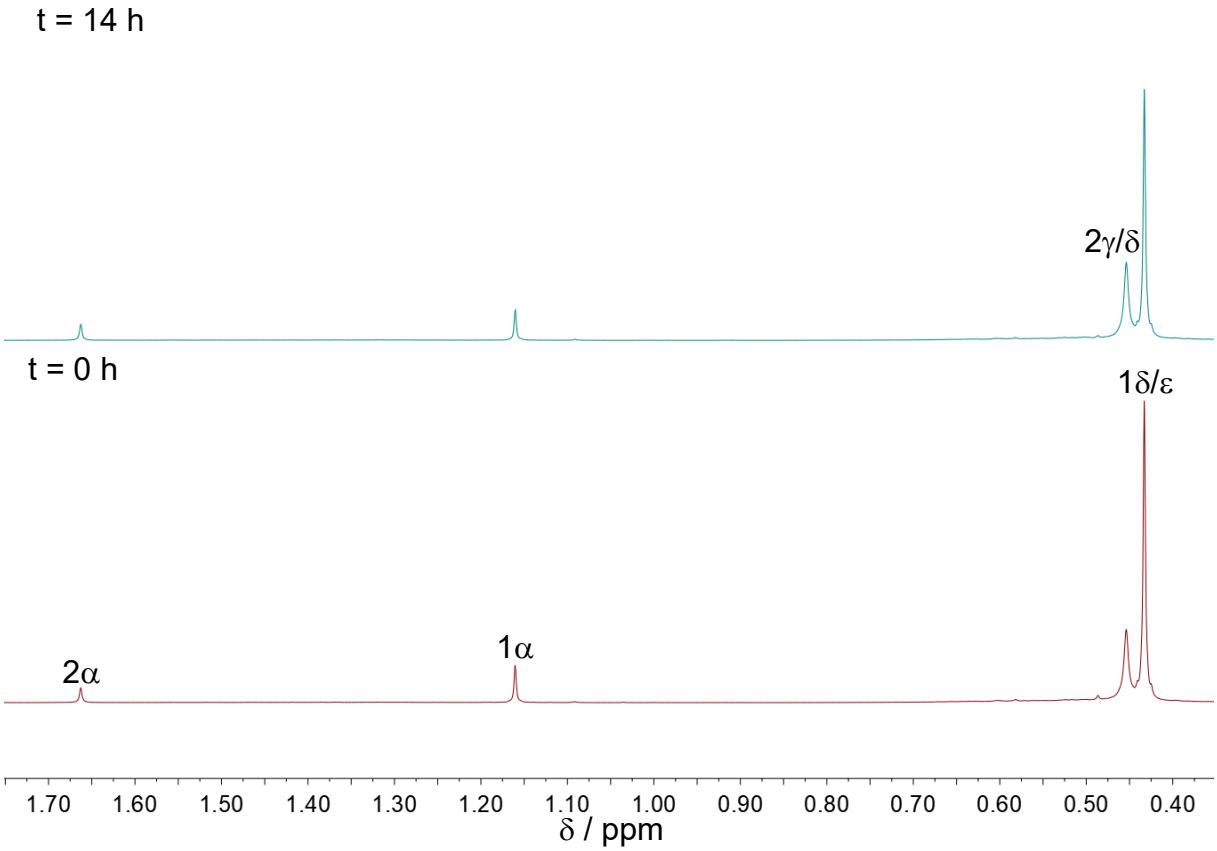

Figure S45. Time-resolved ^{1}H NMR study in [D6]benzene of the dissolved residue of the reaction of $K[Ge_9\{Si(SiMe_3)_3\}_3]$ (60 mg, 0.042 mmol) with pivaloyl chloride (5.2 μL, 0.042 mmol) in 1.2 mL benzene after a reaction time of 16 h at r.t. and after evaporation of benzene to dryness. t abbreviates the period after redissolving products 1 and 2 in [D6]benzene.

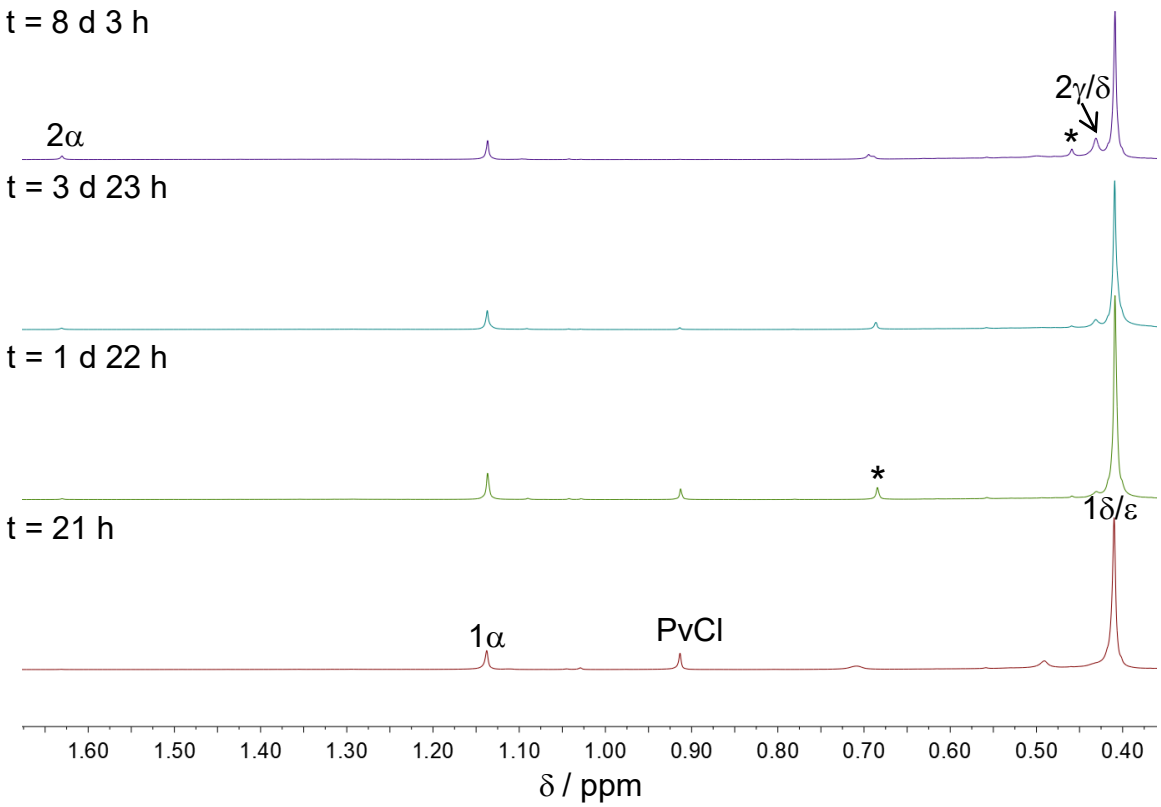

Figure S46. Time-resolved ^{1}H NMR study of the reaction solution of K[Ge$_9${Si(SiMe$_3$)$_3$}$_3$] (30 mg, 0.021 mmol) and pivaloyl chloride (2.6 μL, 0.021 mmol) in 0.6 mL [D8]toluene at 2 °C after reaction time t. Signals marked with * could not be assigned.

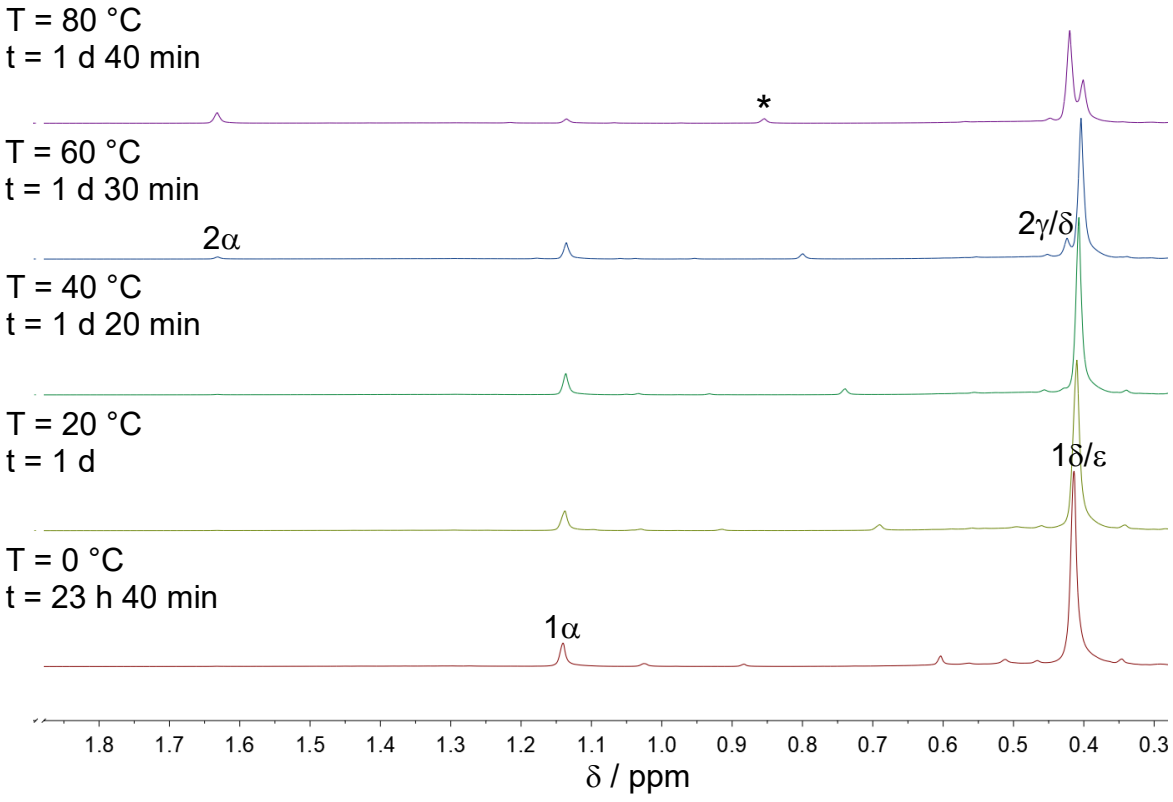

Figure S47. Temperature-resolved ^{1}H NMR study of the reaction solution of K[Ge$_9${Si(SiMe$_3$)$_3$}$_3$] (30 mg, 0.021 mmol) and pivaloyl chloride (2.6 μL, 0.021 mmol) in 0.6 mL [D8]toluene after reaction time t. The compounds were first reacted at 0 °C for 23 h and 40 min before the ^{1}H NMR spectrum at 0 °C was recorded. The temperature was then slowly raised. Signals marked with * could not be assigned.

5 CO-Detection Reaction

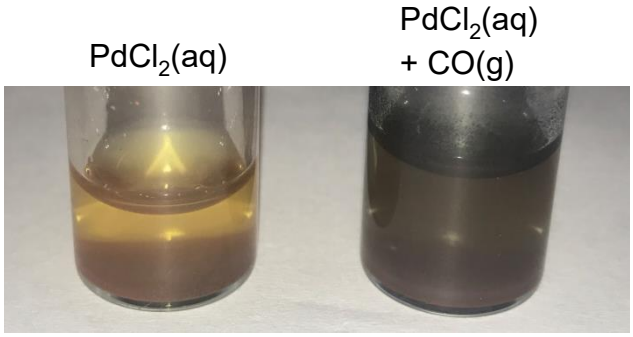

Figure S48. CO detection reaction with a saturated aqueous solution of $PdCl_2$. The gas phase of a reaction solution after almost complete conversion of **1** into **2** (see Figure S49) was injected into a saturated, pale orange aqueous solution of $PdCl_2$. Elemental Pd occurs after 2 minutes and appears as metallic precipitate.

6 Variable-temperature ^{1}H NMR Spectroscopic Investigations of the Neutral Ge_9 Cluster Compounds 1-9

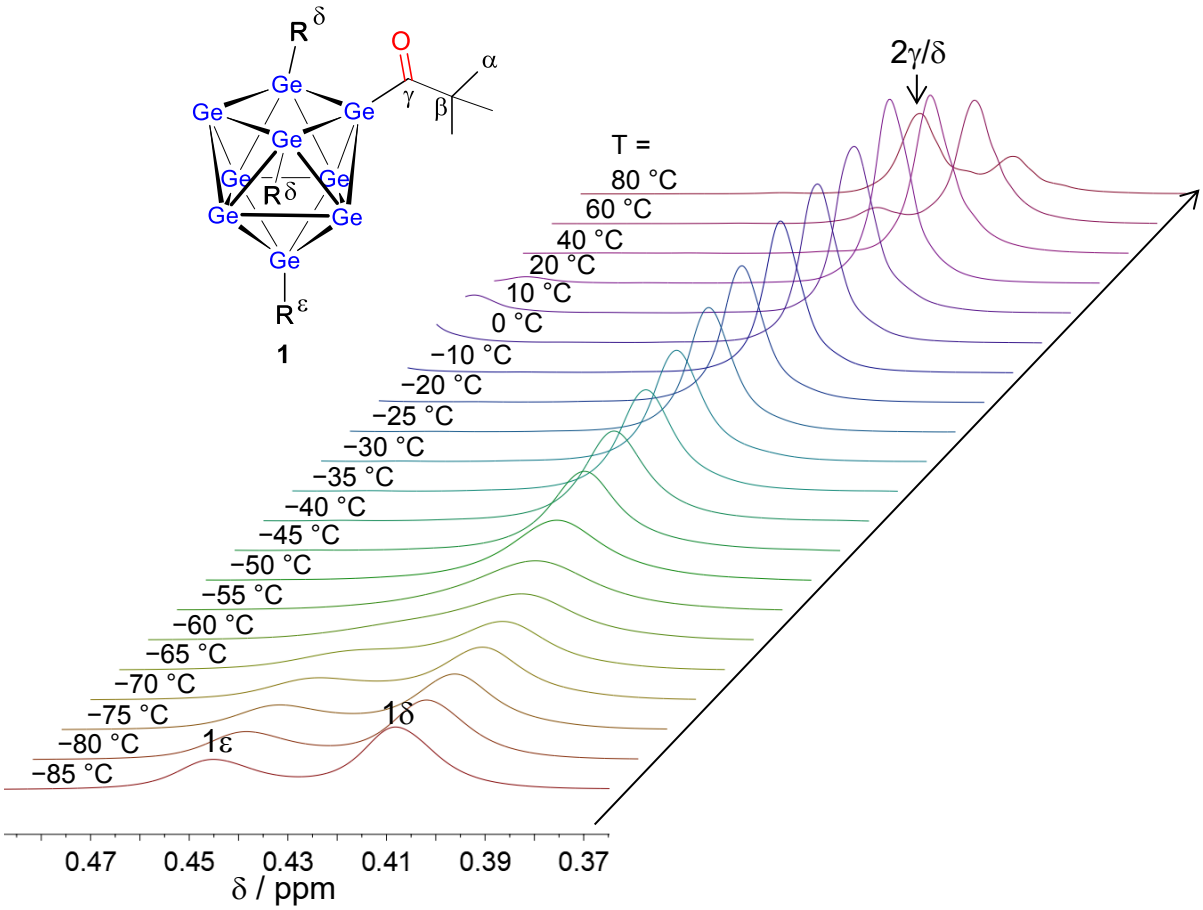

Figure S49. Temperature-dependent ^{1}H NMR spectra in the temperature range from -85 °C to 80 °C of the reaction solution of $K[Ge_9\{Si(SiMe_3)_3\}_3]$ (0.021 mmol, 30 mg) with pivaloyl chloride (0.021 mmol, 2.64 μL) in 0.6 mL [D8]toluene to obtain $[\{Si(SiMe_3)_3\}_3Ge_9(CO)tBu]$ (**1**) after a reaction time of 14.5 h at 2 °C.

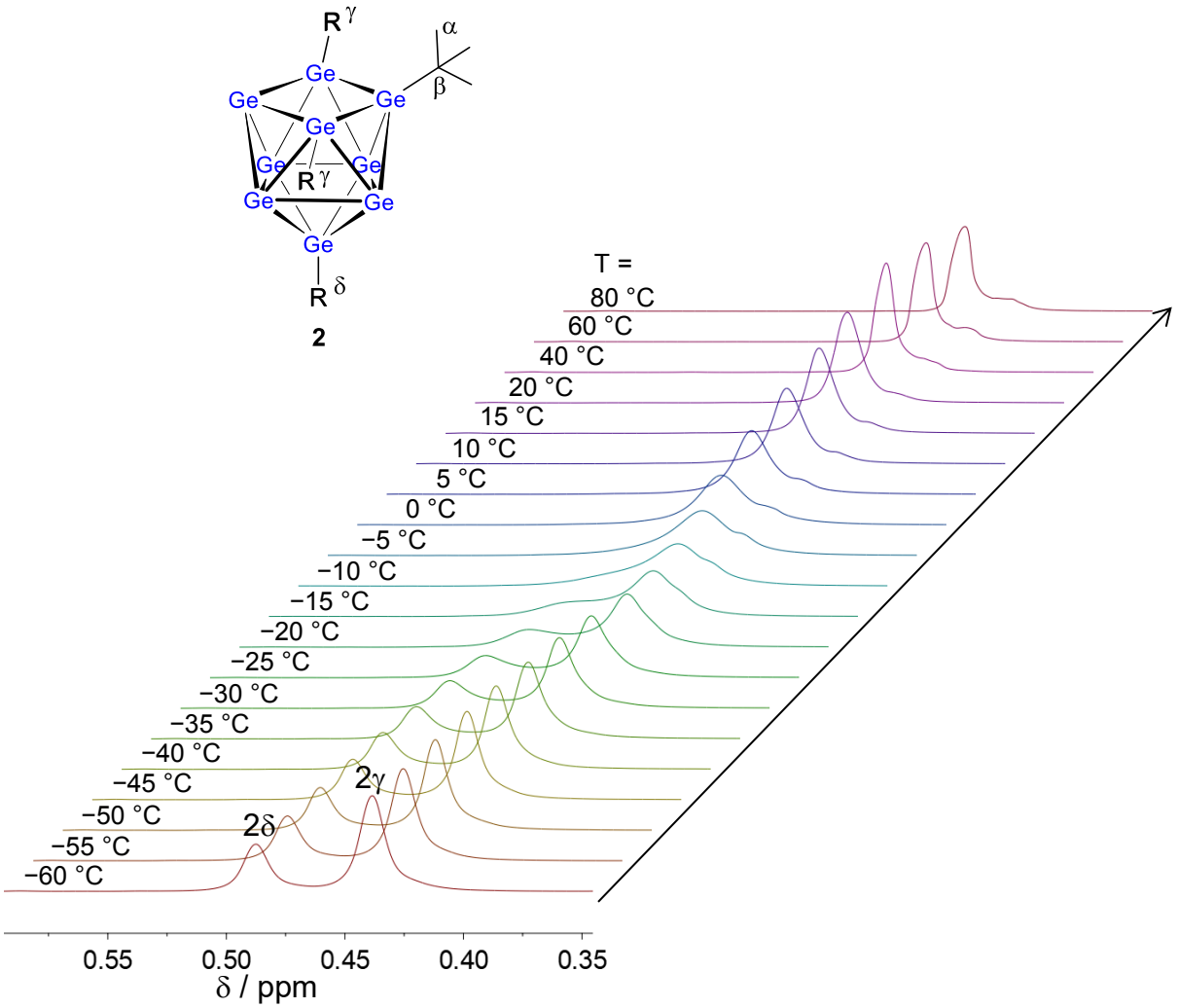

Figure S50. Temperature-dependent ^{1}H NMR spectra of crystals of **2** in [D8]toluene in the temperature-range from −60 °C to 80 °C.

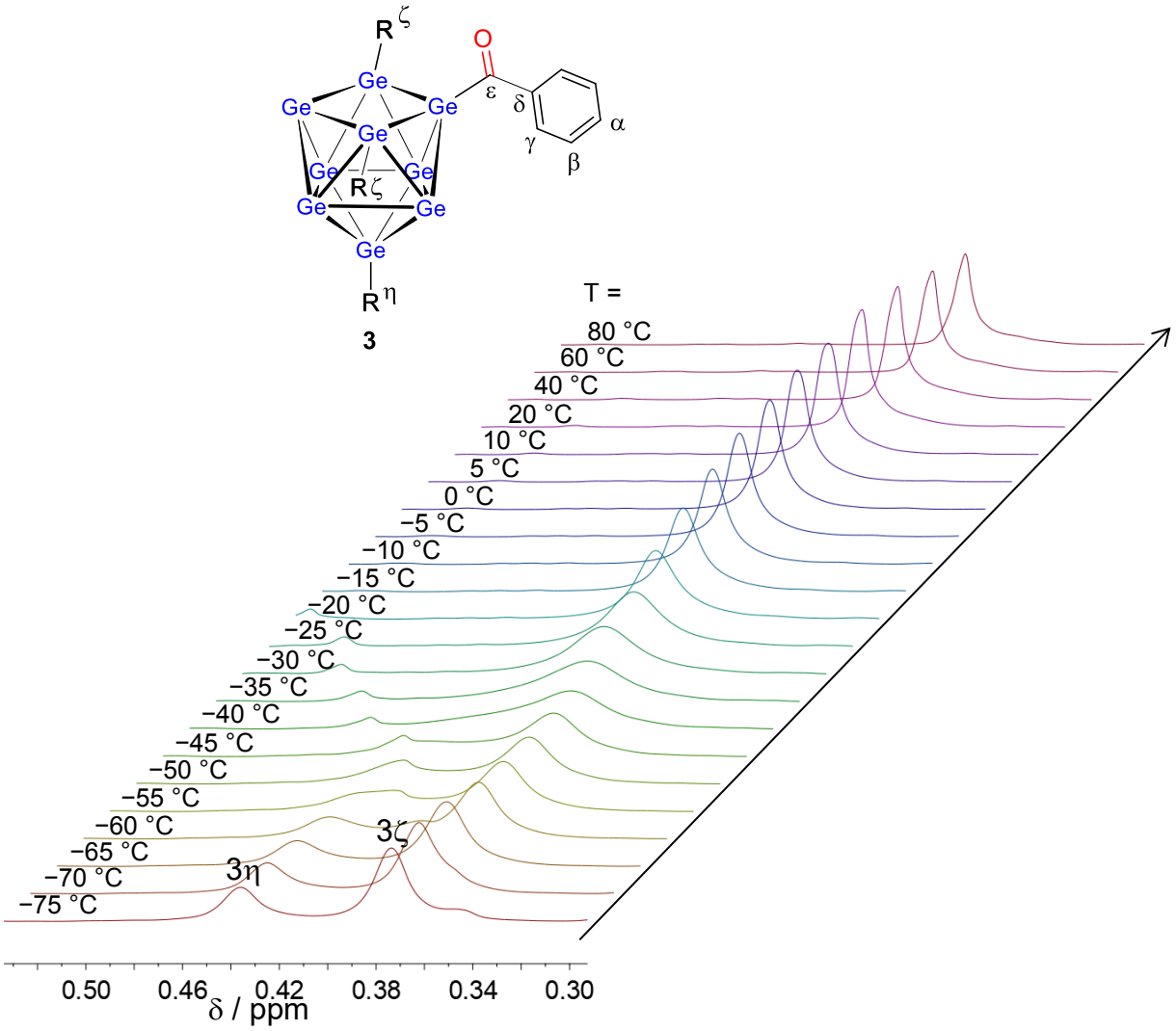

Figure S51. Temperature-dependent ^{1}H NMR spectra in the temperature range from −75 °C to 80 °C of the reaction solution of K[Ge_9{$Si(SiMe_3)_3$}$_3$] (0.021 mmol, 30 mg) with benzoyl chloride (0.021 mmol, 2.44 μL) in 0.6 mL [D8]toluene to obtain [{$Si(SiMe_3)_3$}$_3Ge_9(CO)C_6H_5$] (**3**) after a reaction time of 15 h at r.t..

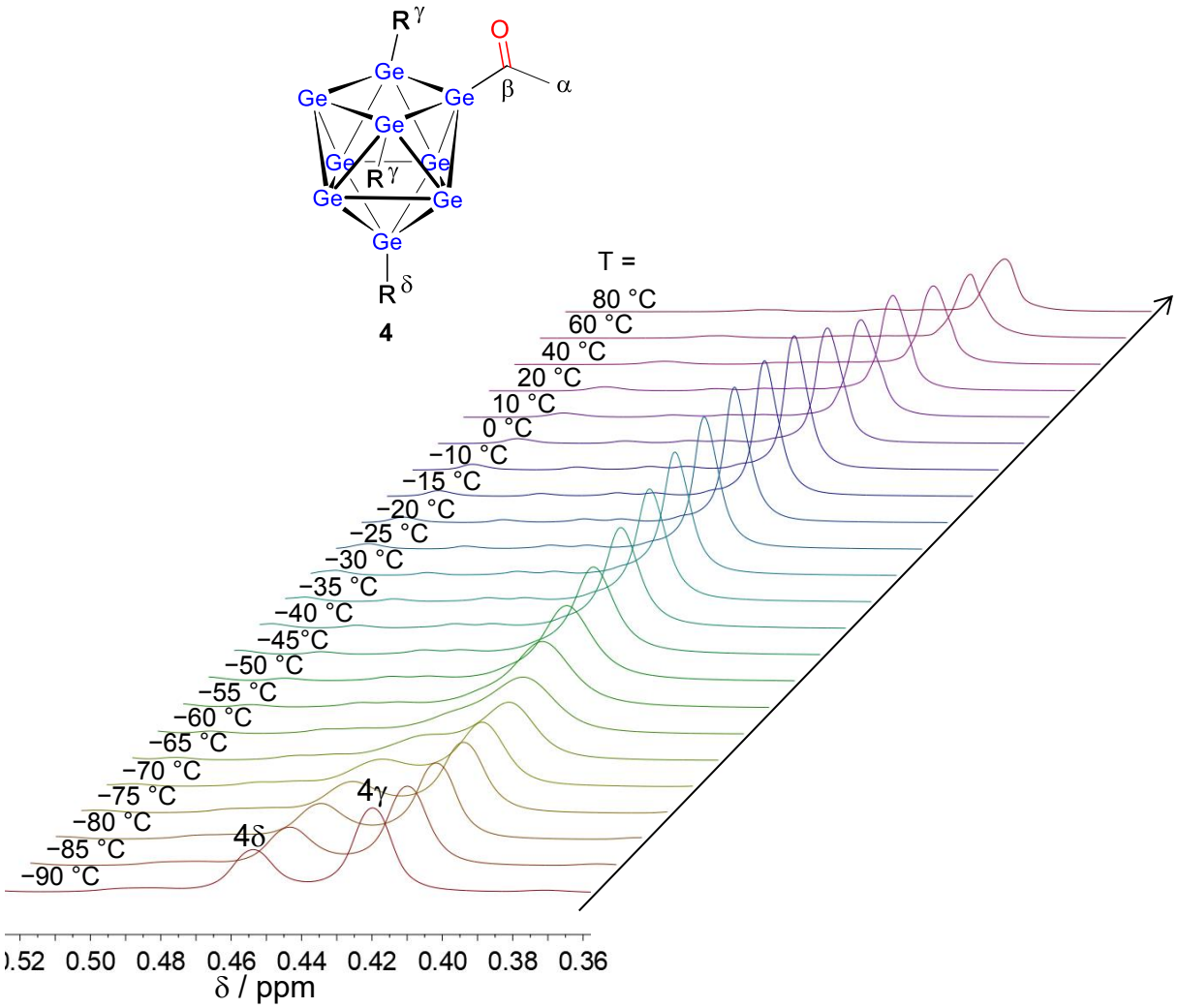

Figure S52. Temperature-resolved ^{1}H NMR study of crystals of 4 in [D8]toluene in the temperature range from −90 °C to 80 °C.

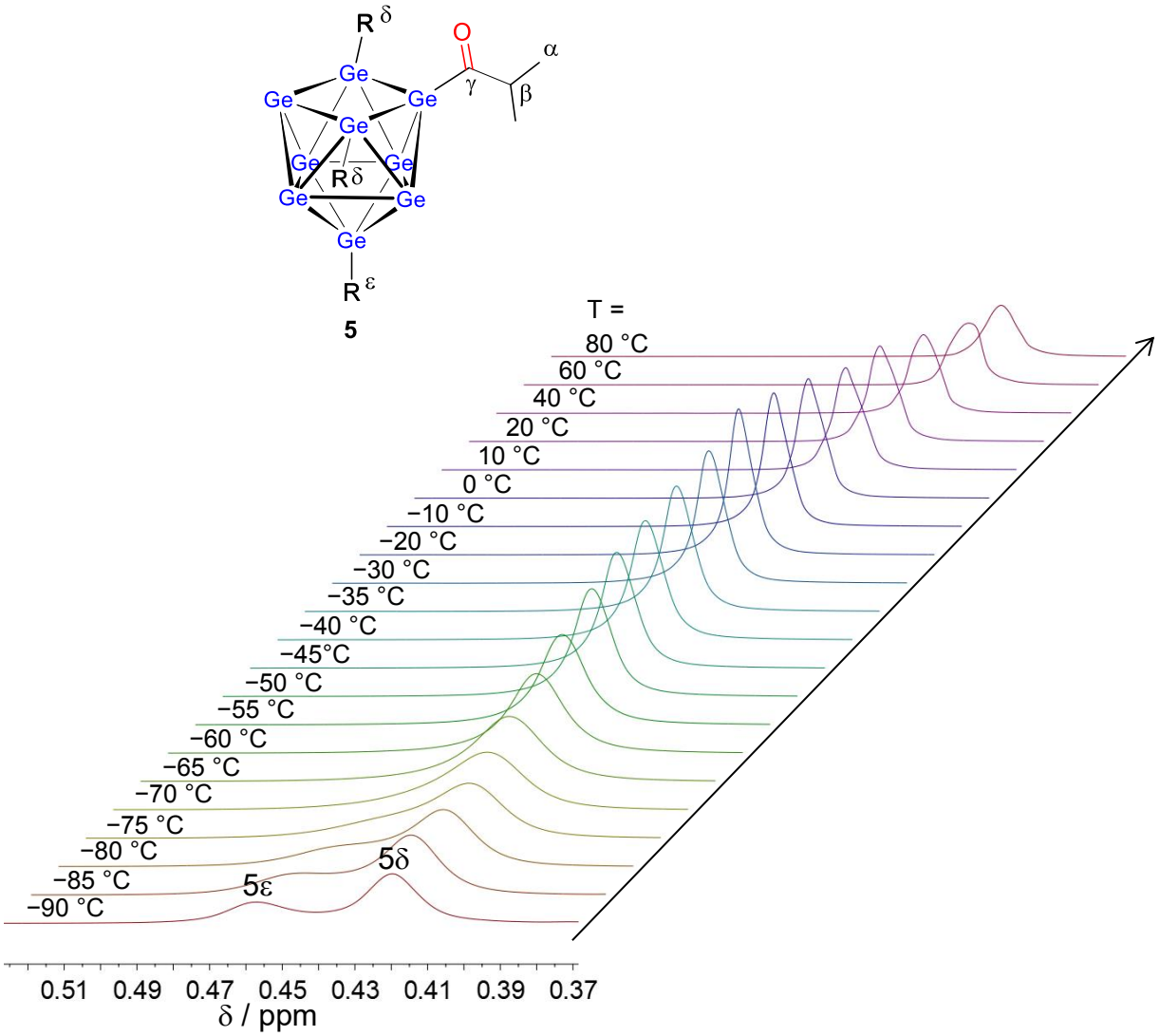

Figure S53. Temperature-resolved ^{1}H NMR study of crystals of **5** in [D8]toluene in the temperature range from −90 °C to 80 °C.

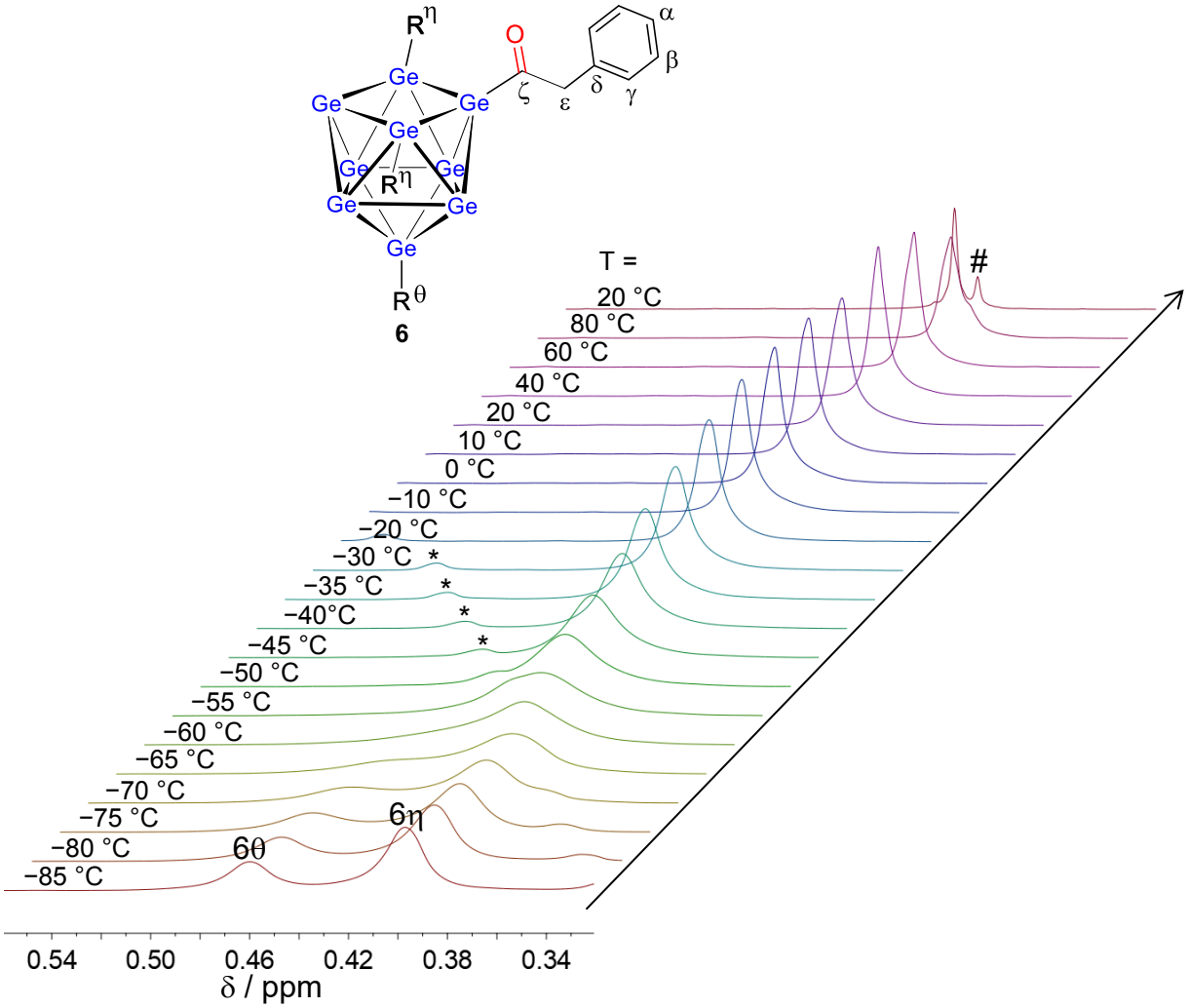

Figure S54. Temperature-dependent ^{1}H NMR spectra in the temperature range from −85 °C to 80 °C of the reaction solution of K[Ge_9{$Si(SiMe_3)_3$}$_3$] (0.021 mmol, 30 mg) with phenylacetyl chloride (0.021 mmol, 2.78 μL) in 0.6 mL [D8]toluene to obtain **6** after a reaction time of 16.5 h at 2 °C. The signals marked with * could not be assigned. The signal marked with # is most likely assigned to the decarbonylated species of **6**.

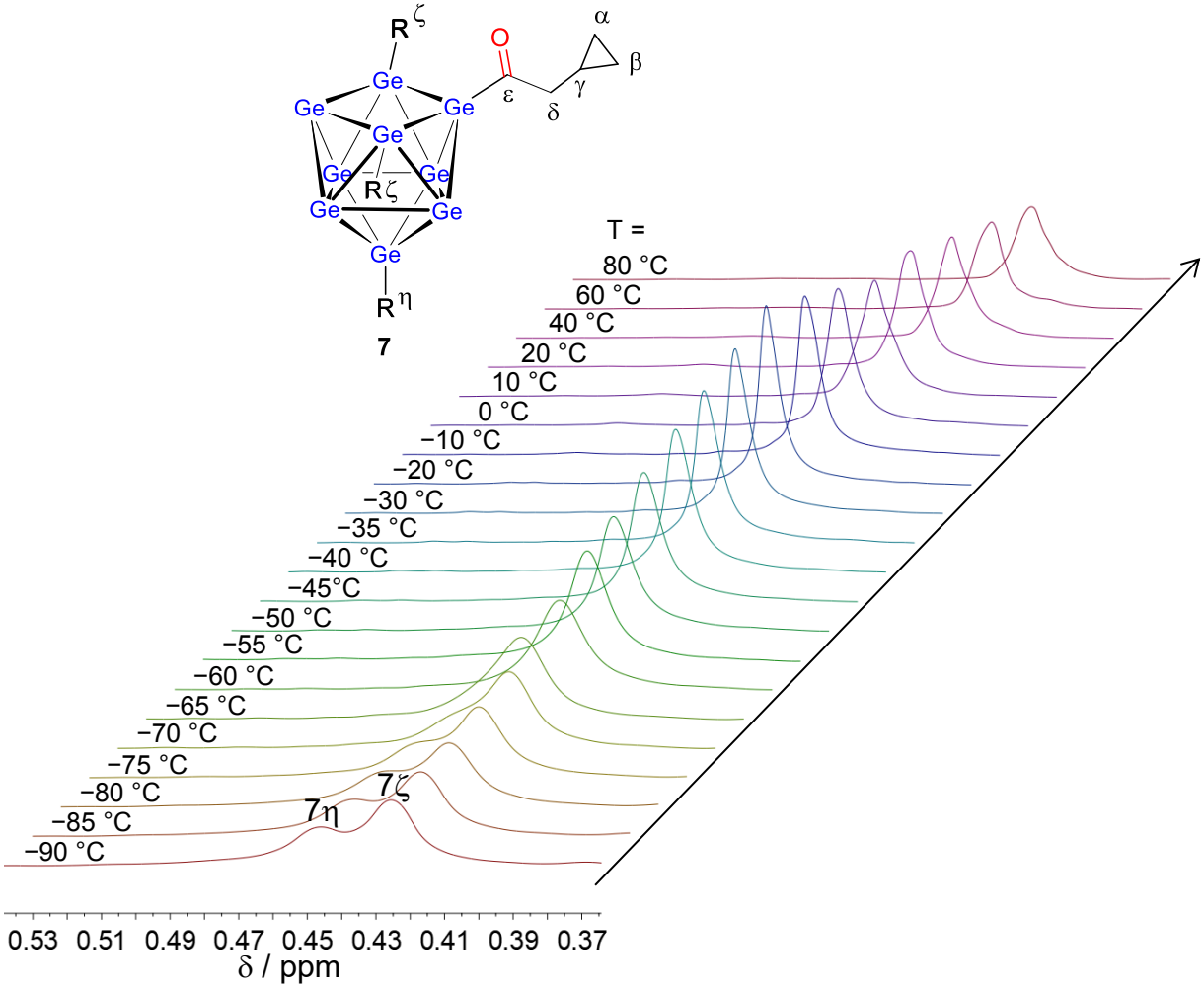

Figure S55. Temperature-dependent ^{1}H NMR spectra in the temperature range from −90 °C to 80 °C of the reaction solution of K[Ge_9{$Si(SiMe_3)_3$}$_3$] (0.021 mmol, 30 mg) with cyclopropylacetyl chloride (0.021 mmol, 2.1 μL) in 0.6 mL [D8]toluene to obtain **7** after a reaction time of 16 h at r.t..

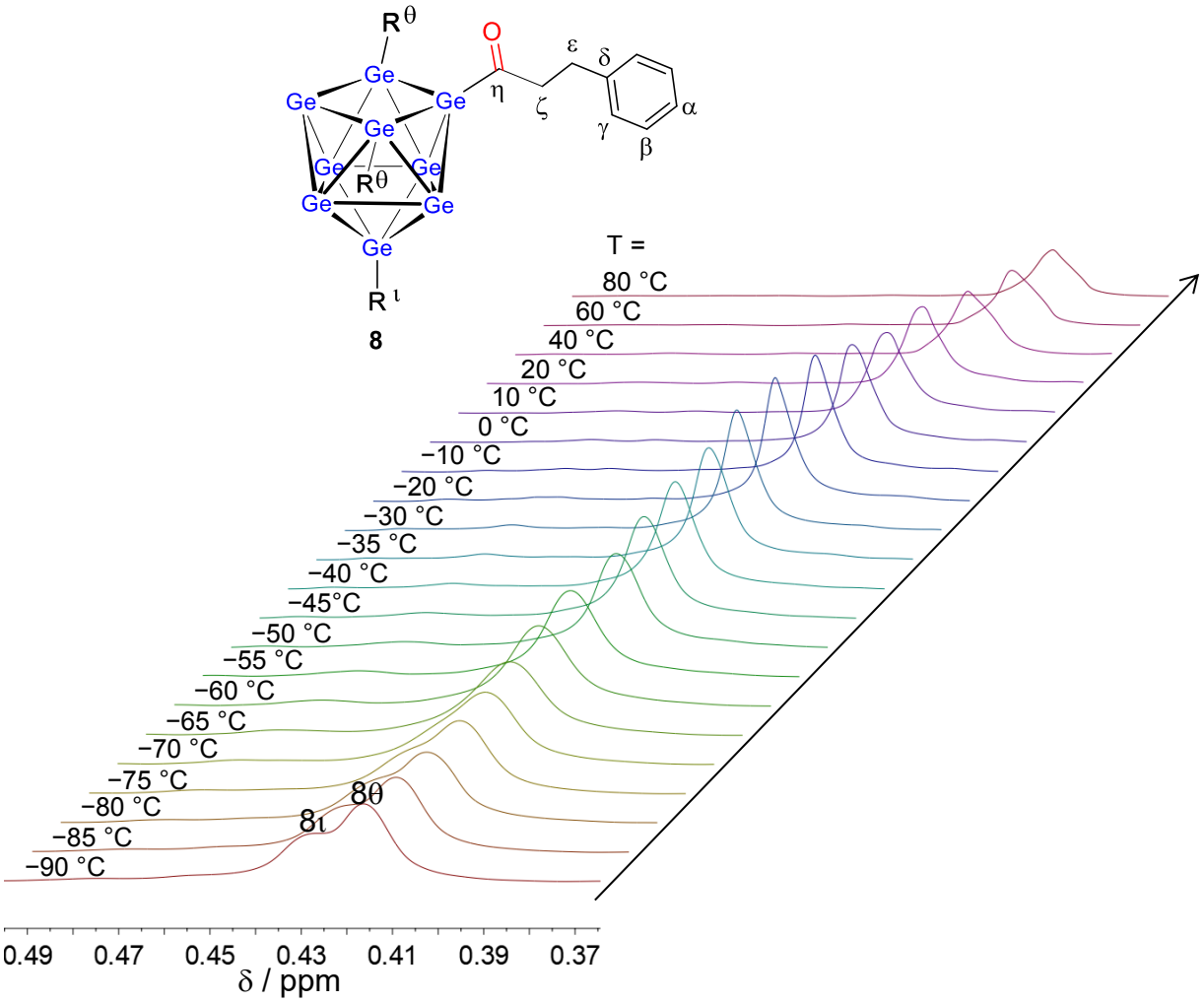

Figure S56. Temperature-dependent ^{1}H NMR study in the temperature range from −90 °C to 80 °C of the crude product **8** in [D8]toluene. The crude product was prepared by mixing $K[Ge_9\{Si(SiMe_3)_3\}_3]$ (0.021 mmol, 30 mg) with hydrocinnamoyl chloride (0.021 mmol, 3.1 μL) in 0.8 mL hexane at r.t. for 16.5 h. The solution was filtered, the solvent evaporated in a vacuum and the residue dissolved in [D8]toluene.

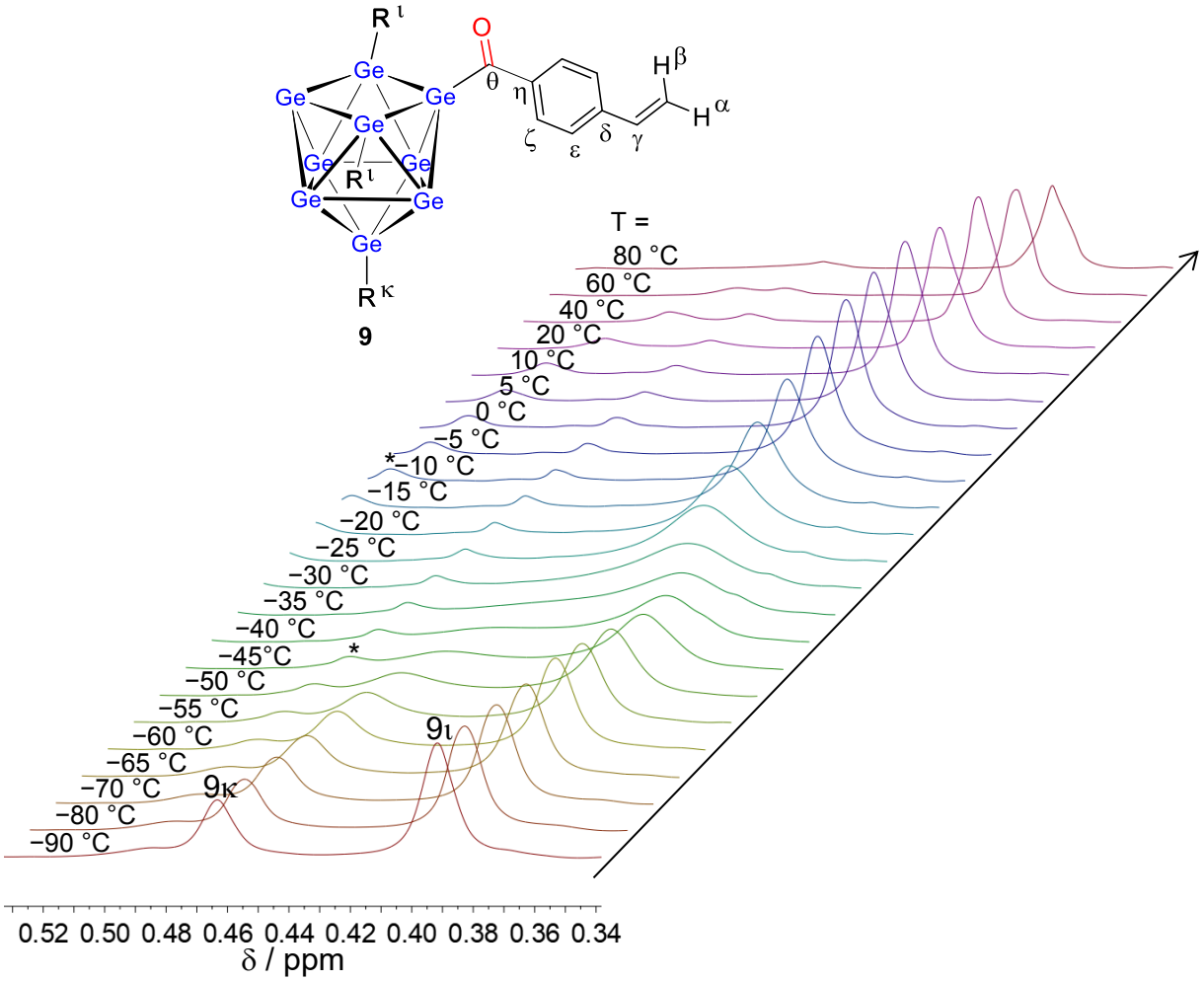

Figure S57. Temperature-dependent ^{1}H NMR study in the temperature range from −90 °C to 80 °C of the crude product **9** in [D8]toluene. The crude product was prepared by mixing K[Ge_9{$Si(SiMe_3)_3$}$_3$] (0.042 mmol, 60 mg) with hydrocinnamoyl chloride (0.042 mmol, 5.8 μL) in 1.2 mL toluene at r.t. for 14 h. The solution was filtered, the solvent evaporated in a vacuum and the residue dissolved in [D8]toluene. Signals marked with * could not be assigned.

Table S4. Coalescence temperatures T_C, calculated rate constants k_r as well as the free activation energies of rotation ΔG in [D8]toluene of neutral acyl-functionalized Ge_9 cluster compounds.

compound	T_C [K]	k_r [s^{-1}]	ΔG [$kJ \cdot mol^{-1}$]
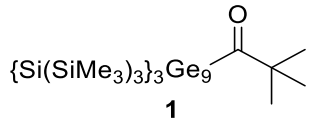 **1**	218	32.9	46.4
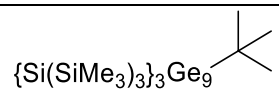 **2**	268	43.5	56.9
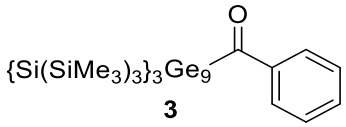 **3**	233	55.1	48.8
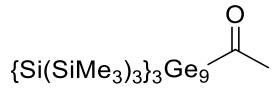 **4**	218	30.2	46.5
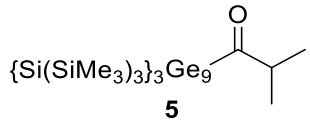 **5**	203	32.9	43.1
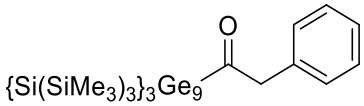 **6**	213	56.0	44.4
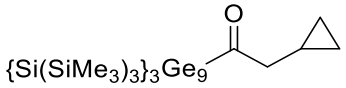 **7**	213	17.8	46.4
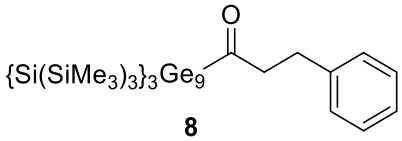 **8**	208	-[a]	-[a]
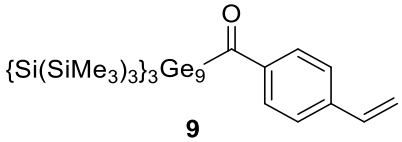 **9**	243	63.1	50.6

7 Mechanism Discussions on the Decarbonylation of 3 and 5

Herein we discuss the decarbonylation mechanism for two other systems that experimentally show no CO formation in the case of compound **3** or CO abstraction with occurring side reactions as is the case for compound **5**.

7.1 $[(SiMe_3)_3Ge_9(CO)C_6H_5]$ (3')

The experiments conducted with the compound $[\{Si(SiMe_3)_3\}_3Ge_9(CO)C_6H_5]$ (**3**) show that after the formation of the Zintl complex with $CO\text{-}C_6H_5$, the complex is stable and no decarbonylation product could be detected.

In Figure S58 we discuss the DFT results for the possible mechanisms for the compound $[(SiMe_3)_3Ge_9(CO)C_6H_5]$ (**3'**) in analogy to Figure 2 in the manuscript.

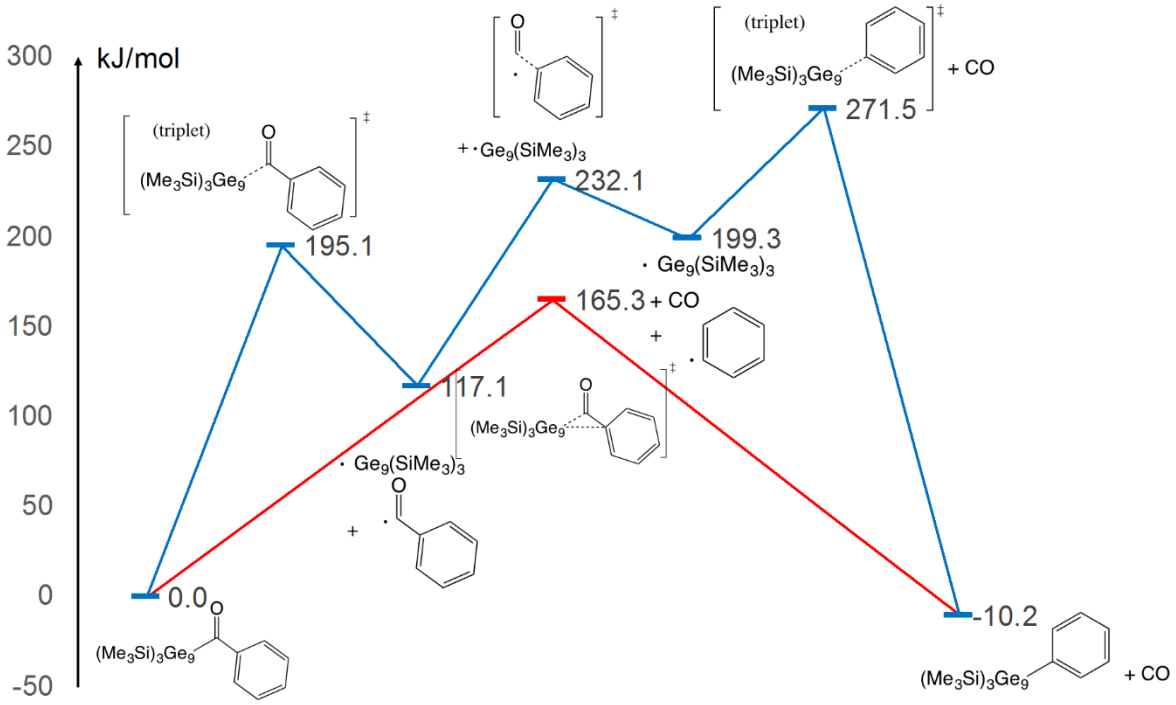

Figure S58. Free Energy (ΔG, kJ/mol) plot over the two compared radical pathways for compound **3'** - red: concerted; blue: stepwise.

In comparison to the compound $[(SiMe_3)_3Ge_9(CO)^tBu]$ (**1'**), the radical pathway for the analogous phenyl-substituted compound **3'** shows very high barriers up to 250-270 kJ/mol. This certainly can be explained by the lower stability of the occurring phenyl radical. In a radical promoting environment, this is indeed an explanation why here the decarbonylation of **3'** is not detectable. But on the other hand, the concerted (covalent) phenyl transfer to the Zintl cluster with CO evolution has a lower barrier than for the pivaloyl substituted complex. As this barrier is still as high as 165 kJ/mol, it may be only a slower alternative.

7.2 $[(SiMe_3)_3Ge_9(CO)CH_2C_6H_5]$ (6')

The experimental observations along compound **6** show that CO can be detected, but the formation of the expected product $[\{Si(SiMe_3)_3\}_3Ge_9CH_2C_6H_5]$ could not be detected.

In Figure S59 we discuss two possible decarbonylation mechanisms for the compound $[(SiMe_3)_3Ge_9(CO)CH_2C_6H_5]$ (**6'**) according to Figure 2.

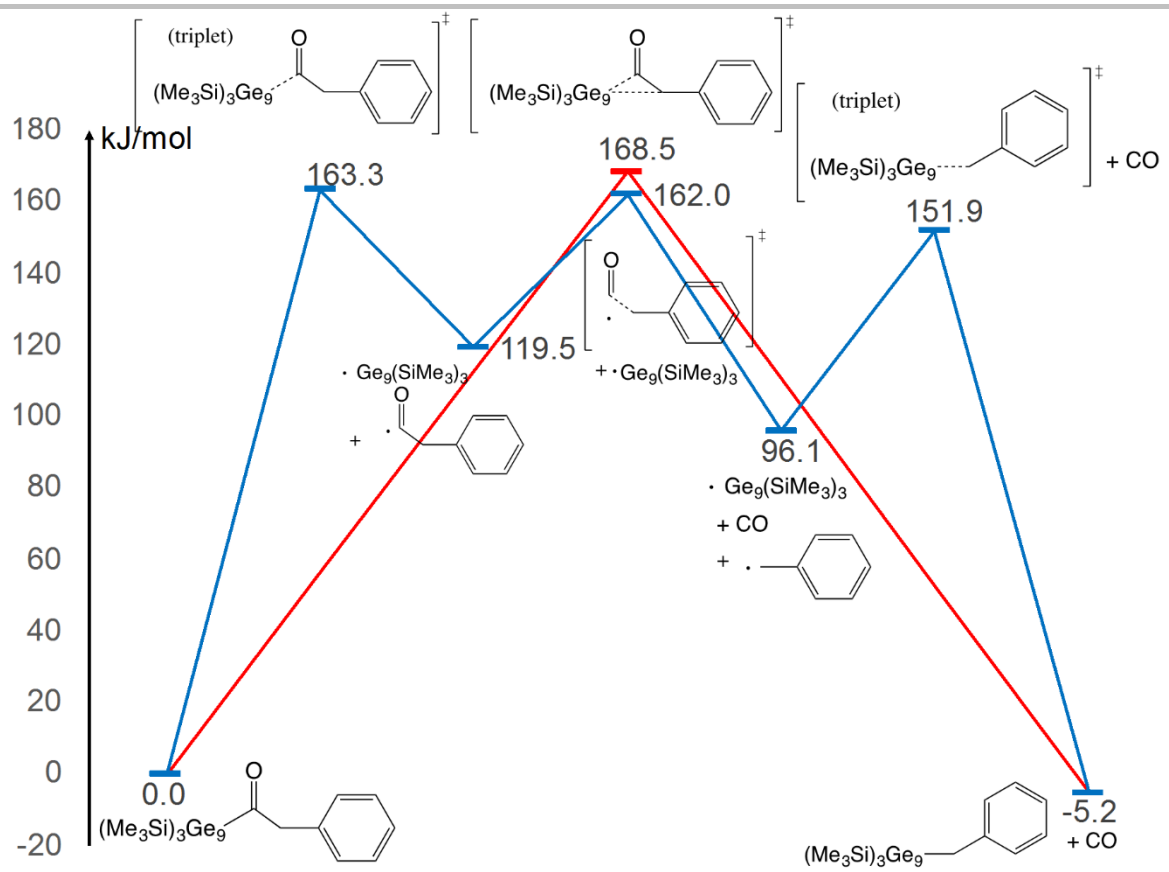

Figure S59. Free Energy (ΔG, kJ/mol) plot over the two compared radical pathways for compound **6'** - red: concerted; blue: stepwise.

Like for the pivaloyl case, the radical pathway is dominant over the concerted decarbonylation pathway, (highest barrier 163.3 kJ/mol versus 168.5 kJ/mol) although the concerted barrier is in the closer range of the barriers from the radical pathway. The CO evolution barrier has a similar height for compound **6'** and **1'**, therefore it is feasible, why CO can be detected experimentally. In contrast to the radical decarbonylation pathway of **1'**, for the radical reaction pathway of **6'**, it is not clear that in the end the benzyl (Bz) radical is quietly undergoing a simple recombination with the Zintl radical. From our results we can see, that the stability of the Bz radical and a higher recombination barrier might give a hint for this observation. The Bz radical is by 23 kJ/mol more stable than the CO-Bz radical and the barrier for the recombination lies at 55.8 kJ/mol. In case of ^{t}Bu versus CO-^{t}Bu radical the energy difference is only 5.6 kJ/mol, showing that both radicals have a similar stability. Additionally, the recombination barrier to form the ^{t}Bu-complex at the Zintl cluster is only 42.2 kJ/mol high. We predict therefore, that the Bz radical once it is formed can undergo further reactions with lower barriers that might even destroy the Ge_9 cluster.

8 Quantum-chemical Calculations: xyz Coordinates, Energies

8.1 Quantum-chemical Calculations on the Decarbonylation of 1'

8.1.1 Starting material / products

$(Me_3Si)_3Ge_9$-CO-^{t}Bu (**1'**)

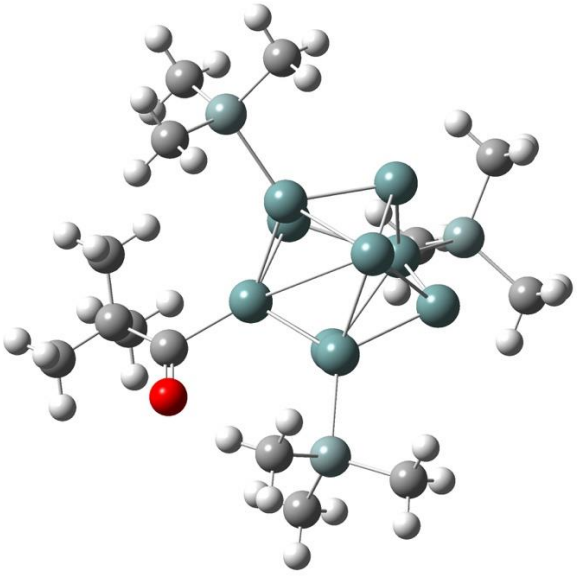

Center Number	Atomic Number	Atomic Type	Coordinates (Angstroms) X	Y	Z
1	32	0	-1.447975	0.077253	0.705139
2	32	0	-0.772221	-1.674556	-0.891849
3	32	0	-0.116583	0.106425	-2.671666
4	32	0	1.686459	-1.391357	-1.440991
5	32	0	0.493902	-1.502823	1.424618
6	32	0	2.374276	-0.045673	0.603693
7	6	0	-3.139261	0.503816	1.788406
8	8	0	-3.662069	1.553351	1.548810
9	6	0	-3.638931	-0.468712	2.855707
10	6	0	-5.040331	-0.055570	3.290468
11	1	0	-5.394544	-0.727368	4.075095
12	1	0	-5.742607	-0.100494	2.456351
13	6	0	-3.643488	-1.887846	2.298324
14	1	0	-2.643028	-2.198468	1.986827
15	1	0	-4.315921	-1.978897	1.442501
16	1	0	-3.981459	-2.582829	3.070056
17	14	0	-1.781384	-3.806023	-1.331481
18	14	0	4.586703	-0.173786	1.502040
19	32	0	-0.639305	1.840905	-0.803175
20	32	0	1.786145	1.433686	-1.391323
21	32	0	0.589859	1.476418	1.501897
22	1	0	-5.048010	0.963799	3.675955
23	6	0	-2.666567	-0.375509	4.036316
24	1	0	-1.650170	-0.643978	3.741262
25	1	0	-2.648599	0.633239	4.452965
26	1	0	-2.987869	-1.064543	4.820855
27	14	0	-1.706439	3.979267	-0.990510
28	6	0	5.474884	-1.604460	0.680632
29	1	0	4.953882	-2.546684	0.860483
30	1	0	5.543394	-1.460587	-0.399278
31	1	0	6.490745	-1.695780	1.076209
32	6	0	5.459748	1.444529	1.141749
33	1	0	5.500433	1.642070	0.068929
34	1	0	4.946111	2.282164	1.617531
35	1	0	6.485071	1.414460	1.521915
36	6	0	4.453628	-0.452082	3.350959
37	1	0	3.927335	-1.381821	3.574918

38	1	0	5.451558	-0.511072	3.795306
39	1	0	3.915260	0.364782	3.835268
40	6	0	-0.686810	5.027962	-2.163496
41	1	0	0.319340	5.193023	-1.773886
42	1	0	-0.595511	4.553265	-3.142326
43	1	0	-1.162383	6.003254	-2.303745
44	6	0	-1.809091	4.767850	0.704428
45	1	0	-0.817418	4.942940	1.124791
46	1	0	-2.328277	5.728760	0.637468
47	1	0	-2.365814	4.126944	1.390413
48	6	0	-3.423312	3.688400	-1.679855
49	1	0	-3.382775	3.198159	-2.654313
50	1	0	-4.002768	3.058643	-1.002143
51	1	0	-3.950286	4.639832	-1.798093
52	6	0	-3.579911	-3.534643	-1.788907
53	1	0	-4.142164	-3.093384	-0.963983
54	1	0	-3.668903	-2.869721	-2.650010
55	1	0	-4.050400	-4.488402	-2.045692
56	6	0	-0.849486	-4.531065	-2.787175
57	1	0	-1.284865	-5.495008	-3.067044
58	1	0	-0.897769	-3.872355	-3.656353
59	1	0	0.202576	-4.688847	-2.543453
60	6	0	-1.649880	-4.936506	0.157969
61	1	0	-2.097750	-5.907893	-0.072941
62	1	0	-0.607350	-5.098447	0.436663
63	1	0	-2.169791	-4.523909	1.024168

HF= -20189.1142004 / NImag=0
Sum of electronic and thermal Enthalpies= -20188.588115
Sum of electronic and thermal Free Energies= -20188.734474

$(Me_3Si)3Ge_9$-^{t}Bu (**2'**)

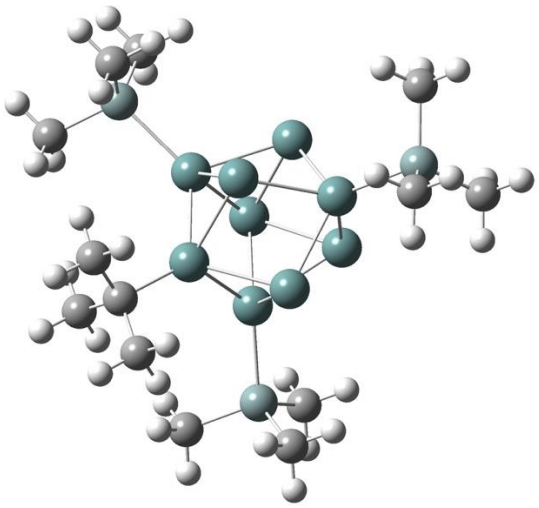

Center Number	Atomic Number	Atomic Type	Coordinates (Angstroms) X	Y	Z
1	32	0	-1.422025	0.003733	1.131458
2	32	0	-0.989392	-1.752285	-0.527640
3	32	0	-0.760964	0.001110	-2.440315
4	32	0	1.293449	-1.419921	-1.565018
5	32	0	0.691314	-1.457870	1.517020
6	32	0	2.327063	-0.004261	0.283192
7	14	0	-1.910789	-3.961083	-0.644095
8	14	0	4.668600	-0.004179	0.762306
9	32	0	-0.980537	1.755857	-0.529209
10	32	0	1.300583	1.411016	-1.568344
11	32	0	0.697643	1.454116	1.518231

12	14	0	-1.899517	3.965516	-0.646705
13	6	0	5.476748	-1.366764	-0.238391
14	1	0	5.066638	-2.343992	0.022921
15	1	0	5.324538	-1.215201	-1.308694
16	1	0	6.553811	-1.387427	-0.048040
17	6	0	5.371069	1.667090	0.287658
18	1	0	5.216379	1.873939	-0.772996
19	1	0	4.898750	2.469049	0.858134
20	1	0	6.446477	1.696207	0.486448
21	6	0	4.886051	-0.313706	2.598274
22	1	0	4.461600	-1.276442	2.889243
23	1	0	5.948898	-0.318398	2.857317
24	1	0	4.396357	0.462184	3.189790
25	6	0	-1.441399	4.660265	-2.326523
26	1	0	-0.358353	4.727993	-2.443940
27	1	0	-1.828060	4.034689	-3.133269
28	1	0	-1.860956	5.663827	-2.444168
29	6	0	-1.196443	5.037768	0.721427
30	1	0	-0.109927	5.105838	0.644572
31	1	0	-1.609259	6.049114	0.656753
32	1	0	-1.436583	4.636115	1.707764
33	6	0	-3.767049	3.863809	-0.483362
34	1	0	-4.196784	3.210281	-1.244889
35	1	0	-4.063330	3.482183	0.495941
36	1	0	-4.208453	4.857899	-0.601731
37	6	0	-3.776505	-3.860494	-0.460648
38	1	0	-4.062640	-3.484768	0.523938
39	1	0	-4.214288	-3.202642	-1.213824
40	1	0	-4.218972	-4.853956	-0.580303
41	6	0	-1.470192	-4.648412	-2.331657
42	1	0	-1.890194	-5.651822	-2.448979
43	1	0	-1.865902	-4.019811	-3.131633
44	1	0	-0.388398	-4.714749	-2.460898
45	6	0	-1.192824	-5.039049	0.711754
46	1	0	-1.605879	-6.050315	0.647342
47	1	0	-0.107169	-5.106283	0.622739
48	1	0	-1.422303	-4.641499	1.702289
49	6	0	-2.922434	0.007259	2.469324
50	6	0	-2.815153	1.260838	3.327502
51	6	0	-4.234412	0.003990	1.694413
52	6	0	-2.813738	-1.240608	3.335663
53	1	0	-1.884113	1.284553	3.896277
54	1	0	-2.867198	2.171942	2.726985
55	1	0	-3.648024	1.286150	4.040694
56	1	0	-4.332192	-0.880836	1.062145
57	1	0	-5.074874	0.006713	2.398847
58	1	0	-4.332371	0.883629	1.054964
59	1	0	-3.647483	-1.263026	4.047930
60	1	0	-2.863040	-2.155660	2.740942
61	1	0	-1.883393	-1.258839	3.905772

HF=-20075.8648207 / NImag=0
Sum of electronic and thermal Enthalpies= -20075.350563
Sum of electronic and thermal Free Energies= -20075.491088

CO

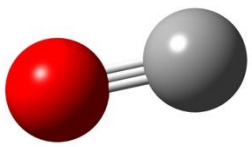

Center Number	Atomic Number	Atomic Type	Coordinates (Angstroms) X	Y	Z
1	6	0	0.000000	0.000000	-0.641924
2	8	0	0.000000	0.000000	0.481443

HF= -113.2309581 / NImag=0
Sum of electronic and thermal Enthalpies= -113.222550
Sum of electronic and thermal Free Energies= -113.244969

8.1.2 TS concerted pathway

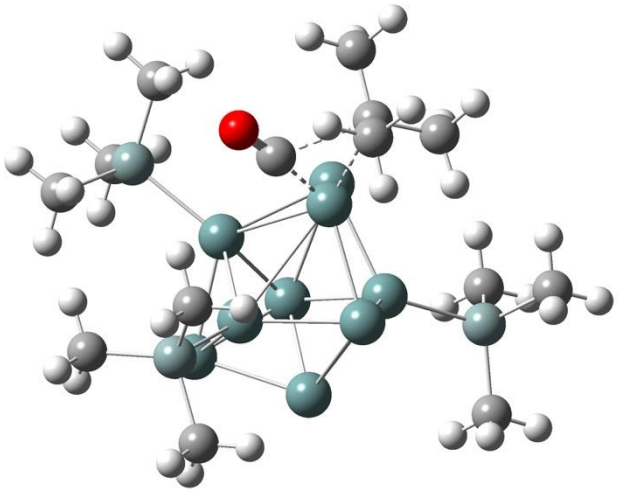

Center Number	Atomic Number	Atomic Type	Coordinates (Angstroms) X	Y	Z
1	32	0	0.118651	1.964470	-0.026344
2	32	0	1.130231	-0.635135	-1.228640
3	32	0	0.817413	-2.889576	0.057051
4	32	0	-1.131189	-1.975714	-1.388968
5	32	0	-0.865942	0.784956	-2.074372
6	32	0	-2.209110	-0.049024	-0.019857
7	6	0	1.808223	2.837701	-0.003904
8	8	0	2.889407	3.251419	0.025263
9	6	0	0.366180	4.452774	-0.088053
10	6	0	0.907531	5.043597	-1.370962
11	1	0	0.562509	6.081260	-1.476585
12	1	0	0.551519	4.497520	-2.249424
13	6	0	-1.161659	4.530762	-0.102617
14	1	0	-1.614219	4.108888	0.798268
15	1	0	-1.602743	4.038434	-0.972859
16	1	0	-1.458319	5.590068	-0.146573
17	14	0	2.934210	-0.714898	-2.821094
18	14	0	-4.606641	-0.153740	-0.001700
19	32	0	1.105721	-0.597346	1.268286
20	32	0	-1.162752	-1.932761	1.426203
21	32	0	-0.908865	0.845180	2.033989
22	1	0	1.998401	5.063759	-1.393560
23	6	0	0.884458	5.159225	1.144511
24	1	0	0.508237	4.699058	2.062583
25	1	0	1.974525	5.179825	1.187515
26	1	0	0.541077	6.202806	1.144126
27	14	0	2.905931	-0.568668	2.865437
28	6	0	-5.268122	1.539688	-0.469192
29	1	0	-4.920119	2.306189	0.226203
30	1	0	-4.946562	1.824964	-1.472872
31	1	0	-6.361945	1.539383	-0.452157
32	6	0	-5.193644	-1.434814	-1.239698
33	1	0	-4.839289	-1.204704	-2.246390
34	1	0	-4.832967	-2.431436	-0.978102

35	1	0	-6.287026	-1.464557	-1.263930
36	6	0	-5.164363	-0.607418	1.730936
37	1	0	-4.803267	0.115873	2.464901
38	1	0	-6.256942	-0.625682	1.783122
39	1	0	-4.793515	-1.592150	2.021480
40	6	0	2.441990	-1.779080	4.218422
41	1	0	1.498229	-1.499623	4.690545
42	1	0	2.334616	-2.790346	3.821786
43	1	0	3.216450	-1.795909	4.990872
44	6	0	3.073005	1.166796	3.553374
45	1	0	2.144206	1.492601	4.025537
46	1	0	3.866727	1.199295	4.305656
47	1	0	3.324419	1.882902	2.768556
48	6	0	4.495778	-1.090542	2.021227
49	1	0	4.396342	-2.073370	1.557065
50	1	0	4.785253	-0.374558	1.249558
51	1	0	5.307978	-1.140358	2.752396
52	6	0	4.358540	-1.702922	-2.109507
53	1	0	4.763892	-1.233626	-1.211619
54	1	0	4.042610	-2.714623	-1.848445
55	1	0	5.165376	-1.776400	-2.844684
56	6	0	2.244765	-1.559059	-4.345411
57	1	0	3.016419	-1.630237	-5.117651
58	1	0	1.901498	-2.569365	-4.115028
59	1	0	1.401293	-1.001857	-4.757138
60	6	0	3.479029	1.033597	-3.220417
61	1	0	4.277124	1.014734	-3.968548
62	1	0	2.651472	1.619735	-3.624783
63	1	0	3.859225	1.549027	-2.336322

HF= -20189.0385228 / NImag=1 (-326.6383 cm^{-1})
Sum of electronic and thermal Enthalpies= -20188.515753
Sum of electronic and thermal Free Energies= -20188.659152

8.1.3 TS / intermediates radical pathway

TS Ge_9-CO radical separation (triplet)

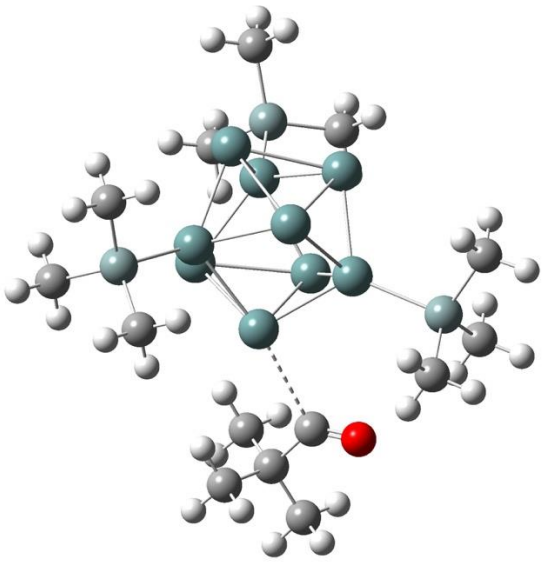

Center Number	Atomic Number	Atomic Type	Coordinates (Angstroms) X	Y	Z

1	32	0	1.470852	0.902180	0.466523
2	32	0	-0.743491	2.193770	-0.110061
3	32	0	-0.116817	1.018630	-2.256216
4	32	0	-2.605798	0.745379	-1.054771
5	32	0	-0.824739	0.676232	1.901375
6	32	0	-2.112824	-1.094387	0.623840
7	6	0	3.833457	-0.407156	1.678980
8	8	0	4.545092	-0.957976	0.919297
9	6	0	4.101027	-0.035692	3.136309
10	6	0	5.376066	-0.722296	3.616333
11	1	0	5.576449	-0.442322	4.653286
12	1	0	6.233281	-0.431812	3.007827
13	6	0	4.251377	1.486015	3.171700
14	1	0	3.355736	1.978996	2.790453
15	1	0	5.106239	1.816229	2.578506
16	1	0	4.408424	1.804071	4.204878
17	14	0	-0.696636	4.588766	-0.130069
18	14	0	-3.603935	-2.755995	1.495998
19	32	0	1.240932	-0.878664	-1.323972
20	32	0	-1.192164	-1.519628	-1.722855
21	32	0	0.362544	-1.623852	0.919096
22	1	0	5.280584	-1.808191	3.568071
23	6	0	2.892861	-0.464680	3.963489
24	1	0	1.978815	0.007103	3.597397
25	1	0	2.752190	-1.546745	3.931752
26	1	0	3.041668	-0.170558	5.005021
27	14	0	2.997419	-1.935652	-2.570628
28	6	0	-3.800880	-2.454297	3.335667
29	1	0	-2.842796	-2.534167	3.852789
30	1	0	-4.207223	-1.460426	3.531971
31	1	0	-4.482667	-3.192658	3.767915
32	6	0	-5.248356	-2.570500	0.615516
33	1	0	-5.674192	-1.578532	0.776956
34	1	0	-5.139253	-2.719177	-0.460444
35	1	0	-5.960400	-3.311920	0.989857
36	6	0	-2.875136	-4.452578	1.179327
37	1	0	-1.906607	-4.561727	1.670928
38	1	0	-3.542539	-5.230618	1.561724
39	1	0	-2.730540	-4.621912	0.110655
40	6	0	2.269438	-2.408133	-4.231418
41	1	0	1.427818	-3.093164	-4.114506
42	1	0	1.915881	-1.528913	-4.773242
43	1	0	3.028979	-2.902258	-4.844632
44	6	0	3.560705	-3.447908	-1.624380
45	1	0	2.739251	-4.149151	-1.467487
46	1	0	4.348036	-3.964055	-2.181839
47	1	0	3.962761	-3.162368	-0.651138
48	6	0	4.394896	-0.709088	-2.775648
49	1	0	4.056576	0.196175	-3.282986
50	1	0	4.805191	-0.428550	-1.804316
51	1	0	5.197839	-1.153419	-3.371448
52	6	0	-1.163763	5.201758	1.579377
53	1	0	-2.162245	4.862666	1.861152
54	1	0	-0.461607	4.841757	2.333760
55	1	0	-1.156346	6.295476	1.603285
56	6	0	1.027692	5.165111	-0.584962
57	1	0	1.072223	6.258199	-0.597111
58	1	0	1.766835	4.801154	0.131119
59	1	0	1.312344	4.801245	-1.573982
60	6	0	-1.941765	5.171800	-1.404383
61	1	0	-1.958125	6.265000	-1.443437
62	1	0	-1.688915	4.800766	-2.399438
63	1	0	-2.947826	4.824708	-1.161990

HF= -20189.0479847 / NImag=1 (-40.7229 cm^{-1})
Sum of electronic and thermal Enthalpies= -20188.523758
Sum of electronic and thermal Free Energies= -20188.671916

$(Me_3Si)_3Ge_9$ radical (doublet)

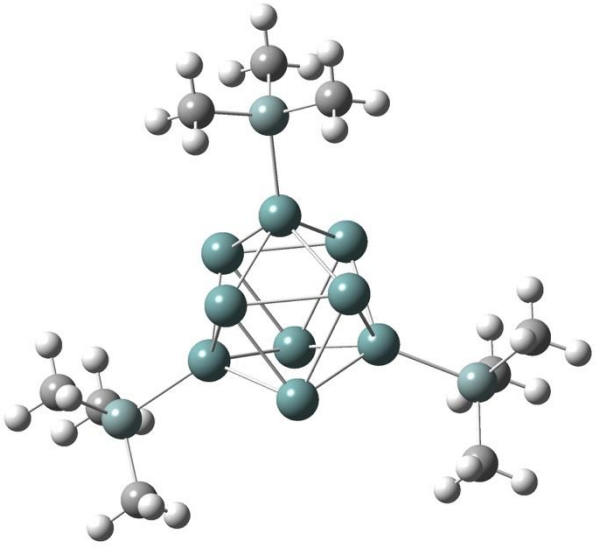

Center Number	Atomic Number	Atomic Type	Coordinates (Angstroms) X	Y	Z
1	32	0	-1.502141	0.527561	-1.623622
2	32	0	-0.398718	2.148318	-0.011290
3	32	0	-1.504724	0.525817	1.592478
4	32	0	1.215912	1.035358	1.594569
5	32	0	1.211143	1.035762	-1.626938
6	32	0	2.067183	-0.731055	-0.016063
7	14	0	-0.821386	4.505395	0.025802
8	32	0	-1.658581	-1.430496	-0.014522
9	32	0	0.297394	-1.576880	1.591284
10	32	0	0.294775	-1.569945	-1.628934
11	14	0	-3.513050	-2.945474	0.026451
12	6	0	-3.729681	-3.528139	1.793922
13	1	0	-2.836363	-4.041743	2.153824
14	1	0	-3.929650	-2.690116	2.464229
15	1	0	-4.571760	-4.223578	1.858572
16	6	0	-3.127033	-4.385404	-1.107972
17	1	0	-2.230123	-4.914517	-0.780929
18	1	0	-3.959144	-5.095632	-1.112776
19	1	0	-2.963336	-4.048032	-2.133102
20	6	0	-5.036798	-2.027172	-0.560015
21	1	0	-5.246206	-1.166976	0.078516
22	1	0	-4.911076	-1.664739	-1.581919
23	1	0	-5.908238	-2.688178	-0.537902
24	6	0	-2.399928	4.840308	-0.925786
25	1	0	-2.310038	4.522124	-1.966012
26	1	0	-3.245632	4.309971	-0.484286
27	1	0	-2.625881	5.910666	-0.915615
28	6	0	-1.004482	5.019205	1.818399
29	1	0	-1.196980	6.094312	1.881755
30	1	0	-1.834895	4.496797	2.296790
31	1	0	-0.097963	4.802533	2.386509
32	6	0	0.632171	5.378208	-0.770714
33	1	0	0.475040	6.460788	-0.758965
34	1	0	1.560002	5.163351	-0.237433
35	1	0	0.760782	5.064887	-1.808425
36	14	0	4.322057	-1.538347	0.026571
37	6	0	5.434138	-0.237995	-0.735869
38	1	0	5.375270	0.701914	-0.184021
39	1	0	6.474438	-0.576304	-0.722311
40	1	0	5.155867	-0.037553	-1.772136
41	6	0	4.779653	-1.836004	1.818738
42	1	0	5.807518	-2.204259	1.887444

43	1	0	4.708780	-0.916096	2.402095
44	1	0	4.121725	-2.576894	2.276613
45	6	0	4.393917	-3.132388	-0.954759
46	1	0	4.092588	-2.971531	-1.991537
47	1	0	5.412543	-3.531447	-0.954651
48	1	0	3.732550	-3.887664	-0.526289

HF= -19918.1392399 / NImag=0
Sum of electronic and thermal Enthalpies= -19917.752814
Sum of electronic and thermal Free Energies= -19917.882094

CO-^{t}Bu radical (doublet)

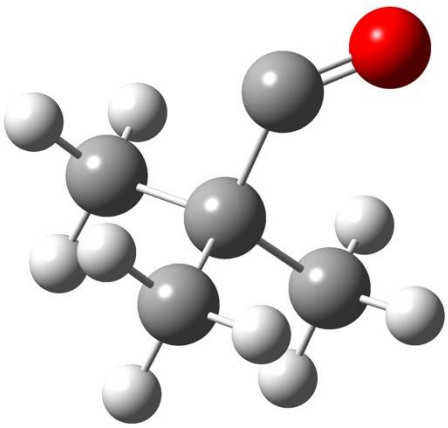

Center Number	Atomic Number	Atomic Type	Coordinates (Angstroms) X	Y	Z
1	6	0	0.143237	-0.003980	1.519452
2	6	0	0.319474	-0.000018	0.005120
3	1	0	-0.406770	0.876960	1.853236
4	1	0	-0.405944	-0.887161	1.848663
5	1	0	1.120831	-0.004849	2.007593
6	6	0	1.055022	-1.251256	-0.471793
7	6	0	1.054508	1.253989	-0.465378
8	1	0	1.144901	-1.263846	-1.559035
9	1	0	2.059152	-1.267923	-0.042077
10	1	0	0.537406	-2.160357	-0.159834
11	1	0	2.058758	1.268704	-0.035876
12	1	0	1.144036	1.272380	-1.552570
13	1	0	0.536674	2.161233	-0.148444
14	6	0	-1.045349	0.001514	-0.682677
15	8	0	-2.118799	0.000421	-0.205000

HF=-270.9056561 / NImag=0
Sum of electronic and thermal Enthalpies= -270.768717
Sum of electronic and thermal Free Energies= -270.809425

TS CO-^{t}Bu separation (doublet)

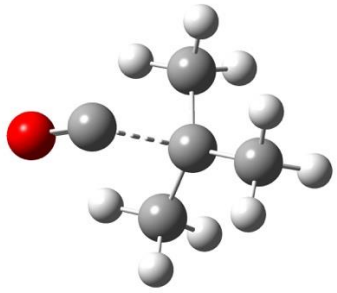

Center Number	Atomic Number	Atomic Type	Coordinates (Angstroms) X	Y	Z
1	6	0	0.427668	-1.496926	-0.308960
2	6	0	0.600167	-0.039911	-0.046017
3	1	0	0.202486	-2.051437	0.604449
4	1	0	-0.366731	-1.685487	-1.034197
5	1	0	1.352640	-1.921965	-0.724979
6	6	0	0.685093	0.854153	-1.237086
7	6	0	1.403185	0.350343	1.146277
8	1	0	0.574814	1.905003	-0.960614
9	1	0	1.665801	0.749670	-1.723477
10	1	0	-0.071938	0.608243	-1.984731
11	1	0	2.474093	0.186326	0.960146
12	1	0	1.271112	1.406689	1.386833
13	1	0	1.132404	-0.238045	2.024965
14	6	0	-1.448363	0.513359	0.627076
15	8	0	-2.280147	-0.005638	0.045483

HF= -270.8835518 / NImag=1 (-230.7379 cm^{-1})
Sum of electronic and thermal Enthalpies= -270.750128
Sum of electronic and thermal Free Energies= -270.794096

^{t}Bu radical (doublet)

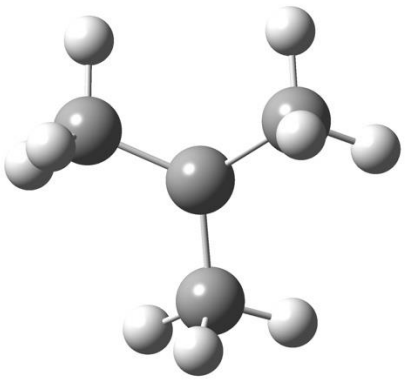

Center Number	Atomic Number	Atomic Type	Coordinates (Angstroms) X	Y	Z
1	6	0	0.742312	1.275826	0.014943
2	6	0	-0.000088	-0.000007	-0.151782
3	1	0	1.738388	1.226165	-0.432658
4	1	0	0.206620	2.117472	-0.431784
5	1	0	0.889905	1.528456	1.078326
6	6	0	-1.476206	0.004863	0.014940

7	6	0	0.733901	-1.280698	0.014937
8	1	0	-1.937387	-0.879255	-0.432913
9	1	0	-1.768635	0.004912	1.078365
10	1	0	-1.931290	0.892863	-0.431439
11	1	0	0.881399	-1.533380	1.078322
12	1	0	0.191891	-2.119077	-0.430283
13	1	0	1.729598	-1.238057	-0.434165

HF= -157.6537087 / NImag=0
Sum of electronic and thermal Enthalpies= -157.529862
Sum of electronic and thermal Free Energies= -157.566566

TS Ge_9-^{t}Bu radical unification (triplet)

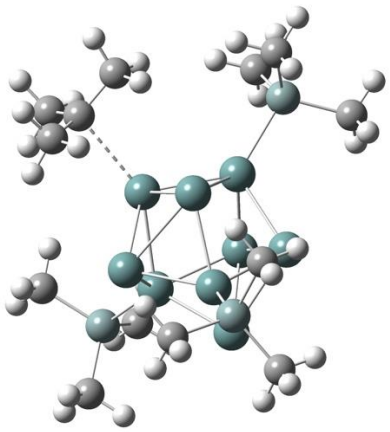

Center Number	Atomic Number	Atomic Type	Coordinates (Angstroms) X	Y	Z
1	6	0	-4.471988	-2.809353	1.259857
2	14	0	-4.529635	-0.973072	0.892600
3	6	0	-5.667905	-0.626968	-0.555845
4	32	0	-2.337089	-0.221597	0.283271
5	32	0	-0.408357	-1.517348	1.303233
6	32	0	1.161554	-1.581320	-0.660800
7	14	0	2.544003	-3.438387	-1.277519
8	6	0	4.320506	-2.849286	-1.375793
9	32	0	-1.695046	1.288158	-1.653766
10	32	0	-1.184402	-1.395224	-1.681507
11	32	0	0.357019	2.139295	-0.393387
12	14	0	1.267443	4.349672	-0.549468
13	6	0	2.389708	4.619685	0.929196
14	32	0	1.692265	0.304763	0.971831
15	6	0	2.962219	-0.419236	3.234471
16	6	0	1.916704	-0.109111	4.250161
17	32	0	-0.766514	1.216384	1.659091
18	32	0	0.898226	0.419138	-2.147220
19	6	0	2.239251	4.494134	-2.145695
20	6	0	-0.147390	5.579117	-0.526134
21	6	0	-5.074468	-0.015375	2.408986
22	6	0	1.962213	-4.043373	-2.952279
23	6	0	2.359146	-4.784808	0.012162
24	6	0	3.251049	-1.863772	2.996284
25	6	0	4.131701	0.507088	3.176133
26	1	0	-4.137300	-3.372254	0.386498
27	1	0	-3.787210	-3.025634	2.081923
28	1	0	-5.465993	-3.171265	1.539126
29	1	0	-4.398475	-0.189284	3.248311
30	1	0	-5.096212	1.058094	2.212525
31	1	0	-6.078623	-0.326668	2.711718
32	1	0	-5.344603	-1.166813	-1.447915
33	1	0	-6.687292	-0.944546	-0.317364
34	1	0	-5.691305	0.437377	-0.796782
35	1	0	0.922733	-4.373835	-2.913300

36	1	0	2.036741	-3.255864	-3.704474
37	1	0	2.577261	-4.886620	-3.280523
38	1	0	1.320433	-5.110123	0.093857
39	1	0	2.966837	-5.652060	-0.262627
40	1	0	2.684241	-4.442095	0.996042
41	1	0	4.427972	-2.054382	-2.116195
42	1	0	4.667192	-2.463238	-0.415472
43	1	0	4.976382	-3.675297	-1.666119
44	1	0	3.054921	3.769450	-2.174928
45	1	0	1.602461	4.317625	-3.014507
46	1	0	2.668473	5.496351	-2.237080
47	1	0	0.236509	6.601532	-0.590486
48	1	0	-0.824114	5.416306	-1.367001
49	1	0	-0.728430	5.491801	0.393945
50	1	0	2.808941	5.629917	0.904751
51	1	0	1.842792	4.502672	1.866780
52	1	0	3.216630	3.907205	0.929031
53	1	0	2.335284	-2.447257	2.875513
54	1	0	3.878463	-2.013006	2.114099
55	1	0	3.796186	-2.293471	3.852274
56	1	0	3.822849	1.554628	3.187699
57	1	0	4.785935	0.354027	4.049089
58	1	0	4.741403	0.338398	2.285688
59	1	0	2.290723	-0.320161	5.265101
60	1	0	1.625806	0.943969	4.229817
61	1	0	1.017581	-0.714897	4.109495

HF= -20075.7924858 / NImag=1 (-102.7278 cm^{-1})
Sum of electronic and thermal Enthalpies= -20075.280884
Sum of electronic and thermal Free Energies= -20075.423866

8.2 Quantum-chemical Calculations on the Decarbonylation of 3'

8.2.1 Starting material / products

$(Me_3Si)_3Ge_9$-CO-Ph

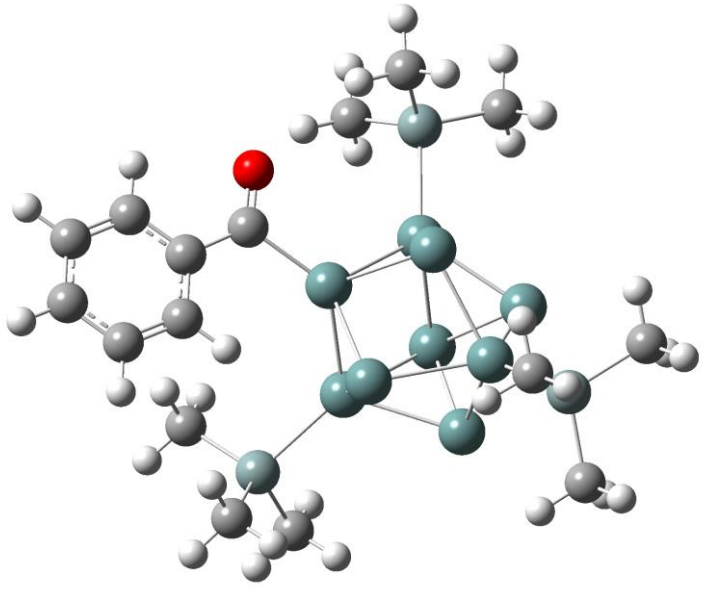

Center Number	Atomic Number	Atomic Type	Coordinates (Angstroms) X	Y	Z

1	32	0	1.268156	0.468481	-0.506161
2	32	0	0.886392	-1.188760	1.273534
3	32	0	-0.495031	0.542818	2.644020
4	32	0	-1.601491	-1.586204	1.523508
5	32	0	-0.004136	-1.707208	-1.160893
6	32	0	-2.314409	-0.795807	-0.791871
7	6	0	2.958559	1.194136	-1.373790
8	8	0	3.046216	2.392480	-1.454877
9	14	0	2.476280	-2.774275	2.113723
10	14	0	-4.225054	-1.679775	-1.926950
11	32	0	-0.222521	2.095786	0.566654
12	32	0	-2.482344	1.045583	0.965641
13	32	0	-0.923803	1.065180	-1.760427
14	14	0	0.188602	4.456473	0.486211
15	6	0	-4.739451	-3.271833	-1.083688
16	1	0	-3.940440	-4.014577	-1.121476
17	1	0	-4.990669	-3.102038	-0.035060
18	1	0	-5.618824	-3.692905	-1.579841
19	6	0	-5.600088	-0.410191	-1.835150
20	1	0	-5.862439	-0.185677	-0.799577
21	1	0	-5.306375	0.524515	-2.316495
22	1	0	-6.495697	-0.785283	-2.339094
23	6	0	-3.739524	-2.002365	-3.708332
24	1	0	-2.920460	-2.721335	-3.770474
25	1	0	-4.590298	-2.407537	-4.264002
26	1	0	-3.418470	-1.083649	-4.202787
27	6	0	-1.260685	5.315708	1.308435
28	1	0	-2.193267	5.109378	0.780237
29	1	0	-1.380155	4.989976	2.343541
30	1	0	-1.102246	6.398214	1.310803
31	6	0	0.371398	4.985440	-1.299172
32	1	0	-0.544219	4.807471	-1.865442
33	1	0	0.603145	6.053793	-1.348749
34	1	0	1.185088	4.436142	-1.776303
35	6	0	1.775368	4.780253	1.427256
36	1	0	1.700802	4.446318	2.463775
37	1	0	2.609671	4.256499	0.956740
38	1	0	2.001784	5.850623	1.429054
39	6	0	4.130252	-1.911405	2.295676
40	1	0	4.512462	-1.578286	1.328592
41	1	0	4.049228	-1.037880	2.945325
42	1	0	4.865751	-2.593158	2.732967
43	6	0	1.836010	-3.336817	3.782857
44	1	0	2.527288	-4.060499	4.224788
45	1	0	1.737152	-2.497044	4.473167
46	1	0	0.858164	-3.813176	3.690846
47	6	0	2.627632	-4.234924	0.947340
48	1	0	3.343225	-4.960741	1.345643
49	1	0	1.666992	-4.736826	0.820025
50	1	0	2.976075	-3.922916	-0.038933
51	6	0	4.033485	0.281803	-1.834708
52	6	0	3.864728	-1.097886	-1.861233
53	6	0	5.243300	0.838344	-2.253142
54	6	0	4.890734	-1.917957	-2.302405
55	1	0	2.918424	-1.530402	-1.550936
56	6	0	6.268753	0.018967	-2.686174
57	1	0	5.355020	1.915151	-2.228204
58	6	0	6.093255	-1.360034	-2.711711
59	1	0	4.751557	-2.991827	-2.330433
60	1	0	7.208802	0.451486	-3.006918

61	1	0	6.897252	-2.000833	-3.054054

HF= -20262.8562689
Sum of electronic and thermal Enthalpies= -20262.361810
Sum of electronic and thermal Free Energies= -20262.505525

$(Me_3Si)_3Ge_9$-Ph

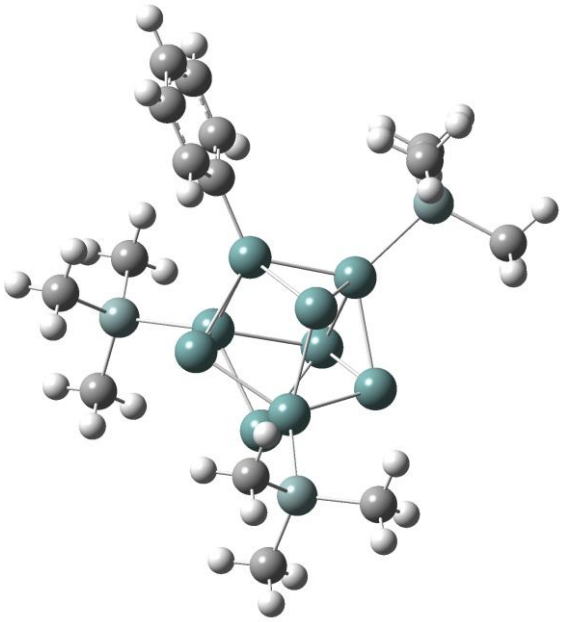

Center Number	Atomic Number	Atomic Type	Coordinates (Angstroms) X	Y	Z
1	32	0	-1.391912	0.013159	0.748448
2	32	0	-0.702586	-1.756631	-0.809485
3	32	0	-0.115055	-0.005871	-2.652335
4	32	0	1.728126	-1.439753	-1.411527
5	32	0	0.562859	-1.494943	1.511279
6	32	0	2.397882	-0.036677	0.612388
7	14	0	-1.822520	-3.868462	-0.957521
8	14	0	4.622164	-0.025183	1.485834
9	32	0	-0.667826	1.760088	-0.816598
10	32	0	1.758785	1.389311	-1.406654
11	32	0	0.600848	1.476243	1.502416
12	14	0	-1.716020	3.908500	-0.967525
13	6	0	5.603157	-1.370518	0.626241
14	1	0	5.159008	-2.352847	0.797622
15	1	0	5.642439	-1.204475	-0.451995
16	1	0	6.629593	-1.390413	1.004121
17	6	0	5.377606	1.657456	1.154630
18	1	0	5.408852	1.873579	0.085090
19	1	0	4.803326	2.448926	1.639945
20	1	0	6.400800	1.694538	1.539819
21	6	0	4.527807	-0.351580	3.329498
22	1	0	4.075551	-1.323174	3.536895
23	1	0	5.531190	-0.343633	3.765276
24	1	0	3.932934	0.411293	3.835298
25	6	0	-0.567465	5.071674	-1.884114
26	1	0	0.376358	5.196173	-1.350583
27	1	0	-0.341052	4.696679	-2.884029
28	1	0	-1.033803	6.055821	-1.989142

29	6	0	-2.063503	4.532891	0.765302
30	1	0	-1.138199	4.680455	1.324702
31	1	0	-2.593572	5.489049	0.719622
32	1	0	-2.684331	3.828213	1.322332
33	6	0	-3.322518	3.705261	-1.914035
34	1	0	-3.145078	3.306622	-2.914631
35	1	0	-4.001723	3.025722	-1.395361
36	1	0	-3.824594	4.671840	-2.016744
37	6	0	-3.425089	-3.612089	-1.897747
38	1	0	-4.074193	-2.901382	-1.382331
39	1	0	-3.238150	-3.230633	-2.903303
40	1	0	-3.965055	-4.559279	-1.988145
41	6	0	-0.716911	-5.069635	-1.877889
42	1	0	-1.216583	-6.037346	-1.982257
43	1	0	-0.480868	-4.701630	-2.878188
44	1	0	0.223697	-5.226519	-1.347260
45	6	0	-2.183508	-4.479061	0.777400
46	1	0	-2.743287	-5.418310	0.735745
47	1	0	-1.261219	-4.654100	1.333839
48	1	0	-2.780080	-3.754206	1.335065
49	6	0	-3.067684	0.034446	1.746158
50	6	0	-4.277816	0.063884	1.054242
51	6	0	-3.082876	0.019985	3.139524
52	6	0	-5.481460	0.078603	1.743783
53	1	0	-4.283124	0.075566	-0.030371
54	6	0	-4.288486	0.034723	3.826917
55	1	0	-2.150055	-0.002858	3.690482
56	6	0	-5.488273	0.063985	3.131390
57	1	0	-6.415984	0.101649	1.195315
58	1	0	-4.288893	0.023377	4.910631
59	1	0	-6.428417	0.075564	3.669907

HF=-20149.6048934
Sum of electronic and thermal Enthalpies= -20149.122034
Sum of electronic and thermal Free Energies= -20149.264434

Molecule CO see chapter 8.1.1.

8.2.2 TS concerted pathway

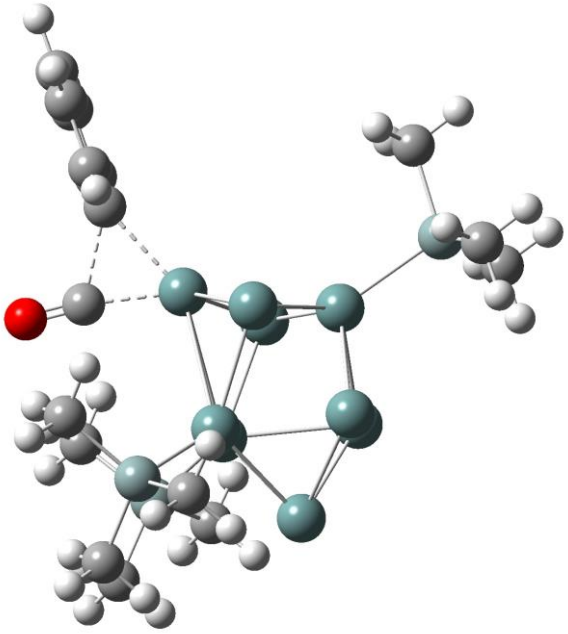

Center Number	Atomic Number	Atomic Type	Coordinates (Angstroms) X	Y	Z
1	32	0	1.103350	1.492436	-0.008823
2	32	0	-1.382044	0.121594	1.245342
3	32	0	-2.592041	-1.835718	0.009663
4	32	0	-0.465938	-2.347734	1.402442
5	32	0	1.072390	-0.039004	2.050259
6	32	0	1.551688	-1.536166	-0.014705
7	6	0	0.394257	3.298518	0.003461
8	8	0	-0.164279	4.315289	0.013799
9	14	0	-2.780431	1.231676	2.857461
10	14	0	3.380123	-3.089550	-0.002835
11	32	0	-1.395059	0.122784	-1.240248
12	32	0	-0.483394	-2.346456	-1.409666
13	32	0	1.049877	-0.034851	-2.071606
14	14	0	-2.823495	1.232389	-2.826097
15	6	0	4.972510	-2.112625	-0.183949
16	1	0	4.987817	-1.550595	-1.119835
17	1	0	5.096770	-1.403290	0.636644
18	1	0	5.833546	-2.787477	-0.180598
19	6	0	3.377191	-4.010159	1.631546
20	1	0	3.445664	-3.318076	2.473334
21	1	0	2.466202	-4.598511	1.755867
22	1	0	4.232097	-4.690883	1.683048
23	6	0	3.196430	-4.283506	-1.437934
24	1	0	3.156840	-3.752542	-2.391147
25	1	0	4.047676	-4.970154	-1.468516
26	1	0	2.284611	-4.876748	-1.347253
27	6	0	-2.890002	0.139057	-4.346867
28	1	0	-1.894032	-0.012440	-4.767139
29	1	0	-3.309699	-0.840755	-4.111343
30	1	0	-3.517032	0.601438	-5.114949
31	6	0	-2.075989	2.900629	-3.242783
32	1	0	-1.076137	2.785992	-3.666127
33	1	0	-2.697734	3.418891	-3.978804

34	1	0	-1.998877	3.537428	-2.359365
35	6	0	-4.534925	1.447276	-2.093328
36	1	0	-4.967559	0.486252	-1.809455
37	1	0	-4.511022	2.082383	-1.206151
38	1	0	-5.198556	1.917461	-2.824976
39	6	0	-4.482339	1.526099	2.129767
40	1	0	-4.437423	2.196659	1.269801
41	1	0	-4.943025	0.591058	1.806125
42	1	0	-5.133789	1.985674	2.878941
43	6	0	-2.887302	0.095783	4.344508
44	1	0	-3.494789	0.558121	5.128174
45	1	0	-3.344682	-0.859479	4.080055
46	1	0	-1.897503	-0.107405	4.757534
47	6	0	-1.979645	2.861135	3.324583
48	1	0	-2.586579	3.378218	4.073683
49	1	0	-0.985478	2.701326	3.746677
50	1	0	-1.878576	3.520224	2.460065
51	6	0	2.339385	3.377250	-0.007837
52	6	0	2.934213	3.770079	1.193272
53	6	0	2.917316	3.782775	-1.212946
54	6	0	4.084721	4.542141	1.189540
55	1	0	2.496033	3.467303	2.139759
56	6	0	4.067819	4.554855	-1.217264
57	1	0	2.465730	3.490163	-2.156329
58	6	0	4.652710	4.934987	-0.015878
59	1	0	4.542064	4.838322	2.126624
60	1	0	4.511944	4.860986	-2.157503
61	1	0	5.552300	5.538888	-0.019017

HF= -20262.7883428 / NImag= 1 (-372.1382 cm^{-1})
Sum of electronic and thermal Enthalpies= -20262.297253
Sum of electronic and thermal Free Energies= -20262.442542

8.2.3 TS / intermediates radical pathway

TS Ge_9-CO radical separation (triplet)

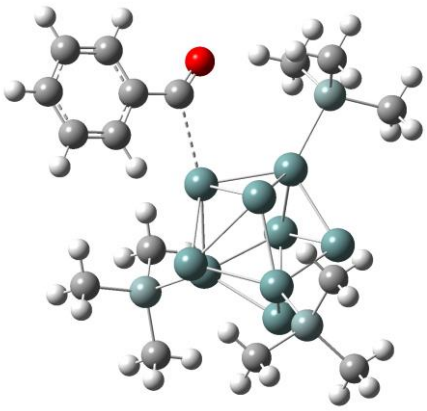

Center Number	Atomic Number	Atomic Type	Coordinates (Angstroms) X	Y	Z
1	32	0	1.517096	0.625439	-0.219823
2	32	0	-0.567493	2.192406	-0.519485
3	32	0	-0.700872	0.543190	-2.429842
4	32	0	-2.790536	0.969422	-0.650580

5	32	0	-0.314632	1.101189	1.737149
6	32	0	-2.117972	-0.602356	1.231200
7	6	0	3.924788	-0.739986	0.558535
8	8	0	4.427012	-1.347363	-0.325704
9	14	0	-0.112579	4.483475	-1.054547
10	14	0	-3.593743	-1.697868	2.767800
11	32	0	0.572160	-1.387974	-1.439227
12	32	0	-1.940561	-1.604996	-1.112352
13	32	0	0.252685	-1.521460	1.058795
14	14	0	1.808069	-2.921278	-2.810007
15	6	0	-2.938375	-3.416110	3.127264
16	1	0	-2.862535	-4.004756	2.210288
17	1	0	-1.946408	-3.373465	3.582484
18	1	0	-3.608284	-3.940857	3.816099
19	6	0	-3.675389	-0.680539	4.340151
20	1	0	-2.691056	-0.594153	4.805836
21	1	0	-4.042829	0.328149	4.138742
22	1	0	-4.351821	-1.151949	5.060302
23	6	0	-5.278169	-1.790451	1.950536
24	1	0	-5.232435	-2.363494	1.021734
25	1	0	-5.994371	-2.279997	2.618211
26	1	0	-5.659397	-0.794537	1.714112
27	6	0	0.588640	-3.667697	-4.021830
28	1	0	-0.216527	-4.192902	-3.503450
29	1	0	0.138915	-2.897769	-4.652819
30	1	0	1.100379	-4.384053	-4.672746
31	6	0	2.547229	-4.232020	-1.698770
32	1	0	1.773919	-4.764510	-1.141045
33	1	0	3.099477	-4.962247	-2.299154
34	1	0	3.241104	-3.781629	-0.986245
35	6	0	3.140004	-1.959469	-3.703359
36	1	0	2.710831	-1.162462	-4.314553
37	1	0	3.833442	-1.513699	-2.987549
38	1	0	3.705789	-2.626896	-4.361434
39	6	0	0.885987	4.551593	-2.638369
40	1	0	1.825948	4.005631	-2.531401
41	1	0	0.333723	4.110558	-3.471215
42	1	0	1.119859	5.589837	-2.895294
43	6	0	-1.744536	5.380880	-1.267931
44	1	0	-1.566468	6.435426	-1.501834
45	1	0	-2.329322	4.947136	-2.082257
46	1	0	-2.346315	5.330493	-0.357887
47	6	0	0.862489	5.214483	0.370588
48	1	0	1.095567	6.264616	0.167125
49	1	0	0.296843	5.166200	1.303740
50	1	0	1.803636	4.679933	0.517959
51	6	0	4.567219	-0.205383	1.771538
52	6	0	3.790287	0.397972	2.754752
53	6	0	5.949475	-0.319142	1.935749
54	6	0	4.390774	0.887026	3.903145
55	1	0	2.718191	0.475538	2.606187
56	6	0	6.544269	0.175213	3.081525
57	1	0	6.535634	-0.794960	1.158072
58	6	0	5.764891	0.777164	4.063661
59	1	0	3.788277	1.355816	4.672181
60	1	0	7.616964	0.093326	3.215026
61	1	0	6.235229	1.163286	4.961163

HF= -20262.7766692 / NImag =1 (-55.2402 cm^{-1})
Sum of electronic and thermal Enthalpies= -20262.284174
Sum of electronic and thermal Free Energies= -20262.431213

$(Me_3Si)_3Ge_9$ radical see chapter 8.1.2.

COPh radical (doublet)

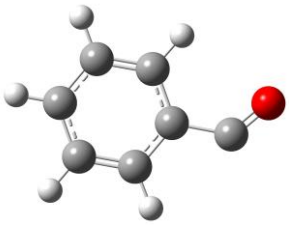

Center Number	Atomic Number	Atomic Type	Coordinates (Angstroms) X	Y	Z
1	6	0	-0.336544	-1.296074	-0.000010
2	6	0	-1.699759	-1.048989	-0.000034
3	6	0	-2.162875	0.259164	-0.000028
4	6	0	-1.269017	1.324804	-0.000002
5	6	0	0.092167	1.083538	0.000015
6	6	0	0.559437	-0.232297	0.000011
7	1	0	0.049650	-2.308295	-0.000009
8	1	0	-2.401535	-1.873831	-0.000054
9	1	0	-3.229138	0.452457	-0.000043
10	1	0	-1.639751	2.342794	0.000004
11	1	0	0.807415	1.897087	0.000032
12	6	0	2.006028	-0.508978	0.000037
13	8	0	2.909592	0.250347	0.000017

HF= -344.6455968
Sum of electronic and thermal Enthalpies= -344.540249
Sum of electronic and thermal Free Energies= -344.578821

TS CO abstraction radical (doublet)

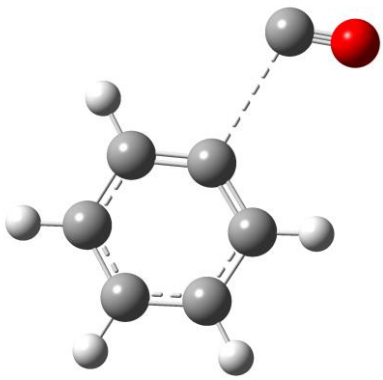

Center Number	Atomic Number	Atomic Type	Coordinates (Angstroms) X	Y	Z
1	6	0	2.832763	-0.607184	-0.000052
2	8	0	3.399992	0.367823	-0.000079
3	6	0	0.294024	-0.168952	0.000147
4	6	0	-0.481295	-1.295479	0.000077
5	6	0	-0.154055	1.123677	0.000103
6	6	0	-1.861504	-1.095234	-0.000045
7	1	0	-0.053337	-2.290644	0.000114
8	6	0	-1.538309	1.297780	-0.000019
9	1	0	0.519783	1.972540	0.000160

10	6	0	-2.380109	0.193331	-0.000092
11	1	0	-2.528496	-1.950110	-0.000103
12	1	0	-1.953375	2.299468	-0.000058
13	1	0	-3.453601	0.338522	-0.000188

HF= / NIMag=1 (-88.8339 cm^{-1})
Sum of electronic and thermal Enthalpies= -344.491495
Sum of electronic and thermal Free Energies= -344.535008

Ph radical (doublet)

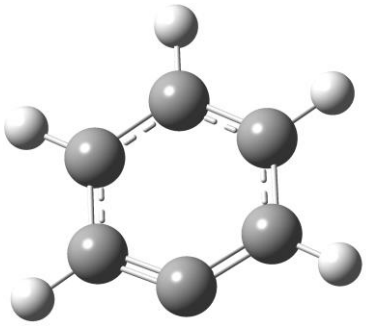

Center Number	Atomic Number	Atomic Type	Coordinates (Angstroms) X	Y	Z
1	6	0	-1.219471	-0.767107	-0.000001
2	6	0	-1.206693	0.627973	-0.000004
3	6	0	-0.000001	1.315096	0.000001
4	6	0	1.206695	0.627969	0.000004
5	6	0	1.219473	-0.767105	-0.000001
6	6	0	-0.000002	-1.388152	-0.000000
7	1	0	-2.152169	-1.318533	-0.000002
8	1	0	-2.143837	1.173344	-0.000005
9	1	0	0.000004	2.398332	0.000002
10	1	0	2.143834	1.173349	0.000008
11	1	0	2.152165	-1.318541	0.000002

HF= -231.3623094
Sum of electronic and thermal Enthalpies= -231.269217
Sum of electronic and thermal Free Energies= -231.302545

TS Ge_9-Ph radical unification (triplet)

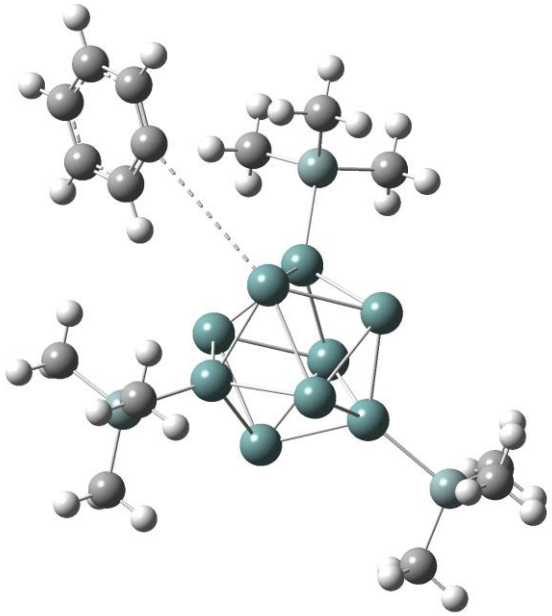

Center Number	Atomic Number	Atomic Type	Coordinates (Angstroms) X	Y	Z
1	6	0	-5.751222	-0.435416	-1.146930
2	6	0	-4.764682	-0.494970	-0.161845
3	6	0	-5.133688	-0.099565	1.095433
4	6	0	-6.373934	0.343963	1.468230
5	6	0	-7.343389	0.395412	0.465788
6	6	0	-7.028876	0.007495	-0.830031
7	32	0	-1.002614	-0.292667	1.567596
8	32	0	-0.143926	-2.060273	-0.036273
9	32	0	1.602198	-1.213164	1.605629
10	32	0	2.754892	0.391468	0.021578
11	14	0	5.103590	0.850368	0.106868
12	6	0	6.001364	-0.489181	-0.846725
13	32	0	-0.851839	1.640847	-0.061891
14	14	0	-2.311973	3.542059	-0.072006
15	6	0	-1.260035	5.075803	-0.300715
16	32	0	1.091662	1.514882	1.569599
17	32	0	-0.915086	-0.299338	-1.697581
18	32	0	1.162684	1.505052	-1.607733
19	32	0	1.674141	-1.224395	-1.605109
20	14	0	-0.903748	-4.331532	0.015233
21	6	0	-2.645292	-4.396680	-0.672259
22	6	0	0.258575	-5.367938	-1.026571
23	6	0	-0.874533	-4.889447	1.803736
24	6	0	5.408724	2.530640	-0.662850
25	6	0	5.613472	0.840252	1.909949
26	6	0	-3.201915	3.586004	1.575076
27	6	0	-3.524703	3.348623	-1.485490
28	1	0	5.811422	-1.474276	-0.414882
29	1	0	5.682511	-0.512549	-1.891160
30	1	0	7.080917	-0.309076	-0.824057
31	1	0	5.089772	2.549632	-1.707349
32	1	0	4.863428	3.312850	-0.130216

33	1	0	6.475503	2.774024	-0.627791
34	1	0	5.413179	-0.128949	2.372036
35	1	0	6.685340	1.044773	1.997622
36	1	0	5.074637	1.602220	2.477499
37	1	0	-0.531005	5.175955	0.506512
38	1	0	-0.714447	5.043419	-1.246402
39	1	0	-1.892178	5.969673	-0.302218
40	1	0	-2.495754	3.647831	2.406115
41	1	0	-3.858458	4.460976	1.620373
42	1	0	-3.814654	2.692235	1.712964
43	1	0	-3.007555	3.265797	-2.444066
44	1	0	-4.143655	2.458325	-1.353060
45	1	0	-4.186115	4.219941	-1.530456
46	1	0	-3.325289	-3.773348	-0.087182
47	1	0	-2.674777	-4.049979	-1.707697
48	1	0	-3.020985	-5.424634	-0.647402
49	1	0	-0.057583	-6.415972	-1.014710
50	1	0	0.268868	-5.027968	-2.064562
51	1	0	1.280872	-5.316072	-0.645661
52	1	0	-1.210296	-5.928754	1.878310
53	1	0	0.132857	-4.825397	2.220880
54	1	0	-1.534525	-4.274379	2.419515
55	1	0	-3.759446	-0.831657	-0.394232
56	1	0	-6.603569	0.641404	2.485311
57	1	0	-5.512722	-0.735342	-2.162016
58	1	0	-8.344575	0.739201	0.703784
59	1	0	-7.788663	0.050434	-1.601961

HF= -20149.4929106 / NImag=1 (-11.0661 cm^{-1})
Sum of electronic and thermal Enthalpies= -20149.012497
Sum of electronic and thermal Free Energies= -20149.157130

8.3 Quantum-chemical Calculations on the Decarbonylation of 6'

8.3.1 Starting material / products

$(Me_3Si)_3Ge_9$-CO-CH_2-Ph (**6'**)

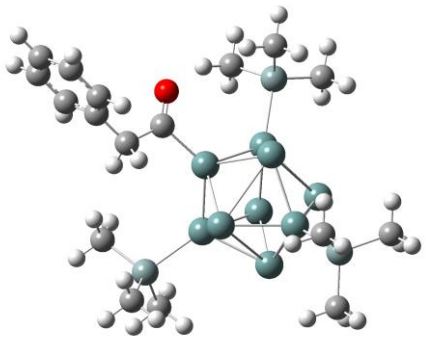

Center Number	Atomic Number	Atomic Type	Coordinates (Angstroms) X	Y	Z
1	32	0	-1.222709	0.158488	0.005846
2	32	0	-0.121751	-1.629553	-1.267469
3	32	0	1.187479	0.144926	-2.657715
4	32	0	2.381005	-1.468146	-0.926280
5	32	0	0.239175	-1.520401	1.355044
6	32	0	2.372783	-0.188149	1.271115
7	6	0	-3.159966	0.459137	0.564949

8	8	0	-3.637787	1.547401	0.446410
9	14	0	-1.035585	-3.725443	-1.990176
10	14	0	4.086434	-0.423103	2.922678
11	32	0	0.140042	1.902563	-1.039306
12	32	0	2.588473	1.346621	-0.750498
13	32	0	0.452320	1.411846	1.545575
14	14	0	-0.723614	4.098595	-1.466851
15	6	0	4.998262	-2.029924	2.610662
16	1	0	4.325013	-2.886197	2.682055
17	1	0	5.451978	-2.041606	1.617881
18	1	0	5.794287	-2.161152	3.349539
19	6	0	5.251563	1.036783	2.776809
20	1	0	5.714297	1.076324	1.788921
21	1	0	4.725353	1.979395	2.938633
22	1	0	6.048518	0.959962	3.522299
23	6	0	3.260769	-0.446488	4.604946
24	1	0	2.550548	-1.271662	4.684489
25	1	0	4.011138	-0.566474	5.391888
26	1	0	2.719421	0.482869	4.791658
27	6	0	0.652701	5.118239	-2.227876
28	1	0	1.499194	5.211968	-1.545244
29	1	0	1.014499	4.667380	-3.153907
30	1	0	0.289764	6.123700	-2.460722
31	6	0	-1.310342	4.841380	0.147538
32	1	0	-0.491745	4.938500	0.862577
33	1	0	-1.731195	5.835806	-0.029613
34	1	0	-2.086391	4.218871	0.597257
35	6	0	-2.156680	3.914477	-2.658891
36	1	0	-1.844514	3.434325	-3.588145
37	1	0	-2.950820	3.312778	-2.212361
38	1	0	-2.572041	4.896098	-2.905546
39	6	0	-2.813442	-3.462092	-2.529364
40	1	0	-3.438878	-3.135247	-1.696154
41	1	0	-2.882529	-2.711614	-3.318847
42	1	0	-3.231364	-4.397683	-2.912611
43	6	0	0.009163	-4.282562	-3.442865
44	1	0	-0.363987	-5.235119	-3.830512
45	1	0	-0.016417	-3.552450	-4.253893
46	1	0	1.051137	-4.420984	-3.148266
47	6	0	-0.959243	-4.984509	-0.604767
48	1	0	-1.361135	-5.943680	-0.945237
49	1	0	0.070147	-5.142065	-0.278113
50	1	0	-1.538986	-4.660768	0.261496
51	6	0	-3.889417	-0.757390	1.107812
52	1	0	-3.853704	-1.509205	0.311375
53	1	0	-3.264886	-1.156402	1.913535
54	6	0	-5.292639	-0.503703	1.563241
55	6	0	-6.354068	-0.569771	0.666645
56	6	0	-5.555238	-0.172278	2.888320
57	6	0	-7.650581	-0.313955	1.084779
58	1	0	-6.163844	-0.824863	-0.370428
59	6	0	-6.850598	0.084225	3.310346
60	1	0	-4.736490	-0.115751	3.597564
61	6	0	-7.902297	0.014060	2.408917
62	1	0	-8.466876	-0.371883	0.374636
63	1	0	-7.038943	0.338334	4.346664
64	1	0	-8.915332	0.212608	2.737526

HF= -20302.1311438
Sum of electronic and thermal Enthalpies= -20301.607384
Sum of electronic and thermal Free Energies= -20301.758312

$(Me_3Si)_3Ge_9$-CH_2-Ph

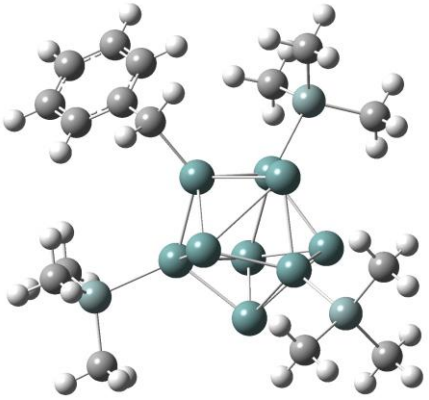

Center Number	Atomic Number	Atomic Type	Coordinates (Angstroms) X	Y	Z
1	6	0	6.573289	-0.036891	-0.712782
2	6	0	5.941294	1.164675	-0.998003
3	6	0	4.671405	1.170713	-1.553106
4	6	0	4.004936	-0.020792	-1.834869
5	6	0	4.655077	-1.220580	-1.549996
6	6	0	5.924916	-1.230469	-0.994875
7	6	0	2.637705	-0.012033	-2.427288
8	32	0	1.179609	-0.004317	-1.064621
9	32	0	-0.897527	1.474673	-1.590198
10	32	0	0.649460	1.752787	0.561532
11	14	0	1.618662	3.939440	0.707872
12	6	0	3.260730	3.785182	1.599806
13	32	0	0.634396	-1.752019	0.565292
14	14	0	1.566997	-3.954769	0.713453
15	6	0	1.817472	-4.658952	-1.007780
16	32	0	-0.915194	-1.458529	-1.585268
17	32	0	-2.625076	0.021650	-0.493227
18	32	0	-1.708652	1.426537	1.421323
19	32	0	0.270280	0.002507	2.453819
20	32	0	-1.723849	-1.401215	1.416000
21	14	0	-4.965910	0.004672	-0.974111
22	6	0	-5.401261	-1.641382	-1.756871
23	6	0	3.208861	-3.825956	1.609890
24	6	0	0.381037	-5.030567	1.687375
25	6	0	-5.873308	0.224640	0.650273
26	6	0	-5.352074	1.415214	-2.145966
27	6	0	0.453411	5.035508	1.684259
28	6	0	1.875194	4.637848	-1.014863
29	1	0	-5.644618	-0.588566	1.341865
30	1	0	-5.597446	1.164217	1.132865
31	1	0	-6.954089	0.232957	0.481490
32	1	0	-5.086751	2.377855	-1.704997
33	1	0	-4.803275	1.311759	-3.083908
34	1	0	-6.421089	1.431071	-2.377843
35	1	0	-5.157014	-2.470341	-1.089885
36	1	0	-6.472322	-1.685071	-1.975257
37	1	0	-4.857978	-1.789871	-2.691907
38	1	0	-0.511536	5.130920	1.183461
39	1	0	0.274613	4.632224	2.682711
40	1	0	0.883246	6.035652	1.794646
41	1	0	0.928051	4.729174	-1.549211

42	1	0	2.328127	5.631706	-0.948669
43	1	0	2.537492	4.007610	-1.611095
44	1	0	3.121283	3.381517	2.604593
45	1	0	3.943336	3.120858	1.066288
46	1	0	3.737398	4.765799	1.690309
47	1	0	3.904306	-3.175330	1.076032
48	1	0	3.073378	-3.416326	2.612817
49	1	0	3.668503	-4.814206	1.705353
50	1	0	0.793300	-6.037977	1.798662
51	1	0	0.206927	-4.624272	2.685440
52	1	0	-0.584276	-5.109120	1.184346
53	1	0	2.250677	-5.661375	-0.938529
54	1	0	0.871235	-4.732552	-1.546445
55	1	0	2.494901	-4.042528	-1.601483
56	1	0	2.466088	0.872288	-3.041033
57	1	0	2.454880	-0.893239	-3.042296
58	1	0	4.190721	2.115770	-1.782510
59	1	0	4.161537	-2.159574	-1.777031
60	1	0	6.442186	2.103526	-0.792454
61	1	0	6.412925	-2.175545	-0.786865
62	1	0	7.566407	-0.043112	-0.280552

HF= -20188.8879849
Sum of electronic and thermal Enthalpies= -20188.375668
Sum of electronic and thermal Free Energies= -20188.515321

Molecule CO see chapter 8.1.1

8.3.2 TS concerted pathway

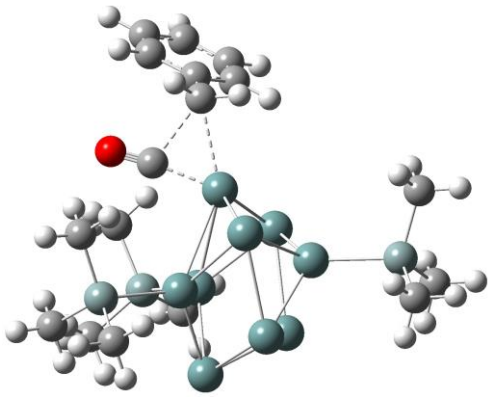

Center Number	Atomic Number	Atomic Type	Coordinates (Angstroms) X	Y	Z
1	32	0	-1.147938	-0.767432	-1.103924
2	32	0	0.594561	1.699446	-0.824673
3	32	0	1.863160	2.163840	1.409624
4	32	0	2.920848	0.563337	-0.330980
5	32	0	1.085227	-0.362212	-2.309311
6	32	0	1.618287	-1.677748	-0.142163
7	6	0	-2.718584	0.278822	-1.516632
8	8	0	-3.586708	1.005653	-1.737769
9	14	0	0.201804	3.708482	-2.091759
10	14	0	3.065194	-3.591932	-0.145020
11	32	0	-0.423657	0.906119	1.316734
12	32	0	1.769105	-0.340014	2.078013
13	32	0	-0.589238	-1.678325	1.225785
14	14	0	-2.116956	1.847456	2.749967

15	6	0	2.269849	-4.922660	-1.203271
16	1	0	1.292715	-5.209424	-0.809421
17	1	0	2.132001	-4.581695	-2.231300
18	1	0	2.900265	-5.816401	-1.225499
19	6	0	4.731328	-3.113061	-0.861162
20	1	0	4.631008	-2.717120	-1.873653
21	1	0	5.219728	-2.351058	-0.250881
22	1	0	5.388037	-3.987127	-0.903424
23	6	0	3.258939	-4.204107	1.617389
24	1	0	2.292302	-4.453695	2.059460
25	1	0	3.881887	-5.103262	1.636936
26	1	0	3.731305	-3.450009	2.249668
27	6	0	-1.874847	1.049716	4.427718
28	1	0	-1.996497	-0.033310	4.368647
29	1	0	-0.879972	1.256992	4.826487
30	1	0	-2.612398	1.438314	5.136190
31	6	0	-3.808960	1.440677	2.056655
32	1	0	-3.947577	0.363648	1.942932
33	1	0	-4.583845	1.810125	2.735192
34	1	0	-3.969492	1.905241	1.082033
35	6	0	-1.875642	3.702475	2.861543
36	1	0	-0.885671	3.948572	3.249920
37	1	0	-1.983415	4.180836	1.886591
38	1	0	-2.622837	4.135368	3.533319
39	6	0	-0.560256	5.003431	-0.971781
40	1	0	-1.541076	4.686762	-0.611956
41	1	0	0.073529	5.202612	-0.105778
42	1	0	-0.692018	5.940476	-1.520666
43	6	0	1.871841	4.275967	-2.724748
44	1	0	1.756631	5.183465	-3.324837
45	1	0	2.552951	4.498026	-1.901205
46	1	0	2.336937	3.512593	-3.351339
47	6	0	-0.948787	3.321615	-3.519732
48	1	0	-1.111280	4.219483	-4.123429
49	1	0	-0.526370	2.550960	-4.167386
50	1	0	-1.921388	2.974598	-3.165878
51	6	0	-3.114808	-1.676895	-2.283795
52	1	0	-3.388405	-1.211323	-3.229087
53	1	0	-2.432343	-2.505736	-2.479203
54	6	0	-4.245422	-2.060433	-1.430916
55	6	0	-5.506302	-1.474192	-1.586528
56	6	0	-4.084702	-2.996647	-0.401743
57	6	0	-6.558453	-1.808587	-0.748792
58	1	0	-5.661450	-0.755360	-2.382670
59	6	0	-5.136866	-3.332036	0.432408
60	1	0	-3.117787	-3.468410	-0.260932
61	6	0	-6.380998	-2.737402	0.266345
62	1	0	-7.526898	-1.344358	-0.895571
63	1	0	-4.985630	-4.064061	1.217344
64	1	0	-7.205200	-3.001425	0.917785

HF= -20302.0690438 / NImag= 1 (-375.3213 cm^{-1})
Sum of electronic and thermal Enthalpies= -20301.548717
Sum of electronic and thermal Free Energies= -20301.694124

8.3.3 TS / intermediates radical pathway

TS Ge_9-CO radical separation (triplet)

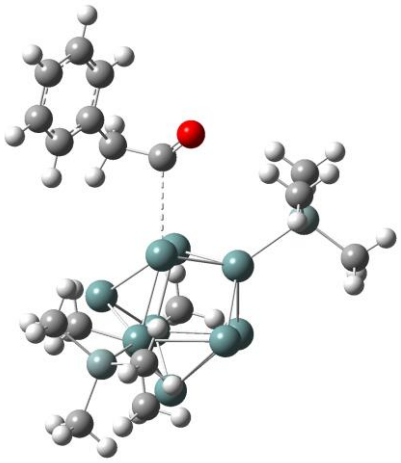

Center Number	Atomic Number	Atomic Type	Coordinates (Angstroms) X	Y	Z
1	6	0	-7.623190	0.835408	2.032916
2	6	0	-7.486199	-0.543888	2.107007
3	6	0	-6.226105	-1.118235	2.147684
4	6	0	-5.084908	-0.320680	2.118534
5	6	0	-5.230568	1.060528	2.037994
6	6	0	-6.491771	1.636267	1.998598
7	6	0	-3.715603	-0.931449	2.135912
8	6	0	-3.325196	-1.578581	0.816687
9	32	0	-1.389854	0.277341	-0.368381
10	32	0	-0.048368	-1.634399	-1.323787
11	14	0	-0.972396	-3.470926	-2.560152
12	6	0	-1.297163	-4.874681	-1.366264
13	8	0	-3.973271	-2.257623	0.106779
14	32	0	0.133755	-1.486005	1.189072
15	32	0	2.300571	-0.151464	1.362458
16	14	0	3.849989	-0.816664	3.065399
17	6	0	5.537276	-0.150718	2.593818
18	32	0	2.433492	-1.362380	-0.882011
19	32	0	2.763426	1.367122	-0.617741
20	32	0	0.355654	2.153889	-0.710788
21	32	0	0.932048	0.399675	-2.457019
22	32	0	0.193623	1.232481	1.641345
23	14	0	-0.463150	4.286798	-1.431705
24	6	0	-1.060162	4.143099	-3.201372
25	6	0	3.276557	-0.083951	4.692447
26	6	0	3.881386	-2.687393	3.158481
27	6	0	-1.876559	4.758074	-0.293176
28	6	0	0.930282	5.533647	-1.304609
29	6	0	0.301412	-3.957015	-3.845481
30	6	0	-2.557310	-2.887342	-3.362012
31	1	0	-2.688679	4.031021	-0.354462
32	1	0	-1.546243	4.809843	0.745988
33	1	0	-2.274955	5.737725	-0.573167
34	1	0	1.295991	5.614594	-0.279332
35	1	0	1.771833	5.251664	-1.940158
36	1	0	0.582122	6.521385	-1.620908
37	1	0	-1.863051	3.408417	-3.285622
38	1	0	-1.441049	5.107179	-3.551334
39	1	0	-0.251859	3.834826	-3.866977
40	1	0	0.509119	-3.129765	-4.526676
41	1	0	1.242465	-4.255048	-3.379621
42	1	0	-0.068146	-4.799759	-4.437196

43	1	0	-2.375952	-2.043056	-4.029604
44	1	0	-2.999434	-3.697205	-3.949981
45	1	0	-3.281892	-2.579581	-2.606029
46	1	0	-0.381726	-5.187890	-0.861341
47	1	0	-2.023964	-4.578241	-0.607986
48	1	0	-1.701089	-5.736761	-1.905433
49	1	0	3.234100	1.005613	4.643675
50	1	0	2.282611	-0.447880	4.959447
51	1	0	3.966678	-0.362352	5.494329
52	1	0	4.591859	-3.017554	3.922141
53	1	0	2.897275	-3.084464	3.414248
54	1	0	4.181116	-3.122155	2.203089
55	1	0	6.277769	-0.434352	3.347511
56	1	0	5.863458	-0.550432	1.631791
57	1	0	5.527552	0.938238	2.519855
58	1	0	-2.948491	-0.203185	2.399286
59	1	0	-3.648328	-1.751923	2.859700
60	1	0	-6.125808	-2.196352	2.199620
61	1	0	-4.347208	1.689393	2.008972
62	1	0	-8.365801	-1.176053	2.134383
63	1	0	-6.589475	2.713896	1.941563
64	1	0	-8.609055	1.283470	2.002717

HF= -20302.0643901 / NImag=1 (-56.0914 cm^{-1})
Sum of electronic and thermal Enthalpies= -20301.542512
Sum of electronic and thermal Free Energies= -20301.696128

$(Me_3Si)_3Ge_9$ radical see chapter 8.1.3

CO-Bz radical (doublet)

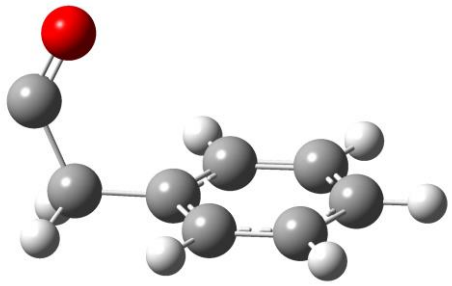

Center Number	Atomic Number	Atomic Type	Coordinates (Angstroms) X	Y	Z
1	6	0	0.591717	1.269157	0.040590
2	6	0	1.899502	1.073715	-0.376892
3	6	0	2.453506	-0.197248	-0.353984
4	6	0	1.692812	-1.270162	0.088809
5	6	0	0.386578	-1.072322	0.506055
6	6	0	-0.176870	0.200212	0.489303
7	1	0	0.163265	2.265551	0.020776
8	1	0	2.486960	1.917152	-0.719559
9	1	0	3.475160	-0.352044	-0.679109
10	1	0	2.119270	-2.265954	0.109977
11	1	0	-0.202924	-1.915828	0.848613
12	6	0	-2.636180	0.059439	-0.146447
13	8	0	-2.505026	-0.468090	-1.185917
14	6	0	-1.600549	0.411466	0.907834

15	1	0	-1.870138	-0.196236	1.777551
16	1	0	-1.794477	1.446531	1.197484

HF= -383.9213505
Sum of electronic and thermal Enthalpies= -383.786768
Sum of electronic and thermal Free Energies= -383.830716

TS CO abstraction radical (doublet)

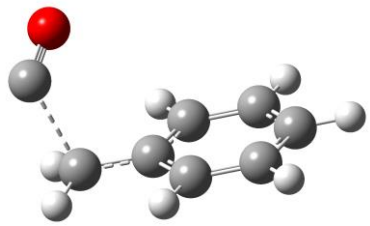

Center Number	Atomic Number	Atomic Type	Coordinates (Angstroms) X	Y	Z
1	6	0	-0.113387	0.355718	0.552007
2	6	0	0.704935	1.296833	-0.096099
3	6	0	1.954811	0.944420	-0.566670
4	6	0	2.420371	-0.356834	-0.412166
5	6	0	1.620863	-1.303713	0.218639
6	6	0	0.370633	-0.955905	0.691831
7	6	0	-1.420857	0.714751	1.014857
8	6	0	-2.753606	0.206301	-0.490539
9	8	0	-2.645263	-0.823993	-0.969231
10	1	0	0.344939	2.312304	-0.219089
11	1	0	2.573951	1.685917	-1.057517
12	1	0	3.400647	-0.631649	-0.781876
13	1	0	1.978725	-2.319151	0.340474
14	1	0	-0.250347	-1.698561	1.180107
15	1	0	-1.909725	0.070714	1.737689
16	1	0	-1.678670	1.762946	1.082894

HF= -383.902164 / NImag=1 (-395.1066 cm^{-1})
Sum of electronic and thermal Enthalpies= -383.770658
Sum of electronic and thermal Free Energies= -383.814502

Bz radical (doublet)

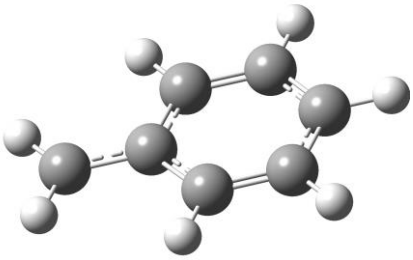

Center Number	Atomic Number	Atomic Type	Coordinates (Angstroms) X	Y	Z
1	6	0	-0.000000	-0.000000	0.987619
2	6	0	0.000000	1.210061	0.250844
3	6	0	0.000000	1.204335	-1.126837
4	6	0	0.000000	0.000000	-1.828168
5	6	0	-0.000000	-1.204335	-1.126837

6	6	0	-0.000000	-1.210061	0.250844
7	6	0	-0.000000	-0.000000	2.388292
8	1	0	0.000000	2.149979	0.791298
9	1	0	0.000000	2.143189	-1.668151
10	1	0	0.000000	0.000000	-2.911117
11	1	0	-0.000000	-2.143189	-1.668151
12	1	0	-0.000000	-2.149979	0.791298
13	1	0	0.000000	-0.927545	2.945140
14	1	0	0.000000	0.927545	2.945140

HF= -270.6806212
Sum of electronic and thermal Enthalpies= -270.559033
Sum of electronic and thermal Free Energies= -270.594662

TS Ge_9-$CH_2C_6H_5$ radical unification (triplet)

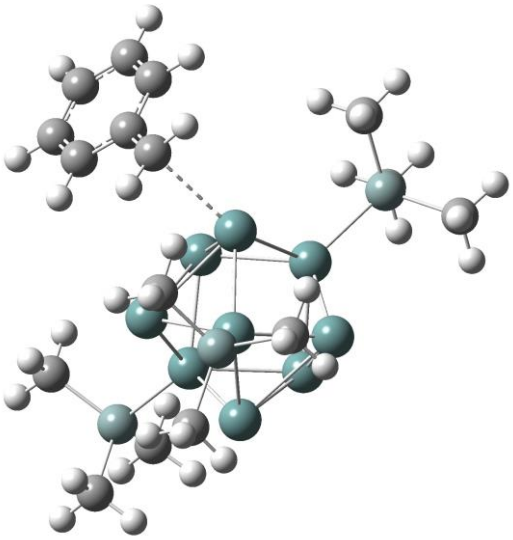

Center Number	Atomic Number	Atomic Type	Coordinates (Angstroms) X	Y	Z
1	6	0	2.749033	1.780469	4.298470
2	6	0	4.113331	1.807854	4.032413
3	6	0	4.731048	0.676938	3.502372
4	6	0	4.000827	-0.464394	3.247941
5	6	0	2.616461	-0.520638	3.521733
6	6	0	2.008976	0.641653	4.046065
7	6	0	1.861695	-1.690221	3.255839
8	32	0	1.036840	-1.337159	0.752357
9	32	0	-1.432599	-1.773132	0.335875
10	14	0	-2.663312	-3.599496	1.274882
11	6	0	-4.486464	-3.172435	1.247113
12	32	0	1.284845	1.337509	0.416625
13	32	0	-1.057846	2.024936	-0.275898
14	14	0	-2.107259	4.113817	0.251892
15	6	0	-1.758822	5.320277	-1.139705
16	32	0	1.498264	-0.215529	-1.565473
17	14	0	3.567526	-0.719014	-2.662956
18	6	0	3.221051	-1.872088	-4.099429
19	32	0	-0.541678	-1.652979	-2.011310
20	32	0	-0.480893	1.054337	-2.552092
21	32	0	-2.534083	0.069924	-1.035823
22	32	0	-1.014405	0.351221	1.629160
23	6	0	-1.355832	4.723313	1.857645
24	6	0	-3.951837	3.846151	0.442034

25	6	0	-2.061032	-3.829522	3.035190
26	6	0	-2.324948	-5.130813	0.250236
27	6	0	4.318393	0.884939	-3.277781
28	6	0	4.704981	-1.533169	-1.413971
29	1	0	-4.390546	3.454922	-0.477688
30	1	0	-4.164523	3.136366	1.243483
31	1	0	-4.448274	4.791254	0.681545
32	1	0	-1.544159	4.018587	2.669814
33	1	0	-0.275417	4.848575	1.764284
34	1	0	-1.788900	5.688708	2.135629
35	1	0	-2.164009	4.959453	-2.086982
36	1	0	-2.217223	6.289497	-0.922293
37	1	0	-0.685995	5.474083	-1.269638
38	1	0	-4.687698	-2.265960	1.820821
39	1	0	-4.836912	-3.008335	0.226504
40	1	0	-5.071915	-3.988251	1.681302
41	1	0	-2.245933	-2.935431	3.633774
42	1	0	-2.583478	-4.667177	3.506403
43	1	0	-0.990167	-4.040239	3.062279
44	1	0	-2.641181	-4.989954	-0.784992
45	1	0	-1.261500	-5.376537	0.245804
46	1	0	-2.870451	-5.986521	0.658851
47	1	0	2.775697	-2.807515	-3.756190
48	1	0	2.534040	-1.415427	-4.814384
49	1	0	4.150661	-2.108541	-4.625715
50	1	0	5.272352	0.689192	-3.776337
51	1	0	3.658240	1.381347	-3.991500
52	1	0	4.502451	1.575843	-2.452886
53	1	0	5.671644	-1.758431	-1.874208
54	1	0	4.879996	-0.878458	-0.557824
55	1	0	4.277160	-2.465915	-1.042111
56	1	0	2.370962	-2.617371	3.027827
57	1	0	0.844167	-1.767163	3.618753
58	1	0	4.489061	-1.341499	2.837464
59	1	0	0.947157	0.624443	4.264910
60	1	0	5.793998	0.692382	3.290964
61	1	0	2.260558	2.656355	4.709167
62	1	0	4.691305	2.701443	4.233251

HF= -20188.8187996 / NImag=1 (-124.5867 cm^{-1})
Sum of electronic and thermal Enthalpies= -20188.309459
Sum of electronic and thermal Free Energies= -20188.455493

9 References

[1] C. Hoch, M. Wendorff, C. Röhr, *J. Alloys Compd.* **2003**, *361*, 206-221.
[2] P. A. Leber, A. J. Nocket, M. F. Wipperman, S. Zohrabian, C. Y. Bemis, M. K. Sidhu, *Org. Biomol. Chem.* **2013**, *11*, 5994-5997.
[3] F. Mäsing, A. Mardyukov, C. Doerenkamp, H. Eckert, U. Malkus, H. Nüsse, J. Klingauf, A. Studer, *Angew. Chem. Int. Ed.* **2015**, *54*, 12612-12617; *Angew. Chem.* **2015**, *43*, 12803-12808.
[4] F. Li, S. C. Sevov, *Inorg. Chem.* **2012**, *51*, 2706-2708.
[5] X-Area, version 1.76.8.1, Stoe & Cie GmbH, Darmstadt **2015**.
[6] G. M. Sheldrick, *Acta Cryst. C* **2015**, *71*, 3-8.
[7] a) A. L. Spek, *Acta Cryst. D* **2009**, *65*, 148-155; b) A. L. Spek, *Acta Cryst. C* **2015**, *71*, 9-18.
[8] Gaussian 09, Revision **E.03**, M. J. Frisch, G. W. Trucks, H. B. Schlegel, G. E. Scuseria, M. A. Robb, J. R. Cheeseman, G. Scalmani, V. Barone, G. A. Petersson, H. Nakatsuji, X. Li, M. Caricato, A. Marenich, J. Bloino, B. G. Janesko, R. Gomperts, B. Mennucci, H. P. Hratchian, J. V. Ortiz, A. F. Izmaylov, J. L. Sonnenberg, D. Williams-Young, F. Ding, F. Lipparini, F. Egidi, J. Goings, B. Peng, A. Petrone, T. Henderson, D. Ranasinghe, V. G. Zakrzewski, J. Gao, N. Rega, G. Zheng, W. Liang, M. Hada, M. Ehara, K. Toyota, R. Fukuda, J. Hasegawa, M. Ishida, T. Nakajima, Y. Honda, O. Kitao, H. Nakai, T. Vreven, K. Throssell, J. A. Montgomery, Jr., J. E. Peralta, F. Ogliaro, M. Bearpark, J. J. Heyd, E. Brothers, K. N. Kudin, V. N. Staroverov, T. Keith, R. Kobayashi, J. Normand, K. Raghavachari, A. Rendell, J. C. Burant, S. S. Iyengar, J. Tomasi, M. Cossi, J. M. Millam, M. Klene, C. Adamo, R. Cammi, J. W. Ochterski, R. L. Martin, K. Morokuma, O. Farkas, J. B. Foresman, and D. J. Fox, Gaussian, Inc., Wallingford CT, **2016**.

[9] M. Ernzerhof, G. E. Scuseria, *J. Chem. Phys.*, **1999**, *110*, 5029-5036.
[10] F. Weigend, R. Ahlrichs, *Phys. Chem. Chem. Phys.*, **2005**, *7*, 3297-3305.

5.7 Challenges in Chemical Synthesis at the Border of Solution-Based and Solid-State Chemistry—Synthesis and Structure of $[CH_3CH_2Ge_9\{Si(SiMe_3)_3\}]^{2-}$

Sabine Frischhut, Wilhelm Klein, and Thomas F. Fässler

published in:

C. R. Chim. **2018**, *10*, 932-937.

CONTENT AND CONTRIBUTION

Within the scope of this publication, the first organo-functionalized twofold silylated Ge_9 cluster $[\{(Me_3Si)_3Si\}_2Ge_9CH_2CH_3]^-$ was synthesized by reaction of $[\{(Me_3Si)_3Si\}_2Ge_9]^{2-}$ with bromo-ethane in acetone. The anion $[\{(Me_3Si)_3Si\}_2Ge_9CH_2CH_3]^-$ was characterized by NMR spectroscopy (^1H, ^{29}Si, ^{13}C, COSY, HMBC, HSQC) and ESI mass spectrometry, but unfortunately could not be crystallized.

Upon addition of the sequestering agent 2,2,2-crypt to the reaction solution containing $[\{(Me_3Si)_3Si\}_2Ge_9CH_2CH_3]^-$, one silyl ligand is abstracted leading to the crystallization of $[K(2,2,2\text{-crypt})]_2[\{(Me_3Si)_3Si\}Ge_9CH_2CH_3]$. The latter was characterized by single crystal X-ray crystallography and comprises a Ge_9 cluster, which carries one silyl ligand and an ethyl-functionality.

$[K(2,2,2\text{-crypt})]_2[\{(Me_3Si)_3Si\}Ge_9CH_2CH_3]$ presents the first example, where a covalently bound silyl ligand, does not point radially away from the cluster core, but lies in the plane, which is described by the open square face of the C_{2v}-symmetric cluster core. Crystal structure determination was assisted by Dr. Wilhelm Klein. The syntheses and characterization of the new compounds were carried out within this work. *In situ* ^1H NMR studies on the desilylation were also carried out within this work.

All obtained data were evaluated within this thesis. The publication was authored within this work. The manuscript was revised by Dr. Wilhelm Klein and by Prof. Dr. Thomas F. Fässler.

C. R. Chimie 21 (2018) 932–937

Contents lists available at ScienceDirect

Comptes Rendus Chimie

www.sciencedirect.com

Full paper/Mémoire

Challenges in chemical synthesis at the border of solution-based and solid-state chemistry—Synthesis and structure of $[CH_3CH_2Ge_9\{Si(SiMe_3)_3\}]^{2-}$

Sabine Frischhut, Wilhelm Klein, Thomas F. Fässler*

Department Chemie, Technische Universität München, Lichtenbergstraße 4, 85747 Garching, Germany

ARTICLE INFO

Article history:
Received 2 March 2018
Accepted 10 April 2018
Available online 10 May 2018

Keywords:
Zintl cluster
Germanium
Crystal structure
Silyl ligand abstraction
Organofunctionalization

ABSTRACT

Polyanionic $[Ge_9]^{4-}$ clusters are accessible in good yields by a solid-state reaction of the elements Ge and K. The nine-atom deltahedral germanium clusters are transformed to silylated species, which in a subsequent reaction allow for addition of an organic moiety. We present a synthetic method for a stepwise ligand exchange reaction at a Zintl ion. Herein, we functionalized the $[Ge_9\{Si(SiMe_3)_3\}_2]^{2-}$ cluster with an ethyl group by a reaction with bromoethane. The obtained anion $[CH_3CH_2Ge_9\{Si(SiMe_3)_3\}_2]^-$ was characterized by NMR spectroscopy and mass spectrometry. After addition of 2,2,2-crypt an abstraction of one silyl ligand was observed resulting in the crystallization of $[K(2,2,2\text{-crypt})]_2[CH_3CH_2Ge_9\{Si(SiMe_3)_3\}]$ representing the first monosilylated Ge_9 Zintl cluster, which carries an additional ethyl group. The latter compound was characterized by single crystal X-ray crystallography, NMR spectroscopy, and elemental analysis.

1. Introduction

A distinctive combination of chemical synthetic protocols for a metamorphosis of the heavier tetrel and pentel elements has been developed over the years. The formation of small charged atom clusters—so-called Zintl clusters—obtained by reacting the respective elements with alkali metals provides precursors for numerous new compounds [1]. In the case of the deltahedral polyanions of tetrel elements Ge, Sn, and Pb, the respective clusters have a good solubility in very polar aprotic solvents. Such nine-atomic clusters provide a source of an "activated" element for the fabrication of novel morphologies such as germanium in the form of an inverse opal structure (Fig. 1) [2].

Therefore, resourcing of capable main-group-element-rich molecules is a synthetic challenge. By adding various organic groups the polyanions reduce their charge and thus allow better solubility in a larger variety of organic solvents. Recently, equipping these Zintl ions with organic groups opened a new field at the border of solid-state chemistry and solution-based reactions of main-group-element-rich molecules [3]. In this context, especially $[Ge_9]^{4-}$ Zintl clusters show multifaceted reactivity toward transition metal compounds and are capable of attaching organic ligands or can undergo follow-up reactions.

The Zintl phases A_4Ge_9 (A = K, Rb) can be easily dissolved in polar solvents, such as ethylenediamine, pyridine, and liquid ammonia [4]. At a maximum, twofold functionalized Ge_9 clusters can be obtained from ethylenediamine solutions. The first *exo*-Ge_9–C bond was obtained in $[Ph–Ge_9–SnPh]^{2-}$ [3a]. Simple nucleophilic substitution reaction of Ge_9^{4-} with alkyl halides resulted in several organofunctionalized deltahedral Ge_9 cluster anions of the form $[R–Ge_9–Ge_9–R]^{2-}$ and $[Ge_9R_2]^{2-}$ in small amounts [5]. The organofunctionalization was further extended to alkenylated cluster entities by a rather complex reaction of Ge_9^{4-} with alkynes in ethylenediamine [5a,6]. The most

* Corresponding author.
E-mail address: thomas.faessler@lrz.tum.de (T.F. Fässler).

https://doi.org/10.1016/j.crci.2018.04.007
1631-0748/

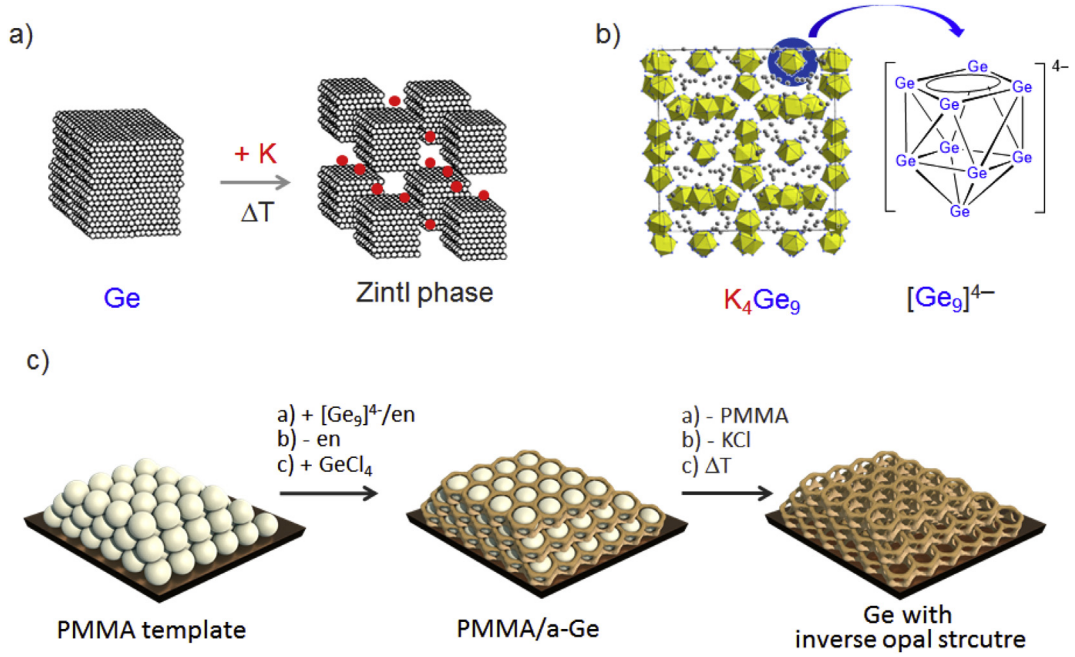

Fig. 1. Formation of a Zintl phase by the reaction of an alkali metal element with a p-block (semi)metal. (b) The Zintl phase K_4Ge_9 comprises discrete $[Ge_9]^{4-}$ cluster anions. (c) Formation of elemental germanium with a novel morphology. Impregnating a PMMA template structure with a $[Ge_9]^{4-}$/en solution, cluster linking/oxidation with $GeCl_4$, and removal of KCl and PMMA results in mesostructured Ge. PMMA, polymethylmethacrylate; en, ethylenediamine.

prominent examples are given by the vinylated clusters $[Ge_9(CH{=}CH_2)_n]^{(4-n)-}$ [7]. The substitution of simple alkynes by dialkynes leads to the isolation of the so-called Zintl triads $[R{-}Ge_9{-}CH{=}CH{-}CH{=}CH{-}Ge_9{-}R]^{4-}$ and $[Ge_9{-}CH{=}CH{-}CH{=}CH{-}Ge_9]^{6-}$ [8]. Due to unforeseen reactions of the deltahedral Ge_9 clusters in ethylenediamine, the focus of research was set more toward reactions of the latter in convenient solvents.

In 2003, Schnepf [3c] reported the soluble anion $[Ge_9(Si(SiMe_3)_3)_3]^-$, which was synthesized by treating metastable Ge(I) bromide with $Li[Si(SiMe_3)_3]$. This complex way of synthesizing the threefold silylated Ge_9 cluster was replaced by the Zintl-route-synthesis, which was developed by Li and Sevov [9], wherein a heterogeneous reaction K_4Ge_9 is treated with 3 equiv of chlorotris(trimethylsilyl) silane in acetonitrile to form $[Ge_9(Si(SiMe_3)_3)_3]^-$. From this anion numerous new compounds emerged and new reactivities of the Ge_9 Zintl cluster were discovered. The attachment of organic moieties and the accompanied introduction of specific functionalities, as is realized in $H_2C{=}CH(CH_2)_nGe_9\{Si(SiMe_3)_3\}_3$ (n = 1, 3), have been reported. For these compounds fluctuation in solution at rt was observed, which is most likely caused by labile-bound silyl ligands or a dynamic cluster framework [10].

Besides, specifically functionalized Ge_9 anions have been achieved by using less sterically demanding silyl ligands, which carry terminal double bonds, for example, $[H_2C{=}CH(CH_2)nPh_2SiGe_9\{Si(SiMe_3)_3\}_2]^-$ (n = 1,2) [11].

Also, the coordination of $[Ge_9\{Si(SiMe_3)_3\}_3]^-$ to transition metals and linkage of two cluster units by coordination to transition metals have been accomplished [12]. Even the neutral organofunctionalized cluster $CH_3CH_2Ge_9\{Si(SiMe_3)_3\}_3$ is capable of coordinating to late transition metals forming the *closo*-cluster $Pd(PPh_3)(CH_3CH_2)Ge_9\{Si(SiMe_3)_3\}_3$ [13].

Only recently, Kysliak and Schnepf developed a synthesis route for the disilylated Ge_9 cluster $[Ge_9\{Si(SiMe_3)_3\}_2]^{2-}$. Remarkably, $[Ge_9\{Si(SiMe_3)_3\}_2]^{2-}$ is formed by reaction of $[Ge_9\{Si(SiMe_3)_3\}_3]^-$ with K_4Ge_9, which enforces the assumption that the silyl ligands are weakly bound to the Ge_9 core [14]. So far, the monosilylated Ge_9 cluster anion $[Ge_9\{Si(SiMe_3)_3\}]^{3-}$ has not been reported.

$[Ge_9\{Si(SiMe_3)_3\}_2]^{2-}$ and $[Ge_9\{Si(SiMe_3)_3\}_3]^-$ readily react with dialkylphosphines R_2PCl to form the species $[Ge_9\{Si(SiMe_3)_3\}_2R_2P]^-$ and $[Ge_9\{Si(SiMe_3)_3\}_3R_2P]$, respectively [15]. Linkage of two $[Ge_9\{Si(SiMe_3)_3\}_2]^{2-}$ entities has been realized in $[\{Si(SiMe_3)_3\}_2Ge_9{-}SiMe_2{-}(C_6H_4){-}SiMe_2{-}Ge_9\{Si(SiMe_3)_3\}_2]^{2-}$ [16].

Herein we present the addition of an ethyl functionality to $[Ge_9\{Si(SiMe_3)_3\}_2]^{2-}$ by the reaction of the latter with bromoethane in acetone. The resulting anion $[CH_3CH_2Ge_9\{Si(SiMe_3)_3\}_2]^-$ was characterized by NMR spectroscopy and electrospray ionization mass spectrometry (ESI MS). In addition, we present the first monosilylated Ge_9 cluster compound carrying an additional ethyl group, which was obtained by addition of 2,2,2-crypt to an acetone solution of $[CH_3CH_2Ge_9\{Si(SiMe_3)_3\}_2]^-$. The compound was crystallized as $[K(2,2,2\text{-crypt})]_2[CH_3CH_2Ge_9Si(SiMe_3)_3]$ and characterized by single crystal X-ray crystallography, NMR spectroscopy, and elemental analysis.

2. Discussion

$[Ge_9\{Si(SiMe_3)_3\}_2]^{2-}$ undergoes a nucleophilic substitution reaction with bromoethane exclusively in THF or

acetone to form the species $[CH_3CH_2Ge_9\{Si(SiMe_3)_3\}_2]^-$ (**1a**), which was unequivocally shown by ESI MS and NMR spectroscopy (Scheme 1, for NMR spectra see Fig. S1 of Supporting information).

The obtained mass spectrum of **1a** is shown in Fig. 2 and matches the *m*/*z* ratio as well as the isotopic pattern of the simulated mass spectrum of the anion $[CH_3CH_2Ge_9\{Si(SiMe_3)_3\}_2]^-$.

Despite the addition of various counter ions, $[CH_3CH_2Ge_9\{Si(SiMe_3)_3\}_2]^-$ could not be crystallized. In case of the addition of 2,2,2-crypt to an acetone solution containing "$K[CH_3CH_2Ge_9\{Si(SiMe_3)_3\}_2]$" (**1**) with the aim of sequestering K^+, the abstraction of one silyl ligand occurred. The peaks in the ^1H NMR spectrum of the residue of the reaction mixture after evaporating the solvent and dissolution in acetone-d_6 show an integral ratio of 27:2:3 for $-Si\{Si(CH_3)_3\}_3$, $-CH_2$, and $-CH_3$ groups, respectively (Supporting information, Fig. S3). The residue was redissolved in acetone and stored at −32 °C for crystallization. Red-brown needle-shaped crystals were obtained. Compound **2** is not stable in the gas phase whereby ESI mass spectra of **2** are not available.

The unit cell of $[K(2,2,2\text{-crypt})]_2[CH_3CH_2Ge_9Si(SiMe_3)_3]$ (**2**) contains two entities of **2a** and four potassium ions complexed with 2,2,2-crypt (Supporting information, Fig. S5). This is consistent with the twofold negatively charged Ge_9 cluster entity **2a** (Fig. 3). Each cluster is equipped with one silyl group and an ethyl moiety. Compound **2a** contains a nearly C_{2v} symmetric Ge_9 cluster core with one open face, and thus, is very similarly shaped to so far reported twofold-substituted Ge_9 Zintl clusters. The Ge–Ge distances within the cluster core range from 2.519(2) (for Ge3–Ge4) to 2.939(2) Å (for Ge5–Ge6), and are typical of twofold-substituted Ge_9 Zintl clusters [6d,7a]. The attachment of ligands to the two atoms Ge1 and Ge3, which are located at the open face Ge1–Ge2–Ge3–Ge4, leads to compression of the Ge distances terminating the open face as compared to those forming the capped square. The Ge1–Si1 distance of 2.423(2) Å is longer than in the crystal structures of $[Ge_9\{Si(SiMe_3)_3\}_2]^{2-}$ (d(Ge–Si) = 2.4097(9) and 2.4071(9) Å) [14] and $[Ge_9\{Si(SiMe_3)_3\}_3]^-$ (d(Ge–Si) = 2.363(2)–2.369(1)Å) [9]. The Ge–Si distance integrates well in this series. The more silyl groups are bound to the cluster the stronger the Ge–Si bond. The Ge3–C1 distance of 2.02(1) Å compares well with the Ge–C distance of 1.973(4) Å in $CH_3CH_2Ge_9\{Si(SiMe_3)_3\}_3$ [10a]. Remarkably, the hypersilyl ligand does not point radially away from the cluster core, as is the case for the silyl ligands in the crystal structures of

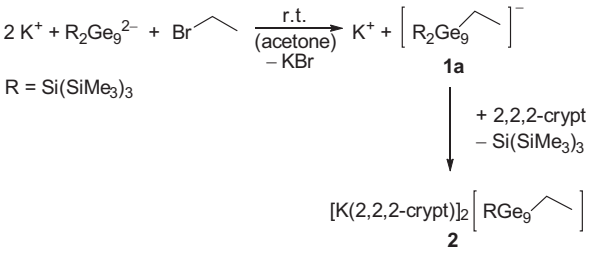

Scheme 1. Reaction of $K_2[Ge_9\{Si(SiMe_3)_3\}_2]$ with bromoethane yielding the anion **1a** and subsequent reaction to **2**.

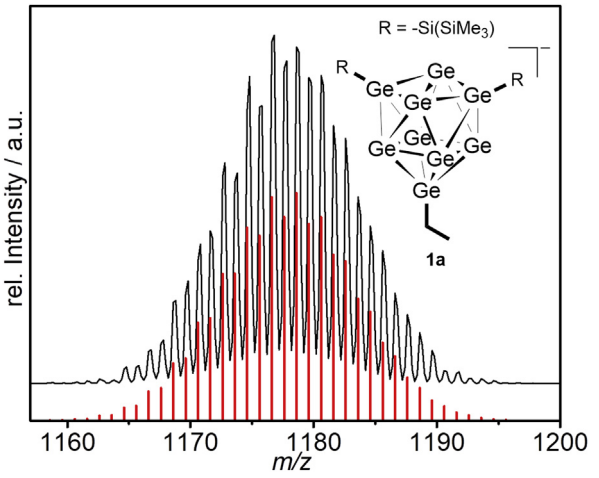

Fig. 2. ESI mass spectrum of a THF solution of **1** and predicted structure of **1a**. The measured spectrum of $[CH_3CH_2Ge_9\{Si(SiMe_3)_3\}_2]^-$ (**1a**) is shown in black. The simulated spectrum is shown as bar graph in red. (For further information see Fig. S2 of Supporting information).

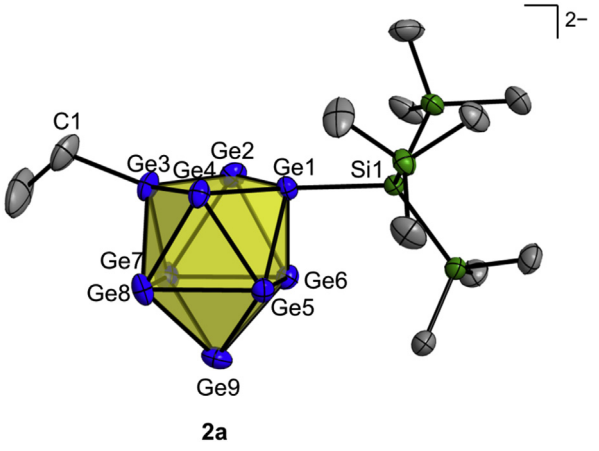

Fig. 3. The twofold negatively charged anion **2a**. All non-hydrogen atoms are shown as ellipsoids at a probability level of 50%. All hydrogen atoms are omitted for clarity.

$[Ge_9\{Si(SiMe_3)_3\}_2]^{2-}$ and $[Ge_9\{Si(SiMe_3)_3\}_3]^-$ but lies in the plane Ge1–Ge2–Ge3–Ge4 (Supporting information, Fig. S6).

In a next step, we further investigated the desilylation of compound **1** by addition of 18-crown-6. The addition of 18-crown-6 to the reaction solution did not lead to the abstraction of one silyl group as was the case for 2,2,2-crypt (Supporting information, Fig. S7). This was shown by the integral ratio of 54:2:3 for $-Si(Si(CH_3)_3)_3$, $-CH_2$, and $-CH_3$ of the ^1H NMR spectrum of the reaction solution. Nevertheless crystallization of **1a** was not successful using 18-crown-6 as a sequestering agent. Presumably, due to the nitrophilicity of the silicon the abstraction of silyl groups is favored when amines like 2,2,2-crypt are present in the solution. Desilylation reactions for germanides have been reported before. Especially KOtBu and fluorides, for example, acyl fluorides have been applied as effective reagents to abstract silyl groups [17].

3. Conclusions

We present a synthetic method for a stepwise ligand exchange reaction at a Zintl ion. The selective organofunctionalization of $[Ge_9\{Si(SiMe_3)_3\}_2]^{2-}$ via the nucleophilic substitution reaction with bromoethane in acetone results in the first step in the anion $[CH_3CH_2Ge_9\{Si(SiMe_3)_3\}_2]^-$. Upon addition of 2,2,2-crypt to the solution desilylation occurs and one silyl ligand is abstracted, which leads to the isolation of the compound $[K(2,2,2\text{-crypt})]_2[CH_3CH_2Ge_9Si(SiMe_3)_3]$. The latter represents the first monosilylated Ge_9 Zintl cluster. The fact that silyl ligands are weakly bound and can be selectively abstracted might lead to a wide range of interesting structures, which contain deltahedral Ge_9 clusters with several different ligands.

4. Experimental section

4.1. General

All manipulations were carried out under a purified argon atmosphere using standard Schlenk techniques. The Zintl phase with the nominal composition K_4Ge_9 was synthesized by heating a stoichiometric mixture of the elements K and Ge (99.999%, Chempur) at 650 °C for 46 h in a stainless steel autoclave [18]. Anhydrous acetone was purchased from VWR Chemicals and stored over molecular sieve (3 Å) for at least 1 day. Chlorotris(trimethylsilyl)silane (≥95.0%, TCI Chemicals) and bromoethane (98%, Sigma–Aldrich) were used as received. 2,2,2-Crypt (Merck) was dried in vacuum for 8 h. 18-Crown-6 (Merck) was sublimed in vacuum. The solvents, acetonitrile and toluene, were obtained from a solvent purificator (MB-SPS). Acetonitrile was stored over molecular sieve (3 Å). The deuterated solvents acetonitrile-d_3 and acetone-d_6 were purchased from Deutero GmbH and stored over molecular sieve (3 Å) for at least 1 day.

4.2. Synthesis of $K_2[Ge_9\{Si(SiMe_3)_3\}_2]$

$K_2[Ge_9\{Si(SiMe_3)_3\}_2]$ was synthesized according to a modified literature procedure [14]. In a glovebox K_4Ge_9 (739 mg, 0.91 mmol) was weighed and introduced into a Schlenk flask and a solution of chlorotris(trimethylsilyl) silane (517 mg, 1.82 mmol) in 24 mL acetonitrile was added. The suspension was stirred at rt for 13 days. After filtering the reaction solution the solvent was evaporated in vacuo. The residue was washed three times with a total amount of 22 mL toluene and the residue was dried in vacuo. An orange solid (518 mg) was obtained. The NMR data match with those reported in the literature.

4.3. Synthesis of $K[CH_3CH_2Ge_9\{Si(SiMe_3)_3\}_2]$ (**1**)

For NMR spectroscopic investigations of **1**, $K_2[Ge_9\{Si(SiMe_3)_3\}_2]$ (30 mg, 0.024 mmol) was treated with a solution of bromoethane (1.8 μL, 0.024 mmol) dissolved in 0.6 mL acetone-d_6. The deep-brown reaction solution was stirred for 21 h at rt and characterized by NMR spectroscopy. ^{1}H NMR (400 MHz, acetone-d_6, 298 K): δ (ppm) 1.28 (m, 2H, CH_2 on ethyl), 1.18 (m, 3H, CH_3 on ethyl), 0.25 (s, 54H, CH_3 on hypersilyl); ^{29}Si NMR (79 MHz, acetone-d_6, 298 K): δ (ppm) −9.38 (*Si*$(CH_3)_3$), −108.56 (*Si*$\{Si(CH_3)_3\}_3$); ^{13}C NMR (101 MHz, acetone-d_6, 298 K): δ (ppm) 20.44 (q, *C*H_3), 4.10 (t, *C*H_2), 3.12 (q, *C*H_3 on hypersilyl); ^{1}H ^{1}H COSY (400 MHz, acetone-d_6, 298 K): δ (ppm)/δ (ppm) 1.27/1.19 (^3J, *C*H_2/*C*H_3); ^{1}H ^{13}C HSQC (400 MHz/101 MHz, acetone-d_6, 298 K): δ (ppm)/δ (ppm) 1.28/4.07 (^1J, *C*H_2/*C*H_2), 1.19/20.40 (^1J, *C*H_3/*C*H_3), 0.25/3.13 (^1J, *C*H_3 on hypersilyl/*C*H_3 on hypersilyl); ^{1}H ^{13}C HMBC (400 MHz/101 MHz, acetone-d_6, 298 K): δ (ppm)/δ (ppm) 1.30/20.34 (^2J, *C*H_2/*C*H_3), 1.17/4.15 (^2J, *C*H_3/*C*H_2); ESIMS (negative ion mode, 4500 V, 300 °C): *m*/*z* 1179 $[CH_3CH_2Ge_9\{Si(SiMe_3)_3\}_2]^-$.

4.4. Synthesis of $\{[K(222\text{-crypt})]_2$ ***2a***$\}$ (**2**)

$K_2[Ge_9\{Si(SiMe_3)_3\}_2]$ (140 mg, 0.11 mmol) was weighed and introduced into a Schlenk tube and a solution of bromoethane (8.5 μL, 0.11 mmol) in 3 mL acetone was added. The reaction solution was stirred for 23 h at rt. After filtering through a glass fiber filter 2,2,2-crypt (86 mg, 0.23 mmol) was added to the red-brown reaction solution. The solvent was evaporated in vacuo to obtain a dark oil, which was characterized by NMR spectroscopy. The oil was dissolved in 0.5 mL acetone and stored at −32 °C for 5 days to obtain 15 mg of red-brown needle-shaped crystals suitable for X-ray crystallography (yield 8%). For NMR spectroscopic investigations of **2**, the crystals were separated from the mother liquor, washed three times with a total amount of 3 mL hexane, and dried at ambient conditions. The crystals were dissolved in acetonitrile-d_3 (for NMR spectra see Fig. S4 of Supporting information). ^{1}H NMR (400 MHz, acetonitrile-d_3, 298 K): δ (ppm) 3.56 (s, crypt), 3.52 (m, crypt), 2.52 (m, crypt), 0.91 (m, 3H, CH_3 on ethyl), 0.82 (m, 2H, CH_2 on ethyl), 0.09 (s, 27H, CH_3 on hypersilyl); ^{1}H ^{1}H COSY (400 MHz, acetone-d_6, 298 K): δ (ppm)/δ (ppm) 0.91/0.81 (^3J, *C*H_3/*C*H_2) elemental analysis calcd (%): C, 32.04; H, 5.95. Found: C, 31.41; H, 5.93.

4.5. X-ray data collection and structure determination

A few crystals of **2** were transferred from the mother liquor into perfluoropolyalkylether under a cold N_2 stream. A single crystal was fixed on a glass fiber and positioned in a 150 K cold N_2 stream. The single-crystal intensity data were recorded on a Stoe StadiVari diffractometer (Mo Kα radiation (λ = 0.71073), Pilatus 300K detector), by using the X-Area software package [19]. The crystal structure was solved by direct methods using the SHELX software [20]. The position of the hydrogen atoms was calculated and refined using a riding model. All non-hydrogen atoms were treated with anisotropic displacement parameters. Crystallographic details of compound **2** are listed in Table 1. CCDC 1826538 contains the supplementary crystallographic data. These data can be obtained free of charge from the Cambridge Crystallographic Data Centre via www.ccdc.cam.ac.uk/data_request/cif. The presence of the elements Si, Ge, and K in the measured single crystal was confirmed by energy dispersive X-ray analysis.

4.6. Energy-dispersive X-ray analysis

The presence of the elements K, Si, and Ge in the single crystal of **2**, which was used to determine the crystal

Table 1
Crystallographic details on **2**.

Compound	**2**
Formula	$C_{47}H_{104}Ge_9K_2N_4O_{12}Si_4$
Formula weight (g mol^{-1})	1761.21
Space group (no)	$P2_1$ (4)
a (Å)	14.682 (1)
b (Å)	15.226 (2)
c (Å)	16.993 (2)
α (deg)	90
β (deg)	90.878 (8)
γ (deg)	90
V (Å^3)	3798.3 (7)
Z	2
T (K)	150 (2)
λ (Å)	0.71073
ρ_{calcd} (g cm^{-3})	1.410
μ (mm^{-1})	3.730
Collected reflections	84,219
Independent reflections	14,793
R_{int}	0.066
parameters/restraints	714/0
R_1 [$I > 2\sigma(I)$/all data]	0.041/0.068
wR_2 [$I>2\sigma(I)$/all data)]	0.076/0.092
Goodness of fit	1.106
max./min differential electron density	0.89/−0.77

structure, was confirmed using a Hitachi TM-1000 tabletop microscope.

4.7. Elemental analysis

Elemental analysis was performed by the microanalytical laboratory at the Department of Chemistry of the Technische Universität München. The elements C, H, and N were determined using a combustion analyzer (Elementar Vario EL, Bruker Corp.).

4.8. NMR spectroscopy

NMR spectra were recorded using a BRUKER Avance Ultrashield AV400 spectrometer. The signals were referenced to the residual proton signal of the deuterated solvents acetone-d_6 (δ = 2.05 ppm) and acetonitrile-d_3 (δ = 1.94 ppm). The chemical shifts are given in δ values in parts per million (ppm).

4.9. Electrospray ionization mass spectrometry

For ESI mass spectrometric investigations samples were prepared as described in Section 4, except instead of the deuterated solvent nondeuterated ones were used. After the reaction time the solvent was removed. A small amount of the residue was characterized by NMR spectroscopy. The residue was then dissolved in THF and filtered through a glass fiber filter. The measurements were carried out on an HCT (Bruker Corp.). The dry gas temperature was adjusted to 125 °C and the injection speed to 240 μL s^{-1}. The measurements were carried out in the negative ion mode.

Acknowledgments

S.F. is grateful to the Fonds der Chemischen Industrie for her fellowship. The authors thank the “Bayerische Staatsministerium für Wirtschaft und Medien, Energie und Technologie” within the program “Solar Technologies go Hybrid” for the financial support. The authors further acknowledge Kevin Frankievicz, B.Sc., for preparation of reaction solutions.

Appendix A. Supplementary data

Supplementary data related to this article can be found at https://doi.org/10.1016/j.crci.2018.04.007.

References

[1] (a) M. Joannis, C. r. hebd. séances Acad. sci. Paris 113 (1891) 795;
(b) C. Kraus, Trans. Am. Electrochem. Soc. 45 (1924) 175;
(c) E. Zintl, J. Goubeau, W. Dullenkopf, Z. Phys. Chem. Abt. A 154 (1931) 1;
(d) D. Kummer, L. Diehl, Angew. Chem. Int. Ed. 9 (1970) 895;
(e) J.D. Corbett, Chem. Rev. 85 (1985) 383;
(f) S. Scharfe, F. Kraus, S. Stegmaier, A. Schier, T.F. Faessler, Angew. Chem. Int. Ed. 50 (2011) 3630.
[2] (a) M.M. Bentlohner, M. Waibel, P. Zeller, K. Sarkar, P. Müller-Buschbaum, D. Fattakhova-Rohlfing, T.F. Fässler, Angew. Chem. Int. Ed. 55 (2016) 2441;
(b) S. Geier, R. Jung, K. Peters, H.A. Gasteiger, D. Fattakhova-Rohlfing, T.F. Fässler, Sustain. Energy Fuels 2 (2018) 85.
[3] (a) A. Ugrinov, S.C. Sevov, J. Am. Chem. Soc. 125 (2003) 14059;
(b) C.B. Benda, J.Q. Wang, B. Wahl, T.F. Fässler, Eur. J. Inorg. Chem. 27 (2011) 4262;
(c) A. Schnepf, Angew. Chem. Int. Ed. 42 (2003) 2624.
[4] S.C. Sevov, J.M. Goicoechea, Organometallics 25 (2006) 5678.
[5] (a) M.W. Hull, S.C. Sevov, J. Am. Chem. Soc. 131 (2009) 9026;
(b) M.W. Hull, A. Ugrinov, I. Petrov, S.C. Sevov, Inorg. Chem. 46 (2007) 2704.
[6] (a) M.W. Hull, S.C. Sevov, Angew. Chem. Int. Ed. 46 (2007) 6695;
(b) M.W. Hull, S.C. Sevov, Chem. Commun. 48 (2012) 7720;
(c) M.W. Hull, S.C. Sevov, J. Organomet. Chem. 721 (2012) 85;
(d) C.B. Benda, H. He, W. Klein, M. Somer, T.F. Fässler, Z. Anorg. Allg. Chem. 641 (2015) 1080.
[7] (a) M.W. Hull, S.C. Sevov, Inorg. Chem. 46 (2007) 10953;
(b) C.B. Benda, R. Schäper, S. Schulz, T.F. Fässler, Eur. J. Inorg. Chem. 2013 (2013) 5964.
[8] (a) M.M. Bentlohner, W. Klein, Z.H. Fard, L.-A. Jantke, T.F. Fässler, Angew. Chem. Int. Ed. 54 (2015) 3748;
(b) S. Frischhut, M.M. Bentlohner, W. Klein, T.F. Fässler, Inorg. Chem. 56 (2017) 10691;
(c) M.M. Bentlohner, S. Frischhut, T.F. Fässler, Chem. Eur. J. 23 (2017) 17089.
[9] F. Li, S.C. Sevov, Inorg. Chem. 51 (2012) 2706.
[10] (a) F. Li, S.C. Sevov, J. Am. Chem. Soc. 136 (2014) 12056;
(b) S. Frischhut, T.F. Fässler, Dalton Trans. (2018), https://doi.org/10.1039/C8DT00321A.
[11] K. Mayer, L.J. Schiegerl, T. Kratky, S. Günther, T.F. Fässler, Chem. Commun. 53 (2017) 11798.
[12] (a) F. Henke, C. Schenk, A. Schnepf, Dalton Trans. 40 (2011) 6704;
(b) C. Schenk, A. Schnepf, Angew. Chem. Int. Ed. 46 (2007) 5314;
(c) C. Schenk, F. Henke, G. Santiso-Quiñones, I. Krossing, A. Schnepf, Dalton Trans. (2008) 4436;
(d) F. Henke, C. Schenk, A. Schnepf, Dalton Trans. (2009) 9141;
(e) F. Li, S.C. Sevov, Inorg. Chem. 54 (2015) 8121;
(f) K. Mayer, L.J. Schiegerl, T.F. Fässler, Chem. Eur. J. 22 (2016) 18794;
(g) F.S. Geitner, T.F. Fässler, Eur. J. Inorg. Chem. (2016) 2688;
(h) L.J. Schiegerl, F.S. Geitner, C. Fischer, W. Klein, T.F. Fässler, Z. Anorg. Allg. Chem. 642 (2016) 1419;

(i) F.S. Geitner, M.A. Giebel, A. Pöthig, T.F. Fässler, Molecules 22 (2017) 1204.
[13] F. Li, A. Muñoz-Castro, S.C. Sevov, Angew. Chem. Int. Ed. 55 (2016) 8630.
[14] O. Kysliak, A. Schnepf, Dalton Trans. 45 (2016) 2404.
[15] (a) F.S. Geitner, J.V. Dums, T.F. Fässler, J. Am. Chem. Soc. 139 (2017) 11933;
(b) F.S. Geitner, C. Wallach, T.F. Fässler, Chem. Eur. J. (2018), https://doi.org/10.1002/chem.201705678.
[16] O. Kysliak, C. Schrenk, A. Schnepf, Inorg. Chem. 56 (2017) 9693.
[17] (a) J. Hlina, C. Mechtler, H. Wagner, J. Baumgartner, C. Marschner, Organometallics 28 (2009) 4065;
(b) J. Radebner, A. Eibel, M. Leypold, C. Gorsche, L. Schuh, R. Fischer, A. Torvisco, D. Neshchadin, R. Geier, N. Moszner, Angew. Chem. Int. Ed. 11 (2017) 3103.
[18] C. Hoch, M. Wendorff, C. Röhr, J. Alloys Compd. 361 (2003) 206.
[19] X-Area, Stoe & Cie GmbH, Darmstadt, 2015.
[20] G.M. Sheldrick, Acta Crystallogr. Sect. C 71 (2015) 3.

SUPPORTING INFORMATION

Challenges in Chemical Synthesis at the Border of Solution-Based and Solid State Chemistry - Synthesis and Structure of $[CH_3CH_2Ge_9\{Si(SiMe_3)_3\}]^{2-}$

Sabine Frischhut, Wilhelm Klein, and Thomas F. Fässler[a]*

1 Characterization of the anion 1a

1.1 NMR spectroscopic characterization of 1a

Figure S1. ^{1}H, b) ^{29}Si, c) ^{13}C, d) ^{1}H ^{1}H COSY, e) ^{1}H ^{13}C HSQC NMR and f) ^{1}H ^{13}C HMBC NMR spectrum of reaction solution of 1 recorded at r.t. in acetone-d_6. Signals marked with # are assigned to toluene which is present in small amounts in the educt $K_2[Ge_9\{Si(SiMe_3)_3\}_2]$. Signals marked with * could not be assigned.

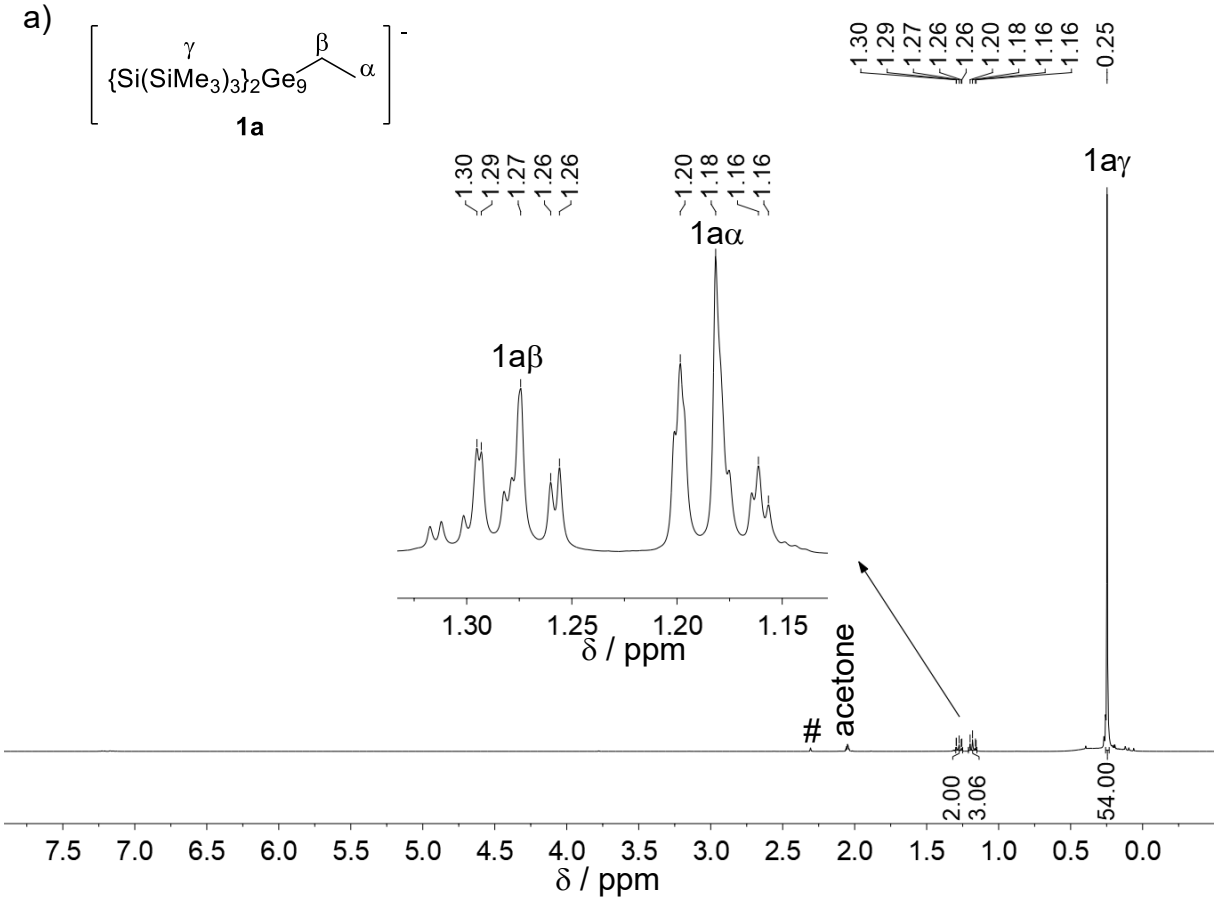

b)

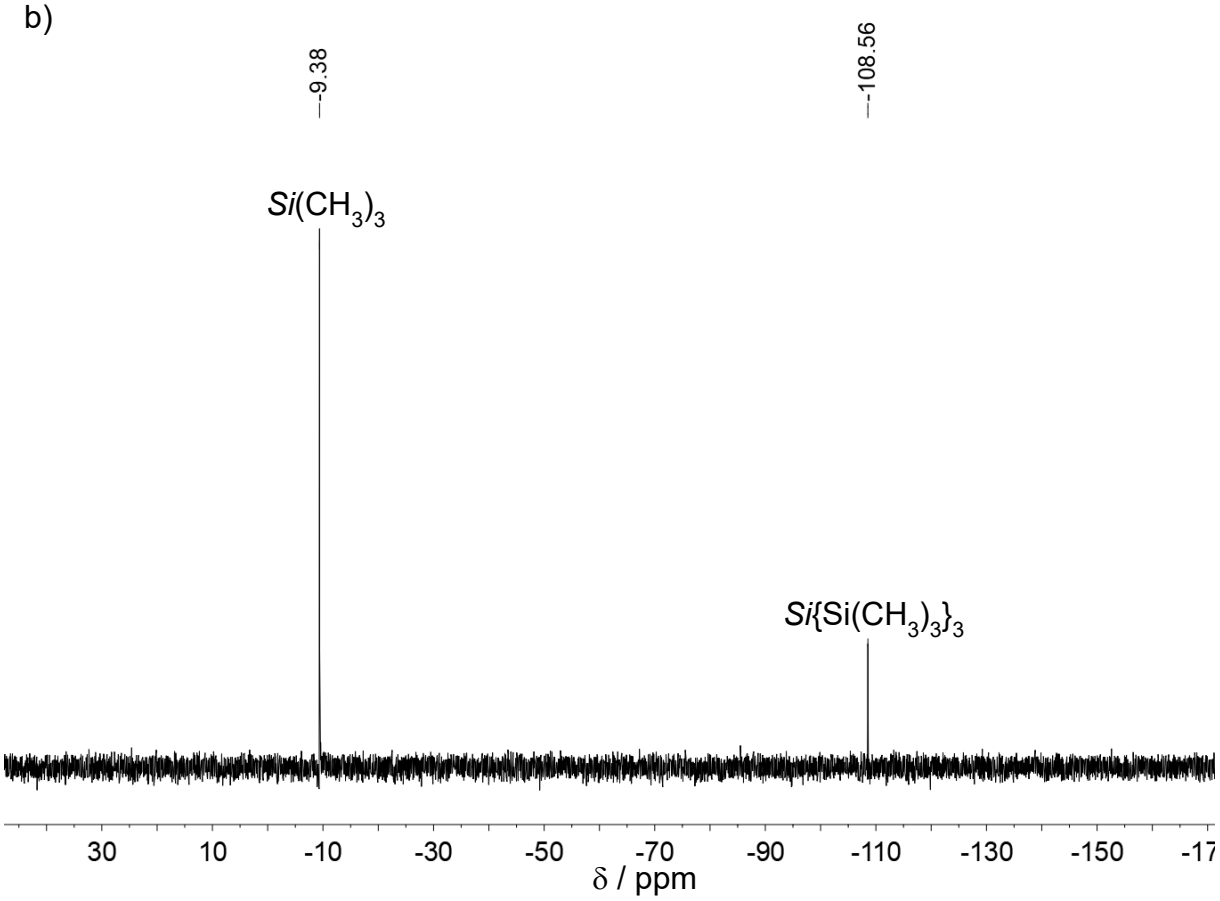
-9.38
-108.56
Si(CH3)3
Si{Si(CH3)3}3
30
10
-10
-30
-50
-70
-90
-110
-130
-150
-17
δ / ppm

c)

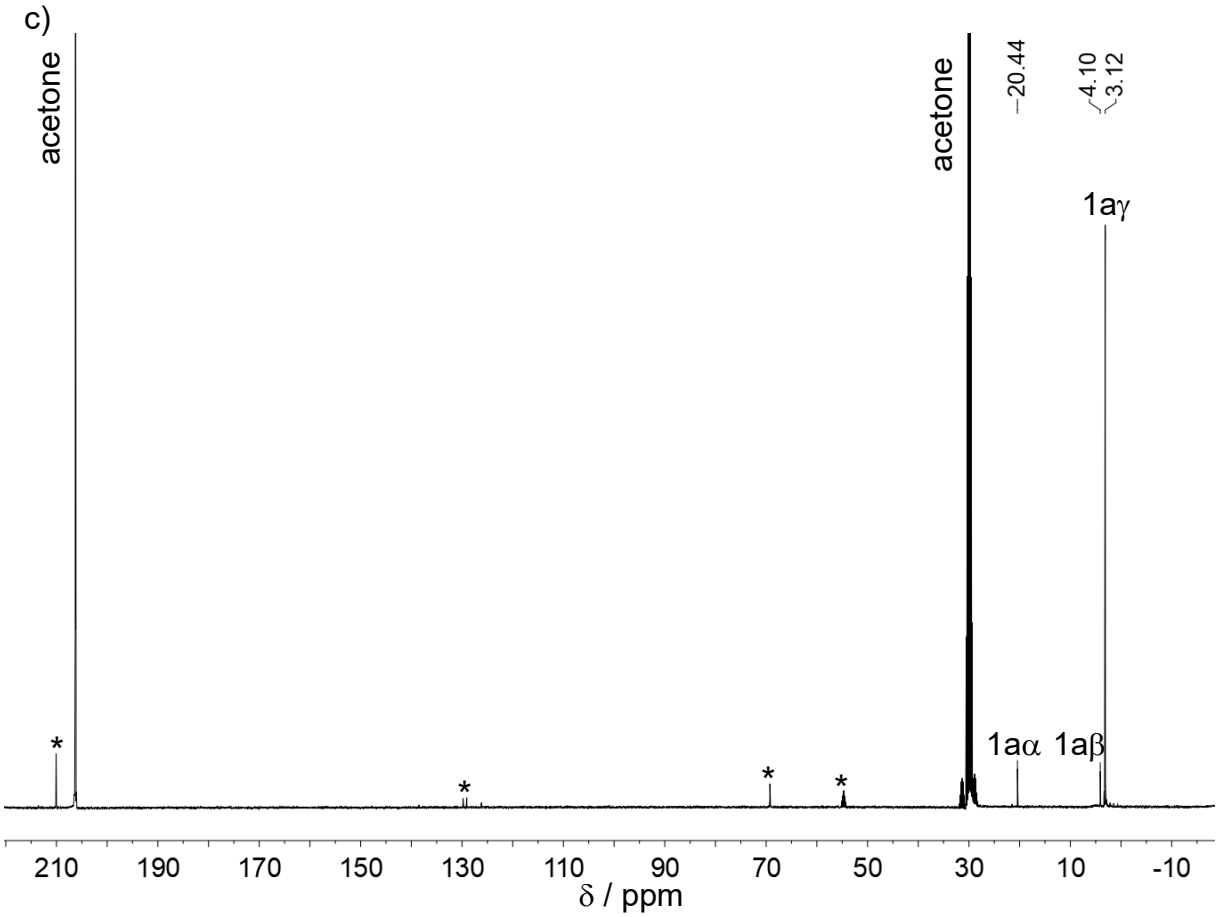
acetone
acetone
20.44
4.10
3.12
1aγ
1aα
1aβ
*
210
190
170
150
130
110
90
70
50
30
10
-10
δ / ppm

d)

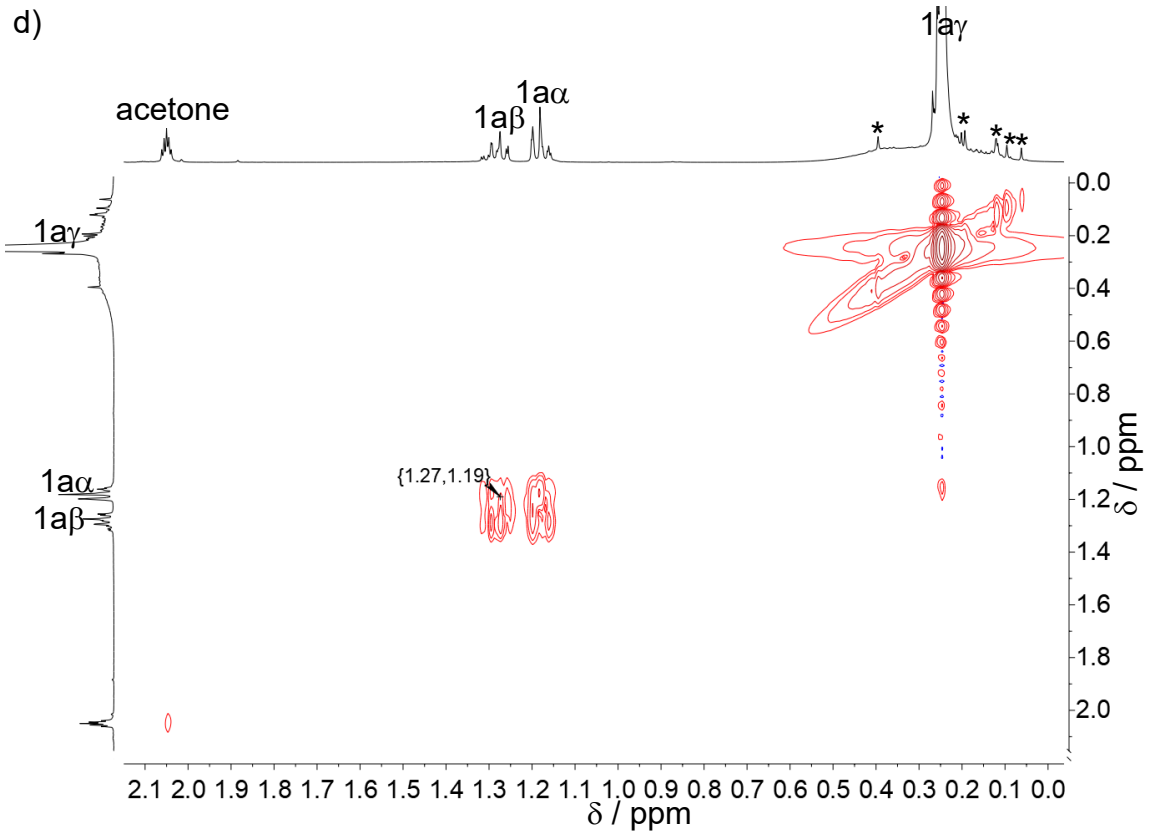
acetone
1aβ
1aα
1aγ
1aγ
1aα
1aβ
{1.27,1.19}
0.0
0.2
0.4
0.6
0.8
1.0
1.2
1.4
1.6
1.8
2.0
δ / ppm
2.1 2.0 1.9 1.8 1.7 1.6 1.5 1.4 1.3 1.2 1.1 1.0 0.9 0.8 0.7 0.6 0.5 0.4 0.3 0.2 0.1 0.0
δ / ppm

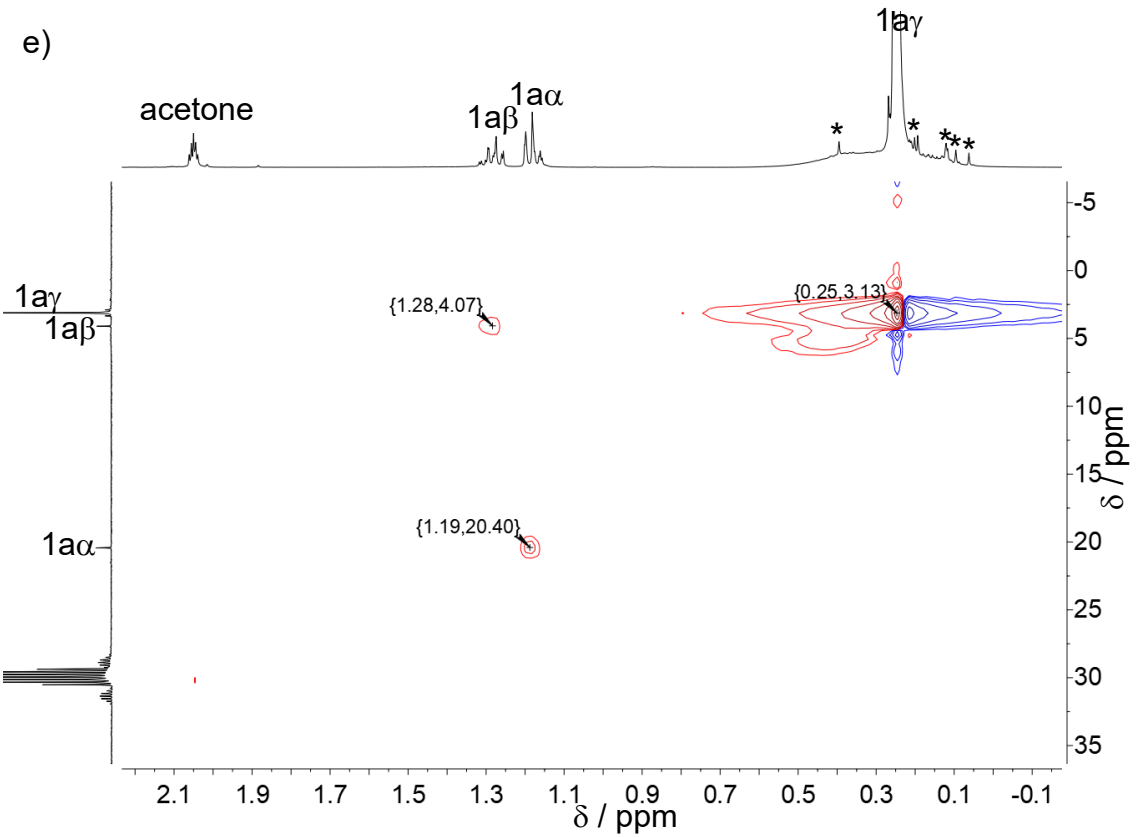
e)
acetone
1aβ
1aα
1aγ
*
{1.28,4.07}
{0.25,3.13}
{1.19,20.40}
1aγ
1aβ
1aα
δ / ppm
δ / ppm

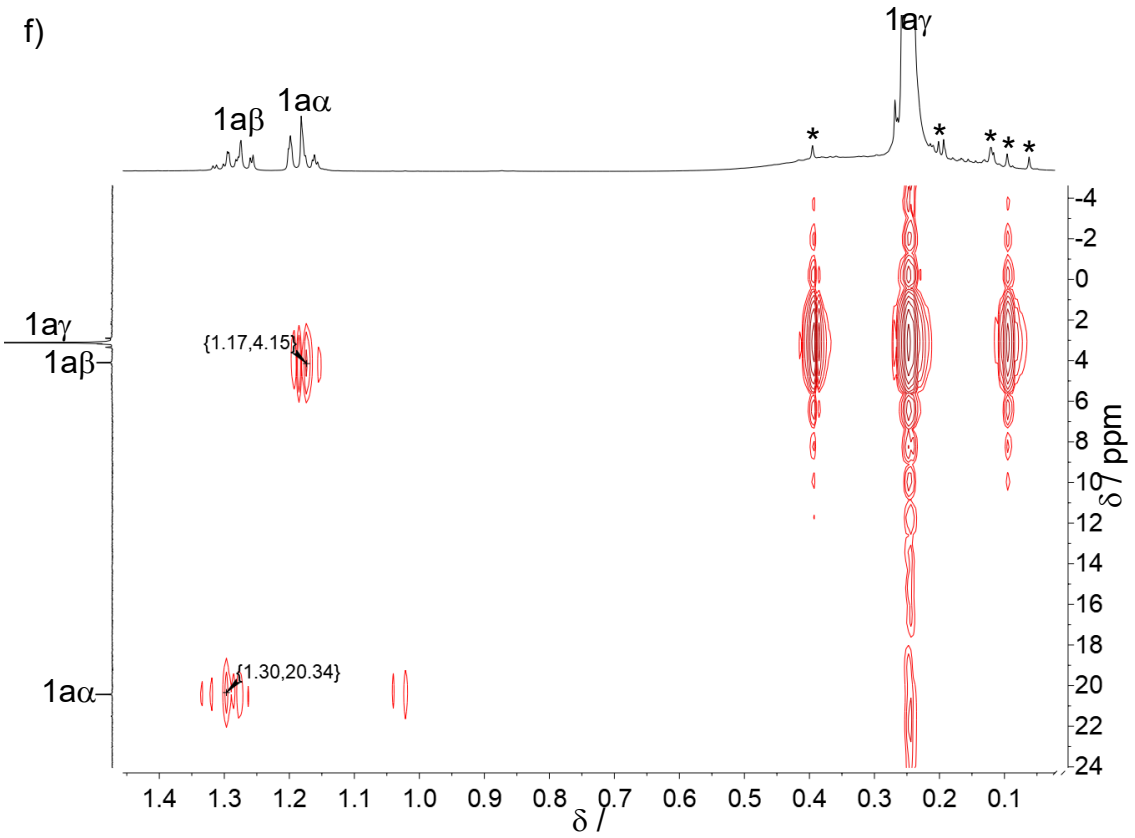
f)
1aβ
1aα
1aγ
*
{1.17,4.15}
{1.30,20.34}
1aγ
1aβ
1aα
δ / ppm
δ /

1.2 ESI mass spectrum of 1a

Figure S2. Relevant section of the measured ESI-MS spectrum of **1** in a thf solution (black) and the simulated spectra of **1a** and $[Ge_9\{Si(SiMe_3)_3\}_3]^-$ shown as bar graphs below in red and blue, respectively. The shown signals are the only signals of relevant intensity observed in the ESI-MS spectrum. **1a** partly reacts to $[Ge_9\{Si(SiMe_3)_3\}_3]^-$ in the gas-phase.

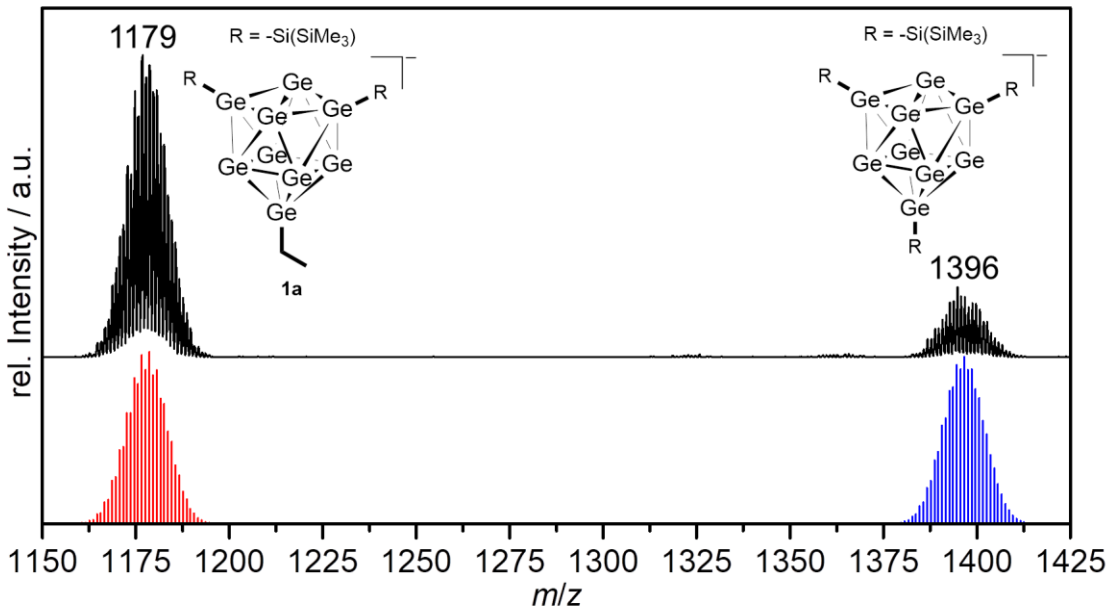

2 Characterization of compound 2

2.1 ^{1}H NMR spectra of 2a

Figure S3. ^{1}H NMR spectrum of the raw product of **2a** recorded in acetone-d_6 at r.t..

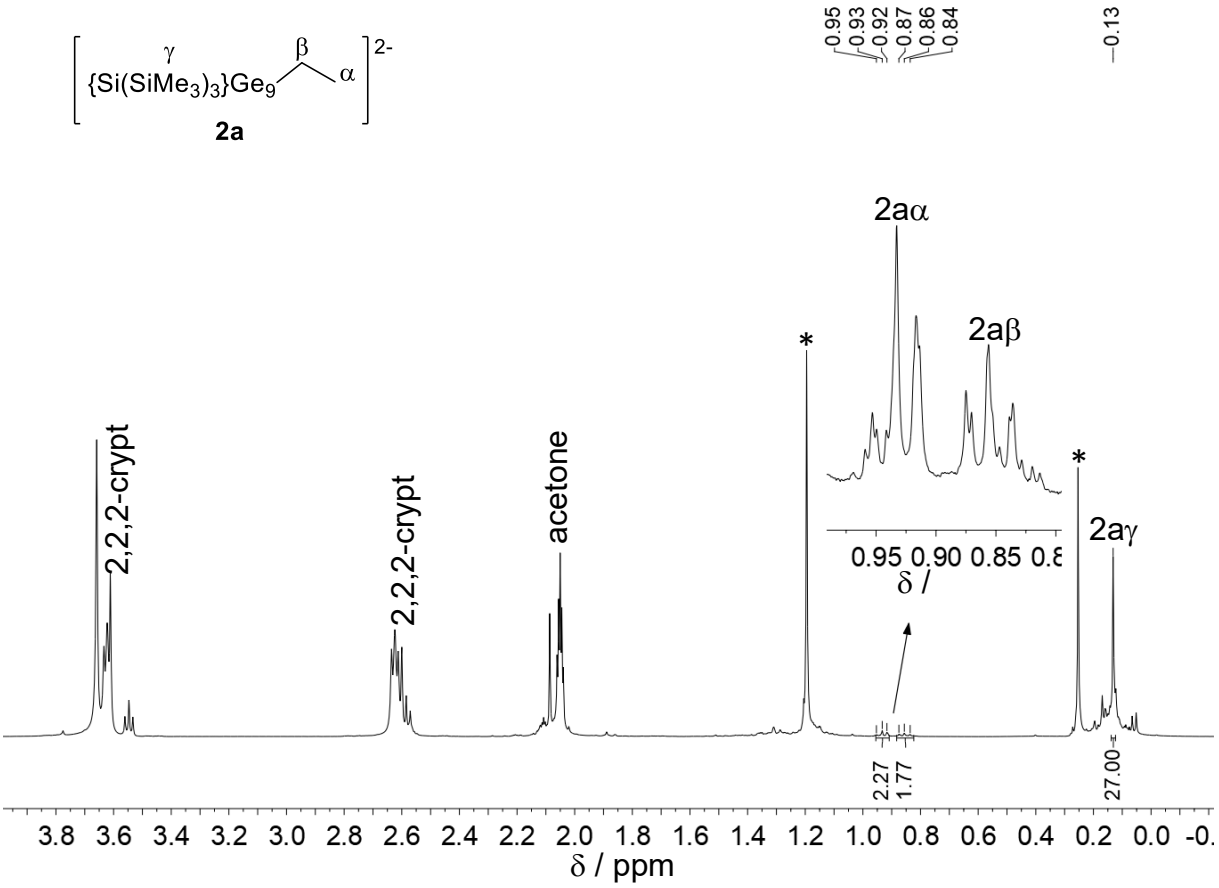
γ
β
α
{Si(SiMe3)3}Ge9
2-
2a
0.95
0.93
0.92
0.87
0.86
0.84
0.13
2aα
2aβ
2aγ
2,2,2-crypt
2,2,2-crypt
acetone
*
*
0.95 0.90 0.85 0.8
δ /
2.27
1.77
27.00
3.8 3.6 3.4 3.2 3.0 2.8 2.6 2.4 2.2 2.0 1.8 1.6 1.4 1.2 1.0 0.8 0.6 0.4 0.2 0.0 -0.
δ / ppm

Figure S4. a) ^{1}H and b) ^{1}H ^{1}H COSY NMR spectrum of crystals of **2** dissolved in acetonitrile-d_3 recorded at r.t..

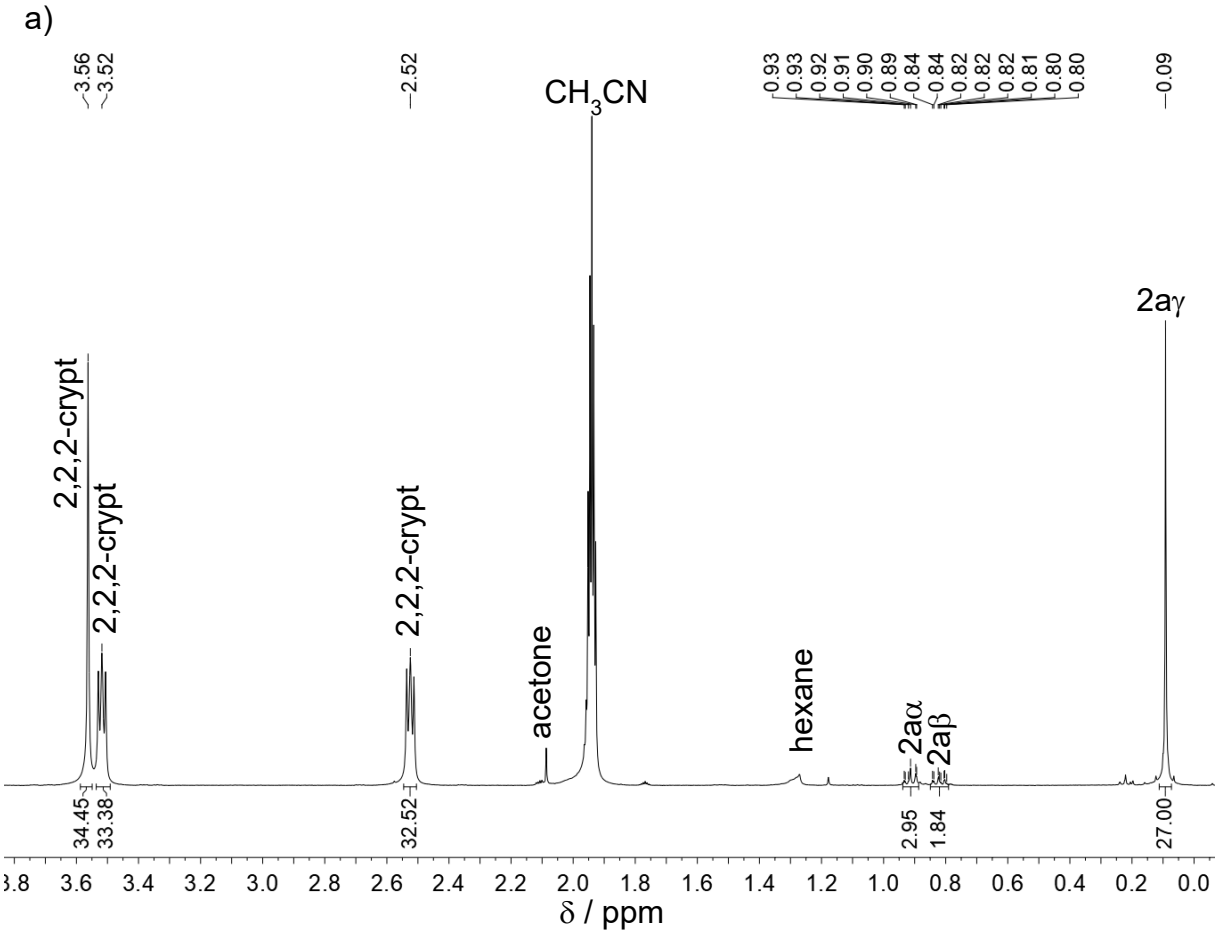

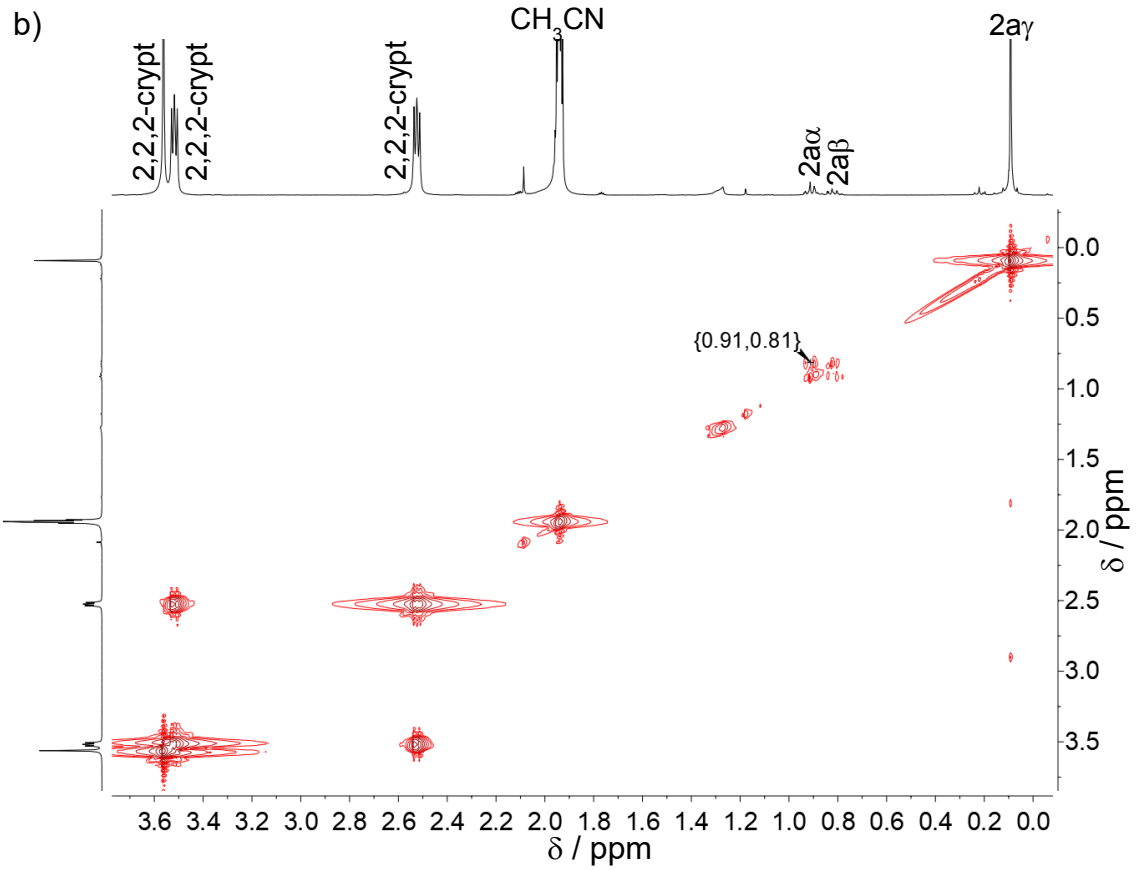

2.2 Crystallographic details on 2

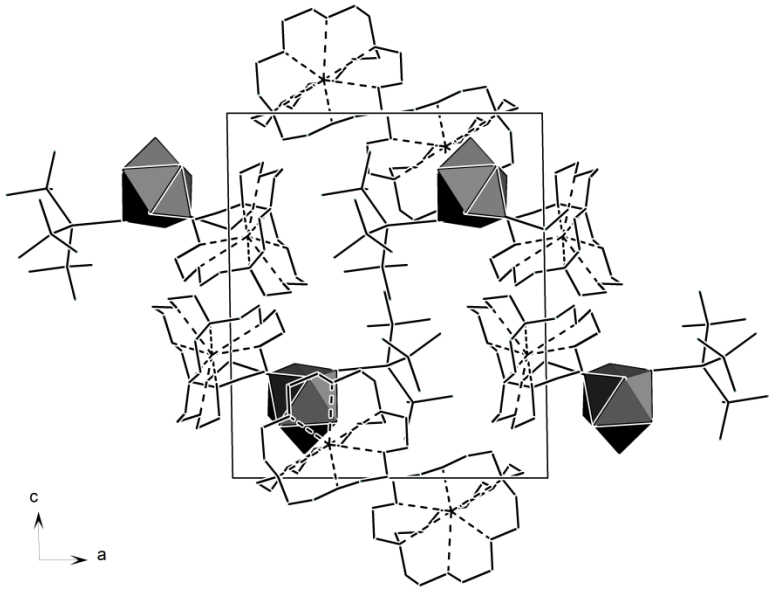

Figure S5. Unit cell of compound **2**. The Ge_9 clusters are shown as grey polyhedra. The organic moieties are shown schematically. All hydrogen atoms are omitted for clarity.

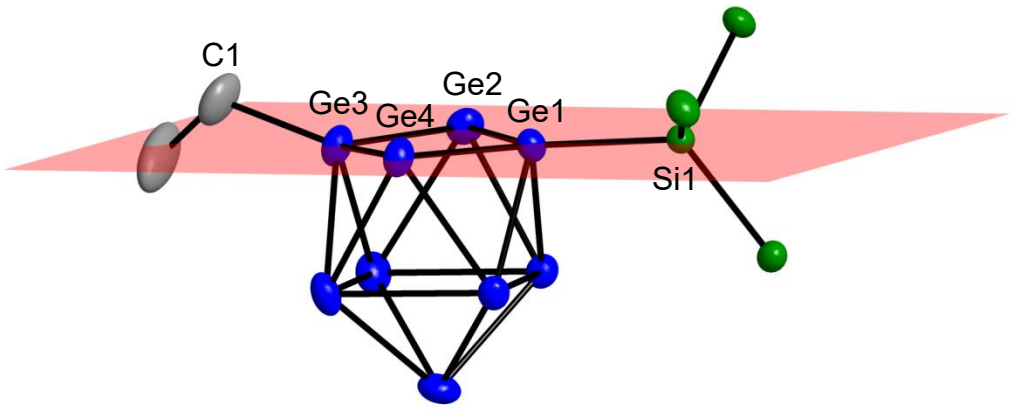

2a

Figure S6. Depiction of **2a** with plane in red which runs through the atoms Ge1, Ge2, Ge3, Ge4 and Si1. All hydrogen atoms as well as the methyl-groups on the hypersilyl ligand are omitted for clarity. All atoms are shown as ellipsoids at a probability level of 50%.

Table S1. Selected bond lengths [Å] in the crystal structure of **2**.

Ge1−Ge2	2.565(1)	Ge4−Ge5	2.620(2)
Ge1−Ge4	2.571(1)	Ge4−Ge8	2.679(2)
Ge1−Ge5	2.607(1)	Ge5−Ge6	2.939(2)
Ge1−Ge6	2.627(1)	Ge5−Ge8	2.717(1)
Ge1−Si1	2.423(3)	Ge5−Ge9	2.587(2)
Ge2−Ge3	2.519(2)	Ge6−Ge7	2.711(2)
Ge2−Ge6	2.623(1)	Ge6−Ge9	2.588(2)
Ge2−Ge7	2.693(2)	Ge7−Ge8	2.873(2)
Ge3−Ge4	2.532(1)	Ge7−Ge9	2.589(2)
Ge3−Ge7	2.596(2)	Ge8−Ge9	2.580(2)
Ge3−Ge8	2.600(2)	C1−C2	1.43(2)
Ge3−C1	2.02(1)		

3 Investigation of a potential desilylation of 1a with 18-crown-6

Figure S7. ^{1}H NMR spectrum of a reaction solution of **1** upon addition of 18-crown-6 recorded in acetone-d_6 at r.t.. $K_2[Ge_9\{Si(SiMe_3)_3\}_2]$ (30 mg, 0.024 mmol) was treated with a solution of bromoethane (1.8 μL, 0.024 mmol) in 0.6 mL acetone-d_6. The reaction solution was stirred for 15.5 h. 18-crown-6 (13 mg, 0.048 mmol) was added to the reaction solution. After 3 h the ^{1}H NMR spectrum was recorded. The ^{1}H NMR spectrum shows that **1a** did not undergo a desilylation.

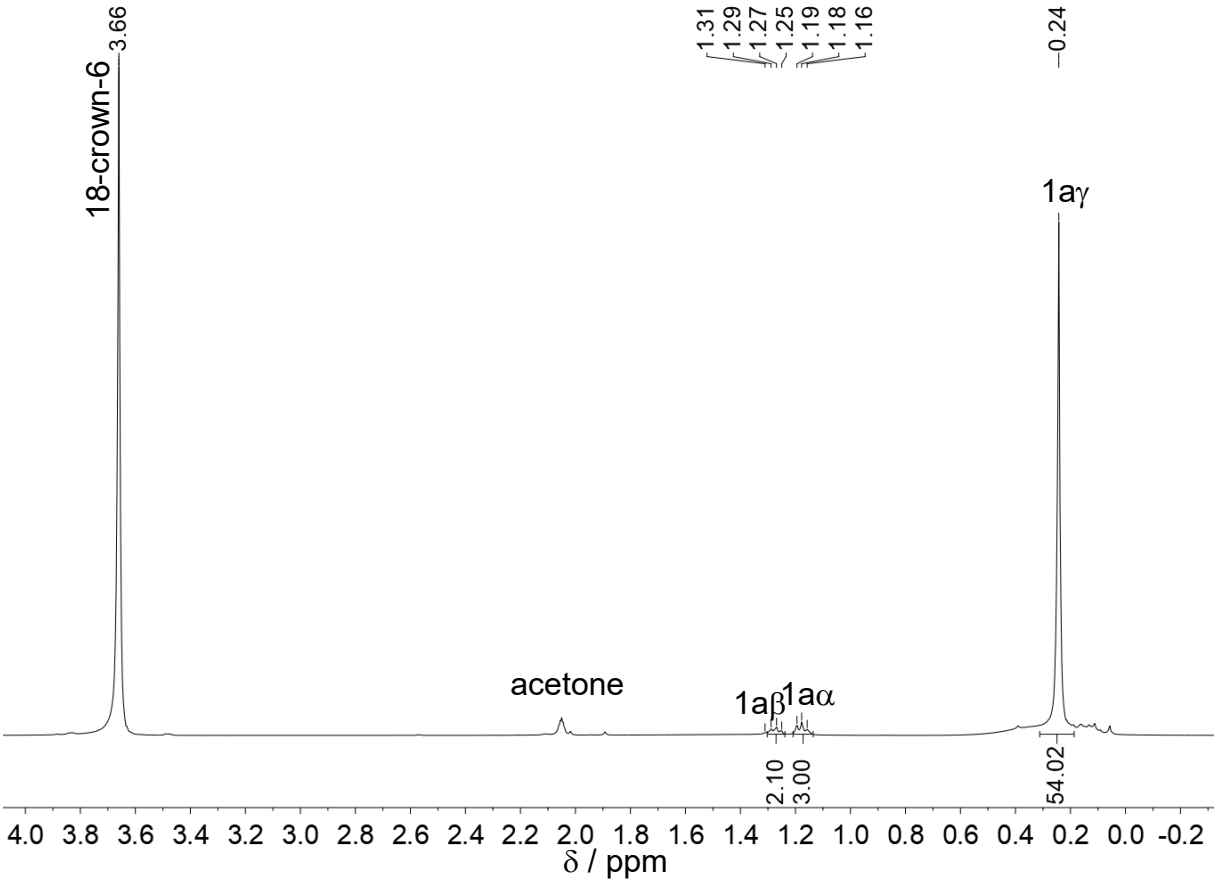

5.8 Acyl-Functionalized Deltahedral Ge_9 Clusters - $[\{(Me_3Si)_3Si\}_2Ge_9(CO)R']^-$ (R' = *t*Bu, Ph, CH_2Ph, $(CH_2)_2Ph$, 9-anthracenyl, Fc)

Sabine Frischhut, Kevin Frankiewicz, and Thomas F. Fässler

Manuscript for publication

5.8.1 Content and Contribution

Within the scope of this work, as a subsequent manuscript for the publication of the neutral acyl-functionalized Ge_9 clusters, the first onefold negatively charged and acyl-functionalized Ge_9 clusters $[\{(Me_3Si)_3Si\}_2Ge_9(CO)R']^-$ (R' = *t*Bu, Ph, CH_2Ph, $(CH_2)_2Ph$, anthracenyl, Fc) were made accessible by reaction of $[\{(Me_3Si)_3Si\}_2Ge_9]^{2-}$ with the respective acyl chlorides Cl(CO)R' in acetone or thf. All anions were characterized by NMR spectroscopy (^1H, ^{29}Si, ^{13}C, COSY, HMBC, HSQC) and ESI mass spectrometry within the scope of this work. B.Sc. Kevin Frankiewicz helped with preparation of reaction solutions.

Remarkably, $[\{(Me_3Si)_3Si\}_2Ge_9(CO)CH_2Ph]^-$ and $[\{(Me_3Si)_3Si\}_2Ge_9(CO)tBu]^-$are stable in solution and the latter does not release CO even at elevated temperatures, unlike the respective neutral compounds $\{(Me_3Si)_3Si\}_3Ge_9(CO)CH_2Ph$ and $\{(Me_3Si)_3Si\}_3Ge_9(CO)tBu$. The corresponding temperature-dependent *in situ* ^1H NMR studies were also performed within this thesis. A silyl ligand abstraction as was the case for $[\{(Me_3Si)_3Si\}_2Ge_9CH_2CH_3]^-$ does not occur upon addition of 2,2,2-crypt.

The data evaluation was performed within this thesis. The manuscript was authored within this work and was revised by Prof. Dr. Thomas F. Fässler.

5.8.2 Manuscript for Publication

Acyl-Functionalized Deltahedral Ge_9 Clusters - $[\{(Me_3Si)_3Si\}_2Ge_9(CO)R']^-$ (R' = *t*Bu, Ph, CH_2Ph, $(CH_2)_2Ph$, 9-anthracenyl, Fc)

Sabine Frischhut, Kevin Frankiewicz, and Thomas F. Fässler[a]*

[a]

Sabine Frischhut, Kevin Frankiewicz, Prof. Dr. T. F. Fässler

Department Chemie, Technische Universität München

Lichtenbergstraße 4, 85747 Garching, Germany

E-mail: thomas.faessler@lrz.tum.de

ABSTRACT

We present a synthesis route towards onefold negatively charged acyl-functionalized Ge_9 clusters. The reaction of $[\{(Me_3Si)_3Si\}_2Ge_9]^{2-}$ with acyl halides (pivaloyl chloride, benzoyl chloride, phenylacetyl chloride, hydrocinnamoyl chloride, 9-anthracenoyl chloride and ferrocenoyl chloride) afforded $[\{(Me_3Si)_3Si\}_2Ge_9(CO)R']^-$ (R' = *t*Bu, Ph, CH_2Ph, $(CH_2)_2Ph$, 9-anthracenyl, Fc). All anions were characterized by NMR spectroscopy (^1H, ^{13}C, ^{29}Si, COSY, HSQC, HMBC) and ESI mass spectrometry. Remarkably, unlike the neutral compound $[\{(Me_3Si)_3Si\}_3Ge_9(CO)tBu]$, $[\{(Me_3Si)_3Si\}_2Ge_9(CO)tBu]^-$ does not eliminate carbon monoxide even at elevated temperatures.

INTRODUCTION

Until recently, twofold negatively charged organo-substituted Ge_9 clusters were only accessible from ethylenediamine solutions in low yields. The most prominent examples are given by the alkenylation products, e.g. the vinylated Ge_9 cluster species $[(H_2C{=}CH)_nGe_9]^{(4-n)-}$ [1-2] or even linked Ge_9 clusters which comprise an extended conjugated π-electronic system $[R{-}Ge_9C_4H_4Ge_9{-}R]^{4-}$ (vinyl or (2*Z*,4*E*)-7-amino-5-azahepta-2,4-dien-2-yl) and $[Ge_9C_4H_4Ge_9]^{6-}$.[3-5] They often show low solubility and, therefore, are difficult to handle in further substitution reactions or follow-up reactions. A more effective way of transferring Ge_9 clusters into less polar solvents, such as acetonitrile or thf, turned out to be a silylation reaction of K_4Ge_9 with chloro-*tris*(trimethylsilyl)silane in acetonitrile.[6] The resulting well-known cluster $[\{(Me_3Si)Si\}_3Ge_9]^-$, which was first synthesized by Schnepf *et al.* by co-condensation reactions with low-valent Ge halides,[7] has been used as starting material for follow-up reactions in recent years, which is traced back to the stabilizing effect of the silyl-ligands due to steric shielding and electronic effects. A wide range of new compounds emerged, which has been reviewed only recently,[8] for instance by coordination of $[\{(Me_3Si)_3Si\}_3Ge_9]^-$ to transition metals,[9-16] by decoration with phosphine-ligands,[17] or alkyl-substitution of the threefold silylated Ge_9 cluster.[18-19] Nevertheless, steric shielding can also be a limiting factor in further reactions. Therefore silylation reactions with a variety of chloro-silanes have been investigated,[15, 20-23] whereas $[(t\mathrm{Bu}_2\mathrm{HSi})_3Ge_9]^-$ was found to be the less steric shielded threefold silylated Ge_9 cluster.[20] A few organo-functionalized Ge_9 clusters emerged, such as $\{(Me_3Si)_3Si\}_3Ge_9Et$[18] and $\{(Me_3Si)_3Si\}_3Ge_9(CH_2)_nCH{=}CH_2$ (n = 1, 2, 3)[19, 24] by reaction of $[\{(Me_3Si)_3Si\}_3Ge_9]^-$ with the respective alkyl halides. However, the attached silyl ligands appeared to be problematic in follow-up reactions with alkyl halides. Only very recently, we reported on a new synthesis approach towards specifically organo-functionalized Ge_9 clusters by reaction of $[\{(Me_3Si)_3Si\}_3Ge_9]^-$ with acyl chlorides. The acylation is applicable to a wide range of acyl chlorides leading to a series of acylated neutral clusters. Remarkably, radical decarbonylation of $\{(Me_3Si)_3Si\}_3Ge_9(CO)t\mathrm{Bu}$ at r.t. is observed to selectively form $\{(Me_3Si)_3Si\}_3Ge_9t\mathrm{Bu}$.[25] The first twofold negatively charged disilylated cluster $[\{(Me_3Si)_3Si\}_2Ge_9]^{2-}$ which is accessible in high yields and easily soluble in less polar solvents was synthesized by Schnepf and coworkers by desilylation of $[\{(Me_3Si)_3Si\}_3Ge_9]^-$ in acetonitrile.[26] $[\{(Me_3Si)_3Si\}_2Ge_9]^{2-}$ serves as a promising starting material in Ge_9 cluster chemistry as it offers more reactive sites than the one-fold negatively charged, sterically

crowded $[\{(Me_3Si)_3Si\}_3Ge_9]^-$. $[\{(Me_3Si)_3Si\}_2Ge_9]^{2-}$ has been applied in the syntheses of mixed silylated Ge_9 cluster species[21, 27], in the reaction with dialkylhalophosphines resulting in $[\{(Me_3Si)_3Si\}_2Ge_9PR_2]^-$,[17, 28] and in a further reaction with bromo-ethane forming $[\{(Me_3Si)_3Si\}_2Ge_9Et]^-$.[29] Just recently, we showed that silyl-ligand abstraction also occurs from $[\{(Me_3Si)_3Si\}_2Ge_9Et]^-$ leading to the monosilylated species $[(Me_3Si)_3SiGe_9Et]^{2-}$.[29] This opens the possibility of a new variety of tailor-made Ge_9 cluster compounds.

In this work, we transferred the acylation of Ge_9 cluster to the twofold silylated species $[\{(Me_3Si)_3Si\}_2Ge_9]^{2-}$ and present its reaction with pivaloyl chloride, benzoyl chloride, phenylacetyl chloride, hydrocinnamoyl chloride, 9-anthracenoyl chloride and ferrocenoyl chloride in acetone or thf at r.t. affording $[\{(Me_3Si)_3Si\}_2Ge_9(CO)R']^-$ (R' = *t*Bu, Ph, CH_2Ph, $(CH_2)_2Ph$, 9-anthracenyl, Fc; Fc = ferrocenyl). The obtained products were characterized by NMR spectroscopy and electron-spray-ionization mass spectrometry (ESI-MS).

RESULTS AND DISCUSSION

The reaction of $K_2[\{(Me_3Si)_3Si\}_2Ge_9]$ with the acyl chlorides Cl(CO)R' (R' = *t*Bu, Ph, CH_2Ph, $(CH_2)_2Ph$, 9-anthracenyl, Fc) affords the anions $[\{(Me_3Si)_3Si\}_2Ge_9(CO)tBu]^-$ (**1a**), $[\{(Me_3Si)_3Si\}_2Ge_9(CO)Ph]^-$ (**2a**), $[\{(Me_3Si)_3Si\}_2Ge_9(CO)CH_2Ph]^-$ (**3a**), $[\{(Me_3Si)_3Si\}_2Ge_9(CO)(CH_2)_2Ph]^-$ (**4a**), $[\{(Me_3Si)_3Si\}_2Ge_9(CO)$-9-anthracenyl$]^-$ (**5a**) and $[\{(Me_3Si)_3Si\}_2Ge_9(CO)Fc]^-$ (**6a**). The addition-elimination reaction exclusively proceeds in acetone and thf (Figure 1 a).

The reaction products were characterized from the reaction solutions in $[D_6]$acetone by NMR spectroscopy (^1H, ^{13}C, ^{29}Si, COSY, HMBC, HSQC; see supporting information). The products were obtained in good purity. ESI mass spectrometric investigations were carried out with the respective thf-reaction solutions. The obtained ESI mass spectra in Figure 1 b-g show the expected *m*/*z* ratios of the anions **1a**-**6a**. The respective simulated patterns are depicted as bar graphs in red below the experimental spectra (for full ESI mass spectra see supporting information).

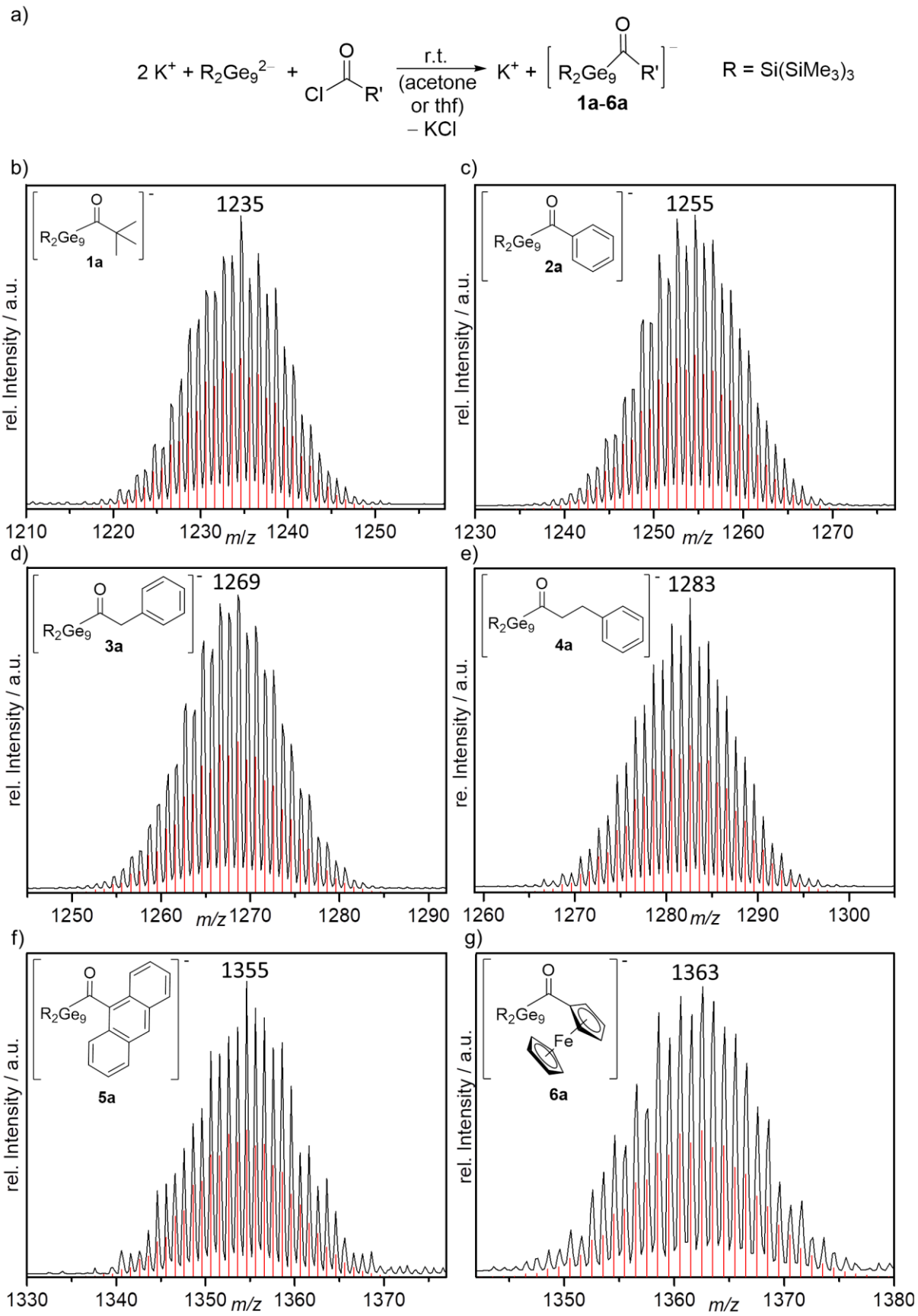

Figure 1. a) Reaction of $K_2[Ge_9\{Si(SiMe_3)_3\}_2]$ with Cl(CO)R' yielding the anions **1a**-**6a.** b)-g) ESI mass spectra of the anions **1a**-**6a** recorded in thf-reaction solutions in the negative ion mode. The measured spectra are shown in black and the corresponding simulated patterns are shown as bar graphs below. R represents the hypersilyl ligands.

Unlike the neutral acylated species $\{(Me_3Si)_3Si\}_3Ge_9(CO)tBu$ and $\{(Me_3Si)_3Si\}_3Ge_9(CO)CH_2Ph$, the respective anions **1a** and **3a** do not undergo CO-elimination even at elevated temperatures (Scheme 1).

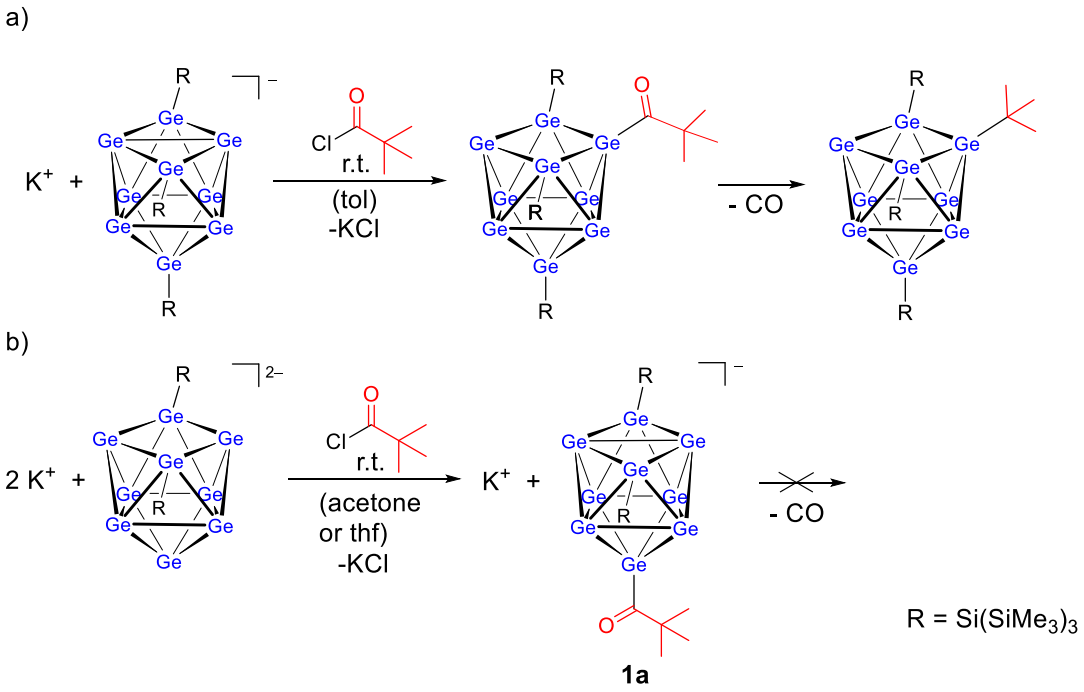

Scheme 1. a) Reaction of $K[\{(Me_3Si)_3Si\}_3Ge_9]$ with pivaloyl chloride yielding $\{(Me_3Si)_3Si\}_3Ge_9(CO)tBu$, which in a subsequent step eliminates CO under formation of $\{(Me_3Si)_3Si\}_3Ge_9tBu$. b) Reaction of $K_2[\{(Me_3Si)_3Si\}_2Ge_9]$ with pivaloyl chloride yielding $K[\{(Me_3Si)_3Si\}_2Ge_9(CO)tBu]$, which does not eliminate CO. R depicts the hypersilyl ligands.

The reason for the absence of the decarbonylation reaction in **1a** remains unknown to date.

CONCLUSION

The successful synthesis of a series of charged acyl-functionalized Ge_9 clusters emphasizes the usefulness of the reaction with acyl chlorides. The variety of obtained organo-functionalized Ge_9 clusters shows that the acylation reaction is an applicable method to introduce functional groups to the silylated species $[\{(Me_3Si)_3Si\}_2Ge_9]^{2-}$. Here, we give six examples of one-fold negatively charged Ge_9 clusters decorated with sterically demanding and less demanding organic substituents, as well as with an organometallic ferrocenoyl fragment. These compounds can be obtained by a facile reaction of $[\{(Me_3Si)_3Si\}_2Ge_9]^{2-}$ with the respective acyl chlorides. Charged functionalized Ge_9 clusters are highly interesting, as they still show reactive sights to attach to surfaces or to add additional functional groups for further specific applications.

EXPERIMENTAL SECTION

General: All manipulations were carried out under a purified argon atmosphere using standard Schlenk techniques. The Zintl phase with the nominal composition K_4Ge_9 was synthesized heating a stoichiometric mixture of the elements K and Ge (99.999%, Chempur) at 650 °C for 46 h in a stainless steel autoclave.[30] Anhydrous acetone was purchased from VWR Chemicals and stored over molecular sieve (3 Å) for at least one day. Chloro-*tris*(trimethylsilyl)silane (TCI Chemicals, ≥95.0%), pivaloyl chloride (Sigma-Aldrich, 99%), benzoyl chloride (Acros Organics, ≥98%), phenylacetyl chloride (Sigma-Aldrich, 98%) and hydrocinnamoyl chloride (Sigma-Aldrich, 98%) were used as received. 9-Anthracenoyl chloride[31] and ferrocenoyl chloride[32] were synthesized according to literature procedures. The solvent thf was obtained from a solvent purificator (MB-SPS) and stored over molecular sieve (3 Å). The deuterated solvent [D_6]acetone was purchased from Deutero GmbH and stored over molecular sieve (3 Å) for at least one day.

Synthesis of "K[{$(Me_3Si)_3Si$}$_2$$Ge_9$(CO)*t*Bu]" (1):

For NMR spectroscopic investigations of **1a**, K_2[{$(Me_3Si)_3Si$}$_2$$Ge_9$] (30 mg, 0.024 mmol) was weighed out into a Schlenk tube in a glovebox and a solution of pivaloyl chloride (3.0 μL, 0.024 mmol) in 0.6 mL [D_6]acetone was added dropwise. A deep-brown solution is formed immediately. The reaction solution was stirred for 22 h at r.t. and was NMR spectroscopically investigated. ^{1}H NMR (400 MHz, [D_6]acetone, 298 K): δ(ppm) 0.96 (s, 9H, 1aα), 0.27 (s, 54H, 1aδ); ^{29}Si NMR (79 MHz, [D_6]acetone, 298 K): δ(ppm) −9.16 (*Si*$(CH_3)_3$), −107.11 (*Si*{Si$(CH_3)_3$}$_3$); ^{13}C NMR (101 MHz, [D_6]acetone, 298 K): δ(ppm) 259.26 (s, 1aγ), 51.82 (s, 1aβ), 27.84 (q, 1aα), 3.13 (q, 1aδ); ^{1}H ^{13}C HSQC (400 MHz/101 MHz, [D_6]acetone, 298 K): δ(ppm)/δ(ppm) 0.96/27.85 (^1J, 1aα/1aα), 0.27/3.14 (^1J, 1aδ/1aδ); ^{1}H ^{13}C HMBC (400 MHz/101 MHz, [D_6]acetone, 298 K): δ(ppm)/δ(ppm) 0.95/51.82 (^2J, 1aα/1aβ); ESI-MS (negative ion mode, 4500 V, 300 °C): *m*/*z* 1235 [{$(Me_3Si)_3Si$}$_2$$Ge_9$(CO)^{t}Bu]$^-$.

Synthesis of "K[{$(Me_3Si)_3Si$}$_2$$Ge_9$(CO)Ph]" (2): For NMR spectroscopic characterization of **2a**, K_2[{$(Me_3Si)_3Si$}$_2$$Ge_9$] (30 mg, 0.024 mmol) was treated with benzoyl chloride (2.8 μL, 0.024 mmol) dissolved in 0.6 mL [D_6]acetone. The purple reaction solution was stirred for 21 h at r.t.. The solution was characterized by NMR spectroscopy. ^{1}H NMR (400 MHz, [D_6]acetone, 298 K): δ(ppm) 7.97 (m, 2H, 2aγ), 7.41 (m, 1H, 2aα), 7.29 (m, 2H, 2aβ), 0.28 (s, 54H, 2aζ); ^{29}Si NMR (79 MHz, [D_6]acetone, 298 K): δ(ppm) −9.05 (*Si*$(CH_3)_3$), −106.09

(*Si*{Si(CH$_3$)$_3$}$_3$); ^{13}C NMR (101 MHz, [D$_6$]acetone, 298 K): δ(ppm) 251.46 (s, 2aε), 145.49 (m, 2aα), 132.94 (s, 2aδ), 128.61 (m, 2aβ), 127.72 (m, 2aγ), 3.12 (q, 2aζ); ^{1}H ^{1}H COSY (400 MHz, [D$_6$]acetone, 298 K): δ(ppm)/δ(ppm) 7.97/7.30 (^3J, 2aγ/2aβ), 7.40/7.25 (^3J, 2aα/2aβ); ^{1}H ^{13}C HSQC (400 MHz/101 MHz, [D$_6$]acetone, 298 K): δ(ppm)/δ(ppm) 7.98/127.57 (^1J, 2aγ/2aγ), 7.42/132.77 (^1J, 2aα/2aα), 7.30/128.43 (^1J, 2aβ/2aβ), 0.29/2.90 (^1J, 2aζ/2aζ); ^{1}H ^{13}C HMBC (400 MHz/101 MHz, [D$_6$]acetone, 298 K): δ(ppm)/δ(ppm) 7.31/145.41 (^3J, 2aβ/2aδ); ESI-MS (negative ion mode, 4500 V, 300 °C): *m*/*z* 1255 [{(Me$_3$Si)$_3$Si}$_2$Ge$_9$(CO)C$_6$H$_5$]$^-$.

Synthesis of "K[{(Me$_3$Si)$_3$Si}$_2$Ge$_9$(CO)CH$_2$Ph]" (3): For NMR spectroscopic investigations of **3a**, K$_2$[{(Me$_3$Si)$_3$Si}$_2$Ge$_9$] (30 mg, 0.024 mmol) was treated with phenylacetyl chloride (3.7 μL, 0.024 mmol) dissolved in 0.6 mL [D$_6$]acetone. The deep-brown reaction solution was stirred for 19 h at r.t.. The reaction solution was characterized by NMR spectroscopy. ^{1}H NMR (400 MHz, [D$_6$]acetone, 298 K): δ(ppm) 7.12 (m, 5H, 3aα/β/γ), 3.86 (s, 2H, 3aε), 0.29 (s, 54H, 3aη); ^{29}Si NMR (79 MHz, [D$_6$]acetone, 298 K): δ(ppm) −9.07 (*Si*Me$_3$), −106.23 (*Si*(SiMe$_3$)$_3$); ^{13}C NMR (101 MHz, [D$_6$]acetone, 298 K): δ(ppm) 253.64 (s, 3aζ), 136.06 (s, 3aδ), 130.55 (m, 3aγ), 128.75 (m, 3aβ), 126.88 (m, 3aα), 66.43 (t, 3aε), 3.13 (q, 3aη); ^{1}H ^{1}H COSY (400 MHz, [D$_6$]acetone, 298 K): δ(ppm)/δ(ppm) 7.10/3.86 (3aα/β/γ/3aε); ^{1}H ^{13}C HSQC (400 MHz/101 MHz, [D$_6$]acetone, 298 K): δ(ppm)/δ(ppm) 7.15/128.76 (^1J, 3aβ/3aβ), 7.10/130.71 (^1J, 3aγ/3aγ), 7.09/126.88 (^1J, 3aα/3aα), 3.86/66.47 (^1J, 3aε/3aε), 0.29/3.18 (^1J, 3aη/3aη); ^{1}H ^{13}C HMBC (400 MHz/101 MHz, [D$_6$]acetone, 298 K): δ(ppm)/δ(ppm) 7.14/135.71 (3aα/β/γ/3aδ), 7.14/128.43 (3aα/β/γ/3aβ), 3.87/135.98 (^2J, 3aε/3aδ), 3.87/130.31 (^3J, 3aε/3aγ); ESI-MS (negative ion mode, 4500 V, 300 °C): *m*/*z* 1269 [{(Me$_3$Si)$_3$Si}$_2$Ge$_9$(CO)CH$_2$C$_6$H$_5$]$^-$.

Synthesis of "K[{(Me$_3$Si)$_3$Si}$_2$Ge$_9$(CO)(CH$_2$)$_2$Ph]" (4): For NMR spectroscopic characterization of **4a**, to K$_2$[{(Me$_3$Si)$_3$Si}$_2$Ge$_9$] (30 mg, 0.024 mmol, 1.0 eq.) a solution of hydrocinnamoyl chloride (3.6 µL, 0.024 mmol, 1.0 eq.) in 0.6 mL [D$_6$]acetone was added. The reaction solution as stirred at r.t. for 20 h. The solution was filtered and characterized by NMR spectroscopy. ^{1}H NMR (400 MHz, [D$_6$]acetone, 298 K): δ(ppm) 7.17 (m, 5H, 4aα/β/γ), 2.84 (m, 2H, 4aζ), 2.67 (m, 2H, 4aε), 0.28 (s, 54H, 4aθ); ^{29}Si NMR (79 MHz, [D$_6$]acetone, 298 K): δ(ppm) −9.09 (*Si*Me$_3$), −106.36 (*Si*(SiMe$_3$)$_3$).

ESI-MS (negative ion mode, 4500 V, 300 °C): *m*/*z* 1283 [{(Me$_3$Si)$_3$Si}$_2$Ge$_9$(CO)(CH$_2$)$_2$C$_6$H$_5$]$^-$.

Synthesis of "K[{(Me$_3$Si)$_3$Si}$_2$Ge$_9$(CO)-9-anthracenyl]" (5): For NMR spectroscopic investigations of **5a**, K$_2$[{(Me$_3$Si)$_3$Si}$_2$Ge$_9$] (30 mg, 0.024 mmol, 1.0 eq.) and 9-anthracenoyl chloride (6 mg, 0.024 mmol, 1.0 eq.) were weighed out in a Schlenk tube and 0.6 mL [D$_6$]acetone were added. The deep-brown reaction solution was stirred for 17.5 h at r.t.. The obtained reaction solution was investigated by NMR spectroscopy. ^{1}H NMR (400 MHz, [D$_6$]acetone, 298 K): δ(ppm) 8.32 (s, 1H, 5aη), 8.08 (d, ^3J = 8.8 Hz, 2H, 5aβ), 7.90 (d, ^3J = 8.4 Hz, 2H, 5aε), 7.37 (m, 2H, 5aδ), 7.28 (m, 2H, 5aγ), 0.25 (s, 54H, 5aκ); ^{29}Si NMR (79 MHz, [D$_6$]acetone, 298 K): δ(ppm) −9.18 (*Si*Me$_3$), −105.92 (*Si*(SiMe$_3$)$_3$); ^{13}C NMR (101 MHz, [D$_6$]acetone, 298 K): δ(ppm) 263.98 (5aι), 147.58 (5aα), 132.19 (5aζ), 128.47 (5aε), 127.20 (5aβ), 126.80 (5aη), 125.91 (5aδ), 125.41 (5aθ), 125.12 (5aγ), 2.98 (5aκ); ^{1}H ^{1}H COSY (400 MHz, [D$_6$]acetone, 298 K): δ(ppm)/δ(ppm) 8.09/7.29 (^3J, 5aβ/5aγ), 7.90/7.37 (^3J, 5aε/5aδ); ^{1}H ^{13}C HSQC (400 MHz/101 MHz, [D$_6$]acetone, 298 K): δ(ppm)/δ(ppm) 8.31/126.88 (^1J, 5aη/5aη), 8.08/127.26 (^1J, 5aβ/5aβ), 7.90/128.55 (^1J, 5aε/5aε), 7.37/125.90 (^1J, 5aδ/5aδ), 7.28/125.19 (^1J, 5aγ/5aγ), 0.25/3.01 (^1J, 5aκ/5aκ); ^{1}H ^{13}C HMBC (400 MHz/101 MHz, [D$_6$]acetone, 298 K): δ(ppm)/δ(ppm) 8.32/147.33 (^3J, 5aη/5aα), 8.31/132.58 (^2J, 5aη/5aζ), 8.31/128.38 (^3J, 5aη/5aε), 8.31/125.19 (^5J, 5aη/5aγ), 8.09/147.37 (^2J, 5aβ/5aα), 8.07/132.09 (^3J, 5aβ/5aζ), 8.08/126.00 (^3J, 5aβ/5aδ), 7.89/132.02 (^2J, 5aε/5aζ), 7.90/125.10 (^3J, 5aε/5aγ), 7.36/132.05 (^3J, 5aδ/5aζ), 7.36/127.14 (^3J, 5aδ/5aβ), 7.27/128.32 (^3J, 5aγ/5aε), 7.27/125.17 (^1J, 5aγ/5aγ); ESI-MS (negative ion mode, 4500 V, 300 °C): *m/z* 1355 [{(Me$_3$Si)$_3$Si}$_2$Ge$_9$(CO)C$_{14}$H$_9$]$^-$.

Synthesis of "K[{(Me$_3$Si)$_3$Si}$_2$Ge$_9$(CO)Fc]" (6): For NMR spectroscopic investigations of **6a**, K$_2$[{(Me$_3$Si)$_3$Si}$_2$Ge$_9$] (30 mg, 0.024 mmol, 1.0 eq.) and ferrocenoyl chloride (6 mg, 0.024 mmol, 1.0 eq.) were weighed out in a Schlenk tube and 0.6 mL [D$_6$]acetone were added to form a bright red solution. The reaction solution was stirred for 16.5 h at r.t.. The solution was investigated by NMR spectroscopy. ^{1}H NMR (400 MHz, [D$_6$]acetone, 298 K): δ(ppm) 4.89 (m, 2H, 6aβ), 4.35 (m, 2H, 6aγ), 4.18 (s, 5H, 6aα), 0.29 (s, 54H, 6aζ); ^{29}Si NMR (79 MHz, [D$_6$]acetone, 298 K): δ(ppm) −9.08 (*Si*Me$_3$), −107.00 (*Si*(SiMe$_3$)$_3$); ^{13}C NMR (101 MHz, [D$_6$]acetone, 298 K): δ(ppm) 244.18 (6aε), 89.99 (6aδ), 71.59 (6aβ), 71.15 (6aα), 70.57 (6aγ), 3.01 (6aζ); ^{1}H ^{1}H COSY (400 MHz, [D$_6$]acetone, 298 K): δ(ppm)/δ(ppm) 4.89/4.36 (^3J, 6aβ/6aγ); ^{1}H ^{13}C HSQC (400 MHz/101 MHz, [D$_6$]acetone, 298 K): δ(ppm)/δ(ppm) 4.89/70.50 (^1J, 6aγ/6aγ), 4.35/71.37 (^1J, 6aβ/6aβ), 4.18/70.93 (^1J, 6aα/6aα), 0.30/2.85 (^1J, 6aγ/6aγ); ^{1}H

^{13}C HMBC (400 MHz/101 MHz, [D$_6$]acetone, 298 K): δ(ppm)/δ(ppm) 4.87/89.85 (^2J, 6aγ/6aδ), 4.86/71.77 (^2J, 6aγ/6aβ), 4.33/89.89 (^2J, 6aβ/6aδ), 4.34/70.56 (^2J, 6aβ/6aγ), 4.16/71.06 (^1J, 6aα/6aα), 0.29/3.00 (^1J, 6aζ/6aζ); ESI-MS (negative ion mode, 4500 V, 300 °C): *m*/*z* 1363 [{(Me$_3$Si)$_3$Si}$_2$Ge$_9$(CO)C$_5$H$_4$-Fe-C$_5$H$_5$]$^-$.

NMR Spectroscopy: NMR spectra were recorded on a BRUKER Avance Ultrashield AV400 spectrometer. The signals were referenced to the residual proton signal of the deuterated solvent [D$_6$]acetone (δ = 2.05 ppm). The chemical shifts are given in δ values in parts per million (ppm).

Electron Spray Ionization Mass Spectrometry (ESI-MS):

For ESI mass spectrometric investigations samples were prepared as described in the experimental sections except instead of [D$_6$]acetone tetrahydrofurane was used. After the reaction time the solvent was removed. A small amount of the residue was characterized by NMR spectroscopy. The residue was then dissolved in thf and filtered over glass fiber filter. The measurements were carried out on a HCT (Bruker Corp.). The dry gas temperature was adjusted to 125 °C and the injection speed to 240 μL s^{-1}.

ACKNOWLEDGMENTS

The authors thank the Bayerisches Staatsministerium für Wirtschaft und Medien, Energie und Technologie within the program “Solar Technologies go Hybrid” for financial support. Moreover, the authors are grateful to B.Sc. Nicole Willeit for preparation of reaction solutions.

REFERENCES

[1] M. W. Hull, S. C. Sevov, *Inorg. Chem.* **2007**, *46*, 10953-10955.
[2] C. B. Benda, J. Q. Wang, B. Wahl, T. F. Fässler, *Eur. J. Inorg. Chem.* **2011**, *27*, 4262-4269.
[3] M. M. Bentlohner, S. Frischhut, T. F. Fässler, *Chem. Eur. J.* **2017**, *23*, 17089-17094.
[4] S. Frischhut, M. M. Bentlohner, W. Klein, T. F. Fässler, *Inorg. Chem.* **2017**, *56*, 10691-10698.
[5] M. M. Bentlohner, W. Klein, Z. H. Fard, L.-A. Jantke, T. F. Fässler, *Angew. Chem. Int. Ed.* **2015**, *54*, 3748-3753.
[6] F. Li, S. C. Sevov, *Inorg. Chem.* **2012**, *51*, 2706-2708.
[7] A. Schnepf, *Angew. Chem. Int. Ed.* **2003**, *42*, 2624-2625.
[8] R. J. Wilson, B. Weinert, S. Dehnen, *Dalton Trans.* **2018**.
[9] F. Henke, C. Schenk, A. Schnepf, *Dalton Trans.* **2009**, 9141-9145.

[10] F. Henke, C. Schenk, A. Schnepf, *Dalton Trans.* **2011**, *40*, 6704-6710.
[11] C. Schenk, F. Henke, G. Santiso-Quiñones, I. Krossing, A. Schnepf, *Dalton Trans.* **2008**, 4436-4441.
[12] C. Schenk, A. Schnepf, *Angew. Chem. Int. Ed.* **2007**, *46*, 5314-5316.
[13] C. Schenk, A. Schnepf, *Chem. Commun.* **2009**, 3208-3210.
[14] O. Kysliak, C. Schrenk, A. Schnepf, *Chem. Eur. J.* **2016**, *22*, 18787-18793.
[15] K. Mayer, L. J. Schiegerl, T. F. Fässler, *Chem. Eur. J.* **2016**, *22*, 18794-18800.
[16] F. S. Geitner, T. F. Fässler, *Eur. J. Inorg. Chem.* **2016**.
[17] F. S. Geitner, J. V. Dums, T. F. Fässler, *J. Am. Chem. Soc.* **2017**, *139*, 11933-11940.
[18] F. Li, S. C. Sevov, *J. Am. Chem. Soc.* **2014**, *136*, 12056-12063.
[19] S. Frischhut, T. F. Fässler, *Dalton Trans.* **2018**, *47*, 3223-3226.
[20] O. Kysliak, T. Kunz, A. Schnepf, *Eur. J. Inorg. Chem.* **2017**, *4*, 805-810.
[21] K. Mayer, L. J. Schiegerl, T. Kratky, S. Günther, T. F. Fässler, *Chem. Commun.* **2017**, *53*, 11798-11801.
[22] O. Kysliak, C. Schrenk, A. Schnepf, *Inorg. Chem.* **2015**, *54*, 7083-7088.
[23] L. J. Schiegerl, F. S. Geitner, C. Fischer, W. Klein, T. F. Fässler, *Z. Anorg. Allg. Chem.* **2016**, *642*, 1419-1426.
[24] S. Frischhut, J. G. Machado de Carvalho, A. J. Karttunen, T. F. Fässler, *Z. Anorg. Allg. Chem.* **2018**, *644*, 1337-1343.
[25] S. Frischhut, W. Klein, M. Drees, T. F. Fässler, *Chem. Eur. J.* **2018**, *24*, 9009-9014.
[26] O. Kysliak, A. Schnepf, *Dalton Trans* **2016**, *45*, 2404-2408.
[27] O. Kysliak, C. Schrenk, A. Schnepf, *Inorg. Chem.* **2017**, *56*, 9693-9697.
[28] F. Geitner, C. Wallach, T. F. Fässler, *Chem. Eur. J.* **2018**, *24*, 4103-4110.
[29] S. Frischhut, W. Klein, T. F. Fässler, *C. R. Chim.* **2018**, *21*, 932-937.
[30] C. Hoch, M. Wendorff, C. Röhr, *J. Alloys Compd.* **2003**, *361*, 206-221.
[31] R. A. Bawa, S. Jones, *Tetrahedron* **2004**, *60*, 2765-2770.
[32] N. M. Saied, N. Mejri, R. El Aissi, E. Benoist, M. Saidi, *Eur. J. Med. Chem.* **2015**, *97*, 280-288.

SUPPORTING INFORMATION

Acyl-Functionalized Deltahedral Ge_9 Clusters - $[\{(Me_3Si)_3Si\}_2Ge_9(CO)R']^-$ (R' = *t*Bu, Ph, CH_2Ph, $(CH_2)_2Ph$, 9-anthracenyl, Fc)

Sabine Frischhut, Kevin Frankiewicz, and Thomas F. Fässler[a]*

[a]

Sabine Frischhut, Kevin Frankiewicz, Prof. Dr. T. F. Fässler

Department Chemie, Technische Universität München

Lichtenbergstraße 4, 85747 Garching, Germany

E-mail: thomas.faessler@lrz.tum.de

1 NMR spectroscopic characterization of 1a

Figure S1. ^{1}H, b) ^{29}Si, c) ^{13}C, d) ^{1}H ^{13}C HSQC NMR and e) ^{1}H ^{13}C HMBC NMR spectrum of reaction solution of **3** recorded at r.t. in [D6]acetone. Signals marked with # are assigned to toluene which is present in small amounts in the educt $K_2[\{(Me_3Si)_3Si\}_2Ge_9]$. Signals marked with * could not be assigned.

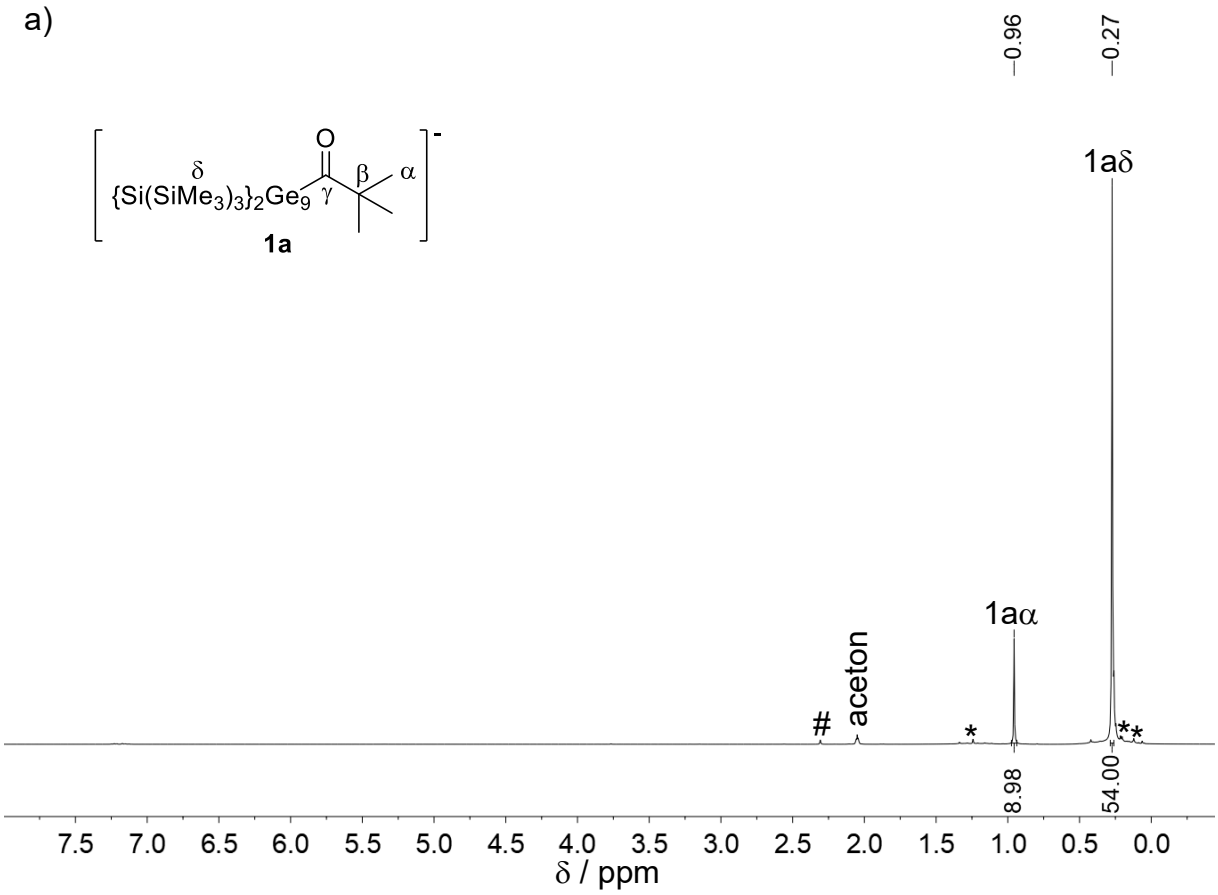

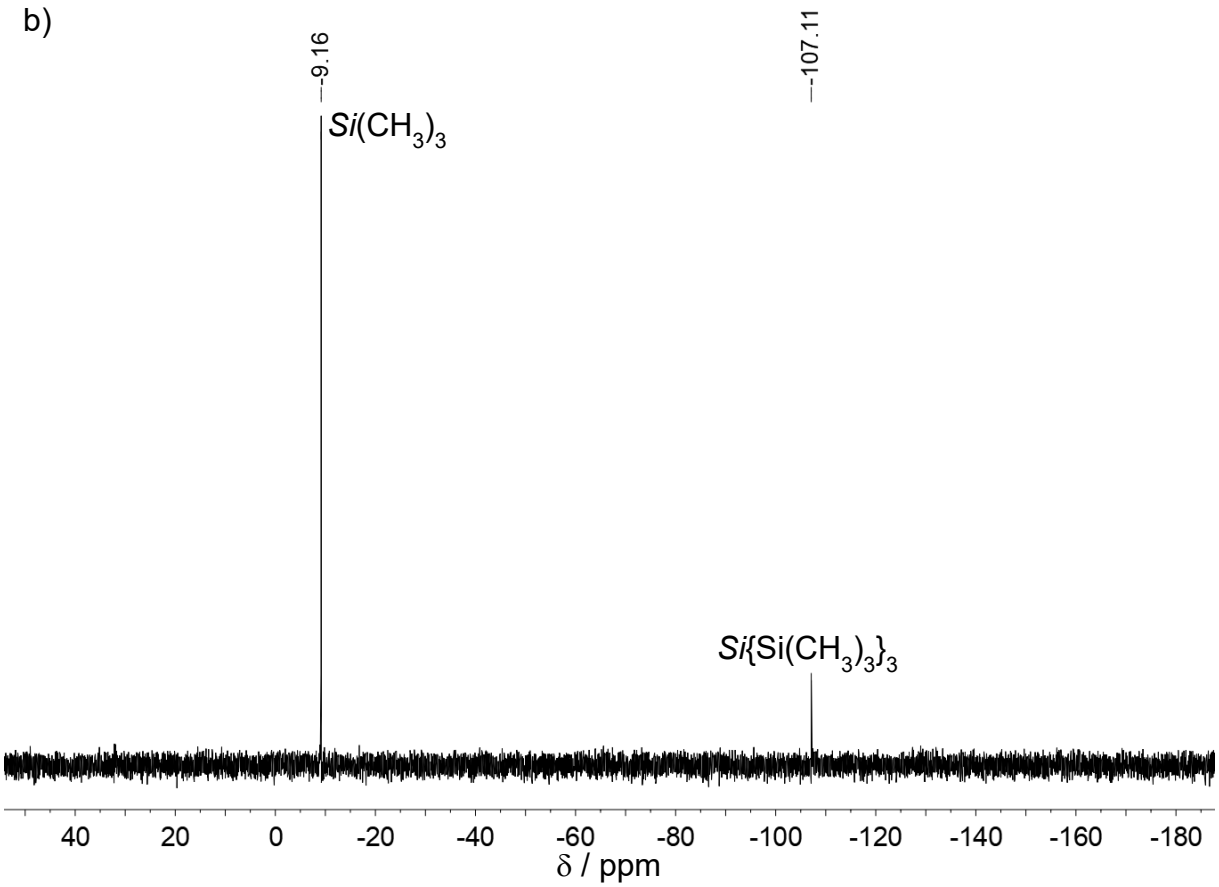
b)
-9.16
-107.11
Si(CH3)3
Si{Si(CH3)3}3
40
20
0
-20
-40
-60
-80
-100
-120
-140
-160
-180
δ / ppm

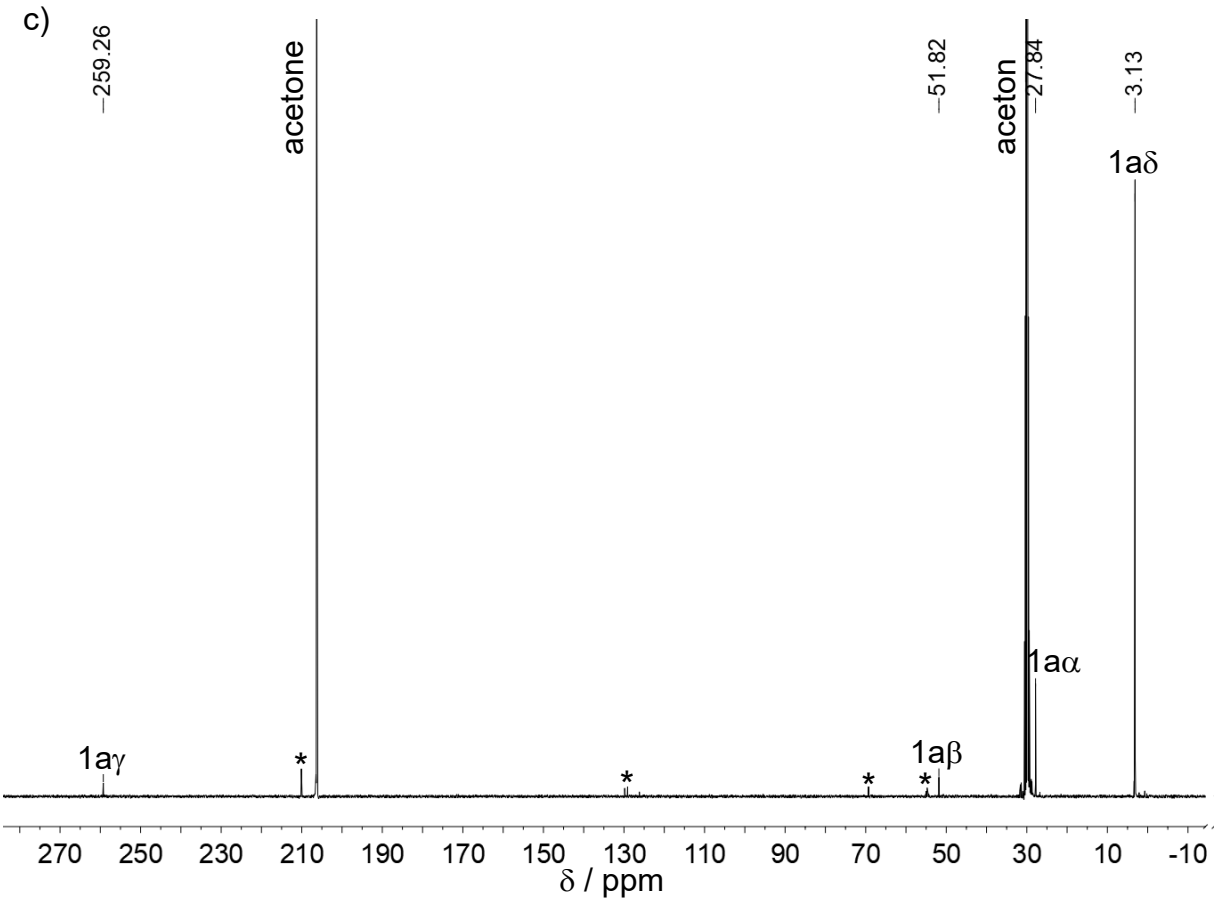
c)
259.26
acetone
51.82
aceton
27.84
3.13
1aδ
1aα
1aβ
1aγ
*
270
250
230
210
190
170
150
130
110
90
70
50
30
10
-10
δ / ppm

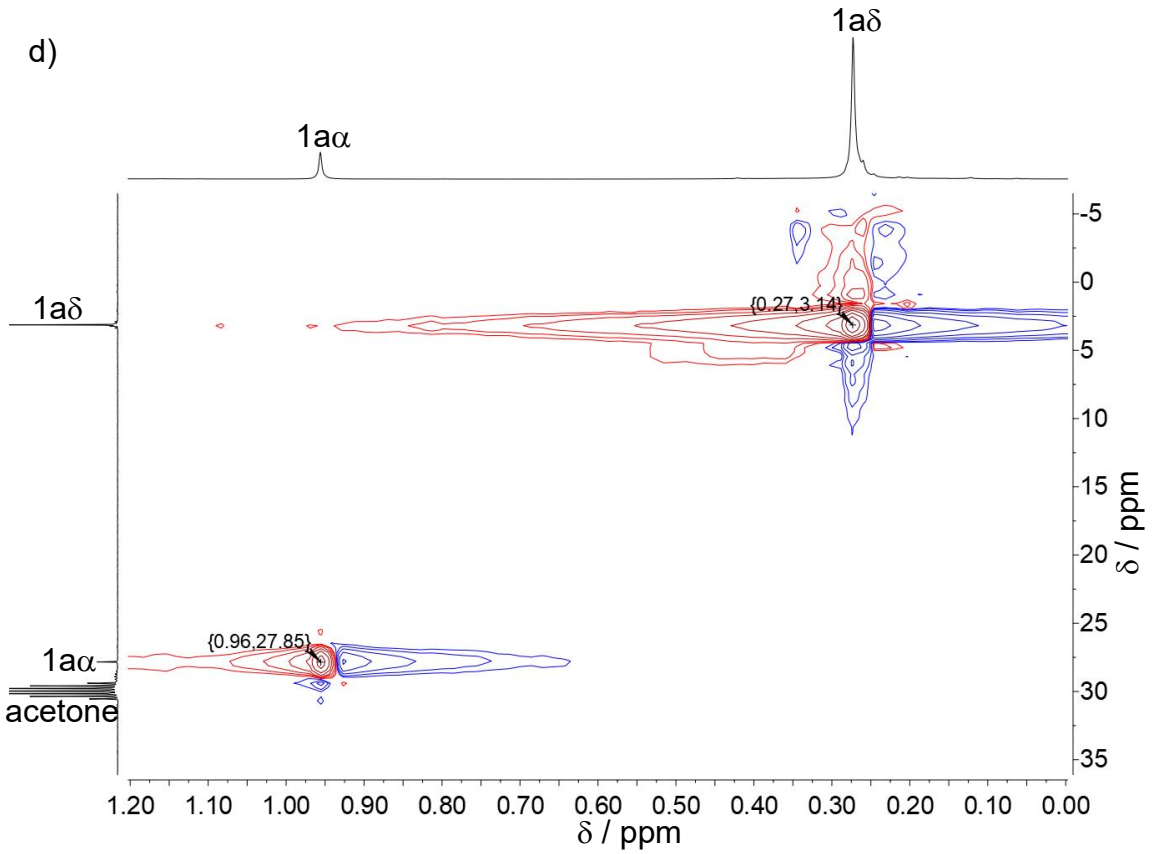
d)
1aδ
1aα
1aδ
{0.27,3.14}
{0.96,27.85}
1aα
acetone
-5
0
5
10
15
20
25
30
35
δ / ppm
1.20 1.10 1.00 0.90 0.80 0.70 0.60 0.50 0.40 0.30 0.20 0.10 0.00
δ / ppm

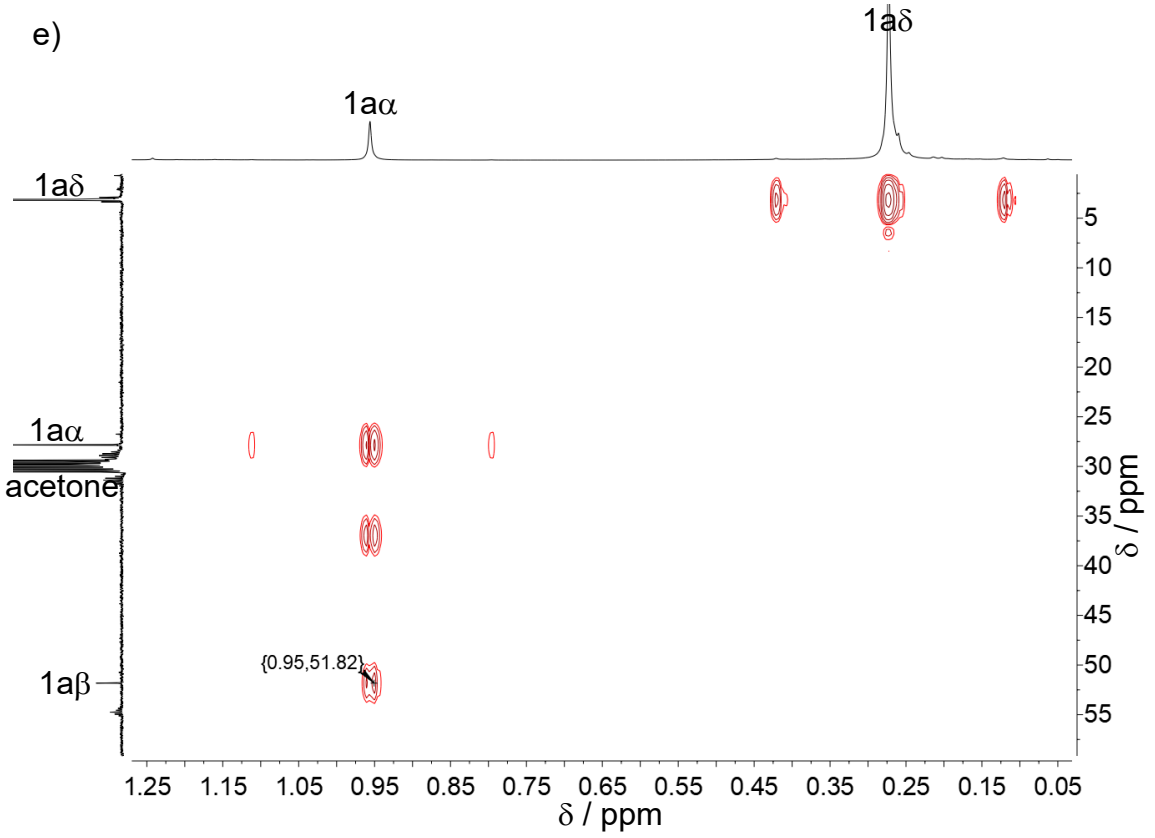
e)
1aδ
1aα
1aδ
1aα
acetone
{0.95,51.82}
1aβ
5
10
15
20
25
30
35
40
45
50
55
δ / ppm
1.25 1.15 1.05 0.95 0.85 0.75 0.65 0.55 0.45 0.35 0.25 0.15 0.05
δ / ppm

2 NMR spectroscopic characterization of 2a

Figure S1. ^{1}H, b) ^{29}Si, c) ^{13}C, d) ^{1}H ^{1}H COSY, e) ^{1}H ^{13}C HSQC NMR and f) ^{1}H ^{13}C HMBC NMR spectrum of reaction solution of **2a** recorded at r.t. in [D6]acetone. Signals marked with * could not be assigned.

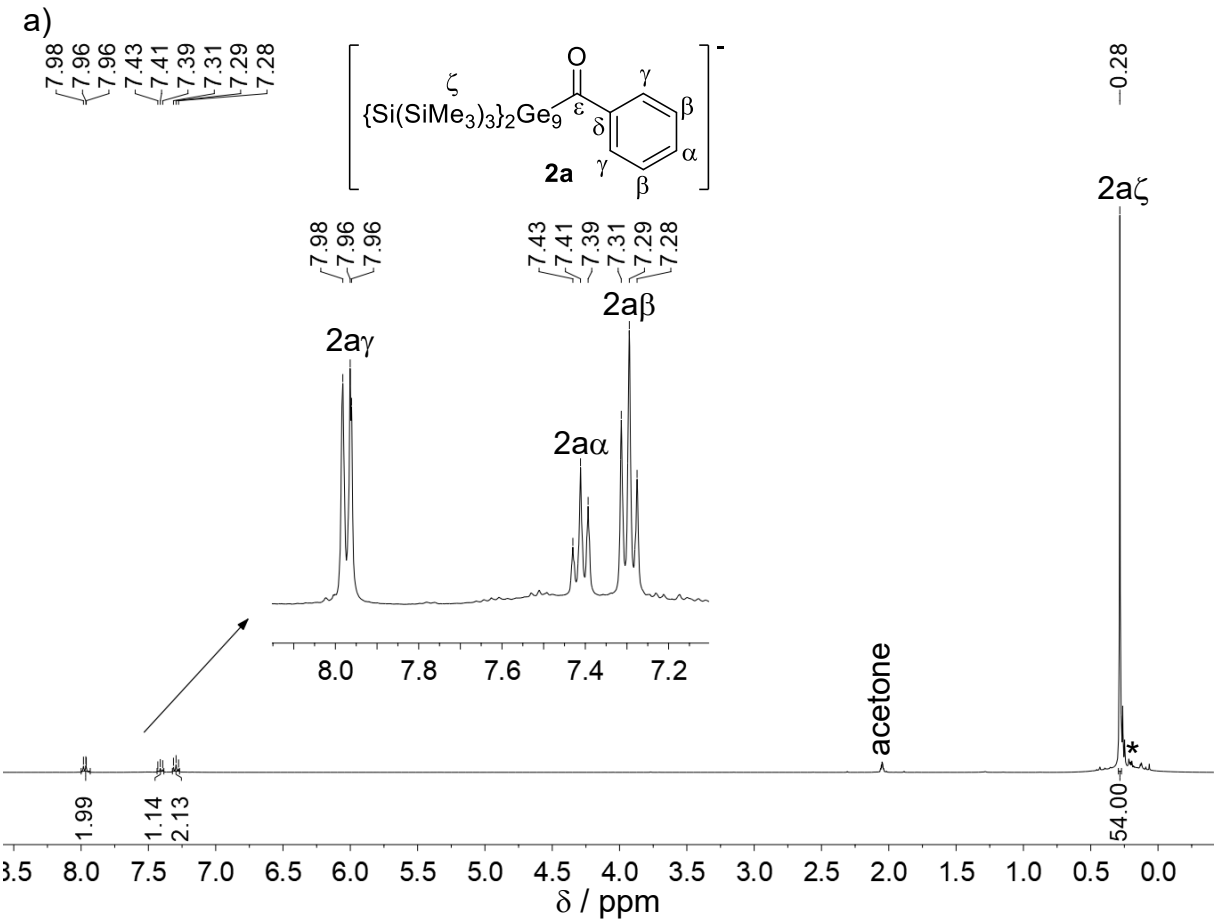

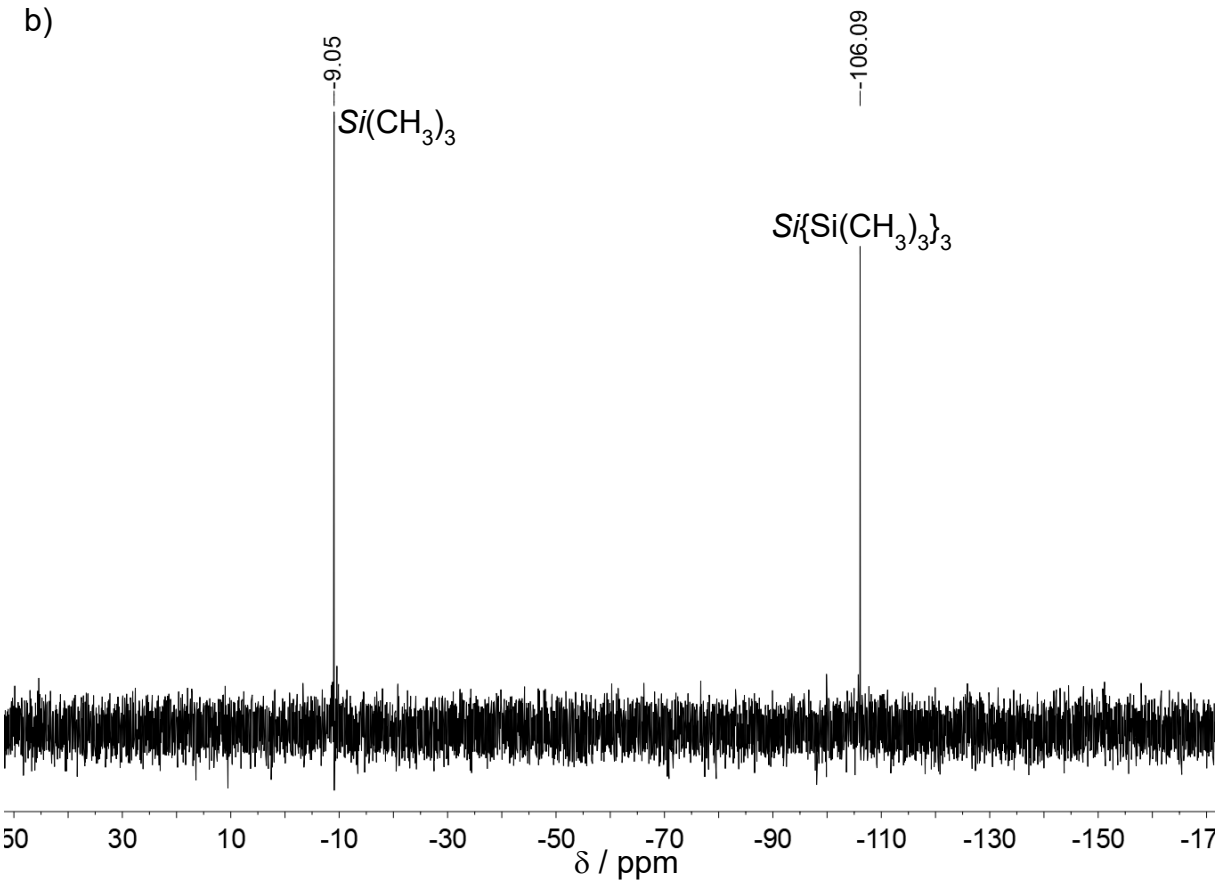
b)
9.05
106.09
Si(CH3)3
Si{Si(CH3)3}3
δ / ppm

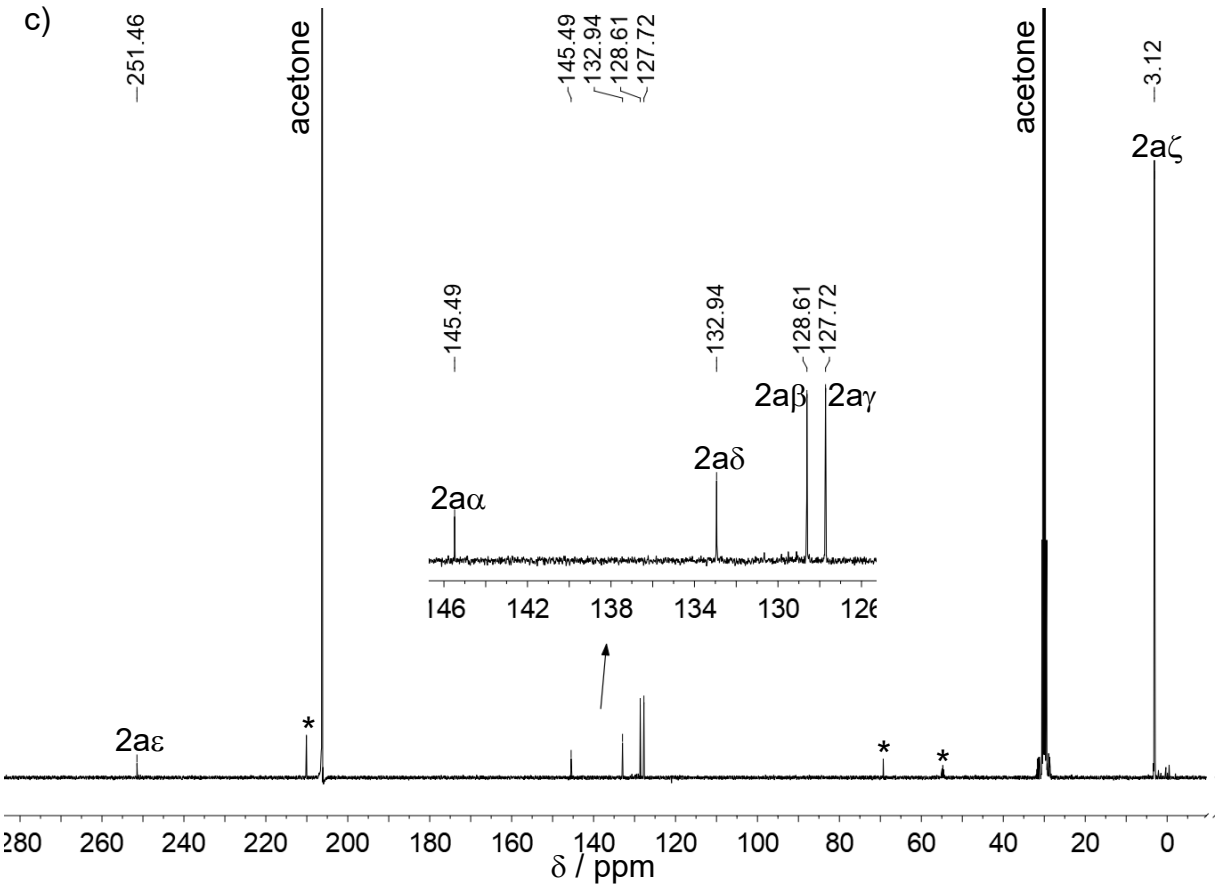
c)
251.46
acetone
145.49
132.94
128.61
127.72
acetone
3.12
2aζ
2aε
2aα
2aδ
2aβ
2aγ
δ / ppm

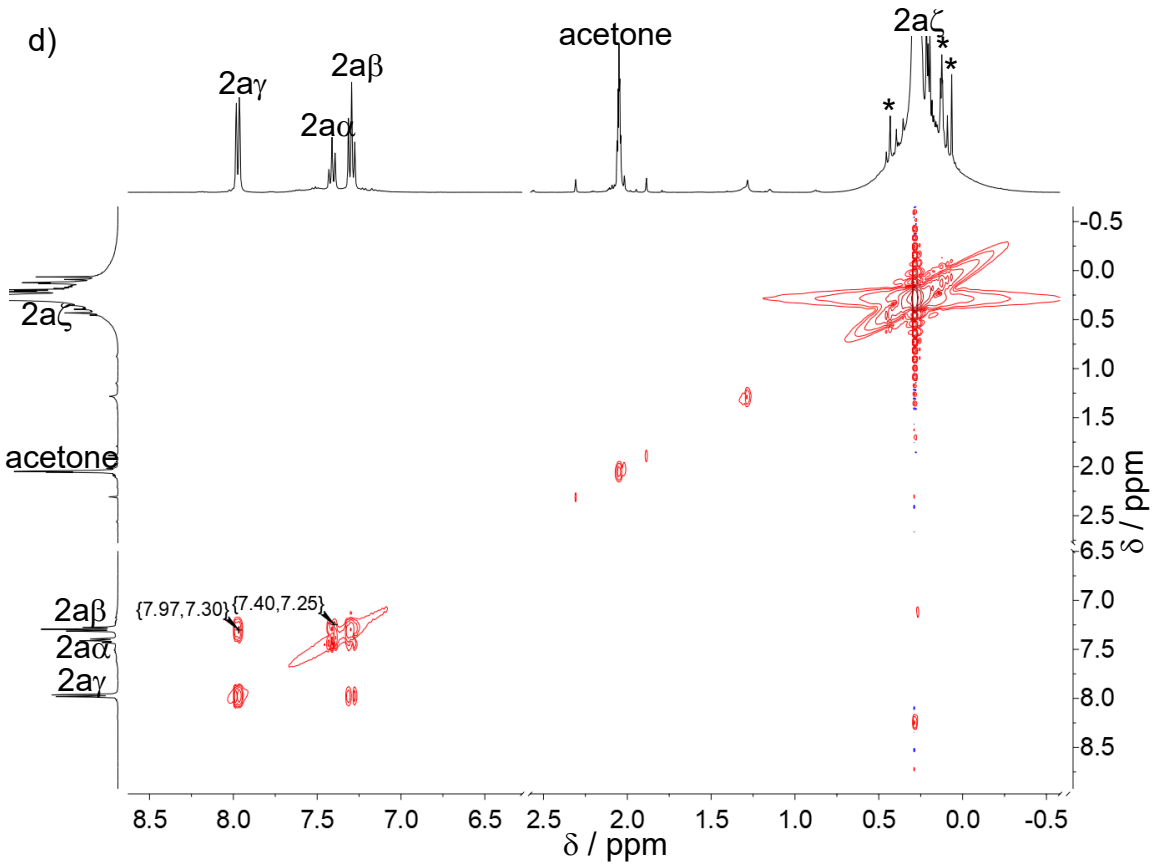
d)
2aγ
2aβ
2aα
acetone
2aζ
{7.97,7.30}
{7.40,7.25}
δ / ppm

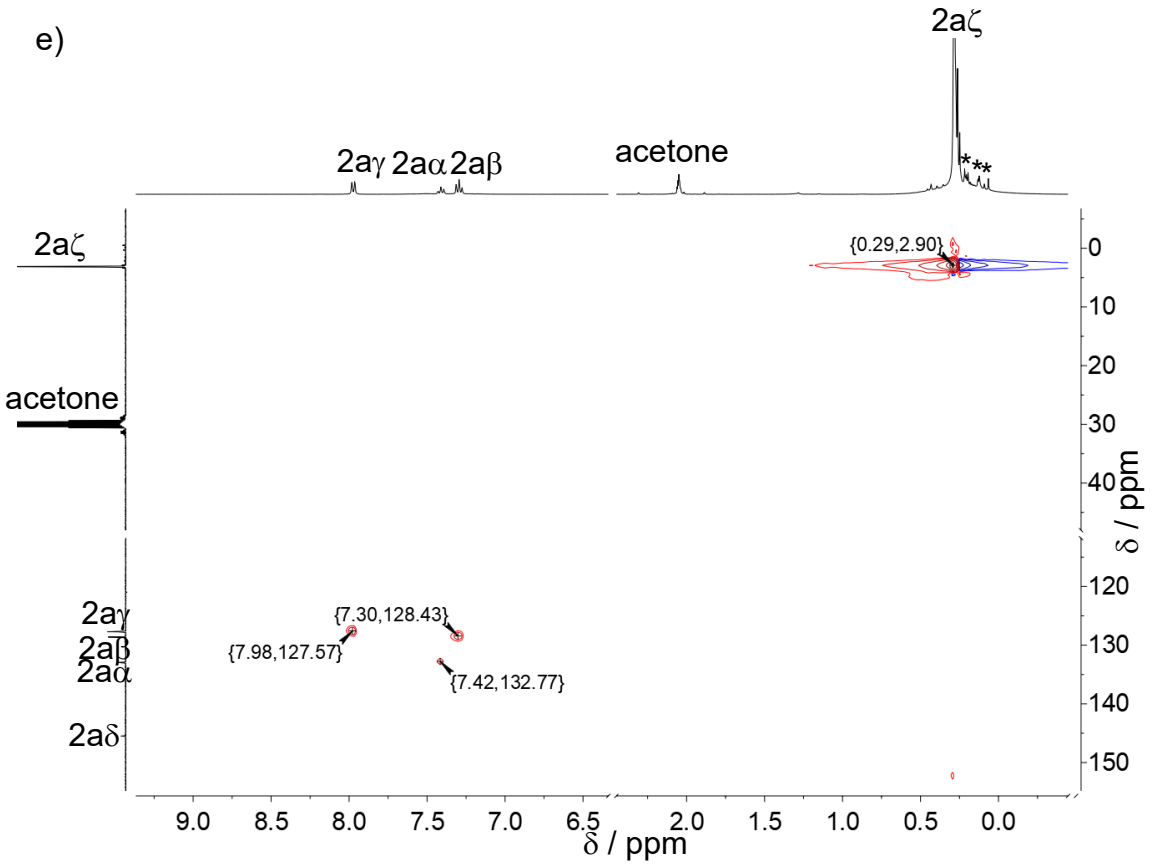
e)
2aγ 2aα 2aβ
acetone
2aζ
{0.29,2.90}
2aδ
{7.30,128.43}
{7.98,127.57}
{7.42,132.77}
δ / ppm

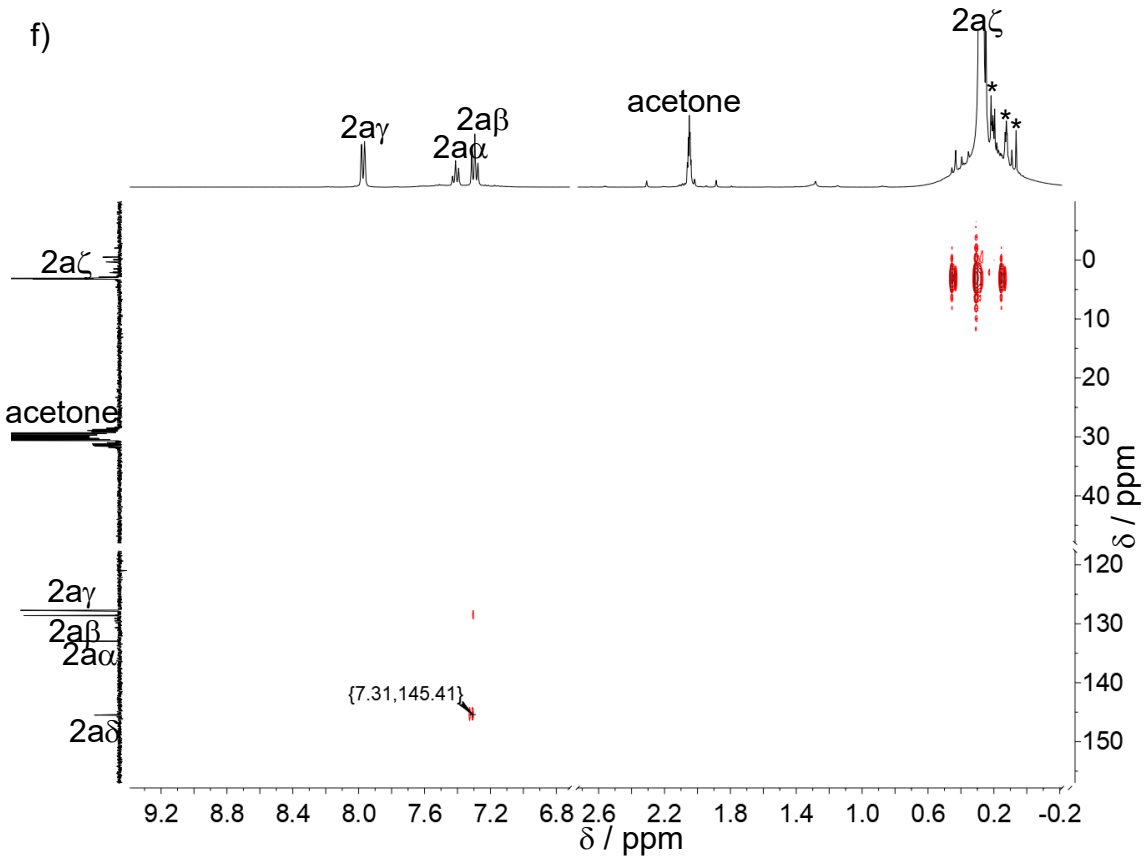

3 NMR spectroscopic characterization of 3a

Figure S35.8.1. ^{1}H, b) ^{29}Si, c) ^{13}C, d) ^{1}H ^{1}H COSY, e) ^{1}H ^{13}C HSQC NMR and f) ^{1}H ^{13}C HMBC NMR spectrum of reaction solution of **3a** recorded at r.t. in [D6]acetone. Signals marked with * could not be assigned.

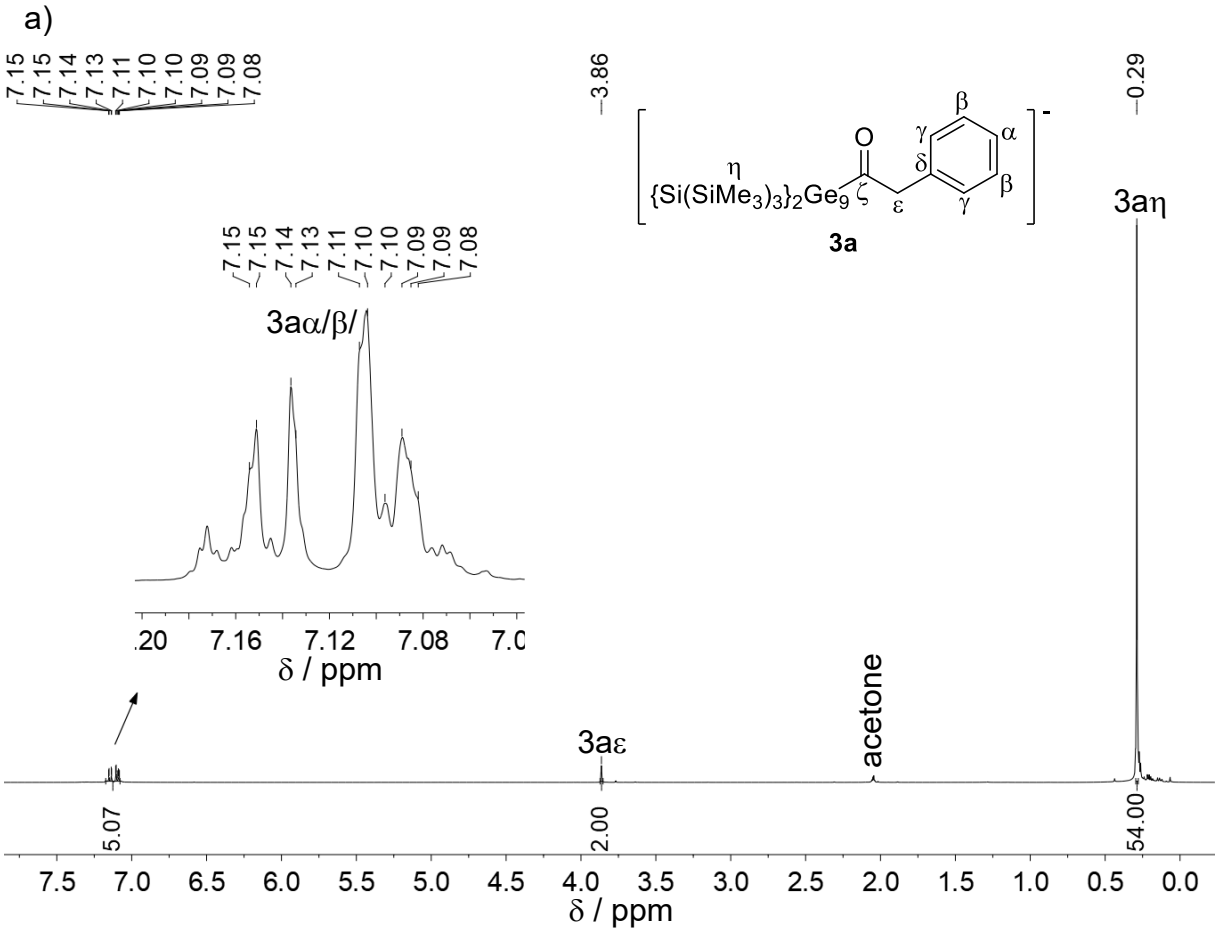
a)
7.15
7.15
7.14
7.13
7.11
7.10
7.10
7.09
7.09
7.08
3.86
0.29
3aη
3aα/β/
3aε
acetone
5.07
2.00
54.00
δ / ppm
3a

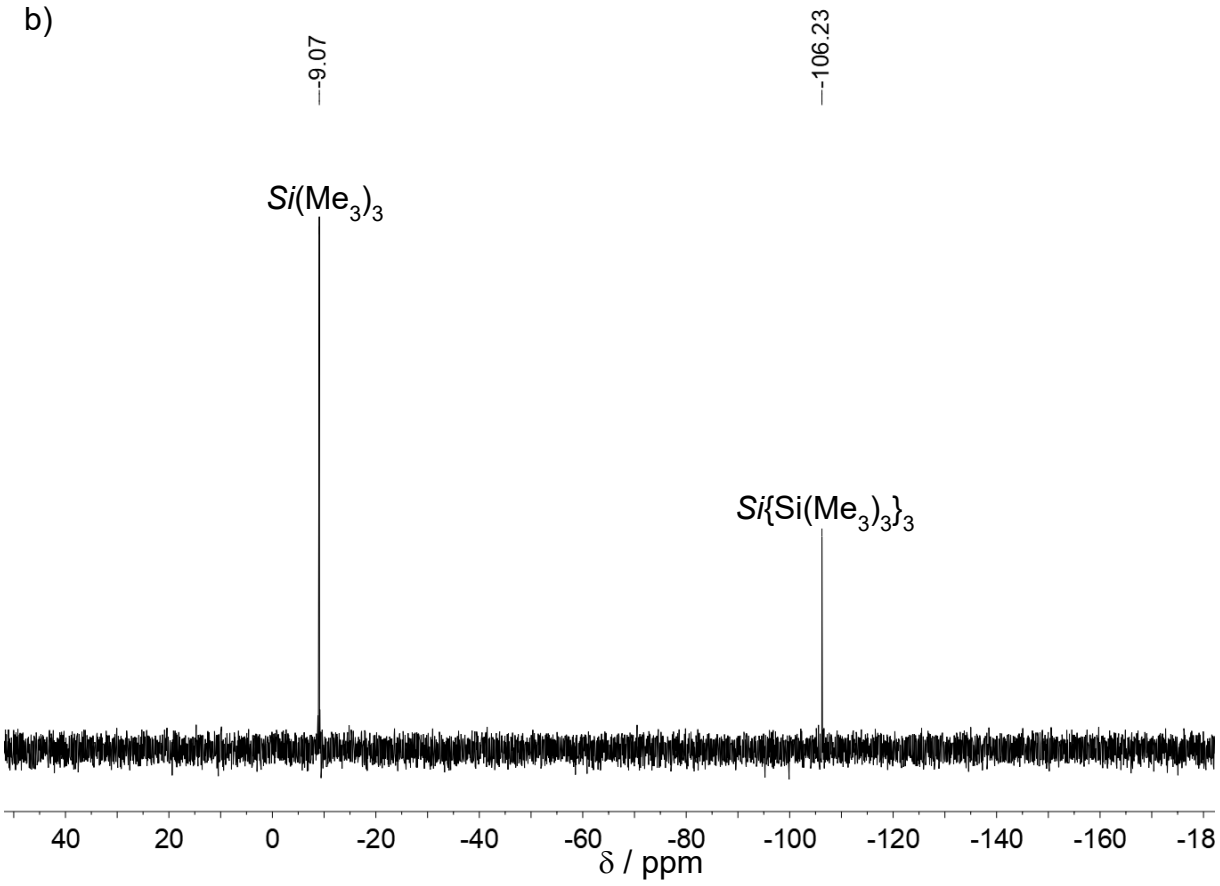
b)
9.07
106.23
Si(Me3)3
Si{Si(Me3)3}3
δ / ppm

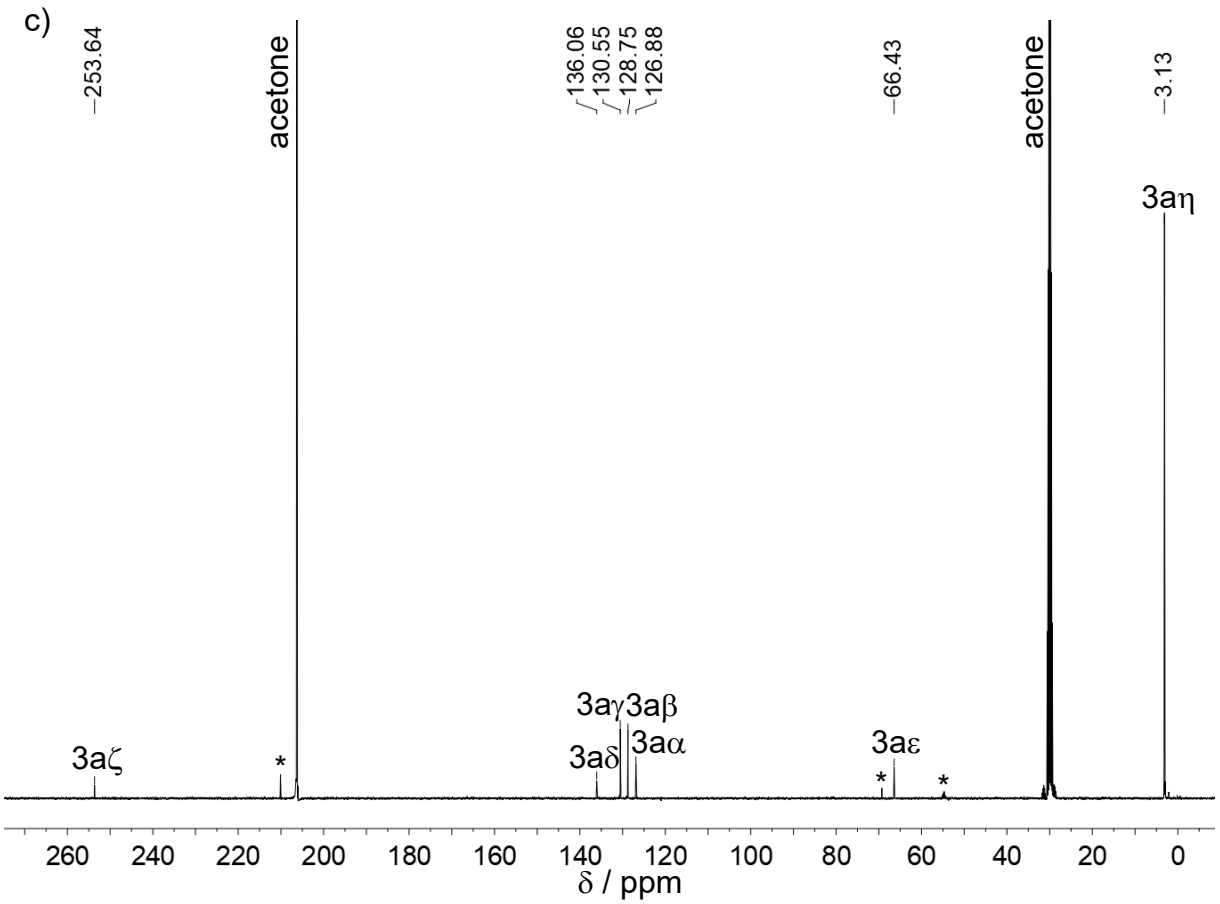
c)
253.64
acetone
136.06
130.55
128.75
126.88
66.43
acetone
3.13
3aη
3aγ
3aβ
3aδ
3aα
3aε
3aζ
*
*
*
260 240 220 200 180 160 140 120 100 80 60 40 20 0
δ / ppm

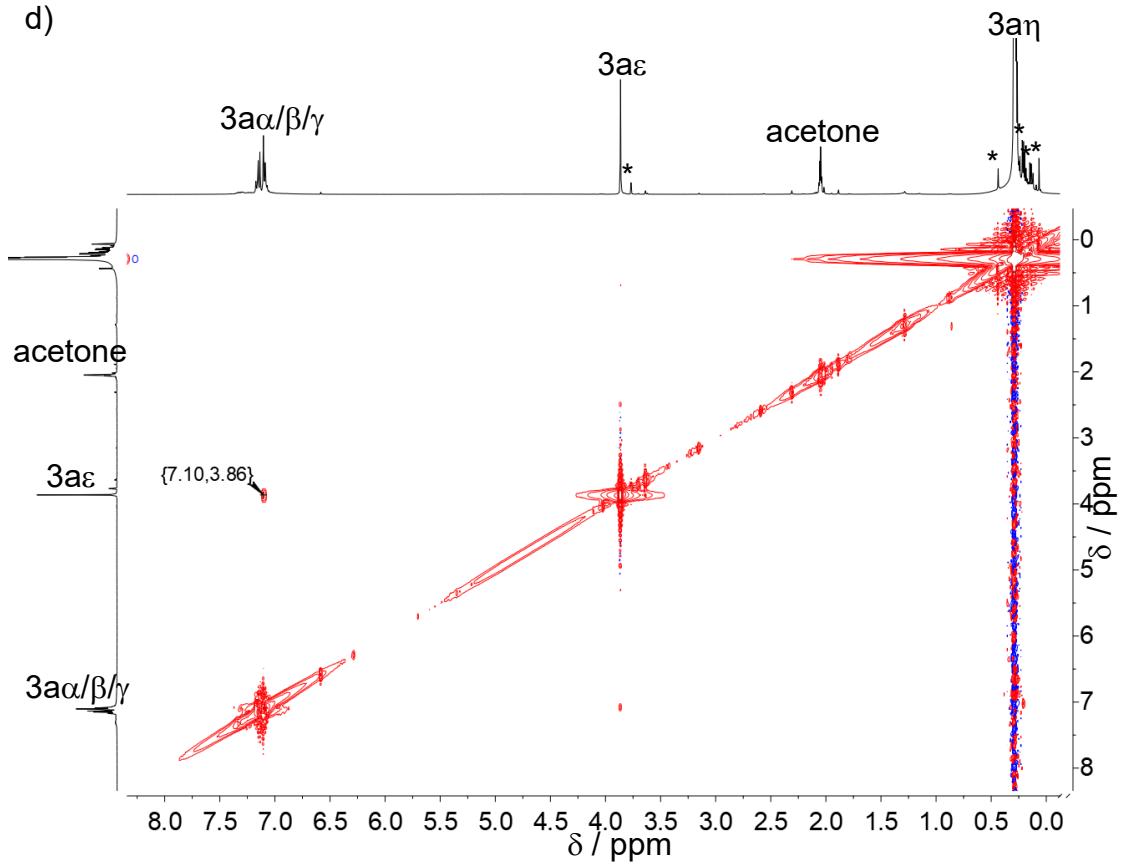
d)
3aη
3aε
3aα/β/γ
acetone
*
*
*
*
acetone
3aε
{7.10,3.86}
3aα/β/γ
0
1
2
3
4
5
6
7
8
δ / ppm
8.0 7.5 7.0 6.5 6.0 5.5 5.0 4.5 4.0 3.5 3.0 2.5 2.0 1.5 1.0 0.5 0.0
δ / ppm

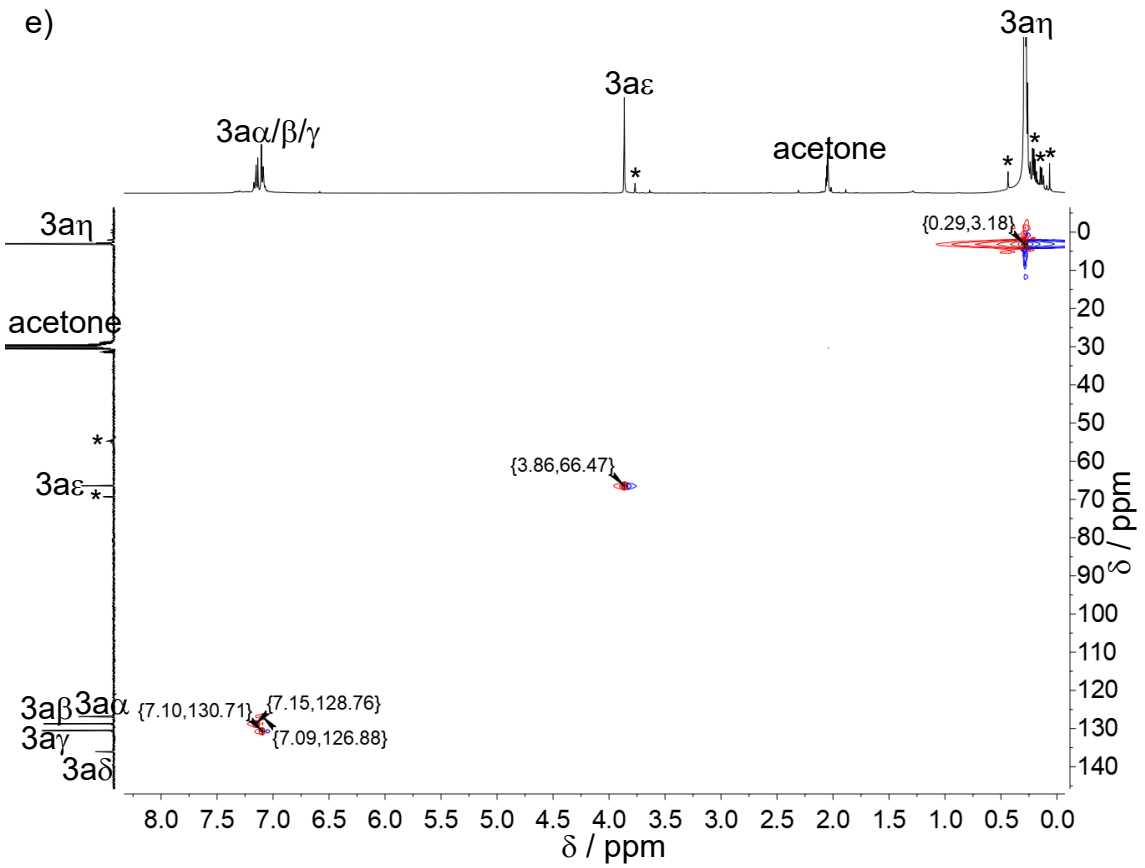
e)
3aη
3aε
3aα/β/γ
acetone
{0.29,3.18}
{3.86,66.47}
{7.10,130.71}
{7.15,128.76}
{7.09,126.88}
3aβ
3aα
3aγ
3aδ
δ / ppm

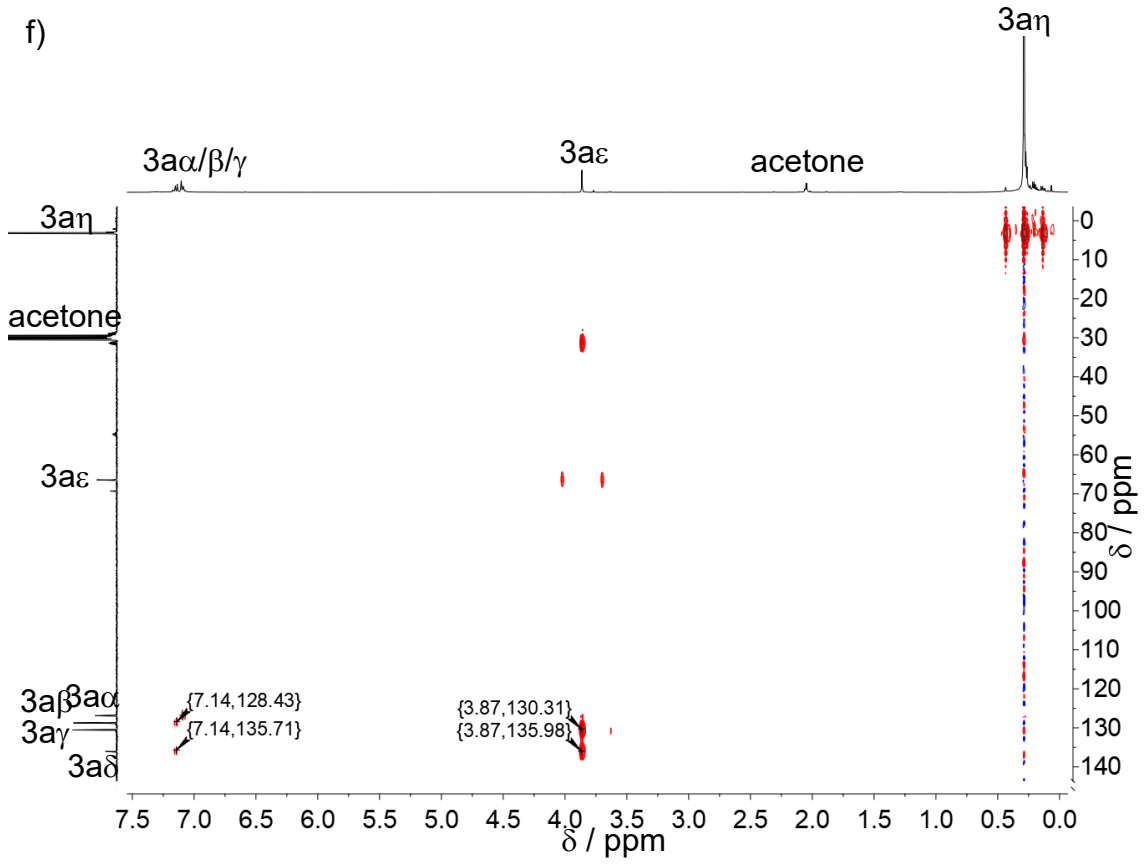
f)
3aη
3aα/β/γ
3aε
acetone
{7.14,128.43}
{7.14,135.71}
{3.87,130.31}
{3.87,135.98}
3aβ
3aα
3aγ
3aδ
δ / ppm

4 NMR spectroscopic characterization of 4a

Figure S4. ^{1}H and b) ^{29}Si NMR spectrum of reaction solution of **4a** recorded at r.t. in [D6]acetone. Signals marked with * could not be assigned. The anion **4a** shows lower stability in solution, thus only ^{1}H and ^{29}Si NMR spectra were recorded.

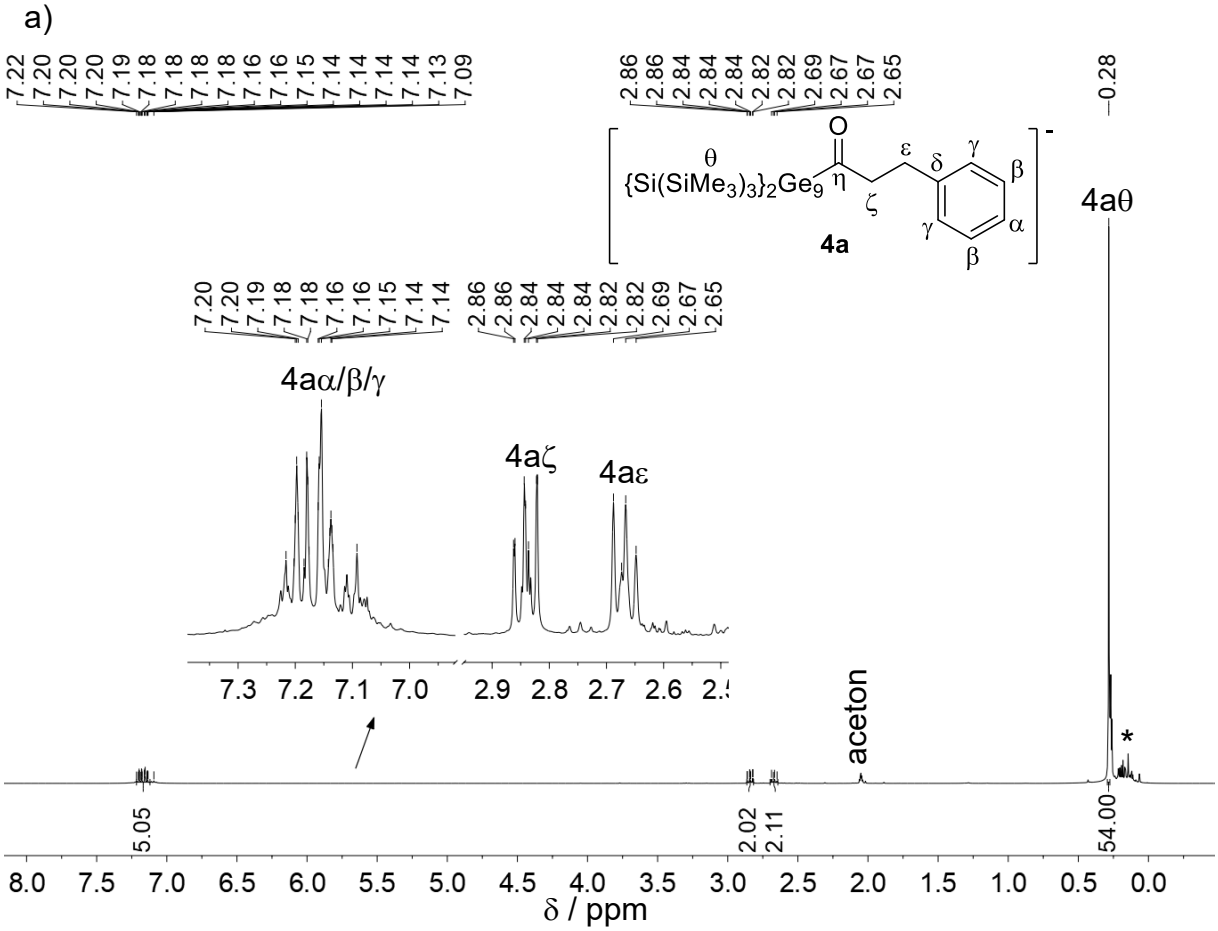

b)

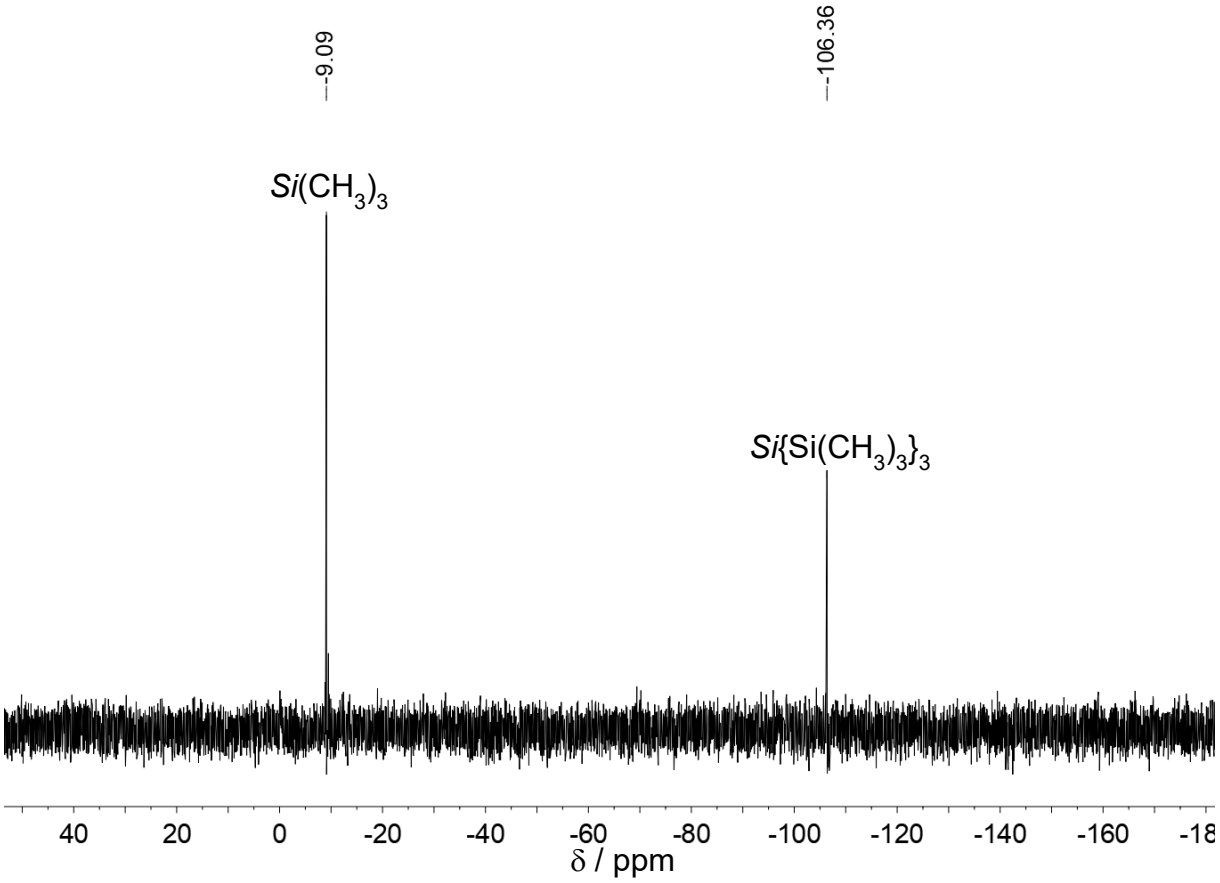
-9.09
-106.36
Si(CH3)3
Si{Si(CH3)3}3
40
20
0
-20
-40
-60
-80
-100
-120
-140
-160
δ / ppm

5 NMR spectroscopic characterization of 5a

Figure S5. a) ^{1}H, b) ^{29}Si, c) ^{13}C, d) ^{1}H ^{1}H COSY, e) ^{1}H ^{13}C HSQC and f) ^{1}H ^{13}C HMBC NMR spectrum of **5a** recorded in acetone-d_6 at r.t.

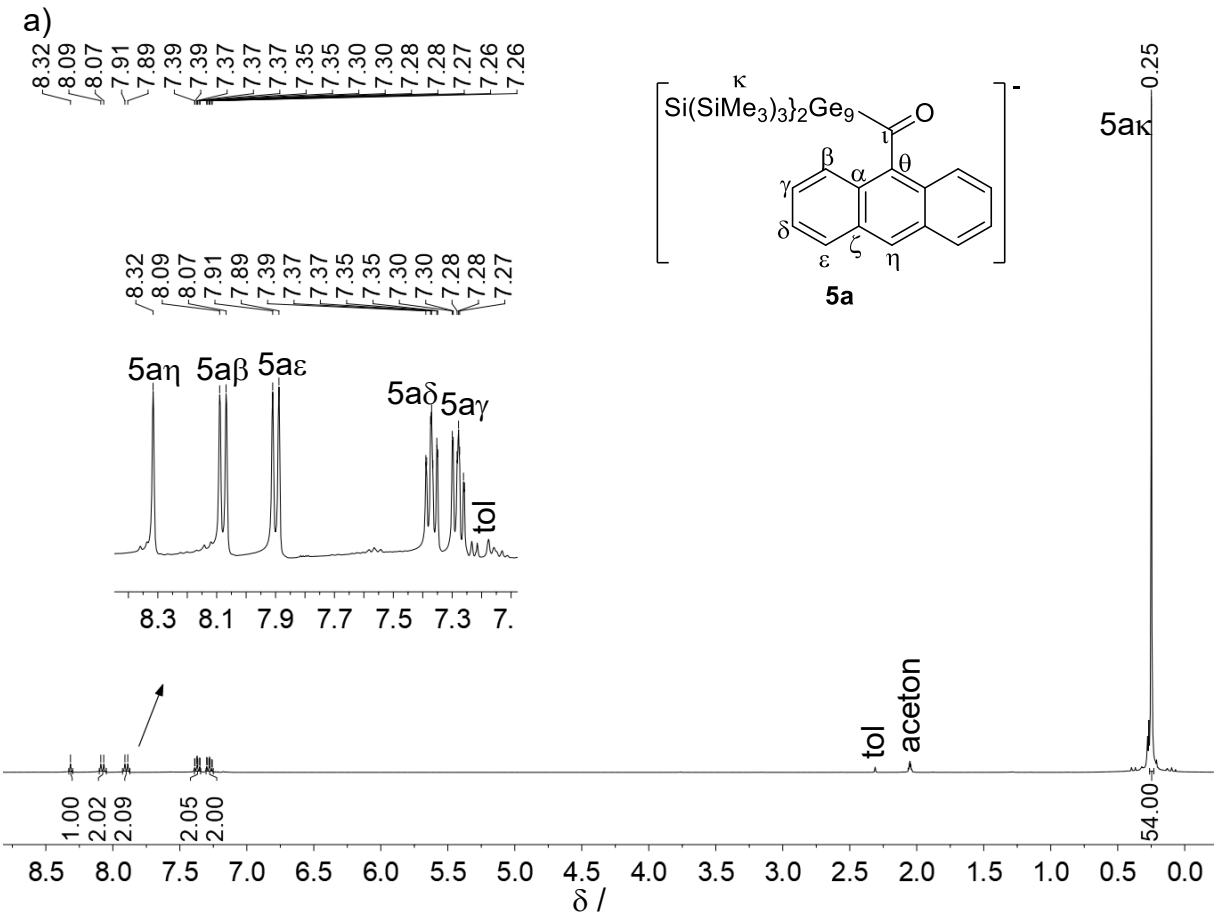

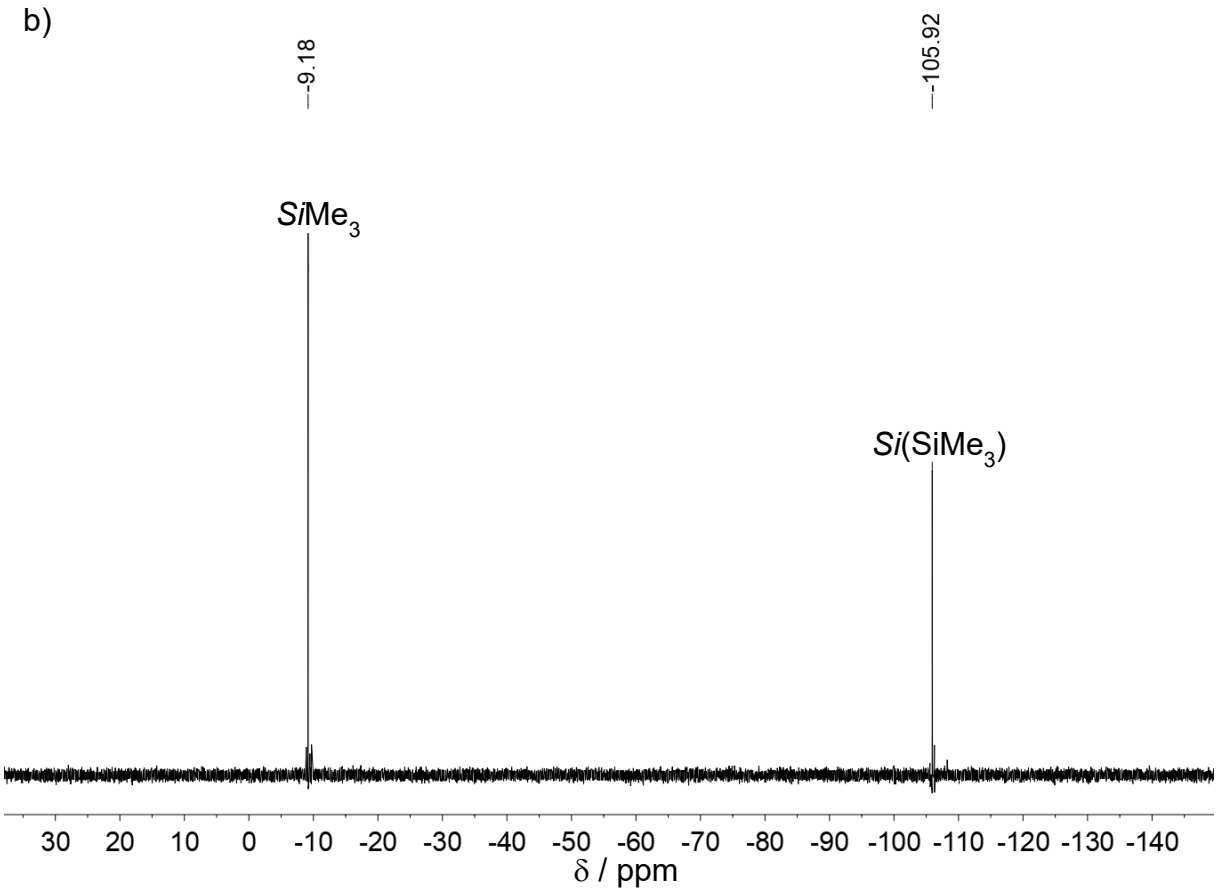
b)
-9.18
-105.92
SiMe3
Si(SiMe3)
30 20 10 0 -10 -20 -30 -40 -50 -60 -70 -80 -90 -100 -110 -120 -130 -140
δ / ppm

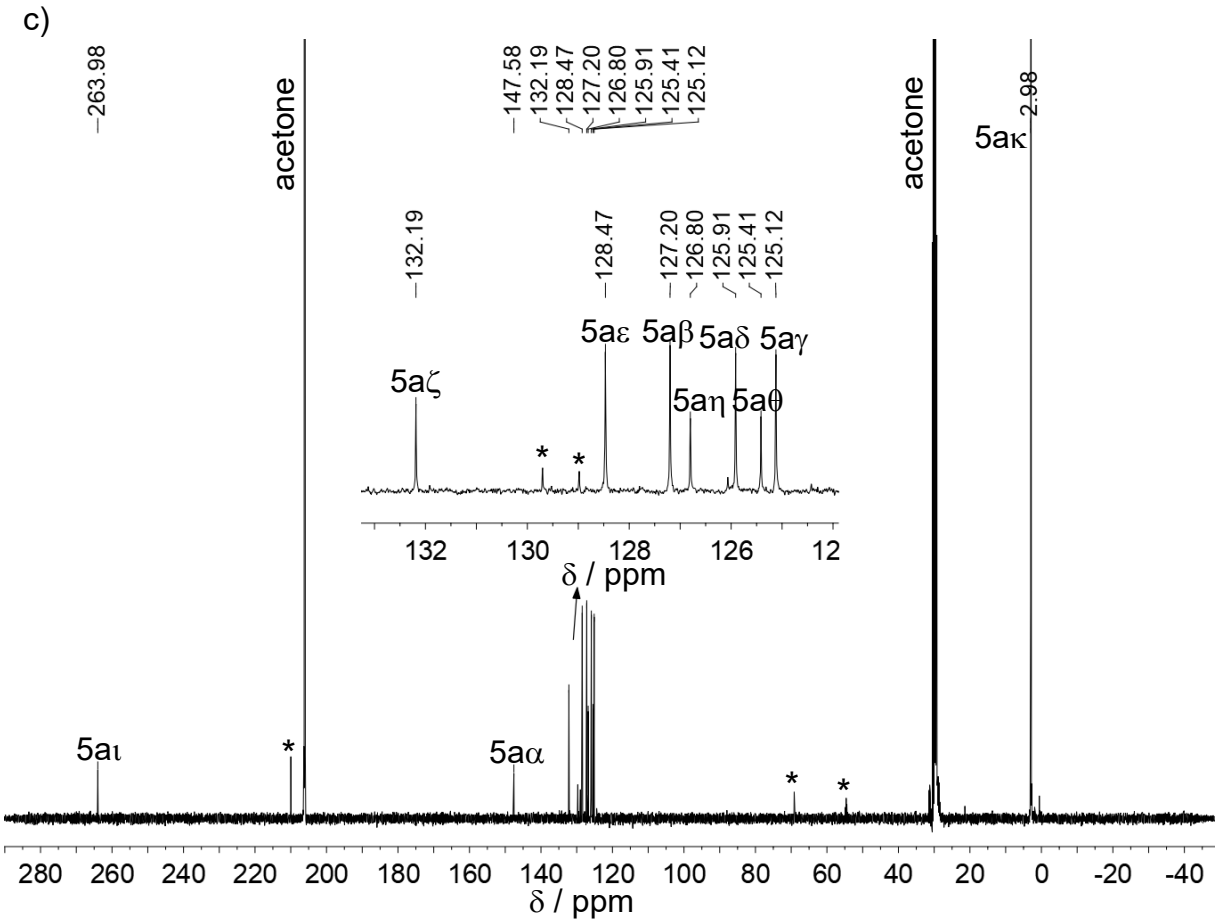
c)
263.98
acetone
147.58
132.19
128.47
127.20
126.80
125.91
125.41
125.12
acetone
5aκ
2.98
5aε 5aβ 5aδ 5aγ
5aζ
5aη 5aθ
132 130 128 126 12
δ / ppm
5aι
5aα
280 260 240 220 200 180 160 140 120 100 80 60 40 20 0 -20 -40
δ / ppm

d)

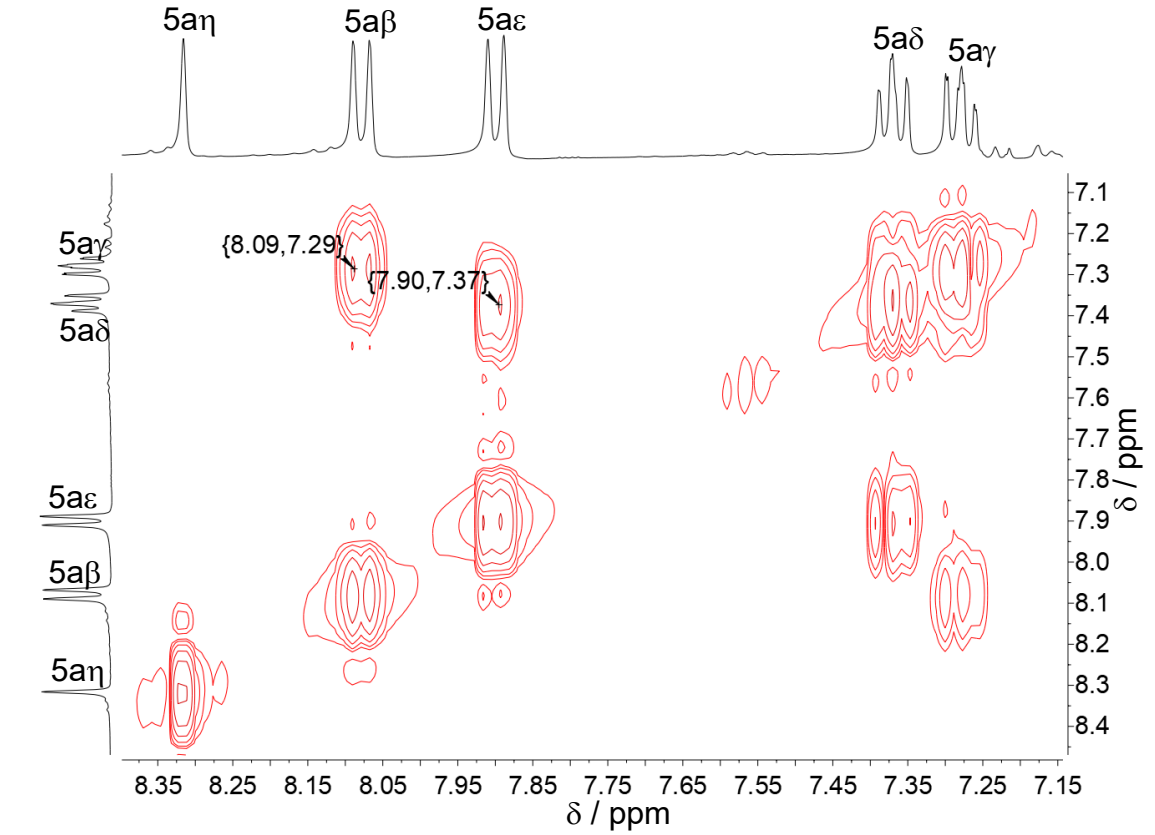
5aη
5aβ
5aε
5aδ
5aγ
{8.09,7.29}
{7.90,7.37}
δ / ppm
δ / ppm

e)

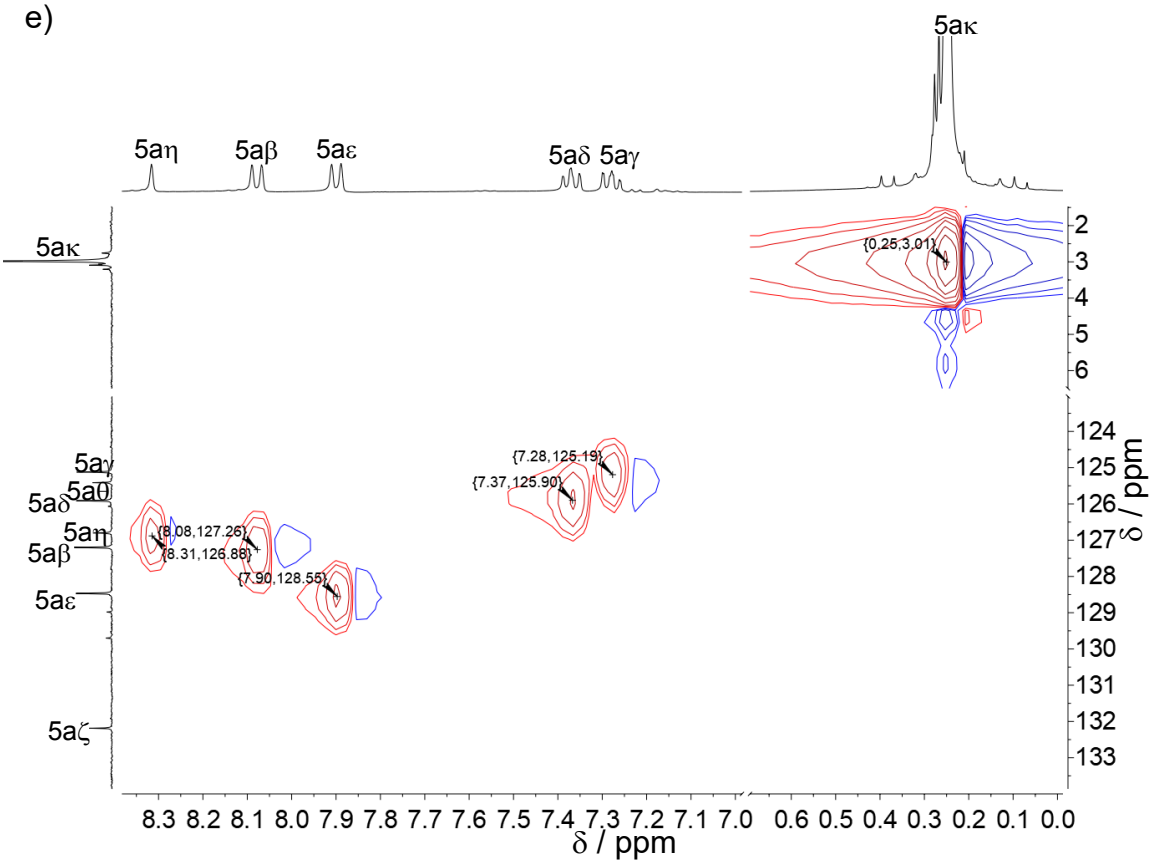
5aκ
5aη
5aβ
5aε
5aδ 5aγ
{0.25,3.01}
{7.28,125.19}
{7.37,125.90}
{8.08,127.26}
{8.31,126.88}
{7.90,128.55}
5aζ
δ / ppm
δ / ppm

f)

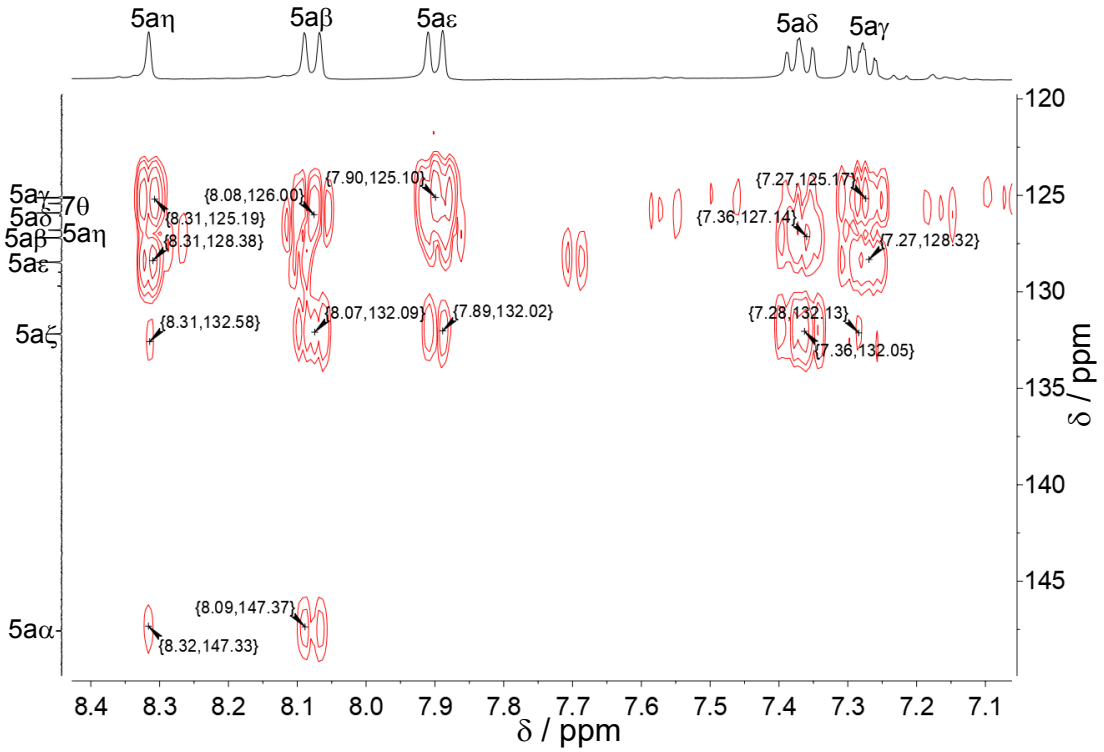
5aη
5aβ
5aε
5aδ
5aγ
5aγ=7θ
5aδ
5aβ=5aη
5aε
5aζ
5aα
{8.08,126.00}
{7.90,125.10}
{8.31,125.19}
{8.31,128.38}
{8.31,132.58}
{8.07,132.09}
{7.89,132.02}
{8.09,147.37}
{8.32,147.33}
{7.27,125.17}
{7.36,127.14}
{7.27,128.32}
{7.28,132.13}
{7.36,132.05}
120
125
130
135
140
145
δ / ppm
8.4
8.3
8.2
8.1
8.0
7.9
7.8
7.7
7.6
7.5
7.4
7.3
7.2
7.1
δ / ppm

6 NMR spectroscopic characterization of 6a

Figure S6. a) ^{1}H, b) ^{29}Si, c) ^{13}C, d) ^{1}H ^{1}H COSY, e) ^{1}H ^{13}C HSQC NMR and f) ^{1}H ^{13}C HMBC NMR spectrum of **6a** recorded at r.t. in [D6]acetone.

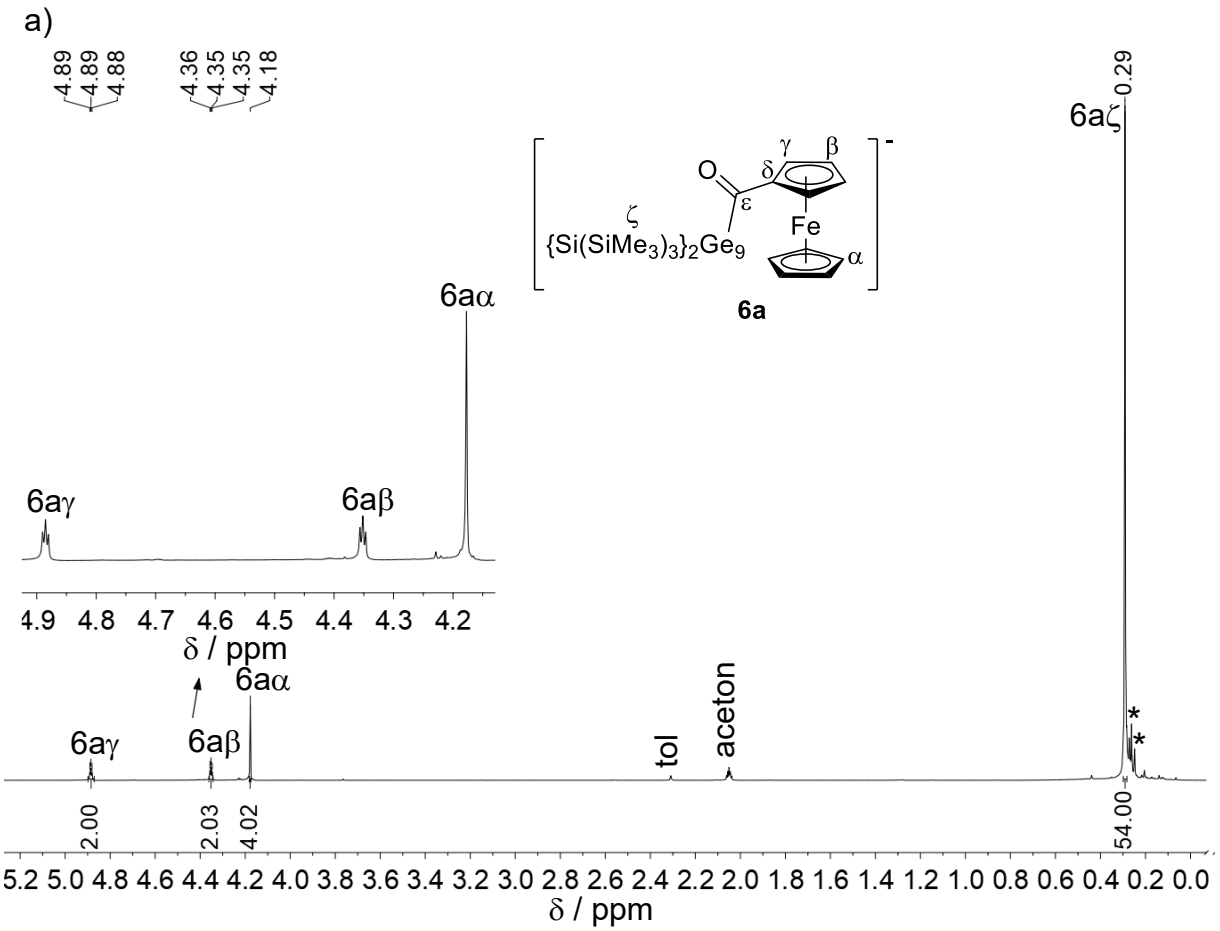

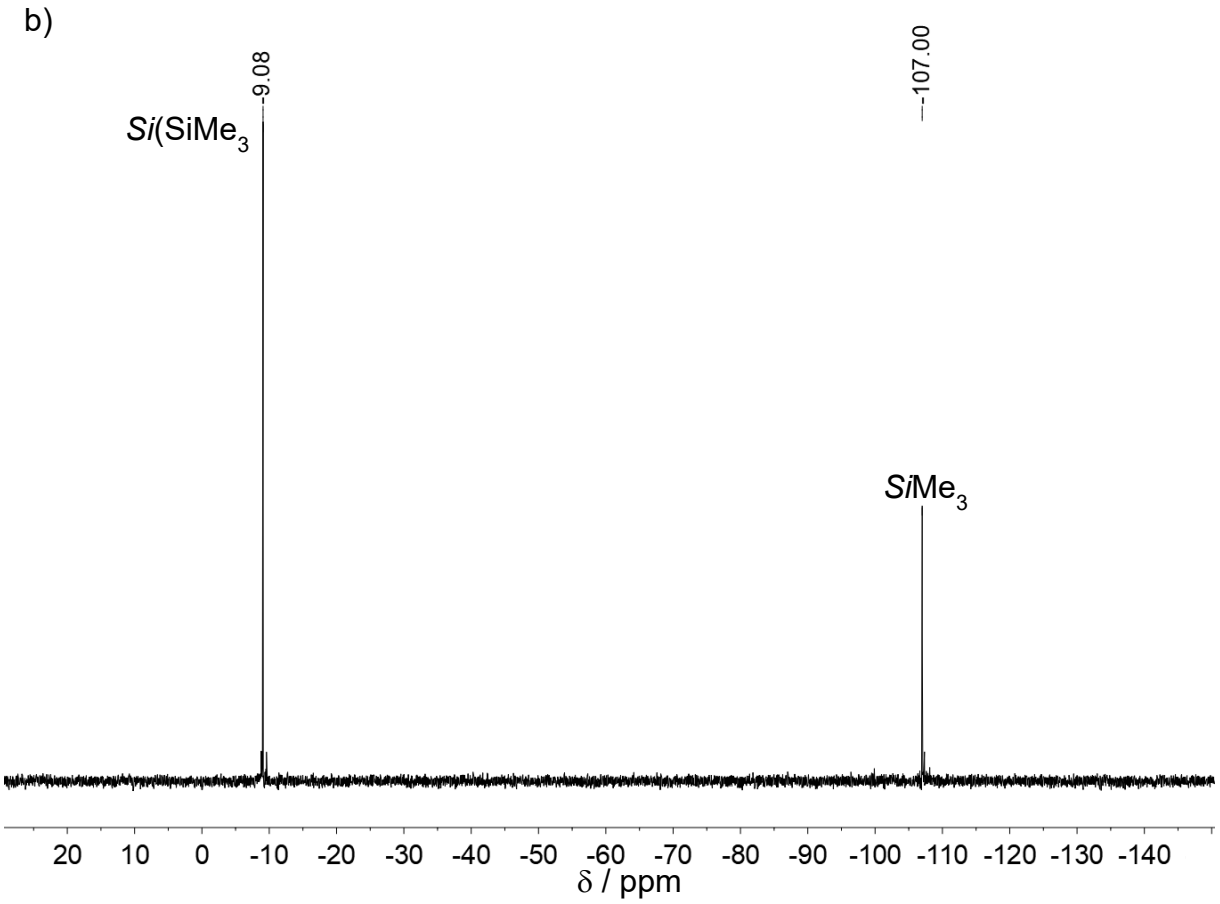
b)
-9.08
Si(SiMe3
-107.00
SiMe3
20 10 0 -10 -20 -30 -40 -50 -60 -70 -80 -90 -100 -110 -120 -130 -140
δ / ppm

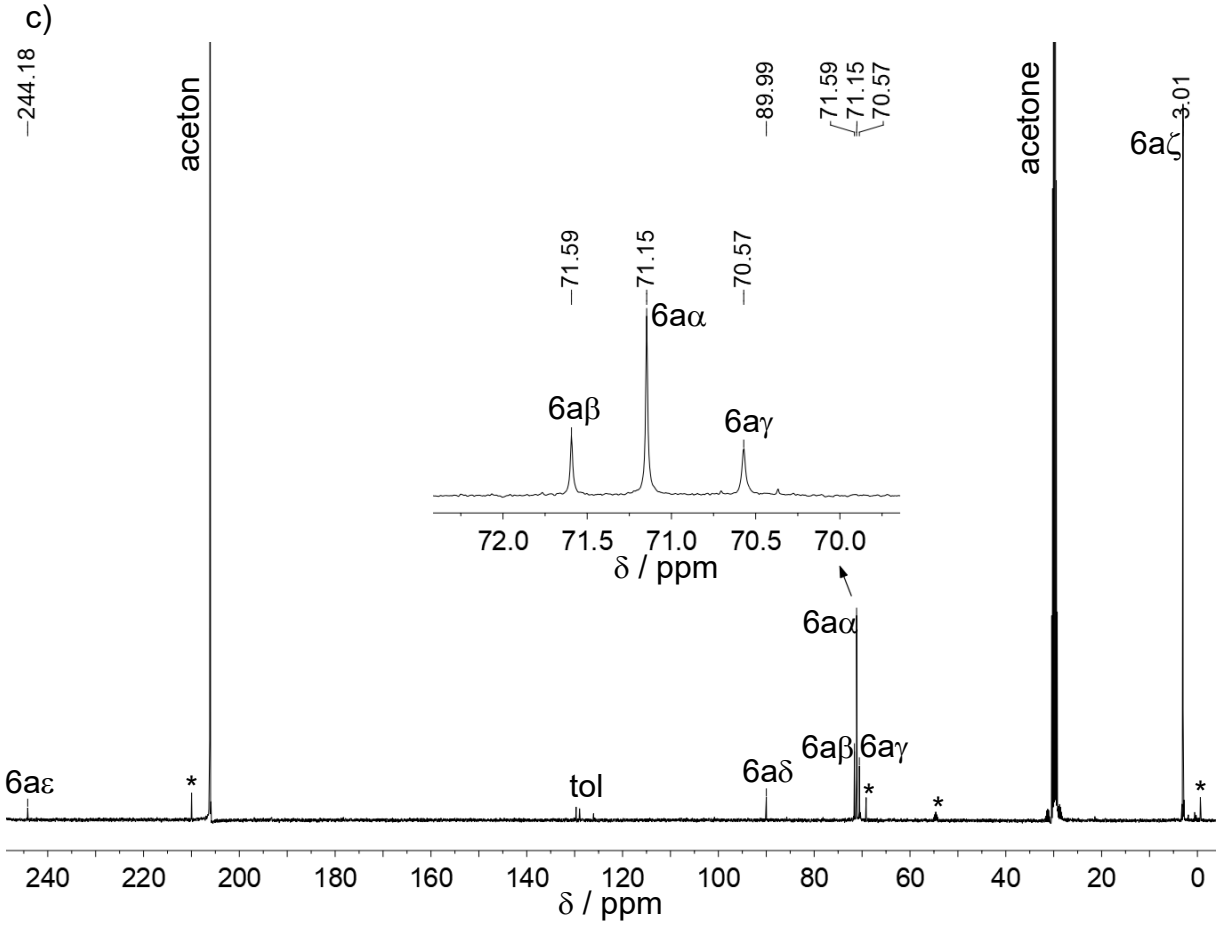
c)
244.18
aceton
89.99
71.59
71.15
70.57
acetone
6aζ
3.01
71.59
71.15
70.57
6aα
6aβ
6aγ
72.0 71.5 71.0 70.5 70.0
δ / ppm
6aα
6aβ
6aγ
6aδ
6aε
*
tol
*
*
*
240 220 200 180 160 140 120 100 80 60 40 20 0
δ / ppm

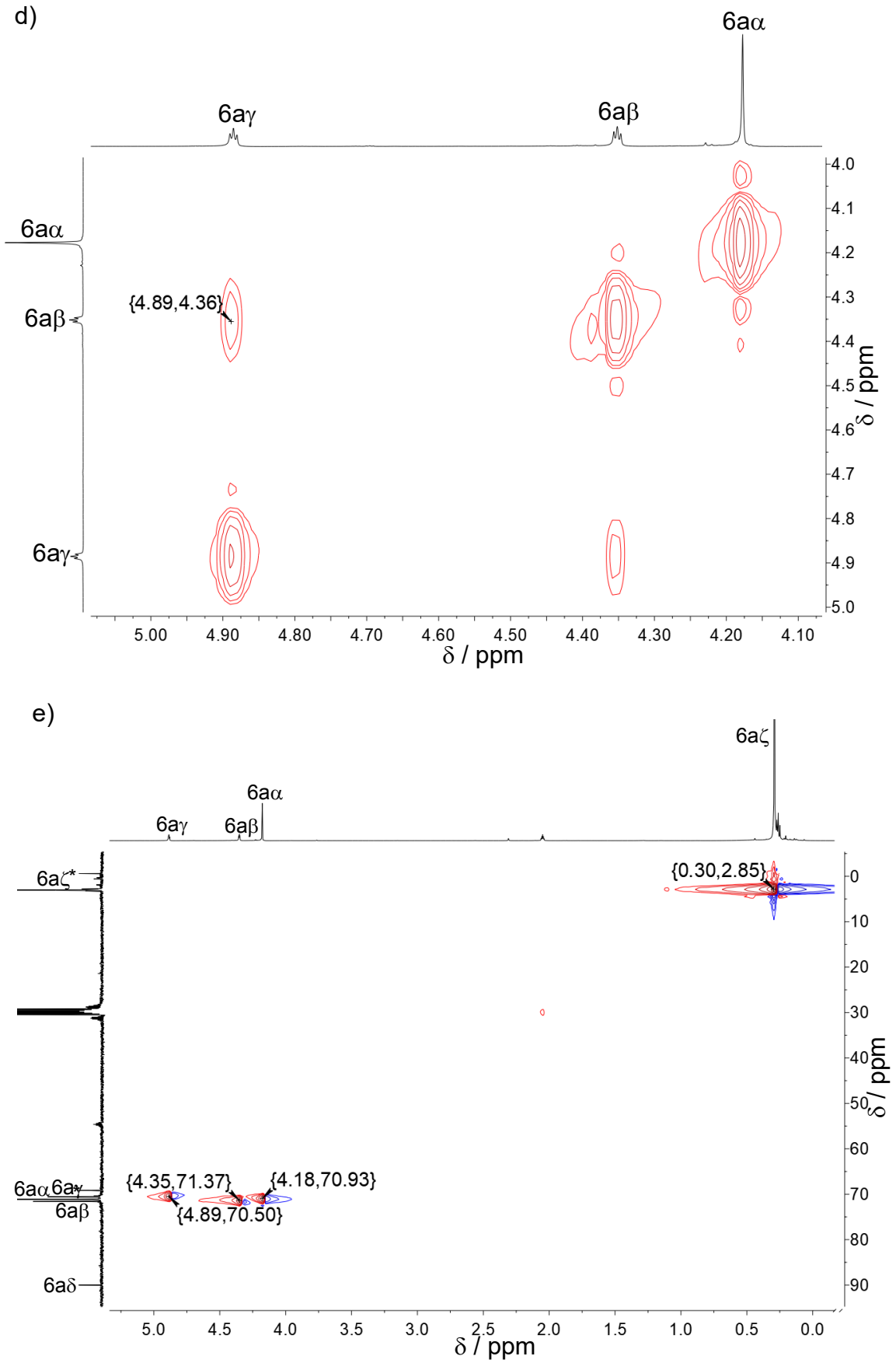
d)
6aα
6aγ
6aβ
{4.89,4.36}
δ / ppm
e)
6aζ
6aα
6aγ
6aβ
6aζ*
{0.30,2.85}
{4.35,71.37}
{4.18,70.93}
{4.89,70.50}
6aδ
δ / ppm

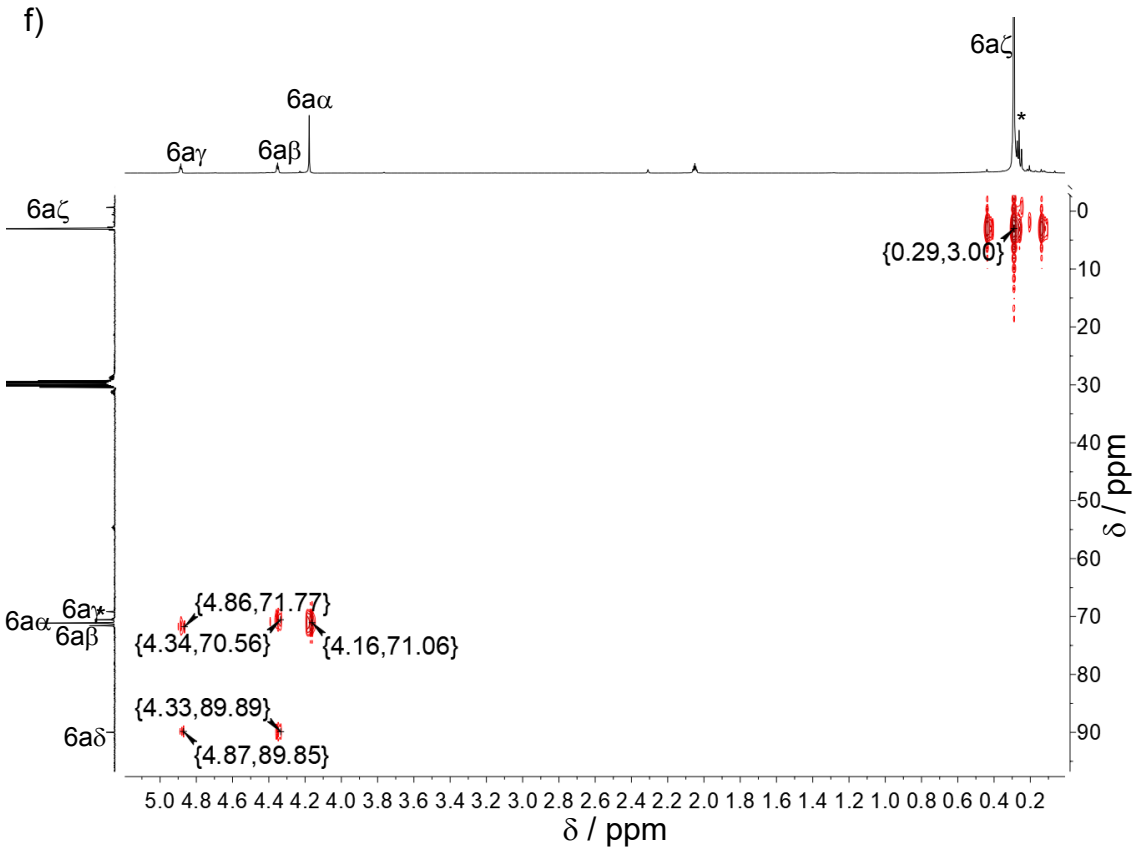

7 ESI mass spectra of reaction solutions containing compounds 1-6

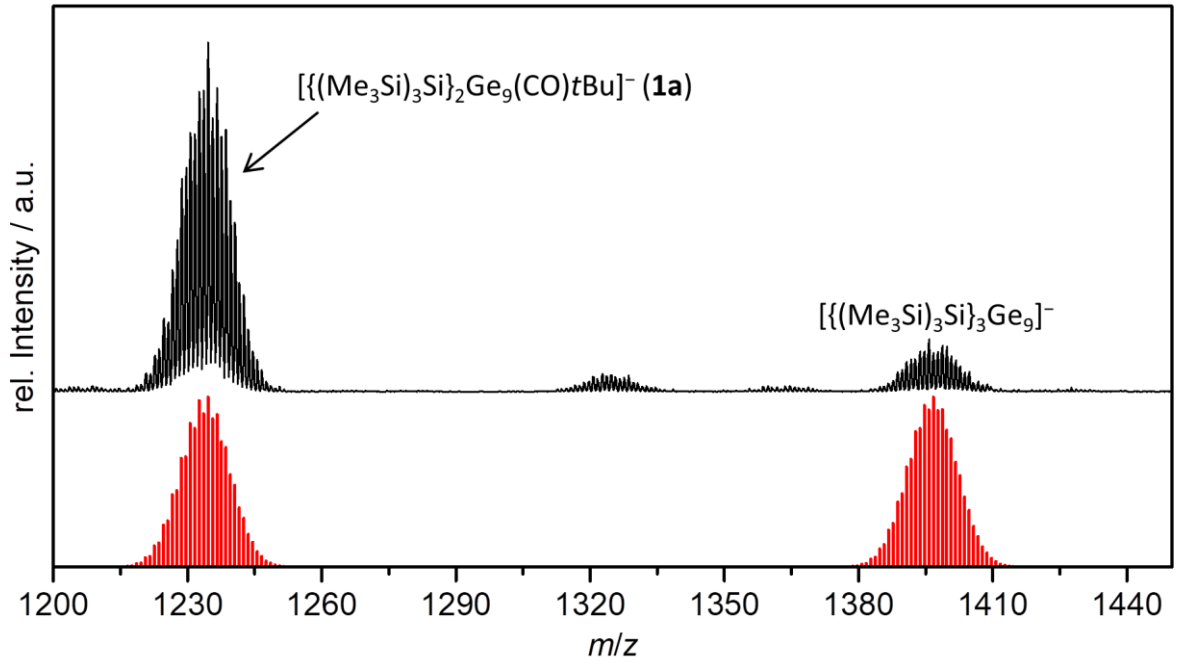

Figure S7. ESI mass spectrum of a thf-reaction solution of **1a** recorded in the negative ion mode. The simulated pattern is shown as bar graph in red below.

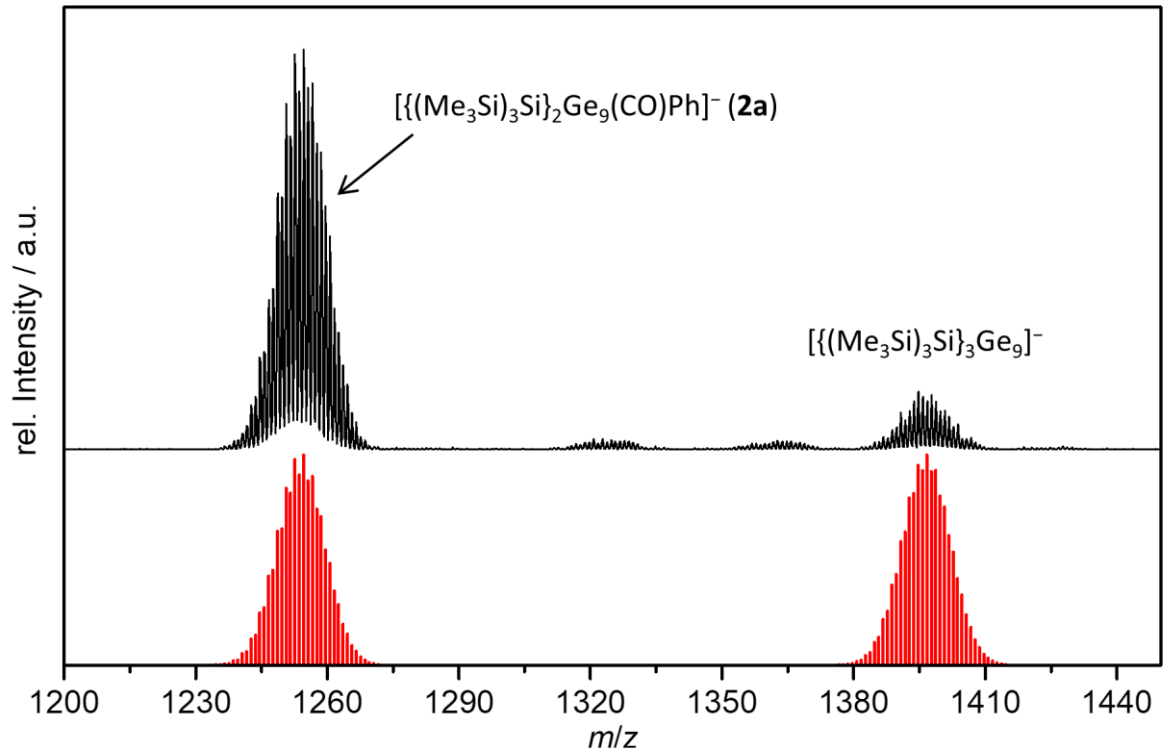

Figure S8. ESI mass spectrum of a thf-reaction solution of **2a** recorded in the negative ion mode. The simulated pattern is shown as bar graph in red below.

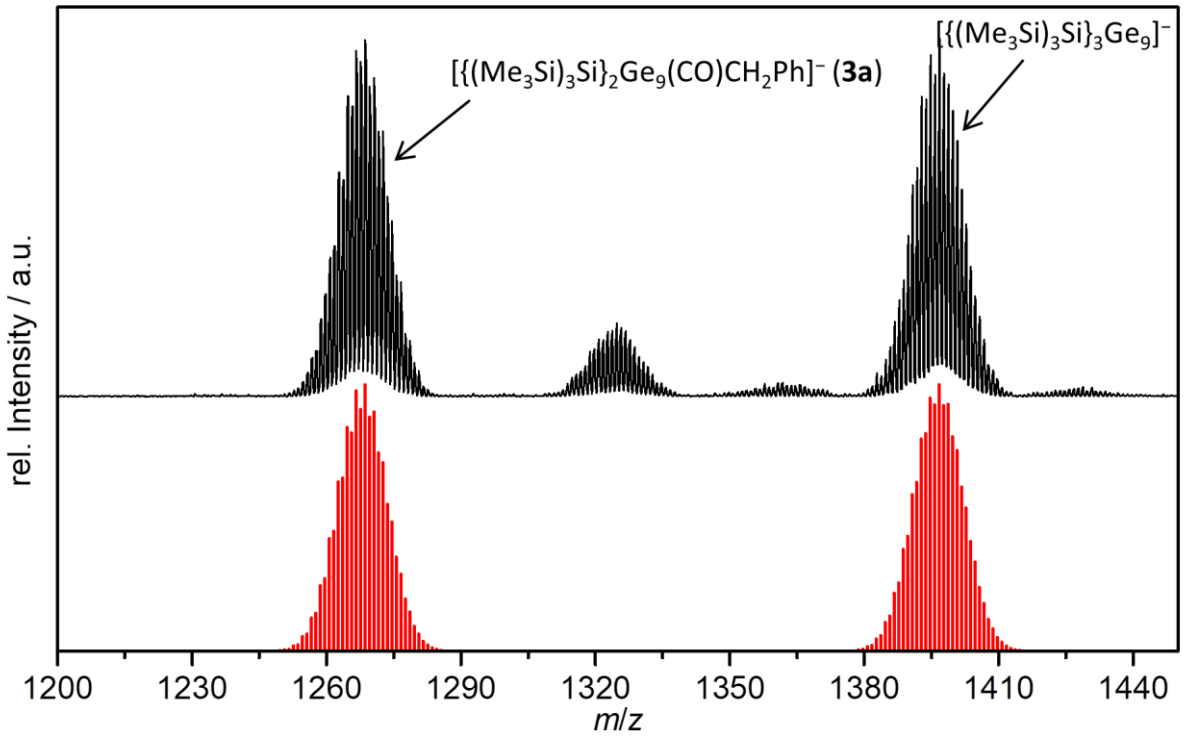

Figure S9. ESI mass spectrum of a thf-reaction solution of **3a** recorded in the negative ion mode. The simulated pattern is shown as bar graph in red below.

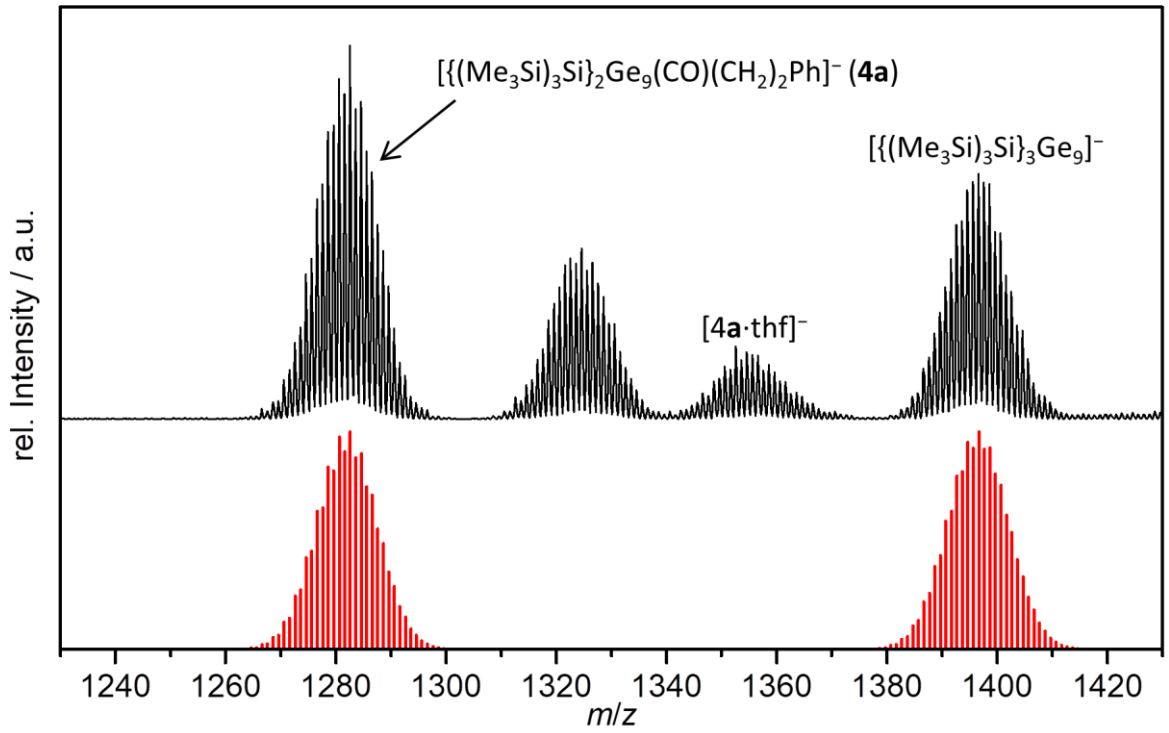

Figure S10. ESI mass spectrum of a thf-reaction solution of **4a** recorded in the negative ion mode. The simulated pattern is shown as bar graph in red below.

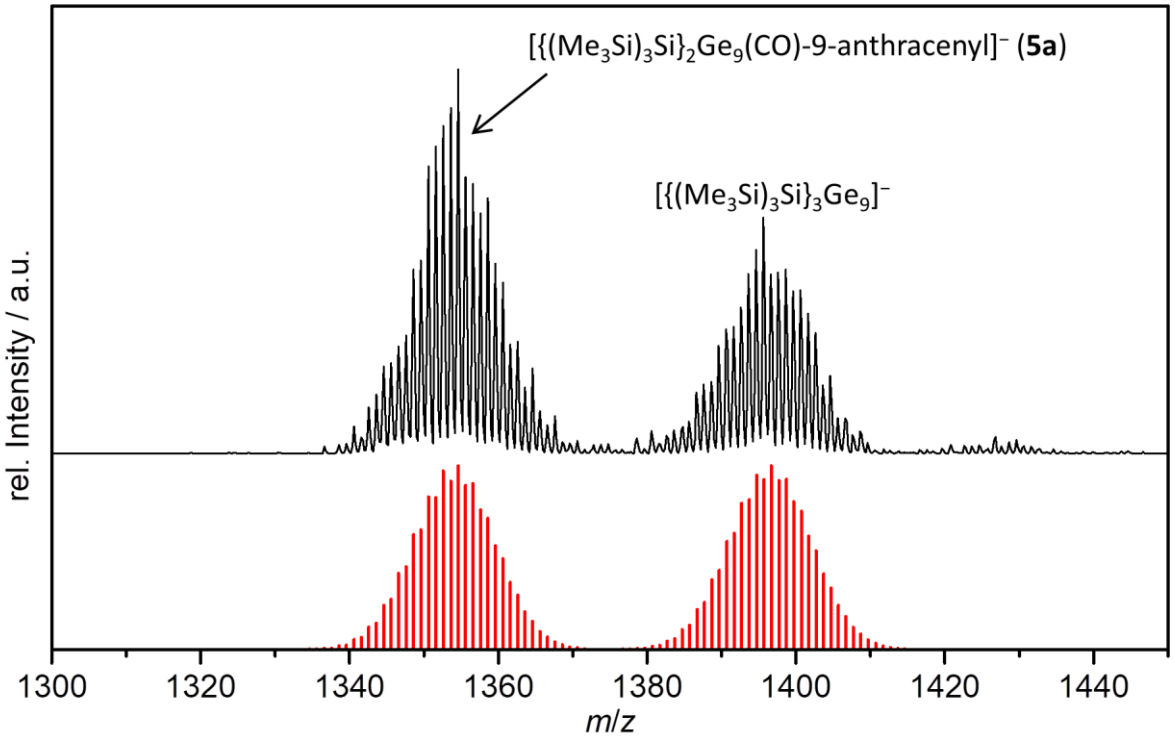

Figure S11. ESI mass spectrum of a thf-reaction solution of **5a** recorded in the negative ion mode. The simulated pattern is shown as bar graph in red below.

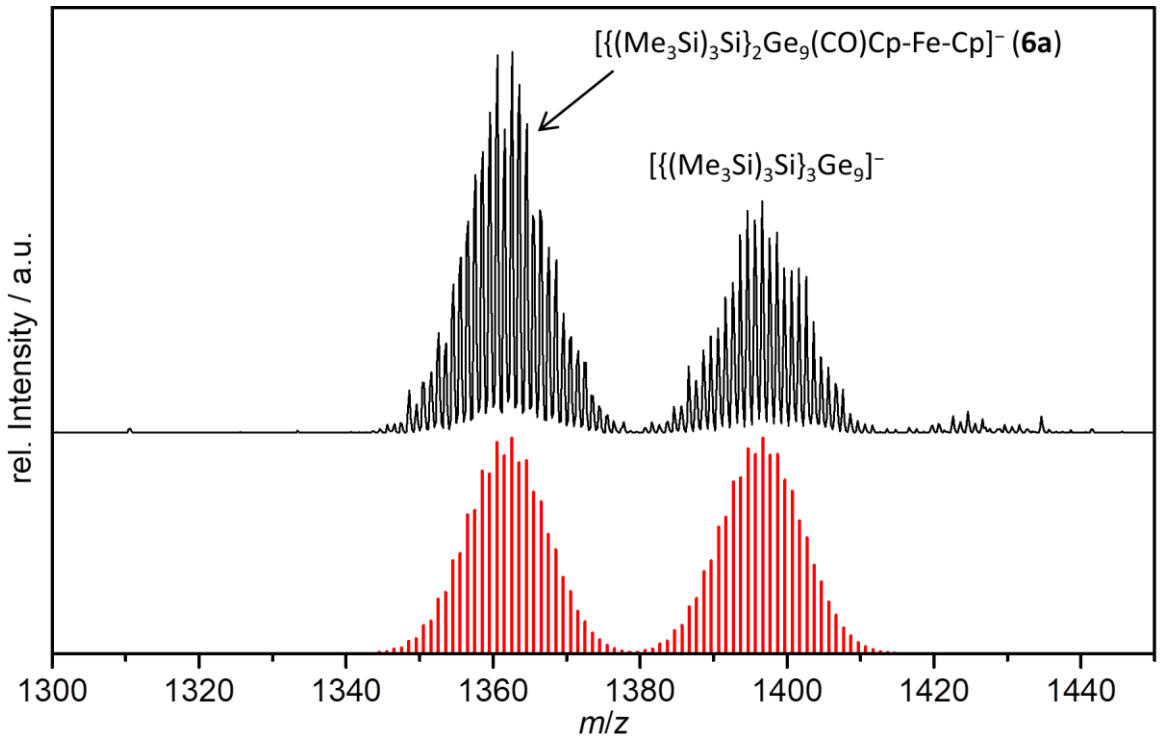

Figure S12. ESI mass spectrum of a thf-reaction solution of **6a** recorded in the negative ion mode. The simulated pattern is shown as bar graph in red below.

5.9 Three-dimensional Covalent Linkage of four Deltahedral Ge_9 Clusters *via* a Central sp^3 Hybridized Ge Atom: Synthesis and Crystal Structure of $K_4[\{Me_3Si)_3Si\}_2Ge_9]_4Ge$

Sabine Frischhut, Peter Jutzi, and Thomas F. Fässler

Manuscript for publication

5.9.1 Content and Contribution

Within the scope of this work the first covalent three-dimensional linkage of Ge_9 clusters was achieved by the linkage of four $[\{(Me_3Si)_3Si\}_2Ge_9]^-$ entities *via* a central Ge(IV) atom. The compound $K_4[\{Me_3Si)_3Si\}_2Ge_9]_4Ge$ was crystallized from a reaction solution of $K_2[\{(Me_3Si)_3Si\}_2Ge_9]$ with $[SiCp^*][B(C_6F_5)_4]$ in the presence of $[Li(OEt_2)_x][B(C_6F_5)_4]$ in fluorobenzene. $K_4[\{Me_3Si)_3Si\}_2Ge_9]_4Ge$ was characterized by single crystal X-ray diffraction and temperature dependent ^1H NMR spectroscopy.

The crystal structure shows that four Ge_9 clusters with C_S-symmetry are interconnected in a tetrahedral arrangement around the central Ge(IV) atom. Each cluster bears a negative charge, and thus, is available for further reactions, which might allow for the build-up of three-dimensional frameworks.

All experiments including syntheses, single crystal X-ray data collection and structure refinement, as well as NMR spectroscopic investigations and data evaluation were carried out within this work. Dr. Wilhelm Klein supported the refinement of single crystal X-ray data.

Prof. Dr. Peter Jutzi generously provided decamethylsilicocene, from which $[SiCp^*][B(C_6F_5)_4]$ is accessible. He also contributed fruitfully to discussions.

The manuscript was authored within this thesis and was revised by Prof. Dr. Thomas F. Fässler.

5.9.2 Manuscript for Publication

Three-dimensional Covalent Linkage of Four Deltahedral Ge_9 Clusters *via* a Central sp^3 Hybridized Ge Atom: Synthesis and Crystal Structure of $K_4[\{Me_3Si)_3Si\}_2Ge_9]_4Ge$

Sabine Frischhut,[a] Peter Jutzi,[b] and Thomas F. Fässler[a]

[a] Sabine Frischhut, Prof. Dr. Thomas F. Fässler
Department Chemie, Technische Universität München
Lichtenbergstraße 4, 85747 Garching, Germany
Email: thomas.faessler@lrz.tum.de

[b] Prof. em. Dr. Peter Jutzi
Department Chemie, Universität Bielefeld
33615 Bielefeld, Germany

ABSTRACT

Nanostructured Ge materials have a high potential for application in semiconductor devices. In this respect, a three-dimensional linkage of Ge_9 clusters is indispensable, which had been unknown to achieve for a long time. We present the first example of four covalently connected Ge_9 clusters, being linked by one sp^3 hybridized germanium atom. $K_4[\{Me_3Si)_3Si\}_2Ge_9]_4Ge$ is synthesized by partly *in situ* oxidation of Ge_9 clusters in a reaction mixture consisting of $K[\{(Me_3Si)_3Si\}_2Ge_9]$, $[SiCp^*][B(C_6F_5)_4]$ and $[Li(OEt_2)_x][B(C_6F_5)_4]$ in fluorobenzene. The structure of $K_4[\{Me_3Si)_3Si\}_2Ge_9]_4Ge$ is determined by single crystal X-ray diffraction. Such three-dimensional linkage of deltahedral Ge_9 clusters is of high interest for the generation of porous high-surface Ge-based structures.

INTRODUCTION

Structured porous semiconductor materials of group 14 are investigated for application in energy storage, sensing, photovoltaics, microelectronics and photonics due to their high surface to bulk atom ratio and their flexibility upon volume change. Especially nanostructured Ge materials show outstanding optical properties strongly depending on the size of particles.[1-2] Compared to silicon, germanium shows increased charge-carrier mobility, which directed the focus of research more towards the synthesis of Ge nanostructured materials.[3] For preparation of such materials several different methods have been applied, e.g. electrochemical deposition[4] and template-driven methods[5-9].

Also, $[Ge_9]^{4-}$ Zintl clusters have been used as precursor to build up amorphous or crystalline Ge nanostructures.[6, 8-11] The reaction of the residue of a K_4Ge_9 solution containing $[Ge_9]^{4-}$ clusters with $GeCl_4$ causes a comproportionation and formation of amorphous germanium. Applying a template allows the amorphous germanium to adapt a mesoporous structure. Retention of the Ge_9 cluster core in the mesoporous structures has not been reported, so far.[8] Yet, intact clusters within such defined 3D structures would lead to an even higher surface to bulk ratio of Ge atoms. To achieve this, a controlled way of covalent linkage of Ge_9 clusters, generating a 3D network, is of special interest.

Already in the early beginning of the investigations on the reactivity of deltahedral Ge_9 clusters in solution, 1D structures, where two or more bare ligand-free Ge_9 clusters are oxidatively coupled and thus, covalently interconnected *via* one or even two covalent bonds, such as in the $[Ge_9–Ge_9]^{6-}$ dimer,[12-14] $[Ge_9=Ge_9=Ge_9]^{6-}$ trimer,[15] $[Ge_9=Ge_9=Ge_9=Ge_9]^{8-}$ tetramer[16] and in the $^1_\infty[Ge_9]^{2-}$ polymer[17-18], were reported (Figure 1). Comparable cables containing deltahedral Ge_9 clusters coordinated to late transition metals were realized in $^1_\infty[Ge_9Hg]^{2-}$ [19-20] and $^1_\infty[Ge_9Zn]^{2-}$ [21]. Covalent linkage of four Ge_9 clusters by connection through sp^3-Ge atom bridges and further coordination to three Au atoms has been achieved in $[Au_3Ge_{45}]^{9-}$. The latter emerged from the reaction of K_4Ge_9 with $[AuCl(PPh_3)]$ in ethylenediamine. Apparently, sp^3-Ge atoms are generated in situ by oxidation of Ge_9 clusters (Figure 1).[22] Kanatzidis and co-workers realized the idea of simple oxidative self-polymerization of $[Ge_9]^{4-}$ in the presence of a cationic surfactant in ethylenendiamine to

generate high-surface mesoporous germanium. The electronic structure is tunable by adsorption of donor acceptor molecules in the interior of the mesopores.[23]

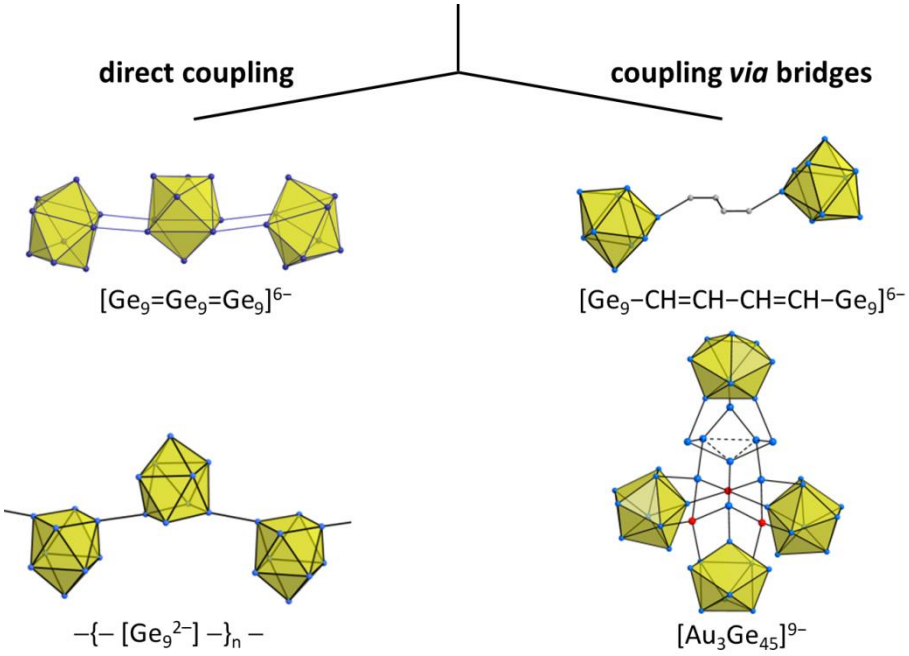

Figure 1. Comparison of the state-of-the-art linked Ge_9 structures containing interconnected deltahedral Ge_9 clusters.

Organo-functionalization of Ge_9 clusters in ethylenediamine made further covalently linked structures accessible, the fullerene triad analogous Zintl triads, where two deltahedral Ge_9 clusters are connected *via* a conjugated organic buta-1,3-dienyl bridge as is given in $[RGe_9-CH=CH-CH=CH-Ge_9-R]^{4-}$ (R = (2*Z*,4*E*)-7-amino-5-azahepta-2,4-dien-2-yl or vinyl) and $[Ge_9-CH=CH-CH=CH-Ge_9]^{6-}$ (Figure 1).[24-26] Successful extended 1D, 2D or 3D linkage *via* organic linking units has not been reported, so far.

In recent years, the silylation of the $[Ge_9]^{4-}$ cluster was found to be very helpful to reduce the charge and this way enhance solubility in convenient solvents. Both, the threefold and twofold silylated clusters, $[\{(Me_3Si)_3Si\}_3Ge_9]^-$ [27] and $[\{(Me_3Si)_3Si\}_2Ge_9]^{2-}$ [28] emerged by reaction of K_4Ge_9 with the respective equivalents of chloro-tris(trimethylsilyl)silane in acetonitrile. Variation of the silyl ligands made several new structures accessible,[29-30] most importantly the Zintl anion $[\{(HC=CH(CH_2)_n)Ph_2Si\}_3Ge_9]^-$ (n = 0, 3).[31] Such Ge_9 clusters, decorated with a terminal double bond has also been realized in the neutral compound $\{(Me_3Si)_3Si\}_3Ge_9(CH_2)_3CH=CH_2$.[32] Both clusters can, in principle, serve as monomer in polymerization reactions forming polymers comprising an organic backbone with Ge_9 clusters attached to it. Using $[\{Me_3Si)_3Si\}_2Ge_9]^{2-}$ as starting point the linkage of two such

entities *via* a third silyl ligand, $[\{(Me_3Si)Si\}_2Ge_9{-}SiMe_2{-}C_6H_4{-}Me_2Si{-}Ge_9\{Si(SiMe_3)\}_2]^{2-}$, was achieved.[33]

In theoretical studies, Takahashi and coworkers predicted the first honeycomb structure consisting of 2D linked deltahedral Ge_9 clusters, which is generated by *in situ* desilylation of $[\{Me_3Si)_3Si\}_3Ge_9]^-$, step-wisely forming $[R_2Ge_9]_2^{2-}$, $[RGe_9]_6^{6-}$ and finally the extended 2D array $[\{Ge_9^-\}_3]_\infty$. The porous structures might have a potential for tunable band gaps.[34]

Experimentally obtained 3D linked deltahedral Ge_9 clusters had not been reported, yet. Nevertheless, according to theoretical studies, oxidative interconnection of Ge_9 Zintl clusters in different directions could result in 2D sheets, fullerene-like cage-structures and three dimensional zeolite-like frameworks.[35] In addition, quantum chemical calculations revealed that $[Ge_9]^{4-}$-analogous $[Si_9]^{4-}$ clusters can in principle be linked *via* a central sp^3 hybridized Si atom, resulting in the formation of the stable anions $[SiCl_{4-n}(Si_9)_n]^{3n-}$, which contain up to four interconnected Si_9 clusters (Figure 2 a).[36] The $[(Si_9)_4Si]^{12-}$ unit can be further interconnected building up the 2D chessboard structure ${}^2_\infty\{[Si_9]Si_2\}_n^{chess}$ as depicted in Figure 2 b.

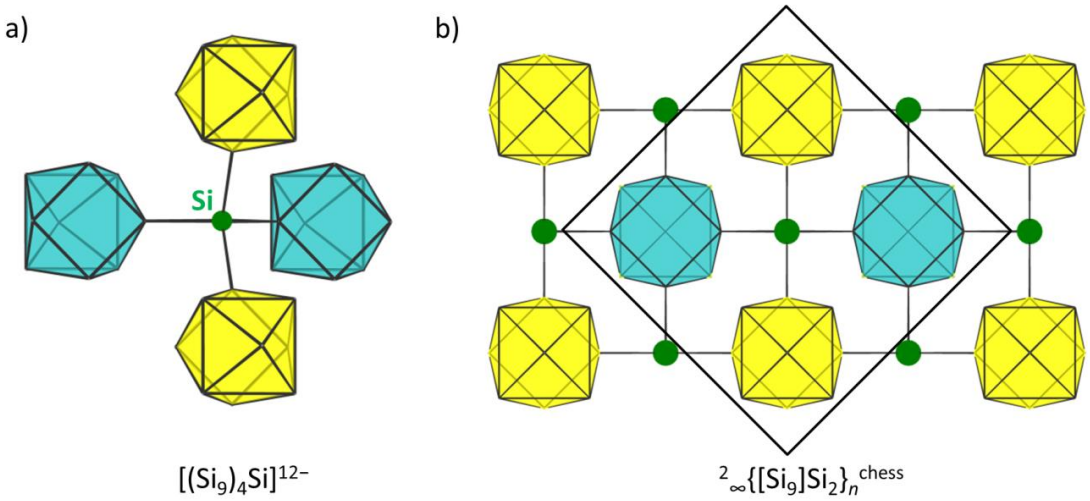

Figure 2. Schematic presentation of interconnected clusters in a) predicted $[(Si_9)_4Si]^{12-}$ [36] and b) predicted ${}^2_\infty\{[Si_9]Si_2\}_n^{chess}$. The different colors indicate different orientations.

During the course of our investigations aiming at the extension of Ge_9 clusters with additional vertices,[21, 37-38] we studied the reaction of $[\{(Me_3Si)_3Si\}_2Ge_9]^{2-}$ with $[SiCp^*]^+$. The reaction of $K_2[\{(Me_3Si)_3Si\}_2Ge_9]$ with $[SiCp^*][B(C_6F_5)_4]$ in the presence of $[Li(OEt_2)_x][B(C_6F_5)_4]$ in fluorobenzene at r.t. results in the unexpected formation of single crystals of

$K_4[\{Me_3Si)_3Si\}_2Ge_9]_4Ge$, which represents the first example of four $[\{(Me_3Si)_3Si\}_2Ge_9]$ entities interconnected *via* a central sp^3 hybridized Ge atom. $K_4[\{Me_3Si)_3Si\}_2Ge_9]_4Ge$ was characterized by single crystal X-ray diffraction and NMR spectroscopy.

DISCUSSION

The reaction of equimolar amounts of $K_2[\{Me_3Si)_3Si\}_2Ge_9]$, $[SiCp^*][B(C_6F_5)_4]$ and $[Li(OEt_2)_x][B(C_6F_5)_4]$ in fluorobenzene at r.t. reproducibly lead to the crystallization of $K_4[\{Me_3Si)_3Si\}_2Ge_9]_4Ge$ (**1**) after storage at −32 °C for two weeks. The formation of **1** is unexpected as fragments of $[SiCp^*][B(C_6F_5)_4]$ do not show up in the product.

Crystal structure

The unit cell of **1** contains four asymmetric units, each of which comprises ten solvent molecules, four potassium cations and one cluster unit $[[\{Me_3Si)_3Si\}_2Ge_9]_4Ge]^{4-}$ (**1a**), indicating a fourfold negatively charged anion **1a**. In the anion **1a**, four $[\{(Me_3Si)_3Si\}_2Ge_9]^-$-clusters are covalently connected through a vertex to a central Ge atom (Ge1) (Figure 3 a). The latter shows a distorted tetrahedral coordination sphere with angles lying in the range of 103.92(2) and 115.15(3)°. The $Ge1-Ge_{cluster}$ *exo*-bond lengths of 2.4174(7) (d(Ge29−Ge1)) to 2.4313(7) Å (d(Ge20−Ge1)) are slightly shorter compared to already known $Ge_{cluster}-Ge_{cluster}$ *exo*-bond lengths of, e.g. 2.488(2) Å in the dimer $[(Ge_9)-(Ge_9)]^{6-}$ [12] and 2.486(1) Å in the polymer $^1_\infty[Ge_9]^{2-}$.[17] In comparison, $Ge_{cluster}-Ge_{atom}$ *exo*-bond lengths in $[Au_3Ge_{45}]^{9-}$ of 2.481(5) to 2.489(5) Å are in the same range as well.[22] These distances are comparable to already known Ge−Ge single bonds.[39]

The four covalently connected Ge_9 clusters are crystallographically independent. The Ge_9 clusters (I-IV) in **1a** are similar in terms of structural characteristics. Figure 2 b gives the structure of cluster I, which is representative of the other clusters II-IV, the relevant structural parameters of clusters I-IV are listed in Table 1.

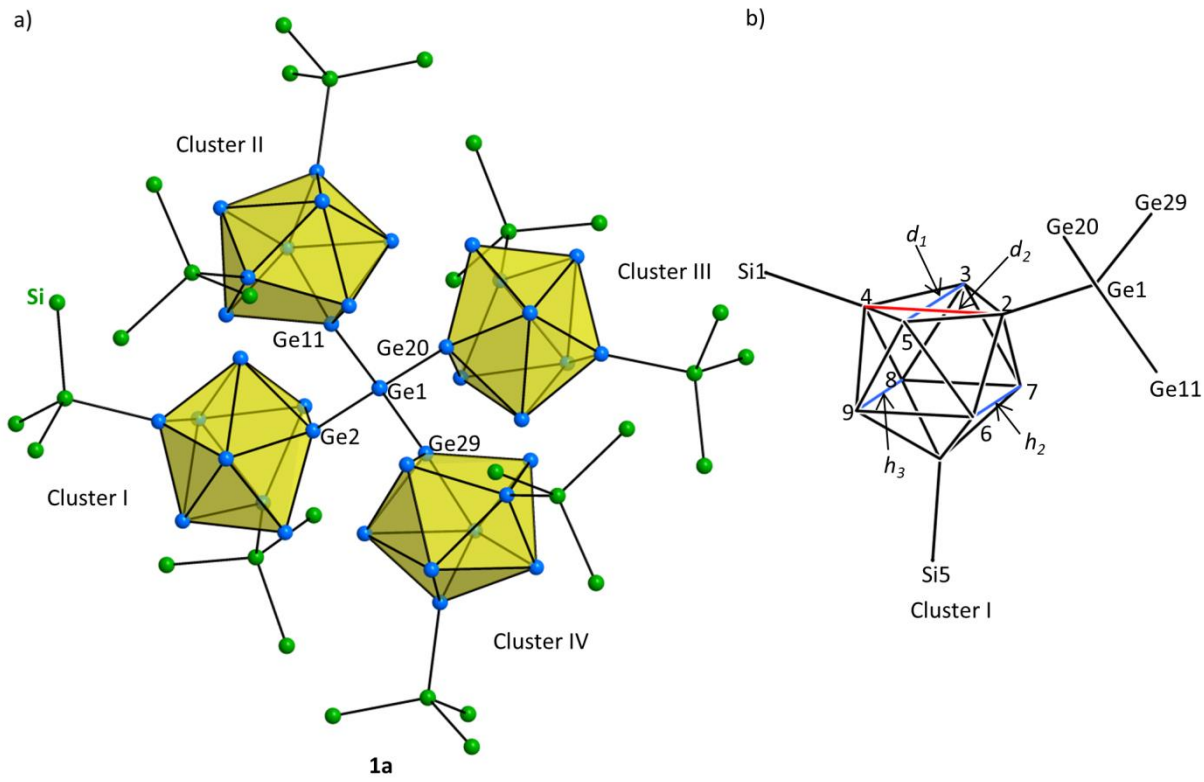

Figure 2. a) Structure of **1a**. The Ge_9 clusters are shown as yellow polyhedra. The methyl groups of the silyl ligands are omitted for clarity. Color code: Ge – blue, Si – green. b) Structure of cluster I including the parameters used for the description of the cluster structure. Values are given in Table 1. d_1 and d_2 reflect the diagonals of the open square face. *h* represents the height of the trigonal prism depicted in blue. h_1 is equal to d_1.

Table 1. Structural parameters of clusters I-IV of the anion **1a**.[40] α represents the dihedral angle. In case of cluster I, α is defined as the angle between the planes Ge2-Ge3-Ge4 and Ge2-Ge5-Ge4.

	cluster I	cluster II	cluster III	cluster IV
d_1 [Å]	3.9190(7)	3.8565(7)	3.9162(7)	3.7730(8)
d_2 [Å]	3.2991(7)	3.3567(7)	3.3104(7)	3.4047(7)
d_1/d_2	1.19	1.15	1.18	1.11
h_2 [Å]	3.1090(7)	3.2146(8)	3.1314(8)	3.3146(8)
h_3 [Å]	3.1310(7)	3.1790(8)	3.1145(8)	3.1846(8)
α [°]	169.8	165.9	169.8	162.1

As indicated in Table 1, the prism height d_1 appears elongated compared to h_2 and h_3, which show similar values, leading to exclusion of a D_{3h}-symmetric cluster core. The ratio of the diagonals d_1/d_2 shows a value significantly above 1. The dihedral angles α, do not significantly deviate from 180°. As a conclusion, the cluster cores adapt a distorted mono-

capped square antiprism with C_{2v}-symmetry, which has so far been typical of two-fold substituted Ge_9 clusters.[41-42] The Ge−Ge bond distances within the cores are very similar and lie in the range of 2.5116(7) Å and 3.2146(8) Å. Each cluster carries two silyl ligands, one of them is situated at a vertex of the open square, and the other one is located at the square-capping vertex. The interconnection of the four clusters by the central Ge1 occurs *via* the vertex of the open square oppositely positioned to the silyl ligand substituted Ge atom.

Each of the four potassium cations belonging to **1** is coordinated by Ge atoms of three different Ge_9 clusters in three different coordination modes. One cluster coordinates to K in an η^4-fashion *via* the open square face, the second cluster in η^2-fashion *via* two neighbored Ge atoms and the third one in η^1-fashion *via* a single Ge atom (Figure 3 a). This in turn means that each cluster is coordinated to three potassium cations in three different coordination modes (see supporting information, Figure S1). The potassium cations are connected *via* a distorted tetrahedron surrounding the inner tetrahedron consisting of Ge atoms of the four connected Ge_9 clusters (Figure 3 b). In addition, two potassium cations (K2 and K4) are additionally coordinated by two solvent molecules. Each cluster of **1a** is one-fold negatively charged.

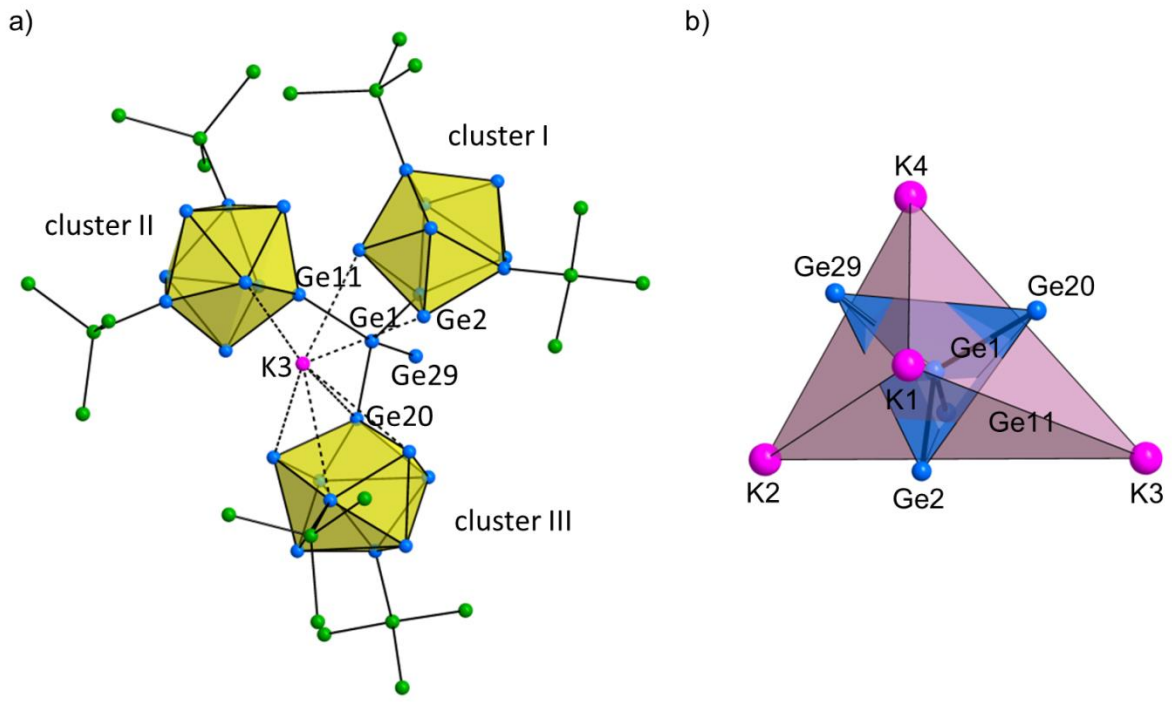

Figure 3. a) Excerpt of the structure of **1**. The Ge_9 clusters are shown as yellow polyhedra. The methyl groups of the silyl ligands are omitted for clarity. b) Interpenetrating tetrahedrons formed by the coordinated potassium cations (depicted in purple) and the germanium atoms bound to the central Ge1 (depicted in blue). All atoms are shown as spheres. Color code: Ge – blue, Si – green, K – pink.

Mechanistic considerations

A solution containing solely 1 equiv. of $K_2[\{Me_3Si)_3Si\}_2Ge_9]$ and 1 equiv. of $[Li(OEt_2)_x][B(C_6F_5)_4]$ in fluorobenzene does not lead to crystallization of the desired product. Therefore, the mechanism of the formation of **1** seems complex and is believed to proceed by stepwise oxidation of the Ge_9 cluster in presence of $[SiCp^*][B(C_6F_5)_4]$ at r.t., which offers comparatively mild conditions for the linkage of four Ge_9 clusters. *In situ* studies revealed, that a simple reaction of $K_2[\{Me_3Si)_3Si\}_2Ge_9]$ with germanium tetrachloride does not lead to the formation of the desired product **1**. Ge_9 cluster fragmentation in solution has been observed in few cases, e.g. the formation of the pristine $[Ge_{10}]^{2-}$ cluster by simple dissolution of Rb_4Ge_9 in ethylenediamine, which shows the flexibility, but also mild oxidation of the $[Ge_9]^{4-}$ clusters in solution.[43] Also, the formation of the latter was observed by reaction of K_4Ge_9 with $Mn_2(CO)_{10}$ in ethylenediamine forming the complex $[Ge_{10}Mn(CO)_4]^{3-}$.[44] The structure of $[Au_3Ge_{45}]^{9-}$ bears four Ge_9 clusters, which are covalently interconnected by *exo*-bonded Ge-bridges. The Ge bridges must be formed by *in situ* oxidation of Ge_9 clusters.[22]

NMR spectroscopic investigations

The isolated crystals of **1** are soluble in fluorobenzene and tetrahydrofurane. Temperature-dependent NMR studies of the isolated crystals of **1** in tetrahydrofurane-d_8 showed only one signal in the region of the silyl ligands, which is rather unexpected. According to the crystal structure each cluster carries two magnetically inequivalent silyl ligands which therefore should show two peaks with an integrals ratio of 1:1. Therefore dynamic behavior of **1** in solution is expected, even though a coalescence temperature could not be detected. So far, dynamic processes in solution have been reported for neutral Ge_9 cluster compounds of the formulae R_3Ge_9R' (R = silyl ligand, R' = organic substituent).[32, 45-46] Upon warming to r.t., **1** decomposes. At temperatures above r.t. most likely the threefold silylated species is formed, which can be concluded from the shifted signal of the silyl ligands from δ = 0.35 ppm to δ = 0.24 ppm in tetrahydrofurane-d_8 (Figure S2, supporting information).

CONCLUSION

With $K_4[\{Me_3Si)_3Si\}_2Ge_9]_4Ge$, the first example of covalent 3D linkage of deltahedral Ge_9 clusters is presented. The compound consists of four interconnected $[\{(Me_3Si)_3Si\}_2Ge_9]^-$ cluster entities and a central sp^3 Ge atom, whereby each cluster bears one negative charge. The anion is an ideal potential candidate for follow-up reactions, especially for building up 3D Ge_9 cluster networks, which might exhibit outstanding electronic properties.

EXPERIMENTAL

General: All manipulations were carried out under a purified argon atmosphere using standard Schlenk techniques. The Zintl phase with the nominal composition K_4Ge_9 was synthesized by heating a stoichiometric mixture of the elements K and Ge (99.999%, Chempur) at 650 °C for 46 h in a stainless steel autoclave.[47] Fluorobenzene (Alfa Aesar, 99%) was dried over calcium hydride. The deuterated solvents tetrahydrofurane-d_8 was purchased from Deutero GmbH, degassed applying freeze-pump-thaw technique and stored over molecular sieve (3 Å) for at least one day. The commercially available reagent $[Li(OEt_2)_x][B(C_6F_5)_4]$ (TCI Chemicals, > 70%) was used as received. $K_2[\{Me_3Si)_3Si\}_2Ge_9]$ and $[Cp^*Si][B(C_6F_5)_4]$ were prepared according to literature procedures.[28, 48]

Synthesis of $K_4[\{Me_3Si)_3Si\}_2Ge_9]_4Ge$ (1): To a suspension of $K_2[\{Me_3Si)_3Si\}_2Ge_9]$ (150 mg, 0.122 mmol) and $[Li(OEt_2)_x][B(C_6F_5)_4]$ (84 mg, 0.122 mmol) in 2 mL fluorobenzene a solution of $[Cp^*Si][B(C_6F_5)_4]$ (103 mg, 0.122 mmol) in 4 mL fluorobenzene was added. The brown-colored solution was stirred for 2.5 h at r.t. The reaction solution was filtered over glass fiber filter and concentrated to approximately 0.75 mL and stored at −32 °C for crystallization. Deep-brown block-shaped crystals suitable for single crystal X-ray crystallography were obtained (yield: 8%) after two weeks. For further spectroscopic analysis the crystals were separated from the mother liquor, washed with 0.2 mL hexane and dried in vacuum. ^{1}H NMR (400 MHz, thf-d_8, 293 K): δ (ppm) 0.35.

X-ray Data Collection and Structure Determination: The crystals were transferred from the mother liquor into perfluoropolyalkylether under a cold stream of N_2. A single crystal was fixed on a glass fiber and positioned in a cold stream of N_2. The intensity data were recorded on a Stoe StadiVari diffractometer (Mo K_α radiation (λ = 0.71073 Å), Pilatus 300K detector), by using the X-Area software package.[49] The crystal structures were solved by Direct Methods and refined using the SHELX software.[50] The positions of the hydrogen atoms were calculated and refined using a riding model. All non-hydrogen atoms were treated with anisotropic displacement parameters except for some solvent molecules. Four solvent molecules of fluorobenzene per unit cell were treated with the Squeeze option of the program Platon.[51-52] Crystallographic details on **1** are listed in Table 1. CCDC xxx contains the supplementary crystallographic data. These data can be obtained free of charge from The Cambridge Crystallographic Data Centre *via* www.ccdc.cam.ac.uk/data_request/cif.

Table 1. Crystallographic details on the crystal structure of **1**.

Compound	**1**·10 FPh
Formula	$K_4C_{132}H_{266}F_{10}Ge_{37}Si_{32}$
fw ($g \cdot mol^{-1}$)	5784.54
space group (no)	P21/n (14)
a (Å)	26.2650(3)
b (Å)	26.1386(3)
c (Å)	36.8175(4)
α (deg)	90
β (deg)	106.585(1)
γ (deg)	90
V ($Å^3$)	24224.8(5)
Z	4
T (K)	150
λ (Å)	0.71073
ρ_{calcd} ($g \cdot cm^{-3}$)	1.586
μ (mm^{-1})	4.778
collected reflections	740071
independent reflections	47576
R_{int}	0.090
parameters/ restraints	1972/ 6
R_1 [$I>2\sigma(I)$ / all data]	0.072/0.048
wR_2 [$I>2\sigma(I)$ / all data)]	0.108/0.099
goodness of fit	1.067
max. / min. diff. el. density	1.60 / −0.86

Electron-Dispersive X-ray (EDX) Analysis: The composition concerning the elements Si and Ge of the single crystal of **1** which was used to determine the crystal structure was analyzed with a Hitachi TM-1000 tabletop microscope.

NMR Spectroscopy: NMR spectra were recorded on a BRUKER Avance Ultrashield AV400 spectrometer. The signals were referenced to the residual proton signal of the deuterated solvent tetrahydrofurane-d_8 (δ = 3.58 ppm). The chemical shifts are given in δ values in parts per million (ppm). The multiplicities are depicted as follows: s – singlet.

Supporting Information (see footnote on the first page of this article):
Further details of the crystal structure of **1**, as well as NMR spectra are given in the Supporting Information.

ACKNOWLEDGMENT

The authors thank the Bayerische Staatsministerium für Wirtschaft und Medien, Energie und Technologie within the program "Solar Technologies go Hybrid" for financial support. Dr. Wilhelm Klein is acknowledged for his help with structure determination. Moreover, the authors thank Nicole Willeit for preparation of reaction solutions, as well as Maria Weindl for temperature-dependent NMR studies.

REFERENCES

[1] A. Stein, *Nature* **2006**, *441*, 1055-1056.
[2] D. D. Vaughn II, R. E. Schaak, *Chem. Soc. Rev.* **2013**, *42*, 2861-2879.
[3] R. Pillarisetty, *Nature* **2011**, *479*, 324.
[4] X. Meng, R. Al-Salman, J. Zhao, N. Borissenko, Y. Li, F. Endres, *Angew. Chem. Int. Ed.* **2009**, *48*, 2703-2707.
[5] G. S. Armatas, M. G. Kanatzidis, *Nature* **2006**, *441*, 1122.
[6] M. G. Kanatzidis, *Adv. Mater.* **2007**, *19*, 1165-1181.
[7] M. H. Park, K. Kim, J. Kim, J. Cho, *Adv. Mater.* **2010**, *22*, 415-418.
[8] M. M. Bentlohner, M. Waibel, P. Zeller, K. Sarkar, P. Müller-Buschbaum, D. Fattakhova-Rohlfing, T. F. Fässler, *Angew. Chem. Int. Ed.* **2016**, *55*, 2441-2445.
[9] S. Geier, R. Jung, K. Peters, H. A. Gasteiger, D. Fattakhova-Rohlfing, T. F. Fässler, *Sustainable Energy Fuels* **2018**, *2*, 85-90.
[10] N. Chandrasekharan, S. C. Sevov, *J. Electrochem. Soc.* **2010**, *157*, C140-C145.
[11] D. Sun, A. E. Riley, A. J. Cadby, E. K. Richman, S. D. Korlann, S. H. Tolbert, *Nature* **2006**, *441*, 1126.
[12] L. Xu, S. C. Sevov, *J. Am. Chem. Soc.* **1999**, *121*, 9245-9246.
[13] R. Hauptmann, T. F. Faessler, *Z. Anorg. Allg. Chem.* **2003**, *629*, 2266-2273.
[14] A. Nienhaus, S. D. Hoffmann, T. F. Fässler, *Z. Anorg. Allg. Chem.* **2006**, *632*, 1752-1758.
[15] A. Ugrinov, S. C. Sevov, *J. Am. Chem. Soc.* **2002**, *124*, 10990-10991.
[16] A. Ugrinov, S. C. Sevov, *Inorg. Chem.* **2003**, *42*, 5789-5791.
[17] C. Downie, Z. Tang, A. M. Guloy, *Angew. Chem. Int. Ed.* **2000**, *39*, 337-340.
[18] C. Downie, J.-G. Mao, H. Parmar, A. M. Guloy, *Inorg. Chem.* **2004**, *43*, 1992-1997.
[19] A. Nienhaus, R. Hauptmann, T. F. Fässler, *Angew. Chem. Int. Ed.* **2002**, *41*, 3213-3215.

[20] M. B. Boeddinghaus, S. D. Hoffmann, T. F. Fässler, *Z. Anorg. Allg. Chem.* **2007**, *633*, 2338-2341.
[21] K. Mayer, L.-A. Jantke, S. Schulz, T. F. Fässler, *Angew. Chem. Int. Ed.* **2017**, *56*, 2350-2355.
[22] A. Spiekermann, S. D. Hoffmann, T. F. Fässler, I. Krossing, U. Preiss, *Angew. Chem. Int. Ed.* **2007**, *46*, 5310-5313.
[23] G. S. Armatas, M. G. Kanatzidis, *Adv. Mater.* **2008**, *20*, 546-550.
[24] M. M. Bentlohner, W. Klein, Z. H. Fard, L. A. Jantke, T. F. Fässler, *Angew. Chem. Int. Ed.* **2015**, *54*, 3748-3753.
[25] S. Frischhut, M. M. Bentlohner, W. Klein, T. F. Fässler, *Inorg. Chem.* **2017**, *56*, 10691-10698.
[26] M. M. Bentlohner, S. Frischhut, T. F. Fässler, *Chem. Eur. J.* **2017**, *23*, 17089-17094.
[27] F. Li, S. C. Sevov, *Inorg. Chem.* **2012**, *51*, 2706-2708.
[28] O. Kysliak, A. Schnepf, *Dalton Trans.* **2016**, *45*, 2404-2408.
[29] K. Mayer, L. J. Schiegerl, T. F. Fässler, *Chem. Eur. J.* **2016**, *22*, 18794-18800.
[30] O. Kysliak, T. Kunz, A. Schnepf, *Eur. J. Inorg. Chem.* **2017**, *4*, 805-810.
[31] K. Mayer, L. J. Schiegerl, T. Kratky, S. Günther, T. F. Fässler, *Chem. Commun.* **2017**, *53*, 11798-11801.
[32] S. Frischhut, T. F. Fässler, *Dalton Trans* **2018**, *47*, 3223-3226.
[33] O. Kysliak, C. Schrenk, A. Schnepf, *Inorg. Chem.* **2017**, *56*, 9693-9697.
[34] A. Muñoz-Castro, K. Takahashi, *J. Phys. Chem. C* **2017**, *121*, 1934-1940.
[35] A. J. Karttunen, T. F. Fässler, M. Linnolahti, T. A. Pakkanen, *ChemPhysChem* **2010**, *11*, 1944-1950.
[36] L.-A. Jantke, T. F. Fässler, *Inorganics* **2018**, *6*, 31.
[37] F. Li, A. Muñoz-Castro, S. C. Sevov, *Angew. Chem. Int. Ed.* **2016**, *55*, 8630-8633.
[38] S. Frischhut, F. Kaiser, W. Klein, M. Drees, F. E. Kühn, T. F. Fässler, *Organometallics* **2018**, *37*, 4560-4567.
[39] W. B. Pearson, *Crystal Chemistry and Physics of Metals and Alloys*, Wiley, New York, **1972**.
[40] C. B. Benda, J. Q. Wang, B. Wahl, T. F. Fässler, *Eur. J. Inorg. Chem.* **2011**, *27*, 4262-4269.
[41] M. W. Hull, S. C. Sevov, *Inorg. Chem.* **2007**, *46*, 10953-10955.
[42] M. W. Hull, S. C. Sevov, *J. Am. Chem. Soc.* **2009**, *131*, 9026-9037.
[43] M. M. Bentlohner, C. Fischer, T. F. Fässler, *Chem. Commun.* **2016**, *52*, 9841-9843.
[44] D. Rios, S. C. Sevov, *Inorg. Chem.* **2010**, *49*, 6396-6398.
[45] F. Li, S. C. Sevov, *J. Am. Chem. Soc.* **2014**, *136*, 12056-12063.
[46] S. Frischhut, W. Klein, M. Drees, T. F. Fässler, *Chem. Eur. J.* **2018**, *24*, 9009-9014.
[47] C. Hoch, M. Wendorff, C. Röhr, *J. Alloys Compd.* **2003**, *361*, 206-221.
[48] P. Ghana, M. I. Arz, G. Schnakenburg, M. Straßmann, A. C. Filippou, *Organometallics* **2018**, *37*, 772-780.
[49] X-Area, version 1.76.8.1, Stoe & Cie GmbH, Darmstadt **2015**.
[50] G. M. Sheldrick, *Acta Cryst. C* **2015**, *71*, 3-8.
[51] A. L. Spek, *Acta Cryst. D* **2009**, *65*, 148-155.
[52] A. L. Spek, *Acta Cryst. C* **2015**, *71*, 9-18.

SUPPORTING INFORMATION

Three-dimensional Covalent Linkage of four Deltahedral Ge_9 Clusters *via* a Central sp^3 Hybridized Ge Atom: Synthesis and Crystal Structure of $K_4[\{Me_3Si)_3Si\}_2Ge_9]_4Ge$

Sabine Frischhut,[a] Peter Jutzi,[b] and Thomas F. Fässler[a]

[a] Sabine Frischhut, Prof. Dr. Thomas F. Fässler

Department Chemie, Technische Universität München

Lichtenbergstraße 4, 85747 Garching, Germany

Email: thomas.faessler@lrz.tum.de

[b] Prof. Dr. Peter Jutzi

Department Chemie, Universität Bielefeld

33615 Bielefeld

1 Structure of **1**

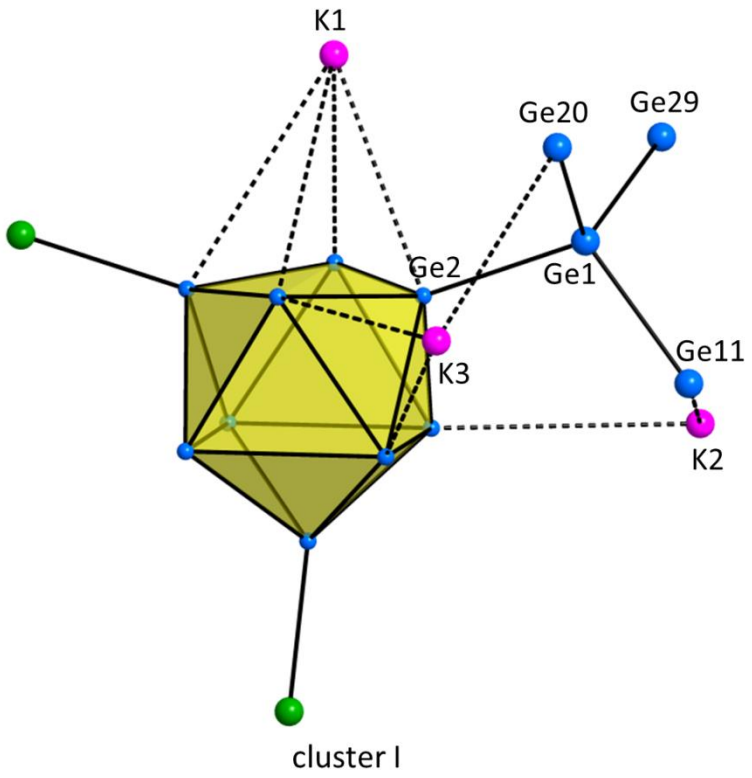

Figure S1. Excerpt of the structure of **1**, highlighting cluster I coordinating to three potassium cations in η^1-, η^2- and η^4-fashion. All atoms are shown as spheres. Trimethylsilyl groups as well as all hydrogen atoms are omitted for clarity. Color code: Ge – blue, Si – green, K – purple.

Table S1. Bond lengths in **1** [Å].

Ge1–Ge2	2.4311(7)
Ge1–Ge11	2.4213(7)
Ge1–Ge20	2.4313(7)
Ge1–Ge29	2.4174(7)

Cluster I		**Cluster II**	
Ge2–Ge3	2.5636(7)	Ge11–Ge12	2.5587(8)
Ge2–Ge5	2.5536(7)	Ge11–Ge14	2.5643(7)
Ge2–Ge6	2.5708(7)	Ge11–Ge15	2.5493(8)
Ge2–Ge7	2.5480(7)	Ge11–Ge16	2.5562(7)
Ge3–Ge4	2.5933(7)	Ge12–Ge13	2.5520(7)
Ge3–Ge7	2.6538(7)	Ge12–Ge16	2.6659(7)

Ge3–Ge8	2.6362(7)	Ge12–Ge17	2.6268(7)
Ge4–Ge5	2.5591(7)	Ge13–Ge14	2.5965(8)
Ge4–Ge8	2.5661(7)	Ge13–Ge17	2.5940(7)
Ge4–Ge9	2.5935(7)	Ge13–Ge18	2.5613(8)
Ge4–Si1	2.395(2)	Ge13–Si9	2.403(1)
Ge5–Ge6	2.6661(7)	Ge14–Ge15	2.6314(7)
Ge5–Ge9	2.6150(7)	Ge14–Ge18	2.6565(7)
Ge6–Ge7	3.1090(7)	Ge15–Ge16	3.2146(8)
Ge6–Ge9	2.7881(7)	Ge15–Ge18	2.7487(7)
Ge6–Ge10	2.5127(7)	Ge15–Ge19	2.5369(8)
Ge7–Ge8	2.8362(8)	Ge16–Ge17	2.8008(7)
Ge7–Ge10	2.5202(7)	Ge16–Ge19	2.4970(7)
Ge8–Ge9	3.1310(7)	Ge17–Ge18	3.1790(8)
Ge8–Ge10	2.5272(7)	Ge17–Ge19	2.5269(8)
Ge9–Ge10	2.5288(8)	Ge18–Ge19	2.5271(7)
Ge10–Si5	2.378(1)	Ge19–Si13	2.369(1)

Cluster III		**Cluster IV**	
Ge20–Ge21	2.5662(7)	Ge29–Ge30	2.5494(8)
Ge20–Ge23	2.5549(7)	Ge29–Ge32	2.5597(7)
Ge20–Ge24	2.5780(7)	Ge29–Ge33	2.5517(8)
Ge20–Ge25	2.5456(7)	Ge29–Ge34	2.5470(8)
Ge21–Ge22	2.5982(8)	Ge30–Ge31	2.5415(7)
Ge21–Ge25	2.6416(7)	Ge30–Ge34	2.6598(8)
Ge21–Ge26	2.6393(7)	Ge30–Ge35	2.6413(7)
Ge22–Ge23	2.5602(7)	Ge31–Ge32	2.5829(8)
Ge22–Ge26	2.5684(7)	Ge31–Ge35	2.5859(8)
Ge22–Ge27	2.5909(7)	Ge31–Ge36	2.5610(8)
Ge22–Si17	2.402(2)	Ge31–Si25	2.394(1)
Ge23–Ge24	2.6573(7)	Ge32–Ge33	2.6199(8)
Ge23–Ge27	2.6226(7)	Ge32–Ge36	2.6804(8)

Ge24−Ge25	3.1314(8)	Ge33−Ge34	3.3146(8)
Ge24−Ge27	2.7844(7)	Ge33−Ge36	2.7277(8)
Ge24−Ge28	2.5116(7)	Ge33−Ge37	2.5324(8)
Ge25−Ge26	2.8297(8)	Ge34−Ge35	2.7794(7)
Ge25−Ge28	2.5128(8)	Ge34−Ge37	2.5007(7)
Ge26−Ge27	3.1145(8)	Ge35−Ge36	3.1846(8)
Ge26−Ge28	2.5294(7)	Ge35−Ge37	2.5293(8)
Ge27−Ge28	2.5310(8)	Ge36−Ge37	2.5314(8)
Ge28−Si21	2.376(1)	Ge37−Si29	2.370(1)

Table S2. Bond angles in **1** [°].

Ge2−Ge1−Ge11	108.35(2)
Ge2−Ge1−Ge20	103.92(2)
Ge2−Ge1−Ge29	113.14(3)
Ge11−Ge1−Ge20	115.15(3)
Ge11−Ge1−Ge29	107.24(3)
Ge20−Ge1−Ge29	109.18(2)

2 ^{1}H NMR spectra of **1**

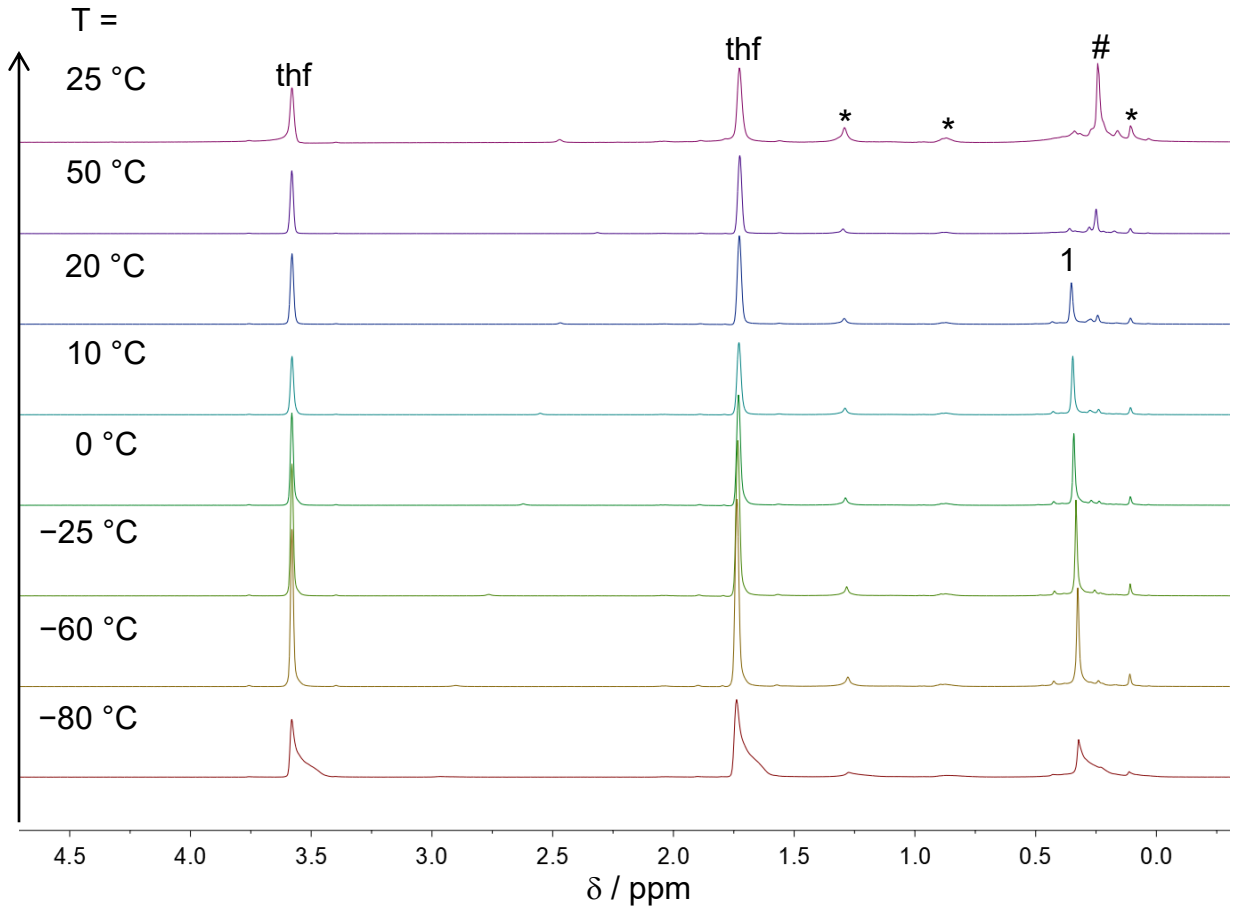

Figure S2. Temperature-dependent ^{1}H NMR study of crystals of **1** dissolved in thf-d_8 at −78 °C. The signal The signal labelled with # most likely derives from $[\{(Me_3Si)_3\}_3Ge_9]^-$. Signals marked with * could not be assigned.

5.10 Capping Nido-Nonagermanide Clusters with *M*-PPh_3 and Dynamics in Solution: Synthesis and Structure of *closo*-[$(Me_3Si)_3Si]_3Et[Ge_9M](PPh_3)$ (*M* = Ni, Pt)

Sabine Frischhut, Felix Kaiser, Wilhelm Klein, Markus Drees, Fritz E. Kühn, and Thomas F. Fässler

published in:

Organometallics **2018**, *37*, 4560-4567.

CONTENT AND CONTRIBUTION

Within the scope of this work, the neutral *closo*-[*M*Ge_9] clusters [{$(Me_3Si)_3Si$}$_3Ge_9CH_2CH_3$]*M*(PPh_3) (*M* = Ni, Pt) were synthesized for the first time by reaction of η^2-ethylene-bis(triphenylphosphine) platinum(0) and η^2-ethylene-bis(triphenylphosphine) nickel(0) with {$(Me_3Si)_3Si$}$_3Ge_9CH_2CH_3$ in toluene at r.t. The accessibility of these *closo*-structures completed the triad, whereby the respective *closo*-[$PdGe_9$] cluster had been reported prior to this work, but was synthesized according to a different synthesis protocol.

All experiments including crystallization and crystal structure analysis were carried out within this work. [{$(Me_3Si)_3Si$}$_3Ge_9CH_2CH_3$]Ni(PPh_3) unexpectedly showed dynamic behavior in solution at r.t., which was revealed by temperature-dependent ^{1}H NMR studies which were evaluated in the scope of this thesis. From the temperature-dependent ^{1}H NMR studies was concluded, that a transformation of the C_S-symmetric structure of [{$(Me_3Si)_3Si$}$_3Ge_9CH_2CH_3$]Ni(PPh_3), which was unequivocally determined by crystallization at −32 °C and single crystal X-ray diffraction, to a different C_S-shaped *closo*-cluster takes place upon heating to temperatures above r.t. This high-temperature isomer most likely is a constitutional isomer and most likely arises from diamond-square-diamond (DSD) rearrangement processes. In contrast, the Pt analogous structure does not show dynamic processes in solution throughout a wide temperature range.

Dr. Felix Kaiser synthesized the educt complexes η^2-ethylene-bis(triphenylphosphine) platinum(0) and η^2-ethylene-bis(triphenylphosphine) nickel(0) and fruitfully contributed to discussions. Dr. Wilhelm Klein assisted with structure determination of the *closo*-[$NiGe_9$] cluster. Dr. Markus Drees performed quantum chemical calculations on the dynamic behavior of the *closo*-[$NiGe_9$] cluster in solution at r.t. to enforce the predicted structures at elevated temperatures.

The publication was authored within this work. The manuscript was revised by Dr. Felix Kaiser, Dr. Wilhelm Klein, Prof. Dr. Fritz E. Kühn and Prof. Dr. Thomas F. Fässler.

ORGANOMETALLICS

Article

Cite This: *Organometallics* 2018, 37, 4560–4567

pubs.acs.org/Organometallics

Capping *nido*-Nonagermanide Clusters with *M*-PPh_3 and Dynamics in Solution: Synthesis and Structure of *closo*-$[(Me_3Si)_3Si]_3Et[Ge_9M](PPh_3)$ (M = Ni, Pt)

Sabine Frischhut,[†] Felix Kaiser,[‡] Wilhelm Klein,[†] Markus Drees,[§] Fritz E. Kühn,[‡] and Thomas F. Fässler*[,†]

[†]Lehrstuhl für Anorganische Chemie mit Schwerpunkt Neue Materialien, Fakultät für Chemie, Technische Universität München, Lichtenbergstraße 4, 85747 Garching, Germany

[‡]Professur für Molekulare Katalyse, Fakultät für Chemie, Technische Universität München, Lichtenbergstraße 4, 85747 Garching, Germany

[§]Lehrstuhl für Anorganische und Metallorganische Chemie, Fakultät für Chemie, Technische Universität München, Lichtenbergstraße 4, 85747 Garching, Germany

Supporting Information

ABSTRACT: In this work, cluster expansion of nine-atomic germanium clusters with nickel and platinum atoms is reported. The compounds $[(Me_3Si)_3Si]_3Et[Ge_9Ni](PPh_3)$ and $[(Me_3Si)_3Si]_3Et[Ge_9Pt](PPh_3)$ are characterized by NMR spectroscopy, elemental analysis, and single crystal X-ray structure analysis. The latter represents the first intermetalloid Ge-Pt cluster with a platinum atom as part of a deltahedron. So far, only one compound of this type has been reported for the homologous Pd. Hence, with these new compounds, metal-coordinated deltahedral Ge_9 clusters are now known for the whole triad of group 10 elements. The cluster compounds are accessible by treating $[(Me_3Si)_3Si]_3EtGe_9$ with η^2-ethylene-bis-(triphenylphosphine)-nickel(0) and η^2-ethylene-bis-(triphenylphosphine)-platinum(0), respectively, in toluene. The crystal structure determination reveals ten-vertex-*closo*-$[Ge_9M]$-cluster cores (M = Ni, Pt) bearing five *exo*-bonded ligands. Unlike the nine-vertex-cluster $[(Me_3Si)_3Si]_3EtGe_9$, the penta-functionalized platinum containing cluster compound $[(Me_3Si)_3Si]_3Et[Ge_9Pt](PPh_3)$ does not show fluctuating behavior in solution over a wide temperature range on the NMR time scale, whereas the $[(Me_3Si)_3Si]_3Et[Ge_9Ni](PPh_3)$ shows highly dynamic processes in solution at ambient temperature.

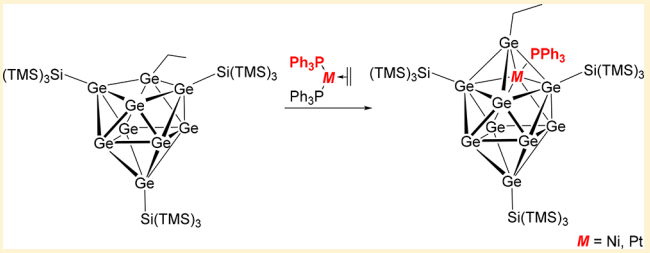

INTRODUCTION

$[Ge_9]^{4-}$ Zintl clusters show multifaceted reactivity toward transition metal compounds. By reacting $[Ge_9]^{4-}$ with diverse transition metal complexes, endohedrally filled cluster species hosting transition metals in the cluster's center, as well as cluster compounds with exohedrally bonded transition metals, are accessible.[1] Therefore, such clusters are candidates to study cluster growth mechanisms for the formation of intermetalloid clusters. The manifold reaction schemes, including stepwise addition and insertion of transition metal atoms to deltahedral cages, flanked by disproportionation reactions allow for the synthesis of a large variety of compounds.[2]

According to the Wade–Mingos rules, $[Ge_9]^{4-}$ represents a *nido*-cluster containing 22 skeleton-bonding electrons.[3] The cluster can be dissolved in highly polar solvents by extraction from the binary Zintl phases A_4Ge_9 (A = K, Rb), e.g., $NH_{3(liq)}$ or ethylenediamine. The transfer of Ge_9 Zintl cluster compounds into less polar and more convenient solvents was achieved by the silylation of the $[Ge_9]^{4-}$ Zintl clusters with chloro-silanes. The first representative was reported by Schnepf et al. through metastable Ge(I)Br,[4] and an even more facile synthesis of $[\{(Me_3Si)_3Si\}_3Ge_9]^-$ is carried out by reacting the Zintl phase K_4Ge_9 with chlorotris(trimethylsilyl)silane in a heterogeneous reaction in acetonitrile. This synthesis route provides access to the stable Zintl anion $[\{Me_3Si)_3Si\}_3Ge_9]^-$, which is highly soluble in acetonitrile, thf, and toluene.[5] The reactivity of the three-fold silylated cluster compound $[\{(Me_3Si)_3Si\}_3Ge_9]^-$ has been studied intensively in recent years, including variation of silyl ligands and the accompanied steric effects. New silylated cluster compounds emerged, such as $[\{(Me_3Si)_2(Ph_3Si)Si\}_3Ge_9]^-$,[6] $[\{(Me_3Si)_3Si\}_2\{(Me_3Si)_2(Ph_3Si)Si\}Ge_9]^-$,[7] and $[\{HtBu_2Si\}_3Ge_9]^-$.[8] Also, the introduction of specific functionalities to the Ge_9 clusters *via* the silyl ligand has been shown by the synthesis of $[\{(Me_3Si)_3Si\}_2\{Ph_2((CH_2)_nCH{=}CH_2)Si\}Ge_9]^-$ and $[\{Ph_2((CH_2)_nCH{=}CH_2)Si\}_3Ge_9]^-$.[9] The silyl ligands can also be formally exchanged by other substituents as is shown in $[\{(Me_3Si)_3Si\}_2PtBu_2Ge_9]$.[10] Stannyl-decorated Zintl anions were realized in $[(SniPr_3)_3Ge_9]^-$.[11] More and more attention has been

Received: July 4, 2018
Published: December 7, 2018

DOI: 10.1021/acs.organomet.8b00459
Organometallics 2018, 37, 4560–4567

Scheme 1. Reaction of $[(Me_3Si)_3Si]_3EtGe_9$ with η^2-Ethylene-bis-(triphenylphosphine)-platinum(0)/η^2-Ethylene-bis-(triphenylphosphine)-nickel(0) in Toluene Yields $[(Me_3Si)_3Si]_3Et[Ge_9Ni](PPh_3)$ (1)/$[(Me_3Si)_3Si]_3Et[Ge_9Pt](PPh_3)$ (2)

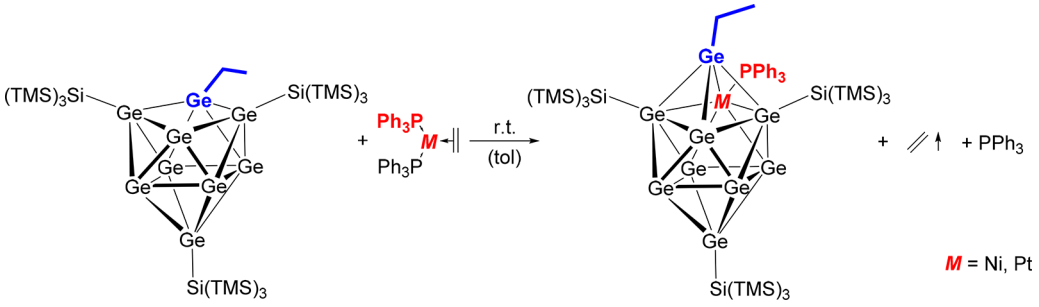

drawn on the three-fold silylated Ge_9 cluster compounds, as they represent excellent starting materials for follow-up reactions in Zintl cluster chemistry. For example, the three-fold silylated cluster compound $[\{(Me_3Si)_3Si\}_3Ge_9]^-$ can undergo nucleophilic substitution reactions with XSnPh$_3$, XSnnBu$_3$, XR′, or Cl(CO)R′ (with X = halide and R′ = organic substituent) to form neutral cluster compounds, which show dynamic behavior in solution.[12]

Also, $[R_3Ge_9]^-$ (R = silyl ligands) readily reacts with late transition metal halides in metathesis reactions. For example, the linkage of two $[\{(Me_3Si)_3Si\}_3Ge_9]^-$ entities can be realized in $[\{Me_3Si)_3Si\}_3Ge_9MGe_9\{Si(SiMe_3)_3\}_3]^{n-}$ for various metals (M = Cu, Ag, Au, n = 1; M = Zn, Cd, Hg, n = 0), where the cluster cores are coordinated to the metal center in an η^3-fashion.[13] With $[\{(Si(SiMe_3)_3)_3Ge_9\}Cu\{Ge_9(Si(SiMe_3)_3)_3\}$-$CuPPh_3]$[14] and $[(CuPiPr_3)_4\{Ge_9(SiPh_3)_2\}_2]$,[15] also larger entities have been reported. Remarkably, the latter contains two $CuPiPr_3$ entities serving as linker by cluster coordination in both Cu-η^1 and Cu-η^2 fashion. Additionally, each Ge_9 cluster core coordinates to one $CuPiPr_3$ entity *via* the Cu atom in an η^4 fashion.

Just recently, also the first *N*-heterocyclic carbene (NHC) adducts of Ge_9 Zintl clusters were reported with $[NHC^{Dipp}M$-$(\eta^3$-$Ge_9[\{Si(SiMe_3)_3\}_3])]$ (M = Cu, Ag, Au) and, thus, for the first time combined NHC and Zintl cluster chemistry, which gave access to several new structures.[10,16]

Cluster expansions have been realized at bare Ge_9 clusters with Zn, Cu, Sn, Pd and also for the heavier homologues Sn_9 with Zn, Cd, Ir, Cr, Mo, W, Ag, Cu, Au, and for Pb_9 with Cr, Mo, W atoms.[1b,16d,17]

Similarly, *nido*-cluster core expansion has been achieved for $[\{Me_3Si)_3Si\}_3Ge_9]^-$, resulting in *closo*-$[[\{Me_3Si)_3Si\}_3Ge_9M$-$(CO)_3]^-$ for M = Cr, Mo, W. The transition metal is introduced into the polyhedral arrangement, forming a distorted bicapped square antiprismatic $[MGe_9]$ core.[18]

With Pd complexes, introduction of three Pd atoms into the cluster scaffold of $[(SniPr_3)_3Ge_9]^-$, followed by merging with a second $[(SniPr_3)_3Ge_9]^-$ unit, was observed.[11,19] Just recently, the first example of a cluster expansion of a neutral Ge_9 cluster, which carries five external ligands $[(Me_3Si)_3Si]_3EtGe_9Pd$-(PPh_3), was reported. The compound with a *closo*-$[PdGe_9]$ core is accessible by the reaction of $[(Me_3Si)_3Si]_3EtGe_9$ with $[Pd(PPh_3)_4]$.[20]

In this work, the related *closo*-$[MGe_9]$ cluster derivatives of the lighter homologue M = Ni and the heavier homologue M = Pt are presented. $[(Me_3Si)_3Si]_3Et[Ge_9Ni](PPh_3)$ (**1**) and $[(Me_3Si)_3Si]_3Et[Ge_9Pt](PPh_3)$ (**2**) were obtained by reaction of $[(Me_3Si)_3Si]_3EtGe_9$ with η^2-ethylene-(bis-triphenylphosphine)-nickel(0) and η^2-ethylene-(bis-triphenylphosphine)-platinum(0), in toluene (Scheme 1), respectively. Both compounds crystallize from *n*-hexane solutions at −32 °C and are investigated by NMR spectroscopy, elemental analysis, and single crystal X-ray diffraction.

RESULTS AND DISCUSSION

Reactions of $[(Me_3Si)_3Si]_3EtGe_9$ with tetrakis(triphenylphosphine)nickel(0) or tetrakis(triphenylphosphine)platinum(0) in analogy to the recently published procedure for the respective palladium species[20] leads to the decomposition of $[(Me_3Si)_3$-$Si]_3EtGe_9$, as monitored in the ^{1}H NMR spectra of the reaction solutions. Consequently, the reactions were carried out with the more readily reactive η^2-ethylene-bis-(triphenylphosphine)-nickel(0) and -platinum(0) complexes where the ethylene ligand is easier to replace. The reaction at room temperature in toluene resulted in the formation of the desired products $[(Me_3Si)_3Si]_3Et[Ge_9M](PPh_3)$ with M = Ni (**1**) and Pt (**2**). The products were extracted with hexane from the solid after removal of toluene, and recrystallized from the hexane solutions at −32 °C.

Single crystal X-ray diffraction of crystals of **1** and **2** unequivocally revealed the formation of a distorted C_S-symmetric bicapped square-antiprismatic *closo*-$[MGe_9]$ core bearing the M atom as a vertex of the square of the antiprism and five ligands that radially point away from the cluster core (Figure 1). The compounds crystallize in the triclinic space group $P\bar{1}$ with one symmetry-independent cluster. The cluster possesses pseudo-C_s symmetry with an approximate mirror plane through the atoms Ni1/Pt1, Ge1, Ge3, Ge6, and Ge8. A triphenylphosphine ligand is coordinated to the Ni/Pt atom which itself coordinates to the five Ge vertices Ge1, Ge2, Ge3, Ge4, and Ge5 of the cluster core. In particular, two hypersilyl groups are bound to the neighboring and opposingly positioned Ge atoms of the square of the antiprism (Ge1 and Ge3).

Both capping atoms bear ligands, namely, the ethyl functionality at the Ge2 atom neighboring the Ni/Pt atom and one of the three hypersilyl groups binds to the Ge6 atom. The Ge−Ge bond lengths within the cluster core in **1** and **2** lie in the range of 2.4682(6)−2.8020(6) Å and 2.4756(8)−2.8885(9) Å, respectively, with Ge1−Ge2 and Ge4−Ge5 being the shortest and longest, respectively. The Ge−Ge bond lengths in **1** appear slightly shorter than the reported ones for the heavier Pd homologue; the Ge−Ge bond lengths in the Pt derivative **2** are similar to those in the lighter Pd homologue.[20] The distances Ge4−Ge9 and Ge5−Ge7 appear elongated (**1**: 3.2429(7) Å and 3.3244(7) Å, **2**: 3.2303(9) Å and 3.3053(9)

DOI: 10.1021/acs.organomet.8b00459
Organometallics 2018, 37, 4560−4567

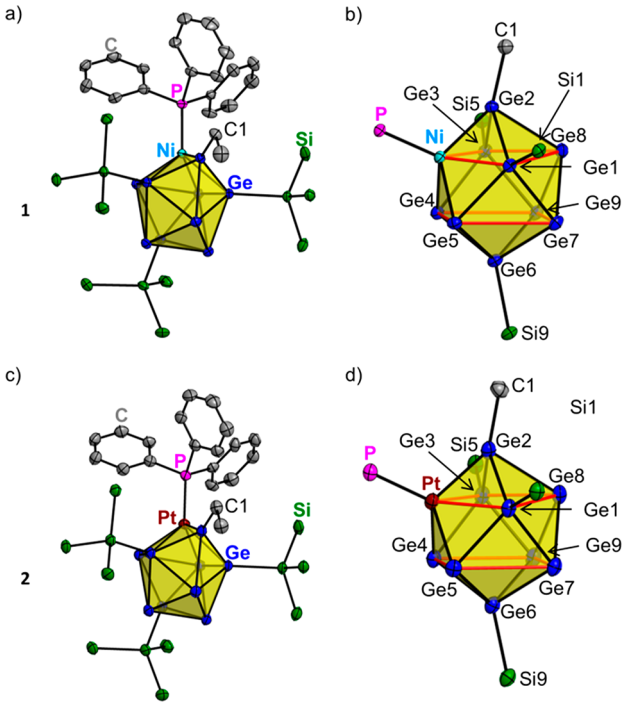

Figure 1. Molecular structures of **1** (a, b) and **2** (c, d). (a/c) The [MGe_9]-cluster cores are depicted as polyhedrons. All hydrogen atoms as well as CH_3 groups on hypersilyl moieties are omitted for clarity. (b/d) The two squares of the underlying quadratic antiprism of the [MGe_9]-polyhedra are highlighted in red. All ellipsoids are shown at a probability level of 50%. Ge - blue, Si - green, C - gray, P - purple, Ni - turquoise, Pt - brown.

Å), compared to the shorter distances Ge4−Ge5 and Ge7−Ge9 (**1**: 2.7638(6) Å and 2.7785(6) Å, **2**: 2.8885(9) Å and 2.7497(9) Å), resulting in a considerably distorted "square", formed by the Ge4-Ge5-Ge7-Ge9 atoms. This has already been observed for neutral, functionalized Ge_9 Zintl clusters.[12a,20] As expected, the average Ni−Ge distance of 2.476 Å in **1** is smaller compared to the average Pd−Ge distance of 2.577 Å and the average Pt−Ge distance of 2.592 Å in **2**. The latter two are rather similar due to similar atom radii of Pd and Pt.[21] The shorter Ni−Ge distances lead to a stronger distortion of the *closo*-cluster core accompanied by a compression of the Ge−Ge distances.

The ^{1}H NMR spectrum of the platinum cluster **2** shows all expected signals at r.t. including the phenyl groups of the phosphine ligands in the range of 7.90−6.99 ppm, the ethyl group, which shows the two expected signals at 2.66 and 2.36 ppm with an integral ratio of 2:3, and two sharp signals at 0.65 and 0.26 ppm in a 1:2 integrals ratio for the three hypersilyl groups. According to the approximate C_S symmetry of the polyhedron, two hypersilyl groups are chemically equivalent (Figure 2).

Even at elevated temperatures up to 90 °C, **2** does not show a change in its nondynamic behavior, as is revealed by temperature-resolved NMR studies (Figure S15, Supporting Information). Thus, the two signals for the hypersilyl groups remain virtually unchanged throughout a wide temperature range.

The ^{1}H NMR spectrum of **1** at r.t. shows broad signals in the region of the H atoms of the hypersilyl ligands at 0.61 and 0.27 ppm, and the ethyl group at 2.86 and 2.25 ppm. The large line widths hint for a dynamic process in solution (Figure S5). Temperature-dependent NMR spectra of **1** show sharp signals at lower temperature up to 0 °C (Figures 2 and 3). The hypersilyl ligands appear as two signals in a 1:2 ratio as expected for a C_S-symmetric cluster. Upon warming to 25 °C, the signals for the hypersilyl and the ethyl ligand progressively broaden and are visually shifted at 25 °C. When further heated up to 80 °C, sharp signals for the hypersilyl ligands at 0.52 and 0.29 ppm in a 1:2 ratio appear in the ^{1}H NMR spectrum (Figure 3a). Also, a new signal set for the ethyl ligand at 2.60 and 1.90 ppm appears with an integrals ratio of 2:3 which still does not show the expected multiplicity at 80 °C (Figure 3b). The signal set of the bound triphenylphosphine ligand does not significantly change in the described temperature range;

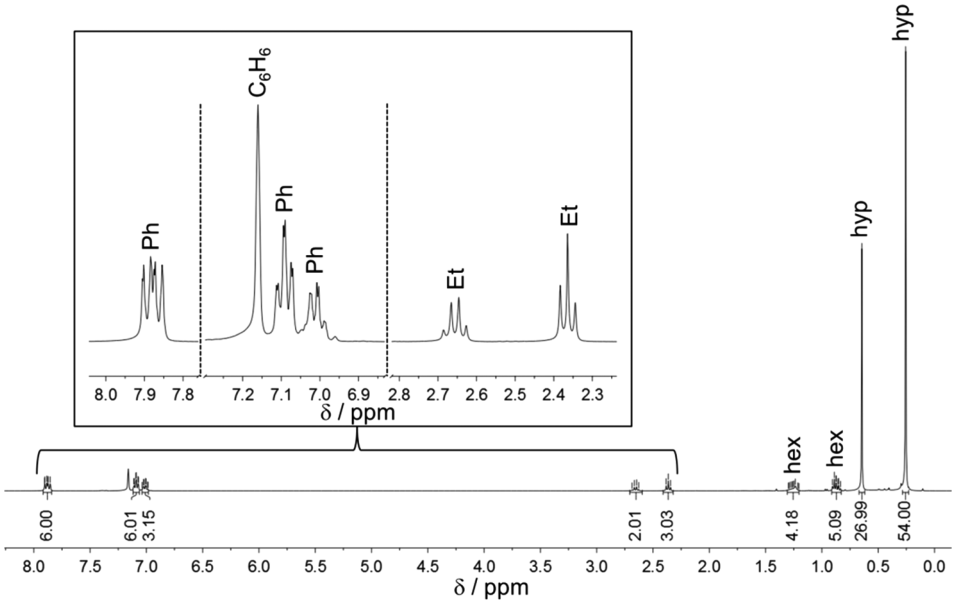

Figure 2. ^{1}H NMR spectrum of dissolved crystals of compound **2**, recorded in [D_6]benzene at r.t. The regions of the phenyl and ethyl groups are shown enlarged. The signals of the hypersilyl groups are marked with "hyp"; the signals of hexane are marked with "hex".

DOI: 10.1021/acs.organomet.8b00459
Organometallics 2018, 37, 4560−4567

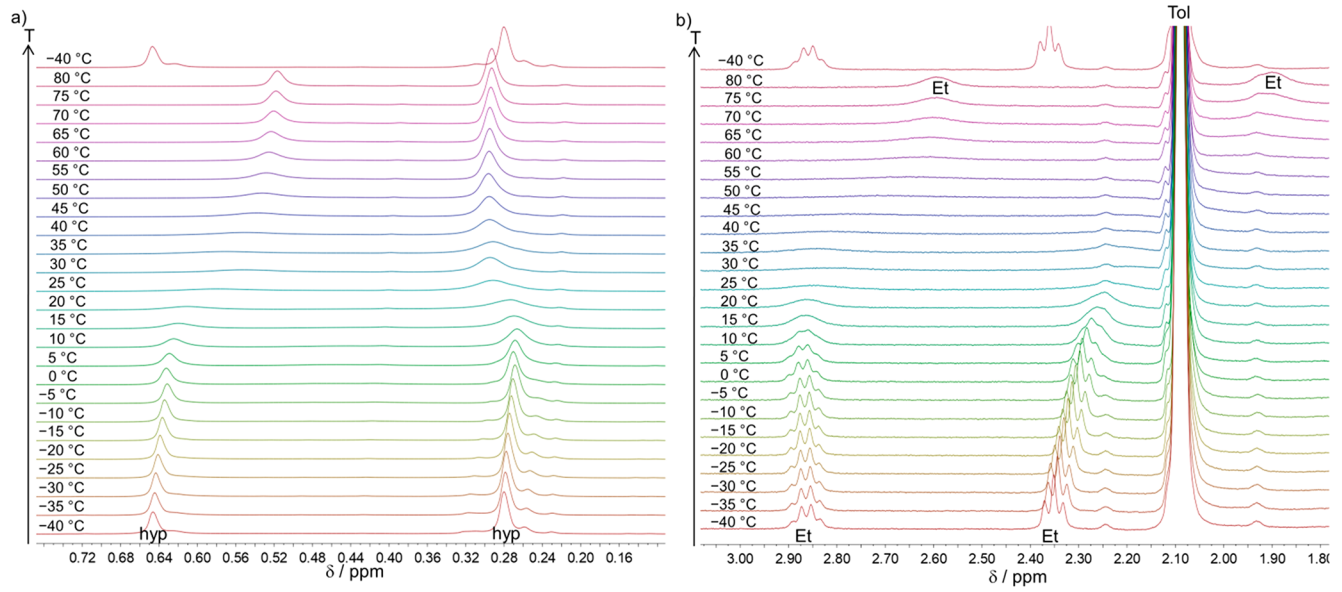

Figure 3. Variable temperature ^{1}H NMR study of crystals of **1** in [D_8]toluene in the range from −40 to 80 °C and subsequent cooling to −40 °C. (a) The signals of the hypersilyl ligands ("hyp") are shown. (b) The signals of the ethyl ligand ("Et") are shown.

however, after increasing time of heating, a signal of low intensity corresponding to free PPh_3 appears (Figure S7). Subsequent cooling to −40 °C leads to the same sharp signal sets as before warming (Figure 2 and Figure S6). Yet, the very weak signal of free PPh_3 remains visible in the ^{1}H NMR spectrum, which hints at slow and irreversible PPh_3 abstraction of **1**. Remarkably, compound **1** is the major component again after heating to 80 °C and subsequent cooling. Variable temperature ^{31}P NMR studies also reveal dynamic temperature-dependent processes in solution (Figure S8, Supporting Information).

Hence, the clusters **1** and **2** do not show the fluctuating behavior as is observed for $[(Me_3Si)_3Si]_3EtGe_9$ in solution at r.t., since the silyl ligands are not all identical. Nevertheless, **1** shows a different dynamic process in solution at r.t., whereby the C_S-symmetry of **1** remains unchanged. This can be concluded from the signal set of two signals for the hypersilyl ligands as well as the corresponding integrals ratio of 1:2 at temperatures above 60 °C in the temperature-dependent ^{1}H NMR spectrum.

Isomerization resulting from rotation of the ethyl group in **1** is feasible, but the reason for the lack of rotational isomerism in **2** in the analogous Pt complex remains unclear. Therefore, we also take constitutional isomerism into account. Scheme 2 shows the two at elevated temperatures possibly formed isomers **1′** and **1′′**, which fulfill the C_S-symmetry.

On the basis of quantum chemical DFT calculations, the energy difference between the two isomers **1** and **1′**, where the position of the Ge2-ethyl fragment is changed with the only ligand-free adjacent Ge8-vertex, is only as high as +7.6 kcal/mol (energy difference between the Pt-analogous isomers **2** and **2′**: +8.1 kcal/mol). Retention of the C_S-symmetry in **1** would also be given when the fragments Ni-PPh_3 and Ge2-ethyl undergo a formal positional change to form the isomer **1′′**. Here, the energy difference of the isomers **1** and **1′′** is +7.2 kcal/mol (energy difference between the Pt-analogous isomers **2** and **2′′**: +9.2 kcal/mol). The energy differences for the isomerization of **1** and **2** are in the same range; however, we do not have any information about transition states. The

Scheme 2. Two Feasible C_S-Symmetric Isomers of 1′ and 1′′ Which Can Be Achieved Based on 1 by the Formal Exchange of Vertices

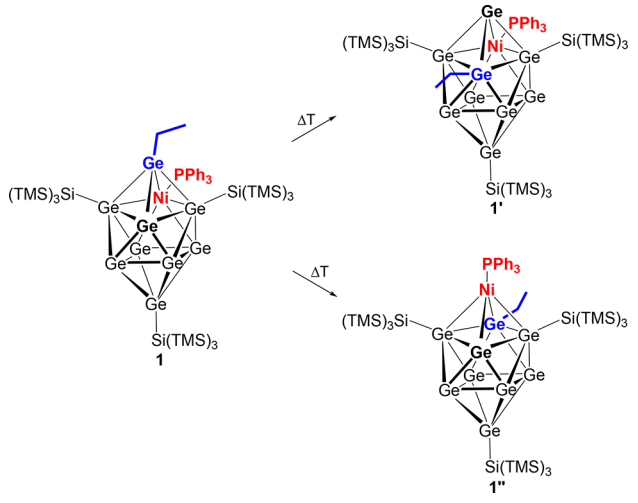

isomerization of **1** most likely proceeds according to a diamond-square-diamond (DSD) rearrangement mechanism. Such cluster rearrangement processes have been described for boranes and carboranes,[22] which are structurally and electronically related to the Ge_9 clusters. Isomerizations analogous to the formation of **1′′** out of **1** are already reported in the literature for *closo*-$[Sn_9Mo(CO)_3]^{4-}$, where the corresponding η^4- and η^5-structures show a dynamic equilibrium.[17g]

The formation of the *closo*-$[MGe_9]$ cluster core (M = Ni, Pt) of **1** and **2** is, similarly to $[(Me_3Si)_3Si]_3Et[Ge_9Pd](PPh_3)$, believed to be initiated by an $M(PPh_3)$ entity capping the triangular face Ge2-Ge4-Ge5 of the *nido*-Ge_9 cluster core, followed by a cluster-opening displacement of the ethyl-functionalized Ge2 vertex.[20]

Currently, investigations on follow-up reactions are ongoing in our laboratories. Among others, the behavior of the PPh_3 ligand and its exchangeability for other ligands is of particular interest to us.

DOI: 10.1021/acs.organomet.8b00459
Organometallics 2018, 37, 4560−4567

CONCLUSION

In this work, we were able to complete the triad of the compounds $[(Me_3Si)_3Si]_3Et[Ge_9M](PPh_3)$ with M = Ni-Pt. The deltahedral Ge_9 Zintl cluster compounds $[(Me_3Si)_3Si]_3Et[Ge_9M](PPh_3)$ [M = Ni (**1**), M = Pt (**2**)] are synthesized by reaction of $[(Me_3Si)Si]_3EtGe_9$ with η^2-ethylene-bis-(triphenylphosphine)-nickel(0) or η^2-ethylene-bis-(triphenylphosphine)-platinum(0). Both compounds **1** and **2** are characterized in solution by NMR spectroscopy as well as in the solid state by elemental analysis and single crystal X-ray diffraction. The nickel derivative **1** shows a strongly distorted *closo*-$[NiGe_9]$ cluster core and most likely undergoes a framework rearrangement in solution at r.t., if compared to the *closo*-$[MGe_9]$ cluster cores of the heavier homologues.

Further investigating the neutral deltahedral Ge_9 Zintl cluster compounds in follow-up reactions is of special interest as neutral, functionalized cluster compounds can be used to build up higher cluster aggregates. After saturating the whole coordination sphere of the neutral Zintl cluster compound $[(Me_3Si)Si]_3EtGe_9$, new interesting structures might be available.

EXPERIMENTAL SECTION

General. All manipulations were carried out under a purified argon atmosphere using standard Schlenk techniques. The Zintl phase with the nominal composition K_4Ge_9 was synthesized heating a stoichiometric mixture of the elements K and Ge (99.999%, Chempur) at 650 °C for 46 h in a stainless steel autoclave.[23] The solvents acetonitrile, toluene, and hexane were dried over molecular sieve in a solvent purification system MB-SPS. *cis*-Dichloro-bis-(triphenylphosphine)-platinum(II) (Sigma-Aldrich), ethylene (≥99.5%, Sigma-Aldrich), chlorotris(trimethylsilyl)silane (≥95.0%, TCI Chemicals), and bromoethane (98%, Sigma-Aldrich) were used as received. $Ni(acac)_2$ was sublimed *in vacuo* (10^{-3} mbar, 160 °C), PPh_3 was recrystallized twice from hot ethanol, and diethyl ether was saturated with ethylene by vigorously passing a stream of ethylene gas through the liquid over a period of 10 min. The deuterated solvents $[D_6]$benzene and $[D_8]$toluene were purchased from Deutero GmbH and stored over molecular sieves (3 Å) for at least 1 day.

Electron-Dispersive X-ray (EDX) Analysis. The elemental composition in the single crystals of **1** and **2** which were used to determine the crystal structure was analyzed with a Hitachi TM-1000 tabletop microscope.

Elemental Analysis. Elemental analysis was performed by the microanalytical laboratory at the Department of Chemistry of the Technische Universität München. The elements C and H were determined with a combustion analyzer (elementar vario EL, Bruker Corp.). Platinum was determined photometrically with tin(II) chloride at 404 nm. Nickel was determined by atomic absorption spectroscopy.

NMR Spectroscopy. All NMR spectra were recorded on a BRUKER Avance Ultrashield AV400 spectrometer. The signals were referenced to the residual proton signal of the deuterated solvents $[D_6]$benzene (δ = 7.16 ppm) and $[D_8]$toluene (δ_{CH3} = 2.09 ppm). The chemical shifts are given in δ values in parts per million (ppm). Variable temperature ^{31}P NMR studies were performed on a BRUKER AV500 cryo spetrometer. Crystals of **1** were dissolved in the deuterated solvent at −78 °C.

DFT Calculations. All calculations have been carried out with the software package Gaussian 09.[24] The level of theory contains the gradient approximated functional PBE[25] and the def2-SV(P)[26] basis set for all elements except Pt. For the latter element, the Dresden-Stuttgart ECP[27] has been used. All optimized structures have been proved by frequency analysis, if we have a ground state (NImag = 0) or a transition state (NImag = 1). All energy values are unscaled ΔG values. Detailed information about the calculated structures (geometry, absolute energy) can be found in the Supporting Information.

Synthesis of η^2-Ethylene-bis-(triphenylphosphine)-nickel-(0). The product was synthesized according to a literature procedure.[28] $Ni(acac)_2$ (1.00 g, 3.89 mmol) and PPh_3 (2.04 g, 7.78 mmol) are dissolved in diethyl ether, and a stream of ethylene gas is passed through the suspension at 0 °C. $AlEt_3$ (469 mg, 4.11 mmol) dissolved in 6.5 mL of hexanes is added over a period of 30 min and stirred for 5 h. The canary yellow precipitate is filtered off with a Schlenk frit, washed three times with diethyl ether, and dried in a vigorous stream of ethylene. The product is isolated as a canary yellow solid. The analytical data match those reported in the literature.

Synthesis of $[(SiMe_3)Si]_3Ge_9Et$. The compound $[(SiMe_3)_3Si]_3Ge_9Et$ was synthesized according to a modified literature procedure.[12a] A solution of chlorotris(trimethylsilyl)silane (357 mg, 1.26 mmol) in 12 mL of acetonitrile is added to K_4Ge_9 (341 mg, 0.42 mmol). The reaction solution is stirred for 21 h at r.t. and filtered over a glass fiber filter. Bromoethane (156 μL, 2.10 mmol) dissolved in 2 mL acetonitrile is added dropwise under vigorous stirring. A brown precipitate is formed; the suspension is stirred for 5 h and then set aside to allow the precipitate to settle down. The supernatant is decanted, and the precipitate is washed three times with a total amount of 24 mL of acetonitrile. The residue is dried *in vacuo* and characterized by NMR spectroscopy (see the Supporting Information).

Synthesis of $[(SiMe_3)Si]_3Et[Ge_9Ni](PPh_3)$ (1). The obtained brown solid of $[(SiMe_3)_3Si]_3Ge_9Et$ (150 mg, 0.11 mmol) and η^2-ethylene-bis-(triphenylphosphine)-nickel(0) (65 mg, 0.11 mmol) are dissolved in 3.2 mL of toluene and stirred for 2 h at r.t. After filtration over a glass fiber filter, the solvent is removed. The residue was extracted with hexane to give a dark-brown solution which was filtered again. After concentration, the solution is stored at −32 °C for crystallization. After 5 days, brown block-shaped crystals of **1** (yield: 27%) suitable for X-ray structure analysis formed. For NMR spectroscopic investigations, crystals of **1** were separated from the mother liquor, washed with acetonitrile, dried *in vacuo*, and dissolved in a deuterated solvent.

^1H NMR (400 MHz, $[D_8]$toluene, 233 K): δ (ppm) 7.76 (m, 6H, phenyl), 7.03 (m, superimposed with signal of toluene, phenyl), 7.951 (m, superimposed with signal of toluene, phenyl), 2.86 (q, 2H, ^3J = 7.6 Hz, CH_2), 2.36 (t, 3H, ^3J = 7.6 Hz, CH_3), 0.65 (s, 27H, $SiCH_3$), 0.28 (s, 54H, $SiCH_3$); $^{31}P\{^1H\}$ NMR (162 MHz, $[D_8]$toluene, 233 K): δ (ppm) 50.99; elemental analysis calcd for **1**·0.5 hex (%): C 33.55, H 6.08, Ni 3.28; found: C 33.23, H 6.08, Ni 3.7.

Synthesis of η^2-Ethylene-bis-(triphenylphosphine)-platinum(0). The compound was synthesized according to a modified literature procedure.[29] *cis*-Dichloro-bis-(triphenylphosphine)-platinum(II) (2.03 g, 2.57 mmol) is suspended in a mixture of 25 mL of dichloromethane and 25 mL of ethanol, cooled to 5 °C, and ethylene is vigorously passed through the stirred suspension *via* cannula. $NaBH_4$ (0.48 g, 12.6 mmol) is added in portions within a period of 10 min, and the solution is stirred at 5 °C for 30 min. 85 mL of ethanol is added, the suspension is stirred for 5 min, and the ethylene stream is turned off. The white precipitate is filtered off, washed with water, ethanol, and pentanes, and slowly dried on air. 1.82 g (2.43 mmol, 95%) of η^2-ethylene-bis-(triphenylphosphine)-platinum(0) is isolated as a white solid. The analytical data match those reported in the literature.[29,30]

Synthesis of $[(SiMe_3)Si]_3Et[Ge_9Pt](PPh_3)$ (2). $[(SiMe_3)_3Si]_3Ge_9Et$ (150 mg, 0.11 mmol) and η^2-ethylene-bis-(triphenylphosphine)-platinum(0) (79 mg, 0.11 mmol) are dissolved in 3.2 mL of toluene and stirred for 3.5 h at r.t. The reaction solution is filtered over a glass fiber filter. After solvent-removal from the red-brown filtrate *in vacuo*, the product is extracted with 2 mL of hexane. After filtration, the solution is concentrated *in vacuo* and stored at −32 °C for crystallization. Red-brown plates of **2** (yield: 32%) suitable for X-ray structure analysis formed within 4 weeks. For NMR spectroscopic investigations, crystals of **2** were separated from the mother liquor, washed with acetonitrile, dried *in vacuo*, and dissolved in a deuterated solvent.

DOI: 10.1021/acs.organomet.8b00459
Organometallics 2018, 37, 4560−4567

^{1}H NMR (400 MHz, [D$_6$]benzene, 298 K): δ (ppm) 7.88 (m, 6H, phenyl), 7.09 (m, 6H, phenyl), 7.01 (m, 3H, phenyl), 2.66 (q, 2H, ^3J = 7.6 Hz, CH_2), 2.36 (t, 3H, ^3J = 7.6 Hz, CH_3), 0.65 (s, 27H, SiCH_3), 0.26 (s, 54H, SiCH_3); ^{1}H ^{1}H COSY (400 MHz, [D$_6$]benzene, 298 K): δ (ppm)/δ (ppm) 7.88/7.09 (phenyl), 2.65/2.37 (^3J, CH_2/CH_3); ^{13}C{^{1}H} NMR (101 MHz, [D$_6$]benzene, 298 K): δ (ppm) 140.8 (s, phenyl), 140.4 (s, phenyl), 134.8 (s, phenyl), 134.7 (s, phenyl), 129.9 (s, phenyl), 129.8 (s, phenyl), 128.3 (superimposed with signal of C$_6$D$_6$, revealed by HMBC and HSQC, phenyl), 47.7 (t, CH_2), 16.1 (q, CH_3), 3.1 (q, SiCH_3); ^{1}H ^{13}C HSQC (400 MHz, 101 MHz, [D$_6$]benzene, 298 K): δ (ppm)/δ (ppm) 7.88/134.4, 7.89/128.0, 7.09/134.4, 7.09/129.6, 7.09/128.0, 7.01/129.6, 2.66/47.3 (^1J, CH_2/CH_2), 2.66/15.70 (^2J, CH_2/CH_3), 2.36/47.35 (^2J, CH_3/CH_2), 2.36/15.70 (^1J, CH_3/CH_3), 0.65/2.72 (^1J, SiCH_3/SiCH_3), 0.26/2.74 (^1J, SiCH_3/SiCH_3); ^{1}H ^{13}C HMBC (400 MHz, 101 MHz, [D$_6$]benzene, 298 K): δ (ppm)/δ (ppm) 7.88/134.6, 7.88/129.9, 7.11/140.7, 7.10/134.7, 7.09/128.4, 7.00/134.8, 2.65/16.5, 2.36/47.7, 0.65/3.2, 0.26/3.3; ^{31}P{^{1}H} NMR (162 MHz, [D$_6$]benzene, 298 K): δ (ppm) 37.79 (s, PtPPh_3); ^{29}Si NMR (79 MHz, 298 K): −9.08 (s, Si[*Si*(CH_3)$_3$]$_3$), −9.83 (s, Si[*Si*(CH_3)$_3$]$_3$), −87.04 (s, *Si*[Si(CH_3)$_3$]$_3$), −94.66 (s, *Si*[Si(CH_3)$_3$]$_3$); elemental analysis calcd for **2**·1.5 hex (%): C 33.42, H 6.11, Pt 9.69; found: C 32.84, H 5.80, Pt 9.6.

X-ray Data Collection and Structure Determination. A few crystals were transferred from the mother liquor into perfluoropolyalkylether under a cold N_2 stream. A single crystal was fixed on a glass fiber and positioned in a 150 K (compound **1**) or 100 K (compound **2**) cold N_2 stream. The single crystal intensity data were recorded on a Stoe StadiVari diffractometer (Mo Kα radiation (λ = 0.71073), Pilatus 300 K detector), by using the X-Area software package.[31] The crystal structure was solved by Direct Methods using the SHELX software.[32] The positions of the hydrogen atoms were calculated and refined using a riding model. All non-hydrogen atoms were treated with anisotropic displacement parameters. Solvent molecules appear partially disordered in the crystal structure of **2**. Crystallographic details of compounds **1** and **2** are listed in Table 1. CCDC 1812801 (**1**) and CCDC 1812802 (**2**) contain the supplementary crystallographic data.

Table 1. Crystallographic Details of Compounds 1·1.5 hex and 2·1.5 hex

	1·1.5 hex	**2**·1.5 hex
formula	$C_{56}H_{122}Ge_9NiPSi_{12}$	$C_{56}H_{122}Ge_9PtPSi_{12}$
fw (g·mol^{-1})	1875.60	2011.98
space group (no.)	$P\bar{1}$ (2)	$P\bar{1}$ (2)
a (Å)	15.167(1)	15.191(1)
b (Å)	15.847(1)	15.708(1)
c (Å)	19.892(2)	19.723(2)
α (deg)	99.133(6)	98.925(7)
β (deg)	106.666(6)	106.532(6)
γ (deg)	99.076(6)	99.084(6)
V (Å^3)	4416.3(6)	4354.5(6)
Z	2	2
T (K)	150(2)	100(2)
λ (Å)	0.71073	0.71073
ρ_{calcd} (g·cm^{-3})	1.410	1.535
μ (mm^{-1})	3.435	4.872
collected reflns	119203	77381
independent reflns	20306	17104
R_{int}	0.066	0.093
parameters/restraints	698/0	752/49
R_1 [all data/$I > 2\sigma(I)$]	0.067/0.040	0.065/0.041
wR_2 [all data/$I > 2\sigma(I)$]	0.099/0.083	0.097/0.089
goodness of fit	1.072	0.96
max./min diff. el. density	0.96/−0.78	2.75/−0.85

The presence of the elements Si, Ge, P, and Pt or Ni in the measured single crystal was confirmed by EDX.

■ ASSOCIATED CONTENT

Supporting Information

The Supporting Information is available free of charge on the ACS Publications website at DOI: 10.1021/acs.organomet.8b00459.

Further details on the crystal structures of **1** and **2**, as well as NMR spectra are provided (PDF)

Cartesian coordinates (XYZ)

Accession Codes

CCDC 1812801 and 1812802 contain the supplementary crystallographic data for this paper. These data can be obtained free of charge via www.ccdc.cam.ac.uk/data_request/cif, or by emailing data_request@ccdc.cam.ac.uk, or by contacting The Cambridge Crystallographic Data Centre, 12 Union Road, Cambridge CB2 1EZ, UK; fax: +44 1223 336033.

■ AUTHOR INFORMATION

Corresponding Author

*Fax: +49-89-289-13186. E-mail: Thomas.Faessler@lrz.tu-muenchen.de.

ORCID

Wilhelm Klein: 0000-0002-6351-9921

Fritz E. Kühn: 0000-0002-4156-780X

Thomas F. Fässler: 0000-0001-9460-8882

Notes

The authors declare no competing financial interest.

■ ACKNOWLEDGMENTS

The authors thank B.Sc. Kevin Frankiewicz for preparation of reaction solutions and Maria Weindl for performing temperature-dependent NMR studies. S.F. and F.K. are further grateful to the Fonds der Chemischen Industrie for their fellowships. This work was supported by funding from TUM.solar in the context of the Bavarian Collaborative Research Project "Solar Technologies Go Hybrid" (SolTech).

■ REFERENCES

(1) (a) Sevov, S. C.; Goicoechea, J. M. Chemistry of Deltahedral Zintl Ions. *Organometallics* **2006**, *25*, 5678−5692. (b) Scharfe, S.; Kraus, F.; Stegmaier, S.; Schier, A.; Fässler, T. F. Zintl Ions, Cage Compounds, and Intermetalloid Clusters of Group 14 and Group 15 Elements. *Angew. Chem., Int. Ed.* **2011**, *50*, 3630−3670.

(2) Benda, C. B.; Waibel, M.; Fässler, T. F. On the Formation of Intermetalloid Clusters: Titanocene (III) Diammin as a Versatile Reactant toward Nonastannide Zintl Clusters. *Angew. Chem., Int. Ed.* **2015**, *54*, 522−526.

(3) (a) Wade, K. The Structural Significance of the Number of Skeletal Bonding Electron-Pairs in Carboranes, the Higher Boranes and Borane Anions, and Various Transition-Metal Carbonyl Cluster Compounds. *J. Chem. Soc. D* **1971**, 792−793. (b) Wade, K. Structural and Bonding Patterns in Cluster Chemistry. *Adv. Inorg. Chem. Radiochem.* **1976**, *18*, 1−66.

(4) Schnepf, A. $[Ge_9\{Si(SiMe_3)_3\}_3]^-$A Soluble Polyhedral Ge_9 Cluster Stabilized by Only Three Silyl Ligands. *Angew. Chem., Int. Ed.* **2003**, *42*, 2624−2625.

(5) Li, F.; Sevov, S. C. Rational Synthesis of $[Ge_9\{Si(SiMe_3)_3\}_3]^-$ from its Parent Zintl Ion Ge_9^{4-}. *Inorg. Chem.* **2012**, *51*, 2706−2708.

(6) Kysliak, O.; Schrenk, C.; Schnepf, A. $\{Ge_9[Si(SiMe_3)_2(SiPh_3)]_3\}^-$: Ligand Modification in Metalloid Germanium Cluster Chemistry. *Inorg. Chem.* **2015**, *54*, 7083−7088.

DOI: 10.1021/acs.organomet.8b00459
Organometallics 2018, 37, 4560−4567

(7) Kysliak, O.; Schnepf, A. $\{Ge_9[Si(SiMe_3)_3]_2\}^{2-}$ a Starting Point for Mixed Substituted Metalloid Germanium Clusters. *Dalton Trans.* **2016**, *45*, 2404−2408.
(8) Kysliak, O.; Kunz, T.; Schnepf, A. Metalloid $Ge_9R_3^-$ Clusters with Various Silyl Substituents: From Shielded to Open Cluster Cores. *Eur. J. Inorg. Chem.* **2017**, *2017*, 805−810.
(9) Mayer, K.; Schiegerl, L. J.; Kratky, T.; Günther, S.; Fässler, T. F. Targeted Attachment of Functional Groups at Ge_9 Clusters via Silylation Reactions. *Chem. Commun.* **2017**, *53*, 11798−11801.
(10) Geitner, F. S.; Dums, J. V.; Fässler, T. F. Derivatization of Phosphine Ligands with Bulky Deltahedral Zintl Clusters - Synthesis of Charge Neutral Zwitterionic Tetrel Cluster Compounds $[(Ge_9\{Si(TMS)_3\}_2)tBu_2P]M(NHCDipp)$ (*M*Cu, Ag, Au). *J. Am. Chem. Soc.* **2017**, *139*, 11933−11940.
(11) Perla, L. G.; Sevov, S. C. A Stannyl-Decorated Zintl Ion $[Ge_{18}Pd_3(SniPr_3)_6]^{2-}$: Twinned Icosahedron with a Common Pd_3-Face or 18-Vertex Hypho-Deltahedron with a Pd_3-Triangle Inside. *J. Am. Chem. Soc.* **2016**, *138*, 9795−9798.
(12) (a) Li, F.; Sevov, S. C. Synthesis, Structures, and Solution Dynamics of Tetrasubstituted Nine-Atom Germanium Deltahedral Clusters. *J. Am. Chem. Soc.* **2014**, *136*, 12056−12063. (b) Li, F.; Muñoz-Castro, A.; Sevov, S. C. $[Ge_9\{Si(SiMe_3)_3\}_3\{SnPh_3\}]$: A Tetrasubstituted and Neutral Deltahedral Nine-Atom Cluster. *Angew. Chem., Int. Ed.* **2012**, *51*, 8581−8584. (c) Frischhut, S.; Fässler, T. F. Synthesis of Low-Oxidation-State Germanium Clusters Comprising a Functional Anchor Group - Synthesis and Characterization of $[(Ge^0)_5(Ge\text{-}R)_3(Ge\text{-}(CH_2)_n\text{-}CH{=}CH_2)]$ with R = $Si(SiMe_3)_3$. *Dalton Trans.* **2018**, *47*, 3223−3226. (d) Frischhut, S.; Klein, W.; Drees, M.; Fässler, T. F. Acylation of Homoatomic Ge_9 Cages and Subsequent Decarbonylation. *Chem. - Eur. J.* **2018**, *24*, 9009−9014.
(13) (a) Schenk, C.; Schnepf, A. $[AuGe_{18}\{Si(SiMe_3)_3\}_6]^-$A Soluble Au−Ge Cluster on the Way to a Molecular Cable? *Angew. Chem., Int. Ed.* **2007**, *46*, 5314−5316. (b) Schenk, C.; Henke, F.; Santiso-Quiñones, G.; Krossing, I.; Schnepf, A. $[Si(SiMe_3)_3]_6Ge_{18}M$ (*M* = Cu, Ag, Au): Metalloid Cluster Compounds as Unusual Building Blocks for a Supramolecular Chemistry. *Dalton Trans.* **2008**, 4436−4441. (c) Henke, F.; Schenk, C.; Schnepf, A. $[Si(SiMe_3)_3]_6Ge_{18}M$ (*M* = Zn, Cd, Hg): Neutral Metalloid Cluster Compounds of Germanium as Highly Soluble Building Blocks for Supramolecular Chemistry. *Dalton Trans.* **2009**, 9141−9145.
(14) Li, F.; Sevov, S. C. Coordination of Tri-Substituted Nona-Germanium Clusters to Cu (I) and Pd (0). *Inorg. Chem.* **2015**, *54*, 8121−8125.
(15) Mayer, K.; Schiegerl, L. J.; Fässler, T. F. On the Reactivity of Silylated Ge_9 Clusters: Synthesis and Characterization of $[ZnCp^*(Ge_9\{Si(SiMe_3)_3\}_3)]$, $[CuPiPr_3(Ge_9\{Si(SiMe_3)_3\}_3]$, and $[(CuPiPr_3)_4\{Ge_9(SiPh_3)_2\}_2]$. *Chem. - Eur. J.* **2016**, *22*, 18794−18800.
(16) (a) Geitner, F. S.; Fässler, T. F. Introducing Tetrel Zintl Ions to N-Heterocyclic Carbenes - Synthesis of Coinage Metal NHC Complexes of $[Ge_9\{Si(CH_3)_3\}_3]^-$. *Eur. J. Inorg. Chem.* **2016**, *2016*, 2688−2691. (b) Schiegerl, L. J.; Geitner, F. S.; Fischer, C.; Klein, W.; Fässler, T. F. Functionalization of $[Ge_9]$ with Small Silanes: $[Ge_9(SiR_3)_3]^-$ (R = *i*Bu, *i*Pr, Et) and the Structures of $(CuNHC^{Dipp})[Ge_9\{Si(iBu)_3\}_3]$, $(K\text{-}18c6)Au[Ge_9\{Si(iBu)_3\}_3]_2$ and $(K\text{-}18c6)_2[Ge_9\{Si(iBu)_3\}_2]$. *Z. Anorg. Allg. Chem.* **2016**, *642*, 1419−1426. (c) Geitner, F. S.; Giebel, M. A.; Pöthig, A.; Fässler, T. F. N-Heterocyclic Carbene Coinage Metal Complexes of the Germanium-Rich Metalloid Clusters $[Ge_9R_3]^-$ and $[Ge_9R^I{}_2]^{2-}$ with R = $Si(iPr)_3$ and R^I = $Si(TMS)_3$. *Molecules* **2017**, *22*, 1204. (d) Geitner, F.; Klein, W.; Fässler, T. Formation of the Intermetalloid Cluster $[AgSn_{18}]^{7-}$ − the Reactivity of Coinage Metal NHC Compounds Towards $[Sn_9]^{4-}$. *Dalton Trans.* **2017**, *46*, 5796−5800.
(17) (a) Mayer, K.; Jantke, L.-A.; Schulz, S.; Fässler, T. F. Retention of the Zn− Zn Bond in $[Ge_9Zn{-}ZnGe_9]^{6-}$ and Formation of $[(Ge_9Zn){-}(Ge_9){-}(ZnGe_9)]^{8-}$ and Polymeric $^1{}_\infty[-(Ge_9Zn)^{2-}-]^1$. *Angew. Chem., Int. Ed.* **2017**, *56*, 2350−2355. (b) Goicoechea, J. M.; Sevov, S. C. Organozinc Derivatives of Deltahedral Zintl Ions: Synthesis and Characterization of *closo*-$[E_9Zn(C_6H_5)]^{3-}$ (*E* = Si, Ge, Sn, Pb). *Organometallics* **2006**, *25*, 4530−4536. (c) Bentlohner, M. M.; Jantke, L.-A.; Henneberger, T.; Fischer, C.; Mayer, K.; Klein, W.; Fässler, T. F. On the Nature of Bridging Metal Atoms in Intermetalloid Clusters: Synthesis and Structure of the Metal-Atom-Bridged Zintl Clusters $[Sn(Ge_9)_2]^{4-}$ and $[Zn(Ge_9)_2)]^{6-}$. *Chem. - Eur. J.* **2016**, *22*, 13946−13952. (d) Scharfe, S.; Fässler, T. F. Varying Bonding Modes of the Zintl Ion $[Ge_9]^{4-}$ in CuI Complexes: Syntheses and Structures of $[Cu(\eta^4\text{-}Ge_9)(PR_3)]^{3-}$ (R = *i*Pr, Cy) and $[Cu(\eta^4\text{-}Ge_9)(\eta^1\text{-}Ge_9)]^{7-}$. *Eur. J. Inorg. Chem.* **2010**, *2010*, 1207−1213. (e) Yong, L.; Hoffmann, S. D.; Fässler, T. F. Crystal Structures of $[K(2.2.2\text{-crypt})]_4[Pb_9Mo(CO)_3]$ - Isolation of the Novel Isomers $[(\eta^5\text{-}Pb_9)Mo(CO)_3]^{4-}$ beside $[(\eta^4\text{-}Pb_9)Mo(CO)_3]^{4-}$. *Eur. J. Inorg. Chem.* **2005**, *2005*, 3663−3669. (f) Yong, L.; Hoffmann, S.; Fässler, T. F. Crystal Structure of Tetrakis [([2.2.2] crypt)potassium] Tricarbonylmolybdenum (0) Nonastannide Ethylenediamine Disolvate, $[K(C_{18}H_{36}O_6N_2)]_4[Mo(CO)_3Sn_9] \cdot 2C_2H_8N_2$. *Z. Kristallogr.-New Cryst.* **2005**, *220*, 53−57. (g) Kesanli, B.; Fettinger, J.; Eichhorn, B. The *closo*-$[Sn_9M(CO)_3]^{4-}$ Zintl Ion Clusters where *M* = Cr, Mo, W: Two Structural Isomers and Their Dynamic Behavior. *Chem. - Eur. J.* **2001**, *7*, 5277−5285. (h) Sun, Z.-M.; Zhao, Y.-F.; Li, J.; Wang, L.-S. Diversity of Functionalized Germanium Zintl Clusters: Syntheses and Theoretical Studies of $[Ge_9PdPPh_3]^{3-}$ and $[Ni@(Ge_9PdPPh_3)]^{2-}$. *J. Cluster Sci.* **2009**, *20*, 601−609.
(18) (a) Henke, F.; Schenk, C.; Schnepf, A. $[Si(SiMe_3)_3]_3Ge_9M(CO)^{3-}$ (*M* = Cr, Mo, W): Coordination Chemistry with Metalloid Clusters. *Dalton Trans.* **2011**, *40*, 6704−6710. (b) Schenk, C.; Schnepf, A. $\{Ge_9R_3Cr(CO)_5\}^-$ and $\{Ge_9R_3Cr(CO)_3\}^-$ a Metalloid Cluster $(Ge_9R_3^-)$ as a Flexible Ligand in Coordination Chemistry [R = $Si(SiMe_3)_3$]. *Chem. Commun.* **2009**, 3208−3210.
(19) Perla, L. G.; Muñoz-Castro, A.; Sevov, S. C. Eclipsed- and Staggered-$[Ge_{18}Pd_3\{EiPr_3\}_6]^{2-}$ (*E* = Si, Sn): Positional Isomerism in Deltahedral Zintl Clusters. *J. Am. Chem. Soc.* **2017**, *139*, 15176−15181.
(20) Li, F.; Muñoz-Castro, A.; Sevov, S. C. $[(Me_3Si)Si]_3EtGe_9Pd(PPh_3)$, a Pentafunctionalized Deltahedral Zintl Cluster: Synthesis, Structure, and Solution Dynamics. *Angew. Chem., Int. Ed.* **2016**, *55*, 8630−8633.
(21) Shannon, R. D. Revised Effective Ionic Radii and Systematic Studies of Interatomic Distances in Halides and Chalcogenides. *Acta Crystallogr., Sect. A: Cryst. Phys., Diffr., Theor. Gen. Crystallogr.* **1976**, *32*, 751−767.
(22) Lipscomb, W. N. Framework Rearrangement in Boranes and Carboranes. *Science* **1966**, *153*, 373−378.
(23) Hoch, C.; Wendorff, M.; Röhr, C. Synthesis and Crystal Structure of the Tetrelides $A_{12}M_{17}$ (*A* = Na, K, Rb, Cs; *M* = Si, Ge, Sn) and A_4Pb_9 (*A* = K, Rb). *J. Alloys Compd.* **2003**, *361*, 206−221.
(24) Frisch, M. J.; Trucks, G. W.; Schlegel, H. B.; Scuseria, G. E.; Robb, M. A.; Cheeseman, J. R.; Scalmani, G.; Barone, V.; Petersson, G. A.; Nakatsuji, H.; Li, X.; Caricato, M.; Marenich, A. V.; Bloino, J.; Janesko, B. G.; Gomperts, R.; Mennucci, B.; Hratchian, H. P.; Ortiz, J. V.; Izmaylov, A. F.; Sonnenberg, J. L.; Williams-Young, D.; Ding, F.; Lipparini, F.; Egidi, F.; Goings, J.; Peng, B.; Petrone, A.; Henderson, T.; Ranasinghe, D.; Zakrzewski, V. G.; Gao, J.; Rega, N.; Zheng, G.; Liang, W.; Hada, M.; Ehara, M.; Toyota, K.; Fukuda, R.; Hasegawa, J.; Ishida, M.; Nakajima, T.; Honda, Y.; Kitao, O.; Nakai, H.; Vreven, T.; Throssell, K.; Montgomery, J. A., Jr.; Peralta, J. E.; Ogliaro, F.; Bearpark, M. J.; Heyd, J. J.; Brothers, E. N.; Kudin, K. N.; Staroverov, V. N.; Keith, T. A.; Kobayashi, R.; Normand, J.; Raghavachari, K.; Rendell, A. P.; Burant, J. C.; Iyengar, S. S.; Tomasi, J.; Cossi, M.; Millam, J. M.; Klene, M.; Adamo, C.; Cammi, R.; Ochterski, J. W.; Martin, R. L.; Morokuma, K.; Farkas, O.; Foresman, J. B.; Fox, D. J. *Gaussian 09*, Revision E.01; Gaussian, Inc.: Wallingford, CT, 2016.
(25) Perdew, J. P.; Burke, K.; Ernzerhof, M. Generalized Gradient Approximation Made Simple. *Phys. Rev. Lett.* **1996**, *77*, 3865.
(26) (a) Weigend, F.; Ahlrichs, R. Balanced Basis Sets of Split Valence, Triple Zeta Valence and Quadruple Zeta Valence Quality for H to Rn: Design and Assessment of Accuracy. *Phys. Chem. Chem. Phys.* **2005**, *7*, 3297−3305. (b) Weigend, F. Accurate Coulomb-

DOI: 10.1021/acs.organomet.8b00459
Organometallics 2018, 37, 4560−4567

Fitting Basis Sets for H to Rn. *Phys. Chem. Chem. Phys.* **2006**, *8*, 1057−1065.
(27) Bergner, A.; Dolg, M.; Küchle, W.; Stoll, H.; Preuß, H. Ab Initio Energy-Adjusted Pseudopotentials for Elements of Groups 13−17. *Mol. Phys.* **1993**, *80*, 1431−1441.
(28) Greaves, E.-O.; Lock, C.; Maitlis, P. Metal−Acetylene Complexes. II. Acetylene complexes of Nickel, Palladium, and Platinum. *Can. J. Chem.* **1968**, *46*, 3879−3891.
(29) Nagel, U. Einfache Synthese von (η^2-Ethen)bis (triphenylphosphan)platin (0). *Chem. Ber.* **1982**, *115*, 1998−1999.
(30) Asaro, F.; Lenarda, M.; Pellizer, G.; Storaro, L. A Multinuclear NMR Study of [Pt0(PPh_3)$_2$(alkene)] Compounds Containing Asymmetric Olefins. *Spectrochim. Acta, Part A* **2000**, *56*, 2167−2175.
(31) *X-Area*, version 1.76.8.1; Stoe & Cie GmbH: Darmstadt, Germany, 2015.
(32) Sheldrick, G. M. Crystal Structure Refinement with SHELXL. *Acta Crystallogr., Sect. C: Struct. Chem.* **2015**, *71*, 3−8.

DOI: 10.1021/acs.organomet.8b00459
Organometallics 2018, 37, 4560−4567

SUPPORTING INFORMATION

Capping *nido*-Nonagermanide Clusters with *M*-PPh_3 and Dynamics in Solution: Synthesis and Structure of *closo*-$[(Me_3Si)_3Si]_3Et[Ge_9M](PPh_3)$ (*M* = Ni, Pt)

Sabine Frischhut,[a] Felix Kaiser,[b] Wilhelm Klein,[a] Markus Drees,[c] Fritz E. Kühn,[b] and Thomas F. Fässler[a]*

[a] Sabine Frischhut, Prof. Dr. Thomas F. Fässler, Lehrstuhl für Anorganische Chemie mit Schwerpunkt Neue Materialien, Fakultät für Chemie, Technische Universität München, Lichtenbergstraße 4, 85747 Garching, Germany.

[b] Dr. Felix Kaiser, Prof. Dr. Fritz E. Kühn, Professur für Molekulare Katalyse, Fakultät für Chemie , Technische Universität München, Lichtenbergstraße 4, 85747 Garching, Germany.

[c] Dr. Markus Drees, Lehrstuhl für Anorganische und Metallorganische Chemie, Fakultät für Chemie, Technische Universität München, Lichtenbergstraße 4, 85747 Garching, Germany.

E-mail: Thomas.Faessler@lrz.tu-muenchen.de

Content

1 Crystallographic details on **1** and **2**

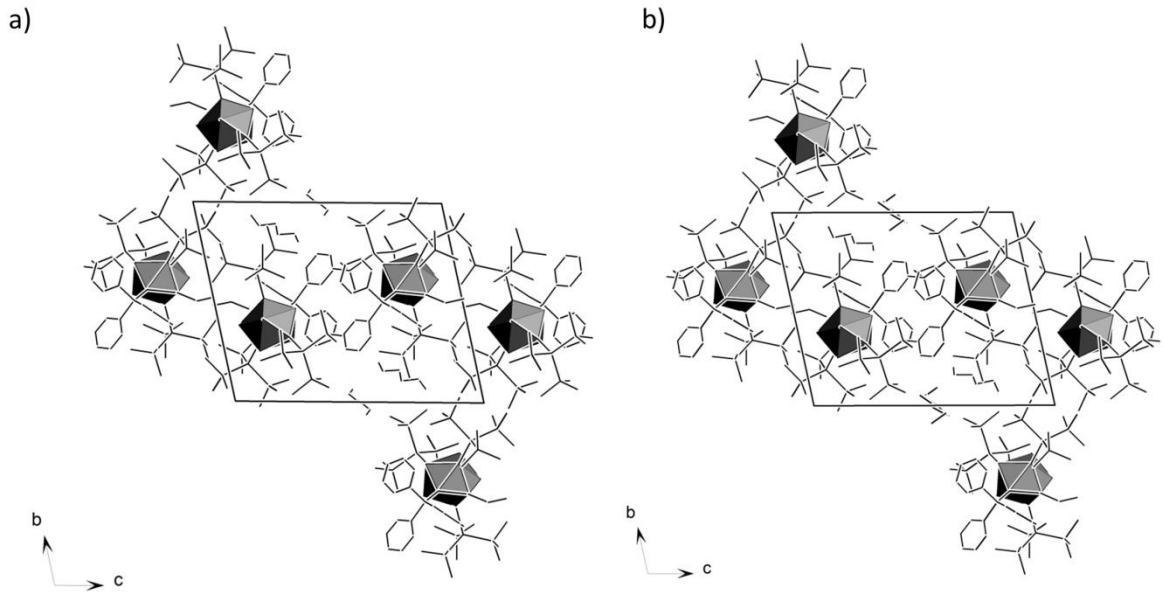

Figure S1. Illustration of the unit cells of a) **1** and b) **2**. [MGe$_9$] cluster cores (M = Ni, Pt) are shown as dark-grey polyhedra. Functionalities and solvent molecules are shown schematically. Hydrogen atoms are omitted for clarity.

Table S1. Selected bond lengths [Å] in **1**.

Ge1 – Ge2	2.4682(6)	Ge3 – Si5	2.422(1)
Ge1 – Ge5	2.5662(6)	Ge3 – Ni	2.6317(6)
Ge1 – Ge7	2.5660(6)	Ge4 – Ge5	2.7638(6)
Ge1 – Ge8	2.7772(7)	Ge4 – Ge6	2.5503(6)
Ge1 – Si1	2.415(1)	Ge4 – Ni	2.4135(6)
Ge1 – Ni	2.6217(7)	Ge5 – Ge6	2.5376(6)
Ge2 – Ge3	2.4730(6)	Ge5 – Ni	2.3984(6)
Ge2 – Ge8	2.7181(6)	Ge6 – Ge7	2.5511(7)
Ge2 – C1	1.983(4)	Ge6 – Ge9	2.5513(6)
Ge2 – Ni	2.3158(6)	Ge6 – Si9	2.398(1)
Ge3 – Ge4	2.5537(6)	Ge7 – Ge8	2.6040(6)
Ge3 – Ge8	2.8020(6)	Ge7 – Ge9	2.7785(6)
Ge3 – Ge9	2.5685(6)	Ge8 – Ge9	2.6111(6)

Table S2. Selected bond lengths [Å] in **2**.

Ge1 – Ge2	2.4756(8)	Ge3 – Si5	2.407(2)
Ge1 – Ge5	2.6032(8)	Ge3 – Pt	2.7676(7)
Ge1 – Ge7	2.5637(8)	Ge4 – Ge5	2.8885(9)
Ge1 – Ge8	2.7613(9)	Ge4 – Ge6	2.5457(8)
Ge1 – Si1	2.404(2)	Ge4 – Pt	2.4990(7)

Ge1 – Pt	2.7672(7)	Ge5 – Ge6	2.5348(8)
Ge2 – Ge3	2.4772(9)	Ge5 – Pt	2.4902(6)
Ge2 – Ge8	2.7432(8)	Ge6 – Ge7	2.5468(9)
Ge2 – C1	1.981(5)	Ge6 – Ge9	2.5460(8)
Ge2 – Pt	2.4365(6)	Ge6 – Si9	2.396(2)
Ge3 – Ge4	2.5880(8)	Ge7 – Ge8	2.5988(8)
Ge3 – Ge8	2.7890(9)	Ge7 – Ge9	2.7497(9)
Ge3 – Ge9	2.5657(8)	Ge8 – Ge9	2.6037(9)

Table S3. Selected bond angles [°] in **1**.

Ni – Ge1 – Ge8	95.26(2)	Ni – Ge2 – Ge8	104.59(2)
Ni – Ge3 – Ge8	94.45(2)	Ge5 – Ge4 – Ge9	90.76(2)
Ge1 – Ni – Ge3	88.02(2)	Ge5 – Ge7 – Ge9	88.83(2)
Ge1 – Ge8 – Ge3	81.72(2)	Ge5 – Ge6 – Ge9	114.87(2)
Ge1 – Ge2 – Ge3	95.24(2)	Ge4 – Ge6 – Ge7	115.07(2)

Table S4. Selected bond angles [°] in **2**.

Pt – Ge1 – Ge8	97.59(2)	Pt – Ge2 – Ge8	106.69(2)
Pt – Ge3 – Ge8	96.93(2)	Ge5 – Ge4 – Ge9	89.34(2)
Ge1 – Pt – Ge3	82.66(2)	Ge5 – Ge7 – Ge9	90.25(2)
Ge1 – Ge8 – Ge3	82.38(2)	Ge5 – Ge6 – Ge9	115.99(3)
Ge1 – Ge2 – Ge3	95.12(3)	Ge4 – Ge6 – Ge7	116.12(3)

2 NMR Spectroscopic Characterization of $[(Me_3Si)_3Si]_3Ge_9Et$

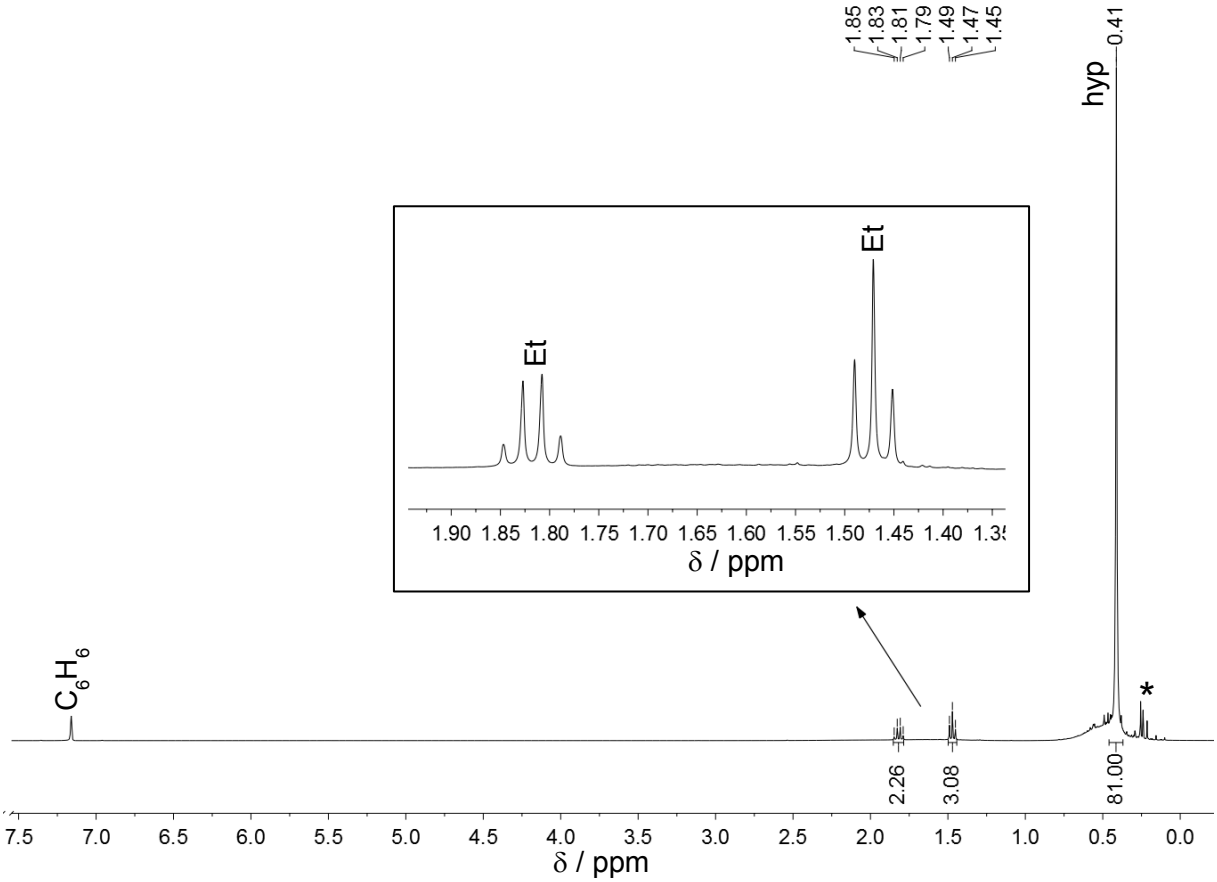

Figure S2. ^{1}H NMR spectrum of the crude product of $[(Me_3Si)_3Si]_3Ge_9Et$ recorded in $[D_6]$benzene at r.t. Signals marked with * could not be assigned.

3 NMR Spectroscopic Characterization of **1**

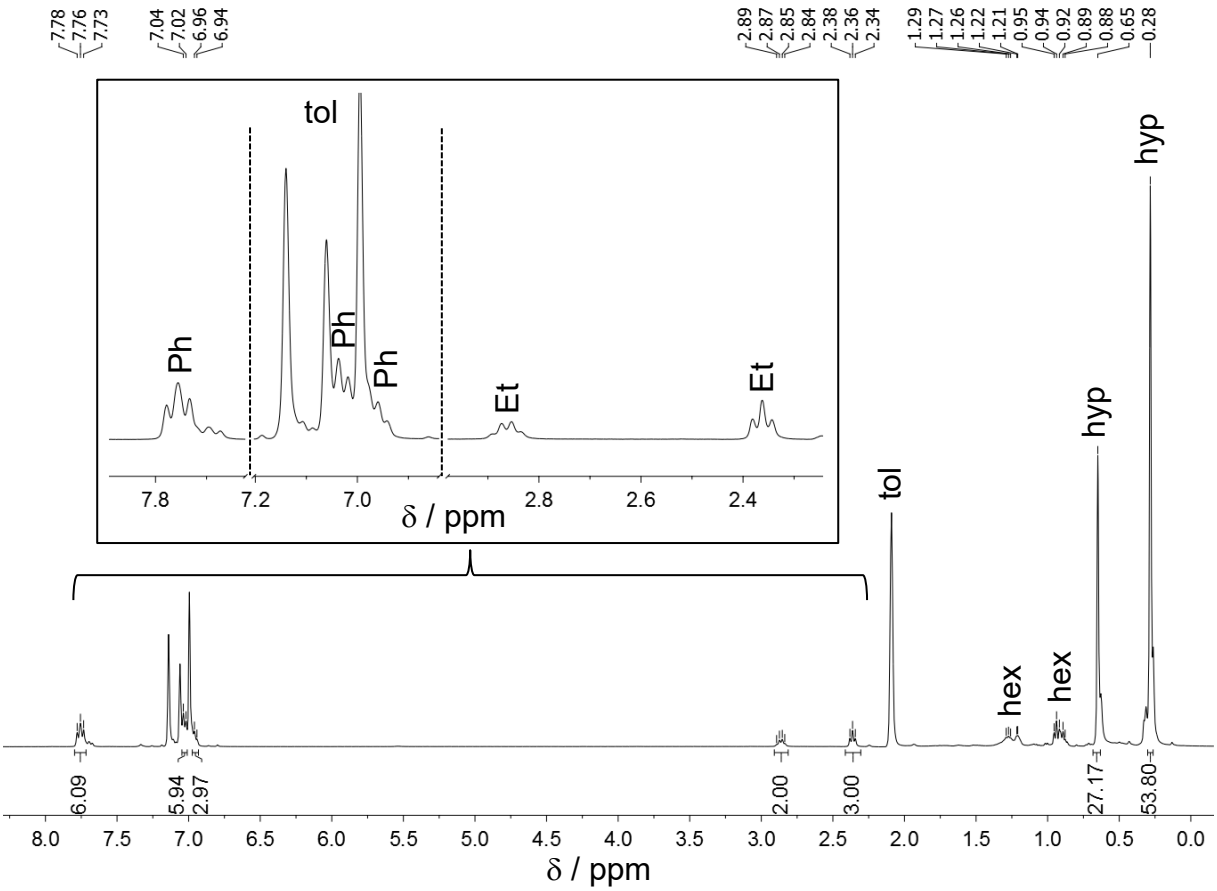

Figure S3. ^{1}H NMR spectrum of dissolved crystals of **1** recorded in [D_8]toluene at −40 °C. The crystals were dissolved at −78 °C to avoid decomposition of the compound. The regions of the phenyl and ethyl groups are shown enlarged. The signals of the hypersilyl groups are marked with hyp, the signals of hexane are marked with "hex".

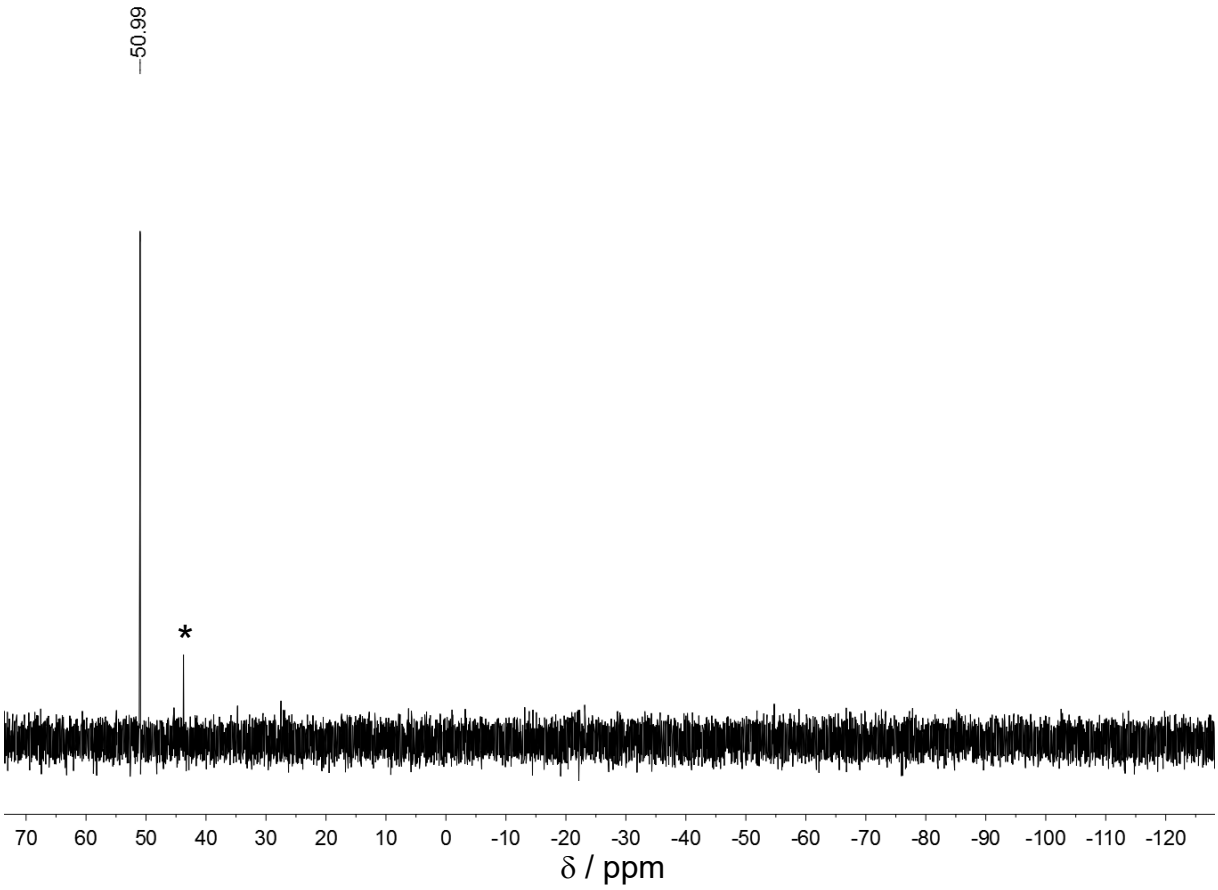

Figure S4. ^{31}P NMR spectrum of dissolved crystals of **1** recorded in [D_8]toluene at −40 °C. The signal marked with * could not be assigned.

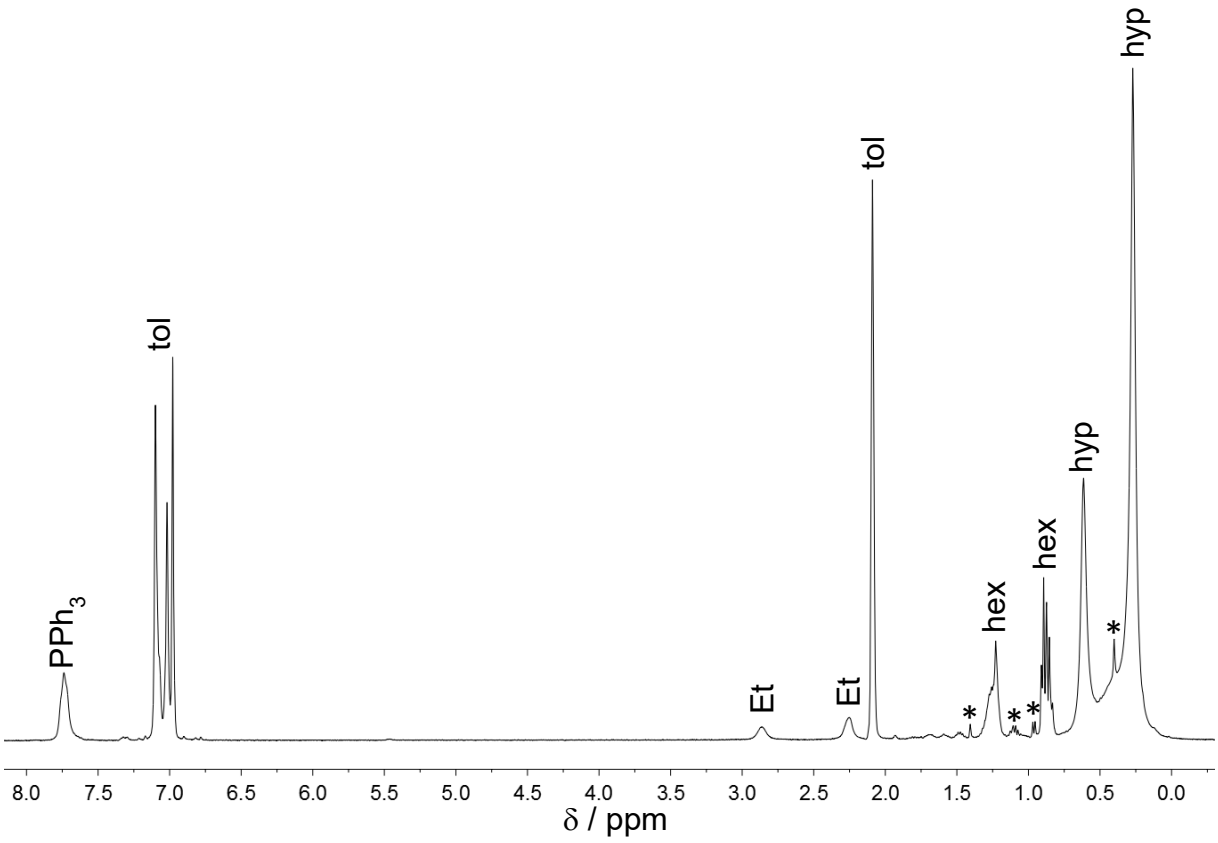

Figure S5. ^{1}H NMR spectrum of dissolved crystals of **1** recorded in [D_8]toluene at 20 °C. The crystals were dissolved at −78 °C.

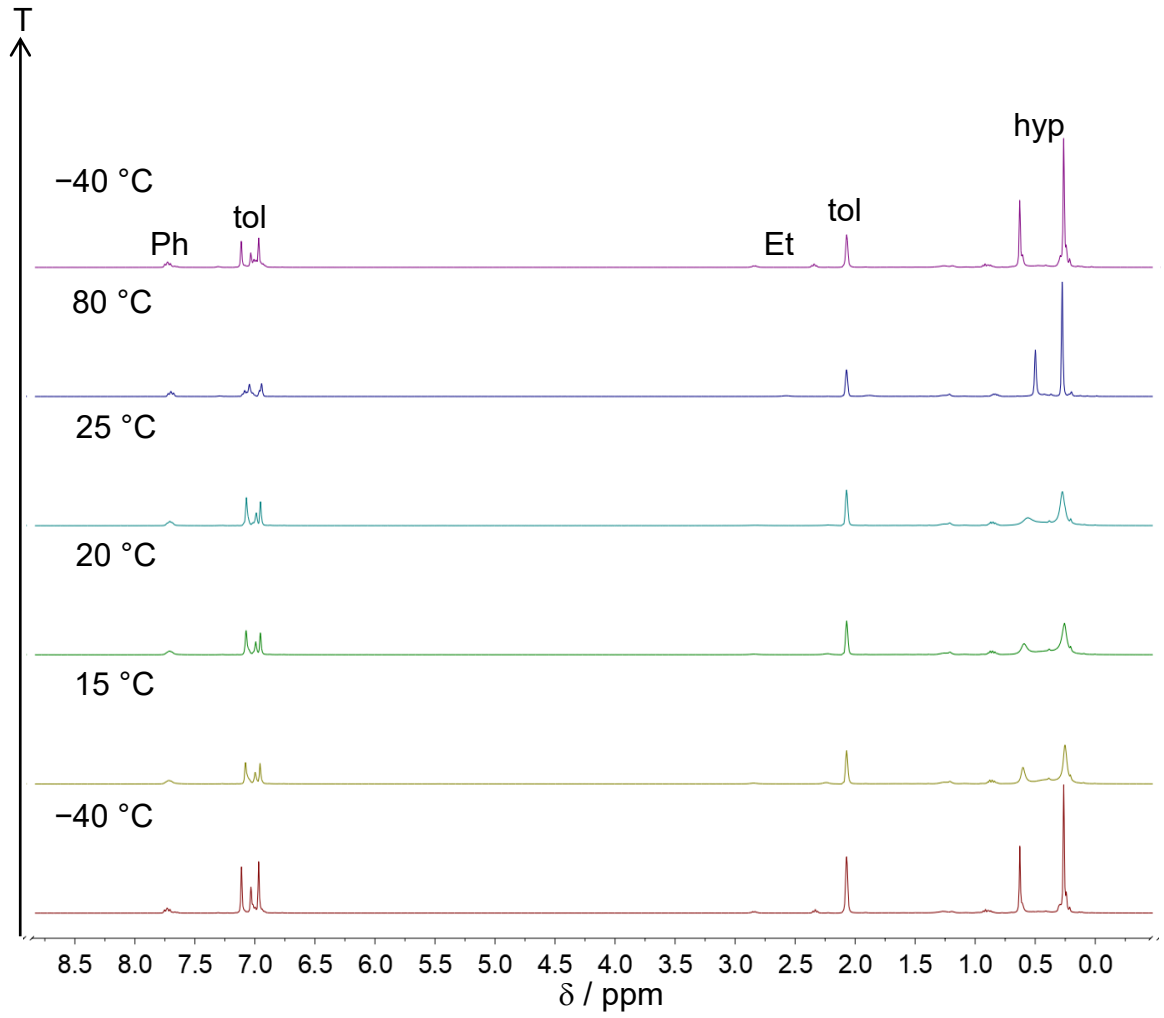

Figure S6. Temperature-dependent ^{1}H NMR spectra of dissolved crystals of **1** recorded in [D_8]toluene.

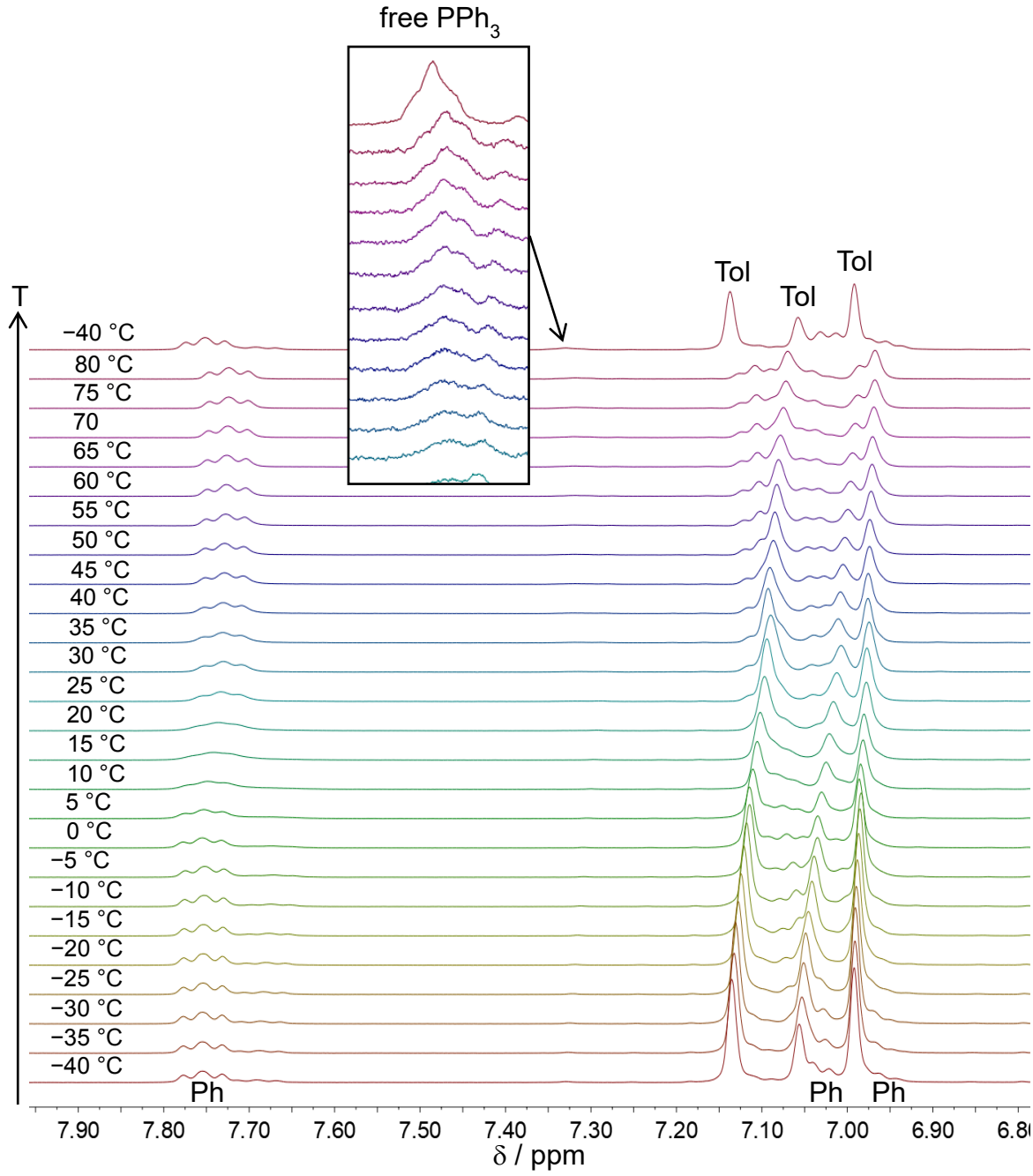

Figure S7. Variable temperature ^{1}H NMR study of crystals of **1** in [D_8]toluene in the range from −40 °C to 80 °C and subsequent cooling to −40 °C. For reasons of clarity only the signals of the triphenylphosphine ligand are shown.

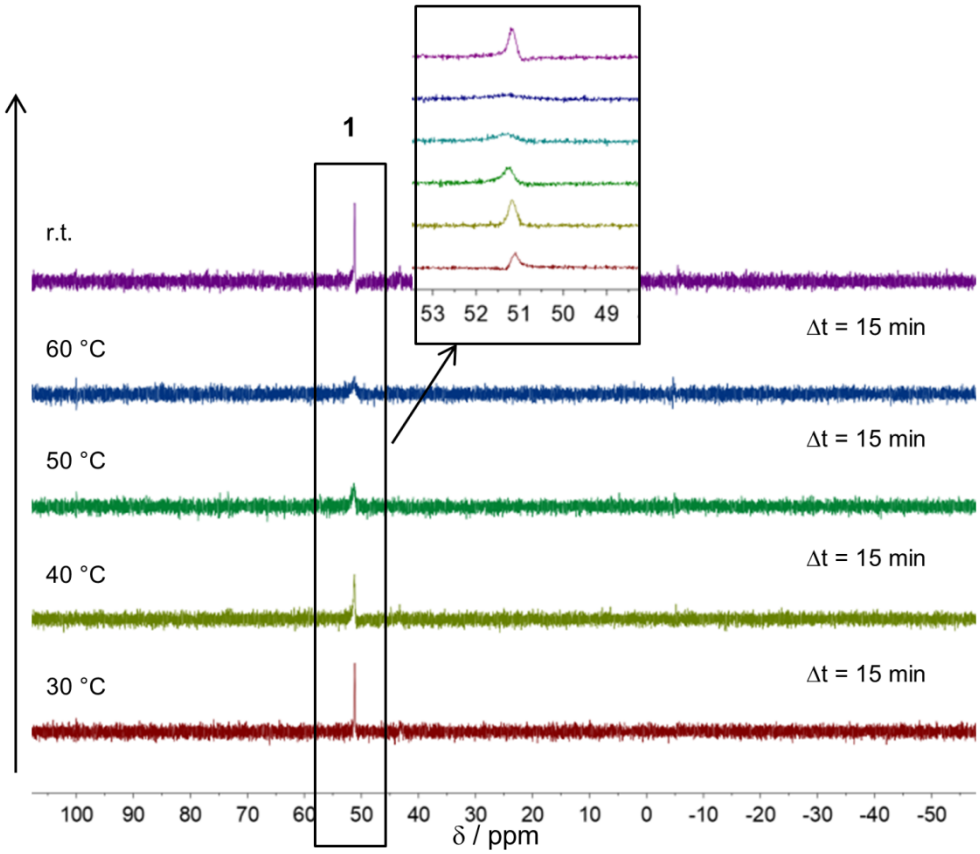

Figure S8. Variable temperature ^{31}P NMR study of crystals of **1** in [D_8]toluene in the range from 30 °C to 60 °C and subsequent cooling to r.t.

4 NMR Spectroscopic Characterization of **2**

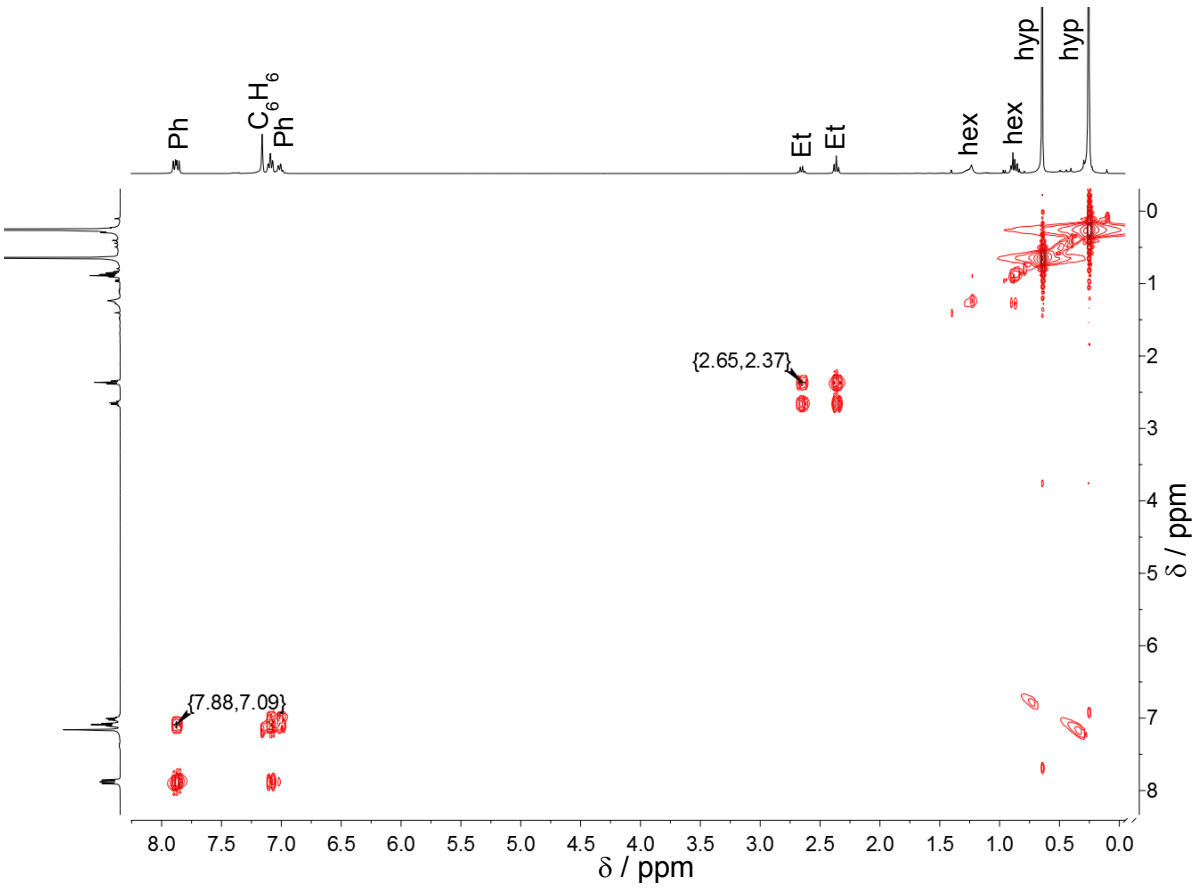

Figure S9. ^{1}H ^{1}H COSY NMR spectrum of dissolved crystals of **2** recorded in [D_6]benzene at r.t.

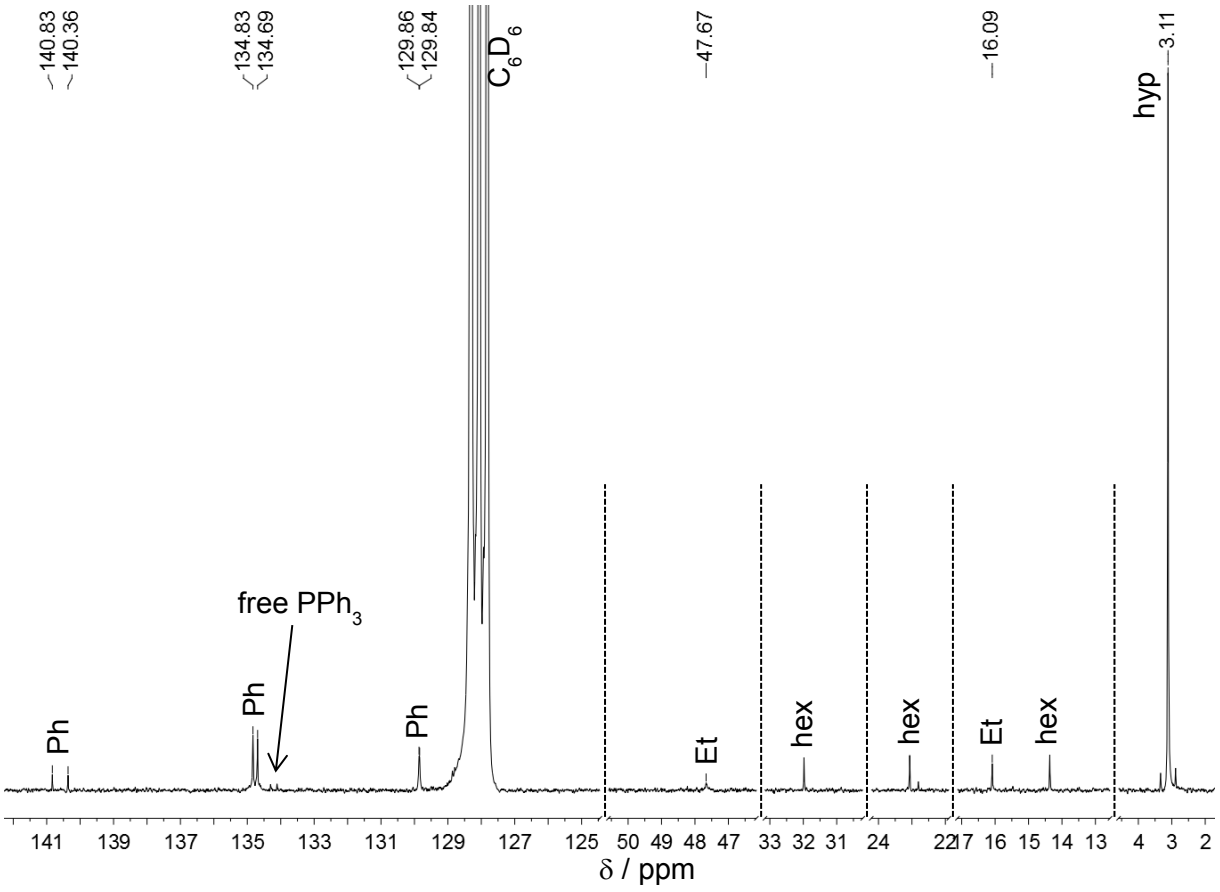

Figure S10. ^{13}C NMR spectrum of dissolved crystals of compound **2** recorded in [D_6]benzene at r.t. Only the relevant regions are depicted for clarity.

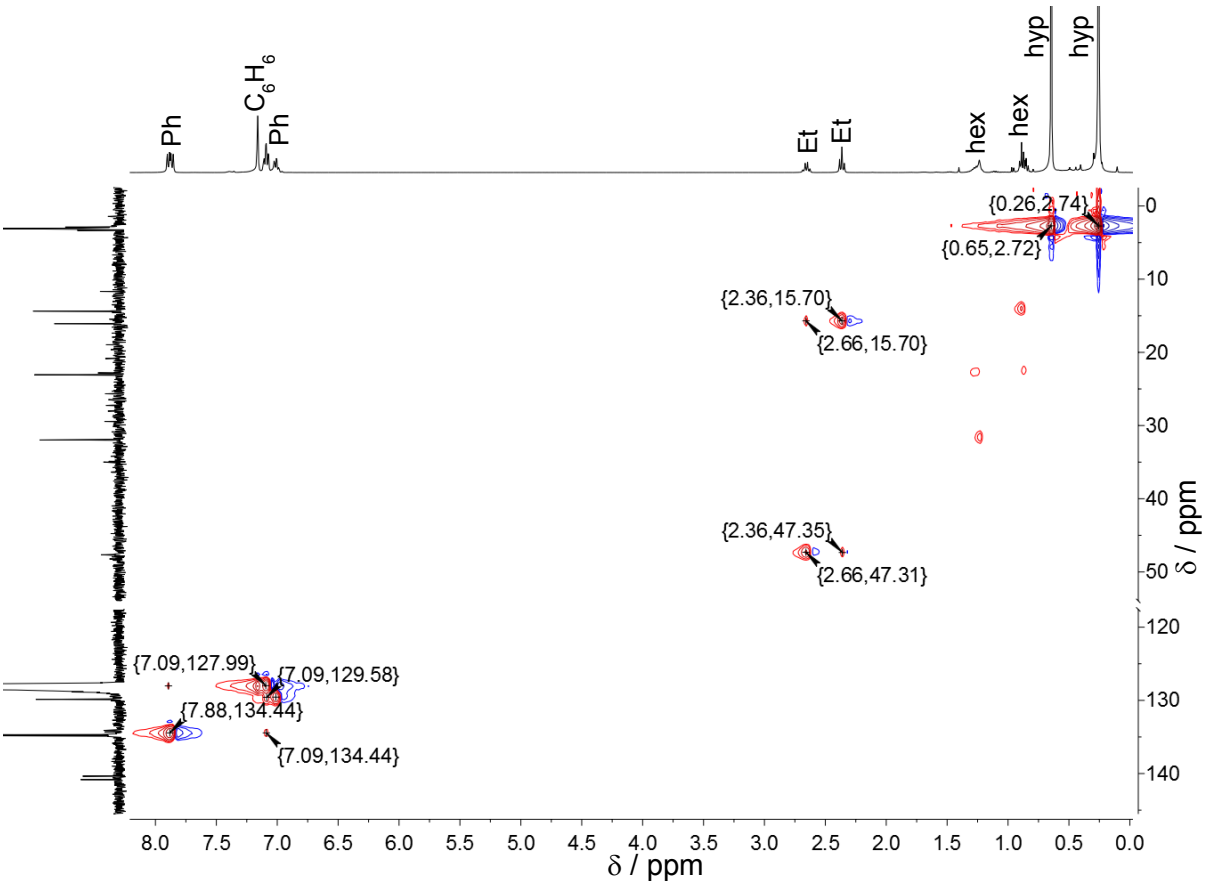

Figure S11. ^{1}H ^{13}C HSQC NMR spectrum of dissolved crystals of **2** recorded in [D_6]benzene at r.t.

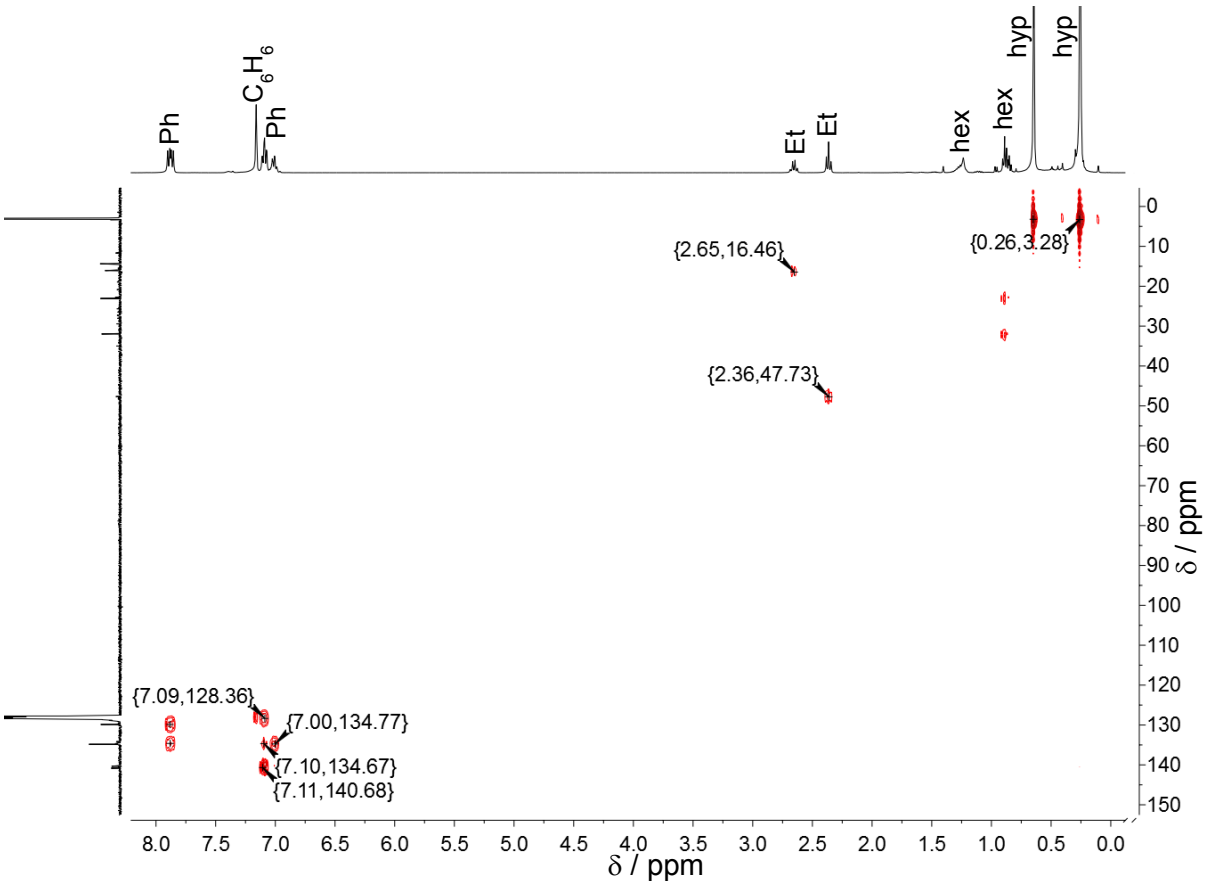

Figure S12. ^{1}H ^{13}C HMBC NMR spectrum of dissolved crystals of **2** recorded in [D_6]benzene at r.t.

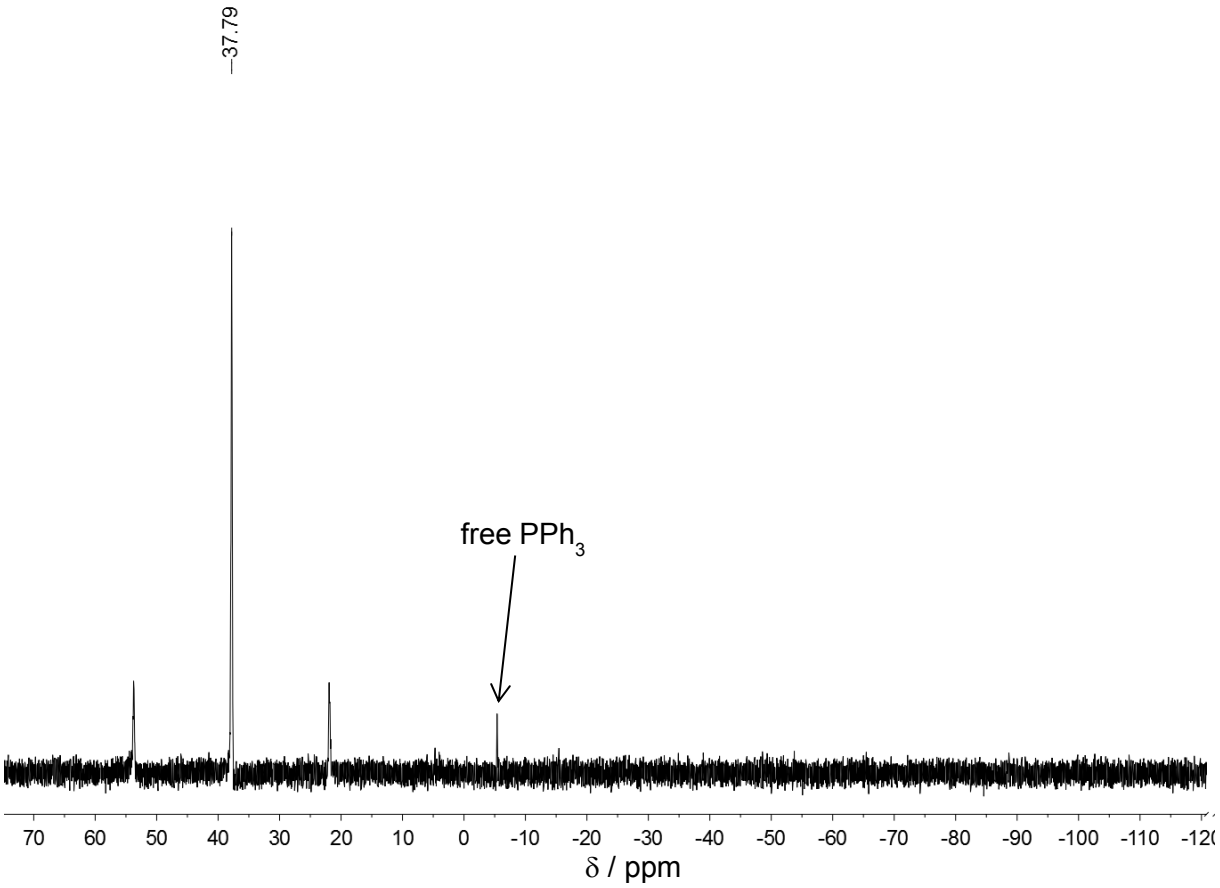

Figure S13. ^{31}P NMR spectrum of dissolved crystals of compound **2** recorded in [D_6]benzene at r.t. The spectrum also shows the coupling of ^{31}P to ^{195}Pt with ^{1}J = 2567 Hz, which is typical for platinum-phosphine complexes.[1]

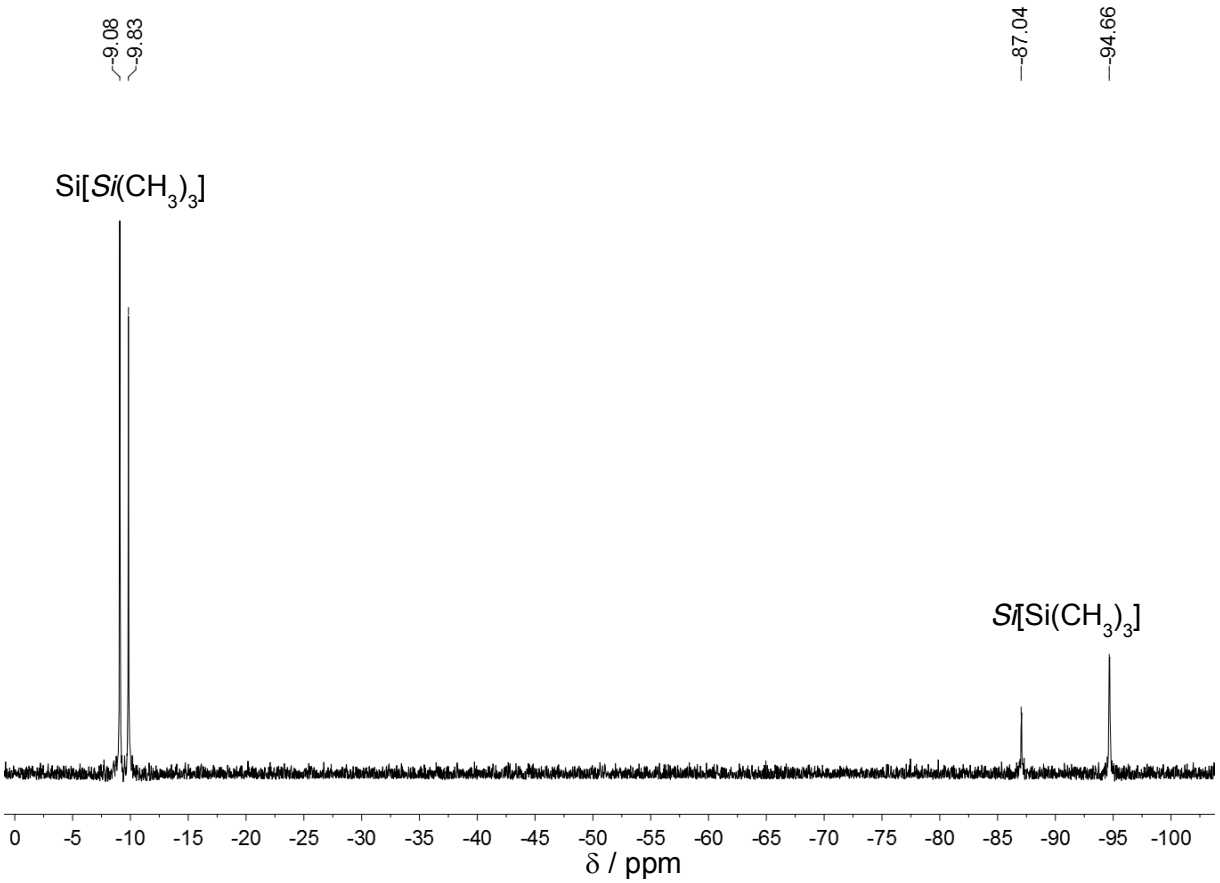

Figure S14. ^{29}Si NMR spectrum of dissolved crystals of compound **2** recorded in [D_6]benzene at r.t.

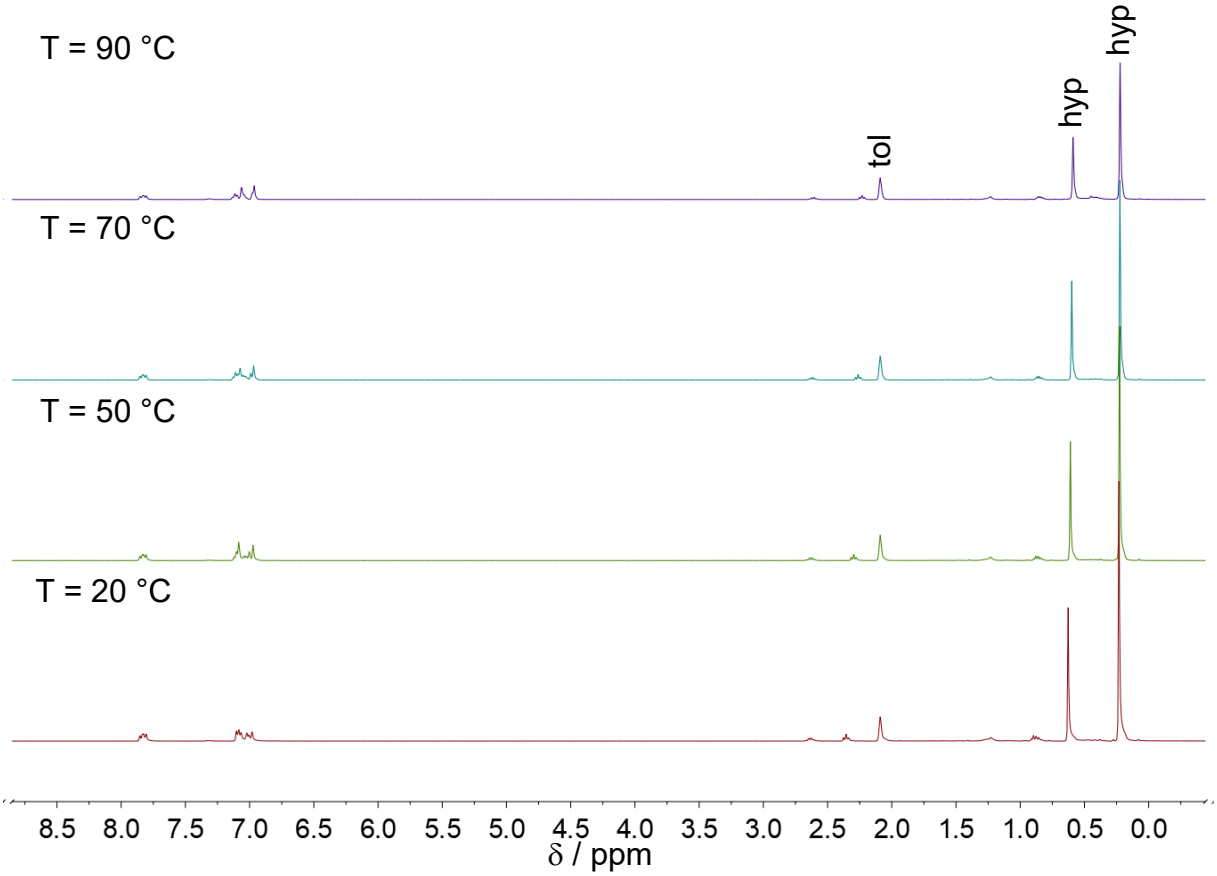

Figure S15. T-resolved ^{1}H NMR study of dissolved crystals of **2** recorded in [D_8]toluene.

5 References

(1) Pidcock, A. *Advances in Chemistry* **1982**, *196*, 1.
(2) Klinger, M.; Schenk, C.; Henke, F.; Clayborne, A.; Schnepf, A.; Unterreiner, A.-N. *Chem*. *Commun*. **2015**, *51*, 12278.

5.11 Deltahedral Ge_9 Cluster-Expansion with Pentamethylcyclopentadienylsilicon(II) Cation

Sabine Frischhut, Jasmin V. Dums, Wilhelm Klein, Peter Jutzi, and Thomas F. Fässler

Manuscript for publication

5.11.1 Content and Contribution

Within the scope of this work, the first Ge_9 Zintl cluster expansion with a tetrel-element atom was achieved. The reaction of $K_2[\{(Me_3Si)_3Si\}_3Ge_9]$ with $[SiCp^*][B(C_6F_5)_4]$ in the presence of lithium cations in fluorobenzene at r.t. for 3 h and subsequent cooling to −32 °C for three days yielded $\{(Me_3Si)_3Si\}_2Cp^*[LiSiGe_9](SiCp^*)_2[Ge_9SiLi]Cp^*\{(Me_3Si)_3Si\}_2$ in very low yield. The compound was synthesized and characterized by single crystal X-ray crystallography within this thesis. The crystal structure was refined under assistance of Dr. Wilhelm Klein.

As was unequivocally shown by the crystal structure, the compound exhibits two coupled *arachno*-$[Ge_9Si]$ icosahedra, each of which bearing six *exo*-bonded ligands. One of the twofive-membered rings of each cluster is capped by a Li atom. The two icosahedra are additionally linked by a covalently side-on bonded Cp*Si−SiCp* bridge. The icosahedra bear one open pentagonal face each. The lithium cation is a capping atom within the *nido*-icosahedron, which does not follow Wade-Mingos rules. The low-valent silicon atom which is integrated into the cluster scaffold is coordinated by a Cp* ligand.

Jasmin Dums performed quantum chemical calculations on the obtained expanded cluster compound.

The incorporation of a low-valent silicon atom into the Zintl cluster scaffold is a break-through in cluster chemistry, as this allows for an easy synthesis of tailor-made metalloid clusters with a distinct number of vertices, including unsubstituted metal atoms.

Prof. Dr. Peter Jutzi contributed by his generous gift of decamethylsilicocene. He contributed significantly to discussions.

The manuscript was authored within this thesis and revised by Prof. Dr. Thomas F. Fässler.

5.11.2 Manuscript for Publication

Deltahedral Ge_9 Cluster Expansion with Pentamethylcyclopentadienylsilicon(II) Cation

Sabine Frischhut[a], Jasmin V. Dums[a], Wilhelm Klein[a], Peter Jutzi[b], and Thomas F. Fässler*[a]

[a] Sabine Frischhut, Jasmin V. Dums, Dr. Wilhelm Klein, Prof. Dr. Thomas F. Fässler
Department Chemie, Technische Universität München
Lichtenbergstraße 4, 85747 Garching, Germany
Email: thomas.faessler@lrz.tum.de

[b] Prof. em. Dr. Peter Jutzi
Department Chemie, Universität Bielefeld
33615 Bielefeld, Germany

ABSTRACT

Compared to siliconoids, deltahedral $[Ge_9]^{4-}$ clusters are easily accessible by extraction from the binary phase K_4Ge_9. The deltahedral disilylated Zintl cluster $[\{(Me_3Si)_3Si\}_2Ge_9]^{2-}$ consists of seven unsubstituted, hemispheroidal germanium vertices. Therefore these clusters provide excellent candidates for investigations on surface structures of semiconductor materials with potentially outstanding, still to explore properties. We report on the first cluster expansion of $[\{(Me_3Si)_3Si\}_2Ge_9]^{2-}$ with the low-valent main group metal compound pentamethylcyclopentadienylsilicon(II) cation in the presence of Li cations in fluorobenzene yielding $\{(Me_3Si)_3Si\}_2Cp^*[LiSiGe_9](SiCp^*)_2[Ge_9SiLi]Cp^*\{(Me_3Si)_3Si\}_2$, consisting of two coupled *arachno*-$[Ge_9Si]$ icosahedra, additionally linked *via* a Si-Si bridge. The compound is characterized by single crystal X-ray crystallography.

INTRODUCTION

Multi-atomic naked metal clusters are the representatives of the transitional region between molecular and solid-state chemistry. Due to their expected exceptional properties, they have been aimed for and studied in nanotechnology in terms of structure-property relations for years.[1] Schnöckel and co-workers introduced the term metalloid clusters, which accordingly include metal clusters that bear both, ligand-free and ligand-substituted metal atoms. The definition also implies that metal-metal contacts predominate metal-ligand contacts.[2] Later, a subterm for Si analogous metalloid clusters was coined by Scheschkewitz, the so-called siliconoids, which bear at least one vertex with a hemispheroidal coordination sphere.[3] The synthesis of such Si clusters has remained a challenge.

A few outstanding, fully ligand-saturated Si clusters, e.g. an octasilacubane[4] and the tetrahedro-tetrasilane, (tBu$_3$Si)$_4$Si$_4$ (Figure 1 a)[5] have been reported, however bearing no unsubstituted Si vertex. The synthesis of such clusters, which is complex and requires several steps, proceeds *via* disilenides as nucleophilic precursors[6] or by reductive dehalogenation of stable low-valent silicon halide precursors.[7-13]

In recent years, the focus in cluster chemistry has been set on siliconoids. The breakthrough towards such stable compounds occurred in 2005 by Scheschkewitz with a five-atomic siliconoid bearing one naked metal atom (Figure 1 b),[14] and by Wiberg and Veith with their Si_8R_6 siliconoid featuring a dumbbell of two ligand-free vertex atoms.[15] These discoveries were followed by pentasilapropellanes with naked bridged Si atoms,[16-17] by the unexpected $Si_{11}R_9$ siliconoid with two unsubstituted Si atoms upon dimerization of two Si_6 units and cleavage of one Si atom,[3] and by the ladderane-like structured siliconoid with two naked Si atoms.[18]

Heteronuclear siliconoids with the heavier congener Ge have also emerged, such as heteronuclear propellanes $R_3Si_3Ge_2$ (Figure 1 c),[19-20] and the homonuclear Ge based metalloid pentagerma[1.1.1]propellane.[21]

The first bottom-up synthesis of a silicon cage anion was achieved by Sekiguchi and co-workers in the isolated tetrahedranyl anion, tris(trimethylsilyl)tetrahedranyllithium (Figure 1 d).[22] An unsaturated anionic siliconoid LiR_5Si_6, which is regarded as the prerequisite to be able to functionalize siliconoids like Zintl clusters, presents the first step towards narrowing

of the gap between siliconoids (naked vertices) and Zintl clusters (negative charge and naked vertices). Functionalization by reaction with various electrophiles yields specifically functionalized siliconoids.[23]

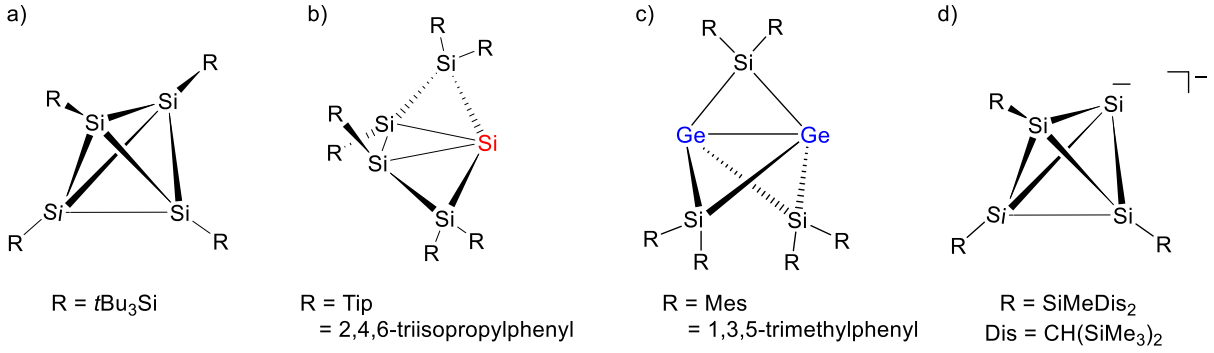

Figure 1. Silicon clusters. a) Fully saturated tetrahedro-tetrasilane,[5] b) R_6Si_5 siliconoid,[14] c) heteronuclear metalla[1.1.1]propellane,[19] d) Tetrasilatetrahedranide[22]. The naked vertex atoms in b) and c) are highlighted.

Unfortunately, all mentioned siliconoids bear more ligand-substituted than naked vertices.

In contrast, deltahedral $[E_9]^{4-}$ Zintl clusters, which bear exclusively naked vertices (*E* = Si, Ge), are easily accessible in one-step syntheses. Especially $[Ge_9]^{4-}$ clusters are well investigated and show flexibility towards incorporation of mostly transition metal atoms into the cluster scaffold.[24-25] Lately, deltahedral Si_9 clusters, which are accessible from the binary Zintl phase $K_{12}Si_{17}$ by dissolution in liquid ammonia have been intensively studied.[26-28] Both, bare Ge_9 and Si_9 clusters can be decorated with two to three silyl ligands forming $[E_9R_3]^-$ or $[E_9R_2]^{2-}$ clusters (*E* = Si, Ge; R = silyl ligand).[29-31]

In contrast to deltahedral Si_9 clusters, specific functionalization of deltahedral Ge_9 clusters has already been reported by reaction with alkyl halides,[32-33] acyl chlorides,[34] reaction with functionalized chlorosilanes[35] or chlorophosphanes.[36-38] Nevertheless, expansion of the Ge_9 cluster core has, so far, only been scarcely reported. $[Ge_{10}]^{2-}$ cluster crystallized from an ethylenediamine solution of Rb_4Ge_9 with (3Z/3*E*)-7-amino-1-(trimethylsilyl)-5-aza-hepta-3-en-1-yne.[39] The reaction was rather unexpected but seems to occur by Ge_9 cluster cleavage in solution. A more straight-forward principle to expand the *nido*-Zintl cluster is given by the reaction of $[Ge_9]^{4-}$ clusters with TlCp and transition metal complexes yielding bare *closo*-$[MGe_9]$ clusters (*M* = Tl or Cu, Sn, Zn, Pd),[40-46] of $[\{(Me_3Si)_3Si\}_3Ge_9]^-$ resulting in *closo*-$[\{(Me_3Si)_3Si\}_3Ge_9Tl]$[47] and *closo*-$[\{(Me_3Si)_3Si\}_3Ge_9M(CO)_3]^-$ for *M* = Cr, Mo, W,[48-49] or neutral

Ge_9 clusters yielding *closo*-[{$(Me_3Si)_3Si$}$_3Ge_9CH_2CH_3$]*M*(PPh_3) (*M* = Ni, Pd, Pt).[25, 50] In all cases the Tl atom or the transition metal is introduced into the polyhedral arrangement forming a distorted bicapped square antiprismatic [*M*Ge_9] core.

So far, E_9 Zintl cluster expansion with low-valent tetrel-element atoms has been unexplored, but is of special interest as this offers an easy and controllable way to access cluster structures with a distinct number of vertices. Especially the pentamethylcyclopentadienylsilicon(II) cation, which is already well understood,[51-52] has been applied as a stoichiometric source of silicon for siliconoid cluster growth.[53]

We herein present the first example of Zintl cluster growth by utilization of the pentamethylcyclopentadienylsilicon(II) cation. The reaction of K_2[{$(Me_3Si)_3Si$}$_3Ge_9$] with [SiCp*][$B(C_6F_5)_4$] in the presence of Li cations in fluorobenzene yielded {$(Me_3Si)_3Si$}$_2$Cp*[LiSiGe_9](SiCp*)$_2$[Ge_9SiLi]Cp*{$(Me_3Si)_3Si$}$_2$, which was characterized by single crystal X-ray crystallography.

DISCUSSION

We successfully expanded a deltahedral Ge_9 cluster by incorporation of one low-valent Si atom into the deltahedral Ge_9 cluster scaffold yielding $\{(Me_3Si)_3Si\}_2Cp^*[LiSiGe_9](SiCp^*)_2[Ge_9SiLi]Cp^*\{(Me_3Si)_3Si\}_2$ (**1**). The reaction proceeded by treating $K_2[\{(Me_3Si)_3Si\}_3Ge_9]$ with $[SiCp^*][B(C_6F_5)_4]$ in the presence of Li cations in fluorobenzene at r.t. for 3 h (Scheme 1). **1** was obtained as a block-shaped deep-brown crystal after storage at −32 °C for 3 days. The structure was determined by single crystal X-ray crystallography.

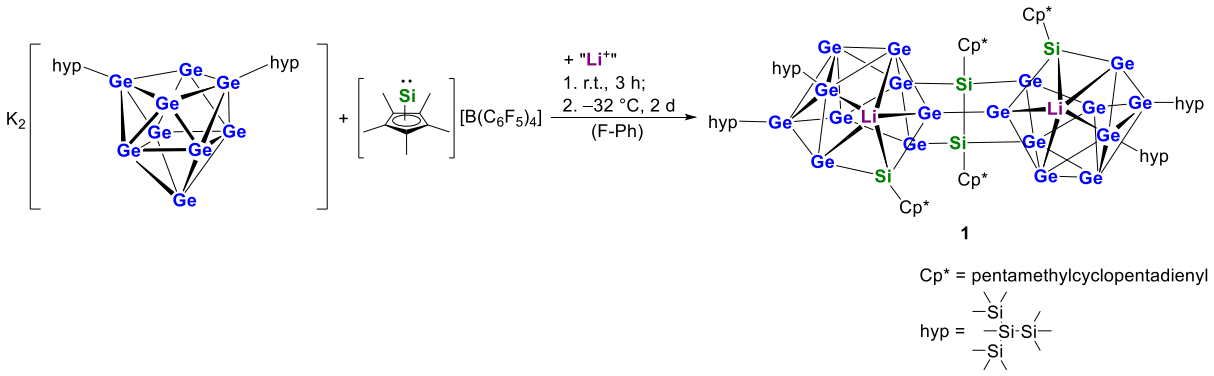

Scheme 1. Reaction of $K_2[\{(Me_3Si)_3Si\}_3Ge_9]$ with $[SiCp^*][B(C_6F_5)_4]$ in the presence of Li cations yielding **1**.

Crystal structure of 1

The structure of **1**, depicted in Figure 2 a, comprises a $[Ge_9Si]$-cluster framework with triangles and two five-membered rings, which can be derived from an icosahedron by removing two non-adjacent vertex atoms (Figure 2 b). Therefore, the Si atom is integrated into the cluster scaffold forming an *arachno*-$[Ge_9Si]$ framework. The Si atom, embedded in the icosahedral framework (Si1), carries a Cp* ligand, which coordinates in η^1-fashion. Hapticity change is often observed for the applied $[SiCp^*]$ cation upon reaction.[52] The two adjacent Ge atoms Ge3 and Ge8 bind a tris(trimethylsilyl)silyl ligand each. Two of the *arachno*-$[Ge_9Si]$ icosahedra are covalently linked *via* the Ge5 vertex. The second cluster arises from point symmetry with the symmetry center being located between the two coupled clusters. The Ge5−Ge5' bond length is determined to be 2.485(1) Å and is typical of oxidatively coupled deltahedral Ge_9 clusters. The *exo*-bond lengths in the coupled Ge_9 clusters $[Ge_9{-}Ge_9]^{6-}$ and the polymer $^1_\infty[Ge_9]^{2-}$ are 2.488(2) and 2.486(1) Å, respectively.[54-55]

In comparison, the intercluster bond lengths in $[Ge_9{=}Ge_9{=}Ge_9]^{6-}$ range from 2.579 to 2.601 Å, indicating a bond order <1.[56] The adjacent vertices Ge1 and Ge6 are connected to Si2 and Si2' of the side-on bridging unit Cp*Si2−Si2'Cp*, respectively. The bond length of d(Si2−Si2') = 2.444(3) Å lies in the range of already observed Si−Si single bonds.[57-58] Apparently, Si2 appears in the formal oxidation state of +IV. One Li atom caps one five-membered ring of the *arachno*-$[Ge_9Si]$ cluster resulting in a *nido*-$[LiGe_9Si]$ icosahedron comprising one open five-membered ring. The Li−Ge distances of d(Li−Ge4) = 2.54(1), d(Li−Ge5) = 2.35(1) and d(Li−Ge8) = 2.19(1) Å appear comparatively short when compared to the *closo*-$[Li_4Ge_{12}]^{8-}$ cluster reported by Sevov and co-workers (d(Li−Ge) = from 2.93(1) to 2.98(1) Å), except for d(Li−Ge9) = 2.93(1) Å, which is in good agreement with the literature.[59] The Li−Si1 bond length of 2.43(1) also appears to be comparatively short (Li−Si single bond: 2.672(9) Å[60]). Li is not further coordinated by any solvent molecule. In total, the formed cluster bears four hemispheroidal, ligand-free Ge vertices (Ge2, Ge7, Ge8, Ge9). The Ge−Ge distances within the *nido*-icosahedron range from 2.5079(9) Å (Ge4−Ge8) to 2.8986(9) Å (Ge1−Ge5), which is in good agreement with so far reported respective bond lengths in substituted deltahedral Ge_9 clusters.[61-62] Ge−Si distances lie in the range of 2.392(2) (Ge4−Si1) and 2.424(2) Å (Ge1−Si1) and compare well with Ge−Si bond lengths in heteronuclear Ge doped siliconoids.[19, 21]

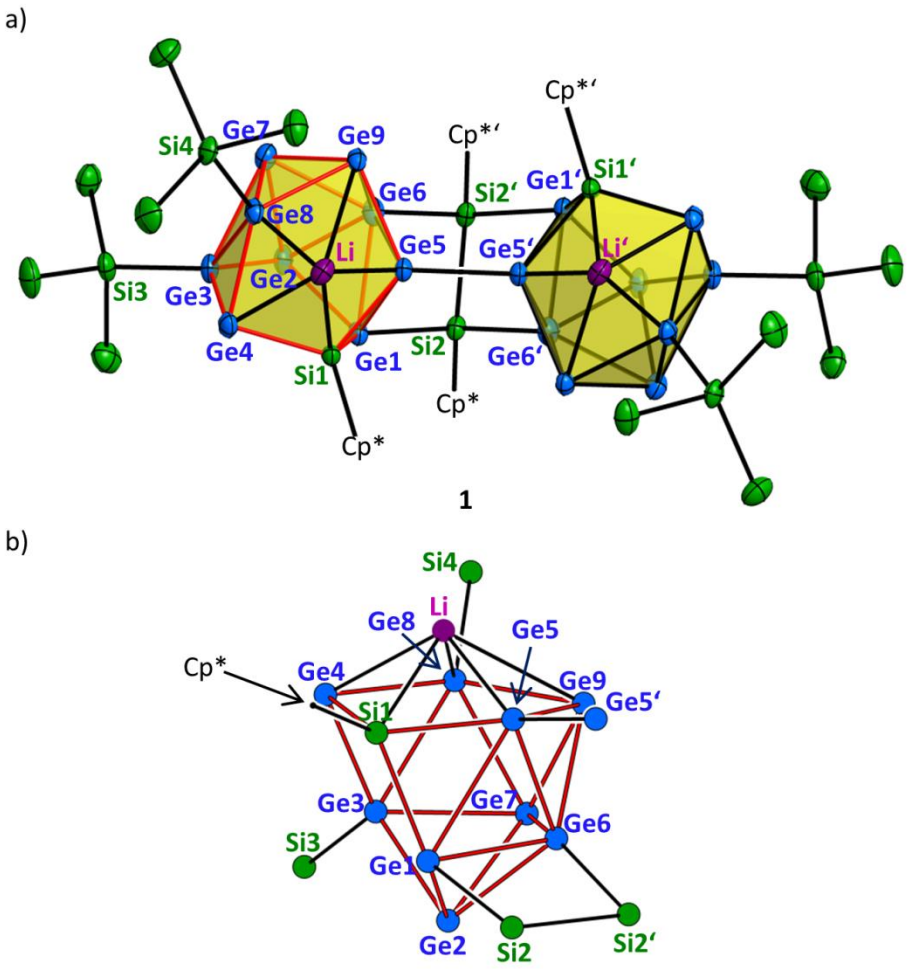

Figure 2. a) Structure of **1**. The *nido*-[LiGe$_9$Si] icosahedra are shown as yellow polyhedra. The methyl groups of the hypersilyl ligands are omitted for clarity. All Cp* ligands are coordinated to Si1 or Si2 in η^1-fashion. All ellipsoids are shown at a probability level of 50%. b) *Arachno*-[Ge$_9$Si] icosahedron highlighted in red. The atoms are shown as spheres. Color code: Ge – blue, Si – green, Li – purple.

The electronic situation in the structure of **1** does not follow Wade-Mingos rules at first sight.[63] Accordingly, the [R$_2$R'$_2$Cp*Ge$_9$Si] cluster (R = tris(trimethylsilyl)silyl; R' = Cp*Si2–Si2'Cp* bridge), which is oxidatively coupled to a second of its kind, comprises 27 skeletal electrons, arising from 4·2 = 8 e$^-$ of the ligand-free vertices and 6·3 = 18 e$^-$ of the substituted tetrel-element vertices, plus 1 e$^-$ from the negative charge. To get a deeper understanding of the electronic situation, quantum chemical calculations on **1** were performed. The structure was optimized in C_2 symmetry and exhibits a HOMO-LUMO gap of 2.17 eV. The structure undergoes a distortion, which results in deviation of the distances of the atoms. Noteworthy, due to rotation of the interconnected [Ge$_9$Si] clusters relative to each other, the distance of the atoms Ge5 and Ge5' appears to be elongated by 17% compared to the respective distance in the crystal structure of **1**. As a consequence, according to the IBO analysis, Ge5 and Ge5' both bear lone pairs and therefore, are not

connected by a chemical bond. Additionally, the IBO analysis shows that the bonding situation of Ge1−Si2, Ge6−Si2', as well as Si2−Si2' is localized, respectively. The population analyses show a positive charged Li (0.35 for Paboon and 0.88 for NPA charges). According to Wade-Mingo's rules of electron-counting, the optimized [$R_2R'_2Cp^*Ge_9Si$] cluster bears 26 skeletal electrons. The ligand-free vertices contribute 5·2 = 10 e^-, the vertices, which carry ligands, contribute 5·3 = 15 e^-, plus 1 e^- coming from the negative charge. This results in an *arachno*-[$R_2R'_2Cp^*Ge_9Si$] icosahedron, which is in good agreement with the structure of **1**. Conclusively, the break-up of the Ge5−Ge5' bond of **1** by simple rotation of the linked clusters leads to the loss of one e^- per cluster, and therefore, to two stable *arachno*-[Ge_9Si] icosahedra with 26 skeletal electrons according to Wade's rules. To date, the quantum chemical calculations have not been completed.

The presence of the Li cations in the product and therefore, also in reaction solution was at first sight unwanted and unforeseen, but arose due to Li impurity in the synthesized [$SiCp^*$][$B(C_6F_5)_4$]. The mechanism of the formation of the presented *nido*-icosahedron most likely proceeds *via* a diamond-square-diamond (DSD) mechanism accompanied by cluster opening. The DSD mechanism can be concluded from the now neighbored hypersilyl substituted Ge atoms Ge3 and Ge8, which in the utilized cluster precursor $K_2[\{(Me_3Si)_3Si\}_3Ge_9]$ had originally been located oppositely to each other.[30] Such DSD mechanisms have been described for deltahedral carboranes and boranes.[64] The formation of **1** also implies redox chemistry, where Si1 is reduced, whereby Si2 and the cluster itself are oxidized.

CONCLUSION

We present the first deltahedral Ge_9 Zintl cluster expansion with a low valent Si atom. The obtained structure shows a distorted *arachno*-[Ge_9Si] icosahedron with one open pentagonal face and one Li-capped five-membered ring. Such reactions might allow for comparatively easy syntheses of metal clusters bearing naked vertices. Such clusters are promising regarding their electronic and structural relations, as well as their expected exceptional properties.

REFERENCES

[1] *Cluster and Colloids* (Ed.: G. Schmid), Wiley-VCH, Weinheim, 1994; Metal Clusters in Chemistry (Eds.: P. Braunstein, L. A. Oro, P. R. Raithby), Wiley-VCH, Weinheim, **1999**.

[2] A. Schnepf, H. Schnöckel, *Angew. Chem. Int. Ed.* **2002**, *41*, 3532-3554.

[3] K. Abersfelder, A. Russell, H. S. Rzepa, A. J. White, P. R. Haycock, D. Scheschkewitz, *J. Am. Chem. Soc.* **2012**, *134*, 16008-16016.

[4] H. Matsumoto, K. Higuchi, S. Kyushin, M. Goto, *Angew. Chem. Int. Ed.* **1992**, *31*, 1354-1356.

[5] N. Wiberg, C. M. Finger, K. Polborn, *Angew. Chem. Int. Ed.* **1993**, *32*, 1054-1056.

[6] D. Scheschkewitz, *Chem. Lett.* **2010**, *40*, 2-11.

[7] C. W. So, H. W. Roesky, J. Magull, R. B. Oswald, *Angew. Chem. Int. Ed.* **2006**, *45*, 3948-3950.

[8] S. S. Sen, H. W. Roesky, D. Stern, J. Henn, D. Stalke, *J. Am. Chem. Soc.* **2009**, *132*, 1123-1126.

[9] Y. Wang, Y. Xie, P. Wei, R. B. King, H. F. Schaefer, P. v. R. Schleyer, G. H. Robinson, *Science* **2008**, *321*, 1069-1071.

[10] R. S. Ghadwal, H. W. Roesky, S. Merkel, J. Henn, D. Stalke, *Angew. Chem. Int. Ed.* **2009**, *48*, 5683-5686.

[11] A. C. Filippou, O. Chernov, B. Blom, K. W. Stumpf, G. Schnakenburg, *Chem. Eur. J.* **2010**, *16*, 2866-2872.

[12] H. Cui, C. Cui, *Dalton Trans.* **2011**, *40*, 11937-11940.

[13] F. Uhlemann, R. Köppe, A. Schnepf, *Z. Anorg. Allg. Chem.* **2014**, *640*, 1658-1664.

[14] D. Scheschkewitz, *Angew. Chem. Int. Ed.* **2005**, *44*, 2954-2956.

[15] G. Fischer, V. Huch, P. Mayer, S. K. Vasisht, M. Veith, N. Wiberg, *Angew. Chem. Int. Ed.* **2005**, *44*, 7884-7887.

[16] D. Nied, R. Köppe, W. Klopper, H. Schnöckel, F. Breher, *J. Am. Chem. Soc.* **2010**, *132*, 10264-10265.

[17] K. Abersfelder, A. J. White, R. J. Berger, H. S. Rzepa, D. Scheschkewitz, *Angew. Chem. Int. Ed.* **2011**, *50*, 7936-7939.

[18] T. Iwamoto, N. Akasaka, S. Ishida, *Nature Commun.* **2014**, *5*, 5353.

[19] D. Nied, P. Oña-Burgos, W. Klopper, F. Breher, *Organometallics* **2011**, *30*, 1419-1428.

[20] D. Nieder, C. B. Yildiz, A. Jana, M. Zimmer, V. Huch, D. Scheschkewitz, *Chem. Commun.* **2016**, *52*, 2799-2802.

[21] Y. Ito, V. Y. Lee, H. Gornitzka, C. Goedecke, G. Frenking, A. Sekiguchi, *J. Am. Chem. Soc.* **2013**, *135*, 6770-6773.

[22] M. Ichinohe, M. Toyoshima, R. Kinjo, A. Sekiguchi, *J. Am. Chem. Soc.* **2003**, *125*, 13328-13329.

[23] P. Willmes, K. Leszczyńska, Y. Heider, K. Abersfelder, M. Zimmer, V. Huch, D. Scheschkewitz, *Angew. Chem. Int. Ed.* **2016**, *55*, 2907-2910.

[24] S. Scharfe, F. Kraus, S. Stegmaier, A. Schier, T. F. Fässler, *Angew. Chem. Int. Ed.* **2011**, *50*, 3630-3670.

[25] F. Li, A. Muñoz-Castro, S. C. Sevov, *Angew. Chem. Int. Ed.* **2016**, *55*, 8630-8633.

[26] L. J. Schiegerl, A. J. Karttunen, J. Tillmann, S. Geier, G. Raudaschl-Sieber, M. Waibel, T. F. Fässler, *Angew. Chem. Int. Ed.* **2018**, *57*, 12950-12955.

[27] C. Lorenz, F. Hastreiter, J. Hioe, N. Lokesh, S. Gärtner, N. Korber, R. M. Gschwind, *Angew. Chem. Int. Ed.* **2018**, *57*, 12956-12960.

[28] T. Henneberger, W. Klein, T. F. Fässler, *Z. Anorg. Allg. Chem.* **2018**, *644*, 1018-1027.

[29] F. Li, S. C. Sevov, *Inorg. Chem.* **2012**, *51*, 2706-2708.
[30] O. Kysliak, A. Schnepf, *Dalton Trans.* **2016**, *45*, 2404-2408.
[31] L. Schiegerl, A. Karttunen, W. Klein, T. F. Fässler, *Chem. Eur. J.* **2018**.
[32] F. Li, A. Muñoz-Castro, S. C. Sevov, *Angew. Chem. Int. Ed.* **2012**, *51*, 8581-8584.
[33] S. Frischhut, T. F. Fässler, *Dalton Trans.* **2018**, *47*, 3223-3226.
[34] S. Frischhut, W. Klein, M. Drees, T. F. Fässler, *Chem. Eur. J.* **2018**, *24*, 9009-9014.
[35] K. Mayer, L. J. Schiegerl, T. Kratky, S. Günther, T. F. Fässler, *Chem. Commun.* **2017**, *53*, 11798-11801.
[36] F. S. Geitner, J. V. Dums, T. F. Fässler, *J. Am. Chem. Soc.* **2017**, *139*, 11933-11940.
[37] F.S. Geitner, C. Wallach, T. F. Fässler, *Chem. Eur. J.* **2018**, *24*, 4103-4110.
[38] F. S. Geitner, W. Klein, T. F. Fässler, *Angew. Chem. Int. Ed.* **2018**, *57*, 14509-14513.
[39] M. M. Bentlohner, C. Fischer, T. F. Fässler, *Chem. Commun.* **2016**, *52*, 9841-9843.
[40] Z.-M. Sun, Y.-F. Zhao, J. Li, L.-S. Wang, *J. Cluster Sci.* **2009**, *20*, 601-609.
[41] S. Scharfe, T. F. Fässler, *Eur. J. Inorg. Chem.* **2010**, *2010*, 1207-1213.
[42] M. M. Bentlohner, L.-A. Jantke, T. Henneberger, C. Fischer, K. Mayer, W. Klein, T. F. Fässler, *Chem. Eur. J.* **2016**, *22*, 13946-13952.
[43] K. Mayer, L.-A. Jantke, S. Schulz, T. F. Fässler, *Angew. Chem. Int. Ed.* **2017**, *56*, 2350-2355.
[44] J. M. Goicoechea, S. C. Sevov, *Organometallics* **2006**, *25*, 4530-4536.
[45] B. Zhou, M. S. Denning, C. Jones, J. M. Goicoechea, *Dalton Trans.* **2009**, 1571-1578.
[46] D. Rios, M. M. Gillett-Kunnath, J. D. Taylor, A. G. Oliver, S. C. Sevov, *Inorg. Chem.* **2011**, *50*, 2373-2377.
[47] F. Li, S. C. Sevov, *J. Am. Chem. Soc.* **2014**, *136*, 12056-12063.
[48] F. Henke, C. Schenk, A. Schnepf, *Dalton Trans.* **2011**, *40*, 6704-6710.
[49] C. Schenk, A. Schnepf, *Chem. Commun.* **2009**, 3208-3210.
[50] S. Frischhut, F. Kaiser, W. Klein, M. Drees, F. E. Kühn, T. F. Fässler, *Organometallics* **2018**, *37*, 4560-4567.
[51] P. Jutzi, A. Mix, B. Rummel, W. W. Schoeller, B. Neumann, H.-G. Stammler, *Science* **2004**, *305*, 849-851.
[52] P. Jutzi, *Chem. Eur. J.* **2014**, *20*, 9192-9207.
[53] K. Leszczyńska, K. Abersfelder, M. Majumdar, B. Neumann, H.-G. Stammler, H. S. Rzepa, P. Jutzi, D. Scheschkewitz, *Chem. Commun.* **2012**, *48*, 7820-7822.
[54] C. Downie, Z. Tang, A. M. Guloy, *Angew. Chem. Int. Ed.* **2000**, *39*, 337-340.
[55] L. Xu, S. C. Sevov, *J. Am. Chem. Soc.* **1999**, *121*, 9245-9246.
[56] A. Ugrinov, S. C. Sevov, *J. Am. Chem. Soc.* **2002**, *124*, 10990-10991.
[57] M. S. Gordon, T. N. Truong, E. K. Bonderson, *J. Am. Chem. Soc.* **1986**, *108*, 1421-1427.
[58] N. Wiberg, H. Schuster, A. Simon, K. Peters, *Angew. Chem. Int. Ed. Engl.* **1986**, *25*, 79-80.
[59] S. Bobev, S. C. Sevov, *Angew. Chem. Int. Ed.* **2001**, *40*, 1507-1510.
[60] H. Dias, M. Olmstead, K. Ruhlandt-Senge, P. Power, *J. Organomet. Chem.* **1993**, *462*, 1-6.
[61] S. Frischhut, M. M. Bentlohner, W. Klein, T. F. Fässler, *Inorg. Chem.* **2017**, *56*, 10691-10698.
[62] M. M. Bentlohner, W. Klein, Z. H. Fard, L.-A. Jantke, T. F. Fässler, *Angew. Chem. Int. Ed.* **2015**, *54*, 3748-3753.
[63] K. Wade, *Inorganic and Nuclear Chemistry Letters* **1972**, *8*, 559-562.
[64] W. N. Lipscomb, *Science* **1966**, *153*, 373-378.

SUPPORTING INFORMATION

Deltahedral Ge_9 Cluster Expansion with Pentamethylcyclopentadienylsilicon(II) Cation

Sabine Frischhut[a], Jasmin V. Dums[a], Wilhelm Klein[a], Peter Jutzi[b], and Thomas F. Fässler*[a]

[a] Sabine Frischhut, Jasmin V. Dums, Dr. Wilhelm Klein, Prof. Dr. Thomas F. Fässler
Department Chemie, Technische Universität München
Lichtenbergstraße 4, 85747 Garching, Germany
Email: thomas.faessler@lrz.tum.de

[b] Prof. em. Dr. Peter Jutzi
Department Chemie, Universität Bielefeld
33615 Bielefeld, Germany

1 Experimental

General: All manipulations were carried out under a purified argon atmosphere using standard Schlenk techniques. The Zintl phase with the nominal composition K_4Ge_9 was synthesized by heating a stoichiometric mixture of the elements K and Ge (99.999%, Chempur) at 650 °C for 46 h in a stainless steel autoclave.[1] Fluorobenzene (Alfa Aesar, 99%) was dried over calcium hydride. The commercially available reagent $[Li(OEt_2)_x][B(C_6F_5)_4]$ (TCI Chemicals, > 70%) was used as received. $K_2[\{Me_3Si)_3Si\}_2Ge_9]$ and $[Cp^*Si][B(C_6F_5)_4]$ were prepared according to literature procedures.[2-3]

Synthesis of $\{(Me_3Si)_3Si\}_2Cp^*[LiSiGe_9](SiCp^*_2)_2[Ge_9SiLi]Cp^*\{(Me_3Si)_3Si\}_2$ (1): To a suspension of $K_2[\{Me_3Si)_3Si\}_2Ge_9]$ (150 mg, 0.122 mmol) in 2 mL fluorobenzene a solution of $[Cp^*Si][B(C_6F_5)_4]$ (103 mg, 0.122 mmol) ($[Cp^*Si][B(C_6F_5)_4]$ was contaminated with Li cations, which most likely came from $[Li(OEt_2)_x][B(C_6F_5)_4]$ impurities) in 4 mL fluorobenzene was added. The brown-colored solution was stirred for 3 h at r.t. The reaction solution was filtered over glass fiber filter and concentrated to approximately 0.75 mL and stored at −32 °C for crystallization. One block-shaped deep-brown single crystal of the size 0.4 x 0.15 x 0.1 mm^3 was obtained after three days, which was suitable for single crystal X-ray crystallography.

X-ray Data Collection and Structure Determination: The crystal was transferred from the mother liquor into perfluoropolyalkylether under a cold stream of N_2. The single crystal was fixed on a glass fiber and positioned in a cold stream of N_2. The intensity data were recorded on a Stoe StadiVari diffractometer (Mo K_α radiation (λ = 0.71073 Å), Pilatus 300K detector), by using the X-Area software package.[4] The crystal structures were solved by Direct Methods and refined using the SHELX software.[5] The positions of the hydrogen atoms were calculated and refined using a riding model. All non-hydrogen atoms were treated with anisotropic displacement parameters. Crystallographic details on **1** are listed in Table S1. CCDC xxx contains the supplementary crystallographic data. These data can be obtained free of charge from The Cambridge Crystallographic Data Centre *via* www.ccdc.cam.ac.uk/data_request/cif.

Quantum Chemical Calculations

The computational analysis of **1** was performed using the Turbomole V7.3 program package[6], with exchange correlation hybrid function after Perdew, Burke and Ernzerhof (PBE0) and def2-TZVP basis sets for all considered elements Li, Ge, Si, C and H.[7-8] Multipole-accelerated resolution-of-the-identity technique was used to speed up the calculations.[9-11] Natural population analysis (NPA)[12] and Paboon charges[13], as well as an intrinsic bonding orbital (IBO)[14] analysis were carried out. For data processing and visualization Jmol[15] and IBOview[16] were used. Additionally, an optimization in a triplet state was tried to carry out, however, did not converge, suggesting a singlet state for **1**. In order to save computing time, the Cp* ligand and the tris(trimethylsilyl)silyl ligands were replaced by Cp and trimethylsilyl ligands, respectively.

2 Crystallographic Details

Table S1. Crystallographic details of **1**·FPh.

Compound	**1**·FPh
Formula	$C_{44}H_{89}FGe_9LiSi_{10}$
fw ($g \cdot mol^{-1}$)	1578.30
space group (no)	C2/c (15)
a (Å)	43.5204(9)
b (Å)	13.5342(3)
c (Å)	24.8107(5)
α (deg)	90
β (deg)	112.631(2)
γ (deg)	90
V ($Å^3$)	13488.5(5)
Z	8
T (K)	150
λ (Å)	0.71073
ρ_{calcd} ($g \cdot cm^{-3}$)	1.555
μ (mm^{-1})	4.160
collected reflections	190412

independent reflections	13275
R_{int}	0.094
parameters/ restraints	614/ 42
R_1 [$I>2\sigma(I)$ / all data]	0.076/0.046
wR_2 [$I>2\sigma(I)$ / all data)]	0.119/0.104
goodness of fit	1.059
max. / min. diff. el. density	1.39 / −1.56

Table S2. Bond lengths [Å] in **1**.

Li−Si1	2.43(1)	Ge3−Ge4	2.5151(9)
Li−Ge4	2.54(1)	Ge3−Ge7	2.7006(9)
Li−Ge5	2.35(1)	Ge3−Ge8	2.6887(9)
Li−Ge8	2.19(1)	Ge4−Ge8	2.5079(9)
Li−Ge9	2.93(1)	Ge5−Ge6	2.6158(9)
Si1−C1	1.947(6)	Ge5−Ge9	2.5615(8)
Si1−Ge1	2.424(2)	Ge5−Ge5’	2.485(1)
Si1−Ge4	2.392(2)	Ge6−Si2’	2.401(2)
Si1−Ge5	2.411(2)	Ge6−Ge7	2.6185(9)
Ge1−Ge2	2.5485(9)	Ge6−Ge9	2.5549(9)
Ge1−Ge5	2.8986(9)	Ge7−Ge8	2.7323(9)
Ge1−Si2	2.426(2)	Ge7−Ge9	2.7487(9)
Ge2−Ge3	2.5188(9)	Ge8−Si4	2.427(2)
Ge2−Ge6	2.5717(9)	Ge8−Ge9	2.5213(8)
Ge2−Ge7	2.8049(9)	Si2−Si2’	2.444(3)
Ge3−Si3	2.417(2)		

References

[1] C. Hoch, M. Wendorff, C. Röhr, *J. Alloys Compd.* **2003**, *361*, 206-221.
[2] O. Kysliak, A. Schnepf, *Dalton Trans.* **2016**, *45*, 2404-2408.
[3] P. Ghana, M. I. Arz, G. Schnakenburg, M. Straßmann, A. C. Filippou, *Organometallics* **2018**, *37*, 772-780.
[4] X-Area, version 1.76.8.1, Stoe & Cie GmbH, Darmstadt **2015**.
[5] G. M. Sheldrick, *Acta Cryst. C* **2015**, *71*, 3-8.
[6] *TURBOMOLE* V7.3, University of Karlsruhe and Forschungszentrum Karlsruhe GmbH, **2016**.
[7] F. Weigend, R. Ahlrichs, *PCCP* **2005**, *7*, 3297-3305.
[8] F. Weigend, M. Häser, H. Patzelt, R. Ahlrichs, *Chem. Phys. Lett.* **1998**, *294*, 143-152.
[9] K. Eichkorn, O. Treutler, H. Öhm, M. Häser, R. Ahlrichs, *Chem. Phys. Lett.* **1995**, 283-290.
[10] M. Sierka, A. Hogekamp, R. Ahlrichs, *J. Chem. Phys.* **2003**, *118*, 9136-9148.
[11] F. Weigend, *PCCP* **2006**, *8*, 1057-1065.
[12] A. E. Reed, R. B. Weinstock, F. Weinhold, *J. Chem. Phys.* **1985**, *83*, 735-746.
[13] C. Ehrhardt, R. Ahlrichs, *Theor. Chim. Acta* **1985**, *68*, 231-245.
[14] G. Knizia, *J. Chem. Theory Comput.* **2013**, *9*, 4834-4843.
[15] Jmol - An Open-Source Java Viewer for Chemical Structures in 3D, The Jmol Team, **2017.**
[16] G. Knizia, J. E. Klein, *Angew. Chem. Int. Ed.* **2015**, *54*, 5518-5522.

6 COMPLETE LIST OF PUBLICATIONS

PUBLICATIONS

8) *Capping Nido-Nonagermanide Clusters with M-PPh_3 and Dynamics in Solution: Synthesis and Structure of closo-[$(Me_3Si)_3Si]_3Et[Ge_9M](PPh_3)$ (M = Ni, Pt)*

S. Frischhut*, F. Kaiser, W. Klein, M. Drees, F. E. Kühn, T. F. Fässler

Organometallics, **2018**, *37*, 4560-4567.

7) On the Affinity between Fullerenes and Deltahedral Zintl Ions: a UV-Vis Spectroscopic Investigation

S. Frischhut*, J. G. Machado de Carvalho*, A. J. Karttunen, T. F. Fässler

Z. Anorg. Allg. Chem., **2018**, *644*, 1337-1343.

6) *Regionales Fonds-Stipendiatentreffen in München*

S. Frischhut*, N. Kunkel*, T. Wylezich*

Nachrichten aus der Chemie, **2018**, *66*, 777.

5) *Acylation of Homoatomic Ge_9 Cages and Subsequent Decarbonylation*

S. Frischhut, W. Klein, M. Drees, T. F. Fässler

Chem. Eur. J., **2018**, *24*, 9009-9014.

4) *Challenges in Chemical Synthesis at the Border of Solution-Based and Solid State Chemistry - Synthesis and Structure of [{$(Me_3Si)_3Si$}$Ge_9(CH_2CH_3)]^{2-}$*

S. Frischhut, W. Klein, T. F. Fässler

C. R. Chim., **2018**, *21*, 932-937.

3) *Synthesis of Low-Oxidation-State Germanium Clusters Comprising a Functional Anchor Group − Synthesis and Characterization of [$(Ge^0)_5(Ge\text{-}R)_3(Ge\text{-}(CH_2)_n\text{-}CH{=}CH_2)$] with R = $Si(SiMe_3)_3$*

S. Frischhut, T. F. Fässler

Dalton Trans., **2018**, *47*, 3223-3226.

2) *On the Mechanism of Connecting Deltahedral Zintl Clusters via Conjugated Buta-1,3-dien-1,4-diyl Functionalities: Synthesis and Structure of* $[Ge_9{-}CH{=}CH{-}CH{=}CH{-}Ge_9]^{6-}$

M. M. Bentlohner*, **S. Frischhut***, T. F. Fässler

Chem. Eur. J., **2017**, *23*, 17089-17094.

1) *Synthesis of Zintl Triads Comprising Extended Conjugated π-Electronic Systems:* $[RGe_9{-}CH{=}CH{-}CH{=}CH{-}Ge_9R]^{4-}$ *(R =* $-CH{=}CH_2$, $-C(CH_3){-}CH{-}CH{-}N(CH_2)_2NH_2$*)*

S. Frischhut, M. M. Bentlohner, W. Klein, T. F. Fässler

Inorg. Chem. **2017**, *56*, 10691-10698.

MANUSCRIPTS FOR PUBLICATION:

Acyl-Functionalized Deltahedral Ge_9 *Clusters* $[\{(Me_3Si)_3Si\}_2Ge_9R']^-$ *(R' = Acyl Functionalities)*

S. Frischhut, K. Frankiewicz, T. F. Fässler.

The Reaction of Ethylenediamine with 1,4-Bis(trimethylsilyl)butadiyne and the Role of Water

S. Frischhut*, M. M. Bentlohner*, T. F. Fässler.

Three-Dimensional Covalent Linkage of four Deltahedral Ge_9 *Clusters via a Central Ge Atom: Synthesis and Crystal Structure of* $K_4[\{Me_3Si)_3Si\}_2Ge_9]_4Ge$

S. Frischhut, P. Jutzi, T. F. Fässler.

Deltahedral Ge_9 *Cluster-Expansion with Pentamethylcyclopentadienylsilicon(II) Cation*

S. Frischhut, J. V. Dums, W. Klein, P. Jutzi, T. F. Fässler.

* These authors contributed equally to this work

CONFERENCE CONTRIBUTIONS

1) *Linking Deltahedral Zintl Clusters with Conjugated Building Blocks to Zintl Triads and Solubility Enhancement by Cation-Exchange*

S. Frischhut*, M. M. Bentlohner, T. F. Fässler

Poster, GDCh Scientific Forum Chemistry 2015, Dresden

2) *Linking Deltahedral Zintl Clusters*

S. Frischhut*, M. M. Bentlohner, T. F. Fässler

Poster, GDCh Scientific Forum Chemistry 2017, Berlin

3) *Zintl Triads as Promising Candidates for Application in Hybrid Solar Cells*

S. Frischhut*, W. Klein, M. M. Bentlohner, T. F. Fässler

Poster, Solar Technologies go Hybrid, 2017, Munich

4) *Functionalization of Ge_9 Zintl Clusters*

S. Frischhut*

Oral presentation, mini-symposium of Fonds der Chemischen Industrie scholars, 2018, Munich

5) *Ge_9 Cluster Expansion with Low-Valent Silicon Compounds*

S. Frischhut*, P. Jutzi, T. F. Fässler

Poster, 9th European Silicon Days, 2018, Saarbrücken

6) *UV-Vis Spectroscopic Investigations on Deltahedral Ge_9 Clusters and Specific Functionalization*

S. Frischhut*, W. Klein, T. F. Fässler

Poster, Solar Technologies go Hybrid, 2018, Würzburg

* presenter